Advances in Pavement Design through Full-scale Accelerated Pavement Testing

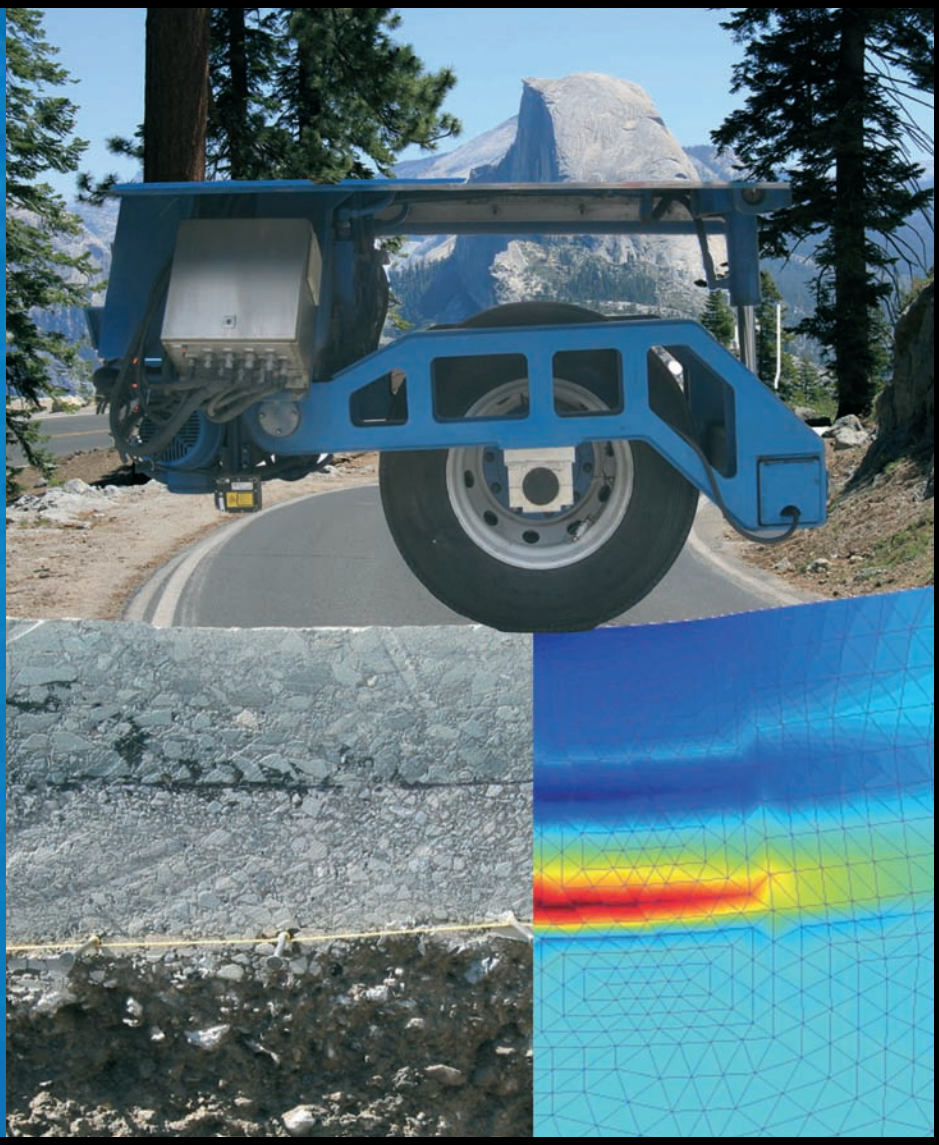

Editor
David Jones

Co-editors
John Harvey, Angel Mateos, Imad Al-Qadi

CRC Press
Taylor & Francis Group
A BALKEMA BOOK

ADVANCES IN PAVEMENT DESIGN THROUGH FULL-SCALE ACCELERATED PAVEMENT TESTING

This page intentionally left blank

PROCEEDINGS OF THE 4TH INTERNATIONAL CONFERENCE ON ACCELERATED PAVEMENT TESTING, DAVIS, CA, USA, 19–21 SEPTEMBER 2012

Advances in Pavement Design through Full-scale Accelerated Pavement Testing

Editor

David Jones
University of California Pavement Research Center, UC Davis, USA

Co-Editors

John Harvey
University of California Pavement Research Center, UC Davis, USA

Angel Mateos
CEDEX Transport Research Center, Madrid, Spain

Imad Al-Qadi
University of Illinois at Urbana-Champaign, USA

CRC Press
Taylor & Francis Group
Boca Raton London New York Leiden

CRC Press is an imprint of the
Taylor & Francis Group, an **informa** business

A BALKEMA BOOK

CRC Press
Taylor & Francis Group
6000 Broken Sound Parkway NW, Suite 300
Boca Raton, FL 33487-2742

Version Date: 2012912

International Standard Book Number-13: 978-0-203-07301-8 (eBook - PDF)

Advances in Pavement Design through Full-scale Accelerated Pavement Testing – Jones, Harvey, Mateos & Al-Qadi (Eds.)
© 2012 Taylor & Francis Group, London, ISBN 978-0-415-62138-0

Table of contents

Part 9: Development and calibration of empirical and mechanistic-empirical pavement design procedures and models

Part 10: Benefit-cost analysis of accelerated pavement testing

Advances in Pavement Design through Full-scale Accelerated Pavement Testing – Jones, Harvey, Mateos & Al-Qadi (Eds.)
© 2012 Taylor & Francis Group, London, ISBN 978-0-415-62138-0

Preface

Every country in the world has aging road and airport infrastructure, and in many instances, it has not been maintained at optimum levels because of funding constraints. As a consequence, pavement engineers are facing an ever-increasing challenge to provide cost-effective approaches to rehabilitate this infrastructure, within constraints of limited financial resources, geometric limitations, traffic control windows, and the need to increase the use of recycled materials. To meet this challenge in this constrained environment, pavement engineers are looking to use better understanding of pavement mechanics, new types of structures, innovative materials and additives, improved materials processing, and new construction techniques. However, the gap remains between mechanistic modeling based on laboratory test characterization and full-scale long-term performance monitoring that lead to the establishment of accelerated pavement testing (APT) facilities. No engineer wants to take the risk of trying something new without a good understanding of how it is going to behave in the long-term and if, when, and how it will fail. In addition, mechanistic models developed based on hypotheses and assumptions and fed by actual materials, traffic and climate data, need validation and calibration with full-scale testing that provides "total system" results in a relatively short period of time compared with the many years required for long-term monitoring. Laboratory testing and scaled down physical simulation can answer some of these questions, but the only true test is to subject the "new" pavement concept to realistic traffic and reasonable environmental conditions. Full-scale accelerated pavement testing, either on test roads or linear/circular test tracks, has proven to be an appropriate alternative to long-term experiments on in-service pavements; it provides quick comparisons between current and new practice and the ability to observe and measure behavior, with minimal risk at relatively low cost.

International conferences dedicated to APT have been held since 1999 to share learning and findings. This fourth conference, APT2012, held in Davis, California in 2012, follows successful conferences in Reno, Nevada in 1999, which focused on the establishment of APT facilities and early findings; Minneapolis, Minnesota in 2004, which focused on operations, results and their implementation; and Madrid, Spain in 2008, which looked at results and implementation from a greater number and variety of APT programs, and explored the benefits versus the costs of APT. Themes of papers for APT2012, which are organized as chapters in this proceedings, cover a range of topics, including the establishment of new facilities arising from the growing interest in and proven benefits of APT, reviews of facilities that have been in operation for a number of years and the impacts that they have had on pavement engineering, findings from studies undertaken since the last conference with a focus on new material developments, and the role of APT in developing and calibrating mechanistic-empirical design procedures and performance models.

Pavement technology has been continually evolving for many decades, much of it supported by APT. Since the AASHO Road Test, which represents one of the first, and probably the most documented, modern APT experiment, to the present, APT facilities have been used to develop solutions for a range of pavement design issues. This has required a continuous adaptation of testing facilities and analysis techniques, needed to better understand and solve future challenges. The Fourth International Conference on APT provides a unique opportunity to explore recent advances as well as to assess future needs and trends, on the basis of the experience from more than 25 APT programs around the world.

After rigorous review by a scientific committee of experts experienced in APT operations, data analysis, and/or implementation of findings from APT experiments, 55 papers from 16 countries were finally accepted for presentation and discussion at the conference and publication in these proceedings.

We would personally like to thank each of the authors for sharing their APT experiences. We would also like to thank the APT2012 Conference Scientific and Organizing Committees, especially the members and friends of the Transportation Research Board's Standing Committee on Full-scale Accelerated Pavement Testing (Committee AFD40), for reviewing the papers and helping to maintain the conference series' high standard.

David Jones, Editor
John Harvey, Angel Mateos, Imad Al-Qadi, Co-editors

Davis, California, 2012

This page intentionally left blank

Advances in Pavement Design through Full-scale Accelerated Pavement Testing – Jones, Harvey, Mateos & Al-Qadi (Eds.)
© 2012 Taylor & Francis Group, London, ISBN 978-0-415-62138-0

Conference Organization

CHAIRPERSONS

John Harvey	University of California, Davis, USA
David Jones	University of California, Davis, USA
Angel Mateos	CEDEX Transport Research Center, Madrid, Spain
Imad Al-Qadi	University of Illinois at Urbana-Champaign, USA

SCIENTIFIC COMMITTEE AND REVIEW PANEL

Chairman David Jones, USA

David Alabaster, New Zealand
Muhammet Akpinar, Turkey
Jean-Maurice Balay, France
Gabriel Bazi, USA
Ronald Blab, Austria
David Brill, USA
Tom Burnham, USA
Al Bush, USA
Bernardo Caicedo, Columbia
Bouzid Choubane, USA
German Claros, USA
Tim Clyne, USA
Nicolas Coetzee, USA
Edel Cortez, USA
George Crosby, USA
Samer Dessouky, USA
Brian Diefenderfer, USA
Louw Du Plessis, South Africa
Mostafa Elseifi, USA
Rebecca Embacher, USA
Glenn Engstrom, USA
Amy Epps Martin, USA
Sigurdur Erlingsson, Sweden
Dulce Feldman, USA
Navneet Garg, USA
Daba Gedafa, USA
Nelson Gibson, USA
Andrew Gisi, USA
Salil Gokhale, USA
Roger Green, USA
James Greene, USA
John Harvey, USA
Gordon Hayhoe, USA
Jaime Hernandez, USA
Gregers Hildebrandt, Denmark
Pierre Hornych, France
Mustaque Hossain, USA
Fred Hugo, South Africa
Jawad Hussain, New Zealand
Maureen Jensen, USA
Yigong Ji, USA
David Jones, USA
Issam Khoury, USA
Erwin Kohler, Chile
Jeremy Lea, USA
Larry Lynch, USA
Joe Mahoney, USA
James Maina, South Africa
Mihai Marasteanu, USA
Angel Mateos, Spain
Rebecca McDaniel, USA
Michael Moffatt, Australia
Tommy Nantung, USA
Kent Newman, USA
Bill Nokes, USA
Hasan Ozer, USA
Manfred Partl, Switzerland
Buzz Powell, USA
Xicheng Qi, USA
Steven Quenneville, USA
Rolf Rabe, Germany
Jan Ritter, Germany
Mary Robbins, USA
Jeffery Roesler, USA
Stefan Romanoschi, USA
Elzbieta Sadzik, South Africa
Luis Loría Salazar, Costa Rica
Shad Sargand, USA
Tom Scullion, USA
Kieran Sharp, Australia
Kyle Shepard, USA
Jean-Michel Simonin, France
Injun Song, USA
Bruce Steven, New Zealand
Wynand Steyn, South Africa
Shelley Stoffels, USA
Marshall Thompson, USA
Erol Tutumluer, USA

Per Ullidtz, Denmark
Hao Wang, USA
Kim Willoughby, USA
Andreas Wolf, Germany
Ben Worel, USA
Rongzong Wu, USA
Richard Yeo, Australia
Hao Yin, USA

YOUNG PROFESSIONAL COMMITTEE

Chairman Arash Rezaei, USA

Brandon Bortz, USA
Erdem Coleri, USA
Fabricio Leiva-Villacorta, USA
Stefan Louw, South Africa
Debakanta Mishra, USA
Songsu Son, USA
Adriana Vargas-Nordcbeck, USA
Richard Willis, USA

ORGANIZING COMMITTEE

Imad Al-Qadi, USA
Helen Bassam, USA
John Harvey, USA
David Jones, USA
Jeremy Lea, USA
Bill Kuhlman, USA
Angel Mateos, Spain
Laura Melendy, USA
David Miller, USA
Richard Willis, USA

Part 1: Overview of accelerated pavement testing

This page intentionally left blank

Advances in Pavement Design through Full-scale Accelerated Pavement Testing – Jones, Harvey, Mateos & Al-Qadi (Eds.)
© 2012 Taylor & Francis Group, London, ISBN 978-0-415-62138-0

A history of modern accelerated performance testing of pavement structures

R.B. Powell
National Center for Asphalt Technology, Auburn University, Alabama, US

ABSTRACT: The type of research conducted at the National Center for Asphalt Technology's (NCAT) Pavement Test Track is known as full-scale Accelerated Performance Testing (APT). APT is the controlled application of a prototype wheel loading, at or above the appropriate legal load limit, to a layered pavement system to determine pavement response and document performance as damage accumulates in a compressed time period. A great variety of APT experiments have been executed over the last hundred years. This document is the result of a literature review on the history and evolution of APT that was foundational to the success of the first research cycle at the NCAT Pavement Test Track.

1 INTRODUCTION

It is difficult to conduct reliable field performance comparisons on open roadways for several reasons. Since user costs and reconstruction expenditures are usually very high when test pavements fail, there can actually be a disincentive to experiment with new methods and materials. When field comparisons are attempted, the quality of construction sometimes varies greatly from region to region. As a consequence of the longer testing period, it is not uncommon for post-construction personnel reassignments to make it difficult to maintain continuity of effort. After construction, there is typically much uncertainty in the number and weight of axle loadings. Lastly, environmental effects can vary significantly from region to region within a single state's jurisdiction.

The type of research conducted at the National Center for Asphalt Technology's (NCAT) Pavement Test Track is known as full-scale accelerated performance testing (APT). It is classified as full-scale because actual vehicles are used to apply the traffic loadings, and it is referred to as accelerated performance because the design traffic that would normally be applied over many years on an open roadway is compressed and applied in only two years. In order to assess the ability of the NCAT study to effectively overcome the difficulties described in the preceding paragraph, the literature relating to the history of APT was reviewed and summarized.

2 BACKGROUND

APT is a type of research that has been utilized in numerous programs around the world to generate comparative results intended to reveal differences in long-term performance potential within a relatively short period of time. The term has been comprehensively defined in the following way:

"*… APT is defined as the controlled application of a prototype wheel loading, at or above the appropriate legal load limit to a prototype or actual, layered, structural pavement system to determine pavement response and performance under a controlled, accelerated accumulation of damage in a compressed time period. The acceleration of damage is achieved by means of increased repetitions, modified loading conditions, imposed climatic conditions, the use of thinner pavements with a decreased structural capacity and thus shorter design lives, or a combination of these factors. Full-scale construction by conventional plant and processes is necessary so that real world conditions are modeled*" (Metcalf, 1996).

Because of the broad spectrum of research conducted globally on pavement performance that will be described in detail in the following paragraphs, a more liberal definition of APT is more applicable. The following verbiage has recently been provided to comprehensively describe APT:

"*… the controlled application of wheel loading to pavement structures for the purpose of simulating the effects of long-term in-service loading conditions in a compressed time period*" (Hugo and Martin, 2004).

Accelerated testing is useful for many reasons. If all performance testing was conducted on open roadways, it would be impossible to fully consider the effect of increasing traffic demands on future performance. For example, the total tonnage that will be shipped by trucks in the United States is projected to increase 49 percent by 2020 (TRIP, 2004). This is a tremendous increase, and would mean that current open roadway performance testing at today's traffic level would only reveal how pavements performed in the past rather than in the future. Additionally, the impact of illegal axle loadings would be beyond the scope of available data.

Lastly, safety considerations would make it impossible to obtain continuous performance data over time.

For this reason, there has been much national and international interest in supporting APT efforts in recent decades. In 1986, the planning document for the Strategic Highway Research Program (SHRP) listed APT as a potential study type in Long-Term Pavement Performance (LTPP) research (TRB-SHRP, 1986); however, no mention is made in subsequent LTPP documents. When asked to reconsider supplementing the LTPP database with APT data in 2002, the SHRP planning committee responded positively but cited concerns of limited resources. Current efforts focus on using APT to generate accelerated data for select Specific Pavement Studies (SPS) sections, which would enhance LTPP while at the same time provide data to relate APT to actual field performance. If these efforts are successful, APT would be used only on off-site locations due to safety concerns to the motoring public (Jones, 2003).

3 FULL-SCALE TEST TRACKS

Full-scale testing has made straightforward contributions to the paving industry over the last century because it does not require significant scale, time, or environmental extrapolation. Of course, the utilization of test tracks has been hindered by cost, which can be prohibitive depending on research funding mechanisms. Throughout the history of the industry, pavement professionals have invested in test tracks when significant changes in either vehicle or pavement technology has rendered the current state of practice inadequate or lacking.

The first asphalt pavement in the US was placed in Newark, NJ in 1870 using asphalt binder and rock asphalt imported from Europe. In 1871, a pavement was placed in Washington, DC using crushed stone and domestic coal tar (Harman et al., 2002). The first significant asphalt project in the US was placed in 1876 on Pennsylvania Avenue in Washington, DC. It covered 45,000 square m and was produced with what was considered at the time the ideal material – Trinidad asphalt (Gillespie, 1992).

A 30,000 square meter project on the same street that was produced with North American rock asphalt provided an opportunity for the first domestic performance comparison test. A finding of equal performance set the stage for greater utilization of non-Trinidad material in the future. More projects followed, and builders' understanding of the engineering principles of asphalt construction deepened. By 1910, refined or petroleum asphalt had permanently overtaken both imported Trinidad and domestic rock asphalt (Gillespie, 1992). Hot-mix asphalt pavements became more prevalent in the United States when the developing refinery and terminal infrastructure made the distribution of liquid asphalt cost effective.

In the early 1900s, highway projects were boosted by the hope of automobile-centered prosperity through a state and national road building movement that promoted the ideal of transcontinental highways (Schauer, 2003). Traffic volumes increased and governments rushed to provide roads that were reliably passable by both automobiles and trucks. Asphalt construction that was used to pave the growing infrastructure with available materials was largely in the hands of private companies, who produced mixes in secrecy under the protection of patents. Fortunately, many of the patents that prevented growth and understanding in the industry began to expire around 1920 (Gillespie, 1992).

The first documented road test in the United States was initiated in 1918 at the Bureau of Public Road's Experimental Farm in Arlington, Virginia. The purpose of this experiment, which was built on the site that would ultimately become Reagan National Airport, was to measure impact forces of different types of wheel loads (Weingroff, 1996).

One of the earliest efforts in the United States to conduct accelerated performance testing to enhance the general understanding of the road building process was the Bates Experimental Road. In 1917, voters in Illinois overwhelmingly approved a $60 million bond issue to finance new highway construction. In order to utilize the most effective designs, the State's Bureau of Public Roads commissioned what would become known as the Bates Experimental Road. Sixty-eight test sections were built near Springfield, Illinois and trafficked in 1922 and 1923 with axle loads that varied between 11 and 58 kN. Trucks equipped with solid rubber tires ran on pavements with brick, asphalt concrete, and Portland cement concrete wearing surfaces to determine which designs lasted the longest under different loading conditions (Mahoney, 2000).

During the 1920s, the automobile and truck manufacturing industries switched from solid rubber to pneumatic tires and from single tires to dual assemblies. These advances led to greater loads and much larger vehicles. By 1932, the American Association of State Highway Officials (AASHO) recommended a legal load of 71 kN for single axles. This limit was raised in 1942 to 80 kN to accommodate larger wartime shipments. In 1946, AASHO recommended a 142 kN tandem axle limit. Between the 1920s and the 1950s, the consistent trend was for more trucks with larger loads (Mahoney, 2000).

Many road tests were conducted in the years before loads changed dramatically as a result of World War II. The Hybla Valley Test was conducted in Virginia by the Bureau of Public Roads, the Highway Research Board (HRB), and the Asphalt Institute. The Pittsburg, California Road Test was conducted using surplus army trucks with solid tires (Pasko, 1998). In a test conducted by the US Army Corps of Engineers on a track in Stockton, California it was first observed that necessary pavement thickness increased directly with the logarithm of axle load repetitions (Hveem, 1948).

The Corps of Engineers has conducted accelerated performance testing (such as the Lockbourne Air Force Base test) of various types for over fifty

years (Mahoney, 2000). Their primary focus has been consistent with the mission of the Department of Defense, which is force projection and sustainment; however, their work also at times addressed the needs of the Federal Aviation Administration and the Federal Highway Administration (Lynch et al., 1999). Numerous mission-oriented Flexible Pavement Laboratory tests were conducted by the Corps at their Vicksburg, Mississippi Waterways Experiment Station (WES) in order to evaluate hot weather performance, and complementary tests were conducted at their Hanover, New Hampshire Cold Regions Research and Engineering Laboratory (CRREL) in order to consider the effect of cold weather (Mahoney, 2000).

Among other advances, these programs produced California Bearing Ratio (CBR) design procedures. Both accelerated and full-scale tests were used to extend California Highway Department design curves to aircraft loads and environmental extremes. Accelerated full-scale pavement testing was later used to incorporate the Marshall stability method for expedient airfields. In the late 1940s, WES experiments concluded that lower loads with higher pressures were more detrimental than higher loads at lower pressures. All research conducted by the Corps prior to the 1970s was conducted in the field (Lynch et al., 1999).

As a consequence of new postwar load limits, a flurry of activity occurred after the end of World War II. The Maryland Road Test was conducted just south of Washington, DC near La Plata, Maryland in 1950 and 1951 by the Bureau of Public Roads (now the Federal Highway Administration, or FHWA) in conjunction with the Highway Research Board (now the Transportation Research Board), several states, truck manufacturers, and other highway-related industries. In this rigid pavement experiment, an existing 1.8 km two-lane highway was carefully inventoried, instrumented, and traversed by 1,000 trucks per day (Pasko, 1998). The test sections for this study are reported to have been built in 1941, likely interrupted by US participation in World War II (Berthelot, 2004).

The WASHO Road Test was conducted in Malad, Idaho from 1952 to 1954 with HRB again directing the project. The focus of the work was flexible pavements with thicknesses of either 50 or 100 mm as part of from 150 to 550 mm of total structural depth. The total cost of this effort was reported to be $650,000, with two thirds of the cost provided by state DOTs. This 1950s figure equates to $84,000 per section in 1999 dollars, encompassing forty-six sections (without replicates) on two loops with four lanes. One unique load was applied per test lane (80 or 100 kN on single axles, 142 or 178 kN on tandem axles), with no traffic allowed in the winter season and limited traffic in the spring. All totaled, 240,000 load applications were applied via 120,000 passes (Mahoney, 2000).

The WASHO Road Test was a collaboration by twelve state DOTs, vehicle manufacturers, petroleum companies, three Universities, the US Army, and the trucking industry (Mahoney, 2000). The study provided valuable experience upon which subsequent testing would be based, but the results could not be used to describe pavement performance in quantifiable terms (Berthelot, 2004).

The AASHO Road Test has had the greatest impact on the practice of pavement engineering through the landmark finding of the well-known "4th power rule" that described the relative damaging effect of axle loads (National Research Council, 1962). It was conducted between 1956 and 1961 on both rigid and flexible pavements off I-80 in Ottawa, Illinois at a total cost of $27 million. Of this total, $12 million was provided by state DOTs and $7 million was provided by the BPR (the balance came from many other smaller sources). In 1999 dollars, the cost per section has been reported to be $172 thousand (Mahoney, 2000).

A total of 468 flexible sections with three surface thicknesses, three base thicknesses, and three subbase thicknesses were installed and tested at the facility, compared with 368 rigid sections, on six test loops that comprised a full factorial experiment. The length of each flexible test section was 30 m, while the length of each rigid test section was 73 m. The project was delayed for five years so it could be modified in consideration of the WASHO test (Mahoney, 2000), and each sponsoring state DOT sent materials for inclusion in the testing program (Berthelot, 2004).

The general practice of pavement engineering in the United States would for decades be determined by results from the full factorial regression analysis conducted on performance data from the AASHO Road Test; however, regional interest in the value of accelerated performance testing persisted. For example, the Penn State Test Track was built at the Pennsylvania Transportation Institute and began testing pavements in 1971 for the purpose of refining pavement design methodology in Pennsylvania and surrounding states (Hugo and Martin, 2004). This project is reported to have contributed significantly to pavement design in the northeastern United States (Mitchell, 1996); however, the facility has not been active in pavements research since 1983 (Hugo and Martin, 2004). Since that time, innovative vehicle research (e.g., the study of hybrid vehicle electrical components) has become a more prominent area of study at that institution (Pennsylvania Transportation Institute, 2005).

With the rise in popularity of APT load simulators (explained in subsequent paragraphs), interest in full-scale test tracks subsided over the next two decades. As experience with load simulation devices revealed their limitations, researchers gradually realized that test tracks and simulators each provided distinct complementary information to engineers on the long-term performance potential of pavements. This movement was encouraged by the notable changes that were occurring in the industry as a result of the Strategic Highway Research Program (SHRP) and Superpave implementation.

Although not an accelerated loading operation, the first facility to emerge from this renewed interest in full-scale test tracks was the Minnesota Road Research Project (MnRoad). Constructed adjacent to I-94

northwest of Minneapolis, MnRoad was opened to traffic in 1994. Twenty-three mainline test sections (nine concrete and fourteen asphalt) were placed into service, along with seventeen with lower traffic volumes. The total cost of construction is reported to have been $25 million. The facility is supported by natural silty clay subgrades that are susceptible to frost action, so four sections were underlain with imported sand in order to vary performance. The two primary objectives of the ten-year project were to facilitate the development, validation and implementation of mechanistic-empirical design procedures, as well as to determine when truck load restrictions should be in place in order to prevent excessive damage during spring thaws (Newcomb et al., 1999).

Also of significant recent interest is the now completed Westrack project. Located about 100 km southeast of Reno at the Nevada Automotive Test Center, Westrack was a $14.5 million project in which robotic tractors were utilized to pull triple trailer trains around a 3 km test oval in the process of applying 4.8 million ESALs. The facility was comprised of twenty-six individual test sections (each with a length of 61 m), eight of which had to be replaced after 2.8 million ESALs (thus, performance data was available for thirty-four total sections). The primary objectives of the experiment were to develop performance related specifications and validate Superpave, which meant that both structure and materials were variables in the experiment (Epps et al., 1999). Traffic began on the desert site in 1997, which was selected from various proposals based on the anticipated mild winters and 100 mm of annual rainfall (Mitchell, 1996).

The federally controlled WesTrack project generated an increased interest within state departments of transportation in accelerated performance pavement testing. Where WesTrack was intended to answer broad questions of national significance, many states wanted the opportunity to direct research that would answer local questions important to their individual jurisdictions. In response to this increased interest, in the mid-1990s NCAT began the planning process to develop a cooperatively funded accelerated loading test facility in eastern Alabama. After several years of planning with representatives from regional departments of transportation, the concept of the cooperatively funded NCAT Pavement Test Track would become a reality.

4 LOAD SIMULATION DEVICES

The development and proliferation of a great variety of load simulation devices after the completion of the AASHO road test would lead many to believe that such technologies are a recent phenomenon, but this is not the case. At the same time that engineers in the United States were focusing on vehicle-pavement interaction through various full-scale tests (e.g., Arlington, Bates, etc.), engineers in the United Kingdom (UK) were working to develop and refine clever and cost-effective load simulation technologies.

APT research was first conducted in the UK at the Transport Research Laboratory in 1912 with the introduction of the National Physical Laboratory's "Road Machine." The device was later transferred to the Road Research Laboratory (RRL). It ran like a carousel, spinning a 13 kN load at a speed of 14 km/h around a 10 m diameter test bed. The device simulated vehicle wander and operated inside a housing with environmental control. Initial work with the "Road Machine" examined the use of asphalt mixes over concrete (Brown and Brodrick, 1999).

In 1933, the original device was replaced by the "Road Machine 2," which propelled a 22.5 kN load at a speed of 48 km/h around a 34 m diameter test bed. The next generation "Road Machine 3" was implemented in 1963, which increased the capability of the simulations to 68.5 kN at a maximum speed of 25 km/h. Work with the #3 unit focused primarily on investigating elastic responses in layered asphalt systems, concluding that elastic theory worked well for cool, stiff pavements but that the viscous effect at higher temperatures introduced important uncertainties. "Road Machine 3" was effectively replaced by the Pilot Scale Facility, when the laboratory moved in the late 1960s, in which a manually driven truck trafficked 28 m by 7 m by 2 m deep test pits (Brown and Brodrick, 1999).

At about this same time, another APT device was constructed at Washington State University in the United States. This facility was a full-scale circular test track that became operational in 1967. It is reported that the Washington circular track was the first US facility designed for modern accelerated performance testing (Hugo and Martin, 2004).

Other APT technologies were evolving simultaneously in the late 1960s. The first prototype unit that would eventually become known as the Heavy Vehicle Simulator (HVS) was under development in South Africa by the Council for Scientific and Industrial Research (CSIR) at this time. Although a production unit would not be completely refined until the late 1970s, HVS research provided the dominant influence in the development of South African pavement engineering capability. It is considered a fundamental tool in developing appropriate pavement structural design and analysis methods, and has been a catalyst for the close cooperation between South African road authorities and researchers ever since. Modern versions of the machine have been built to provide dynamic load simulation as well as an option for super heavy aircraft-type loadings (Kekwick et al., 1999).

Meanwhile, APT technology was progressively evolving in Europe. The Nottingham Pavement Test Facility was commissioned in 1973 in the UK as a half-scale laboratory-housed machine to serve as a theoretical test bed. It was a separate and distinct operation from the Pavement Test Facility at the Road Research Laboratory (RRL), which would not be built until 1985. The Nottingham device loads isolated test pits that are 4.8 m by 2.4 m by 1.4 m deep; however, there was no capability to vary water content in the

sealed pits during a test. It is reported that the device is still used constantly for comparative testing. Loading can be varied from zero to 15 kN via a 150 mm wide tire that travels at a speed of up to 16 km/h. Test temperature can be controlled between 15 and 30°C and up to 600 mm of wander can be imposed (Brown et al., 1999).

The Danish Road Testing Machine (RTM) became operational at about this same time (1973) under the ownership of the Danish Road Institute and the Danish Technical University in Lyngby. It is an indoor, full-scale facility that is 27 m long and 2.5 m wide. The actual test section is 9 m long and 2 m deep. The RTM operates within a 4 m wide by 3.8 m high climate chamber that uses heating and cooling equipment to maintain test temperatures between –20 and 40°C. Groundwater can be automatically raised or lowered as desired. Loads can be applied by either single or dual wheels at loads of up to 65 kN. The maximum velocity of the load assembly is 30 km/h, which accommodates up to 10,000 load repetitions in a workday. The lateral position of the wheel can be automatically changed during testing to simulate wander (Larsen and Ullidtz, 1998).

Although it is reported that one linear APT and two circular APTs were placed into service in Europe between 1975 and 1980 (Mateos, 2002), global implementation of the technology was not embraced until several years later, at a time when many countries faced growing transportation challenges. For example, only one third of Australia's 800,000 km network of roads has paved surfaces. The loading limits of unbound granular pavements were not well defined by this time, but the continent was in the midst of a twenty-year, fourfold increase in overland freight shipments. For this reason, the Accelerated Loading Facility (ALF) was developed and implemented at an initial cost of $1 million as a successor to their Economics of Road Vehicle Limits study (a quarter-scale linear test track). Between the year the program was implemented (1983) and 1999, over 120 different pavement types had been studied. As continued evidence of the practical nature of their work, recent studies with the Australian ALF have investigated alternative materials and maintenance intervention options (Sharp, 1999).

The French Nantes facility was also commissioned in the following year (1984). Reported to have been inspired by the AASHO Road Test, this unique design utilizes a carousel that travels at a maximum speed of 100 km/h via a robust central power source. Adjustable load axle assemblies are mounted at the ends of 20 m long adjustable travel arms, on which between 90 to 150 kN single or multiple axles may be mounted. Although originally built with only one unit, the facility now utilizes three carousels designed for unattended night and weekend operation. In the first 15 years of operation, 50 million loadings were applied in 180 experiments at a reported total cost of between $500,000 and $700,000 per test. Experiments have ranged from product evaluations and model development to load configuration experimentation and examination of equivalency laws (Gramsammer et al., 1999). Each of the three annular test tracks have an outside diameter of 40 m and an inside diameter of 28 m. The research pavements slope two percent to the interior with a circumference of 110 m. The mean radius of each track, which may have up to four different pavement structures, is 17.5 m. Only one of the three existing tracks is built inside an isolating concrete pit with moisture control capabilities (the other two are built on natural soils) (Turtschy and Sweere, 1999).

Another Pavement Test Facility was constructed in 1985 at the UK's Road Research Laboratory to allow the existing Nottingham Pavement Test Facility to continue to serve as a theoretical test bed. The RRL device, which supported more practical APT research, applied wheel loads of up to 98 kN at speeds of up to 20 km/h on pavements built in 28 m by 10 m by 3 m deep test pits. The length of each test section is 7 m, and different wheel configurations can be studied in either bi- or unidirectional loading with or without wander (Brown and Brodrick, 1999).

Australian ALF technology was first imported to the United States in 1986 and placed into service at FHWA's Pavement Test Facility (PTF), which is located just outside of Washington, DC at the Turner-Fairbank Highway Research Center in McLean, Virginia. The primary objective of the PTF is to develop and verify new specifications, designs, and test procedures using two separate ALF machines that run tests on alternative pavement designs (structures or materials) or on identical pavement designs but in alternative loading configurations (e.g., by varying tire pressure or axle loading). Each device is capable of applying 35,000 axle passes per week at a load ranging from 44 to 100 kN traveling at a speed of 17.5 km/h on a test bed that accommodates twenty-four full-scale test sections, each 14 m by 4 m, with environmental control (Mitchell, 2005). As an example of the type of research conducted at the PTF, a Superpave validation experiment was initiated in 1994 in which rutting and fatigue were measured in forty-eight test sites over twelve lanes in a effort to study binder properties and performance prediction testing (Sherwood et al., 1999).

Another unique European design has been utilized for Spain's APT, operational in Madrid since 1988. The CEDEX test oval has two 75 m straight sections connected by curves, which produces a total length of 304 m. Each tangent can support up to three 20 m test sections (since only 67 m of the tangents lie within curve transitions). Concrete pits that are 2.6 m deep by 8 m wide (with the capability of being flooded) completely isolate test sections, with sprinklers and covers provided to simulate different performance environments. The CEDEX load bogie runs around a concrete rail on the interior of the oval. Electric power for the guidance apparatus and load assembly is provided via guide rail. A typical dual tire load is 63.5 kN, and at least two bogies can run simultaneously. The device has the capability of simulating wander, with 400 mm

of transverse movement control across a 1.3 m wide wheelpath (Turtschy and Sweere, 1999). The initial cost for the CEDEX track is reported to have been $2 million. So far, curve research has been limited to surface courses and roadway paints because of the higher shearing forces (Ruiz, 1999).

An example of a highly functional completely indoor design was built in Christchurch, New Zealand in 1989. The Canterbury Accelerated Pavement Testing Indoor Facility (CAPTIF) is housed in a hexagon shaped building 26 m wide and 6 m high. An annular tank that is 4 m wide and 1.5 m deep confines the bottom and sides of test pavements that are built in the tank using small dozers, pavers, etc. The resulting track has a median diameter of 18.5 m and a circumference of 58 m. Loading is applied by either spring- or airbag-suspended Simulated Loading and Vehicle Emulators (SLAVEs) with loading arm radii that can be set differently allowing for the testing of multiple wheelpaths on a single track. The CAPTIF facility was used in the DIVINE program (Dynamic Interaction Vehicle Infrastructure Experiment), which was intended to quantify performance differences related to initial material and construction variability and performance differences due to variability in wheel loadings induced by varying tire-suspension dynamics (Kenis and Wang, 1999).

In recent decades, APT technology has also been deployed in Asia. Stabilized bases under asphalt pavements are widely used in China, but most of the early research was with light vehicles at low traffic levels. China's Research Institute of Highways (RIOH) bought an ALF unit from Australia in 1989 to facilitate work on stabilized bases under heavy loads and high traffic levels. Their initial testing program was completed in 1991, but work continues with stabilized bases due to the economy of this method of construction and its continued use in their developing infrastructure. In its current configuration, their ALF can apply loads varying from 50 to 80 kN at speeds of up to 20 km/h over 12 m long test lengths. The device can apply 400 load cycles per hour in a unidirectional manner, typically with a dual wheel across a normally distributed wheelpath. Environmental factors are not controlled at this facility (Shutao et al., 1999).

Although the growth of APT facilities in Europe stalled in the early 1990s, work continued on developing programs. Construction of the LINTRACK facility located in Delft, Netherlands began in 1987, with proof testing completed in 1991. This device can apply loads between 15 and 100 kN via single or dual tires with up to 2 m of wander. At a speed of 20 km/h, approximately 1,000 bi-directional wheel passes can be applied in a testing hour. The device has provisions for environmental control of experimental pavements that can be built with normal paving equipment. The propulsion system for the load application mechanism is a steel cable wrapped around a powered drum, and the entire assembly operates in a 23 m by 6 m by 5 m shed. Testing is conducted on the middle 3.5 m of test pavements, with 4 m on either end for acceleration and deceleration of the load wheel (thus, 11.5 m total trafficked length) (Houben and Dommelen, 2005). It is reported that LINTRACK is mobile and can be used to test in-service pavements (Mateos, 2002).

At the same time that European efforts were leveling off, the continued utilization of ALF technology at the PTF site in Virginia was encouraging more American interest in APT. An original linear device was subsequently built in 1991 at Indiana's Purdue University. The Purdue APT is an indoor facility consisting of an environmental building over an isolated concrete test pit. Heating is applied via plumbing in the pit through which hot water is cycled. A load carriage rolls back and forth down a movable reaction beam at an average speed of 8.3 km/h (with or without up to 250 mm of wander) to apply traffic to dual test pavements. Testing can either be conducted unidirectionally (in which the wheel is lifted for the return trip down the beam) or in a bi-directional manner (without lifting). Loads of up to 89 kN can be applied via single or dual wheels, although 40 kN is the typical load. Each paving lane is placed at a width of 3 m, where two tests are conducted on each lane (thus, each test lane is 1.5 m wide). Separate 1.5 m wide concrete slabs lie at the bottom of the test pit in order to simulate the asphalt over concrete roadways common in Indiana (Galal and White, 1999).

Australian ALF technology was next utilized in the United States at the Louisiana Transportation Research Center (LTRC) Pavement Research Facility (PRF) located in Port Allen, Louisiana (across the Mississippi River from Baton Rouge). The first PRF-ALF experiment in 1992 compared historically prevalent flexible crushed stone and in-place soil cement stabilized base construction to alternative base construction methods suitable for semi-tropical climates. In this study, 6 million ESALs were applied to nine test lanes via the second ALF of its type in the United States (the first was at the Virginia PTF). The Louisiana PRF device is equipped such that 43 to 85 kN loads can be applied unidirectionally at 17 km/h, which produces up to 8,100 passes daily (Metcalf et al., 1999).

There was also interest in the development of APT technology in South America at this time. For example, a traffic simulator was designed and built between 1992 and 1994 at the Rio Grande do Sul Federal University in Brazil. The resulting structure is 15 m long by 4.3 m high and 2.5 m wide and holds a half axle with dual wheels. The running speed for the Brazilian device is 6 km/h over a 7 m travel path, and testing can be conducted with up to 400 mm of imposed wander (Merighi et al., 2001).

The age and condition of the US transportation infrastructure has influenced the proliferation of domestic APT programs. In 1993, CSIR worked with Dynatest and the California Department of Transportation (Caltrans) to validate the use of HVS technology in providing reconstruction guidance for California's aging system. As a result of this successful effort, two South African HVS systems were placed in service at Berkeley in 1994 (Pavement Research

Center, 2005). The objective of their ongoing research is to design rehabilitated pavements for a thirty-year service life with minimum thickness, maximum constructability, and minimum maintenance. The use of in-place reclamation and recycled materials has also featured in their studies. Their strategy consists of HVS testing, laboratory tests, and mechanistic-empirical design. At the time when their program was initiated, approximately one third of California's total 24,000 centerline km pavement infrastructure required corrective maintenance or rehabilitation (Harvey et al., 1999).

In 1995, a completely different approach to APT was introduced via the first operational tests of the Mobile Load Simulator (MLS) in Victoria, Texas. In the MLS design, six full standard tandem axles travel around an elliptical path as they traffic a section of pavement, lift off, pass back over (inverted) to the starting position, and traffic the section again (thus, traffic is applied in a unidirectional manner). This action occurred inside a 31 m by 4.5 m by 6 m tall environmental enclosure that is transportable. The cost to develop the original prototype over a period of five years is reported to have been $3.4 million, although it is estimated that any future units would only cost $2 million to produce. The six tandem axle assemblies are loaded with up to 150 kN each and travel at a speed of 18 km/h, which produces 6,000 axle repetitions per hour. Research efforts thus far have been intended to investigate new materials, determine load damage equivalency, and investigate truck component-pavement interaction (Hugo et al., 1999).

A new type of linear tester was constructed in Lancaster, Ohio in 1997 as a joint venture between Ohio State University and Ohio University. The Accelerated Pavement Loading Facility is used to evaluate both asphalt and concrete test pavement installed in a test pit that is 13.7 m by 11.6 m by 2.4 m deep. The device applies up to a 133 kN load via either single or dual tire assemblies. The entire assembly is enclosed in a room in which the environment can be controlled between –10 and 55°C, but large doors on both ends of the building are provided to facilitate conventional construction. Recent testing on the performance of asphalt pavements was followed with testing on ultra-thin whitetopping placed on rutted asphalt from a prior study (Edwards and Sargand, 1999).

Another new linear tester was installed at Kansas State University in 1997 (Hugo and Martin, 2004). The "K-APT" was installed inside a 651 square meter building, and consists of two 1.8 m deep pits of varying width at a length of 6.1 m. Loading can be applied in either a uni- or bi-directional manner with a movable load frame. In the K-APT design, an air suspension tandem axle with pneumatic loading moves back and forth via a drive belt assisted by spring reversal on either end of the travel path. It is reported to take 15 seconds for a complete down and back loading cycle, which produces a wheel speed of 8 km/h over a 4.3 m research length. The typical load configuration in Kansas testing is 150 kN on dual wheels (Vijayanath et al., 1999). Temperature can be controlled (from above via infrared heaters and from below via a subsurface heating system) between –23°C and 66°C (K-State Engineering, 2002). It is also possible to control the water table during testing. Research is funded through a group known as the Midwest States Accelerated Testing Pooled Funds Program, which includes DOTs in Iowa, Kansas, Missouri and Nebraska (Hugo and Martin, 2004).

Even though many European programs were fully developed by this time, several new facilities were placed into service in the late 1990s. The Danish Asphalt Rut Tester (DART) was designed and installed at the Danish Road Institute in 1997 for the purpose of testing wearing courses. Denmark has 870 km of motorways, with about 300 km overlaid with hot-mix asphalt. DART was developed to test slabs since small laboratory rut testing devices only evaluate single mixes and Denmark was interested in overlay performance (i.e., composite structures). The device is capable of applying up to a 65 kN load at a travel speed of up to 5 km/h using normally distributed wander. Composite test slabs of all the bound layers are typically removed from a roadway that is in need of an overlay and transported to the laboratory. The size of the resulting test pavement typically runs about 120 cm by 150 cm by 5 to 25 cm (depending on the thickness of bound layers in the existing structure). Slabs are cut such that the DART will traffic the overlaid pavement in the same direction that traffic will be applied in the field. Tests are run at temperatures that simulate the anticipated performance environment between 25 and 60°C. DART is equipped with a built in laser profilometer. The performance of the overlaid pavement in the field is predicted based on results from laboratory-overlaid slabs (Nielsen, 1999).

It has become more common for agencies to avoid the necessity of inventing complex machinery by investing in production testing equipment when initiating an APT program. The HVS and the ALF are examples of commercially available technologies; however, the development of HVS user groups in recent years has arguably made it a more popular choice. For example, Finland and Sweden have operated a joint HVS-Nordic research program since 1997 that is shared and transported between countries. It is reported that $17 million was spent on this program between 1994 and 2001. The device utilizes either dual or single wheels to apply loads that vary between 20 and 110 kN at a speed of up to 15 km/h. It is fully mobile with environmental control (Hugo and Martin, 2004).

Likewise, the Corps of Engineers turned to the HVS when they decided to standardize their accelerated performance testing in the late 1990s. Until the 1970s, all of their APT testing had been conducted in the field. In the 1980s, these tests were moved indoors to accommodate greater environmental control and to facilitate mechanistic measurements. As part of this overall strategy, the US Army Engineer Research and Development Center (ERDC) chose two HVS units for

deployment at their CRREL facility in New Hampshire in 1997 as well as at their WES facility in Mississippi in 1998 (Lynch et al., 1999). Although the Corps had HVS units produced to suit their specific needs, it is not possible to build a simple linear beam loading unit that will simulate extreme loading scenarios. Because of new, heavy-duty aircraft, the FAA custom built a 270 m by 18 m enclosed facility at the William J. Hughes Technical Center that began testing in 1998. It is a rail-based vehicle that drives two landing gear trucks, each containing as many as six wheels that can be loaded up to 340 kN. Operating speed can be varied between 8 and 24 km/h (Merighi et al., 2001).

Many countries continue to develop proprietary technology to address their own specific loading situations. The CEFET research center of Sao Paulo, Brazil has developed one such APT device. The CEFET-SP system uses a dual wheel truck axle in a simulator that can either be used in the laboratory or taken to remote field projects. Their unit applies a load of 120 kN at a speed of 2.5 km/h over a travel path that is only 1 m long. The simplicity of the device means that size has been minimized, where the entire length of the current machine is only 4 m. It is reported that 50,000 loadings can be applied in a 24-hour operating cycle, and because it is relatively simple it can be assembled at remote field locations in about two hours (Merighi et al., 2001).

Another newly developed proprietary technology is located at the University of Minnesota and is known as the Minnesota Accelerated Loading Facility (Minne-ALF). Proof testing for the Minne-ALF was completed in 1999 on concrete pavement. The unit has a peak speed of 65 km/h, which produces an average speed of 44 km/h over the 2.75 m travel path. In the current design, a 40 kN load is applied to a 3.7 m by 4.6 m test slab; however, it is possible to increase the load up to 100 kN if a slower speed is utilized. The rocker beam design applies the full load in one direction and a partial load in the other direction in order to produce the benefit of unidirectional loading while avoiding the dynamics of lost contact. This option is said to be important when testing load transfer in concrete pavement, which was the subject of initial proof testing. It is reported that 172,000 load cycles are currently possible in the laboratory-based device in a test day (Snyder and Embacher, 1999).

Even more recently, the Florida Department of Transportation initiated an APT program in October of 2000. Their HVS Mark IV model is capable of applying loads of between 31 and 200 kN at a speed of 13 km/h, and is equipped with an automated laser profiler for measuring rut depths while the system is operating. Wander is adjustable from zero to 750 mm, and the system can apply up to 14,000 unidirectional loadings in a day. Florida took advantage of the previously stated benefits of purchasing a commercially available APT, and the time between their initial investment and the production of useful data was very short. In order to have greater confidence in their HVS results, Florida sponsored research on the 2003 NCAT Pavement Test Track to validate past HVS research (FDOT, 2005).

Also in 2000, the Accelerated Transportation Loading System (ATLaS) was developed by the Advanced Transportation Research and Engineering Laboratory with funding from the state of Illinois. ATLaS' wheel carriage can be outfitted with single or dual wheels from either trucks or aircraft. The device is positioned by gantry crane, and test loads (which can be either bi- or unidirectional) are transmitted to the wheels via hydraulic ram. Initial testing has focused on continuously reinforced concrete pavements (Hugo and Martin, 2004).

A completely different type of APT was placed in service at the German Federal Highway Research Institute in 2001. Testing is based on the concept that the passage of a single tire can be approximated by progressive load applications that are induced by a hydraulic actuator-based pulse mechanism. A load of up to 56 kN is applied for 0.025 seconds via a 300 mm diameter load plate. This is intended to represent a maximum legal load traveling at 60 km/h. A 2.1 m by 1.8 m section of test pavement is automatically loaded in a progressive distribution that is similar to an in-service pavement subjected to moving traffic. Six million impulses can be applied to a test pavement in 30 days via a frequency of 145 impulses per minute (Golkowski, 2002).

There are reported to be several other APT facilities that have been active in Europe for an unknown period of time. For example, the Zurich IVT-ETH test track consists of an annular concrete pit that is 2 m wide by 2 m deep (thus, ground water can be controlled) with a median diameter of 32 m. The loading system consists of three arms, each with dual wheels that are individually driven by electric motors. Speed in the Zurich APT can be varied up to a maximum of 80 km/h (Turtschy and Sweere, 1999).

The Shell Laboratory Test Track (LTT) is located at the Shell Research and Technology Centre in Amsterdam. It is a circular track with an outside diameter of 3.3 m and a width of 0.7 m. Wheel loadings are 20 kN at a velocity of 16 km/h. Temperature of testing can be controlled up to a maximum of 60°C (Lijzenga, 1999).

In Asia, there is another unique and noteworthy APT. The Chinese linear track is loaded with an automated vehicle that travels back and forth via electrical power. Test sections are 60 m in total length, but 7.5 m on either end is neglected due to acceleration and deceleration (leaving 45 m in the middle for pavement research). Ramp areas on either end are sloped at 5 percent in order to utilize gravity to slow the vehicle down and limit wear and tear on braking and acceleration components. The load vehicle runs on ten tires placed on three axles at a maximum speed of 30 km/h. The average travel cycle takes one minute to move down to the opposite end and return. The facility is capable of running continuously for seven days without service, and the load vehicle is built primarily with parts provided by Nissan to avoid proprietary engineering

and maximize reliability. It is reported to have been used in the study of recycled pavements (Mitsui, 2002).

Although it is unclear how to best categorize the project (test track or load simulator), the Public Works Research Institute of China operates a small test track (630 m by 7 m) that is tied into a larger test track (870 m by 7 m) through turnouts. Buried cables run along the sides of each facility for guidance purposes. Three automated vehicles simulate wander as they use the magnetic signal from the cables to navigate either or both track(s). Test vehicles are loaded to 44.1 kN on steer axles and 58.8 kN on drive axles, where the load on drive axles can be incremented using 19.6 kN metal weights up to a maximum capacity of 156.8 kN. The design speed of the facility is 40 km/h, which made it possible to apply 750,000 loadings between 1997 and 2000 (Sakamoto, 2001).

It is reported that twenty-eight APT facilities are currently operational, with fifteen located in the United States. These figures are almost certainly an underestimate, as they are based on the results of a survey completed by known facilities. Most are tests at fixed sites; however, there are some that focus on field studies in the belief that there is improved vehicle-pavement-environment interaction. Benefit-cost ratios varying from 1:1 to greater than 20:1 have been reported (Hugo and Martin, 2004).

The majority of European APT facilities (known in Europe as ALT) were commissioned in the period between 1975 and 1985. As of 2002 (at the time the referenced article was written), Europe was reported to have ten full-scale facilities (where full-scale pavement sections were tested by full-scale rolling wheels), two hydraulic actuator-based pulse load facilities (in Bergisch Gladbach, Germany and Dresden, Germany), and several small-scale facilities. Several countries host circular track facilities not well-reported in English literature, including Romania and Slovakia. The reported timeline lists one in 1965, two in 1970, three in 1975, six in 1980, eight in 1985, ten in 1990, ten in 1995, and eleven in 2000 (Mateos, 2002).

5 COLLABORATION

In order to advance the science of APT, both international and domestic collaborative efforts have been undertaken. The European Cooperation in the field of Scientific and Technical Research (COST) effort was founded in 1971 to encourage coordinated cooperation between members of the European Union in research and development. The Brussels-based organization provides a framework in which research facilities, universities and companies cooperate in a broad range of activities primarily in areas of basic research and pre-competitive research. COST is officially composed of fifteen members from the European Union; however, since 1989 non-COST countries have been able to participate in individual programs (COST, 2004). The COST 347 Group is responsible for coordinating APT efforts throughout Europe.

The coordinating organization in the United States is TRB Committee AFD40: Full-Scale and Accelerated Pavement Testing (formerly A2B09), which was transitionally formed in 2000 from Task Force A2B52. The scope of AFD40 states that the committee is concerned with APT via conventional or accelerated traffic conducted in either the laboratory or the field with mobile or fixed equipment. The objectives of the group are to assimilate significant worldwide accomplishments from the past and the present, recommend approaches for future practice, use the Internet as a clearinghouse for timely issues, and support the formal transfer of information through reports and presentations. There are approximately twenty-two official members of AFD40, including representatives from government, industry and academia. (TRB A2B09, 2003).

6 SUMMARY

As discussed in this paper, a tremendous variety of APT experimentation has been attempted over the last hundred years. Communication and collaboration between groups like COST 347 and AFD40 is essential in avoiding duplication of effort and developing future experiments that optimize the investment of scarce research funding. It is expected that strategically planned APT research will continue to play an important role in society's efforts to minimize the life cycle cost of the roadway transportation infrastructure.

REFERENCES

Berthelot, C.F. 2004. *Road Performance Modeling*. Transportation Research Centre, University of Saskatchewan.

Brown, S.F. and Brodrick, B.V. 1999. *25 Years' Experience with the Pilot-Scale Nottingham Pavement Test Facility*, University of Nottingham.

COST. 2004. *COST: European Cooperation in the Field of Scientific and Technical Research*. Project Web, http://www.bbw.admin.ch/html/pages/forschung/cost/cost-haupt-e.html.

Edwards, W.F., and Sargand, S.M. 1999. Response of an Ultra-Thin Whitetopping Pavement to Moving Wheel Loads. *Proceedings 1st International Conference on Accelerated Pavement Testing.* Reno, NV.

Epps, J.A., Leahy, R.B., Mitchell, T., Ashmore, C., Seeds, S., Alavi, S. and Monismith, C.L. 1999. WesTrack – The Road to Performance Related Specifications.*Proceedings 1st International Conference on Accelerated Pavement Testing.* Reno, NV.

Florida Department of Transportation. 2005. FDOT Accelerated Pavement Testing and Research Program, www.dot.state.fl.us/statematerialsoffice/pavement/research/apt/index.htm, Florida Department of Transportation.

Galal, K., and White, T. 1999. INDOT-APT Test Facility Experience. *Proceedings 1st International Conference on Accelerated Pavement Testing.* Reno, NV.

Gillespie, H.M. 1992. *A Century of Progress: The History of Hot-Mix Asphalt*, National Asphalt Pavement Association, 1992.

Gramsammer, J., Kerzreho, J. and Hugues, O. 1999. *The LCPC's APT Facility*, French Civil Engineering and Pavement Research Laboratory.

Harman, T., Bukowski, J.R., Moutier, F., Huber, G., and McGennis, R. 2002. *The History and Future Challenges of Gyratory Compaction: 1939 to 2001*. Transportation Research Board, Washington, DC.

Harvey, J., Long, F., and Prozzi, J.A. 1999. Application of CAL/APT Results to Long Life Flexible Pavement Reconstruction.*Proceedings 1st International Conference on Accelerated Pavement Testing.* Reno, NV.

Houben, L.J.M. and van Dommelen, A.E. 2005. LINTRACK, http://vbk.ct.tudelft.nl/LINTRACKhome, Delft University of Technology.

Hugo, F., Fults, K., Chen, D., Smit, A. and Bilyeu, J. 1999. An Overview of the TxMLS Program and Lessons Learned. *Proceedings 1st International Conference on Accelerated Pavement Testing.* Reno, NV.

Hugo, F. and Epps-Martin, A. 2004. *Significant Findings from Full-scale Accelerated Pavement Testing*. NCHRP Synthesis 325, Transportation Research Board, Washington, DC.

Hveem, F.N. 1948. A New Approach to Pavement Design, *Engineering News Record* Reprint, McGraw-Hill Publishing Company, Inc.

Jones, D. 2003. *Considerations for Supplementing Long Term Pavement Performance Data with Data from Accelerated Performance Testing*. Report DJ-2003/2 to LTPP Committee, Washington, DC.

Kekwick, S.V., Theyse, H.L. and Kleyn, E.G. 1999. *Development of a Long-Term Accelerated Pavement Testing Programme and Structural Design Models*. Transportek, CSIR.

Kenis, W. and Wang, W. 1999. Pavement Variability and Reliability. *Proceedings 1st International Conference on Accelerated Pavement Testing.* Reno, NV.

Kansas State University. 2002. Kansas State Engineering Testing Lab for Civil Infrastructure: Accelerated Testing Laboratory.

Larsen, H.J.E. and Ullidtz, P. 1998. *Development of Improved Mechanistic Deterioration Models for Flexible Pavements*. Report 89, Danish Road Institute.

Lijzenga, J. 1999. *The Stiffness Relation in the Rutting Prediction Model of the Shell Pavement Design Method*. Shell International Oil Products BV, Amsterdam.

Lynch, L., Janoo, V. and Horner, D. 1999. US Army Corps of Engineers Experience with Accelerated and Full-Scale Pavement Investigations. *Proceedings 1st International Conference on Accelerated Pavement Testing.* Reno, NV.

Mahoney, J. 2000. *Accelerated Pavement Testing – An Overview*. University of Washington, Seattle, Washington.

Mateos, A. 2002. COST 347: Work Package 1 – ALT Facilities in Europe, *ALT Matters, Issue 2*. COST 347.

Merighi, J.V., Fortes, R.M., Teixeira, E.S.L. and Lima, D.C. 2001. A Study of HMA Rutting Performance Using Accelerated Pavement Testing. *Second International Symposium on Maintenance and Rehabilitation of Pavements and Technological Control*, Auburn, AL.

Metcalf, J.B. 1996. *Application of Full-scale Accelerated Pavement Testing*. NCHRP Report 235, Transportation Research Board, Washington, DC.

Metcalf, J.B., Romanoschi, S.A., Li, Y. and Rasoulian, M. 1999. The First Full-scale Accelerated Pavement Test in Louisiana: Development and Findings. *Proceedings 1st International Conference on Accelerated Pavement Testing.* Reno, NV.

Mitchell, T. 2005. *Pavement Testing Facility*. Turner Fairbank Highway Research Center.

Mitchell, T. 1996. WesTrack: The Road to Solutions, *Public Roads, Vol. 60, No. 2*.

Mitsui Engineering and Shipbuilding Company. 2002. *Recycled Asphalt Pavement Endurance Test System*. Tokyo, Japan.

National Research Council. 1962. *Special Report 61E – The AASHO Road Test, Report 5*. Pavement Research, Highway Research Board, Washington, DC.

Newcomb, D.E., Engstrom, G., Van Deusen, D.A., Siekmeier, A. and Timm, D.H. 1999. Minnesota Road Research Project: A Five-Year Review of Accomplishments. *Proceedings 1st International Conference on Accelerated Pavement Testing.* Reno, NV.

Nielsen, C.B. 1999. *Accelerated Testing of Permanent Deformation in Hot Rolled Asphalt Concrete Overlaid with Rut Resistant Asphalt Wearing Courses*. Danish Road Institute.

Pasko, T.J. 1998. Concrete Pavements – Past, Present and Future, *Public Roads, Vol. 62 No. 1*.

University of California Pavement Research Center. 2005. http://www.its.berkeley. edu/pavementresearch/.

Pennsylvania Transportation Institute. 2005. www.pti.psu.edu/, Penn State University.

Ruiz, A. 1999. *The CEDEX Full-scale Test Track*, Spanish Center for Research on Public Works.

Sakamoto, T. 2001. Public Works Research Institute, Ministry of Land, Infrastructure and Transport, Japan.

Schauer, P. 2003. The Trip to Town: Rural Transportation Patterns and Developments Since 1900. *Transportation Research News, No. 225*. Transportation Research Board, Washington, DC.

Sharp, K.G., Johnson-Clarke, J.R. and Fossey, D.W. 1999. A Review of the Australian ALF Program. *Proceedings 1st International Conference on Accelerated Pavement Testing.* Reno, NV.

Sherwood, J.A., Xicheng, Q., Romero, P., Stuart, K., Naga, S., Thomas, N.L., and Wogawer, W. 1999. Full-Scale Pavement Fatigue Testing from FHWA Superpave Validation Study. *Proceedings 1st International Conference on Accelerated Pavement Testing.* Reno, NV.

Shutao, M., Liufu, H., Daoxin, W., Jinan, S. and Yongqi, L. 1999. The Performance of Stabilized Base Pavements Under Accelerated Loading. *Proceedings 1st International Conference on Accelerated Pavement Testing.* Reno, NV.

Snyder, M. and Embacher, R. 1999. *Minne-ALF Project Overview and Retro-Fit Dowel Study Results*. Report No. Mn/DOT 2000-02, Minnesota Department of Transportation.

The Road Information Program (TRIP). 2004. *America's Rolling Warehouses: The Impact of Increased Trucking on Economic Development, Congestion and Traffic Safety*. Washington, DC.

Transportation Research Board Committee A2B09. 2003. *Committee on Full-scale/Accelerated Pavement Testing, Triennial Self-Evaluation of Committee Activities*. Transportation Research Board. Washington, DC.

Turtschy, J. and Sweere, G. 1999. *Long Term Pavement Performance Modeling Based On Accelerated Pavement Testing*. Forum of National Highway Research Laboratories.

Vijayanath, B., Wu, Z., Hossain, M. and Gisi, A.J. 1999. Instrumentation of the Superpave Test Sections at the Kansas Accelerated Testing Laboratory. *Proceedings 1st International Conference on Accelerated Pavement Testing.* Reno, NV.

Weingroff, R. 1996. Milestones for US Highway Transportation and the Federal Highway Administration, *Public Roads*, Vol. 59 No. 4.

Advances in Pavement Design through Full-scale Accelerated Pavement Testing – Jones, Harvey, Mateos & Al-Qadi (Eds.)
© 2012 Taylor & Francis Group, London, ISBN 978-0-415-62138-0

A decade of full-scale accelerated pavement testing

W.J.vdM. Steyn
University of Pretoria, Pretoria, South Africa

ABSTRACT: Full-scale Accelerated Pavement Testing (f-sAPT) has been conducted for almost 50 years in various forms. The NCHRP requested an evaluation of the last decade of f-sAPT to assess the status quo, identify major developments and trends, as well as the general perception of US Departments of Transport and f-sAPT operators regarding the role and impact of f-sAPT. This paper summarizes the results of the synthesis and captures developments and trends in f-sAPT since 2000, with a focus on the specific areas of major developments, changes in operating procedures, and the effect that f-sAPT in general is perceived to have had on the development of pavement engineering. It is concluded that the judicious use of f-sAPT contributes to and supports the body of knowledge regarding the way that pavement materials and structures react to controlled traffic and environmental loads.

1 INTRODUCTION

Full-scale accelerated pavement testing (f-sAPT) forms a vital link between the laboratory evaluation of materials used in pavement layers and the field behavior of these materials when combined into pavement structures. For many years f-sAPT provided pavement engineers with knowledge that improved their understanding of pavement materials and structures, as well as their behavior under typical traffic and environmental loading. It formed the basis for developing various theories about pavement behavior and supports most of the current pavement design methods.

The f-sAPT narrative over the last decade is well defined through a focus on the keynote addresses and syntheses of the three International Accelerated Pavement Testing (APT) Conferences (IAPTC) held since 1999 (Mahoney 1999, Hugo 1999, Hugo 2004, Prozzi 2008, Dawson 2008).

Mahoney (1999) identified the expectations for the future of APT at the 1st IAPTC as:

- Improved analytical data analysis techniques;
- More APT devices in service;
- New and improved non-destructive testing (NDT) equipment complementing APT;
- Improved practices resulting from APT;
- More services and options from the private sector;
- Increased use of the Internet for a variety of pavements and APT activities, and
- Formation of APT consortia.

Hugo (1999) (1st IAPTC) stated that a successful long-term APT program requires an extensive laboratory program and a cooperative approach with industry, followed by rapid and extensive implementation of the findings. Partnering and cooperation between different programs to ensure economic use of APT was deemed important, while supplemental tools for APT have become useful and indeed valuable as diagnostic tools in their own right. The incorporation of an improved understanding of loading conditions should be supported to enable improved modeling of pavement response modes through improved links between APT, long term pavement performance and real life. APT is seen as the proving ground for newly developed models over the full spectrum of pavement engineering, including new environmental condition models.

Hugo (2004) (2nd IAPTC) opened the 2nd IAPTC indicating that the overall goal of APT programs is to improve performance and economics of pavements through using APT to simulate the behavior of an equivalent in-service pavement under conventional traffic and prevailing environmental conditions. Closer linkages between pavement management systems (PMS), in-service highways, and long term monitoring (LTM) programs were again highlighted, while the need for cooperation was addressed through identifying the need to carefully formulate new APT studies with due regard to the incorporation of the extensive volume of significant findings from completed APT studies.

Prozzi (2008) (3rd IAPTC) focused on the long standing link between APT and the history of pavement design and highlighted the close relationship between the Transportation Research Board (TRB) and APT and the importance of international collaboration in transportation research. The differences between APT and LTM, long-term effects, the need for improved modeling and showing tax-payers the benefits of what is done were highlighted. Major needs for APT were identified as improved pavement structural

information required to support upgrading of the transportation system, accurate performance prediction, focus on marginal materials, and improvements in the performance of rehabilitated pavements. A summary synthesis indicated that APT covers all major pavement response modes, material, and pavement types; it needs advance modeling and quantitative methods to be beneficial to practitioners; it pays off through producing significant savings in pavement life cycle costs; and opportunities exist for private funding and international collaboration.

Based on the keynotes and syntheses, the importance of technical research excellence to enable the most economical use of scarce natural resources to enable a sustainable transportation network, supported by international cooperation, is visible through developments reported at the series of IAPTCs.

The objective of the latest NCHRP synthesis on f-sAPT (Steyn, 2012) was to collate and analyze the research conducted in the area of f-sAPT over the period 2000 to 2011. NCHRP Syntheses 235 (Metcalf, 1996) and 325 (Hugo and Epps-Martin, 2004) reported on information pertaining to APT projects until early 2000. The following topics were specifically included in the synthesis scope:

- Evaluation of the operational f-sAPT programs;
- Discussion of material related issues as researched through f-sAPT;
- Discussion on pavement structure related research using f-sAPT;
- Application of f-sAPT in the evaluation and validation of new mechanistic-empirical (M-E) pavement design methods, and
- Identification of the future needs and focus of f-sAPT.

The overall finding from this synthesis is that the judicious use of f-sAPT contributes to and supports the body of knowledge regarding the way that pavement materials and structures react to controlled traffic and environmental loads.

Over the last decade, f-sAPT programs have expanded and research findings have been published on a wide range of topics. More than 30 f-sAPT programs are currently active in the United States and internationally. Presentations and publications stemming from the TRB annual meetings, other conferences and journals added to the increase in APT research findings. The synthesis (Steyn, 2012) makes it clear that f-sAPT research has generated significant findings, and that the application of these findings has expanded into the broad field of pavement engineering.

Metcalf (1996) defined f-sAPT as "the controlled application of a prototype wheel loading, at or above the appropriate legal load limit to a prototype or actual, layered, structural pavement system to determine pavement response and performance under a controlled, accelerated, accumulation of damage in a compressed time period. The acceleration of damage is achieved by means of increased repetitions, modified loading conditions, controlled climatic conditions (e.g., temperature and/or moisture), the use of thinner pavements with a decreased structural capacity and thus shorter design lives, or a combination of these factors. Full-scale construction by conventional plant and processes is necessary so that real world conditions are modeled." This definition has also been used in the latest synthesis.

Research and developments conducted outside the focus period of the latest synthesis (Steyn, 2012) (thus pre-2000) were excluded as these have been covered extensively in the previous syntheses. The absence of information on some topics, as well as the absence of discussion on early developments by various f-sAPT programs is thus the result of this limited period focus. It is strongly suggested that the various syntheses on f-sAPT and relevant NCHRP reports be read as a series of documents to obtain an extensive understanding of developments in f-sAPT.

This paper summarizes the major issues emanating from the latest synthesis (Steyn, 2012). It begins with the study background, followed by a broad evaluation of operational f-sAPT programs. Information focusing on materials, pavement structures, vehicle-pavement-environment interaction, pavement modeling and analysis, and f-sAPT impacts and economic analyses is covered. Finally, expected future developments in f-sAPT are discussed followed by the major conclusions from the synthesis.

2 BACKGROUND TO SYNTHESIS

The information available for the synthesis consisted of the responses to an extensive on-line web-questionnaire; information obtained from published journal and conference papers from 2000 to 2011 (published until May 2011 – more than 500 references cited); discussions with interested and affected parties regarding f-sAPT, and meeting minutes and presentations of the TRB Full-Scale Accelerated Pavement Testing (AFD40) committee. The TRB AFD40 committee functions as a full TRB committee and tracks presentations and papers linked to its activities through an active website and communication with members (TRB 2011).

2.1 *General f-sAPT perceptions*

Three groups of respondents were targeted through the questionnaire. These included a group of specialists who have worked in the field of f-sAPT, but are no longer currently actively involved (five respondents), representatives of all 50 US States Departments of Transport (DOT), and known US and international f-sAPT program representatives.

All 50 US State DOTs were invited to participate through invitations sent to the staff responsible for pavements in accordance with the AASHTO Subcommittee on Design membership list. The responses received from 38 US State DOTs indicated that 32

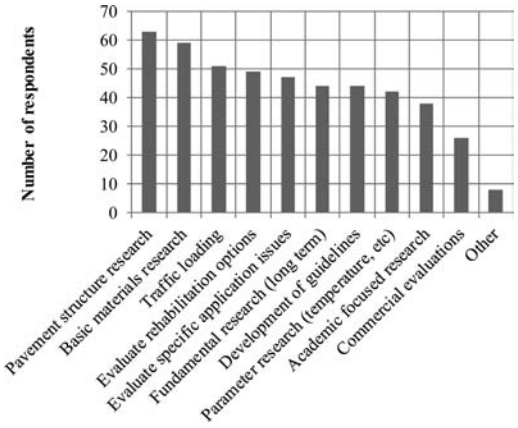

Figure 1. Anticipated roles of f-sAPT according to respondents.

states are interested in APT while six states are neither involved nor planning to become involved in APT work.

Forty-three known US and international operators and owners of f-sAPT devices were invited to respond to the questionnaire. This is an increase of 15 over the number identified in the previous synthesis Hugo and Epps-Martin, 2004), although only 29 of these programs responded and completed the questionnaire. Most active f-sAPT devices were included in the respondents. Where details were not supplied by programs through the questionnaire, details of the programs were identified through papers and websites.

A total of 72 unique responses were obtained from the combination of US State DOTs, specialists, and APT programs. Fifty-six (77 percent) of the respondents viewed the importance of f-sAPT as high with only three holding the view that the importance is low. The major roles seen for f-sAPT are pavement structure and basic materials research, while commercial evaluation of products is deemed as playing a smaller role (Figure 1). Thirty-nine respondents viewed the future of f-sAPT as a normal part of operations and growing. The major benefits of f-sAPT are viewed as improved structural and material design methods, performance modeling, and evaluation of novel materials and structures.

3 CURRENT F-SAPT PROGRAMS AND EQUIPMENT

APT systems can be divided into full-scale systems (f-sAPT) and small-scale systems. F-sAPT systems are those where a standard truck tire (or combination of tires) is used for applying the loads to the pavement while small-scale systems are those where a scaled-down version of a truck tire and tire load is applied to the pavement (the synthesis (Steyn, 2012) focused only on f-sAPT). F-sAPT can be divided into tests tracks, circular, and linear tracking devices. The synthesis provides a summary of the current US and international f-sAPT programs and organizations. It covers traffic loading equipment, environmental control systems, instrumentation, and analysis equipment, and is based on the questionnaire survey results, literature review and selected discussions. Only a summary of the data are provided in this paper.

3.1 *F-sAPT programs*

Implementation of an f-sAPT facility and associated test program is a long-term action that requires considerable investments (Balay and Mateos, 2008). The program cost typically exceeds the initial price of the facility and the construction cost of the experimental pavements, as laboratory testing, pavement surveys, pavement and facility maintenance, data analysis, and reporting have to be included to develop a good f-sAPT program. Road authorities have to be involved from the start to assist in defining the broad scope of the project, support during the research and implementation of the outputs to common pavement practice. In recent years, increased emphasis has been placed on f-sAPT with various f-sAPT facilities utilized throughout the US and internationally. Brown et al (2004) views the primary reason for this increase in the use of f-sAPT facilities as the need to quickly and safely develop answers to emerging pavement issues within a reasonable period of time.

In 1996 there were 35 f-sAPT facilities around the world, of which 19 had active research programs in place (Metcalf, 1996). Since then there has been an increase in interest in f-sAPT and a move to enhance national and international interaction. This has led to two broad cooperative activities: in the US, the creation of the TRB technical committee on Full-scale and Accelerated Pavement Testing (AFD40) and in Europe, the establishment of the Cooperation for Science and Technology (COST) Pavement Research with Accelerated Loading Testing Facilities Program (COST 347).

Thirty-two of the respondents to the questionnaire own an f-sAPT device, while 38 of the respondents have some form of access to an f-sAPT device. Of those respondents who have access to an f-sAPT device, 23 own the device, two rent the device and the remainder access the device through other means (i.e. sharing, part of a consortium, etc.). Selected details regarding the actual f-sAPT device characteristics are summarized in Table 1.

Much of the benefit from f-sAPT has derived from comparison studies of known materials and configurations against novel and innovative materials and configurations where some equivalency between the two has provided sufficient confidence to apply the novel solution. This short-term pay-off has been complemented by progress in the understanding of material behavior and pavement performance.

A substantial improvement in the combination of laboratory materials characterization, f-sAPT and full scale pavement performance observations occurred

Table 1. Selected details of f-sAPT devices types.

Description	Number of respondents	
Type of f-sAPT device	22 Mobile	10 Fixed
Linear or non-linear trafficking	29 Linear	3 Non-linear
Uni or bi-directional loading	29 Uni-directional	3 Bi-directional also
Field site or fixed site	28 Field site	4 Fixed site
Roads or airfields	31 Roads	1 Airfield
Fixed device or trucks	30 Fixed device	2 Trucks

Table 2. Typical f-sAPT test types conducted.

	Often	Infrequently	Never
Dedicated constructed test sections (normal construction)	16	5	4
Dedicated constructed test sections (test pit)	9	9	5
In-service field test sections	6	9	9
Rehabilitation option comparison	10	9	5
Other	4	4	2

during the last decade. Uncertainties related to f-sAPT traffic versus real traffic and the effects of real time environmental cycles still require improved understanding and modeling.

Feedback on the current research programs of the various facilities focused on a wide scope of all the major possible topics also reported in literature. The majority of the focus is on hot-mix asphalt (HMA), as well as studies with environmentally focused topics such as warm-mix asphalt (WMA) and recycling. Considerable evaluation of materials models for the *Mechanistic Empirical Pavement Design Guide* (MEPDG) has also been undertaken. Future planned research programs focus on similar topics, although some programs mentioned a decline in funding and a lack of future planning after current work is completed. Table 2 summarizes the types of f-sAPT experiments typically conducted by the programs. The main focus is on dedicated constructed test sections. It is reported that 44 percent of the funding is short-term with 33 percent long-term and the remainder (23 percent) intermittent funding. Respondents mainly select projects based on official research programs (19 programs); however, there are still seven programs indicating that projects are selected on an ad hoc basis.

Most f-sAPT programs make use of the standard types of measurements (i.e. permanent deformation/strain, elastic deflection/strain) in some form, as well as basic environmental data (moisture and temperature, depending on the material and test conditions). F-sAPT programs consistently upgrade and improve their f-sAPT devices and instrumentation. Examples of currently planned new developments include implementation of new f-sAPT devices (at least three programs), improvements in control and load monitoring systems and software, upgrades of data acquisition systems, and instrumentation packages (in-depth deflection, dynamic rutting, wireless technology, moisture and pressure sensors, fiber optic sensors etc.), installation of camera systems for identifying and measuring cracks, commissioning of dedicated materials testing laboratories, and f-sAPT device automatic fault finding systems.

Twenty programs use a combination of f-sAPT and laboratory testing to augment their data generation for analysis process, while selected use of LTM data (referring to both Strategic Highway Research Program (SHRP) Long Term Pavement Performance (LTPP) sections, as well as local field section monitored over a number of years that are not part of the SHRP LTPP sections) and field studies also occur (12 programs).

F-sAPT programs use various methods to disseminate the outputs from their programs to industry. The most popular mechanism is conferences, meetings, and journals (21 programs), with the least popular websites and news releases (8 programs). Programs view the main opportunities to disseminate f-sAPT research information as focused pavement engineering conferences and journals, with 28 respondents indicating that they have been actively involved in the various international APT conferences since 1999.

Spreadsheet based systems are used to store data at some stage of the research. Approximately 50 percent of respondents have dedicated databases where all data are ultimately stored and from where further analyses are conducted.

Sixteen of the f-sAPT device owners make data available to non-APT users for analyses, while 12 programs share their data with other f-sAPT programs. Consequently, 52 of the respondents use data from their own f-sAPT programs or databases for research, while 19 of the respondents use data originating from other organizations. The majority of respondents (50) combine data from more than one test section in their research.

Most f-sAPT programs (18) indicated that a need still exists to generate knowledge and expand the understanding of materials and pavements in an environment where traffic demands evolve and constant improvements in performance models potentially lead to more cost effective application of limited road infrastructure budgets.

3.2 *Associations and committees*

Formation of associations of f-sAPT programs occurred actively during the last decade. These associations are formed around specific loading devices or funding programs with the general objective of

Table 3. List of active f-sAPT associations and committees.

Association/Committee	Website
Consortium of Accelerated Pavement Testing (CAPT)	http://rip.trb.org/browse/dproject.asp?n=27614
Cooperation for Science and Technology (COST)	http://www.cost.eu/domains_actions
Forum of European National Highway Research Laboratories (FEHRL)	www.fehrl.org
Heavy Vehicle Simulator International Alliance (HVSIA)	http://www.hvsia.co.za
Mobile Load Simulator (MLS) User Group	No active website
Transportation Engineering and Road Research Alliance (TERRA)	http://www.terraroadalliance.org/about/index.html
Midwest States Accelerated Pavement Testing Pooled Funds Program	No active website
Transportation Research Board Committee on Full Scale/Accelerated Pavement Testing (AFD40)	http://wweb.uta.edu/faculty/sroman/AFD40/

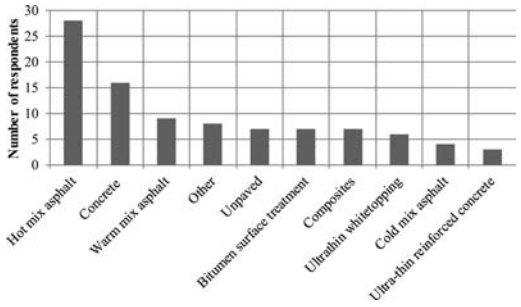

Figure 2. Surfacing materials evaluated with f-sAPT.

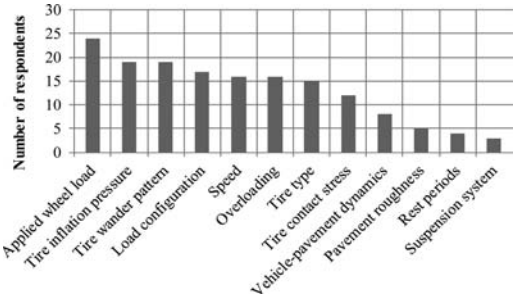

Figure 3. Load characteristics related to observed f-sAPT performance.

improving the cost effectiveness of the overall programs through cooperative efforts of program planning, data analysis, and device improvements. A list of the identified associations is shown in Table 3 with their associated contact details.

4 PAVEMENT MATERIALS AND STRUCTURE EVALUATION

The synthesis (Steyn, 2012) evaluated f-sAPT work conducted on specific pavement materials, as well as the response obtained from different pavement structures and the effect of loading and environmental conditions on the test results. It covered the full range of typical pavement materials and combinations of materials.

The most popular surfacing material evaluated by respondents is HMA, followed by traditional concrete, with most of the other surfacing types only being evaluated by less than 30 percent of the respondents (Figure 2). WMA was interestingly (as a relatively novel material) the third-most evaluated surfacing. For pavement base layers, granular materials have been evaluated the most often, followed by a group of base materials including asphaltic, cemented, and recycled, while the various unstabilized materials were most often used for subbase and subgrade materials.

Traditional cracking (incorporating all types of structural fatigue) and rutting structural distress types for HMA surfacings and concrete pavements were most often evaluated, while permanent deformation was most often evaluated as the structural distress type for base and subbase layers. Fewer respondents include functional distress in their evaluations, with the second-most selected option in the questionnaire indicating that functional distress is not deemed applicable for evaluation using f-sAPT. This is probably influenced by the large number of f-sAPT devices that use short pavement sections for testing (as opposed to test tracks).

Most programs used wheel load as the load characteristic to which they related f-sAPT data, with the tire-related properties (inflation pressure, type, contact stress) starting to play a more prominent role (Figure 3). The material properties used to explain performance (Figure 4) are mostly typical properties that are known to affect structural performance of materials. Respondents mostly rated unconventional materials and compaction as the aspects of pavement engineering that may enhance construction and rehabilitation of pavements that were evaluated in their f-sAPT programs.

Apart from the major emphasis on HMA rutting, a developing trend is the evaluation of environmentally sensitive materials such as WMA and recycled asphalt (RA), as well as the focus on pavement life extension through application of HMA overlays and various types of thin concrete overlays. Aging effects of HMA is addressed to a degree, although accelerated artificial aging of HMA is not necessarily providing similar results to real time-aged HMA. Although some f-sAPT on granular materials is still being conducted, the applications are limited. A number of miscellaneous unique applications of f-sAPT were identified,

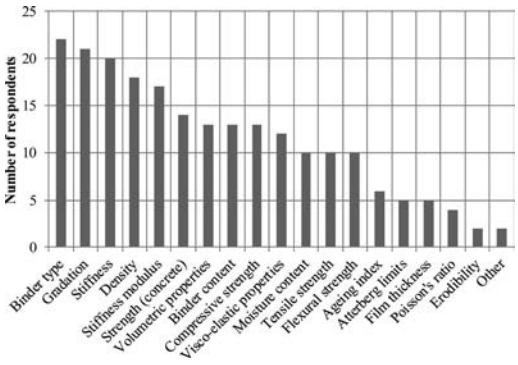

Figure 4. Material properties related to observed f-sAPT performance.

including the testing of pipes in trenches, snow melting systems, and the use of f-sAPT data to assist in calculating road user charges and pay factors.

5 VEHICLE-PAVEMENT-ENVIRONMENT INTERACTION

The specific interaction between the loading device and the pavement structure with a focus on the linkages to real traffic loading and the environment were evaluated and typically incorporated the effects of load equivalence, tire types, real-life environmental effects, etc. F-sAPT aims to evaluate pavement sections under a range of loading and environmental conditions in order to improve the knowledge of the potential performance of the pavement layers and structure under a full range of operational conditions. Using this philosophy, it is standard f-sAPT practice to select a range of vehicular loading conditions, as well as environmental conditions for different tests and obtain the response of the pavement under the specific selected conditions. The outputs of these tests are combined to develop a model of pavement response under expected field conditions.

The majority of respondents relate their f-sAPT data to pavement temperature and ambient air temperature (between 18 and 24 respondents), with a limited number of respondents evaluating the effects of rainfall, drainage, ageing, and humidity. Most respondents (between 11 and 17) control the pavement and ambient temperature during tests, with moisture control being a secondary parameter that is controlled or monitored (between 7 and 9 respondents). The improved characterization of loading conditions is mirrored by the use of more complicated materials models that can react to these input conditions and provide improved models of the materials' load responses.

The focus on temperature monitoring and control is probably related to the high percentage of HMA type f-sAPT evaluations conducted. The major effects of tire contact stresses and loading conditions on pavement response were highlighted by many researchers and are shown to be incorporated as a factor in many of the test programs evaluated. Improved measurement systems, as well as novel analysis techniques for incorporating actual tire-pavement contact stresses into analyses, allows for an improved understanding and appreciation of this parameter. The loading effects caused by wide-based and also aircraft tires are being evaluated at various f-sAPT facilities. A limited number of facilities incorporate LTM of existing pavements into their research, although it is appreciated that it is an important link between f-sAPT and real life data.

The combination of f-sAPT data with laboratory, LTM and field data differs between projects and depends mainly on the requirements of the specific project. F-sAPT is almost always combined with and supported by laboratory data, with field data used for calibration with real environment and traffic. Some respondents make use of replicate sections on public roads that become the field sections and almost serve the role of LTM sections, although they are not monitored in the same way as the SHRP LTPP sections. F-sAPT is clearly viewed as one of the available tools and not as the ultimate answer to all questions.

6 MODELING AND ANALYSIS

F-sAPT programs employ a range of modeling and analysis methods in analyzing data from their programs. The application of f-sAPT in the *Mechanistic Empirical Pavement Design Guide* (MEPDG) and other mechanistic-empirical (M-E) pavement design methods specifically received attention during the last decade. Most of the modeling and analysis work evaluated, focused on improving the materials models for the various M-E design models, thereby reducing the risk of design as more appropriate parameters are incorporated into the design, and the effect of each of the parameters are better understood.

The increased use of finite element methods (FEM) in cases of analyzing moving loads (as opposed to static load analysis) where factors such as mass inertia and stress rotation are incorporated into the model; the increased use of materials models that are not simply linear elastic, but which incorporate the effects on non-linearity, viscosity, and environmental sensitivity (i.e., moisture and temperature); the increased use of detailed definition of the applied loads in terms of both load history and contact stress patterns, and the increased cognizance given to the effects of the environment on pavement response are highlights in the latest f-sAPT modeling efforts.

It appears as if a process is driven on several fronts where improved computer capacity allows the complexity of calculations to increase without becoming too time and resource consuming, the understanding of materials properties are improving with the parallel development of appropriate laboratory and field instruments, and tests to obtain these parameters for different materials and the subsequent modeling is improved through the combination of these factors. Most of the M-E methods operate on a multi-level

basis, where pavements of lesser importance where higher risk can be tolerated are designed using a simplified version of the system, and pavements where very little risk can be tolerated are designed using the most complex version of the M-E method.

It does, unfortunately, appear that a lot of the modeling is still focused on the surfacing layers and that the effect and contribution of lower layers are generalized and simplified, even though these effects may sometimes affect the surfacing and other upper layers significantly. It is specifically the strength-balance of the pavement (providing a pavement structure where layers are not over-strained or over-stressed due to a lack of support or protection) that often appears to be ignored in test planning and modeling.

The majority of respondents use elastic layer theory for most backcalculation, deflection, and stress/strain analyses. Iterative methods are mainly used for backcalculation, while elasto-plastic and visco-elastic layer theory are applied in limited instances. This is probably because these model properties are typically material related (i.e., visco-elastic methods for asphalt materials).

Although attempts are being made to incorporate more advanced model formulations to closer predict material behavior, the use of linear-elastic layered theory still provides reasonable results in some cases. The development of advanced pavement design methods and the use of f-sAPT data for the calibration of these methods, analysis of advanced pavement response models, and improved pavement design methods is becoming a more common activity. Several major initiatives in the development of prominent pavement design methods that incorporated f-sAPT (such as the Australian, South African, Minnesota, and other approaches) have been covered in previous syntheses (Metcalf 1996, Hugo and Epps-Martin, 2004).

7 IMPACTS AND ECONOMIC ANALYSIS

7.1 *Impacts*

Respondents viewed improved structural and material design methods, evaluation of novel materials, improved performance modeling, and the development of performance related specifications as the major benefits of f-sAPT (Figure 5). The most significant findings from f-sAPT in the last decade contain a vast collection of specific topics focusing on all aspects of pavement engineering. Issues around materials characterization, pavement modeling, pavement behavior and performance, pavement design method development and calibration, benefits of specific materials and technologies, and economic impacts of f-sAPT programs provide a small sample of these highlights. Aspects that do stand out are the number of respondents indicating that technologies that are viewed as environmentally friendly such as WMA and the use of RA are significant in their programs.

The most significant international findings of f-sAPT in the last decade can be summarized on a

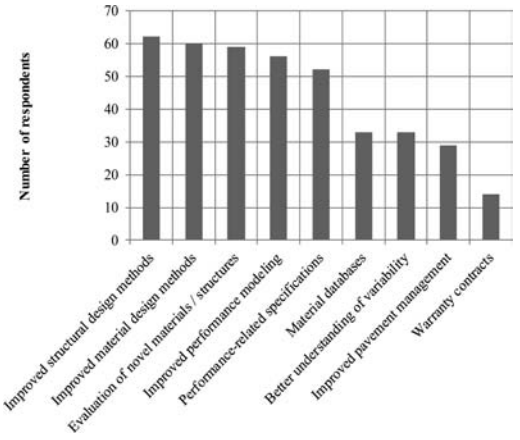

Figure 5. Major benefits of f-sAPT.

strategic level as the calibration of pavement design methods (specifically the *MEPDG* and California Mechanistic Empirical design methods [*CalME*]), development of databases of information on pavement performance that are shared between different pavement research programs, cost savings through implementing f-sAPT, and the development of improved instrumentation and analysis methods. In terms of more practical examples, issues such as an improved understanding of failure mechanisms of top-down cracking, critical strain limits in HMA, the effect of adequate layer compaction, variability of materials and layer properties, improved understanding of the links between various materials' laboratory and field behavior and the effect of various real environmental conditions and traffic on pavement behavior and performance are seen as major international findings.

Feedback indicates that the various f-sAPT facilities are conducting focused research that addresses questions that affect the quality and performance of their sponsor's pavement infrastructure positively through an improved quantification of risks associated with the use of various technologies, as well as improving the general understanding of material and pavement behavior and performance.

The educational benefits of f-sAPT were also evaluated in the questionnaire, and were identified as being mainly visible in the opportunity of providing students and young engineers with the funding, topics, and technical support to pursue studies in pavement engineering through detailed analyses of full-scale pavement behavior. At least 55 specific students could be identified as having been involved with graduate studies linked to f-sAPT in the past decade.

7.2 *Economic analysis*

Benefit-cost ratio (BCR) is mostly used to evaluate the economic benefit of f-sAPT programs. Nine programs conduct economic evaluations, with most evaluations conducted after the research has been

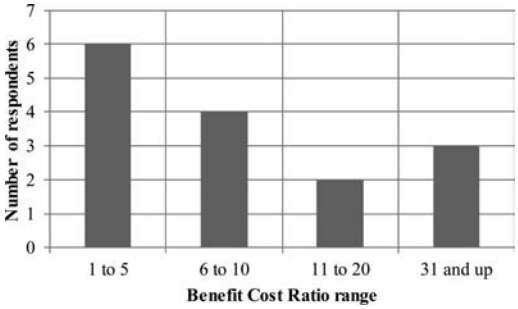

Figure 6. Estimates of BCR for f-sAPT facilities.

Table 4. Summary of Benefit Cost Ratios (BCRs) from questionnaire and literature.

Origin	BCR
UCPRC 1	3.2 to 9.5
Australia	1.4 to 11.6
South Africa	2.2 to 10.2
Caltrans I710	5.3 and 32.4
Louisiana	5.3
MnROAD	8.9

completed (8 respondents). Four programs use BCR information as input in their research planning. Feedback from clients and sponsors is in some cases used to evaluate the benefit, albeit not in economic or objectively measured terms. The benefit of cost avoidance or avoidance of implementation of a costly action that is proven to be ineffective during f-sAPT is also seen as a strong indicator of the success of some f-sAPT programs. Estimates of BCR from respondents (Figure 6) indicate that the majority (6 respondents) estimate their BCR at between one and five. The number of respondents drops for the next two categories (6 to 10 and 11 to 20) and increases again for the over 31 BCR group.

Based on published literature, the ranges of BCR are shown in Table 4. It was important to ensure that the same factors were included in the comparative analyses and that similar analysis procedures were followed. The data in Table 4 indicates that the ranges are broadly between 1.4 and 11.6 (excluding the high Caltrans example where user costs were included in the analysis). This relates well with the 10 respondents who indicated a BCR of between one and ten for their facilities (Figure 6). The main difference between the data in Figure 6 and Table 4 is that those in Figure 6 are mostly estimated while those in Table 4 are calculated.

The credibility of this type of analysis lies in the acceptance of the results by road authorities and practitioners. One of the criticisms of BCR is the effect of inputs, assumptions and subjectivity on results as reflected in the sensitivity analysis. Sensitivity analysis is recommended as it enables examination of these effects for interpretation and use of BCR values.

8 FUTURE DEVELOPMENTS

8.1 *Continued trends*

Hugo and Epps-Martin (2004) identified the following four items for future research:

- In situ field performance of pavements tested in f-sAPT;
- Closer association between f-sAPT and in-service pavement evaluations, LTPP studies, and PMS to validate f-sAPT results;
- Exploration of vehicle-pavement-environment interaction to enhance the ability to do quantitative performance prediction of different pavement structures under specific conditions, and
- Prudent use of available information and collaborative research efforts to improve the reliability of findings and establish confidence limits.

Evaluating these four items in the light of the information covering the period 2000 to 2011, it is evident that the f-sAPT community is probably moving in the right direction, although it may be slow and with deviations in some areas.

The importance of having in-service sections for performance evaluation and validation of f-sAPT data (LTM section) is appreciated by most, and there are a number of cases where such validations have been attempted. The problem currently is in the linkage with good information regarding the performance trend of the field sections. Mostly, these sections are not as well monitored as the original f-sAPT sections, and it often becomes difficult to obtain reliable traffic and environmental data for a field section. The costs of a long-term field evaluation are often a hindrance to ensuring that long-term data are collected regularly.

Vehicle-pavement-environment interaction is receiving ample attention in current programs, and the majority of reports at least indicate the conditions under which specific tests were conducted. This includes tire type and conditions, temperature and moisture content at which a test was conducted, and the speed at which the test was run. Although all these parameters are not necessarily controlled during the test, the fact that researchers appreciate their importance is already a step forward. The importance of incorporating these aspects into modern pavement design methods also forces improved evaluation of the methods to control and measure these parameters during f-sAPT, as well as during normal trafficking of pavements.

Collaborative research has increased significantly during the last decade. The development of associations has led to improved communications around common interests and facilities. Different facilities and programs are also using data collectively to evaluate models developed at specific facilities and to validate the applicability of specific models and design methods. This allows for data originating from other programs and countries to be analyzed using a model developed under different conditions, and the

robustness of models is thus evaluated. The regular international APT conferences and the work conducted at TRB's AFD40 committee also ensure constant communication between role-players. Prudent use of technology such as videoconferencing allows meetings to be organized with international colleagues, fostering the relationships and the multiple uses of data.

The most significant strategic level findings from f-sAPT in the last decade focus on issues around materials characterization, pavement modeling, pavement behavior and performance, pavement design method development and calibration, benefits of specific materials and technologies, economic impacts of f-sAPT programs, calibration of pavement design methods, development of databases of information on pavement performance that are shared between different pavement research programs, cost savings through implementing f-sAPT findings, and the development of improved instrumentation and analysis methods.

8.2 *New trends*

Many of the trends identified in the synthesis are known issues, but which did not receive the required attention in the research and testing environment as would be expected. Issues such as the stress rotation within pavement layers that affects the performance as indicated in the synthesis, non-linear, elasto-plastic, elasto-visco-plastic and other complex models are being incorporated into research and analysis procedures more often. The active use of these models and techniques should be pursued to gain further improvements in the area of pavement behavior based on f-sAPT.

Economic evaluation of f-sAPT programs is receiving more attention. It appears as if the majority of f-sAPT programs are satisfied that they get good data from the programs, and that more detailed BCR-type analyses are not required. More attention and time are rather focused on the technical analyses and issues around pavement provision and maintenance.

Continuous improvements in computer technology allow the use of more complex models that provide data much closer to real pavement response to loads. These more complex models also incorporate the details of tire-pavement contact stress area and magnitudes.

Respondents to the questionnaire indicated that research into the following broad topics should lead to future significant findings from f-sAPT:

- More detailed focus on vehicle-pavement interaction (including improved load and contact stress models);
- Improved environment-pavement interaction (including climate change issues);
- Development of, and improvements in, performance related specifications;
- Improved *MEPDG* validation;
- Evaluation of sustainable pavement solutions (energy efficient technologies and re-use of available infrastructure), and
- Improved reliability in pavement design.

The increased use of dedicated airfield facilities is visible in the academic literature. The special load magnitudes and wheel configurations used on aircraft require more specific instrumentation and monitoring equipment than that on more traditional f-sAPT programs.

9 CONCLUSIONS

These conclusions are based on the information gained from the questionnaire, as well as the published literature. The synthesis on f-sAPT contributes to the body of knowledge by evaluating developments and advances around f-sAPT between 2000 and 2011. The overall conclusion is that the judicious use of f-sAPT contributes to, and supports the body of knowledge regarding the way that pavement materials and structures react to controlled traffic and environmental loads. Through well-planned studies, the f-sAPT work conducted over the last decade highlighted the following strategic findings that provide important information to the pavement engineering community to ensure the sustainable and efficient supply of cost effective pavement-related infrastructure.

- General perceptions regarding f-sAPT indicate that it is important, with a major role to be played in pavement structure and basic materials research. The future of f-sAPT is perceived as growing and being a normal part of pavement research operations, benefiting improved structural and material design methods, performance modeling and evaluation of novel materials and structures.
- Many programs share their facilities and data in order to expand their database. The formation of associations of f-sAPT users with the general objective of improving the cost effectiveness of overall programs through cooperative efforts of program planning, data analysis, and device improvements, is evident.
- A wide scope of topics is addressed in the research conducted by the various programs, with the major focus on HMA materials. A developing trend is the evaluation of sustainable materials such as WMA and RA, as well as the focus on pavement life extension through application of HMA overlays and ultra-thin whitetoppings (UTW).
- Respondents view temperature as the most important environmental parameter to relate f-sAPT data with, and to control during tests – probably related to the high percentage of HMA type f-sAPT evaluations conducted. The major effects of tire contact stress and loading conditions on pavement response were highlighted by many researchers and are shown to be incorporated as a factor in many of the test programs evaluated for this synthesis.

– Improved characterization of loading conditions is mirrored by the use of more complicated materials models that can react to these input conditions and model the response of the various materials more realistically. Many programs actively focus on the validation of models incorporated in the *MEPDG* and *CalME* pavement design procedures, thereby reducing the risk involved in pavement design as more appropriate parameters are incorporated, and the effect of each are better understood.
– Improved computing technology allows the complexity of calculations to increase without becoming too time- and resource-consuming, while the understanding of materials properties is improving with the parallel development of appropriate laboratory and field instruments and tests to obtain these parameters for different materials.
– Improved structural and material design methods, evaluation of novel materials, improved performance modeling, and the development of performance related specifications are perceived as the major benefits of f-sAPT.
– Perceptions regarding the way that f-sAPT has changed the pavement engineering world focused on proving new techniques and materials and development of a fundamental understanding of pavement structures.
– Evaluation of economic benefits of f-sAPT has come to the forefront during the past decade with more programs reporting attempts at performing BCR type evaluations of their research programs. It appears that general international economic conditions forces researchers to prove the benefit of their research much more and identify, analyze, and quantify the direct and indirect benefits obtained from f-sAPT. Estimates of BCR from respondents ranged broadly between 1.4 and 11.6.
– It is evident that the f-sAPT community is moving towards the future with a focus on calibration of f-sAPT outputs with in-service pavement data, specifically with a view to incorporating environmental and real traffic issues that cannot be modeled using f-sAPT.
– Questionnaire respondents indicated that issues such as a more detailed focus on vehicle-pavement interaction (including improved load and contact stress models), environment-pavement interaction (including climate change issues), development of, and improvements in, performance related specifications, improved *MEPDG* validation, evaluation of sustainable pavement solutions (energy efficient technologies and re-use of available infrastructure), and improved reliability in pavement design are important future focus areas.

ACKNOWLEDGEMENTS

The project that this paper has been based on was funded by the National Research Council through their National Cooperative Highway Research Program, and their support in conducting the project and permission to publish information from the project is acknowledged.

REFERENCES

Balay, J.M. and Mateos, A. 2008. Implementation of APT Facilities in developing countries. In *Proc. 3rd International Conference on Accelerated Pavement Testing*, Madrid, Spain, October 1–3, 2008.

Brown, R., Powell, B., West, R. and Timm, D. 2004. Update on NCAT test track. *In Proc. 2nd International Conference on Accelerated Pavement Testing*, Minneapolis, Minnesota, September 26–29, 2004.

Dawson, A. 2008. Who needs APT? – We all need APT. In Proc. *3rd International Conference on Accelerated Pavement Testing*, Madrid, Spain, October 1–3, 2008.

Hugo, F. and Epps-Martin, A. 2004. Significant findings from full-scale accelerated pavement testing, *Synthesis of Highway Practice 325. Transportation Research Board, National Research Council*, Washington, D.C., 2004, 201 pp.

Hugo, F. 1999. Conference synthesis and view ahead. In Proc. *International Conference on Accelerated Pavement Testing*, Reno, Nevada, 18–20 October 1999.

Hugo, F. 2004. Opening overview. In Proc. *2nd International Conference on Accelerated Pavement Testing*, Minneapolis, Minnesota, September 26–29, 2004.

Mahoney, J.P. 1999. Accelerated Pavement Testing – an overview. In Proc. *International Conference on Accelerated Pavement Testing*, Reno, Nevada, 18–20 October 1999.

Metcalf, J.B. 1996. Application of full-scale accelerated pavement testing. *Synthesis of Highway Practice 235. Transportation Research Board, National Research Council*, Washington, D.C., 1996. 117 pp.

Prozzi J. 2008. Conference synthesis. In Proc. *3rd International Conference on Accelerated Pavement Testing*, Madrid, Spain, October 1–3, 2008.

Steyn, W.J.vdM. 2012. *Full-scale accelerated pavement testing, 2000 to 2011*. NCHRP Project 20–05. Synthesis Topic 42–08. National Cooperative Highway Research Program (NCHRP), Transportation Research Board (TRB), National Research Council, Washington D.C. 2011 (final draft submitted at date of writing paper).

TRB Full-Scale Accelerated Pavement Testing (AFD40) committee meetings website. 2011. http://www3.uta.edu/faculty/sroman/AFD40 (accessed on 26 September 2011).

Part 2: Establishment of new accelerated pavement testing facilities

This page intentionally left blank

Advances in Pavement Design through Full-scale Accelerated Pavement Testing – Jones, Harvey, Mateos & Al-Qadi (Eds.)
© 2012 Taylor & Francis Group, London, ISBN 978-0-415-62138-0

PaveLab and heavy vehicle simulator implementation at the National Laboratory of Materials and Testing Models of the University of Costa Rica

J.P. Aguiar-Moya, J.P. Corrales, F. Elizondo & L. Loría-Salazar
PITRA-LanammeUCR, University of Costa Rica, Costa Rica

ABSTRACT: The LanammeUCR is an academic entity attached to the Civil Engineering Faculty of the University of Costa Rica. The Transportation Infrastructure Program (PITRA) of LanammeUCR, works directly with the Costa Rican government performing applied research, auditing and technology transfer. It is funded from a law that assigns 1% of the fuel tax collected in Costa Rica to LanammeUCR with the main objective of ensuring the efficiency of road investments in the country. To meet this objective, PITRA has allocated a considerable component of its funds towards the acquisition of high technology/state-of-the-art equipment such as an falling weight deflectometer, road surface profiler, Geo3D, and dynamic testing equipment for material characterization, among others. With the goal of improving the design and construction of pavements structures, as well as better understanding the different materials used, LanammeUCR decided to acquire a Heavy Vehicle Simulator (HVS) with instrumentation. With this Accelerated Pavement Testing (APT) equipment, LanammeUCR will be fully equipped to monitor the performance of different pavement structures and materials, and new and improved pavement technologies, and to develop and calibrate a mechanistic-empirical design guide for local weather, materials, and traffic conditions. This paper summarizes the draft plan for the design of the APT facility that will be constructed at LanammeUCR. The facility includes a saturation system to simulate pavement conditions during Costa Rica's intense rainy season.

1 INTRODUCTION

Since the early 1990's it was evident that the state of the Costa Rican transportation infrastructure was rapidly deteriorating. This condition worsened due to the lack of supervising and planning from the Administration (Ministry of Transportation and Public Works). To make matters even worse during this decade, the component of the national budget that was destined towards road investment was drastically reduced (MOPT, 2011). This was a consequence of policies at the macroeconomic level regarding public spending, resulting from investment adjustment programs established under the guidance from the International Monetary Fund (IMF).

The reduction in road spending resulted in an accelerated deterioration of the country's transportation infrastructure. Additionally, establishing contacts with the private sector to perform new construction or maintenance activities was a difficult process due to the complexities of the adjudication procedure and the lack of budget. In order to address these issues, the National Transportation Council (CONAVI) was created in 1998 as established by Law 7798 with the objective of planning, programming, administrating, financing, performing, and supervising the maintenance and expansion of the national road network.

However, mostly due to lack of funding, the emphasis of road investment quickly shifted from new construction to maintenance of the existing infrastructure. This changed the role of the DOT to that of comptroller and supervisor. This change in priorities still remains, but is currently complemented by construction of new projects by means of concessions awarded to the private sector.

In 2002, Law 8114 destined economic resources for the maintenance and rehabilitation on the national road network. Additionally, the law assigned responsible supervising entities to ensure the quality of the national and municipal road networks. Part of the responsibilities assigned by law to LanammeUCR are those of performing applied research in topics related to road infrastructure that should result in the improvement of materials and pavement structures in use, and updating the national specifications at least every ten years.

Consequently, LanammeUCR has been working on characterization of local materials, improvement of asphalt mixtures to be used locally, and evaluation of the national road network since 2002. However, development of a pavement design procedure is difficult since new construction projects are limited.

Additionally, partly due to lack of knowledge in proper mixture and structural design, and partly due to deficient construction practices and poor quality control/quality assurance (QC/QA), most pavement projects still fail a few days after construction. Therefore, long term monitoring of properly designed and constructed road projects, from construction to failure,

has been rather limited. This is an important setback in the objective of developing a structural design guide for Costa Rica since calibration or development of field pavement deterioration models is not possible.

To address this issue, and with the goal of properly characterizing the deterioration of new pavement structures, or rehabilitated pavement structures, the possibility of constructing and using full scale pavement test sites has been evaluated since 2005. After a detailed analysis of the different options/methods that are currently used worldwide to evaluate full scale pavement test section, it was determined that the best option for Costa Rica and LanammeUCR was to invest in an accelerated pavement testing (APT) facility. The facility will be equipped with a Heavy Vehicle Simulator (HVS) Mark VI model. This mobile machine will allow for accelerated trafficking of controlled or field test sections and will be capable of simulating 20 years of road deterioration in just a few months.

In conjunction with the acquisition of the HVS, the construction of a building that will house test tracks that can accurately simulate soil saturation conditions is being built with the intention of running the HVS under controlled conditions prior to taking the HVS to evaluate pavement test sections in the field.

All of the previous discussion is encompassed in the mid- and long-term research plan that has been established by Pitra and its Materials and Pavements Division. The plan establishes a line of research whose objectives will culminate in the development of new specifications to address all the material, climatic, traffic conditions associated with the country, and eventually, in the development of a mechanistic-empirical pavement design guide for Costa Rica. In this sense, the development of the APT program is a tool that will not only aid in the evaluation of natural scale test sections, but will also allow for the development of pavement deterioration and performance prediction models for the country. All of the previous will be complemented with materials and pavement research that has been performed at LanammeUCR for the past several years, and which is envisioned to continue in the future.

2 LANAMMEUCR

The National Laboratory of Materials and Testing Models (LanammeUCR) is an academic entity that is attached to the Civil Engineering Faculty at the University of Costa Rica (Figure 1). The LanammeUCR was founded in the 1950s and since its establishment, has focused its efforts towards applied research, development of professional engineers, and technology transfer in the fields of civil and transportation infrastructure.

LanammeUCR's main objective is the generation of specialized information and its transfer. Additionally, LanammeUCR lends its services and expertise to both the public (local and municipal governments, Regional governments) and private sectors to ensure that the latest technological processes are applied.

Figure 1. LanammeUCR facilities.

In an effort to ensure the competitiveness of the laboratory, LanammeUCR has ensured that the quality of the results it generates are accurate, repeatable, and trustworthy. In order to do so, the testing procedures that are used need to be validated and follow proper QC/QA tests. Consequently, since 2001, LanammeUCR implemented a quality assurance system following the ISO/IEC 17025 specification entitled: "*General requirements for the competence of testing and calibration laboratories*".

Additionally, in 2002, LanammeUCR accredited the first set of laboratory procedures with the Costa Rican Accreditation Entity (ECA), and since then the scope of the accreditation has been widened to include 77 testing procedures and several calibration procedures.

2.1 *Transportation infrastructure program (Pitra)*

As a part of the Faculty of Civil Engineering, LanammeUCR encompasses programs in several areas such as transportation infrastructure, seismic engineering and risk management, structural, and geotechnical engineering. The Transportation Infrastructure Program (Pitra) is in itself subdivided into several units that specialize in evaluation of the road network, technical auditing, management of the municipal network and bridges, and production of technical specifications. All in all, Pitra is composed of a team of 40 technicians, 52 engineers, 2 lawyers, 5 chemists, 17 administrative personnel, and 24 undergraduate research assistants.

Additionally, to complement all of these units, there is a Materials and Pavements Program that complements the work of the other units by means of applied research in different pavement related issues. The Materials and Pavements Program focuses mainly on granular materials and soils, asphalt mixtures, material chemistry, preservation techniques, and pavement evaluation and monitoring.

Current research activities are aimed towards analysis and evaluation of physical, mechanical, and chemical properties of the different materials that are used in the road infrastructure, development of specifications for materials adapted to Costa Rican conditions, development and calibration of pavement infrastructure performance models, and in the mid- to long-term, development of a structural design guide for the

country, and eventually, for the region. All of the previous is fundamental to ensuring good performance of the national road infrastructure since material, climatic, and traffic conditions are very particular to the region and as such need to be properly understood.

More recently, research is being performed in coordination with other units of Pitra to expand the focus of research from specific pavement and pavement infrastructure related topics, to a more comprehensive transportation perspective that includes bridge and structural analysis, geotechnical analysis, traffic and safety research.

To aid Pitra, and Pitra's Materials and Pavements Program in performing applied research and its other functions, LanammeUCR established a pavements laboratory. In 1997, the pavements laboratory consisted of a Marshall hammer, 2 viscometers, and 1 penetrometer. However, since then the pavements laboratory has grown and currently includes a conventional HMA laboratory, a dynamic analysis laboratory, a rheology and materials laboratory, and a field laboratory. All of the previous is complemented with a civil infrastructure laboratory capable of evaluating concrete and aggregates, soils, full-scale structures and resistance of materials.

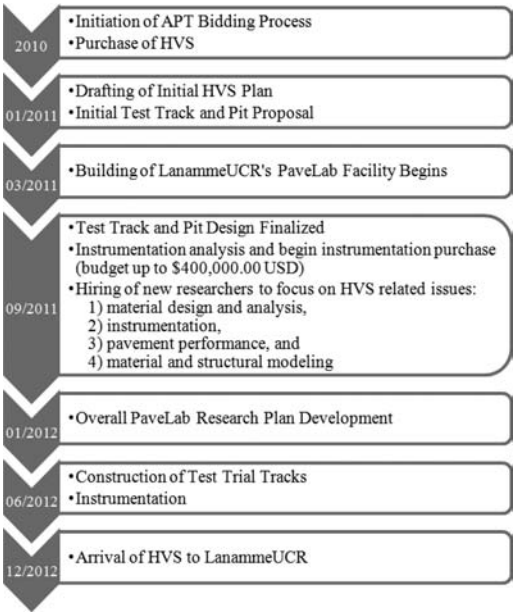

Figure 2. PaveLab project schedule.

2.2 *Law 8114*

As mentioned previously, Law 8114 was implemented to ensure the quality of the national road network. As part of the law (Article 6), several responsibilities are assigned to LanammeUCR to ensure that the previous conditions are met. These responsibilities can be summarized as:

1 Programs to educate and certify laboratory technicians
2 Technical audits of active projects
3 Biannual evaluation of the entire paved road network
4 Annual evaluation of roads and bridges awarded to concessioners
5 Updating the national road and bridges specification manual once every ten years
6 Technical audits of laboratories involved in the road industry
7 Technical advice to the heads of the DOT, Vice Minister, and Minister
8 Professional development courses and technology transfer activities aimed at inspectors and engineers, and
9 Research on topics related to the problems that the national paved road infrastructure is facing.

To ensure that LanammeUCR can perform these activities, Law 8114 assigns approximately 1% of the total fuel tax that is collected in Costa Rica. Pitra was created because of the responsibility that LanammeUCR holds towards Costa Rica. Internally, Pitra manages the funds to ensure that its assignments defined by law are met. Consequently, it is through appropriate planning that a percentage of the funds from Law 8114 have been budgeted towards the purchase of high technology/state-of-the-art equipment for the pavement laboratories within LanammeUCR and for the field evaluation laboratory.

It is through this budget geared towards equipping the laboratory to perform applied research that the purchase of an HVS and construction of the APT facility (PaveLab) is being undertaken. Additionally, part of the budget is also going towards instrumentation for the HVS and for hiring specialized personnel to be involved in the material design and analysis, instrumentation, pavement performance, and material and structural modeling.

3 LANAMMEUCR

As previously stated, in 2005 the possibility of using APT facilities began to be analyzed, mainly because of the need for evaluating the long term performance of existing pavement structures and new technologies that have proven effective in the laboratory but have not yet been used in the field. All of the previous discussion is within the scope of the responsibilities defined by Law 8114, and the research plan established internally by Pitra.

In 2009, the HVS was entered into the budgetary reserve for the upcoming years. From that point in time, the PaveLab Project has been scheduled and planned as shown in Figure 2.

PaveLab's research and testing plan is still under development and it is the intention of LanammeUCR to form an APT Committee with the public sector (DOT, National Road Association, Construction Chamber, and the Association of Professional Engineers and Architects) to ensure that the testing that

is performed as part of the HVS Plan will be for the benefit of the country.

Based on the most recent planning, it is expected that initial HVS testing will be performed in two main phases:

1 From 2013 to 2015 it is expected that the HVS will be used in controlled experiments within LanammeUCR PaveLab's facilities, using the saturation testing pits. This will allow comparison of different types of HMA mixtures and soil stabilization methods that are currently used or that are intended for future use in the country.
2 In a second phase starting in 2016, testing activities will not only be performed at LanammeUCR facilities, but the equipment will be taken to the field to evaluate different projects.

It is planned that initial research will involve the comparison of HMA mixtures with modified and neat binders in order to quantify the improvement associated with including a modifier. This is very important since the use of modified binders in Costa Rica has been very limited and because only one type of binder is produced by the national refinery. However, due to the climatic and traffic diversity in the country, the availability of several binder options is a necessity.

Most of the data analysis will be performed by Pitra's Materials and Pavement Program. However, through the PaveLab APT Committee, it is expected that the results will be spread to the engineering community so that they make an impact on pavement design and construction practices in the Region. Additionally, because of LanammeUCR's attachment to the Universidad de Costa Rica's Civil Engineering Faculty, an undergraduate and graduate thesis program will be developed to ensure that the information generated by the HVS can be used to its greatest potential.

Please note that PaveLab's Research and Testing plan is still under development and is subject to change based on research performed prior to the start of operation in 2013, and based on the input of the different sectors that are involved.

4 PAVELAB'S HVS

The HVS model acquired by LanammeUCR is the Dynatest/CSIR HVS Mark VI, which was the latest model released by Dynatest prior to the purchase date. This equipment does not have self propulsion or self powering features. However, its redesign and new features offer a great range of testing options. Some of the characteristics of this model are as follows:

– The HVS Mk VI can apply at least 26,000 bidirectional passes or 13,000 unidirectional passes of the load carriage in a 24 hour period, along an 8 m test section.
– The HVS load levels are between 30 and 100 kN (7–22.5 kips). Loading up to 200 kN (45 kips) is possible with an aircraft wheel and ballast options.

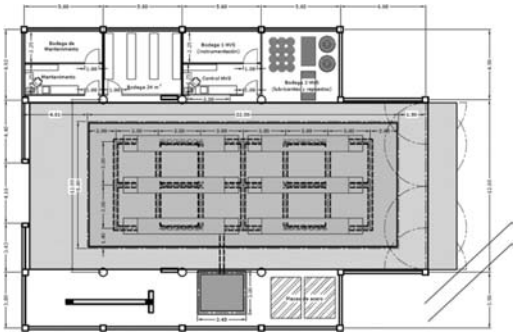

Figure 3. Plan view of the HVS building with the test pit in the middle.

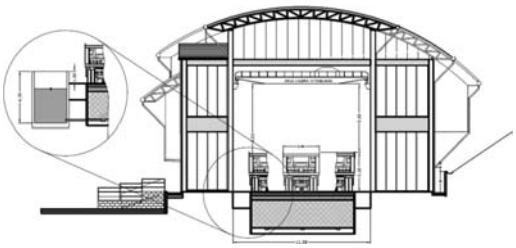

Figure 4. Lateral view of the HVS building, the detail corresponds to the water system.

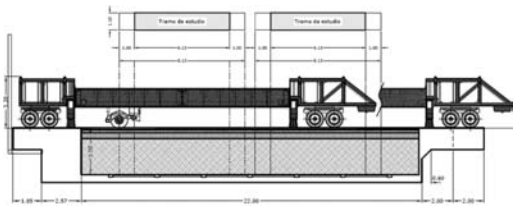

Figure 5. Lateral view of the HVS location over the pit.

– The maximum wheel speed is 12.8 km/hr ± 3 km/hr (8 mph ± 2 mph). The speed can be increased to 20 km/hr when using the beam extension.
– The equipment is capable of shutting itself down automatically at a programmed number of passes. Also, in case of a malfunction, the HVS can be stopped within one pass by two different mechanisms.
– The HVS is capable of duplicating traffic wander or wheel distribution by means of integrated mechanisms.
– The equipment can be operated in a range of temperatures varying from −15°C to 40°C (5°F to 105°F).
– Some of the new features that this model has in comparison to the previous models are:
  - A redesigned frame and a simplified hydraulic system based on the HVS Mk V carriage design.
  - The possibility of a beam extension, which allows higher testing speeds and a longer test track.

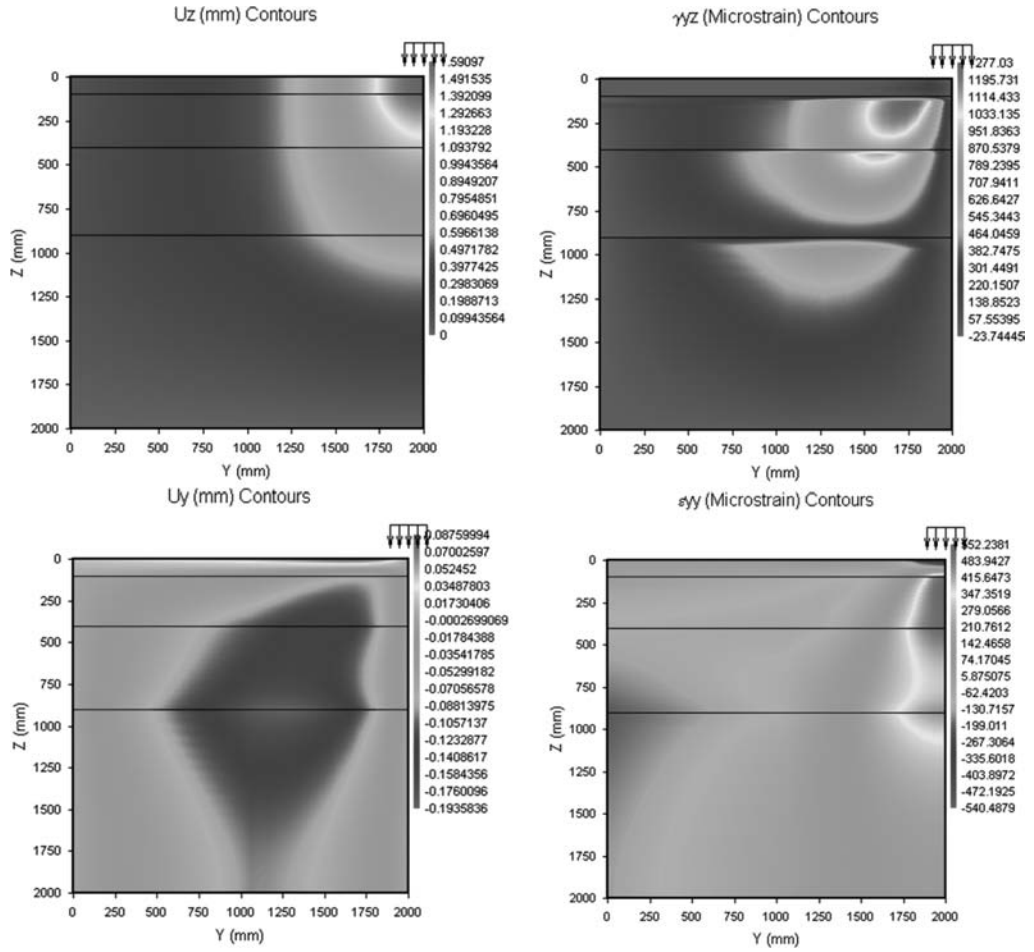

Figure 6. Example of *EverStressFE* analysis for a simple structure under a standard 40 kN load.

- Easier towing due to the reduced weight.
- The HVS Mk VI wheels are turntable mounted, which makes it more maneuverable on site. This feature will be of special help to LanammeUCR, because of space limitations within the PaveLab facility that is being prepared for the equipment.

Also, as mentioned previously, LanammeUCR will also destine $400,000 to the acquisition of part of the instrumentation that the equipment requires in order to gather more data for further analysis. The selection of instrumentation is based on past experience at other APT facilities (Choubane et al., 2011; Jones et al., 2002). Some of the equipment and parts that are planned to be purchased are the following:

– Dynamic loading equipment
– Automated onboard 3D laser profiler
– Pavement Data Acquisition System
– Dynatest PAST II and SOPT sensors
– Stress in Motion Sensor (SIM Pad)
– Multi Depth Deflectometer with 3 Levels
– Crack Activity Meter (CAM)

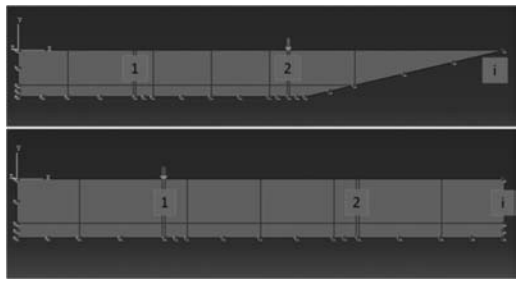

Figure 7. Analyzed test pit sections using FEM.

Each of these additional components is considered to be of great importance for the development of the HVS program in Costa Rica. Furthermore, a yearly evaluation of the different new equipment alternatives will be performed to ensure that new components are developed or acquired so that the equipment capabilities can keep up with the state of the practice.

4.1 *APT facility*

The APT facility that will house the test tracks for the PaveLab program will be located at the new Laboratory of Road Safety and Enforcement. This building is part of LanammeUCR and is expected to be ready by the first quarter of 2012. Even though the facility is be part of this new project, its construction is completely independent from the rest of the structure to make sure that it meets the necessary power requirements, the emergency power supply requirements, and the weather-proofing and sound isolation necessary for optimal operation.

Figures 3 through 5 show the current layout of the APT facility. As shown, there will be six test areas (green rectangles) distributed on a 22 m by 9 m pit. To control the water table, a gravity operated water distribution system will be constructed adjacent to the test pit as shown on Figures 3 and 4 (blue colored). The overall design of the test pits is based on experience at other APT facilities (Hugo et al., 2004).

Several analyses were made to determine the optimal dimensions of the test pit. An initial analysis was made using the *EverStressFE* software package, defining simple pavement structures. These first results were used to evaluate the necessary depth to dissipate the stresses on the structure. An example of this analysis is shown in Figure 6. As shown, the stresses generated by the HVS (40 kN load) are negligible below a depth of 2 m. Similar analysis with loads up to 200 kN were also performed. This was used to estimate the optimal dimensions for the test pit.

In general, it was observed that the higher stresses/strains occurred in the area between the surface and approximately 1.0 m below the surface. More importantly, it was found that in general, a test pit depth over 2.5 m was adequate to ensure that the monitored stresses and strains would be similar to those in the field under the same loading conditions.

Finite element method (FEM) analysis was also used to check the stresses and strains estimated previously for a pavement structure subjected to a maximum load of 40 kN. The 40 kN load is equivalent to an applied wheel pressure of 120 psi over a circular area with 124 mm radius. It is important to clarify that even though the HVS can apply a load up to 100 kN (on its basic configuration), the 40 kN load was considered as the typical load applied by a single truck tire. For the FEM analysis, *ABAQUS* was used to solve the model.

Based on the FEM analysis, the same loading condition was analyzed under two different scenarios as shown in Figure 7:

1 A pit with a ramp to facilitate the entrance of construction equipment, and
2 A pit without a ramp access.

In both cases, it was assumed that testing would be performed on two sections along the longitudinal direction. For the analysis, the depth of the pit was set to 2.5 m to expand on the results previously obtained using *EverStressFE*. The results from these analyses are shown in Figures 8 and 9.

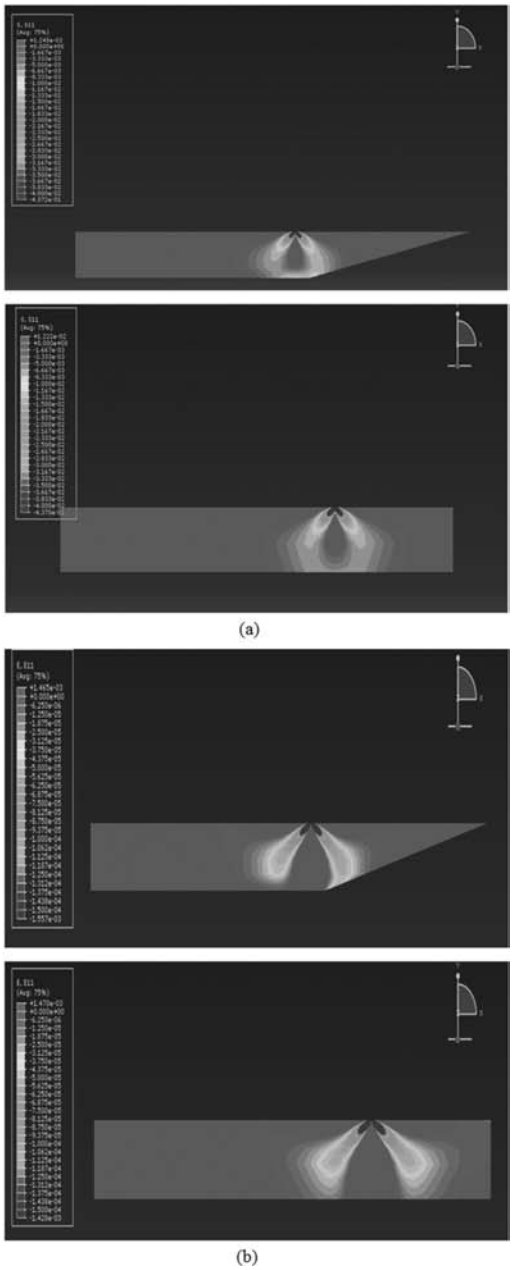

Figure 8. (a) Horizontal stresses and (b) horizontal strains for test section close to test pit ramp.

The results shown on the figures correspond to the application of the load at the extreme of the test section (closest to the test pit edge which is the critical condition due to the ramp configuration – load point. 2). All the data generated by the FEM was subsequently analyzed using spreadsheets. A selection of the results is shown in Figure 10.

Even though the figure does not show significant differences on the dissipation of the stresses and strains

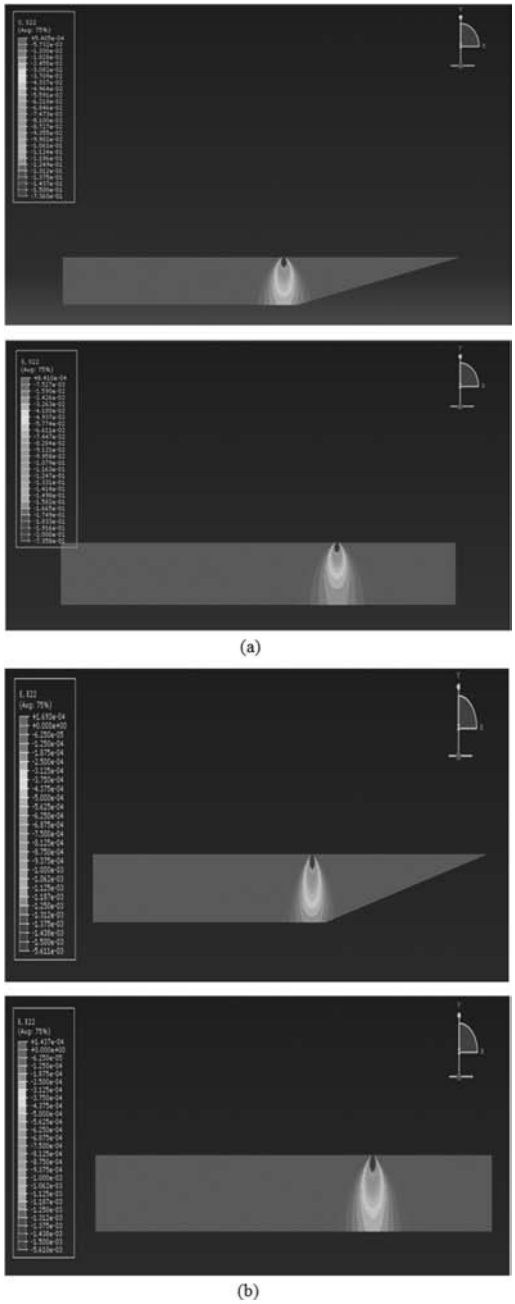

(a)

(b)

Figure 9. (a) Vertical stresses and (b) vertical strains for test section close to test pit ramp.

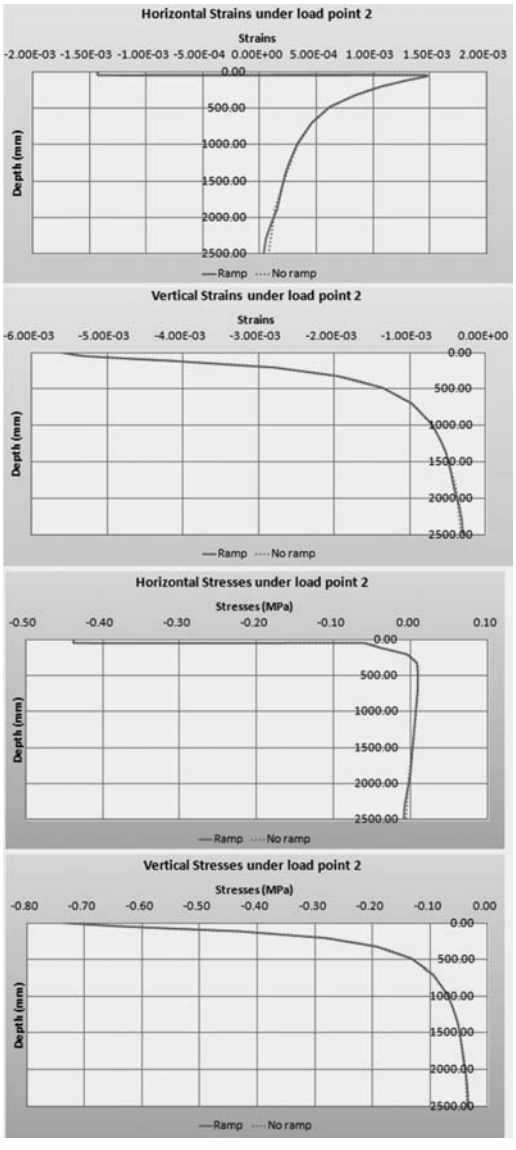

Figure 10. Horizontal and vertical stresses and strains for both geometric loading conditions.

(when comparing the use of an access ramp to not using it), the figure does indicate a slight difference in stresses and strains between the condition with a ramp and no ramp. Furthermore, the construction of the access ramp to the test pit would incur in a loss of available testing area within the test pit.

Finally, after analyzing all the data from this exercise and reviewing the literature with regards to typical test pit construction for other HVS sites, it was decided that the best working configuration for the HVS in Costa Rica would be: no access ramp and 3 m of depth. The decision of not using a test ramp is based on the fact that the use of the ramp significantly reduced the effective test area of the test pit: by eliminating the ramp, one additional test section can be allocated within the test pit.

Additionally, a 3 m deep test pit was selected after considering that higher testing loads might be applied in the future and this slight increase in test pit depth can accommodate an increase in applied load. This decision was later confirmed by the expertise of other HVS owners, and Dynatest, whose help and strong

support have been fundamental in the design of this project.

5 CONCLUDING REMARKS

LanammeUCR was founded primarily to improve the quality of life of the Costa Rican' people and their competitiveness as a nation. LanammeUCR is one of the few laboratories in the region capable of: providing reliable road analysis to the public and private sectors, assessment of the country's entire paved road network, accurate evaluation of material quality, instruments for optimizing current decision processes, and tools for transfer and implementation of existing and new technologies.

With a focus on meeting the objectives set for LanammeUCR, PaveLab is initiating an APT program. The idea of acquiring an HVS is based on the mid- and long-term research plan of the institution that is geared towards meeting LanammeUCR's commitment with Costa Rica. PaveLabs's testing will be based on research that is aimed towards the development of new specifications for the country, and that will eventually lead to the development of a Costa Rican mechanistic-empirical pavement design guide. In this sense, the PaveLab's HVS is a tool that will allow evaluation of full-scale pavements in a natural, but controlled environment, and facilitate the generation of pavement deterioration models for the country that will indicate to the pavement designers what type of pavements have proven effective or not, and under what type of conditions. It will also allow the Administration to check if the DOT, their subcontractors (private companies), and the newer modality – concessionaries – are designing and constructing pavements that can meet the expectations, both functional and structural, of the users.

REFERENCES

Asamblea Legislativa. *Ley 7798 – Creación del Consejo Nacional de Vialidad*. Normativa y Jurisprudencia de Costa Rica. 1998.

Asamblea Legislativa. *Ley 8114 – Ley de Simplificación y Eficiencia Tributaria*. Normativa y Jurisprudencia de Costa Rica. 2002.

Choubane, B., Greene, J. and Sheppard, K. 2011. *Instrumentation of Florida's Accelerated Pavement Testing Facility*. FDOT, State Materials Office. Gainesville, FL.

Dassault Systèmes, 2009. *DS Simulia Abaqus 6.9 User's Manual*. Providence, RI.

Davids, B. 2011. *EverStressFE Manual*. http://www.civil.umaine.edu /everstressfe/. Website accessed on 09/28/11.

Hugo, F. and Epps Martin, A.L. 2004. *Significant Findings from Full-Scale Accelerated Pavement Testing*. NCHRP Synthesis 325. Washington, D.C.

International Organization for Standardization. 2005. *ISO/IEC 17025 – General requirements for the competence of testing and calibration laboratories*. Geneva, Switzerland.

Jones, D. and Morton, B. 2002. *HVS operations: Protocol for instrumentation, data collection and data storage – 2nd Draft*. CSIR Report TR-2002/22. Pretoria, South Africa.

Ministerio de Obras Públicas y Transportes. 2011. *Presentación de Carreteras*, Dirección de Planificación Sectorial. http://www.mopt.go.cr/planificacion/carreteras/presentacion.asp. Website accessed on 09/28/11.

Advances in Pavement Design through Full-scale Accelerated Pavement Testing – Jones, Harvey, Mateos & Al-Qadi (Eds.)
© 2012 Taylor & Francis Group, London, ISBN 978-0-415-62138-0

The Universidad de los Andes linear test track apparatus

B. Caicedo, J. Monroy, S. Caro & E. Rueda
Department of Civil and Environmental Engineering, Universidad de los Andes, Bogotá, Colombia

ABSTRACT: This paper describes the development of a new apparatus to perform accelerated loading tests on pavement structures. This apparatus is the main component of the laboratory of physical modeling of pavements at the University of Los Andes in Bogotá Colombia. The components of this laboratory are: (i) a concrete pit 11.4 m long, 3.2 m wide and 3.5 m deep; the pavement structure is constructed in this pit and it allows the control of the water table and the environmental conditions over the pavement surface; (ii) the linear loading test apparatus, and (iii) a mini asphalt plant that simplifies tests with modified asphalt materials. The loading apparatus is a linear test track that applies the load of a half axle truck (dual tires with maximum load of 75 kN). This new linear test track has an original control system based on the combination of an electrical frequency power controller, and a set of air springs. The air springs absorb the energy of the moving load when slowing down close to the ends of the track, and it allows generation of energy during the acceleration process. This system permits high velocities while saving energy. This paper describes the main components of the apparatus and present some results of a first test carried out using this new APT device.

1 INTRODUCTION

The Universidad de los Andes has, since 2000, owned an APT facility as the main component of the laboratory of physical modeling of pavements. The first APT apparatus used at Los Andes University was an outdoor circular machine developed at the end of the 1990's (Caicedo and Perez, 2000; Balay and Mateos, 2008). Each of the two rolling modules included an electrical motor (22 kW) contributing to maximum speed of 40 km/h. The mean radius of rotation of the wheels was 11 m and the apparatus could accommodate simulated transverse wandering up to 3 m in width. The beam was supported by a hydraulic jack to continuously control the load applied by the wheels to the pavement structure. The maximum load applied was 65 kN on each dual-wheel. This first version of the facility was able to apply up to 200,000 loading cycles per week to the test track, which was 35 m long and 4 m wide. This apparatus was the first APT facility operating in Colombia.

Two main studies were performed with this first APT machine between 2000 and 2005. The first one studied the behavior of rubber modified asphalt mixtures, and it was funded by the World Bank (Pérez, 2000). The second was dedicated to studying soil stabilization techniques, and was funded by the Colombian Ministry of Transportation.

In 2007, this circular APT facility was transformed into an indoor linear APT facility. Some of the components of the previous machine were re-used, e.g., the main beam supporting the rolling loads and one of the motors. In the new apparatus, the wheels are pulled by an electrical AC motor that is equipped with a control system. Air spring absorbers are used in order to harness a large part of the kinetic energy as the wheel movement reverses at each extremity of the main beam. This system allows test speeds up to 20 km/h.

This new linear APT facility is located in a laboratory in which temperature and surface water condition can be controlled (the later with the use of several sprinklers). The pavement structure is constructed in a waterproof concrete pit 3.4 m deep, allowing the complete control of the water table during the tests. The test track is 11 m long, including 8 m for the testing zone, and 3.5 m wide. The device applies transverse wandering of the wheels during the test, up to 0.5 m on each side of the wheelpath centerline.

The main objective of this paper is describing the main components of the new apparatus, and presenting some results from the first test carried out using it. Consequently the results presented in the paper are only validation results for the APT apparatus and the behavior of the tested pavement structure is not presented.

2 TEST FRAME

The linear test track apparatus has a set of two steel beams with rails to guide linear displacement of the loading carriage. The frame span is 11.4 m; however, the allowable displacement of the loading carriage is limited to 9 m. The loading carriage has four air springs (two in each direction of the movement) that help

to transform the kinetic energy of the carriage into potential energy in the springs (Figure 1). This energy accumulation smoothes the deceleration process and assists in collecting kinetic energy for redirecting the carriage in the opposite direction.

The loading carriage has a secondary bogie that controls the transversal displacement of the wheels in +/−0.5 m increments from the center of the longitudinal assembly. The purpose of this transversal displacement is to avoid any channelization of the wheels.

The longitudinal beams are attached to two concrete walls. These walls constitute the reaction system of the air springs. The beams can be attached to the walls at different vertical positions. In this way, it is possible to control the location of the loading device according to the level of the surface of the pavement. Furthermore, the possibility of changing the vertical position also permits the use of a pulse loading device that can be installed on the beams.

2.1 *Wheel load assembly*

The wheel assembly consists of a half single-axle system with dual wheels. The load on the wheels is controlled by a different air spring. The pressure of the air spring is controlled by a manual air pressure control (Figure 2). The air spring of the loading system also acts as a suspension system. The loading system permits a maximum load on the dual wheels of 75 kN, which corresponds to a maximum single axle load of 150 kN.

2.2 *Control system for longitudinal displacement*

Reaching high velocities in the wheel assembly on a linear test track apparatus is a challenging task. This is because the system needs to reduce the velocity, change the direction of the displacement, and accelerate again; all in a very short distance. Therefore, it is important and convenient to store kinetic energy to reduce the power required by the motor.

In order to achieve high velocities, the test track presented in this paper uses a combination of air springs, which work as an energy storage system and an electric motor (with power of 22 kW). This motor is controlled by a speed control device and a programmable controller (PLC).

The combination of the two sources of energy (i.e., air springs and electric motor) requires carefully synchronization of both acceleration modes. In other words, it is important to compute the distance at which the movement is controlled by the air springs, and the distance at which the movement is controlled by the electric motor.

The characteristics of the displacement on the air spring regime can be calculated using dynamic equations of linear movement (neglecting energy losses due to the interaction between the pavement and the wheels):

$$\frac{dV}{dt} = \frac{A_{as} dp_{as}}{m_L} \tag{1}$$

where, V is the velocity of the loading device, t is time, m_L is the mass of the loading device, A_{as} is the area of the loading surface of the air spring, and p_{as} is its internal pressure.

Equation 1 can be solved for an initial velocity of the air spring regime. This initial velocity is chosen to avoid overpressure in the air spring. In fact, during compression the air spring reduces its volume, and then its pressure grows according to:

$$p_{as} = p_0 \frac{v_o}{v_{as}(X_{as})} \tag{2}$$

where p_o and v_o are the initial pressure and initial volume of the air spring, respectively, and v_{as} (X_{as}) is the volume corresponding to a length of X_{as}.

Figure 3 shows the results of the calculated velocities obtained using Equations 1 and 2. The maximum

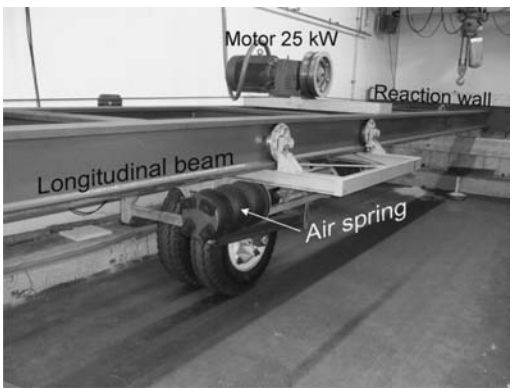

Figure 1. Components of the test track (longitudinal direction).

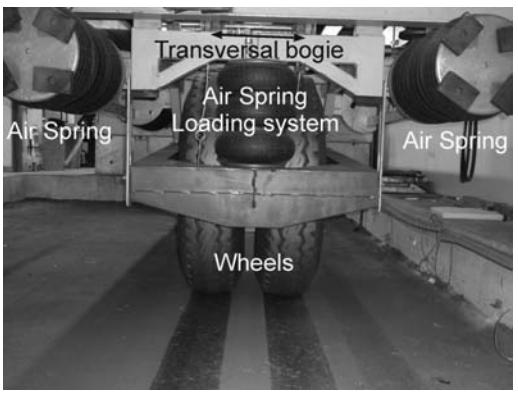

Figure 2. Components of the test track (transversal direction).

velocity for this calculation is 20 km/h, and the initial velocity of the air spring regime is 10.8 km/h. In the current configuration, the apparatus does not have a velocity sensor to measure the actual velocity reached under operation, but it will be included in further tests.

Figure 4 describes the different control regimes of the apparatus depending on the length of the longitudinal displacement of the loading carriage.

3 ENVIRONMENTAL CONDITIONS

An indoor APT facility has both advantages and disadvantages. The main advantage is the ability to control environmental conditions, while the main disadvantage is the difficulty related to duplicating natural conditions.

Colombia is located in a tropical region and, therefore, pavement structures are not subjected to freeze-thaw cycles. Instead, climatic variations of interest in Colombia are related mainly to rainfall (effecting ground moisture) and high temperatures. To control these two environmental conditions, the APT facility is located in a closed room, and the test pavement is constructed in a waterproof concrete pit 3.4 m deep (Figure 5).

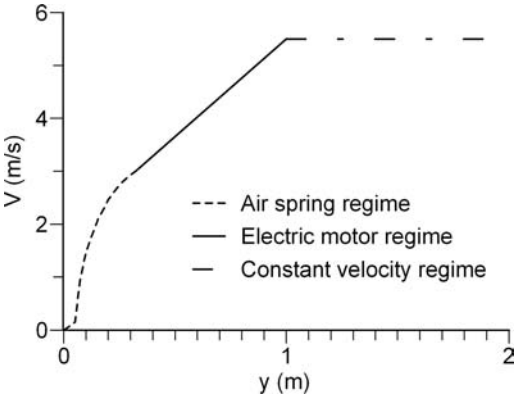

Figure 3. Calculated velocity of the loading device in each control regime.

4 INSTRUMENTATION AND DATA ACQUISITION SYSTEM

Performance of pavement structures is studied by measuring different variables related to the environmental and mechanical response of the pavement. Some of the sensors used were adapted from commercial devices, while others were developed at Los Andes University.

Instrumentation is divided into two different sets of sensors: 1) environmental sensors, and 2) mechanical sensors. This differentiation relates to the different measuring rates that are required for the data

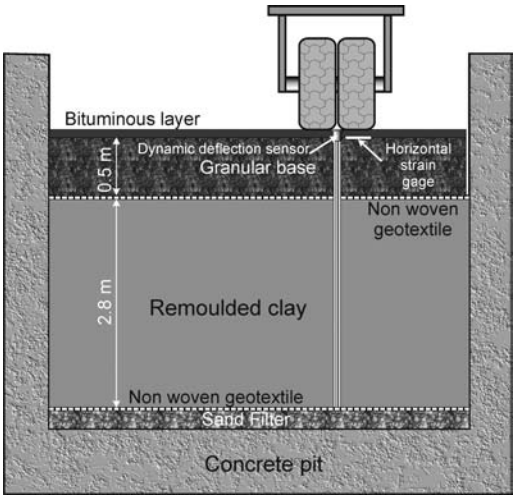

Figure 5. Schematic drawing of the concrete pit and pavement structure.

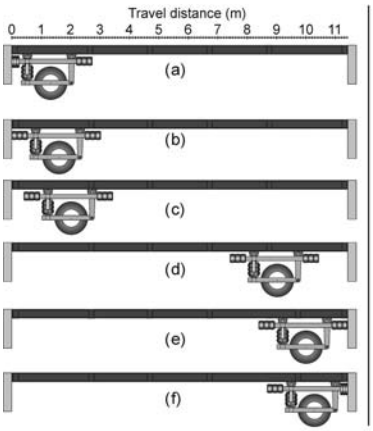

Test Cycle	V (km/h)	Length (m)
Air spring cycle, air spring compressed to its minimum length. Electric motor in freewheel	0	0
Air spring at its maximum length Start of electric motor cycle	10.8	0.32
Electric motor cycle, end of acceleration phase Start of the constant velocity phase	20.0	1.0
End of constant velocity phase Start of electric motor controlled deceleration	20.0	8.0
End of motor controlled cycle Motor set to freewheel cycle	10.8	8.68
Air spring cycle Electric motor in free wheel	0	9.0

Figure 4. Different stages in the control system.

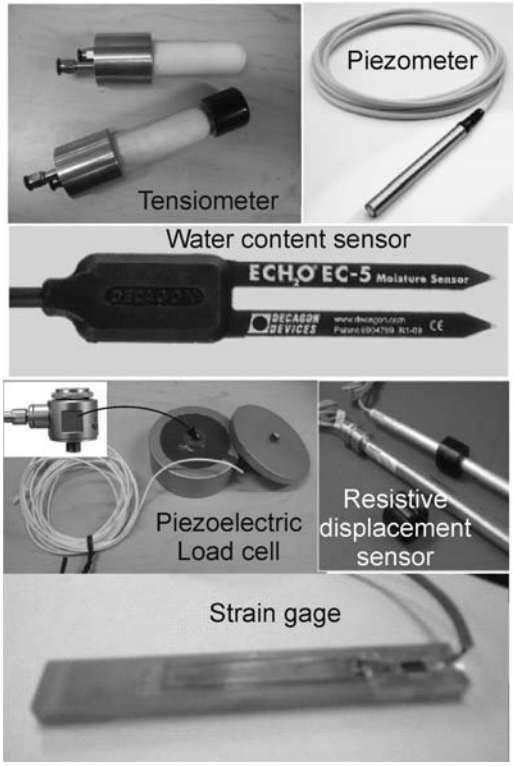

Figure 6. Set of environmental and mechanical sensors used in the APT facility.

acquisition process, and to the different signal levels characterizing both groups of sensors (Figure 6). Environmental sensors include:

- Thermocouples to measure temperature,
- Capacitive sensors to measure soil moisture,
- Tensiometers to measure suction in the different layers of the pavement structure, and
- A piezometer to measure the position of the water table.

Due to the characteristics of the moving loads in pavements, mechanical sensors and data acquisition must have dynamic capacity. The set of mechanical sensors includes:

- Strain gages to measure tensile strains, developed at Los Andes University. These gages were made in a machined piece of glass fiber material with an omega strain gage glued on its surface and protected with silicone rubber,
- Piezoelectric load cells to measure vertical stresses at different levels in the pavement structure. It is important to mention that these load cells were commercially developed for applications other than in pavements. Therefore, the load cell was placed in a steel casing and embedded in silicone rubber,
- A resistive sensor to measure vertical displacements (dynamic deflection). This sensor—developed to work under water—is housed in a steel casing glued to the surface of the pavement. To measure the displacement, this sensor uses a rigid bar that is embedded in the bottom of the concrete pit as a fixed reference,
- A transverse profiler to manually measure the development of rutting on flexible pavements. This is made with an aluminum square, attached to different sections of the walls of the concrete pit. The measurements of this instrument are acquired by means of a digital indicator.

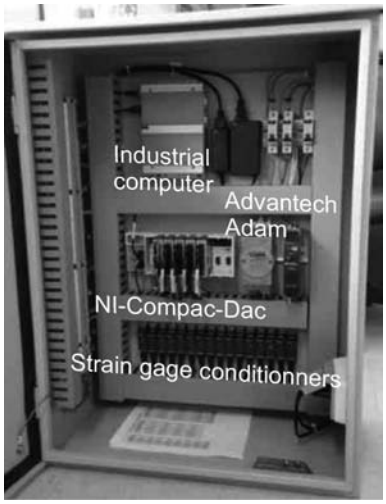

Figure 7. Data acquisition system.

The data acquisition system (Figure 7) consists of *Adam* modules constructed by *Advantech*, and *Compac-Dac* modules made by *National Instruments*. The *Adam* modules have low data acquisition rates (10 samples/second), and a precision of 16 bits. These modules are used for capturing environmental data. The *Compac-Dac* module has a high data acquisition rate (100,000 samples/second), and it can hold different modules adapted to each kind of measurement. In this case, each conditioning module has different requirements; for example, the module adapted to measure strain has a precision of 24 bits, which is appropriate for this kind of measurement. Figure 8 shows a typical response of two of the main dynamic sensors: horizontal strain gauge (Figure 8a), and the dynamic deflection sensor (Figure 8b).

5 CONSTRUCTION OF THE TEST SECTION

As described previously, the pavement structure is constructed in a concrete pit. This method is advantageous for controlling environmental variables (e.g., the position of the water table), but it requires a careful preparation of the subgrade. One of the main interests of the APT facility at Los Andes University is studying the performance and response of pavements in the city of Bogotá, which are constructed over a lacustrine deposit of soft soils. For this reason, the pit was

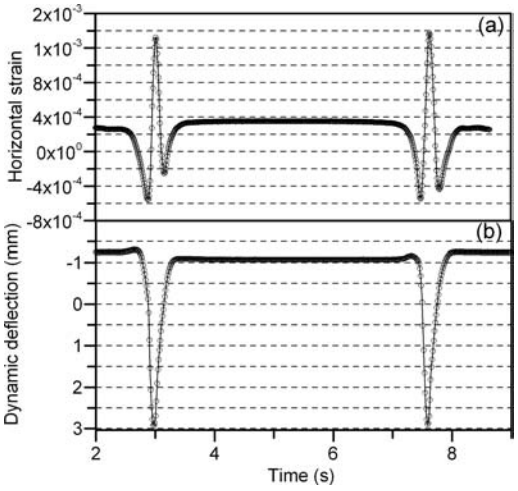

Figure 8. Typical response of two sensors: horizontal strain gauge (Figure 8a), and dynamic deflection sensor (Figure 8b).

Figure 9. Compaction of the pavement layers with small equipment.

filled with a first layer of granular material protected with non-woven geotextile, and then with a 2.8 m-thick layer of soft clay compacted using a rammer. Afterwards, another double layer of non-woven geotextile was placed over the reconstructed subgrade, and over this layer the pavement structure is constructed.

As the test section is constructed in the concrete pit, it is necessary to use specialized equipment typically smaller than that used in conventional construction. Small-sized vibratory equipment shown in Figure 9 is used to achieve compaction specifications.

Construction of test pavements is usually conducted by pavement contractors.

6 TEST CONDUCTED AT THE APT AT LOS ANDES UNIVERSITY

Two pavement simulations have been performed in the new APT facility at Los Andes University. The first was coordinated with the road authority in the city of Bogotá. The second is investigating the use of geocells as a reinforcement of unbounded granular bases. This study is still in progress.

The study carried out for the city of Bogotá analyzed the effects on pavement performance of the different kind of buses used in the public transport system of the city. This study was relevant since most of the urban

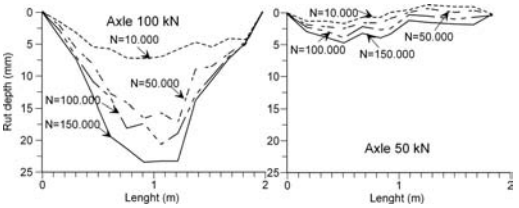

Figure 10. Rutting measured for the different axle loads.

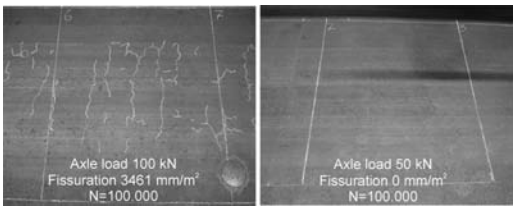

Figure 11. Fatigue cracking measured for the different axle loads.

roads in the city of Bogotá were originally constructed without a proper structural pavement design, and the use of heavy buses is rapidly deteriorating the road network. As part of this project, an optimization model was developed to manage the problem of heavy busses in Bogotá. This model, which requires deterioration curves of the roads for different axle load as an input, allows choosing the appropriate size of the buses and optimizing the cost of the infrastructure (Caicedo et al. 2012).

The performance of a weak pavement structure constructed with a soft subgrade below 50 cm of unbound granular material, and surfaced with 7 cm of dense-graded hot mix asphalt (HMA) mixture was studied under two axle loads: 100 kN and 50 kN. Tests were carried out at half of the maximum velocity of the apparatus (10 km/h). Typically, these pavement structures suffer rapid deterioration under heavy loads, which is evidenced by the development of rutting and fatigue cracking. Figures 10 and 11 present an example of the rut profiles measured at the middle of the test track (where the velocity is constant) after trafficking with the different axle loads.

7 SUMMARY AND CONCLUSIONS

This paper describes a new linear APT apparatus designed and constructed at Los Andes University in Bogotá, Colombia. This APT facility uses a combination of an electronic control system, to power an electric motor, and an air-spring system to store the kinetic energy from the moving wheels. The combination of these two modes is used to reach higher than typical velocities (20 km/h) for a linear APT facility of this size. The linear APT facility at the University of Los Andes was a new development from an initial circular APT facility constructed a decade ago. The use of both types of APT facilities has been useful

to compare the advantages and disadvantages of both configurations:

- The circular APT permitted the use of typical field construction equipment but the construction costs of the track were higher than the construction costs of the linear track.
- The circular APT operated at higher velocities than the linear track device.
- The construction of the linear track requires small equipment; these are not used in large field construction projects, but are typically used for maintenance activities of pavements.
- In the linear APT it is easier to control the environmental conditions in comparison to the circular facility.

After proving the performance of the APT apparatus presented in this paper, Los Andes University is proposing to the authorities of the city of Bogotá to use the APT to improve the design methodologies currently used in the city.

REFERENCES

Balay J.M. and Mateos, A. 2008. Implementation of APT Facilities in Developing Countries, *Proceedings 3rdInternational Conference on Accelerated Pavement Testing*. Madrid, Spain.

Caicedo B. and Pérez, R.S.A. Desarrollo del Carrusel de Fatiga de la Universidad de los Andes, *Revista de Ingeniería Universidad de Los Andes, Universidad de Los Andes, v.1, n.12*, p. 25–30, 2000.

Caicedo B., Ocampo, M. and Sanchez-Silva, M. 2012. An integrated method to optimise the infrastructure costs of bus rapid transit systems. In *Structure and Infrastructure Engineering, DOI: 10.1080/15732479.2010*.499951.

Pérez R.S.A. and Munevar, S. 2000. *Primera experiencia colombiana en el Carrusel de Fatiga*, Disertaciones, Maestría en Ingeniería Civil, Universidad de Los Andes, Los Andes.

Advances in Pavement Design through Full-scale Accelerated Pavement Testing – Jones, Harvey, Mateos & Al-Qadi (Eds.)
© 2012 Taylor & Francis Group, London, ISBN 978-0-415-62138-0

Design and implementation of a full-scale accelerated pavement testing facility for extreme regional climates in China

D. Zejiao, T. Yiqiu & L. Meili
Harbin Institute of Technology, Harbin, China

ABSTRACT: A new full-scale accelerated pavement testing facility is being designed and implemented in Beijing, funded by the National Development and Reform Commission (NDRC), People's Republic of China. This facility is designed as a loop consisting of two semi-circular and two straight test tracks, around which a pilotless vehicle with the maximum weight of 45,000 kg and maximum speed of 60 km/h moves repeatedly. The facility is enclosed, allowing control of environmental conditions including temperature, moisture and ultraviolet radiation. This facilitates testing under simulated extreme conditions experienced in different regional areas throughout China. A general description of components of this system, including the Auto-Vehicle Loading Subsystem, Environment Conditioning Subsystem, Data Collection, Central Controlling Subsystem, and the Testing Loop Subsystem, is summarized together with the proposed system capabilities or parameters. The factors considered during the design phase of this facility are discussed, including the pavement section geometries. A three-dimensional finite element asphalt pavement model subjected to the proposed moving automobile was established to obtain the dynamic response of the designed pavement section and evaluate its dimensions. The result shows that the proposed dimensions of the designed pavement section are appropriate according to the response variation along the pavement section.

1 INTRODUCTION

With the rapid development of expressway construction in China, more and more pavement researchers and engineers have realized the importance of Accelerated Load Test (ALT) in pavement evaluation. It is widely accepted that ALT is the most direct and efficient way to understand structural behavior of pavements, which is crucial to the structural design, performance prediction, and maintenance decisions. In addition, ALT is also a powerful tool to identify the causes of premature failure and the effects of heavy traffic and different regional climate conditions.

Design and construction of a new full-scale accelerated pavement testing facility in Beijing has been in progress since 2007, funded by the National Development and Reform Commission (NDRC), People's Republic of China. It is defined as an Accelerated Loading Facility for Pavement Structures and Materials in Different Regional Climates. It is within the framework of The 11th Five-Year National Grand Infrastructure Technology Program "*Research and Evaluation Facility for Grand Infrastructure Material Service Safety*". This facility was designed as an oval loop consisting of two semi-circular and two straight test tracks, around which a pilotless vehicle with a maximum weight of 45,000 kg and a maximum speed of 60 km/h moves. The facility is enclosed, allowing control of environmental conditions including temperature, moisture and ultraviolet radiation. This facilitates testing under simulated extreme conditions experienced in different regional areas throughout China.

When designing a full-scale pavement accelerated testing facility, it is desirable to have a full-scale pavement and test under actual traffic and environment conditions, so that realistic performance can be simulated. However, very large structures and long testing times may significantly increase the operational costs, thereby reducing the usability of the facility. Accelerated loading facilities can be generally categorized into three types based on their scale and capabilities. First, large full-scale tracks, such as the AASHO Road Test (1956), MnROAD (1993), WestTRACK (1995) and NCAT (2001) are large and generally carry realistic vehicle loads. However, environmental conditions cannot be controlled, operation time is relatively long, and costs are comparatively high. Second, linear loading facilities, for example, HVS initially started in South Africa (1971), ALF from Australia (1984) and MLS of TxDOT (1995), are movable accelerated testing equipment. The advantage of this type of equipment is the lower operating costs and smaller testing areas, but limited test section length and lower testing speeds can be a disadvantage. Third, circular testing facilities, such as LCPC in France and CEDEX in Spain, have circular or loop tracks, which allow loading speeds similar to actual traffic levels. The facility presented in this paper can be classified into the third category

Table 1. Accelerated load facility subsystems.

Subsystem	Detail					
Testing Loop	Total length (m)	Straights (m)	Curves (m)	Width (m)	Chamber height (m)	Pavement depth (m)
	200	$40 \times 2 = 80$	$60 \times 2 = 120$	4.5	7.5	3.0
Auto-Vehicle	Wheel spacing (m)	Wheelbase (m)	Traveling mode	Axle load (kN)	Speed@20kN (km/h)	Speed@45kN (km/h)
	$\leq$1.4	3.1	Auto navigation with orienting wheel	25 to 225	$\leq$60	$\leq$20
Environment Conditioning	Pavement temp. (°C)	Internal temp. (°C)	Air temp. (°C)	Rain intensity (mm/h)	Water level (m)	Ultraviolet intensity (10^4 μW/cm^2)
	-15 to $+60$	-5 to $+30$	-40 to $+50$	0 to 25	2	0.2 to 5.0

(i.e., circular loading). However, unlike some other facilities, the whole operation is carried out in a closed space, allowing climate conditions to be simulated.

2 COMPONENTS OF THE DESIGNED ACCELERATED FACILITY

The designed accelerated loading facility consists of the Auto-Vehicle loading subsystem, environment control subsystem, data collection and central control subsystem, the testing loop subsystem. Details of these systems are summarized in Table 1 and discussed in more detail in the following sections.

2.1 *Auto-vehicle loading subsystem*

The test vehicle is unpiloted. Axles are designed to be changeable to reflect different vehicle loadings. The axle load ranges from 100 kN to 225 kN, which means the total vehicle weight can reach as high as 45 tons. The maximum loading is used to evaluate heavy duty pavements and to accelerate the testing in some cases. The maximum traveling speed is set to 60 km/h for axle loadings of 100 kN, which is the standard axle load according to the Chinese pavement design specification. For the higher axle loading of 225 kN, the maximum operating speed is reduced to 20 km/h for safety considerations. The overall structural design for the Auto-Vehicle is shown in Figure 1.

The Auto-Vehicle is restrained between the interior and exterior wall of the test track by four orienting wheels. Two high-powered servo motors are used to drive the two front traction wheels through retarders. The loading level is determined by the number of attached 500 kg weights. The Auto-Vehicle's steel frame consists of longitudinal, transverse and vertical steel beams which are welded into an integral truss. The mid bottom steel frame is designed to lower the centroid of the loading

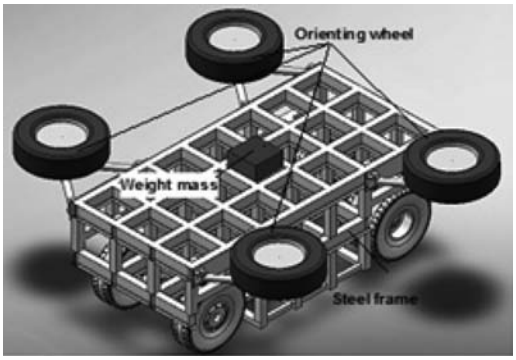

Figure 1. Structural design of Auto-Vehicle.

system, which provides stability and reliability of vehicle motion. The dimensions of the Auto-Vehicle are 4.5 m $\times$ 2.7 m $\times$ 2.0 m, wheelbase is 3.1 m and wheel spacing is 1.4 m.

One of the most important factors taken into consideration during the design of the Auto-Vehicle Loading Subsystem was how to eliminate the centrifugal force induced while changing direction. The four orienting wheel modules are designed to partially achieve this. Each orienting wheel module includes an assembly plate linked with the aforementioned steel cage, two hydraulic damping and orienting wheels pushing against the ambilateral walls, as shown in Figure 2.

2.2 *Environment conditioning subsystem*

The environment conditioning subsystem is used to simulate the different regional climates throughout China. The primary parameters of this component, including air temperature, pavement surface temperature, internal pavement temperature, rain intensity, ultraviolet intensity, and water table, are fully controlled and coupled in some cases to achieve certain prescribed climate conditions.

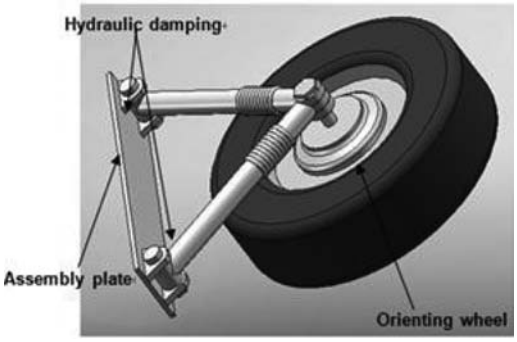

Figure 2. Orienting wheel modules.

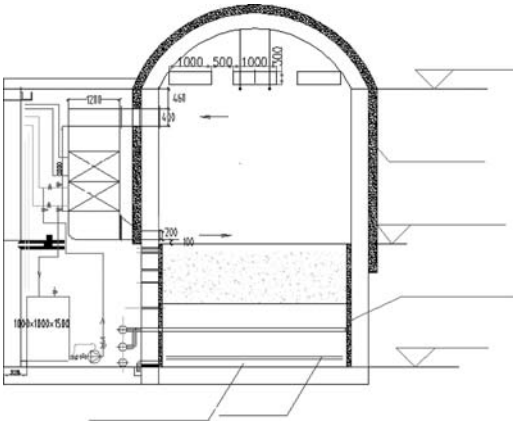

Figure 3. Temperature controlling components.

This subsystem comprises a temperature unit, moisture unit, radiation unit, and wind unit. Testing temperatures are as follows:

- Air temperature: $-40°C$ to $+50°C$
- Pavement surface temperature: $-15°C$ to $+60°C$
- Internal pavement temperature: $-5°C$ to $+30°C$.

The reference point for internal pavement temperatures is 2 cm below the surface. Three heat sources are used including heating/cooling from an air conditioning system blowing over the pavement surface, heating/cooling conduction using pipelines embedded in the soil subgrade, and radiation from infrared devices (Figure 3).

The moisture controlling unit is designed to simulate rainfall and groundwater effects on the pavement structure. Sprayers along the interior wall are used to simulate rainfall or fog. The rainfall intensity can be varied between 1 mm/h and 25 mm/h. Salt water can also used to simulate coastal climates. A seepage pipe is installed at a depth of 2.0 m to control groundwater conditions and prevent seepage (Figure 4).

In the ultraviolet radiation unit, one hundred sets of ultraviolet tubes radiate the pavement surface simulating natural ultraviolet aging conditions of high altitude mountain areas in southwestern China. Each

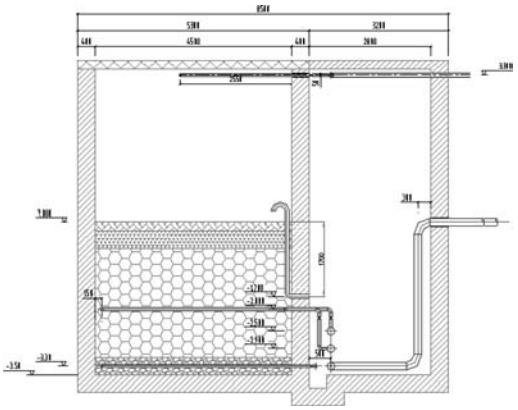

Figure 4. Moisture controlling components.

set consists of three tubes with wavelengths of 365 nm, 354 nm and 308 nm, respectively. Single wavelength radiation cannot reflect typical ultraviolet radiation from natural sunshine. The ultraviolet units are distributed evenly along the straight test track in three rows, with each row having a separated power switch so that the overall radiation intensity can be changed when necessary. The ultraviolet radiation intensity is adjustable from 2,000 $\mu W/cm^2$ to 50,000 $\mu W/cm^2$.

2.3 *Data collecting and central controlling subsystem*

The data collection and central controlling subsystem is the "brain" of the whole facility and is divided into two units, including a system monitoring and controlling unit and a pavement information collecting and processing unit.

The system monitoring and controlling unit is designed to implement real-time monitoring on the Auto-Vehicle and each environmental conditioning unit, and to adjust instantly according to the feedback information and the prescribed target setting. The system monitoring and controlling parameters for the Auto-vehicle operation include speed, spatial location, and operation status, and for the environment system includes air temperature, surface temperature, pavement internal temperature, soil temperature, air moisture, soil moisture, water table, ultraviolet intensity, and infrared intensity. All these data are collected instantaneously, and corresponding adjustment signals are returned to the related controlling unit according to the predetermined parameters. Figure 5 shows the flow chart for the system monitoring and controlling unit.

The pavement information collection and processing unit collects dynamic responses from the test pavement and is coupled to the climate controlling and Auto-Vehicle loading subsystems. These responses include stress, three directional strains, temperature, water table, soil pressure, pore pressure, and moisture, all of which may vary according to the requirements of the particular accelerated loading test. Specific data

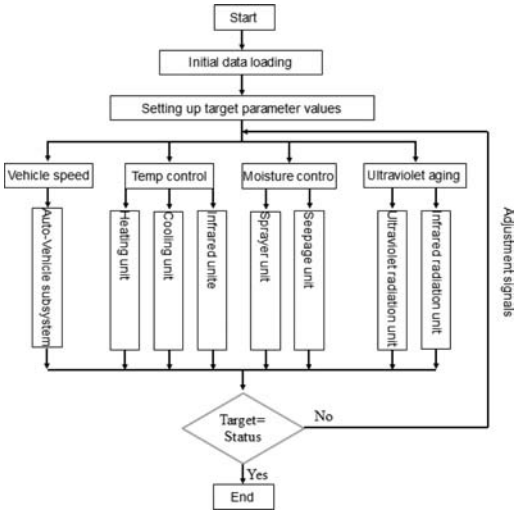

Figure 5. Flow chart for system monitoring and controlling unit.

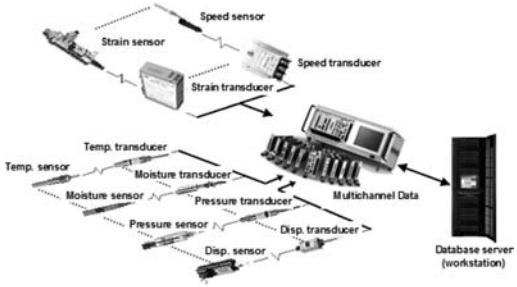

Figure 6. Multichannel data collection in the information collecting and processing unit.

collected by the system monitoring and controlling unit, especially those from the environmental control and Auto-Vehicle loading subsystems, may also be used in the pavement information collecting and processing unit. Figure 6 shows an illustration of this designed unit.

2.4 *Testing loop subsystem*

The Auto-Vehicle testing loop subsystem is illustrated in Figure 7. It has a similar shape to that of a 400 m athletic track, which allows a relatively high travelling speed compared to linear loading facilities. It contains two straight tracks joined by two semicircular tracks. The straight tracks are designed as full environment controlled segments, which can fulfill all designed accelerated tests. The semicircular tracks are used for evaluating the effects of cornering and vehicle steering on pavements.

Each straight track consists of a 36-m long testing segment and 2-m transition segment on each end. Tracks are 4.5 m wide and 3 m deep. The environment conditioning chamber is 7.5 m tall, with 4.5 m above

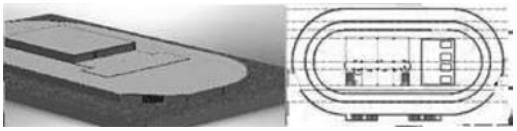

Figure 7. Plan design of testing loop.

ground level. The chamber is made of steel reinforced concrete, and special anti-seepage and heat preservation measures have been implemented to guarantee the prescribed environment conditions. As shown in Figure 7, the material laboratory and office building is located in the middle of the testing loop.

The curved segments of the track have a 7.5° superelevation to accommodate centrifugal loading forces. All interior walls and the exterior walls of the straight tracks are designed to bear an impact force of 200 kN, while the exterior walls on the curved sections are designed to bear a 300 kN impact. The track construction allows for smooth and safe operation of the Auto-Vehicle.

3 THREE-DIMENSIONAL FINITE ELEMENT SIMULATION IMPLEMENTATION

Acceptable pavement segment sizes are discussed in Dong et al. (2009), based on a static finite element analysis. A three-dimensional finite element asphalt pavement model subjected to a distributed moving vertical load was established to obtain the dynamic response of the designed pavement segment and check its boundary effects. The finite element analysis software, *ABAQUS*, in the implicit dynamic analysis mode was used for this study. In order to fulfill the non-uniform distributed surface moving load, a *FORTRAN* subroutine *DLOAD* was developed for this study (Dong, 2010). The actual pavement structure and material properties from the Liuhuan Expressway in Beijing, considered representative of pavement structures in China (Liu, 2010), were used as input for the model.

3.1 *Three-dimensional finite element model*

A 3-D finite element model was developed to simulate the Liuhuan expressway which is used as a typical tested pavement structure at the facility (Figures 8 and 9). The in-plane dimensions of the 3-D finite element model are 4,500 mm (width) × 2,520 mm (length). Symmetry was considered in the FE model to simulate the full dual-tire axle loading. A fine mesh was generated around the loading area along the wheel-path and a relatively coarse mesh was utilized farther away from it. The element size at the loading area is 15 mm in the direction of traffic, 16 mm laterally, and 20 mm vertically. When dynamic loads travel along the loading path at a speed of 60 km/hour, the loading time on each element was found to be 0.0009 sec. To improve the rate of convergence, an 8-node linear brick reduced-integration elements (C3D8R) was used.

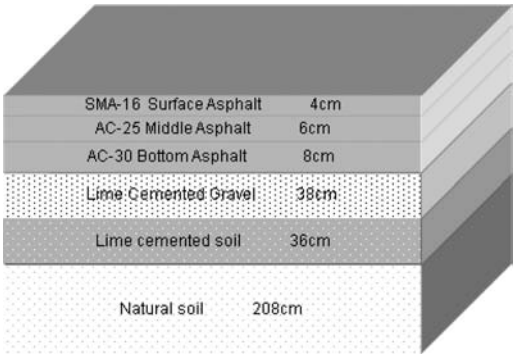

Figure 8. Pavement structure and material used in FE simulation (Liuhuan Expressway).

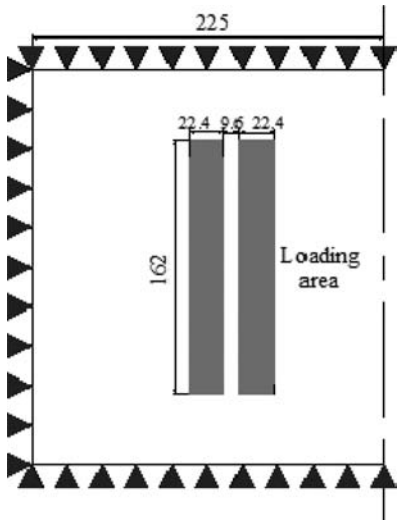

Figure 9. Planar geometries and meshing of FE model.

For the FE model in an implicit dynamic analysis, infinite elements (CIN3D8, 8-node 3-D linear infinite element) were used to simulate the far-field region in the longitudinal boundaries. The bottom and lateral boundaries were only fixed in the normal direction of the related surface to simulate the actual boundaries of the designed test section.

3.2 *Material characterization*

Visco-elastic properties from dynamic modulus testing, following the test method in NCHRP Report 465 (NCHRP, 2002), were used to characterize the asphalt layers. In this test, a UTM-100 was used to apply a sinusoidal force on the test specimens. After an initial preconditioning, the selected dynamic load with frequencies of 25, 10, 5, 1, 0.5 and 0.1 Hz was applied to the specimen and the axial deformation measured by extensometers was recorded. Each specimen was tested at temperatures of -10, 4.4, 21.1, 37.8 and 54.4°C, respectively. The dynamic modulus in the frequency domain was converted to the relaxation modulus in the time domain using the approximation method proposed by Schapery and Park (2009). In order to obtain the necessary visco-elastic material parameters for the *ABAQUS* analyses, the Prony series, time dependency, WLF equation, and temperature dependency of the asphalt mixture need to be defined. Details on the laboratory test setup, conversion process for the Prony series, and additional material properties can be found in Dong et al. (2007). Tables 2 through 4 summarize the elastic, visco-elastic and temperature parameters used in this analysis.

Table 2. Elastic parameters of analyzed asphalt pavement structure.

Material	Layer	Elastic modulus (MPa)	Poisson ratio	Density (kg/m^3)	Damping factor
SMA-16	Surface asphalt	1,550	0.35	2,400	–
AC-25	Middle asphalt	1,250	0.35	2,400	–
AC-30	Bottom asphalt	2,450	0.35	2,400	–
Lime cemented gravel	Base	10,000	0.25	2,100	0.05
Lime cemented soil	Subbase	2,000	0.35	1,900	0.05
Soil	Subgrade	250	0.4	1,900	0.05

Table 3. Prony parameters of asphalt mixture.

	g_i		
τ_i	SMA-16	AC-25	AC-30
0.00001	0.7490	0.3933	0.3696
0.0001	0.1063	0.2357	0.2011
0.001	0.0643	0.1867	0.1942
0.01	0.0290	0.1168	0.1223
0.1	0.0145	0.0438	0.0574
1	0.0068	0.0153	0.0235
10	0.0036	0.0044	0.0100
100	0.0017	0.0007	0.0041
1000	0.0013	0.0018	0.0027

Table 4. Parameters of WLF Equation of asphalt mixture.

Material	t_0	C1	C2
SMA-16	21.1	41.1	388.9
AC-25	21.1	7.3	93.0
AC-30	21.1	9.2	96.5

3.3 *Moving distributed load*

Figure 10 represents the simplified model used in the FE analysis for a dual-tire, at half axle load. The developed model simulates the tire imprint by considering the dimension of each tire rib separately (10 ribs for a dual-tire assembly). Each tire rib is divided into two elements laterally and 10 to 12 elements longitudinally depending on the length. Table 5 represents the dimension of the tire ribs and the proposed loading amplitudes used in this analysis. The distance between the two tires was set to 9.6 cm which is divided into six elements laterally.

Dynamic variation of tire pressures with time steps is assumed to be a half sine curve, with no difference between the entrance and exit of the tire imprint. This is taken as a representative loading model which may be slightly different from the field measured distribution of contact stress presented in Yoo et al. 2007 and 2009).

3.4 *Dimension evaluation*

The effective loading length of each testing segment varies between 8 m and 12 m, which is similar to that of the linear loading facility. The variation of dynamic response along the lateral and vertical direction within pavement was selected to evaluate the feasibility of the proposed width and depth. The centerline of the dual-tire was used as a reference line (Distance is set to zero, $l = 0$). The analysis points are shown in Figure 11.

The time histories and distributions of the dynamic responses, including three directional strain and stress, were analyzed in detail in Dong (2009). All the responses varied with the lateral distance from the centerline of the dual-tire. Figure 12 presents vertical strain and vertical stress variation with lateral distance.

Vertical strain decreases with depth, and the maximum vertical strain occurs in the upper layer. Minimal strain occurs in the base layer as this semi-rigid layer has a much higher modulus compared to the other layers. As the depth increases, the strain in the soil also decreases to an insignificant level. As for the lateral distributed points, the maximum vertical strain occurs at the central rib of the tire, and the strain amplitudes decrease with the distance from the center rib. At a point $l = 0.4$ away from the central point, the strain is much smaller than at the central points. The same was observed with the distribution of vertical stress, as shown in Figure 13.

Results of this analysis show that the dimensions of the test pavement segments proposed in the preliminary design course are acceptable.

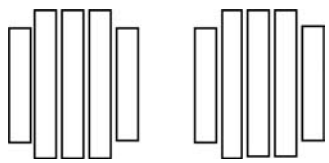

Figure 10. Simplified vertical distributions of dual-tire load.

4 SUMMARY AND CONCLUSIONS

The design of a full-scale accelerated loading facility for extreme regional climates started in 2007, and is

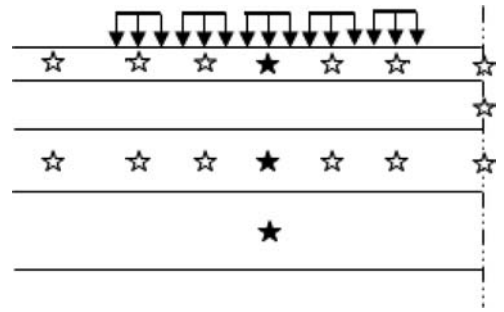

Figure 11. Analysis points for dynamic response of asphalt pavement.

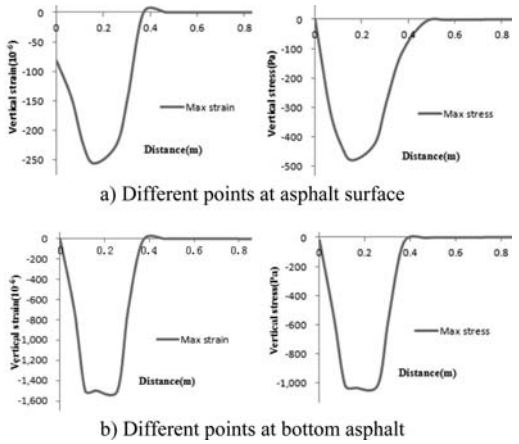

Figure 12. Time histories of vertical strain and stress for different points.

Table 5. Parameters of double-tire loading.

Parameter	Rib 1	Groove 1	Rib 2	Groove 2	Rib 3	Groove 3	Rib 4	Groove 4	Rib 5
Pressure (kPa)	780	–	1430	–	1560	–	1430	–	780
Length (cm)	15.0	–	18.0	–	18.0	–	18.0	–	15.0
Width (cm)	3.2	1.6	3.2	1.6	3.2	1.6	3.2	1.6	3.2

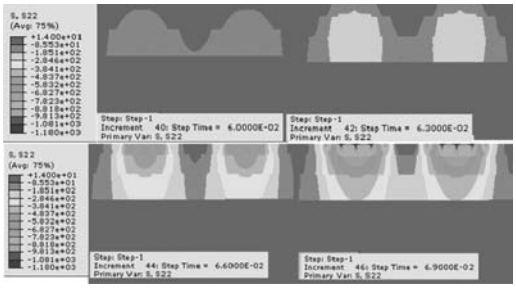

Figure 13. Spatial distribution of vertical stress at different loading times.

proposed to be finished at the end of 2012. This facility was designed as an oval loop over which a pilotless vehicle moves around repeatedly. The facility is fully enclosed to facilitate complete control of environmental conditions. This facility includes an Auto-Vehicle loading subsystem, environment control subsystem, data collection and central control subsystem, and a testing loop subsystem.

The total length of the testing loop is 200 m with two 40 m straight sections and two 60 m semicircular sections. Axle loads range from 25 kN to 225 kN, and the maximum speed is 60 km/h. Pavement temperatures can be controlled between −15°C and 60°C, which covers typical field climate conditions in China. Moisture and ultraviolet aging are also fully controlled.

A three-dimensional finite element asphalt pavement subjected to a non-uniform moving load was developed to check the appropriateness of the proposed dimensions of the testing segments. Dynamic response variation along the lateral and vertical direction was analyzed. Results show that the dimensions of the test pavement segments proposed in the preliminary design course are acceptable.

ACKNOWLEDGEMENTS

The authors would like to express gratitude to the design and support group of the full-scale accelerated loading facility including, Prof. Guo Bin, Prof. Yao Yingxue, Prof. Ma Guangfu, Prof. Li Bingxi, Prof. Wu Sigang, Prof. Gao Dong, Prof. Jiang Baocheng, Associate Prof. Fu Zhongbin, Associate Prof. Zhou Liang, Associate Prof. Liu Guangyi, Associate Prof. Jiang Ye, Associate Prof. Li Chuanjiang, Assistant Prof. Li Yunliang, Dr. Chen Fengchen, Prof. Sun Dongbai, Prof. Zhang Weidong, Prof. Wang Linbing, Assistant Prof. Sun Fengyan and Prof. Jin Ying. Support, cooperation, and funding from the National Center for Material Service Safety are also acknowledged. The authors would also like to express special appreciation to Mr. Li Shenglong for the finite element analysis work presented.

REFERENCES

Dong, Z.J., Tan, Y.Q. and Cheng, F.C. 2009. Preliminary design of testing segment for Accelerated Loading Facility based on finite element simulation analysis, *ASCE Geotechnical Special Publication (GSP 190): Asphalt Material Characterization, Accelerated Testing, and Highway Management*, Changsha, pp. 72–78.

Dong, Z.J., Tan, Y.Q., Cao, L.P. and Liu. H. 2009. Combining Strain Measurement and FEM Simulation to Obtain Dynamic Response of Asphalt Pavement. *International Journal of Pavement Research and Technology, Vol. 02, No.05*, pp. 231–235.

Dong, Z.J. 2010. *Structural behavior of asphalt pavement based on intelligent monitoring technology and nonlinear dynamic simulation*. Postdoctoral Report of Harbin Institute of Technology, 2010.

Liu, H. 2010. *Mechanism of flow rutting and anti-rutting technology for asphalt pavement with semi-rigid base*. Doctoral Dissertation of Harbin Institute of Technology, 2010.

NCHRP Report 465. 2002. *Simple performance test for Superpave mix design: Appendix A–Test method for dynamic modulus of asphalt concrete mixtures for fatigue cracking*, Transportation Research Board Report, National Research Council, Washington D.C.

Park, S.W. and Schapery, R.A. 2009. Methods of interconversion between linear viscoelastic materials functions. Part I–A numerical method based on Prony series. *International Journal Solids and Structures, Vol. 36, No. 11*, pp. 1653–1675.

Yoo, P.J. and Al-Qadi, I.L. 2007. Effect of Transient Dynamic Loading on Flexible Pavements. *TRB 2007 Annual Meeting CD-ROM*, Washington, DC.

Yoo, P.J. 2007. *Flexible pavement dynamic response analysis and validation for various tire configurations*. Doctoral Dissertation of University of Illinois at Urbana-Champaign.

This page intentionally left blank

Part 3: Review of the impact of accelerated pavement testing programs on practice

This page intentionally left blank

Advances in Pavement Design through Full-scale Accelerated Pavement Testing – Jones, Harvey, Mateos & Al-Qadi (Eds.)
© 2012 Taylor & Francis Group, London, ISBN 978-0-415-62138-0

Significant findings from the first three research cycles at the NCAT Pavement Test Track

R. West & R.B. Powell
National Center for Asphalt Technology, Auburn University, Alabama, US

ABSTRACT: The NCAT Pavement Test Track is a unique accelerated pavement testing facility that has now been operational for over 10 years. It is a cooperative project with individual test sections sponsored by highway agencies and commercial interest groups. This paper highlights key findings since the first heavily loaded tractor-trailer made the inaugural 2.7-km journey around the track over a decade ago. Test track findings have already resulted in numerous improvements in current asphalt pavement specifications, and the research will continue to pay dividends for years to come. Findings span the industry areas of mix design, aggregate and binder characteristics related to performance, structural design and tire-pavement interaction. This report is a summary of findings related to each of these five areas.

1 INTRODUCTION

The NCAT Pavement Test Track is a unique accelerated pavement testing facility that unites real-world pavement construction with live heavy trafficking for rapid testing and analysis of asphalt pavements. It is funded and managed as a cooperative project among highway agencies and industry sponsors. The track, shown in Figure 1, is a 2.7-km oval with 46 different 60-m test sections that are sponsored on three-year cycles. Each sponsor has specific research objectives for their section(s) and shared objectives for the track as a whole. Three cycles have been completed since the test track opened in 2000, and a fourth cycle will end in 2011.

The track sections are trafficked by a fleet of heavily loaded tractor-trailers that circle the track five days per week for 16 hours per day, applying 10 million equivalent single-axle loads (ESALs) to the pavements during each three-year research cycle. A picture of the heavy triple-trailer trains in service at the NCAT Pavement Test Track, with each axle loaded at the federal legal bridge standard, is shown in Figure 2. Pavement performance within each section is continuously monitored to evaluate rutting, fatigue cracking, roughness, texture, friction and noise. At the end of each cycle, test sections either remain in place for additional evaluation during the next cycle or are replaced, as determined by the section sponsor.

Test sections can be classified as either surface mix performance sections, which are built on a robust cross-section that limits distresses to the experimental surface layers, or as structural sections of different thicknesses that more closely resemble real-world pavements. Structural pavement sections have embedded strain and pressure sensors to analyze pavement response to loads for validation of mechanistic-empirical pavement design procedures. All sections are also equipped with temperature sensors throughout the pavement depth. Construction materials are often long-hauled from other states as required by sponsors in order to build 60-m test sections that are truly representative of sponsors' roadways.

2 BACKGROUND

The first cycle began in 2000 with the loading of 46 test sections. The only variable among the sections in

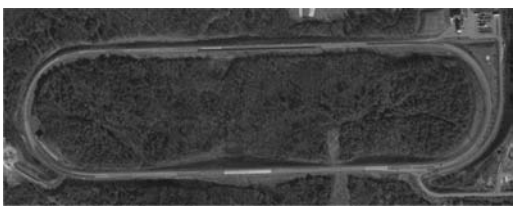

Figure 1. Satellite photo of the NCAT Pavement Test Track.

Figure 2. Accelerated truck traffic on the NCAT Pavement Test Track.

the first cycle of tests was the properties of the mixtures in the top 100 mm. This cycle was completed in 2002 after 10 million ESALs had been applied to the sections. This traffic level is representative of up to 20 years of traffic on typical rural interstate highways.

The second cycle of tests began in 2003 when parts of the test track were reconstructed. Eight sections were completely removed down to the subgrade and reconstructed to evaluate different thicknesses of hot-mix asphalt (HMA). Some of these structural sections used modified asphalt, and others used neat asphalt in adjacent sections. The structural section experiments marked the beginning of using the test track to examine issues relating to mechanistic pavement design. Each of these structural sections was built with embedded stress and strain gauges to measure the section's response to traffic throughout the cycle. Fourteen other sections from the original construction were milled and overlaid with a new surface mix to be evaluated. The remaining sections were left in place to evaluate the effects of two more years of traffic (another 10 million ESALs) and environmental exposure on durability.

The third research cycle began in 2006, with a combination of new and old sections in service. Eight original sections built in 2000 (all surface mix performance sections) remained in place and accumulated 30 million ESALs by the end of the third cycle in 2008. Sixteen sections (12 mix performance and four structural) from the second cycle also remained in place and had accumulated 20 million ESALs at the end of the third cycle. Twenty-two new sections (15 mix performance and seven structural) were built in 2006.

The fourth cycle began in 2009 and will be completed in late 2011. Three of the original surface mix performance sections built in 2000 remain in place and will have accumulated 40 million ESALs by the end of the fourth cycle. Eleven sections from the 2003 track (nine mix performance and two structural) remain in place and will have accumulated 30 million ESALs. Nine sections from the 2006 track (eight mix performance and one structural) remain in place and will have accumulated 20 million ESALs. Twenty-three new sections (nine mix performance and 14 structural) were built in the current research cycle.

3 RESEARCH FINDINGS

A number of findings from the test track have been used by the various sponsors to improve their materials specifications and pavement design policies. The majority of the research findings can be categorized into one of the following areas: (1) mix design, (2) aggregate characteristics related to performance, (3) binder characteristics related to performance, (4) structural design and (5) tire-pavement interaction. This report is a summary of findings related to each of these five areas.

3.1 *Mix design*

3.1.1 *High RAP mixtures*

Six test sections in the third cycle were devoted to evaluating the performance of pavements with both moderate (20 percent) and high (45 percent) reclaimed asphalt pavement (RAP) contents. Results indicate that high RAP content mixes can provide excellent rutting performance and durability. Field performance through four years does not indicate that using a softer virgin binder grade significantly improves performance for high RAP content mixes (Willis et al., 2009).

In the current cycle, sections were built with 50 percent RAP in the surface, intermediate and base layers to further assess the cracking resistance of high RAP mixes. In one section, the virgin binder is a regular PG 67-22 binder, and in the other section the same binder was foamed to facilitate production as warm-mix asphalt (WMA). Preliminary results from laboratory beam testing at measured track strain levels provide favorable fatigue expectations for high RAP content mixes run as both HMA and WMA. Another surface mix performance section was milled and inlaid with gravel containing 45 percent RAP and PG 67-22 binder. Porous friction course (PFC) surfaces in three other sections were placed with 15 percent RAP.

3.1.2 *Warm-mix asphalt*

MeadWestvaco donated materials to produce and construct an early version of its Evotherm WMA in the fall of 2005. These two WMA test sections opened to heavy traffic immediately after construction, near the end of the 2003 research cycle, and this new technology proved to be very resistant to rutting (Prowell, 2007). Both sections remained in service throughout the 2006 track, exhibiting durability and rutting performance comparable to HMA for 10.5 million ESALs. One section remains in service on the 2009 track. Durability of WMA has been found to be comparable to HMA through six years and more than 19 million ESALs.

In the current cycle, data shows that WMA sections built with both a foamed asphalt technology and an additive technology have the same structural response to heavy loads and environmental effects as HMA. These sections were also opened up to heavy traffic after construction in August 2009 and have proven to be resistant to rutting. As previously mentioned, the fatigue expectation for all WMA sections exceeds expectations for the HMA control. The track is now being used by state DOTs as an approval mechanism for new WMA technologies (Powell and Taylor, 2011).

3.1.3 *Stone-matrix asphalt mixtures*

Through the first four cycles of the NCAT Pavement Test Track, 21 stone-matrix asphalt (SMA) sections have been put to the test (eight on the 2000 track, eight on the 2003 track, three on the 2006 track and two on the 2009 track). Excellent performance of the SMA test sections in the first cycle prompted several states to use this premium mix type to extend pavement life for heavy traffic highways. Specific test sections

using crushed gravel aggregate in an SMA performed as well as other SMA sections, allowing states with limited native quarried stone to implement SMA at a much lower cost. Other test sections were built to compare SMA and Superpave mixes on a life-cycle cost basis. After five years and 20 million ESALs, both sections had less than 2 mm of wheel-path deformation, but the Superpave section was showing an increasing trend of macrotexture—an indicator of raveling—and some cracking at the longitudinal joint. In contrast, the higher binder content SMA section exhibited only a slight change in macrotexture with no cracking (Timm et al., 2006).

3.1.4 *Open-graded friction course mixtures*

Several highway agencies have sponsored test sections to evaluate the performance of open-graded friction course (OGFC) mixes with different aggregates and construction techniques. The Georgia DOT sponsored two test sections to assess how aggregates with different percentages of flat and elongated particles would affect performance. Results showed that more cubical aggregate reduced the permeability and capacity to eliminate water spray compared to less cubical and lower cost aggregate (Powell, 2009). The Tennessee DOT sponsored an OGFC mixture using a hard limestone that had excellent performance, including superior friction results, prompting TDOT to begin placing OGFC on some routes for the first time in 2005. The Mississippi DOT continues to assess an all-gravel OGFC placed in 2006, which has already withstood over 19 million ESALs. The Florida DOT is currently evaluating an OGFC mixture containing 15 percent RAP.

One of the most interesting test sections on the track has been the twin-layer OGFC placed in 2006. This section has a 9.5 mm nominal maximum aggregate size (NMAS) OGFC surface layer on top of a 12.5 mm NMAS OGFC layer. Both OGFC layers were placed with a special (and very large) paver built specifically to simultaneously place two HMA layers (Powell, 2009). After five years the twin-layer OGFC surface continues to be the quietest and most effective section at eliminating water spray on the track.

Although the enhanced safety and reduced-noise benefits of OGFC mixtures are well documented, test track research is currently assessing the structural contribution of the OGFC surface layer and how OGFC may be able to minimize top-down cracking when a heavy tack coat is used. OGFC surfaces have been found to reduce the recurrence of surface cracking in underlying dense mixes intentionally produced with a susceptibility to surface cracking, providing the most protection when placed in a bonded application with a spray paver.

3.1.5 *Critical air voids level for acceptance*

The Indiana Department of Transportation sponsored test track research to identify the lowest limit for air voids, one of the most used pay-factors for pavement quality. Because the focus of the experiment was rutting performance, cold weather climate differences between Alabama and Indiana were not a concern. A series of short sections constructed with surface layers having low QC air voids were subjected to the test track's heavy trafficking. The surface mixes were intentionally produced to have QC air voids between 1.0 and 3.5 percent by adjusting the mix gradation and increasing the asphalt content. Results showed that the rate of rutting significantly increased when QC air voids were less than 2.75 percent, indicating that removal and replacement of surface layers is appropriate below that level (Willis et al., 2009). It is important to note that the Indiana DOT experiment used only mixes with neat asphalt binder. Other sections on the track with surface mixes containing modified binders with air voids less than 2.5 percent have held up well under the extreme traffic on the track (Brown et al., 2002, Willis et al., 2009). A photograph of one of the Indiana sections built with low QC voids is shown in Figure 3.

Figure 3. Significant rutting in test section with low QC air voids.

3.1.6 *Comparison of mix design methods*

In the first cycle, the Oklahoma DOT built two test sections to compare the performance of mixes designed with the Superpave system to mixes designed by ODOT's standard Hveem-based mix design. Although both sections exhibited good performance on the track, less rutting was observed in the Superpave section (Brown et al., 2002). This test track study gave ODOT the confidence to move forward with implementing Superpave.

3.1.7 *Fine-graded versus coarse-graded mixtures*

During the early years of Superpave implementation, there was a strong push toward coarse-graded mixtures for improving rutting resistance; however, that notion was called into question when the results of Westrack showed that a coarse-graded gravel mix was less resistant to rutting and fatigue cracking than a fine-graded mix with the same aggregates. In the first cycle of the NCAT Pavement Test Track, the issue was examined more completely. Twenty-seven sections were built with a wide range of aggregate types comparing coarse-, intermediate- and fine-graded mixtures. NCAT Pavement Test Track results showed that fine-graded Superpave mixes perform as well as coarse-graded and intermediate-graded mixes under

heavy traffic and tend to be easier to compact, less prone to segregation, and less permeable (Brown et al., 2002). Based on these findings, many state highway agencies revised their specifications to allow the use of more fine-graded mix designs.

3.1.8 *Increased durability*

Test track research has shown that higher asphalt contents improve mix durability, leading to longer pavement life. More asphalt can be incorporated into the mixture by reducing the compactive effort required during mix design. Several states placed mixes on the test track that were designed with 50 to 70 gyrations in the Superpave gyratory compactor (SGC) that have withstood the heavy loading on the track with excellent performance (Timm et al., 2006, Willis et al., 2009).

3.1.9 *Top-down cracking*

Florida's pavement management system has shown that top-down cracking is the state's most prevalent form of pavement distress. University of Florida research has indicated that the best method for predicting resistance to top-down cracking is the energy ratio, which is determined from properties of the surface mixture and stress conditions in the pavement structure. Florida DOT has sponsored test track sections in past and current cycles to validate the energy ratio concept and to determine ways to mitigate this mode of distress. Test sections have shown that using a polymer-modified binder in dense-graded surface layers increases a mixture's energy ratio and improves the pavement's resistance to top-down cracking (Willis et al., 2009). The current cycle is assessing how a heavy tack coat applied with a spray-paver during construction of an OGFC layer may provide added resistance to the start or severity of top-down cracking.

3.1.10 *Thin overlay using a 4.75 mm nominal maximum aggregate size mixture*

Thin HMA overlays (less than 30 mm thick) are a common treatment for pavement preservation. Currently, about half of U.S. states utilize 4.75 mm nominal maximum aggregate size (NMAS) mixtures in thin overlay applications. An advantage of the 4.75 mm mixtures is that they can be placed as thin as 13 mm, allowing the mix to cover a much larger area than thicker overlays. In the second test track cycle, the Mississippi DOT sponsored a test section of 4.75 mm NMAS surface mix containing limestone screenings, fine crushed gravel and a native sand. The section has been in place for eight years and carried more than 29 million ESALs with only 7 mm of rutting and no cracking. This section is proof that well-designed 4.75 mm NMAS mixes are a tough and durable option for pavement preservation.

3.2 *Aggregate characteristics*

3.2.1 *Effect of aggregate toughness on performance*

The South Carolina DOT used the test track to evaluate how an aggregate with an excessive Los Angeles Abrasion loss would hold up through plant production, construction and performance in a real pavement. Although the aggregate did break down more than other aggregates through the plant, the resulting asphalt mixture performed well on the track. Rutting performance on the track was similar to that of other sections, and there were no signs of raveling, as indicated by texture changes (Timm et al., 2006). Based on these results, South Carolina changed its specifications to allow the use of this aggregate source with higher LA abrasion loss.

In another test section, South Carolina was interested in assessing the polishing behavior of a different aggregate material. A surface mixture with the aggregate was designed, produced and placed on the track. Friction tests conducted at regular intervals of traffic applications showed a sharp decline in skid resistance, indicating that the aggregate was not suitable for use in surface mixes (Timm et al., 2006). The test track enabled South Carolina to make this assessment within a year without placing the driving public at risk. Mississippi and Tennessee DOTs constructed sections to observe how blending limestone into gravel mixes effects pavement performance and friction test results. Both states concluded that mixes containing all local crushed gravel will provide satisfactory performance (Powell, 2006).

Missouri DOT constructed three test sections on the 2003 track to determine the possibility of adjusting the quality requirements for SMA aggregates without compromising performance. Before that time, only one in-state source of material could be used. As a result of this experiment, Missouri was able to revise the specification and reap the benefits of lower-cost SMA mixes through increased competition and reduced haul cost.

3.2.2 *Elimination of the restricted zone*

Part of the original Superpave mix design procedure included a restricted zone within the gradation band for each nominal aggregate size. Test track sections with a variety of aggregate types proved that mixtures with gradations through the restricted zone could have excellent rutting resistance (Brown et al., 2002). The restricted zone was subsequently removed from the Superpave specifications.

3.3 *Binder characteristics*

3.3.1 *Effect of binder grade on rutting*

Superpave guidelines recommend using a higher PG grade for high traffic-volume roadways to minimize rutting. Results from the first cycle of testing indicated that, on average, permanent deformation was reduced by more than 50 percent when the high-temperature grade was increased from PG 64 to PG 76 (Brown et al., 2002). This two-grade bump is typical of many projects on high traffic-volume roadways. This information validated one of the key benefits of modified asphalt binders. The Florida DOT had conducted accelerated testing of its own using a Heavy Vehicle Simulator

(HVS) to determine at what depth it would be possible to discontinue the use of modified binders without sacrificing improved rutting performance. Two sections of the 2003 track were subsequently used to validate these findings by comparing their performance with those used in the HVS experiment. Results on the NCAT Pavement Test Track were comparable to results in the HVS, giving Florida confidence to implement its previous findings (Powell, 2008).

3.3.2 *Increasing the binder content in mixtures containing modified binders*

In the first cycle, the Alabama Department of Transportation also sponsored test sections to evaluate mix designs with an extra 0.5 percent asphalt content. Performance of those sections on the track showed that increasing the asphalt content of mixes produced with modified binders did not affect rutting resistance; however, mixes produced with neat binders were more sensitive to changes in asphalt content (Brown et al., 2002). Furthermore, the performance of test sections containing neat asphalt was consistent with the finding previously described. For mixtures with modified binders, low lab-compacted air voids are not a good indicator of rutting.

3.3.3 *Comparison of different types of binder modification*

The effect of binder modifiers on the performance of dense SMA and PFC mixes was a major focus of the 2000 track. Excellent performance was observed in all mixes produced with modified binders, regardless of the type of modifier used (Brown et al., 2002).

In the current cycle, Missouri DOT sponsored two sections to compare the performance of a surface mix containing an SBS-modified binder and a ground tire rubber-modified binder. Both binders graded as PG 76-22. To date, comparisons of the two sections show that both binders provide excellent and essentially equivalent performance.

3.4 *Structural design*

3.4.1 *Engineering response of pavement structures to load and environment*

Over the past three cycles, 18 test sections have been instrumented with stress and stain gauges to measure actual responses of pavement structures to loading and environmental conditions. The stress and strain measurements at the bottom of asphalt layers have correlated well with predicted values, using layered-elastic models for a wide range of pavement materials and thicknesses at high speeds (Timm et al., 2006). This important finding validates the use of such models in mechanistic-based pavement structural design methods, including *PerRoad* and the *Mechanistic-Empirical Pavement Design Guide (MEPDG)*.

3.4.2 *Revision of the asphalt layer coefficient for pavements*

Although many highway agencies are preparing for implementation of the MEPDG, thousands of projects continue to be designed using the pavement design method developed more than 50 years ago that was based on the AASHO Road Test. In simplified terms, the current method relates the expected decrease in pavement serviceability to the design traffic divided by the structural capacity of the pavement structure. The pavement's structural capacity is calculated by summing the products of the thickness of each layer multiplied by an assigned layer coefficient that represents the relative structural contribution of that layer.

When 225 mm pavements were found to be the perpetual equivalent of the original robust track foundation, the Alabama DOT funded a study to examine the layer coefficient for structural asphalt layers. The performance and loading history of all 14 structural sections built on the NCAT Pavement Test Track in the second and third cycles were analyzed. These test sections represented a broad range of asphalt thicknesses, mix types, bases, and subgrades. The analysis indicated that the asphalt layer coefficient should be increased from 0.44 to 0.54 (Peters-Davis and Timm, 2009). This increase in the layer coefficient translates directly to an 18.5 percent reduction in the design thickness for new pavements and overlays. ALDOT implemented the new layer coefficient in its pavement design practice in 2010 and estimates this change will save $50 million per year in construction costs.

3.4.3 *Strain threshold for perpetual pavements*

Analysis of data from in-situ pavement instrumentation from three cycles of the test track indicates that these pavements can withstand higher levels of strain than suggested by lab tests without accumulating fatigue damage (Willis et al., 2009). This may allow pavement engineers to design perpetual pavements with thinner cross-sections and, thus, make HMA more competitive against other pavement types in life-cycle cost comparisons.

3.4.4 *High polymer inlays for rehabilitation of failed pavement structures*

The track is often used for high risk, high reward research that may not be suitable for assessment on in-service roadways. In one such experiment, a full depth asphalt pavement on a soft clay subgrade that failed near the end of the 2006 research cycle was first rehabilitated for the 2009 research cycle using a conventional 125-mm mill and inlay. When the section failed a second time after less than half the traffic that produced the original failure, it was decided to rehabilitate the section again using the same high polymer mix that had performed well in another (significantly thinner) test section.

The second rehabilitation of the failed section consisted of a 144-mm mill and inlay, which is the total thickness of the high polymer mix in the thinner section. Traffic applied to the high polymer rehabilitation has now surpassed the level needed to completely fail the original conventional rehabilitation, with no indication that another failure is pending. Based on

this positive finding, high polymer inlays are being considered on at least four projects in two different states as a way to salvage structures that have exhibited structural failures.

3.5 *Tire-pavement interaction*

3.5.1 *New generation open-graded friction course mixes*

Each cycle of the test track has featured sections with new-generation OGFC mixtures using a variety of aggregate types. Testing has shown that OGFC surfaces, also known as porous friction courses, eliminate water spray, improve skid resistance and significantly reduce tire-pavement noise.

3.5.2 *Friction performance*

Several agencies have sponsored test sections to evaluate the performance of OGFC mixtures with a range of aggregate types. Examples of aggregates used in OGFC surfaces on the test track include granite, limestone, slag, and other gravels. Ongoing research is explaining the correlation between friction results on the test track with laboratory conditioning and friction testing. This work will reduce the cost, time and risks associated with field evaluation of new pavement surfaces and could provide new opportunities for research on building safer roads.

3.5.3 *Tire-pavement noise and pavement surface characteristics*

The noise generated from tire-pavement interaction is substantially influenced by the macrotexture and porosity of the surface layer. Tire-pavement noise testing on the track indicates that the degree to which these factors influence noise levels is related to the weight of the vehicle and to tire pressures. For lighter passenger vehicles, the porosity of the surface, which relates to the degree of noise attenuation, is the dominant factor. For heavier vehicles (with higher tire pressures), the macrotexture of the surface and the positive texture presented at the tire-pavement interface has a greater influence (Smit and Waller, 2007).

3.5.4 *High-precision diamond grinding to remove bumps for smoother roads*

A good way to level high areas in the pavement surface that can occur in the construction and maintenance of HMA is through high-precision diamond grinding. When performed on transverse joints at the test track, this grinding process resulted in a very smooth and tight surface (Timm et al., 2006). None of the numerous joints leveled with the grinding equipment during each research cycle have exhibited any performance issues. Some of the leveled areas have been in service for 11 years with no performance problems. No sealing was applied to these treated surfaces.

3.6 *Prediction testing*

3.6.1 *Performance tests to predict rutting*

Pavement engineers are interested in identifying a reliable test that can predict rutting performance. Through each cycle, NCAT has conducted several performance tests on the mixtures placed at the track, including dynamic modulus, repeated load tests and wheel-tracking tests. Although the amount of rutting for most of the test sections at the track has been low, sufficient rutting was observed to determine if trends exist between the performance tests and actual rutting measured on the track. The results have shown that dynamic modulus has no correlation with rutting. The Asphalt Pavement Analyzer (APA) is a popular test for assessing rutting potential and has consistently provided reasonable correlations with test track performance (Powell, 2006). As a result of this testing at the track, several state DOTs implemented specifications requiring the use of the APA on new mix designs. Based on a correlation between APA results and rutting on the track in the third cycle, an APA criteria limit of 5.5 mm was established for heavy-traffic pavements (Kandhal and Cooley, 2008).

In the last few years, several researchers have recommended a repeated-load axial deformation test known as the Flow Number (FN) test for predicting rutting. Although no consensus has been reached regarding several variations of the test method, NCAT has used a confined test with 69 kPa and a repeated axial stress of 483 kPa. A strong correlation was found between the results of the FN test using these conditions and rutting on the track (Willis et al., 2009). A minimum FN criterion of 800 cycles was recommended for heavy traffic pavements.

3.6.2 *Using energy ratio to predict top-down cracking*

As previously described, the University of Florida and Florida DOT have developed a promising method for predicting the susceptibility of surface layers to top-down, load-related cracking. This method was validated on the test track in the third cycle. Two test sections were built with identical structures, except for the surface layers. One surface mix was designed with a low energy ratio, and the other was designed with a high energy ratio. As expected, the section with the low energy ratio exhibited top-down cracking first, with cracks appearing after 1.9 million ESALs. The section with the higher energy ratio surface layer carried 50 percent more traffic before cracks appeared. This research demonstrated that top-down cracking is a phenomenon that can be replicated in experimental pavements and that the energy ratio method can correctly assess the relative performance of surface mixes to this mode of distress (Willis et al., 2009).

3.6.3 *Dynamic modulus prediction*

In mechanistic-based pavement design methods, the dynamic modulus (E^*) is a basic input for HMA, since this property characterizes the rate of loading and temperature dependency of HMA. Three predictive dynamic modulus models and laboratory-measured E^* values for mixes placed on the 2006 NCAT Pavement Test Track were compared to determine which model most accurately reflected E^* values determined

in laboratory testing. The Hirsch model proved to be the most reliable E^* model for predicting the dynamic modulus of an HMA mixture (Willis et al., 2009).

4 SUMMARY

The NCAT Pavement Test Track is a unique accelerated pavement testing facility that has now been operational for 11 years. It is a cooperative project with individual test sections sponsored by highway agencies and commercial interest groups. There have been numerous significant findings since the first heavily loaded tractor-trailer made the inaugural 2.7-km journey around the track a decade ago, many of which are summarized in this paper. Test track findings have already resulted in numerous improvements in current asphalt pavement specifications, and the research will continue to pay dividends for years to come. Findings span the industry areas of mix design, aggregate and binder characteristics related to performance, structural design and tire-pavement interaction.

ACKNOWLEDGEMENTS

The Pavement Test Track is managed by NCAT, who is responsible for daily operations and the completion of associated research. Funding for the NCAT Pavement Test Track has been provided under a cooperative agreement by the following entities:

- Alabama Department of Transportation
- Florida Department of Transportation
- Georgia Department of Transportation
- Indiana Department of Transportation
- Mississippi Department of Transportation
- Missouri Department of Transportation
- Nebraska Department of Roads
- North Carolina Department of Transportation
- Oklahoma Department of Transportation
- South Carolina Department of Transportation
- Tennessee Department of Transportation
- Texas Department of Transportation
- Wisconsin Department of Transportation
- Federal Highway Administration
- Cargill Deicing Technology
- Kraton Polymers
- Lake Asphalt of Trinidad and Tobago
- Oldcastle Materials
- Polycon
- Shell Sulfur Solutions

REFERENCES

Brown, E. R., Cooley, L. A., Hanson, D., Lynn, C., Powell, R. B., Prowell, B.D. and D. Watson. 2002. *NCAT Test Track Design, Construction, and Performance*. NCAT Report 02-12. National Center for Asphalt Technology, Auburn University.

Kandhal, P. and Cooley, L.A. 2008. *Accelerated Laboratory Rutting Tests: Evaluation of the Asphalt Pavement Analyzer*. NCHRP report 508, Transportation Research Board, Washington, DC.

Peters-Davis, K., and Timm, D. 2009. *Recalibration of the Asphalt Layer Coefficient*. NCAT Report 09-03. National Center for Asphalt Technology, Auburn University.

Powell, R.B. 2006. *Predicting Field Performance on the NCAT Pavement Test Track*, Ph.D. Dissertation. Auburn University, Auburn, Alabama.

Powell, R.B. 2008. Comparing Field Performance Under a Heavy Vehicle Simulator to Rutting Performance at the NCAT Pavement Test Track. *Proceedings of the 3rd International Conference on Accelerated Pavement Testing*.

Powell, R.B. 2009. Construction and Performance of Georgia's Permeable Surface Mixes on the 2006 NCAT Pavement Test Track. *CD-ROM Proceedings of the 88th Annual Transportation Research Board*.

Powell, R.B. and Taylor, A. 2011. Design, Construction and Performance of Sulfur-Modified Mix in the WMA Certification Program at the NCAT Pavement Test Track. *Proceedings of the 2nd International Conference on Warm-Mix Asphalt*.

Prowell, B., Hurley, G., and Crews, E. 2007. Field Performance of Warm Mix Asphalt at the NCAT Test Track. *CD-ROM Proceedings of the 86th Annual Transportation Research Board*.

Smit, A. and Waller, B. 2007. *Sound Pressure and Intensity Evaluations of Low Noise Pavement Structures with Open-Graded Asphalt Mixtures*. NCAT Report 07-02. National Center for Asphalt Technology, Auburn University.

Timm, D., West, R., Priest, A., Powell, R.B., Selvaraj, I., Zhang, J. and Brown, E.R. 2006. *Phase II NCAT Test Track Results*. Report 06-05. National Center for Asphalt Technology, Auburn University.

Tran, N., Taylor,A., Timm, D., Robbins, M., Powell, R.B. and Dongre, R. 2009. *Evaluation of Mixture Performance and Structural Capacity of Pavements Using Shell Thiopave*. NCAT Report 10-05. National Center for Asphalt Technology, Auburn University.

Willis, R., Timm, D., West, R., Powell, R.B., Robbins, M., Taylor, A., Smit, A., Tran, N., Heitzman, M. and Bianchini, A. 2009. *Phase III NCAT Test Track Findings*, NCAT Report 09-08. National Center for Asphalt Technology, Auburn University.

This page intentionally left blank

Advances in Pavement Design through Full-scale Accelerated Pavement Testing – Jones, Harvey, Mateos & Al-Qadi (Eds.)
© 2012 Taylor & Francis Group, London, ISBN 978-0-415-62138-0

A ten year review of Florida's accelerated pavement testing program

J. Greene & B. Choubane
Florida Department of Transportation, Gainesville, Florida, US

ABSTRACT: The need for faster and more practical evaluation methods under closely simulated in-service conditions prompted the Florida Department of Transportation (FDOT) to initiate an Accelerated Pavement Testing (APT) program in 2000. The main objective of this program is to continuously improve the performance of Florida's pavements in a cost-effective manner. Technology transfer and implementation are also of primary importance. The APT program recognizes that such efforts are essential to reap expected dividends from this investment. All research results and aspects of innovations arising from this program are implemented as soon as practical. Over the ten years of its existence, the Florida APT program has investigated flexible, rigid, and composite pavements. This paper provides a ten year review of FDOT's APT program. The evolution of the APT facility and program are described. Results from several projects are summarized and benefits from implemented technology and practices are highlighted.

1 INTRODUCTION

The evaluation and validation of emerging technologies and innovative concepts require assessing their in-service long-term performance. In respect to pavements, the cumulative effects of traffic loading and environmental conditions on the material properties and pavement response are critical in assessing performance and establishing failure modes. The primary disadvantage of such an investigative approach is the extensive time period and expense required to obtain long-term performance information.

The need for faster and more practical evaluation methods under closely simulated in-service conditions prompted the Florida Department of Transportation (FDOT) to initiate an accelerated pavement testing (APT) program in 2000. APT is generally defined as a controlled application of a realistic wheel load to a pavement system simulating long-term, in-service loading conditions. APT allows monitoring of a pavement system's performance and response to accumulation of damage within a much shorter time period. The primary objective of FDOT's APT program is to continuously improve the performance of Florida's pavements. As such, technology transfer and implementation of research findings are of primary importance.

2 ENHANCEMENTS TO FDOT'S HVS

Accelerated loading is performed using a Heavy Vehicle Simulator (HVS), Mark IV model. The HVS can apply wheel loads between 30 and 200 kN (7 and 45 kips) along a 9 m (30 ft.) test strip. Dual or single tires can be used. The effective test segment within this span is 6 m (20 ft.). The remaining 2 m (5 ft.) at either end of the test strip allows the HVS wheel to load and unload while accelerating and decelerating. A chain-driven carriage system allows uni- or bi-directional load applications. Wheel wander of up to 76 cm (30 in.) can be induced. The HVS can apply up to 24,000 passes per day in the bi-directional mode and 14,000 passes per day in the uni-directional mode. Florida's standard loading protocol consists of a 40 kN (9 kip) load with 10 cm (4 in.) of wander applied uni-directionally. General HVS properties are listed in Table 1. Additional information on how the loading protocol was established is detailed elsewhere (Byron et al. 2004).

2.1 *Environmental control*

A temperature control system was developed and installed during 2001.The primary components of the system include insulated panels and radiant heaters. The insulated panels originally consisted of aluminum sheeting with a Styrofoam core. The panels were redesigned in 2006 with lightweight materials to allow for placement without the use of a forklift.

Three pairs of 2.7 m (9 ft.) long radiant heating elements are mounted on both sides of the HVS test beam. These elements are independently controlled to provide six heating zones. They are also adjusted automatically to maintain a constant temperature at a depth of 5 cm (2 in.). A test temperature of 50°C (120°F) is standard for experiments to investigate rutting potential of asphalt mixtures. Figure 1 shows the HVS with the insulated panels attached.

Table 1. HVS properties.

Parameter	Specification
Weight	50 + tons
Length	75 ft. (22.9 m)
Tested section length	20 ft. (6.1 m)
Width	12 ft. (3.7 m)
Load range	7 to 45 kips (30 to 200 kN)
Wheel speed	2 to 8 mph (3 to 13 km/h)
Max. passes per day	14,000 (uni-directional) 24,000 (bi-directional)
Max. rut depth	4 in. (10 cm)
Tire types	Goodyear Unisteel G149 RSA, 11R22.5 (Dual Tire) Goodyear G286 A SS, 425/65R22.5 (Super Single) Michelin X One XDA-HT Plus, 445/50R22.5 Michelin X One XDA-HT Plus, 455/55R22.5
Tire wander	0 to 30 in. (0 to 76 cm)
Environment control	Insulated panels and heater system

Figure 1. Insulated panels used for temperature control.

2.2 *Laser profiling system*

A laser profiling system was added to the HVS in 2001 to automatically determine rut depth. The profiling system consists of two 16 kHz lasers mounted 76 cm (30 in.) apart on either side of the load carriage as shown in Figure 2. These lasers, model SLS 5000^{TM} manufactured by LMI Silicon, are specified to be accurate to within ±0.2% of the measurement range. Data is collected at a 4 km/h (2.5 mph) operating speed.

Rut measurements are collected at predetermined intervals in the form of longitudinal and transverse profiles. At each predetermined number of loaded passes the profile measurements are taken following a directional pattern as shown in Figure 3. In such a pattern, the lasers, while traveling with the unloaded carriage, survey an area of approximately 6.1 m (20 ft.) in length and 1.5 m (5 ft.) in width in a series of 61 fluid and continuous sweeps. The profiles are automatically acquired using the laser-based system at a rate of 16 kHz and averaged at 100 mm (4 in.) intervals. Following this process, a total of 58 transverse profiles are generated at any given number of load passes. The

Figure 2. Laser profiling system for rut depth measurement.

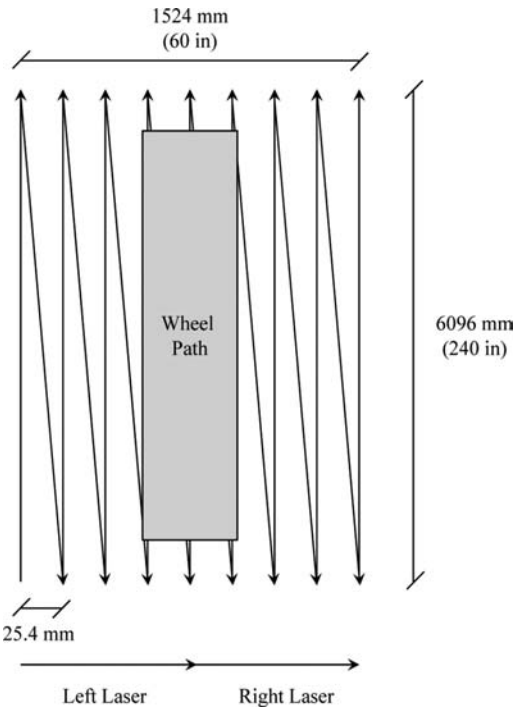

Figure 3. Path of laser profiler for measuring pavement surface profile.

resulting file comprises a data array of 58 rows and 134 columns and is used to produce a three dimensional surface profile of the entire test section. Profile measurements take approximately 15 minutes to complete. The initial profile (profile after construction and before loading) is used as the reference (baseline) to estimate the rut depths. A typical three dimensional surface profile is shown in Figure 4.

2.3 *HVS condition based maintenance*

The HVS represents a significant investment and requires considerable attention to maintain efficient operations. In 2003, a condition based maintenance program was initiated to monitor the HVS health, prevent failures and minimize downtime through the

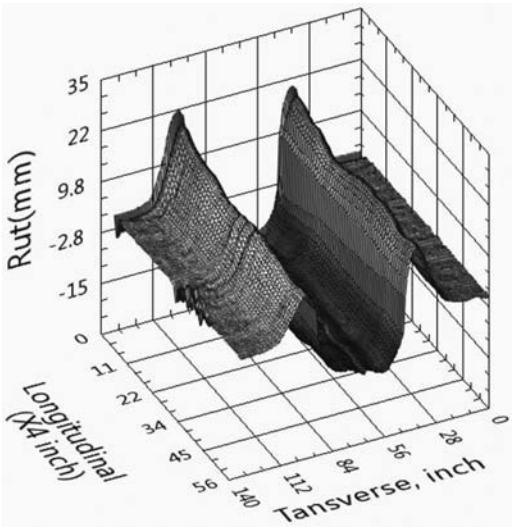

Figure 4. Three dimensional surface profile.

Table 2. HVS condition based maintenance sensors.

Sensor	Qty	Location	Objective
Power monitor	3	Inside power boxes	Detect power fluctuations
Thermocouple	16	Electronic enclosures	Detect overheating and fan failures
Accelerometer	5	Main motor	Monitor motor vibration
Laser rangefinder	1	Between main beams	Determine wheel location
Hydraulic tank sensor	2	Hydraulic tank	Detect hydraulic leaks
Hydraulic fluid sensor	2	Hydraulic tank	Monitor hydraulic fluid quality
Tire pressure sensor	2	Valve stem pressure	Monitor inflation
Infrared temp sensor	1	Near test tire	Monitor tire temperature
Camera	1	In view of test track	Monitor test section for leaks and obstructions

integration of additional sensors. The sensors installed on the HVS have been a tremendous aid in not only developing routine maintenance schedules but also in troubleshooting and detection of issues before they become critical. As a result of this effort, the HVS has become much more efficient and downtime is minimal. Table 2 summarizes the sensors used to monitor the HVS.

3 FDOT'S APT ASSETS

3.1 *APT facility*

The APT facility is housed within the State Materials Research Park in Gainesville. The test site originally consisted of eight linear test tracks with each test track

Figure 5. HVS and test tracks.

measuring 46 m (150 ft.) long and 3.7 m (12 ft.) wide. Seven of the test tracks were extended an additional 90 m (300 ft.) in 2011. The original test tracks are shown in Figure 5. The supporting soil layers consist of a 27 cm (10.5 in.) limerock base over a 30 cm (12 in.) mixture of limerock and native A-3 soil (as classified by the AASHTO soil classification system). Two additional 15 m (50 ft.) long test tracks are enclosed by a sump with an interconnecting channel system for controlling the water table.

3.2 *Accelerated pavement aging system*

Cracking is the most predominant flexible pavement distress in Florida. Investigations of distressed flexible pavements have shown that a great number of cracks originate from the surface. The most recent theories presented in NCHRP 1-42A regarding the mechanisms of top-down cracking indicate that aging of the asphalt pavement surface and the ability of the pavement to heal after loading are critical (Roque et al. 2010). In 2005, FDOT designed an accelerated pavement aging system (APAS) that uses heat as the primary force to rapidly age the pavement and limit its healing ability. Stiffness gradients due to the advanced oxidation levels at the surface are also induced. The APAS can be programmed to apply heat for extended periods, cycle heat on and off and spray water to rapidly cool the pavement. The APAS measures 3 m (10 ft.) wide by 7.3 m (24 ft.) long. Twelve 3 m (10 ft.) long radiant heaters equally spaced along the width of the APAS are used to heat the pavement to 90°C (194°F). Two thermocouples per heater are installed at the pavement surface and at a depth of 5 cm (2 in.) to monitor and adjust the temperature. Water can be sprayed at 163 liters (43 gal.) per minute from 65 nozzles evenly distributed along the APAS to cool the pavement from 90°C to 30°C (194°F to 86°F) in approximately 7 minutes. A standard procedure to determine appropriate heating periods is under development. The APAS is shown in Figure 6.

The APAS has successfully been used to promote top-down and bottom-up cracking under APT loading. Figure 7 shows crack measurements made during an APT fatigue cracking study. Sections with greater aging levels cracked earlier although the rate of cracking was similar for all sections.

Figure 6. Accelerated pavement aging system.

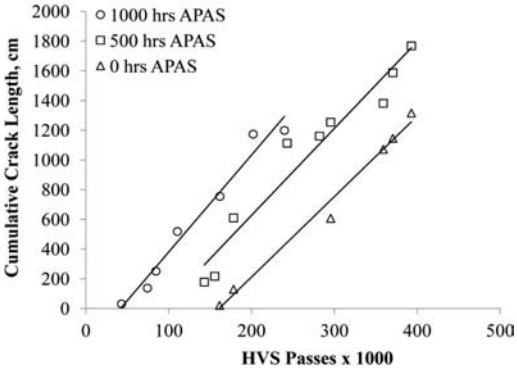

Figure 7. Fatigue cracking due to different aging levels.

3.3 *Material laboratories and pavement testing*

The SMO is equipped with state-of-the art asphalt, concrete and soil laboratories. Extensive collaboration and coordination with the asphalt laboratory has been essential since flexible pavements have made up the bulk of the APT experiments. The asphalt research laboratory includes Superpave binder and mixture test equipment. Cores are often tested in indirect tensile (IDT) mode to determine tensile strength, creep strength, and resilient modulus. The dynamic modulus and flow number are determined with an Asphalt Mixture Performance Tester (AMPT).

Initial pavement properties are measured using nondestructive test devices. Ground Penetrating Radar (GPR) is used to estimate newly constructed asphalt density and thickness. Pavement layer stiffness is assessed using a Falling Weight Deflectometer (FWD). Cores are taken for verification purposes at locations selected from the GPR and FWD data. The FWD and Portable Seismic Properties Analyzer (PSPA) have been used to measure the change in pavement stiffness due to loading, accelerated aging, and elevated water table.

3.4 *Pavement instrumentation*

Pavement response is generally recorded in terms of deflection, strain or stress. Environmental effects such as temperature and moisture are also often critical to pavement performance. Strain is usually measured near the bottom and surface of HMA layers and at selected points near the center, edges, and joints of concrete slabs. Vertical stress distributions through the depth of unbound base and embankment layers are used for settlement and rutting analyses; therefore, pressure sensors are typically placed in the base and subgrade. Linear variable displacement transducers (LVDT) have been used to measure the thermal movement of concrete slabs. Table 3 lists the most common pavement instrumentation used by FDOT. More detailed information on instrumentation use and installation is provided elsewhere (Greene et al, 2011a).

Table 3. Commonly used pavement instrumentation.

Sensor	Location	Objective
Thermocouple	Various depths	Pavement temp
H-gauge	Bottom of asphalt	Asphalt strain due to tire loads
Foil gauge	HMA surface	Surface strain due to tire or thermal loads
Concrete strain gauge	Top and bottom of concrete near center, edges and joint	Concrete strain
Pressure cell	Granular layers	Granular layer stress
Moisture probe	Granular layers	Granular layer moisture

Pavement instrumentation is connected to a National Instruments (NI) data acquisition (DAQ) system mounted on a custom made portable enclosure. The enclosure is temperature controlled and rated for outdoor use (NEMA 4X). A wireless link between the main HVS control room computer and the outdoor DAQ enables control from indoors where further processing can be performed using fully-automated NI *LabVIEW* software. When the HVS tire is traveling at 11 km/h (7 mph), it takes approximately 6.5 seconds for the tire to traverse the test section. Stress and strain data is often collected in windows of up to 50 seconds to capture the response of at least three passes of the loaded tire. Data is typically scanned at 1,000 Hz. Other sensor information such as temperature from thermocouples, moisture data, and LVDT data is acquired at different frequencies depending on the objective.

A LabVIEW program is used to merge instrumentation and related HVS data and to identify critical strain and stress components. All of this information is recorded in a spreadsheet for further analysis. The resulting processed file contains the following information:

1. Time of data collection
2. Wheel location
3. Pass number
4. Wheel load

Table 4. Major APT experiments.

Year	Experiment	Findings and Outcomes	Source
2001	Evaluation of polymer modified asphalt binders	Rutting resistance improvement was found even when modified binder was limited to the final structural layer. Revised design manual and specification.	Tia et al. 2002; Gokhale et al. 2005
2003	Assessment of APT loading	FDOT HVS load parameters were standardized.	Byron et al. 2004
2004	Early strength requirement of slab replacement concrete	Required flexural strength was defined in terms of slab temp. gradient. A concrete stress/strain prediction model was developed. The maturity method was verified.	Tia et al. 2005
2005	Coarse and fine graded Superpave evaluation	Fine graded mixtures performed as well as coarse graded mixtures. Revised design manual and specification.	Choubane et al. 2005
2006	Thin concrete overlay evaluation	Developed a model for predicting stress/strains for traffic and thermal loads. Design recommendations were made.	Tia et al. 2007
2007	Asphalt mixture cracking assessment	Developed the APAS and a crack initiation model using fracture mechanics and IDT testing.	Roque et al. 2007
2008	Evaluation of asphalt strain gauge repeatability	Strain gauges were found to be repeatable when pavement was less than 104°FC (40°F).	Gokhale et al. 2009
2009	Impact of wide-base tires on pavement damage	Wide-base tires were found to perform as well as a standard dual tire. A model to predict pavement response due to tire type was developed.	Greene et al. 2010
2010	Gradation based mixture performance evaluation method	Validated gradation evaluation method to optimize asphalt gradations. Mix design spreadsheet was modified to monitor future gradations.	Greene et al. 2011b
2010	SAMI contribution to rutting	An asphalt rubber membrane interlayer (ARMI) was found to contribute to instability rutting.	Greene et al. 2012

5. Pavement and ambient temperature
6. Strain/stress information (e.g. strain magnitude and duration)

4 OVERVIEW OF RESEARCH PROJECTS

The development, planning and execution of the APT program are conducted on an annual cycle with support from the FDOT Central Offices and Districts and through partnerships with the Florida's University System, industry and the Federal Highway Administration (FHWA). Throughout the year, research needs that address issues affecting Florida's roadways are collected from the Central and District offices. A formal process is initiated in the fall when critical research topics are solicited from academia, the FHWA, industry, as well as FDOT offices. Research needs are classified according to the following three categories:

1. Critical issues that should be addressed by APT
2. Critical issues not applicable to APT but should be performed with in-house resources
3. Critical issues that should be addressed through a contracted effort

Over the 10 years of its existence, the Florida APT program has investigated flexible, rigid, and composite pavements. Specific aspects that have been assessed include asphalt mixture gradation, the use of polymer modified binder, damage due to tire types, effect of stress-absorbing membrane interlayers (SAMI), environmental effects (i.e. asphalt aging), early strength gain requirement of concrete for slab replacement and thin concrete overlays. Table 4 summarizes the major APT experiments. Table 5 summarizes the asphalt and concrete materials used for the APT experiments.

5 IMPACT OF APT RESEARCH

Over the first ten years, FDOT's APT program has provided a significant impact on Florida's roadways. Engineers have successfully used the APT facility to gain insight into new pavement technology and design methods that laboratory testing alone could not provide. Several APT projects have been conducted in collaboration with Florida universities. Some of these projects involved contracting directly with universities while others simply involved sharing data for graduate level research projects. Eight Ph.D. dissertations and one Master's thesis have been completed using Florida APT data. Table 6 lists these academic research reports.

Most important is the impact that the APT program has had on pavement construction and design practices. FDOT's Flexible Pavement Design Manual and construction specifications have been revised based on research performed on polymer modified binders and gradations of Superpave mixtures. APT research showed new generation wide-base tires generate similar or less damage to Florida pavements as the standard dual.

Table 5. Pavement structure and materials.

Experiment	Structure	Materials
Evaluation of polymer modified asphalt binders	4 in. SP-12.5 mm	Limestone, SBS modified PG 76-22 binder, and PG 67-22 binder
Assessment of APT loading	4 in. SP-12.5 mm	Limestone, SBS modified PG 76-22 binder, and PG 67-22 binder
Early strength requirement of slab replacement concrete	9-in. plain jointed concrete pavement (12 ft. by 16 ft. slabs)	Dowels and various cement levels 6 hr compressive strength of 900 to 1,700 psi, and 24 hr compressive strength of 2,770 to 4,750 psi
Coarse and fine graded Superpave evaluation	4 in. fine and coarse SP-12.5 mm	Georgia granite, and PG 67-22 binder
Thin concrete overlay evaluation	4, 5 and 6 in. thick bonded concrete overlay (6 ft. by 6 ft. and 4 ft. by 4 ft. joints) and 6, 8 and 10 in. thick unbounded concrete overlay (6 ft. by 6 ft. joints)	Compressive strength of 2,400 psi at 24 hours and 28 day compressive strength of 5,800 psi
Cracking assessment of asphalt mixtures	6 in. SP-12.5 mm	Georgia granite and PG 67-22 binder
Evaluation of asphalt strain gauge repeatability	1.5 in. FC-12.5 mm and 2 in. SP-12.5 mm	Georgia granite and PG 67-22 binder
Impact of wide-base tires on pavement damage	Two 2-in. lifts of SP-12.5 mm and 1/2 in. OGFC	Georgia granite, PG 67-22 binder, asphalt rubber binder (FC-5)
Gradation based mixture performance evaluation method	Two 2-in. lifts of SP-12.5 mm	Georgia granite, PG 67-22 binder
SAMI contribution to rutting	SP-12.5 mm overlays of 2 to 4 in. and 1/2 in. ARMI	Georgia granite, PG 67-22 binder, asphalt rubber binder

Table 6. Thesis and dissertations using FDOT APT data.

Year	Deliverable	Thesis/Dissertation Title	Source
2002	Master's Thesis	Evaluation of Superpave mixtures with and without polymer modification by means of APT	Kim 2002
2005	Ph.D. Dissertation	Analysis and verification of stresses and strains and their relationship in failure in concrete pavements under HVS loading	Kumara 2005
2006	Ph.D. Dissertation	Identification and assessment of the dominant aggregate size range of asphalt mixtures	Kim 2006
2007	Ph.D. Dissertation	Creation of a laboratory testing device to evaluate instability rutting in asphalt pavements	Novak 2007
2007	Ph.D. Dissertation	Evaluation of concrete mixes for slab replacement using the maturity method and APT	Mano-khoon 2007
2007	Ph.D. Dissertation	Analysis, testing and verification of the behavior of composite pavements under Florida conditions using a HVS	Tapia 2007
2009	Ph.D. Dissertation	Interstitial component characterization to evaluate asphalt mixture performance	Guarin 2009
2009	Ph.D. Dissertation	Development and evaluation of an HMA fracture mechanics based model to predict top-down cracking in HMA layers	Zou 2009
2009	Ph.D. Dissertation	Effects of truck tire type and tire-pavement interaction on top-down cracking and instability rutting	Wang 2009

It can be difficult to assess the economic benefits of any research program. Often, it takes years for the actual benefit to be realized. Other times, research may find that current practices are ineffective and should be stopped. It is clear, however, that the economic benefit from the first APT experiment alone has produced significant cost savings. FDOT has not had polymer modified mixtures in place long enough to fully

quantify the additional life that can be expected but Von Quintus et al. 2007 estimated an additional five to ten years may be possible. According to the 2011 data from FDOT's Estimates Office, structural asphalt cost approximately $125,000 per lane mile. On average, FDOT resurfaces approximately 500 Interstate and Turnpike lane miles annually. Pavements resurfaced on these facilities require the use of polymer modified mixtures. If a modest increase in pavement life of just two years is realized, the reduction in annualized cost assuming a 3.5% discount rate is approximately $1,000 per lane mile per year, or $500,000 per year for the total Interstate and Turnpike pavements resurfaced. The total annualized savings is considered conservative since pavement life is likely extended greater than two years and polymer modified mixtures are also used on pavements outside of the Interstate and Turnpike systems.

One of the important aspects of the polymer modified asphalt research was not only to provide evidence of the effectiveness of polymers to improve pavement performance, but also to identify the optimum location to place modified asphalt binders. FDOT's Flexible Pavement Design Manual was revised to specify the use of PG 76-22 asphalt binder in the final structural course for traffic level D roadways (10 to >30 million ESALs) and the final two structural layers for traffic level E roadways (≥30 million ESALs). According to the most recent data from FDOT's Estimates Office, polymer modified mixtures cost an average $7/ton more than unmodified mixes. Due to APT research approximately 300,000 tons of traffic level D mixtures were not required to include polymer modified asphalt binder during 2010 and again in 2011. A savings of approximately $2.1 million was achieved each year. Again, this estimate is likely conservative since pay items (such as structural asphalt) are not recorded for lump sum contracts which include many larger projects.

In 2005, FDOT revised the Flexible Pavement Design Manual to reflect APT findings that fine-graded asphalt mixtures performed as well or better than coarse-graded mixtures. Previously, all traffic level D and E mixtures were required to be coarse-graded mixtures. According to discussions with industry, a cost savings of $2 to $5 per ton of asphalt mix is achieved by using fine-graded mixtures as opposed to coarse-graded mixtures. This cost savings comes from improved workability. Since the change, contractors use fine-graded mixtures almost exclusively. Considering that on average FDOT paves just over 5 million tons per year and approximately 30% of that total consists of traffic level D and E mixtures an annual cost savings of at least $3 million is achieved.

The APT program has become a critical component of FDOT's research program. The success of the program can be attributed to the careful selection of research projects that address critical issues and prolong the life of Florida's roadways. Technology transfer and implementation of research results is also vital and must continue as governments struggle with budgets for infrastructure investment. It is anticipated that the APT program will continue to provide a significant benefit to FDOT.

REFERENCES

Byron, T., Choubane, B. and Tia, M. 2004. Assessing Appropriate Loading Configuration in Accelerated Pavement Testing. *Proceedings, 2nd International Conference on Accelerated Pavement Testing*, Minneapolis, MN.

Choubane, B. Gokhale, S., Sholar, G. and Moseley, H. 2005. Evaluation of Coarse and Fine-Graded Superpave Mixtures Under Accelerated Pavement Testing. In*Transportation Research Record, Journal of the Transportation Research Board, No 1974*, National Research Council: pp. 120–127.

Greene, J., Toros, U., Kim, S., Byron, T. and Choubane, B. 2010. Impact of Wide-Base Tires on Pavement Damage. In *Transportation Research Record, Journal of the Transportation Research Board, No 2155*, National Research Council: pp. 82–90.

Greene, J., Choubane, B. and Sheppard, K. 2011a *Instrumentation of Florida's Accelerated Pavement Test Facility*. Florida Department of Transportation, Gainesville, FL.

Greene, J., Kim, S. and Choubane, B. 2011b. Accelerated Pavement Testing and Gradation-Based Performance Evaluation Method. In *Transportation Research Record, Journal of the Transportation Research Board, No 2225*, National Research Council: pp. 119–127.

Greene, J., Kim S., Datre, N. and Choubane, B. 2012. Effect of a Stress Absorbing Membrane Interlayer on Instability Rutting. CD-ROM. *Transportation Research Board of the National Academies*.

Gokhale, S., Choubane, B., Byron, T. and Tia, M. 2005. Rut Initiation in Asphalt Mixtures as Generated Under Accelerated Pavement Testing. In *Transportation Research Record, Journal of the Transportation Research Board, No. 1940*, National Research Council: pp. 136–145.

Gokhale, S., Byron, T., Iyer, S. and Choubane, B. 2009. Evaluation of Pavement Strain Gauge Repeatability: Results from Accelerated Pavement Testing. In *Transportation Research Record, Journal of the Transportation Research Board, No 2094*, National Research Council: pp. 30–40.

Guarin, A. 2009. *Interstitial Component Characterization to Evaluate Asphalt Mixture Performance*. Ph.D. Dissertation, University of Florida.

Kim, H.J. 2002. *Evaluation of Superpave Mixtures With and Without Polymer Modification by Means of Accelerated Pavement Testing*. Master's Thesis, University of Florida.

Kim, S. 2006. *Identification and Assessment of the Dominant Aggregate Size Range of Asphalt Mixture*. Ph.D. Dissertation, University of Florida.

Kumara, W. 2005. *Analysis and Verification of Stresses and Strains and their Relationship in Failure in Concrete Pavements under HVS Loading.* Ph.D. Dissertation, University of Florida.

Manokhoon, K. 2007. *Evaluation of Concrete Mixes for Slab Replacement Using the Maturity Method and Accelerated Pavement Testing*. Ph.D. Dissertation, University of Florida.

Novak, M. 2007. *Creation of a Laboratory Testing Device to Evaluate Instability Rutting in Asphalt Pavements*. Ph.D. Dissertation, University of Florida.

Roque, R., Guarin, A., Wang, G., Zou, J. and Mork, H. 2007. Develop Methodologies/Protocols to Assess Cracking Potential of Asphalt Mixtures Using Accelerated

Pavement Testing. *Contract BD545-49.* Tallahassee, Florida: Florida Department of Transportation.

Roque, R., Zou, J., Kim, Y., Thirunavukkarasu, S., Underwood, B. and Guddati, M, 2010. *Top-Down Cracking of Hot Mix Asphalt Layers: Models for Initiation and Cracking.* Project 1-42A. Washington D.C.: National Cooperative Highway Research Program.

Tapia, P. 2007. *Analysis, Testing and Verification of the Behavior of Composite Pavements under Florida Conditions using a Heavy Vehicle Simulator*. Ph.D. Dissertation, University of Florida.

Tia, M., Roque, R., Sirin, O. and Kim, H.J. 2002. *Evaluation of Superpave Mixtures With and Without Polymer Modification by Means of Accelerated Pavement Testing.* Contract BC-354. Tallahassee, Florida: Florida Department of Transportation.

Tia, M. and W. Kumara. 2005. *Strength Requirement of Concrete for Slab Replacement Using Accelerated Pavement Testing*. Contract BC-354. Tallahassee, Florida: Florida Department of Transportation.

Tia, M., Wu, C.L., Tapia, P. and Kumara, W. 2007. *Evaluation of Feasibility of Using Composite Pavements in Florida by Means of HVS Testing*. Contract BD-545. Tallahassee, Florida: Florida Department of Transportation.

Wang, G. 2009. *Effects of Truck Tire Type and Tire-pavement Interaction on Top-Down Cracking and Instability Rutting*, Ph.D. Dissertation, University of Florida.

Von Quintus, H., Mallela, J. and Buncher, M. 2007. Quantification of the Effect of Polymer Modified Asphalt on Flexible Pavement Performance. In *Transportation Research Record, Journal of the Transportation Research Board, No 2001*, National Research Council: pp. 141–154.

Zou, J. 2009. *Development and Evaluation of an HMA Fracture Mechanics Based Model to Predict Top-Down Cracking in HMA Layers.* Ph.D. Dissertation, University of Florida.

Advances in Pavement Design through Full-scale Accelerated Pavement Testing – Jones, Harvey, Mateos & Al-Qadi (Eds.)
© 2012 Taylor & Francis Group, London, ISBN 978-0-415-62138-0

Fourteen years of accelerated pavement testing at Kansas State University

M. Hossain, B.S. Bortz & H. Melhem
Kansas State University, Manhattan, Kansas, US

S.A. Romanoschi
University of Texas at Arlington, Arlington, Texas, US

A. Gisi
Kansas Department of Transportation, Topeka, Kansas, US

ABSTRACT: The Accelerated Pavement Testing (APT) program at Kansas State University (KSU) has been in existence for the past 14 years. The Midwest States Accelerated Pavement Testing Pooled Funds Program, a consortium of the Departments of Transportation of Iowa, Kansas, Missouri, and the Nebraska Department of Roads, has been the sponsors for the majority of the tests. Sixteen full-scale pavement tests have been completed since 1997. The majority of the tests were done for side-by-side comparison of new products or processes for both asphalt and concrete pavements. These tests successfully evaluated new products or practices and verified current pavement designs and/or practices for four Midwestern states. Results of a multi-year experiment are now being used for calibration of the new *Mechanistic-Empirical Pavement Design Guide* (*MEPDG*) procedure models in Iowa, Kansas, and Missouri. This paper summarizes the confirmation of practices and improvements in highway pavement design and construction that have resulted from the tests conducted at this APT facility. Major findings along with the lessons learned from these experiments are described.

1 INTRODUCTION

The accelerated pavement testing (APT) program at Kansas State University (KSU) has been active for over 14 years. The sixteenth full-scale pavement test is now complete and the seventeenth and eighteenth experiments are underway. The APT machine is located at the KSU Civil Infrastructure Systems Laboratory (CISL) in Manhattan, Kansas. The equipment was designed and fabricated by an industrial partner, Cardwell International, Ltd. under a grant by the Kansas Technology Enterprise Corporation (KTEC). The building housing the APT facility was made possible by private donations from alumni of the KSU College of Engineering. Shortly after the APT facility was placed in service, the Midwest States Accelerated Pavement Testing Pooled Funds Program, a consortium of the departments of transportation of Iowa, Kansas, Missouri, and the Nebraska Department of Roads, was formed with the Kansas Department of Transportation (KDOT) as the lead agency. The technical advisory committee of this program selects and funds the projects at this facility. The 16 projects that have been conducted thus far are:

- APT 1: Rutting of cold in-place recycled, fly-ash stabilized base with a thin asphalt overlay.
- APT 2: Comparing three different types of shear transfer devices in jointed portland cement concrete pavements (PCCP).
- APT 3: Comparison of KDOT Superpave (SM-2C) with Marshall (BM-2C) overlay mixes over existing/previously tested PCCP under radiant heat conditions.
- APT 4: Testing 8 in. of an asphalt concrete mix on grade compared to 5 in. of the same mix placed on 5 in. of reclaimed asphalt milling.
- APT 5: Milling a 2-in. layer from the surface and replacing it with a new hot-mix asphalt (HMA) overlay.
- APT 6: Rutting performance of Superpave mixtures with different ratios of river sand.
- APT 7: Pilot instrumentation of a Superpave test section
- APT 8: Effectiveness of thin non-dowelled, non-reinforced PCCP overlays on highly distressed PCCP.
- APT 9: Performance of non-dowelled, non-reinforced PCCP on drainable and semi-permeable bases.
- APT 10: Effectiveness of epoxy-coated steel and fiber reinforced polymer (FRP) dowels in PCCP joint repair.
- CISL 11: Performance of foamed asphalt stabilized base in full-depth reclaimed asphalt pavement.
- CISL 12: Evaluation of chemically stabilized subgrade soil.
- CISL 13: Thin bonded rigid overlay on PCC and HMA pavements.

– CISL 14: Verification of mechanistic-empirical design models for flexible pavements.
– CISL 15: Geocelluar confinement systems on unpaved roads.
– CISL 16: Geocelluar confinement systems on low-volume paved roads.

2 DESCRIPTION OF THE FACILITY

The CISL laboratory that houses the APT program is an indoor facility 5,575 sq.ft. (540 m^2) in area. Three test pits, two 20 ft × 16 ft. × 6 ft. (6 m × 5 m × 1.8 m) pits and one 20 ft. × 12 ft. × 6 ft. (6 m × 3.7 m × 1.8 m) environmental pit, provide space to construct a variety of pavement test sections. The CISL laboratory also houses a falling weight deflectometer (FWD) calibration facility and a 500 kip (2,225 kN) outdoor structural testing frame. A 20 kip (89 kN) overhead bridge crane and an outdoor staging area for soils and aggregate provide functionality. Two 14 ft. × 20 ft. (4.3m × 6.1m) overhead doors allow access to the pits (Lewis, 2008).

2.1 *APT machine description*

The APT machine consists of a 42 ft. (12.8 m) reaction frame with single or dual axle assemblies. The dual wheel axle assemblies are belt driven using a 20-HP electric motor and a variable frequency drive to control speed and direction (Lewis, 2008). Testing speed is approximately 7 mph (11 km/h) and it is capable of 100,000 wheel load applications (bi-directional) per week. It has a 40 kip (178 kN) loading capacity and is capable of uni-directional or bi-directional loading. Load is applied and removed with hydraulic cylinders through an on-board pump. Up to 12 in. (300 mm) of wander can be applied with a user-defined interface.

2.2 *Changes to the APT machine*

Over the last 14 years, considerable improvements have been made to the APT machine. The original loading assembly was an actual trailer bogie (tandem axle) from a tractor-trailer. Load was applied with air bags using an air suspension system. An on-board air compressor applied the load. The loading capacity was 17.5 kip (78 kN), the same as the load rating of the axles. The desire to increase the loading capacity required a larger air compressor to be remotely installed and a system was developed to transport the air to the moving bogie shown in Figure 1. Later, in order to increase the load, the load application system was redesigned using hydraulics exclusively. However, in order to apply single axle loads, one of the dual axles needed to be disabled and chained in the "up" position. This resulted in a difference in load in one direction while testing in the bi-directional mode. As the reaction frame was rated for fatigue at 40 kip (178 kN), to apply an axle load above 20 kip (89 kN), a single axle was needed. A custom single axle capable of higher loads was designed and improvements to the hydraulic and suspension systems were incorporated (Lewis, 2008).

Figure 1. Original APT machine configuration.

Figure 2. Single axle configuration.

In an effort to accentuate the capability of the machine in terms of the number of load applications, another upgrade was completed. The original analog control system using relay logic had limited safety systems and required manual monitoring of the equipment. Consequently the facility could not be operated continuously due to staff limitations. In order to perform testing 24 hours a day, 7 days a week, automated control and safety features to stop the machine were needed. This was achieved with load cells, transducers, and safety systems. At the same time, it was also decided to incorporate the ability to provide wheel wander so that the loading would more realistically simulate truck load applications on in-service pavements. The wander system uses screw jacks to move the frame for lateral wander. The wander is applied in a truncated normal distribution as shown in Figure 3. A full wander of +6 in. to −6 in (152 mm) takes 676 passes to complete.

3 INSTRUMENTATION AND DATA ACQUISITION

In order to assess rutting on flexible pavements accurately, a transverse profiler was constructed at CISL

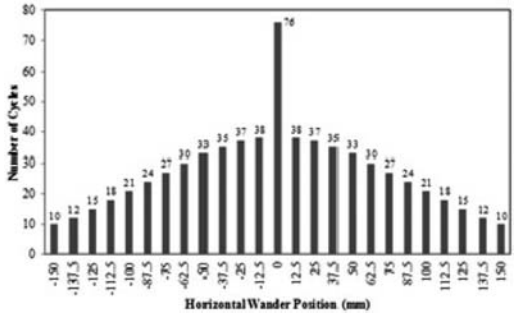

Figure 3. Traffic wander distribution.

Figure 4. Transverse profiler.

(Figure 4). It consists of a 14 ft. (4.3 m) aluminum tube with a 2-in. (50 mm) square cross section. Stands on each end allow for height adjustment and individually adjustable feet allow for level correction. A Chicago Dial Indicator digital gauge with a resolution of 0.001 in. (0.025 mm) is attached to the beam with a movable mount. The indicator has a digital output and software to upload output data into a spreadsheet format. Fixed reference points are mounted at each end of the pavement to be profiled and measurements are taken at 0.5 in. (12.5 mm) intervals.

Strain gauges have been used extensively at CISL. For asphalt pavements, a *Texas Measurements type PML-60-2L* concrete embedment strain gauge is modified. Two aluminum "H" bars are machined and attached using epoxy. These bars help bond the gauge to the base of the asphalt layer. High temperature TFE insulated wires are attached to the gauge. Although failure rate has been at or above 15% during construction, the lower cost of these gauges allows for redundancy and a significant cost saving. *Geokon model 3500* soil pressure transducers are used to measure pressure on top of the subgrade. These transducers have been very reliable and have been used at CISL since 1999. Thermocouples are constructed from the *Omega* thermocouple extension wire. *Campbell Scientific* time domain reflectometer (TDR) probes are used to measure soil moisture. Linear variable differential transformers (LVDT) have been used for slab movement monitoring at the concrete pavement joints.

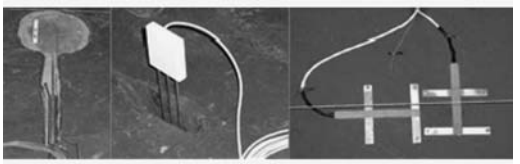

Figure 5. Various instruments used at CISL.

Figure 5 shows the various types of instrumentation used at CISL (Lewis, 2008).

A *National Instruments SCXI* data acquisition system was initially used to collect data. The signal-conditioning hardware and associated software were developed in-house to acquire data from in situ sensors, load cells, and position transducers all within the same acquisition system and time base. Recently, a cDAQ system from National Instruments has been used for data collection. The cDAQ system allows multiple interchangeable modules to be used with an electronic chassis and a simple USB interface with a personal computer (PC). For this setup, three types of terminal block modules were used with the cDAQ-9178 chassis. A thermocouple module (NI 9211, 4-channel, +/−80 mV, 24-bit differential analog input), two quarter-bridge input modules (NI 9235, 120 ohm, 8-channel, 24-bit, 2.5 ex) and an analog input module (NI 9205, 32-channel, +/−10 V, 16-bit) were installed in the chassis for data collection. The cDAQ system interfaced with a PC equipped with *LabVIEW 2009* through a simple USB 2.0 connection.

Non-destructive test equipment is used for quality control and to measure pavement response. A nuclear moisture density gauge, a Geogauge, and a lightweight falling weight deflectometer (LFWD) are used to evaluate subgrade condition (density and moisture). KDOT provides CISL with pavement deflection data from the FWD tests with their Dynatest and Jils FWDs. A Portable Seismic Property Analyzer for Pavements (PSPA-P) is also available.

4 ENVIRONMENTAL CAPABILITIES

One of the unique capabilities of the CISL laboratory is that it can duplicate natural conditions, such as freeze-thaw cycling and rapidly changing temperature conditions. Refrigerant compressors and a boiler can heat or cool a glycol and water mixture from −25°F (−32°C) to 140°F (60°C) (Melhem, 1997). The mixture is circulated through surface heat exchangers (Figure 6) and u-tubes in the subgrade soil of the environmental pit.

Since pavement materials and soil are poor conductors of heat, achieving set point temperatures or changing those is a time consuming process. Infrared radiant electric heaters have been employed with some success in creating differential temperatures between the pavement surface and the subgrade. However,

Figure 6. Surface heat exchangers.

Figure 7. Environmental chamber.

maintaining uniformity throughout the test section has been difficult at best (Lewis, 2008). The ambient temperatures within the building vary with the seasons as the building has heating but not cooling. In order to overcome this limitation, an environmental chamber around the APT machine was constructed (Figure 7). Walls of lightweight aluminum and insulating foam now enclose the machine. Heating/cooling units on both ends maintain temperatures between 100°F (38°C) and 60°F (15°C) on the test sections.

5 PCCP JOINT TESTING

The PCCP tests are time consuming. Thus a pulse load system (an MTS system with hydraulic power supply and actuators) was developed that can be placed across the PCCP joint so that each actuator applies a load on one side of the joint (Figure 8). A hydraulic pump produces a servo-valve controlled load, resulting in alternating loads on the two actuators. The cyclic loading is produced by an oscillating signal generated by an electronic device that includes a timer, relay, cycle counter, and frequency adjustment.

6 PAST EXPERIMENTS AT CISL

Past experiments conducted at CISL can be grouped into the following categories:

– Evaluation of new products or practices (Lewis, 2008);

Figure 8. Joint testing system.

– Verification of current designs and/or practices; (Melhem et al., 2003; Melhem, 1997), and
– Calibration of the *Mechanistic-empirical Pavement Design Guide* (*MEPDG*) procedure models.

6.1 *Evaluation of new products*

The APT facility at the CISL laboratory was initially developed to evaluate an innovative and patented load transfer device, called *X-FLEX*, for portland cement concrete pavements (PCCP) (Melhem, 1997). This was accomplished in the APT 2 experiment (comparison of three different types of shear transfer devices in jointed PCCP). Three 20-ft. (6 m) long and 75 in. (2 m) wide PCCP lanes were constructed side-by-side with a joint in the middle. The pavement section consisted of 9 in. (230 mm) of PCCP over 4-in. (100 mm) fly ash stabilized cold in-place recycled (CIPR) base and compacted, AASHTO A-4 soil subgrade. In those test lanes, one lane had conventional steel dowels spaced at 12 in. (300 mm) center to center, one had fiberglass tubes filled with a special high-strength concrete mix, and the *X-FLEX* system in the remaining lane. A crack was initiated at the joint, using a folded sheet metal plate. The joints were loaded using the PCCP joint tester described earlier. A total of 4.7 million load (20,000 lbs or 89 kN) repetitions were applied from mid-May to late August of 1997. Since the experiment involved proprietary products, no results were publicly disclosed (Melhem, 1997).

Alternative load transfer devices for PCCP joint repair were evaluated in APT 10 (effectiveness of epoxy-coated steel and fiber-reinforced polymer [FRP] dowels as PCCP joint repair). The experiment was a follow up of APT 9 (performance of non-dowelled, non-reinforced PCCP on drainable and semi-permeable bases [Melhem et al. 2003]). That experiment evaluated the effect of unbound drainable base types (permeable and semi-permeable) on the performance of PCCP. These bases were being used by the Kansas Department of Transportation (KDOT) and the Missouri Department of Transportation (MODOT), respectively, at that time. Both base materials were crushed stones with a top size of 1.0 in. (25 mm). The percentages of fines (passing US No.

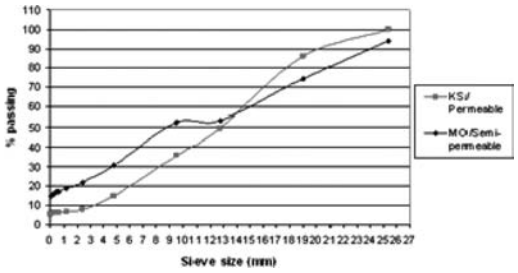

Figure 9. Gradation for permeable and semi-permeable base materials.

200) sieve were 6% and 15%, respectively, for the permeable and for the semi-permeable bases as shown in Figure 9. The permeability of the semi-permeable materials was between 530 and 630 m/day (Melhem et al., 2003).

Two lanes were constructed in two pits with edge drains (with 4 in. pipes) on one side of each lane. The permeable and semi-permeable aggregate bases were about 7 ft. (2.6 m) wide, 4 in. (100 mm) thick and built over compacted, silty (AASHTO A-4) subgrade. The top 6 in. (150 mm) of the subgrade was treated with lime and compacted to 95% density. To facilitate drainage, the subgrade was underlain by 12 in. (300 mm) of pea gravel. The base was compacted with a vibratory plate compactor. The PCCP slab thickness was 6 in. (150 mm). The slabs were restrained in the pit at the ends with reinforcing bars welded to the pit rail. Contraction joints were sawed 5 ft. (1.7 m) from each end of the slabs, leaving a 10-ft. (3.3 m) section in the middle. The sections were loaded uni-directionally with 300,000 repetitions of a single axle load of 22 kips (98 kN) under alternating heating and cooling cycles. A measured quantity of water was also added directly to the surface using a system of pipes. Severe pumping was observed on the semi-permeable section while there was no pumping on the permeable section. Cracking was also prevalent on the semi-permeable section and more severe than that on the permeable section (Melhem et al., 2003). This test validated KDOT's drainage policy for PCCP that was in effect at that time.

The distressed lane with the semi-permeable base was repaired in the APT 10 experiment. Full depth slab replacement was completed and a longitudinal crack was repaired with epoxy injection. Dowel bar retrofit was also undertaken. One-inch (25-mm) diameter steel dowels were paced in the joint on one end and 1.5 in. (37 mm) fiber reinforced plastic (FRP) dowels were placed in the joint on the other end. A working transverse crack was also retrofitted with 1 in. (25 mm) diameter FRP dowels. Loading consisted of 22 kip (98 kN) unidirectional single axle loads. Test duration was 10 days and a total of 21,355 repetitions were applied. The results showed that 1 in. (25 mm) conventional steel dowels performed much better than 1.5 in. (37 mm) FRP dowels (Melhem et al., 2003). This study confirmed existing practices of using steel dowels in the Midwestern states.

In the CISL 12 experiment (evaluation of chemically stabilized subgrade soil), four chemical stabilizers; portland cement, fly ash, lime, and a proprietary product, were evaluated (Romanoschi et al., 2008). The experiment entailed constructing four flexible pavement structures in two pits and subjecting them to full-scale accelerated loading.

The pavement cross-section consisted of 6 in. (150 mm) stabilized subgrade over compacted clay (AASHTO A-7-6) subgrade, and 3 in. (75 mm) of Superpave 0.75 in. (9.5 mm) nominal maximum aggregate size mixture. The test pavements were loaded in pairs using a tandem axle with dual wheels and a 30 kip (136 kN) load, and a single axle with a 26 kip (118 kN) load. Accelerated loading was done in bi-directional mode, at a speed of about 7 mph (12 km/h). The lateral wander applied in this experiment followed a truncated normal distribution with a standard deviation of 6 in. (150 mm) and maximum wander of 12 in. The tire inflation pressure was maintained at 100 psi (690 kPa) and was verified weekly. The dynamic wheel load was monitored with load cells installed on each wheel. Around 800,000 repetitions of the 30 kip tandem axle were applied to the lime and proprietary stabilizer pavement sections (Romanoschi et al., 2008). The pavement sections in the other pit (portland cement and fly ash) received 1,300,000 passes of the 30 kip tandem axle followed by 700,000 passes of the 26 kip single axle. Earlier, the pavement structure where the embankment soil was treated with a proprietary stabilizer failed after 45,000 passes of the 30 kip tandem axle, due to lack of sufficient support underneath the HMA surface layer. Severe cracking and rutting developed on that section. In order to continue testing the adjacent lime stabilized test section, the failed HMA layer and 2 in. (50 mm) of stabilized embankment soil were removed. The remaining soil was re-compacted. A 2 in. (50 mm) sand layer was placed and compacted, and 4 in. (100 mm) of portland cement concrete was poured, finished, and cured for 28 days. Loading on the lime-treated section was continued to a total of 800,000 repetitions while 1.3 million load repetitions were applied to the portland cement and fly ash-treated sections. With these load repetitions, all three sections exhibited only rutting in the wheel path. Because no cracking or other distresses were observed, these three sections were compared based on permanent deformation and rut depths computed from the measured transverse profiles. It should be noted that no water was added to these pavement sections. The subgrade moisture content remained relatively unchanged during testing since the pavements were constructed in the pit and the asphalt concrete surface layer was paved wall-to-wall. The results indicated that portland cement and lime were the most effective stabilizers for the soil types tested (Romanoschi et al., 2006). These stabilizers resulted in lower vertical compressive stresses at the top of the subgrade and lower rut depth at the pavement

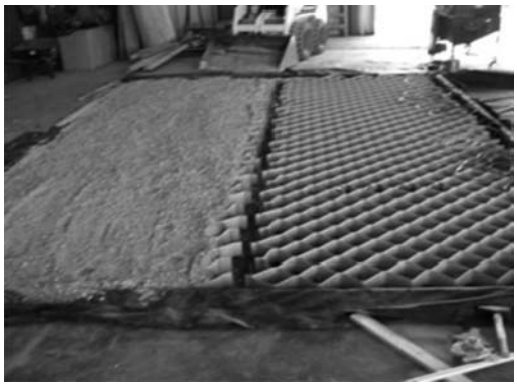

Figure 10. Geocell confinement systems.

surface than the fly ash-treated soil. After more than two million axle load repetitions, the pavement with cement stabilized soil exhibited significantly less surface cracking than the pavement with fly ash stabilized soil. The proprietary product proved to be ineffective in stabilizing the non-sulfate clayey soil used in this experiment. The unconfined compressive strength measured on the laboratory-prepared samples of soil stabilized with the proprietary chemical product was similar to that of the untreated soil indicating that no strengthening occurred.

Geocells are three-dimensional honeycomb-like structures filled with an in-fill of available granular materials that can improve the shear strength of in-fill materials. A new type of Geocell, manufactured with *NEOLOY*™ polymeric alloy (NPA, a nano-composite alloy of polyester/polyamide nano fibers, dispersed in polyethylene matrix), shown in Figure 10 was evaluated in the CISL 15 and CISL 16 experiments. CISL 15 studied different Geocell configurations or heights (200, 150, 100 and 75 mm), in-fill materials (crushed stone [AB-3], quarry waste [limestone screening], reclaimed asphalt pavement [RAP] and sand), and cover thickness (25 mm vs. 50 mm). These sections were unpaved. The sections were loaded with an 18 kip (89 kN) single axle load and 90 psi (627 kPa) tire pressure. The results indicated that 75-mm Geocells and 50-mm cover were the best combination, and that the crushed stone and RAP were the best infill materials (Han et al., 2010).

CISL 16 studied the recommended NPA Geocell design (75 mm) with 2-in. (50-mm) cover under 2-in. (50 mm) and 4-in. (50 mm) HMA layers. Three in-fill materials (crushed stone [AB-3], quarry waste [limestone screening], and RAP) were studied. Eight lanes with two as control with AB-3 base and the remainder with three in-fill materials and 2-in. (50mm) and 4-in. (100-mm) HMA layers were constructed and tested. The results show that quarry waste was the weakest infill material. However, the 2-in. (50-mm) HMA layers were too thin since all sections had 12.5 mm rutting (0.5 in.) after 10,000 repetitions of an 18 kip (89 kN) single axle load. All sections with 4-in. (100 mm) HMA did not reach failure rut depth (12.5 mm) after 1.2 million repetitions of this load (Bortz et al., 2012).

Figure 11. Foamed asphalt stabilized material production (Romanoschi et al., 2004).

6.2 *Evaluation of new practices*

Foamed asphalt stabilization was studied in the CISL 11 experiment (Performance of foamed asphalt stabilized base in full-depth reclaimed asphalt pavement) (Romanoschi et al., 2004). The experiment consisted of testing 6, 9, and 12 in. (150, 230, and 300 mm) foamed asphalt stabilized bases against a control section with 9-in. (230 mm) of crushed aggregate base. All sections had a 3-in. (75-mm) HMA surface. The research idea was developed by the Iowa Department of Transportation (IADOT) and CISL personnel worked closely with the IADOT and Wirtgen technicians to design and construct the project successfully. The laboratory mix design was conducted by the IADOT Central Materials Laboratory in Ames, Iowa. Sample aggregates, RAP, soil, and the asphalt binder (PG 64-22) to be used in the project were shipped to IADOT to develop the mix design. A Wirtgen Foamed Bitumen Laboratory Plant (WLB 10) was used in the mix design process. The foamed asphalt stabilized base material was produced at the CISL in a portable Wirtgen plant, operated by a Wirtgen technician. The plant consisted of a two-bin aggregate blending system and a chamber for mixing foamed asphalt with the full depth reclaimed material blend of RAP, aggregate, and soil, which was stockpiled at the site. Figure 11 shows the production of the foamed asphalt stabilized material. The stockpiled stabilized material was transferred into the pit in the CISL with a bucket loader and compacted in 3-in. (75-mm) layers to achieve the required thickness. Compaction was done with a steel-wheeled vibratory roller. The asphalt layer was constructed with a 12.5-mm NMAS Superpave mixture designated as SM-12.5B in Kansas. The combined aggregate gradation (dry) of this mixture passes below the maximum density line in the sand sizes. The mixture had 6.4% PG 64-22 asphalt content. All sections were instrumented with pressure cells, strain gauges, TDR gauges, and thermocouples.

Loading was applied using a 17 kip (75 kN) single axle with dual wheels for the first 100,000 passes.

Figure 12. Strain gauges and fixture setting.

Thereafter, 400,000 passes of a 30 kip (134 kN) tandem axle with dual wheels were applied. A fixed wheel path (zero lateral wander) was maintained and loading was bi-directional throughout the experiment. The tire inflation pressure was maintained at 100 psi (697 kPa). All testing was performed at room temperature. No moisture was added.

The results of this research proved that the foamed asphalt stabilized RAP material is very uniform and can be placed and compacted easily. The material can be effectively used as base material in flexible pavements. The permanent deformation on the pavements with the foamed asphalt stabilized base was between 0.25 (6 mm) and 0.5 in. (12.5 mm), after 100,000 passes of the 17 kip (75 kN) single axle and 400,000 passes of the 32 kip (134 kN) tandem axle. These values were comparable to those on sections with the Kansas AB-3 granular base. Based on the observed permanent deformation at the pavement surface and pressure on the top of the subgrade, 1.0 in. of foamed asphalt stabilized RAP material is equivalent to 1.0 to 1.25 in. of conventional Kansas AB-3 granular base. The structural layer coefficient of the foamed asphalt stabilized RAP material, determined from FWD data analysis, was found to be 0.17 (Romanoschi et al., 2004).

Thin concrete overlays over existing PCCP and asphalt pavements were studied in CISL 13 (thin bonded rigid overlay on PCC and HMA pavements) (Romanoschi et al. 2009). The objective of this study was to determine the response and failure modes of thin concrete overlays. Four pavement structures were built and tested in this experiment. Two thin concrete overlays (4 and 5 in. [100 and 125 mm thick]) were constructed on a 5-in. (125 mm) thick PCC pavement, and two thin whitetopping (TWT) pavements, with 4-in. (100 mm) and 6-in. (150 mm) thick PCC overlays were constructed on a 5-in. (125 mm) HMA layer. The thicknesses were selected by the technical advisory committee of the pooled fund program. The pavements were instrumented to measure the strains at selected locations in each PCC overlay section. Strain gauges and thermocouples were embedded in the pavement to monitor response, as shown in Figure 12.

The TWT pavement structure was not subjected to any special condition such as, heating or cooling, or moisture. Each of the four pavements was loaded with approximately two million passes at indoor ambient conditions. The lateral wander applied in this experiment followed the truncated normal distribution discussed earlier. The applied single axle load was approximately 26 kips (128 kN), equally distributed between the two pavements (13 kips or 64 kN on each pavement). The wheel load was monitored with load cells installed on each wheel. The thin concrete overlays failed due to loss of support underneath the slab resulting in transverse cracking. No loss of bond between the PCC overlay and the supporting slab was observed. The 4-in. (100-mm) TWT exhibited a transverse crack at the middle of the slab, while the 6-in. (150 mm) TWT had no cracks at the end of testing. During loading, all pavements experienced loss of support in the subgrade under the joints which caused an increase in the maximum longitudinal strains at the mid-span of the slabs. The absence of debonding suggests that environmental factors (high daily or seasonal temperature gradients, presence of water at the interface, etc.) or improper surface preparation may have caused the loss of bonding between the thin PCC overlays and the existing pavement (Romanoschi et al., 2009).

6.3 *Verification of current designs and practices*

Various design, rehabilitation, and paving material practices of the Kansas Department of Transportation, Nebraska Department of Roads and Missouri Department of Transportation have been evaluated in the APT 1, APT 3 through APT 6, and APT 9 experiments. APT 9 is discussed above. The other experiments are briefly described below.

APT 1 was essentially a “shakedown” experiment for the then newly built APT machine to verify whether the wheel load assembly and drive mechanism worked effectively. However, the performance of the cold in-place recycled material (CIPR) test section was evaluated at the same time (Melhem, 1997).

In this study, a 12-ft. (3.8-m) wide by 20-ft. (6.6-m) long test section consisting of a 3 in. (75 mm) HMA layer (19 mm NMAS aggregate) over a 4-in. (100 mm) RAP-fly ash base, 6-in. (150 mm) aggregate subbase (KDOT AB-3), and 60 in. (1.5 m) AASHTO A-4 soil subgrade. The pavement was underlain by 11 in. (280 mm) of pea gravel to facilitate drainage and 9 in. (230 mm) reinforced concrete slab to prevent ground water seepage. The RAP material was placed in a layer at the required thickness and 10% ASTM Class C fly ash (by weight) was spread uniformly on the RAP. Water was added to the materials with a soaker hose to produce a consistency at which the materials could be worked (mixed) with a roto-tiller. The material was compacted with a small steel-wheel roller. Paving was done using a Blaw kNox paver using mixture from a local drum-mix plant. At that time, the plant was producing asphalt mix for paving a local arterial road.

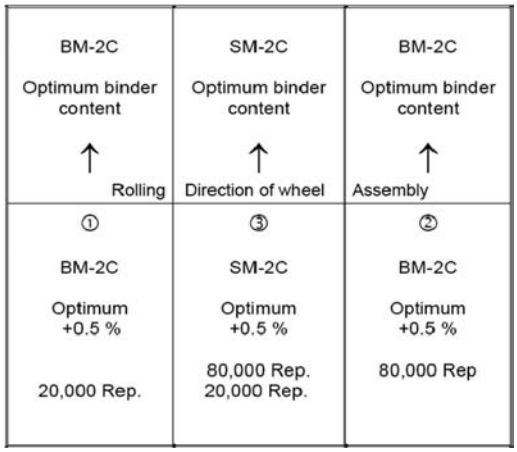

Figure 13. Layout of test sections in APT 3.

Compaction of the HMA was accomplished with a steel-wheeled roller. The section was loaded with a 34 kip (76 kN) tandem axle. Severe rutting (up to 1 in. [25 mm]) was observed after 30,000 load repetitions. The ruts were repaired with HMA and loading continued up to 145,000 repetitions when the maximum rut depth of approximately 1 in. (25 mm) was again reached. No cracking was visible at that time (Melhem, 1997). After repairing with another patching material, loading continued up to 168,000 repetitions when the maximum rut depth of approximately 1 in. (25 mm) was again reached and the patch cracked. However, the remaining pavement did not crack.

KDOT started implementing Superpave mixture design in the late 1990s and APT 3 was initiated to compare the KDOT Superpave 3/4 in. (19 mm) NMAS mix (SM-2C) with the Marshall mix of the same NMAS (BM-2C) (Melhem, 1999). The previously tested PCC slabs in the APT 2 experiment (steel and FRP dowels) were used. The overlays were tested at elevated temperatures using radiant heaters. The asphalt overlays were about 4 in. (100 mm) thick and were placed as three adjacent lanes of about 76 in. (1.9 m) wide each on top of the existing 9-in. (230-mm) concrete sections. Each of the three 20-ft. (6.1 m) long strips was divided into two sections placed parallel to the direction of the testing wheels. Mix binder contents on these two sections were optimum and optimum plus 0.5%, respectively (Figure 13). The pavement surface temperature was maintained at 122°F (50°C) with infrared radiant heaters during loading. The strips were tested in pairs such that two adjacent lanes were each loaded with one half of the moving tandem axle (34 kip [150 kN]). The standard wander configuration was used.

The center and north lanes were tested first for up to 80,000 load repetitions. At that stage rutting in the north lane was about 1.2 in. (31 mm). The tandem axle was moved to the center and south lanes, which were tested for an additional 20,000 load repetitions. Thus the north lane had 80,000 repetitions, while the central lane had a total of 100,000 repetitions and the south lane had 20,000 repetitions. Results from a visual inspection and transverse profile analysis concluded that the sections with optimum binder content performed slightly better than those with the higher binder content. Moreover, it was apparent that the SM-2C mix had better rut resistance than the BM-2C mix (Melhem, 1999).

The APT 4 experiment, requested by the Nebraska DOR, investigated the use of compacted RAP as granular base course material (Melhem, 1999). The test pavement layout consisted of two 8-ft. (2.5 m) wide lanes side-by-side. The pavement structure of the first lane was an 8-in. (200 mm) layer of HMA (50-blow Marshall design) on compacted, fine-grained silt-clay subgrade. The second lane had 5 in. (125 mm) of HMA on 5 in. (125 mm) of compacted RAP on the same subgrade soil. Infrared radiant heaters were used to maintain an HMA surface temperature of 90°F (32°C). The sections were loaded with a standard 18 kip (80 kN) single axle with dual tires at an air pressure of 90 psi (620 kPa) in a bi-directional mode with no wander. Rutting, HMA strains, vertical pressure at the top of the subgrade, and HMA densities were monitored in this experiment for up to 67,000 load repetitions. The performance of the sections was comparable.

In the APT 5 experiment, mill and inlay repairs of the APT 4 test sections were tested. The existing pavements were milled to a depth of 2 in. (50 mm) and inlaid with 2 in. (50 mm) of a KDOT Marshall design mix (3/4 in. NMAS or BM-2C). Loading conditions were the same as in APT 4. The wheelpaths used in APT 4 were also matched. The in-laid sections received 84,000 repetitions of an 18 kip (80 kN) single axle and an additional 16,000 repetitions of an overloaded 22 kip (98 kN) axle. Both sections showed comparable performance after a total of 167,000 load repetitions (Melhem, 1999).

In APT 6, the performance of two sections with fine graded, 12.5 mm (1/2 in.) NMAS Superpave mixtures (SM-2A) with varying percentages (15 to 30%) of river sand, was evaluated. The sections had a 6 in. (150 mm) HMA layer over a 9-in. (230-mm) aggregate base (KDOT AB-3) and 57-in. (1.5 m) soil subgrade. The subgrade consisted of a typical silty-clay soil (AASHTO A-4). A 34 kip (150 kN) tandem axle with dual wheels and 90 psi (620 kPa) tire pressure was used for loading. All load applications were done at 98°F (38°C) temperature at the middle of the SM-2A layer (Melhem and Sheffield, 2000). The results show that the section with 30% sand rutted much more than that with 12% sand. Partly based on the results of this study, maximum natural sand content in Superpave mixes in Kansas has been limited to 35%.

6.4 *Calibration of the Mechanistic-Empirical Pavement Design (MEPDG) procedure*

Experiment CISL 14 (verification of mechanistic-empirical design models for flexible pavements) was

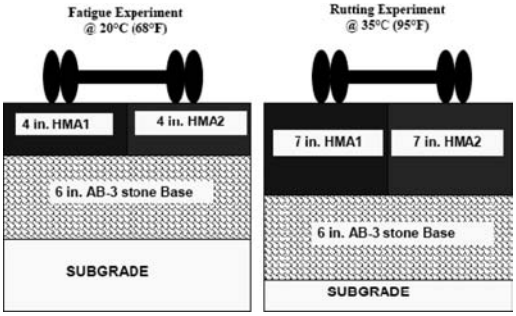

Figure 14. Typical CISL 14 test sections design.

a multi-agency effort to provide calibration of the *MEPDG* for Iowa, Kansas, and Missouri through testing of their Superpave mix flexible pavements. The calibration of the design models for flexible pavements encompassed three major tasks:

- Verification of the models to predict mechanical properties of pavement materials from conventional, local material properties such as dynamic modulus of asphalt concrete from aggregate gradation, binder viscosity, and resilient modulus; resilient modulus of unbound materials from gradation or classification data; and elastic modulus of stabilized materials from compressive strength data.
- Verification of the mechanistic structural model that calculates the response (stresses, strain, and deflections) of the flexible pavement structure under a given wheel loading for a given pavement structure, with known layer thickness and material stiffness.
- Verification or calibration of pavement performance models, transfer functions, and empirical functions that relate the distresses in the pavement structure to the magnitude of the pavement response for local pavement configurations (Lewis, 2008).

CISL 14 was conducted to assess these tasks. Twelve experimental pavement structures were constructed at the CISL and tested between 2006 and 2009. Three pairs of sections were used to study fatigue cracking behavior in flexible pavements. The remaining three section pairs were used to study rutting behavior in asphalt concrete pavements. In total, six asphalt mixes were used, two for each of the three participating states. One fatigue cracking and one rutting pavement were built for each mix. Figure 14 shows an example of four test sections, a fatigue cracking pair and rutting pair, built in two pits to test the two asphalt concrete mixes of one state.

The pavement sections were constructed in three layers: an asphalt concrete surface layer, a 6-in. (150 mm) unbound granular base course over 65 in. (1.7 m) of A-7-6 clayey soil subgrade layer. The fatigue cracking sections had a 4-in. (100-mm) nominal thickness for the asphalt concrete surface layer and were loaded at a pavement surface temperature of 68°F (20°C). The rutting sections had a 7-in. (178-mm) nominal thickness for the asphalt concrete surface layer and were loaded at a pavement surface temperature of 95°F (35°C). The sections were loaded with a 20 kip (100 kN) single axle load. Wander was provided by moving the entire frame of the APT machine in the lateral direction with a maximum lateral wander of ±6 in. (±150 mm). Transverse profiles at the pavement surface were measured periodically during loading to record the evolution of rut depth with number of load repetitions. Instrumentation was embedded in the experimental pavement sections during construction. Strain gauges were used to measure horizontal and vertical strains at the bottom of the HMA layer. LVDTs were used to measure the dynamic and permanent vertical deformation in each layer. Pressure cells were used to measure the vertical compressive stress below the base layer. Thermocouples were used to measure the temperature at the surface and two additional depths in each pavement structure. Accelerated loading was applied first to the Kansas pavements. The rut test pavements exhibited more than 0.75 in. (19 mm) of rutting after 400,000 passes of the 20 kip (100 kN) single axle. The Kansas fatigue cracking test sections received 2 million passes. Missouri and Iowa rut test sections received more than 700,000 passes. The Iowa sections failed in rutting (maximum rut depth of 0.5 in [12.5 mm]) after 100,000 passes since the mixture had a binder content much higher than the design asphalt content. Missouri fatigue cracking test sections received 2.2 million load repetitions with no signs of distresses. Rutting remained under 0.25 in. (6 mm) on both lanes. Testing of the Iowa fatigue sections ended after 1,000,000 repetitions with no signs of fatigue cracking. Detailed data analysis was in progress at the time of preparing this paper.

7 CONCLUSIONS

The accelerated pavement testing (APT) program at Kansas State University (KSU) is now about 15 years old. The APT testing machine is located at the KSU Civil Infrastructure Systems Laboratory (CISL) in Manhattan, Kansas. Sixteen full-scale pavement tests have been completed since 1997. These tests successfully evaluated new products or practices and verified current pavement designs and/or practices for four Midwestern states. Results of a multi-year experiment are now being used for calibration of the *Mechanistic-empirical Pavement Design* (*MEPDG*) procedure in Iowa, Kansas and Missouri.

REFERENCES

Bortz, B.S., Hossain, M., Halami, I. and Gisi, A. 2012. *Accelerated Pavement Testing of Low-Volume Paved Roads with Geocell Reinforcement.* Paper submitted for possible presentation and publication at *APT 2012*. Davis, California in the conference proceedings.

Han, J., Pokharel, S.K., Yang, X.M., Manandhar, C., Leshchinsky, D., Halahmi, I. and Parsons, R.L. 2010. Performance of geocell-reinforced RAP bases over weak subgrade under full-scale moving wheel loads. Invited for a special issue, submitted for possible publication in *Journal of Materials in Civil Engineering, ASCE*.

Lewis, P. 2008. Lessons Learned From the Operations Management of an Accelerated Pavement Testing Facility. *Proceedings of the 3rd Intl. Confc. on Accelerated Pavement Testing.* Madrid, Spain.

Melhem G., Swart, R. and Walker, S. 2003. *Accelerated Testing For Studying Pavement Design and Performance (FY 2001): Evaluation of the Performance of Permeable and Semi-Permeable Unbound Granular Bases under Portland Cement Concrete Pavement (PCCP) Slabs and Alternate Load Transfer Devices for Joint Repair.* Final Report No. FHWA-KS-02-7, Kansas Department of Transportation, Topeka.

Melhem, H.G. 1999. *Accelerated Testing for Studying Pavement Design and Performance*. FY97-98, Report No. FHWA-KS-99-2, Kansas Department of Transportation, Topeka, KS.

Melhem, H.G. 1997. *Development of an Accelerated Testing Laboratory for Highway Research in Kansas.* Report No. FHWA-KS-97/5, Kansas Department of Transportation, Topeka, KS.

Melhem, H.G. and Sheffield, F. 2000. *Accelerated Testing for Studying Pavement Design and Performance.* FY99, Report No. FHWA-KS-99-7, Kansas Department of Transportation, Topeka, KS.

Romanoschi S., Dumitru, A., Lewis, C.P. and Hossain, M. 2009 *Thin Bonded Rigid Overlays on PCC and HMA.* Final Report No. FHWA-KS-08-8, Kansas Department of Transportation, Topeka, KS.

Romanoschi S., Dumitru, A., Lewis, C.P. and Dumitru, O. 204. *Performance of Foamed Asphalt Stabilized Base In Full-Depth Reclaimed Asphalt Pavement.* Final Report No. FHWA-KS-03-8, Kansas Department of Transportation, Topeka, KS.

Romanoschi S., Lewis, A. and Dumitru, O. 2008. *Evaluation of the Chemical Stabilized Subgrade Soil.* Final Report No. FHWA-KS-07-8, Kansas Department of Transportation, Topeka, KS.

Romanoschi, S., Banda, A., Hossain, M. and Gisi, A. 2006. Evaluation of Chemically Stabilized Clay Soil Embankments with Accelerated Pavement Testing. In the *Transportation Research Record 1952, Journal of the Transportation Research Board*, National Research Council.

Romanoschi, S.A., Hossain, M., Gisi, A.J. and Heitzman, M. 2004. Accelerated Pavement Testing of Contaminated Recycled Asphalt Pavement Material When Stabilized with Foamed Asphalt. In the *Transportation Research Record 1896, Journal of the Transportation Research Board*, National Research Council,pp. 199–207.

Advances in Pavement Design through Full-scale Accelerated Pavement Testing – Jones, Harvey, Mateos & Al-Qadi (Eds.)
© 2012 Taylor & Francis Group, London, ISBN 978-0-415-62138-0

The implementation of accelerated pavement testing findings into industry practice in New Zealand

B.D. Steven
Beca Infrastructure Ltd, Christchurch, New Zealand

D.J. Alabaster
NZ Transport Agency, Christchurch, New Zealand

B.D. Pidwerbesky
Fulton Hogan Ltd, Christchurch, New Zealand

ABSTRACT: New Zealand has been running a nationally funded APT program since 1968, which has produced a number of outcomes that have been implemented into New Zealand practice. Pavement response measurements allowed the national roads authority to adopt the mechanistic based Austroads Pavement Design Guide in 1995 and have also contributed to the development and verification of RLT testing protocols and have helped calibrate and benchmark LTPP sites. Projects have been either initiated due to issues arising from the performance of in-service pavements or where new construction technologies or materials have been proposed. These projects have included pavement curvature prior to the placing of thin asphalt surfaces, foamed bitumen stabilization, aggregate specifications, pavement loading at various levels for High Productivity Vehicle regulations, and a study on the dynamic effects of various vehicle suspensions.

1 INTRODUCTION

New Zealand has been conducting a nationally funded accelerated pavement testing (APT) program since 1968 (Williman and Paterson, 1971). The current accelerated testing machine (Canterbury Accelerated Testing Indoor Facility, CAPTIF) has been in continuous service for the last 25 years. This paper will describe some of the outcomes from the APT program that have been implemented into practice in New Zealand.

The APT projects completed in New Zealand have been initiated by a need to either: further the fundamental understanding of pavement response and performance; or to understand the impact of a change in the design methodology or regulations; or to investigate/replicate the causes of in-service pavement issues/problems.

The predominant pavement construction in New Zealand is a thin surfaced unbound granular pavement, where the main design criterion is the vertical compressive strain at the top of the subgrade. It has been recognized that the accumulation of permanent or plastic strain in the pavement is a function of the elastic strain and that although the strain at the top of the subgrade is used as the design criteria, this criteria is in fact a proxy for the elastic strains, and thus plastic strains throughout the entire pavement structure. Structural asphalt pavements are used in heavily trafficked urban areas and in recent years, modified and stabilized pavement construction techniques have been used in greenfield construction (pavements not subjected to traffic during construction) and pavement rehabilitation for moderate to heavily trafficked pavements.

Pavement failure in New Zealand is defined as a rut depth of 25 mm for the unbound granular pavements. The chipseal surfacing has sufficient flexibility and ductility to account for the gradual deformation (rutting) of the pavement over time.

2 THE CANTERBURY ACCELERATED PAVEMENT TESTING INDOOR FACILITY

CAPTIF is located in Christchurch, New Zealand. It consists of an indoor 58 m long (on the centerline) circular track contained within a 1.5 m deep by 4 m wide concrete tank, so that the moisture content of the pavement materials can be controlled and the boundary conditions are known. A centre platform carries the machinery and electronics needed to drive the system. Mounted on this platform is a sliding frame that can move horizontally by 1.0 m. This radial movement enables the wheelpaths to be varied laterally and can be used to have the two "vehicles" operating in independent wheelpaths. An elevation view is shown in Figure 1.

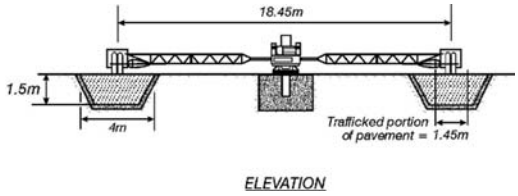

Figure 1. Elevation view of CAPTIF.

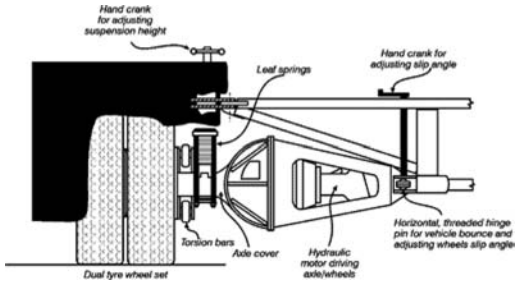

Figure 2. Elevation of the SLAVE unit.

At the ends of this frame, two radial arms connect to the Simulated Loading and Vehicle Emulator (SLAVE) units shown in Figure 2. These arms are hinged in the vertical plane so that the SLAVEs can be removed from the track during pavement construction, profile measurement, etc., and in the horizontal plane to allow vehicle bounce.

CAPTIF is one of the few accelerated pavement test facilities in the world in that it was specifically designed to generate realistic dynamic wheel forces. Most other accelerated pavement testing facility designs, that CAPTIF is aware of, attempt to minimize dynamic loading. The SLAVE units at CAPTIF are designed to have sprung and unsprung mass values of similar magnitude to those on actual vehicles and use, as far as possible, standard heavy vehicle suspension components. The net result of this is that the SLAVEs apply dynamic wheel loads to the test pavement that are similar in character and magnitude to those applied by real vehicles. The configuration of each vehicle, with respect to suspensions, wheel loads, tire types and tire numbers, can be identical or different for simultaneous testing of different load characteristics.

The following types of data have been collected during projects as required:

- Pavement vertical compressive strain (non-coupled inductive coil technology)
- Pavement vertical compressive stress (pressure cell technology)
- Pavement horizontal tensile strains (H-bar technology)
- Transverse pavement profiles/rutting (rolling wheel/LVDT profile beam)
- Longitudinal pavement profiles (vehicle mounted laser/accelerometer system)
- Pavement deflection (FWD and deflection basin measurements from a continuous measurement Benkelman beam)
- Pavement and air temperatures
- Pavement moisture conditions
- Dynamic wheel forces
- Pavement construction data (material density, particle size distributions, layer thicknesses)

The development and operation of the vertical strain measurement systems at CAPTIF has been described in detail in a companion paper. The current vertical soil strain system is the fourth system to be used at CAPTIF and is now based on a National Instruments hardware platform. Steven (2007) described the verification of the system with independent deflection measurements and showed that the integrated vertical strains were within 15% of the measured surface deflections for a range of applied loads. These findings have given confidence that the measured strains were representative of the actual in-service response of the pavement structure.

3 INTEGRATION OF APT DATA INTO DESIGN

The majority of projects that have been conducted at CAPTIF have incorporated sub-surface instrumentation into the pavement, thus allowing a substantial volume of pavement response data to be collected over the last 25 years. This data has been used by researchers and engineers to validate or calibrate various pavement response and design models/methods.

3.1 *Design criteria*

In 1987, Pidwerbesky (1995) commenced a series of pavement tests, measuring the vertical strains for a range of pavement designs (varying thicknesses of aggregate layers over a common subgrade). The results from these tests were used to test the subgrade strain criterion from the Shell Pavement Design Manual (Shell, 1978) and the Austroads Pavement Design Guide (Austroads, 2008) by the analysis of the recorded verses predicted vertical compressive strains in the subgrade. This work showed that the recorded strains were up to three times the magnitude predicted by the previous design models. Previous subgrade strain models were reviewed in detail in Pidwerbesky (1995), and modifications to the subgrade strain criterion were proposed in Pidwerbesky et al. (1997). The findings from this work gave the national roads authority (Transit New Zealand at the time) additional information to allow the adoption of the 1992 Austroads Pavement Design Guide in 1995 for the design of pavements in New Zealand. Prior to 1995, pavement design had been undertaken using a CBR/ESA design chart.

3.2 *Laboratory and field correlations*

In 2000, pavement response and performance data was used to compare the results from repeated load

triaxial tests (RLTT) and linear elastic modeling (Arnold et al., 2001). Three pavements were constructed at CAPTIF from aggregates that ranged from premium to unacceptable with respect to the current aggregate specifications based on the particle size distribution and type of fine particles.

In contrast to the CAPTIF pavement test, the RLTT tests on the three materials showed little differences in moduli values. Further, the RLT derived moduli were significantly lower than those determined from measured stresses and strains. The use of RLTT derived moduli in mechanistic pavement design using *CIRCLY* resulted in stresses and strains at critical locations (i.e., near the top of subgrade) is close to those measured. The method using the Austroads auto-sublayering feature and the RLTT derived moduli appropriate to the bulk stress for the top layer produced the closest match between computed and measure pavement response. The sublayering system divides a material into five layers, sets the stiffness of the top sub-layer to the user specified stiffness, and then calculates a modular ratio based on the user specified stiffness and the stiffness of the next material down in the pavement structure to ensure a gradual change in the modulus profile of the pavement.

Permanent deformation modeling gave the same material ranking for deformation resistance as the CAPTIF test for both the linear and exponential methods of extrapolating the permanent strain results from the RLTT. The linear method of predicting deformation showed the greatest difference in the magnitude of deformations between the three materials. Further, the linear method was the only method that would have rejected the use of the material, which was sabotaged with additional fines added. It was therefore recommended that this method (linear extrapolation) be used for material evaluation.

3.3 *Advanced pavement models*

Arnold (2004), Steven et al. (2007), Werkmeister et al. (2005) and Gonzales (2009) have used the CAPTIF datasets to develop and calibrate research grade pavement response models. However these models require material data that is not routinely or easily measured in the laboratory, making the adaptation of more sophisticated pavement models for pavement design difficult. In addition, the models generally require the use of a calibration factor to allow the model response to be matched to field results. Arnold and Werkmeister (2010) developed a protocol for interpreting RLTT test results that allow the performance of new or alternative materials to be compared against proven and accepted materials.

Steven et al. (2007) developed a finite element model that used RLTT resilient modulus data to determine the element stiffnesses in the FEM to predict stress, strain, and surface deflection under both wheel and FWD loading. Once the RLTT/field calibration factor had been determined for one load level, the model was accurate (within 10%) for other load levels. This work showed that the generalized material model initially proposed by Uzan (1985), and currently used in the new AASHTO pavement design model, was appropriate and could be implemented into an FEM model. However, the integration of the material model into the FEM model was fraught with difficulties as a number of assumptions were required with respect to either material properties or the numerical implementation of the FEM code.

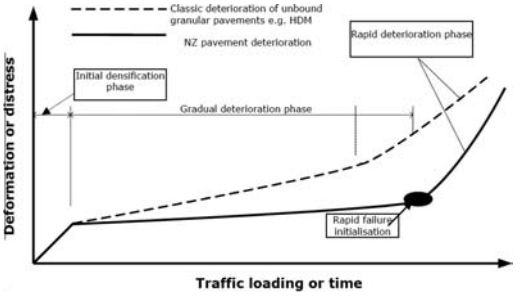

Figure 3. Comparing the default HDM rut model with observed rut progression in New Zealand.

3.4 *Long-term pavement performance models*

In addition to using CAPTIF measurements for the development of pavement design models, the data has also been used to help calibrate pavement deterioration models for use in pavement management systems (Henning et al., 2007). Rutting data from the CAPTIF pavements was combined with data from New Zealand's Long Term Pavement Performance program and used to develop a three stage pavement rutting model as shown in Figure 3 (initial densification, stable rut rate progression, and failure and/or accelerated deterioration) that has been used as a simpler alternative to the HDM-4 rutting model for unbound granular pavements.

4 INTEGRATION OF APT DATA INTO CONSTRUCTION

A number of projects have been either initiated due to issues arising from the performance of in-service pavements or where new construction technologies or materials have been proposed. These types of projects have been undertaken to either help understand the mechanisms of distress or to compare the performance of the new material/technology with the accepted and proven materials that are currently in use in New Zealand.

4.1 *Pavement curvature and open graded porous asphalts*

In most countries, porous asphalts are typically laid on top of structural asphalt layers. In New Zealand structural asphalt is generally prohibitively expensive

and porous asphalt (layer thickness <40 mm) is used directly on chipseal-surfaced unbound granular pavements. In the late 1980s, rule-of-thumb guidelines were developed to try to prevent fatigue cracking. Recent pavement failures on major projects have highlighted that the current rule-of-thumb design procedures are inadequate. Instead more rigorous design procedures that employ current modern mechanistic pavement design practices (e.g., *CIRCLY*) or falling weight deflectometer (FWD) data are required.

This research (Alabaster and Fussell, 2007) which was carried out in 2004 and 2005 aimed to achieve the following objectives:

- Develop a horizontal tensile strain versus fatigue life curve that can be applied to the base of an open-graded porous asphalt (OGPA) layer;
- Establish a relationship between basecourse surface curvature (D0-D200) and OGPA fatigue life, and
- Evaluate the extension to fatigue life of using enhanced binders in OGPA; with the aim of improving the fatigue design aspects of road noise reducing surfaces.

Two accelerated pavement tests were undertaken at CAPTIF. The first test was an attempt to develop a horizontal tensile strain versus fatigue life curve and establish a relationship between basecourse surface curvature and fatigue life. The results of this test were surprisingly positive and, with the agreement of the project's Steering Group, the second test concentrated on examining extension of fatigue life by initial trafficking rather than using enhanced binders.

The objectives were based on the traditional view of thin asphalt behavior applied in the Austroads Pavement Design and Rehabilitation Guides and existing research into asphalt behavior. The first objective was not achieved as it was not possible to find instrumentation of a scale that would not interfere with the performance of the thin surfaces. In the second objective, deformation was found to lead to surface failure before fatigue occurs. As a result of the findings from this second objective, the third objective was modified in agreement with the Steering Group to examine this problem in more depth and attempt to extend surface lives by initial trafficking.

Three of the sections of the first test showed that when high basecourse curvatures are measured, pavement deformation sufficient to cause pavement failure occurs before classic fatigue failure of the surfacing layer develops. Another section in the first test showed that, if pavements are constructed well, then applying low noise surfaces immediately after construction is possible.

The laboratory fatigue results contradict current wisdom that OGPA is more tolerant of deflection than asphalt concrete. However, without being able to generate fatigue in the OGPA layer at CAPTIF, this finding could not be validated.

The second test showed that the pavements could tolerate more deflection if initial trafficking was undertaken. The current deflection criteria are conservative even if factors such as temperature and ageing are considered.

From analysis of the FWD readings from the first test, a conservative approach would consider that all deflections having curvatures over 250 μm are unacceptable (i.e., on pavements with design loadings over 100,000 ESALs [equivalent single axle loads]) and that such results would require additional analysis. In this additional analysis, pavements with basecourse of known good rut resisting performance and a degree of saturation below 60% could be identified, and surfaced immediately.

The second test suggested that surfaces failing the performance and saturation criteria would be acceptable after an initial trafficking of 100,000 ESALs. This trafficking would reduce initial deformation and thus lead to acceptable surface life.

In this case, if Resource Management Act (RMA) noise requirements need to be met at the highway opening, the speed limit could be lowered while the chipseal surface is trafficked. If lowering the speed limit is not practical, the basecourse could be modified to increase its resistance to deformation, and then the OGPA applied.

4.2 *Aggregate compaction during pavement construction*

The majority of pavements in New Zealand consist of a granular base with a chipseal surfacing. The specifications for constructing these pavements call for the compaction level to be closely controlled and monitored using nuclear density gauges. For basecourse layers, the average dry density is required to be greater than 98% of the value obtained by the vibrating hammer compaction test and all values are to be greater than 95% of maximum dry density (MDD). There have been a number of high-profile early failures in New Zealand (rut depths greater than 20 mm observed early in the pavement life) associated with 'greenfield' pavements (pavements not subjected to traffic during construction) where the granular layers were thicker than 400 mm. It is uncertain if the rutting was due to poor construction control, difficulties in measuring the density of thick layers with a gauge operating in backscatter mode, or because of a lack of traffic on the pavement. In response, a research project was initiated at CAPTIF (Patrick and Werkmeister, 2010) to investigate the effect of constructing the basecourse and subbase to a range of densities.

The intention was to construct three pavement sections to 85%, 90%, and 95% of MDD. The 450-mm basecourse layer was constructed in three 150-mm lifts which were compacted using a vibratory plate compactor. Due to the relatively tight radius of the test track it is very difficult to use a full-sized vibratory roller and the plate compactor is usually used for compaction. It was found impossible to construct each layer to the specific density. This was especially noticeable with the target of 85% of MDD. After spreading

and lightly compacting the layer, the percentage of MDD was over 88%.

The results from the CAPTIF test demonstrated that the initial post construction deformation of a thin-surfaced granular pavement was affected by the compaction level achieved in the pavement, although the depth of the rut was relatively small and there was little difference between the different levels of initial compaction.

The results of the RLTT and FEM modeling support the above conclusions in that a degree of compaction of 88% MDD would not result in significant rutting in the pavement. The testing and modeling suggested that after one million load applications the difference in rut depth of a 450-mm thick granular layer that had been compacted to 88% MDD and one that had been compacted to 95% MDD would be approximately 3 mm. The rut depths were calculated using a transfer function that was based on elastic strain, layer thicknesses, and applied load cycles.

The results of the FE calculations indicate that the maximum vertical elastic strains and vertical compressive stress induced by a three-tonne roller drum (high-amplitude dynamic load with static drum weight) in the upper part of the basecourse are smaller than the stresses and elastic strains induced by a 40 kN dual wheel for the pavements investigated, but considerably higher in the lower part of the basecourse when the same wheel load is applied.

It would appear that as the compaction system does not build up residual stresses in the pavement, when traffic loading does occur granular material is moved in such a way that there is a buildup of those stresses that can resist the wheel loading.

It was postulated that the shear deformation found in the field is associated not just with post-construction rutting, but is exacerbated by water ponding in the ruts and then being forced through the surface by vehicle tires.

4.3 *Particle shape and grading*

Steven et al. (2000) studied the effect of particle shape and gradation on the performance of unbound basecourse aggregates in a 1987. Aggregates consisting of different combinations of rounded (30%, 50% and 70%) and angular, crushed particles were created, for three different particle size distributions using Talbot's equation:

$$P_d = \left[\frac{d}{D}\right]^n \qquad (1)$$

where: P_d is the percentage of the sample passing a sieve size, d; d is the sieve size (mm); D is the largest particle size in the sample (mm); and n is the gradation exponent.

The values for the gradation exponent (n), 0.4, 0.5 and 0.6, represent the lower limit, midpoint and upper limit of the gradation envelope for New Zealand primary basecourse aggregate. A total of nine basecourse

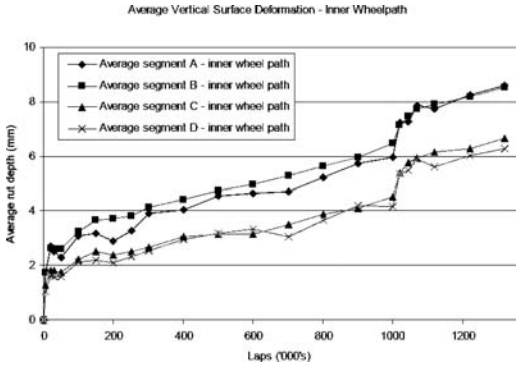

Figure 4. Rut depth verses load cycles for RCC (Segment D) and natural aggregates (Segments A–C).

aggregates were created. These aggregates were placed in nine sequential segments in the track. After loading with 54,000 ESALs, the subgrade deformation was similar for all test segments, while the basecourse deformation differed. Particle shape had the greatest effect on the performance of the aggregates, compared with gradation. Aggregates consisting of 30% or less angular particles could not be compacted and were replaced during construction. The best performance was achieved with aggregates of 70% or more angular particles, which is required by the New Zealand basecourse aggregate specification.

A laboratory study (Arnold et al., 2007) was undertaken to determine the effect of grading/particle size distribution on permanent deformation in multi-stage repeated load triaxial (RLT) tests. Results showed the coarse gradings, with a Talbot's exponent n-value of 0.8, had the least amount of permanent deformation for high moisture contents near saturation. Finer gradings with an n-value of 0.3 had the least deformation in all of the tests in dry conditions at less than 70% of optimum moisture content. Similar performance in terms of permanent deformation was obtained if variations of the n-value were less than 13%.

4.4 *Recycled crushed concrete*

In 2000, a section of a test pavement was constructed with recycled crushed concrete (RCC) as the basecourse aggregate (de Pont et al., 2001). The RCC was crushed to produce a grading that was compliant with the basecourse grading envelope. After loading of in excess of 1×10^6 ESALs, the performance of the RCC was comparable to the natural basecourse aggregate (Figure 4) and partly as a result of this trial, RCC is now a permitted basecourse aggregate, providing it meets the requirements of the basecourse specification.

4.5 *Modified basecourse aggregates*

A recently completed project (Gonzalez et al., 2009) looking at stabilized pavements was initiated by the introduction of foamed bitumen stabilization (FBS) in

Table 1. FBS pavements and rutting performance.

Section	Bitumen (%)	Cement (%)	Surface deformation under outer wheelpath/heaving at Nc cycles (mm) 200k	1.0M	1.326M
B00C10	0.0	1.0	3/0	6/4	14/18
B12C10	1.2	1.0	2/0	6/0	7/3
B14C10	1.4	1.0	2/0	6/0	7/3
B28C10	2.8	1.0	2/0	6/0	8/3
B00C00	0.0	0.0	6/0	10/2	15/17
B22C00	2.2	0.0	4/0	9/2	17/14

New Zealand. The initial test in this projected examined the performance of FBS aggregate with a varying amount of active filler (cement) and binder. The pavements tested are listed in Table 1 and showed that the best performance was from aggregates stabilized with a combination of cement and lime. After the application of 1.326×10^6 ESALs, the surfacing was cut in the FBS/cement sections to allow water to infiltrate the FBS material and loading resumed for an additional 42,000 ESALs. The 1.2% binder section exhibited significant deformation and surface cracking while the 1.4% and 2.8% binder sections had no appreciable change in condition.

These results showed that foam bitumen and cement had a significant effect on improving the performance of the materials studied. Material samples taken for indirect tensile strength (ITS) and repeat load triaxial (RLT) laboratory tests. Results showed that the ITS test was a good predictor of the pavement performance and produced a clear trend, while RLT results were inconclusive.

4.6 *Lime stabilized subbases*

In this early (1988) experiment (Steven et al. 2000), three pavements were constructed, two with lime-stabilized clay subbases of 150 mm and 250 mm thickness, and the third with an unmodified high quality, well-graded, crushed aggregate. The laboratory CBR of the unstabilized and stabilized clay specimens was 5% and 20%, respectively. For all three pavements, the surfacing was a 30 mm thick layer of hot-mix asphalt and the basecourse was a 150 mm thick layer of high quality, well-graded crushed aggregate. The subgrade had an unsoaked CBR of 3%.

Elastic deflections and permanent deformation of the pavement surface were measured. Pavement failure was defined as vertical surface deformation of 25 mm. The pavement containing the 150-mm thick lime-stabilized layer performed significantly better than the same thickness of unstabilized aggregate. Increasing the stabilized subbase thickness by 100 mm yielded a fifteen-fold increase in the life of the pavement.

This experiment showed that stabilizing the top of weak subgrades was preferential to using additional aggregate layers, as the lower aggregate layers could not be compacted to a level that would provide a sound platform on which to compact the upper aggregate layers.

5 INTEGRATION OF APT DATA INTO OPERATION

There have been two major projects looking at the operational aspects of APT; one looking at dynamic loading on pavement wear, and another looking at the effects of increased axle masses on pavement wear.

5.1 *Dynamic loading on pavements*

Conventional pavement design and management practice is based on the static axle loads of the vehicles that traffic the pavement. Since the AASHO road test of the late 1950s it has been assumed that the pavement wear generated by an axle is proportional to some power of its static axle load. The most commonly used value for this power is four. Real axle loads are, of course, not static but dynamic and vary with suspension type and vehicle load as well as speed and road surface profile. Two vehicles with the same static axle loads can generate very different dynamic loads. It has been postulated that the use of suspensions that reduce the level of dynamic loading will generate less pavement wear for the same level of static load. This seems intuitively reasonable and has been shown theoretically using the fourth power relationship between load and wear described above together with some assumptions regarding the load distribution. If the hypothesis is correct these “road-friendly” suspensions offer an attractive opportunity to pavement managers. Pavements could carry the same traffic load for less wear or alternatively carry more traffic load for the same wear. Any policy initiatives to encourage greater use of “road-friendly” suspensions require an understanding of the relationship between dynamic wheel loads and pavement wear. In New Zealand the situation is further complicated by the fact that most of pavements are thin-surfaced unbound granular structures. The behavior of these pavements is different from that of the asphalt concrete (AC) flexible pavements extensively used in the European and North American networks. Most of the international body of research on flexible pavements relates to these AC pavements (for example, the fourth power relationship between loads and wear) but results from these countries have still been applied to the New Zealand style thin-surfaced pavements.

This research project consisted of a series of three accelerated pavement tests to determine the relationship between different levels of dynamic loading and pavement performance and life (Pidwerbesky et al., 1999). The tests were undertaken at CAPTIF between 1993 and 1998. Originally the Simulated Loading and Vehicle Emulator (SLAVE) units, which are a "quarter truck" type of vehicle that applies the pavement loads at CAPTIF, were fitted with a multi-leaf two stage steel

spring suspension. In order to undertake this project and as part of the general improvements and development at CAPTIF, the SLAVE units were modified to allow fitting with two other suspension configurations.

For each of the tests the two SLAVE units were fitted with different suspension configurations, but with the same static load, and operated in separate parallel wheelpaths on the same pavement. The two different suspensions resulted in different levels of dynamic loading being applied to the pavement under the vehicles. By monitoring the performance and life of these two wheelpaths, the influence of dynamic loading could be determined.

The first test involved a New Zealand style thin-surfaced pavement structure with a design life, based on the National Roads Board (NRB) design charts, of 350,000 ESALs. One of the SLAVE units was fitted with the original multi-leaf steel spring while the other was fitted with a modern steel parabolic leaf spring and a viscous damper. Wide-base single tires were used to maximize the separation between the two wheelpaths and the static wheel load was 37 kN which is approximately equal to half the reference weight for an axle fitted with wide single tires (7.2 tonnes). Thus each load cycle would apply approximately one ESAL to the pavement. This pavement failed after only 35,000 load cycles. At this point the surface profile had deteriorated to the extent that it was not possible to continue operating the facility safely. Although the parabolic spring suspension, being a more modern design, had been expected to be more "road-friendly" than the multi-leaf steel spring this was not the case. From the start the dynamic loads generated by the SLAVE with the parabolic spring were higher than those from the multi-leaf at the test speed. An analysis of the suspension characteristics showed that although the parabolic spring had less hysteresis than the multi-leaf spring it was stiffer. Similarly although it had viscous damping (a positive feature) the damping levels were too low to be effective. Part of the reason for these poor characteristics was that the suspension was designed for the SLAVE maximum wheel load of 60 kN and consequently was considerably over-rated for the actual load of 37 kN. This situation has parallels with in-service vehicles. Many of the vehicles in the fleet are sourced from countries with higher allowable axle loads than New Zealand and it is not uncommon for these vehicles to be fitted with suspensions that are rated for these higher loads. The wheelpath trafficked by the parabolic spring suffered the most damage which was in accord with the pattern and magnitude of the dynamic loads. In spite of the premature failure of this pavement and consequently the small amount of data that was collected, it was possible to show a correlation between dynamic wheel forces, and pavement profile and profile change. While this relationship had long been postulated this was the first time anywhere in the world that it had been measured.

The second pavement in the test series was undertaken as part of the OECD DIVINE (Dynamic Interaction between Vehicles and Infrastructure Experiment). To meet the requirements of the OECD scientific expert group overseeing the experiment and the interests of all the member countries, a thicker AC pavement design was specified. While the asphalt layer was still relatively thin (85 mm) by European and North American highway standards, so that the failure conditions might be achieved within a reasonable timeframe, it was thick enough for its behavior to be considered representative of asphalt concrete flexible pavements. The inclusion of a thicker pavement in this series of tests has the merit of providing a link between the performance of conventional AC surfaced flexible pavements and the thin surfaced unbound granular structures used in New Zealand. For this test one of the SLAVE units was fitted with the multi-leaf steel spring while the other was fitted with an airbag spring and viscous damper. The static wheel load was set to 49 kN and again wide-base single tires were used. The higher wheel load was in line with European practice and was also chosen to accelerate the wear. A 10 m section of the pavement was intensively instrumented. The test proceeded for 1.7 million load cycles when it was terminated for time and cost reasons. At this point the pavement had still not reached the preset failure criteria and at the rate of wear that was occurring could have lasted up to three million load cycles or more. This compares with most modeling predictions for this pavement of a life of 500,000 load cycles or less.

The two different suspensions systems provided significantly different levels of dynamic loading with the steel more than twice as high as the air. A localized rut formed in the wheelpath being trafficked by the steel suspension early in the test, but then stabilized. This rut appears to have been the result of a combination of high dynamic loading and a local weakness in the pavement, which was not detectable in the structural capacity measurements done at construction. Because of the complication of this rut many of the analyses were undertaken on two data sets – a complete set comprising the whole pavement and a reduced set with data from the rutted section removed.

Without the data from the rutted section of pavement the mean levels of both rutting and cracking were similar in both wheelpaths. For the complete data set both rutting and cracking were higher for the wheelpath trafficked by the steel suspension. However, the variation in both rutting and cracking was significantly higher in the wheelpath trafficked by the steel suspension even for the reduced data set. Correlation analysis showed moderate relationships between dynamic wheel forces and the surface profile changes (rutting, longitudinal profile changes, and vertical surface deformation) for the steel suspension and very weak relationships for the air suspension. Conversely the relationship between initial pavement strength and surface profiles changes is much stronger for the air suspension than for the steel. This implies that the surface profile changes in the pavement are related to both the initial structural capacity and the level of dynamic loading. If the level of dynamic loading is

kept low, as with the air suspension, then the surface profile changes are driven by the variations in structural capacity. If the pavement structure is also uniform then the pattern of wear will also be uniform. On the other hand, with high dynamic loads, an initial local pavement weakness will lead to some local pavement deformation that will stimulate a dynamic response. This will result in a pattern of dynamic loading that will contribute to further surface profile changes. The net effect is that the wear is more localized with areas of more severe damage and other areas with less.

The third test was undertaken on a New Zealand style thin-surfaced pavement design similar to the first test with the same vehicle and loading configuration as the second test. Although the design life of this pavement was 94,000 load cycles, when the test was terminated at 300,000 load cycles the preset failure criteria had not been met. The key pavement wear factor for this pavement was permanent deformation. The mean level of wear was similar for the two wheelpaths but the variation in wear was related to the level of dynamic loading. As with the previous pavement there was a moderate correlation between pavement wear and dynamic wheel loads and also between wear and pavement structural capacity. The degree of correlation was approximately the same for both wheelpaths.

Overall it appears that pavements at CAPTIF last much longer than the design life predicted by the old NRB design charts and by many of the pavement life models, possibly up to three times or more as long. This phenomenon has also been observed on previous pavement tests. However, the Austroads design guide, which was adopted by Transit New Zealand in 1995, predicts pavement load cycle limits that are much closer to those observed at CAPTIF. The main differences between CAPTIF pavements and in-service pavements appear to be the reduction in environmental influences at CAPTIF, the relatively high degree of quality control of materials and construction, and the accelerated testing, which reduces ageing effects. If these are the reasons for an increased pavement life at CAPTIF then it implies that some pavement wear can be attributed to environmental, construction quality, and ageing effects rather than loading. This has major implications for road pricing and user charges policies.

The mean level of pavement wear observed for the last two tests appears to be independent of dynamic loading. While this might be interpreted as indicating a first power relationship between load and wear rather than a fourth power, this is not necessarily the case. The difference in mean wear that would be expected by applying a fourth power to the different dynamic loads is relatively small. Given the accuracy of the measurements the possibility of a fourth power relationship cannot be conclusively eliminated. Lower powers (between one and four) could also fit the data. The Austroads load cycles versus subgrade strain relationship uses a power of 7.14. While the pavement life values predicted by this relationship seem to have some validity it is difficult to see any evidence for the power value being this high.

The variations in pavement wear around the track are related to both the dynamic loading and to the variations in structural capacity of the pavement. These relationships, while expected, have never been measured anywhere before. Lower dynamic loads would result in a more even distribution of pavement wear. If the maintenance intervention criteria are set as a level of roughness or a maximum rut depth, this will increase the interval between interventions. Improving the uniformity of pavement structures by better construction practices and quality assurance should similarly reduce the frequency of maintenance required.

The mechanisms of pavement damage observed were different to those predicted in the design models. In particular, compression of the basecourse layer was a significant contributor to the permanent deformation. With the second pavement most of the cracking in the AC layer initiated from the top of the layer rather than the bottom, as predicted by most models. This phenomenon has been reported elsewhere.

Partly as a result of the outcomes from this research, Transit New Zealand elected not to proceed with vehicle mass limits based on suspension type.

5.2 *Increased axle masses*

The road freight transport industry in New Zealand has successfully lobbied to increase its efficiency. This has been achieved through increases in the allowable mass limits for heavy vehicles on selected routes. Prior to this approval being granted, CAPTIF undertook a series of tests from 1999 to 2004 (Arnold et al., 2004) to investigate the effect of increasing mass limits on the life of pavements, and how much more pavement rehabilitation and maintenance will be required.

The aim of this testing was to compare the effect of mass (of 8, 10 and 12 tonne single axle dual loads) on pavement wear for a range of pavements that are more typical of those used on New Zealand roads. Two major accelerated pavement tests of one million passes were used to monitor pavement wear as indicated by rutting. After these passes had been applied, the loads were increased from 8 tonnes to either 10 or 12 tonnes, and a further 300,000 to 400,000 cycles were applied.

One of the features of CAPTIF is that the SLAVE can simultaneously traffic two wheelpaths, each with a different axle load. Therefore the same pavement can be trafficked with two separate loads, but subjected to the identical environmental and age conditions. Two different aggregate gradings were used in the pavement construction, one was a finer grading with the fines content >10% and the other was the typical coarsely graded M4 aggregate. When the load on the 40 kN vehicle was increased part way through each test, the section with finely graded aggregates had no change in the rate of rutting (Figure 5) whereas the sections with the M4 graded aggregates had a step change in the rate of rutting (Figure 6), almost replicating the

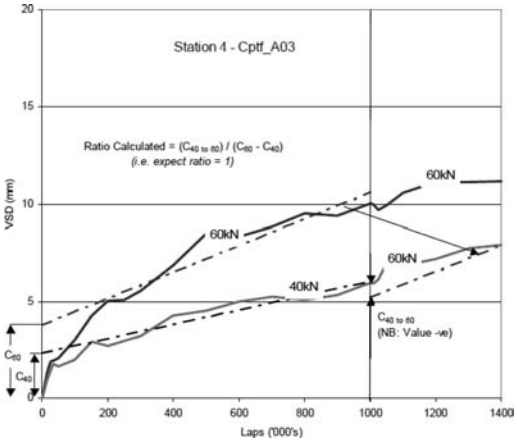

Figure 5. Effect of loading on a fine graded aggregate.

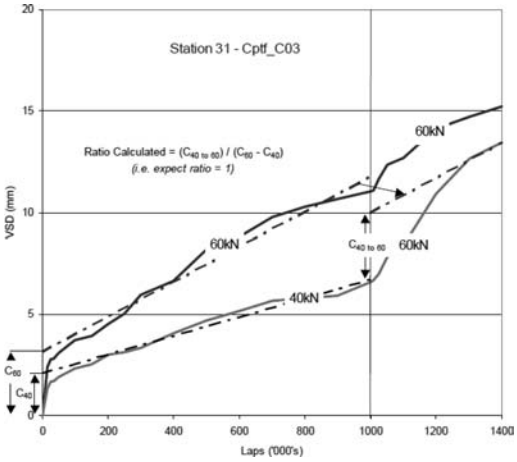

Figure 6. Effect of loading on coarse graded aggregate.

behavior of a new pavement undergoing the initial post-construction densification.

The CAPTIF pavements were all surfaced with 25 mm of asphalt concrete. Two additional tests were conducted on chipseal-surfaced pavements to compare the rate of surface texture depth deterioration between 8 and 10 tonne axle loads and 8 and 12 tonne axle loads. The results from these tests showed that an increase in mass limits is likely to reduce the life of chipseal surfacings on New Zealand roads. This reduction was previously found on a private forestry road used by vehicles with axle loads nearly double the current legal limit in New Zealand.

Overall it was found that the load equivalency factor (damage) exponents ranged from 1.1 to 3.4, all less than the historical value of 4.0 (Fourth Power Rule) and that the rate of rut progression was linear, after the initial post construction densification had occurred. The damage exponent was related to the pavement strength and was lower for the higher strength pavements. These findings have not been incorporated into the pavement design process.

Subsequent to the completion of this research, vehicle operators can apply for a "High Productivity Vehicle" status for a particular vehicle on specified routes. The approval of specific routes is based on the pavement condition and the capacity of bridges, etc. Permit charges for HPVs are still partly based on the Fourth Power Law calculations.

6 CONCLUSIONS

The outputs from New Zealand's APT program have been utilized to help understand and influence work in the design, construction, and operation of roads in New Zealand and other countries. Through the development of verified and robust in-pavement instrumentation for the measurement of key pavement parameters, pavement response data has been used to help develop pavement models and design processes, including both fundamental response models and through the LTPP program.

The impacts of construction related issues including material and construction quality, early performance of pavements have been studied at CAPTIF, either as a result of actual pavement issues or through the desire to test alternative materials and/or techniques.

There have been two extensive studies completed that have had the potential to influence the operation of the freight industry in New Zealand, one based around vehicle dynamics and pavement wear and the other around the effect of increased axe limits on pavement wear. The vehicle dynamics study made original contributions to the area of study, but did not result in any change to the operating environment. The second study, looking at increased axle limits, has contributed to the limited increase in axle limits in New Zealand.

ACKNOWLEDGEMENTS

The authors would like to acknowledge the New Zealand Transport Agency and its predecessors for its support in funding the CAPTIF research program.

Opinions expressed in this paper are those of the authors and do not necessarily reflect the policy of the New Zealand Transport Agency.

REFERENCES

Alabaster, D. and Fussell, A. 2006. *Fatigue design criteria for low noise surfaces on New Zealand roads.* Land Transport New Zealand Research Report 307. 58pp

Arnold, G., Alabaster, D. and Steven, B. 2001. *Prediction of Pavement Performance from Repeat Load Tri-Axial (RLT) Tests on Granular Materials.* Transfund New Zealand Research Report No. 214.

Arnold, G. 2004. *Rutting of Granular Pavements.* PhD Thesis, University of Nottingham, Nottingham, UK.

Arnold, G., Steven, B., Alabaster, D. and Fussell, A. 2004. *Effect on Pavement Wear of Increased Mass Limits for Heavy Vehicles – Concluding Report.* Land Transport New Zealand Research Report 281. 80pp.

Arnold, G., Werkmeister, S. and Alabaster, D. 2007. *The effect of grading on the performance of basecourse aggregate.* Land Transport New Zealand Research Report 325. 51 pp.

Arnold, G. and Werkemeister, S. 2010. *Pavement thickness design charts derived from a rut depth finite element model.* NZ Transport Agency research report no. 427. 84pp.

Austroads. 2008. *Guide to Pavement Technology Part 2: Pavement Structural Design.* Austroads Publication AGPT02/08. 263pp.

de Pont, J., Steven, B., Alabaster, D. and Fussell, A. 2001. *Effect on Pavement Wear of an Increase in Mass Limits for Heavy Vehicles.* Transfund New Zealand Research Report No. 207. 55pp.

Gonzales, A. 2009. *An Experimental Study of the Deformational and Performance Characteristics of Foamed Bitumen Stabilized Pavements*. PhD Thesis, University of Canterbury, Christchurch New Zealand.

Gonzalez, A., Cubrinovski, M., Pidwerbesky, B. and Alabaster, D. 2009. Full-Scale Experiment on Foam Bitumen Pavements in an Accelerated Testing Facility. *Transportation Research Record 2094*: 21–29.

Henning, T.F.P., Roux, D.C. and Alabaster, D. 2007. *Benchmarking pavement performance between Transit's LTPP and CAPTIF programmes.* Land Transport New Zealand Research Report 319. 98 pp.

Patrick, J. and Werkmeister, S. 2010. *Compaction of thick granular layers.* NZ Transport Agency Research Report No. 411. 40pp.

Pidwerbesky, B.D. 1995. Strain response and performance of subgrades and flexible pavements under various loading conditions. *Transportation Research Record 1482*: pp. 87–93.

Pidwerbesky, B.D., Steven, B.D. and Arnold, G. 1997. Subgrade strain criteria for limiting rutting in asphalt pavements. *Eighth International Conference on Asphalt Pavements. 2: 1529–1544*. University of Washington, Seattle, Washington, USA.

Pidwerbesky, B., de Pont, J. and Steven, B. 1999. *The Relationship between Dynamic Wheel Loads and Road Wear*. Transfund New Zealand Research Report No. 144. 88pp.

Shell. 1978. *Shell Pavement Design Manual*. Shell International Petroleum Co. Ltd., London.

Steven, B., Sharp, K. and Arnold G. 2000. *Comparison of Accelerated Pavement Test facilities in New Zealand and Australia.* Transfund New Zealand Research Report No. 198. 115pp.

Steven, B., Alabaster, D. and de Pont, J. 2007. Elastic Nonlinear Finite Element Analysis of a Flexible Pavement Subjected to Varying Falling Weight Deflectometer Loads. *Transportation Research Record 2016.* pp.31–38.

Uzan, J. 1985. Characterization of Granular Material. *Transportation Research Record, 1022*, pp.52–59.

Werkmeister S., Steven B.D, Alabaster D.J., Arnold G. and Oeser, M. 2005. 3D Finite Element analysis of accelerated pavement test results from New Zealand's CAPTIF Facility, Bearing Capacity of Roads, Railways and Airfields: *Proceedings of the 7th International Symposium on the Bearing Capacity of Roads and Airfields (BCRA)*, Trondheim, Norway, pp.24–26.

Williman, A. and Paterson, W.D.O. 1971. A Track for the Accelerated Testing of Highway Pavements. *New Zealand Engineering 26(3)*, March, pp. 73–77.

Advances in Pavement Design through Full-scale Accelerated Pavement Testing – Jones, Harvey, Mateos & Al-Qadi (Eds.)
© 2012 Taylor & Francis Group, London, ISBN 978-0-415-62138-0

History of construction contracting methods used at MnROAD

B.J. Worel & T.R. Clyne
Minnesota Department of Transportation, Maplewood, Minnesota, US

ABSTRACT: MnROAD was built in the early 1990s and has seen 26 construction events throughout its nearly 20 years of operations. MnROAD has three roadway segments that consist of various 500 foot test cells. There are currently 30 Mainline cells (on Interstate I-94), 24 Low Volume Road cells (trafficked by a Minnesota Department of Transportation [MnDOT] 80,000 pound 5-axle truck), and some specialized cells located in other locations around the facility. As test cells fail other test cells are designed and reconstructed to keep each of the road segments operational. Since cells are designed to fail, each cell has a different life span and failures can occur at any time. MnROAD is owned and operated by MnDOT, and most construction events have been limited to "traditional" design-bid-build practices. Over the years MnROAD has stretched what is considered "typical" in the way partnerships have been developed to encourage designs using non-standard specifications, new and innovative construction methods, and finance with other partners all while working in a system that is rich in a traditional contracting process. This paper's purpose is to document the past construction events that have taken place over the years and highlight what has worked and what has been problematic for MnROAD as a MnDOT (state government) run facility. Its audience and focus is directed to help MnROAD and other agencies struggling to incorporate research into construction. The paper will also suggest other contracting options that incorporate innovative research into future construction.

1 INTRODUCTION

MnROAD was constructed by the Minnesota Department of Transportation (MnDOT) between 1990 and 1993, as a full-scale accelerated pavement testing facility, and was opened to traffic in 1994. Located near Albertville, Minnesota (40 miles northwest of Minneapolis-St. Paul), MnROAD is one of the most sophisticated, independently operated pavement test facilities of its type in the world. Its design incorporates thousands of electronic in-ground sensors and an extensive data collection system that provide opportunities to study how traffic loading and environmental conditions affect pavement materials and performance over time. Along with the sensor data MnROAD collects field performance data (rutting, cracking, ride), which is all captured into the MnROAD database for researchers to use worldwide. MnROAD currently (2010) consists of three unique road segments with the following statistics (Figure 1):

- Interstate "Mainline"
  - 3.5 miles long
  - "Live" public traffic
  - 28, 500 vehicles per day
  - 12.7% trucks
  - 30 test cells
- Low Volume Road "LVR"
  - 2.5 mile closed-loop
  - Loaded by a MnROAD-operated 18-wheel, 5-axle, 80,000-lb tractor-semi-trailer
  - Simulates the conditions of rural roads
  - 24 test cells
- Farm Loop
  - Built on site in the stockpile area
  - Two test cells tested (2008–2010)
  - Testing using variety of farm equipment
  - Supporting pooled fund study TPF-5(148)

One of MnROAD's unique features is that when a test cell fails or the research is complete MnROAD is able to remove that cell and replace it with another. Typical successful replacement activities include having a balance between construction funding, sensor installations, developed research, and implementation plans. If one these four elements is missing, the final product tends to be of limited use. Each proposed project uses these criteria to determine what future construction should be pursued for it to provide mutual benefits for both MnROAD partners and state and county engineers. Current research ideas are typically developed by a combination of number of different organizations. These organizations include Minnesota Department of Transportation, the Transportation Engineering Road Research Alliance (TERRA), and the Local Road Research Board (LRRB). External partners have also have contacted MnROAD directly or worked though the organizations listed above to develop written partnership agreements to facilitate

Figure 1. Arial view of MnROAD.

the research. MnDOT works closely with its partners but has the final say on what research is ultimately pursued.

This paper separates the 26 MnROAD construction events into three unique categories. These include 15 traditional MnDOT design-bid-build, seven construction using procurement (purchase orders), and four public-private partnerships. Each of these will be examined by providing some background, an example, and discussion on the pros and cons related to the construction efforts MnROAD has undertaken as a state government operated facility.

2 TRADITIONAL (DESIGN-BID-BUILD) CONSTRUCTION

The traditional MnDOT contracting method is design-bid-build where MnDOT designs the roadway; contactors develop a bid, and then build the project if they are the low bidder. This approach involves many practices that tend to discourage innovation related to construction practices and the use of non-traditional materials. MnDOT has recognized that in some circumstances construction contracts need to be done in other ways. One alternative MnDOT has successfully used is design-build contracting where a contractor is rewarded for innovation to develop the best, fastest, and most economical solution for the needed project. MnDOT has completed ten design-build contracts, most notably the reconstruction of the I-35W bridge in Minneapolis, which allowed MnDOT and the contractor to work together to reestablish this critical link in record time though innovative contracting. Even with these contracting options, MnDOT still relies on their standard contracting options, with 15 construction events using design-bid-build as shown in Table 1. These can be split into two categories. The first being individual regular contracts and others include tying into an existing state contract and using the existing pay factors to have the work completed at MnROAD.

A recent example of a traditional design-bid-build construction is the 2010 SHRP-II Composite Pavement experiment developed through a partnership agreement with Applied Research Associates. MnROAD agreed to take in the funds to do the construction (develop plans, special provisions, bids, construction inspection, and payments) and assist in the research (purchase/install sensors, collect sensor data, and monitor field performance over time). This partnership was somewhat non-traditional but for the most part MnDOT let a normal contract. Both parties wanted an experienced contractor and ARA did not want to take the risks involved in doing the contracting themselves.

Some of the interesting challenges for developing a contract for ARA included use of:

- Two concrete pavers used in tandem (wet on wet construction) – something that no local contractors have ever attempted.
- Recycled coarse aggregate in the concrete mix that had not been used in Minnesota in the last 30 years.
- A gradation, uncommon to Minnesota but used in Europe, for the dense graded high quality concrete upper layer. This needed to be custom prepared.
- A new curing compound and retarder that the contractor had no experience with.
- A brushed exposed aggregate finish as part of the European design. The contractor did not have the same equipment and had to bid the job not knowing exactly how it was going to be done.
- A Stone Matrix Asphalt (SMA) in one of the test cells. Minnesota currently does not use SMA pavements and local contractors do not have much experience with the design and construction of them.

Meetings were held to assist potential contractors and the research team to better understand how to build and best contract construction of the test cells. These meetings were designed to help exchange information and possibly reduce the contractor's risk before they committed to the bid. They also helped MnDOT to form the plans and special provisions for bidding. MnDOT first held an informational meeting coordinated by the State Concrete Paving Association of Minnesota and the MnDOT construction office so MnDOT and ARA could get feedback on the innovative construction and materials from three local concrete contractors. Contractor's feedback included providing a location at MnROAD for construction of a "practice slab" using the two pavers, three different concrete mixes, and help in developing a sense of how to do the exposed aggregate surface before the work was done on the mainline interstate. MnDOT, the University of Minnesota, and ARA then developed the plans and special provisions for the design-bid-build contracting process. A second formal pre-bid meeting was held to re-assess the plans and special provisions to help answer any questions before bids were submitted by potential contractors. It was hoped that this would keep the bid price as low as possible (to stay within

Table 1. MnROAD construction – traditional MnDOT (design-bid-build).

Year	Construction Activity	# of Cells	Construction Notes	Constr. Costs * (×1,000)
90-93	Original construction Phase-I	23 ML 14 LVR	SP 8680-109, SP 8680-123, SP 8680-124, SP 8680-125, SP 8680-129. MnDOT using regular federal construction funds	25,000
97	Superpave inlay	2 ML	SP 8680-136. Tied to existing state job using MnDOT purchase order for cost overrun. Research plans and mix designs	58
97	Whitetopping	6 ML	SP 8697-170. MnDOT and FHWA	116
99	Superpave & large stone base	5 LVR	SP 8816-040. MnDOT	328
99	Microsurfacing	2 ML	Tied to existing state job using MnDOT purchase order for cost overrun. MnDOT Specification	5
00	Thin PCC and doweled PCC	3 LVR	SP 8816-040. MnDOT	226
00	60” culvert design	1 LVR	SP 8816-040. MnDOT and FHWA funding	100
03	Microsurfacing	9 ML	Tied to existing state job using a MnDOT purchase order (OPERA Funds) for cost overrun. MnDOT Specification	15
04	Whitetopping on HMA	4 ML	SP 8816-607. MnDOT and FHWA	161
06	GeoComposite barrier drain	2 LVR	SP 8680-152. MnDOT, NCHRP & pooled fund study	130
07	Construction, Phase-II	6 LVR 2 Farm	SP 8680-156. MnDOT, FHWA, partners and pooled funds	390
08	Construction, Phase-II	16 ML 8 LVR	SP 8680-157. MnDOT, FHWA, partners and pooled funds	2,234
10	SHRP-II composite pavement	3 ML	SP 8680-159. Partnership though ARA	707
11	Stabilized FDR	1 LVR	SP 8680-166. MnDOT	65
11	Concrete overlay	2 ML	SP 8680-165. MnDOT and FHWA	464

*not adjusted to current year dollars

ARA’s construction budget) by helping the contractors understand the innovative construction and reduce perceived risks. Despite these meetings, initial bids were rejected because they were higher than both the engineers estimate and ARA’s budget, but only due to the lack of experience on SMA paving. Consequently, despite ARA’s desire to include an SMA section, a high quality Superpave mix was instead accepted for the rebidding of this project.

The other type of traditional design-bid-build projects are those where MnROAD ties into another existing MnDOT projects. The 1997 Superpave inlay of two test cells is an example, where the contractor on a nearby state-contracted job was asked if they were willing to do additional work under their existing contract. Typically extra amount labor and materials can be added to the contract at the agreed amount provided the cost does not exceed 10% of the original contract amount. MnROAD and/or the research partners pay the difference. This is one of the easiest and fastest ways to get a qualified contractor to build test cells at MnROAD, but requires a contractor to be in the area, agree to do the extra work under their existing contract, and fall within the timeframe needed for MnROAD. In many instances, the timing does not work out to do this type of contracting making this option of limited use for MnROAD’s research needs.

Some interesting challenges have arisen when the research goals require non-traditional construction practices. Special provisions need to be written so contractors can bid the project, field inspection can be done, and the contractor paid for their work. Some examples include:

- Developing plans for the 60 in. culvert project when researchers wanted half of the pipes installed using “poor” construction methods and compaction. This allowed researchers to measure the effects of poor and correct installations, but was difficult to develop special provisions for the MnDOT inspector to demand.
- Installation of large stone base materials without segregation when MnDOT and the contractors did not have experience with these materials.
- Installing pervious base materials specified by researchers that may not support construction equipment in the field.
- Construction of roller compacted concrete when no contactor had constructed this material and no inspectors had experience with it.
- Spread and blend high carbon fly ash for base stabilization with specialized equipment.
- Fractionate RAP piles (separate into different size fractions), develop mix designs, and introduce the fractionated RAP into the mix.

These examples and interesting challenges demonstrate some of the research pros and cons related to traditional design-bid-build contracting:

Research Pros

- Allows for typical construction methods and practices

Table 2. MnROAD construction – contracted though procurement.

Year	Construction Activity	# of Cells	Construction Notes	Constr Costs*
2000	Oil gravel	2 LVR	MnDOT purchase order to cover the costs. Research plans and mix designs	40,000
2003	MiniMac	4 ML	MnDOT purchase order to cover the material costs. MnDOT equipment and labor	15,000
2004	Mesabi hard rock HMA & PCC	2 LVR	MnDOT purchase order to cover the costs (MnDOT, MnDNR, NRRI partnership). Research plans and mix designs	75,000
2005	Flexible slurry	4 LVR	MnDOT purchase order to cover the costs (MnDOT and LRRB partnership). Research plans and mix designs	25,000
2008	Chip seal	1 LVR	MnDOT purchase order to contract the contractor. FHWA partnership through a pooled fund	5,000
Many	Partial depth concrete patching	many	MnDOT purchase order to cover the costs along with partnerships	Minimal
Many	HMA crack sealing & patching	many	MnDOT purchase order to cover the costs along some partnerships	Minimal

*not adjusted to current year dollars

– Skilled contracted workers – consistent workmanship
– Established formal contract and contracting process
– Less risk to MnDOT and its partners compared to other contracting methods
– Allows experienced MnDOT inspectors to assist researchers who tend to have limited field experience.

Research Cons

– MnDOT traditional construction process can be limiting when developing special provisions to use new materials and construction practices. This is especially true when the process is not completely known and field modifications are needed to accomplish/learn in the field.
– Contractors are being asked to be flexible in the field to allow researchers to learn from the construction, but contractors have a contract and schedule to keep.
– Typical design-bid-build contracting is very detailed and time consuming, which can impact some partnerships that want to do something quicker especially for small construction efforts.
– Non-typical construction, small quantities, researcher needs, and sensor installations tend to result in higher bids because a contractor perceives a higher risk to work on these types of projects.

3 MNDOT RESEARCH CONSTUCTION USING PROCUREMENT

MnROAD has used procurement (purchase orders) to build on seven efforts since 1994. These types of jobs are typically smaller construction efforts that are usually less expensive. They can be broken into two major types. The first is when MnDOT funds both a contractor's labor and materials using a purchase order. The second is when a purchase order is used to purchase only the materials and MnDOT supplies the labor and equipment. A list of these construction events are shown in Table 2.

MnROAD has used purchase orders to contract both the contractor and materials needed for smaller construction and maintenance needs over the years. Examples include crack sealing of HMA test cells, chip seals including the ones done in 2008 and the fog seals done since 2008 for the aging pooled fund study, which requires 100 ft. of fog seal each year for five years. These efforts are controlled by MnDOT purchasing rules that require that the total funds do not exceed a certain amount. Note MnDOT's purchasing rules have changed over the years but typically a purchase is acceptable if the total value is less than $25,000.

Some examples of this type of contracting using purchase orders involve purchasing only the materials and having MnDOT forces do the work with in-house equipment and labor. This system was used for the 2003 MiniMac surfacing, 2004 Messabi hard rock HMA paving, and the multiple crack sealing and concrete patching efforts. In most instances, the extra coordination needed pays off in terms of time-saved, although MnDOT does not consider its own labor costs since contracting for own labor is not required. If MnROAD has other offices do the work, funds are transferred between the offices. MnROAD has learned some lessons related to this type of contracting, including during the 2011 partial depth concrete patching. This work involved using MnDOT's Bridge Office equipment to grind out and shot blast the 135 failed concrete areas. Patch materials were purchased using purchase orders and donations from different material suppliers. The patches were placed by MnROAD research staff with the assistance of the material suppliers. As with other similar efforts, MnROAD staff realized that they do not have the trained skilled concrete finishers, the work is physically demanding, and time consuming in that staff are taken away from other normal activities.

Table 3. MnROAD construction – private partnerships.

Year	Construction Activity	# of Cells	Construction Notes	MnDOT Constr Costs
2005	Concrete pervious parking lot	1	Partnership agreement, ARM donated materials and labor	0
2006	Concrete pervious side walk	1	Partnership agreement, ARM donated materials and labor	0
2007	Diamond grinding Cell 37	1 LVR	Verbal agreement, pooled fund study	0
2008	Stabilized FDR	3 ML	Partnership agreement, Road Sciences built the cells	0

Both of these types of efforts have the following pros and cons related to research being completed though procurement efforts.

Research Pros

- Quick turn around
- Cheaper construction costs (but this does not include internal MnDOT research staff costs)
- Less standard, but more flexible construction/ contracting rules to follow
- Keeps mainline or LVR open to traffic when a test cell fails unexpectedly and repairs are needed quickly.
- Typically involves partnerships.

Research Cons

- The follow-up long term research focus may be missed.
- Typically done for lower cost/effort test cells but most projects cannot be done using procurement.
- Heavy involvement from others to donate equipment and staff which can be difficult to coordinate.
- Sometimes less skilled workmanship (you get what you pay for).
- Less construction quality control.
- Can involve high demands on internal research staff to do the labor along with their normal job duties.

4 PRIVATE PARTNERSHIPS

MnROAD has also utilized a form of private partnership to accomplish four different construction efforts for the MnROAD research facility. These are similar to many of the partnerships developed though procurement, but are almost always constructed entirely by private partnerships. These partnerships are not a true public-private partnership where MnDOT provides opportunities for an outside partner to construct, maintain, and operate a facility such as a toll road or bridge. MnROAD research partnerships are typically with close trusted groups that have a common research focus and are considered a low risk to MnDOT and the driving public, since traffic delays to the public can be avoided if anything goes wrong. This allows MnDOT to not require bonding to ensure work gets completed and simplifies the private partnership process down to a written partnership agreement. Table 3 lists the private partnerships that have been completed at MnROAD.

One of the first successful private partnerships was done with Aggregate Ready Mix of Minnesota (ARM) and its members. This included both the 2005 construction of a pervious concrete parking lot and a pervious sidewalk in 2006. Both these efforts were relatively small in scale and were not located on the LVR or Mainline. ARM agreed to develop the mix designs, provide the construction equipment, some construction labor, and technical expertise, hired a University of Minnesota student to follow-up on the research, and agreed to repair the pavements after the study was complete. MnROAD assisted with the removal of the existing parking lot and sidewalk, sensor instrumentation, and assisted with the construction. Both parties formed a partnership agreement and shared the responsibilities. The positive findings from these initial field trials allowed MnROAD to have the confidence to construct pervious concrete and porous asphalt test cells on the LVR in 2008 for real traffic loadings.

Another example of a successful private partnership was the 2007 partnership with Diamond Surfacing. This partnership was though a MnROAD pooled fund study, *TFP-5(134) PCC Surface Characteristics*, which involved using laboratory findings from Purdue University to formulate a full-scale study at MnROAD. Diamond Surfacing donated the expertise and insight needed to develop the cutter heads required, provided equipment and construction labor needed to grind three stripes in Cell 37, each measuring 18 in. wide by 500 ft long. These different concrete surfaces were then monitored for friction and noise before the study determined them to be ready for implementation on three MnROAD mainline concrete test cells. This partnership and study is allowing state agencies to have a new rehabilitation tool to develop smoother, quieter, and safer surfaces for the driving public, but has also benefited Diamond Surfacing by allowing them to work with researchers to produce a long lasting product that may become a more common rehabilitation technique. This partnership has continued to flourish and has become a key area of interest and successful research at MnROAD.

The third project involved a partnership with RoadScience, in which three mainline test cells were reconstructed using stabilized full-depth reclamation (FDR) on existing older cracked HMA test cells. The construction took place in 2008 and the research is still ongoing. This was the first time MnROAD provided three cells to a partner to fund the design and construction of the test cells needed for the study. MnDOT

and RoadScience entered into a partnership agreement where no funds were transferred between parties. The design was developed and agreed upon between both parties. Road Science then developed the plans and special provisions for construction, hired the contractor directly, inspected the job, and made payments. MnDOT was responsible for purchasing and installing sensors, collecting pavement performance data, and conducting the research evaluation. This has also been a successful research partnership and provided a method to get test cells reconstructed at minimal cost.

Listed below are some pros and cons related to this type of partnership.

Research Pros

- Partners are involved and engaged for the entire study.
- Partners have common research goals.
- Good relationships including a high level of trust.
- Contractor can sometimes be more innovative when working with a non-government agency.
- No MnDOT construction contract (plans, paperwork, payments, inspection, etc.) that requires research staff time.

Research Cons

- Risk is taken by MnDOT. If something goes wrong with construction and extra funds are needed, MnDOT legally is responsible.
- Partnership agreements are typically not fool-proof legal documents and MnDOT is the owner of the property.
- Decisions can be made outside of the agencies control since the partner is leading the effort.

5 COMMON ISSUES AFFECTING INNOVATION AND CONSTRUCTION

No matter what contracting method is utilized for construction at accelerated pavement testing facilities, some common issues should be taken into consideration from the experiences gained at MnROAD. When it comes to judging a product or technique agencies may only give a product one opportunity to prove itself, which is not always appropriate. If the field trial fails or under-performs for any reason, agencies typically never try it again. This is also true for MnROAD and other accelerated pavement testing facilities, and can negatively impact future innovation and experimentation.

Short test cells sometimes render construction difficult. Understanding the products and working with key experts helps to produce a consistent product needed to evaluate the design in the field. Materials and equipment limitations both need to be considered when designing experiments. MnROAD has 500 ft. test cells and has been able to develop meaningful research with these limitations:

- Individual operators and equipment affect the final outcome no matter how many inspectors are on site. MnROAD works to make sure everyone understands the research needs before work is started. For example, HMA thicknesses have varied from 2.5 to 3.5 in. in a 500 ft. test cell with 50 engineers watching the paver operator work.
- Weather can affect the final product. For example, variable initial curl is built into a concrete pavement depending on the weather on the day of construction. This affects the final product and needs to be documented.
- Contractors are often asked to do something outside of their normal expertise. For example, the use of new equipment, techniques, or materials requires practice before a consistent and quality product can be produced. Contractors are geared for profit orientated production type projects, which often do not support innovation. Communication with the contractor is important.
- Equipment and expertise required for certain types of construction may not be available in a specific area. This must be taken into account when developing contracts.
- Certain construction materials may not be readily available for research needs. This also affects local contractors who may not have experience constructing with materials from other areas.

6 CONCLUSIONS

MnROAD is almost 20 years old and has over 26 construction events that have been used to promote innovation in materials and the construction industry. Three basic types of construction contracting have taken place over the years including traditional design-bid-build, research construction using procurement, and the use of private partnerships. Through these experiences, MnROAD has learned the following:

- Each of the contracting methods works equally well and can be used depending on the needs of the research partners. Each method has its pros and cons that need to be considered to insure a successful project.
- Successful research has a balance between construction funding, sensor installations, well thought out research plans, and an implementation plan to use the results. MnROAD staff have found that if any one of these elements is missing, the final product tends to be of limited use.
- Communication, trust, and common goals have helped develop successful research partnerships. Organizations such as TERRA and the LRRB have proven essential in the successful development of useful products.
- Partnership agreements are essential in most successful research projects. This helps form common construction, research, and implementation goals where each party has a stake in the final product.

– When designing new test cells at an accelerated pavement testing facility, owners need to understand the limitations that short test cells, construction equipment, materials, and people have on the success of the construction efforts and ultimate research results. Good communication is important throughout. The entire process also needs to be documented for researchers to understand what may have influenced the true performance of the cell. Not every failure is a predictor of future performance of a certain design or material.
– Complete construction documentation is needed for researchers to understand any influences construction may have on the pavement or material performance. Not every failure is the fault of the design or materials used.
– Future focus of research needs and possible construction at MnROAD needs to be focused on the customer.

ACKNOWLEDGEMENTS

The authors gratefully acknowledge all who have participated in the research efforts at MnROAD. This includes MnDOT staff, the Minnesota Local Road Research Board (LRRB), FHWA and other research partners who have financially supported the research facility. The authors also acknowledge the MnROAD staff for their efforts over the years, which have helped make MnROAD a successful accelerated pavement testing facility.

REFERENCES

Current and Past Construction Reports and Research <http://www.dot.state.mn.us/mnroad/construction/index.html> Accessed 15 March 2012.

This page intentionally left blank

Advances in Pavement Design through Full-scale Accelerated Pavement Testing – Jones, Harvey, Mateos & Al-Qadi (Eds.)
© 2012 Taylor & Francis Group, London, ISBN 978-0-415-62138-0

International case studies in support of successful applications of accelerated pavement testing in pavement engineering

F. Hugo
Stellenbosch University, Stellenbosch, South Africa

M. Arraigada
Swiss Federal Laboratories for Materials Science and Technology, Switzerland

L. Shu-ming
Tongji University, Shanghai, China

T. Zefeng
Communication Research Institute of Liaoning Province, China

R.Y. Kim
Construction and Environmental Engineering, North Carolina State University, US

ABSTRACT: Accelerated Pavement Testing (APT) offers a unique proven methodology to investigate performance of different material and pavement structures under various conditions. Case studies using Mobile Load Simulator (MLS) equipment provide well-documented information in support of this statement. The international selection of typical cases provides pavement engineers (and managers) insight into some of the lessons learned and application of the knowledge gained in respect of distress and failure mechanisms. Case studies from China, Europe, and United States are presented. These cover applications of asphalt materials including pavement surfacing, stone matrix asphalt, Guss asphalt, and full-depth asphalt. Trafficking under wet and dry as well as artificially heated conditions, are discussed. Structural compositions include a steel bridge deck surfacing, a full-scale and comparative scaled pavement, and a sandy subbase subjected to the influence of a high water table. The paper reports on a synthesis of facets of analyses and findings from the case studies including both laboratory and field applications.

1 INTRODUCTION

At the Third International Accelerated Pavement Testing (APT) Conference in 2008, the findings of three APT case studies were reported and discussed by Hugo et al., (2008). The same procedure was used in a paper presented at the recent Conference on Asphalt Pavements in Southern Africa (CAPSA) conference in South Africa for reporting on a number of APT case studies (Hugo et al., 2011). In particular, the effect of slow moving traffic resulting in harsh operational conditions for asphalt materials was discussed. It was apparent that there was considerable benefit gained from conducting syntheses of APT studies.

Full-scale Mobile Load Simulator (MLS) equipment, developed after the 2006 MLS prototype, was recently used for APT studies in Europe and China during 2009 and 2010. In two of the case studies, the one-third scale model mobile load simulator (MMLS3) was incorporated in the studies. The findings that were reported by the respective researchers provide noteworthy information (Pugliessi et al., 2010). This paper will provide a synthesis of the findings from selected case studies. It will include a review of findings from an earlier Accelerated Loading Facility (ALF) study in the USA that was linked to APT with the MMLS3. The information should provide a useful basis for application by pavement design engineers. The case studies were selected to relate to monitoring and evaluation of distress and failure mechanisms impacting on pavement performance in APT studies.

Fifteen distress mechanisms that were identified in the course of the synthesis study are shown in Table 1. The extent of this is apparent. Twelve of these features in the case studies were selected for discussion in this paper.

Details pertaining to each of the case studies will not be presented except where appropriate for the purpose of supporting the conclusions in the case study. Readers are referred to the respective references that were reviewed for more information. The broad spectrum of the distress mechanisms covered by the case studies is apparent from the extent to which each relates to a number of distress or failure mechanisms.

Table 1. Summary of distress and failure mechanisms relating to pavement performance identified during the APT case studies

	Case study/location				
Distress/failure mechanism	1 – CRILP Bridge deck	2 – CRILP HMA study	3 – EMPA Full-depth HMA	4 – NCSU Fatigue study	5 – Tongji Full-depth HMA
Fatigue cracking		X			
Stiffness				X	X
GPR response (voids)			X		
Debonding	X				
Response	X	X	X		X
Friction loss	X				
Surface degradation	X	X			
Rutting/deformation	X	X	X		
Scaled performance			X	X	X
Heating	X	X			X
Bleeding		X			
Stripping	X	X			
Water table					X

Against the background of the case studies in Table 1, the following primary objectives were selected for review:

- Evaluation of surfacing options for a steel bridge deck in China (CS1).
- Trafficking of stiff full-depth pavements under both wet and dry conditions as well as artificially heated conditions in China (CS2) and Switzerland (CS3).
- Comparison of fatigue distress on a model pavement and a full-scale test pavement in USA (CS4).
- Influence of a high water table on the structural performance of a stiff full-depth pavement in China (CS5).

Details relating to the respective APT facilities will not be presented unless required for better understanding of the respective case studies. In this regard the following general information relating to the full-scale MLS testing system is provided.

2 MLS APT EQUIPMENT

The MLS full-scale equipment is fully described on the MLS website (www.mlstestsystems.com), but can be summarized as follows:

Two full-scale machine sizes are available, MLS10 and MLS66. The operational systems are identical except for the respective lengths of the machines. The MLS66 has six bogies with load wheels, while the MLS10 has four. They have similar test wheel load capacity but, due to the differences in length, the MLS10 only has one load wheel on the pavement surface at a time.

The MLS66 has two load wheels on the pavement for part of the rotational cycle. The system comprises an endless chain of test wheels rotating in a vertical plane at nominally 22 km/h. The bogie chain is housed in a structure with travelling wheels back and front and is capable of manoeuvring on the test site using a hydraulic powered motor. The structural shell can be lifted to allow testing and inspection of the pavement during stoppages. Heaters can be used internally to heat and control the pavement to a maximum surface temperature of 70°C. The pavement can also be wetted artificially to simulate rain conditions during trafficking. The entire machine can be shifted sideways during trafficking by hydraulic power to simulate lateral wander of traffic. The load on the pavement can be monitored as the bogie traverses the test section and the pavement surface can be monitored to track surface deformation.

The full-scale MLS machines have been utilized for APT studies in Mozambique, South Africa, Switzerland, Austria, and China. In several instances the studies included the use of the MMLS3 a one-third scaled version of the MLS to supplement the full-scale APT. In the same vein the MMLS3 has been used in conjunction with other full-scale APT equipment such as the Accelerated Load Facility (ALF) and the Heavy Vehicle Simulator (HVS).

3 CASE STUDY 1: BRIDGE DECK SURFACING IN LIAONING PROVINCE, CHINA

The Communication Research Institute of Liaoning Province (CRILP) in China acquired a MLS66 full-scale and a one-third scale MMLS3 machine. These were delivered in August 2009. Two major contract studies have been completed by CRILP to date. The details in their reports on the projects serve as the basis for the first two case studies discussed below.

3.1 *Study background*

The steel bridge deck surfacing (SBD) project was undertaken to compare the performance of two types

Structure No 1 (Epoxy-gravel) Structure No 2 (Gussasphalt)

Structure 1: Resin-Asphalt (RA)	Structure 2: Gussasphalt (GA)
35mm Stone Matrix Asphalt	35mm Stone Matrix Asphalt
25mm Resin-Asphalt Concrete	25mm Gussasphalt Mixture
Epoxy-Gravel Adhesive Layer	ELIMINATION water Proofing
Bridge Steel Deck	Bridge Steel Deck

Figure 1. Details of the bridge deck surfacing tested in the Shenyang laboratory in Liaoning.

of pavement surfacing for the deck of a steel bridge that will serve for the coastal road crossing the Liao River. This was the first full-scale APT study by CRILP. The SBD-project was carried out indoors in the CRILP laboratory in Shenyang.

The project client built the bridge section before the formal test and the suppliers of the two pavement types placed the layers on the steel deck of the bridge section between March and June, 2010. A schematic of the construction is shown in Figure 1.

The surfacing layers tested were a Liaoning rut resistant resin asphalt concrete (RA) and Guss asphalt (GA). The latter is a high temperature mix, hot poured asphalt extensively used in Germany. After placement it cools to an impervious deformation resistant layer.

The objective of the test was to compare performance of the two pavement structures for rut-resistance, water-proofing and skid resistance. A special foundation pit was excavated in the laboratory floor with retaining walls alongside to enable the MLS66 to travel longitudinally. The suspended bridge sections were supported at both ends. After completion of the bridge structure, 2.9 million APT load applications were applied on the two surfacings.

3.2 *Test results*

Figure 2 shows one of the transverse pavement profiles after zero, 100,000, 600,000, 1.1 million, 1.5 million, 2.3 million, and 2.9 million 75 kN load repetitions on dual tires mounted on each of the six bogies. Profiles of the respective pavements on the deck were recorded with the MLS profilometer and calculated.

The progressive rutting in terms of load applications on the two bridge surfacings is shown in Figure 3. There was a "step" jump in the curves between 1.1 and 1.3 million repetitions. This was due to the effect of different temperatures applied during the test. The first 800,000 load applications were applied at ambient temperature (i.e. 10 – 25°C) and the next 400,000 load applications at 45°C. The pavement profile did not

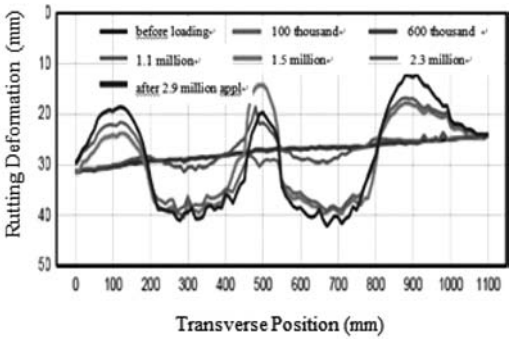

Figure 2. Typical transverse pavement profile of the two adjacent overlays relative to trafficking intervals.

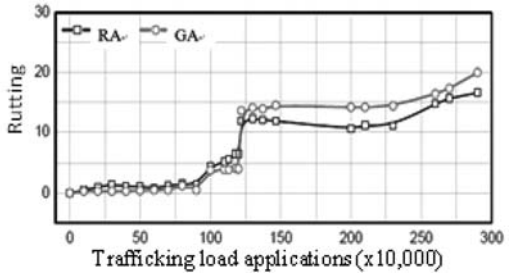

Figure 3. Comparative rutting of RA and GA on the BDS under MLS66 trafficking.

change as much as expected during this period, and the temperature was therefore increased to 55°C. At this temperature, the rutting rate increased suddenly and consequently the temperature was reduced back to 45°C until completion of the test.

3.3 *Findings from the SBD surfacing performance*

Findings from the SBD surfacing study include:

- The rut-resistant resin-asphalt pavement structure had better comparative rutting performance than the Guss-asphalt pavement.
- The artificial heating successfully controlled the testing conditions.
- Waterproofing and skid resistance of the two structures was similar.
- There was no evidence of stripping but the Guss-asphalt showed some evidence of bleeding.
- There was no evidence of debonding of the pavement layers.

3.4 *Case study 1 conclusions*

The following conclusions were drawn from the study:

- The study provided confidence for selecting the rut-resistant resin-asphalt pavement structure as the better surfacing for the bridge, subject to economic evaluation.

– The APT test protocol was considered reasonable as a basis for similar future studies.
– The testing efficiency of the project was considered cost-effective in terms of time and lessons learned.

4 CASE STUDY 2: TWO HIGHWAY ASPHALT PAVEMENT STRUCTURES IN LIAONING PROVINCE, CHINA

This project was the first field APT after the MLS66 arrived in Liaoning. The project site is located in Xinbin County, Liaoning Province.

The project compared the performance of two highway structures; a rubberized asphalt pavement and a conventional provincial highway pavement. Details on the two test sections constructed are summarized in Table 2. Four test sections were displaced longitudinally and constructed adjacent to each other.

Trafficking was conducted under ambient conditions on each pavement structure with no temperature control. This was followed by a limited number of load applications on sections of each pavement structure under controlled temperature with traffic wander. The test site and equipment is shown in Figure 4 and test results are summarized in Table 3.

4.1 *Findings from structural performance*

The two pavement structures were evaluated in terms of rut-resistance, fatigue-resistance, and shoving under comparable conditions. Direct comparisons between the two sections could not be made because of the different pavement structures; however the following observations were made:

– The conventional section had better performance in terms of rut-resistance than the rubberized asphalt section under channelized trafficking.
– Shoving performance was similar on both sections.
– The rubberized asphalt exhibited cracking after about 1.7 million load applications (Figure 5). In contrast there was no cracking on the conventional section.

Table 3. Case Study 2 rutting performance summary.

Test details	Temp. (°C)	Repetitions	Max. Rut Depth (mm)
Conventional			
Ambient temp.	8∼41	2,240,000	8
Controlled temp.	45	110,000	4
	50	360,000	15
Total repetitions		2,710,000	
Rubberized asphalt			
Ambient temp.	3∼40	2,200,000	20
Controlled temp.	35	13,000	12
	45	20,000	17
	55	24,000	23
Total repetitions		2,257,000	

Figure 4. MLS66 on the RubAP/LAC test sections at Namzamu.

Figure 5. Close-up view of transverse crack on rubberized asphalt.

Table 2. Case Study 2 test section description (on in situ subgrade with resilient modulus not less than 70 MPa).

Layer		Material and layer thickness (mm)			
		Conventional (LAC) 730 mm		Rubber Asphalt (RubAP) 540 mm	
Asphalt Surface	Upper	Stone matrix asphalt-13L (13 mm)	35	Rubber asphalt (ARAC-16)	50
	Middle	LAC-20 (20 mm)	60		
	Lower	LAC-25 (25 mm)	80		
Seal coat		Slurry seal on emulsified asphalt prime	5	Rubber asphalt chip seal	10
Binder course		–	–	Graded crushed macadam	120
Subbase		Cement stabilized macadam	200	Cement stabilized macadam	180
Bottom subbase		Cement stabilized sand and gravel	200	Cement stabilized sand and gravel	180
Cushion layer		Graded sand gravel	150	–	–

– The performance provided useful information on failure mechanisms of the two pavement structures and differences in performance provided good information for exploring fatigue designs for the two pavement systems.
– The rubberized asphalt experiment provided adequate performance to justify further research on the use of this material. It also exposed the team to aspects of construction quality that need to be monitored.

5 CASE STUDY 3: STIFF FULL-DEPTH PAVEMENTS IN SWITZERLAND

This case study focuses on a synthesis of data obtained through the interactive relationship between full-scale and scaled APT with specific emphasis on the strains in the top asphalt layer. It relates to field APT trials by the Federal Institute for Materials Testing and Research (EMPA) as a part of its efforts to gain confidence in its ability to conduct APT with the MLS10 it had acquired. In a joint venture between EMPA and the National University of Rosario (UNR) in Argentina, MMLS3 tests were used to evaluate the ability of the scaled trafficking system to measure strains under the scaled wheel load for comparison with strains that were measured under the full-scale trafficking (Pugliessi et al., 2010; Pugliessi, 2011).

5.1 *Study background*

Three pavement structures were constructed near the A4 Westring motorway close to Zürich (Figure 6), and instrumented with horizontal strain gauges, temperature sensors, and accelerometers. The primary purpose of the study was to evaluate the response and performance of a heavy duty full-depth asphalt pavement subjected to trafficking by an MLS10.

A series of 120-mm long *Kyowa* strain gauges were installed (transversal and longitudinal) 30 mm and 110 mm deep in the asphalt during the construction of the test sections (Figure 7). The three sections were tested with the MLS10 (Arraigada et al., 2012).

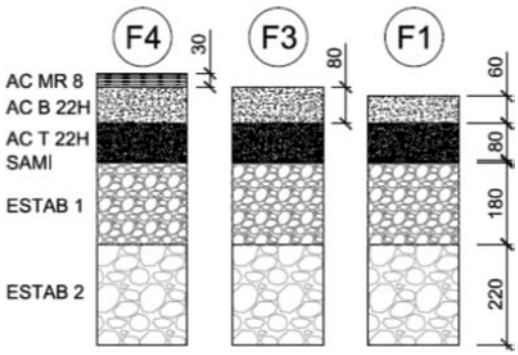

Figure 6. Schematic of three pavement structures at Filderen (Pugliessi et al., 2010).

After completion of the tests a 190 mm asphalt slab was cut from Section F4 (Figure 8) of the full-scale pavement and transported to the laboratory for temperature conditioning and subsequent MMLS3 testing. A 10 mm interlayer of cement/sand mix was spread between the 190 mm asphalt block and an underlying 300 mm concrete block prior to seating the slab on it. The slab was instrumented to measure strains (Figure 9). The MMLS3 was then straddled over the asphalt block for trafficking (Figure 10).

The strain gauges were reconnected and the block tested at different temperatures and speeds, under limited load applications. Only strain measurements were

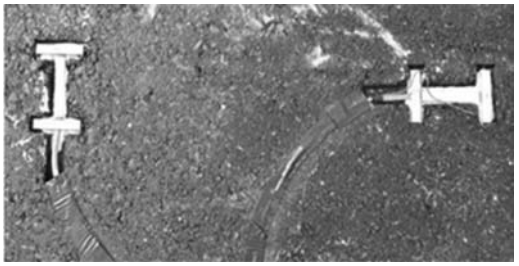

Figure 7. Strain gauges prior to asphalt covering.

Figure 8. Extraction of asphalt slab from test pavement.

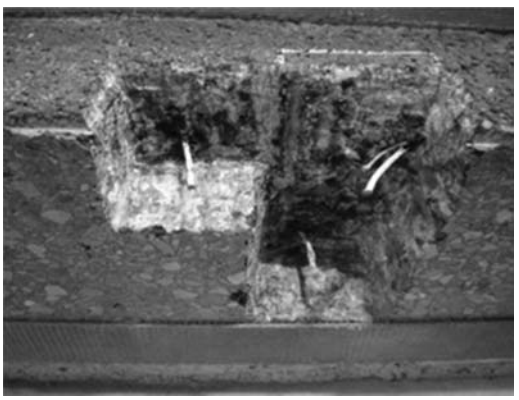

Figure 9. Cables for monitoring strains under lab trafficking.

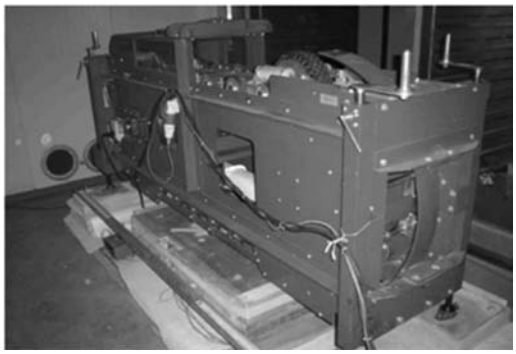

Figure 10. MMLS3 trafficking of extracted slab.

Table 4. Input parameters for *BISAR* linear-elastic analyses of MMLS3 and MLS10 wheel loads.

Temp. °C	Layer stiffnesses for *BISAR* analyses (MPa)		
	Layer 1	Layer 2	Layer 3
1,200 reps/hour (both machines)			
20	1,000	3,000	3,000
25	870	2,200	2,230
35	700	1,500	1,500
7,200 reps/hr (MMLS3), 6,000 reps/hr (MLS10)			
20	3,480	7,645	7,930
25	2,480	5,020	5,060
35	870	2,200	2,230

MMLS3 Wheel Load: 2.1 kN at 600 kPa.
MLS10 Wheel Load: 65 kN at 800 kPa.

taken since rutting was minimal and stresses were not considered. Comparisons were made between the strains measured under the scaled and full-scale tests and those predicted by analytical procedures, specifically finite element analyses and *BISAR* linear elastic analyses (Pugliessi, 2011; Arraigada et al., 2012).

Strain data under MLS10 trafficking were collected at different ambient temperatures (no artificial heating was used) and trafficking speeds. In contrast, the MMLS3 trafficking was done at predetermined temperature levels. The temperature was controlled manually at the predetermined levels.

Cores from the test pavement samples were tested in the laboratory to measure indirect tensile stiffness of the asphalt under different temperatures and trafficking frequencies.

Elastic strains were analyzed with *BISAR*, using the input parameters listed in Table 4. Results are summarized in Tables 5 and 6 (Partl and Arraigada, 2011; Arraigada et al., 2012).

5.2 *Summary of findings*

Findings from the study are summarized as follows:

- All strains increased as the temperature was increased, as expected.
- At 20°C and trafficking at 1,200 reps/hr and 7,200 reps/hr, all measured longitudinal strains under full-scale and MMLS3 were closely related to values calculated by *BISAR*. The Indirect Tensile stiffness measurements by Pugliessi (2011) according to EN 12697-26 (2004**)** Annex C were used as input data for the analyses.
- At 25°C and 35°C and 7,200 reps/hr the longitudinal strain correlation was slightly less than those recorded at 20°C.
- At 25°C and 35°C and 1,200 reps/hr, the discrepancy between calculated and measured MMLS3 longitudinal strains became much larger especially as the temperature increased. The reason for this is not clear and requires further investigation. No 1,200 reps/hr tests were done under MLS10 trafficking.
- At 20°C, 25°C, and 35°C at 7,200 reps/hr, the transverse strains under MMLS3 trafficking were closely related to values that were calculated by *BISAR*. In contrast the transverse strains under MMLS3 trafficking at 1,200 reps/hr did not correlate as well.
- The transverse strains under the MLS10 did not correlate at any of the three temperatures at 6,000 reps/hr. Furthermore, the discrepancy increased as the temperature increased. The reason for this was not investigated.
- It is, however, noteworthy that this is somewhat similar to the response of the longitudinal strain under the MMLS3 at 25°C and 35°C. The increase in strain in both scenarios (MLS10 and MMLS3) would naturally lead to harsh conditions for rutting performance. In the one case due to increased temperature but in the other also as a result of slow trafficking. The importance of performance evaluation under slow heavy trafficking is apparent (Hugo et al., 2011).
- From a critical surveillance of the data in Table 5, the question arose whether some of the discrepancies between strains could be related to the strain gauges being slightly out of line. To evaluate this hypothesis, strains were measured with the MMLS3 offset 50mm from the identified gauge positions. The elastic strains were calculated to reflect measurement 4 mm on either side of the identified position as well as on it. The analytical calculated strain values were used as a guideline for estimating the perceived position of the gauges. It was concluded that the strain gauges were about 4 mm further from the identified position (i.e. at 54 mm).

5.3 *Case study 3 conclusions*

There was close agreement between measured and calculated strains under both MMLS3 and MLS10 trafficking. It was apparent that the strain measurements at a depth of 30 mm under the MMLS3 trafficking, were compatible with strains that had been measured under the full-scale MLS10 at the same

Table 5. Measured and calculated strains under MMLS3 wheel centre and between MLS10 dual tires (longitudinal and transverse).

	Calculated Strain (με)		Measured Strain (με)		Calculated Strainr (με)		Measured Strain (με)	
Temp (°C)	Long.	Trans.	Long.	Trans.	Long.	Trans.	Long.	Trans.
MMLS3	1,200 repetitions/hour				7,200 repetitions/hour			
20	−56	56	−66	30	−20	−20	−23	22
25	−74	74	−121	54	−30	−30	−43	32
35	−104	104	−207	105	−74	−74	−77	67
MLS10	1200 reps/hr				7200 reps/hr			
20	−28	−28	Not	Not	−8	15	−12	87
25	−38	−38	tested	tested	−14	22	−15	143
35	−57	−57			−38	51	−23	382

Table 6. Comparative MMLS3 strains with machine off-set from strain gauge (measured and calculated).

			Calculated Strain (με)		Measured Strain (με)		Measured Strain (με)	
Temp (°C)	Offset (mm)	Stiffness* (MPa)	Long.	Trans.	Long.	Trans.	Long.	Trans.
MMLS3			3,600 reps/hour		2,720 reps/hour		4,240 reps/hour	
20	46	2,200	−14	14				
	50		−12	14	−9	9	−8	8
	54		−10	14				
25	46	2,200	−19	18				
	50		−16	20	−13	15	−10	11
	54		−14	19				

*Layer stiffness: 2,200 MPa/5,000 MPa/5,500 MPa

depth in the pavement structure. This is considered to be a significant advance in the knowledge required to be able to monitor strain levels within pavement structures under MMLS3 trafficking. Overall, the findings serve as a basis for application in asphalt pavement evaluation and related future research.

6 CASE STUDY 4: FATIGUE PERFORMANCE AND CRACKING

Fatigue performance is a primary aspect that normally requires extensive trafficking that can become expensive. As a result such tests are generally fewer in number. Failure mechanisms related to cracking include changes in stiffness of the structure, and debonding. In an APT study of the performance of a pavement that was constructed at the FHWA Turner-Fairbank Highway Research Center in McLean, Virginia (Kim, 1997), stress wave tests were conducted on a 100 mm thick pavement with an AC-5 surface layer. Trafficking was carried out with the FHWA Accelerated Load Facility (ALF).

In a subsequent study of a scaled pavement using the MMLS3 at North Carolina State University, Lee (2003), compared the trend of the stress wave results on a local pavement structure to those reported by Kim and Kim (1996). Figure 11 compares the phase velocities at the center of the wheel-trafficked area and the cumulative crack length in terms of the number of wheel applications for both the MMLS3 and ALF. It can be seen that the phase velocity (and therefore AC stiffness) decreases as the number of loading cycles increase in both cases of the MMLS3 and ALF.

6.1 *Findings related to the full-scale and scaled APT fatigue*

The physical characteristics of the performance of the two pavements were very similar. This is evident from the study findings.

Figure 11 demonstrates that prior to the appearance of visible surface cracks, after 125,000 load applications, the phase velocities had already significantly reduced. The reduction in phase velocity indicates that the structural degradation in the model pavement test is similar in character, although at a somewhat slower initial rate than observed for the ALF results. This observation suggests that the proposed non-destructive evaluation technique (NDE) using stress wave technique measurements (WCM) could be successfully implemented to investigate fatigue damage evaluation especially for thin AC layers and overlays.

This process may allow the optimum time for maintenance/rehabilitation of a thin AC layer pavement to be determined before cracks appear on the pavement surface.

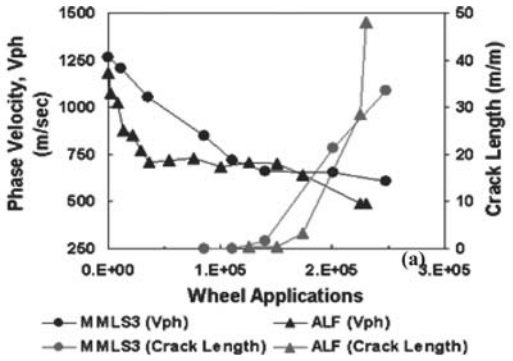

Figure 11. Phase velocity and cumulative surface crack length as a function of wheel applications (Lee, 2003).

The early reduction is attributed to structural degradation of the pavements due to the initiation, propagation, and densification of micro-cracks (Kim and Kim, 1996). Figure 11 also demonstrates that the phase velocity decreases significantly prior to appearance of surface macro cracks. This observation suggests that the optimum time for maintenance/rehabilitation may be long before cracks appear on the pavement surface. Lee and Kim (2004) commented on this phenomenon and stated that the optimum time may be better determined by the change in the phase velocity than by a visual condition survey of the pavement surface. Similar findings were reported by (Lee et al., 1997) in full-scale studies with the TxMLS on Highway 59 in Victoria, Texas where PSPA was used.

6.2 *Case study 4 conclusions*

It is apparent that transfer of findings between APT systems is feasible and likely to be cost beneficial provided the test systems are compatible. Furthermore, the available tools for monitoring progressive change during APT trafficking are invaluable for detecting micro-fracturing before distress becomes visible at the surface.

7 CASE STUDY 5: FULL-DEPTH ASPHALT PAVEMENTS ON SAND SUBGRADE IN CHINA

The Tongji University MLS66 was initially commissioned in the new APT laboratory. Subsequently it was deployed to conduct a field test to determine the effect of a variation in the water table depth on rutting of a full-depth asphalt pavement supported by cement stabilised subsurface layers. An experimental pavement was constructed on the G40 highway on Chong-ming Island. This highway will connect Shanghai and the inland city of Xi'an. The scope of the experiment included evaluation of the performance of a fine sand subbase with a high water table in the pavement structure. The fine sand is abundant in this region, but it has not been widely used as road subbase.

7.1 *Background to the field study*

The APT project was undertaken in July, 2010. The APT experiments involved both full-scale MLS66 and the MMLS3 tests. Comprehensive details pertaining to the MLS66 study are presented in the paper by Wu et al. (2012). The laboratory MMLS3 tests were used to assist with the selection of appropriate asphalt mixes for the study.

The test pavements were constructed concurrently as Track I and II. Both had similar asphalt and cemented layers. These were supported on imported fine sand subbase layers placed on a graded macadam layer overlying the in situ clay. Track I had a 1.5 m sand layer and Track II a 3 m sand layer. After construction, the average ground water table was about 2 m below the pavement surface.

The asphalt structure consisted of a surface layer of 40 mm SMA-13 (PG70 penetration grade) binder modified with SBS mixed rubber particles), an intermediate layer of 80 mm AC-20C (modified with 15% by weight rock asphalt), and 80 mm AC-25C (modified with 20% rock asphalt). The bitumen content of the natural rock asphalt was on average 22.3% with a penetration value of 6.1 and a softening point of 84.5°C. The binder in the AC-20C and AC-25C layers was unmodified PG70. The rock asphalt was added during mix production.

The imported base consisted of 540 mm aggregate stabilized with 4% cement. The top 600 to 800 mm of the sand subbase was treated with 3.5% cement, giving the material a resilient modulus of at least 40 MPa. The sand layers were compacted to 93% of laboratory density.

Trafficking with the MLS66 was carried out with an axle load of 75 kN, which is 50% heavier than the standard axle load in China, and a tire pressure of 800 kPa. The MMLS3 laboratory study was done on gyratory compacted briquettes in the conventional test bed, and 2.8 kN axle load and 710 kPa tyre pressure. Four asphalt mixtures were evaluated namely SMA13, OGFC13, AC13 and AC20 (AC is a traditional dense-graded asphalt mixture and the number in the mix type represents the maximum nominal aggregate size in mm). Track I was heated intermittently during trafficking. Track II was tested at ambient temperature.

7.2 *Test results*

The following test results are relevant to the context of this case study. Readers are also referred to (Wu et al. 2012) for more detailed information.

- After more than one million MLS66 APT applications, the total vertical displacement of the fine sand subbase was about 1.5 mm. Strain data showed that the modulus of the sand had remained constant.
- The temperature range of Track I was controlled and less variable than that of Track II, where temperatures varied with ambient temperature. Despite the MLS66 being covered by a structural

Table 7. Temperature range in MLS66 test tracks.

Depth (mm)	T_I (°C)	Average T_I(°C)	T_{II} (°C)	Average T_{II}(°C)
40	43–58	53	22∼46	31
80	43–59	52	16∼39	27
120	45–65	56	–	–
160	43–59	53	24∼36	29
200	37–48	44	25∼35	30

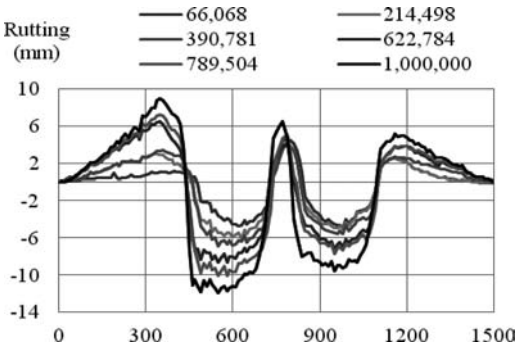

Figure 12. A typical MLS66 transverse profile for Track I (Wu et al., 2012).

shell, the weather affected the temperature and the water level especially when during rain. During trafficking the water table depth varied between 1.9 and 2.3 m. The temperature range of the two tracks during trafficking is presented in Table 7.

– The temperature of the MMLS3 test bed was controlled by a closed loop water circulation system set at 60 C. A thermocouple was laid in the middle of two samples 25 mm below the surface of the asphalt to measure the central section temperature in one test. Actual temperatures were found to have varied between 55 and 65°C.

7.3 *Analyses of performance and rut data*

Both Tracks I and II had two measuring positions referenced as 3 and 4. A typical transverse profile of one of these positions is shown in Figure 12 as it developed during the trafficking. Two maximum points, across the test section were chosen, namely Max1 and Max2. Max1 is defined as the peak rut depth made by trafficking wheel 1 or 2 at the specific measuring position. Max2 is defined as the peak rut depth of the adjacent dual wheel.

The rut depth points were first normalised to a zero reading then normalised with a line across the rut depth values at 0 mm and 1,500 mm across the test section. The Max1 and Max2 points were then selected as the baseline, yielding a total of eight sets of data, respectively, four sets per track. The eight sets of data were consolidated into a single composite averaged curve respectively for heated and ambient performance.

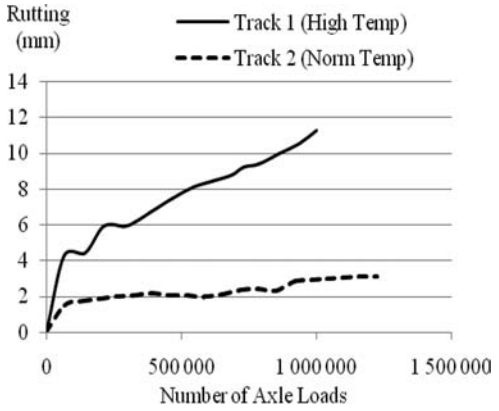

Figure 13. Composite of averaged rutting performance under heated and ambient temperature.

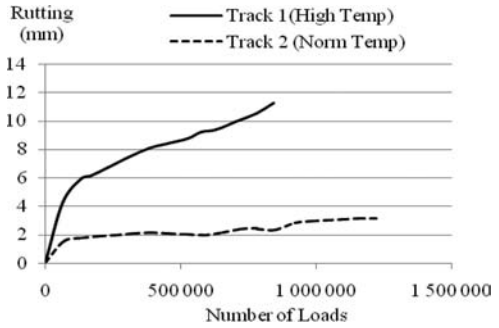

Figure 14. Averaged rutting performance after removal of the axle loads when no rutting occurred under heated trafficking.

The final rut depth at 1 million load repetitions for Track I was 11.3 mm and that of Track II was 3.1 mm.

In Figure 13, two periods where no rutting occurred (i.e., 50 to 100,000 repetitions and 200,000 to 300,000 load repetitions) during trafficking under controlled temperatures are apparent. The reason for this was not clear and was not considered important. It was decided to remove these loading periods from the analyses of the rutting performance (Figure 14). An example of a similar experience treated in a similar manner was found in the NCAT test track literature (Smit et al., 2003).

The modified data points for the two tracks are shown in Figure 15, with plotted power trend lines. Two trend lines, namely 1 and 2, were plotted on Track I. Trend line 1 was plotted by using an appropriate mathematical function. The final predicted rutting was the same as the observed line (predicted 11.1 mm at 1 million axle loads compared to observed of 11.3 mm) before the deletion of the "no-rutting" areas. As an alternative Trend line 2 was plotted on the data which gave a final rut depth of 12 mm at 1 million axle loads. It is apparent that the final rut depth is dependent on the course of events in the early trafficking life of the pavement.

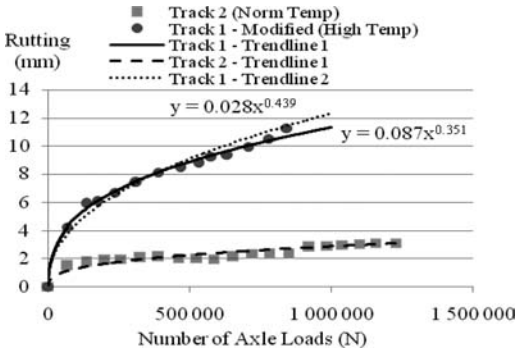

Figure 15. Averaged rutting performance based on extension of the trend line of the heated conditions to compensate for the deleted axle loads.

Wu et al. (2012) further summarized the findings as follows:

- Rutting performance on Track I was influenced by the artificially heated conditions. Two stages are apparent: (1) from 0 to about 66,000 repetitions, where the rate of rutting was 0.6 mm per 10,000 repetitions, and (2) from 66, 000 to 1 million repetitions when the rate of rutting was 0.2 mm per 10,000 repetitions.
- Less rutting was recorded on Track II due to the lower temperatures. The same to distinct periods as Track I were observed, but rates were rutting rates were 0.4 mm and 0.05 mm per 10,000 load repetitions, respectively.
- During trafficking, no fatigue cracking was observed on the surface. A forensic trench through the pavement revealed that the vertical deformation originated from the surface material's deformation and shear flow.

MMLS3 rutting profiles in terms of load applications were compiled for the four laboratory mixes and results of the SMA-13 and AC-20C mixes are shown in Figure 16. The AC-25C was not tested and was assumed to be similar to the AC-20C since this was reported to be the case with the AC-13C that was tested. It should be noted that these values reflect only downward deformation in line with regular rut definitions. This is in contrast to the peak-to-peak maximum rut values that were used as the basis of the analysis by Wu et al. (2012).

7.4 *Analyses and findings from field and laboratory APT result comparisons*

The rut information from Track I was analyzed to enable a comparison between actual full-scale rutting and MMLS3 predicted rutting from the tests on gyratory compacted specimens. Comparisons with Track II were not made due to varying pavement temperatures on this test. Ruting data of the asphalt mixes under MMLS3 trafficking were analysed by a method akin to the so-called "Direct Method" described by Huang

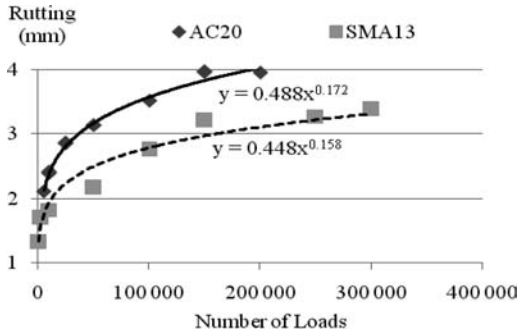

Figure 16. MMLS3 rutting profiles of SMA13 and AC-20C mixes.

Table 8. Actual vs predicted rut rates for Track 1 (mm/10,000 load applications).

Load period	Actual (mm)	Predicted (mm)
0–66,000	0.64	1.88
66,000–330,000	0.12	0.15
330,000–1,000,000	0.07	0.05
66,000–1,000,000	0.08	0.08

(1993). This approach has been used successfully in a variety of rutting studies (Hugo et al, 2011; DPG, 2008).

Two factors are relevant in this method. In principle the dynamic trafficking stress in the briquette under MMLS3 trafficking and the linear elastic stress at the midpoint of the respective asphalt layers is taken as the basis for the vertical stress correlation factor (VSCF). The other factor is the ratio between briquette thickness and the respective layers defined as the thickness correlation factor (TCF). The actual rutting under the MMLS3 trafficking, for each mix, is extrapolated by fitting a trend line to reach the anticipated design number of highway traffic axles. This is generally determined by a power function (Rutmmls). These functions are used as the basis for calculating the predicted rutting (Rut_{pred}) of the different pavement layers.

$$Rut_{pred} = VSCF \times TCF \times Rut_{mmls} \quad (1)$$

The predicted rutting for Track I was calculated by summing the first three layers, whilst bringing the rutting factors into consideration. By using the predicted rutting, a trend line was taken as the basis to predict the rutting at 1 million load repetitions. The results of the analyses are shown in Figure 17. This prediction was then compared to the adapted full-scale performance of Track I (Figure 15) in Figure 18. The rutting rates for the adapted full-scale performance and the adapted predicted performance on the basis of the MMLS3 tests were calculated as shown in Table 8.

It is apparent that the respective rutting rates matched poorly for the initial test period when most of

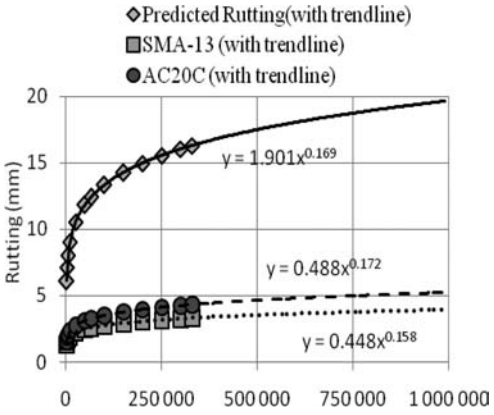

Figure 17. Performance prediction of Track I on the basis of analytical procedures using MMLS3 data.

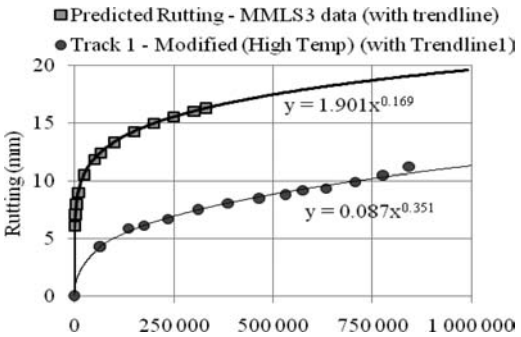

Figure 18. Comparison of the adapted rutting performance on Track I to the predicted rutting from MMLS3 laboratory tests.

the rutting occurred (i.e., 0 – 66,000). Thereafter the deformation rate trends matched relatively well during the secondary phase of rutting.

There are two possible reasons for the discrepancy in performance prediction. The MMLS3 rutting test results presented in Figure 16 show that the rut depths of the mixes after 100,000 load applications exceeded the limit of 2.4 mm for rut depth that would probably apply for the trafficking conditions prevalent at the test site according to the MMLS3 Test Protocol (DPG1.2008). This would have categorized both the SMA mix and the AC-20C mix as unsuitable. However, these results were most likely exacerbated, if not primarily caused by the temperature differences between the field and the laboratory studies discussed above. This appears to be the same conclusion reached by Wu et al (2012).

7.5 *Case study 5 conclusions*

The following conclusions are made based on the observations in this case study:

– The rutting performance predicted from the MMLS3 tests (approximately 20 mm), did not match full-scale performance (approximately 12 mm). It was concluded that the primary reason for the discrepancy was related to the differences in heated temperature of the laboratory tests (55 to 65 C) compared to those under the MLS66 trafficking (on average 53 to 56°C).
– The independent downward rutting analyses yielded comparative results that differentiated more between Track I (4 mm) with controlled heating than Track II tested at ambient temperatures (2.5 mm). This is ascribed to the differences in upward heave on Track I during early trafficking compared to Track II (Wu et al., 2012).
– The findings and related discussions on rates of rutting by Wu et al (2012), who analysed in terms of peak-to-peak rut, differ from those discussed in this paper, which focussed on downward rutting only.
– The exclusion of the 150,000 load applications that had not caused any rutting during the early trafficking phase with supplement at the end of trafficking appeared to have only minimal effect on the final rut depth (11.3 mm vs. 12 mm). This was despite the virtual increased rate of rutting during the early trafficking phase.
– The results of the rutting study with the MLS66 on Chong-ming Island provided an opportunity for further evaluation of the rutting limits set for the MMLS3 Protocol (DPG1.2008). It also served to compare “rates of deformation” under MMLS3 and MLS66 trafficking particularly during the secondary phase of rutting.

8 CONCLUSIONS FROM THE SYNTHESES OF THE FIVE CASE STUDIES

The five APT case studies discussed in this paper provided valuable information pertaining to the evaluation of performance and failure mechanisms of asphalt pavements, including:

– The results from the APT on the bridge structure demonstrated the benefit of evaluating solutions for deck surfacing prior to embarking on full-scale bridge construction.
– The case studies provided a better understanding of the benefit of APT in evaluating design procedures with materials not yet used in a region or country such as China.
– Evaluation of response of asphalt through strain measurements proved feasible with scaled and full-scale MLS APT trafficking.
– Extraordinary strains arising from slow trafficking and increased temperature in terms of longitudinal and transverse strains observed under MLS APT warrants investigation.
– Stiffness monitoring during APT and surveillance of field performance of pavements was once again confirmed as an invaluable tool.
– It is apparent that transfer of findings between different APT systems is feasible and likely to be cost beneficial.

– The beneficial use of “rates of deformation” for evaluating rutting was apparent both for full-scale and scaled APT.

ACKNOWLEDGMENTS

This paper is a collaborative international effort between the co-authors and their respective associates. The case studies report on projects that involved researchers and associated staff from different organizations and companies. Permission to use the findings and related information is appreciated. A list of project associates is given below excluding the authors. The final responsibility for the views expressed in the paper rests solely with the authors.

– CRILP APT project team: Fan Xinhua, Pr Eng, Director of Research and Development Center, Liu YunQuan, Pr Eng, Chen Qian, Assistant Engineer, and Zhang Huaizhi, Engineer, and the Shanghai Yangtze River Tunnel and the Bridge Construction and Development Co., Ltd.
– Tongji University project team: Professor Ye Fen, Professor Ling Jian-ming, Wu Jin-ting, Wang Sheng, Zhi Hong-fei, Zhao Qian-qian, Zhou Ji-zhao, Qian Jin-song, and Zhang Hua-jin.
– EMPA Filderen project team: Professor Dr Manfred Partl.
– School of Engineering, National Univ of Rosario Argentina: Eng Andrés Pugliessi, Eng MSc. Fernando Martínez, and Eng MSc Silvia Angelone.
– MLS Test Systems project team: Nic van der Westhuizen, Data Analyst and Engineer.

REFERENCES

Arraigada, M., Pugliessi, A. and Partl, M. 2012. *Initial Test Results of the New Mobile Load Simulator MLS10 in Switzerland.* Submitted for publication in APT 2012 proceedings.

DPG1. 2008.*Method for evaluation of permanent deformation and susceptibility to moisture damage of bituminous road paving mixtures using the Model Mobile Load Simulator (MMLS3*). Best Practice document developed under the auspices of the Road Pavement Forum (RPF) and approved for use and distribution at the bi-annual meeting held in Pretoria, South Africa.

Huang, Y.H. 1993. *Pavement Analysis and Design.*, New York, NY: Prentice Hall Inc.

Hugo, F., Bowker, I., Liebenberg, J. and Rossmann, D. 2011. Evaluation of Performance of Asphalt Paving Mixes under Harsh Conditions using the MMLS3, In *10th Conference on Asphalt Pavements for Southern Africa*, CAPSA.

Hugo, F, De Vos, E.R., Tayob, H., Kannemeyer, L. and Partl, M. 2008. Innovative Applications of the MLS10 for Developing Pavement Design Systems, In *Third International Conference on APT in Madrid.*

Kim, Y. and Kim, Y.R. 1997. In-situ evaluation of fatigue damage growth and healing of asphalt concrete pavements using stress wave method, *Transportation Research Record, No. 1568*, Transportation Research Board of the National Academies, pp. 106–113.

Kim, Y. 1997. *Nondestructive Evaluation of Damage Growth and Healing in Asphaltic Surface Layers Using Stress Wave Technique* Dept. of Civil Engineering, North Carolina State University.

Lee, S.J. and Kim, Y.R. 2004. Development of Fatigue Cracking Test Protocol and Life Prediction Methodology Using the Third Scale Model mobile Load Simulator, In *Fifth Intl RILEM Conference on Cracking in Pavements* – Mitigation, Risk Assessment and Prevention, pp. 29–36, Limoges, France.

Lee, N.K.J., Hugo, F. and Stokoe, K.H. 1997. Detection and Monitoring of Cracks in Asphalt Pavements under Texas Mobile Simulator Testing, *Transportation Research Record, No 1570*, Journal of the Transportation Research Board, pp. 10–22, Washington, D.C.

Lee, S.J. 2003. *Long-Term Performance Assessment of Asphalt Concrete Pavements Using the Third Scale Model Mobile Loading Simulator and Fiber Reinforced Asphalt Concrete*, PhD Dissertation. North Carolina State University.

Partl, M.N. and Arraigada, M. 2011. Der neue Mobile Load Simulator MLS10. *Strasse u Autobahn*, 62, Nr 4, pp. 252–257.

Pugliessi, A. 2011. *Relationship between Mobile Load Simulators MMLS3 and MLS10*, M Eng thesis, National University of Rosario (UNR), Argentina.

Pugliessi, A. et al. 2010. Utilización de Simuladores Móviles de Carga MMLS3 y MLS10 para el Estudio de Pavimentos, *XXXVI Asphalt Meeting Buenos Aires*, 2010.

Smit, A.dF., Hugo, F., Rand, D. and Powell, B. 2007. Model Mobile Load Simulator Testing at National Centre for Asphalt Technology Test Track, *Transportation Research Record No 1832*, Journal of the Transportation Research Board, Washington, D. C.

Wu, J. et al. 2012. *Rutting Resistance of Asphalt Pavements with Semi-rigid Base under Full-scale Trafficking of High and Normal Temperature*, Paper submitted for publication in APT 2012 Proceedings.

Part 4: Instrumentation for accelerated pavement testing

This page intentionally left blank

Advances in Pavement Design through Full-scale Accelerated Pavement Testing – Jones, Harvey, Mateos & Al-Qadi (Eds.)
© 2012 Taylor & Francis Group, London, ISBN 978-0-415-62138-0

Semi-automated crack analysis system for the Heavy Vehicle Simulator

K. Sheppard, J. Greene & B. Choubane
Florida Department of Transportation, Gainesville, Florida, US

J. White & J. Fletcher
University of North Florida, Gainesville, Florida, US

ABSTRACT: The condition of Florida roadways is documented through annual surveys conducted by the State Materials Office (SMO) of the Florida Department of Transportation (FDOT). This survey has shown that the majority of the deficient flexible pavements are due to cracking. Based on these circumstances, FDOT's Accelerated Pavement Testing (APT) program has placed a greater focus on deficiencies in the evaluation of crack development and crack resistance. As part of this effort, a computer based program has recently been developed to assist with the identification and quantification of pavement cracks from digital images. A digital camera mounted in front of the wheel carriage on the Heavy Vehicle Simulator (HVS) collects the images at regular intervals during testing to document initiation and the progression of crack development. This paper provides a description of the crack analysis system and offers an example of its use.

1 INTRODUCTION

The condition of Florida roadways is documented through annual surveys conducted by the State Materials Office (SMO) of the Florida Department of Transportation (FDOT). This survey has shown that the majority of the deficient flexible pavements are due to cracking. Based on these circumstances, FDOT's Accelerated Pavement Testing (APT) program has placed a greater focus on deficiencies in the evaluation of crack development and crack resistance. In 2005, FDOT developed an accelerated pavement aging system (APAS) to better simulate the aging effect on flexible pavements constructed for APT research. Models and laboratory tests have been developed to predict asphalt pavement cracking based on APT and laboratory research performed in Florida (Roque et al. 2002; Roque et al. 2007). Validation of pavement response models and the effectiveness/reliability of pavement design methods rely on the accuracy of distress measurements made on full-scale test sections constructed specifically for APT or in-service pavements.

To better document crack initiation and development, a camera system and computer program have recently been developed to assist with the identification and quantification of pavement cracks from digital images. A digital camera mounted in front of the wheel carriage on the Heavy Vehicle Simulator (HVS) collects the images at regular intervals during testing to document initiation and the progression of crack development. This paper provides a description of the crack analysis system and offers an example of its use.

2 OBJECTIVE

The objective of this paper is to provide information on the development of a semi-automated method to document crack initiation and development through an image-based analysis method. This method has been found to require less time than manual measurements and provides accurate representations of crack patterns, quantity of cracks, and types of cracks.

3 FDOT'S HEAVY VEHICLE SIMULATOR

FDOT uses a HVS, Mark IV to apply accelerated loading to pavement sections. The HVS is electrically powered (using a external electric power source or electricity from an on-board diesel generator), fully automated and mobile. The HVS functionality has been enhanced to include automated laser profiling and test track temperature control capabilities.

The HVS can apply wheel loads between 7 and 45 kips (using dual or wide-base single tires) at speeds of between 2 mph and 7 mph along a 26 foot test strip. The effective test segment within this test span is approximately 20 feet in length. The initial three feet and final three feet allows for acceleration and deceleration of the test wheel. Testing is typically conducted in a uni-directional mode. Tire wander can be applied if desired. A complete description of the test facility has been presented elsewhere (Byron et al. 2004). The HVS is shown in Figure 1.

Figure 1. FDOT's Heavy Vehicle Simulator.

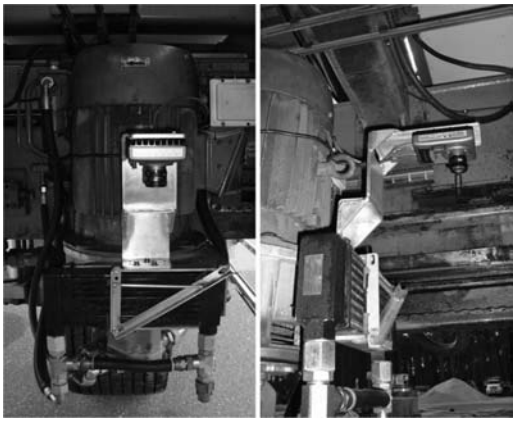

Figure 2. NI Smart Camera and bracket.

4 AUTOMATED PAVEMENT DISTRESS COLLECTION SYSTEMS IN APT

Several commercial vendors and consultants offer automated pavement distress analysis services and collection vehicles. These techniques include sophisticated sensors and analysis systems. The goal is to collect network level distress data at highway speeds and then process the data in the office. This method has gained interest over the years since risk to the pavement inspector and travelling public is minimized. Currently the most common technique to collect pavement distress data is through digital images and laser profilers. This technology can also be leveraged for APT. A laser profiler was added to FDOT's HVS in 2001 to automate rut depth measurement (Byron et al. 2005). The system includes two 16 kHz laser profilers mounted on either side of the HVS wheel. Collection of profile data can be performed in less than 15 minutes and data analysis is automated. This enhancement to the HVS has provided a highly accurate method to determine a three dimensional profile of the entire test section. Recently, a semi-automated image-based crack analysis system developed and implemented as part of HVS testing is expected to provide similar benefits.

4.1 *HVS camera system*

The camera system used for crack measurements is a National Instruments (NI) NI1742 *GigE Smart Camera* and is mounted facing downward on a custom fabricated bracket attached to the HVS load carriage. The camera has a 533 MHz built-in processor, 128 MB system memory, two gigabit Ethernet ports, 640×480 resolution (0.3 megapixel), two analog inputs and two analog outputs. The distance from the pavement and lens focal length were investigated to ensure adequate coverage of the test section width. Despite the relatively low resolution, this camera was selected for its built-in processor, data storage capability and compatibility with the current NI software used in FDOT's HVS data collection system. These features greatly assist with management of data over a limited network bandwidth. Higher resolution cameras with these features are available but were not considered at the time due to cost. The camera and custom bracket are shown in Figure 2.

4.2 *Digital image collection process*

Multiple images are necessary to capture the full test section length. To automatically collect images, the unloaded wheel carriage is moved from one end of the test section to the other at 2 to 3 mph (3 to 5 km/h). The camera includes input and output terminals that can be used to trigger the image acquisition or trigger other devices such as lights, valves, or other sensors. A proximity sensor is used to detect targets installed on the side rail of the HVS test beam and automatically trigger the camera to collect images at predefined distances. Camera scans are taken at regular pass intervals in order to monitor crack development.

All HVS data is sent over one network and traffic must be properly managed so that the network is not overloaded. The digital images are stored in a buffer on the camera and then split into smaller packets before they are sent over the network. The images are then transmitted over a wireless bridge/router to the main vehicle control unit (VCU) computer and then to the host computer inside the HVS control room for processing. The smaller packets are rejoined using another program running on the host PC inside the HVS control room and saved for further processing.

Since the camera is mounted in front of the tire, it is not possible to obtain images representing the first three feet of the test section. However, the first and last three feet of the test section are typically excluded from rut depth and crack measurements due to acceleration and deceleration of the tire at these locations. At the present time, cracks are marked with a silver paint pen or light colored crayon prior to data collection. It is anticipated that in the future, a higher resolution camera will make fully automated analysis possible.

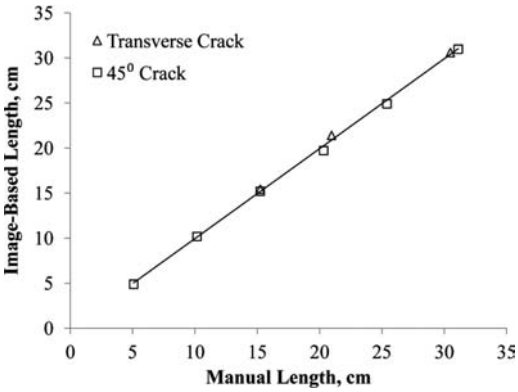

Figure 3. Comparison of manual and image measured simulated crack lengths.

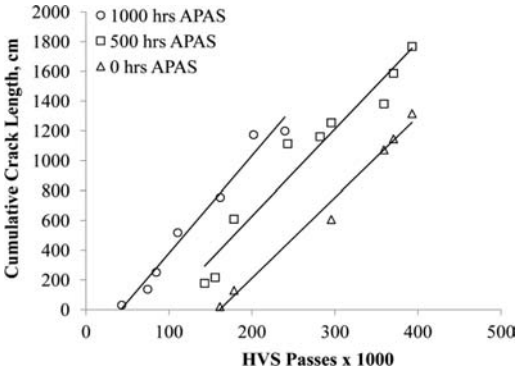

Figure 4. Crack progression due to different aging levels.

4.3 *Semi-automated crack analysis*

All device control and image processing is done using NI Vision Development software. NI software has primarily been used for data acquisition, data processing and machine control. The Vision Development software was recently developed by NI as a result of the growing need for automated inspection and image analysis. It allows for quick and efficient program development since it is a visual based programming language.

Once the images are saved to a specified location on the host computer the user can select all of the test track images that will be pieced together to form a panorama image of the tested area. During analysis the program crops the outside edges of the image so that only the applicable test track area remains. A grid of closely spaced dots of known distance was used to correct image distortion and also to programmatically transform pixel coordinates to real world units. The program applies a threshold to the image in order to detect the cracks that are manually marked before the scan is taken. The threshold identifies pixels within a defined intensity range and selects them for further processing. Since lighting is not controlled during the collection of the images the threshold is manually set by maximizing the detected pixels and minimizing spurious returns. Small objects that are smaller than a specified radius are filtered to minimize false positives. Once the threshold is selected and applied, the program recognizes detected adjacent pixels as a crack. A subroutine joins adjacent crack endpoints if the cracks are within 1 inch (25 mm) of each other and on the same axis. Finally, the positions and lengths of the cracks are determined. After processing, the image is overlaid with position and length information for each crack and the data is exported to an Excel spreadsheet. Figure 3 shows a comparison of manual and image-based measurements of simulated cracks. Lines were painted on the test track to represent cracks oriented in the transverse and 45° orientations. As the figure suggests, the image-based measurements accurately estimates the length of both sets of simulated cracks.

5 IMPLEMENTATION

Previous crack inspections of APT test sections consisted of marking cracks with a paint pen or crayon, measuring the location, length and direction of each crack and then photographing the cracks. The crack information was then manually entered into a spreadsheet. This process becomes time intensive as multiple cracks begin to develop and could be considered potentially hazardous since the inspector has to crawl under the HVS. Inspections of sections with advanced cracking often took more than 30 minutes. In the semi-automated technique, cracks are still highlighted with a paint pen or crayon but a considerable amount of time and effort required measuring the length and position of cracks is no longer necessary. Furthermore, a single panoramic image documenting the crack length and position is provided.

The semi-automated crack analysis system was first implemented during an experiment to investigate the rate of cracking due to the effect of three different aging levels. The APAS was used to apply accelerated aging to these pavement sections. The effect of aging on the asphalt material was characterized through laboratory testing and APT. As each test was initiated the test section was visually inspected for cracks in the morning and in the late afternoon. Once an initial crack was observed the camera system was used to document the crack location, length and direction. During the remainder of the test the camera system was used to analyze the crack development each morning after scheduled daily maintenance activities. At this rate, cracks were typically imaged and analyzed at increments of approximately 10,000 passes of the HVS wheel load. Several hundred thousand passes are often required for cracks to initiate and progress to a sufficient level. Figure 4 shows the crack progression developed due to different aging levels. Aging levels were defined by the total amount of time the pavement was heated to 195°F (90°C) with the APAS. Current crack initiation and propagation research has focused on establishing appropriate pavement conditioning levels in the laboratory and with the APAS to represent aging levels seen in the field. Cores showed

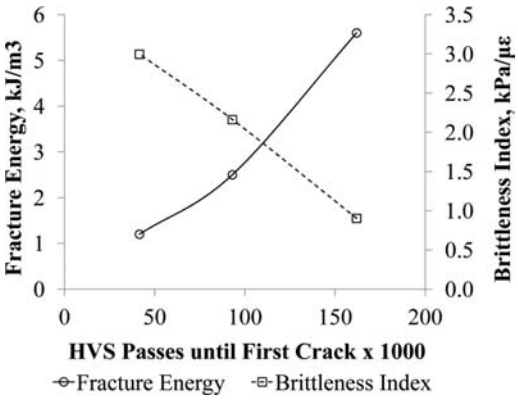

Figure 5. Material properties and crack initiation relationships.

that the cracks generated from the bottom of the asphalt and migrated to the surface. The asphalt material was 3 inches (7.5 cm) thick for all three sections. Figure 5 shows the relationships of laboratory tested material properties and the initial observations of a crack on the pavement surface. The brittleness index refers to the ratio of the asphalt mixture's indirect tensile strength and failure strain. Recent research funded by FDOT has suggested that ductile asphalt material has a brittleness index of less than 1.0 while brittle material has an index greater than 2.5 (Roque et al. 2012). Figure 6 shows a portion of the panoramic image of the test section conditioned using 1,000 hours of the APAS. The crack position and length are overlaid on the image.

6 OTHER IMAGE-BASED HVS APPLICATIONS

FDOT implemented a condition based HVS maintenance program to prevent failures and minimize downtime. The primary focus of this program has been to integrate additional sensors to the HVS to monitor its "health" and performance. Following the successful implementation of the image-based crack analysis system, research has been initiated on the use of a *Matrox GatorEye* camera to automatically inspect the test track area. The camera, shown in Figure 7, is permanently installed at one end of the HVS test beam and continuously collects images of the track. A program developed with the NI Vision Development software monitors the current test track image with a previously collected image for abrupt changes that might be the result of a fluid spill or a test track obstruction. Currently the program monitors the track for darker areas that would represent spilled fluid. Lighting of the test track is also being investigated to optimize the monitoring program. Patches of sunlight on the track throughout the day can interfere with the program's calibrations, so panels have been manufactured to help ensure standard lighting. The future goal is for the program to automatically detect significant changes in the

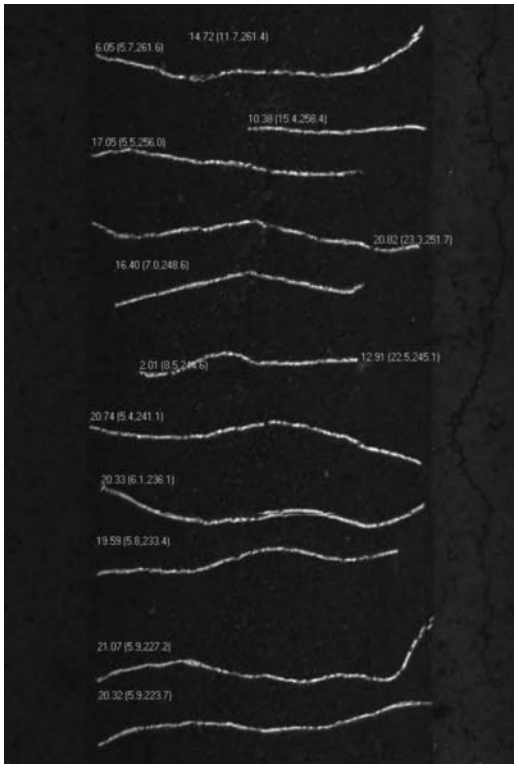

Figure 6. Processed image and information overlay.

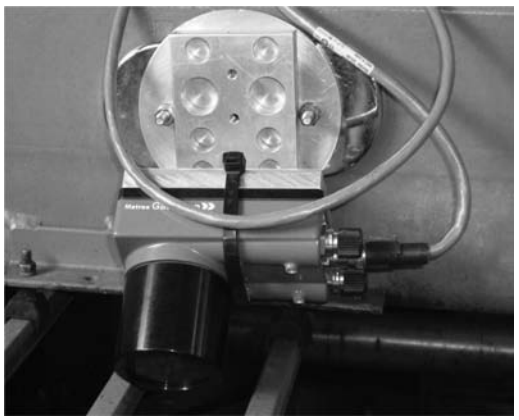

Figure 7. Matrox GatorEye camera.

test track surface and activate an audible warning to alert the HVS monitor for closer inspection.

7 SUMMARY AND RECOMMENDATIONS

FDOT has implemented an image based analysis system to document the initiation and development of cracks during APT research. The system provides a method to accurately document the progression of cracks throughout the accelerated loading period and

reduces the manpower and time required to conduct pavement inspections. Currently, cracks are still manually highlighted with a paint pen or light crayon. The crack analysis program determines the location, length, and orientation of the highlighted cracks. To eliminate manual inspection altogether, a higher resolution camera is necessary to detect unmarked cracks. It is anticipated that this process will continue to improve with time and provide more accurate and objective measurements of cracks.

REFERENCES

Byron, T., Choubane, B. and Tia, M. 2004. Assessing Appropriate Loading Configuration in Accelerated Pavement Testing. *Proceedings, 2nd International Conference on Accelerated Pavement Testing*, Minneapolis, Minnesota.

Byron T., Gokhale, S. and Choubane, B. 2005. Laser Based Technology for Automated Rut Measurement in Accelerated Pavement Testing. *CD-ROM, 84th Annual Meeting of the Transportation Research Board Compendium of Papers*, Washington DC.

Roque, R., Birgisson, B. Zhang, Z., Sangpetngam, B. and Grant, T. 2002. *Implementation of SHRP Indirect Tension Tester to Mitigate Cracking in Asphalt Pavements and Overlays.* Contract No. BA-546. Tallahassee, Florida: Florida Department of Transportation.

Roque, R., Guarin, A., Wang, G., Zou, J. and Mork, M. 2007. *Develop Methodologies/Protocols to Assess Cracking Potential of Asphalt Mixtures using Accelerated Pavement Testing.* Contract No. BD545-49. Tallahassee, Florida: Florida Department of Transportation.

Roque, R., Simms, R., Chen, Y., Koh, C. and Lopp, G. 2012. *Development of a Test Method that Will Allow Evaluation and Quantification of the Effects of Healing on Asphalt Mixture.* Contract No. BDK-75-977-26. Tallahassee, Florida: Florida Department of Transportation.

This page intentionally left blank

Advances in Pavement Design through Full-scale Accelerated Pavement Testing – Jones, Harvey, Mateos & Al-Qadi (Eds.)
© 2012 Taylor & Francis Group, London, ISBN 978-0-415-62138-0

The CAPTIF unbound pavement strain measurement system

F.R. Greenslade & D.J. Alabaster
NZ Transport Agency, Christchurch, New Zealand

B.D. Steven
Beca Infrastructure Ltd., Christchurch, New Zealand

B.D. Pidwerbesky
Fulton Hogan Ltd., Christchurch, New Zealand

ABSTRACT: The Canterbury Accelerated Pavement Testing Indoor Facility (CAPTIF) has been measuring elastic strain in unbound pavements for more than 40 years. This paper documents a brief history of the approaches used at CAPTIF, the validation of the systems, the development of the latest system which has been built on a scientific/industrial measurement platform from National Instruments (NI), and potential improvements into the future.

1 INTRODUCTION

One of the fundamental measurements that have been recorded at the Canterbury Accelerated Pavement Testing Indoor Facility (CAPTIF) is elastic strains in the subgrade and pavement. As New Zealand roads consist primarily of thin surfaced, unbound granular pavements, the sensors used for this measurement have been inductive coil sensors because the free-floating coils cause the least disturbance to the materials compared with other strain-measuring devices. The principal of operation involves the mutual inductance coupling of two co-axial sensors embedded within the subgrade or pavement layers. One of the coils is excited with an alternating current signal (transmitter coil). The other coil (receiver coil) returns an induced alternating current signal due to the magnetic coupling between them. The coupling is extremely sensitive to axial spacing and hence can be directly related to strain. CAPTIF has used and modified a variety of coil induction strain measurement systems, the first reported measurements were published in 1972 (Patterson, 1972). The following is a summary of those systems.

1.1 *Bison system*

CAPTIF started using the original 'Bison' equipment in the early 1970's. It had been developed by E.T Selig at State University of New York at Buffalo (Selig, 1969). The Bison apparatus could measure one coil pair at a time. A dial on the front of the device was used to 'null' the signal before a voltage reading was measured from an output using a voltmeter. It was flexible in that it could be used at different spacing ranges and could be used with different coil diameters. By the early 1990's, the Bison system at CAPTIF evolved to include manual switching (multiplexing) of coil pairs so that multi-coil pair installations could be measured. A Hewlett-Packard datalogger was added to record measurement values at high speed so that resilient strains could be recorded.

1.2 *Saskatchewan system*

In the mid 1990's a new coil measurement system was purchased from DDR Technologies Ltd, Saskatchewan, Canada. This system had been developed for the APT facility operated by Saskatchewan Highways and Transportation Department. It used coils produced by the Bison Company. The Saskatchewan system had some advantages. It was capable of measuring a vast number of channels by daisy chaining together more electronic modules. The system was controlled by a personal computer (PC) with software written in the "*C*" language, which could be altered to accommodate CAPTIF's specialized requirements. The oscillation frequency of the transmitter circuits was set to 150 kHz which caused a fast generation and decay of the magnetic coupling. This allowed a much faster switching time between coil pairs and therefore many coil pairs could be measured in one pass of the vehicle. A disadvantage of the system was that in order to enable the system to operate at higher frequencies each coil pair had to be tuned to that frequency. Cable lengths (6 m) were critical to achieve the 'tuned circuit' due to their capacitance. Additional tuning circuitry was necessary to achieve

the ‘tuned’ state. CAPTIF encountered a major problem with this system. The coils would tend to drift off tune during a project and therefore did not match their calibration equations. The Saskatchewan system was abandoned when the Bison Company ceased operation and production of Bison coils stopped.

1.3 *Emu system*

Around the year 2000, CAPTIF purchased the εmu system developed by Nottingham University. The εmu had manual controls and so in order to automate the system it was modified and a multiplexor system developed to allow multiple channels to be read. The multiplexor system and data acquisition was achieved with the use of *National Instruments* (NI) data acquisition cards installed inside a PC. Software was developed using NI *Labview*. The NI hardware and software proved to be both reliable and flexible.

Nottingham University provided instructions to build the εmu system and its coils so CAPTIF was no longer restricted to the use of Bison coils. The εmu system employed a more traditional approach than the Saskatchewan system and so avoided the tuning problems. The CAPTIF implementation of this system experienced electronic drift typically found with custom built electronic designs of its era. The drift did not effect the excellent capabilities of measuring resilient strains; however, it limited it’s capability to measure permanent (plastic) strains.

1.4 *CAPTIF system*

Since the NI hardware had proved reliable with the εmu system, CAPTIF decided to investigate the use of NI hardware for the coil excitation and signal conditioning. The induction process occurring in the coil pair functions in a very similar way to a common displacement sensor known as the Linear Variable Displacement Transducer (LVDT). NI produces a module (SCXI-1540) specifically for controlling and measuring LVDT’s and in 2006 this was trialed to assess whether it would be suitable for strain coils. Initially a selection of coils with different wire thickness and numbers of coil turns was tested to determine which coil design produced the best output. Once the coil selection was determined, a high grade pre-amplifier was developed to boost the signal from the receiver coil to a range that was suitable for use with the SCXI-1540. These trials were very successful. The system proved very accurate, repeatable, and stable. The stability was such that CAPTIF felt confident that the system could be used to measure permanent strains in pavement tests, which was previously not possible in previous systems because of the electronic drift.

Based on this successful trial, CAPTIF decided to develop a complete system based on NI hardware. This system comprised of an industrial NI PXI-SCXI-chassis fitted with an embedded controller running a *Microsoft Windows* operating system and NI *Labview* software.

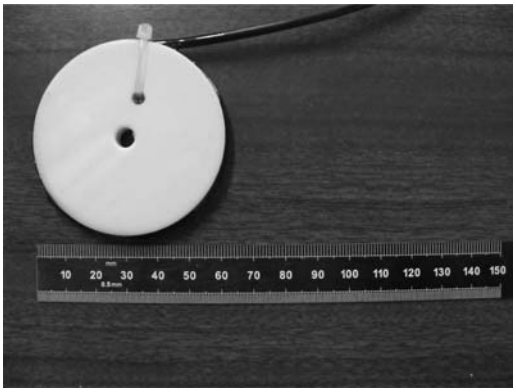

Figure 1. CAPTIF strain coil.

The chassis was also fitted with a multiplexor switch, a data acquisition card and the SCXI-1540 LVDT module. A termination panel was designed for connecting the coils and included the pre-amp circuitry. The industrial chassis and termination panels are installed in a standard industrial cabinet.

2 HARDWARE

The CAPTIF system has been developed to measure strains or displacements that occur between pairs of inductive coils that are buried within pavement layers. It can be used to measure the elastic strain generated by moving vehicles and can detect permanent strains caused by repeated vehicle loading.

2.1 *Inductive coils*

The inductive coils consist of a circular plastic disk with a groove cut into the perimeter in which copper wire is wound around to form an inductive circuit (Figure 1).

The inductive coils are used as a pair. One of the pair becomes the transmitter in which an alternating current is driven from an electronic source. This has the effect of generating an alternating magnetic flux field around the coil. The receiver coil is placed within this magnetic flux field and this causes an alternating current to be generated within the receiver coil. This phenomenon is known as mutual induction. The magnitude of the generated signal is proportional to the distance between the coils. This relationship is not linear (because the magnetic flux density gradient is not linear). The receiver coil output is measured by electronic detection circuits. Thus a pair of coils will provide a non-contact strain measuring device. The magnetic flux occurring in the coil pair can be influenced by metallic objects and external magnetic radiation. It is advisable to keep moving metallic objects at least 300 mm away. Where coils need to be placed higher in the pavement large metallic moving objects will generate an additional response in the

receiving coils which can be corrected for in later data processing.

2.2 *LVDT technology*

LVDT's are commonly used in scientific and industrial applications. The electronic technology to measure LVDT's has become very accurate and reliable. LVDT's use the same principle of operation as strain coils, therefore it is possible to use the electronic circuits that have been devised to work with LVDT's with the strain coils. The NI SCXI-1540 is an electronic module that has been specifically designed to measure LVDT's. It includes electronic circuits that generate alternating current sources for excitation of sensors as well as signal conditioning circuits for detecting alternating current signals. The SCXI-1540 is the heart of CAPTIF system.

2.3 *Hardware main components*

The CAPTIF system consists of the following components:

1. An NI PXI-1050 chassis. This is a combination chassis that is divided into two parts. The first part accepts PXI format cards. The second part accepts SCXI-format signal conditioning cards.
2. An NI PXI-8184 embedded controller, which acts as a stand alone computer. It runs a real time operating system and controls the PXI and SCXI-buses. It runs the data acquisition and control software and communicates via Ethernet connection to external computers. It has onboard memory and a hard drive.
3. An NI SCXI-1540 LVDT module (described above).
4. An NI PXI-6221 data acquisition card (DAQ), which converts the analog signal output from the SCXI-1540 to digital data.
5. An NI PXI- 2576 multiplexor to enable switching of the coil pairs to the SCXI-1540.
6. A CAPTIF designed termination panel, which provides coil cable connectors and connects via ribbon cable to the PXI-2576. It also incorporates the CAPTIF designed pre-amplifier circuit that boosts the receiver coil signal before entering the SCXI-1540.

2.4 *Hardware operation*

The transmitter coil of each inductive coil pair is routed from the termination panel via the PXI-2576 to the excitation terminals of channel zero on the SCXI-1540. The excitation signal is a 10 kHz 3.5 Vpp alternating current signal. The transmitter coil induces an alternating current signal in the receiver coil, which outputs a very small voltage in the region of 30 mVrms at 75 mm coil spacing. This signal is routed from the termination panel via the PXI-2576 back to the CAPTIF pre-amplifier on the termination panel which feeds directly into the channel zero input terminals of the SCXI-1540. The pre-amplifier has a fixed gain of 100. The SCXI-1540 has gain set to one. The output from channel zero of the SCXI-1540 is read in the PXI-6221 DAQ. The voltage range is set to ± 5 V for plastic strain measurements.

To measure resilient strains, the static-loaded coil voltage is first measured. An equivalent voltage is then applied from an analog output to the non-referenced single ended (NRSE) input on the PXI-6221. Then the dynamically loaded coil voltage is measured with respect to this NRSE input. Therefore the difference between the initial static-loaded coil voltage and the changing coil voltage generated by the transient load can be measured. Because the voltage difference is so small the range is set to ± 200 mV, which allows a much higher resolution of the very small resilient strains.

The PXI-2576 is configured to be a dual 32×1 multiplexor. This allows up to 32 transmitter coils and 32 receiver coils to be routed to the SCXI-1540. A coil pair sequence is pre-programmed into the software. The multiplexor is set to the first coil pair and a static-loaded coil voltage is measured (this is used as the reference for the resilient strain measurement). As a vehicle approaches it triggers a photo-electric sensor (SUNX VF2-RM5-3). The photo-trigger is input into the trigger terminal on the PXI-6221, which initiates a dynamic measurement to be taken. The coil pair is sampled continuously at an appropriate speed to enable a trace of the resilient strain to be recorded. Once the measurement is taken the multiplexor is set to the next coil pair. The process of taking an static-loaded coil measurement and a triggered resilient strain measurement repeats until all the coil pairs have been measured. For a 32 pair coil array this will take 32 passes of the vehicle.

2.5 *Resolution specifications*

The NI PXI-6221 employs a 16 bit analog to digital converter (DAC). The CAPTIF system utilizes the DAC in two modes. When taking a plastic strain measurement the DAC is set to an input range of ± 5 V. Therefore the calculated resolution will be $10\,\text{V}/2\hat{}16 = 152.6$ uV. At a coil spacing of 75 mm a 152 uV change in output is approximately equal to 0.009 mm. This equates to 118 microstrain. When taking a resilient strain measurement, the range of the DAQ Card is set ± 0.2 V. The calculated resolution will be $0.4\,\text{V}/2\hat{}16 = 6.1$ uV. This equates to 4.72 microstrain. However, due to electrical noise these calculated resolutions cannot in practice be achieved.

2.6 *Practical resolution*

All analog sensors and electronic devices have an inherent electrical noise, which is superimposed on the signal of interest. Electronic amplifier circuits will also amplify the noise as well as the signal. The CAPTIF system in the resilient strain measurement mode records about 5 mV of noise at a 75 mm coil spacing. In order to determine strain resolutions less than 500 microstrain it is necessary to process the data

Figure 2. CAPTIF test facility.

to remove the noise. This can be done in post processing of the captured raw data or can be done by using the inbuilt software filter. Using the inbuilt filter, resilient strains of less than 50 microstrain can typically be resolved. It may be possible with the use of more sophisticated hardware and software filtering to remove more electrical noise and get resolutions closer to the calculated hardware resolutions.

2.7 *Improvements*

CAPTIF is about to trial a higher specification data acquisition card, the NI-PXI-6289. The analog to digital converter is an 18 bit device. The calculated resolution would then be 29.5 microstrain for plastic strain measurements. The smallest range on this device is ± 0.1 V, which equates to a calculated resolution of 0.59 microstrain for resilient strain measurements. Practical limits due to electrical noise need to be considered; however, some improvement is expected. The PXI-6289 has onboard hardware filters to remove noise, which will be experimented with.

3 SOFTWARE

The CAPTIF system uses custom software to provide control, data acquisition, data storage, and communication. The software has been written using NI *Labview*. The embedded controller runs a *Windows 7* operating system. Drivers are loaded on to the controller and allow operation of the PXI hardware by the *Labview* software. The software was developed on the PXI controller and runs remotely from a PC over Ethernet.

3.1 *A typical CAPTIF project and coil layout*

The CAPTIF APT facility (Figure 2) consists of a circular concrete tank in which a pavement is constructed. The circular pavement is normally divided into six sections (Figure 3). Each section can be a different pavement material. A test machine with a rotating chassis and two loading vehicles is mounted on a central pedestal. A photoelectric beam is used on each section of pavement to act as a trigger for the data acquisition when a vehicle passes through it.

A common coil layout (Figure 4) used at CAPTIF captures strains in thee dimensions. The main

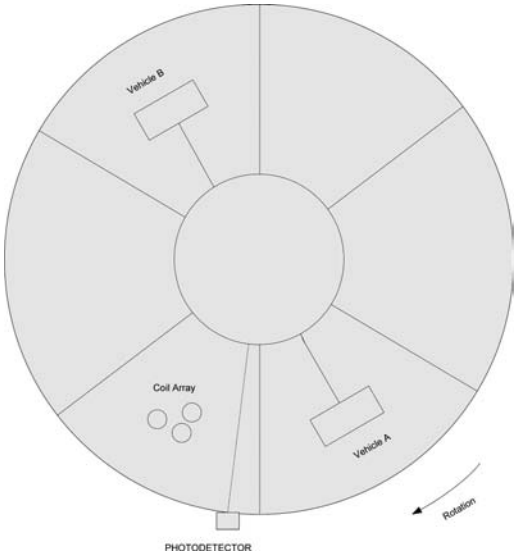

Figure 3. Plan view of typical CAPTIF pavement layout.

vertical stack has seven pairs and will extend through the basecourse and the subgrade material. Two further stacks are arranged around the main stack so that longitudinal and transverse strains can be measured. These 'side' stacks also measure the vertical strains and act as a check against the main stack. Each section of the pavement will contain at least one of these arrays and measurements will be triggered by a specific photo-detector for that array.

3.2 *Software programs*

CAPTIF has developed three software programs for the system. All programs access a pre-configured layout file. This file is resident on the hard disc drive and has all the information pertaining to the coil pair array. It includes a unique pair number, the transmitter and receiver coil numbers, and what multiplexor circuits they are connected to.

3.2.1 *Calibration software*

This software is used for calibrating the coils and is used with the coil calibration jig (Figure 5). A pair is selected from the layout file and then measurements are recorded at pre-determined coil spacings (Table 1). The relationship between the coil spacing and voltage output is logarithmic and the software calculates a calibration equation that takes the form:

$$y = \ln(x) + b \tag{1}$$

where: y = mm, and x = volts (Figure 6).

3.2.2 *Static strain software*

This software is used to log plastic strain measurements from the coil sensors. It is normally left running continuously during the life of the project. At a pre-determined lap or time interval a sequence is initiated whereby all the coils in the array are measured

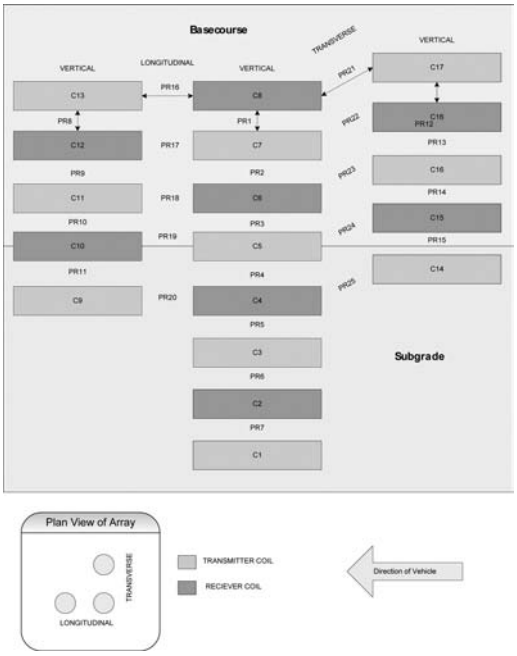

Figure 4. Cross section of coil array used at CAPTIF.

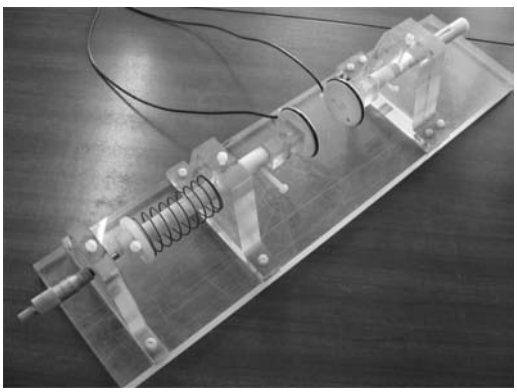

Figure 5. Jig used to calibrate the strain coil pair.

and recorded. A plot of displacement values with load cycles at each coil pair (Figure 7) is produced with the data.

3.2.3 *Dynamic strain software*

This software records the resilient strains caused by separate loading events and has been designed to suit the operation of the CAPTIF test track facility. A typical resilient strain record for a single coil pair is shown in Figure 8. In this case the coil data has been directly converted to displacement (mm) and data has been captured as a trace of 4,000 samples at a sampling frequency of 3,000 samples/sec.

The user has control over a number of parameters:

- **Rate**: This is the number of samples per second that the data acquisition system will record. A higher sampling rate gives a higher temporal resolution to the event.
- **Samples per channel**: Sufficient samples must be recorded to capture the whole transient event.

Table 1. Typical calibration data.

Date:	12/09/2010		
Pair:	S		
tx coil no:	1		
rx coil no:	2		
plane:	V		
tx mux:	19		
rx mux:	52		
80	3.4293		
78	3.6624		
76	3.9172		
74	4.1955		
72	4.5003		
80	3.4286		
78	3.6623		
76	3.9165		
74	4.1950		
72	4.4989		
80	3.4274		
78	3.6635		
76	3.9181		
74	4.1973		
72	4.5010		
Cal curve equation $mm = A\ln(X) + b$			
A:	b:	scale:	residue:
−29.286	116.029	0.01902	0.0014

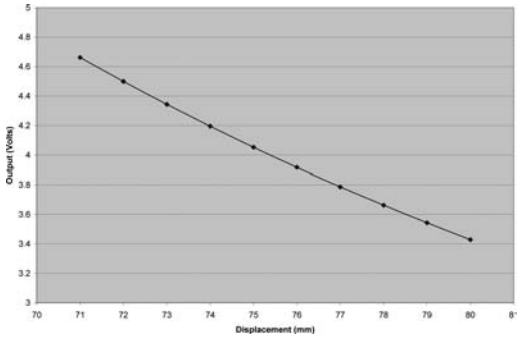

Figure 6. Typical calibration curve.

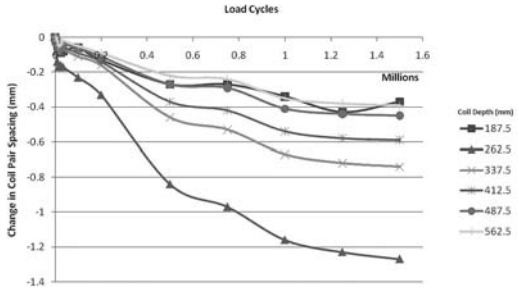

Figure 7. Load cycles vs. change in coil pair spacing at coil pair mid points.

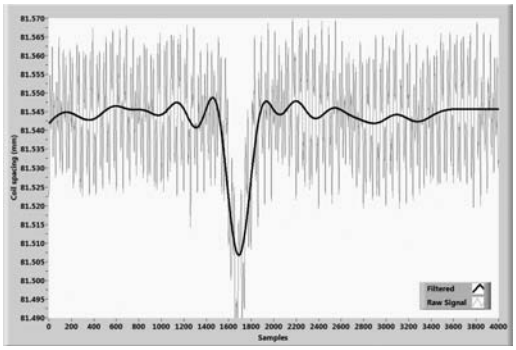

Figure 8. Output from dynamic strain software.

- **Start delay**: A time delay is normally entered so that recording does not start immediately after the photo-detector has been triggered. This vehicle takes a finite time to reach the coil array after passing through the detector. Data collected during this passage would be redundant.
- **Laps**: The number of vehicle laps to record in the data file.
- **Input range**: Enables selection of high or low resolution.
- **Use photo-trigger?**: The data capture can be initiated by a photo-trigger or a software trigger.
- **Save**: Saves the data to a file
- **Filter**: Employs a software filter to remove unwanted noise. This filter applies a 16th order Butterworth filter with a pass-band of 0.45 Hz to 10 Hz. It is only used in this case to smooth the data for viewing. The un-filtered data is saved to file for later processing by the project researchers.

The dynamic strain software operates as follows:

1. The setup parameters for the test are entered on the front panel.
2. The vehicle is run up to the required speed.
3. The software is 'RUN'.
4. The software loads the coil layout file.
5. The software switches in the first pair of the array.
6. The software waits for a trigger.
7. Data is acquired for that pair.
8. The software plots a graph of the coil voltage measured.
9. The software then switches to the next coil in the layout file and waits for a new vehicle trigger.
10. The process is repeated until all the coil pairs have been tested.
11. The full set of coils will be tested again a number of times according to the number of LAPS set.
12. A data file is stored on the hard disk.

The data file is stored on the PXI machine disk. The data is the raw displacement (mm) measured from each coil pair. A peak strain value is also calculated and recorded.

The dynamic strain software is run at predetermined 'lap intervals' during the life of the project.

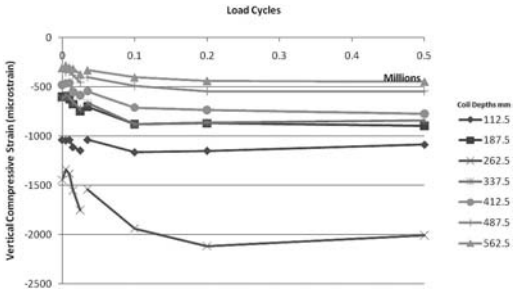

Figure 9. Load cycles vs. peak vertical strain at coil pair mid points.

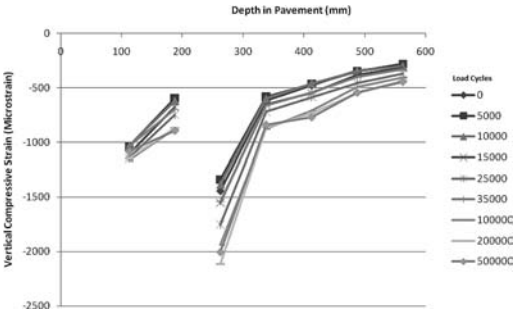

Figure 10. Depth vs. peak vertical strain at varying load cycles.

After the resilient strains have been recorded the dynamic strain software is stopped and the static strain software is set running again to record the plastic strains.

Figure 9 presents the peak vertical compressive strain for a stack of coils during the early stages of a project. The break in readings at 35,000 cycles indicates where a thin surface was applied and the load on the vehicles was raised from 40 kN to 50 kN.

A more traditional plot of strain with depth is presented in Figure 10. The brake in the plot illustrates the change from the unbound basecourse layer to the subgrade layer.

4 VALIDATION

4.1 *Static strain validation with profilometer*

Figure 11 presents a comparison of the change in coil spacings against vertical surface deformation (VSD), which was measured on the pavement surface with a transverse profile beam. There is a strong relation between the surface measurements and the coil changes, as expected. The relationship is not one to one because the coil pairs do not extend fully to the bottom of the concrete tank (pavement boundary), do not extend fully to the surface of the pavement, and are slightly offset from the peak VSD reported.

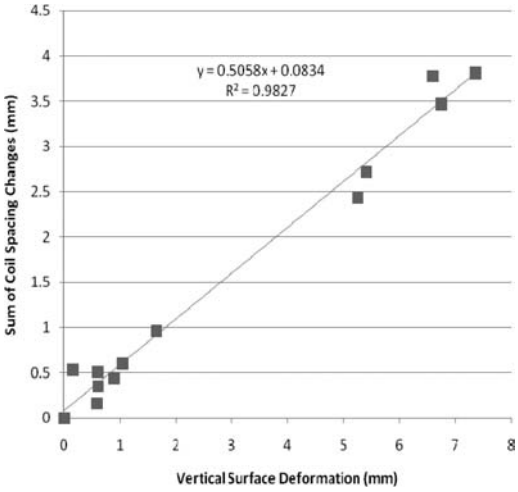

Figure 11. Vertical surface deformation vs sum of coil spacing changes.

4.2 *Dynamic strain (Emu system) validation with surface deflectometer and Falling Weight Deflectometer (FWD)*

In order to verify the accuracy of the εmu soil strain system, the measured strains were integrated over the depth of the pavement and compared against the surface deflections measured with the CAPTIF Deflectometer (a modified Benkelman beam with continuous deflection readout) and a Dynatest FWD (Steven, 2005). In order to reduce the effect that the vehicle speed might have on the results, the strain data for comparing the deflectometer results was captured when the loading vehicles were moving at a steady speed of 6 km/h over the coils. The strain data for the FWD results was captured as the FWD was dropped over the coils. The pavement response was measured under three different loading configurations for the deflectometer check and under four different drop heights for the FWD check. These checks were done on the pavement constructed for the CAPTIF PR3-0404 research project after the application of 600,000 load cycles. The pavement construction was 25 mm asphalt wearing course over 275 mm premium aggregate basecourse over silty subgrade with a California Bearing Ratio of 10%. In order to integrate the measured strains over the full depth of the pavement, several assumptions were made to account for the sections of pavement that were not monitored by the soil strain system. These assumptions were:

– To calculate a linear regression for the basecourse strains, the resulting line of best fit was extrapolated to the top of the basecourse and to the basecourse/subgrade interface. A linear extrapolation was chosen because the strains measured at the three depths showed that the strains varied linearly with depth;

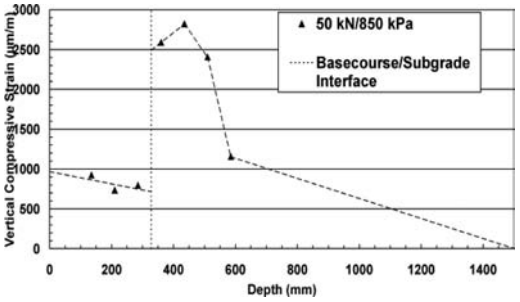

Figure 12. Strain profile at Station 9 for 50 kN/850 kPa wheel load at 6 km/h, PR3-0404 pavement.

– There was zero strain in the thin asphalt concrete layer. This layer was 30 mm thick, therefore any compression of the layer would be small compared to the overall deflection/compression of the pavement structure;
– To fit a straight line to the top two strain points in the subgrade and to extrapolate this line up to the basecourse/subgrade interface to determine the strain at the top of the subgrade, and
– The strain decreased at a constant rate from the measured value at lowest coil pair to a value of zero at the bottom of the pavement tank (1,500 mm).

The different steps in the computations carried out to integrate the strains are detailed below:

1. The as-constructed thicknesses of the asphalt concrete and basecourse layers were determined from the construction records.
2. The actual strain coil depths below the surface were calculated from the construction records.
3. A straight line was fitted to the basecourse strains (three values) using a least squares method. The fitted line was extrapolated to the asphalt concrete/basecourse and basecourse/subgrade interface depths in order to determine the basecourse strains at the top and bottom of the basecourse layer.
4. The extrapolated basecourse strains were integrated over the thickness of the basecourse layer to calculate the compression in the basecourse layer.
5. A straight line was fitted to the top two strain points in the subgrade and this line was extrapolated up to the basecourse/subgrade interface to determine the strain at the top of the subgrade.
6. The subgrade strains were integrated over the gauge length of the coil pairs and summed to calculate the compression in the subgrade layer.
7. The calculated deflections were compared with the measured deflection from the loading vehicle or FWD.

A representative plot of the strain versus depth and the lines that are fitted to the strains is shown in Figure 12. The area under the dashed line is calculated in order to determine the surface deflection. A summary

Table 2. Results from strain integration calculations for a rolling wheel.

Station 9			
Load/Pressure (kN/kPa)	40/650	40/850	50/850
Integrated deflection (mm)	1.155	1.205	1.388
Deflectometer deflection (mm)	1.065	1.098	1.281
% Difference	8.5%	9.8%	8.4%
Absolute difference (mm)	0.090	0.107	0.107
Station 23			
Load/Pressure (kN/kPa)	40/650	40/850	50/850
Integrated deflection (mm)	1.139	1.161	1.349
Deflectometer deflection (mm)	1.167	1.146	1.310
% Difference	−2.4%	1.3%	3.0%
Absolute difference (mm)	−0.028	0.015	0.039
Station 37			
Load/Pressure (kN/kPa)	40/650	40/850	50/850
Integrated deflection (mm)	0.855	0.860	1.039
Deflectometer deflection (mm)	0.710	0.686	0.805
% Difference	20.5%	25.3%	29.0%
Absolute difference (mm)	0.145	0.174	0.234

of the calculations for the strain/deflections measured by the deflectometer is shown in Table 2.

The calculated results for Stations 9 and 23 are within the range of −2.4 to +9.8% of the measured values. This is considered an acceptable result given the various assumptions that were made. The calculated results for Station 37 show a greater variation against the measured values, with calculated values ranging from 20.5 to 29.0% of the measured values. A possible reason for the bigger percentage difference for the Station 37 results is that the actual deflection and strain values are lower than the other two stations (approximately 0.73 versus 1.18 mm and 1,151 versus 2,355 and 3,960 microstrain for the average strains at the top of the subgrade), and any inaccuracies in the assumptions will have a bigger effect on the computed deflections.

The same procedure was followed for the FWD measurements. In this test, the FWD weights were dropped from four different heights and the response of the strain coils was recorded for each drop height. The FWD contractor carried out the testing in two visits to the CAPTIF facility. Due to other work requirements, the contractor was required to use two different FWD machines for the two visits, even though the visits were only three days apart.

A summary of the calculations for the strain/deflections measured by the FWD is shown in Table 3. The deflections obtained by integrating the strains from the FWD loading show a greater difference with the deflections measured by the FWD device. For this comparison, the differences are up to 25%, although most (13 of 16) of the differences are 15% or less and 14 of the 16 measurements have differences that are less than 0.150 mm.

In conclusion, these measurements show that the strains measured by the εmu soil strain system are realistic, and that they can be verified against an independent measurement method.

Table 3. Results from strain integration calculations for the FWD.

Station 9 (FWD A)				
FWD load (kN)	25.3	33.2	51.8	71.7
Integrated deflection (mm)	0.735	0.947	1.369	1.773
FWD deflection (mm)	0.642	0.837	1.200	1.426
% Difference	14.5	13.1	14.1	24.3
Absolute difference (mm)	0.093	0.110	0.169	0.347
Station 23 (FWD A)				
FWD load (kN)	23.8	31.2	48.3	67.6
Integrated deflection (mm)	0.624	0.808	1.219	1.556
Deflectometer deflection (mm)	0.578	0.765	1.184	1.413
% Difference	8.0	5.7	3.0	10.1
Absolute difference (mm)	0.046	0.043	0.035	0.143
Station 9 (FWD B)				
FWD load (kN)	20.3	42.5	57.1	70.8
Integrated deflection (mm)	0.603	1.129	1.424	1.658
Deflectometer deflection (mm)	0.502	1.023	1.324	1.550
% Difference	20.1	10.3	7.5	7.0
Absolute difference (mm)	0.101	0.106	0.100	0.108
Station 37 (FWD B)				
FWD load (kN)	20.4	42.7	57.5	71.3
Integrated deflection (mm)	0.473	0.811	1.034	1.216
Deflectometer deflection (mm)	0.359	0.713	0.899	1.067
% Difference	31.8	13.7	15.0	13.9
Absolute difference (mm)	0.114	0.098	0.135	0.149

5 CONCLUSIONS

CAPTIF has used, evaluated and modified various strain coil systems over many years. Each system has provided useful and appropriate data according to the state-of-the-art technology of the day. This data has been validated with data output from other measurement devices. Some coil systems proved better suited for resilient strains and others for plastic strains. CAPTIF's new system, using 'off-the-shelf' electronic modules has excellent stability and resolution. It provides the best performance to date for combined resilient and plastic strain measurement.

ACKNOWLEDGMENTS

The authors acknowledge specific input from Alan Fussell, and Frank Adams who installed the system at the CAPTIF facility. The authors also gratefully acknowledge New Zealand Transport Agency for funding the CAPTIF project.

REFERENCES

Patterson,W.D.O. 1972. *The measurement of Pavement Deformations using Induction Coils.* Road Research Unit, National Roads Board, Wellington, New Zealand.

Selig, E.T. 1969. *A New Technique for Soil Strain Measurement.* State University of New York, Buffalo, NY.

Steven, B.D. 2005. *The Development and Verification of a Pavement Response and Performance Model for Unbound Granular Pavements.* PhD Thesis, University of Canterbury, Christchurch, New Zealand.

Advances in Pavement Design through Full-scale Accelerated Pavement Testing – Jones, Harvey, Mateos & Al-Qadi (Eds.)
© 2012 Taylor & Francis Group, London, ISBN 978-0-415-62138-0

Detection of debonding and vertical cracks with non destructive techniques during accelerated pavement testing

J-M. Simonin, V. Baltazart, P. Hornych, J-P. Kerzrého, X. Dérobert,
S. Trichet, O. Durand, J. Alexandre & A. Joubert
LUNAM Université, IFSTTAR, Bouguenais, France

ABSTRACT: This paper presents an experiment conducted on the pavement fatigue carrousel of IFSTTAR. Several defects (debonded areas or transverse vertical cracks) were intentionally incorporated during construction. Before the start of the loading planned in March 2012, different non-destructive test techniques were used to detect and locate these artificial defects. Two different electromagnetic wave techniques were tested: Ground Penetrating Radar (GPR) with horn or coupled antennas and a higher frequency system (step frequency radar). Deflection basin measurements with a Falling Weight Deflectometer (FWD) were also taken. Another technique based on Frequency Response Function (FRF) in intermediate frequency domain (100–10,000 Hz) to detect and locate the defects showed interesting results. Further measurements will be made with these different techniques during the experiment to assess the evolution of the defects. It will also allow comparison of the ability of each technique to detect such damage, to precisely quantify their limits of application, and to optimize the survey process of roads.

1 INTRODUCTION

The French road network mostly completed more than 30 years ago, and consists mainly of old bituminous pavements. Some of them have also been maintained several times with thin overlays (less than 8 cm thick). On these pavements, considerable damage such as potholes and alligator cracking has been observed in recent years, in particular after periods of heavy rain or freeze/thaw. Frequently, this type of damage is assumed to be associated with moisture effects linked to interface debonding between the overlays and the old pavement. These debonding mechanisms have a large influence on the residual life of the pavement, and thus their early detection is a very important issue for pavement maintenance (Savuth, 2006).

To detect such interface damage, selected non-destructive techniques (NDT), such as electromagnetic techniques (ground penetrating radar, step-frequency radar, or infra-red) or mechanical techniques (from static deflection and radius of curvature measurements to seismic wave propagation methods), appear as promising approaches. They could also be efficient to detect and survey internal cracks.

This paper compares measurements with different NDT to detect and locate debonding and internal cracks, performed before the start of an experiment carried out on the large pavement fatigue carrousel of IFSTTAR in Nantes. These techniques will be used to survey the roadway during the planned loading phase.

2 DESCRIPTION OF THE FULL SCALE EXPERIMENT

2.1 *Description of the accelerated testing device*

The pavement fatigue carrousel of IFSTTAR (Figure 1) is a large scale circular outdoor test facility, unique in Europe by its size (120 m long) and loading capabilities (maximum loading speed of 100 km/h equating to a loading rate of one million cycles per month). Different to most ALT equipment, it is able to test pavements to failure in a few weeks. The machine comprises a central motor unit and four arms that can be equipped with different wheel configurations. The circular test track can be divided into several different test sections, loaded simultaneously. The width of the test track (6 m) allows for the application of traffic loads on the same track at two different radii.

2.2 *Description of the test site*

This study is part of a full scale experiment started on the test track in March 2011, investigating low traffic pavements with two different thicknesses of asphalt layer, namely 8 cm and 14 cm. A quarter of the fatigue test track has been dedicated to this study (Sector B). This 25 m long pavement section, consists of two bituminous layers (8 cm thick base layer, and 6 cm thick wearing course), over a granular subbase. Several types of defects were intentionally incorporated into the base layer or at the interface between the

Figure 1. The pavement fatigue carrousel at IFSTTAR.

two asphalt layers. A vertical crack was also included in a hydraulic pavement on another sector. The vertical crack was made by sawing the hydraulic base layer, and then covering it with a new 4 cm thick bituminous overlay.

The experiment will be performed in two parts. The first part consists of loading the outer radius (19 m), during 1.2 million load cycles (Hornych et al., 2012). This first part of the experiment is outside the scope of this paper, and concerns mainly the testing of pavements with geogrid reinforcement. The second part will start in the spring of 2012, and will consist of loading the inner radius (16 m), where the section with defects is located. Before the start of the loading on the inner radius, different non destructive techniques were performed to evaluate the initial state of the pavement, and to evaluate the capacity of the equipment to detect the defects. The results of these initial tests are presented in this paper. Similar tests will be performed during the accelerated test, to characterize the state of the different defects after different numbers of loads, until the failure of the pavement.

2.2.1 *Material characteristics and pavement construction*

The pavement structures were built on the existing subgrade of the test track, which is sand with 10% fines, and sensitive to water. The modulus of this subgrade is approximately 70 MPa.

The structure built on this subgrade includes the following layers:

- A granular subbase consisting of 30 cm of 0/31.5 mm unbound granular material (UGM). After construction, this base was covered with a spray seal.
- A bituminous base layer, consisting of 8 cm of road base asphalt material (RBA) (0/14 mm grading).
- A bituminous wearing course, consisting of 6 cm of bituminous concrete (BC) (0/10 mm grading).

The main characteristics of the bituminous materials are given in Table 1. Complex modulus tests on trapezoidal specimens (NF EN 12 697-31 2008) were performed on the two bituminous mixes. The standard elastic moduli obtained for the two materials at 15°C and 10 Hz are also given in Table 1.

Table 1. Composition and characteristics of the bituminous mixes.

Fractions	BC (Class 2)	RBA (Class 3)
0/2 (%)	29.3	32.47
2/6 (%)	25.52	19.1
6/10 (%)	38.75	9.55
10/14 (%)	–	33.43
Filler (%)	0.95	0.95
Bitumen 30/50 (%)	5.5	4.49
E Modulus (MPA)	11,320	12,670

Table 2. Different defects and characteristics introduced into test track.

Defect zones	Type	Dimensions, m (length × width) (m)	Position, m, R = 16 m along radius
I-1	sand	0.5 × 2.0	2.5, 3.0
I-2	geotextile	0.5 × 2.0	3.5, 4.0
I-3	tack coat free	0.5 × 2.0	4.5, 5.0
I-4-I-9	geotextile	0.5 × 0.5	6.5, 9.0
I-10	geotextile	3.0 × 1.0	9.5, 12.5
I-11	sand	1.5 × 2.0	13.5, 15.0
I-12	geotextile	1.5 × 2.0	17.0, 18.5
I-13	tack coat free	1.5 × 2.0	20.5, 22.0

2.2.2 *Debonded interface*

The construction of the pavements was carried out by a road construction company, using standard equipment. Rectangular debonded areas of different size and longitudinal or transversal direction were created artificially, using different techniques (sand, plastic film, or absence of tack coat) and are summarized in Table 2. They are located at the interface between the two bituminous layers. Figure 2 presents a photograph of the debonded areas before the wearing course construction.

The debonded areas I-1, I-2 and I-3 are 2 m wide and 0.5 m long, and centered on the radius of 16 m. I-4 to I-9 are small defects, 50 × 50 cm, with a geotextile interface, located in and outside the wheel paths. I-10 is a 3 m long by 0.5 m large defect, centered in the wheel path. I-11 to I-13 are bigger debonded areas, 2 m wide by 1.5 m long, with different types of interface (sand, geotextile or without tack coat).

Figure 3 shows a map of the experimental section, with the location of the different defects. These defects were centered on the radius R = 16 m, which corresponds to the centre of the wheelpath when the pavement is loaded. The total width of the wheelpath (with lateral wandering) will be approximately 1.0 m (between 15.5 m and 16.5 m).

2.2.3 *Artificial cracks*

A transverse vertical crack was introduced by sawing in another sector of the test track, where an

Figure 2. Interface defects before wearing course construction.

older pavement structure was retained from a previous experiment (Figure 4). The structure included the following layers:

- 20 cm of a granular subbase of 0/20 mm unbound granular material;
- Part of an old bituminous base layer, consisting of 4 cm of Road Base Asphalt Material (0/14 mm grading);
- A base layer consisting of 13 cm of a Fiber Reinforced Cement Concrete (FRCC);
- A bituminous wearing course consisting of 4 cm of bituminous concrete (0/10 mm grading).

The wearing course was milled off in a square area of 2 m by 2 m. The FRCC base layer was then sawed

Figure 4. Sawing of a transverse vertical crack inside the fiber reinforced cement concrete layer.

with a 2.5 mm thick disk to a depth of 40 mm. Finally, a new wearing course was laid on this area to cover the internal crack. Other vertical cracks may be created during the experiment.

3 PAVEMENT INVESTIGATION

The main objective of the experiment is to compare different NDT techniques (FWD, inclinometer, Colibri, radar) used to detect different geometrical characteristics of artificial defects. Other objectives are to follow the evolution of the defects during loading, and to evaluate their effect on pavement performance. This will be helpful in optimizing pavement monitoring with the different NDT methods.

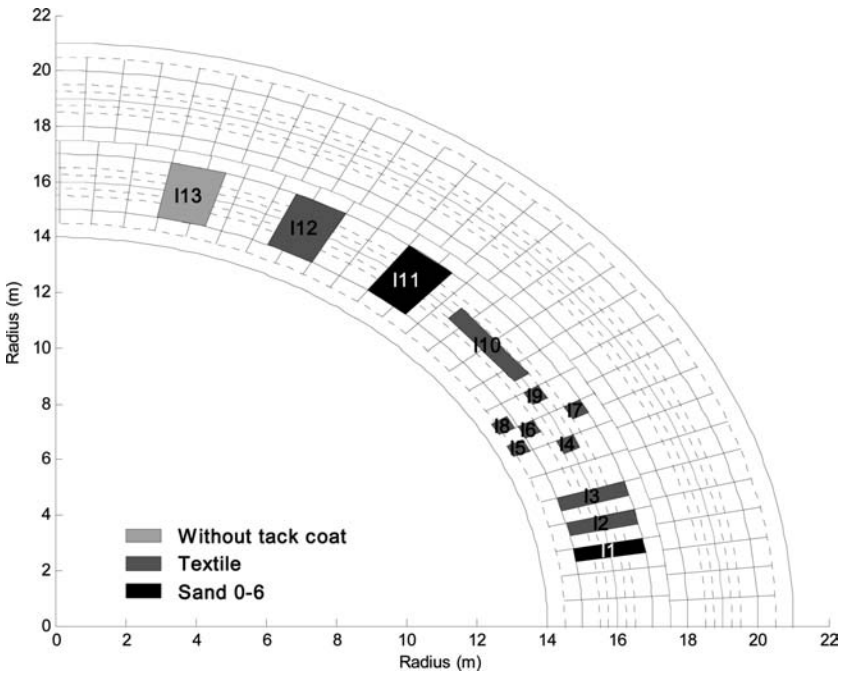

Figure 3. Map of the different debonded areas in sector B.

It is planned to:

– Characterize the initial state of the pavement (these results are presented in this paper).
– Repeat the NDT tests after different load levels:
  - After 10,000 loads, when the structure is consolidated;
  - After 50,000, 100,000 and 150,000 loads to survey the structure;
  - When visual surveys indicate the start of distress in the structure (e.g., cracking, rutting).
– Analyze in detail the final state of the pavements, using NDT tests, and also by coring and excavation of trenches, to compare the actual state of the pavement with the NDT results.

The structure will be investigated using the following methods:

– Three radar devices: two classical with a coupled 2.6 GHz antenna and a Horn 2.0 GHz antenna, and a step frequency radar which uses a network analyzer;
– The Colibri apparatus, which is based on the frequency response function (FRF) presented below;
– FWD tests, to estimate deflection basins under a dynamic load;
– Inclinometer measurements, to estimate the radius of curvature of the deflection basin under a rolling load.
– Benkelman beam, to measure the deflection basin under a rolling load.

The project will also consider evaluating other NDT methods used in civil engineering such as impact echo, pulse echo, wave propagation, infra-red methods, if available technically feasible.

3.1 *Radar probing techniques*

Over the past few years, radar systems have emerged as a powerful non-destructive testing (NDT) technique for pavement surveys (Scullion, 1995; Saarenketo, 2000; Cardimonda et al., 2003; FHWA, 2010) including assessing defects such as segregation, stripping, and cracking (Forest, 2004). Radar systems have several major advantages, such as a high data acquisition rate and global monitoring through quasi-continuous measurements. Radar systems take advantage of the penetration capability of electromagnetic (EM) waves to image any dielectric contrast within the subsurface. Within the scope of this paper, the capabilities of the two existing radar techniques (i.e., pulse and step-frequency radar) are compared on a qualitative basis to detect debonding embedded in the pavement section.

3.1.1 *Radar measurement principle*

As shown in Figure 5, the transmitting antenna (Tx) sends a radar wavelet into the medium. Scattered echoes are generated by any dielectric contrast within the medium and propagate back to the receiving antenna (Rx). The vertical structure of the pavement,

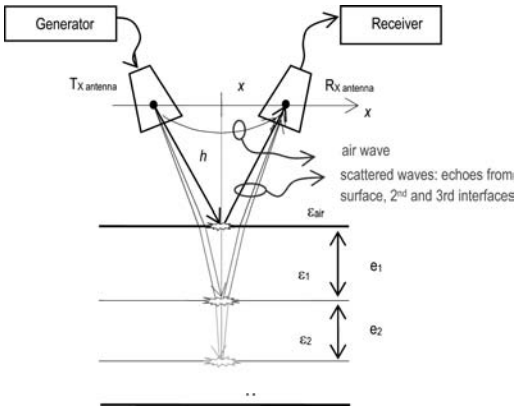

Figure 5. Radar principle and antenna configuration: The zero-offset mode is the conventional radar configuration for pavement survey, when Tx and Rx antennas are co-localized at x=0; CMP radar configuration consists in moving Tx and Rx apart at different x values (multioffset).

which provides a horizontally stratified medium, can then be measured by the radar data through echo detection and amplitude analysis. At vertical incidence, defining Δt_1 and v_1 as the travel time and the wave velocity, respectively, the thickness of a pavement layer is given by the following equation:

$$e_1 = v_1 \, \Delta t_1 / 2 \tag{1}$$

Radar techniques typically require some core samples of the pavement structure to determine the wave speed v_1, with respect to the light speed c_O. However, further amplitude analysis of successive echoes enables the use of a coreless technique for which, the wave speed v_1 is retrieved from the echo amplitudes A1 and A0, associated with the top surface echo amplitude and the amplitude of the Tx pulse, respectively, according to:

$$v_1 = c_o \left(\frac{1 - A_1/A_0}{1 + A_1/A_0} \right) \tag{2}$$

Radar data consists of vertical profiles of electromagnetic wave amplitudes (or A-scan) recorded at each location along the track. The data vectors collected along the track are gathered into a data matrix which is called the B-scan image.

For detection purposes, data processing mostly aims at selecting the maximum echoes from the vertical profile (signal amplitude) and at performing accurate time delay estimation. Layer thickness estimation is based on the time delay of primary echoes.

3.1.2 *Application to debonding*

For the analysis of radar signals, a debonded interface is considered as a thin layer with different electromagnetic properties. A major limitation of radar techniques remains in the size and thickness of this interface with

respect to the wavelength as well as the time resolution. When the thickness of the defect is greater than about half of the wavelength, (Derobert, 2004), two separate echoes are generated, and the thickness of the defect can be determined using Equation 1. When defects are thinner than this limit, as is the case in this experiment, the two echoes overlap each other, merging into an apparent single echo with longer time duration. According to (Gregoire, 2001), thickness up to a tenth of the wavelength of the GPR pulses can still be detected provided that accurate waveform analysis at high signal to noise ratios can be completed. The advanced signal processing techniques which have been used to perform UTAS (ultra thin asphalt surface) pavement survey in (LeBastard et. al., 2007) may overcome the latter limitation by an additional approximate factor of four.

Classical data processing used to date to detect debonding in pavements consists of performing an amplitude survey of the echo attached to the interface between the wearing course and the base layer (Simonin et al., 2012). Any spatial variation of that echo amplitude along the radar profile (Bscan) with respect to an intact zone would reveal debonded areas. As shown in Section 3.1.4, the shorter pulses provided by the step-frequency radar enhances the amplitude variations due to overlapping echoes.

3.1.3 *Pulse and step-frequency radar technologies*

Impulse radar was the first technology used in the GPR community. The pulse is usually a Ricker-type with a smooth spectrum and without any zero within the bandwidth, as shown in Figure 6 (bottom). In the 1990s, step-frequency technology enabled larger bandwidth and better measurement flexibility. Based on a network analyzer, the Tx antenna successively radiates monochromatic waves (i.e., one single frequency at a time) into the road pavement. The received signal is synthesized in the time domain by an inverse Fourier transform. Network analyzers have increased in speed and some commercial step-frequency radars are now able to collect data at traffic speeds. Moreover, step-frequency technology has moved a step further by providing surface probing capability thanks to array antenna technology and appropriate processing.

For the experiment, Tx and Rx antennas were set 20 cm apart and located 40 cm above the pavement surface. Both systems have roughly the same footprint on the pavement surface, i.e., the same spatial integration on the surface. A 2.6 GHz ground-coupled GSSI antenna was also used for qualitative comparison. The ground-coupled configuration insures better signal to noise ratio and allows finer spatial resolution.

The first system uses GSSI impulse radar with 2 GHz air-coupled antennas. The antennas are fixed to a trolley which is manually moved. A fine spatial sampling is achieved (40 profiles per meter) and is controlled by a survey wheel. A B-scan profile was recorded along the radius 16 m (Figure 7a).

The second system is a step-frequency within a bandwidth of 0.7 to 7.4 GHz and uses Vivaldi Rx and

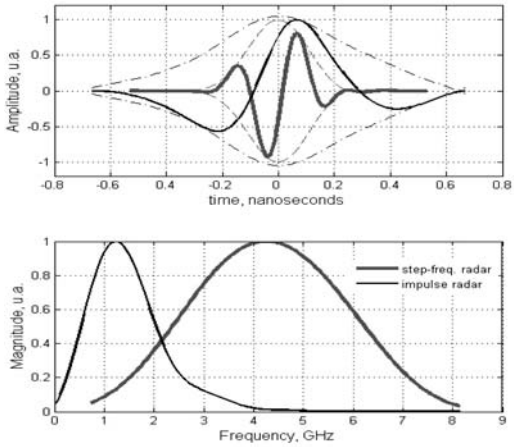

Figure 6. Measured radar pulses in both the time (top) and the frequency domains (bottom) for the two radar systems, i.e., the 2 GHz impulse radar (black line) and the step-frequency system (thick gray line).

Tx antennas (Gibson, 1979; Langley et al., 1996). The ultra-wide band antennas have been especially designed for pavement survey application at the Electronics, Antennas and Telecommunications Laboratory (LEAT) at the Nice-Antipolis University. They use the "stripline" technology, display a small lateral dimension and yield a bandwidth of 800 MHz to 8 GHz in a bi-static air-coupled configuration. This frequency range induces a central frequency around 4 GHz and a resolution about twice that of the impulse technique. The antennas were mounted behind a car and the B-scans were recorded over a smaller range from the I-13 defect to the end of the I-11 defect along the same radius as before, i.e., 16 m. The B-scan profile in Figure 8b was collected at very low speed. The spatial sampling only allowed four profiles per meter, due to the data acquisition capacity, but plans are in place to improve this sampling rate.

3.1.4 *Experimental results on the carrousel*

Figure 7a presents the radar Bscans which were collected with the 2 GHz impulse radar along the 16 m radius. Qualitative comparison with the 2.6 GHz ground-coupled radar is shown in Figure 7b.

Vertical white lines identify the different defect zones shown in Figure 3. Four zones are labeled A to D with the following defects: A – I-1 to I-3 (0.5 m long defects), B – I-4 to I-9 (small square geotextile defects), C - I10 (3 m long geotextile defects), D – I-11 to I-13 (1.5 m large defects). Despite this marking, data interpretation required further investigation.

The horizontal trace corresponds to the first echo on the pavement surface. Vibrations of the trolley were removed using conventional post-processing. The second echo corresponds to the interface to detect distress between the wearing course and the base layer. The third echo corresponds to the bottom of the base layer. The narrowest defects in Regions A and B could hardly

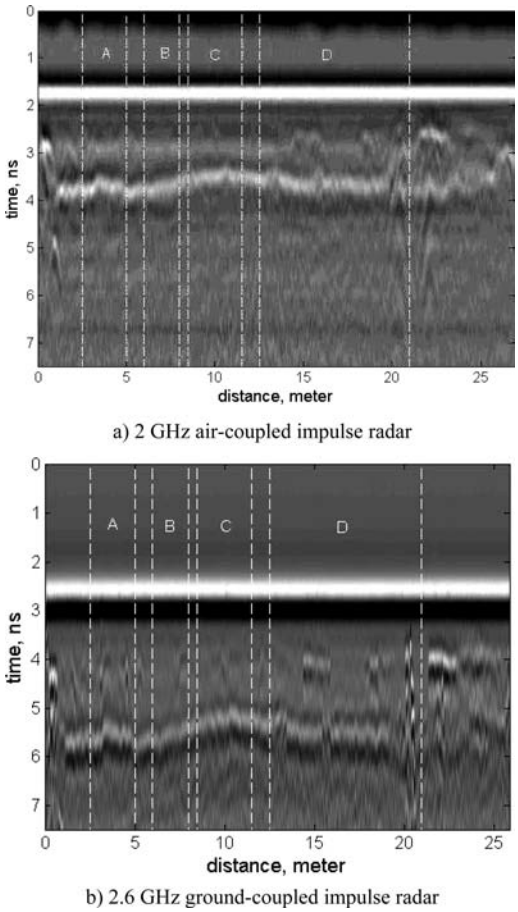

Figure 7. 2 GHz impulse air-coupled and 2.6 GHz impulse ground-coupled B-scan radar images over the four defect zones, A to D.

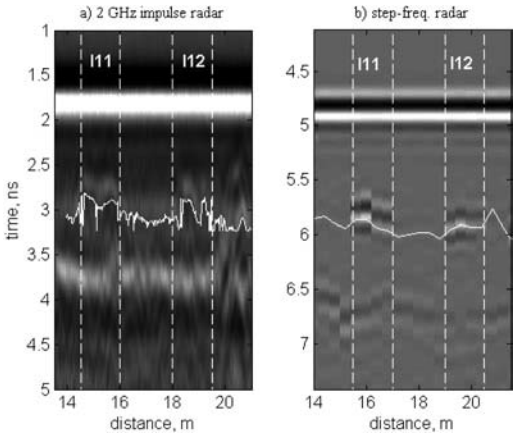

Figure 8. Bscan images obtained by the two radar technologies over the "D" zone shown in Figure 7, including sand (I-11) and geotextile (I-12) interface defects; a) impulse radar (zoom on Figure 7a); b) step-frequency radar.

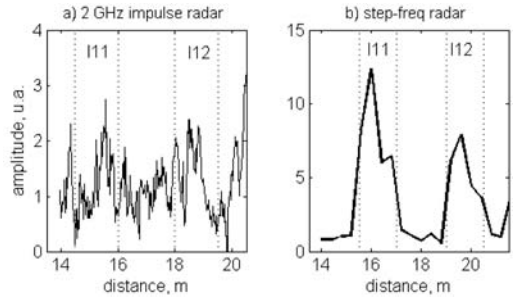

Figure 9. Debonding detection on the Bscans shown on Figure 8: Variations along the longitudinal profile of the echo amplitude attached to the wearing course interface.

be detected. At the end of the B-scan, some hyperbolas revealed embedded metal instrumentation within the pavement.

For debonding detection, attention was focused on the largest defects in Region D (I-11 to I-13 in Table 2). Stronger echoes than expected were observed for I-13 and will be investigated further with cores that will be taken at the end of the experiments. Figure 8a shows a magnified image of the I-11 and I-12 defects to simplify the comparison with the step-frequency Bscan shown in Figure 8b. Vertical white dashed lines indicate the defect delimitations. The echo from the interfaces between the wearing course and the base layer are shown as white lines. This echo was automatically detected by selecting the maximum of the amplitude within an appropriate time window.

The amplitude variations of the echo along the distance are used to detect debonding. Then, taking the echo on the zone with no distress between I-11 and I-12 as the reference signal, the two defects can be seen in Figure 8 using both a smaller delay shift and some contrast in the signal amplitude. The variations of that echo along the longitudinal profile are shown in Figure 9. For the 2 GHz impulse radar in Figure 9a, the location of the defects is difficult because of both the noise and the limited contrast amplitude over the defects (with regards to the zone with no distress). In Figure 9b, the shorter pulses provided by the step-frequency radar enhance the amplitude variations over the debonded areas. The amplitude variation is about five times larger over the defects. Clearly, data interpretation of the step-frequency Bscans is more intuitive and readily reveals the location of the defects.

This first comparison of the different radar measurement techniques shows the better efficiency of ground-coupled antennas when locating small objects, and the better capability of the step-frequency technique to detect debonded areas. However, the proposed step-frequency procedure requires further optimization to be used for routine measurements. Special coring over the I-13 defect is planned at the end of the experiments to investigate the origin of the stronger than expected echo. Further data collection is also planned over the embedded artificial crack (discussed in Section 2.2.3).

3.2 *Impulse method based on frequency response function*

Several NDT methods use an impulse load to test structures. The characteristics of the impulse load lead to different phenomena being observed, which are analyzed with different methods. A falling weight deflectometer (FWD) impulse contains energy only in the low frequency domain (<100 Hz). This method measures the deflection bowl from the centre of the load to a distance up to 2 m. Other methods use measurements further from the impulse position to estimate propagation wave velocities (Rayleigh or Lamb) in a higher frequency domain (several kHz). In the same frequency domain, pulse echo or impact echo methods generate compression or shear waves close to the impact point. These methods observe multiple reflections at layer interfaces to estimate bonding condition or interface depth. Usually the load impulse is not measured. For intermediate frequency (100 to 10,000 Hz), impulse loads can be measured and analyzed with a modal testing theory (Ewins, 2000) to calculate the Frequency Response Function (FRF). Based on IFSTTAR experience, a methodology has been developed to calculate a damage indicator sensitive to interface damage or reflective cracking (Simonin et al., 2009a,c; Simonin et al., 2012).

3.2.1 *Principle of the method*

Roadways constitute continuous structures on which the complex frequency response function (FRF) can be measured. The Colibri apparatus (Figures 10 and 11) is a completely automated system for dynamic investigation of pavements. It includes:

- A hammer with a force-cell to measure the shock application;
- An accelerometer placed at 0.10 m from the impact to measure the surface response, held by a spring mass system;
- An optical sensor to control the level of the impact.
- An engine to raise the hammer and produce the impact.
- An electric jack enabling the lowering and raising of the system on the road surface as well as the placement of the sensors when the Colibri is mounted on a vehicle;
- Electronics, data acquisition systems, and a computer to manage the measurement sequences and to store the data.

During a measurement sequence, the system is positioned on the road surface. The engine raises the hammer to the appropriate level and then drops it, applying a wide-band dynamic impulse to the pavement to determine the inertance FRF, $A(f)$, at each test point. The FRF is the ratio between the harmonic acceleration response and the harmonic force. Signals (force and acceleration) are recorded by the computer. Usually, the test is repeated three times to achieve satisfactory signal processing. If the system is mounted on a vehicle, the computer controls the vertical displacements of the Colibri system using the electric

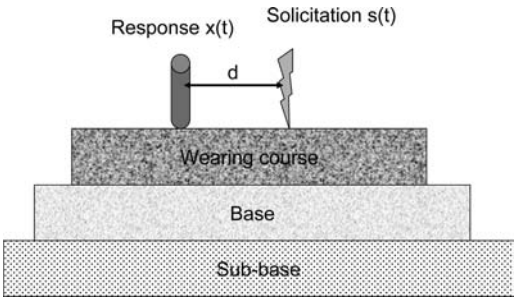

Figure 10. Principle of dynamic investigation test.

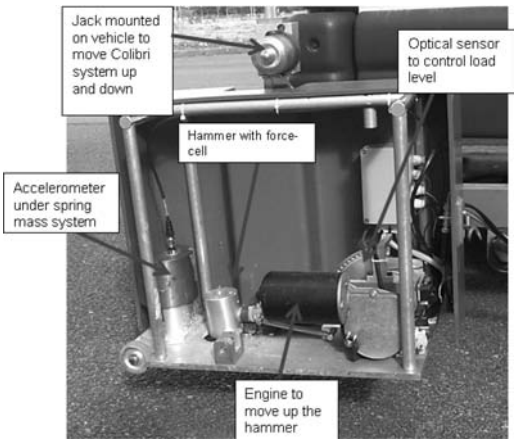

Figure 11. The Colibri prototype.

jack, allowing automatic measurements at different locations.

For a healthy structure, the impulse generates vibrations of the whole pavement. When a structure includes a defect (interface or crack), low frequency vibration modes appear which correspond to the vibration of a part of the structure (above the delamination or close to the crack). The inertance modulus estimated for the delaminated structure is higher than that of the healthy structure, increasing at each eigen frequency. Thus, a difference of inertance can be observed in a sensitive frequency band. This band and particularly the lowest frequency, depends on the characteristics of the defect (extension, depth, nature).

3.2.2 *Application to pavement investigation*

Application to pavement investigation (Simonin et al., 2009a,c) entails collecting the inertance function along a roadway section. The process then compares the FRF modulus by defining a reference FRF representative of the healthy structure and then identifying an FRF which is significantly different from this reference function. It should be noted that the reference function is related to the investigated roadway. Structure (materials and layer thicknesses) is assumed to be homogeneous. The measurement variations are then representative of the presence of damage, which lead to a weaker structure.

For each measurement point, i, a spectral analysis of a series of tests is used to calculate the inertance, $A(f,i)$, and the coherence function, $\gamma(f,i)$, between the pavement response and the applied solicitation. These functions depend on the frequency, f, and on the measurement point. The coherence function estimates the dependence of the output signal compared to the input signal. It is a real value ranging between 0 (no dependence) and 1 (full dependence). A minimum threshold of coherence (usually 0.8) is chosen to validate the calculation of the inertance. This threshold can be adapted according to the specifics of the study. For each frequency and each measurement point, the FRF is validated if the coherence value is higher than this threshold. Thereafter, the analysis is restricted to the population of validated measurements. In a homogeneous zone, data are then processed in two steps:

– Estimation of a reference function representative of the healthy structure;
– Calculation of a normalized damage.

To estimate the reference function modulus, it is assumed that a part of the test was carried out in a zone with no distress. This can be achieved by investigating an un-trafficked zone such as an emergency lane. In practice the set of modulus, $|A(f_k,i)|$, measured at a fixed frequency, f_k is usually considered. The reference value at this frequency, $|A_{ref}(f_k)|$, is defined as a percentile of the selected population. The 20th percentile is usually adopted, which allows obtaining a low value representative of the healthy structure and eliminating abnormal measurements. This set of reference values is used to build the reference transfer function representative of the healthy structure, $|A_{ref}(f_k)|$.

Inertance modulus increases with frequency. The FRF modulus, $|A(f_k,i)|$, is normalized using the modulus of the reference function. For each frequency and each measurement point, the damage, $D(f_k,i)$, is calculated using Equation 3. This value varies between 0 and 1. The matrix, D, represents the damage on the road section for the different frequencies. It can be presented as a "damage map" where:

– The X-coordinate is the abscissa along the road section;
– The Y-coordinate is the frequency band;
– Colors or level of gray represent the level of damage.

$$D(f_k,i)=\begin{cases}0 \text{ if } |A(f_k,i)|<|A_{ref}(f_k)| \\ 1-\dfrac{|A_{ref}(f_k)|}{|A(f_k,i)|}\end{cases} \quad (3)$$

3.2.3 *Application on the test site*

The Colibri prototype was used to investigate the experimental pavement section with the different debonded areas. A longitudinal profile at the 16 m radius and several transverse profiles were investigated. Measurements were made at points spaced at a distance of 0.05 m, and each individual measurement included three impacts. A 2 m long profile was also recorded above the internal crack.

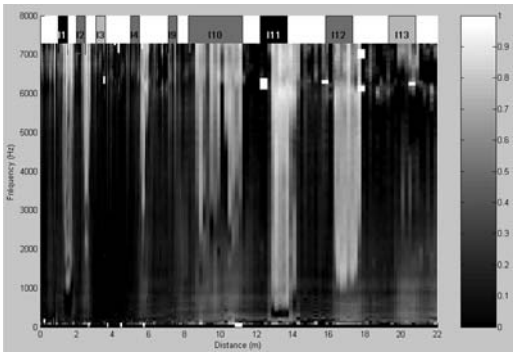

Figure 12. Results of Colibri measurements on the pavement with defects (longitudinal profile).

Figure 12 shows the analysis of a longitudinal profile at the 16 m radius. The picture shows the damage level, as a function of the distance (X) and the frequency (Y). The level of gray represents the damage level from 0 (black) to 1 (white). The designed debonded areas are indicated at the top of the picture. The dynamic investigation method allows reasonably accurate detection and location of the areas with defects. The frequency range of the response also appears to provide an indication of the nature of the defect. Areas without tack coat, for instance, (I-3 and I-13) are only sensitive to the higher frequencies. It should also be noted that there is some difference between the designed and measured position of the defects. Three reasons could explain these differences. First, they could be due to construction, as positioning such objects during construction is always difficult. Second, during construction, the geotextile or sand could have been displaced by the finisher. Third, it is difficult to position the Colibri system along the circular track with 1.0 cm accuracy. Measurement results confirm that the Colibri system is able to detect and locate the debonded areas and to make a distinction between them. This confirms previous experience with this methodology.

Figure 13 shows a longitudinal profile above the vertical internal crack (2.5 mm wide, 40 mm deep) in the FRCC base layer. A clear influence of this internal crack can be observed in the frequency range (500 to 2,500 Hz). Colibri results were also affected at high frequency ranges (>1,500 Hz) at the end of the profile (Distance > 0.5 m). A poorly bonded interface during the construction explains this result. Colibri measurements are therefore sensitive to vertical and horizontal internal cracks.

3.3 *Deflection basin measurements*

Several devices are used to measure deflection basins. Falling weight deflectometer, Benkelman Beam or Lacroix Deflectograph are the most commonly used.

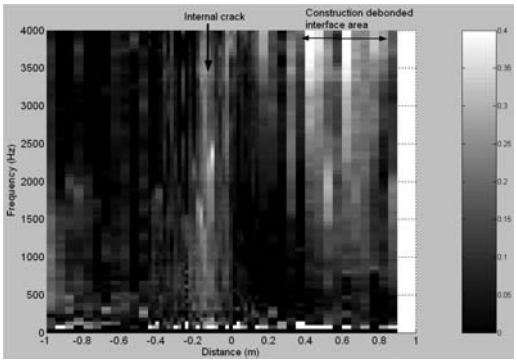

Figure 13. Results of Colibri measurements on the pavement with internal crack.

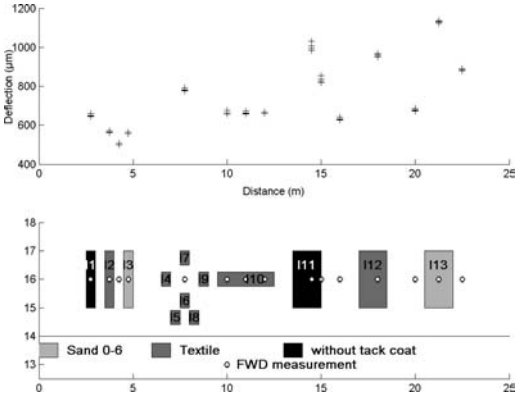

Figure 14. Results of FWD measurements on the pavement with defects (longitudinal profile).

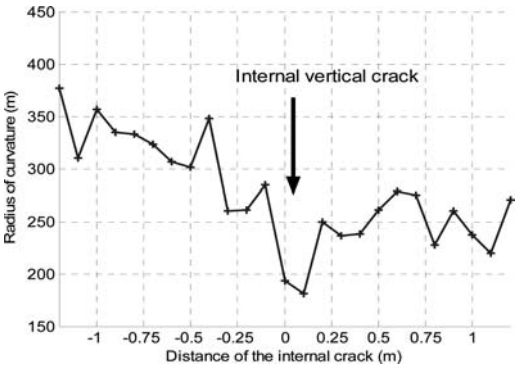

Figure 15. Results of inclinometer measurements used for crack detection.

The load application is the main difference between these devices. FWD applies an impulse dynamic load and measures deflection at different distances from this load while other systems use a rolling load and measure the deflection bowl in a fixed point. If the maximum deflection is a common indicator, other deduced parameters cannot be compared. For example the radius of curvature close to the maximum deflection can be estimated with a Benkelman beam or a Deflectograph. It can't be compared with the difference in deflection between the central sensors and those at different distances form the load.

Measurement of radius of curvature is current practice in France. This parameter is more sensitive to internal defects such as interface debonding than maximum deflection (Savuth, 2006; Simonin, 2009b). An accurate measurement of the radius of curvature usually uses an inclinometer (Queroy and Brun, 1974) which can be placed on the road surface or be attached to the beam of a Lacroix deflectograph. FWD, Benkelman beam and inclinometers are commonly used to survey pavements on the fatigue test track. Evolution of deflection and also radius of curvature with time and distance will be estimated during the experiment.

FWD tests were performed along a longitudinal profile at the 16 m radius, on the pavement section with defects. Four load levels were applied and the test was repeated four times at each level. Figure 14 compares FWD measurements at the highest load level ($\approx$74 kN) along the profile. The first graph shows the maximum deflection at each measurement point. The second graph locates the debonded areas (and their type) and the measurement points. Deflections varied from 500 μm to 1,136 μm depending on the measurement point. High deflection values were clearly obtained above or close to the biggest debonded areas (I-11, I-12, I-13). Small debonded areas were much more difficult to detect, with deflection values close to those obtained on areas without defects, except perhaps for the measurement point situated between the small defects I-4 to I-9. It is also difficult to precisely locate the position of the defect, and to make a clear difference between the different defect types using only the maximum deflection. The deflection bowl from the seven sensors will be analyzed in detail later in the study to try to identify other differences between the measurement results. This will include spatial and time analysis of the response of each sensor.

Another measurement technique that will be investigated in this experiment is the measurement of the deflection bowl with an inclinometer under a rolling load. A small measurement interval will be used with this method to estimate the variation of the deflection bowl in the presence of interface defects.

Some tests with the inclinometer method have already been performed in a previous full scale experiment, and gave interesting results. In that experiment, a transverse crack was sawn in the base layer (bituminous material) and covered with a bituminous wearing course 5 cm thick. The radius of curvature was estimated with an inclinometer. Tests were performed every 10 cm along a 2 m long longitudinal profile. Figure 15 shows the measured values of the radius of curvature. The internal crack is located close to the abscissa 0. The level of measurement clearly decreases at the distance 0 and 0.10 m which correspond to the influence zone of the internal crack.

In future experiments, use of the inclinometer is planned for monitoring the evolution of cracks. A comparison with other techniques will be made. The results could also be helpful to define a suitable methodology for continuous deflection measurements, in relation to prototypes which have already been developed (Simonin, 2009b; Rasmussen, 2002).

4 CONCLUSION AND OUTLOOK

This paper presents the first part of an experiment performed on the IFSTTAR APT facility to evaluate the use of different NDT techniques for the detection of different defects (debonding, cracks), and their evolution under traffic.

A pavement section with different artificial defects (debonding, cracks) has been built and tests performed using different investigation methods, before the start of loading of the pavement. These first results show some potential and limitations of the different methods, and will help to define adequate monitoring procedures, with each apparatus. They also point out some research needs.

Radar measurements are easy to perform even at traffic speed to continuously detect layer interfaces and calculate thicknesses. They can also give an indication of the probability of interface debonding. The antenna choice (central frequency) is of primary importance. The SFR technique, which allows increasing the frequency band, gives a high resolution picture which is useful to detect internal debonding. It has also been shown that contact antennas, analyzing a smaller surface area, are more useful for detecting small defects. Radar techniques are adapted to a first estimation of interface state along a long itinerary. Some research is still needed to optimize the individual signal or image processing, to obtain an interface damage indicator.

Dynamic investigation with the Colibri prototype confirms that the method is able to detect and locate interface debonding or internal cracks, but at a much slower measurement rate. A new apparatus will be finished in 2012, and will improve this aspect (about 5 seconds per measurement, compared with 40 seconds presently). It will be possible to investigate several hundred meter long sections to provide the road engineer with a picture of the internal damage of the road base and wearing course. The good results obtained with this method have led to an interest in evaluating other mechanical methods in the dynamic domain. The impact echo method or Rayleigh or Lamb wave propagation methods could give absolute values of the mechanical properties of the materials (Rayleigh or compression wave velocity, mechanical impedance of interfaces). However, measuring equipment would need to be improved before these methods could be satisfactorily used in pavement applications.

Maximum deflection measurements show sensitivity to the presence of debonding. However, this method measures the global response of the whole pavement structure, and consequently the measurements are sensitive to the performance of all the pavement layers, and not only to the specific defect being investigated. A limitation of the FWD is that it applies an impulse-dynamic load at fixed points and measures the response at the surface and thus cannot be used to make quasi-continuous measurements (i.e., every 10 cm for example) to detect small debonded areas even if it is sensitive to such defects. However, FWD remains necessary to backcalculate the modulus of pavement structures, including the subgrade.

Tests on the APT section show that radar devices and Colibri are able to detect and locate interface defects. Colibri and inclinometer devices could be used to detect internal cracks. During the loading phase, the test site will be surveyed with the different methods to evaluate the evolution of the defect with loading, and to estimate when a method can be used to accurately detect a defect (a damage level). Other methods such as pulse echo and impact echo methods will also be considered.

REFERENCES

Adous, M. 2006. *Electromagnetic characterization of civil engineering materials within the 50 MHz-13 GHz bandwidth. PhD* (in French). Nantes University. France.

Cardimonda, S. et al. 2003. Automated Pavement Analysis in Missouri Using Ground Penetrating Radar, *Proc. 2nd Conf. Appl. Of Geophys. and NDT Method. to Transp. Facilities and Infrastr. California, USA, FHWA-WCR-02-001*, 10 p.

Dérobert, X. 2004. Step-frequency radar technique applied on very-thin layer pavements. In: *Surface-penetrating radar. Daniels D.J. (ed), Instit. Electrical Engineers. London (UK). 2nd ed*, pp. 386–394.

Ewins, D-J. 2000. *Modal testing: theory, practice and application.* Second edition. Letchworth. Research studies press LTD.

FHWA report. 2010. *Step Frequency Ground Penetrating Radar Characterization and Federal Evaluation Tests*. Publication No. FHWA-HRT-10-037.

Gibson, P.J. 1979, The Vivaldi aerial, Digest of 9th Eur. Micr. Conf., Brighton, pp 120–124.

Grégoire, C. 2001. *Fracture characterisation by ground penetrating radar*. Ph D. Kath. Univ. Leuven. BE.

Hornych, P. Kerzrého, J-P. Sohm, J., Chabot, A. Trichet, S. Joutang, J-L. and Bastard, N. 2012. Full scale tests on geogrid reinforced flexible pavement on the French fatigue carrousel. In *Accelerated Pavement Testing. Proc of the 4th Int. Conf. on Accelerated Pavement Testing.* Davis, CA.

Langley, J.D.S., Hall, P.S. and Newham, P. 1996, Balanced antipodal Vivaldi antenna for wide bandwith phased arrays, *IEE Proc. on Microwave Ant. Prop., vol 143, No 2, April.*

Le Bastard, C. et al. 2007. Thin pavement thickness estimation using GPR with high and super resolution methods. *IEEE Trans. on Geosc. Rem. Sensing. Vol. 45, No.8.* pp 2511–2519.

Le Bastard, C., Baltazart, V. and Wang, Y. 2010. Modified ESPRIT (M-ESPRIT) algorithm for time delay estimation in both any noise and any radar pulse context by a GPR. *Signal Processing. 90*, pp. 173–179.

NF EN 12 697-31, 2008. *Test methods for hot mix asphalt. Specimen preparation by gyratory compactor.*

Pinel N., Le Bastard, C., Baltazart, V., Bourlier, C. and Wang, Y. 2011. Influence of surface roughness on thin layer thickness evaluation: *Application to the theoretical study of road layers, IET Sonar and Navigation, 5 (6)*. pp 650–656

Queyroi, D. and Brun, Y. 1974. *One application of the LCP precision inclinometer*. Bulletin de Liaison des Ponts et Chaussées.

Rasmussen S., Krarup, J.A. and Hildebrand G. 2002. Non-contact Deflection Measurement at High Speed. *Bearing Capacity of Roads, Railways and Airfiels. Balkema.* pp 53–60.

Saarenketo, T. and Scullion, T. 2000. Road evaluation with ground penetrating radar. *Journ. Appl. Geophy*s. 43 pp. 119–138.

Savuth, C. 2006. *Contribution à l'auscultation structurelle des chausses mixtes : détection des défauts d'interface à l'aide de la déflexion*. Ph D. INSA de Rennes. France.

Scullion, T. and Saarenketo, T. 1995. Ground Penetrating Radar Technique in Monitoring Defects in Roads and Highways. *Proc. Symp. Appl. Geophys. to Eng. and Env. Prob., SAGEEP, Orlando, Florida*. pp. 63–72.

Simonin, J-M. Lièvre, D. and Dargenton, J-Ch. 2009a. Structural roadway assessment with frequency response function. pp. 459–466 *Bearing Capacity of Roads and Airfields. Proc. Intern. Conf.*

Simonin, J-M. Cottineau, L-M. Muzet, V. Heinkele, C. and Guillard, Y. 2009b. Deflection measurement: The need of a continuous and full view approach. pp. 467–476. *Bearing Capacity of Roads and Airfields. Proc. Intern. Conf.*

Simonin, J-M. Odéon, H. Delaval, E. Lièvre, D. and Dargenton, J-C. 2009c *Auscultation dynamique des structures de chaussée, méthode d'essai LPC n° 70*. 48p. LCPC editor.

Simonin, J-M. Fauchard, C. Hornych, P. Guilbert, V. Kerzrého, J-P. and Trichet, S. 2012. Detecting unbounded interface with non destructive techniques. *Rilem conference. Craking in pavements. Delft. Netherlands.*

This page intentionally left blank

Advances in Pavement Design through Full-scale Accelerated Pavement Testing – Jones, Harvey, Mateos & Al-Qadi (Eds.)
© 2012 Taylor & Francis Group, London, ISBN 978-0-415-62138-0

Rut depth measurement method and analysis at the FAA's National Airport Pavement Test Facility

I. Song & R. Aponte
SRA International, Inc, Linwood, New Jersey, US

G. Hayhoe
FAA William J. Hughes Technical Center, Atlantic City, New Jersey, US

ABSTRACT: The FAA developed and modified a truss profiler, which is independent of pavement profiles, that is used to monitor rutting of flexible pavements at the National Airport Pavement Test Facility (NAPTF). The truss profiler was developed to replace the more labor-intensive and time-consuming straightedge measurements. Transverse profiles corresponding to the cumulative number of load repetitions applied during traffic tests were measured using a laser displacement sensor mounted and running on a customized 20 m (66 ft.)-long aluminum truss. The profiler is capable of measuring ruts caused by 10-wheel aircraft gear configurations having dual-wheel spacing of 137 cm (54 in.) in two traffic lanes. Maximum transverse measuring width is 18.3 m (60 ft.) and upheaval outside the wheel track areas is included in all rutting measurements. The profiles reported in this paper were measured on a flexible pavement test track with a single 12-ft.-wide traffic lane. The collected profile data was processed using an FAA developed computer program to calculate the maximum rut depth, upheaval, and straightedge-simulated rut depth measured relative to the initial transverse (baseline) profiles. Trafficked profiles were shifted vertically (and/or horizontally), and rotated to compensate for differences in the setup of the profiler. The method of rut depth measurement is presented and the accuracy of the profiler is reviewed. Possible errors in measurements such as truss fluctuations in temperature, structural curvature, and cross slope of the pavement are identified. Detailed descriptions of the adjustment methods used to correct for the identified errors are presented. The geometric changes of the transverse profiles are shown with increasing number of load repetitions superimposed on the untrafficked baseline profiles. Analysis of the profiles shows the effects of lateral wander, loading induced stress, and tire pressure on a Hot Mix Asphalt (HMA) pavement surface layer. The processed rutting performance data obtained from the NAPTF test pavements are presented and discussed. Specific discussions include characterization of HMA failures showing tertiary flows from the collected data.

1 INTRODUCTION

The Federal Aviation Administration (FAA) operates the National Airport Pavement Test Facility (NAPTF), a full-scale airport pavement test facility located at the William J. Hughes Technical Center near Atlantic City, New Jersey. Both flexible and rigid pavements are constructed and tested at the facility. Permanent deformation test results collected from flexible pavements are presented in this paper. The procedures for data collection and processing by an FAA developed profiling system were used. Monitored accumulation of the permanent deformation corresponding to the number of repeated wheel load passes is analyzed.

The FAA's profiling equipment, which runs on rails at the sides of the test pavement, is operated independently of the test pavement surface and was developed to measure the permanent deformation from wide aircraft gear configurations and wandering under typical airport pavement loading conditions. The rut depths with increasing load numbers, based on the untrafficked baseline profiles at different test conditions, are computed using geometric straightedge simulations on the collected profile lines. The computed rut depths from the simulation showed typical HMA pavement performance, including tertiary flow.

2 TEST CONDITIONS

The flexible pavement was constructed on a CH clay subgrade known as DuPont clay. The pavement structure consists of 43 cm (17 in.) of econocrete as a stabilized base (P-306) (FAA, 2011) and a 13 cm (5 in.) HMA surface layer (P-401). The HMA layer was placed with two different mix designs. The mixes used the same aggregate and aggregate grading, but different asphalt binders. One mix had a straight PG 64-22 asphalt binder and the other had a polymer modified PG 76-22 binder. A hydronic heating system was embedded in the econocrete at its base to control the temperature of the HMA at a temperature

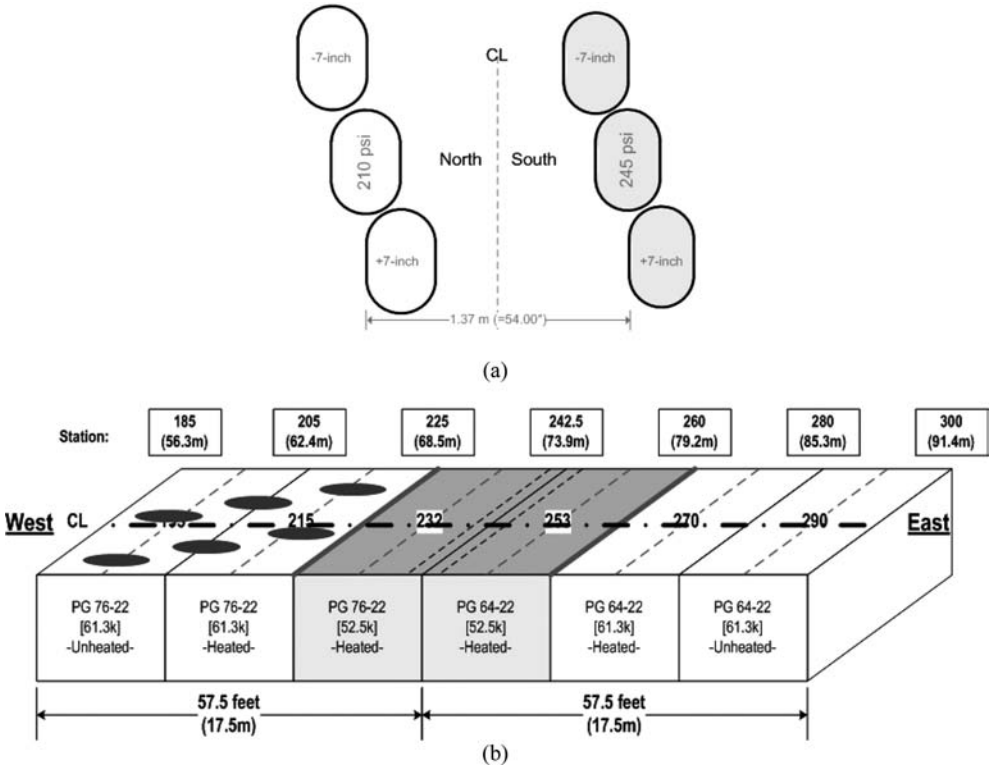

Figure 1. Trafficking conditions for the high tire pressure test area (a) foot prints for wander pattern with 7 in. spacing; (b) loading conditions. The dotted blue lines show the position of the transverse profile measurements.

representative of high temperature airport operations. The as-constructed dimensions of the high tire pressure (HTP) test pavement structure are 35 m (115 ft.) long and 3.7 m (12 ft.) wide.

Dual tires with 137 cm (54 in.) spacing mounted on one of the loading modules on the NAPTF test vehicle were used for the test loading. The tires were inflated with the dead weight of the module on the tires and with the tires at ambient temperature. Inflated tire pressures were 1.45 MPa (210 psi) and 1.69 MPa (245 psi) for the North and South wheels respectively. Higher tire pressures up to approximately 1.5 MPa (218 psi) and 1.75 MPa (254 psi) were reached during testing.

Wheel loads were 23.8 MT (52,500 lbs) and 27.8 MT (61,300 lbs) with the load application pattern as indicated in Figure 1. The wander pattern of +18 cm (7 in.) (toward the south), 0 (equal distances from the centerline to each tire), and −18 cm (7 in.) (toward the north) is shown in Figure 1a and the loading pattern is shown in Figure 1b. The loads were applied at a trafficking speed of 0.305 m/s (1 ft./s) from west to east. The module was unloaded at the east end and returned to the west end at 1.22 m/s (4 ft./s), after which the wander position was changed and the loading pattern repeated.

3 DATA COLLECTION

Transverse profiles were measured during trafficking at the middle of each test item, 6.1 m (20 ft.) apart, as shown in Figure 1b. The measurements were made at approximately every 21 passes or whenever significant changes were observed.

Since traffic testing at the NAPTF is conducted on a pavement area 18.3 m (60 ft.) wide, the transverse profiles were measured with the FAA's 20 m (66 ft.) long truss profiler equipped with a non-contact vertical displacement transducer as shown in Figure 2. The profiler runs on the rail system which is used for supporting and guiding the NAPTF test vehicle. The supporting points of the transverse profiler located on the rail are capable of maintaining the same vertical reference points for the transverse profiles with pavement surface condition changes. This vertical reference point minimizes any possible profile distortions from the lateral locations of the profiler placed within the depression or upheaval areas.

The truss profiler is operated by moving an infrared laser to monitor the vertical displacement of the pavement, and an incremental rotary encoder as a distance measuring instrument (DMI) on a trolley rolling along the steel flange of an aluminum truss type beam. The

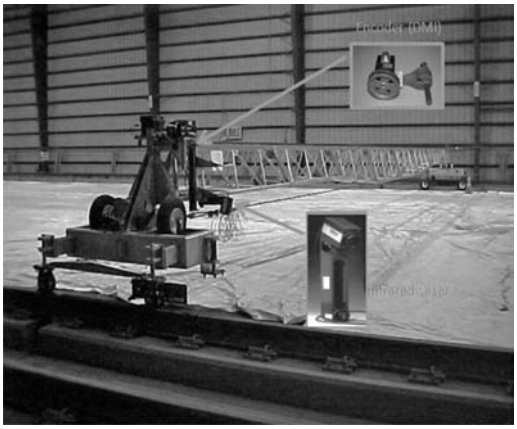

Figure 2. Laser mounted truss type FAA transverse profiler.

laser footprint is oval in shape and the size is approximately 2.5 mm (0.1 in.) × 5 mm (0.2 in.). The laser adopted for the profiler has a measuring range of 100 mm (4 in.) to 1,024 mm (40.4 in.) with a stand-off distance of 390 mm (15.4 in.) to 1,200 mm (47.3 in.) (LMI, 2011). The signal acquisition box is assembled to collect data using a USB digital data acquisition unit and software (MCC, 2011).

4 DATA PROCESSING

The collected profile data is processed using software developed by the FAA. A screen shot of the program is presented with an example transverse profile in Figure 3.

Reference profile lines were taken at a designated calibration section without any load applications. They were used as an input parameter for a subroutine in the program to compensate for any unexpected vertical deformations from environmental condition changes. The pavement profiles before loading were used as base profile lines for each pavement test section to compute rut depth. The rut depth accumulation started from the baselines is mathematically computed to depict HMA pavement performance. The straightedge simulation is performed on each profile line to compute the amount of maximum depression and upheaval in the pavement section. Specific sections of the profiles were cut and rotated for geometric comparisons.

4.1 *Calibration of beam curvature for baseline profiles*

Since the FAA customized truss profiler is made from a steel rail on an aluminum truss structure, the different metal expansions at the top and bottom of the profiler leads to a "sagging" shape as shown in Figure 4.

The δ_T in Equation 1 is the thermal deformation due to the thermal expansion coefficient, α, metal length, L, and temperature changes, ΔT, from a reference

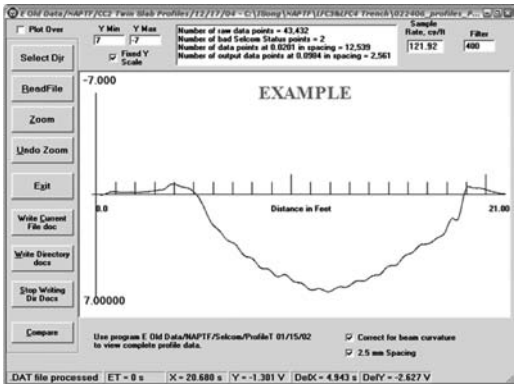

Figure 3. Screenshot of the FAA profile processing software with a transverse profile example.

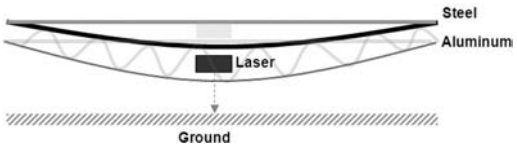

Figure 4. Temperature induced profiler shape changes.

point. In general, the thermal expansion coefficient is approximately 13.0×10^{-6} m/m K (7.3×10^{-6} in/in °F) and 22.2×10^{-6} m/m K (12.3×10^{-6} in/in °F) for steel and aluminum respectively (TET, 2011). The thermal deformation is defined as follows:

$$\delta_T = \alpha \times L \times \Delta T \tag{1}$$

A calibration profile line showing consistent transverse profiles independent of ambient temperature changes is selected inside the NAPTF facility. The calibration line profile measured at the same time of profile measurement on the test pavement becomes a reference point to adjust the amount induced by ambient temperature changes. Equation 2 compensates the vertical discrepancies of the data points along the full length of the profiler. The compensations are performed for every profile data point at each pass number, *n*. This equation makes an ideally perfect straight truss profiler and is set as an initial (base) profile line before the start of trafficking to monitor permanent deformation relative to the initial conditions:

$$P_{\mathrm{i,n}} = \left| r_{\mathrm{i,n}} - x_{\mathrm{i,n}} \right| \tag{2}$$

where $P_{\mathrm{i,n}}$ = the processed profile data at pass number n; $r_{\mathrm{i,n}}$ = the reference profile data at pass number n; $x_{\mathrm{i,n}}$ = the profile data at pass number n, and i = the profile data sequences from the 1st to the ith.

Figure 5 shows an example of the beam curvature corrections in the program before test pavement profiling. Notice the change in the reference profile when the beam curvature correction function is activated.

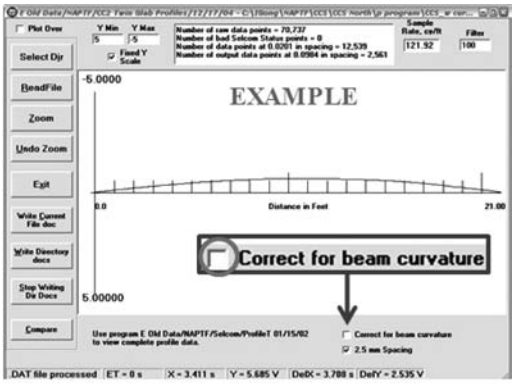

(a)

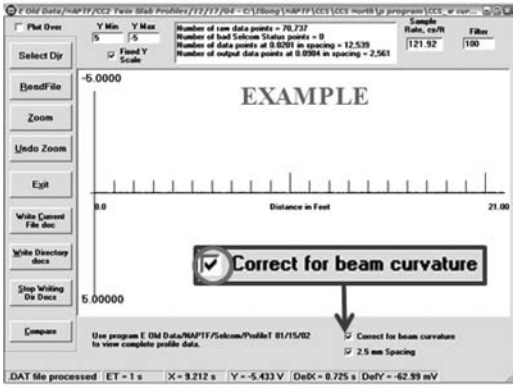

(b)

Figure 5. Beam curvature correction function in the FAA profile data processing software (a) without beam curvature correction; (b) with beam curvature correction.

4.2 *Sectioning transverse profile*

Traffic wandering was considered in the full-scale pavement testing to simulate, in some measure, in-service runway traffic conditions. For the purpose of computing rut depth and upheaval, horizontal traffic zones were divided based on test conditions such as loading and pavement materials or specific analysis purposes. The sectioned profiles were first shifted vertically and rotated to make both start and end elevations equal to zero. A vector rotation can be conducted in terms of a typical linear transform matrix. The vector A in Equation 3 rotates each vector by an angle θ in the counterclockwise direction. The matrix A representing the transformation will have $(\cos\theta, \sin\theta)^T$ as its first column and have $(\sin\theta, \cos\theta)^T$ as its second column:

$$A = \begin{pmatrix} \cos\theta & -\sin\theta \\ \sin\theta & \cos\theta \end{pmatrix} \tag{3}$$

The procedures are depicted in Figure 6. The portion of the profile to be sectioned is marked by dashed vertical

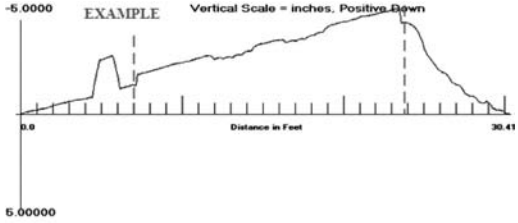

(a)

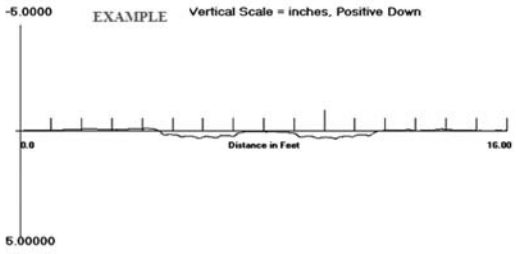

(b)

Figure 6. Transverse profile processing (a) sectioning; (b) shifting and rotation for rut depth calculations.

lines. The sectioned profile is shifted vertically and rotated so that the end points have values of zero.

4.3 *Straightedge simulation*

Straightedges are widely used to measure pavement depressions because of their simple and easy methods of use. Standards for their use are specified in (ASTM, 2011) and in FAA Advisory Circular (AC) 150/5370-10F (FAA, 2011). However, the measurement process is time consuming and the accuracy is questionable due to the procedures to identify the measurement location of maximum deviation between straightedge and pavement surface. The profiler with 2.5 mm (0.1 in.) sample spacing was developed to replace the more labor-intensive and time-consuming straightedge measurements, especially for in-service airfield runways.

Song and Hayhoe (2006) have written about straightedge simulation in their paper. As they discussed, a certain length of straightedge moves along the pavement surface profiles and the maximum vertical distance between the straightedge and the pavement surface profiles is calculated for each location along the profile. There are two methods in common use for the measurement of maximum deviation. As illustrated in Figure 7, the first one is to measure the maximum distance to the pavement surface between the straightedge support points and the other is make the measurement over the full length of the straightedge.

Straightedge simulation methods were utilized to determine the maximum depression, rut depth, and upheavals at pre-determined longitudinal locations as marked in Figure 1. Figure 8 illustrates the change in maximum rut depth with increase in traffic by overlaying transverse profiles in the same figure and

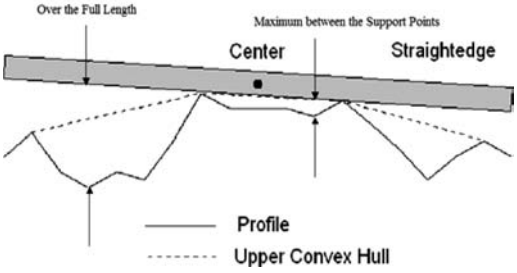

Figure 7. Straightedge calculation methods.

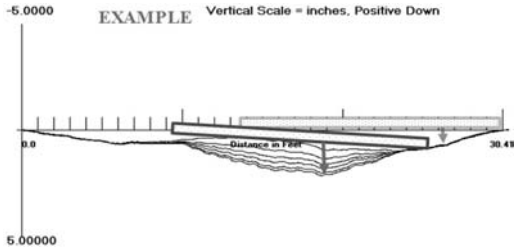

Figure 8. Maximum rut depth determination utilizing the straightedge simulation method.

by application of the straightedge simulations on the gathered profiles. In the simulation, as seen in Figure 8, the rectangle, representing a 5 m (16 ft.)-long physical straightedge, was shifted horizontally to find the locations corresponding to the maximum pavement depression with increased traffic numbers.

4.4 *Rut depth measurement*

Since permanent deformation in asphalt pavements is one of the most significant distresses affecting performance of the pavement, the procedures to calculate rut depth are critical for HMA pavement evaluation.

The rut depth occurring either through consolidation or through plastic flow was monitored with increasing traffic numbers. As described above, the HMA surface depression from the peak elevation to the bottom elevation was measured through straightedge simulation procedures. Rutting is caused by the progressive movement of materials under repeated loads either in the asphalt concrete layer or in the underlying layers. Hence, geometric analyses were also added to monitor the upheaval mostly caused by lateral shear flow of the materials under the surface.

The gathered rut depth data were of downward and upward elevation changes relative to initial (base) profile lines. This step is to determine the relative rut depth and upheaval at given locations as the maximum difference between the two profiles at given intervals during the traffic test.

5 RESULTS AND ANALYSIS

The data processing and research results are presented and discussed. Only the results of temperature induced truss beam curvature changes in the data processing steps are presented because the other processing steps have been presented earlier as examples. Rut depth progress from the HMA test sections at the NAPTF with different loading conditions such as load level and tire pressures are also presented.

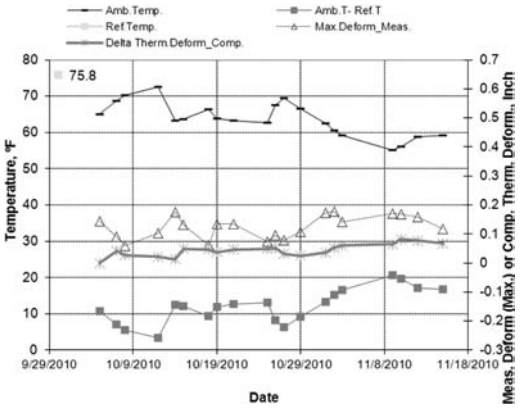

Figure 9. Measured maximum vertical displacement changes in the profiler with ambient temperature changes.

5.1 *Profiler movements by temperature changes*

The different thermal expansion coefficients for steel and aluminum affect the vertical movements of the truss beam. This movement causes errors in the rut depth calculations. To avoid these errors, measured profiles were adjusted based on the comparisons shown in Figure 9. Ambient temperature changes from approximately 15.0°C (59°F) to 22°C (72°F) were monitored and are shown as the top line in the chart. The relative temperature changes from the reference temperature, 24.3°C (75.8°F), are marked with squares in the figure. Maximum vertical movements of the beam are shown with triangles and varied up to approximately 2.5 mm (0.1 in.) over the ambient temperature range.

Thermal deformations of the two metals were computed using Equation 1 and are plotted in Figure 9 with asterisk shapes. The thermal expansion coefficient, a, is the only parameter affecting thermal deformation, δ_T, because the total length of metal, L, and temperature changes, ΔT, are the same for the two materials. The computed discrepancy also follows the ambient temperatures, although it is not as good as measured. The coefficient of determination, R^2, value between measured and computed thermal deformation discrepancy was 0.6229 by linear regression curve fitting as shown in Figure 10. One of the reasons for the relatively low R^2 value could be related to the computations based on the assumptions that each of the materials is continuous and has equal volume. However, the truss profiler has 4 separate bolted truss sections and the steel is placed only on the top of the truss to provide a guide rail to operate the profiling system trolley.

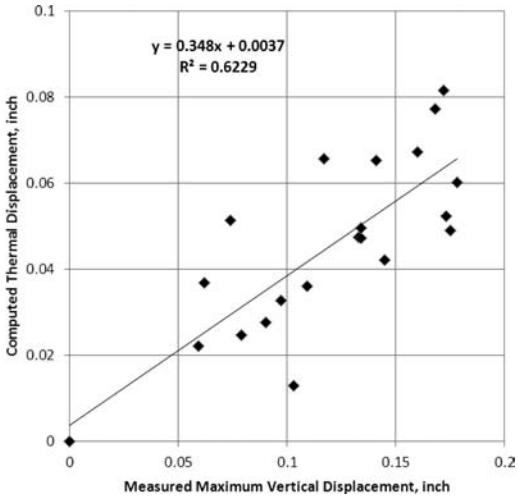

Figure 10. Correlations between measured maximum vertical displacement and computed thermal displacement.

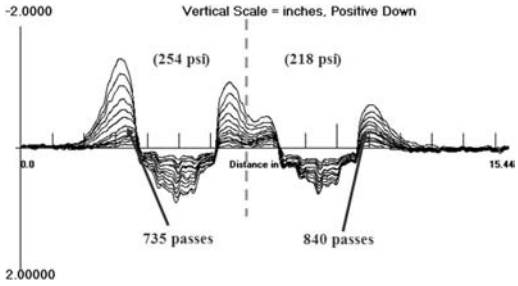

Figure 11. Transverse profiles at increasing traffic repetitions from the 1.5 MPa (218 psi) and 1.75 MPa (254 psi) wheel paths at 27.8 MT (61,300 lbs) wheel load.

5.2 *Rut depth*

When asphalt concrete is subjected to repeated loading, it hardens with accumulating plastic deformation causing consolidation. If there are no other maintenance activities, or the material heals rapidly, it will reach a point where it is sufficiently stiff for microcracks to initiate and grow. The asphalt concrete starts accumulating more plastic deformation after the initiation of microcracks, which is commonly called "tertiary flow" (Song, 2004). The accumulated stresses from traffic loads after completing the consolidation stages in pavement sub layers, causes these materials to move laterally to the non-trafficked zones depending on their adhesion strengths.

The measured transverse profiles were processed to simulate measurements made with a straightedge. Figure 11 illustrates transverse profile comparisons between 1.50 MPa (218 psi) and 1.75 MPa (254 psi) contact tire pressures at increasing traffic repetitions.

The graphical illustrations in Figure 11 show significant increase in upheaval rates from 735 and 840 load repetitions for higher and lower tire pressures respectively.

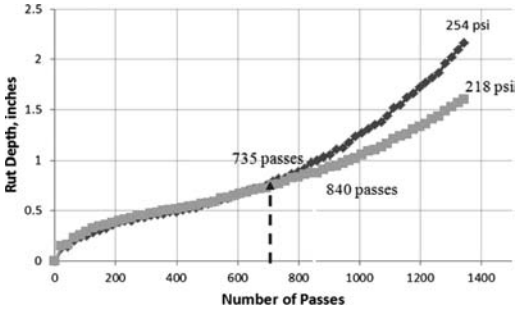

Figure 12. Rut depth changes with different tire pressures at 27.8 MT (61,300 lbs) wheel load in the PG 64-22 test sections.

The increases in computed rut depths for different tire pressures are plotted versus traffic repetitions in Figure 12. Similar results to those shown in Figure 11 were observed from rut depth computations utilizing straightedge simulations. Figure 12 shows rut depth changes with different tire pressures at 27.8 MT (61,300 lbs) wheel load in the PG 64-22 test section also indicates inflection points at 735 and 840 load repetitions for tire pressures of 1.75 MPa (254 psi) and 1.50 MPa (218 psi) respectively. Both inflection points match well with the findings from geometric analyses. The shear stress after consolidation of the pavement materials induced lateral movement of the sublayer materials at the two inflection points. The accumulated plastic flow is expressed as exponential rut depth increases for traffic applications after the two inflection points.

The pavement test sections using PG 76-22 binder have not been completed, and trafficking will continue until they show tertiary flow similar to the PG 64-22 test sections.

6 CONCLUSIONS

An infrared laser operated truss beam profiler used for monitoring pavement transverse profiles was developed. Using the profiler, data processing protocols for collecting transverse profile data to compute rut depth simulating field straightedge measurement were developed. The procedures include beam curvature corrections caused by different thermal expansion coefficients of the steel and aluminum components in the truss profiler and/or structural irregularity.

The vertical movements of the transverse profiler beam caused by ambient temperature changes were quantified and used for compensating the collected transverse profile data. A reference profile line concept was introduced and utilized to subtract the measured data at each pavement condition.

The transverse profiler was successfully used to measure the performance of flexible pavement test sections with the transverse profile line shape changes monitored at increasing pass numbers. The traditional hot mix asphalt failure stages of primary, secondary, and tertiary flow based on the rut depth charts and

stacked profile lines from the full-scale traffic testing were seen in the results.

ACKNOWLEDGEMENT AND DISCLAIMER

The work described in this paper was supported by the FAA Airport Technology Research and Development Branch, Manager, Dr. Satish K. Agrawal. The contents of the paper reflect the views of the authors who are responsible for the facts and accuracy of the data presented within. The contents do not necessarily reflect the official views and policies of the FAA or SRA International, Inc. The paper does not constitute a standard, specification, or regulation.

REFERENCES

ASTM International. 2011. Standard Test Method for Measuring Rut-Depth of Pavement Surfaces Using a Straightedge. *Annual Book of ASTM Standards (ASTM E1703/E1703M – 10) volume 04.03.*

Federal Aviation Administration (FAA) 2011. *Standards for Construction of Airports. Advisory Circular 150/5370-10E*: 195–208 & 230–232.

LMI Technologies Accessed September 23, 2011. *OptocatorTM Laser Sensors Manual*: www.lmi3D.com.

Measurement Computing Corporation (MCC). Accessed September 23, 2011. http://www.mccdaq.com.

Song, I. 2004. *Damage Analysis in Asphalt Concrete Mixtures Based on Parameter Relationships.* College Station, Texas: Texas A&M University.

Song, I. and Hayhoe, G.F. 2006. Airport Pavement Roughness Index Relationships Using the Federal Aviation Administration (FAA) Profiling System. *ASCE T&DI Airfield and Highway Pavement Specialty Conference – Meeting Today's Challenges with Emerging Technologies*, Atlanta, Georgia: 741–752.

The Engineering ToolBox (TET). Accessed September 23, 2011. http://www.engineeringtoolbox.com.

This page intentionally left blank

Advances in Pavement Design through Full-scale Accelerated Pavement Testing – Jones, Harvey, Mateos & Al-Qadi (Eds.)
© 2012 Taylor & Francis Group, London, ISBN 978-0-415-62138-0

Direct measurement of residual stress in airport concrete pavements

H. Yin
Gemini Technologies, Inc., Egg Harbor TWP, New Jersey, US

E. Guo
Consultant, Basking Ridge, New Jersey, US

F. Pecht
FAA Technical Center, Atlantic City International Airport, New Jersey, US

ABSTRACT: The current Federal Aviation Administration design procedures for airport concrete pavements do not directly consider top-down cracking. However, this distress has been repeatedly observed in full-scale tests conducted at FAA's National Airport Pavement Test Facility (NAPTF) and AIRBUS in Europe. Generally, the maximum load stress related strain near the slab bottom is mostly higher than the strain near the surface. Therefore, the cause of early appearance of top-down cracks remains unknown. Neither minimizing the curling nor increasing the slab thickness could effectively control cracks initiated from the surface. For top-down cracking, the total stress is considered a key factor. This is the sum of residual stress that exists in the pavement before a load is applied and the load induces any stress. Therefore, direct measurement of residual stress appears to be a new approach towards a better estimation of the total stress. Two testing methods, coring and saw-cutting, have been investigated, improved upon, and evaluated through a number of FAA sponsored research projects. Some residual stress measurements using both methods are presented. Future work will focus on the effects of residual stress on top-down cracking risk for field practice.

1 INTRODUCTION

Current concrete pavement design specifications use the maximum tensile stress as the failure indicator to predict service life and pavement performance. It must be noted that this is the total stress on the concrete slab causing the rupture. The AC150/5320 6E (FAA 2008) design method uses the load associated stress as the total stress, while the *Mechanistic Pavement Design Guide (MEPDG)* (AASHTO, 2002) predicts the total stress using mechanistic models. In the mechanistic models, upon certain assumptions, the maximum stresses are typically calculated using laboratory measured material properties and approximate loading configurations. However, the residual stress, which exists in concrete slabs even before traffic loads are applied, is one factor that has not been adequately considered in any design procedures.

Residual stresses in concrete pavements diminish a pavement's ability to sustain its designed load. When capacity is reduced by residual stress, a pavement is vulnerable to premature failure necessitating costly repairs or replacement. While ASTM E837 (2001) presents a test method for measuring residual stresses in steel, no similar testing method exists for concrete.

An innovative means of measuring the residual stress in concrete slabs was recently developed at the FAA's National Airport Pavement Test Facility (NAPTF) (Pecht et al., 2008) and built on by work at the University of Illinois under the FAA Center of Excellence for Airport Technology (CEAT) program (Mark and Lange, 2010). In this procedure, a surface strain gauge is glued to the slab. Then saw cuts are made on both sides of the gauge to a sufficient depth to release the residual stress. After allowing sufficient time for the heat generated by the saw cutting operation to dissipate, the difference between the initial and final strain gauge readings is proportional to the residual stress. A conceptual relationship between the total strain, load induced strain, and residual strain is given in Figure 1.

As shown in Figure 1a, during the measurement, the initial reading of the strain gauge was set to zero. After a wheel load was applied at the slab corner, the strain gauge recorded about 40 microstrains. A total of seven core drills were then made. If the drilling completely releases the normal stress, the true normal stress at the circle edge should be zero (Kirsch, 1898). Since the drill bit cannot be set exactly at the edge of the strain gauge, only a portion of the stress was released. The strain reading was reduced after each drilling operation as the gauge was pushed to one side by the generated heat. During the waiting period the heat effects diminished gradually and the strain readings became

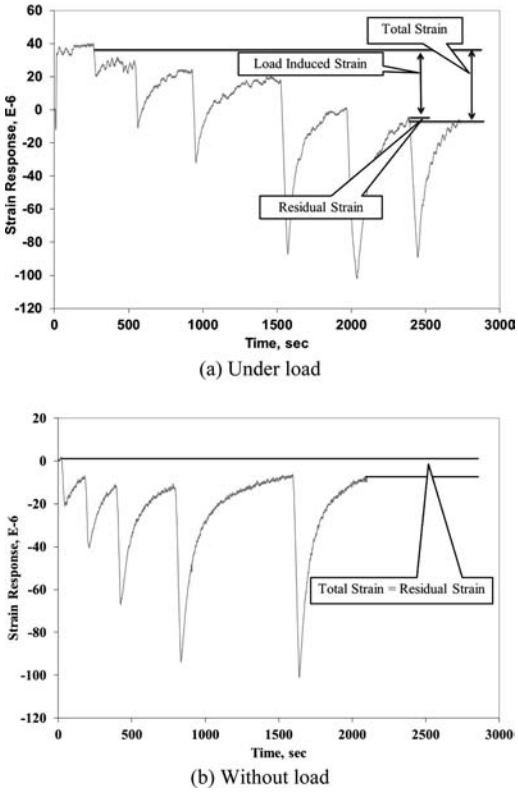

Figure 1. Typical residual strain measurements.

steady. The difference between two successive readings indicates the stress related strain released by each drilling. The drilling was stopped when the sixth and seventh readings were close to each other, about -7 microstrains. Consequently, the residual strain would be $0 - (-7) = 7$ microstrains in tension. Another typical residual stress measurement is given in Figure 1b. For this case, since no load was applied, the total strain was simply the measured residual strain, i.e., 8 microstrains. Note that the magnitude of residual strain is independent of load application.

2 BACKGROUND

2.1 *Residual stress in concrete*

Residual stresses exist in concrete pavements and structures due to material volume changes, temperature, and moisture gradients, changes in support conditions and structural restraints. Unlike stresses associated with live and dead loads, residual stresses are neglected by pavement and structural design procedures and are routinely unknown and overlooked. Yet, in some circumstances, the magnitude of residual stress can rise to a significant fraction of the strength, thus diminishing the ability for the concrete to sustain its design load. Unfortunately, there is no method to quantify the magnitude of the residual stresses which lead to the much earlier appearance of top-down cracks compared to bottom-up cracks. The early appearance of top-down cracks has been repeatedly observed in all construction cycles (CC) at the NAPTF (Guo and Marsey, 2001; Guo, 2005; Stoffels et al., 2008; Guo and Hayhoe, 2011) and full-scale tests at Airbus (Fabre and Balay, 2008).

2.2 *Top-down cracking in airport concrete pavements*

Early top-down cracks appear to be more caused by high moisture gradients than from temperature gradients (Bissonnette et al., 2007; Daiutolo, 2008). This type of distresses cannot be rationally explained using load induced strain because the measured maximum tensile strains near the bottom are mostly higher than those near the slab surface (Guo, 2005, 2008, 2010). However, consideration must also be given to the total stress operating on the concrete slab, and which leads to the rupture. This is the sum of the load-related stress and the residual stress. The total stress at the slab surface could be higher than that at the bottom of slab. It is impossible to estimate the total stress based upon the total strain because, as a pavement deteriorates, distresses will manifest themselves as a result of the altered stress state. Therefore, the relationship between deflection and the stress related strain is not valid (Guo et al., 2009).

Small airports occasionally need to accommodate aircraft movements heavier than that for which the pavement was designed. For these thinner concrete slabs, the risk of top-down cracking becomes a major concern for allowing or denying the limited operations. Field surveys of medium and large airports have also shown that top-down cracks have to be considered for terminal pavements where heavy airplanes irregularly move near the slab corners.

3 PROBLEM STATEMENT

3.1 *Early top-down cracks cannot be controlled by minimizing curling*

As mentioned in the previous sections, top-down cracking risks appears to be appreciable higher than bottom-up cracking if the measured cracking strains are assumed to be close to the strains induced by the total critical stress. Since 2002, most concrete test pavements at NAPTF have been routinely watered for curling control (Daiutolo, 2008; Stoffels et al., 2008). Consequently, the appearance of cracks was significantly delayed compared to CC1 tests (Brill, 2009). Even so, detailed distress maps (example in Figure 2) show that top-down corner cracks occurred much sooner than the bottom-up and top-down cracks longitudinal. During CC4, similar observations were obtained (Stoffels et al., 2008). Even though the curling of both CC2 and CC4 had been carefully controlled, top-down cracks still developed in the non-trafficked areas.

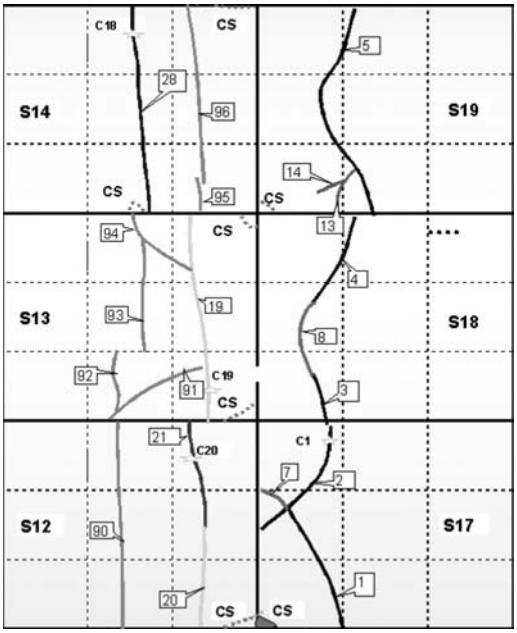

Figure 2. Top-down cracks (Number 1 to 6) were observed much earlier than the bottom-up cracks (Number 19, 20, 21, and 95) in CC-2 (Ricalde and Daiutolo, 2005).

3.2 *Early top-down cracks cannot always be avoided by increasing slab thickness*

All of the above observations were obtained from test sections with a thickness between 6 and 12 in. During full-scale tests conducted in France (Fabre and Balay, 2008), large numbers of corner cracks were observed in slabs as thick as 15 in. Full length longitudinal cracks were also observed in non-trafficked areas due to heavy gear loads applied on both sides of the slab. Similar full depth longitudinal cracks were also observed in the transition section with 17-in. thick slabs at the FAA's NAPTF (Guo and Pecht, 2007). An 830 psi concrete flexural strength still did not preserve the slabs. Although efforts were made to conduct mechanistic analysis for calculating load induced stress at all possible trafficked positions, the calculated values were never close to the flexural strength. However, field distress surveys revealed that corner cracks do not frequently occur on thick (16 in.) runways.

3.3 *Early observed top-down cracks cannot be adequately investigated using mechanistic analysis*

Several mechanistic models are available for predicting "temperature induced" (non-traffic) critical stresses (Mohamed and Hansen, 1997; Ioannides and Khazanovich, 1998; Liang and Niu, 1998; Bissonnette, 2007). One such model utilizes the "built-in curling" concept and deflection measurements (Rao and Roesler, 2005). Assuming that the following nonlinear factors of temperature gradient through the slab, moisture gradient through the slab, built-in temperature gradient, differential drying shrinkage, and creep are independent of each other, the total amount of curling can be represented as a temperature difference, or the total effective linear temperature difference (TELTD). Guo et al. (2009) demonstrated that it is not always a reliable procedure to use deflection to calculate stress with the linear elastic assumption. Yu et al. (1998) also observed the disagreement of deflection and stress relationship from measurements and mechanistic analysis. In addition, variability in material properties (Bazant and Planas, 1997), localized environment (Grasley, 2006), creep effects (Nilson et al., 2004), and interface condition (Guo et al., 2009) could also contribute to the prediction errors when using mechanistic analysis.

4 OBJECTIVE

As presented in the previous sections, mechanistic approaches cannot always adequately explain why top-down cracks occur earlier than bottom-up cracks.

Theoretically, the total stress can only be obtained by selecting a reference point at which the stress is "zero". From an experimental point of view, both coring and saw cutting can reduce the stress to zero perpendicular to the drilling/cutting line. Then, the reading after drilling/cutting subtracted from the reading before drilling/cutting is the "total stress related strain".

The objective of this research work was to investigate, evaluate, and improve the direct measurement of residual stress in concrete. This would allow top-down cracking risks in airport concrete pavements to be better assessed and design procedures to be improved.

5 DEVELOPEMENT OF RESIDUAL STRESS MEASUREMENT PROCEDURES

5.1 *Coring method*

A series of residual stress measurements using the coring method were initially conducted on beams, single slab, and multiple slabs (Guo et al., 2008). In addition, the reliability of the testing procedure was thoroughly evaluated (Guo and Pecht, 2007). The relative effects for stress release on beams were investigated by 3D FEM model (Li, 2009). For demonstration purposes, two examples of residual stress measured using the coring method are given in Figures 3a and 3b.

The coring method introduces minimal damage to existing pavements. Test results have proven to be repeatable and reliable (Guo and Pecht, 2007, Pecht et al., 2008). In addition, the coring method can be further improved by two-sided drilling.

5.2 *Saw-cut method*

The coring method was replaced by a two-sided saw-cut method. The saw-cut procedure minimizes the heat released and significantly reduces the time

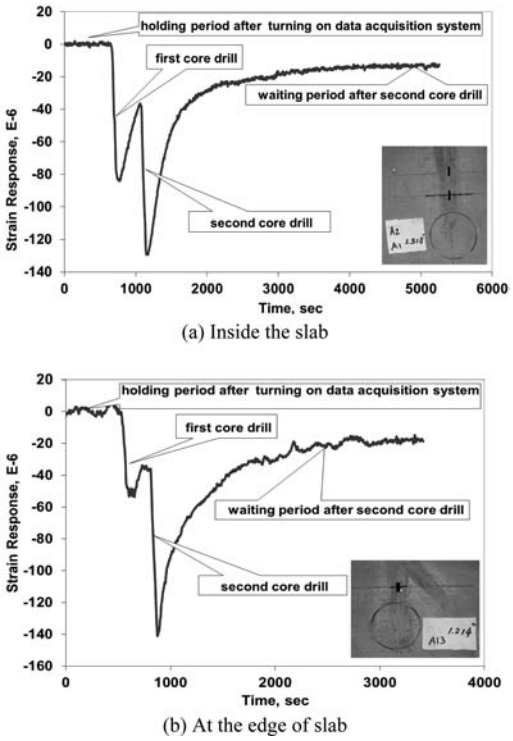

Figure 3. Residual stress measured using coring method.

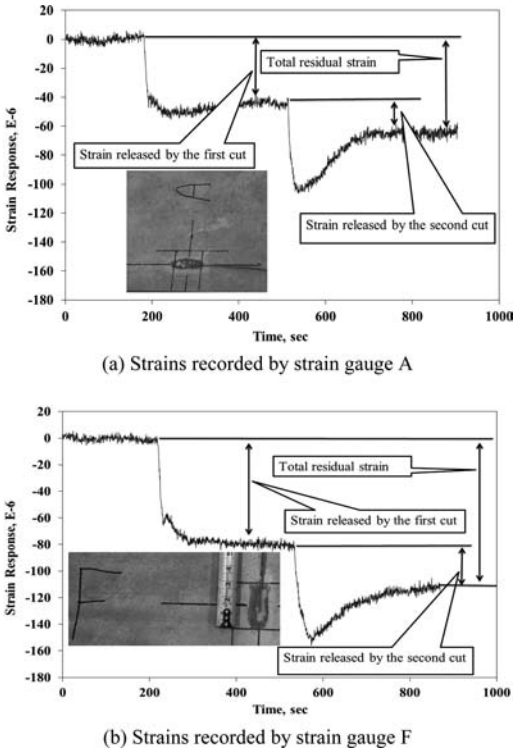

Figure 4. Residual stress measurements using saw-cut method.

required to drop the temperature back to the initial state (Mark, 2009; Mark and Lange, 2010). Since 2009, numerous laboratory and field tests have been conducted by the Engineering Research and Development Center (ERDC), US Army Corps of Engineers, to evaluate the two test methods (Bianchini and Gonzalez, 2011).

Practically, the saw-cut procedure can be completed in a few seconds but core drills may take up to several minutes. In addition, the saw-cut procedure requires much shorter waiting periods for the gauge response to steady. Since strain gauges are very sensitive to environmental changes, such as wind, the test must be completed as quickly as possible in the field. Therefore, the saw-cut (notch) procedure was selected for full-scale tests at NAPTF.

At the NAPTF, measurements of residual stress using the saw-cut procedure were conducted on June 30, 2011. Since all existing cracks initiated from the slab edge and only critical stress at the joint is considered in current design specifications (FAA, 2008), all gauges were installed at the transverse joints. Two cuts on each side of the gauge were made to a depth of 1.0 to 1.2 in. To better understand the effect of each cut, a waiting period was proposed between two successive cuts. It is critical that the "zero reference point" for the strain reading is recorded at the same stress state, before and after the saw cut. This ensures that the difference between the two readings is the desired "total stress related strain". Cutting generates heat and induces new stresses. This additional stress must be controlled to a negligible level. Readings from two strain gauges are presented in Figure 4. It is clear that most stress was released by the first cut. However, significantly different strain gauge readings (about 40 microstrain variation) are present between gauge A and F. While small discrepancies of the layer material properties and subgrade support resulting in dissimilar results on the same slab are common, it is unclear whether these factors can range widely enough to produce the strain responses depicted in Figure 4.

As illustrated in Figures 3 and 4, the released strains exhibit three distinguishable characteristics:

1. During each core drill or saw cut, the strain reading decreases sharply due to the heat being generated on one side of the gauge;
2. After each core drill or saw cut, the strain reading increases because of the cooling from the other side of the gauge. The reading rises smoothly and then gradually tends toward a steady state;
3. The strain reading will not change when the saw cutting depth reaches a certain point, which indicates all stresses that could have been released are released.

The advantages of direct measurements of residual stresses can be summarized as follows:

1. Direct measurement avoids dealing with variability in material properties, localized environment,

creep effects, and interface conditions, which are extremely difficult to accurately address in any mechanistic analysis;
2. A common practice for estimating load induced response is to subtract the initial gauge reading from the peak value. However, it can be theoretically proven that the normal stress perpendicular to the saw cut (notch) must be zero along the cutting line. Thus, it is possible to measure residual strain, total strain, and then further estimate related stresses.
3. Though the residual stress can not be entirely released, most of it can be released if a double (two-side) cutting procedure is followed and the spacing between the cut and the gauge is small enough (e.g., less than 0.5 in.).

6 CRITERIA FOR RELIABLE RESIDUAL STRESS MEASUREMENT

The strain readings in Figure 4 are considerably higher than previous results (Figure 3). Some very high strains were also reported in Castaneda (2011), and Bianchini and Gonzalez (2011). Castaneda (2011) measured a load induced strain of 380 microstrains in an uncracked single slab. Given that related stress would be up to 2,000 psi, the existence of microcracks on the concrete surface could be one explanation of such high residual strains.

It is known that measured pavement responses are not as stable and precisely repeatable as analytical solutions. A qualitatively sound and acceptable precise range of residual stress on slab surfaces (i.e., 0–50, 50–100, or 100–150 psi) rather than exact values, is of importance for practical applications.

To ensure reliable measurements of residual stress, four criteria are proposed:

1. The concrete surface needs to be carefully prepared so that micro cracks are minimized.
2. Strain gauges need to be correctly installed and gauge readings must be carefully evaluated (Guo and Pecht, 2007).
3. Saw cuts must be made one at a time. The second cut should not be made until the strain reading has steadied. A waiting period is required for each cut.
4. The strain curve must follow the pattern, as previously shown in Figures 1, 3, and 4.

7 CONCLUSIONS AND RECOMMENDATIONS

High surface stress induced early top-down cracks have been repeatedly observed in full-scale tests at FAA's NAPTF and Airbus in Europe. Neither the measured load stress related strains nor mechanistic analysis can reasonably explain this phenomenon.

The total stress is the sum of pre-existing residual stress and the load induced stress. Therefore, direct measurement of the residual stress is an innovative means towards the better estimation of the total stress. Testing procedures have been investigated, improved upon, and evaluated through a number of FAA sponsored research projects. Based on residual stress measurements from the NAPTF, both coring and saw-cut methods showed promise as viable techniques for measuring stresses in plain airport concrete pavements.

It is important to note the nonlinearity of residual stress, which results from differential drying and improper compaction in the plastic state of the freshly cast concrete. In addition, a given measurement of residual stress only indicates the surface stress state at the time of testing. The stress state changes over time as the pavement experiences daily and seasonal temperature cycles. Thus, it is prudent to repeat the testing over time in order to better understand the residual stress state.

Assessing the top-down cracking risk in airport concrete pavements is challenging due to complex environmental conditions, slab geometry, and pavement use. Field practice calls for a standardized testing procedure to measure residual stress.

ACKNOWLEDGEMENTS

This work was supported by the FAA Airport Technology Research and Development Branch, Manager, Dr. Satish K. Agrawal. Special thanks are given to Dr. Gordon F. Hayhoe for his technical leadership in test planning and organization and to Mr. Chuck Teubert for his test management. The contents of the paper reflect the views of the authors, who are responsible for the facts and accuracy of the data presented. The contents do not necessarily reflect the official views and policies of the FAA. The paper does not constitute a standard, specification, or regulation.

REFERENCES

AASHTO. 2002. *Mechanistic-Empirical Pavement Design Guide*.

ASTM E837-01. *Standard Test Method for Determining Residual Stresses by the Hole-Drilling Strain-Gage Method.*

Bazant, Z.P. and Planas, J. 1997. *Fracture and Size Effect in Concrete and Other Quasibrittle Materials*.

Bianchini, A. and Gonzalez, C.R. 2011. *Field Evaluation of Curling And Warping In Rigid Pavements With Respect To Temperature And Moisture Gradients And Depth.* Report submitted to FAA, U.S. Army Engineer Research And Development Center.

Bissonnette, B, Attiogbe, E.K., Miltenberger, M.A. and Fortin, C. 2007. Drying Shrinkage, Curling, and Joint Opening of Slabs-on-Ground, *ACI Materials Journal.*

Brill, D. 2009. *Calibration of FAARFIELD Rigid Pavement Design Procedure.* Technical report DOT/FAA/AR-09/57.

Castaneda, D.I. 2011. *New Field Testing Procedure For Measuring Residual Stress In Plain Concrete Pavements And Structures,* MSc Thesis, University of Illinois at Urbana-Champaign.

Daiutolo, H. 2008. Control of Slab Curling in Rigid Pavements at the FAA National Airport Pavement Test Facility,

3rd *International Conference on Accelerated Pavement Testing*, Madrid, Spain.

FAA. 2008. *FAA Advisory Circular, Airport Pavement Design and Evaluation.* AC150/5320 6E.

Fabre, M. and Balay, M.J. 2008. The Airbus Pavement Experimental Programme and High Tire Pressure Test, 3rd *International Conference on Accelerated Pavement Testing*, Madrid, Spain.

Grasley, Z.C. 2006. *Measuring and Modeling the Time-Dependent Response of Cementitious Materials to Internal Stresses*. PhD Thesis, University of Illinois at Urbana-Champaign.

Guo, E. and Marsey, W. 2001. Verification of Curling In PCC Slabs at FAA National Airport Pavement Test Facility, *ASCE Special Edition for Conference Advantaging Airfield Pavements.*

Guo, E. 2005. Crack Propagation in Concrete Slab Observed at the FAA's NAPTF, *Proceedings of Workshop on Fracture Mechanics for Concrete Pavements: Theory to Practice*.

Guo, E., Pecht, F. and Ricalde, L. 2008. Pavement Strength Measured by Full Scale Test, Pavement Cracking, Mechanisms, *Modeling, Detection, Testing and Case Histories*.

Guo, E. and Pecht. F. 2007. Application of Surface Strain Gages at the FAA's NAPTF, *FAA World Wide Airport Technology Transfer Conference*, Atlantic City, NJ.

Guo, E, Pecht, F.E., Ricalde, L., Barbagallo, D. and Li, X. 2008. Data Analysis On Residual Stresses Measured In Concrete Beams, *Proceedings of the 9th International Conference on Concrete Pavements*, San Francisco, CA.

Guo, E., Daiutolo, H., Ricalde, L. and Wang, Q. 2009. Interface Effects on the Load Induced Responses of a Curled Single Slab, *CD-ROM Proceedings 88thTRB Annual Meeting*. Washington, DC: Transportation Research Board.

Guo, E. and Gordon, H. 2010. Three-Stage Failure Mechanisms of Concrete Pavement – Failure Stage One: Initiation of Cracks, 7*thInternational DUT-Workshop on Design and Performance of Sustainable and Durable Concrete Pavements*, Alcazar de la Reina, Carmona.

Guo, E. and Gordon, H. 2011 Top-Down and Bottom-Up Cracking Mechanism in Failure Stage Two of Airfield PCC Pavements,*Seminar on Airfield Pavements, XXIVth World Road Congress*.

Ioannides, A.M. and Khazanovich, L. 1998. Nonlinear Temperature Effects on Multilayered Concrete Pavements, *Journal of Transportation Engineering, ASCE, Vol. 124, No. 2*.

Kirsch. 1898. *VDI, Volume 42*. See Reference by Timoshenko 1953, page 407.

Li, X. 2009. *Forming Process and Measurement Method Study on Residual Stress in Cement Concrete*, PhD Thesis, Harbin Institute of Technology, China.

Liang, R.Y. and Niu, Y.Z. 1998. Temperature and curling stress in concrete pavements: Analytical Solutions. *Journal of Transportation Engineering, ASCE , Vol. 124*.

Marks, D.G. 2009. *Development Of Residual Stress Measurement For Concrete Pavements Through Cantilevered Beam Testing*, MSc Thesis, University of Illinois at Urbana-Champaign.

Marks, D.G. and Lange, D.A. 2010. Development of Residual Stress Measurement for Concrete Pavements through Cantilevered Beam Testing, *FAA Worldwide Airport Technology Transfer Conference*, Atlantic City, NJ.

Mohamed, A. and Hansen, W. 1997. Effect of Nonlinear Temperature Gradient on Curling Stress in Concrete Pavements, *Transportation Research Record, Journal of the Transportation Research Board, No.1568*. Washington, DC: Transportation Research Board.

Nilson, A, Darwin, D. and Dolan, C. 2004. *Design of Concrete Structures, 13th Edition*, McGraw-Hill Company, Inc.

Pecht, F., Guo, E. and Gagnon, J. 2008. Core-ring Strain Gage Procedure for Measuring Residual Stress in a Concrete Beam, *Proceeding of 6th International Conference on Road and Airfield Pavement Technology*, Kaparo, Japan.

Rao, S. and Roesler, J.R. 2005. Non-destructive Testing of Concrete Pavements for Characterization of Effective Built-in Curling, *Journal of Testing and Evaluation, Volume 33*, Issue 5.

Ricalde, L and Daiutolo, H. 2005. New Rigid Pavement Construction and Testing at the FAA National Airport Pavement Test Facility (NAPATF), 5*thInternational Conference on Road and Airfield Pavement Technology and Exhibition on Road and Airfield Construction and Management*, Seoul, Korea.

Stoffels, S., Morian, D., Ioannides, A., Wu, S., Sadasivam, S., Yeh, L. and Yin, H. 2008. *Improved Overlay Design Parameters for Concrete Airfield Pavements.* Final Report, IPRF Project FAA-01-G-002-04-2.

Yu, H.T, Khazanovich, L. and Darter, M.I. 1998. Analysis of Concrete Pavement Responses to Temperature and Wheel Loads Measured from Instrumented Slabs. *Transportation Research Record, Journal of the Transportation Research Board, No. 1639*. Washington, DC: Transportation Research Board.

Advances in Pavement Design through Full-scale Accelerated Pavement Testing – Jones, Harvey, Mateos & Al-Qadi (Eds.)
© 2012 Taylor & Francis Group, London, ISBN 978-0-415-62138-0

A modular data acquisition system for heavy vehicle simulator tests

R.Z. Wu, J.D. Lea & D. Jones
University of California Pavement Research Center, University of California, Davis, US

ABSTRACT: This paper describes the design and fabrication of a Data Acquisition (DAQ) system that uses the latest hardware and software technology. Two systems were built to work with two active Heavy Vehicle Simulators (HVS) at the University of California Pavement Research Center (UCPRC). The new DAQ systems replaced the old ones that were built in 2005. The upgrade was considered necessary because the data acquisition hardware used in the old systems were no longer actively supported by the vendor. The new system maintains the ability to measure temperature, displacement, strain, pressure (voltage) and surface profile. In addition, the new system can also measure resistance and current. A modular design was adopted to facilitate future upgrades without having to replace all of the components. It also allows sharing and balancing of the DAQ needs between the two HVS units. It is believed that the design of the new DAQ system is sufficiently generic and can provide useful information for other accelerated pavement testing programs.

1 INTRODUCTION

Data collection is an essential part of any accelerated pavement testing (APT). It collects data on pavement condition and responses that are required for analysis and drawing conclusions from the tests. The software and hardware that are used for data collection are herein referred to as a data acquisition (DAQ) system. Depending on the specific needs of an APT program, the DAQ system used can be very different and is typically custom built.

This paper presents a modular DAQ system that has been developed for the Heavy Vehicle Simulators at the University of California Pavement Research Center (UCPRC). Although the specific details of the system may not be readily applicable to other APT programs, it is believed that the general design will be helpful for institutions that are starting an APT program, or for other APT programs that are considering upgrading or replacing their DAQ systems.

Data of potential interest to researchers in a typical HVS test can be divided into three categories based on the parameter being measured: (1) pavement condition and response; (2) loading parameters such as tire pressure and wheel load; and (3) ambient environment conditions such as rainfall and air temperature. The DAQ system discussed in this paper is focused on data related to pavement only. At UCPRC, loading parameters are obtained by monitoring network traffic on the private HVS local area network (LAN), while an automatic weather station is installed next to the test tracks for logging on-site weather conditions.

The UCPRC has been actively running HVS tests since it first acquired two machines and the associated DAQs in 1994 (Harvey, et al. 1996). The DAQ systems were upgraded once in 2005 to a DAQ board based system and has since been incrementally enhanced without changing the overall structure. The system is able to measure temperature, displacement, strain, pressure, and to drive a laser profilometer. A list of the sensors and instrumentation that can be connected to the old UCPRC DAQ system is shown in Table 1.

Table 1. List of sensors and instrumentations that can be connected to the old UCPRC DAQ system.

Sensor or instrumentation	Measurement type	Sensor type
Thermocouple	Temperature	Type-K
Road Surface Deflectometer (RSD)	Displacement	AC LVDT
Multi-Depth Deflectometer (MDD)	Displacement	AC LVDT
Joint Deflection Measurement Device (JDMD)	Displacement	DC LVDT
Strain gauge	Strain	Wheatstone bridge
Pressure cell	Pressure	Wheatstone bridge
Laser profilometer (PRF)	Distance	Laser

Although still functional, problems with the 2005 DAQ systems include:

- Issues with the DAQ hardware:
  - The DAQ boards are no longer supplied by the vendor
  - The DAQ boards are not supported by the latest version of hardware driver and consequently the software can not be upgraded

- The DAQ boards require a very old technology that is no longer available in modern PCs, which makes it impossible to upgrade the controller PC

– It is difficult to transfer the DAQ capacity between the two systems because too many functions are packed into the signal conditioning box. Adding a component to the box requires considerable wire re-routing. There is also insufficient space in the box for additional components.
– The current DAQ software does not record HVS wheel speed along with deflection and strain measurements.

To address these issues, two new DAQ systems were designed and built that use the latest hardware and software platform available. The new system has a modular design so that components can be independently removed, replaced and added, and the software uses the most current hardware driver, and adds the capability to record wheel speed to the DAQ software.

This paper presents the design of the new DAQ hardware including demand analysis, hardware selection and implementation, and describes the methods used in the software to collect synchronize pavement responses and HVS wheel speed.

2 HARDWARE DESIGN

This section describes how the decisions were made about the hardware components as well as the overall modular design of the system.

The components of a DAQ system can be divided into four groups:

– A controller, typically a personal computer (PC), that runs the DAQ software and drives the DAQ hardware;
– The DAQ hardware that converts analog signals into digital values that can be read by the controller;
– The signal conditioners that convert the raw signal from sensors or instrumentation into quantities readable by the DAQ hardware; and
– The sensors or instrumentation that measure pavement response or conditions.

One of the key objectives for the new system was to be able to replace each one of the above components without significantly affecting any of the other components. Also, it was decided to use off-the-shelf components wherever possible so that individual components can be replaced with minimal downtime.

2.1 *Demand analysis*

Determining the demand requirements of a new DAQ system before designing it is critical. There is considerable variability in terms of data collection capability in the hardware offered by various vendors. A clear demand analysis allows one to reach the balance between system capability and budget.

The first aspect of demand covers the kind of sensors that the new DAQ should support. As mentioned above, the 2005 DAQ system measured temperature, displacement, strain, and pressure through a range of sensor types, and drove a laser surface profilometer. The new system would thus need to accommodate the same measurements, all of which are routinely used in UCPRC studies, as a minimum requirement, as well as be able to accommodate additional sensor types, such as those based on resistance and current. For example, certain pressure cells provide a temperature reading with a thermister, which is essentially a sensor with resistance varying with temperature.

Another critical aspect of demand analysis for the new DAQ system is the sampling rate of each quantity being measured. Different quantities need to be sampled at different rates depending on whether they are static or dynamic. From an HVS testing perspective, dynamic quantities are those that vary with position of the wheels while static quantities do not. Dynamic quantities include deflection, strain and pressure, while static quantities include pavement temperature and permanent deformation.

Dynamic quantities were sampled at every 7.4 mm of wheel movement in the 2005 DAQ system, which is believed to be sufficiently fast for the HVS, which can run at a speed of up to 20 km/h. This implies a sampling rate of:

$$R_{Dynamic,HVS} = \frac{20 \times 10^6/3600}{7.4} = 750(Hz) \qquad (1)$$

where $R_{Dynamic,Hvs}$ is the required sampling rate or dynamic quantities during HVS tests.

The second consideration for dynamic quantities is the need to measure pavement response from a falling weight deflectometer (FWD). A typical FWD load pulse is 0.025 seconds. Assuming a minimum of 20 samples per load pulse, the sampling rate required for recording FWD responses is:

$$R_{Dynamic,FWD} = \frac{1}{0.025/20} = 800(Hz) \qquad (2)$$

where $R_{Dynamic,FWD}$ is the required sampling rate for dynamic quantities during FWD testing.

Combining the requirements for recording pavement response under HVS trafficking and FWD loading, the overall required sampling rate was rounded off to 1,000 Hz to allow for some redundancy. In addition, the raw data sampling rate was increased by a factor of 10 to 10,000 Hz. This allows resampling at 1,000 Hz by taking an average of every 10 readings to filter out noise.

Another important consideration for the HVS DAQ system is that it has limited needs for real time hardware control. In fact, the only device it needs to control is the laser profilometer.

Table 2. DAQ modules selected for each system.

Module	Signal Type	Quantity Type	Sampling Rate (kS/s/Ch)*	Available Channels	Number of Modules
NI cDAQ-9401	Digital I/O, Counter	Control	N/A	8	1
NI cDAQ-9221	Voltage (+/−60V)	Dynamic	100	8	1
NI cDAQ-9205	Voltage (+/−10V)	Dynamic	15	16	2
NI cDAQ-9237	Strain, Pressure Cell	Dynamic	50	4	1
NI cDAQ-9203	Current	Dynamic	25	8	1
NI cDAQ-9213	Temperature	Static	0.075	16	1
NI cDAQ-9219	Universal	Static	0.1	4	1

*: kS/s/Ch = 1000 samples per second per channel

2.2 *DAQ hardware selection*

Once the demands are determined, the actual DAQ hardware can be selected to satisfy these demands. The decision involves selecting: (1). individual DAQ modules for each parameter to be measured; and (2). the hardware platform that combines all of the DAQ modules into a synchronized system.

National Instrument (NI) products were selected for building the DAQ system because they provide a complete solution that allows fast software development and hardware integration. NI products are divided into various form factors, among which *PXI* and *CompactDAQ* are the two most versatile options based on the number of modules they support. After comparing *PXI* and *CompactDAQ systems*, a decision was made to use the *CompactDAQ* system because it satisfies all of the demands and is less expensive than the *PXI* system. An NI cDAQ-9178 8-slot USB chassis was selected along with eight modules (see Table 2). Note that the NI cDAQ-9188 8-slot Ethernet chassis was initially selected but was replaced because its communication with the PC controller was not fast enough for driving the profilometer. The maximum sampling rates for the modules measuring dynamic parameters are all faster than 10,000 Hz per channel.

2.3 *Modular design*

In order to achieve a modular design, the following components were separated from each other:

- The controlling PC
- The DAQ hardware
- The signal conditioners, and
- The sensors and instrumentation.

A hardware diagram of the new DAQ system is shown in Figure 1, with shading inside the text box indicating each of these components. Most of the sensors can be directly connected to the DAQ hardware because the *CompactDAQ* modules provide the required signal conditioning for strain, temperature, and resistance. Alternating current (AC) LVDTs such as those used in MDDs and RSDs require a signal conditioner to convert the AC output into standard direct current (DC) output that can be connected to the NI cDAQ-9205 that reads voltage. DC LVDTs such as those used in JDMDs require voltage excitation, which needs to be supplied in a separate conditioner box.

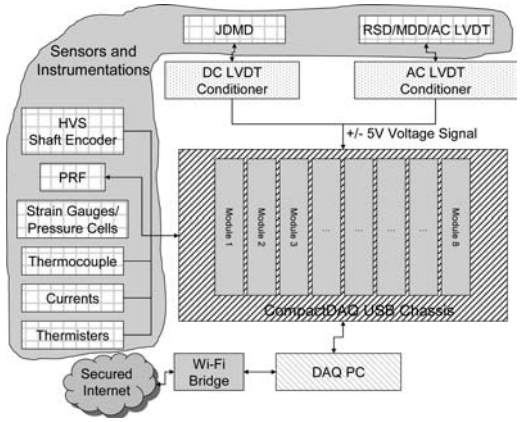

Figure 1. Hardware diagram of the new DAQ system, shading in each text box indicates component type.

The modular design shown in Figure 1 allows replacement of any component without affecting the other components, and the DAQ hardware can be upgraded relatively easily if the *CompactDAQ* system becomes obsolete.

3 IMPLEMENTATION

This section describes how the design discussed in Section 2 was physically built. All of the hardware shown in Figure 1 was designed to be connected to a centralized location where the DAQ PC drives the DAQ hardware during data collection. The signal conditioners, DAQ hardware, DAQ PC and network hardware are all mounted in an open-frame standard 48 cm rack. The sensors and instruments connect to the rack-mount system using cables. Figure 2 shows a schematic of the rack-mount system.

The DC LVDT stack shown in Figure 2 contains only a power supply unit to provide the necessary excitations. Each of the AC LVDT stacks contain five AC LVDT conditioner circuits and a power supply unit. The *CompactDAQ* stack contains only the DAQ hardware, i.e., the 8-slot chassis and its modules.

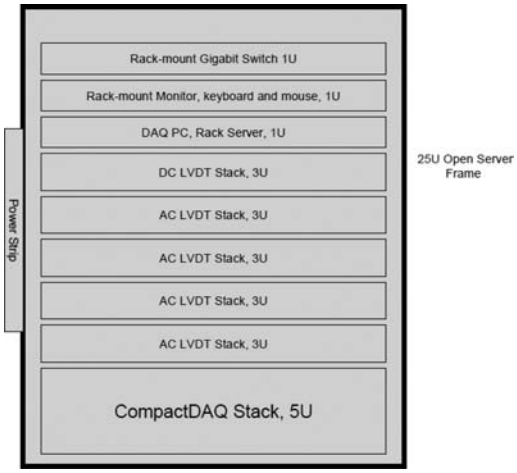

Figure 2. Schematic of the new rack-mount DAQ system.

4 SOFTWARE DESIGN

The 2005 DAQ software did not require a complete rewrite. Instead, it was upgraded to use the latest device driver and then enhanced to incorporate new features that were considered useful. This section discusses the overall framework and features added to the software.

4.1 *Overall framework*

The HVS DAQ software records pavement responses and status during both trafficking and data collection breaks. Static quantities such as pavement temperature are sampled at slow rates (such as 1 Hz for temperature) and the sampling of different quantities does not require synchronization. On the other hand, dynamic quantities are sampled at a much higher rate (around 1 kHz depending on the wheel speed) and consequently the sampling needs to be synchronized so that all quantities correspond to the pavement responses at exactly the same time.

For collecting dynamic quantities, signals provided by the HVS are used for timing and triggering in order to synchronize the data collected. Figure 3 shows a schematic of the driving mechanism for the HVS and some of the sensors related to HVS wheel movements. The HVS carriage unit is connected to a chain that is in turn driven by a rotating sprocket at one end of the machine. An encoder is installed on the shaft of the driving sprocket to record the shaft rotation. A proximity sensor is installed at each end of the HVS to control start, stop and turn around actions.

Figure 4 shows how the signals from the HVS sensors are used during data collection. A single pulse is generated by the proximity sensors whenever the wheels return to or leave the section ends. This pulse is used to trigger data collection. The DAQ software also keeps track of these proximity sensor signals and determines the direction of the wheels. The shaft encoder outputs a series of signals in the form of a pulse

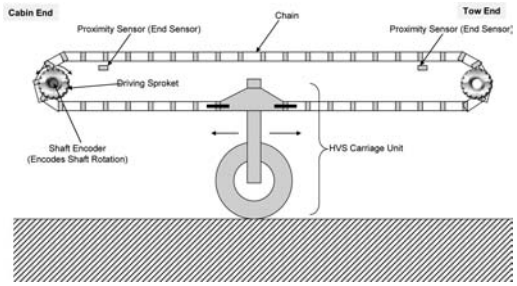

Figure 3. Schematic of HVS driving mechanism and layout of sensors related to wheel movement.

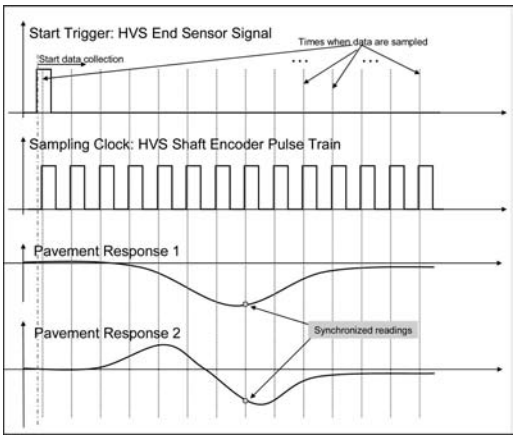

Figure 5. Triggering and timing of synchronized data collection for dynamic data parameters.

train with a resolution of 1,000 pulses per shaft rotation that indicates direction and amount of shaft rotation. This pulse train is referred to as the HVS Clock, and data collection is synchronized by triggering at the same time and using the same sampling clock. In the 2005 DAQ system, the HVS Clock was subdivided into 125 pulses per shaft rotation before it was used as the sampling clock. The new DAQ software has the same triggering and timing mechanism, but does not subdivide the HVS Clock. Consequently, eight times more data is collected compared to the 2005 system. The raw data are then re-sampled at 1/8 of the HVS Clock rate by taking an average of every eight readings resulting in better quality data, especially if noise levels are high.

4.2 *Recording HVS wheel speed*

Compared to the 2005 system, one of the major enhancements to the DAQ software is the ability to record a synchronized instantaneous wheel speed for the pavement responses collected. This allows studies of the effect of wheel speed on pavement response and performance.

The key to measure wheel speed is the digital counter in the NI-cDAQ 9178 chassis that can be

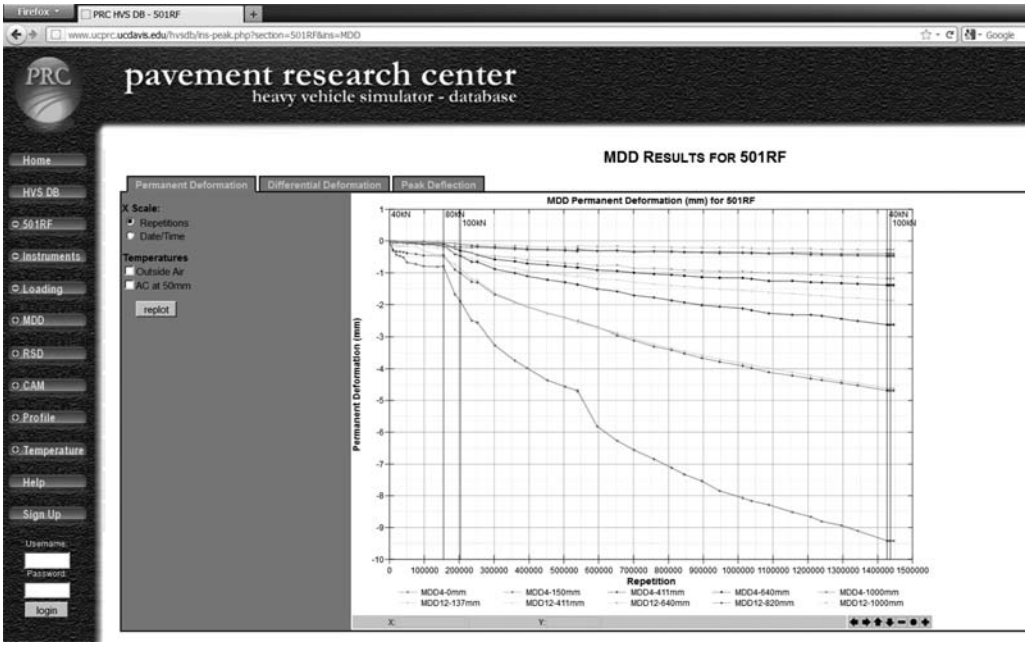

Figure 4. Screenshot of the web-interface for UCPRC HVS database.

accessed using digital modules such as NI cDAQ-9401. A digital counter can measure the frequency of a given pulse. Given that the HVS wheel moves a distance of 7.4 mm for each pulse in the HVS Clock, HVS wheel speed can be calculated by measuring the frequency of the HVS Clock.

4.3 *Data storage and access*

The data collected are stored in text format to allow effective revision control. They are loaded into a *PostgreSQL* database server (Lea and Popescu, 2003) using a loader program that is written as an *Excel*® spreadsheet. The loader program conducts various quality checks before accepting the data. Once loaded, the data can be accessed through a web interface that provides various built-in plots (example of screenshot in Figure 5). The data can also be queried and exported using standard database engines that are available in various programming languages such as *Matlab*®, *Java*® and *Visual Basic*®.

5 SUMMARY AND CONCLUSIONS

This paper describes the design and fabrication of a new data acquisition (DAQ) system for accelerated pavement testing devices. The hardware of this DAQ system follows a modular design that separates the DAQ hardware from the other components. The main goal is to have a system that allows each of the key components to be independently repaired and/or upgraded without affecting the other components. The new system also allows for relatively easy transfer of DAQ capacity between two APT units, which is important because different HVS tests can have very different DAQ needs.

Although the discussion presented in this paper is specific to Heavy Vehicle Simulators, it is believed that the ideas are sufficiently generic to be applicable to other accelerated pavement testing programs.

ACKNOWLEDGEMENT AND DISCLAIMER

This work was undertaken with funding from the California Partnered Pavement Research Program of the California Department of Transportation (Caltrans), Division of Research and Innovation, which is greatly appreciated. The opinions and conclusions expressed in this paper are those of the authors and do not necessarily represent those Caltrans, or the Federal Highway Administration. The authors would also like to acknowledge the staff at the accelerated pavement testing facility at Florida State Department of Transportation for their assistance.

REFERENCES

Harvey, J.T., 1996. *Initial CAL/APT Program: Site Information, Test Pavement Construction, Pavement Materials Characterizations, Initial CAL/APT Test Results, and Performance Estimates.* Davis and Berkeley: University of California Pavement Research Center. Report for the California Department of Transportation.

Lea, J. and Popescu, L. 2003. *The Design and Implementation of the Pavement Research Center Heavy Vehicle Simulator Database*. Davis and Berkeley: University of California Pavement Research Center. Report for the California Department of Transportation.

This page intentionally left blank

Advances in Pavement Design through Full-scale Accelerated Pavement Testing – Jones, Harvey, Mateos & Al-Qadi (Eds.)
© 2012 Taylor & Francis Group, London, ISBN 978-0-415-62138-0

Simulating the effects of instrumentation on measured pavement response

F. Leiva-Villacorta & D.H. Timm
Auburn University, Auburn, Alabama, US

ABSTRACT: Asphalt strain gauge installation procedures have typically used hot mix sieved through a 4.75 mm screen, hand placed over the gauges and hand compacted prior to roller compaction which has led to a high gauge survival rate. This finer mix in the immediate vicinity of the gauge could theoretically yield lower moduli and higher strains. The objective of this study was to evaluate the potential effect of using a finer mix as gauge cover on pavement response. Finite element analysis was used to simulate a three-layered pavement structure containing a patch of sieved material at the bottom of the asphalt concrete layer. Tensile strain responses were calculated at the bottom of the asphalt concrete layer under a single load for all structures with and without the finer mixture. The results were compared to a previously defined benchmark of 30 $\mu\varepsilon$ which was more likely to be exceeded with layers thinner than 5 in. and moduli between 200 and 500 ksi.

1 INTRODUCTION

Mechanistic-empirical (M-E) pavement design relies on the accuracy of mechanistic models to compute critical pavement responses and predict pavement performance. As researchers continue to develop and refine models, gauges embedded in pavement sections at accelerated pavement test (APT) facilities have proven useful in providing measured responses as a basis of comparison. One such APT facility, the National Center for Asphalt Technology (NCAT) Test Track, has been using embedded gauges since 2003 in so-called "structural" pavement sections (Timm et al., 2004, Timm, 2009). Though asphalt strain gauge installation procedures have evolved incrementally with each successive reconstruction cycle at the Test Track, they all have used hot mix sieved through a 4.75 mm screen, hand placed over the gauges and hand compacted prior to regular roller compaction. This procedure protects the gauges during construction and has lead to a high gauge survival rate. However, this process introduces finer mix in the immediate vicinity of the gauge which could yield lower moduli and higher strain. Therefore, the level of significance of the potential error induced by the use of finer mix as gauge cover needed to be determined.

2 BACKGROUND

Pavement instrumentation is an important tool to monitor in situ pavement material performance and critical structural responses under environmental and loading conditions. The NCAT Test Track is a facility where instrumentation is used to study many issues pertaining to mechanistic-empirical (M-E) design. Inclusion of instrumented sections started in 2003 (second cycle) where eight sections were utilized for a structural experiment. Currently, that number has been doubled to sixteen sections.

A typical structural section at the Test Track contains 12 strain gauges and two pressure cells (Figure 1). One earth pressure cell is placed at the top of the base material layer and the other on top of the subgrade material layer. The strain gauge array is centered along the outside wheel path of the pavement structure. The array consists of two rows of three longitudinal gauges and two rows of three transverse gauges. Each asphalt gauge has an offset of 2 ft. from the next closest gauge (Timm et al., 2004). All these devices are connected to a data acquisition system. During gauge installation, trenches for the conduits containing the cables and cavities for pressure cells were excavated. Prior to the placement of the next layer these elements were hand-backfilled and hand-compacted. Finally, all the asphalt strain gauges were covered with the respective mix sieved through the No. 4 sieve prior to compaction by rollers (Figure 2).

Information obtained from the last two Test Track research cycles related to the installation of gauges, methodology for data collection, and data analysis has been well documented (Timm et al., 2004, Timm, 2009). This information includes full details of not only gauge installation but also analyses of variability on gauge response (Willis and Timm, 2009). Gauges placed in different areas and tested under the same loading conditions can return different measurements based on material property (i.e., density) variability. A 30 $\mu\varepsilon$ difference was previously set as the benchmark for the Test Track for between-gauge precision under live traffic (Willis and Timm, 2009). In addition, it was noted that almost 75% of the data points

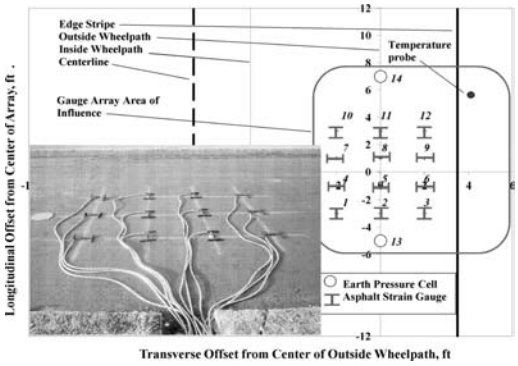

Figure 1. Sensor arrangement.

Figure 2. Procedure followed to protect the gauges during construction.

fell below the 5% within-gauge repeatability standard set by the gauge manufacturer and that 100% of the data points fell below 10% within-gauge repeatability under falling weight deflectometer loading. Other studies have indicated that a ±30% to ±35% difference in measured strains from a single gauge could be expected due to traffic loading on thin (less than 3 in.) asphalt concrete layers (Siddharthan et al., 2005, Howard et al., 2008).

The entire installation process incorporates complexity during construction which may involve time delays and additional difficulty in quality control (Llenin et al., 2006). Inclusion of objects with lighter density (asphalt strain gauges made out of nylon coated with a Teflon polymer) that do not belong to a typical pavement structure, and the use of finer material to cover them, may provide a localized zone of low density and higher binder content. One study suggested that settlement over the gauge array due to poor compaction has led to premature failure in terms of fatigue cracking (Hugo et al., 1997). Another study suggested that variation in construction techniques seemed to have a significant effect on rutting performance (Mulvaney, 2004). A recent study (Leiva-Villacorta and Timm 2011) performed at the NCAT Test Track indicated that the presence of pavement instrumentation and the construction process had no effect on the uniformity of the density of the mat. However, the effect of gauge installation (finer mix in the immediate vicinity of the gauge) on measured pavement response has yet to be evaluated.

When linear elastic materials are considered in flexible pavement modeling, stresses and strains can be calculated using multilayer elastic theory (Huang, 2004). In this approach, the wheel load is circular and the pavements are considered infinite in horizontal extent. Thus, displacements, stresses and strains are axisymmetric in relation to the center of the load. The superposition principle can be used to determine the influence of all wheel loads because the problem is considered linear. However, there is a trend in the pavement industry to substitute flexible pavement analysis based on the multilayer elastic theory by analysis based on the finite element method (NCHRP, 2004). Axisymmetric modeling calculates pavement behavior using a two-dimensional mesh revolving around a central axis by assuming identical stress states exist in every radial direction; therefore, loading is circular. An axisymmetric configuration has been utilized successfully by different researchers (Cho et al., 1996, Thompson et al., 1985, Helwany et al., 2000) for simulating pavement structure and traffic loading interaction.

Finally, different studies have reported significantly different simulated tensile asphalt strains ($\pm 100\,\mu\varepsilon$) compared to asphalt strain measurements obtained from accelerated pavement testing facilities (Timm et al., 2006, Taylor and Timm, 2009, Howard and Warren, 2009). This has been observed as a common behavior either when multilayer elastic theory was used (Timm et al., 2006, Taylor and Timm, 2009) or when a finite element method was used (Howard and Warren, 2009). However, this behavior has yet to be attributed to the presence of asphalt gauges and the gauge installation process.

3 STUDY OBJECTIVE

The objective of this study was to evaluate the potential effect of using a finer mix as gauge cover on pavement response.

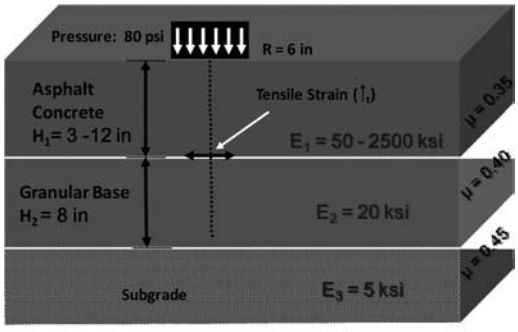

Parameters

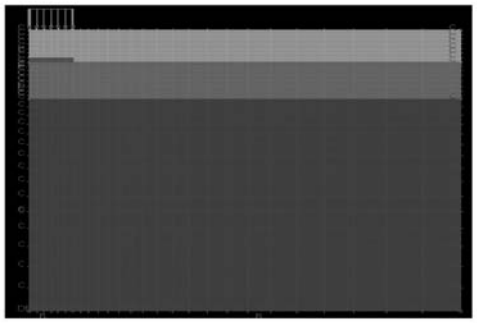

FEA simulation

Figure 3. Parameters used in FEA simulation.

4 SCOPE

To accomplish the objective, a three-layered pavement structure containing a 12 in. diameter by 1 in. thick patch of sieved material at the bottom of the asphalt concrete (AC) was simulated using finite element analysis (FEA). The total AC thickness and the modulus were varied while the thickness of the base layer, the base modulus, and subgrade modulus were fixed parameters. The moduli of the unsieved mixture and sieved mixture/patch were varied following the complex modulus master curve of a 19.0 mm mixture and 9.5 mm Superpave mixture with an extra 10% reduction, respectively. Tensile strain responses were calculated at the bottom of the AC layer under a simulated falling weight deflectometer load for all structures with and without the finer mixture. The results were compared to a previously defined benchmark of 30 $\mu\varepsilon$ for between-gauge precision. Finally, critical scenarios that could potentially have a negative effect on pavement response were incorporated into a simulated NCAT Test Track section subjected to a dual tire load on a single axle.

5 METHODOLOGY

Figure 3 shows the material properties and load utilized in the FEA simulation. The depth of examined pavement section was fixed to 50-times the radius of the loading area and the investigated length of horizontal direction was fixed at 20-times the loading radius. These boundary conditions were fixed in accordance with the findings of several researchers (Cho et al., 1996, Thompson et al., 1985, Helwany et al., 2000) using a combination of finite elements and infinite elements. Materials were assumed to be linear-elastic and the FE analyses were performed under an axisymmetric condition. The software *ADINA 7.5 – 900* node version was utilized to perform the analyses for all structures with and without the finer mixture. The selected moduli of the unsieved AC layers were 50, 100, 200, 500, 750, 1,000, 1,500, 200 and 2500 ksi. These values were selected from the complex modulus master curve of a 19.0 mm Superpave mixture. Since no master curve was available for a 4.75 mm mixture containing the same aggregate source and asphalt binder of the previous mixture, the moduli of a 9.5 mm mixture was reduced by 10% to simulate the finer 4.75 mm mixture. The 19.0 mm mixture and 9.5 mm mixture were selected from the control mixes utilized in the 2009 Test Track.

The selected thicknesses for the AC layer were 3, 5, 7, 9 and 12 in. Tensile strain responses were calculated at the bottom of the unsieved AC layer for all structures and compared to layered elastic analysis results. Tensile strain responses were then calculated at the bottom of the AC layer for all structures with the finer mixture. Relative differences were analyzed in terms of AC modulus and thicknesses and conclusions were made based on observed trends and benchmark analysis.

6 RESULTS AND DISCUSSION

One key element to build the finite element model was to determine the moduli of the unsieved and sieved AC mixtures. First, 19.0 mm mixture and 9.5 mm mixture master curves were selected from the control mixes from the 2009 Test Track. Second, specific moduli were selected from the 19.0 mm master curve to represent the unsieved AC mixture moduli. Third, each selected unsieved AC layer modulus was paired (same frequency/temperature) with a 9.5 mm mixture modulus. Finally, an extra 10% reduction was applied to the paired 9.5 mm mixture moduli to create the moduli of the sieved mixture (4.75 mm mixture). An example of this process can be seen in Figure 4. For this example, a 1,000 ksi modulus was first selected for the 19.0 mm mixture and then the corresponding modulus for the 9.5 mm mixture was found to be 757 ksi. Finally, to obtain the modulus of the 4.75 mm mixture, a 10% reduction was applied to 757 ksi resulting in 688 ksi.

The application of the extra 10% reduction of the moduli was based on previous observations that the air void content of the hand-compacted sieved mixture was 1% to 2% higher (Leiva-Villacorta and Timm, 2011) and that the voids in the mineral aggregate (VMA) should also increase (AASHTO, 2007) for finer mixtures (1% to 2%). The Hirsch model shown in

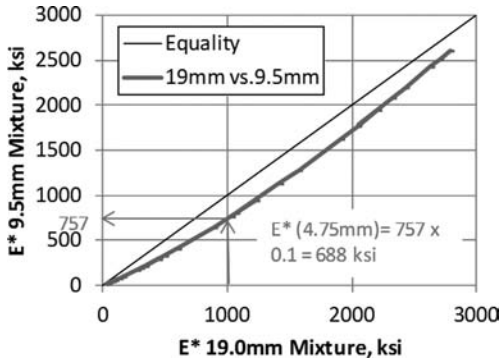

Figure 4. Process used to obtain 4.75 mm E* values from Control mixtures.

Equation 1 (Christensen et al., 2003) was used to determine how much the modulus of the 9.5 mm mixture should decrease based on the increment in air voids content and VMA for binder properties obtained at three frequencies (0.1, 1 and 10 Hz) and at three temperatures (40, 70 and 100°F). The end result indicated that, on average, a 10% reduction in modulus could be expected from the 9.5 mm mixture to a 4.75 mm mixture.

Table 1 shows the moduli of the unsieved and sieved mixtures used in the FEA simulations. The differences in moduli varied from 12% to 43% and were higher at intermediate moduli (of the 19.0 mm mixture) in the range of 200 ksi and 750 ksi. In order to explain why the differences in moduli were not constant, a comparison plot of the moduli of the 19.0 mm mixtures versus the moduli of the 9.5 mm mixture is shown in Figure 4. Note how the 19 mm vs. 9.5 mm curve is close to the equality line for lower moduli and then the curve separates from the line as the modulus increases to finally approach the equality line at higher moduli. This indicates that differences in moduli between mixtures were not only variable but higher at intermediate moduli (of the 19.0 mm mixture) in the range of 200 ksi and 750 ksi and lower at the extremes.

$$|E^*| = P_c\left[4{,}200{,}000\left(1-\frac{VMA}{100}\right)+3|G_b^*|\left(\frac{VFA\times VMA}{10{,}000}\right)\right] + (1-P_c)\left[\frac{1-\frac{VMA}{100}}{4{,}200{,}000}+\frac{VMA}{3|G_b^*|VFA}\right]^{-1} \quad (1)$$

where

$$P_c = \frac{\left(20+\frac{3|G_b^*|VFA}{VMA}\right)^{0.58}}{650+\left(\frac{3|G_b^*|VFA}{VMA}\right)^{0.58}} \quad (2)$$

Table 1. Simulated mixture moduli.

Mixture Modulus (ksi)		
Unsieved	Sieved	% Difference
50	32	36.0
100	58	42.0
200	114	43.0
500	300	40.0
750	465	38.0
1,000	688	31.2
1,500	1,140	24.0
2,000	1,640	18.0
2,500	2,200	12.0

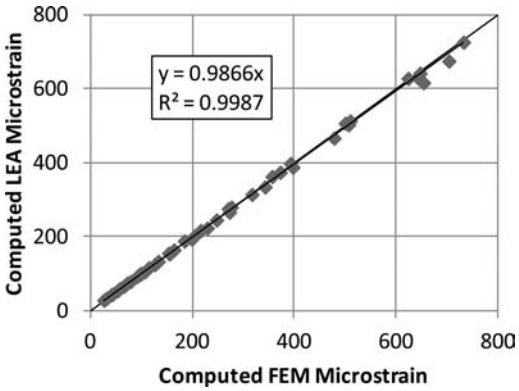

Figure 5. Verification of FEA results using LEA.

$$VFA = \left(\frac{VMA - airvoids}{VMA}\right)\times 100 \quad (3)$$

| E*| = dynamic modulus of the mix (psi); VMA = voids in the mineral aggregate; VFA = voids filled with asphalt and $|G_b^*|$ = dynamic shear modulus of the binder (psi).

Another important step taken prior to evaluating the potential effect of using a finer mix as gauge cover on pavement response was the verification of the FEA simulation and making sure the calculated results were consistent with layered-elastic analysis (LEA). The results obtained from the FEA simulation for the structure with the unsieved AC layers (without the finer mixture patch) were compared and verified with the software *WESLEA*. Figure 5 shows that a good match was obtained between computed FEA and LEA strain responses. This also indicates that the key elements used to build the FE model (number of nodes and mesh configuration) were properly selected to produce reliable pavement responses.

Figure 6 shows the plot of the longitudinal and transverse microstrain calculated along a horizontal distance from the center of the applied load for a structure with and without the finer mixture. The modulus of the unsieved mixture for this exercise was 500 ksi with an AC thickness of 7 in. Only a small section of

the calculated longitudinal and transverse strain values, within 10 in. from the center of the load, was affected by the presence of the finer mix (Figure 6.a). A closer look indicated this small section was mostly located in the tensile portion of the simulated strain trace (Figure 6.b). It is important to mention a discontinuity seen at the edge of the patch (6 in.) in the longitudinal strain series. This is due to the modulus ratio $E_{sieved}/E_{unsieved}$ being less than 1.0. The sieved mixture has lower resistance to deformation than the unsieved mixture. The effect is a discontinuity at the edge of the patch. Beyond the patch, in a radial distance, the tensile strain tended to follow the same path observed for the case without the sieved mixture. For this example, the maximum calculated tensile strains for the unsieved and sieved mixture conditions were 216 $\mu\varepsilon$ and 240 $\mu\varepsilon$, respectively and were located at the center of the load. A relative difference of 24 $\mu\varepsilon$ between these conditions could potentially produce an erroneous pavement response of 11.0%. An analysis of the level of significance of the relative differences and errors are discussed later in this paper.

Figure 7 shows a comparison between calculated strain responses with and without the sieved mixture for all the scenarios (variable AC modulus and variable AC thickness). The overall effect on pavement response was to always increase the tensile strain. This conclusion was obtained from the slope of the curve which indicates that on average, simulated strain responses using the finer mixture tended to be around 6.3% higher than the simulated strain responses without the finer mixture. An average absolute error (AAE) of 7.542% was also calculated, using Equation 4, to have an analytical/statistical parameter. This value of AAE was below the previously reported 10% strain variability under FWD testing (Willis and Timm, 2009) and it was significantly below the 30% difference due to traffic loading (Siddharthan et al., 2005). In other words, the theoretical differences are significantly smaller than testing variability in the field.

$$AAE = \frac{\sum \left| \frac{Strain_s - Strain_u}{Strain_u} \right|}{n} \times 100\% \qquad (4)$$

where $Strain_s$ = sieved mix strain, $Strain_u$ = unsieved mix strain and n = number of data points.

A one sample T-test was performed to evaluate the overall effect of the computed AAE. The results shown in Table 2 indicated that there is enough evidence to conclude that on average the percent difference (error) was lower than 10% at a significance level of 0.05. Thus, the potential error introduced by the use of a finer mix as gauge cover on measured response can be considered insignificant.

The effect of the variables AC total thickness and AC modulus of the unsieved mixture on the relative difference in strain responses were analyzed and the results are shown in Figure 8. When varying the

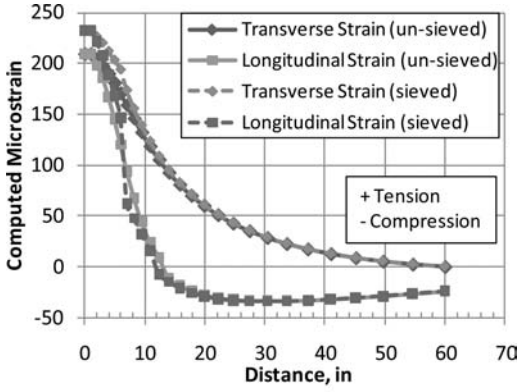

a. Horizontal strain vs. radial distance

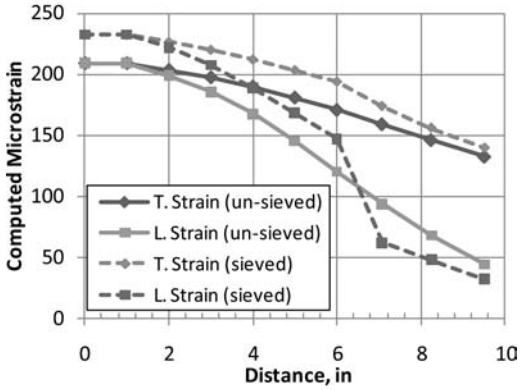

b. Close up of affected section

Figure 6. Effect of the finer mixture.

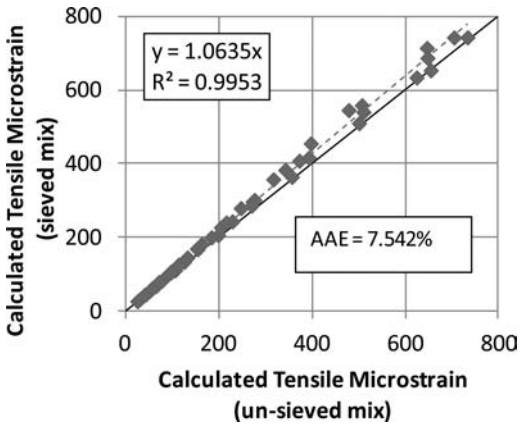

Figure 7. Overall effect on pavement response.

AC modulus of the AC layer with the unsieved mixture (Figure 8.a), the relative difference was found to have a peak value for intermediate moduli (200 and 500 ksi). These results were expected to show a peak value because the higher differences in moduli

Table 2. One Sample T-test (% Error).

Mean	Std. Dev.	SE Mean	95% Upper Bound	T-value	P-value
7.54	3.59	0.54	8.44	−4.60	<<0.05

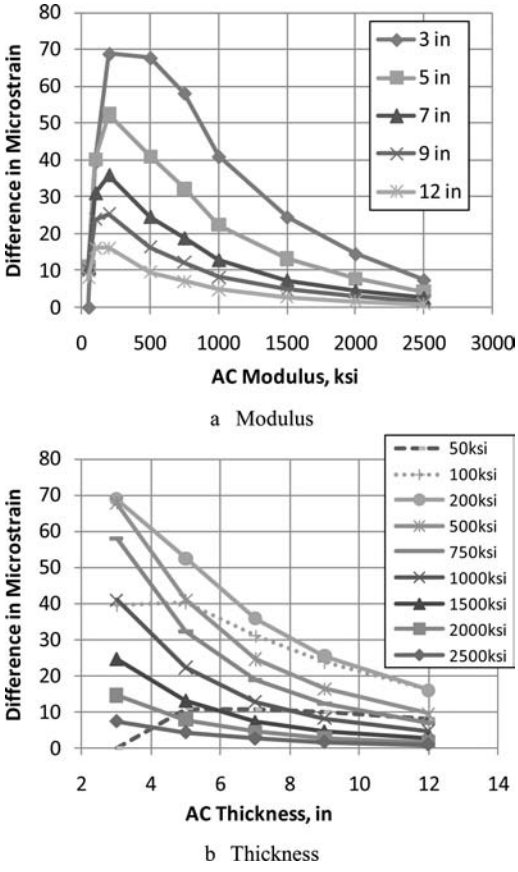

Figure 8. Modulus and thickness effects on microstrain differences.

between sieved and unsieved mixtures ranged from 100 ksi to 750 ksi as shown in Table 1. Above 500 ksi the relative difference tended to decrease rapidly for the structure with a total AC thickness of 3 in. As the thickness was increased the sensitivity of the results due to the change in the AC moduli tended to reduce (lower slopes for thicker AC layers).

Figure 8.b shows that the relative difference tended to decrease as the total AC thickness was increased. In general, it was found that the thicker the AC layer the lower the relative difference. Relative differences were as high as 75 με and as low as 1.0 με. The 200 ksi, 500 ksi, 750 ksi and 1,000 ksi curves seemed to be more sensitive to the change in thickness due to the higher observed slope. These results were expected

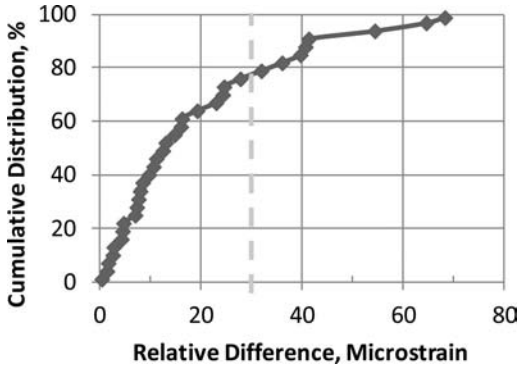

Figure 9. Analysis of relative difference.

because the higher gaps in moduli between sieved and unsieved mixtures were obtained for these scenarios (see Table 1). On the other hand, the 1,500 ksi, 2,000 ksi and 2,500 ksi rapidly converged to differences of 1.0 με because of the smaller gap in moduli between sieved and unsieved mixtures. Finally, the 50 ksi and 100 ksi curves do not follow the general trend and the results were smaller at 3 in. compared to 5 in. of AC. These results can be explained by the so-called critical thickness for thinner AC layers. An increase in tensile strains is expected as the thickness of the AC layer decreases. At this critical thickness a maximum tensile strain is obtained and for thinner layers, below it, smaller tensile strains are obtained.

The cumulative distribution plot of relative differences, shown in Figure 9, indicates that 25% of the relative differences were above 30 με (Siddharthan et al., 2005). This value was previously set as the benchmark for the Test Track for between-gauge precision. Further investigation showed that 25% of the results exceeding the benchmark were due to AC layers thinner than 7 in. with moduli between 200 and 500 ksi. Once again these results were expected to be in this range because the higher differences in moduli between sieved and unsieved mixtures ranged from 100 ksi to 750 ksi as shown in Table 1. Therefore, errors in pavement response tended to increase as the differences in moduli between sieved and unsieved mixtures increased. Errors in pavement response also tended to increase for thinner AC layers.

A benchmark analysis of the combined effect of total AC thickness and modulus on pavement response was performed and the results are shown in Figure 10. When considering the factor "thickness", the average relative difference for the simulated structure with a thickness of 3 in. was the only scenario that exceeded the benchmark of 30 με and had a percent error larger or equal to 10%. When considering the factor "modulus" of the unsieved mixture, the average relative difference for simulated structures with moduli between 200 and 500 ksi also had a percent error larger or equal to 10%. Therefore, special attention is needed during the data screening process for these critical scenarios (structures with AC layers below

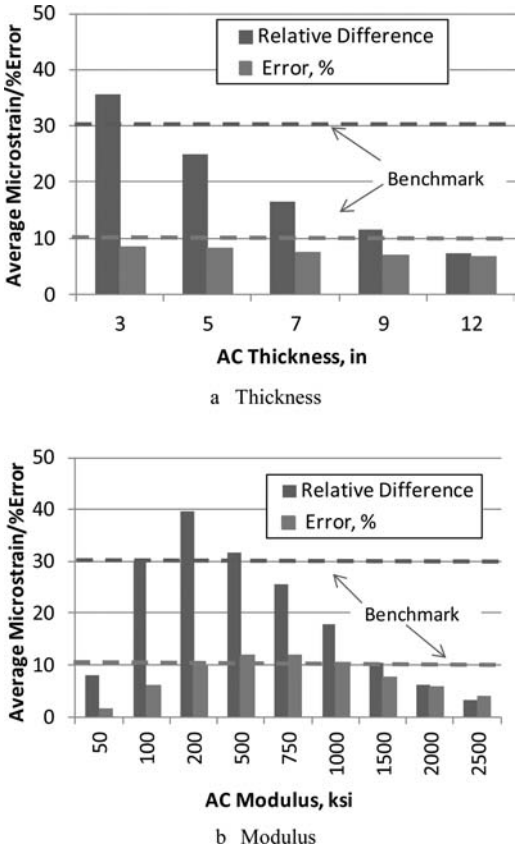

Figure 10. Benchmark analyses.

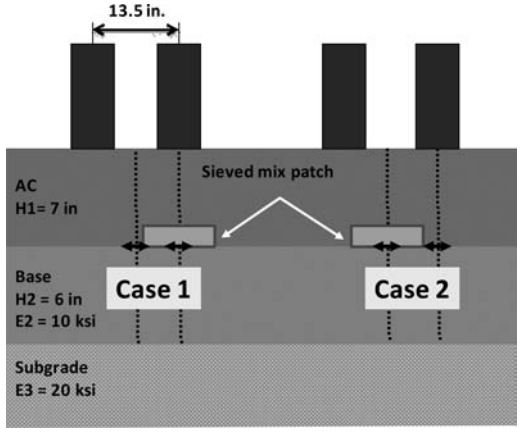

Figure 11. Schematic of simulated dual tire load.

5 in. and moduli between 200 and 500 ksi). However, based on previous studies where errors were found to be about 30% for thin AC layers (Siddharthan et al., 2005, Howard et al., 2008), a benchmark of 30% would not be exceeded by any of the scenarios shown in this study. Furthermore, no sections have been placed at the Test Track with less than 5 in. of AC.

The results obtained up to this point were used to evaluate the effect of traffic on the finer mixture on the control section built at the NCAT Test Track in 2009. A single dual tire load of 10,000 lb (5,000 lb per tire) at 100 psi pressure was simulated as the traffic load. The moduli of the unsieved AC layer were set to 50, 100, 200, 500 and 750 ksi which could potentially have a significant effect on strain responses. The moduli of the base and subgrade layers were set to 10 ksi and 20 ksi, respectively. A higher subgrade modulus compared to the base modulus is a unique characteristic of the Test Track (Taylor and Timm, 2009). The Test Track control section was designed to have 7 in. of total AC and 6 in. of unbound base. Two cases were simulated using the FE method: Case 1 with the sieved mixture patch directly below one tire and Case 2 with the center of the patch located at mid distance between the tires. Figure 11 shows a schematic of the two cases. Tensile strain responses were evaluated at two critical locations: directly below the center of one tire and at mid-distance between the tires to obtain the maximum tensile strain. The same critical locations were used in a control case (with no patch). The maximum tensile strains were also obtained for this simulated condition.

The differences in maximum tensile strain responses considering the structure with and without the sieved mix patch are shown in Table 3. The maximum tensile strain for these conditions was obtained from either the midpoint between the tires or directly below one tire. It was found that AC layers with moduli equal or below 200 ksi could potentially exceed the benchmark of 30 με. In addition, the maximum microstrain difference did not occur at the highest difference in mixtures moduli as observed for the single 80 psi load. Instead, the maximum difference in microstrain was found at lowest AC modulus and the trend was to decrease as the AC modulus was increased. The load magnitude (100 psi) and dual load configuration maybe responsible for this trend. In addition, modeling a granular base material with lower modulus than the subgrade may also be responsible for this trend.

The relative errors shown in Table 3 were for all cases below the previously discussed 10% benchmark and consequently can be considered as insignificant. Therefore, the differences higher that 30 με which were obtained at relatively high strain responses could be considered insignificant for practical purposes. Nevertheless, special consideration is needed during the data screening process for these critical scenarios.

7 SUMMARY

Based on the results of this study, the following observations were made:

– Simulation of a finer mixture patch located at the bottom of the AC layer produced higher tensile strains with differences ranging from 1 to 70 με and errors ranging from 0.5 to 15%.

Table 3. Simulated strain responses under dual tire load.

Unsieved mix modulus (ksi)	% Diff. between sieved & unsieved moduli	Diff. in pavement response (με*)	% Error
50	36	41.5	5.0
100	42	37.8	6.5
200	43	31.5	8.3
500	40	17.1	8.5
750	38	12.0	8.0

*Maximum tensile strain considering the patch for either case minus maximum tensile strain without the patch.

- Simulated thinner AC layers showed higher relative differences and as the thickness was increased the difference tended to decrease.
- The relative differences were found to be higher at intermediate moduli (100 to 750 ksi).
- A benchmark of 30 με was more likely to be exceeded with AC layers thinner than 5 in. and sections with moduli between 200 and 500 ksi.
- A benchmark 10% error was more likely to be exceeded with AC layers thinner than 5 in. and sections with moduli between 200 and 750 ksi.
- Benchmarks of 30 με and 10% error were obtained for gauge repeatability under FWD testing. Relative differences and errors below these limits can be considered insignificant.
- A benchmark of 30% error due to traffic loading on thin AC layers was not exceeded (less than 3 in.). Errors below this limit can be considered insignificant.
- For the control section from the NCAT test track benchmarks of 30 με could potentially be exceeded for AC layers with moduli equal or less than 200 ksi.

8 CONCLUSIONS AND RECOMMENDATIONS

Based on the analyses performed in this study, the following conclusions and recommendations can be made:

- The use of a finer mix as gauge cover can potentially produce higher measured strain responses. These results are more likely to occur when differences in moduli between sieved and unsieved mixtures are the highest.
- This effect seemed to be more evident for thinner AC layers (less than 5 in.) and intermediate to low moduli (50 to 750 ksi).
- From a practical point of view, ensuring that the gauge is seated and placed properly is very important for response measurement. By using the same mixture (after removing the coarse portion), a fair degree of uniformity can be expected.
- Given that the sieved mix truly had lower modulus, the use of stiffer binders with fine mixes designed to protect the gauges could offset the reduction in modulus.
- The applicability of the results found in this study is limited to the analyzed materials and structures. Further investigation is needed to analyze the effect of the base and subgrade materials properties, the effect of moving loads, and the environment.

REFERENCES

AASHTO M323-07. 2007. *Standard Specification for Superpave Volumetric Mix Design.* ADINA System user manuals. Bathe, K. J. 1996. Finite Element Procedures. Prentice-Hall.

Cho, Y., McCullough, B.F. and Weissmann, J. 1996. Considerations on finite-element method application in pavement structural analysis. *Transportation Research Record. 1539*, Transportation Research Board, Washington, D.C.

Christensen, Jr., D.W., T. Pellinen, and R.F. Bonaquist. 2003. Hirsch Model for Estimating the Modulus of Asphalt Concrete. *Journal of the Association of Asphalt Paving Technologists* from the Proceedings of the Technical Sessions, Vol. 72, pp 97-121, Lexington, KY.

Helwany, S., Dyer, J. and Leidy, J. 2000. Finite-element analyses of flexible pavements. *Journal of Transportation Engineering.* Vol. 124(5).

Howard I.L., and Warren K.A. 2009. Finite-Element Modeling of Instrumented Flexible Pavements under Stationary Transient Loading. *Journal of Transportation Engineering*, Vol. 135, No. 2.

Howard, I.L., Warren K.A., Eamon, C. and Lord C.R. 2005. *Variability Analysis of Thin Instrumented Flexible Pavements.* Submitted to the 87th Annual Meeting of the Transportation Research Board, Washington, D.C.

Huang, Y.H. 2004. *Pavement Analysis and Design.* Prentice Hall, Inc., Englewood Cliffs.

Hugo, F., Scullion, T. Lee, N., Fults, K. and Visser, T. 1997. A Rational Evaluation of Pavement Performance Using the Texas Mobile Load Simulator. *Proceedings of the 8th International Conference on Asphalt Pavements*, Seattle, Washington.

Leiva-Villacorta, F. and Timm D.H. 2011. Effects of Asphalt Pavement Instrumentation on In Situ Density. *Proceedings, TandDI Congress 2011: Integrated Transportation and Development for a Better Tomorrow*, American Society of Civil Engineers, Chicago, IL.

Llenin, J.A., Pellinen, T.K. and Abraham, D.M. 2006. Construction Management of a Small-Scale Accelerated Pavement Testing Facility. *Journal of Performance of Constructed Facilities.* Volume 20:3.

Montgomery D.C. 2008. *Design and Analysis of Experiments.* 7th ed., John Wiley and Sons, INC.

Mulvaney, R. 2004. Minnesota Department of Transportation. MnROAD Mainline Rutting Forensic Investigation. *2nd International Conference on Accelerated Pavement Testing*. Minneapolis, Minnesota.

NCHRP/TRB, 2004. *Guide for Mechanistic-Empirical Design of New and Rehabilitated Pavement Structures, Appendix RR: Finite Element Procedures for Flexible Pavement Analysis.* Project I-37A.

Siddharthan, R.V., Sebaaly, P.E., El-Desouky, M., Strand, D. and Huft, D. 2005. Heavy Off-Road Vehicle Tire-Pavement Interactions and Response. *Journal of Transportation Engineering*, Vol. 131.

Taylor, A.J. and Timm, D.H. 2009. *Mechanistic Characterization of Resilient Moduli for Unbound Pavement Layer Materials*. National Center for Asphalt Technology: NCAT Report 09-06.

Timm, D.H. et al. 2006. Phase II NCAT test track results. Rep. No.06-05, National Center for Asphalt Technology (NCAT), Auburn, Ala.

Timm, D.H. 2009. *Design, Construction and Instrumentation of the 2006 Test Track Structural Study.* National Center for Asphalt Technology: NCAT Report 09-01.

Timm, D.H., Priest, A.L. and McEwen, T.V. 2004. *Design and Instrumentation of the Structural Pavement Experiment at the NCAT Test Track*. Report No. 04-01. National Center for Asphalt Technology, Auburn University, Ala.

Thompson, M.R. and Elliot, R.P., 1985. ILLI-PAVE-Based Response Algorithms for Design of Conventional Flexible Pavements. *Transportation Research Record 1043*, TRB, Washington, D. C.

Willis, R. and Timm D. 2009. Repeatability of Asphalt Strain Measurements under Falling Weight Deflectometer Loading.*Transportation Research Record: Journal of the Transportation Research Board, No. 2094*, Washington, D.C.

This page intentionally left blank

Part 5: Accelerated pavement testing on asphalt concrete pavements

This page intentionally left blank

Advances in Pavement Design through Full-scale Accelerated Pavement Testing – Jones, Harvey, Mateos & Al-Qadi (Eds.)
© 2012 Taylor & Francis Group, London, ISBN 978-0-415-62138-0

Accelerated loading, laboratory, and field testing studies to fast-track the implementation of warm mix asphalt in California

D. Jones, R.Z. Wu & B. Tsai
University of California Pavement Research Center, University of California, Davis

C. Barros & J. Peterson
California Department of Transportation

ABSTRACT: The use of Warm-Mix Asphalt (WMA) has increased substantially in recent years and considerable funding has been allocated to research on the topic. Some road authorities have implemented its use based only on results from limited testing, while other states have adopted a more conservative approach. Given the significant differences to Hot-Mix Asphalt (HMA) practice and fears of a moratorium on the use of the technology if unexplained problems occur, the California Department of Transportation decided to follow a more conservative approach, by designing and implementing a phased comprehensive study. Phase 1 investigated rutting behavior of three different WMA technologies against an HMA control in an accelerated loading test with associated laboratory testing assessing rutting and fatigue performance and moisture sensitivity. A number of controlled pilot studies were also constructed during this phase. Phase 2 investigated the effects of the same three WMA technologies on moisture sensitivity in an accelerated loading test. Phase 3 investigated the use of seven different WMA technologies in rubberized asphalt following the same testing program used in Phase 1. The findings have been used to prepare a WMA technology approval process and a framework for statewide implementation that resulted in over one million tonnes of warm-mix asphalt being placed on state highways in the 2011 paving season. This paper provides an overview of the California WMA study and summarizes the results of the accelerated load and laboratory testing completed to date.

1 INTRODUCTION

The California Department of Transportation (Caltrans) has an interest in warm-mix asphalt with a view to reducing stack emissions at plants, to allow longer haul distances between asphalt plants and construction projects, to improve construction quality (especially during nighttime closures), and to extend the annual paving season. However, the use of a warm-mix asphalt technology requires the addition of additives (including water) into the mix, and changes in production and construction procedures, specifically related to temperature, which could influence performance of the pavement. Therefore, Caltrans and the University of California Pavement Research Center (UCPRC) initiated a phased research study including laboratory testing, accelerated load testing and full-scale field studies to assess concerns related to these changes before statewide implementation of the technology was approved. This is a somewhat more cautious approach compared to some other states, but was implemented to ensure that performance is fully understood and that any future pavement failures on projects using warm-mix asphalt are explainable and do not lead to a moratorium on the use of warm-mix asphalt. History has shown that potentially promising technologies are abandoned simply because of a poor understanding of changed design, production and/or construction procedures. Accelerated pavement testing was an integral component in understanding the effects of long-term truck traffic, and reducing the risk of implementation on routes with high truck volumes. This paper describes the study phases completed to date (Jones, et al., 2008, 2009, 2011a, 2011b), the findings of which have been used to prepare a warm-mix asphalt technology approval process and to guide statewide implementation.

Warm-mix technology names are used in this paper for clarification purposes only. Caltrans and the UCPRC do not endorse the use of any specific warm-mix technology.

2 PROJECT OBJECTIVES

The objectives of the California warm-mix asphalt study are to:

– Determine whether the use of additives (including water), introduced to reduce production and construction temperatures of asphalt concrete, influence mix production processes, construction

procedures, and the short-, medium-, and/or long-term performance of hot-mix asphalt.
– Use research findings to guide the implementation of warm-mix asphalt.

A workplan (Jones, et al., 2007) was prepared for meeting these objectives. Research tasks included monitoring the production of different warm mixes and hot-mix controls; monitoring the construction of test tracks with the mixes including the measurement of emissions; sampling of raw materials during production and specimens from the test tracks for laboratory testing; laboratory testing to assess rutting and fatigue cracking performance, and moisture sensitivity; accelerated load testing to assess rutting and fatigue cracking performance, and moisture sensitivity; monitoring the construction and performance of a series of pilot projects on in-service pavements; and preparing specifications and other documentation required for implementing the use of warm-mix asphalt in California. Research has been undertaken in phases. This paper describes the first three phases, which included:

– *Phase 1:* A laboratory and accelerated load test to assess the performance of three different warm-mixes and a hot-mix control in a conventional dense-graded mix. A test track was built for the study. Laboratory testing on both plant-mixed, field-compacted and laboratory-mixed, laboratory-compacted specimens included assessments of rutting performance, fatigue/reflective cracking performance, and effects on moisture sensitivity. Technologies assessed included *Advera®*, *Evotherm DAT®*, and *Sasobit®*. The test track was constructed at the Graniterock Company's Aromas quarry and asphalt plant.
– *Phase 2:* An accelerated load test to assess moisture sensitivity, using the same test track used in the Phase 1 study.
– *Phase 3:* A laboratory and accelerated load test to assess the performance of seven different warm-mixes against two hot-mix controls in a gap-graded rubberized asphalt mix. A new test track was built for the study. Paving emissions were also measured. Laboratory testing protocols were the same as those followed in Phase 1. Technologies assessed included *Advera®*, *Astec Double-Barrel Green®*, *Cecabase®*, *Evotherm DAT®*, *Gencor Ultrafoam®*, *Rediset WMX®*, and *Sasobit®*. Mixes were produced at two different asphalt plants (Granite Construction's Sacramento plant and George Reed Construction's Marysville plant) to accommodate the two different water injection technologies. Mix designs were prepared for each plant. The test track was constructed at the University of California Pavement Research Center (UCPRC) at the University of California, Davis.

The field testing phase, which was undertaken concurrently with the other phases, is described in another paper. More than 20 test sections were constructed around the state on roads covering a range of traffic volumes and climate regions. Most field studies were on thin overlays including open-graded friction courses. Ongoing research includes studies on binder aging in warm-mix asphalt and the use of warm-mix technologies in mixes containing high percentages of reclaimed asphalt.

3 TESTING PROTOCOLS

3.1 *Laboratory*

Plant-mixed, field-compacted laboratory testing was conducted on specimens sawn or cored from 500 mm × 500 mm slabs sawn from the test track approximately six weeks after construction. Laboratory-mixed, laboratory-compacted specimens were prepared using aggregates and binder collected on the days that the mixes were produced for the test tracks. Tests included shear (AASHTO T-320 [Permanent Shear Strain and Stiffness Test]), beam fatigue (AASHTO T-321 [Flexural Controlled-Deformation Fatigue Test]), and moisture sensitivity (AASHTO T-324 [Hamburg Wheel Track Test] and Caltrans CT-371 [Tensile Strength Retained, similar to AASHTO T-283]). In addition to the above, laboratory-mixed, laboratory-compacted specimens were subjected to an open-graded friction course durability test (Cantabro [ASTM D-7064]). Typical experimental plans used in previous UCPRC studies were adopted for this study to facilitate later comparison of results.

3.2 *Accelerated load testing*

Accelerated pavement testing was undertaken with a Heavy Vehicle Simulator (HVS). The test section layout, test setup, trafficking, and measurements followed standard UCPRC protocols (Jones, 2005). The pavement temperature at 50 mm was maintained at 50°C ± 4°C in all phases to assess rutting potential under typical pavement conditions. Infrared heaters inside a temperature control chamber were used to maintain the pavement temperature. In the moisture sensitivity study, each section was presoaked with water for a period of 14 days prior to testing. A 150 mm high soaking dam was constructed around each test section and a row of 25 mm diameter holes was drilled to the bottom of the upper lift of asphalt (i.e. 60 mm), 250 mm away from the section and 250 mm apart. During testing, a constant flow of preheated water (50°C) was maintained across the section at a rate of 15 L/hour to induce moisture damage.

All trafficking was carried out with a dual-wheel configuration, using radial truck tires (11R22.5- steel belt radial) inflated to a pressure of 720 kPa, in a channelized, unidirectional loading mode. Loads started at 40 kN and were increased to 60 kN after 150,000 load repetitions and to 80 kN after a further 100,000 load repetitions. Load was checked with a portable weigh-in-motion pad at the beginning and end of each test as well as after each load change.

Table 1. Phase 1 and Phase 2 test track data.

Parameter	Control	Advera	Evotherm	Sasobit
Binder content (%)[1]	5.3	5.1	5.2	4.5
Prod temp (°C)	155	120	120	120
Pave temp (°C)[2]	135	105	105	117
Ambient temp (°C)	20	20	20	20
Air voids (%)	5.6	5.4	7.1	7.0

[1]Target 5.2%; [2]Behind screed

Table 2. Phase 3 test track data (Mix Design #1).

Parameter	Control	Gencor	Evotherm	Cecabase
Binder content (%)[1]	7.7	7.9	7.7	7.7
Rubber content (%)	18	18	18	18
Prod temp (°C)	160	140	125	130
Pave temp (°C)[2]	154	128	120	128
Ambient temp (°C)	10	10	10	10
Air voids (%)	4.9	6.3	6.2	6.4
Hveem Stability[3]	27	28	27	27

[1]Target 7.3%; [2]Behind screed; [3]Immediate, no curing

Table 3. Phase 3 test track data (Mix Design #2).

Parameter	Control	Sasobit	Advera	Astec	Rediset
Binder content (%)[1]	7.7	8.0	7.6	8.4	10.0
Rubber content (%)	19	19	19	19	19
Prod temp (°C)	166	149	145	145	140
Pave temp (°C)[2]	137	137	130	125	126
Ambient temp (°C)	10	10	10	10	10
Air voids (%)	11.6	8.5	10.7	9.1	8.4

[1]Target 8.3%; [2]Behind screed

Rutting was measured with a laser profilometer and pavement temperatures were monitored using thermocouples imbedded in the pavement. Dedicated nearby weather stations monitored ambient temperature, rainfall, relative humidity, wind speed and direction, and solar radiation.

4 TEST TRACK DESIGN AND CONSTRUCTION

Test tracks were designed and constructed using conventional techniques and equipment and in conformance to Caltrans specifications. The Phase 1 and 2 test track consisted of two 60-mm asphalt concrete layers, over 300 mm crushed stone base, over 250 mm of crushed stone subbase, over bedrock. The Phase 3 test track consisted of a 60 mm rubberized asphalt concrete layer, over a 60 mm hot-mix asphalt layer, over 400 mm of crushed stone base, over compacted subgrade.

The Phase 1 test track was constructed in late summer with mild ambient temperatures. The Phase 3 test track was constructed in early spring with low ambient temperatures and a cold wind. This was intentional to quantify the potential benefits of using warm-mix asphalt for early season paving.

Haul distance for the Phase 1 test track was approximately 1.0 km and consequently there was no heat loss during the haul. Haul distances from the two asphalt plants for the Phase 3 test track were 60 minutes and 120 minutes respectively. Key data for the asphalt concrete on the two test tracks are provided in Tables 1 through 3.

5 SUMMARY OF LABORATORY TEST RESULTS

5.1 *Air void content*

Air-void contents were higher and more variable on the specimens removed from the test track compared to the specimens prepared in the laboratory. There was a bigger variation in the rubberized mixes compared

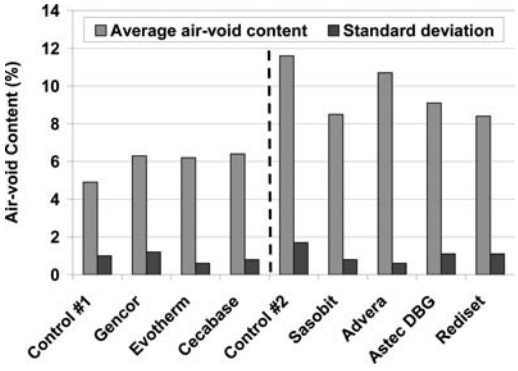

Figure 1. Air void content for Phase 3 test track (Average determined from 65 specimens per mix).

to the dense-graded mixes. This was attributed to a number of reasons including better compaction control and more consistent temperatures in the laboratory compared to the field. The higher air-void contents recorded during construction of Mix Design #2 in the Phase 3 study (Figure 1) were attributed to difficulty with compaction due to higher than expected temperature loss during the longer haul, which resulted in compaction temperatures being lower than optimal. This was expected on the Control section, but should have been better considered by the technology providers when setting production temperatures on the warm-mixes.

5.2 *Rutting performance*

Rutting performance on the specimens removed from the test tracks showed similar trends to the accelerated load test results (discussed in Section 6), with no significant differences between the hot-mix controls and the warm-mixes (example for Phase 1 in Figure 2). Results varied on laboratory prepared specimens, depending on whether the mix was conditioned (four hours at 135°C) prior to specimen preparation or not. On unconditioned specimens, rutting performance on the warm mixes was generally poorer than the controls. This was attributed to less oxidation of the binder and consequent lower initial stiffness of the mixes. On conditioned specimens (typically four hours at compaction temperature), performance was closer to the test track specimens.

5.3 *Fatigue/reflective cracking performance*

There was no significant difference in fatigue cracking performance between the warm-mix and hot-mix specimens in any of the studies, except the *Sasobit* specimens with low binder content from the Phase 1 study, which showed reduced performance, as expected (Figure 3). Laboratory prepared specimens at the correct binder content performed similar to the Control specimens. A limited study to assess small reductions in binder content to counter lower mix stiffness as a

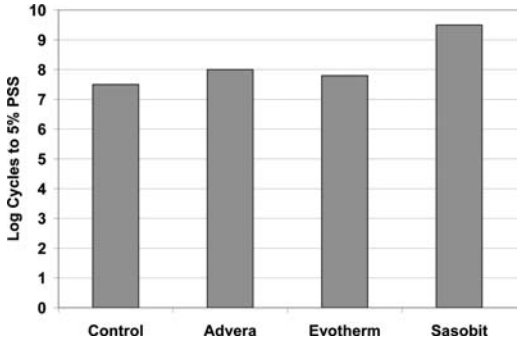

Figure 2. Phase 1 shear test results for specimens removed from test track (PSS = Permanent Shear Strain).

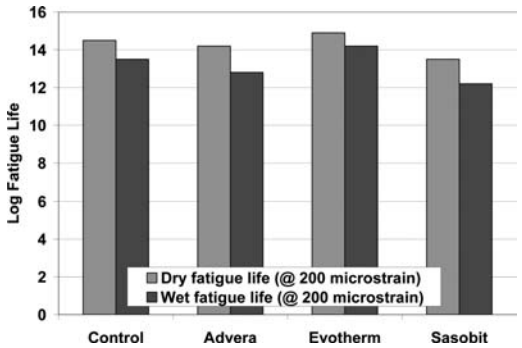

Figure 3. Phase 1 fatigue test results for specimens removed from test track (Tested at 200 microstrain at 20°C).

result of reduced binder aging resulted in a reduction in fatigue performance.

5.4 *Moisture sensitivity*

In the Phase 1 study, Hamburg Wheel Track and tensile strength retained results were generally poor for all mixes (Figure 4), with unconditioned laboratory prepared specimens having lowest performance. In the Phase 3 study, only results for specimens removed from the test track were available at the time of preparing this paper, with results similar for all specimens with little evidence of moisture sensitivity (Figure 5).

5.5 *Open-graded friction course durability*

There was no significant difference in durability between the warm-mix and hot-mix specimens in tests conducted on the Phase 1 aggregates, despite slightly higher drain-down on the warm-mix specimens.

6 SUMMARY OF ACCELERATED LOAD TESTS

6.1 *Phase 1: Early rutting performance on dense-grade*

Testing on the four sections was started in October 2007 and ended in April 2008. The duration of the tests on the four sections varied from 170,000 to 285,000

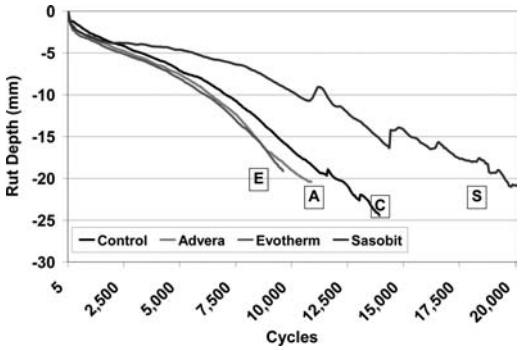

Figure 4. Phase 1 Hamburg Wheel Track test results for specimens removed from test track (C = Control, A = Advera, E = Evotherm, S = Sasobit).

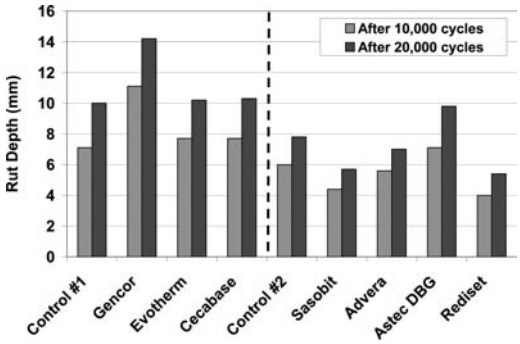

Figure 5. Phase 3 Hamburg Wheel Track test results for specimens removed from test track.

load repetitions. A range of daily average temperatures was experienced; however, the pavement temperatures remained constant throughout HVS trafficking.

Rutting behavior (average maximum rut) for the four sections is compared in Figure 6. The duration of the embedment phases on the *Advera* and *Evotherm* sections were similar to that of the Control; however, the depth of the ruts at the end of the embedment phases on these two sections was slightly higher than the Control. In both instances, this was attributed to less oxidation of the binder during mix production because of the lower plant temperatures and is unlikely to relate to early rutting on in-service pavements with typical California traffic volumes. However, it remains a concern on thick warm-mix pavements with very high truck traffic. Additional binder testing to study effects of the additives and aging at different production temperatures on binder properties is currently being undertaken in Phase 4 to better understand the issue. Rutting behavior on the warm-mix sections followed trends similar to that of the Control in terms of rut rate (rutting per load repetition) after the embedment phase. Note that the performance of the *Sasobit* section cannot be directly compared with the other three sections given that the binder content of this mix was 0.7 percent lower than the other mixes.

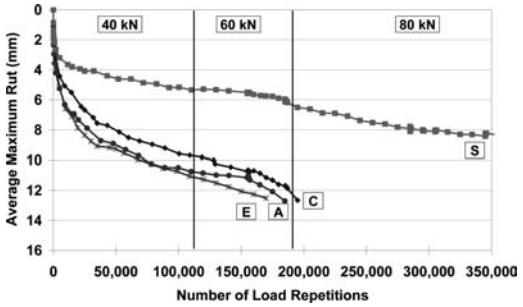

Figure 6. Phase 1 rutting (C = Control, A = Advera, E = Evotherm, S = Sasobit).

6.2 *Phase 2: Moisture sensitivity on dense-grade*

Testing on the four sections was started in June 2008 and ended in May 2009. The duration of the tests on the four sections varied from 352,000 to 620,000 load repetitions. A range of daily average temperatures was experienced during the four seasons of testing; however, the pavement temperatures remained constant throughout HVS trafficking.

Rutting behavior (average maximum rut) for the four sections is compared in Figure 7. The duration of the embedment phases on the warm-mix asphalt sections were shorter than the control, opposite to the behavior in the first phase. Binder extractions and testing is currently being undertaken to better understand this observation. Embedment phases were noted at each load change on all sections.

There was a distinct difference in rutting performance of the *Advera* and *Sasobit* sections compared to the Control and *Evotherm* sections, in that the latter two sections rutted at a notably faster rate than the former two sections. The Control and *Evotherm* sections were predominantly shaded by an adjacent structure for much of the day, while the *Advera* and *Sasobit* sections had sun for most of the day. Binder testing is being undertaken to determine if different aging played a role in this behavior, and the findings will be reported in a separate publication. Trafficking was terminated on the *Advera* and *Sasobit* sections before the failure criterion was met in the interests of completing the study. In forensic investigations undertaken after testing, none of the sections showed any indication of moisture damage, which contradicted the laboratory Hamburg Wheel Track and Tensile Strength Retained test results.

6.3 *Phase 3: Early rutting performance on rubberized asphalt*

This phase was considered as two sub-projects given that mixes came from two different asphalt plants with different mix designs (7.3% binder content on Mix Design #1 compared to 8.3% on Mix Design #2). Load testing was conducted concurrently on both mixes using two Heavy Vehicle Simulators. Testing was started in June 2010 and ended in December 2010.

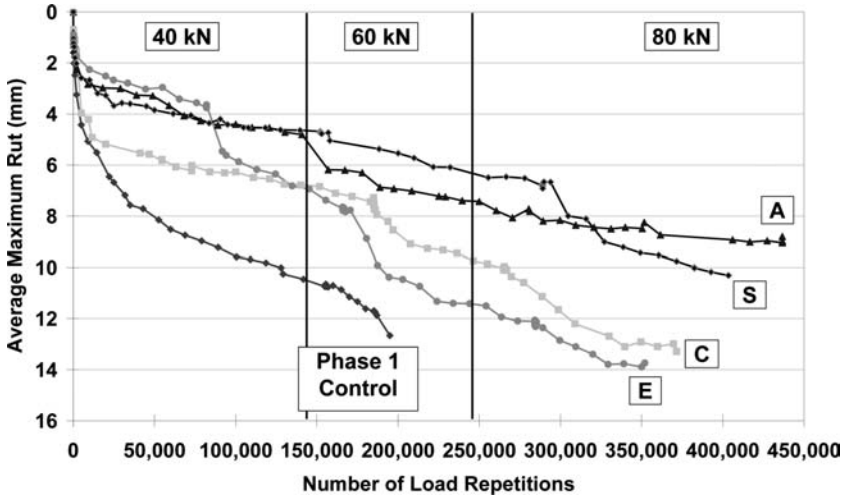

Figure 7. Phase 2 rutting (C = Control, A = Advera, E = Evotherm, S = Sasobit).

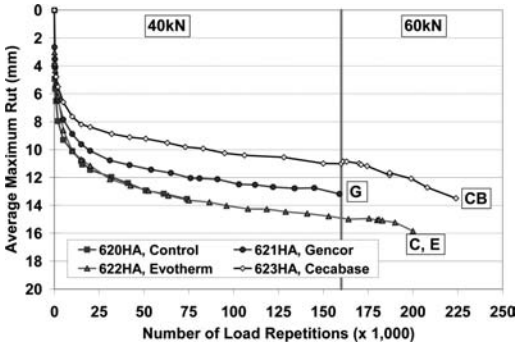

Figure 8. Phase 3, Mix Design #1 rutting (C = Control, E = Evotherm, G = Gencor, CB = Cecabase).

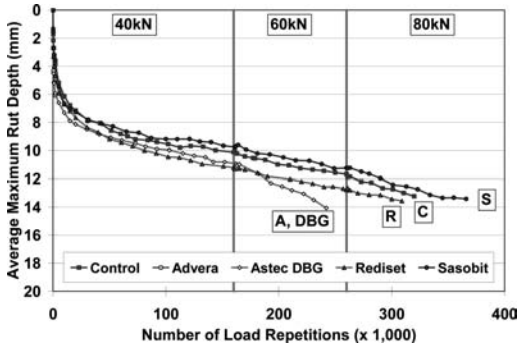

Figure 9. Phase 3, Mix Design #2 rutting (C = Control, A = Advera, DBG = Astec DBG, R = Rediset, S = Sasobit).

On the first project (Control, *Cecabase*, *Evotherm DAT*, and *Gencor UltraFoam*), the duration of the tests varied between 85,000 and 225,000 repetitions; with performance generally better on the warm-mix sections compared to the Control. On the second project (Control, *Advera*, *Astec Double-Barrel Green*, *Rediset*, and *Sasobit*), the duration of the tests varied between 225,000 and 375,000 repetitions with most sections performing in a similar way, but with two sections showing some load sensitivity at higher loads. This behavior was later attributed to subgrade moisture conditions identified during a forensic investigation.

Rutting behavior (average maximum rut) for the two projects is compared in Figures 8 and 9 respectively. In the first project, the embedment phases on two of the warm-mix sections were shorter than the Control. Embedment on the third warm-mix was the same as the Control. In the second project, embedment phases were similar for all mixes.

Differences in performance were related to air-void content, actual binder content, and lift thickness which varied slightly between the mixes. The binder content

Figure 9. Portable flux chamber for measuring emissions during paving.

of the *Rediset* mix was significantly higher than the other mixes (i.e., 1.7 percent higher than the design binder content). Compaction on the second project was generally poor, which was attributed to the longer

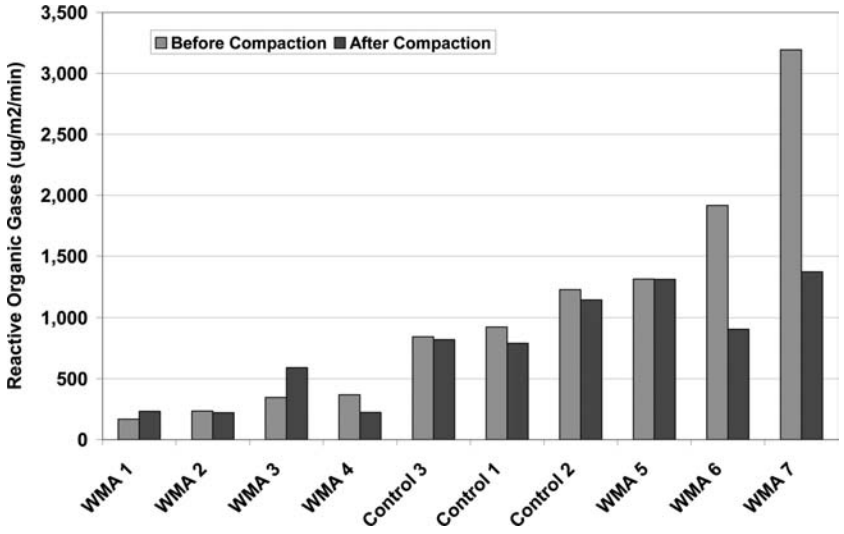

Figure 10. Reactive organic gas emissions during Phase 3 paving.

haul (approximately 2.5 hours) and cold temperatures during placement.

7 EMISSIONS TESTING

The purpose of the emissions study was to develop and assess equipment for accurately measuring surface emissions during hot- or warm-mix asphalt paving operations. A transportable flux chamber (Figure 9) was fabricated to obtain direct measurements of reactive organic gas (ROG) emissions and to estimate the fluxes of volatile organic compounds (VOCs) and semi-volatile organic compounds (SVOCs) for different asphalt mixes and production temperatures. A comprehensive validation study was carried out during the Phase 3 study to verify the applicability of the method in characterizing organic compounds in emissions during construction (Farshidi, et al., 2011).

Although trends in emission reduction from the time of placement until after final compaction were similar for all the mixes tested, significant differences were noted in the alkanes' concentration of the emissions from the Control mixes from the two asphalt plants and from the different warm mix technologies (Figure 10). In some instances, the warm mixes had higher concentrations than the control. For example, the second highest emission concentration recorded was on one of the warm-mix sections placed at the lowest temperature recorded of all the sections. Consequently, any generalization with regard to emissions reduction during the placement of asphalt through the use of warm-mix technologies is inappropriate and should be restricted to comparisons of specific WMA technologies against HMA controls.

Preliminary results from this study indicate that the method developed is appropriate for accurately quantifying and characterizing VOC and SVOC emissions during asphalt paving. Based on the results obtained to date, the study is being extended to assess other gaseous and particulate polycyclic aromatic hydrocarbons (PAH) emissions during paving. Collection of PAHs through a fine particulate filter followed by a sorbent-backed filter with further gas chromatographic/mass spectrometric (GC/MS) analysis is being investigated. The results will be used to quantify the potential benefits of using warm-mix asphalt technologies in reducing reactive organic gas emissions, and to more accurately assess the contribution of emissions from asphalt paving to total ROG emissions for specific areas.

8 KEY OBSERVATIONS

The following key observations have been made from the study results to date:

- Smoke and haze typical on construction projects using hot-mix asphalt are significantly reduced on warm-mix projects. However, actual emissions during paving vary between technologies and the temperatures at which they are placed. Consequently, generalizations about reduced emissions from warm-mix asphalt when compared to hot-mix asphalt should not be made.
- Compaction on warm-mix sections is similar to that on hot-mix sections if similar rolling patterns are followed and the temperatures do not drop too low. Warm-mixes cool at a slower rate than hot-mixes and consequently there is a longer time window to complete compaction. However, periods of mix tenderness are also generally longer and breakdown rollers may need to be held back to accommodate this.
- In the Phase 1 experiment, production and compaction temperatures were set. Two of the technologies showed considerable tenderness during

breakdown rolling, indicating that the placement temperatures were on the high side and consequently the breakdown and intermediate rollers were held back until the mix had cooled down to an appropriate level. Contractors may be inclined to reduce the binder content to minimize this problem. This is **NOT** advised; rather the approach of delaying the start of breakdown rolling by a few minutes should be followed. Reduced binder content could lead to a stiffer mix that is more susceptible to raveling and early reflection cracking, especially in thin overlays.

- In the Phase 3 experiment, production and compaction temperatures were set by the individual warm-mix technology provides in discussion with the asphalt plant operator. In certain instances, compaction temperatures may have been a little low, which resulted in poor compaction on some sections. Ambient temperatures and haul time need to be closely monitored in the setting of these temperatures to ensure that adequate compaction can still be achieved. The focus should not be solely on trying to reduce production temperatures.
- Laboratory rutting performance of warm-mix asphalt specimens prepared according to standard procedures with no additional conditioning is generally poorer than hot-mix specimens prepared in the same way, indicating that some early rutting is possible until the binder oxidizes to the same extent as that of hot-mix asphalt. This implies that early rutting is possible in the first few months after construction on thicker warm-mix asphalt projects that carry heavy truck traffic. Longer rut embedment phases on the warm-mix sections compared to the hot-mix section in the Phase 1 accelerated loading study support this observation. No difference in rutting was observed on any of the other accelerated loading tests or on any of the field sections monitored to date, indicating that the problem is probably limited to applications in thicker pavements (the Phase 1 test track was 120 mm thick, whereas all other experiments varied between 38 mm and 50 mm). Reductions in the binder content should not be considered to counter this effect.
- No increase in moisture sensitivity was noted on any of the warm-mix sections assessed in this study. However, measurements at the asphalt plants indicated that the moisture contents of the warm-mixes were generally higher than the hot-mix controls, although all were within Caltrans specification (i.e., 1.0 percent by mass of mix), indicating that the potential for moisture related problems does exist if aggregate moisture contents are not closely monitored.

9 CONCLUSIONS

A comprehensive, phased research study has revealed that warm-mix asphalt will provide equal performance to hot-mix asphalt in most instances. Reduced binder aging as a result of lower production temperatures appears to have a short-term influence on rutting performance, which could result in a faster initial rut rate on thicker pavements under heavy truck traffic for the first few months in hot climates. Accelerated pavement testing was beneficial in understanding this rutting behavior and in assessing the potential for increased moisture sensitivity due to the lower production temperatures. Based on the results and conclusions from the research conducted to date, coupled with training and workshops for district staff, Caltrans is implementing the use of warm-mix asphalt statewide on pavements in all traffic classes, with over a million tons of warm-mix placed in a full spectrum of applications in 2011. Results from the research, and specifically the accelerated pavement testing, were considered a fundamental component in understanding potential risks of implementation, especially on high truck traffic routes and in those areas with moisture sensitive aggregates.

ACKNOWLEDGEMENTS

This paper describes research activities that were requested and sponsored by the California Department of Transportation (Caltrans), Division of Research and Innovation, and the California Department of Resources, Recycling, and Recovery (CalRecycle). Caltrans and CalRecycle sponsorship is gratefully acknowledged. The assistance and interest of the warm-mix technology providers, Graniterock Company, Granite Construction, Teichert Construction, George Reed Construction, and the HVS test crew under the direction of Mr. Peter Miller is also gratefully acknowledged. The contents of this paper reflect the views of the authors and do not necessarily reflect the official views or policies of the State of California or the Federal Highway Administration. This paper does not constitute a standard, specification, or regulation.

REFERENCES

Farshidi, F., Jones, D., Kumar, A., Green, P. and Harvey, J.T. 2011. Direct Measurements of Volatile and Semi-Volatile Organic Compounds from Hot- and Warm-Mix Asphalt. *Transportation Research Record, Journal of the Transportation Research Board, No 2207*. Washington, DC: Transportation Research Board of the National Academy of Sciences.

Jones, D., Wu, R., Tsai, B.W., Lu, Q. and Harvey, J.T. 2008. *Warm-Mix Asphalt Study: Test Track Construction and First-Level Analysis of Phase 1 HVS and Laboratory Testing.* Davis and Berkeley, CA: University of California Pavement Research Center. (RR 2008 11).

Jones, D., Wu, R., Tsai, B.W., and Harvey, J.T. 2009. *Warm-Mix Asphalt Study: First-Level Analysis of Phase 2 HVS and Laboratory Testing and Forensic Investigation.* Davis and Berkeley, CA: University of California Pavement Research Center. (RR-2009-02).

Jones, D., Wu, R., Tsai, B.W., and Harvey, J.T. 2011a. *Warm-Mix Asphalt Study: Test Track Construction and First-Level Analysis of Phase 3a HVS and Laboratory*

Testing, and Forensic Assessment. (Mix Design #1). Davis and Berkeley, CA: University of California Pavement Research Center. (RR-2011-02).

Jones, D., Wu, R., Tsai, B.W., and Harvey, J.T. 2011b. *Warm-Mix Asphalt Study: Test Track Construction and First-Level Analysis of Phase 3a HVS and Laboratory Testing, and Forensic Assessment. (Mix Design #2).* Davis and Berkeley, CA: University of California Pavement Research Center. (RR-2011-03).

Jones, D. and Harvey, J. 2007. *Warm-Mix Asphalt Study: Workplan for Comparison of Conventional and Warm-Mix Asphalt Performance using HVS and Laboratory Testing.* Davis and Berkeley, CA: University of California Pavement Research Center. (WP-2007-01).

Jones, D. 2005. *Quality Management System for Site Establishment, Daily Operations, Instrumentation, Data Collection and Data Storage for APT Experiments*. Pretoria, South Africa: CSIR Transportek. (Contract Report CR-2004/67-v2).

This page intentionally left blank

Advances in Pavement Design through Full-scale Accelerated Pavement Testing – Jones, Harvey, Mateos & Al-Qadi (Eds.)
© 2012 Taylor & Francis Group, London, ISBN 978-0-415-62138-0

Assessment of response and performance of perpetual pavements with warm mix asphalt surfaces at the Ohio Accelerated Pavement Load Facility

I. Khoury, S.M. Sargand, A. Al-Rawashdeh & W. Edwards
Ohio Research Institute for Transportation and the Environment, Ohio University, Athens, Ohio, US

ABSTRACT: A controlled environment study of perpetual pavement was conducted at the Ohio Research Institute for Transportation and the Environment's Accelerated Pavement Load Facility (APLF). The surface layer of each section consisted of one of the Warm Mix Asphalts (WMA), *Aspha-min*, *Sasobit*, and Evotherm, or a hot-mix control. The test sections were divided into northern and southern halves, with the northern halves having a full 16 in. (400 mm) perpetual pavement; the southern halves had intermediate layer thicknesses decreasing in 1.0 in (25 mm) increments, which was compensated for by increasing the thickness of the dense-graded aggregate base. Instrumentation in the southern half was used to measure temperature, subgrade pressure, deflections, and longitudinal and transverse strains at the base of the fatigue resistance layer. The temperature was set to 40°F (4.5°C), 70°F (21°C), and 104°F (40°C), in that order. At each temperature, Rolling Wheel Loads (RWL) of 6,000 lb (26.7 kN), 9,000 lb (40 kN), and 12,000 lb (53.4 kN) were applied at selected lateral shifts and the sensor responses measured before and after being subjected to 10,000 passes of 9,000 lb (40 kN) RWL at ∼5 mph (8 km/h). Profiles were measured after 100, 300, 1,000, 3,000, and 10,000 passes to assess consolidation of each surface.

1 INTRODUCTION

Warm Mix Asphalt (WMA) is a relatively new technology which was introduced in 1995 in Europe. WMA is gaining attention all over the world because it offers several advantages over conventional asphalt concrete mixes. The benefits include (1) Reduced energy consumption in the asphalt mixture production process; (2) Reduced emissions, fumes, and undesirable odors; (3) More uniform binder coating on aggregate, which should reduce mix surface aging; and (4) Extended construction season in temperate climates.

WMA requires the use of additives to reduce the temperature of production and compaction of asphalt mixtures. It offers an alternative to hot-mix asphalt (HMA), which is produced at temperatures between 280°F (138°C) and 320°F (160°C). Warm mix asphalt is compacted at a temperature range of 250°F (121°C) to 275°F (135°C). Several techniques have been used to improve the workability of asphalt mixes at a lower temperature. These include (*www.warmmixasphalt.com/WmaTechnologies.aspx*):

- *Aspha-min*, the addition of sodium aluminum silicate or zeolite to the asphalt mix (*www.aspha-min.de/en/html/overview.html*).
- *Sasobit*, the addition of a paraffin-wax compound extracted from coal gasification (*www.sasolwax.com/Sasobit_Technology.html*)
- *Evotherm*, the addition of an emulsion to improve the coating and workability of WMA mixes (*www.meadwestvaco.com/Products/*).

A fourth common technique is *WAM Foam*, which uses a foaming action to reduce the working temperature. This technique was excluded from the study at the request of the project sponsor. WMA techniques were used to reduce the viscosity of asphalt binder at certain temperatures and to dry and fully coat the aggregates at a lower production temperature than conventional hot-mix asphalt. The reduction in mixing and compaction temperatures of asphalt mixtures can lead to a 30 percent reduction in both fuel energy consumption and emissions, depending on the WMA technology used and the moisture content of the aggregates (APAO, 2003).

"Perpetual pavement" is the term given to the unique design of a long-life flexible pavement. The structural integrity of the pavement is intended to last at least 50 years, while only the top wearing surface would periodically be milled and replaced to eliminate surface distresses. This relatively quick fix reduces user delays and rehabilitation costs, offsetting the higher initial cost. The removed surface layer can also be recycled, saving material resources.

The main focus of the perpetual pavement concept is to eliminate bottom-up fatigue cracking while still providing a durable product. When pavements undergo cyclic traffic loading, the bottom layer of the pavement structure becomes fatigued from induced strain, where cracks begin to develop and then propagate into the upper layers, eventually making their way to the surface. To combat this problem, the perpetual pavement design is thicker than conventional designs. As the pavement structure becomes thicker, the strain under

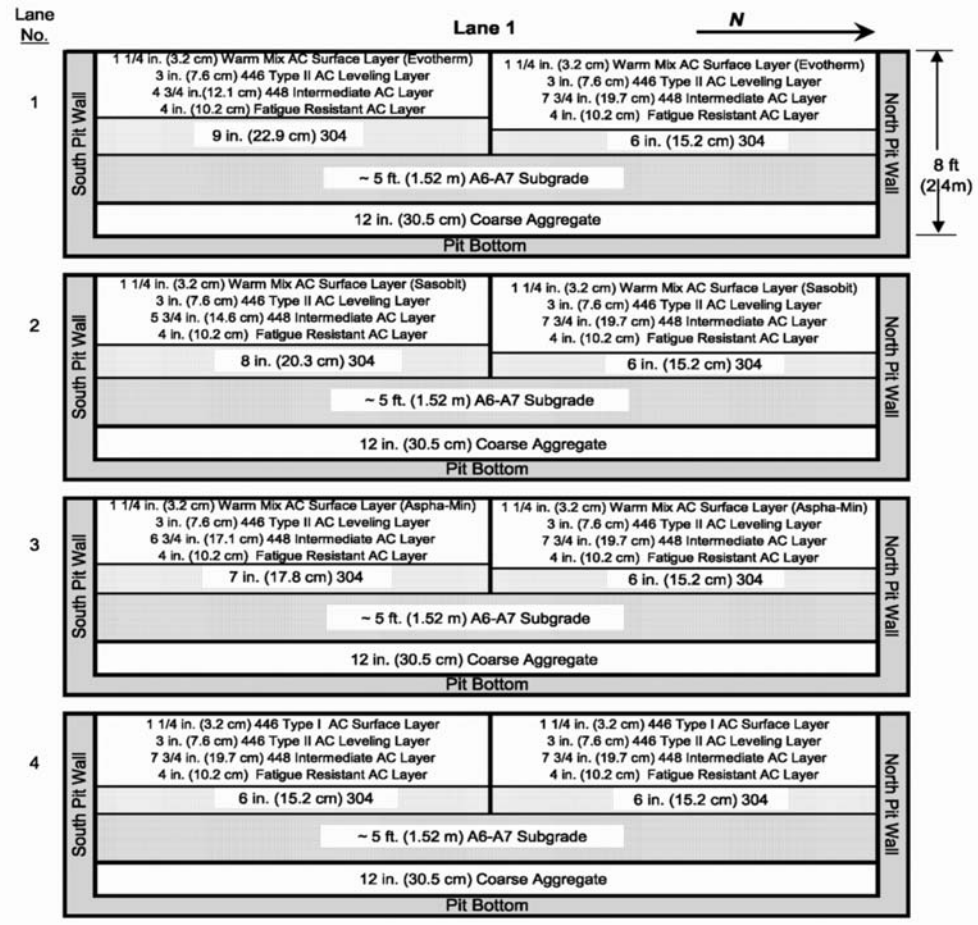

Figure 1. APLF test section profile view diagram showing pavement structure build-up in each 8 ft. (2.4 m) lane. The 3 ft. (0.9 m) pave margins at the outer edges of Lane 1 and Lane 4 are not shown.

load at the bottom of the hot-mix asphalt (HMA) pavement layer decreases, thus reducing damage due to loading and increasing the fatigue life of the pavement. It is believed that once the strain is lowered below some threshold, known as the endurance limit, then fatigue cracking as a result of tensile strain at the bottom of the HMA will never occur (Brown and Timm, 2006). The endurance limit is currently accepted as 70 microstrains ($\mu\varepsilon$) for most perpetual pavement designs, though some claim a higher endurance limit of 100 $\mu\varepsilon$ is suitable. Perpetual pavements are normally comprised of three distinct layers; a rut and wear resistant top layer, a rut resistant intermediate layer, and a special fatigue resistant bottom layer.

The fatigue resistance layer, or "rich" bottom layer, is the main difference between conventionally thick asphalt pavement designs and the perpetual pavement design. This layer has slightly higher asphalt binder content and lower air voids, making it more flexible. Given the appropriate thickness, this layer can be designed so that the endurance limit is never exceeded. The higher asphalt content is also designed to improve the layer's resistance to moisture.

The Ohio Department of Transportation (ODOT) tested the perpetual pavement concept on the westbound lanes of the US Route 30 bypass of Wooster in Wayne County, Ohio (WAY-30), which was constructed in 2005. The pavement consisted of 16 in. (400 mm) of asphalt in four layers built on 6 in. (150 mm) of dense-graded aggregate base (DGAB). Two test sections were instrumented by the Ohio Research Institute for Transportation and the Environment (ORITE). A weather station was also used to monitor environmental conditions. Controlled vehicle tests with single axle and tandem axle loads and other monitoring, such as falling weight deflectometer (FWD) measurements and gathering of environmental data, were conducted during different seasons over the next four years. The perpetual pavement performed well over this period, and the critical stress at the base of the fatigue resistance layer (FRL) was

exceeded only by the heaviest loaded vehicles travelling at extremely low speeds that were expected to rarely, if ever, occur in practice (Sargand et al., 2008; Sargand, 2010).

ODOT then decided to sponsor a second research project that would test different thicknesses of perpetual pavement in ORITE's Accelerated Pavement Load Facility (APLF), along with selected formulations of warm-mix asphalt (WMA) on the surface layer. The project also included a field study of a road resurfacing project using the same formulations of WMA, along with analyses of the energy consumption and cost savings, and laboratory testing of the material properties. These aspects are reported separately (Sargand, 2009; Hurley et al., 2009). In order to maintain continuity with the WAY-30 study, the same endurance level of 70 $\mu\varepsilon$, was used.

2 OBJECTIVES

The following are the primary objectives of this research:

- Examine the influence of pavement thickness on the tensile strain developed at the bottom of the perpetual pavement layer.
- Document the performance of perpetual pavements containing three types of WMA and one conventional wearing course, and to monitor pavement response in the form of deflections, strains, and pressures in and under perpetual pavements.

3 ABOUT THE APLF

ORITE's APLF at Ohio University's Lancaster Campus is a state-of-the-art indoor test facility for road pavements. A full-scale two-lane test road (24 ft. [7.3 m] wide, 45 ft. [13.7 m] long) can be built from the soil layer up inside the building. The environment can be temperature controlled from 10°F (−12°C) to 130°F (44°C); humidity is also controlled and moisture can be added to test its effect on subgrade soil. A rolling tire load from 9,000 lb (40 kN) to 30,000 lb (133 kN) can be applied to simulate a passing truck, up to 500 times per hour. The wheelpath can be adjusted ±10 in. (250 mm). The pavement test section can be fully instrumented so that deflections, strains, and pressures in all layers under the wheel load can be measured, along with longer term responses such as curling and warping of concrete pavement slabs. The APLF allows for testing road materials and construction techniques on a small scale with a full-width installation under extreme conditions, without having to risk experimentation on in-service pavements.

4 CONSTRUCTION AND INSTRUMENTATION OF THE TEST PAVEMENTS

The test pavement constructed for this project at the APLF included a total of eight pavement sections containing three types of WMA and one conventional wearing course placed on two thicknesses of perpetual pavement cross sections along each lane, as shown schematically in Figure 1. The 38 ft. (11.6 m) width of the APLF was divided into four 8 ft. (2.4 m) wide lanes, one for each surface treatment, with 3 ft. (0.9 m) borders at the edge of the pit. Each lane was divided into a north and south half of 22.5 ft. (6.9 m) length. The northern pavement sections each had the same profile with perpetual pavement thickness 16 in. (405 mm), with the only difference between each being the type of warm- or hot-mix asphalt used in the 1.25 in. (32 mm) surface layer. The perpetual pavement was constructed in the same manner as that constructed on the US Route 30 test road in Wayne County (Sargand et al., 2008).

The four southern sections had progressively thinner perpetual pavement depths of 16 in. (400 mm), 15 in. (380 mm), 14 in. (355 mm), and 13 in. (330 mm). The different section thicknesses in the southern part of the APLF were designed to provide data useful to future verifications of perpetual pavement analysis and design procedures. The different surface mixes had negligible impact on the perpetual pavement behavior and stresses in the lower layers of asphalt.

The 16 in. (400 mm) perpetual pavements were built up from the bottom in the following layers, as shown in Figure 1: 12 in. (300 mm) coarse aggregate topped by ∼5 ft. (∼1.5 m) of type A6-A7 subgrade soil, a 6 in. (150 mm) dense-graded aggregate base (DGAB, ODOT Item 304), a 4 in. (100 mm) fatigue resistant layer, a 7.75 in. (200 mm) intermediate AC (ODOT Item 448) layer, a 3 in. (75 mm) AC leveling layer of ODOT Item 446 Type II, and a 1.75 in. (32 mm) surface layer of ODOT Item 446 Type I HMA or one of the WMA mixes. For the southern half of each WMA lane, the intermediate layer (ODOT Item 448) was reduced by 1 in. (25 mm), 2 in. (50 mm), or 3 in. (75 mm) and the DGAB increased a corresponding amount to keep the surface of each pavement structure at the same elevation.

The conventional asphalt mixes were delivered to the APLF from the Shelley and Sands Asphalt Plant located in Logan, Ohio, while the WMA mixes were brought in from the plant site established near the GUE-541 project, and are the same as used at the field site. All sections were supported on a uniform dense-graded aggregate base (DGAB) and subgrade. Subgrade moisture was not varied throughout the project in an effort to limit the number of variables to be monitored and used in the analysis. Figure 2 has photographs of the sensors and the paving operations in the APLF.

The southern sections of the APLF were instrumented to measure dynamic response to load in the form of strains, pressure, and deflections. Figure 3 shows the sensor layout along the centerline of the lane. The instrumentation consisted of four *Dynatest PAST II AC* strain gauges oriented to measure longitudinal and transverse strain 1.0 in. (25 mm) above the bottom of the fatigue resistant AC layer, two

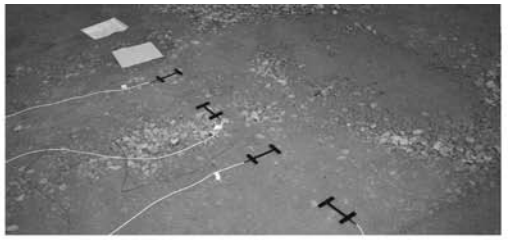

(a)

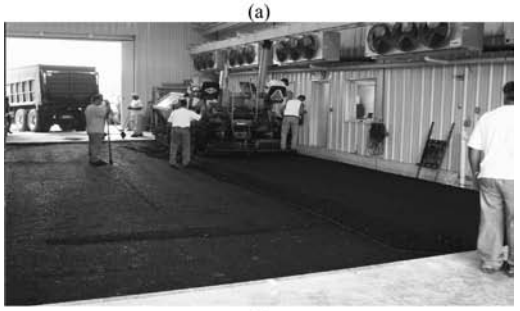

(b)

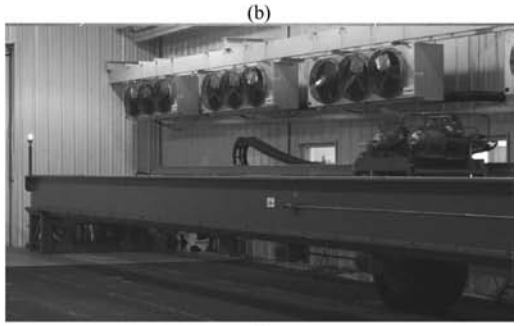

(c)

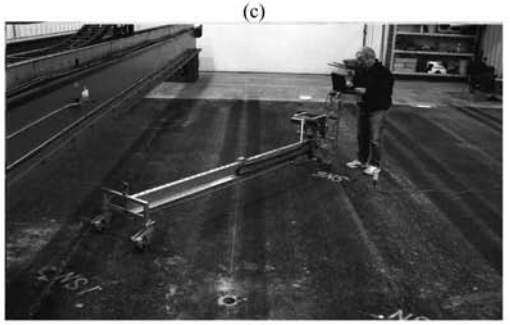

(d)

Figure 2. Views inside the APLF: (a) placement of sensors; (b), paving test sections; (c), load wheel behind beam; (d), using ORITE profilometer to measure a pavement surface profile.

Micro Sensors GHSD 750 LVDTs and one *Geokon* Earth Pressure Cell, all spaced 18 in. (450 mm) apart longitudinally along the lane centerlines to measure the dynamic response of the four perpetual pavements of different thickness. The two LVDTs were installed so that one measured surface deflection referenced to the top of the subgrade and the second deflection to a depth of approximately 5 ft. (1.5 m) below the pavement surface. A hole for the deep LVDT was

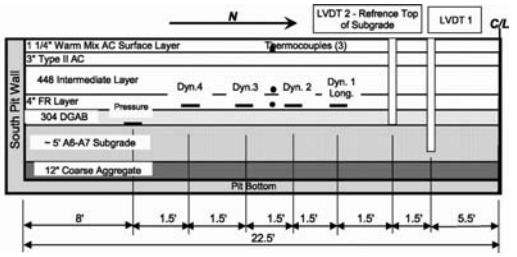

Figure 3. Profile view showing sensor locations along centerline in southern section of each APLF lane (not to scale).

drilled about 3 ft. (0.9 m) into the 304 aggregate, lined with PVC pipe, capped to keep it clean, and referenced for future drilling through the pavement to install the LVDT. Thermocouples were also placed 1.0 in. (25 mm) below the surface, at the center and 1.0 in. (25 mm) above the bottom of the AC to monitor pavement temperature during the tests.

Installation proceeded as follows: The pressure cell was placed on the finished subgrade before placement of the aggregate for the DGAB layer. Upon completion of the DGAB layer, strain gauges were installed by sieving out large particles from a portion of the hot fatigue resistant mix, placing a 1.0 in. (25 mm) thick pad of the sieved material on the aggregate, laying the gauge on the pad, covering it over with another in. (25 mm) of sieved material, hand compacting the asphalt encasing the strain gauge, and then letting the paver complete placement of the fatigue resistant layer. Thermocouples were held in place with loose AC ahead of the paver. After all paving was completed, holes were drilled through the AC and the two LVDTs were installed as shown in Figure 3. An infrared camera was used during the APLF test section construction to document WMA cooling throughout the placement and compaction processes.

Each specific section was tested at low, medium, and high temperatures of 40°F (5°C), 70°F (21°C), and 104°F (40°C), respectively, applied in that order to the pavement. Once the temperature of the asphalt had stabilized and initial sensor measurements taken, 10,000 passes were applied using a 9,000 lb (40 kN) single-axle dual-tire load moving at a constant speed of 5 mph (8 km/h). A second set of sensor readings under loads was taken after the set of passes was completed. During the 10,000 passes of the load, periodic visual condition surveys were performed to document the development of distress as the number of loads applied to the pavement increased. Surface profile surveys were also obtained with a profilometer (traveling laser instrument) that monitored rutting development as the loading of the pavement sections progressed under the three planned temperature levels. If rutting under the constant 9 kip (40 kN) single axle load equaled 0.5 in. (12.5 mm), testing was discontinued on that strip.

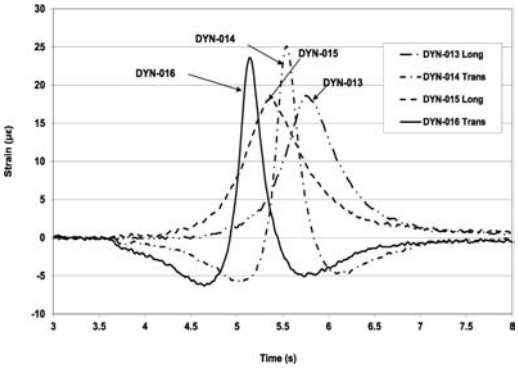

Figure 4. Example data for longitudinal and transverse strain as function of time during loaded rolling wheel pass in Fatigue Resistance Layer (FRL) in APLF.

5 RESULTS

5.1 *Strains under Fatigue Resistance Layer (FRL) in perpetual pavements*

Rolling wheel loads (RWL) of 6,000 lb (27 kN), 9,000 lb (40 kN), and 12,000 lb (54 kN) were applied by the speed-controlled tire at 5 mph (8 km/h) before and after the set of 10,000 runs (load wheel passes) with a 9,000 lb (40 kN) load rolling in a bidirectional mode at 5 mph (8 km/h) with no wheel wander applied at each temperature. It required about one week to apply the 10,000 bidirectional loading cycles. During each measurement session, each load was applied four times across the section along four different parallel tracks laterally shifted by the following amounts from the sensor line: 1.0 in. (25 mm), 3 in. (75 mm), −4 in. (−100 mm), and −9 in. (−225 mm), where positive is east (left) of the sensor line. The rolling wheel and associated beam can be seen in Figure 2c.

Figure 4 shows the longitudinal and transverse strains under the fatigue resistance layer (FRL) of the 13 in. (330 mm) perpetual pavement section at 40°F (4.5°C) as the load wheel ran from north to south. As the wheel approached the first longitudinal strain gauge (DYN-016 in Figure 4) a compression strain developed on that gauge, indicated by the negative value at approximately time = 4.7 seconds. When the wheel was directly over the gauge at time = 5 seconds, a tensile strain developed on the same gauge. Then, a compression strain developed as the wheel left the gauge, signified by the negative strain at time = 5.8 seconds. For the transverse strain gauge (DYN-015 in Figure 4), only a tensile strain is observed, peaking at about time = 5.3 seconds. The other two traces, DYN-014 and DYN-013 in Figure 4 for the second longitudinal and second transverse strain gauge mimic the curves of the other gauges. This process was repeated every time the axle load passed over the pavement. The repeated compression and tension strain in the longitudinal direction caused a permanent deformation in the asphalt layer, which manifests as rutting and fatigue cracking after sufficient repetitions.

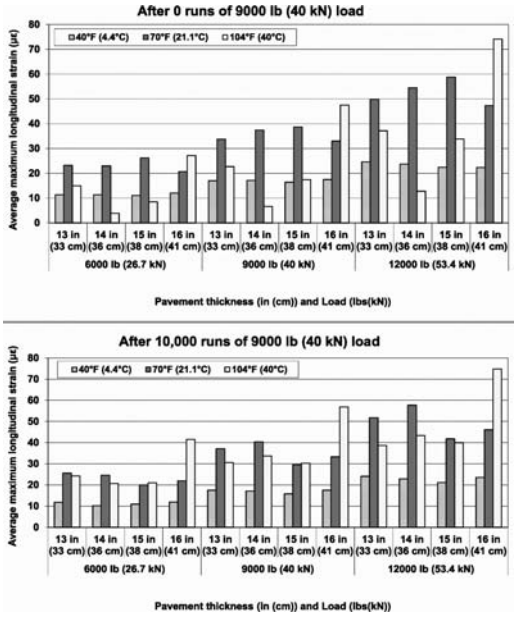

Figure 5. Longitudinal strain in Fatigue Resistance Layer (FRL) in APLF after 0 runs (top) and 10,000 runs (bottom).

The data collected from the graph in Figure 4 were recorded as follows: the two peak values of the longitudinal strains were determined (time = 5 seconds for DYN-016 and time = 5.3 seconds for DYN-014 in the figure) and these two values averaged for entry into the appropriate place in the appropriate table as a longitudinal strain. Similarly, the two peaks for the other two sensors (DYN-015 and DYN-013) were averaged to obtain the transverse strain values for the tables.

Figures 5 and 6 show the longitudinal and transverse strains in microstrains (με), respectively, in the fatigue resistance layer before applying the rolling wheel load (top) and after 10,000 runs of the wheel with a 9,000 lb (40 kN) load (bottom). The longitudinal strain for the conventional mix increases with increasing load and ambient temperature. The data indicate that the transverse strains observed in the FRL under the thinner pavements are considerably higher than in the FRL under the full-depth 16 in. (400 mm) pavement. This trend holds at all temperatures and under all loads, and is most pronounced under the highest load at the highest temperature. That said, the magnitude of the longitudinal strains remained below the critical design parameter of 70 με at all times, with a few exceptions under the 12 kip (54 kN) test load at the high temperature. Because the APLF conditions represent a uniform high temperature of 104°F (40°C) without a gradient, these results represent extreme conditions not likely to occur in the field. In addition, the full-depth section with the thickest intermediate layer performed about as well as the other sections. This suggests that it may be possible to maintain perpetual pavement conditions in a thinner pavement structure compensated for by a thicker and stiffer base.

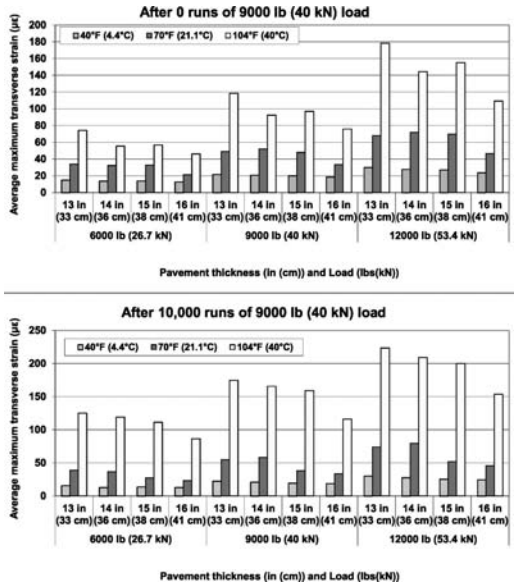

Figure 6. Transverse strain in Fatigue Resistance Layer (FRL) in APLF after 0 runs (top) and 10,000 runs (bottom).

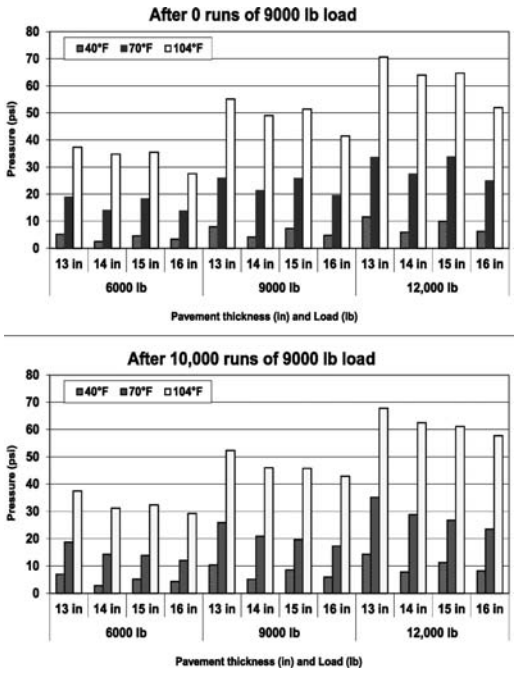

Figure 7. Pressure under base with load on wheelpath after 0 runs (top) and 10,000 runs (bottom).

5.2 *Pressure under base layer*

Figure 7 shows the pressure under the wheelpath under the base layer (304) after zero runs (top) and 10,000 runs (bottom) at ambient temperatures of 40°F (4.5°C), 70°F (21°C), and 104°F (40°C). The highest pressure was measured under the base layer of the

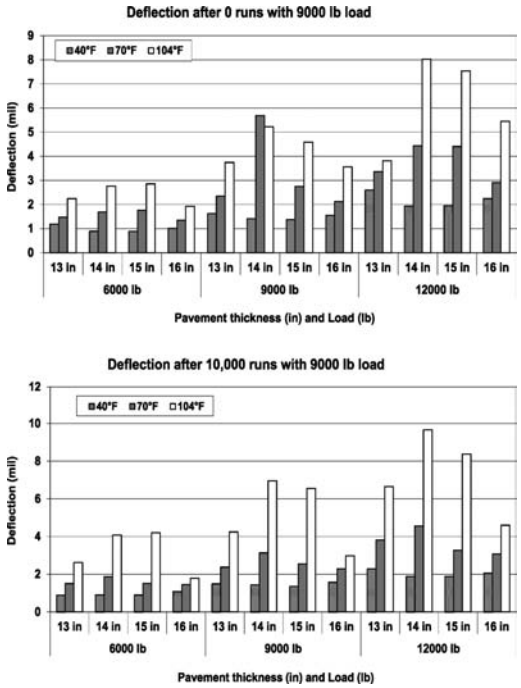

Figure 8. Deflection of subgrade layer after 0 runs (top) and 10,000 runs (bottom) along the wheelpath.

thinnest AC section. As with the strain measurements, the RWLs applied during measurement were 6,000 lbs (27 kN), 9,000 lbs (40 kN), and 12,000 lbs (54 kN) at each temperature. The pressure under the aggregate base increased with increasing load and the ambient temperature of the facility. The difference in the pressure at each section is very small. The lowest pressure measured was under the full-depth section at different loads and different ambient temperatures. This may be due to the greater thickness of the Item 448 (intermediate AC) layer in this section and the greater stiffness of the conventional HMA mix on the surface. The pressure under the base layer was almost the same after zero and 10,000 runs for the same applied load and ambient temperature.

5.3 *Subgrade deflection*

Figure 8 shows the deflections of the subgrade layer under each section after zero runs (top) and 10,000 runs (bottom) under 6,000 lb (26.7 kN), 9,000 lb (40 kN), and 12,000 lb (53.4 kN) loads at the three different ambient temperatures. The deflections of subgrade layer under the thinner AC sections were very similar to those under the full-depth AC. The change in deflections for the thinner sections and control section was very small with respect to the changes in load and temperature. This suggests that any effect that might have come from the reduction in Item 448 layer thicknesses was mitigated by the compensatory increase in the DGAB thickness. The thickness of the subgrade

layer was uniform under all sections. Because of these differences in the thicknesses of the Item 448 layer and DGAB in the instrumented sections resulted in differences in the depths of the strain gauges between the sections, strain responses under rolling wheel loads cannot be directly compared across lanes.

Wheel load responses measured on pavement sections in the APLF also would not be expected to agree with dynamic responses measured on the same pavement sections in the field because of dramatically different temperature distributions at the two sites. Field sections are exposed to daily temperature cycles where surface warming and cooling can generate significant gradients within the pavement layer over a 24-hour cycle. APLF sections are maintained at a constant air temperature, thereby reducing any gradients in the pavement to a few degrees. This difference in gradient will have a major impact on measured responses.

5.4 *Falling weight deflectometer testing in APLF*

The overall test plan for the APLF installation consisted of measuring dynamic responses and surface rutting in the pavement sections at 40°F (4.5°C), 70°F (21°C) and 104°F (40°C), as follows:

1. Measure dynamic deflections with an FWD at nominal loads of 6,000 lb (27 kN), 9,000 lb (40 kN), and 12,000 lb (54 kN) in all eight sections (North (16 in. [400 mm] AC) and South (variable depth AC) portions for each of Lanes 1-4.
2. Measure dynamic deflection, strain and pressure with sensors installed in the southern sections of the test lanes during FWD loading and as 6,000 lb, 9,000 lb, and 12,000 lb loads were applied with rolling dual tires at 5 mph (8 km/h). The rolling tire measurements are reported above.
3. Periodically measure surface profiles in all eight sections as 10,000 rolling wheel loads were applied at 9,000 lbs.

After air temperature in the facility had been maintained at 40°F (4.5°C) sufficiently long for temperature to stabilize throughout the test pad, dynamic deflections were measured with the FWD, and dynamic responses were measured with the embedded pavement sensors as loads were applied with the FWD and rolling dual tires. Lateral surface profiles were measured across the wheelpaths after 0, 100, 300, 1,000, 3,000, and 10,000 passes of the rolling dual wheels. Similar data were then collected at nominal air temperatures of 70°F (21°C) and 104°F (40°C). For each of the three series of tests, the temperature of the pavement surface was near the air temperature. At 70°F (21°C), temperature was nearly uniform through the pavement. At 40° F (4.5°C), and 104°F (40°C), there was a slight gradient of increasing and decreasing temperatures, respectively, toward the bottom of the asphalt concrete.

While the FWD load was dropped over seven sensors embedded in each of the four instrumented pavement sections, outputs from the embedded sensors were recorded with a *Megadac 5108A* data acquisition system at the three loads and three temperatures. The top portion of Table 1 contains a summary of maximum sensor responses recorded during the second drop and normalized to a 9,000 lb (40 kN) load. LVDT data referenced to the top of the subgrade were not included in the table. The bottom portion of Table 1 contains sensor responses (average maximum longitudinal strain, average maximum transverse strain, maximum vertical deflection from the deep LVDT, and maximum vertical pressure) measured along the centerline of the pavement sections under the 9,000 lb. (40 kN) rolling dual tire load at three temperatures. FWD deflections, not shown in the table, agreed with the LVDT readings within 1.0 mil (25 μm).

5.5 *Surface rutting*

Previous testing in the APLF showed that AC consolidation progresses at a near linear rate on a log-log plot of average depth vs. number of load applications, and that power trend lines, of the form $y = ax^b$, fit the data quite well. For these tests, therefore, profiles were averaged at two locations in each of the eight pavement sections at 0, 100, 300, 1,000, 3,000 and 10,000 load cycles to provide a good distribution of points along the logarithmic application axis.

Surface deformations were measured with a 10-ft. (3 m) long rolling wheel profilometer developed by ORITE, which measures elevations to at least 5-mil (127 micron) accuracy at 0.5 in. (12.5 mm) intervals along the profile path. This profilometer is shown in Figure 1d. To avoid any effects from loads being applied in adjacent lanes, profiles were skewed across the eight-foot wide lanes so that the profiler feet were located along the lane edges. Profiler lateral position and elevation were referenced by fender washers epoxied to the pavement for the profiler feet to sit on during each set of measurements.

The eight pavement sections were identified by lane number and north or south end of the lane (i.e., 1S or 2N). The two profile locations within each pavement section were further identified by adding a north or south indicator to the section identifier (i.e., 1SS, 1SN, 2SS or 2NS). To minimize any vertical offsets which occasionally occurred at the ends of a profile, all profiles were aligned by: 1) moving profiles vertically so the average of the first five points matched the average of the same five points on the reference profile, and 2) rotating the profiles around the first point until the average of the last five points on each profile matched the average of the last five points on the reference profile.

Figure 9 shows a typical profile history measured in Section 1S at 104°F (40°C). The heavy line is the initial reference profile recorded after completion of the 40°F (4.5°C) and 70°F (21°C) tests.

This plot shows:

1. Changes in the lateral profile of the pavement surface as repeated rolling wheel loads were applied to the pavement. These profile changes are the

Table 1. Measured sensor responses under FWD load plate and under rolling wheel load, after 10,000 runs.

Section	1S	2S	3S	4S
Surface Mix	Evotherm	Sasoblt	Aspha-min	HMA Control
Total thickness	13″ (33.0 cm)	14″ (35.6 cm)	15″ (38.1 cm)	16″ (40.6 cm)
Measured responses from embedded sensors under FWD load normalized to 9000 lb (40 kN)				
Nominal air temperature	Average longitudinal tensile strain (με)			
40°F (4.4°C)	12.5	20.2	16.1	10.1
70°F (21.1°C)	30.4	42.7	16.7	36.3
104°F (40.0°C)	55.6	70.5	52.2	51.6
	Average transverse tensile strength (με)			
40°F (21.1°C)	17.3	22.7	18.0	15.1
70°F (21.1°C)	39.6	40.0	22.3	32.3
104°F (40.0°C)	51.3	49.8	51.3	47.6
	Vertical pressure on subgrace (ps (kPa))			
40°F (21.1°C)	1.21 (8.35)	0.77 (5.32)	1.06 (7.34)	0.63 (4.36)
70°F (21.1°C)	3.06 (21.2)	2.52 (17.4)	2.27 (15.6)	1.42 (9.79)
104°F (40.0°C)	4.34 (29.9)	3.19 (22.0)	3.97 (27.4)	4.25 (29.3)
	Deep LVDT deflection (mil (μm))			
40°F (21.1°C)	1.91 (48.5)	2.03 (51.5)	1.82 (46.2)	1.48 (37.6)
70°F (21.1°C)	2.04 (51.8)	4.42 (112)	2.20 (55.9)	2.34 (59.4)
104°F (40.0°C)	6.43 (163)	4.84 (123)	4.34 (109)	3.86 (98.0)
Measured responses from embedded sensors under rolling wheel load of 9000 lb (40 kN)				
Nominal air temperature	Average longitudinal tensile strain (με)			
40°F (4.4°C)	17.6	17.1	15.8	17.6
70°F (21.1°C)	37.2	40.4	29.6	33.3
104°F (40.0°C)	30.6	33.7	30.3	56.9
	Average transverse tensile strength (με)			
40°F (21.1°C)	22.5	21.2	19.5	18.8
70°F (21.1°C)	54.9	58.3	38.1	33.6
104°F (40.0°C)	174.8	165.7	159.1	116.2
	Vertical pressure on subgrace (ps (kPa))			
40°F (21.1°C)	1.50 (10.3)	0.74 (5.1)	1.24 (8.6)	0.86 (6.0)
70°F (21.1°C)	3.75 (25.9)	3.03 (20.9)	2.84 (19.6)	2.51 (17.3)
104°F (40.0°C)	7.59 (52.3)	6.66 (46.0)	6.64 (45.8)	6.22 (42.9)
	Deep LVDT deflection (mil (μm))			
40°F (21.1°C)	2.24 (56.7)	1.97 (50.0)	1.80 (45.7)	1.93 (49.0)
70°F (21.1°C)	4.00 (102)	4.62 (117)	2.99 (75.9)	2.97 (75.4)
104°F (40.0°C)	7.47 (190)	11.1 (282)	9.95 (253)	7.23 (184)

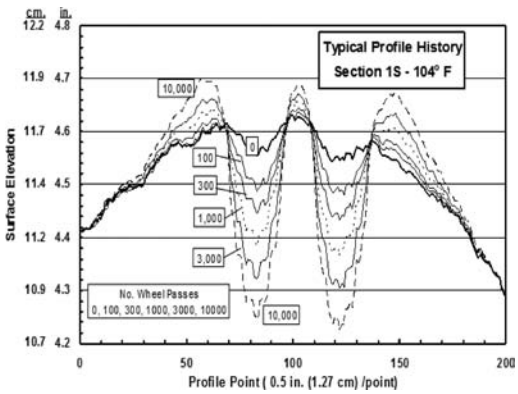

Figure 9. Profile history in Section 1S.

result of permanent deformations in the pavement structure, which include zones of downward consolidation under the tires and upward shoving/heaving outside the tires. Consolidation and shoving/heaving were calculated as areas by integrating incremental differences in elevation from a reference profile. The depth of consolidation was calculated as the linear change in elevation under the tires from the initial reference profile and, if the height of shoving/heaving were also used, it would be calculated similarly outside the tires.

Rut and rutting are general terms often used to describe the depth or extent of consolidation in pavement wheelpaths. Rut depth is a linear difference in elevation between certain high and low points on a profile. Unfortunately, however, the calculation of rut depths varies with procedures used to measure profiles and define ruts. In this study, average depth of consolidation was used to define deformation under the tires.

Long straightedges are the most practical method of measuring ruts in the field since references are usually not available to compare profiles. While ruts measured vertically from a straightedge laid across the wheelpath to the lowest point in the

wheelpath are what drivers feel on the road and what ponds water, they usually contain elements of consolidation and shoving/heaving. In a controlled setting like the APLF, however, referenced profiles make it possible to monitor consolidation and shoving/heaving separately. This information provides a more detailed picture of how pavement structure, AC mix properties, and temperature affect surface deformation.

2. Zones of AC consolidation are bounded by inflection points on the profiles, the lateral position of which remained stable throughout 10,000 loading cycles. The positions of these points varied slightly over the 16 profiling locations on the test pad, probably due to slight variations in the layout of the reference washers and the location of the profiler on the washers, but were very close to the edges of the rolling tires in all profiles.
3. Initial consolidation in the wheelpaths was caused by earlier testing at 40°F (4.5°C) and 70°F (21°C), both of which resulted in minimal surface deformation and were considered as seating runs for the 104°F (40°C) tests. Because of equipment malfunctions, approximately one year was required to complete all rolling wheel tests at three temperatures in the APLF, instead of the anticipated three months. As a result, it was difficult to compare as-built profiles with subsequent profiles because of changing test temperatures in the facility and loading in adjacent lanes which caused some minor surface deformation over time. In general, there was little change in profiles at 40°F (4.5°C), minimal deformation under the tires at 70°F (21°C), and substantial consolidation under the tires and shoving/heaving outside the tires at 104°F (40°C). The as-built profile in Figure 9 can be approximated by continuing the zero pass line from before the left tire up to the zero pass peak between the tires and on past the right tire to form a smooth concave surface.
4. If rut depth was measured with a straightedge after 10,000 loading cycles, it would be about 0.45 in. (115 mm), of which 0.3 in. (8 mm) is the depth of consolidation and 0.15 in. (4 mm) is the height of shoving/heaving. A rut depth of 0.5 in. (12.5 mm) is often used as a criterion to grind or overlay AC pavements.

Undulations within the consolidated portion of the profiles were likely caused by the five treads in each tire, which remained in the same lateral position for all passes of the tires due to the lack of wander in the rolling wheel tests.

From the data such as that shown in Figure 9, average depth of consolidation as a function of wheel passes was graphed, and the parameters for the power law ($y = ax^b$) determined for each section. Table 2 summarizes the average trend line parameters calculated for each of the eight pavement sections at 104°F (40°C), the temperature at which the asphalt showed the greatest consolidation.

Figure 10 compares the five 16-inch (400 mm) thick AC sections where the only variable was surface mix.

Table 2. Average depth of consolidation parameters for each pavement section.

Mix	Section	AC Depth (in.)	Trendline Parameters at 104°F (40°C) a (in.)	b	R^2
Evotherm	1N	16	0.0083	0.3677	0.98
	1S	13	0.0083	0.3567	0.98
Sasobit	2N	16	0.0059	0.3868	0.99
	2S	14	0.0048	0.3918	0.99
Aspha-min	3N	16	0.0103	0.3232	0.99
	3S	15	0.0048	0.4028	0.97
HMA Control	4N	16	0.0037	0.4179	1.00
	4S	16	0.0032	0.4387	0.99

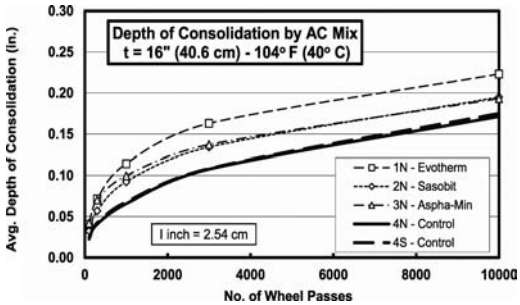

Figure 10. Linear plot of consolidation depth for each AC surface mix as a function of number of passes at high temperature.

Each curve represents the average of two locations in each section. The plot shows: 1) excellent agreement between redundant Sections 4N and 4S, 2) higher early consolidation in the three warm AC mixes than in the conventional mix, and 3) especially high consolidation in the *Evotherm* mix. The plot also shows slightly reduced slope between 1,000 and 10,000 cycles for the warm AC mixes in Sections 1N, 2N, and 3N, as compared to the standard AC mix Sections 4N and 4S. In summary, the three warm mix AC mixes, and especially the *Evotherm* mix, exhibit more early consolidation than the standard ODOT Type I 446 mix, but this difference may be slowly mitigated as the long term rate of consolidation for the conventional mix was slightly higher than that for the warm AC mixes.

While intercept-a, as the calculated consolidation at one load cycle, is a preliminary indicator of early consolidation, it is not necessarily a reliable measure of early consolidation, as shown in Figure 10 and Table 2. The *Evotherm* mix in Section 1N clearly had the most early consolidation, but intercept-a in Table 2 is larger in Section 3N than in Section 1N. This can be explained since the Aspha-Min mix in Section 3N has about equal consolidation as the *Evotherm* mix in Section 1N at 100 and 300 cycles, but tapered off after 300 cycles to give an overall flatter slope-b and a higher

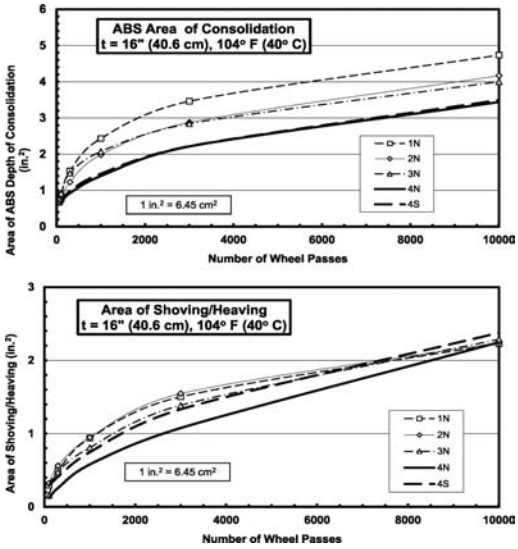

Figure 11. Linear plots of area of ABS net consolidation area (top) and area of shoving/heaving (bottom) for each AC surface mix as a function of number of passes at high temperature.

intercept-a when extrapolated back to one cycle in the trend line equation.

As noted earlier, surface profiles were divided into zones of consolidation and shoving/heaving as delineated by profile inflection points located just inside the edges of the rolling tires. The lateral position of these inflection points remained quite stable throughout the 10,000 loading cycles. Since detailed profiles were obtained with the profilometer, it was of interest to separate AC deformation into areas of negative consolidation under the two tires, areas of positive shoving/heaving between and outside the tires, and net deformation being the arithmetic sum of consolidation and shoving/heaving. These areas were calculated by integrating changes in elevation across profiles and plotting these values versus the number of loading cycles to determine if there were certain trends which might further characterize the effects of surface mix and AC thickness on deformation. Figure 9 shows how areas of consolidation and shoving/heaving expanded with an increasing number of load applications. Since all profiles were skewed across the wheelpaths, the calculated areas were adjusted to bring them perpendicular to the wheelpath. This adjustment was not necessary for average consolidation since it was calculated solely from the average of elevations measured between the inflection points, which remained the same for perpendicular and skewed profiles.

Plots of ABS area of consolidation at the top of Figure 11 are identical in shape to curves in Figure 10 for average depth of consolidation. This is because these areas are a product of the depth multiplied by a constant width across the wheelpath. This adjusted profile length is essentially the same for all profiles and, therefore, cancels out as a variable in the area calculations. The bottom of Figure 11 shows similar profile areas calculated for shoving/heaving in the five 16-inch (400 mm) thick AC sections. As expected, the area of shoving/heaving is less than the area of consolidation, indicating an overall net consolidation. In summary, warm AC mixes had higher initial and higher long term consolidation, higher initial shoving/heaving which quickly dissipated, and persistent higher net consolidation than the conventional AC mix.

6 CONCLUSIONS

6.1 *Warm mix asphalt*

All three of the warm mix asphalt surfaces appeared to experience more consolidation than the HMA control surface during the initial stages of application of the wheel load. After the initial consolidation, further consolidation of each pavement was about equal. The difference was about twice as great for *Evotherm* than for the other two WMA mixes. In the long term, this constant difference in consolidation represents a relatively small portion of total consolidation experienced by the pavement. The NCAT report also noted significantly greater rutting for the *Evotherm* mix in their test (Hurley et al., 2009).

The AC consolidation measured with a straightedge includes components under the tires and shoving/heaving between and outside the tire edges. These components progress according to a power equation of the form $y = ax^b$ as loading cycles accumulate. If no tests had been performed at 40°F (4.5°C) and 70°F (21°C), more initial consolidation would have been observed in all four lanes, and constants *a* and *b* would have been somewhat different, although relative deformations would likely have remained the same.

6.2 *Perpetual pavement*

The strains measured in the fatigue resistant layer (FRL) did not show significant differences between the different sections in the APLF. It thus appears that the reduction of a perpetual pavement thickness from 16 in. (400 mm) to 13 in. (330 mm) accompanied by a corresponding increase in the thickness of the base structure will respond about equally well to loads.

At the highest APLF temperature of 104°F (40°C), the highest longitudinal strains exceeded the FRL design strain. However, the uniformly distributed high temperature in the APLF pavement structure led to the high strains and represented an extremely harsh condition. Under real world conditions, a temperature gradient would exist between the hot surface and the cooler subgrade, which would be expected to reduce the strain at the bottom of the AC layer.

The transverse and longitudinal strains under FWD loading were about equal, as expected. At 104°F (40°C) and under a 9,000 lb. (40 kN) load, transverse strain 1.0 in. (25 mm) from the bottom of the AC, surface deflection and pressure on the subgrade were

much larger under tires traveling at 5 mph (8 km/h) than under the FWD load plate.

ACKNOWLEDGEMENTS

This research was sponsored by the Ohio Department of Transportation and the Federal Highway Administration. The authors would like to acknowledge the contributions of the technical liaisons and project panel members to the original research project, particularly Roger Green, Dave Powers, and the Ohio DOT Office of Research and Development. The authors also acknowledge the contributions of ORITE Research Engineer Wallace Richardson and graduate students Andrew Wargo and Carlos Vega-Posada.

REFERENCES

APAO. 2003. *Warm mix asphalt shows promise for cost reduction, environmental benefit.* Salem, OR: The Asphalt Pavement Association of Oregon.

Brown, R. and Timm D.H. 2006. "The Thick Of It", *Roads and Bridges, Volume 44, Number 2*.

Hurley, G.C., Prowell, B.D. and Kvasnak, A. 2009. *Ohio Field Trial of Warm Mix Asphalt Technologies: Construction Summary*. Final Report 09-04. Auburn, AL: National Center for Asphalt Technology.

Sargand, S.M., Figueroa, J.L. and Romanello, M. 2008. *Instrumentation of the Way-30 Test Pavements*, Technical Report No. FHWA/OH-2008/7 for the Ohio Department of Transportation, State Job No. 14815.

Sargand, S.M., Figueroa, J.L., Edwards, W. and Al-Rawashdeh, A.S. 2009. *Performance Assessment of Warm Mix Asphalt WMA Pavements*. Technical Report No. FHWA/OH-2009/08 for the Ohio Department of Transportation, State Job No. 134312.

Sargand, S.M. and Figueroa, J.L. 2010. *Monitoring and Modeling of Pavement Response and Performance, Task A: Ohio*. Technical Report No. FHWA/OH-2010/3A for the Ohio Department of Transportation, Pooled Fund Project TPF-5121, State Job No. 134287.

This page intentionally left blank

Advances in Pavement Design through Full-scale Accelerated Pavement Testing – Jones, Harvey, Mateos & Al-Qadi (Eds.)
© 2012 Taylor & Francis Group, London, ISBN 978-0-415-62138-0

Structural evaluation and short-term performance of sustainable pavement sections at the NCAT pavement test track

A. Vargas-Nordcbeck & D.H. Timm
Auburn University, Auburn, Alabama, US

ABSTRACT: As state agencies have started to transition from an empirical pavement design method to a Mechanistic-Empirical (ME) approach, it has become necessary to further evaluate the material properties and structural characteristics of newer sustainable pavement technologies. The objective of this study was to evaluate pavement responses and short-term performance for different sustainable pavement sections placed at the National Center for Asphalt Technology (NCAT) Test Track. The Test Track was reconstructed in the summer of 2009 and part of the experiment included six new structural sections built using several sustainable technologies. Falling Weight Deflectometer (FWD) testing and strain and pressure measurements under live traffic loads were obtained periodically under different environmental conditions. Results indicated that pavement responses changed significantly for some sustainable sections. Field performance measurements showed that rut depths were influenced by the use of sustainable technologies, but all sections performed well overall with less than 10 mm of rutting. No cracking had been observed in any of the sections after 20 months of operation and over 8 million applied ESALs.

1 INTRODUCTION

The asphalt industry has been developing sustainable paving technologies and practicing green-construction techniques since the 1960's through the reduction in emissions from asphalt plants (APAI, 2008). A sustainable pavement can be defined as a safe, efficient, and "environmentally friendly" pavement that meets today's transportation needs without jeopardizing the ability to meet such needs in the future (Chappat, 2003). Recent advances in this area include technologies that focus on low consumption of energy for production and placement, conservation of natural resources, noise reduction, and improvement of the quality of stormwater runoff.

Warm mix asphalt (WMA) describes a group of technologies which allow a reduction in the temperatures at which asphalt mixes are produced and placed. While hot-mix asphalt (HMA) is typically produced in the temperature range of 280°F to 335°F, WMA mixes can be produced in the range of 220°F to 275°F by using technologies that reduce mixture viscosity and improve workability. This temperature reduction provides environmental benefits such as reduced emissions, fumes and odors, and energy savings (Anderson et al., 2008). The improved workability offers paving benefits including the ability to pave in cooler temperatures, longer haul distances, improved compaction, and use of higher reclaimed asphalt pavement (RAP) percentages (D'Angelo et al., 2007).

Lower production temperature of the asphalt mixtures also results in a reduction of binder aging, which can lead to more flexibility and resistance to cracking in service. However, there is concern that a potentially softer binder could contribute to loss of stability in hot weather and increase rutting susceptibility (Newcomb, 2006). Additionally, since some WMA use water as a workability aid, WMA mixes may be more susceptible to moisture damage (Anderson et al., 2008).

Another approach to sustainable asphalt pavements is the inclusion of high RAP percentages in the mix. High RAP is defined as using 25 percent or more RAP in an asphalt mixture by weight of the total mix (Copeland, 2011). The maximum amount of RAP allowed in HMA varies for each state and is generally under 30% for surface courses, but can increase for binder and base courses (FHWA, 2008). Although the use of high RAP mixes has economic and environmental benefits such as conservation of energy, preservation of resources, and reduction of waste materials, their design and construction can be challenging due to the presence of aged binder that can cause problems with workability and compactability.

Finally, porous friction courses (PFC) are gap-graded HMA mixtures designed to have a large number of voids so that water can drain through and over their surface (Roberts et al., 1996). PFCs provide safety improvements including reduction in splashing and hydroplaning, improved visibility of road markings during rain events, as well as higher wet

frictional resistance, particularly at high speeds (Kandhal, 2002). Environmental benefits include reduction of tire-pavement noise due to the sound absorbing negative texture generated by mixture air voids (Smit and Waller, 2007) and reduction in pollutants commonly observed in highway runoff such as total suspended solids and metals (Berbee et al., 1999; Barrett, 2006).

PFCs are typically assigned no or minimal structural contribution for pavement design. However, some researchers have indicated that PFCs are structurally comparable to conventional dense-graded mixes (Kandhal, 2002; Poulikakos et al., 2003). Performance issues for this type of mixture are generally related to moisture susceptibility and raveling. Rutting and cracking do not appear to be a significant factor.

As state agencies have started to transition from an empirical pavement design method to a mechanistic-empirical (ME) approach, it has become necessary to further evaluate the material properties and structural characteristics of these newer technologies. This information is important for accurate performance prediction and design of efficient pavement structures because the ME design method relies on mechanistic models that calculate structural responses (stresses, strains, and deflections) based on material properties, environmental conditions, and loading characteristics; as well as on empirical models that predict pavement performance from the calculated responses and material properties.

2 OBJECTIVE

The objective of this study was to evaluate the pavement responses and short-term performance of sustainable pavement sections under full-scale accelerated pavement testing.

3 SCOPE OF WORK

To accomplish the aforementioned objective six full-scale instrumented test sections were constructed in 2009 at the National Center for Asphalt Technology (NCAT) Test Track. All sections had the same design cross-section and the mixtures were designed to have similar gradations and volumetric properties. Deflection testing was conducted routinely to quantify the seasonal behavior of the pavement layer moduli. Strain and pressure measurements were taken approximately once a week under live traffic loads and under different environmental conditions. Field performance was monitored on a weekly basis.

Comparisons between sections were first achieved by performing statistical regressions of each measured property versus mid-depth pavement temperature in each of the sections. Hypothesis tests were conducted at 95% confidence level for the regression coefficients to determine if the trends were similar for the sections. Additionally, a post ANOVA Tukey's test with 5% significance level was used to compare the measured responses at a reference temperature. A detailed explanation of the statistical procedures used is beyond the scope of this study and can be found elsewhere (Devore, 2000).

4 TEST FACILITY AND SECTIONS

This study was based on data from the NCAT Test Track Phase IV research cycle. The NCAT Test Track is a 1.7 mile closed loop full-scale accelerated testing facility located in Opelika, Alabama. A fleet of tractor-trailers operates five days per week for 16 hours per day, applying a total of 10 million 18,000 lb equivalent single axle loads (ESALs) to the 200-ft test sections over a two-year period. Reconstruction for this research cycle was carried out during the summer of 2009, with paving operations performed between July 3 and August 11. Traffic operations started on August 28, 2009 and are currently ongoing.

As part of the fourth research cycle, the Group Experiment (GE) was created to include structural sections built using several sustainable technologies. A total of three WMA sections were placed including a foam-based (water injection) section, an additive-based section, and a foamed-based section containing 50% RAP, respectively. A control HMA section and a control HMA section with 50% RAP were also placed. Finally, a section with permeable surface (PFC) and the same intermediate and base layers as the control was included. During construction, all pavement sections included in this study were embedded with a gauge array to measure horizontal asphalt strain, vertical aggregate base pressure, and vertical subgrade pressure in the center of the outside wheelpath. Additionally, in each section four temperature probes were bundled together and installed in the pavement to measure temperature at the top, middle and bottom of the asphalt concrete (AC) and 3.0 in. into the underlying aggregate base layer. A detailed report on the instrumentation plan is documented elsewhere (Timm, 2009).

Table 1 shows a description of each section. The letters "S" and "N" in the section column denote the tangent of the Test Track in which the sections were located (South or North).

All sections were paved in three lifts and paving was performed by the same contractor using the same crew. All mixtures were produced at the same plant. With the exception of the PFC surface lift in Section S8, each lift of the south tangent sections were paved on the same day in a continuous process, keeping the plant settings constant while varying the production temperature. Similarly, both north tangent sections were placed in the same manner. Table 2 shows the production temperature for each mixture.

All GE sections had a design asphalt thickness of 7 in. over 6 in. of aggregate base and a stiff subgrade underneath. The as-built layer thicknesses at the gauge array determined from surveyed depths during construction are shown in Figure 1. These thicknesses were used to adjust the measured vertical pressures to the design cross section to account for differences due to construction variability.

Table 1. Section description.

Section	Description	Abbreviation	Lift	NMAS (mm)	Virgin Binder
S8	PFC surface with same intermediate and base lifts as the control	PFC	Surface Intermediate Base	12.5 19.0 19.0	PG 76-22 PG-76-22 PG-67-22
S9	Control	Control	Surface Intermediate Base	9.5 19.0 19.0	PG 76-22 PG-76-22 PG-67-22
S10	Foam-Based WMA	WMA-F	Surface Intermediate Base	9.5 19.0 19.0	PG 76-22 PG-76-22 PG-67-22
S11	Additive-Based WMA	WMA-A	Surface Intermediate Base	9.5 19.0 19.0	PG 76-22 PG-76-22 PG-67-22
N10	50% RAP HMA	HMA-RAP	Surface Intermediate Base	9.5 19.0 19.0	PG-67-22 PG-67-22 PG-67-22
N11	50% RAP WMA (Foam-Based)	WMA-RAP	Surface Intermediate Base	9.5 19.0 19.0	PG-67-22 PG-67-22 PG-67-22

Table 2. Production temperatures.

	Production Temperature (°F)					
Lift	S8	S9	S10	S11	N10	N11
Surface	335	335	275	250	325	275
Intermediate						
Base	325	325				

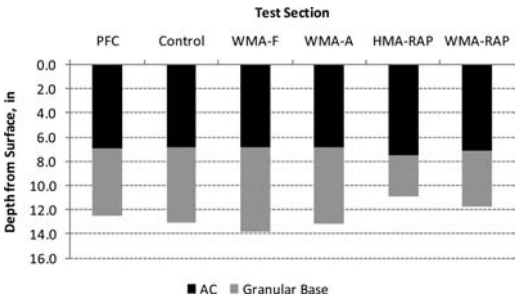

Figure 1. As-built pavement cross sections.

5 FIELD MEASUREMENTS

This study includes data collected from August 2009 to April 2011. During trafficking operations, strain and pressure measurements were taken approximately once a week under live traffic loads and under different environmental conditions. A fleet of five triple-trailer vehicles operated 16 hours per day, five days a week. On each date of data collection, three passes of each truck traveling approximately 45 mph were obtained along with pavement temperatures.

Horizontal strains were measured at the bottom of the AC layer in the longitudinal and transverse directions using CTL gauges with a range of $\pm$1,500 $\mu\varepsilon$, while vertical pressures were measured at the top of the granular base and at the top of the subgrade using Geokon model 3500 earth pressure cells with a full-scale capability of 36.3 psi. Figure 2 shows a schematic of the gauge arrangement used in all test sections. This configuration includes six asphalt strain gauges in each direction (longitudinal and transverse), allowing for redundancy to be built into the system, so that in the event of gauge failure, paired gauges help ensure that at least one measurement is made.

This study focused only on longitudinal tensile strain and vertical subgrade pressure. Longitudinal strain was selected since previous studies at the Test Track had shown that longitudinal strains were about 36 percent higher than transverse strain measurements (Priest and Timm, 2006; Timm and Priest, 2008). Vertical subgrade pressure was used since classic pavement design procedures are based on limiting the vertical response at the top of the subgrade to prevent rutting (Haddock, 2002). Data were subdivided by axle type (i.e., steer, single and tandem). Only the single axle data are presented in this study because they represent the majority of axle passes on each section. Additionally, the values shown correspond to the "best hit" on each section for each test date, which was defined as the 95th percentile of the readings obtained on a given test date.

Falling weight deflectometer (FWD) testing was performed three times per month to quantify the seasonal behavior of the pavement layer moduli. FWD testing was conducted at three predetermined random locations per test section. At each random location, testing was performed in the inside, outside, and between the wheelpaths. A Dynatest 8000 FWD was used with nine sensors spaced at 0, 8, 12, 18, 24, 36, 48, 60, and 72 in. from load center and a load plate

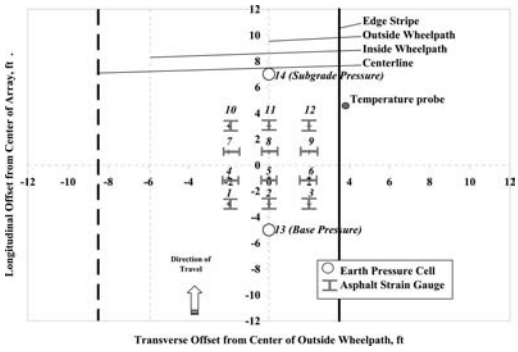

Figure 2. Schematic of instrumentation.

with a radius of 5.91 in. and a split configuration to ensure good seating on the pavement surface. Three repetitions of the FWD at four load levels (approximately 6, 9, 12 and 16 kips) were completed at each location. Mid-depth temperatures were obtained at the time of testing. The data presented in this report correspond to the measurements taken at the gauge array with the 9 kip load. The pavement layer moduli were backcalculated from deflection data using *EVERCALC 5.0* for a three-layer cross-section (asphalt concrete, aggregate base, and subgrade soil). Since the same aggregate base and subgrade were used throughout the Test Track, this study focuses only on the asphalt concrete layer moduli. Data were filtered to eliminate results with root-mean-square error (RMSE) exceeding 3 percent.

5.1 *Strain and pressure*

The mid-depth pavement temperature was used to correlate the measured responses (strain and pressure) to temperature. Previous studies at the Test Track have shown the effectiveness of using mid-depth temperature for these correlations (Priest and Timm, 2006; Willis and Timm, 2009). The relationship between these parameters follows an exponential function, as shown in Equation 1:

$$response = k_1 e^{k_2 T} \quad (1)$$

where response = pavement response (microstrain or subgrade pressure (psi)); T = Mid-depth AC temperature (°F); and k_1, k_2 = Section-specific regression coefficients.

Figures 3 and 4 show the longitudinal strain and the vertical subgrade pressure versus mid-depth temperature for each of the test sections. Peak pressure readings were determined from a baseline established just prior to a truck pass to mitigate the effects of daily and seasonal temperature changes on internal cell pressure. To determine if the response-temperature relationships were statistically similar among the sections, hypothesis tests were performed on the intercepts (k_1) and slopes (k_2). In most cases, at 95% confidence level

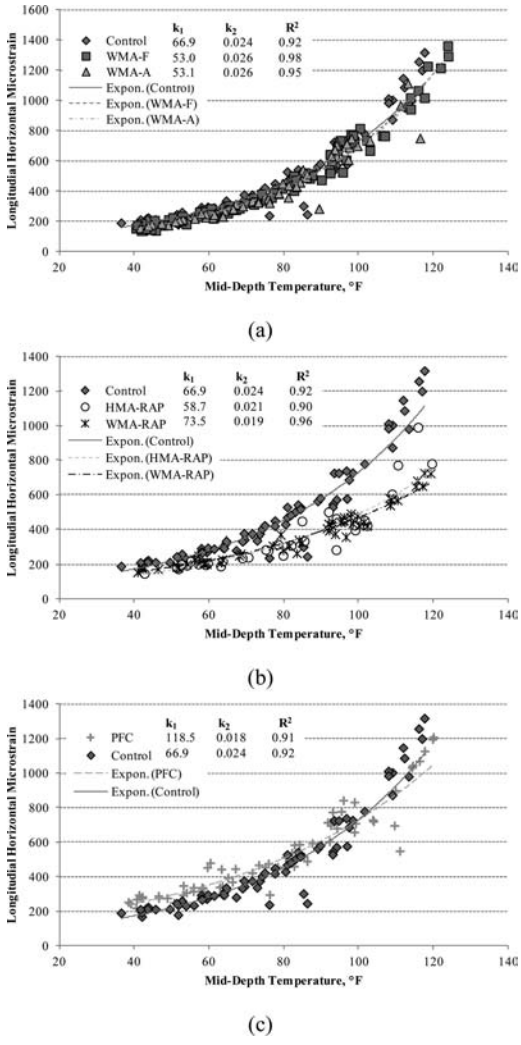

Figure 3. Longitudinal strain versus temperature for a) control vs. WMA, b) control vs, high RAP and c) control vs PFC.

there was no evidence that the regression coefficients of the sustainable sections were statistically different from the control. As expected, the PFC section exhibited higher responses under load, especially at high temperatures (higher intercept and lower slope). In the WMA-RAP and HMA-RAP sections strain and pressure were less influenced by temperature, respectively. The lower slopes are presumably due to the presence of binder with more aging.

To compare the different test sections fairly, it was necessary to normalize the responses to a reference temperature of 68°F by dividing Equation 1 with reference temperature (T_{ref}) by the same equation with measured temperature (T_{meas}) and solving for temperature-normalized response ($response_{Tref}$), as shown in Equation 2.

$$response_{Tref} = response_{Tmeas} e^{k_2 (Tref - Tmeas)} \quad (2)$$

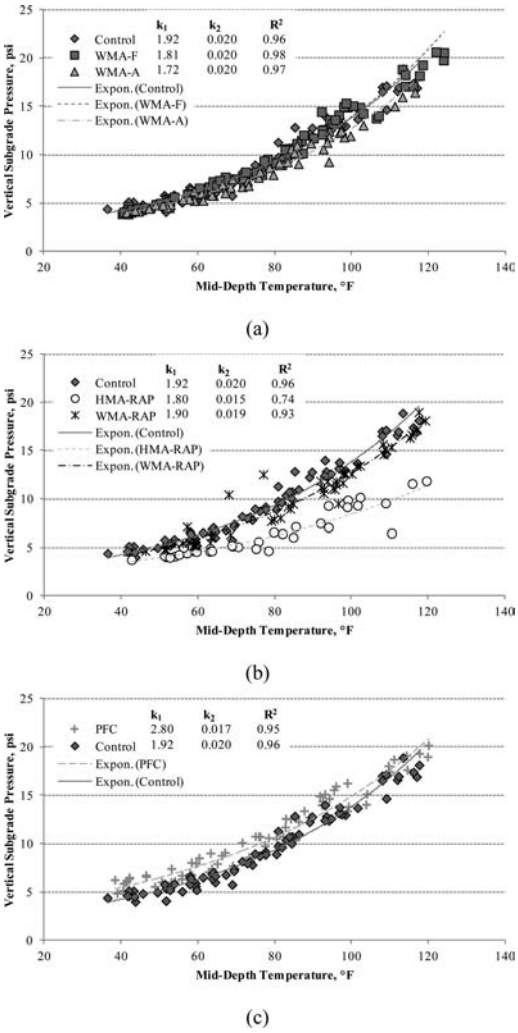

Figure 4. Subgrade pressure versus temperature for a) control vs. WMA, b) control vs, high RAP and c) control vs PFC.

where $response_{Tref}$ = normalized response (microstrain or subgrade pressure (psi)) at reference temperature T_{ref}; $reponse_{Tmeas}$ = measured response (microstrain or subgrade pressure (psi)) at temperature T_{meas}; T_{ref} = mid-depth reference temperature (°F); T_{meas} = measured mid-depth temperature at time of test (°F); and k_2 = section-specific regression coefficient from Figures 3 and 4.

Because pressures are also dependent on the thickness of the pavement layers, it was necessary to apply a correction to account for slight differences in as-built pavement thickness. The correction factors were obtained based on theoretical relationships between layer thickness and longitudinal strain or vertical pressure from layer elastic analysis. Each section was modeled using the software *WESLEA*; the layer moduli were backcalculated from FWD testing and the thicknesses were varied in half-inch increments

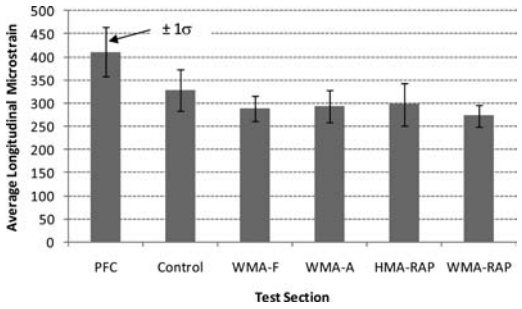

Figure 5. Average longitudinal microstrain at 68°F.

from 5.5 to 8 in. for the AC layer and from 3 to 7.5 in. for the aggregate base layer. The pavement responses were plotted against AC and aggregate base thickness and the data series were fitted using a power function as shown in Equation 3.

$$response = aH^b \tag{3}$$

where response = microstrain or subgrade pressure (psi); H = AC or aggregate base thickness (in); and a, b = regression coefficients.

The correction factor was found by dividing the right hand side of Equation 3 with reference thickness (H_{ref}) by the same term with measured thickness (H_{meas}).

$$CF = \frac{H_{ref}^b}{H_{meas}^b} \tag{4}$$

where H_{ref} = reference thickness (7 in for AC, 6 in for aggregate base); H_{meas} = as-built thickness measured at the center of the gauge array (in); and b = section-specific regression coefficient.

Although differences during construction were subtle, this correction allowed for a more fair comparison of the test sections. Figures 5 and 6 illustrate the average temperature-normalized and thickness-corrected longitudinal strain and subgrade pressure, respectively. A Tukey's post ANOVA test was performed to compare the different sections. At 95% confidence level, the strain of the PFC section was significantly higher than the control. Conversely, the strain of the WMA and high RAP sections was significantly lower than the control.

For subgrade pressure, the PFC section was also significantly higher than the control. All other sections, with the exception of WMA-F were lower than the control. It should be noted that while the HMA-RAP section exhibited the lowest pressure, the use of the WMA technology increased the vertical stress in section WMA-RAP at a level comparable to the virgin mixtures.

Theoretically, a plot of temperature normalized responses over time should resemble a flat line. Although the asphalt concrete is expected to become stiffer over time and respond differently under load,

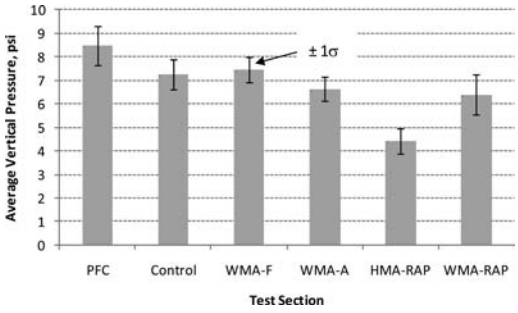

Figure 6. Average subgrade pressure at 68°F.

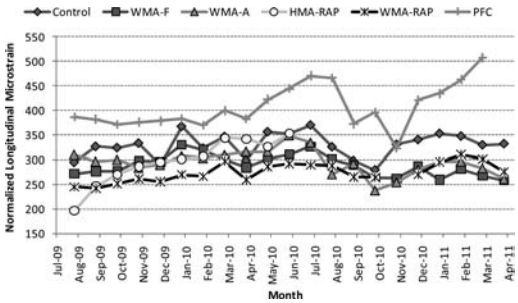

Figure 7. Average monthly normalized microstrains.

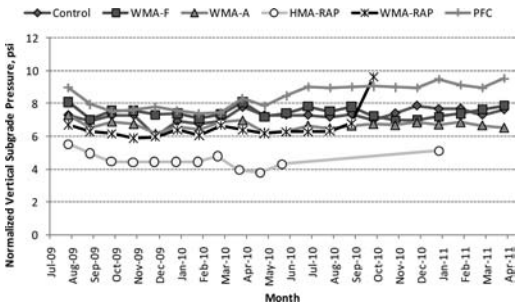

Figure 8. Average monthly normalized subgrade pressures.

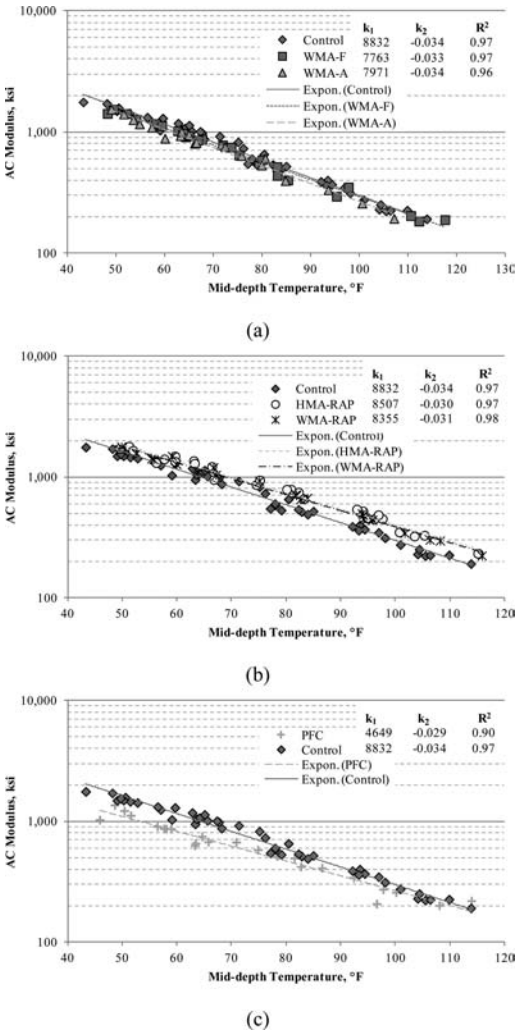

Figure 9. Backcalculated AC modulus versus temperature for a) control vs. WMA, b) control vs, high RAP and c) control vs PFC.

large variations from the average in the short term may be an indication of damage in the pavement structure. Figures 7 and 8 plot the monthly averages for normalized strain and subgrade pressure, respectively. Most sections exhibited low variability over time. The PFC started showing erratic responses in the early spring of 2010, which may suggest that its structural capacity was reduced. The HMA-RAP section had increasing microstrain over time, but relatively stable vertical pressures. It is possible that this trend could be related to the lower correlations found between responses and temperature compared to the other sections. In the WMA-RAP section, there was an abrupt increase in subgrade pressure in the last recorded data. After that point, it was not possible to obtain additional measurements, and the high pressure was likely due to equipment malfunction and not pavement failure.

5.2 *Backcalculated AC modulus*

The backcalculated AC modulus obtained from FWD testing was also dependent on pavement mid-depth temperature and followed a function similar to the one shown in Equation 1. The moduli of each section and the regression coefficients are shown in Figure 9. Hypothesis tests performed on the intercepts (k_1) and slopes (k_2) indicated that only the PFC and WMA-F sections had intercepts lower than the control, while the PFC section and the high RAP sections (HMA-RAP and WMA-RAP) had slopes higher than the control. This means that in general the modulus of the PFC section was lower than the control, which was expected because PFCs contain very little mastic (binder and fine aggregate) to stiffen the mix; most of the stiffness comes from stone-on-stone contact of the coarse aggregate. This is consistent with the trends observed

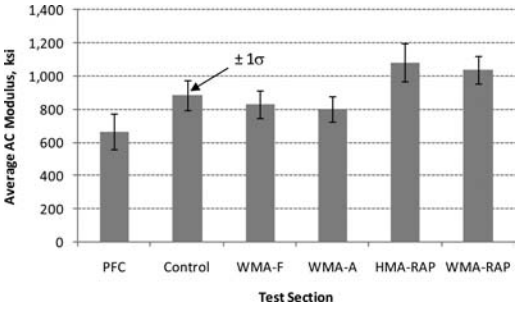

Figure 10. Average AC modulus at 68°F.

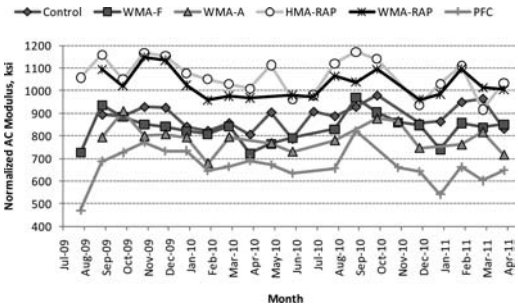

Figure 11. Average monthly normalized AC moduli.

for the pavement responses, where strain and pressure were higher than the control.

On the other hand, the high RAP sections had higher moduli at all temperatures due to the presence of stiffer aged binder. The moduli of these sections were less susceptible to changes in temperature than the control, a trend also observed for strain and pressure. The WMA-F section exhibited slightly lower modulus at low temperatures but was comparable to the control at higher temperatures.

Figure 10 shows the average temperature-normalized moduli for all test sections. Results were normalized to 68°F using the same procedure applied for strain and pressure. Statistical testing indicated that there were significant differences among all sections. However, from a practical perspective, it can be observed that the differences between the control and WMA sections were under 100 ksi, making them comparable. Similarly, the difference between the high RAP sections is relatively small. Therefore, although statistical differences exist among the sections, for practical purposes the sections can be divided into three groups: PFC, control and WMA sections, and high RAP sections.

The temperature normalized moduli over time plotted in Figure 11 show the same general trends observed in Figure 10. The PFC section had higher variability over time, which was also observed for strain and pressure. The HMA-RAP section also exhibited erratic results, particularly in the second half of the analysis period. High variability in this section was also noted in the dynamic pavement responses and its cause is not clear at this point in the experiment. Further analysis

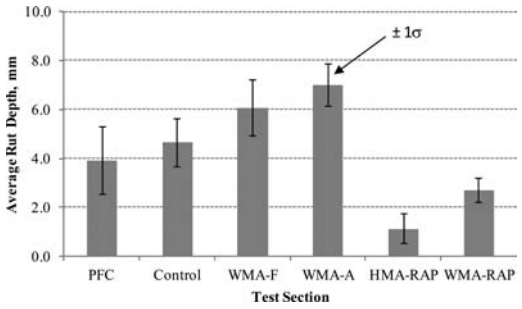

Figure 12. Average rut depths as of 4/25/2011.

will be performed in the forensic stage of the research cycle to address this issue.

6 PERFORMANCE

All sections were tested regularly to assess pavement performance. Field performance evaluations focused on the middle 150 ft. of each 200-ft. test section to eliminate the effects of transitions near section ends. Field rut depths were measured approximately monthly on each of the sections using the Alabama Department of Transportation (ALDOT) method, which uses a 4-ft-long level with a dial gauge. Readings were taken in each wheel path along three predetermined random locations within each section and the averages were computed. Sections were also manually inspected for cracking on a weekly basis and crack maps were developed to determine the extent and to monitor the progression of cracking.

Figure 12 shows the average rut depths as of April 25, 2011, when nearly 8 million ESALs had been applied. Tukey comparisons at 95% confidence level indicated that there was no statistical difference between the virgin WMA sections (WMA-F and WMA-A) and that these sections had higher rut depths than the control. Conversely, the two high RAP sections (HMA-RAP and WMA-RAP) did not exhibit significant differences and had the least rutting. The PFC section was statistically similar to the control section. Overall, the results were as expected because the WMA-F section exhibited higher pressures than the control while the high RAP mixes had lower pressures and higher moduli. Although the WMA-A section had lower pressures than the control, it had relatively higher permanent deformation. This could be due to accumulated damage in the AC layer that had not yet manifested as cracking. Further monitoring and forensic analysis will be required to determine the cause. The PFC section had higher subgrade pressures than the control, but its aggregate structure, which relies on stone-on-stone contact, allows the mixture to withstand traffic loads without experiencing significant permanent deformation. It is important to note that all sections have performed very well, with rut depths less than 10 mm.

As of April 25, 2011, the cut-off date for this research, cracking had not been observed in any of

the sections. Although the PFC section showed erratic behavior over time, it did not show signs of surface cracking. Further monitoring and forensic evaluation will be required to determine if any damage had occurred deeper in the pavement structure.

7 CONCLUSIONS

This study evaluated the structural responses of sustainable pavement sections under traffic loads and their short-term performance in terms of rutting and cracking. The following conclusions were reached:

- The use of sustainable pavement technologies appeared to have an effect on pavement properties. In general, WMA sections and sections containing high RAP percentages had strains and pressures lower than the control. The PFC section had higher strains and pressures than the control.
- Although statistical differences existed among the AC moduli of the sections, from a practical perspective sections were divided into three groups: PFC (with the lowest modulus), control and WMA sections, and high RAP sections (with the highest moduli). The modulus versus time relationship of each section was consistent with the trends observed for strain and pressure versus time.
- The use of WMA technologies appeared to increase rutting susceptibility of the mixtures. The PFC and high RAP sections exhibited less rutting than the control. However, after 20 months of operation and nearly 8 million applied ESALs, all sections had performed very well, with rut depths less than 10 mm. No cracking had been observed.
- Based on temperature normalized results over time, it is possible that the PFC section had experienced some damage that was not yet visible in the pavement surface. The high variability observed in the high RAP sections could be related to instrumentation problems. Further monitoring and forensic evaluation will be conducted at the end of the research cycle.

ACKNOWLEDGEMENTS

The authors wish to thank the following state departments of transportation for their continued cooperation and support of this research: Alabama, Florida, North Carolina, Oklahoma, and Tennessee. The Federal Highway Administration also deserves special recognition for their support and cooperation.

REFERENCES

Anderson, R.M., Baumgardner, G., May, R. and Reinke, G. 2008. *Engineering Properties, Emissions, and Field Performance of Warm Mix Asphalt Technologies*. NCHRP 9-47 Interim Report, Transportation Research Board of the National Academies.

Asphalt Paving Association of Iowa (APAI) 2008. *The Iowa Asphalt Report, The Green Issue*.

Barrett, M. 2006. *Stormwater Quality Benefits of a Porous Asphalt Overlay. Center for Transportation Research*. Report No. FHWA/TX-07/0-4605-2, Austin, Texas.

Berbee, R., Rijs, G., de Brouwer, R. and van Velzen, L. 1999. *Characterization and Treatment of Runoff from Highways in the Netherlands Paved with Impervious and Pervious Asphalt*. Water Environment Research, 71(2).

Chappat, M. 2003. *The Environmental Road of the Future: Life Cycle Analysis*. Colas Group.

Copeland, A. 2011. *Reclaimed Asphalt Pavement in Asphalt Mixtures: State of the Practice*. Report No. FHWA-HRT-11-021, Federal Highway Administration, McLean, Virginia.

D'Angelo, Harm, J., Bartoszek, E., Baumgardner, J., Corrigan, G.M., Cowsert, J., Harman, T., Jamshidi, M., Jones, W., Newcomb, D., Prowell, B., Sines, R. and Yeaton, B. 2007. *Warm-Mix Asphalt: European Practice*. International Technology Scanning Program, Federal Highway Administration.

Devore, J.L. 2000. *Probability and Statistics for Engineering and the Sciences*. Duxbury Thomson Learning, California.

FHWA. 2008. *User Guidelines for By-product and Secondary Use Materials in Pavement Construction*. FHWA Publication FHWA-RD-97-148, Federal Highway Administration, Washington DC.

Haddock, J.E., Hand, A.J. and Fang, H. 2002. *Contributions of Pavement Structural Layers to Rutting of Hot Mix Asphalt Pavements*. NCHRP Report 468, National Academy Press, Washington D.C.

Kandhal, P. 2002. *Design, Construction, and Maintenance of Open-Graded Asphalt Friction Courses*. Information Series 115. National Asphalt Pavement Association, Lanham, MD.

Newcomb, D. 2006. *An Introduction to Warm Mix Asphalt*. National Asphalt Pavement Association.

Poulikakos, L., Takahashi, S. and Partl, M. 2003. *A Comparison of Swiss and Japanese Porous Asphalt through Various Mechanical Tests*. Presented at the 3rd Swiss Transport Research Conference, Monte Verità/Ascona.

Priest, A.L. and Timm, D.H. 2006. *Methodology and Calibration of Fatigue Transfer Functions for Mechanistic-Empirical Flexible Pavement Design*. NCAT Report 06-03, National Center for Asphalt Technology, Auburn University.

Roberts, F.L., Kandhal, P.S., Brown, E.R., Lee, D.Y. and Kennedy, T.W. 1996. *Hot Mix Asphalt Materials, Mixture Design, and Construction*. NAPA Education Foundation, Lanham, MD, Second Edition.

Smit, A.d.F. and Waller, B. 2007. *Sound Pressure and Intensity Evaluations of Low Noise Pavement Structures with Open Graded Asphalt Mixtures*. NCAT Report 07-02, National Center for Asphalt Technology, Auburn University.

Timm, D.H. and Priest, A.L. 2008. *Flexible Pavement Fatigue Cracking and Measured Strain Response at the NCAT Test Track*. Paper No. 08-0256 Presented at the 87th Transportation Research Board Annual Meeting, Washington D. C.

Timm, D.H. 2009. *Design, Construction and Instrumentation of the 2006 Test Track Structural Study*. NCAT Report 09-01, National Center for Asphalt Technology, Auburn University.

Willis, J.R. and Timm, D.H. 2009. *Field-Based Strain Thresholds for Flexible Perpetual Pavement Design*. NCAT Report No. 09-09, National Center for Asphalt Technology, Auburn University.

Advances in Pavement Design through Full-scale Accelerated Pavement Testing – Jones, Harvey, Mateos & Al-Qadi (Eds.)
© 2012 Taylor & Francis Group, London, ISBN 978-0-415-62138-0

Evaluation of a rubber modified asphalt mixture at the 2009 NCAT test track

J.R. Willis, R.B. Powell & M.C. Rodezno
National Center for Asphalt Technology, Auburn, Alabama, US

ABSTRACT: While some state agencies look at using recycled products in asphalt mixtures as a means to become more environmentally-friendly, other states and contractors are investigating materials like Ground Tire Rubber (GTR) as a substitute for polymer modification in asphalt binders. The Missouri Department of Transportation recently built two test sections at the National Center for Asphalt Technology (NCAT) Pavement Test Track to validate the use of GTR as a substitute for Styrene-Butadiene-Styrene (SBS) in asphalt mixtures. The Test Track sections were monitored weekly over a two year period for field performance including rutting, smoothness, and texture using an inertial profiler. Monthly crack maps were also developed to assess mixture cracking. Additionally, each mixture was sampled for laboratory characterization in terms of stiffness, rutting, cracking, and moisture susceptibility using standard laboratory procedures. Based on the gathered data, GTR mixtures can be used as an adequate polymer substitute without sacrificing asphalt mixture performance.

1 INTRODUCTION

The utilization of scrap tire rubber in asphalt started in the mid-1960s when ground rubber was placed in asphalt surface treatments, such as chip seal applications. Later on, in the 1970's, ground tire rubber (GTR) asphalt chip seals were used as a stress absorbing membrane interlayer (SAMI). Its use extended to hot mix asphalt (HMA) and has continued to evolve due to the rubber's enhancement of mixture performance including improved rutting resistance, thermal reflectivity, and resistance to fatigue cracking. Other benefits reported include reduction in maintenance, improved ride, good skid resistance, and noise reduction (Kaloush et al., 2002; Huang et al., 2002; Way, 2000).

In terms of environmental issues, the disposal of scrap tires is a major waste management concern due to used tires being placed in scrap tire piles. Additionally, some studies have shown that the addition of GTR does not contribute significantly to any increase in undesirable compounds such as carbon dioxide (CO_2) emissions (Gunkel, 1994). Arizona, California, Florida, and Texas have successfully developed and specified the most rubberized asphalt products. It was reported that together, these states reused over 35.6 million tires in asphalt paving applications from 1995 to 2001 (RPA, 2002).

When GTR asphalt mixtures are evaluated, it is important to distinguish between the different processes and applications that are currently used. The processes of applying GTR in asphalt mixtures can be divided into two broad categories, a dry process or a wet process. In the dry process, crumb rubber is blended with the aggregate before the asphalt binder is added into the mix. The crumb rubber particles in this process are generally coarser than those in the wet process and are considered as part of the aggregate gradation (Huang, 2002). In the wet process, the GTR is blended with the asphalt binder and is then mixed with the aggregate. When asphalt cement and crumb rubber is blended together, the crumb rubber swells and softens. Some of the factors that influence this reaction include blending temperature, the reaction time, the type and amount of mechanical mixing, the size and texture of the crumb rubber and the aromatic component of the asphalt cement (TFHRC, 2005). In general, crumb rubber is added to an asphalt binder to improve the binder properties by reducing the binder's temperature susceptibility. In the United States, the addition of GTR is typically conducted using the asphalt rubber-wet process.

While environmental stewardship is important, some state agencies and contractors are investigating GTR asphalt mixtures as a substitute for using polymers in asphalt mixtures such as styrene-butadiene-styrene (SBS). If GTR mixtures can perform equivalently to polymer modified mixtures, state agencies and contractors will have additional tools they can use to develop, produce, and construct more cost-effective, environmentally friendly asphalt pavements.

1.1 *Objective and scope*

The objective of this research was to determine if GTR asphalt could adequately replace SBS in dense-graded mixtures without sacrificing mixture performance. To

accomplish this objective, an asphalt mixture containing 11% 30–40 mesh rubber and an SBS-modified asphalt mixture were placed on the National Center for Asphalt Technology (NCAT) Test Track. The field performance of these two mixtures was monitored using visual observations and inertial profilers for 10 million equivalent single axle loads (ESALs) to determine if there was any overall difference in mixture rutting, cracking, texture, and smoothness. Additionally, mix was sampled during construction and taken to the NCAT laboratories where standard asphalt mixture performance tests were used to characterize the mixtures in terms of rutting, cracking, moisture damage, and stiffness.

2 TEST FACILITY

The NCAT Test Track is a 1.7 mile closed loop full-scale accelerated loading facility located near Opelika, Alabama. During each two and a half year research cycle, test sections are trafficked with approximately 10 million equivalent single axle loads (ESALs) using a fleet of triple-trailer vehicles. In addition to the field performance measurements, a complete laboratory characterization of the binders and mixtures is conducted to validate field performance with laboratory test results.

3 MATERIALS

In 2009, the Missouri Department of Transportation built two test sections at the NCAT Pavement Test Track to determine if GTR would be an adequate substitute for SBS in asphalt mixtures. These two test sections were constructed on perpetual foundations to ensure the distresses (whether they be cracking or rutting) were indicative of the surface mixture's performance and not the subgrade or base material. All perpetual sections included a minimum of 23 in. of asphalt materials (Brown et al., 2002).

The subgrade for the experiment was an improved roadbed material, also documented as track soil, taken from rock formations in the west curve of the Test Track and compacted to 95% of Proctor maximum density. A densely crushed granite base layer was built in a 6 in. lift above the track soil. The final layer separating the unbound materials from the bound materials was a non-woven geotextile fabric. This layer was designed to allow the flow of water through the layer, but not allow fines to pump to the surface or through the pavement layers (Brown et al, 2002).

The first mixture was a 12.5 mm nominal maximum aggregate size (NMAS), 2.5 percent SBS-modified dense-graded Superpave mixture designed at 100 gyrations. The mixture was placed on the perpetual buildup. The second mixture used a similar aggregate skeleton and compactive effort; however, instead of modifying the asphalt with polymer, a PG 67-22 asphalt binder was modified with a terminally blended 11% rubber binder to bump the high temperature grade. The rubber was −40 mesh material. Both mixtures were constructed 1.75 in. thick at 93 percent density. Quality control gradations and volumetrics for both mixtures are given in Table 1.

Table 1. Test Track materials.

Sieve Size	GTR	SBS
Percent Passing – Gradation (%)		
3/4″	100	100
1/2″	97	96
3/8″	89	86
#4	59	55
#8	37	34
#16	22	21
#30	13	13
#50	9	9
#100	7	7
#200	5.6	5.4
Mix Information		
Design Gyrations	100	100
Virgin Binder Grade	67-22	76-22
Binder Additive	GTR	SBS
Binder Content (%)	6.0	5.4
Effective Binder Content (%)	5.1	4.5
Voids in Mineral Aggregate (%)	15.0	14.8
Air Voids (%)	3.3	4.5
Dust Proportion	1.1	1.2

The primary difference between the two mixtures is the asphalt content. The GTR modified asphalt mixture had an additional 0.6 percent asphalt in the mixture. This reduced the mixture's air voids to 3.3 percent.

3.1 *Laboratory characterization*

While field validation is the ultimate proof of mixture performance, laboratory characterization is used to predict pavement distresses in the field once the mixture has been subjected to trafficking. The two binders used in this study were graded using the Superpave performance grade (PG) specification. The mixtures were tested for resistance to moisture damage, cracking, and permanent deformation. In addition to assessing the mixtures' susceptibility to these distresses and the stiffness of the material was determined using a dynamic modulus protocol.

3.2 *Binder properties*

Binders in the asphalt mixtures were sampled from the tank at the plant and then tested in the NCAT binder laboratory to determine the performance grade (PG) in accordance with AASHTO M 320-10.

Table 2 summarizes the true grade and performance grade of each binder. The results confirmed that all the binders used in the construction of the two sections were PG 76-22 binders as requested by the Missouri Department of Transportation.

Table 2. Grading of binders.

Mix	True Grade	Performance Grade
GTR	81.7 – 25.0	76 – 22
SBS	76.6 – 26.3	76 – 22

Table 3. Average TSR results.

Mix	Conditioned Tensile Strength (psi)	Unconditioned Tensile Strength (psi)	Tensile Strength Ratio
SBS	148.1	171.4	0.86
GTR	203.3	220.0	0.92

While both binders were classified using the PG system as PG 76-22 binders, there was a 5.1°C difference in the high temperature true grade of the binders. While this difference was a result of the binder being engineered to meet the elastic recovery specification for Missouri, the GTR binder is expected to be stiffer at hotter temperatures and thus more resistant to rutting.

3.3 *Moisture susceptibility*

Moisture susceptibility testing was performed in accordance with AASHTO T 283-07. Six specimens of each mix were compacted to a height of 95 mm and an air void level of 7 ± 0.5 percent. The conditioned specimens were vacuum saturated to the point at which 70 to 80 percent of the internal voids were filled with water. These samples then underwent a freeze-thaw cycle as specified in AASHTO T 283-07.

The indirect tensile strength was determined using a Pine Instruments Marshall Stability press which loads the sample at a rate of 2 in./min. AASHTO M323-07 recommends a tensile strength ratio (TSR) value of 0.8 and above for moisture resistant mixes.

Table 3 provides the average conditioned tensile strength, average unconditioned tensile strength, and tensile-strength ratio for each mixture. While the GTR mixture had a higher TSR value, the TSR values for both mixtures exceeded the criterion of 0.80 suggesting the mixtures should be resistant to moisture damage.

Two-sample t-tests ($\alpha = 0.05$) were conducted to compare the tensile strengths of the two mixtures in both the conditioned and unconditioned states. The GTR mixture was statistically stronger in indirect tension at room temperature than the SBS mixture in both the conditioned ($p = 0.001$) and unconditioned ($p = 0.006$) states.

3.4 *Dynamic modulus*

Dynamic modulus testing was performed to assess the stiffness of both the SBS and GTR mixtures. Samples for this testing were prepared in accordance with AASHTO PP 60-09. The target air void level for the test samples is not specified in this method; however, the samples were prepared at $7 \pm 0.5\%$ air voids. This air void level was selected as a common target air void level for pavements compacted in the field. Three samples from each mix were prepared for testing to collect sufficient data to construct the dynamic modulus master curve.

Table 4. Temperatures and frequencies used for dynamic modulus testing.

Test Temperature (°C)	Loading Frequencies (Hz)
4.0	10, 1, 0.1
20.0	10, 1, 0.1
40 or 45	10, 1, 0.1, 0.01

Testing was performed in an IPC Global Asphalt Mixture Performance Tester (AMPT). Dynamic modulus testing was performed to quantify the stiffness behavior of the asphalt mixture over a wide range of testing temperatures and frequencies. The temperatures and frequencies used for the Test Track mixes were those recommended by AASHTO PP 61-09. For this methodology, the high test temperature was dependent on the high PG grade of the base binder in the mixture. Table 4 shows the general outline of temperatures and frequencies used. Since both binders graded as PG 76 binders, the mixtures were tested with a high test temperature of 45°C.

Dynamic modulus testing was performed in accordance with AASHTO TP 79-09. This testing was performed unconfined. Test data were screened for data quality in accordance with the limits set in AASHTO TP 79-09. Variability of dynamic modulus values at specific temperatures and frequencies were checked to have a coefficient of variation (COV) at or below 13%. All data were also checked for reasonableness (reduction in moduli with increasing temperature or slower loading).

The data were then analyzed for two specific purposes. First, the data were used to generate a master curve for each individual mix per the methodology in AASHTO PP 61-09. The master curve uses the principle of time-temperature superposition to shift data at multiple temperatures and frequencies to a reference temperature so that the stiffness data can be viewed without temperature as a variable. This method of analysis allows for visual relative comparisons to be made between multiple mixes.

Figure 1 shows the unconfined master curves of the two mixtures. The mixture performance at the low temperature high frequency (right side) portion of the master curve shows equivalent mixture stiffness. At the intermediate temperatures, there is some slight deviation between the stiffnesses of the mixtures (middle of the curves). However, more separation in the master curves is noticed at the high temperature low frequency portion of the curve. An ANOVA analysis

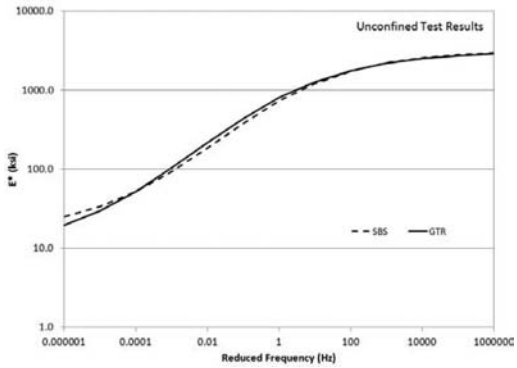

Figure 1. Dynamic modulus master curves.

($\alpha = 0.05$) conducted on the data showed that while temperature ($p = 0.000$) and frequency ($p = 0.000$) were significant in determining mixture stiffness, using GTR instead of SBS did not statistically alter the stiffness of the material ($p = 0.446$).

It should be noted that stiffness alone does not quantify mixture performance. Dynamic modulus data should be coupled with pavement performance equations and/or performance tests to fully validate how the mixture will perform in the field.

3.5 *Rutting*

To characterize the rutting susceptibility of the mixtures in this study, the two mixtures were tested using loaded wheel testers and a repeated loading test.

3.5.1 *Asphalt Pavement Analyzer (APA)*

The rutting susceptibility of the GTR and SBS mixtures were evaluated using the APA. Only surface mixtures are evaluated using the APA. Testing was performed in accordance with AASHTO TP 63-09. The samples were prepared to a height of 75 mm and an air void level of 7 ± 0.5 percent. Six replicates were tested for each mix. The samples were tested at a temperature of 64°C (the 98 percent reliability temperature for the high PG grade of the binder). Typically, these samples are tested at the high binder PG grade. However, for the Test Track, a constant testing temperature for all mixes was desired to facilitate relative comparisons between the mixes. The samples were loaded with a steel wheel (loaded to 100 lbs) resting atop a pneumatic hose pressurized to 100 psi for 8,000 cycles. Manual depth readings were taken at two locations on each sample after 25 loading cycles and at the conclusion of testing to determine the sample rut depth (Table 5).

A statistical two-sample *t*-test of the rut depths from the six samples ($\alpha = 0.05$) was unable to distinguish any difference between the rut depths measured in the GTR and SBS mixtures.

The APA test results are also appropriate for determining a rate of secondary rutting for each mixture. Rutting typically occurs in three stages: primary, secondary, and tertiary. The confined state provided by the molds prevents the mixture from truly ever achieving tertiary flow. Therefore, once the mixture has overcome the stresses induced during primary consolidation, it is possible to determine the rate at which secondary rutting occurs.

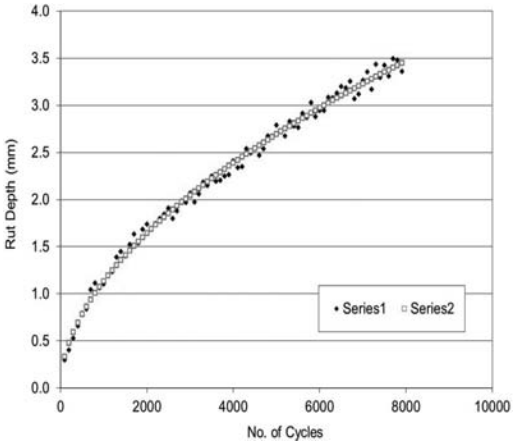

Figure 2. Example rate of rutting plot for two samples in center mold.

Table 5. APA test results.

Mix	Average Rut Depth (mm)	Coefficient of Variation (%)	Rate of Rutting (mm/cycle)
SBS	1.41	24.3	0.0000516
GTR	1.37	17.5	0.0000568

The secondary rate of rutting was calculated in the APA by fitting a power function to the rut depths automatically measured for two samples from the left, right and center molds of the APA during testing (Figure 2). These three average rates were then used to calculate a singular rate of rutting for each mixture. The primary consolidation of a sample can be seen as the initial steep line when comparing rut depth to the number of cycles; however, as the slope of the line decreases, the samples move into secondary consolidation. The rate of rutting was determined by finding the slope of the power function at the 8,000th loading repetition. The results of this analysis are given in Table 5.

While the GTR mixture had a numerically smaller rut depth, the rate of rutting was slightly higher than that of the SBS mixture. This suggests that the GTR mixture will perform better under initial consolidation; however, it accrued rutting faster than the SBS mixture. Overall, the differences between the SBS mixture and GTR mixture were small and it is not expected the difference would contribute significantly in terms of field performance.

3.5.2 *Flow number (F_n)*

The determination of the F_n for the mixtures was performed using the AMPT. Testing was performed using

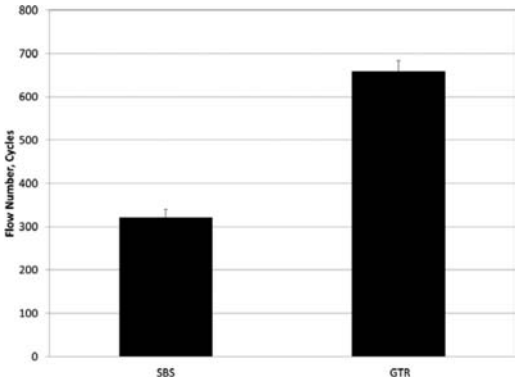

Figure 3. Flow number test results.

three new specimens for each of the surface courses of the two test sections. F_n tests were conducted at a temperature of 59.5°C which is the *LTPPBind* 3.1 50% reliability temperature for the Test Track location at 20 mm from the surface of the pavement based on recommendations from NCHRP Report 673 (Advanced Asphalt Technologies, 2011). The specimens were tested at a deviator stress of 87 psi without confinement. The tests were terminated when the samples reached 10 percent axial strain. For the determination of tertiary flow, the Francken model (Biligiri et al., 2007) was used (Equation 1). Non-linear regression analysis was used to fit the model to the test data.

$$\varepsilon_p(N) = aN^b + \langle c(e)^{dN} - 1 \rangle \quad (1)$$

where $\varepsilon_p(N)$ = permanent strain at 'N' cycles; N = number of cycles; and a, b, c, d = regression coefficients.

The average flow number for both the SBS and GTR mixtures are given in Figure 3 with error bars signifying ±1 standard deviation. Numerically, the GTR mixture was able to withstand over twice as many repeated loads as the SBS mixture before reaching tertiary flow. A two-sample *t*-test ($\alpha = 0.05$) confirmed statistically the GTR mixture had superior resistance to permanent deformation ($p = 0.028$) using the flow number test.

3.5.3 *Summary*

While the APA test results suggest the two mixtures have overall equivalent resistance to permanent deformation, the flow number test suggests the GTR mixture is more resistant to rutting. The difference in the true high temperature grade of the binder suggests the flow number ranking is correct. In either case, the objective of the research was met. Both rutting tests showed the GTR and SBS mixtures would have at least equivalent rutting resistance.

3.6 *Low temperature cracking*

The critical cracking temperature where the estimated thermal stress exceeds the tested indirect tensile strength of a mixture can be used to characterize the low temperature cracking performance of asphalt mixtures. This type of analysis could be referred to as a 'critical temperature analysis.' A mixture exhibiting a lower critical cracking temperature than those of the other mixtures would have better resistance to thermal cracking. Both the SBS and GTR mixtures were evaluated using a critical temperature analysis for this study. To estimate the thermal stress and measure the tensile strength at failure, the indirect tensile creep compliance and strength tests were conducted for three replicates of each mix as specified in AASHTO T 322-07. A thermal coefficient of each mixture was estimated based on its volumetric properties and typical values for the thermal coefficient of asphalt and aggregate. This computation is explained in more detail below.

The IDT system, which has been used to predict thermal stress development and low temperature cracking in asphalt mixtures, was used to collect the necessary data for the critical cracking temperature analysis. The testing was conducted using an MTS load frame equipped with an environmental chamber capable of maintaining the low temperatures required for this test. Creep compliance at 0°C, −10°C, and −20°C and tensile strength at −10°C in accordance with AASHTO T 322-07 were measured. These temperatures are specified as a function of the low temperature PG grade of the binder in AASHTO T322-07. The creep test applies a constant load to the asphalt specimen for 100 seconds while the horizontal and vertical strains are measured on each face of the specimen using on-specimen instrumentation.

Four samples were prepared for each mix. The first sample was used to find a suitable creep load for that particular mix at each testing temperature. The remaining three samples were tested at this load for the tested data set. Specimens used for the creep and strength tests were 38 mm to 50 mm thick and 150 mm in diameter. Samples were prepared to 7 ± 0.5% air void content.

Theoretical and experimental results indicate that for linear visco-elastic materials, the effect of time and temperature can be combined into a single parameter through the use of the time-temperature superposition principle. The creep compliance mastercurve can be generated from an appropriate set of creep compliance tests under different temperature levels by shifting the creep compliance data to a curve based on a reference temperature. This reference temperature is typically the lowest creep compliance test temperature (−20°C for this study). The relations between real time t, reduced time ξ, and a shifting factor a_T are given as Equation 2.

$$\xi = t/a_T \quad (2)$$

An automated procedure to generate the mastercurve was developed as part of the Strategic Highway Research Program (SHRP) (Buttlar et al., 1998). The system requires the measurement of creep compliance test data at three different test temperatures. The final products of the system are a generalized

Table 6. IDT critical temperature analysis.

Mix	Average Strength (MPa)	Failure Time (hours)	Critical temperature (°C)
GTR	4.67	4.6	−25.0
SBS	4.39	4.5	−24.4

Maxwell model (or Prony series), which is several Maxwell elements connected in parallel, and temperature shifting factors. The generalized Maxwell model and shifting factors are used for predicting thermal stress development of the asphalt mixture due to change in temperature.

In addition to thermo-mechanical properties, it is required to estimate the thermal coefficient of the asphalt mixture for the critical temperature analysis. The linear thermal coefficients, α, of the given asphalt mixtures were estimated in Equation 3 (Jones et.al., 1968).

$$a_{mix} = \frac{(VMA \times B_{AC} + V_{AGG} \times B_{AGG})}{(3V_{TOTAL})} \quad (3)$$

where α_{MIX} = linear coefficient of thermal contraction of the asphalt mixture (1/°C); B_{AC} = volumetric coefficient of thermal contraction of the asphalt cement in the solid state (3.45×10^{-4}/°C) (11); B_{AGG} = volumetric coefficient of thermal contraction of the aggregate (1×10^{-6}/°C), VMA = percent volume of voids in the mineral aggregate; V_{AGG} = percent volume of aggregate in the mixture; and V_{TOTAL} = 100 percent.

Based on the above parameters, the change in thermal stress for each mixture was estimated at the cooling rate of 10°C per hour starting at 20°C. The finite difference solution below developed by Soules et al. (1987) was used to estimate thermal stress development based on the Prony Series coefficients.

A complete description of the thermal stress analysis can be found in Hiltunen and Roque (1994) and Kim et al. (2008).

Table 6 shows the average strength, failure time, and critical temperature of both the GTR and SBS mixtures. The GTR mixture performed either equivalently or better than the SBS mixture in terms of having a higher strength, slightly longer time until failure, and lower critical temperature. It should be noted that both critical temperatures are well below the required -16°C for the region of testing. Therefore, both mixtures should adequately resist low temperature cracking.

3.7 *Surface cracking*

The energy ratio has been developed to assess a mixture's resistance to top-down or surface cracking (Roque et al., 2004). To determine this mixture property, three specimens, 150 mm diameter by approximately 38 mm to 50 mm. thick, cut from gyratory compacted samples, were prepared, and one set of indirect tension tests including resilient modulus, creep compliance, and tensile strength was performed at 10°C.

To evaluate the top-down cracking performance of a given pavement, tensile stress, σ, obtained at the bottom of the asphalt layer using elastic layer analysis, and mixture properties (resilient modulus, M_r, power function parameters, D_1 and m, tensile strength, St, and dissipated creep strain energy at failure, $DCSE_f$) are required as inputs of the top-down cracking model. Stress was assumed to be 150 psi. In this model, each property can be obtained from the three mixture tests.

The resilient modulus is obtained in a load control mode by applying a repeated haversine waveform load with a loading period of 0.1 seconds followed by a rest period of 0.9 seconds and is determined from the stress-strain curve. The power function parameters are obtained by fitting the creep compliance curve performed using a constant load control mode, and the tensile strength and dissipated creep strain energy at failure are determined from the stress-strain curve developed during strength testing. The detailed testing procedures and data interpretation methods for the resilient modulus, creep compliance, and tensile strength tests are described elsewhere (Roque and Buttlar, 1994; Roque et al., 2004; Buttlar and Roque, 1994; Roque et al., 1997).

Table 7 summarizes the ER data for two mixtures tested in this phase of the research. The values of energy ratio determined would be the indicators of cracking performance of the sections with different binders. Again, the energy ratio is calculated by analyzing multiple test samples to arrive at a singular value. Therefore, statistical analyses could not be completed on these data.

Only slight differences in the energy ratio of the two mixtures were observed in the data analysis. The SBS mixture had a slightly lower ER. This suggests that the GTR mixture would perform slightly better that the SBS in terms of surface cracking.

Current recommendations suggest that a minimum ER of 1.95 is needed if trafficking is less than one million ESALs per year (Roque et al., 2004). While the Test Track trafficking is higher than this requirement, both mixtures were more than twice the required ER.

4 FIELD PERFORMANCE

The field performance of mixtures placed at the NCAT Test Track is routinely assessed. An inertial profiler is used to measure rutting and pavement smoothness, and texture on a weekly basis. Monthly crack maps of the sections are drawn to assess the cracking potential of the mixture.

After 10 million ESALs of trafficking, neither mixture has shown signs of cracking. Wireline rut depths were measured for the SBS and GTR sections of 4.8 and 3.8 mm, respectively. Thus, neither mixture has

Table 7. Energy Ratio Test Results.

Property	Mix	
	GTR	SBS
m-value	0.408	0.410
D_1(E-07)	5.50	6.51
S_t (MPa)	2.71	2.37
M_r (GPa)	10.69	10.34
FE (kJ/m^3)	4.1	5.1
$DSCE_{HMA}$ (kJ/m^3)	3.76	4.83
Stress (psi)	150	150
A (E-08)	4.50	4.68
$DSCE_{MIN}$ (jK/m^3)	0.85	0.97
ER	4.96	4.43

shown signs of significant rutting in the field. Additionally, both mixtures have maintained texture near or below 0.5 mm for the entire 10 million ESALs. Therefore, raveling is not considered to be a problem with either mixture at this point in this phase of trafficking.

The primary difference between these two test sections is roughness. Final international roughness index (IRI) measurements between the two test sections showed the SBS section had an IRI of 103.1 in/mile while the GTR test section had a roughness of 52.3 in/mile. Initially, the SBS section was constructed rougher than the GTR test section. Over time, neither test section has become rougher.

5 CONCLUSIONS AND RECOMMENDATIONS

Based on this research the following conclusions can be drawn about plant-produced rubber-modified asphalt mixtures.

- The addition of GTR and SBS modified PG 6722 binders to PG 7622 binders did not effect the PG grading; however, there was a difference of 5°C in the high temperature true grade of the binders. This difference was engineered to meet Missouri's elastic recovery specification.
- When designed and constructed properly, GTR and SBS mixtures can have equivalent field performance in terms of cracking, rutting, and smoothness.
- The SBS mixture had 0.5 mm more texture than the GTR mixture; however, this was not due to raveling or pavement distresses.
- The GTR and SBS mixtures had equivalent stiffness, moisture damage resistance, and resistance to rutting in the APA. The GTR mixture had a higher flow number than the SBS mixture.
- The GTR mixture had higher tensile strengths than the SBS mixture in both low temperature and moisture damage testing.
- The GTR mixture had a slightly lower critical temperature than the SBS mixture.
- The GTR mixture had a higher energy ratio than the SBS mixture meaning it might be slightly less susceptible to surface cracking. Both mixtures passed the criterion for trafficking of 1,000,000 ESALs per year.

Based on these results, the following recommendations are made.

- State agencies should consider GTR mixtures as an appropriate substitute for SBS modified asphalt mixtures.
- Proper care should be taken during the design and construction phases to ensure the mixtures placed are high quality and meet appropriate quality control standards.

ACKNOWLEDGEMENTS

The authors of this paper would like to thank the Missouri Department of Transportation and OldCastle Materials Group for the support of this work.

REFERENCES

Advanced Asphalt Technologies, LLC. 2011. *A Manual for Design of Hot Mix Asphalt with Commentary*. NCHRP Report 673, National Academies of Sciences, Transportation Research Board.

Biligiri, K.P., Kaloush, K.E., Mamlouk, M.W. and Witczak, M. 2007. Rational Modeling of Tertirary Flow of Asphalt Mixtures. *Transportation Research Record* 2001: 63–72.

Brown, E.R., Cooley, L.A., Hanson, D., Lynn, C., Powell, B., Prowell, B. and Watson, D. 2002. *NCAT Test Track Design, Construction, and Performance*. NCAT 02-12, National Center for Asphalt Technology, Auburn University.

Buttlar, W.G. and Roque, R. 1994. Development and Evaluation of the Strategic Highway Research Program Measurement and Analysis System for Indirect Tensile testing at Low Temperatures. *Transportation Research Record* 1454: 163–171.

Buttlar, W.G., Roque, R. and Reid, B. 1998. Automated Proecdure for Generation of Creep Compliance Master Curve for Asphalt Mixtures. *Transportation Research Record* 1630: 28–36.

Gunkel, K. 1994. *Evaluation of Exhaust Gas Emissions and Worker Exposure from Asphalt Rubber Binders in Hot Mix Asphalt*. Wildwood Environmental Engineering Consultants, Inc., Michigan Department of Transportation.

Hiltunen, D.R. and Roque, R. 1994. A Mechanics-Based Prediction Prediction Model for Thermal Cracking of Asphaltic Concrete Pavements. *Journal of the Association of Asphalt Paving Technologists* 63: 81–117.

Huang, B., Mohamad, L.N, Graves, P.S. and Adabie, C. 2002. Louisiana Experience with Crumb Rubber-Modified Hot-Mix Asphalt Pavement. *Transportation Research Record* 1789: 1–13.

Jones, G.M., Darter, M.I. and Littlefield, G. 1968. Thermal Expansion-Contraction of Asphaltic Concrete. *Journal of the Association of Asphalt Paving Technologists* 37: 56–97.

Kaloush, K.E., Witczak, M.W., Way, G.B., Zbrorowski, A., Abojaradeh, M. and Sotil, A. 2002. *Evaluation of Arizona Asphalt Rubber Mixtures Using Advanced Dynamic*

Material Characterization Tests: Final Report, Arizona State University, Tempe, AZ.

Kim, J. Roque, R. and Birgisson, B. 2008. Integration of Thermal Fraction in the HMA Fracture Model. *Journal of the Association of Asphalt Paving Technologists* 77: 631–662.

Roque, R., Birgisson, B., Drakos, C. and Dietrich, B. 2004. Development and Field Evaluation of Energy-Based Criteria for Top-down Cracking Performance of Hot Mix Asphal. *Journal of the Association of Asphalt Paving Technologists* 2004: 229–260.

Roque, R. and Buttlar, W.G. 1992. The Development of a Measurement and Analysis System to Accurately Determine Asphalt Concrete Properties Using the Indirect Tensile Mode. *Journal of the Association of Asphalt Paving Technologists* 61: 304–332.

Roque, R., Buttlar, W.G., Ruth, B.E., Tia, M., Dickison, S.W. and Reid, B. 1997. *Evaluation of SHRP Indirect Tension Tester to Mitigate Cracking in Asphalt Concrete Pavements and Overlays*. Final Report. Florida Department of Transportation B-9885, University of Florida, Gainesville, Florida.

Rubber Pavement Association. 2002. Air Quality Issues and Best Management Practices with the Production of Asphalt-Rubber Asphalt Concrete. http://www.asphaltrubber.org/ari/Emissions/RPA_Environmental_Issues_With_AR2002.pdf.

Soules, T.F., Busbey, R.F., Rekhson, S.M., Markovsky, A. and Burke, M.A. 1987. Finite-Element Calculation of Stresses in glass Parts Undergoing Viscous Relaxation. *Journal of the American Ceramic Society* 70 2: 90–95.

Turner Fairbanks Highway Research Center. 2005. *User Guidelines for Waste and Byproduct Materials in Pavement Construction*. Federal Highway Administration, Washington, D.C.

Way, G.B. 2000. Flagstaff I-40 Asphalt Rubber Overlay Project: Nine Years of Success. *Transportation Research Record* 1723: 45–52.

Advances in Pavement Design through Full-scale Accelerated Pavement Testing – Jones, Harvey, Mateos & Al-Qadi (Eds.)
© 2012 Taylor & Francis Group, London, ISBN 978-0-415-62138-0

Accelerated performance of a failed pavement on a soft clay subgrade after rehabilitation with high polymer mix at the NCAT pavement test track

R.B. Powell
National Center for Asphalt Technology, Auburn University, Alabama, US

ABSTRACT: The Pavement Test Track is a full-scale, accelerated performance test facility for flexible pavements managed by the National Center for Asphalt Technology (NCAT) at Auburn University. Forty-six unique 60-m test sections are installed around a 2.7-km oval and subjected to accelerated damage via a fleet of tractors pulling heavy triple trailers. Methods and materials that produce better performance for research sponsors are identified so that future pavements can be constructed based on objective life cycle comparisons. In this study, a 250-mm thick, full depth asphalt pavement that failed near the end of the previous research cycle was first rehabilitated using conventional methods. When the section failed a second time after less than half the traffic that produced the original failure, it was decided to rehabilitate the section again using the same high polymer mix that had performed well in another test section. Traffic applied to the high polymer rehabilitation has now surpassed the level needed to completely fail the original conventional rehabilitation, with no indication that another failure is pending. An overview of the original construction and subsequent rehabilitation of the failed pavement on a soft clay subgrade are included in this paper, with a focus on comparing the performance of the conventional rehabilitation with the high polymer content asphalt inlay.

1 INTRODUCTION

The Pavement Test Track (www.pavetrack.com is a full-scale, accelerated performance test facility for flexible pavements managed by the National Center for Asphalt Technology (NCAT) at Auburn University. Forty-six unique 60-m test sections are installed around a 2.7-km oval and subjected to accelerated damage via a fleet of tractors pulling heavy triple trailers. Methods and materials that produce better performance for research sponsors are identified so that future pavements can be constructed based on objective life cycle comparisons. In this study, a 250-mm thick, full depth asphalt pavement that failed near the end of the previous research cycle was first rehabilitated using conventional methods. When the section failed a second time after less than half the traffic that produced the original failure, it was decided to rehabilitate the section again using the same high polymer mix that had performed well in another test section.

2 CONSTRUCTION

The Oklahoma Department of Transportation (ODOT) sponsored two new structural test sections on the 2006 NCAT Pavement Test Track in order to study the perpetual pavement thickness design concept. These sections (N8 and N9, shown in Figure 1) represented the thickest cross-sections yet built as part of the structural response experiment. The original stiff (200,000 Pa) subgrade under these two ODOT sections was removed and replaced with a soft (40,000 Pa) subgrade that was more representative of design soils in Oklahoma. Section N8, the first of the two ODOT sections, was mechanistically under designed with 250 mm of asphalt (50-mm rich bottom layer, 150 mm of dense Superpave mix, and a 50-mm stone matrix asphalt (SMA) surface). The second section, N9, was designed to be a perpetual pavement with a total HMA thickness of 350 mm. The rich bottom layer was increased in the thicker section to 75 mm and an additional 75-mm Superpave lift was added. In both sections, the rich-bottom layer was simply a mixture designed to 2% air voids rather than 4% in the other Superpave layers (thus, a higher binder content). Detailed information on the design, production, and placement of all the layers in both sections are available on the project website and well documented in other publications (Willis et al., 2009).

3 ACCELERATED PERFORMANCE

Test sections on the NCAT Pavement Test Track are loaded with heavy triple trailer trains with an average gross vehicle weight of 689 kN (89 kN target per single axle) driven by human drivers at a cruise speed of 72 km per hour. Individual single axles are loaded to optimize the efficiency of pavement damage, which

Figure 1. Locations of Sections N8 and N9 on the NCAT pavement test track.

Figure 2. Accelerated truck traffic with the NCAT fleet.

averages approximately 11.8 ESALs per truck pass. Each vehicle in the five truck fleet (shown in Figure 2) laps the track approximately 400 times a day in order to induce damage in experimental pavements. A design lifetime of pavement damage (10 million equivalent single axle loadings, or ESALs) is compressed into a 2-year trucking cycle in order to load test pavements in an accelerated manner. Both surface performance and subsurface (high-speed) pavement response are measured weekly in order to provide all the necessary information for comprehensive life cycle modeling.

As seen in Figure 3, high-speed strain instrumentation revealed that longitudinal strains (routinely higher than transverse strains, shown as the average of six gauges) at the bottom of the slightly thinner section (N8) were approximately twice as high as longitudinal strains measured on the thicker section (N9) at 20°C before the influence of any damage effects. Because this is the standard test temperature for beams in the laboratory, it often serves as the basis of comparison for in-service pavements. Lower strain levels in Section N9 led researchers to believe it could actually be perpetual, meaning that the structure would be thick enough to prevent the initiation of a crack at the bottom of the lower lift of HMA (Timm et al., 2009). Strain levels measured in Section N8 were thought to be high enough that "bottom up" cracking could cause the type of deep, expensive failure that perpetual pavement designs aim to avoid.

As predicted, roughness began to increase on the thinner section as a result of cracks propagating up from the bottom of the pavement. As seen in Figure 4, roughness in the thinner section began to increase

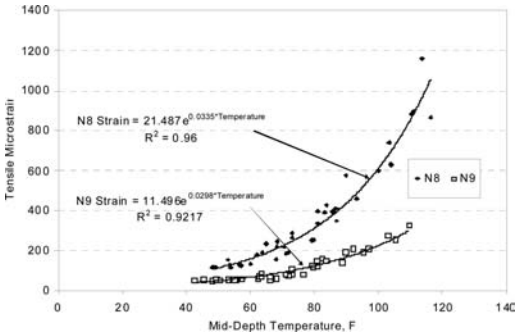

Figure 3. Strain measurement comparisons.

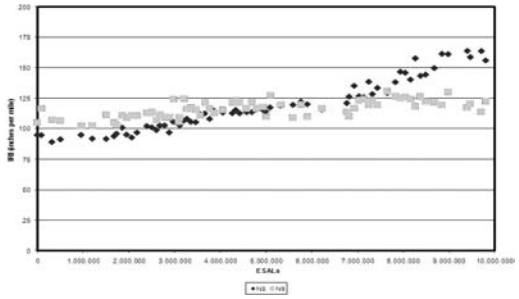

Figure 4. Changing roughness as a function of accumulating traffic damage.

after approximately 6.8 million ESALs. After approximately 8.3 million ESALs, extensive cracking was visible on the surface. By the end of the 10 million ESAL traffic cycle on the 2006 NCAT Pavement Test Track, Section N8 was in need of rehabilitation. The terminal crack map for this section, which shows extensive alligator cracking as interconnected cracked areas, is shown in Figure 5. A forensic investigation confirmed that cracking and rutting extended all the way down to the top of the subgrade. Consistent with the expectation for a perpetual pavement, the thicker section (N9) did not exhibit any distresses through the entire 10 million ESAL research cycle.

4 CONVENTIONAL REHABILITATION

The initial rehabilitation of the failed section consisted of a 125-mm mill and inlay, which is ODOT's standard practice for the type of structural failure observed. The 125-mm inlay consisted of 75 mm of dense Superpave mix under 50 mm of stone matrix asphalt SMA. The mixes used for this inlay were identical to the original mixes placed in the structure in the summer of 2006. At the request of ODOT researchers, geotextile fabric interlayers were used in two different areas of the inlay in order to determine if they would affect the onset of reflective distresses. As seen in Figure 6, an untreated control area was maintained for each type of fabric.

As seen in Figure 7, cracking again appeared in the rehabilitated section (one crack in an area with

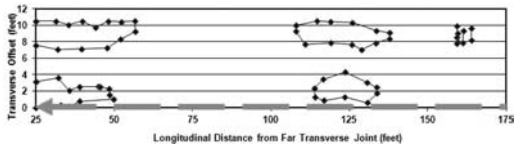

Figure 5. Terminal crack map for thinner Section N8 after 10 million ESALs.

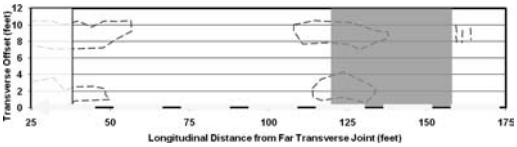

Figure 6. Fabric placement in rehabilitated section (prior cracking in dashed line).

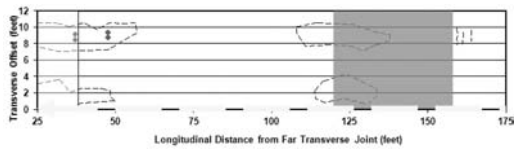

Figure 7. Recurrence of cracking after 2.7 million ESALs.

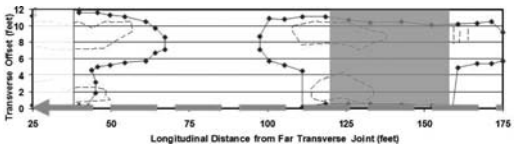

Figure 8. Terminal cracking after 3.8 million ESALs.

a geotechnical fabric and one in the adjacent control area) after approximately 2.7 million ESALs. Although cracks generally took longer to form in the areas of the mat where the fabric interlayers were placed, pavement condition in the area in which a fabric interlayer was installed deteriorated more rapidly after cracking was observed. Cracking after the application of approximately 3.8 million ESALs is shown in Figure 8. The cracked area between 30 and 55 m developed completely in a single week of accelerated traffic (approximately 100,000 ESALs). It is believed that micro-cracking in the surface SMA in both the cracked areas allowed water to flow into the mat, creating a failure plane at the fabric interface; however, forensic testing confirmed that distresses extended all the way to the bottom of the failed pavement. The complete failure of the rehabilitated structure is evident in Figure 9.

5 HIGH POLYMER REHABILITATION

A high polymer mix appeared to be a viable option to rehabilitate the failed section because no distresses at all had been observed in a relatively thin, high strain pavement included in the 2009 Group Experiment

Figure 9. Photo of failed conventional rehabilitation

(GE) (Timm et al., 2011). Additionally, an order of magnitude increase in fatigue life has been observed by other researchers in the laboratory in mixtures blended with high polymer binders (Klutz et al., 2009). It was thought the full depth distresses in the failed section would produce the types of high strain conditions these materials have been shown to resist.

The 144-mm thick GE section (N7) that had exhibited good performance consisted of three lifts of HMA using a binder modified with approximately three times the styrene-butadiene-styrene (SBS) polymer normally used. The 56-mm base lift and 56-mm intermediate lift each contained 7.5 percent polymer and 19-mm stone, while the 32-mm thick wearing course was designed with a 9.5-mm NMAS aggregate blend. Oklahoma officials supported using the high polymer design but proposed changing the size of stone in the base course to 9.5-mm, in effect duplicating the wearing course composition and thickness. In order to optimize the cracking resistance of the smaller NMAS lower layer, it was produced with lower air voids for a rich bottom approach. The thickness of the intermediate layer was increased to 80 mm to accommodate the change in the lower layer. A consensus on this design change was reached among NCAT, representatives from the polymer supplier, and the Oklahoma DOT. No fabric interlayers were used in the second rehabilitation.

6 PERFORMANCE COMPARISON

Improvements in the mechanistic response of the pavement structure resulting from the high polymer rehabilitation are well documented in other publications (Timm et al., 2012). Traffic applied to the new surface (shown in Figure 10) has significantly surpassed the level needed to completely fail the original conventional rehabilitation, with no indication that another failure is pending. A plot of roughness and macrotexture measured on the section for both the conventional and high polymer rehabilitation efforts is shown in Figure 11. Here, it is seen that the upward trend in the original rehabilitation began after approximately

Figure 10. High polymer rehabilitation after traffic surpassed original failure.

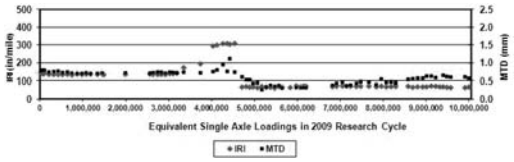

Figure 11. Measured roughness and macrotexture for entire 2009 research cycle.

3.0 million ESALs. The high polymer rehabilitation was completed at the 4.6 million ESAL mark, meaning that over 5.4 million ESALs had been applied at the completion of the 10 million ESAL research cycle with no sign of the increase in roughness that typically precedes structural cracking. This represents an 80 percent improvement in performance compared to the original conventional rehabilitation effort.

7 IMPLEMENTATION

This positive experience with high polymer rehabilitation attracted the attention of state DOTs with specific and challenging rehabilitation needs. For example, the Alabama Department of Transportation (ALDOT) contacted NCAT researchers seeking feedback on the suitability of using this method for three unique infrastructure projects. Following a comprehensive review of data provided by ALDOT, all three projects were considered to be potential candidates for high polymer rehabilitation. General information for these projects is provided in the following paragraphs.

7.1 *Prevention of reflective cracking*

The first project was on a roadway that was being rehabilitated in the summer of 2011 using conventional methods. Cracked pavement was milled to accommodate the placement of new binder and surface mix. After the binder mix was placed, but before it could be overlaid with new surface mix, project personnel observed intermittent cracking in both the inside and outside wheelpaths. A map of observed cracking is shown in Figure 12. The enhanced strain tolerance of high polymer mix made it an attractive option for use

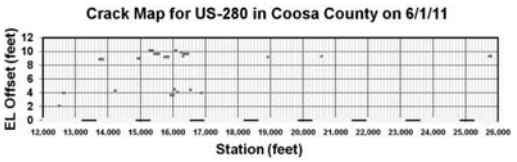

Figure 12. Observed cracking in binder mix prior to placement of new surface.

Figure 13. Localized failure with pumping on Interstate I-59 in Tuscaloosa.

on this project; however, ALDOT was unable to negotiate an acceptable price for the changed scope of work with the original contractor. The Department decided to overlay the cracked binder mix with conventional surface mix, as planned, and then let the project again using high polymer mix in the future when cracking begins to reflect through to the surface.

7.2 *Improving structural capacity*

The second project was a section of interstate I-59 in Tuscaloosa County that was exhibiting structural failures in stretches of asphalt pavement that connect a series of relief bridges through a flood plain. Forensic testing indicated structural deficiencies that could only be corrected by significantly increasing structural capacity. A picture of a localized failure is included as Figure 13. Complete reconstruction was not considered to be a viable option, and increasing the thickness of the existing pavement would have required costly bridge jacking to maintain grade. In a sense, this project was very similar to the failed Section N8 on the NCAT Pavement Test Track. High polymer mix was recommended as a cost effective way to improve structural capacity of the failed pavement.

7.3 *Preventing the recurrence of rutting*

The third candidate project was on a stretch of US-231 in Pike County that runs through Troy, Alabama. This section of roadway is subjected to heavy traffic and a high percentage of loaded trucks. Numerous intersections require trucks to decelerate and accelerate intermittently throughout the project. A history of rutting prompted ALDOT to choose SMA binder and surface mixes for rehabilitation back in the summer of 2008. Rutting quickly returned later that

Figure 14. Forensics on rutted SMA pavement on US-231.

same year. Forensic investigations revealed deformation of the SMA binder (shown in Figure 14), which led the Department to patch the affected areas using completely new mix designs for replacement SMA binder and surface mix. Rutting has since returned throughout the project. A high polymer Superpave mix was recommended for the next rehabilitation based on excellent rutting performance on the NCAT Pavement Test Track.

8 CONCLUSIONS AND RECOMMENDATIONS

Several important conclusions can be drawn from the findings of this experiment that may have a significant impact on pavement rehabilitation practices on the open infrastructure:

- Geotextile fabric interlayers appeared to delay the onset of reflective cracking; however, they may have accelerated the failure process after cracking was initiated;
- Rehabilitation using high polymer mix lasted significantly longer than rehabilitation using conventional mix. Approximately 80 percent more traffic had been applied as of the end of the 2009 research cycle;
- The life cycle cost of the high polymer inlay could be fully assessed by leaving the section in place with traffic continuation for the 2012 research cycle;
- Rehabilitation using high polymer mix can be implemented by state DOTs in the interim by conservatively using the findings from the unfailed surface in the current research cycle that showed an 80 percent improvement in performance; and
- The long term performance of the three potential high polymer rehabilitation projects under consideration by ALDOT should be documented in order to improve the decision making process for future projects.

ACKNOWLEDGEMENTS

The Pavement Test Track is managed by NCAT, who is responsible for daily operations and the completion of associated research. Funding for the NCAT track has been provided under a cooperative agreement by the following entities:

- Alabama Department of Transportation
- Florida Department of Transportation
- Georgi Department of Transportation
- Mississippi Department of Transportation
- Missouri Department of Transportation
- North Carolina Department of Transportation
- Oklahoma Department of Transportation
- South Carolina Department of Transportation
- Tennessee Department of Transportation
- Federal Highway Administration
- Kraton Polymers
- OldCastle Materials
- Polycon
- Shell Sulfur Solutions
- Lake Asphalt of Trinidad and Tobago

REFERENCES

Kluttz, R.Q., Molenaar, A.A.A. van de Ven, M.F.C., Poot, M.R., Liu, X., Scarpas, A. and Scholten, E.J. 2009. Modified Base Courses for Reduced Pavement Thickness and Improved Longevity. *Proceedings of the International Conference on Perpetual Pavement*, Columbus, OH.

Timm, D., Powell, B., Willis, R. and Kluttz, R. 2012. Pavement Rehabilitation Using High Polymer Asphalt Mix. *Proceedings of the 91st Annual Transportation Research Board*, Washington, DC.

Timm, D.H., Gierhart, D. and Willis, J.R. 2009. Strain Regimes Measured in Two Full Scale Perpetual Pavements. *Proceedings, International Conference on Perpetual Pavement*, Columbus, OH.

Timm, D., Robbins, M. and Kluttz, R. 2011. Full-Scale Structural Characterization of a Highly Polymer-Modified Asphalt Pavement. *CD-ROM Proceedings of the 90th Annual Transportation Research Board*, Washington, D.C.

Willis, J., Timm, D., West, R.C., Powell, R., Robbins, M., Taylor, A., Smit, A., Tran, N., Heitzman, M. and Bianchini, A. 2009. *Phase III NCAT Test Track Findings*. Report No. 09-08, National Center for Asphalt Technology, Auburn University.

This page intentionally left blank

Advances in Pavement Design through Full-scale Accelerated Pavement Testing – Jones, Harvey, Mateos & Al-Qadi (Eds.)
© 2012 Taylor & Francis Group, London, ISBN 978-0-415-62138-0

Evaluation of a heavy polymer modified asphalt binder using accelerated pavement testing

J. Greene, B. Choubane & P. Upshaw
Florida Department of Transportation, Gainesville, Florida, US

ABSTRACT: As part of its Accelerated Pavement Testing (APT) program, the Florida Department of Transportation (FDOT) initiated, in 2001, an experiment to evaluate the effects of polymer modifiers on the rutting performance of Superpave mixes using a Heavy Vehicle Simulator (HVS). That study led to the use of PG 76-22 asphalt binder on the final structural course for traffic level D roadways (10 to >30 million ESALs) and the top two structural courses for traffic level E roadways (≥ 30 million ESALs). As a follow up, a study was conducted to evaluate the performance of stiffer polymer-modified binders meeting PG 82-22 requirements for focused use on intersections and other low speed facilities with concentrated heavy loads. This paper describes the research approach and findings. It is anticipated that the localized use of a PG 82-22 asphalt binder will significantly improve pavement performance at locations with historically excessive rut depths.

1 INTRODUCTION

In 2001, the Florida Department of Transportation (FDOT) conducted an experiment to assess the rutting resistance of a polymer modified PG 76-22 asphalt binder on Superpave mixtures through Accelerated Pavement Testing (APT). This study led to the use of PG 76-22 asphalt binder on the final structural course for traffic level D roadways (10 to >30 million ESALs) and the top two structural courses for traffic level E roadways (≥30 million ESALs). The Florida Flexible Pavement Design Manual also recommends consideration of a PG 7622 asphalt binder at intersections or other facilities with slow moving and concentrated truck loads. Annual statewide pavement condition surveys have indicated that pavements rated as deficient due to excessive rutting have steadily decreased over the last 10 years. However, localized failures still occur at locations with concentrated truck traffic at low speeds. In response to this, a follow-up APT study was recently conducted to evaluate the performance of a polymer-modified asphalt binder meeting PG 82-22 requirements. This paper describes the research approach and findings.

2 OBJECTIVE

The objective of this study was to evaluate the rutting and fatigue resistance of three asphalt binder types: (1) a polymer modified PG 82-22, (2) a polymer modified PG 76-22, and (3) an unmodified PG 67-22. Accelerated pavement testing (APT) and laboratory testing was used to accomplish this goal.

3 BACKGROUND

Recent studies have indicated that increased rutting resistance can be achieved with the use of a PG 8222 asphalt binder (Powell 2011, Prowell 1999, Thomas et al. 2007). A limited laboratory evaluation conducted by FDOT also showed that rutting potential decreased as percent modified asphalt binder increased. The study consisted of a 12.5 mm fine graded mixture of granite and sand. In light of this evidence FDOT has begun to investigate the potential benefits of using a PG 82-22 asphalt binder at locations with a history of extensive rutting. As a first step towards implementation, FDOT recently drafted a developmental specification to allow PG 82-22 asphalt binder on a case-by-case basis. While the cost of PG 82-22 asphalt binder is currently $100/liquid ton more than PG 76-22 asphalt binder and $250/liquid ton more than an unmodified PG 67-22 asphalt binder, it is anticipated the heavy polymer asphalt binder will increase the life of these facilities and reduce the hazards that accompany rutted roadways such as hydroplaning.

4 EXPERIMENT DESIGN

To allow for a faster and a more practical assessment under closely simulated in-service conditions, APT was considered to address the objectives of this study. APT is generally defined as a controlled application of a realistic wheel loading to a pavement system simulating long-term, in-service loading conditions. This allows the monitoring of a pavement system's performance and response to accumulation of damage

Figure 1. FDOT's HVS and APT test tracks.

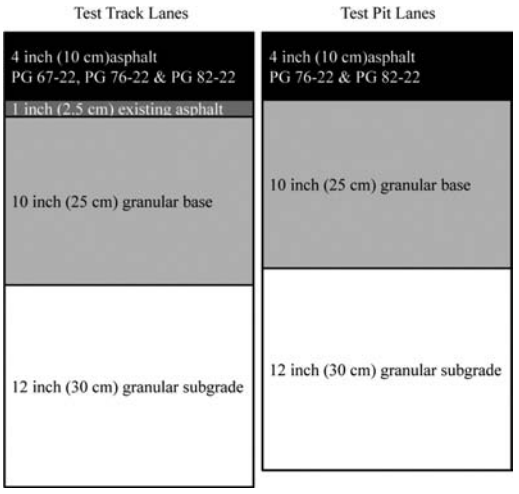

Figure 2. Test track and test pit pavement structures.

within a much shorter time frame. In Florida's APT program, the accelerated loading is performed using a Heavy Vehicle Simulator (HVS), Mark IV model. The HVS is electrically powered (using an external electric power source or electricity from an on-board diesel generator), fully automated, and mobile. The HVS and test tracks are shown in Figure 1. A complete description of the test facility has been presented elsewhere (Byron et al. 2004, Choubane et al. 2005).

Three test track lanes measuring 12 ft. (3.7 m) wide and 150 ft. (46 m) long were constructed for the APT portion of the study that focused on rut depth measurements. Two additional test lanes measuring 50 ft. (15 m) long were constructed on test pits which allowed control of the water table. The water table was raised to the bottom of the base on the test pit lanes to weaken the granular base layer so that fatigue tests could be conducted. Each lane consisted of two 2 in. (5 cm) lifts of 12.5 mm fine graded Superpave mixture of granite material and 5.1% asphalt binder. The construction of each lane was similar except for the asphalt binder type which included an unmodified PG 67-22, a Styrene Butadiene Styrene (SBS) modified PG 76-22, or an SBS modified PG 82-22. The primary difference in the modified binders was the amount of SBS polymer that was used. Approximately 1 in. (2.5 cm) of existing hot-mix asphalt (HMA) remained after a milling operation prior to resurfacing of the test track lanes. The asphalt lanes constructed on the test pits was paved directly on the base surface. Figure 2 illustrates the pavement structures for both test track lanes and test pit lanes. A minimum of three sections per lane were designated for rutting tests to account for construction variability. During HVS testing, the pavements were heated to 50°C (120° F) and trafficked with a 455 mm wide base single tire (Michelin X One XDA-HT Plus 455/55R22.5) loaded to 9,000 pounds (40 kN) and inflated to 100 psi (689 kPa). A wheel wander of 4 in. (10 cm) was used for each test. A previous FDOT study showed that when compared to a standard dual tire, the 455 mm wide base single tire produced similar rut depths (Byron, et al, 2004). Of the two lanes constructed on the test pits, one lane included a modified PG 76-22 binder and the other a modified PG 82-22 binder. The test pit dimensions allowed only one test per binder type. Two strain gauges were placed at the bottom of the asphalt layer to measure the longitudinal strain. A Goodyear G286 A SS, 425/65R22.5 (Super-Single) loaded to 12,000 pounds (53 kN) and inflated to 110 psi (758 kPa) was used to load the test pits without wheel wander.

5 MATERIAL PROPERTIES

5.1 *Asphalt binder properties*

The asphalt binder was blended by the supplier to meet the requirements of PG 67-22, PG 76-22, and PG 82-22 asphalt binders according to the current FDOT specifications. FDOT is currently considering the PG+ system but has not yet adopted the new grading system. The PG 82-22 asphalt binder included approximately six percent SBS polymer modifier which is double that of the PG 76-22 asphalt binder.

Dynamic Shear Rheometer (DSR) tests were performed according to AASHTO T-315 on the original asphalt binder at the upper temperature of each binder grade. A considerable difference in G*/sin δ was observed for the different asphalt binders. FDOT specifies a minimum G*/sin δ of 1.0 kPa and a maximum phase angle (δ) of 75° for a PG 76-22 original asphalt binder. A developmental specification requires a phase angle of 65° for a PG 82-22 original asphalt binder. Both polymer modified asphalt binders met the respective requirements. Figures 3 and 4 show the DSR properties for each asphalt binder for comparison.

The Multiple Stress Creep Recovery (MSCR) evaluates an asphalt binder's potential for permanent deformation and can be measured using the DSR. Ten creep/recovery cycles are performed with a stress of 0.1 kPa applied for one second with a nine second rest period. The stress level is then increased to 3.2 kPa

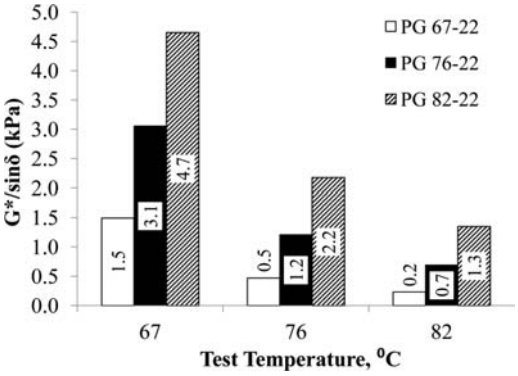

Figure 3. G*/sin δ measurements.

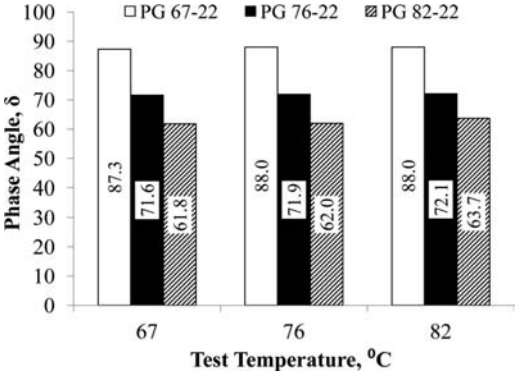

Figure 4. Phase angle measurements.

Table 1. AASHTO specifications for MSCR data.

Asphalt binder grade	Standard (S)	Heavy (H)	Heavy Very (V)	Extreme (E)
Traffic level/ speed	<10 million ESALs or >45 mph	10–30 million ESALs or 15–45 mph	>30 million ESALs or <15 mph	>30 million ESALs and <15 mph
J_{nr} max, kPa	4.0	2.0	1.0	0.5
J_{nr} max difference, %	75	75	75	75

for an additional ten cycles. Specifications have been developed based on the non-recoverable creep compliance (J_{nr}) and are shown in Table 1 (AASHTO, 2010). Asphalt binder samples were collected from the plant and conditioned in a rolling thin film oven (RTFO). MSCR tests were performed on the RTFO residue at a temperature of 64°C. A summary of the MSCR test results are shown in Table 2.

5.2 *Mixture properties*

Several standard quality control (QC) tests were performed to verify the uniformity and quality of the mixtures. Table 3 shows that the gradation, percent asphalt binder, and percent air voids from samples retrieved from trucks delivering the mix were within normal ranges. During construction of the test lanes there was some concern that adequate density would be difficult to obtain on the lane with the PG 82-22 asphalt binder due to the increased stiffness. The contractor applied compaction effort following the paver earlier for the PG 82-22 lane so that compaction temperatures were higher. The developmental specification states that compaction temperature for a mixture using PG 82-22 asphalt binder should not exceed 340°F (171°C). Additional passes of the roller were also applied. A non-nuclear Pavement Quality Indicator (PQI) device was used to estimate the compacted asphalt mixture density after each pass of the roller. Table 4 summarizes the compaction effort for each lane. The bottom lift for the PG 67-22 lane was slightly less dense than desired but the average core density of this lane was considered acceptable. It should be noted that more than 20 cores were used to determine the average density for the PG 76-22 and PG 82-22 lanes and only three cores were used for the PG 67-22 lane.

Table 2. Summary of MSCR data.

Asphalt binder	J_{nr} 0.1 kPa	J_{nr} 3.2 kPa	Difference	Grade
PG 67-22	2.243	2.443	8.2%	S
PG 76-22	0.414	0.461	10.1%	E[1]
PG 82-22	0.149	0.157	4.9%	E

[1]Borderline

An Asphalt Pavement Analyzer (APA), Hamburg wheel tester, and Asphalt Mix Performance Tester (AMPT, testing flow number) were used to evaluate the rut potential of the mixtures in the laboratory. APA tests (AASHTO T340) were conducted at a temperature of 64°C for 8,000 cycles (16,000 passes) utilizing a 100 pound (445 N) load applied to a 100 psi (689 kPa) hose. Hamburg (AASHTO T324) samples were tested submerged in water at a temperature of 50°C (120°F) for 10,000 cycles (20,000 passes) utilizing a 158 pound (700 N) load. The Flow Number was determined using a confining stress of 10 psi (69 kPa), a contact stress of 7 psi (50 kPa), a creep deviator stress of 100 psi (689 kPa), and a test temperature of 130°F (54°C). The Flow Number test was conducted according to AASHTO T79. Table 5 summarizes the laboratory data. As indicated by literature and previous FDOT laboratory tests, rutting resistance increased as the amount of polymer was increased.

6 ACCELERATED PAVEMENT TESTING

Rut depth measurements were obtained periodically using a laser-based profiling system mounted on the underside of the HVS wheel carriage. The data showed

Table 3. Average volumetric properties.

Sieve Size/ Mixture QC Test	Design Values		Truck Samples		
	JMF	Range	PG 67-22	PG 76-22	PG 82-22
4/3 in. (19.0 mm)	100	100	100.0	100.0	100.0
1/2 in. (12.5 mm)	98	90–100	97.3	97.4	97.8
3/8 in. (9.5 mm)	88	NA-90	86.3	86.1	86.6
#4 (4.75 mm)	59	–	57.8	57.4	57.5
#8 (2.36 mm)	40	28–50	39.2	38.5	39.1
#16 (1.18 mm)	29	–	28.7	27.9	28.4
#30 (600 μm)	22	–	22.1	21.4	21.7
#50 (300 μm)	12	–	13.2	12.8	13.0
#100 (150 μm)	4	–	4.9	4.7	5.0
#200 (75 μm)	2.0	2–10	2.8	2.7	2.8
% Binder	5.1	4.7–5.5	4.9	4.8	4.7
% Air voids	4.0	2.8–5.2	3.3	4.0	4.0

Table 4. Average compaction properties.

Compaction Parameter[1]	PG 67-22		PG 76-22		PG 82-22	
Lift	1	2	1	2	1	2
Vibe passes	1	1	2	2	2	2
Static passes	5	3	2	2	4	4
Temp. (°F)	310	305	320	330	340	340
Temp. (°C)	154	152	160	166	171	171
% density	90.8	92.1	92.2	93.3	94.1	94.1

[1]Using a 25,000 lb. (11,340 kg) Caterpillar CB634C roller

Table 5. Laboratory rut potential tests.

Binder Grade	APA in. (cm)	Hamburg in. (cm)	Flow No
PG 67-22	4.9 (12.4)	4.7 (11.9)	73
PG 76-22	4.0 (10.2)	3.9 (9.9)	152
PG 82-22	2.1 (5.3)	2.1 (5.3)	280

rutting decreased as the amount of polymer modifier increased. After 100,000 passes, the lane with PG 82-22 and PG 76-22 polymer modified asphalt binders rutted approximately 0.5 and 0.8 times less than the lane without polymer modified asphalt binder, respectively. Figure 5 shows the average rut history of three sections for each test lane. Multiple tests were performed to account for construction variability. No individual rut profile measured on the PG 82-22 lane overlapped an individual rut profile of the PG 76-22 lane after approximately 30,000 passes of the HVS. In other words, the worst performing section on the PG 82-22 lane was still better than the best section on the PG 76-22 lane after initial densification/distortion of the mixture. The same was true for the PG 76-22 lane and the PG 67-22 lane.

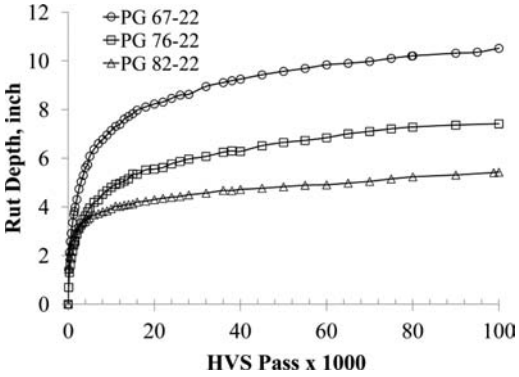

Figure 5. Average rut profiles.

Shear deformation and densification are the primary causes for rutting of flexible pavements. One method used by FDOT and others to determine the portion of rutting generated from shear flow is to estimate the area or volume of accumulated material at the edge of the rutted wheel path and compare it to the empty area or volume below the wheel path (Gokhale et al. 2005, Harvey and Popescu, 2000, Drakos, 2003). It can be reasonably assumed that the material at the edge of the wheel path is displaced by shear flow. If the area of displaced material is equal to the area of the material below the wheel path, it can be assumed that the majority of rutting was due to shear flow. In general, as the amount of polymer modifier increased, a larger shear to wheel path area ratio was measured. Figure 6 illustrates the transverse profiles after 100,000 passes. Table 6 summarizes the rut and shear data for several pass levels and indicates that densification was more prevalent early in the test, but that shear becomes dominant within a few thousand passes. It should be noted that the rut depth for the transverse profile is found through establishing a straight line between the sheared materials at the edge of the wheel path and determining the greatest distance to the bottom of the wheel path.

HVS rut depth correlations with mixture and binder laboratory tests are presented in Figures 7 and 8. In general, the correlations were as expected. Approximately linear correlations were found with HVS rut depth and each laboratory indicator. Additional tests would be necessary to properly describe the relationships.

Several hundred thousand passes were completed on the test pits without observation of any fatigue cracking. Tensile strain was measured at different times to capture the pavement response at different temperatures. The temperature range was different for each test pit lane since testing was conducted a few months apart. Figure 9 shows the measured tensile strain. For comparison, strain data is included from a previous experiment that had the same pavement structure, similar aggregate and gradation and used an unmodified PG 67-22 asphalt binder. It should be noted that the Michelin 455 mm wide base tire loaded

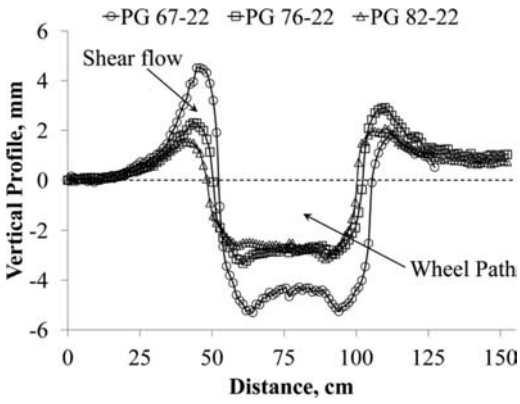

Figure 6. Vertical profile at 100,000 passes.

Table 6. Shear and rut depth summary.

Pass #	PG 67-22 Rut in. (mm)	PG 76-22 Rut, in. (mm)	PG 82-22 Rut, in. (mm)
100	0.06 (1.5)	0.03 (0.8)	0.06 (1.5)
5,000	0.24 (6.1)	0.16 (4.1)	0.14 (3.6)
100,000	0.41 (10.4)	0.29 (7.4)	0.21 (5.3)
	Shear Area/ WP Area	Shear Area/ WP Area	Shear Area/ WP Area
100	0.21	0.44	0.23
5,000	0.60	0.50	0.28
100,000	0.72	0.45	0.27

Shear Area = Area of displaced material due to shear WP Area = Area of displaced material in wheel path.

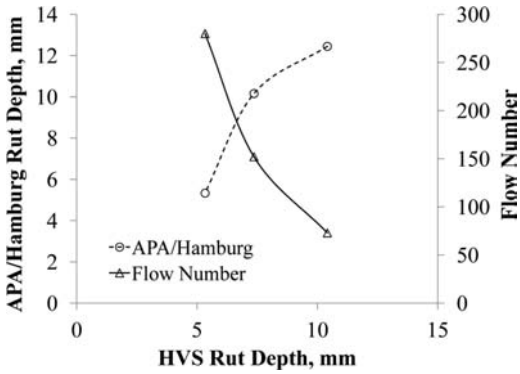

Figure 7. Laboratory and HVS rut potential correlations.

to 12,000 pounds (53 kN) and inflated to 100 psi (689 kPa) was used for the earlier experiment with the PG 67-22 asphalt binder.

Both modified binders appear to have better fatigue performance than the unmodified binder. Fatigue life can be estimated using a number of different transfer equations. One such transfer equation is presented in AASHTO's *Mechanistic Empirical Pavement Design Guide (MEPDG)*. The MEPDG equation is shown below:

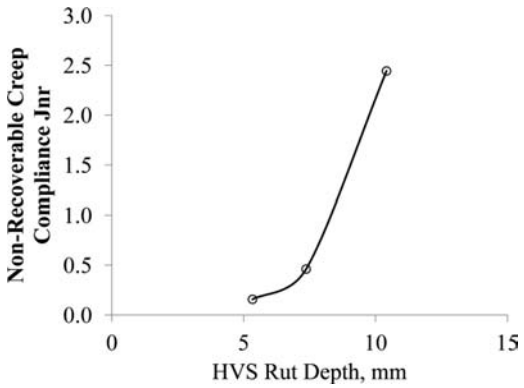

Figure 8. MSCR and HVS rut depth correlation.

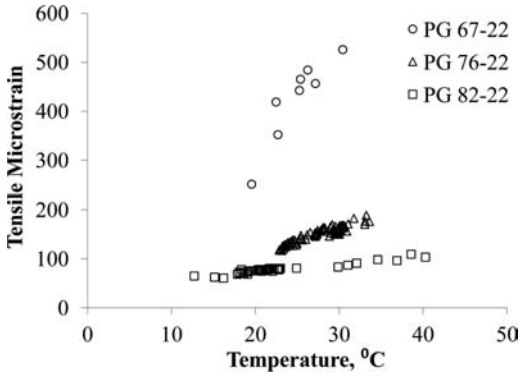

Figure 9. Strain measurements.

$$N_f = 0.00432 \times K \times C \times \left(1/\varepsilon_t\right)^{3.9492} \left(1/E\right)^{1.281} \quad (1)$$

where:
N_f = repetitions until fatigue failure (50% cracking of lane area)
K = thickness calibration
C = regional or national calibration factor
ε_t = tensile strain
E = asphalt modulus, psi
h_{ac} = thickness of asphalt layer, in.

At 68°F (20°C), the fatigue life of the PG 82-22 and PG 76-22 sections are approximately 136 and 20 times greater than the PG 67-22 section, respectively. Furthermore, the fatigue life of the PG 82-22 section is approximately seven times greater than the fatigue life of the PG 76-22 section.

7 IMPACT OF THE RESEARCH

FDOT District Engineers are seeking solutions for pavements with histories of excessive rutting where existing strategies have not worked. Often these pavements are at locations with concentrated and slow

moving truck traffic. The HVS is an ideal tool to investigate these harsh conditions. This study has shown that a PG 82-22 asphalt binder has an increased rutting resistance compared to existing asphalt binders. The mixture with the PG 82-22 asphalt binder rutted 0.5 and 0.7 times as much as the mixtures with the PG 67-22 and PG 76-22 asphalt binders, respectively. In addition, strain data indicated that the fatigue life of a mixture with PG82-22 asphalt binder may be increased as much as seven times more than a mixture with PG 76-22 asphalt binder. Currently, there are five upcoming projects that will use PG 82-22 asphalt binder. These projects are located on ramps and intersections with rut depths which are often greater than 1 in. (2.5 cm). It is anticipated that the implementation of the PG 8222 asphalt binder will improve asphalt pavement performance at these locations.

REFERENCES

American Association of State Highway and Transportation Officials (AASHTO). 2010. *Standard Specification for Performance-Grade Asphalt Binder Using Multiple Stress Creep Recovery (MSCR) Test*. AASHTO Designation: MP 19-10, Washington DC.

Byron, T., Choubane, B. and Tia, M. 2004. Assessing Appropriate Loading Configuration in Accelerated Pavement Testing. Proceedings of the *2nd International Conference on Accelerated Pavement Testing*, Minneapolis, Minnesota.

Choubane, B., Gokhale, S., Sholar, G. and Moseley, H. 2005. Evaluation of Coarse and Fine-Graded Superpave Mixtures Under Accelerated Pavement Testing. In *Transportation Research Record, Journal of the Transportation Research Board, No 1974*, National Research Council, Washington DC., pp. 120–127.

Drakos, C.E. 2003. *Identification of a Physical Model to Evaluation Rutting Performance of Asphalt Mixtures*. University of Florida.

Gokhale, S., Choubane, B., Byron, T. and Tia, M. 2005. Rut Initiation in Asphalt Mixtures as Generated Under Accelerated Pavement Testing. In *Transportation Research Record, Journal of the Transportation Research Board, No. 1940*, National Research Council, Washington D.C., pp. 136–145.

Harvey, J. and Popescu, L. 2000. Accelerated Pavement Testing of Rutting Performance of Two Caltrans Overlay Strategies. In *Transportation Research Record, Journal of the Transportation Research Board, No. 1716*, National Research Council, Washington D.C., pp. 116–125.

Powell, R.B. 2011. Rehabilitation of a Failed Pavement With High Polymer Mix. In *Oklahoma Asphalt, Volume 10, No. 2*, Oklahoma Asphalt Pavement Association, Oklahoma City, Oklahoma, pp. 4–11.

Prowell, B.D. 1999. Development of Rutting Criteria for the Asphalt Pavement Analyzer. *International Conference on Accelerated Pavement Testing*. Reno, Nevada.

Thomas, T.D., Littlefield, J.C., Pittman, J., Plummer, R.C., Easterling, J.R. Owens, J.R. and M.S. Buchanan. 2007. *Hot Mix Asphalt Characterization for the 2002 AASHTO Design Guide.* FHWA/MS-RD-07-166, Federal Highway Administration, McLean, Virginia.

Advances in Pavement Design through Full-scale Accelerated Pavement Testing – Jones, Harvey, Mateos & Al-Qadi (Eds.)
© 2012 Taylor & Francis Group, London, ISBN 978-0-415-62138-0

Accelerated pavement testing of low-volume paved roads with geocell reinforcement

B.S. Bortz & M. Hossain
Kansas State University, Manhattan, Kansas, US

I. Halami
PRS Mediterranean Ltd, Tel-Aviv, Israel

A. Gisi
Kansas Department of Transportation, Topeka, Kansas, US

ABSTRACT: Geocellular confinement systems (geocells) are three Infrastructure System Laboratory (CISL) of Kansas State University. Three of the four lanes had 75-mm geocell-reinforced bases and 25-mm cover of three different in-fill materials; crushed limestone, AB-3; quarry by-products; and Recycled Asphalt Pavement (RAP). The fourth test lane was the control section consisting of 300-mm crushed stone (AB-3) base. The sections were paved with a 50-mm Superpave Hot-Mix Asphalt (HMA) layer. All sections were instrumented to measure the strains at the bottom of the HMA layer and stresses on top of the subgrade. The sections were loaded with 50,000 and 70,000 repetitions of an 80-kN single axle load of the Accelerated Pavement Testing (APT) machine. The failure rut depth was 12.5 mm. All sections except the control section had this rut depth by 10,000 repetitions. The calculated and measured responses show that on three test sections, stresses on top of the subgrade exceeded the unconfined compressive strength of the soil. The test sections were redesigned and reconstructed. The redesigned sections consisted of 100-mm geocell- reinforced bases, 50-mm cover, and an HMA layer of 100 mm. The same infill materials were used in the test sections. The control lane had a depth of 200 mm. These sections were also instrumented. All sections carried 1,200,000 repetitions of the 80-kN single axle loads with rut depths not exceeding 10 mm. Based on these results, a mechanistic-empirical design methodology for low-volume paved roads with geocell-reinforced bases is being developed.

1 INTRODUCTION

Low volumes road account for approximately 80% of the world's road infrastructure. A majority of these roads are farm-to-market roads. In Kansas, these roads have historically been surfaced with hot-mix asphalt (HMA). Due to dwindling budgets, highway and road agencies now have tighter budgets to maintain these low-volume roads and there is a need for economical innovations in their rehabilitation. Currently, most road reconstruction consists of stabilizing the subgrade, via mechanical compaction, the addition of a cement or lime (or combination of the two) stabilized subbase, placement of a thick base layer over the subgrade/subbase before placing the HMA layer. However, there is growing interest in the use of geosynthetics to reinforce the soil in different applications including road base construction.

Geosynthetics are defined by the American Society for Testing and Materials (ASTM, 2004) as, "a planar product manufactured from polymeric material used with soil, rock, earth, or other geotechnical engineering related material as an integral part of a man-made project, structure, or system." Different types of geosynthetics exist with different functions. These functions can be grouped as: separation, reinforcement, filtration, drainage, and containment (Koerner, 1994). Transportation engineers have been working on the use of geosynthetics in pavement structures since the mid 1970's. A combination of geotextile and geo-grid reinforcements has been shown to increase bearing capacity when placed over a weak subgrade and they can increase the load distribution capacity by confining the soil particles. Geocellular confinement systems (geocells) are a type of geosynthetic that have seen an increasing interest as reinforcement in the base courses of pavement structures.

Geocellular confinement systems (geocells) are three-dimensional (3-D) honeycomb-like structures filled with an in-fill of granular material, as shown in Figure 1. Such containment, or confinement, vastly improves granular material shear strength. The geocells are made of strips of polymer sheet or geotextile connected at staggered points so when the strips are pulled apart a large honey-comb mat is formed. These

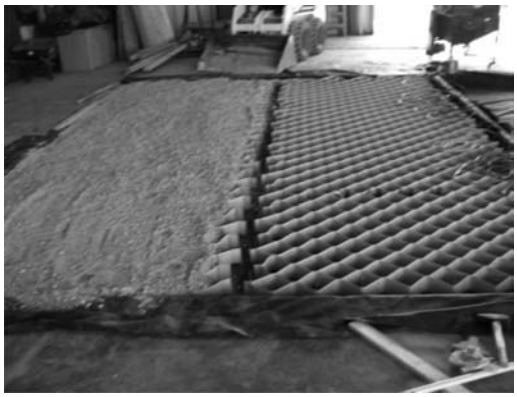

Figure 1. Geocellular confinement systems.

geocells provide both a physical containment of an in-fill geo material and a transfer of load through the geocells (Koerner, 1994). Geocells can protect a weak subgrade by reducing the penetration of base materials into the soft grade by high lateral confining stresses and contact wall friction of the cell and soil (Bathurst, 1989).

Originally, geocells were made from high-density polyethylene (HDPE) strips ultrasonically welded together. Currently, other materials are being used in manufacturing geocells. Geocells can be shipped to the job site in a collapsed configuration increasing shipping efficiency. At the job site, they are placed directly on the surface of the subsoil and propped open in an accordion fashion with an external stretcher assembly. They are then filled with an in-fill material and compacted (Koerner, 1994). Some advantages of using geocells include: construction expediency, low labor skill requirements, and low hauled-in tonnage requirements (Webster, 1979). Krishnaswamy et al. (2000) showed that geocells can be effective over soft clay foundations even with poor quality in-fill materials.

Currently, geocells, due to their 3-D structure, have more widespread use for confinement applications than any other planar geosynthetic reinforcement (Yuu et al., 2008). However, most studies have demonstrated the use of geocells for increasing bearing capacity and reducing settlement of soft soil foundations (Dash et al. 2001, Dash et al. 2003, Dash et al. 2004, and Sitharam et al. 2005). Even though these studies have demonstrated that geocells can provide outstanding soil confinement and perhaps enhance the performance of base courses on weak subgrade, the acceptance of geocells for unpaved and paved roads is still limited due to the lack of accepted design methods and research (Yuu et al., 2008). Bathurst and Jarrett (1989) showed that geocell-reinforced bases had higher load capacity over soft peat subgrades, while Giroud and Han (2004) showed that geocells can stiffen the base layer, reducing normal stresses while reorienting the shear stresses on the subgrade that limit the lateral movement of base material and subgrade soil. Thus, geocells have the possibility to be an economical option in rehabilitation of pavements by reducing base layer and HMA overlay thicknesses needed over a marginal or weak subgrade, and allowing the use of lower quality in-fill materials because of the confining nature of the geocell.

Results for geocells uses in foundation footings have been very positive. Dash et al. (2003 and 2004) showed the increase in bearing capacity of soft subgrade materials while reducing both surface heave and settlement. Geocells used in tandem with other geosynthetics, such as a geotextile or geogrid, have shown to strengthen the soil layer. In these studies, geocells worked by confining the failure wedges under load which typically develop in unreinforced soils. Movement of the soil is resisted by the tensile hoop strength developed by the geocells walls and the passive resistance of the full adjacent cells (Mandal and Gupta, 1994).

Some common problems often occur when reconstructing roadways over soft subgrade. The subgrade is usually over excavated so new subgrade and/or base material replaces the old subgrade. However, this can be difficult if there are shallow utilities in the area. Also in many areas, bridge clearances have to be maintained so raising the pavement elevation is not an option. If contractors are forced to keep the soft subgrade in place, they can treat the subgrade with a cementitious material that can be expensive. The subgrade can be mechanically stabilized with a compactor but this leaves the subgrade exposed to the climate which can delay the project in the event of rain. Geocells can be used to strengthen a subgrade and increase the resilient modulus without increasing the cross section of the pavement structure (Al-Qadi and Hughes, 2000).

In 2009, the University of Kansas and Kansas State University conducted joint research on unpaved geocell-reinforced bases over weak subgrade. The geocells and materials used in that test are the same that are being used in the current tests discussed in this paper. Three different base materials were used in that study: crushed stone (AB-3), reclaimed asphalt pavement (RAP), and quarry waste (Pokharel et al., 2011 and Han et al., 2010). The study resulted in the following conclusions for geocell-reinforced unpaved roads:

- A 170-mm geocell reinforced base can outperform a 300-mm crushed stone, AB-3 base.
- RAP was the best performing in-fill material in unpaved sections.
- Geocells increased the stress distribution angle (Pokharel et al., 2011).
- A thicker (50 mm to 75 mm) cover is needed to minimize traffic damage to the geocells (Han et al. 2010).

The need for full-scale and rapid testing of pavement structures has led to Accelerated Pavement Testing (APT) programs. APT can test new technologies and the impacts of these technologies on different pavement configurations. Lately, some departments of transportation in the western states such as, Oregon,

Utah, and California, have begun requiring APT for approval of geosynthetics in pavement projects.

2 STUDY OBJECTIVE

The main objectives of this study are to:

- Test a geocell design with different in-fill materials and a thin HMA overlay under real world traffic on a marginal subgrade, using accelerated pavement testing (APT).
- Develop a design method for geocell-reinforced paved roads considering the quality of the in-fill material.
- Construct a three-dimensional (3-D) finite element (FE) model using the commercial FE software *Abaqus*. The developed model will be calibrated with the results from the APT of the geocell-reinforced sections.
- Prepare recommendations to formulate a mechanistic design method for geocell-reinforced paved roads.

3 STUDY APPROACH

To achieve the study objectives, four lanes of pavement test sections were constructed at the Civil Infrastructure System Laboratory (CISL) of Kansas State University (KSU). Three out of these four lanes were geocell-reinforced and had different in-fill materials. The fourth test lane was the control section consisting of crushed stone, AB-3 base. Three types of in-fill materials including crushed limestone (AB-3), quarry by-products (QW), and reclaimed asphalt pavement (RAP), were used in this study. In the "first" test, the control and QW lanes were loaded with 70,000 repetitions and the AB-3 and RAP lanes were loaded with 50,000 repetitions of an 80-kN single axle. Due to excessive rutting, a thin overlay was placed over all sections. A thicker cross section for the "second" test was designed and constructed using the same in-fill materials. Those sections have been loaded with 1,200,000 repetitions without any failure.

4 FACILITY AND EQUIPMENT

CISL houses an accelerated pavement testing (APT) machine and three pits for constructing test sections. The reaction frame of the APT machine covers a distance of 12.8 m and applies an 80-kN single axle load with air-bag suspension on dual tires. The wheel assembly is belt driven by a 20-HP electric motor, while the load is controlled by hydraulic pressure. The tire pressure can be variable but 552 kPa was used in this study. The pits are approximately of the same size at 6.1-m long, 4.9-m wide, and 1.8-m deep. The moving wheel has a frequency of 0.167 Hz (i.e. six seconds per pass) at a speed of 11.3 km/hr with a constant speed over the length of the test pit (Lewis, 2008).

5 MATERIAL PROPERTIES

5.1 *Geocells and geotextile*

The geocells used in this study are NEOLOY™ polymeric alloy (nano-composite alloy of polyester/polyamide nano fibers, dispersed in polyethylene matrix) (NPA) geocell (Han et al., 2010). The polymeric alloy has a similar flexibility at low temperatures as HDPE, along with an elastic behavior similar to engineering thermoplastics. The NPA geocell had a wall thickness of 1.1 mm and two perforations of 350 mm^2 each on one pallet of the NPA geocell. The NPA geocells materials have a tensile strength of 19.1 MPa and secant elastic modulus of 355 MPa at 2% strain (Han et al., 2010). The tensile test was performed at 23°C and at a strain rate of 10% per minute. The geotextile used as a separator between the subgrade and the base was a 3.5-oz non-woven geotextile.

5.2 *Subgrade*

An AASHTO (American Association of State Highway and Transportation Officials) A-7-6 clay was used for the subgrade construction. The optimum moisture content of this material was 21% with a maximum dry density of 1,610 kg/m^3 (Han et al., 2010). In the first test, an approximate CBR of 6%, measured by dynamic cone penetrometer (DCP), was achieved in the pits at a moisture content of 21%. Plastic Limit (PL), Liquid Limit (LL), and percent finer than 75 μm sieve tests were found to be 22%, 43%, and 97.7%, respectively. The Plasticity Index was 21 (Bortz et al., 2011). In the second test, a CBR of 12% was achieved at a moisture content of 18%.

5.3 *Base course*

All infill materials used in this study were the same as those used in previous studies (Han et al., 2010 and Pokharel et al., 2011).

5.3.1 *AB-3*

Crushed limestone, AB-3, was used in the control section with no geocells as well in a test lane with geocell reinforcement. AB-3 is a well-graded base material that is used in a variety of low-volume road applications in Kansas. Pokharel et al. (2011) found a mean particle size of (d_{50}) of 4.4 mm, a coefficient of curvature of 1.55, and a coefficient of uniformity of 21. The maximum dry density and optimum moisture content of the material was 2,130 kg/m^3 and 10.2%, respectively and CBR was 45%. In the first test the AB-3 was compacted at a moisture content of 9.2% in the control lane and 9.0% in the geocell lane. In the second test, the AB-3 was compacted at a moisture content of 6.7% in the control lane and at 6.3% in the geocell-reinforced lane.

5.3.2 *Quarry waste*

About 22 million tons of crushed rock is produced in Kansas annually. It is estimated that about 35%

to 40% of this is reduced to fines commonly called quarry waste (QW). Some of this QW is used in hot-mix asphalt production or in agricultural applications, leaving leaves approximately 10% to 20% (2 million to 4.4 million tons) stockpiled or land filled annually in Kansas (Rockers and Moses, unpublished data). The QW in this study was sourced from a local quarry in Kansas. Pokharel et al. (2011) found the mean particle size (d_{50}) of 1.3 mm, a coefficient of curvature of 2.3, a coefficient of uniformity of 24, a maximum dry density of 2,060 kg/m^3, an optimum moisture content of 11%, and CBR of 19%. In the first and second tests, the QW was compacted at moisture contents of 10.6% and 6.8%, respectively.

5.3.3 *Reclaimed Asphalt Pavement (RAP)*

Nationwide, approximately 100 million tons of reclaimed asphalt pavement (RAP) is produced each year. Approximately 80 million tons is reused in various aspects of pavement construction (NAPA, 2011). The RAP in this study was collected from a local asphalt plant in Manhattan, Kansas. Han et al. (2010) found the RAP had a maximum dry density of 1,810 kg/m^3, an optimum moisture content of 6%, and a CBR value of 10% at 5% moisture content and 8% at the optimum moisture content. In the first and second tests, the RAP was compacted at moisture contents of 6.4% and 10.4%, respectively.

5.4 *Hot Mix Asphalt*

The base layer was paved over with a 50-mm hot-mix asphalt (HMA) layer for the first test. The HMA was produced and laid by a local asphalt contractor. A Superpave mixture with 12.5 mm nominal maximum aggregate size (NMAS) and fine gradation, known as SM-12.5A in the Kansas Department of Transportation (KDOT), was used. The aggregate blend consisted of 26% 19-mm rock, 17% 9.5-mm chips, 20% manufactured sand and 17% concrete sand. A PG 70-28 binder was used. The in-place density was 92% (2,250 kg/m^3) in the first test and 92% (2,259 kg/m^3) in the second test of the theoretical maximum specific gravity. The mixture air void content at N_{design} was 4.04%.

6 TEST SETUP

6.1 *Test sections*

In this study, two pits were divided into two lanes (6.1 m long by 2.45 m wide) each for a total of four lanes. For the first test, the subgrade for each lane was a clay (A-7-6) compacted to a CBR of about 6%. In the second test, the subgrade was compacted to a CBR of 12%. The latter CBR value of 12% was based on the analysis of in-situ DCP data from Kansas Department of Transportation projects. A non-woven geotextile was used to separate the base and subgrade. Based on the recommendations from Pokharel et al. (2011) and Han et al. (2010), the geocells were laid out in a near circular pattern with a dimension of 250 mm in the wheel direction (also the seam direction), 210 mm in the transverse direction and an height of 75 mm. The NPA geocells were filled and compacted, and then covered with 25-mm of infill material. This cover was considered too thin after noting that the geocells were exposed in some places during construction. The reinforced base layer was paved over with 50-mm HMA of a Superpave mixture with 12.5 mm NMAS as shown in Figure 2. The second test consisted of a thicker cross section of the reinforced and HMA layers. The height of the NPA geocells was increased to 100 mm with a 50-mm infill cover. The thicker in-fill cover helped in better compaction of the in-fill materials. The HMA layer thickness was increased to 100 mm of the 12.5-mm NMAS as shown in Figure 3.

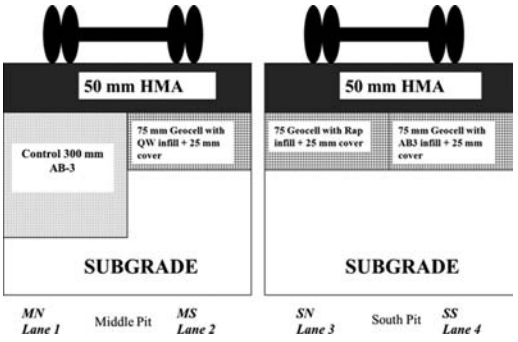

Figure 2. First test cross sections.

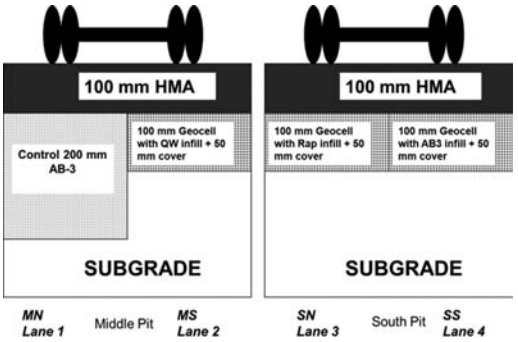

Figure 3. Second test cross sections.

The APT machine has the capabilities to wander laterally while applying passes. A wander of $\pm$150 mm was programmed into the machine. The wander was applied in a truncated normal distribution as shown in Figure 4. A full wander of +150 mm to −150 mm took 676 passes to complete.

6.2 *Instrumentation*

All four lanes were instrumented with pressure cells on top of the subgrade and two strain gauges at the bottom of the HMA layer. Thermocouples were also placed below the HMA layer. The NPA geocells were

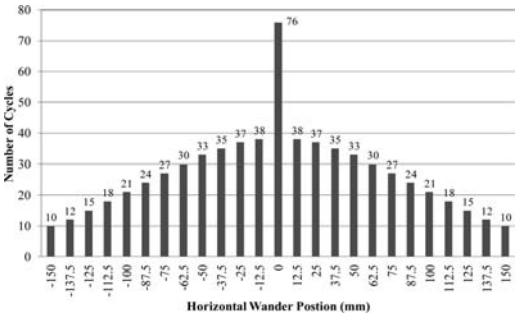

Figure 4. Truncated wander of APT machine.

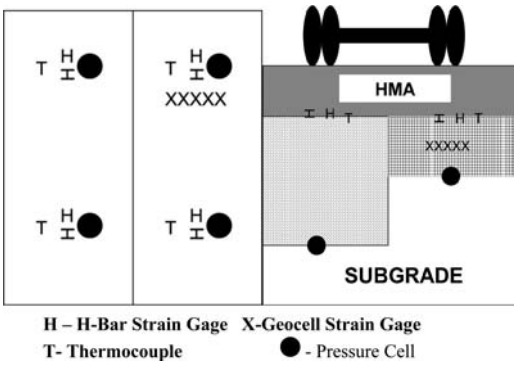

Figure 5. Instrumentation of test pits.

instrumented with five strain gauges per lane. The instrumentation layout is shown in Figure 5.

The pressure cells were Geokon Model 3500 cells. The H-Bar strain gauges were Texas Measurements TML-60-2L gauges epoxied to two pieces of aluminum to form the H-Bar as suggested by Lewis (2008). The thermocouples used were Type T. The strain gauges embedded on the body of NPA geocells were Vishay C2A-06-250LW-120. During placement of the HMA layer, some of the HBar gauges were damaged. Seventy-five percent of the gauges survived the initial construction.

7 ACCLERATED PAVEMENT TESTING RESULTS

7.1 *Rut depths*

All lanes were subjected to the moving wheel test. The rut depths were measured using a transverse profiler. The profiler is a 4.27-m long piece of aluminum tubing with a 50-mm square cross section. A Chicago Dial Indicator digital gauge is mounted to a movable slide on the beam. The gauge produces a digital output and sends the data to a spreadsheet. Three fixed reference points, at every 1.5 m of lane length, were placed on the HMA on the outside of the lanes. Measurements were taken every 12.5 mm across the middle 3,650 mm

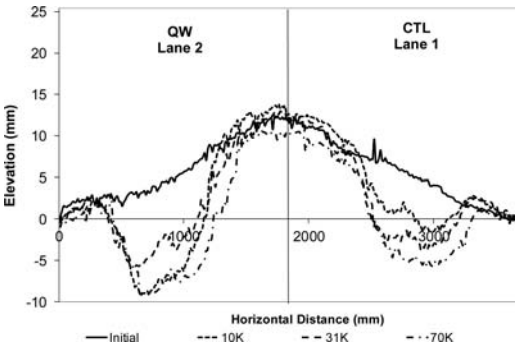

Figure 6. Typical profiles of test lanes (Control and QW) in the middle pit during the first test.

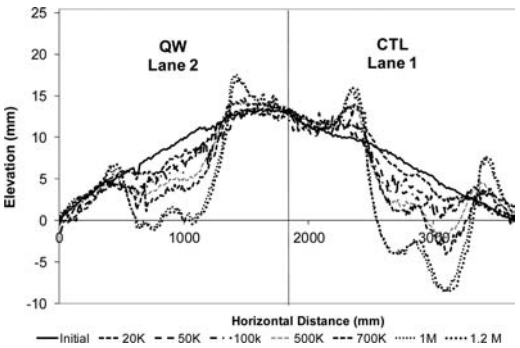

Figure 7. Typical profiles of test lanes (Control and QW) in the middle pit during the first test.

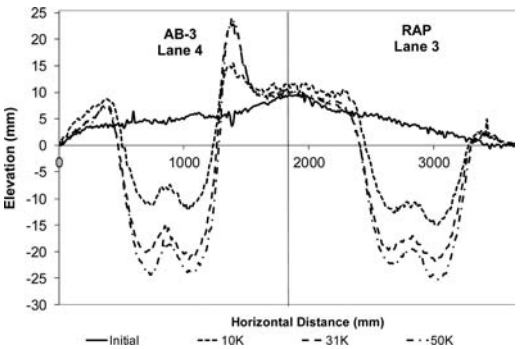

Figure 8. Typical profiles of test lanes (AB-3 and RAP) in the south pit during the first test.

(Lewis 2008). Typical profiles for each pit can be seen in Figures 6 through 9.

In the first test, the QW lane heaved at an isolated area after 10,000 passes. The rut depths at the blow out at 10,000 and 20,000 passes were 13 mm and 18 mm, respectively, as shown in Figure 10. An attempt was made to repair the heave using asphalt-patching materials. However, heaving continued and after another 10,000 passes, a 12.5-mm thick steel plate was used to cover the area of heaving. This was necessary to continue testing for the rest of the QW lane and the

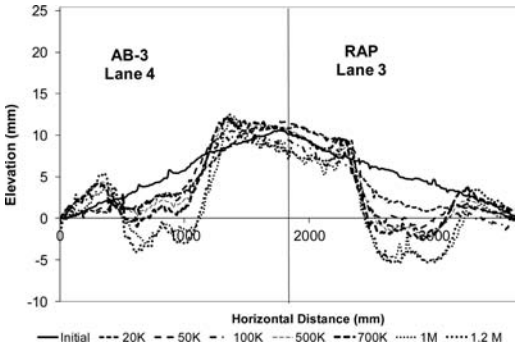

Figure 9. Typical profiles of test lanes (AB-3 and RAP) in the south pit during the second test.

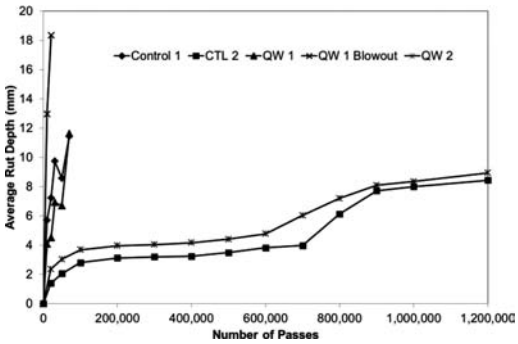

Figure 10. Middle pit rut depths.

control lane. Some of the materials placed in the rut to support the plate were pushed into the wheelpath in the QW lane. This decreased the rut depth as illustrated in Figure 10. However, by 70,000 passes, the rutting had returned to its original depth before the plate was placed over the heaved area. The heave was later found to have been caused by subgrade failure. No geocells were found at that locale when part of the HMA was removed.

The middle pit (containing control and QW lanes) received 70,000 passes while the south pit (RAP and geocell-reinforced AB-3) received only 50,000 passes due to scheduling of a 38-mm overlay. The failure rut depth was 12.5 mm. All sections except the control section had this rut depth by 10,000 repetitions. The overlay results are not presented in this paper.

In the second test, most of the rutting occurred in the first 50,000 passes but the rut depths were considerably lower than the failure rut depth. The comparable average rut depths can be seen in Figures 10 and 11. The average rut depth was calculated using the rut depths at the middle 125 mm of the wheel path across three different places. The second test did not result in rut depths over 10 mm after 1,200,000 passes.

7.2 *Vertical Stress*

Pressure cells were placed above the subgrade and just below the geotextile. The pressure was recorded for a

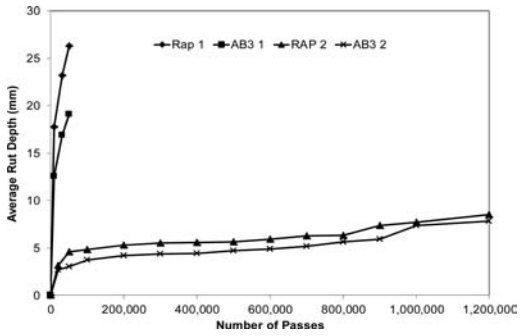

Figure 11. South pit rut depths.

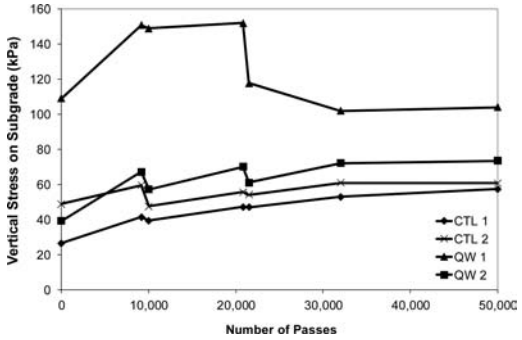

Figure 12. Vertical stress results in the middle pit during the first test.

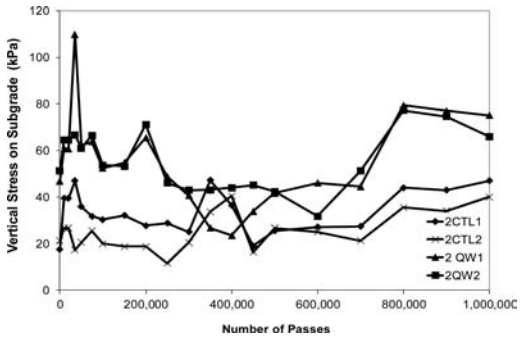

Figure 13. Vertical stress results in the middle pit during the first test.

full wander cycle (676 passes). The top 50 peak pressures were averaged and are presented in Figures 12 through 15. In the first test, after repeated loads, the stress on the QW section increased rapidly and then remained somewhat constant. This high stress coincided with the heaving observed on this section. It should be noted that the stress at 10,000 repetitions is much higher than the unconfined compressive strength of 105 kPa of the subgrade soil. The stress decreased after repair of the section and placement of the plate. It then increased slowly for the remainder of the test.

The pressure cell results were much lower in the second test. This was expected due to the increase in total

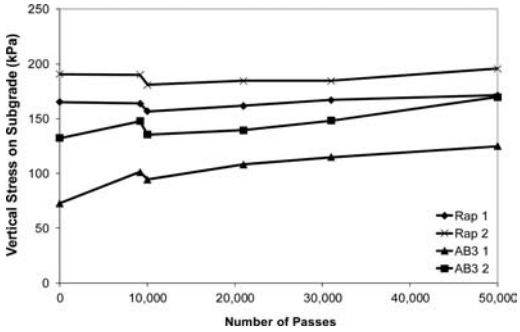

Figure 14. Vertical stress results in the south pit during the first test.

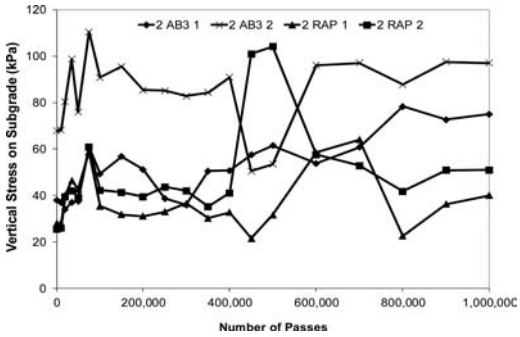

Figure 15. Vertical stress results in the south pit during the second test.

pavement thickness above the subgrade, resulting in applied stresses well below the unconfined compressive strength of the subgrade. The control lane, and thickest section, produced the lowest pressure on the subgrade, as expected.

7.3 *FWD testing and data analysis*

Falling weight deflectometer (FWD) tests were performed on the paved sections. During FWD testing, seven sensors were used at offset locations of 0, 203, 305, 457, 610, and 914 mm. From the FWD results, the modulus of each layer was backcalculated using the software package *EVERCALC* from the Washington State Department of Transportation. To minimize the root mean square (RMS) error, deflections from only the first four sensors were used in the backcalculation process. This choice of sensors was used to take into account the shallow subgrade (the CISL APT pits are underlain by a 230-mm thick reinforced concrete slab) and the effects of the concrete walls of the pits. Experience has shown that this confinement tends to affect only the outer sensors. The layer moduli were used in the *KENPAVE* software in the *KENLAYER* program for computing strain at the bottom of the HMA layer and stress at the top of the subgrade. The calculated responses were compared with the measured responses under the moving wheel load. Tables 1 and 2 list these responses. The control

Table 1. *KENLAYER* comparison of pressure on subgrade.

	Pressure on subgrade			
	Control Lane 1		QW Lane 2	
First Test				
KENLAYER (kPa)	58.3		121.7	
Sensor	1	2	3	4
Measured (kPa)	29.5	54.1	130.0	56.6
% Difference	49.5%	7.3%	−6.8%	53.5%
Second test				
KENLAYER (kPa)	39.9		43.2	
Sensor	1	2	3	4
Measured (kPa)	32.2	22.9	52.8	54.4
% Difference	19.3%	42.5%	−22.1%	−25.8%
	RAP Lane 3		AB3 Lane 4	
First test				
KENLAYER (kPa)	130.5		132.0	
Sensor	1	2	3	4
Measured (kPa)	186.1	222.6	92.5	157.4
% Difference	−42.6%	−70.6%	29.9%	−19.2%
Second test				
KENLAYER (kPa)	52.2		54.1	
Sensor	1	2	3	4
Measured (kPa)	46.4	81.3	35.2	48.2
% Difference	11.0%	−56.0%	35.0%	10.9%

lane had the lowest pressure on the subgrade from both calculation and measurements since it is thicker than the rest. Overall, the second test produced response results closer to the predicted values than the results from the first test. This was attributed to the thin layers and high load levels.

7.4 *Strain at the bottom of the HMA layer*

The strain at the bottom of the HMA layer was measured using the H-Bar strain gauges. Table 2 lists both calculated and measured strains. The measured strain is the average recorded by the surviving strain gauges in each lane. The high strain measured in the QW lane was a prelude to the heaving in the first test. The lower than expected strain in the RAP and AB-3 lanes could be attributed to the beam effect described by Pokharel et al. (2011) and Han et al. (2010). The base and HMA layers acted like a beam and moved together reducing the strain at the interface. This strain was significantly reduced in the second test due to the higher HMA thickness.

As can be seen in the rutting, stress, and strain results, the control outperformed the reinforced section in the first test. After some theoretical calculations using *KENLAYER*, the control section was considered to be "overdesigned" compared to the reinforced sections. The vertical stress on the subgrade and strains below the HMA in reinforced sections were calculated

Table 2. *KENLAYER* comparison of strain at the bottom of HMA Layer.

	Micro strain (Below HMA)			
	Control	QW	Rap	AB3
First test				
KENLAYER	−363	−857	−922	−902
Measured	−369	−633	−429	−273
% Difference	−1.62%	−638%	53.45%	69.75%
Second test				
KENLAYER	−162	−190	−246	−254
Measured	−140	−146	−220	−220
% Difference	13.90%	23.04%	14.90%	13.21%

to be over 200% higher than that of the control section. The results of the overdesign of the control section lead to the reduction of the control thickness in the second test. The variation of strains in the first test was again attributed to the combination of thin layers and heavy load.

8 FINITE ELEMENT MODELING

Finite element modeling (FEM) is a numerical method that provides approximations to solutions to boundary value problems. The anticipated FEM in this study will include lessons and information from previous modeling efforts. The asphalt pavement layer will be modeled using a creep model as suggested by Onyango (2009) along with non-linear modeling of the subgrade per Hadi and Bodhinayake (2003). The base layer, subgrade, and geocell material properties will be modeled using validated properties proposed by Yang (2010), Pokharel et al. (2011), and Han et al. (2010) since the materials used are the same in all studies. The loading will follow Onyango (2009) with 80-kN load and wheel wander.

The asphalt material properties will be derived from laboratory testing. *Abaqus* has no predefined parts such as the *FLAC*^{3D} geogrid. The geocell models will need to be developed within *Abaqus*. The anticipated process for this will include partitioning the base layer in the shape of the geocells and applying skin reinforcement to the partitioned sides, as shown in Figure 16. This will enhance the results of the shapes of the geocells compared to the diamond shapes used by Yang (2010).

In the part module, each section will be built with the appropriate (three) layers. The step module will be used to apply a pressure load of 552 kPa on two tire prints 208 mm wide and the entire length of the studied section as shown in Figure 17. The load will be applied in the simplified fashion (Huang, 1995; Hua, 2000; and Fang, 2001). The speed of the APT machine translates into a load duration of 0.05 seconds per pass. The boundary conditions will be fixed at the bottom (encastre: $U1 = U2 = U3 = UR1 = UR2 = UR3 = 0$),

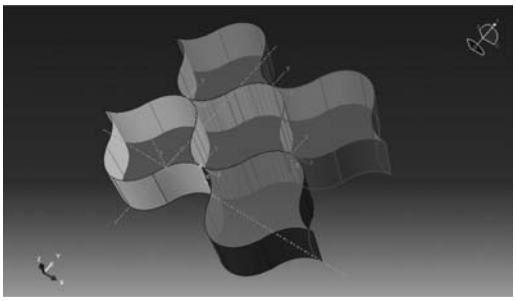

Figure 16. Geocell part.

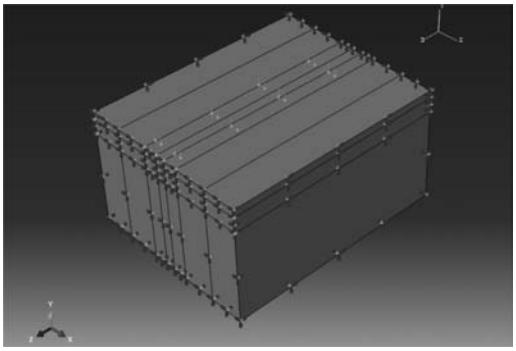

Figure 17. Pit assembly.

while the axi-symmetry ($U1 = UR2 = UR3 = 0$), will simulate the other half of the lane. To simulate the longitudinal distance of the lane, Z-Symmetry ($U3 = UR1 = UR2 = 0$) will be used on the sides parallel to the x-axis, as shown in Figure 17.

9 CONCLUSIONS

In this study, three polymeric alloy geocell reinforced bases with quarry waste, reclaimed asphalt (RAP), and crushed limestone (AB-3) as in-fill materials, and one control section with AB-3 base course were studied under accelerated pavement testing. The first test involved "thin" cross sections, which rutted and failed prematurely. High stresses and strains were recorded in this first test. In the second test "thicker" cross sections were built and performed very well. In the second test, all the sections were loaded with 1,200,000 passes, and lower stresses and strains were recorded along with less rutting. The following conclusions can be drawn from this study.

- A 50-mm cover over the geocells ensures a better compaction and simplifies construction.
- A 75-mm thick geocell reinforced base layer approaches the maximum capacity of the geocells with a thin HMA overlay. A 100-mm thick geocell enhances the load-bearing capacity of the base layer.

– The subgrade must be protected in order to ensure better performance of the paved road. The applied stress on top of the subgrade should be less than the unconfined compressive strength of the soil.
– A 50 mm HMA layer is too thin for the standard wheel load. A minimum thickness of 100 mm for the HMA layer is recommended for geocell pavements similar to those described in this paper. The thicker HMA layer spreads the vertical stress over a wider area.
– Geocells are a viable tool for low-volume road maintenance and reconstruction when designed and constructed properly. Cost/benefit ratios are being calculated for the consideration of geocells.

ACKNOWLEDGEMENTS

This project was funded by the Midwest States Accelerated Pavement Testing Pooled Funds Program. PRS Mediterranean, Ltd. in Israel gave continued support throughout the study and provided the NPA geocells. The authors would like to thank Mr. Randy Testa, Mr. Luke McIntosh, and Ms. Quinn Stenzel for help during the lane construction and testing. Professor Jie Han of the University of Kansas and his students passed along the knowledge learned in a previous study and helped in the construction of the geocell layers.

REFERENCES

ASTM D 4439-04. 2004. *Standard terminology for geosynthetics ASTM*. Philadelphia, PA.

Al-Qadi, I.L. and Hughes, J.J. 2000. Field evaluation of geocell use in flexible pavements. *Transportation Research Record, Vol. 1709*, pp. 26–35.

Bathurst, R.J. and Jarrett, P.M. 1989. Large-scale model tests of geocomposite mattresses over peat subgrades. *Transportation Research Record, Vol. 1188*, pp. 28–36.

Bortz, B.S., Hossain, M., Halami, I. and Gisi, A. 2011. Innovative uses of quarry waste and reclaimed asphalt pavement, *Proceedings of the International Conference on Sustainable Design and Construction*, Kansas City, Missouri, March.

Dash, S.K., Rajagopal, K. and Krishnaswamy, N.R. 2001. Strip footing on geocell reinforced sand beds with additional planar reinforcement. *Geotextiles and Geomembranes, Vol. 19, No.8*, pp. 529–538.

Dash, S.K., Sireesh, S. and Sitharam, T.G. 2003. Model studies on circular footing supported on geocell reinforced sand underlain by soft clay. *Geotextiles and Geomembranes, Vol. 21, No. 4*, pp. 197–219.

Dash, S.K., Rajagopal, K. and Krishnaswamy, N.R. 2004. Performance of different geosynthetic reinforcement materials in sand foundations. *Geosynthetics International, Vol. 11, No. 1*, pp. 35–42.

Fang, H. 2001. *Rational approach to rutting rehabilitation decisions*. Ph.D. Dissertation, Purdue University, West Lafayette, IN.

Giroud, J.P. and Han, J. 2004. Design method for geogrid-reinforced unpaved roads. I. Development of Design Method. *ASCE Journal of Geotechnical and Geoenvironment Engineering, Vol. 130, No. 8*, pp. 775–786.

Hadi, M.N.S. and Bodhinayake, B.C. 2003. Non-linear finite element analysis of flexible pavements. *Advances in Engineering Software, Vol. 34*, pp.657–662.

Han, J., Pokharel, S.K., Yang, X.M., Manandhar, C., Leshchinsky, D., Halahmi, I. and Parsons, R.L. 2010. Performance of geocell-reinforced RAP bases over weak subgrade under full-scale moving wheel loads. Invited for a special issue, submitted for possible publication *in Journal of Materials in Civil Engineering, ASCE, 2010*.

Hua, J. 2000. *Finite element modeling analysis of accelerated pavement testing devices and rutting phenomenon*. Ph.D. Dissertation, Purdue University, West Lafayette, IN.

Huang, H. 1995. *Analysis of accelerated pavement tests and finite element modeling of rutting phenomenon*. Ph.D. Dissertation, Purdue University, West Lafayette, IN.

Koerner, R.M 1994. *Designing with geosynthetics. Third Edition*, Prentice Hall, New Jersey.

Krishnaswamy, N.R., Rajagopal, K. and Madhavi Latha, G. 2000. Model studies on geocell supported embankments constructed over a soft clay foundation. *Geotechnical Testing Journal, Vol.23, No. 1*, March, pp. 45–54.

Lewis, P. 2008. Lessons learned from the operations management of an accelerated pavement testing facility. *Proceedings of the 3rd Intl. Conference On Accelerated Pavement Testing*, Madrid, Spain, October.

Mandal, J.N. and Gupta, P. 1994. Stability of geocell-reinforced soil. C*onstruction and Building Materials. Vol. 8, No. 1*, pp. 55–62.

MAPA. *Asphalt Pavement Recycling Facts*. <http://moasphalt.org/facts/environmental/facts.htm> Jan. 11, 2011.

Onyango, M. 2009. *Verification of mechanistic prediction models for permanent deformation in asphalt mixes using accelerated pavement testing*. Ph.D. Dissertation, Kansas State University, Manhattan, KS.

Pokharel, S.K., Han, J., Manandhar, C., Yang, X.M., Leshchinsky, D., Halahmi, I. and Parsons, R.L. 2011. Accelerated pavement testing of geocell-reinforced bases over weak subgrade. *Proceedings of the 10th International Conference on Low-Volume Roads*, July 24–27, Lake Buena Vista, Florida, USA.

Sitharam, T.G., Sireesh, S. and Dash, S.K. 2005. Model studies of a circular footing supported on geocell-reinforced clay. *Canadian Geotechnical Journal, Vol. 42, No. 2*, pp. 693–703.

Webster, S. 1979. *Investigation of beach sand trafficability enhancement using sand-grid confinement and membrane reinforcement concepts; Report 1, sand test sections 1 and 2*. Technical report GL-79-20. U.S. Army Engineer Waterways Experiment Station Geotechnical Laboratory.

Yang, X. 2010. *Numerical analyses of geocell-reinforced granular soils under static repeated loads*. Ph.D. Dissertation, University of Kansas, Lawrence, KS.

Yuu, J., Han, J., Rosen, A., Parsons, R.L. and Leshchinsky, D. 2008. Technical review of geocell-reinforced base courses over weak subgrade. *Proceedings of the First Pan American Geosynthetics Conference and Exhibition*, March 2–5, Cancun, Mexico.

This page intentionally left blank

Advances in Pavement Design through Full-scale Accelerated Pavement Testing – Jones, Harvey, Mateos & Al-Qadi (Eds.)
© 2012 Taylor & Francis Group, London, ISBN 978-0-415-62138-0

Accelerated pavement testing of two flexible road pavements to assess long-term structural performance

J. Ritter, R. Rabe & A. Wolf
Federal Highway Research Institute, Bergisch Gladbach, Germany

ABSTRACT: This paper presents the results of an accelerated pavement testing project conducted by Germany's Federal Highway Research Institute (BASt). The main objective of the project was to evaluate the long-term structural performance of flexible road pavements under simulated heavy vehicle traffic. For this purpose two test sections of different strengths were subjected to dynamic impulse generator loading to simulate heavy vehicle loading. During loading, the condition of the pavement was monitored by periodic deflection measurements with a Falling Weight Deflectometer (FWD) and measurements of the transverse profile. Embedded sensors provided information on the dynamic mechanical response of the pavement under loading. The results showed a significant increase in the elastic strain at the bottom of the asphalt base course and a decrease in the bearing capacity. Furthermore structural bottom-up cracking in the asphalt base course was detected. A first approach to estimate the vertical propagation of cracks in asphalt pavement layers on the basis of the measured FWD surface deflections is presented.

1 INTRODUCTION

The maintenance of the German federal trunk road network is a task of increasing urgency. The network comprises about 12,800 km (7,954 mi) of federal highways and more than 41,000 km (25,476 mi) of federal trunk roads. Due to its central location in Europe and the expansion of the European domestic market, current studies predict further growing numbers of heavy vehicle road traffic (Progtrans, 2007). Additionally the age structure of the pavements, in particular in the old federal states of Germany, shows that a substantial part was built more than 30 years ago (BMVBS, 2011). These circumstances imply a heavy burden for the maintenance of the federal trunk road network and a demand for a systematic and efficient use of limited financial resources for road maintenance measures.

The German Federal Highway Research Institute BASt currently carries out a comprehensive research program of full-scale accelerated pavement testing at BASt's indoor pavement test facility to provide scientifically based knowledge about the long-term structural performance of flexible road pavements Ritter, 2010). The test facility allows the dynamic testing of entire road pavement structures under controlled environmental conditions.

This paper describes the results from the testing of two flexible road pavements of similar construction type but different thickness and strength, built according to the German pavement design guide RStO 01 (FGSV, 2001a).

The main objectives of the project are the description of the structural performance under continuous accelerated simulated traffic loading until failure, with emphasis on the long-term performance of bearing capacity, and the description of the influence of construction properties on structural performance. This fundamental research is intended to provide a basis for the later development of performance models for the structural condition assessment of flexible road pavements.

2 RESEARCH PROGRAM AND EQUIPMENT

2.1 *Research program*

The test sections were subjected to a continuous simulated heavy vehicle traffic loading to achieve structural failure. The condition of the test pavements was monitored with non-destructive measuring methods including transverse surface profile measurements with a laser profilometer and deflection measurements using a falling weight deflectometer (FWD) at regular intervals.

Surface deflections were measured in the center of the rectangular loading area and in the unloaded area of each test section. The measuring point in the unloaded area was used as a reference point to evaluate the influence of temperature changes. Strain gauges and soil pressure cells, installed at various depths in the pavement, were used to measure dynamic mechanical responses of the pavement under loading. Thermocouples recorded the temperatures at different depths in the asphalt layers.

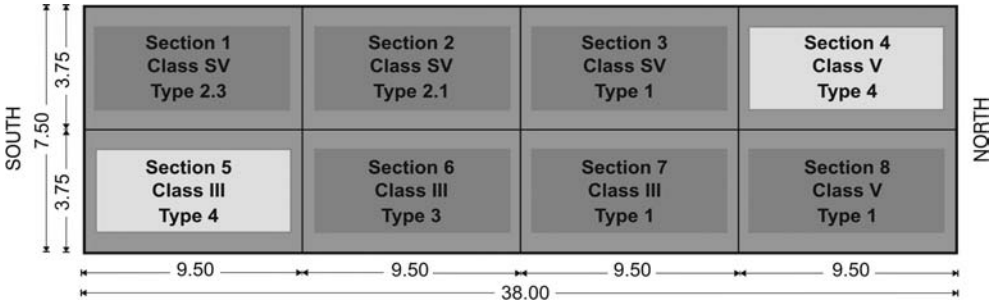

Figure 1. Plan view of the test track and the test sections.

After completion of loading, asphalt samples were taken from the weaker sections to determine changes in the layer thickness and to analyze cracking.

2.2 *Test pavement construction*

The accelerated testing was performed at the Federal Highway Research Institute's full-scale pavement test facility. The test facility consists of a concrete tank, 38 m (125 ft.) long, 7.5 m (24.5 ft.) wide, and 3.5 m (11.5 ft.) deep, which can accommodate entire pavement structures from the subsoil to the wearing course.

The current test track is divided into eight sections, each 9.5 m (31.2 ft.) long and 3.75 m (12.3 ft.) wide (see Figure 1). Two steel frames, each carrying one hydraulic impulse loading generator, can move forwards and backwards on two rails parallel to the test track. The entire test facility is located inside an air-conditioned laboratory, which allows testing under controlled climatic conditions. The air conditioning system is set to maintain an average air temperature of 20°C (68°F). During testing, the air temperature varied between 15°C (59°F) and 25°C (77°F). The simulation of a changing ground water level was not part of the program. The ground water level was kept below the formation level more than 90 cm (35.4 in.) below the pavement surface during the test program.

In the scope of this project, test Sections 4 and 5 were subjected to continued simulated heavy vehicle loading. These sections were constructed according to Construction Type 4 "asphalt base and gravel base on a subbase" of the German pavement design guideline RStO 01 (FGSV, 2001a) for flexible road pavements (see Figure 2). Both pavements had a 4 cm (1.6 in.) thick stone mastic asphalt SMA 0/8 S (Pen 50/70 binder type) wearing course for heavy vehicle traffic. Section 4 had an 8 cm (3.1 in.) thick asphalt concrete AC 0/22 CS (Pen 70/100 binder type) base course laid on a 20 cm (7.9 in.) gravel/sand base 0/32. The 58 cm (22.8 in.) strong subbase consisted of the same gravel/sand-mixture used for the base. Section 5 featured an additional 4 cm (1.6 in.) thick asphalt concrete AC 0/16 S binder course on a 10 cm (3.9 in.) asphalt base. Furthermore the aggregate base and subbase of Section 5 were built with a higher bearing capacity

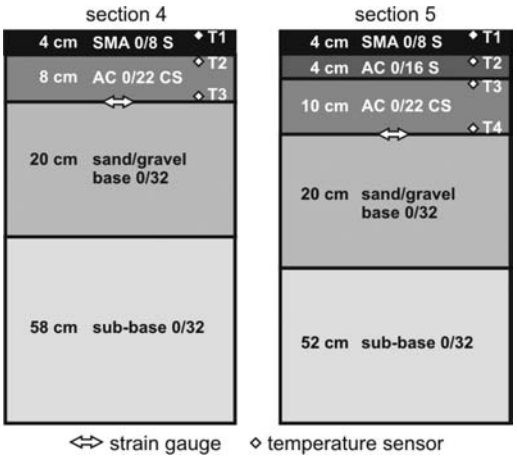

Figure 2. Cross-section of pavements in Section 4 and 5.

compared to Section 4. The bearing capacity was determined using the static plate load test with a maximum load of 50 kN on a circular loading plate with 30 cm (11.8 in.) diameter.

According to the RStO 01 (FGSV, 2001a) the pavement in Section 4 was designed for up to $0.3 \cdot 10^6$ 10-t-ESALs over a design service life of 30 years (RStO 01 Construction Class V), whereas the stronger pavement in Section 5 was designed for up to $3.0 \cdot 10^6$ 10-t-ESALs (RStO 01 Construction Class III).

The test sections each had a uniform depth of 90 cm (35.4 in.) from the surface of the asphalt pavement to the surface of the subgrade. The actual pavement was constructed inside a concrete tank with a total depth of up to 3.5 m (11.5 ft.). Layers of filter gravel, subsoil (silt) and granular subgrade were placed in the concrete tank, followed by the actual road pavement of 90 cm (35.4 in.) thickness.

With the exception of the asphalt binder and the asphalt wearing course, which were laid by paver and compacted with vibrating rollers, the asphalt base course, the granular subbase and the subgrade were placed manually and compacted with a plate vibrator.

All materials were in accordance, at the time of construction, with the valid German regulations ZTV Asphalt-StB 01 (FGSV, 2001b) and ZTV T-StB

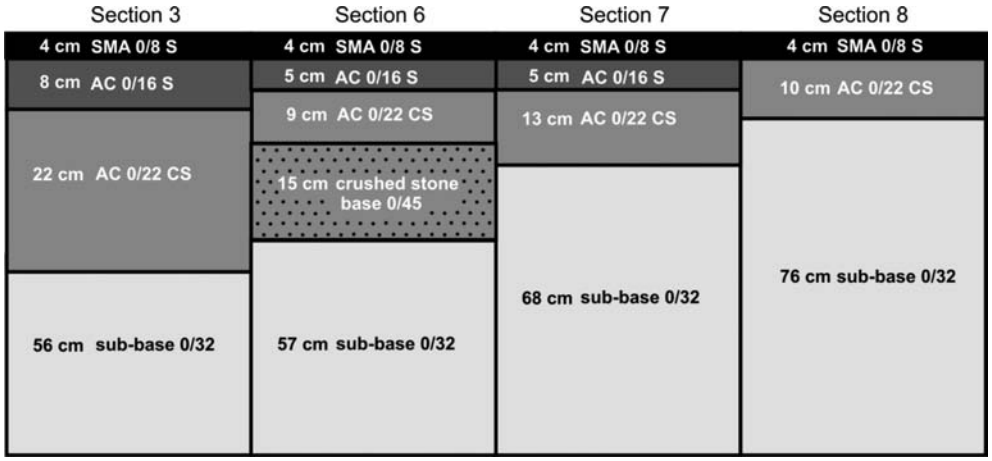

Figure 3. Cross-section of pavements on Sections 3, 6, 7 and 8.

(FGSV, 2002) with the exception of minor variations. Control checks during construction showed that all technical regulation requirements were met at almost all of the test points. Only a few test points showed that the bulk density of the asphalt wearing course and asphalt base course as well as the deformation modulus and the density of the granular base fell slightly below the required values. These anomalies was attributed mostly to the manual compaction, but were considered acceptable and thus accepted.

Deflection data from FWD measurements on Sections 3, 6, 7, and 8 (Figure 3) were used to establish a cracking prediction model described in Section 4.4 below.

Sections 3, 7, and 8 were built according to Construction Type 1 "asphalt base course on a granular subbase course" according to the RStO 01 (FGSV, 2001a) for flexible road pavements. The construction of the pavements varies according to the particular construction class (see Figure 3). The construction of Section 6 refers to Construction Type 3 "asphalt base course on a coarse aggregate base on granular subbase" according to the RSt0 01.

2.3 *Test section instrumentation*

The pavement was equipped with sensors for measuring the mechanical response of the structure under loading (Rabe, 2004). These sensors were purpose-designed and manufactured for accelerated pavement testing at the Federal Highway Research Institute (Rabe, 2004). This paper considers only the strain measurements in the longitudinal direction at the bottom of the asphalt base inside the loading area, and the asphalt temperatures measured with thermocouples.

The construction of the strain sensor is shown in Figures 4 and 5. The sensor consists of two strain gauges fixed on each side of a strip of fiber reinforced epoxy resin. The use of two strain gauges within a bridge circuit allows the compensation of unwanted bending strain of the sensor. The strain gauges are shielded with

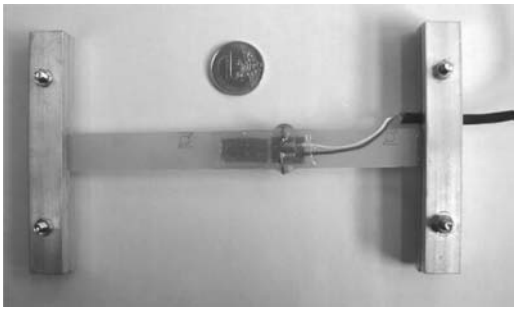

Figure 4. Asphalt strain gauge without cover (Rabe, 2004).

Figure 5. Asphalt strain gauge with cover (Rabe, 2004).

an aluminum profile to protect them from mechanical impact and hot asphalt during paving. Forces are transmitted from the asphalt to the strain gauges via anchor profiles at both ends of the sensor (Rabe, 2004). The strain gauges were installed in both longitudinal and transverse directions at the bottom of the asphalt base course (see Figure 2).

Embedded thermocouple elements were used to measure the temperature at various depths inside the asphalt layers in each test section (Rabe, 2004).

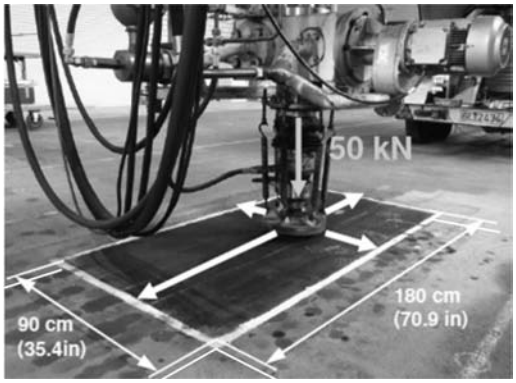

Figure 6. Hydraulic impulse generator and loading area.

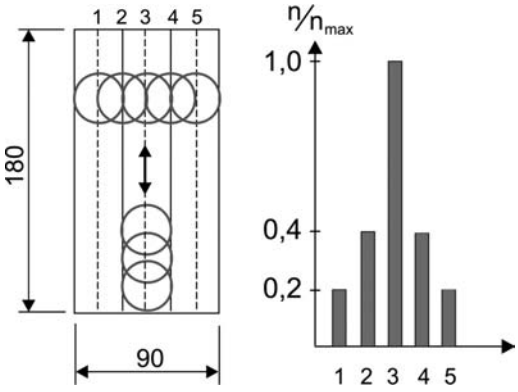

Figure 7. Lateral distribution of the impulse pattern.

2.4 *Loading equipment used on the test sections*

A mobile hydraulic impulse generator was used for the loading of the test sections (Figure 6). The impulse generator simulates a moving wheel by applying short impulses to the pavement surface while continuously moving forwards and backwards in a longitudinal direction at a speed of 2 mm/s and a frequency of approximately 120 impulses per minute.

The impulse load of 50 kN is transmitted to the pavement via a 2 cm (0.8 in.) rubber layer underneath the impulse generator loading plate, resulting in an average contact pressure of 0.707 MPa at a given radius of the loading plate of 15 cm (6.0 in.). The duration of the load impulse is 0.025 s; followed by a rest period of 0.414 s.

Only a partial area of the test section was loaded, termed the "loading area". The dimensions of the loading area are 180 cm (70.9 in.) in length and 90 cm (35.5 in.) in width (Figures 6 and 7).

To simulate in-situ lateral wheel wander the impulse generator allows a shift of ±45 cm from the center line of the loading area in a lateral direction. The loading was distributed over five parallel tracks with a spacing of 15 cm (6.0 in.) between the centerline of each track according to the distribution shown in Figure 7.

For the interpretation of measuring results, a representative number of load repetitions, N, was determined to account for the center position of the measuring points. N is calculated using the complete number of impulses in the center track and half the number of impulses in the adjacent tracks on either side.

Due to the very different nature of the impulse loading and the impact of a passing wheel, it is not possible to establish an accurate equivalency between the number of load impulses and the number of passing wheels. Therefore, the described number of load repetitions N was used for the following evaluations.

Further information on the BASt APT equipment can be obtained from (Rabe, 2004 and 2008).

3 RESULTS AND DISCUSSION

3.1 *General information*

Loading was halted on Section 4 after about 14 million impulses when surface deflections indicated no further increase in deflection. The loading of Section 5 had to be interrupted due to technical reasons after approximately 32 million load impulses. At this point measuring results indicated continuing increases in deflection. No specimens were taken from Section 5 after completion of this loading cycle so as to provide an undisturbed pavement for continuing loading in a follow-up project.

3.2 *Structural damage*

After the loading of Section 4 terminated 11 beams 130 cm (51.2 in.) × 15 cm (6.0 in.) × 13 cm (5.1 in.) were cut from the asphalt pavement and analyzed visually in a forensic study. Distinctive cracking was clearly visible in the asphalt base course. Figure 8 shows beam sample #7 which was located near the center of the loading area (see Figure 9). The sample exhibits numerous longitudinal bottom-up cracks distributed in a lateral direction.

The cracks originated from the bottom of the asphalt base and propagated upwards, mainly along larger grains inside the bituminous mortar. The cracks stop at the interface between the asphalt wearing course and asphalt base course. No penetration into the asphalt wearing course was observed.

Occurrence of cracks in the loaded area was general higher than in the unloaded area. A strict relationship between the position of the crack's origin on the sample and the lateral load distribution could not be derived.

Figure 10 provides information on the average length of the cracks as a function of the lateral position of the sample. The term "vertical length" refers to the vertical length of the crack measured from the bottom of the asphalt base course to the top end of the crack. The growth of the crack parallel to the asphalt surface was not considered. The result shows that analogous

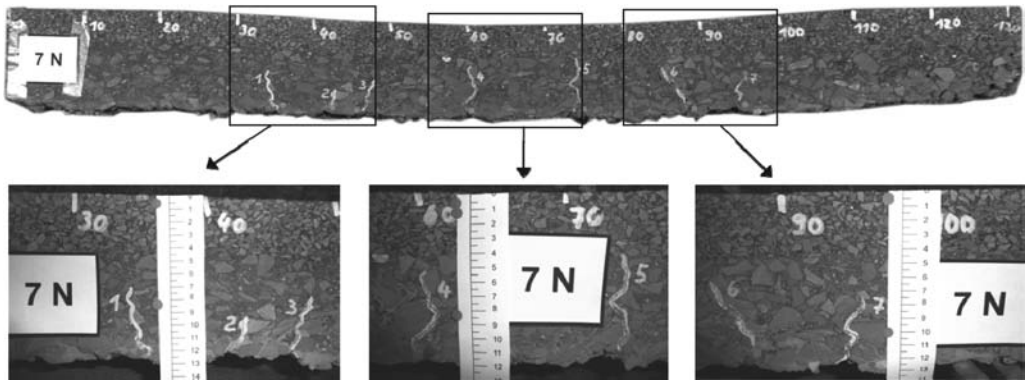

Figure 8. Example for crack propagation originating from the bottom of the asphalt base course (sample 7N).

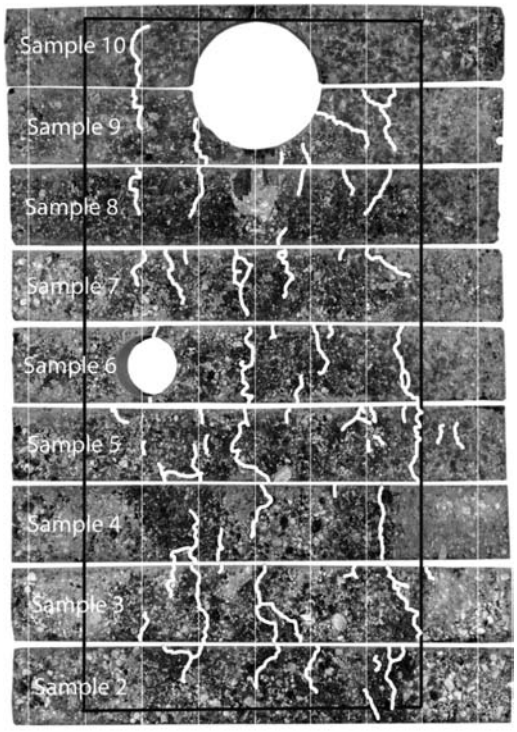

Figure 9. Cracking at the underside of the asphalt base course (vertical grid: 15 cm, cracking highlighted, loading area marked).

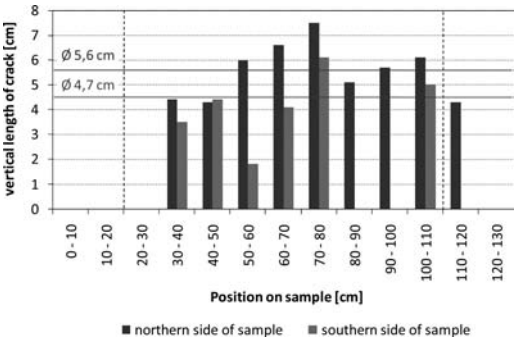

Figure 10. Average vertical length of cracks in the asphalt base course as a function of the lateral position and the side of the sample (loading area and average value of crack length are marked).

to the lateral load distribution, the length of the cracks decreases with increasing distance from the center of the loading area.

The crack mapping at the bottom of the asphalt base course was reconstructed by joining the photographs of the single samples together. The resulting cracking map is presented in Figure 9. Cracks, the borders of the loading area, and a 15 cm (6.0 in.) grid are highlighted.

Figure 9 shows that most cracks do not continue across the whole length of the asphalt base in the longitudinal direction. Some cracks can be traced over a large number of asphalt samples whereas a substantial part of the cracks end in between adjacent samples. Overall, the crack pattern suggests a predominantly longitudinal progress of cracks at the underside of the asphalt base course.

The observed bottom-up cracking is in accordance with the common assumption that load-induced fatigue cracking initiates at the bottom of the asphalt layers at the point of maximum tensile stress. It should be noted that in the case of Section 4, the cracking cannot be solely traced back to the fatigue of the asphalt due to repeated loading. As mentioned in Section 3.3, the asphalt pavement was subjected to bending caused by rutting of the granular base, which induced permanent tensile strains at the bottom of the asphalt base. These strains were then superimposed by those induced by the impulse loading which then resulted in fatigue cracking.

Crack propagation through the entire asphalt layers was not observed despite continued effort to cause total failure of the pavement in Section 4. The results

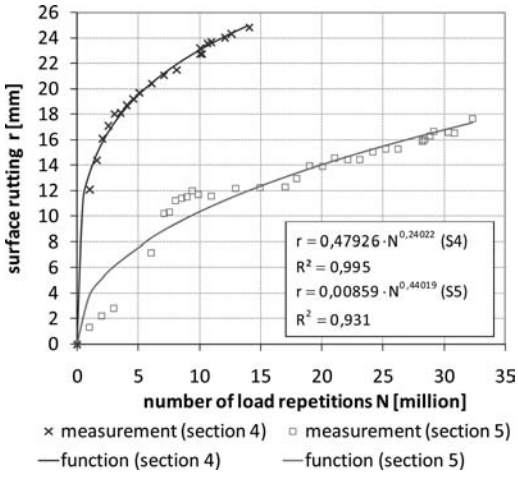

Figure 11. Permanent deformation as a function of the number of load repetitions.

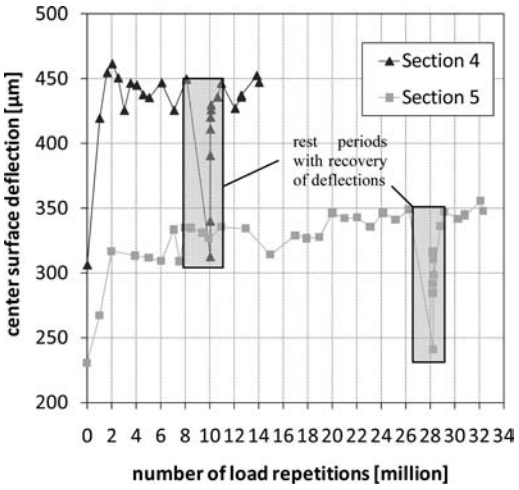

Figure 12. Normalized center deflection as a function of the number of load repetitions on Sections 4 and 5.

suggest that the interface between the base and the wearing course can prevent cracks from propagating to the surface.

3.3 *Permanent deformation*

Results from the transverse profile measurements are presented in Figure 11. The values show the maximum permanent deformation measured in the center of the loading area.

The results show that the rutting depth in Section 4 (weaker construction) was higher than in Section 5 (stronger construction). The rate of deformation was also greater in the weaker section and vice versa. The regression between the maximum rut depth and the number of load repetitions can be described with a power function with reasonably good agreement ($R^2 > 0.9$).

Analysis of the asphalt samples taken from Section 4 in the loaded and unloaded area provided valuable information on the observed rutting.

The comparison of thickness of the asphalt layers in the loaded and unloaded area showed them to be almost identical, giving no indication of plastic deformation of the asphalt. From this observation it is clear that the rutting occurred only in the granular layer underneath the asphalt, resulting from post-compaction under loading ("secondary rutting"). It is assumed, that the use of the plate vibrator contributed to the observed post compaction.

3.4 *Bearing capacity*

3.4.1 *Normalization of deflections*

Surface deflections were measured under an FWD target load of 50 kN in the loaded and unloaded areas of both sections. To compensate the effects of small deviations from the target load, the measured deflections were normalized to the reference value of the target load impulse ($F = 50$ kN) under assumption of a linear relationship between the load and the resulting deflection.

The measured deflections were also normalized to a reference temperature of 20°C (68°F) to account for the influence of temperature changes observed during testing. The asphalt temperature ranged from 15°C (59°F) to 25°C (77°F) during testing, depending on the depth of measurement. The approach applied for the normalization is based on the correlation between the deflections measured in the unloaded and therefore damage-free area of each test section and the average temperature of the asphalt pavement over the period of the test series.

The relationship between the temperature and deflection can be described reasonably well with a linear function. A correction factor was derived from the linear relationship, which was added or subtracted from the measured deflection. As the reliability of the data decreased with growing distance from the center of the loading plate the normalization was limited to deflections measured within a distance of 600 mm (23.5 in.) from the load center.

3.4.2 *Development of the center deflection*

The normalized center deflections as a function of the number of load repetitions are shown in Figure 12. Both sections show a significant loss of bearing capacity as derived from the increasing values of the center deflection under loading. The two sections can be distinguished by the total increase of values and the rate of development. The total increase defined as the difference between the values before and after loading was higher in the weaker section (141 µm) compared to the stronger section (118 µm). As the deflection measured in the unloaded condition is lower in the stronger pavement than in the weaker pavement the total increase as a percentage was found to be similar (46% compared to 51%). An average deflection was determined with

a linear regression of the relevant value for the "after loading" state to minimize the influence of scatter of values.

An initial rapid growth of values followed by an interval of almost linear development was observed in both sections. As the second interval characterized by a linear development was reached after less load repetitions in Section 4 (approximately 1.63 million impulses) compared to Section 5 (approximately 2.01 million impulses), it was concluded that the rate of deterioration was higher in the weaker section. This complies with the expectation that under equal loading a thin asphalt pavement will show a shorter service life and vice versa.

On Section 4 a leveling of deflection values was observed whereas the results show a continuing increase in deflection on Section 5 at the end of the measurement series. A progressive development of values was not observed in either section.

The sudden decrease of values after about 8 million impulses (Section 4) and about 26 million impulses (Section 5) was caused by long interruptions due to necessary maintenance of the hydraulic impulse generator. After a rest period of several weeks the bearing capacity expressed by elastic deflections recovered significantly, indicating some type of healing effect occurring during the rest period. After loading was continued, the deflections resumed the same trend as that prior to the rest period. A similar observation is described in Groenendijk (1994) who suggests recovering processes or thixotropic effects in the asphalt as possible causes. A follow-up project has been initiated at the BASt testing facility to focus on this aspect.

3.4.3 *Development of layer moduli derived from backcalculation*

The software *EVERCALC 5.0* (WSDOT, 2001) was used to determine the layer moduli on the basis of the surface deflections normalized to the reference temperature (T = 20°C, 68°F). A simplified linear-elastic three-layer-system consisting of an asphalt layer, a gravel/sand base, and a subgrade was used as a model for the calculation. The bottom of the concrete tank underneath the pavement structure was accounted for by assuming a stiff layer of 30,000 MPa at 3.1 m (10.2 ft.) depth. The layer moduli derived from backcalculation are shown in Figures 13 and 14. The values of the layer moduli are related to the modulus of the unloaded condition (E = 1.0, N = 0).

The development of layer moduli is characterized by the following aspects: The values of the layer moduli decrease with increasing number of load repetitions. Exempted from this is the modulus of the subgrade in Section 4 which shows a contrary increase. The asphalt layer on Section 5 also showed a greater loss of stiffness compared with Section 4, whereas the stiffness of the gravel/sand base shows a uniform trend. Analogous to the center deflection, a continuous decreasing trend in values on Section 5 was observed compared to the leveling of values in Section 4.

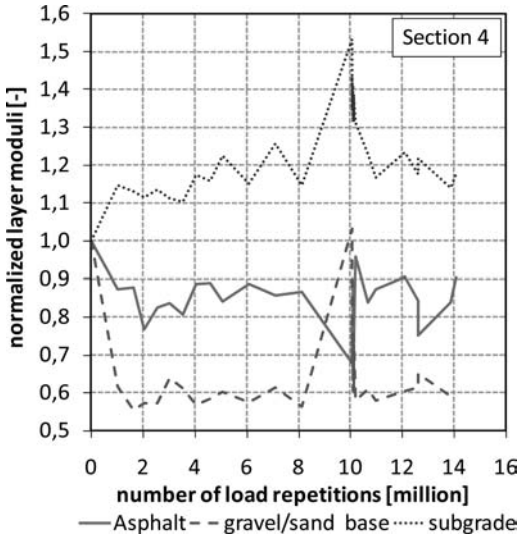

Figure 13. Layer moduli from backcalculation in Section 4.

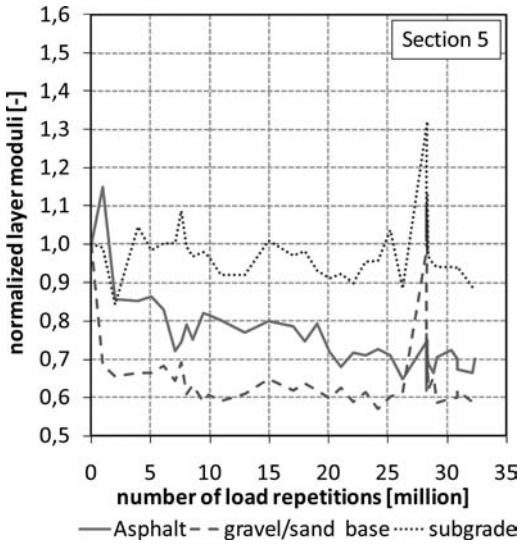

Figure 14. Layer moduli from backcalculation in Section 5.

The observed increase in stiffness of the subgrade was interpreted as a sign of post-compaction of this layer due to the repeated loading in Section 4. This supports the assumption that the permanent deformation is considered secondary rutting in the granular base (see discussion in Section 3.3).

3.5 *Development of measured longitudinal strain*

The asphalt strain and subgrade stress was recorded in each measuring cycle when the impulse generator passed the center track of the loading area in longitudinal direction.

Whereas a wheel moving on a pavement surface results in a continuous loading, the impulse generator

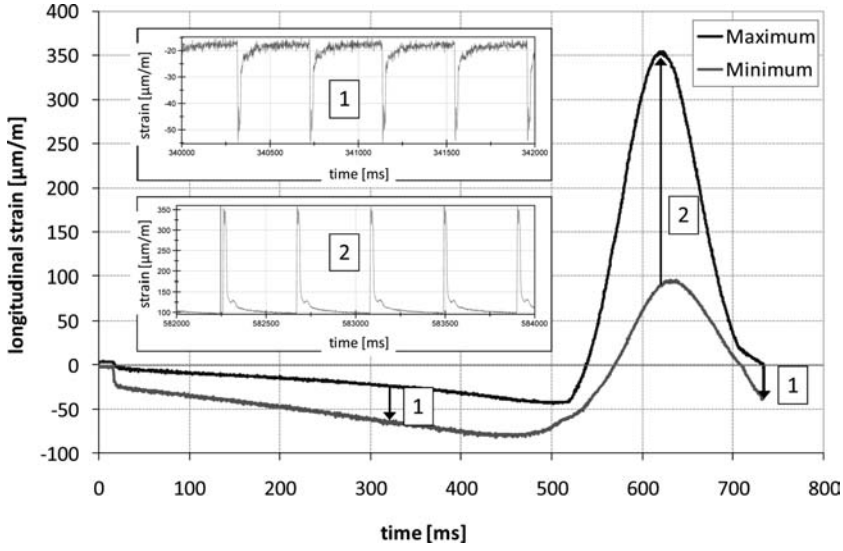

Figure 15. Example for longitudinal strain curves measured at the bottom of the asphalt base (unloaded condition, Section 4).

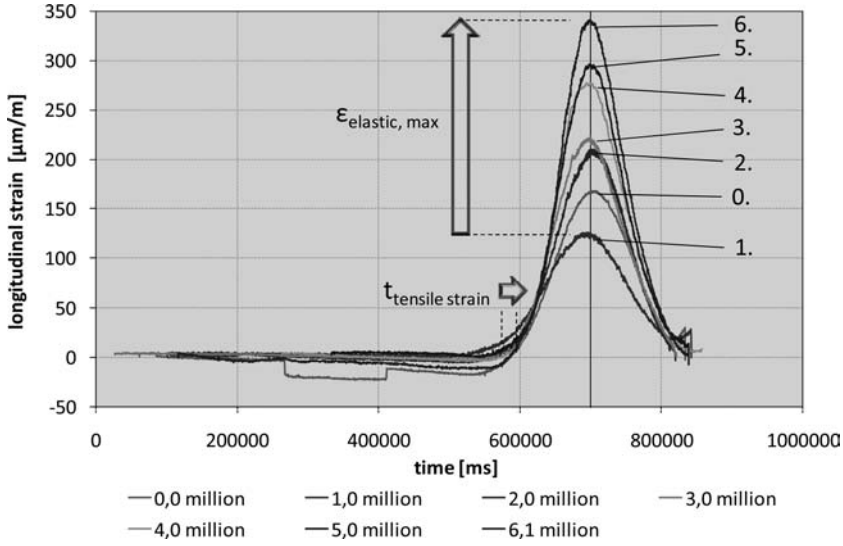

Figure 16. Maximum longitudinal strain curves as a function of the number of load impulses on Section 5.

exerts a sequence of short single impulses. Figure 15 shows example measured strains when the impulse generator passed the center track of the loading area in the longitudinal direction. The envelope curves for the maxima and minima values of strain are shown. Additionally the signals of single impulses are depicted in detail to illustrate the distribution of compressive strain (1) and tensile strain (2) inside the envelope curve.

The curves show the distinctive change from compressive strain to tensile strain in the longitudinal direction at the bottom of the asphalt base course caused by the passing impulse generator. In contrast to a passing wheel the impulse generator moves significantly slower and lacks the continuity of loading of a passing wheel (Rabe, 2008).

Figure 16 shows the curves computed from measurements at different times of loading. The results show that the maximum value of the elastic strain $\varepsilon_{elastic,max}$ increases with increasing accumulated loading with the exception of measurement #1. The period of tensile strain $t_{tensile\ strain}$ also increases (not recognizable in Figure 16). This observation can be reproduced using linear elastic multi-layer theory to calculate the strain at the bottom of the asphalt layers, assuming

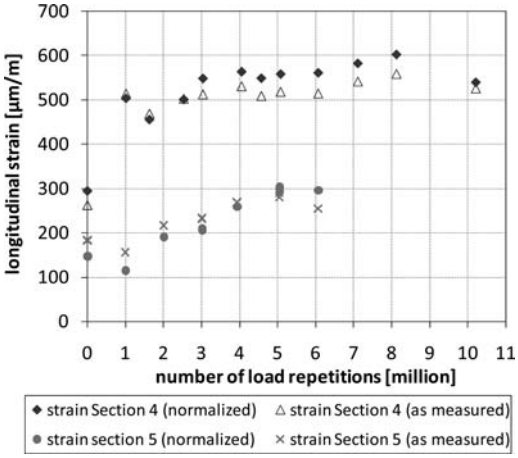

Figure 17. Longitudinal strain at the bottom of the asphalt base as a function of the number of load repetitions on Sections 4 and 5 (normalized/measured).

a successive decrease of stiffness of the asphalt. It is concluded that the results suggest a loss of structural strength.

A comparison of both sections is shown in Figure 17. The measurement results are presented by reducing the curve to the value of the maximum elastic strain. The value of the elastic strain was determined from the difference between the maximum and minimum curves at a given time.

The values were normalized to the reference temperature of 20°C (68°F). As a systematic empirical analysis of the correlation between elastic strain and the asphalt temperature could not be carried out, an analytical approach similar to Groenendijk (1994) was used. In brief this approach is based on a correction factor which is derived from calculating the strain at the bottom of the asphalt pavement assuming varying layer moduli to simulate temperature changes, using linear elastic layer theory.

The elastic strain plotted against the number of load repetitions shows an increase in longitudinal strain under continued loading on both sections. Consistent with the higher thickness of the pavement in Section 5 compared to Section 4 the measured strains are generally lower in view of both the unloaded and loaded condition. The results also indicate a lower increase of strain in the thicker asphalt pavement for the values before and after loading.

The rate of deterioration was lower in the stronger pavement. On Section 4, an initial period with a rapid increase/retardation followed by a period with a predominant linear trend was observed. This does not match the development of values in Section 5, which had a more linear trend with generally slower development.

In comparison to the measured strains, the calculated strains assuming a three-layer-system and using the layer moduli determined from backcalculation show considerably lower values in both unloaded and loaded conditions.

On Section 4, the measured strain increases from 295 to 603 µm/m (0 to 8.1 million impulses). In comparison the calculated strain increases from 159 to 212 µm/m in the same interval. The same tendency was observed on Section 5 where the measured strain increases from 184 to 256 µm/m whereas the calculated values increase from 110 to 140 µm/m (0 to 6.07 million impulses).

The observed differences indicate that the evaluation of measured results from embedded sensors requires considerable care. Calibration of the sensors, technical design properties, and the quality of the interaction between the surrounding asphalt and the sensor can all significantly influence the measurement results. The results obtained in this study suggest an application of sensors for comparative studies rather than providing absolute mechanical values.

3.6 *A pragmatic approach for the prediction of cracking*

The analysis was extended to measuring results from Sections 3, 6, 7 and 8 to further interpret the data from Sections 4 and 5. These sections are also part of the test track as shown in Figure 1. FWD measurements with a target load of 50 kN were carried out at an average asphalt temperature of 19°C (66.2°F) on all sections.

A relationship between the center deflections and those for the total area of asphalt was determined. As depicted in Figure 18 the relationship between the measured center deflection and the asphalt thickness can be reasonably well described with a power function. The center deflections measured in the unloaded conditions were plotted against the total thickness of the asphalt layers. The regression shows a good correlation ($R^2 = 0{,}987$). The function was then extrapolated beyond the measured data to account for thinner asphalt pavements with accordingly higher deflections than measured in the scope of this project. The given values refer to a maximum reference load impulse of 50 kN.

Values obtained from pavements with different construction type fitted well in the approximation function. Consequently, in this context the influence of the construction type was not significant, analogous to a basic principle of the RStO 01 (FGSV, 2001a) that pavements of the same construction class show an equivalent structural strength independent of the construction type.

The prediction of the effective thickness of the asphalt pavement is demonstrated in the diagram in Figure 19 using Section 4 as an example. In this context the term “effective thickness” is defined as the thickness of the asphalt pavement that is not affected by significant structural damage (e.g., cracking).

The first point marks the unloaded condition. The predicted thickness of the asphalt layer of 12 cm (4.7 in.) is consistent with the actual thickness of the

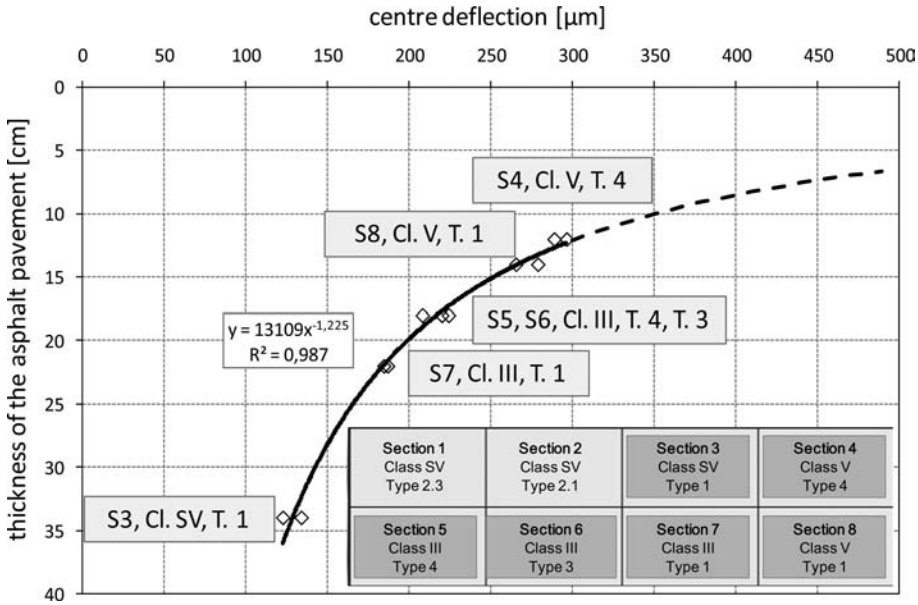

Figure 18. Center deflection as a function of thickness of the asphalt layers derived from the construction type according to the RStO 01 (FGSV, 2001a).

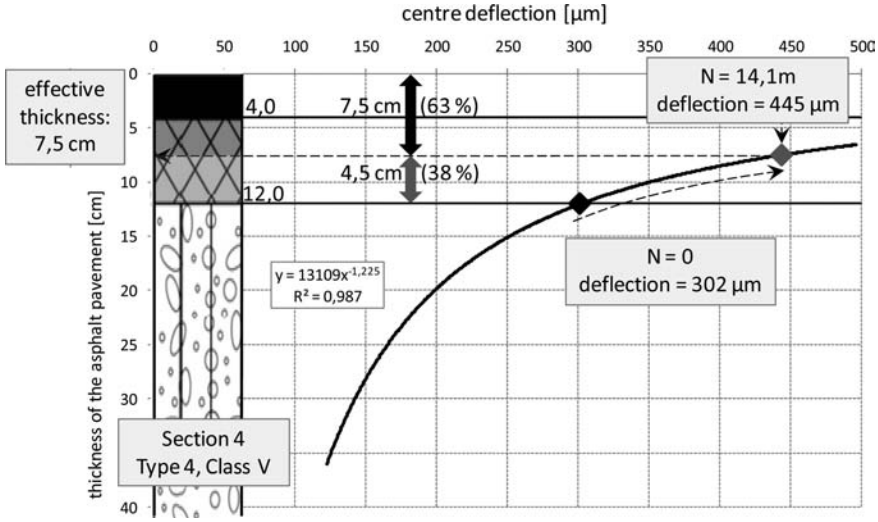

Figure 19. Prediction of the effective thickness of the asphalt layers on Section 4 after 14.1 million load impulses.

asphalt pavement. The second point represents the asphalt pavement after being subject to repeated loading with 14.1 million load impulses. Based on the measured deflection after loading (445 µm) and the extrapolated approximation function, the remaining thickness of the undamaged asphalt pavement was predicted to amount to 7.5 cm (3 in.). Consequently 4.5 cm (1.8 in.) or 38% of the 12 cm (4.7 in.) thick asphalt pavement was considered to show structural damage after 14.1 million load impulses.

The predicted effective thickness of the asphalt pavement in Section 4 was confirmed by the determination of the crack propagation on samples taken from this section after loading. As depicted in Figure 10, the average length of cracks across the whole asphalt base course was 5.1 cm (2 in.). Consequently the effective thickness of the asphalt pavement is 6.9 cm (2.7 in.). On the basis of the results from the FWD measurements, a remaining effective thickness of the asphalt layers of 7.5 cm (3 in.) was predicted.

The accurate determination of the remaining effective thickness appears promising for the evaluation of the structural condition of flexible road pavements on the basis of surface deflection measurements. Verification of the approach by testing on Section 5 and on in-service pavements is planned in view of developing a pragmatic approach for the estimation of the remaining life on the basis of the measured deflection and the cumulated heavy vehicle traffic load.

4 SUMMARY, CONCLUSIONS AND OUTLOOK

4.1 *Summary*

Accelerated pavement testing was conducted at Germany's Federal Highway Research Institute on two flexible full-scale road pavements. The pavements were continuously loaded to achieve structural failure. Periodic condition monitoring was carried out simultaneously with the loading. Both pavements comprised an asphalt base course on a granular gravel/sand base laid on a granular subbase. The stronger pavement had an additional binder course, thicker total asphalt concrete as well as a thicker granular base layer. The weaker test section was loaded with about 14 million load impulses. The loading was terminated when no further increase in deflection was measured. Due to technical reasons the loading in the stronger section had to be stopped after about 32 million load repetitions despite a continuing increase in deflection measurements.

4.2 *Conclusions*

The main findings of the project are:

- Structural failure was achieved in the test section with the weaker construction, which showed distinctive cracking in the asphalt base course. The repeated loading resulted in a decrease in the structural strength, which was concluded from the observed increase in surface deflections, the decrease of layer moduli derived from backcalculation of FWD deflections, and the increase in longitudinal elastic strain at the bottom of the asphalt base course. The asphalt pavement was subject to plastic deformation as a result of post-compaction of the underlying unbound layers. It was concluded that the superposition of permanent strain induced by plastic deformation and strains due to repeated loading caused the propagation of cracks in the asphalt base course.
- The stronger pavement in Section 5 showed a deterioration of structural strength characterized by increasing surface deflections and decreasing layer moduli as well as increasing longitudinal strain. The rate of deterioration in this section was slower than in the weaker section. The total increase in the center deflections relative to the unloaded condition was similar on both sections if the differences in bearing capacity are taken into consideration.
- The change in bearing capacity under repeated loading resembles a power function in both sections ($0 < \text{exponent} < 1$). An initial sharp decrease was followed by a longer-lasting interval with an almost linear development. A progressive decrease in the bearing capacity at the end of the service life was not observed despite continued loading on both test sections.
- A relationship between the center deflection and the effective thickness of the asphalt layers was observed. On the basis of this relationship, a pragmatic approach to predict the propagation of bottom-up-cracking was developed. The estimated and measured length of cracks showed a reasonably good agreement.
- The longitudinal strain as a critical parameter for the mechanistic design of flexible pavements was derived from backcalculation of surface deflections and from strain gauge measurements at the bottom of the asphalt base. In this case the calculated strain was significantly lower than the actual measured strain.
- The cracking observed in the weaker section was characterized as "bottom-up-cracking" and supports the theoretical assumption that traffic-induced structural damage of asphalt pavements initiates at the bottom of the asphalt layers where the maximum values of the tensile strain occur.
- Termination of crack propagation at the interface between the two asphalt courses could be the reason for the slowing in the change in bearing capacity observed on the weaker section.

4.3 *Outlook*

Loading on Section 5 will be resumed in a follow-up project to obtain further knowledge on the crack propagation and the recovery of the bearing capacity in rest periods.

In the long term the untested sections (Sections 1, 2, 3, 6, 7 and 8) will be analyzed in a similar way to that described in this paper to further understand behavior of the different construction classes and types.

The results will also be used to verify analytical methods in combination with material testing, and to verify performance models for the prediction of remaining service life of flexible pavements.

REFERENCES

Federal Ministry of Transport, Building and Urban Affairs (BMVBS). 2011.*Maintenance management of the federal trunk roads, Germany.* Federal Highway Research Institute (BASt).

Forschungsgesellschaft für Straßen- und Verkehrswesen (FGSV). 2001a. *Richtlinien für die Standardisierung des Oberbaus von Verkehrsflächen – RStO 01*, Cologne, Germany.

Forschungsgesellschaft für Straßen- und Verkehrswesen (FGSV). 2001b. *Zusätzliche Technische Vertragsbedingungen und Richtlinien für den Bau von Fahrbahndecken aus Asphalt – ZTV Asphalt-StB 01*, Cologne, Germany.

Forschungsgesellschaft für Straßen- und Verkehrswesen (FGSV). 2002. *Zusätzliche Technische Vertragsbedingungen und Richtlinien für Tragschichten im Straßenbau – ZTV T-StB 95, edition 1995, version 2002*, Cologne, Germany.

Groenendijk, J., Vogelzang, C.H., Molenaar, A.A.A. and Dohmen, L.J.M. 1994. Performance tests under accelerated loading with the LINTRACK test facility in the Netherlands, *Proceedings of the 4th International Conference on the Bearing Capacity of Roads and Airfields*, Minneapolis, Minnesota, USA.

ProgTrans AG, 2007. *Abschätzung der langfristigen Entwicklung des Güterverkehrs in Deutschland bis 2050, Final Report*. Basel, Switzerland.

Rabe, R. 2004. *Bau einer instrumentierten Modellstraße in Asphaltbauweise zur messtechnischen Erfassung der Beanspruchungssituation im Straßenaufbau*. Project AP 03 342, Final Report, Federal Highway Research Institute (BASt), Bergisch Gladbach, Germany.

Rabe, R. 2008. Pavements under permanent stress – A closer look inside a structure, *Proceedings of the 3rd International Conference on Accelerated Pavement Testing*, Madrid, Spain October 1–3.

Ritter, J. 2010. *Dauerbelastungsversuche an einer Modellstraße zur vergleichenden Beurteilung des Tragverhaltens unterschiedlicher Bauweisen*. Project AP 06 000, Final Report, Federal Highway Research Institute (BASt). Bergisch Gladbach, Germany.

Washington State Department of Transportation (WSDOT). 2001. *EVERCALC© 5.0*, Washington, USA.

Advances in Pavement Design through Full-scale Accelerated Pavement Testing – Jones, Harvey, Mateos & Al-Qadi (Eds.)
© 2012 Taylor & Francis Group, London, ISBN 978-0-415-62138-0

Evaluation of a flexible pavement structure in an accelerated pavement test

Th. Saevarsdottir
University of Iceland, Reykjavik, Iceland

S. Erlingsson
University of Iceland, Reykjavik, Iceland
Swedish National Road and Transport Research Institute, VTI, Linköping, Sweden

ABSTRACT: A flexible test road structure was built and tested in an Accelerated Pavement Test (APT) using a Heavy Vehicle Simulator (HVS) to investigate the performance behavior for validation in a mechanistic performance design. The structure was instrumented to measure the responses at different locations due to different wheel loadings and various tire pressures, with single and dual tires. The permanent deformation manifested on the surface as rutting was measured. The responses gained from various tire loads and pressures were analyzed using three approaches; all layers linear-elastic, the base nonlinear and base and subbase nonlinear. The measurements taken after 100,000 load repetitions were compared with the measurements taken in the beginning of the test. Some softening effect was noticed in the asphalt layers and was taken into account in the analysis. The observed accumulation of permanent deformation of the unbound layers was modeled using a three parameter model. Generally good agreement was established between the measured and calculated values.

1 INTRODUCTION

Today, most of traditional highway pavement design is done with empirical methods that are developed and based on long-term experience. Empirical methods are mainly used due to the complex behavior of pavements. The behavior depends on many factors such as the applied load, the material used, the thickness of the layers and the environmental conditions. The main limitation of empirical methods is that they cannot be extrapolated with confidence beyond the conditions on which they are based. To be able to develop mechanistic design methods the behavior and properties of the materials used needs to be properly understood. These methods need to consider and realistically model the response of granular layers (base and subbase) under various traffic loadings. In thin pavements the granular base and subbase layers, show a complex elasto-plastic behavior under external loading. Therefore it is important to compare the results of numerical analyses with actual measurements of stresses, strains and deflections in a full scale pavement structure in order to model their behavior adequately. The development of accelerated pavement tests (APT) of instrumented pavement structures has increased the understanding of pavement behavior and built a foundation for new, more sophisticated design methods.

An APT using a Heavy Vehicle Simulator (HVS) was performed at the Swedish Road and Transport Research Institute (VTI) test facility in Linköping, Sweden, between May and September 2005. The test is referred to as SE10, and the results are used in this analysis. The HVS is a linear full-scale accelerated road-testing machine with a heating/cooling system. The pavements were constructed by normal road construction equipment in a test pit that is 3 m deep, 5 m wide and 15 m long. The length of the tested structure was 6 m (Wiman, 2006 and 2010).

The main purpose was to get good direct measurements of stresses and strains in the thin pavement structure as well as to evaluate the performance of the structure. This increases understanding of necessary complexity of the numerical model needed to capture the main structural behavior.

2 PAVEMENT STRUCTURE

The pavement was tested at VTI's full-scale indoor pavement test facility under constant environmental conditions. The structure consisted of 10.7 cm thick Hot Mix Asphalt (HMA), divided into a 3.3 cm surface course (AC pen 70/100; $d_{max} = 16$ mm) and a 7.4 cm bituminous road base (AC pen 160/220; $d_{max} = 32$ mm). Under the asphalt were two layers of unbound crushed rock (granite), an 8.8 cm base layer (0–32 mm) and a 45 cm subbase layer (0–90 mm) overlying a subgrade of fine graded sand (Wiman, 2001 and 2010). A cross section of the structure is shown in Figure 1 together with the configuration of the instrumentation used.

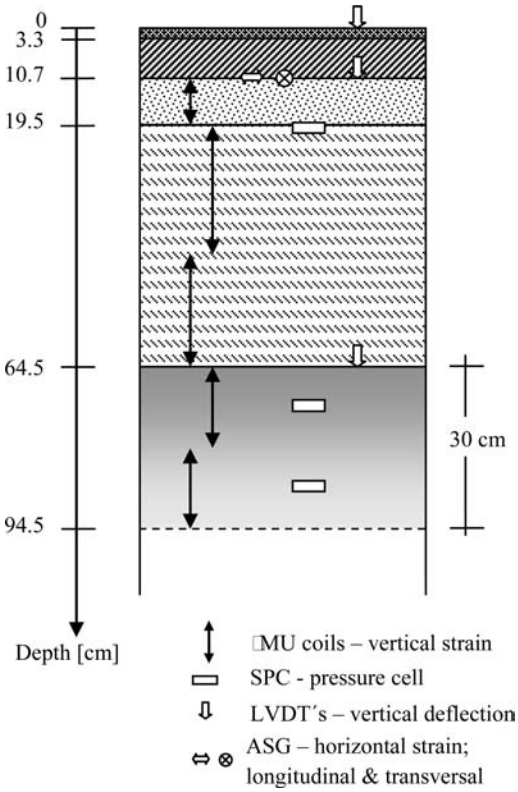

Figure 1. A cross section of pavement structure SE10 as well as the vertical location of the instrumentation.

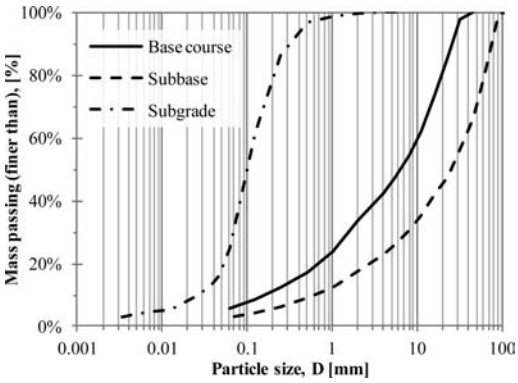

Figure 2. Grain size distribution curves of the unbound materials in the pavement.

The grain size distribution curves of the unbound layers of the pavement are shown in Figure 2. The subgrade consisted of silty sand with a high fines content of about 25% and over 90% of the grains under 0.5 mm. The subbase had a fines content of about 3% and a maximum aggregate size of $d_{max} = 90$ mm whilst the base material had a fines content of about 6% with $d_{max} = 32$ mm (Wiman, 2010).

3 HVS TESTING PROJECT

The pavement structure, SE10, was instrumented to measure response and performance. The instrumentation (see Figure 1) consisted of (Wiman, 2010):

- εMU coils (inductive coils) were used to measure the vertical strain (elastic and permanent), at five depth intervals and three coils at each depth range.
- Soil pressure cells (SPC) were used to obtain stresses, placed at three depths with three sensors at each depth.
- Linear variable differential transducers (LVDT's) were used to measure the vertical deflection in relation to the bottom of the test pit and over the base and subbase.
- Eight asphalt strain gauges (ASG) (H-bar) were used to measure the tangential strain at the bottom of the asphalt bound layers, four gauges measured in the longitudinal and four in the transverse direction.

The test was divided into three phases:

- Pre-loading phase, of 20,000 load repetitions applying light loading.
- Response phase, to get information on the response due to various loadings.
- Main accelerated loading test, with more than one million load cycles applied.

In all phases bidirectional loading was applied. The pre-loading step was performed with a 30 kN single wheel load with a tire pressure of 700 kPa. Wheel passes were distributed evenly in the lateral direction to achieve even compaction in the 70 cm wide wheel path. In the response phase, the response of the structure was estimated from both single wheel and dual wheel configurations using various tire pressures and axle loads. The centre to centre spacing of the dual wheel configuration was 34 cm. The lateral distribution of the loading followed a normal distribution where the wander was divided into eleven segments, from plus to minus 25 cm in 5 cm intervals. In the main accelerated load test phase, development of permanent deformation was monitored using a dual wheel configuration with 120 kN axle load and 800 kPa tire pressure. The response of the pavement structure was measured regularly during the main accelerated testing phase (Wiman, 2006 and 2010; Erlingsson, 2007 and 2010). The first 490,000 load repetitions have been analyzed and modeled.

4 RESPONSE BEHAVIOR OF THE STRUCTURE

In this section all figures are drawn in the case of a dual tire loading combination; taken under the centre of one of the wheels; with 120 kN axle load; 800 kPa tire pressure; a rolling wheel speed of 12 km/h and a constant temperature of 10°C.

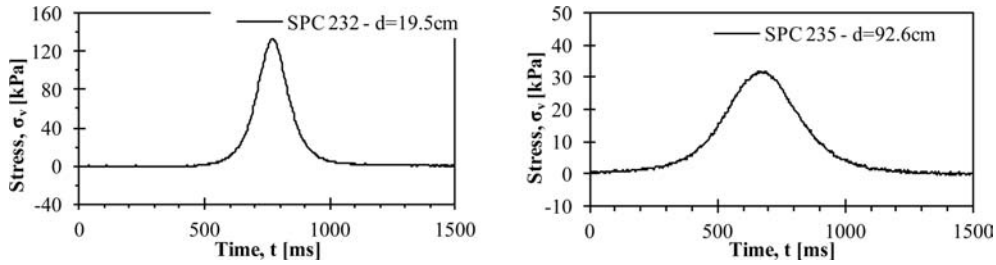

Figure 3. Induced vertical stress registration of two SPC sensors, at depths of 19.5 and 92.6 cm.

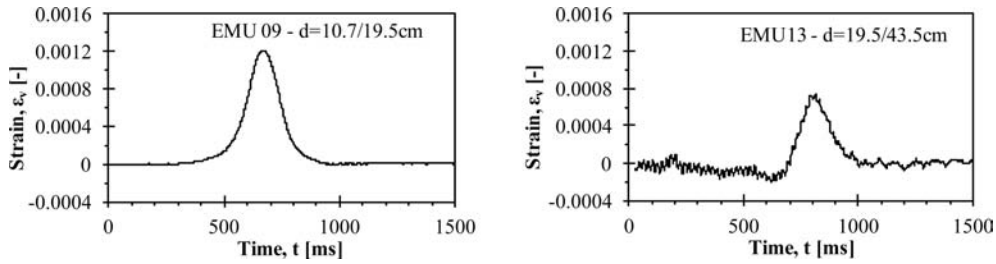

Figure 4. Induced vertical strain registration of two εMU sensors, for depth ranges from 10.7 to 19.5 cm and 19.5 to 43.5 cm.

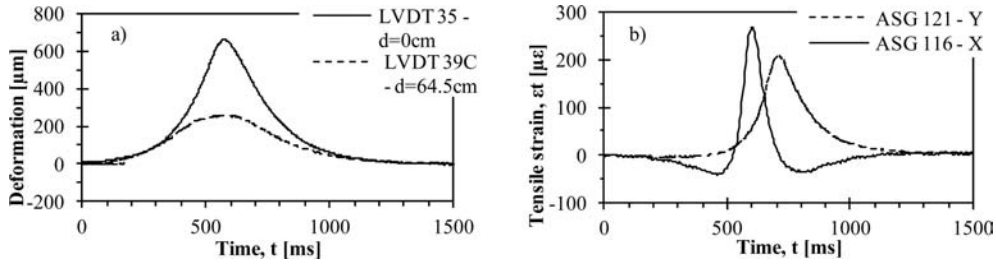

Figure 5. a) Induced deformation registration of two LVDTs, from bottom of test pit to surface and depth of 64.5 cm and b) Induced tensile strain registration of ASG gauges at bottom of bituminous base, where X is longitudinal and Y is transverse direction.

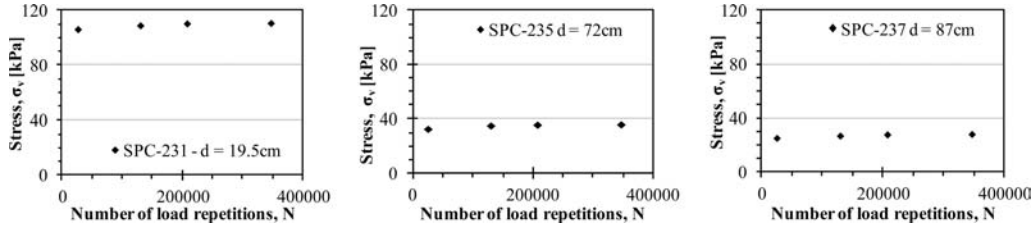

Figure 6. Induced vertical stress as a function of load repetitions, at depths of 19.5, 72 and 87 cm.

Figures 3 to 5 show a typical registration from the sensors of the structural responses. The registrations of the measurements were generally smooth with minimal noise in the signal. The signal recorded form the εMU coils in the subgrade layer was somewhat noisier, but in these instances a moving average was used to estimate the sensor readings.

On Figures 6 to 8 the development of sensor registration as a function of load repetitions N is shown. The vertical stress was measured on the centre line of the wheel path at three depths; 19.5 cm which is at the bottom of the base layer and at 72 cm and 87 cm in the subgrade. From Figure 6, which shows stress development, it can be noticed that the registered vertical

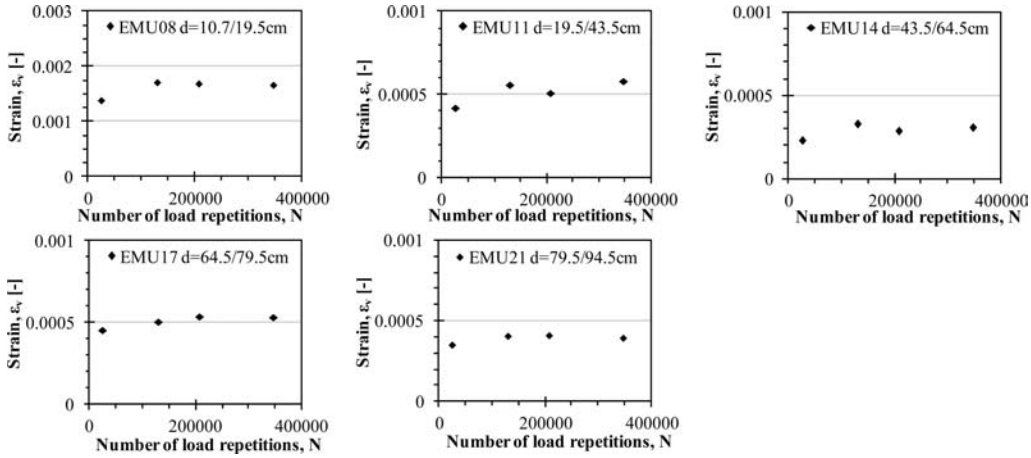

Figure 7. Induced vertical strain as a function of load repetitions, at depth ranges from 10.7 to 19.5 cm etc.

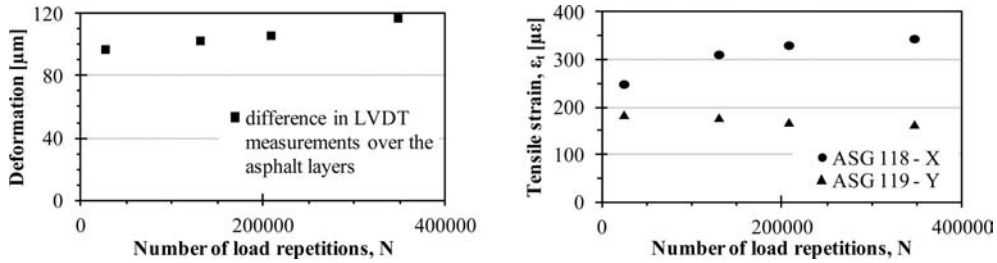

Figure 8. a) Difference in induced deformation measured with LVDTs from bottom to top and bottom to bottom of asphalt bound layers (10.7 cm) and b) induced tensile strain as a function of load repetitions at bottom of bituminous base, where X is longitudinal and Y is transversal direction.

stress was reasonably constant for the first 400,000 load repetitions examined here.

Similarly, the vertical strain was measured on the centre line of the wheel path over five depth intervals; 10.7–19.5 cm (over the base layer); 19.5–43.5 cm (over the upper part of the subbase); 43.5–64.5 cm (over the lower part of the subbase); 64.5–79.5 cm (over the top of the subgrade) and 79.5–94.5 cm (over a part of the subgrade) (see Figure 1).

In Figure 7, which shows strain development, the registered vertical strain was reasonably constant between 100,000 and 400,000 load repetitions, but showed an increase after the first 20,000 load repetitions in all layers, indicating weakening of the materials. This was attributed to softening of the HMA taking place between 20,000 and 100,000 load repetitions, causing more strain to reach the unbound layers. In Figure 8a the difference in deformation measured with LVDTs, from the bottom of the concrete pit to the surface and to 10.7 cm depth, which is the interface between the bound and unbound layers, is plotted as a function of load repetitions. The figure shows that the difference increases as the load repetitions increase. The average difference is around 8%. On Figure 8b, the development of the tensile strain at the bottom of the bound layers (10.7 cm depth) is presented. The strain increases as the number of load repetitions increases due to the softening of the HMA.

5 RESPONSE MODELING

The pavement structure was modeled in an axisymmetric analysis. The HMA and the subgrade were treated in the analysis as linear elastic materials where stiffness of the HMA was adjusted according to the ambient temperature. Using cylindrical co-ordinates the elastic stress-strain relationship can be written as:

$$\begin{bmatrix}\sigma_r\\ \sigma_\theta\\ \sigma_z\\ \tau_{rz}\end{bmatrix}=\frac{M_r}{(1+\nu)(1-2\nu)}\begin{bmatrix}1-\nu & \nu & \nu & 0\\ \nu & 1-\nu & \nu & 0\\ \nu & \nu & 1-\nu & 0\\ 0 & 0 & 0 & \frac{1-2\nu}{2}\end{bmatrix}\begin{bmatrix}\varepsilon_r\\ \varepsilon_\theta\\ \varepsilon_z\\ \gamma_{rz}\end{bmatrix} \quad (1)$$

where M_r is the material stiffness (resilient modulus) and ν is the Poisson's ratio of the unbound material.

The stiffness modulus for granular materials is generally stress dependent. A number of relationships exist to describe the stress dependency of the stiffness modulus. One of the most common and also one of the simplest is the $k-\theta$ expression (May and Witczak,

Table 1. Material parameters of different layers used in response analyses.

Layer and Test Condition		Linear (LIN) E/M_r [MPa]	Nonlinear Base (NONL base) k_1 [−]	Nonlinear Base (NONL base) k_2 [−]	Nonlinear Base and Subbase (NONL bsb) k_1 [−]	Nonlinear Base and Subbase (NONL bsb) k_2 [−]
Asphalt concrete	Begin*	5,000	–	–	–	–
	Moist**	4,500				
Bituminous base	Begin*	1,500	–	–	–	–
	Moist**	1,350				
Unbound base		130	713	0.6	713	0.6
Unbound subbase		190	–	–	2,060	0.6
Subgrade		50	–	–	–	–

E – Young's modulus of bound materials; Mr – Resilient stiffness of unbound materials, *N = 20.000–30.000; **N > 100.000

1981; Uzan, 1985; Gomes-Correia et al., 1999; Lekarp et al., 2000). In a normalized form this equation is frequently written as:

$$M_r = k_1 p_a \left(\frac{3p}{p_a}\right)^{k_2} \tag{2}$$

where k_1 and k_2 are experimentally determined constants, p is the mean normal stress level of the loading, i.e., $p = 1/3(\sigma_r + \sigma_\theta + \sigma_z)$, and p_a is a reference pressure, $p_a = 100$ kPa.

This relationship has been shown to capture the main behavior characteristics of unbound granular materials under various rolling wheel loading situations (Huang, 2004; Erlingsson, 2007).

In this paper the responses where calculated using a multi-layer elastic theory (MLET) using the *Kenlayer* computer program (Huang, 2004).

6 PERMANENT DEFORMATION PREDICTION MODELING

The accumulation of vertical strain in the pavement materials was modeled according to the procedure used in the *Mechanistic-Empirical Pavement Design Guide* (*MEPDG*) (ARA Inc., 2004) which is based on best fit approaches from laboratory testing. For the unbound layers (base course, subbase and subgrade) a simple three parameter work hardening model was used (Tseng and Lytton, 1989):

$$\hat{\varepsilon}_{pl}(N) = \varepsilon_0 \cdot e^{-\left(\frac{\rho}{N}\right)^{\beta}} \tag{3}$$

where N is the number of load repetitions and ε_0, ρ and β are regression parameters.

According to the *MEPDG*, the deformation in unbound materials is found by modifying the Tseng and Lytton method (ARA Inc., 2004):

$$\delta_a(N) = \beta_1 \left(\frac{\varepsilon_0}{\varepsilon_r}\right) e^{-\left(\frac{\rho}{N}\right)^{\beta}} \varepsilon_v h \tag{4}$$

where δ_a is the permanent deformation in the layer; ε_r is resilient strain imposed in lab test to obtain ε_0, ρ and β; ε_v are the average vertical resilient strains in the layer obtained from the primary response model; h is the thickness of the layer and β_1 is a calibration factor for different granular layers.

After numerous modifications a reasonable calibrated relationship was obtained and models provided to find the regression parameters. In the approach used, the granular layers are divided into sub-layers (i) and the total deformation occurring in each layer is determined by summing the permanent deformation over the sub-layers:

$$\delta_a(N) = \sum_{i=1}^{n} \delta_a(N)_i = \sum_{i=1}^{n} \beta_1 \left(\frac{\varepsilon_0}{\varepsilon_r}\right) \cdot e^{-\left(\frac{\rho}{N}\right)^{\beta}} (\varepsilon_v)_i h_i \tag{5}$$

where n is the total number of sub-layers.

7 MATERIAL PROPERTIES

The material parameters for all layers of the pavement used in the numerical analyses of its response are given in Table 1. The calculations were performed with three different models:

- All material models are linear elastic (LIN)
- All material models are linear elastic, but the base material was assumed stress dependent (NONL base)
- Bound material layers and subgrade material models are linear elastic, but base and subbase material models are stress dependent (NONL bsb).

It was considered appropriate to treat the subgrade as a linear elastic material since low stress levels were measured and therefore elastic theory provides adequate results.

Results from plate load tests (PL), falling weight deflectometer tests (FWD) during construction, indirect tension tests (ITT) of the bituminous layers, and repeated load triaxial (RLT) tests of the unbound layers were all used for estimating the material parameters.

Table 2. Material parameters of the unbound layers used to predict the permanent deformation.

Layer	W [%]	β [−]	ρ [−]	$\varepsilon_0/\varepsilon_r$ [−]	β_1 [−]
Unbound base (granular)	6	0.19	6,564	22.1	0.4
Unbound subbase (granular)	6	0.19	6,564	22.1	0.8
Subgrade	15	0.13	450,180	28.6	1.2

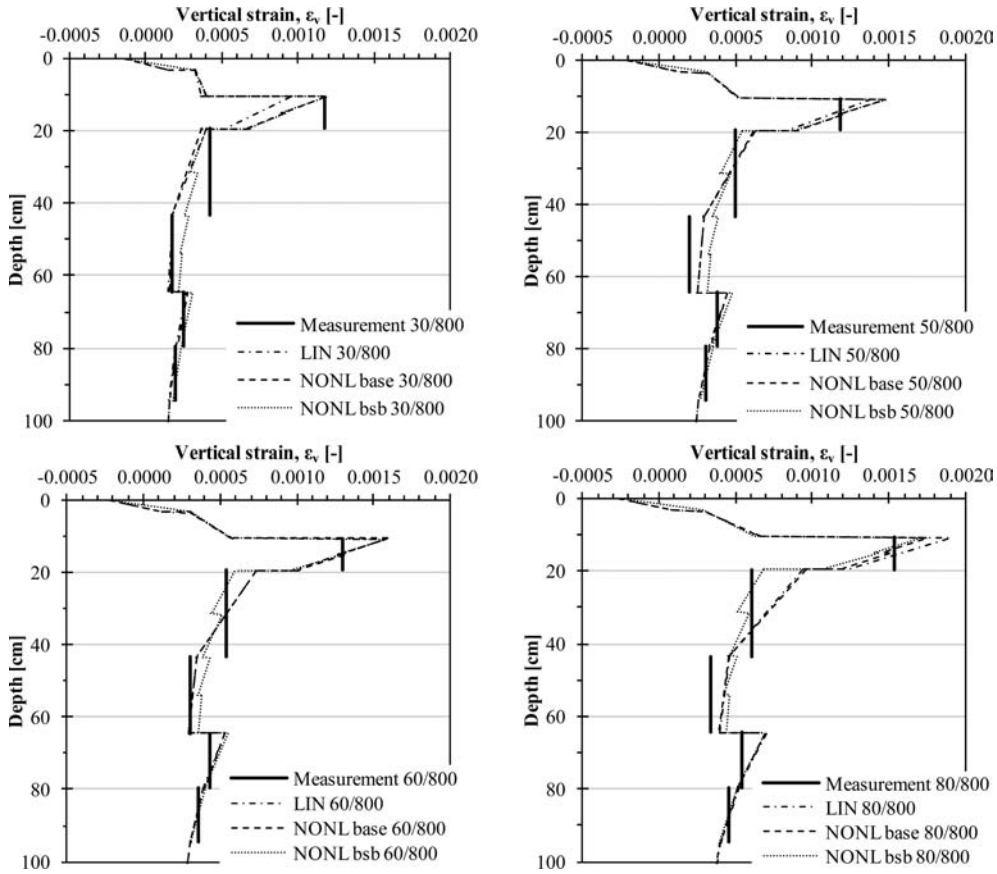

Figure 9. Vertical resilient strain as a function of depth, tested with dual wheel configuration with 800 kPa tire pressure and various wheel loading a) 30/800, b) 50/800, c) 60/800 and d) 80/800.

The final material parameters were selected to establish a good agreement between the responses (under the centre of one of the tires) of an applied dual wheel load of 120 kN axle with 800 kPa tire pressure and calculations. This configuration was chosen given that most measurements had been carriedout with this loading. These parameters were verified with other load cases as discussed in Section 8. Measurements for the various load cases were taken between 20,000 and 30,000 load repetitions. For responses after 100,000 load repetitions, the stiffness of the asphalt bound layers was reduced by 10% as measurements show some softening effect in the bound layers (see Figures 7 and 8). In all cases the Poisson's ratio (ν) was set to 0.35. The unit weights, γ, were 24 kN/m^3 for the asphalt concrete and the bituminous base, 20 kN/m^3 for the unbound base, 19 kN/m^3 for the unbound subbase and 16 kN/m^3 for the subgrade layer.

The base and subbase both consisted of crushed rock (granite), with similar grain size distribution but the base layer had grain size between 0 and 32 mm whereas the subbase had aggregates up to 90 mm. The higher stiffness of the subbase in Table 1, compared to the base was attributed to better compaction of the subbase layer. Compaction has a significant influence on the stiffness of unbound materials. Van Niekerk et al. (2000) showed that the resilient modulus (M_r) changed significantly with increased compaction, but samples were compacted to 97–105% of maximum Proctor density. Van Niekerk et al. also showed that at

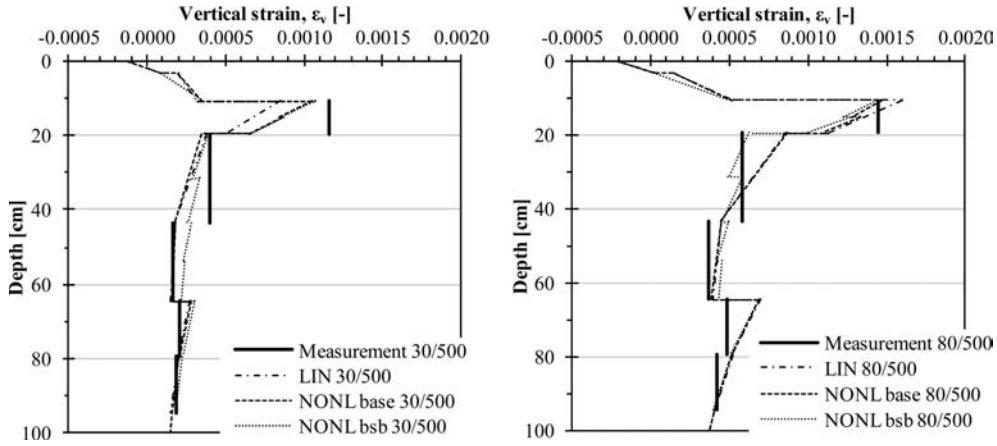

Figure 10. Vertical resilient strain as a function of depth, tested with 500 kPa tire pressure and various wheel loading a) 30/500, b) 80/500.

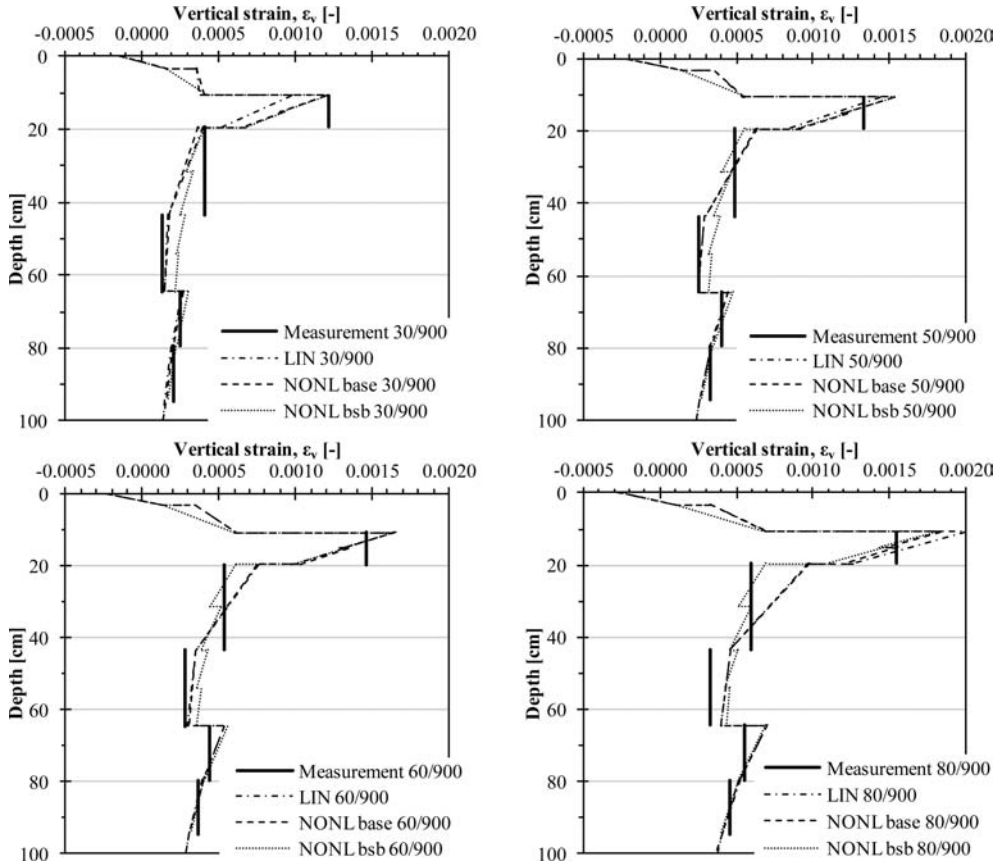

Figure 11. Vertical resilient strain as a function of depth, tested with 900 kPa tire pressure and various wheel loading a) 30/900, b) 50/900, c) 60/900 and d) 80/900.

a constant sum of principle stresses of 100 kPa the M_r was 127 MPa for 97% degree of compaction (D.o.C.) and 257 MPa for 103% D.o.C., or 50% difference in resilient modulus with 6% increase in D.o.C.

The parameters used in the permanent deformation prediction are listed in Table 2. The material properties ρ, β and $\varepsilon_0/\varepsilon_r$ were obtained using equations developed by ARA Inc. (2004) to fit the *MEPDG* model described

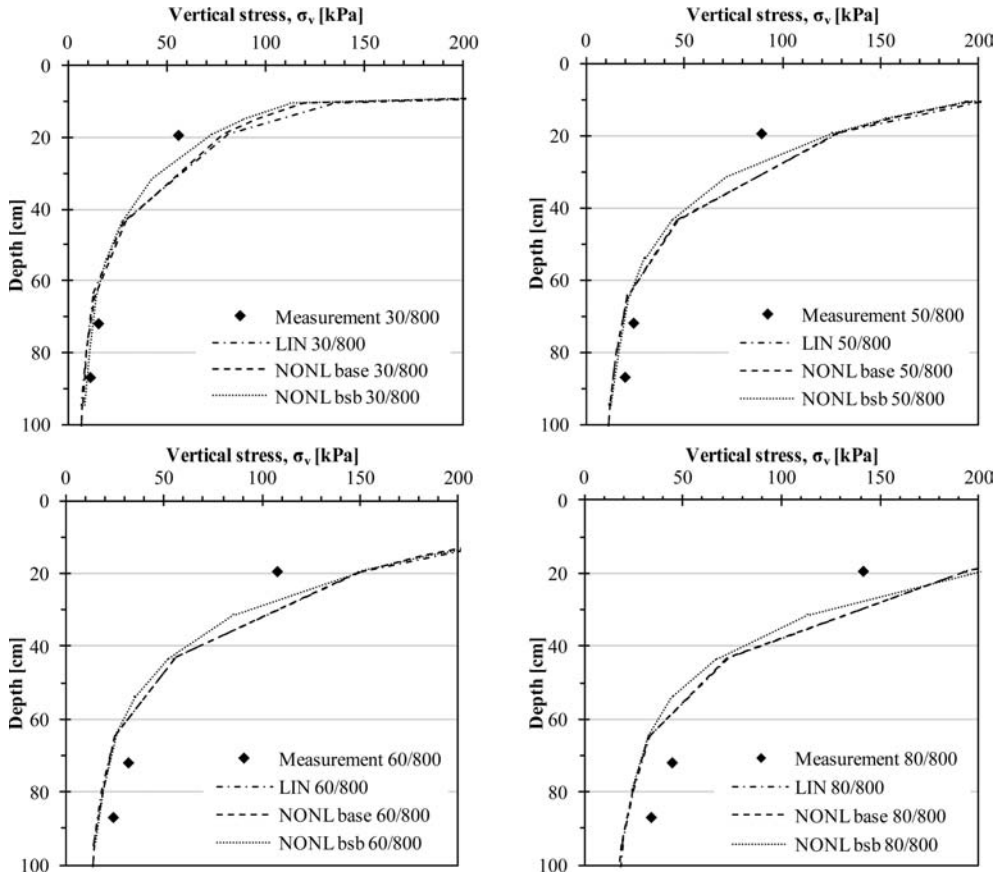

Figure 12. Vertical induced stress as a function of depth, tested with 800 kPa tire pressure and various wheel loading a) 30/800, b) 50/800, c) 60/800 and d) 80/800.

earlier and the calibration factor β_1 was used to obtain a reasonable resemblance between the measured and calculated values.

8 RESPONSE ANALYSIS

The figures in this section show the results of calculated and measured vertical stresses and vertical strains as a function of depth. In all cases the average value of the gauges at the same depth is shown, with loading consisting of a dual wheel configuration and a profile taken under the centre of one of the tires. Both the load as well as the pressure varied, with the axle loads being 60, 100, 120 and 160 kN (dual wheel loads of 30, 50, 60 and 80 kN) and the tire pressure being 500, 800 and 900 kPa. On the figures; 30/800 indicates a 30 kN wheel load and 800 kPa tire pressure, 80/900 indicates an 80 kN wheel load and 900 kPa tire pressure, etc.

When comparing responses due to different load and pressure the measurements were taken between 20,000 and 30,000 load repetitions. The figures generally show good agreement between the measured and calculated strains, for both linear and nonlinear (stress dependent) calculations. However, induced vertical stress is harder to capture in calculations. It is known that the measurement of vertical stresses in coarse grained materials is difficult, which might partly explain the observed difference between stress measurements and calculations.

In Figures 9 to 11, the vertical lines are the average of the measured values for a certain depth interval whilst the dotted lines represent the calculated strain. Using a nonlinear model for both the base and subbase layers gave the best results, but the linear elastic model for all layers also gave a reasonable outcome. It should be noted that the linear elastic model appears to underestimate the vertical strain at low tire load and pressure values and overestimate the vertical strain at high tire load and pressure.

In Figures 12 to 14 the black diamonds are the average of measured vertical stress values for a certain depth whilst the dotted lines represent the calculated values. Because the combined asphalt bound layers are just over 10 cm thick and reasonably stiff the vertical stress decreases rapidly with depth. In the base layer the vertical stress was down to 50–150 kPa depending on applied load and pressure. All the models gave similar results, overestimating the stress in the base and underestimating them in the subgrade, especially

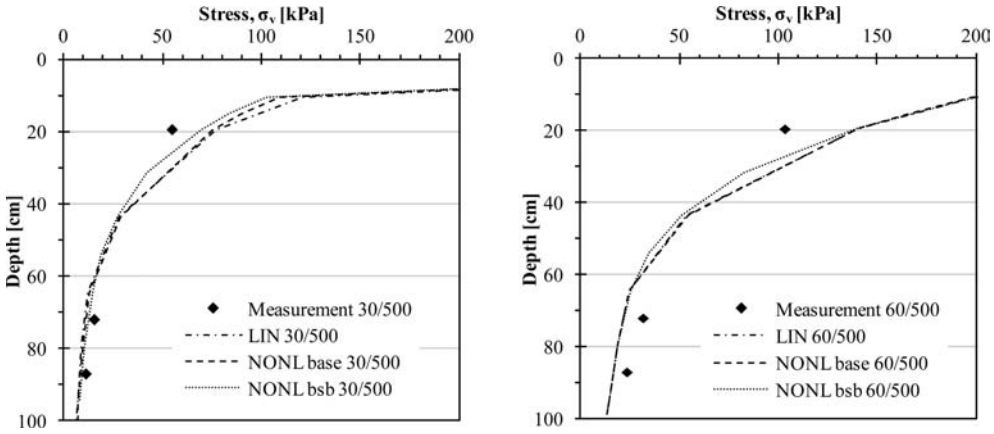

Figure 13. Vertical induced stress as a function of depth, tested with 500 kPa tire pressure and a) 30/500 and b) 60/500.

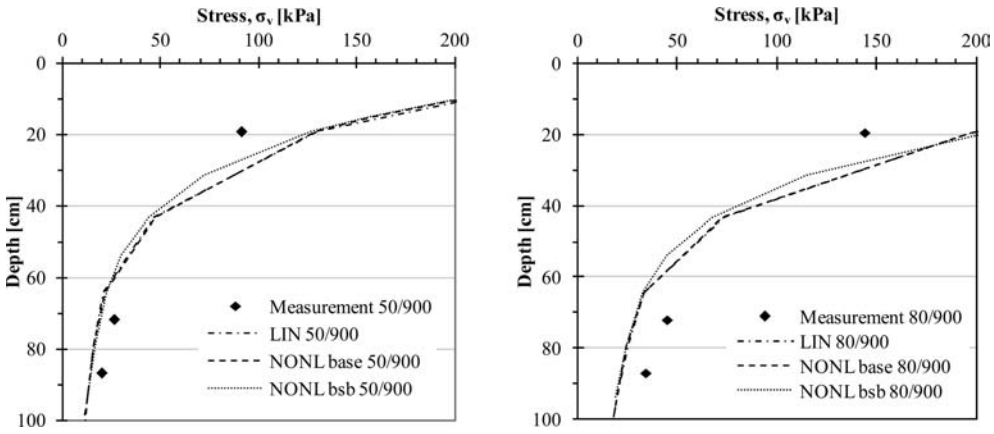

Figure 14. Vertical induced stress as a function of depth, tested with 900 kPa tire pressure and a) 50/900 and b) 80/900.

when the load was high. Nevertheless, the slope of the stresses harmonizes well in the subgrade.

9 PERFORMANCE PREDICTION

In Figure 15, the vertical strains are compared between the initial measurements taken between 20,000 and 30,000 load repetitions and measurements taken later into the test or after 100,000 load repetitions. The stiffness of the asphalt bound layers was decreased by 10% for the later stages as both εMU and LVDT measurements showed signs of softening of the asphalt bound layers.

The vertical lines in Figure 15 are the average of measured vertical strains for a certain depth interval whilst the dotted lines represent the calculated strain. All three models gave similar results, underestimating the vertical strain in the base and subgrade layers but nevertheless giving reasonable results after decreasing the stiffness of the asphalt bound layers.

Figure 16 shows the measurement of accumulated permanent deformation as a function of load repetition and the predicted deformation according to the *MEPDG* model compared. This is done for the base course, subbase and the top 30 cm of the subgrade. The subbase and subgrade were divided into two sections as with the εMU coils (see Figure 1) and added together to get the total deformation of the layers. The lateral wander was not taken into account here, but this should not have a significant impact as it only changes the linearity of the *MEPDG* model, which is adjusted with the calibration factor, β_1.

A calibration factor was adjusted to get reasonable correlation between the measured and calculated values (Table 2). The measurements in the base layer match well with the calculated values but in the other two cases the calculations and measurement fit well for the first 300,000 load repetitions but after that the slope of the measured values increases. This is not captured by the model. The reason for this change in behavior is not known. The authors considered two possible reasons for this; micro-damage or cracks in the bound layers causing higher loads in the unbound part of the structure or gradual change of accumulation of permanent deformation from predominately consolidation to

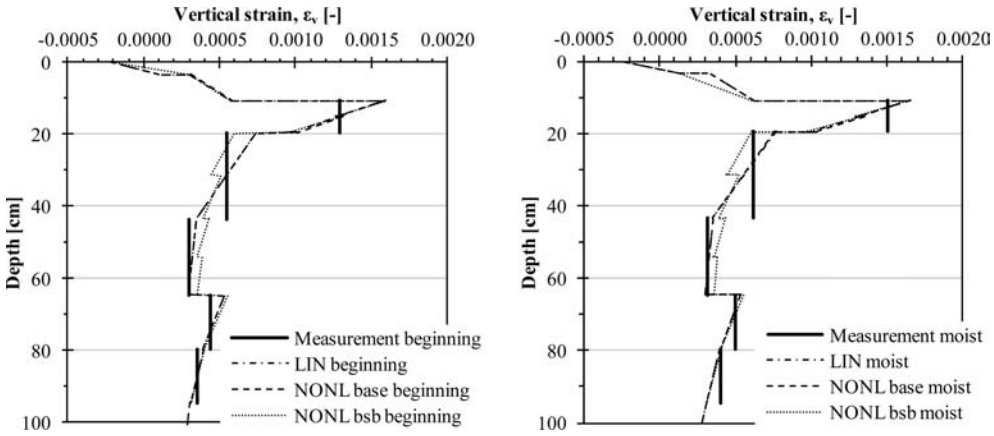

Figure 15. Vertical resilient strain as a function of depth in the beginning or between 20,000 and 30,000 load repetitions and in moist state after 100,000 load repetitions, tested with 800 kPa tire pressure and 120 kN axle load.

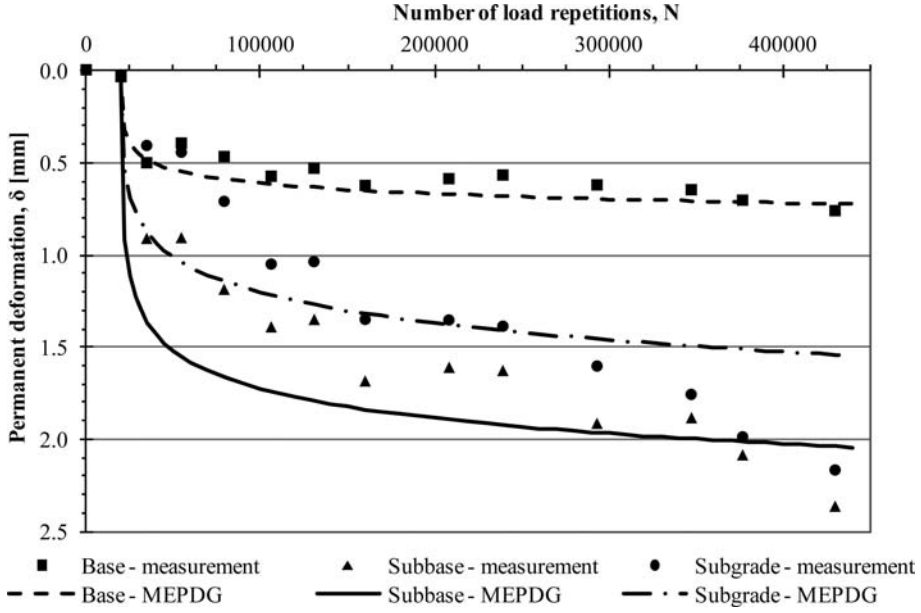

Figure 16. Permanent deformation in the unbound layers as a function of load repetitions. The testing was done with a dual wheel configuration, 800 kPa tire pressure and 120 kN axle load.

shear flow driven deformation. The first explanation is proven wrong as Figures 6 and 7 show no change in the vertical stress and strain measurements after 300,000 load repetitions. That leaves the latter explanation as a possible cause. This would have caused a rapid structural failure which could not be verified due to changes in the test setup after 490,000 load repetitions.

10 CONCLUSIONS

Responses of a pavement structure were monitored while testing with an HVS using various applied loads and tire pressures. These responses were analyzed using three different material approaches; all layers linear, the base layer assumed stress dependent, and the base and subbase both stress dependent. In general good agreement was established between the induced vertical measured and calculated strain values for a broad range of wheel load and tire inflation cases. Larger deviation in vertical stresses was observed between calculations and measurements. This might be due to difficulties in measuring vertical stresses in coarse grained materials.

When looking at the vertical strain the nonlinear models gave better results but the linear model gave adequate results if consideration is given to the fact that the model tends to underestimate the vertical strain at

low tire load and pressure and overestimate at high tire load and pressure.

Measurements taken in the beginning of the test were compared with measurements taken later on under the same load conditions. Both measurements and calculations indicate some softening in the asphalt layers with time, as the vertical strain in the unbound layers, deformation difference over the asphalt layers, and the tensile strain at the bottom of the asphalt layers all increase as more load repetitions are applied. In the calculations, 10% reduction in the stiffness of the asphalt layers was estimated after 100,000 load repetitions.

The *MEPDG* model correlated reasonably well with permanent deformation occurring in the unbound layers for approximately the first 300,000 load repetitions, thereafter the measured deformation rate increased compared to the calculated values. This might be explained by a gradual change from predominately consolidation to shear flow driven deformation. The calibration factors that corresponded best with measurements were 0.4, 0.8 and 1.2 for base, subbase and subgrade, respectively. In the *MEPDG*, field calibration factors of 1.673 and 1.35 are suggested for unbound granular base and subgrade, respectively. These values are higher than found in this study; however one must bear in mind that the values here are based on an accelerated pavement test carried out in a constant environment which does not cater for seasonal climate variations.

ACKNOWLEDGEMENTS

The work described in this paper was sponsored by the Icelandic Road Administration (ICERA) and data used from the Swedish National Road and Transport Research Institute (VTI).

REFERENCES

ARA Inc. 2004. *Guide for the Mechanistic-Empirical Design of New and Rehabilitated Pavement Structures*. Final report, NCHRP 1-37A. Transportation Research Board of the National Academies, Washington, DC. USA.

Erlingsson, S. 2007. Numerical Modelling of Thin Pavements Behavior in Accelerated HVS Tests. *Road Materials and Pavement Design. Vol 8/4*. pp. 719–744.

Erlingsson, S. 2010. Impact of Water on the Response and Performance of a Pavement Structure in an Accelerated Test. *Road Materials and Pavement Design. Vol. 11/4*. pp. 863–880.

Gomes-Correia, A., Hornych, P. and Akou, Y. 1999. Review of models and modeling of unbound granular materials. In: Gomes-Correia (ed.) *Unbound granular materials – Laboratory testing, in-situ testing and modeling*. A.A. Balkema, Rotterdam. pp. 3–15.

Huang, Y.H. 2004. *Pavement Analysis and Design*. 2nd edition. Pearson Education Inc., Prentice Hall and Education Inc., Upper Saddle River, New Jersey, USA.

Lekarp, F., Isacsson, U. and Dawson, A. 2000. State of the Art. I: Resilient Response of Unbound Aggregates. *ASCE Journal of Transportation Engineering. Vol. 126. No. 1*. pp. 66–75.

May, R.W. and Witczak, M.W. 1981. Effective Granular Modulus to Model Pavement Response. *Transportation Research Record 810*. Transportation Research Board, National Research Council, Washington DC. pp. 1–9.

Tseng, K-H. and Lytton, R. L. 1989. Prediction of Permanent Deformation in Flexible Pavement Materials. Implication of Aggregates in Design, Construction, and Performance of Flexible Pavements, *ASTM STP 1016*. H. G. Schrauders and C. R. Marek (eds). American Society for Testing and Materials, Philadelphia. pp. 154–172.

Uzan, J. 1985. *Characterization of Granular Materials. Transportation Research Record 1022*, Transportation Research Board, National Research Council. Washington, DC. pp. 52–59.

Van Niekerk, A.A., Scheers, J. van, Muraya, P. and Kisimbi, A. 2000. The Effect of Compaction on the Mechanical Behavior of Mix Granulate Base Course Materials and on Pavement Performance. *HERON. Vol. 45. No. 3.* ISSN 0046-7316. pp. 197–218.

Wiman, L.G. 2001. *Accelerated load testing of pavements; HVS-NORDIC tests in Sweden 1999.* Swedish National Road and Transport Research Institute (väg- och transportforskningsinstitut – VTI), Linköping, Sweden. VTI rapport 477A.

Wiman, L.G. 2006. *Accelerated load testing of pavements; HVS-Nordic tests at VTI Sweden 2003–2004.* Swedish National Road and Transport Research Institute (väg- och transportforskningsinstitut – VTI), Linköping, Sweden. VTI rapport 544A.

Wiman, L.G. 2010. *Accelererad provning av vägkonstruktioner; Referensöverbyggnad enligt ATB Väg*. Swedish National Road and Transport Research Institute (väg- och transportforskningsinstitut – VTI), Linköping, Sweden. (*In Swedish*) VTI rapport 628.

This page intentionally left blank

Advances in Pavement Design through Full-scale Accelerated Pavement Testing – Jones, Harvey, Mateos & Al-Qadi (Eds.)
© 2012 Taylor & Francis Group, London, ISBN 978-0-415-62138-0

How low is too low? Assessing the risk of low air voids using accelerated pavement testing

E. Levenberg
Technion – Israel Institute of Technology, Technion City, Haifa, Israel

R.S. McDaniel
North Central Superpave Center, Purdue University, West Lafayette, Indiana, US

T.E. Nantung
Indiana Department of Transportation, West Lafayette, Indiana, US

ABSTRACT: Various forms of asphalt pavement distress can be attributed, in many cases, to low air voids in mixtures during production and placement. When low air voids are encountered during production, the specifying agency must decide whether to require the material that has already been placed to be removed and replaced or whether it can be left in place. This study was conducted, in part, in the INDOT/Purdue Accelerated Pavement Testing (APT) Facility to develop a decision-support tool for dealing with such events that is based on projected rutting performance of the pavement system. The responses to repetitive APT wheel passes of test pavements with low air voids in either the surface or intermediate course were measured using a laser based system. The permanent deformation of the top pavement layers is used, in conjunction with simplified mechanistic analysis and engineering judgment, to formulate the desired decision-support tool.

1 INTRODUCTION

Various forms of asphalt pavement distress can be attributed, in some cases, to low air voids in the mixtures during production. The most notable of these include permanent deformation in the form of rutting or shoving (or both) and sometimes flushing/bleeding. The occurrence of low air void contents (AVCs) may originate during plant production as a result of an accidental increase in binder content or mix fines (or both), or during the construction phase as a result of overcompacting an adequately designed and produced mix. When low air voids are encountered during production, the specifying agency must decide whether to require the placed material to be removed and replaced or whether it can be left in place, typically with a reduction in pay. The performance of the low air void mixture may or may not be problematic, depending on several factors, including the severity of the deficiency in air voids, other mix attributes, the location of the low void mixture within the pavement structure, and the environmental and traffic conditions at the paving location.

1.1 *Literature review*

The two most common asphalt mixture design methods, namely Marshall (Asphalt Institute, 1997) and Superpave (AASHTO, 2004; AASHTO, 2007), use air void content as the main element that determines binder content. Traditionally, AVC is considered by the pavement engineering community to be one of the most important factors that affect mixture behavior and pavement performance. In the typical Marshall methodology, the design AVC ranges between 3 to 5%. In the standard Superpave methodology the design AVC is fixed at 4%. In a recent study Christensen and Bonaquist (2006) re-evaluated this target value for the Superpave system. The study concluded that a design AVC in the range of three to five percent is adequate for all Superpave mixture types (i.e., surface, intermediate and base), for all aggregate gradations (i.e., dense, coarse and fine), and for all binder grades.

Currently there are no widely accepted, rational mechanisms for quantifying the impact of low air voids on pavement performance. There are, however, numerous reports in the literature documenting the potential for poor performance when these mixtures are used. During the development of the Marshall design methodology (Foster, 1982), it was found that surface asphalt concrete (AC) mixtures constructed to an in situ AVC of 2.5% or less shoved under traffic loads during hot weather conditions. These mixtures were predominantly dense graded, having a maximum aggregate size of 19.0 mm (0.75 in.). The Marshall study also evaluated dense graded sand-asphalt mixes having maximum aggregate size of 4.75 mm (0.19 in.). These mixes exhibited instability at in-place AVCs

higher than 3%. This resulted in a 2% translation of the AVC requirement range, for these latter mixes only, to 5 to 7% (instead of 3 to 5%).

In a study of in-place rutting, Brown and Cross (1989) looked at pavements that experienced premature rutting and at pavements that had no rutting after more than ten years of service. They used coring, trenching and laboratory tests to assess the source of the ruts. The researchers concluded that a low AVC in situ or in recompacted specimens was a good indicator for rutting and pointed to a previous study with similar results (Huber and Herman, 1987). Another study set out specifically to identify mix design parameters that may affect rutting (Brown and Cross, 1992). In that research 42 pavements were sampled from 14 different states. Based on coring, trenching and laboratory tests, the following conclusions were made: (i) pavements that rutted had in-place AVCs below 3%; and (ii) most of the observed rutting was confined to the top 75 to 100 mm (3 to 4 in.) of the pavement.

Somewhat in contradiction to the above studies, reported field experience can also be found in which mixes designed and constructed with low AVCs behaved adequately. The following lists several examples. Davis (1988) reported that dense graded large stone mixes, with maximum aggregate sizes of 50 mm (2 in.) or larger, behaved extremely well with no rutting or cracking at in-place AVCs of 3% or less; these mixes also had very soft 'lively' binders. During the WesTrack experiment (FHWA, 1999), the AC mixture in test section #43 was designed to a target AVC of 1.7%. After paving, the average in-place AVC of the corresponding test section was also very low: 1.6%. Despite this fact, this mix experienced minimal rutting/shoving compared to all other sections in the experiment. In addition, low void AC mixtures had been suggested in the context of perpetual pavements to provide increased fatigue resistance at the bottom of the asphalt course (Harvey and Tsai, 1996). Pavements designed according to this concept are so-called rich-bottom pavements. For example, researchers in California (Harvey, et.al., 1999) proposed a pavement reconstruction strategy which included a bottom AC layer that is 50 to 75 mm (2 to 3 in.) thick, designed to an AVC of 2%. Detailed reports on such mixture designs and "rich-bottom" construction can be found in other publications (Monismith, et.al, 2001; Scullion, 2006; Willis and Timm, 2006).

1.2 *Indiana's practices and issues*

The Indiana Department of Transportation (INDOT) uses the Superpave system for designing all asphalt mixture types and selects the design binder content as that which provides 4.0% air voids at the design number of gyrations (N_{design}), which is based on the design traffic level. INDOT accepts hot mix asphalt based on the produced volumetric properties – specifically the binder content, air void content at N_{design} and voids in the mineral aggregate (VMA) at N_{design}. In addition, in-place density and smoothness are also pay factors. During production, plate samples are removed from the mat behind the paver screed. Portions of these plate samples are compacted in the gyratory compactor to the design gyrations, and, after cooling, the bulk specific gravity and VMA of the specimens are determined. Mixtures placed with air void contents below 2.0% risk removal and replacement at the contractors' expense. Mixtures with air void contents between 2.0% and 4.0% are accepted at a lower rate of payment, as determined by the INDOT Failed Materials Committee. The Failed Materials Committee adjudicates the non-complying material on a case-by-case basis; using engineering judgment, they try to consider in their decision such factors as how low the air void content is, the traffic level, the depth of the failed material within the pavement structure, and other mitigating circumstances.

Based exclusively on experience, without a rational decision-making process, the Department carries a higher risk level of accepting an inferior product that may not perform as intended. At the same time, contractors face the increased risk of reduced pay or the cost of removal and replacement when there is a possibility the material will perform acceptably. Consequently, INDOT initiated a research project to evaluate the impact of low air voids on rutting performance in order to develop a decision-support tool for determining whether to accept or reject a mixture with inadequate air voids and for assessing a monetary penalty if the material is allowed to remain in place.

2 OBJECTIVE

The objective of the overall research project was to develop a decision-support tool to help determine and balance risk when accepting or rejecting asphalt mixtures with low air voids. The aim is for the development to be founded on projected rutting performance that is, in turn, based on Accelerated Pavement Testing (APT) results and mechanistic considerations. This paper describes the associated APT study and its findings.

3 EXPERIMENTAL SCOPE

This project involved two experiments. First, INDOT sponsored two test sections at the National Center for Asphalt Technology (NCAT) Test Track in 2006 (Phase III). In one section, a low air void content was obtained by increasing the binder content; in the other, the low air void content was achieved mainly by a change in the aggregate gradation (and a small change in the binder content). NCAT divided each section in two and targeted approximately 1% and 2% air voids in the two subsections. Another test section on the Track served as the control, with approximately 4% AVC. In all cases, the 50 mm (2 in.) surface mixtures of the existing structures at NCAT were replaced with the low void content mixtures. The results suggested that acceptable rutting performance can be expected

Figure 1. The INDOT/Purdue APT Facility.

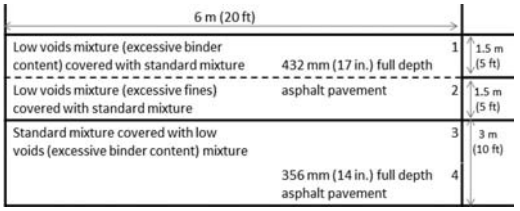

Figure 2. Layout of test sections in the APT Facility.

Table 1. Proportions of Mix Components by Mass of Mix.

		Low voids mix (%)	
Mixture component	Standard mix (%)	Excess binder	Excess fines
Coarse aggregate	46.0	45.2	40.0
Natural sand	10.0	10.0	11.0
Manufactured sand	24.0	24.0	29.0
RAP	15.0	15.0	15.0
Virgin PG 64-22	5.0	5.8	5.0
Total binder	5.7	6.5	5.7

if the AVC is above 2.75%. At AVCs below this level, the rutting rate increased dramatically (Willis, et al., 2009).

The second experiment undertaken for this study, and the focus of this paper, made use of the INDOT/Purdue APT Facility, shown in Figure 1. This facility comprises an enclosed, climatically controlled building where pavement sections can be constructed in a 6 m by 6 m (20 ft. by 20 ft.) pit using full-scale construction equipment. The pit is 1.8 m (6 ft.) deep to allow a subgrade to be constructed below the pavement. A carriage spans the pit, and the loading mechanism is moved across using an elevator motor. A downward force of up to 89 kN (20,000 lbs) can be applied to the pavement through half of a single axle, equipped with either dual tires or a super single tire. The load can be applied in one direction (i.e., unidirectional mode) or two directions; lateral wheel wander can also be simulated in the test. Rutting distress is in effect accelerated because of the relatively slow speed of travel of 8 km/h (5 mph). The temperature in the APT facility can be increased up to 60°C (140°F) by heating the ambient air with suspended heaters. Surface rutting profiles are measured transversely across each lane using a laser based system. The operation of the APT and analysis of the resulting measurements are described hereafter.

4 TESTING LAYOUT AND MATERIALS

At the beginning of this study, two perpetual pavement design sections remained in place in the APT facility from a previous study. The total AC thickness in Lanes 1 and 2, shown in Figure 1, was 430 mm (17 in.), and the AC thickness in Lanes 3 and 4 was 355 mm (14 in.). Both were supported by a two-layered subgrade composed of 405 mm (16 in.) of cement stabilized soil overlying untreated soil. The top 100 mm (4 in.) of the pavement was milled and removed in 2009 so that the low void mixture experiment could proceed. Embedded gauges targeting mechanical responses remained in the pavement structure from the previous experiment. However, after construction it was found that most of the instrumentation was out of scale and could not be reliably used any further.

New mixtures were placed in two 50 mm (2 in.) lifts over the existing perpetual structure. In Lanes 1 and 2, the lower 50 mm (2 in.) lift consisted of a low air void content mixture while the top 50 mm (2 in.) complied with standard design specifications. Excessive binder content was the cause for the low voids in Lane 1, while in Lane 2 the low voids were due to excessive fines content. The top 100 mm (4 in.) in Lanes 3 and 4 were composed of a standard mixture 50 mm (2 in.) thick overlaid by a low voids mixture due to excessive binder content. The above described configuration is shown in Figure 2.

The three mix types placed in the APT sections were based on an existing mix design used by a local producer to pave several roads in the area. The mix was a 9.5 mm surface mix with a PG 64–22 binder with an N_{design} of 75 gyrations (for a traffic volume of 300,000 to 3,000,000 equivalent single axle loads). The mixes were composed of dolomite coarse aggregate, dolomite manufactured sand, reclaimed asphalt pavement (RAP) and natural sand. The proportions of the various components of the mixtures are shown in Table 1.

5 LOADING CONDITIONS AND RUTTING MEASUREMENTS

APT loading was carried out using a super single tire inflated to 0.7 MPa (100 psi), making a circular contact area with the pavement with a 165 mm (6.5 in.) radius. Thirteen load 'packages' were executed, each containing 1,000 wheel passes, applied in unidirectional mode

Table 2. Application Order of Loading Packages in Lane 3.

Loading package #	Cumulative number of passes	Lateral offset (mm)	Lateral offset (in.)
1	1,000	0	0
2	2,000	0	0
3	3,000	−125	−5
4	4,000	−75	−3
5	5,000	0	0
6	6,000	+50	+2
7	7,000	−75	−3
8	8,000	0	0
9	9,000	+125	+5
10	10,000	−125	−5
11	11,000	+100	+4
12	12,000	−25	−1
13	13,000	0	0

without wander. Every single 'package' was composed of ten 'sets' of 100 wheel passes having different loading intensities increasing from 8.9 kN to 89 kN (2,000 to 20,000 lbs.). In addition, each loading package was assigned an individual lateral carriage position, i.e., different wander position relative to the center of the tested lane (refer to Table 2).

In terms of climate, the goal was to maintain a constant temperature level of 30 C (86 F) in the pavement throughout the experiment. An embedded "temperature tree" was used to monitor the prevailing temperature at various depths. In actuality, the temperatures varied within the range of 24.4 to 31.7°C (76 to 89 F).

Surface profile measurements were collected repeatedly during testing using a laser beam assembly along seven cross sections, spaced 0.3 m (1 ft.) apart, located before and after the middle of the tested lane (lengthwise). To better understand the evolution and source of any surface rutting, changes in layer thicknesses were also monitored. To accomplish this, at least partially, holes were drilled in the pavement so that their bases/bottoms served as targets for the laser beam. These holes were relatively narrow and protected by nylon sleeves 25 mm (1 in.) in inner diameter; the sleeves were glued to the drill-hole sides along the circumference to prevent closure under loading. Each sleeve was installed flush with the surface and extended to one-third to one-half of the drilled depth, enabling the layer thickness to change at the measurement point.

Figure 3 shows a 'drill' plan, not drawn to scale, presenting a close-up view of the central area of a 6 m (20 ft.) long test section. Five drill-hole lines are shown, spaced 0.30 m (1 ft.) apart before and after the middle of the test section. Five holes were drilled in each line, symmetrically spread around the centerline of the test lane at 125 mm (5 in.) intervals. The drill depths along the LH, LH−2 and LH+1 lines were 50 mm (2 in.); the holes in lines LH−1 and LH+2 extended to a depth of 100 mm (4 in.) below the pavement surface. Once the array of holes was installed and

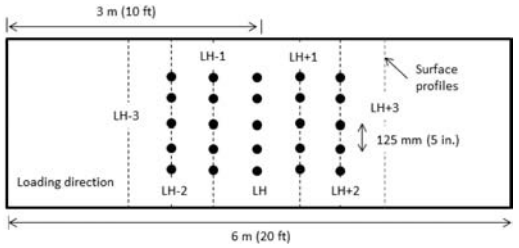

Figure 3. Layout of drill holes and surface profile measurements in test lanes.

before any loading was applied to the pavement, ten replicate surface profiles were measured along the five lines, capturing the drill points. Ten replicate profiles were also measured along two additional lines that did not consist of any holes (LH-3 and LH+3 in the figure). The resulting dataset served as the benchmark for all subsequent load induced deformations.

6 MEASUREMENTS AND ANALYSIS

The laser profile measurements collected during the 13,000 passes are analyzed hereafter. The measurements from Test Lane 3 (see Figure 2), where the low voids mixture was placed on top of a standard mix, are addressed first. The surface profile evolution along the LH-3 line (refer to Figure 3) is shown in Figure 4. If a virtual straightedge is placed on the surface, resting on the heaving noticed on both sides of the chart, the maximum rutting level is seen to be about 6 mm (0.25 in.). The tire treads can also be seen in the central part of the figure – between transverse locations 400 and 700 mm. Figure 5 shows the rutting along the LH line with the 50 mm (2 in.) holes. In this figure the vertical deformation of the bottom of the holes relative to their initial elevations is also shown – after 13000 passes. It may be seen that, similar to Figure 4, the overall rutting level is about 6 mm (0.25 in.). Additionally, this figure reveals that the top low voids lift is roughly "responsible" for 50% of the observed/overall surface rutting.

An attempt to analyze the profile lines that included 100 mm (4 in.) holes, namely LH−1 and LH+2 was unsuccessful. After viewing the available measurements it was realized that the laser was failing to reach the bottom of the holes. The reason for this is the inability of the automatic positioning system to repeatedly return to the same location (lengthwise). This experimental aspect will be improved upon in future studies. The results from Lanes 1 and 2 are not shown here due to space limitations. However, the overall findings are similar to the findings from Lane 3; i.e., the maximum rutting level was about 6 mm (0.25 in.) and the top lift is not the only contributor to the observed surface rutting.

A mechanistic model was used to extend the APT study and examine the rutting behavior when a low

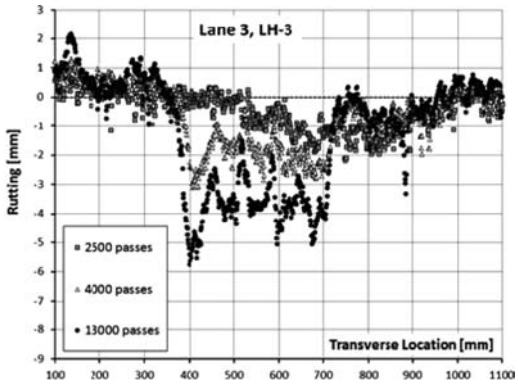

Figure 4. Selected laser profiles for APT lane 3 – line LH-3 (refer to Figure 3).

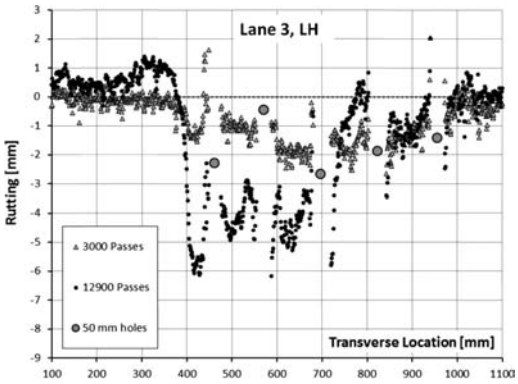

Figure 5. Selected laser profiles for APT lane 3 – line LH (refer to Figure 3).

void layer is located deeper in the pavement system. A relatively simple model was selected, in which the pavement is idealized as a four layered system, consisting of (Lane 3): 355 mm (14 in.) of asphalt, 405 mm (16 in.) of cement treated soil, 1,070 mm (42 in.) of untreated soil, and the concrete floor of the test pit (semi-infinite). The constitutive response of all four layers was assumed to be linear (isotropic) elastic, obeying the constitutive relation (summation convention applies):

$$\varepsilon_{ij}^{e} = \frac{s_{ij}}{2G} + \frac{\sigma_{kk}}{9K}\delta_{ij} \qquad (1)$$

in which ε_{ij}^{e} is the elastic strain tensor, s_{ij} is the deviatoric component of the stress tensor σ_{ij}, G is the shear modulus, and K is the bulk modulus.

After assuming the Poisson's ratios for each layer, moduli values were obtained from FWD testing carried out at a temperature level of 32°C (90°F). This temperature level is slightly higher than the prevailing temperature during the APT study, but the resulting backcalculated moduli are considered more representative given that the loading speed of the APT carriage was slow (Levenberg, et.al., 2009). By simulating the super single wheel movement, the layered model was utilized to compute the history of stresses in the asphalt lifts along a cross-section (e.g., line LH in Figure 3). Computations were performed every 25 mm (1 in.), both in the vertical direction (i.e., downward in the pavement) to a depth of 325 mm (13 in.) and also in the transverse direction to an offset distance of 1,000 mm (3.3 ft.) from the line of travel (i.e., a grid of 41×7 points). The wheel movement was simulated quasi-statically, by applying the load at different distances (lengthwise) from the cross section; 28 distances were used for this purpose, spaced unevenly between 0 mm and 2,000 mm (6.5 ft.). Because of the linear nature of the model, superposition and symmetry considerations could be used to generate the full stress history in the asphalt lifts during the entire 13,000 passes of the APT carriage from the above calculations.

In order to simulate rutting originating from the asphalt layer, a visco-plastic (VP) constitutive model was assumed for each of the asphalt lifts. In analogy with the linear elastic constitutive model, Equation 1, the VP equation takes the form:

$$\dot{\varepsilon}_{ij}^{vp} = \frac{s_{ij}}{\eta_G} + \frac{\sigma_{kk}}{\eta_K}\delta_{ij} \qquad (2)$$

in which $\dot{\varepsilon}_{ij}^{vp}$ is the VP strain-rate tensor, η_G represents viscosity resisting shear deformation, and η_K represents a viscosity resisting bulk deformation. As can be seen, when η_K increases towards infinity no isotropic VP strains can develop in the material, only VP shear deformations; this condition has the potential to represent a low voids mix for which VP deformations will be predominantly shear related. For standard mixtures, VP strains will develop under load in both shear and volumetric modes. Also, η_G in standard mixes is expected to be higher compared to η_G in a low void mix, representing the greater resistance to shear deformation of the former. The choice for Equation 2 was inspired by studies dealing with the permanent deformation (compaction) of ice and snow (Ambach and Eisner, 1983).

It should be noted that in order to generate realistic results using this simple VP model, neither η_G nor η_K can be considered constant; they should depend on temperature, age/time and possibly on VP strain history. None of these dependencies is explored herein. Temperature is assumed constant; time/age effects are ignored due to the short duration of the APT experiment; and VP strain history is not included because it introduces nonlinear behavior that precludes the use of superposition and therefore dramatically increases the computational cost.

At this point, the computed stress history in a cross-section (from the layered model) after 13,000 passes of the APT carriage (considering wander and different loading levels) is used as input for the VP model. Initially, only the top two lifts, having a combined thickness of 100 mm (4 in.), were assumed to contribute to the observed rutting as the remainder of the structure had already endured loading from a previous study. The necessary viscosities were subsequently

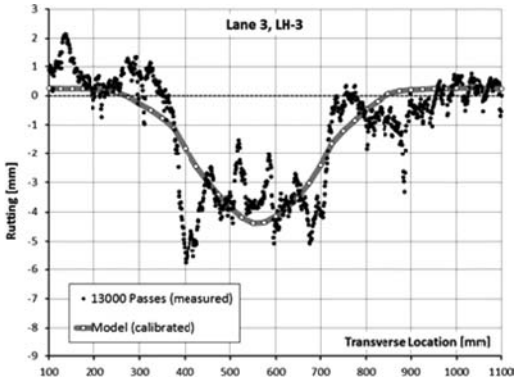

Figure 6. Surface rutting data and calibrated model.

obtained from inverse analysis by matching the measured rutting in the experiment. The match obtained for Lane 3 is shown in Figure 6.

One indication for the reasonableness of the modeling effort was that the resulting shear viscosity (η_G) of the standard mix was much higher than the shear viscosity of the low voids mix. Also, as expected, the bulk viscosity (η_K) of the low voids mix was much higher than the bulk viscosity of the standard mix.

Using the calibrated viscosity values for the low voids mix, such an asphalt lift having a thickness of 50 mm (2 in.) was virtually inserted into the APT pavement at different depths from the top. When placed (in the model) under a surface lift made of standard mix, the results from Lanes 1 and 2 were adequately reproduced. This provided further confidence that the model was functioning appropriately. When the low voids mixture was placed further down from the pavement surface, below additional 50 mm (2 in.) lifts made of standard mix, the overall rutting level at the surface did not improve, only the width of the rut increased slightly. More details will be provided in a forthcoming report.

7 CONCLUSIONS AND RECOMMENDATIONS

The APT measurements in this study indicate that similar rutting performance should be expected if a low void mix is placed as a surface layer or placed 50 mm (2 in.) below the surface underlying a standard mix. The cause of the low voids, whether it originates from excessive binder content, or excessive fines, did not appear to impact the behavior. Using mechanistic considerations, deeper positions for the low voids mix were explored, and it was found that surface rutting is negatively affected even if such a layer is placed deeper in the pavement, up to a depth of 300 mm (12 in.). Hence, combining the APT and NCAT study findings, the following is recommended for high traffic intensities (Table 3). The extension for low traffic level is based on engineering judgment.

The proposed decision support tool in Table 3 is provisional, based on preliminary analysis of limited data from the APT and NCAT studies. The table is formulated as a rough guide, not taking explicitly into account the specifics of the low void mix (e.g., maximum aggregate size or other factors), details about the pavement system, in situ climatic conditions, and as-built layer properties and volumetrics. This is done intentionally so that it could gain practical acceptance by allowing room for engineering judgment on the part of the decision makers.

Table 3. Proposed decision support tool.

AVC [%]	Traffic intensity (20 year)	
	Low	High*
3.0	1	1
2.9	1	2
2.8	2	2
2.7	2	2
2.6	2	3
2.5	3	3

*ESALs>10,000,000

1	Accept without monetary reduction
2	Consider leaving mix in-place with monetary reduction
3	Reject mix

ACKNOWLEDGMENTS

This paper is based on research sponsored by the Indiana Department of Transportation and Federal Highway Administration under SPR-2813. The contents of this paper reflect the views of the authors, who are responsible for the facts and the accuracy of the data presented herein. The contents do not necessarily reflect the official views or policies of the Indiana Department of Transportation or the Federal Highway Administration at the time of publication. This report does not constitute a standard, specification, or regulation.

REFERENCES

AASHTO. 2004, Standard Practice for Superpave Volumetric Design for Hot-Mix Asphalt HMA, *AASHTO Designation R 35-04, Association of American State Highway and Transportation Officials*, Washington, DC.

AASHTO. 2007, Standard Specification for Superpave Volumetric Mix Design, *AASHTO Designation M 323-07, Association of American State Highway and Transportation Officials*, Washington, DC.

Ambach, W. and Eisner, H. 1983, Effective Shear Viscosity and Effective Bulk Viscosity of Firn of a Temperate Glacier, *Proceedings of the Second Symposium on Applied Glaciology Colbeck, S.C. Ed., Annals of Glaciology 4*, pp. 10–12.

Asphalt Institute 1997, *Mix Design Methods*, MS-2, Sixth Edition, p. 141, Lexington, KY.

Brown, E.R. and Cross, S.A. 1989, A Study of In-place Rutting of Asphalt Pavements, *Journal of the Association of Asphalt Paving Technologists*, Vol. 58, pp. 1–39, Lino Lakes, MN.

Brown, E.R. and Cross, S.A. 1992, *A National Study of Rutting in Hot Mix Asphalt HMA Pavements*, NCAT Report 92-5, National Center for Asphalt Technology, Auburn University, Auburn, AL.

Christensen, D.W. and Bonaquist, R.F. 2006, *Volumetric Requirements for Superpave Mix Design*, National Cooperative Highway Research Program, NCHRP Report 567, p. 57, Transportation Research Board, Washington, DC.

Davis, R.L. 1988, *Large Stone Mixes: A Historical Insight*, NAPA Report IS 103/88, National Asphalt Pavement Association, Lanham, MD.

FHWA. 1999, *Performance of Coarse-Graded Mixes at WesTrack-Premature Rutting*, FHWA Report RD-99-134, Federal Highways Administration, Washington, DC.

Foster, C.R. 1982, *Development of Marshall Procedures for Designing Asphalt Paving Mixtures*, NAPA Report IS-84 National Asphalt Pavement Association, Lanham, MD.

Harvey, J.T. and Tsai, B.W. 1996, Effects of Asphalt Content and Air Void Content on Mix Fatigue and Stiffness, *Transportation Research Record 1543*, Journal of the Transportation Research Board, Washington DC, pp. 38–45.

Harvey, J., Long, F. and Prozzi, J.A. 1999, Application of CAL/APT Results to Long Life Flexible Pavement Reconstruction, *Proceedings of the Accelerated Pavement Testing Conference*, Reno, Nevada.

Huber, G.A. and Herman, G.H. 1987, Effect of Asphalt Concrete Parameters on Rutting Performance, *Journal of the Association of Asphalt Paving Technologists*, Vol. 56, pp. 33–61, Lino Lakes, MN.

Levenberg, E., McDaniel, R.S. and Olek, J. 2009, *Validation of NCAT Structural Test Track Experiment Using INDOT APT Facility*, Report Number FHWA/IN/JTRP-2008/26, Joint Transportation Research Program, Indiana Department of Transportation and Purdue University, West Lafayette, IN.

Monismith, C.L., Long, F. and Harvey, J.T. 2001, California's Interstate-710 Rehabilitation: Mix and Structural Section Designs, Construction Specifications, *Journal of the Association of Asphalt Paving Technologists*, Vol. 70, pp. 762–799, Lino Lakes, MN.

Scullion, T. 2006, *Perpetual Pavement Design in Texas: State of the Practice*, Report FHWA/TX-06/0-4822-1, Texas Transportation Institute, Texas A&M University, College Station, Texas.

Willis, R.J. and Timm, D.H. 2006, *Forensic Investigation of a Rich Bottom Pavement*, NCAT Report 06-04, National Center for Asphalt Technology, Auburn University, Auburn, AL

Willis, R., Timm, D., West, R., Powell, B., Robbins, M, Taylor, A., Smit, A., Tran, N., Heitzman, M. and Bianchini, A. 2009, *Phase III NCAT Test Track Findings*, National Center for Asphalt Technology, NCAT Report 09-08, Auburn University, Auburn, AL.

This page intentionally left blank

Advances in Pavement Design through Full-scale Accelerated Pavement Testing – Jones, Harvey, Mateos & Al-Qadi (Eds.)
© 2012 Taylor & Francis Group, London, ISBN 978-0-415-62138-0

Exploratory evaluation of cracking performance of a 4.75 mm NMAS overlay using full-scale accelerated loading

X. Qi, X. Li & N.H. Gibson
Turner Fairbank Highway Research Center, Mclean, Virginia, US

T. Clark
Virginia. Asphalt Pavement Association, Richmond, Virginia, US

K. McGhee
Virginia Department of Transportation, Charlottesville, Virginia, US

ABSTRACT: State transportation agencies have begun to develop and implement specifications for 4.75 mm Nominal Maximum Aggregate Size (NMAS) Superpave mixes with some specifications based on recommendations from a study conducted by the National Center for Asphalt Technology. These mixes restore surface texture and ride quality but also have advantages such as optimal use of available aggregates, accommodation of Reclaimed Asphalt Pavement (RAP), and application as an impermeable, thin preservation treatment. A trial 4.75 mm NMAS from Virginia DOT was placed as a thin treatment on existing accelerated pavement test sections. The objectives of this study were to conduct full-scale load testing to gain confidence in a new mix design and to explore the ability of this thin treatment to curtail top down cracking. Several sub-sections, which were reserved and left unloaded from a preceding study, received a 25 mm thick mill-and-fill with the 4.75 mm NMAS mix. The construction produced a test section where half of the loaded wheel path was paved with the 4.75 mm NMAS mix allowing a direct comparison of cracking performance with and without the thin treatment. Full scale accelerated aging was utilized to compare the fatigue cracking performance for four combinations; with and without 4.75 mm NMAS treatment each with and without aging. Crack maps illustrated that the unaged 4.75 mm mixture's cracking performance exceeded the life of the sections without the treatment. Estimates of the increase in life provided by this thin treatment exceed 8 years. Forensic coring has shown top-down cracking to be the predominant distress. When aged, however, the 4.75 mm treatment provided no additional life, but performed as well as an aged section without the treatment.

1 INTRODUCTION

1.1 *Background*

An aging highway infrastructure combined with increasingly limited resources and rapidly growing traffic volumes can benefit from preservation practices to extend service life. Recently, the use of Superpave 4.75 mm nominal maximum aggregate size (NMAS) asphalt concrete (AC) in a thin overlay has gained more attention as a possible pavement preservation strategy. A 2004 National Center for Asphalt Technologies (NCAT) survey of state agencies indicated that several states were using 4.75 mm NMAS mixtures or mix types reasonably close to the AASHTO criteria for 4.75 mm mixes. The survey also confirmed that more agencies were interested in using 4.75 mm NMAS mixes in the future (West et al, 2011). Thin lift 4.75 mm NMAS mixes not only restore surface texture and ride quality but also have advantages such as providing a use for screening stockpiles and leveling courses to decrease construction time.

In May 2010, a trial 4.75 mm NMAS developed by Virginia DOT and Superior Paving Corporation, Inc. was placed as a thin treatment on existing accelerated pavement test sections at the FHWA pavement testing facility (PTF). Three pavement subsections which were reserved and left unloaded from a preceding study received a 25-mm thick mill-and-fill inlay with the 4.75 mm NMAS mix. The construction produced a test section where half of the loaded wheelpath was paved with the 4.75 mm NMAS mix allowing a direct comparison of cracking performance with and without the thin treatment. Full scale accelerated aging was utilized to compare the fatigue cracking performance for four combinations with and without a 4.75 mm NMAS treatment each with and without aging.

1.2 *Objectives*

The objectives of this study were to conduct full-scale load testing to gain confidence in a new mix design and to explore the ability of this thin treatment to

Table 1. Aggregate gradation of 4.75 mm job mix formula and production.

Sieves #	Bealton sand	#10	RAP	Nat. Sand	Bag House	Mix Design	Gradation Check
¾″ (19 mm)	100	100	100	100	100	100	100
½″ (12.5 mm)	100	100	99.8	100	100	100	99.7
3/8″ (9.5 mm)	100	100	95	100	100	99.1	97.0
#4 (4.75 mm)	96	96	67	98	100	92.3	87.6
#8 (2.36 mm)	62	66	50	86	100	68.7	60.1
#16 (1.18 mm)	38	45	39	66	100	45.7	43.1
#30 (0.60 mm)	26	33	29	36	100	31.9	31.0
#50 (0.30 mm)	17	24	21	12	100	21.6	21.4
#100 (0.15 mm)	10	18	14	5	98	14.7	15.1
#200 (.075 mm)	5.2	12.4	9.3	2.5	95	10.3	10.4
Blend %	26	44	20	10	1	–	–

Table 2. Volumetric properties of 4.75 mm job mix formula and production.

				Produced Mix Gmm From FHWA: 2.595 From Contractor: 2.584	
Specification Criteria Ndesign = 50 gyrations			Job Mix	FHWA aggregate	Contractor's aggregate
Volumetrics		Virginia DOT	Formula	$G_{SB} = 2.813$	$G_{SB} = 2.789$
VTM (%)	Design	5	4.4	–	
	Production	3–6	–	4.21–3.98	
VFA (%)	Design	70–75	74	–	
	Production	70–80	–	75.1–76.2	74.0–75.2
VMA (%)		16.5 min.	16.9	16.9–16.7	16.2–16.0
V_{be} (%)		–	–	14.96	14.86
Dust to Binder (effective asphalt)		1–2	1.98	1.99	2.11

curtail top down cracking (i.e. one of the objectives was to exclude oxygen from the underlying section). This paper summarizes the design and construction of the as-built 4.75 mm NMAS mix, accelerated pavement aging and testing, and the results obtained from the accelerated pavement testing to date. The laboratory evaluation of the 4.75 mm NMAS mix has been reported elsewhere (Li et al, 2012).

2 MATERIALS AND MIX DESIGN OF 4.75 MM MIX

The aggregate blend for the 4.75 mm NMAS mix is 44% fine aggregate screening, 26% manufactured sand, 20% fine recycled asphalt pavement (RAP) and 10% natural sand. The aggregate gradations are summarized in Table 1. The virgin binder was a PG 76-22. It can be seen from Table 1 that the final mix design met almost all Superpave mix design criteria for 50 gyrations recommended by NCAT (James et al, 2003). Specifically, it has as high as 10% passing the 0.075 mm sieve, 30% to 54% passing on the 1.18 mm sieve, over 16% VMA (voids in mineral aggregate) and approximately 75% VFA (voids filled with asphalt). The dust-to-binder ratio is above 1.5 and the volume of effective binder is less than 13.5%; both criteria recommended by NCAT study for good rutting resistance mixtures (West et al, 2011).

The gradation and asphalt content was checked for the production mix obtained during construction by extraction using trichloroethylene (TCE) solvent. Two replicates were tested and the average gradation is shown in the last column in Table 1. Consistent gradation between design and production was found on the smaller sieves, but with larger differences on the coarser aggregates. The asphalt binder was extracted and recovered following AASHTO T319. The recovered mix binder graded as a PG 82-22, which suggests that the RAP likely increased the high temperature grade by one grade while leaving the low temperature grade unaffected. The asphalt content, VFA, VMA and ratio of dust to effective binder content of the produced mix meet most design targets at 50 gyrations. Volumetric properties are provided in Table 2.

The VMA can be marginally within or outside the allowable production range specified by Virginia DOT depending on whether the contractor's or FHWA's maximum specific gravity and aggregate bulk specific gravity are used.

Given this was production and not laboratory produced material, the mix was still within production tolerance, which is 5.7% for two samples per VDOT SM-4.75 specifications and did not meet the design gradation for 9.5 mm NMAS. Consequently, the

conclusions reached from this project were not jeopardized by the slight deviation from design gradation ranges.

3 EXISTING MATERIAL AND STRUCTURE

The thin 4.75 mm NMAS overlay was placed on existing sections available for additional full scale tests that remained after transportation pooled fund study TPF-5(019) was completed. Details of the structural configuration and materials in the accelerated pavement testing experiment are described in the literature (Gibson et al, 2012). The pavement structure contains an asphalt concrete (AC) layer placed on top of a crushed aggregate base (CAB) over a relatively stiff AASHTO A-4 subgrade (decomposed bedrock). The AC layer thickness before the inlay was 150 mm. The total thickness of the AC and CAB layers is 660 mm. The AC mix design for the test lanes was an identical, dense, coarse graded 12.5 mm nominal maximum aggregate mix, but with different binder types. The three binders in the structural AC layers underneath the inlay used an unmodified control (Lane 8), unmodified air blown (Lanes 10), and a relatively soft base binder heavily modified with styrene-butadiene-styrene (Lane 9). Lane 9 is still under loading and data are not reported here.

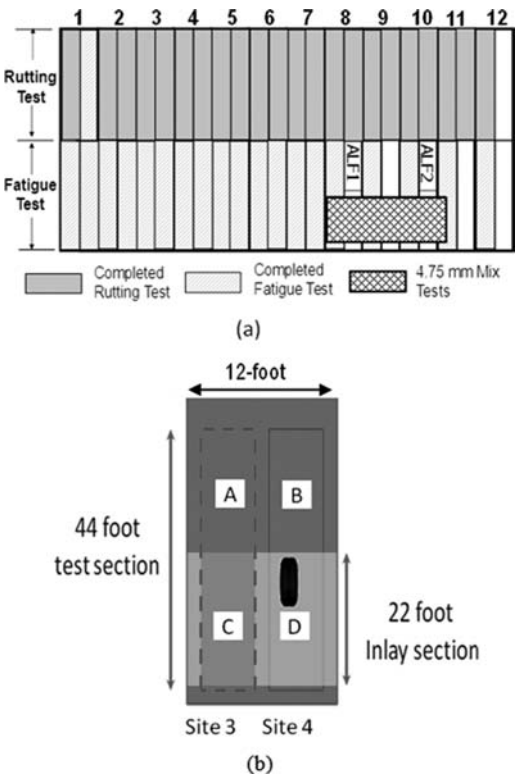

Figure 1. Layout of ALF test sites with 4.75 mm NMAS inlay; (a) inlay sections within overall pavement test facility and (b) dimensions of inlay within a test lane.

4 CONSTRUCTION OF 4.75 MM NMAS INLAY

A layout of the inlay within the pavement test facility is provided in Figure 1a. An inlay rather than an overlay was constructed in order to avoid any wheel dynamics caused by a transition or bump when the ALF trolley traveled from one sub-section to another. As shown in Figure 1b, the 4-m wide and 13.2-m long (12-ft. by 44-ft.) lane contains two testing sites at each end where the left site is designated as Site 3 and the right as Site 4. Each site was then further divided into two subsections. The end of each lane was labeled with four subsections A, B, C and D as shown in Figure 1b. Only Sections C and D were inlaid with the 4.75 mm mix.

The top 25 mm (1 in.) layer of the original pavement was milled with a hard joint around all edges. A tack coat of CRS-1 at 0.07 gallons/square yard was applied just before paving. The mixture was produced at a local asphalt mixture plant and transported to the ALF site with a distance of approximately 18 miles. The mix was then dumped into a Roadtec SB-2500B material transfer vehicle (MTV), which fed a Blaw-Knox PF3200 rubber tire paver. Paving started from the eastern side and moved transversely toward the western side. The lay-down temperature was measured by an infrared thermometer and averaged about 124°C (255°F). The mix was produced using a water foaming technique in anticipation of a longer than ideal haul duration through a traffic congested region. The mix appeared workable and no problems associated with an overly stiff mix were observed. A 15,000 lb roller was used for the breakdown and an 8,000 lb roller was used finishing. The initial roller pattern was two vibratory passes and one static pass. Additional static compaction was made to further lower the air voids while monitoring with nuclear density gauges targeting a 10% air void content. Photographs of construction are provided in Figure 2.

Three slabs were cut from Lane 8 for Virginia DOT to verify the air void content and measure the permeability. One slab had an air void content of 10.4% and the other two had air void contents of 13.1% and 13.2%, respectively. The permeability test revealed coefficient of permeability values of 142×10^{-5}, 708×10^{-5} and 772×10^{-5} cm/sec for the three specimens. This is higher than that recommended by the NCAT study and the pavement may be more susceptible to permeability related distress in areas with high air voids. A total of 18 extra field cores were also taken from various locations a few days after the construction to check the final air void content by using the saturated surface-dry method (AASHTO T-166). The average in-place air void content from this testing was 13.2% with a range of 10.4% to 16.3%. This is noticeably higher than the target value but is consistent with that of the four field validation projects, reported by the NCAT study (West et al, 2011). This was mostly attributed to the types of

(a)

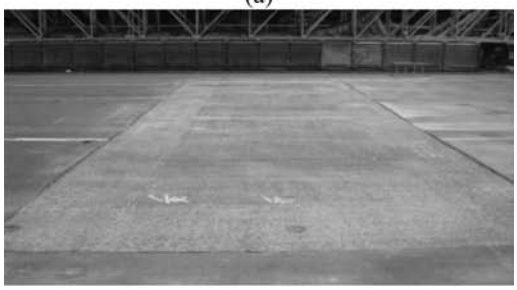

(b)

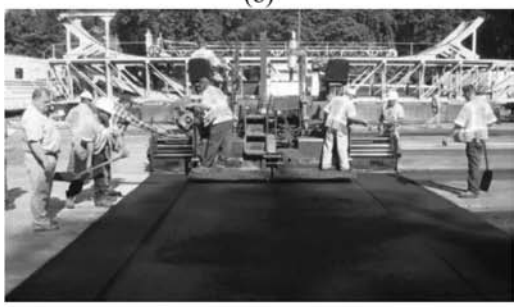

(c)

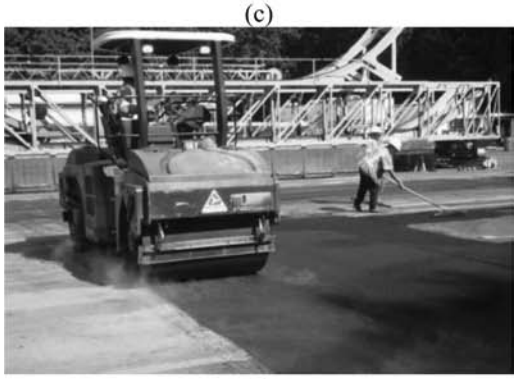

(d)

Figure 2. 4.75-mm Mix inlay construction: (a) milling operation, (b) after milling, (c) paving, (d) compaction.

rollers used. It is now recommended that larger rollers (27,000 lb) are used for construction rather than the 15,000 lb and 8,000 lb roller used for breakdown and finish rolling in this study.

Table 3. Summary of historical sequence for Lane 8 and Lane 10.

Lane 8 (control PG 70-22 binder) Including Site3 (sections A, C) and Site4 (sections B, D)	Lane 10 (Air Blown binder) Including Site3 (sections A, C) and Site4 (sections B, D)
Built in summer 2002	Built in summer 2002
Site 3 original fatigue loading in Dec 2005 to May 2006 and then completed over Feb 2008 to Mar 2008	Site 3 original fatigue loading in Dec 2005 to May 2006
Site 4 reserved and left untouched with natural aging and weathering from construction up to Apr 2010	Site 4 reserved and left untouched with natural aging and weathering from construction up to Jun 2010
Four weeks of accelerated aging with radiant heaters from Apr to May 2010	4.75 mm NMAS inlay installed Jun 2010
4.75 mm NMAS inlay installed Jun 2010	Eight weeks of accelerated aging with radiant heaters between Jun and Aug 2010 (for both Section B and D)
Four weeks of accelerated aging between Jun and Jul 2010. During this time only the aging was applied to the section without the inlay (Section B). The 4.75 mm treatment (Section D) was left unaged	Reserved site 4 is loaded between Oct 2010 to Feb 2011
Reserved site 4 is loaded between Sept 2010 to Apr 2011	

5 NATURAL AND ACCELERATED PAVEMENT AGING

The pavement sections used in this study were subjected to natural and accelerated pavement aging. Table 3 summarizes the historical sequence of both Lane 8 and Lane 10. The accelerated aging used radiant heaters to heat the pavement continuously at 74°C for a period of 8 weeks before loading. The equivalency of the full scale accelerated aging to normal pavement aging has been discussed in another paper (Gibson etc. 2012). The 8 weeks of full scale accelerated aging is equivalent to 12 to 18 months of natural aging depending on the pavement depth.

6 FULL-SCALE ACCELERATED PERFORMANCE TESTING

The split layout of the 4.75 mm NMAS inlay within the wheel path allowed the performance of the ALF sections with and without the treatment to be characterized at the same time. Specifically, a comparison between A and B subsections in both lanes can be used

to quantify the effect of aging on cracking in a conventional pavement without any treatment. Whereas, the performance between C and D subsections in Lane 8 quantifies the ability of a new unaged thin overlay to delay cracking in the treatment of an aged pavement. The comparison between C and D subsections in Lane 10 investigated the ability of a thin overlay in an aged condition to delay cracking in an aged pavement. This activity evaluates a preservation strategy which maintains the structural integrity before any cracking distresses initiate or the perpetual pavement scenario where milling and resurfacing is a corrective action.

The accelerated loading for cracking was carried out at an intermediate temperature of 19°C for both natural and accelerated aged sections. Lateral wander was programmed and the tire type was a 425 super single. The tire load and inflation pressure was 71 kN and 827 kPa respectively. The ALF devices were stopped at regular intervals for both pavement performance assessment and ALF machine maintenance. Stops were more frequent earlier in loading to observe any immediate changes in rutting or rapid cracking and thereafter the stopping interval times were gradually increased. Cracks were manually traced onto clear Mylar plastic sheets as they formed at the surface of the pavements. Different color pens were used to correspond to the number of load repetitions. Two approaches were used to process the data. One was to measure the total crack length and the other was to measure the percentage of area cracked in the loaded area; about 1.0 m wide and 10 m long (3.4 ft. × 33 ft.). A cracked area was considered to be fatigued when individual cracks had grown and met each other forming a network of cracks. The loaded area was divided into 30 cm × 30 cm (1 ft. × 1 ft.) unit sections used to quantify the percent cracked area.

Rutting was measured at the center of the wheel path despite the test section being carried out at an intermediate temperature of 19°C, a temperature widely believed to produce less significant permanent deformation. Rut depth was quantified by essentially the change in the thickness of the asphalt layer due to permanent deformation. A Layer Deformation Measurement Assembly (LDMA) installed in the asphalt uses an aluminum plate on top of the crushed aggregate base as a reference for steel rods fitting within holes drilled through the asphalt layer.

7 TESTING RESULTS AND DATA ANALYSIS

7.1 *Measured ALF fatigue cracking*

Full-scale fatigue cracking performance at 19°C for Lane 8 is quantified in Figures 3 and 4. Normally fatigue cracking in this type of APT experiment is measured from the entire site's loaded area. However, since Site 4 in Lane 8 and Lane 10 evaluated the 4.75 mm mix using a half-site subsection, the performance of these subsections needed to be compared against the equivalent subsection in neighboring Site 3

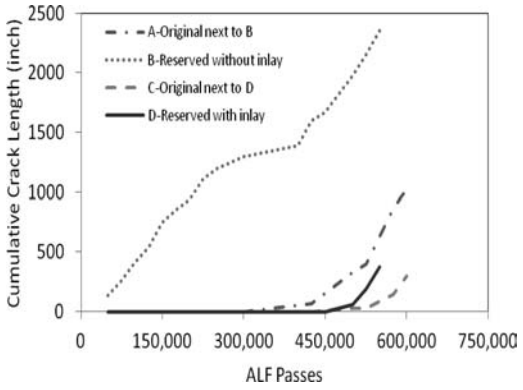

Figure 3. Cumulative crack length for Lane 8.

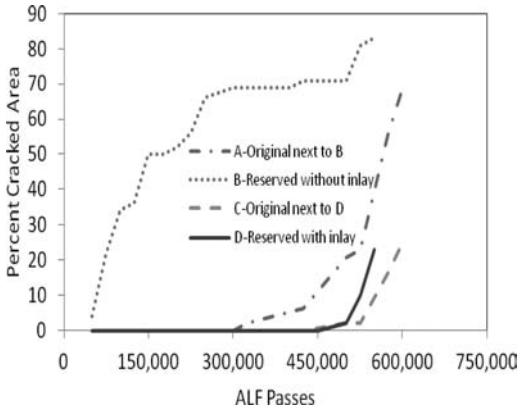

Figure 4. Percentage of cracked area for Lane 8.

that were tested at a much younger unaged condition. As seen from Figures 3 and 4 for Lane 8, the unaged 4.75 mm NMAS inlay (Subsection D) first cracked at about 425,000 passes which was slightly lower than the 500,000 passes needed to produce an initial crack in the corresponding neighboring Subsection C. This indicates that these subsections had almost the same fatigue cracking performance. In contrast, the aged Subsection B without the treatment cracked with much less loading at 50,000 passes. This illustrates that unaged, strain-tolerant treatments have a potential ability to delay aging related top-down cracking. Note that Subsections A and C in Site 3 were loaded at an age of about 3.3 years after construction; the neighboring Subsection B was naturally aged to about 7.7 years then accelerated-aged to an older condition (i.e., possibly equivalent to an additional 4+ years or a total age of about 11.7+ years). Subsection D is the same as Subsection B but with the top 25 mm (1-in.) removed and replaced with a 4.75 mm inlay which performed equivalent to Subsection C. Therefore, the net gain in fatigue cracking life for Subsection D with the inlay treatment is potentially about eight years (11.7+ years subtract 3.3 years equal to 8+ years).

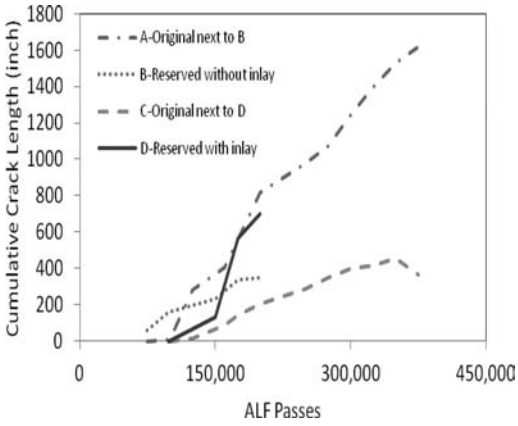

Figure 5. Cumulative crack length for Lane 10.

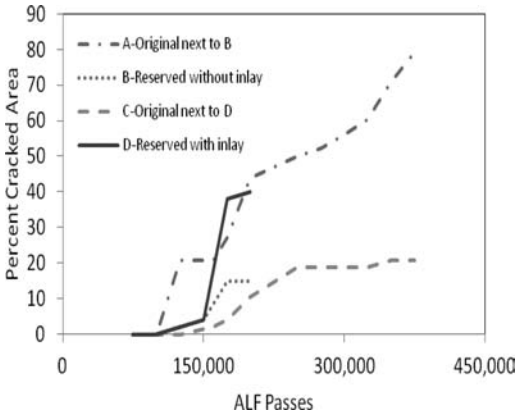

Figure 6. Percentage of cracked area for Lane 10.

Note that the impact of aging is dramatic as seen in Figures 3 and 4 which compare Subsection A to Subsection B without any treatment. Obviously, the accelerated aging in this experiment reduced pavement fatigue life significantly for both the existing AC pavement and the 4.75 mm NMAS overlay pavement.

The relative performance of an aged treatment is shown for Lane 10 in Figures 5 and 6. The performance of the aged inlay Subsection D is nearly identical to the performance of the aged Subsection B without the treatment. This illustrates that once thin overlays become brittle with age there is little to no benefit and preservation should be considered again.

7.2 *Cracking initiation location*

A series of cores were taken from the selected unaged and aged pavement sections after fatigue loading to determine if aging caused a different type of fatigue cracking, i.e., top-down or bottom-up cracking. The sides of the cores were examined for the presence of cracks propagating from the top-down or from the bottom-up as shown in Figure 7. A schematic representation of the vertical direction of cracking with depth

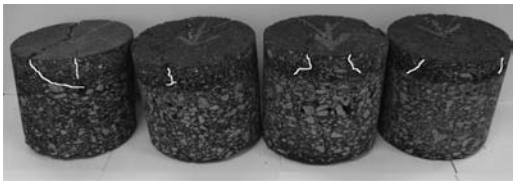

Figure 7. Photographs of cores taken to inspect for direction and depth of cracking.

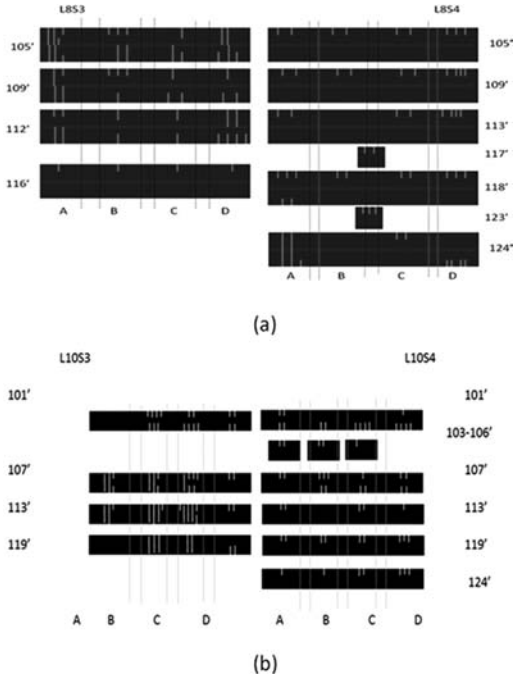

Figure 8. Top-down/bottom-up Cracking Patterns from Pavement Cores. [a] Cracking patterns of Lane 8 Site 3 (unaged) and Lane 8 site 4 (aged) [b] Cracking patterns of Lane 10 Site 3 (unaged) and Lane 10 site 4 (aged).

taken from core measurement surveys is shown in Figure 8. The transverse coring and associated schematic is meant to simulate a trench cut across the pavement at different stations to map the crack patterns with depth. As seen from the figure, the top-down cracks were the predominant type of cracking on the aged sections, which confirms the anecdotal body of knowledge that aging causes flexible pavements to be more prone to cracking in a top-down pattern.

For Lane 10 Site 4, the crack depth was also measured during the core survey. The average and standard deviation of the crack depths were 22.4 mm and 14.9 mm for the aged subsection while the inlay subsection had an average and standard deviation of 13.4 mm and 4.7 mm, respectively. This indicates that the extent of crack propagation was different for the subsections with and without the inlay treatment although they cracked initially almost at the same ALF

loading applications as discussed previously. The inlay treatment might have delayed the crack propagation.

Overall, cracking in the thin overlay appeared not to extend to depths deeper than the thickness of the overlay. The implications of this are important from a preservation standpoint because it suggests that thin overlays keep the distresses concentrated within their layers and significantly delay more structural cracking below.

8 SUMMARY AND CONCLUSIONS

This study evaluated the cracking and rutting performance of a 4.75 mm NMAS thin overlay lift using Full-Scale Accelerated Loading and various laboratory tests. A trial 4.75 mm NMAS from Virginia DOT was placed as a thin treatment over existing accelerated pavement test sections. The construction produced a test section where half of the loaded wheelpath was paved with the 4.75 mm NMAS mix allowing a direct comparison of cracking performance with and without the thin treatment. Full scale accelerated aging was utilized to compare the fatigue cracking performance for four combinations of pavement, with and without the 4.75 mm NMAS treatment, and with and without aging.

The unaged 4.75 mm NMAS overlay performed much better in fatigue cracking resistance than the untreated existing pavement in Lane 8 while the aged 4.75 mm NMAS overlay performed nearly the same as the untreated existing pavement in Lane 10. Therefore, thin 4.75 mm NMAS overlays used as a preservation treatment have the ability to significantly delay the aging related top down cracking, but once such thin layers becomes brittle with age that benefit is lost.

Cores cut from the pavement sections after accelerated loading indicate that top-down cracks were the predominant type of cracking for the aged sections. Therefore, the accelerated aging rendered the pavement more prone to top-down cracking.

ACKNOWLEDGEMENTS

The authors thank Dave Helmick and Dickie Maddox from Superior Paving whose cooperation and assistance was vital to the trial section. Dennis Lim, Jason Metcalf and Mario Tinio in the Accelerated Load Facility at the FHWA Turner-Fairbank Highway Research Center are recognized for providing their expert attention in the performance data collection, cutting pavement cores, and running the laboratory tests.

REFERENCES

Gibson, N., Qi, X., Andriescu, A. and Copeland, A. 2012. Recommended Asphalt Binder Fatigue Performance Specification from Full-Scale Accelerated Pavement Tests Considering Aging Effects. *Proceedings 4th International Conference on Accelerated Pavement Testing.*

Gibson, N., Qi, X., Shenoy, A. Al-Khateeb, G., Kutay, M., Andriescu, A., Stuart, K., Youtcheff, J. and Harman, T. 2001. *Full-Scale Accelerated Performance Testing for Superpave and Structural Validation.* Report FHWA-HRT-11-045. FHWA, U.S. Department of Transportation, 2011.

James, R., Cooley, A. and Buchanan, S. 2003. Development of Mix Design Criteria for 4.75 mm Superpave Mixes. *Transportation Research Record 1819, TRB*, National Research Council, Washington DC, 2003, pp. 125–133.

Li, X., Gibson, N., Qi, X., Clark, T. and McGhee, K. 2012. Laboratory and Full-Scale Evaluation of 4.75 mm NMAS Superpave Overlay, *CD-ROM Proceedings 2012 Annual Transportation Research Board Meeting.*

West, R., Heitzman, M., Rausch, D. and Julian, G. 2011. *Laboratory Refinement and Field Validation of 4.75 mm Superpave Designed Asphalt Mixtures.* Research Report. National Center for Asphalt Technology.

This page intentionally left blank

Advances in Pavement Design through Full-scale Accelerated Pavement Testing – Jones, Harvey, Mateos & Al-Qadi (Eds.)
© 2012 Taylor & Francis Group, London, ISBN 978-0-415-62138-0

Rutting resistance of asphalt pavements with fine sand subgrade under full-scale trafficking at high and ambient air temperature

J. Wu, F. Ye, J. Ling, J. Qian & S. Li
School of Transportation Engineering, Tongji University, Shanghai, China

ABSTRACT: The rutting performance of an asphalt pavement structure with a fine sand subgrade and a high ground water table was evaluated with full-scale trafficking tests with the Mobile Load Simulator 66 (MLS66) on Chong-ming Island, Shanghai. The purpose was to establish the reliability of the design with fine sand. There were two test sections with the same asphalt pavement structure but different subgrade depths. Track I was designed with a shallow 1.5 m fine sand subgrade and Track II was designed with a medium 3.0 m fine sand subgrade. The two tracks were constructed using traditional procedures on the natural clay subgrade covered with a layer of graded macadam. The asphalt pavements consisted of three asphalt layers (total 200 mm) and two cement-treated aggregate layers (total 540 mm, with 5% cement). The top 600 mm to 800 mm of the subgrade was treated with 3 to 4% cement. Track I was subjected to 1 million load applications at elevated temperature for 15 days and 1.1 million load applications were applied on Track II at ambient air temperature for 17 days. Profile and temperature data were collected. Pavement profiles and diagnostic excavation indicated that pavement deformation originated from compression and shear flow of the asphalt materials. No fatigue cracking was observed. The influence of the fine sand subgrade and its depth on pavement rutting was negligible. Cores and pit surveys showed that the top asphalt layer of 120 mm thickness was significantly affected by trafficked loading and temperature. The rate of rutting and total deformation volume of asphalt at high temperature was 1.5 times that of the test at ambient air temperature during early trafficking, about three times more thereafter. The rate of deformation on Track I was almost twice as fast as that of Track II. It is concluded that thick asphalt pavement with cement- treated-aggregate base will have good rutting resistance and can be expected to be a perpetual structure.

1 INTRODUCTION

In China, highway traffic volume is increasing rapidly, both in volume and axle weights (Lu, 2006). Motivated by economic benefits, the proportion of multi-axle, overloading and high tire pressure in traffic composition is increasing, and a channelized trafficking phenomenon is becoming serious. Consequently rutting is one of the main modes of premature failure in asphalt roads in China and has been a focus of research. Compared to the traditional laboratory tests and field observation, Accelerated Pavement Testing (APT) is preferable (Hugo and Epps-Martin, 2004) because it not only can simulate real traffic, but also can apply many load applications to achieve long-term service performance in a relatively short time.

APT has been widely applied in the research of rutting. Epps et al. (2003) used TxMLS (Texas Mobile Load Simulator) and MMLS3 (one-third scale Model Mobile Load Simulator) for stress analysis and stress distribution, then modified methods for pavement performance prediction through comparison of theoretical values with measured ones. Khaled and White (1999) modeled increase of rutting or permanent deformation when temperature rises or loading speed decreases, likewise when load or tire pressure increases. Leif (1999) indicated that rutting was relatively large in thin pavements in the initial loading phase based on APT, but that they can bear considerable trafficking in the dry state. Moisture content had considerable influence on the acceleration of pavement failure. Pavement life was 2.5 to 5 times longer in a low moisture content state than in high moisture content when rutting was 10 mm. Zhou and Scullion (2002) proposed a program named *VESYS* based on results from APT to predict rutting behavior. This had a better correlation with measured values from field tests. Southeast University, Tongji University and Chongqing Transportation Research Institute (Yang et al., 2006; Zhou et al., 2008; Huang et al., 2000; Hua et al., 2006; Su et al., 2008) conducted research on rutting resistance and prediction using a circular track test. The results showed that rutting was not excessively affected by flexible and semi-rigid subgrade, and rutting mainly occurred in the pavement within 200 mm. It decreased when high viscosity asphalt or polyester fibers SMA were used. Zhou (1997) applied dynamic loading of 50 kN through a large circular test, and discussed the forming process and law of rutting under high temperature compared to

SHRP (Strategic Highway Research Program) related results. Meng et al. (2008) recommended evaluating rut upheaval deformation through Accelerated Loading Facility (ALF) tests since there was good consistency between rutting deformation volume and rutting depth. Xu and Meng (2004) suggested that rutting resistance of asphalt pavement with flexible base was basically equivalent to pavements with semi-rigid base through ALF tests.

The previous research provided good information about test selection, survey measurements and test plans for the current study. The National Natural Science Foundation of China and Shanghai Science and Technology Commission funded research for this paper. The purpose was to evaluate the performance of a fine sand subgrade with a high water table under the same asphalt pavement structures. If found reliable in the accelerated test, the design will be used for the construction of the G40 highway, which is one part of a national highway network that will connect the coastal city of Shanghai with the inland city of Xi'an. Chong-ming Island is located at the mouth of the Yangtze River. It is the terminal of the G40 highway where fine sand is abundant. Although commonly found, there is little published data on the performance of this sand in pavement structures. In order to evaluate the performance of asphalt pavements on shallow, fine-sand subgrades with high water tables, an APT project was undertaken on Chong-ming Island in July, 2010.

This paper introduces the rutting performance analysis and trend development from the APT. Regression models of rutting against load applications were developed and corresponding correlation analyses undertaken. Rutting trends at high and ambient air temperatures of the asphalt pavement with semi-rigid base were analyzed in terms of several comparative indices.

2 GENERAL INFORMATION ABOUT THE TESTS

2.1 *APT equipment*

An MLS66 was used for the accelerated loading. It exerts a half-axle load via dual tires on the pavement surface, simulating heavy truck traffic for design or evaluation purposes (Figure 1). Its dimensions are 15 m × 2.87 m × 3.5 m (length × width × height), and the effective loaded trafficked length is 6 m. The machine comprises a rigid outer frame with six wheel carriages referred as bogies, each fitted with dual 305/70R22.5 tires. The bogies run along two sets of vertical endless looped elliptical guide rails. Maximum loading of the dual tires is 75 kN. The load is applied through two hydraulic cylinders pressurized from on-board hydro-pneumatic nitrogen accumulator tanks on the bogies. The bogies can travel at a speed of up to 6 m/s (22 km/h), equating to 6,000 axle load applications per hour.

A schematic of the MLS66 is shown in Figure 2 (MLS66 operation manual, 2010). Each bogie-chain is equipped with aluminum reaction plate sets and 12 pairs of steel wheels with diameters of 250 mm running on steel guides. There are 32 linear induction motors (LIMs) fixed in rigid frames and attached to the main structural frame. LIM aluminum reaction plates are mounted on the moving reciprocating bogie chain. The latter is then driven by electro-magnetic forces and the wheel bogies are driven along the endless rail loop. They are cooled by recycled cooling water with an onboard water pump, heat exchanger and air fan.

2.2 *Pavement structure*

Two test tracks were constructed using conventional procedures on the in-situ natural clay subgrade covered with a layer of graded macadam. Track I had a shallow subgrade filled with 1.5 m fine sand, while Track II had a typical subgrade filled with 3.0 m fine sand. This fine sand is the local material on Chongming Island. The gradation curve of the fine sand is shown in Figure 3 (Zhang et al, 2008). The fine sand subgrade was constructed layer by layer and the mean degree of compaction was 96%. The mean resilient

Figure 1. Accelerated pavement testing device MLS66.

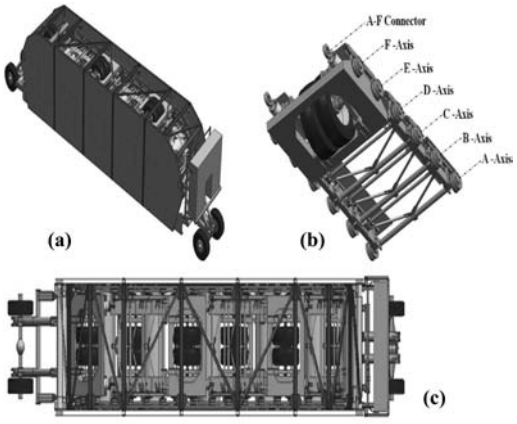

Figure 2. MLS66 structures (a) Overall structure; (b) Wheel frame structure; (c) Plan view.

modulus at the top of the subgrade top was 43.2 MPa. During preliminary observations of the roadbed, the measured underground water level was 2 m below the road surface.

The base layer was 36 cm of cement stabilized macadam (4% cement), and the subbase layer was 18 cm of cement stabilized macadam (3% cement). Both layers were compacted to 96% of laboratory determined density.

The pavements of Track I and Track II consisted of the same materials, and were constructed at the same time. Structure details are provided in Table 1 and the design gradation curves of the asphalt layers in Figure 4. All material tests followed the prescribed standards of the Research Institute of Highway Ministry of Transport (JTJ 052-2000, JTG E40-2007). Core-drilling specimens of the asphalt mixture (three cores per layer) were taken after construction and tested. The results are listed in Table 2 and Table 3.

2.3 *Testing plan*

In most regions of China, the highest air temperature in summer can reach more than 35°C, and the maximum temperature of the asphalt pavement can reach 60°C to 65°C (Lu, 2008). In order to simulate the effect of the loading environment, the pavement of Track I, was heated artificially to the most unfavorable conditions. During daytime, heating plates were placed next to the test tracks. At night, the trafficked area was covered with the heating plates, as shown in Figure 5. Following suggestions from MLS Company, the heating plate temperature was set to 70°C and thermostatically controlled. Accumulated loading repetitions of Track I reached 1 million. Track II was tested at ambient air temperature. Considering that the rutting rate might be slower, total repetitions of wheel loading was increased to 1.1 million.

Fiber Bragg Grating (FBG) strain sensors and thermal resistance temperature sensors (Pt100) were installed at the bottom of each layer of pavement as shown in Figure 6. Two additional temperature sensors were installed 20 mm below the surface in the upper asphalt layer. The thermocouples connected to the heated plates were used to measure the temperature at a depth of 2 mm from the surface.

Loading on the dual tires was set to 75 kN, which simulates a half-axle load 50% higher than the standard axle load in China. According to the H-K method proposed by Heukelom and Klomp (1964), loading parameters were calculated based on Equation 1.

$$\frac{p_i}{p} = \left(\frac{P_i}{P}\right)^{\frac{1}{3}} \quad (1)$$

where, P_i, P = the conversion and standard axle load respectively; p_i, p = the corresponding wheel pressure of P_i and P respectively.

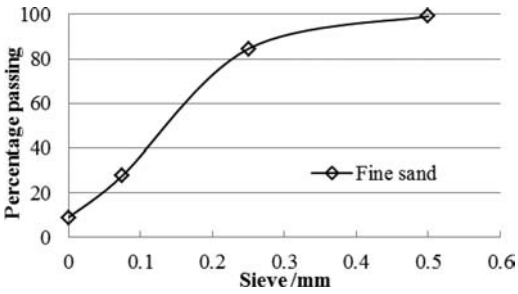

Figure 3. Gradation curve of fine sand.

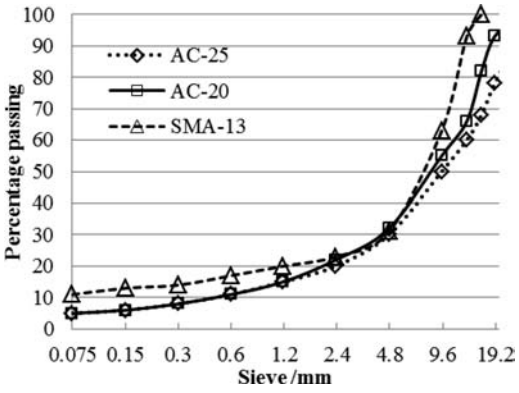

Figure 4. Designed gradation curve of three asphalt layers.

Table 2. Test results of asphalt mixture.

Asphalt mixture	DS number/mm	Residual Stability %	TSR %
SMA-13	8432	91.7	87.1
AC-20	3725	90.7	88.2
AC-25	2493	87.2	89.7

Table 1. Surface structure.

Layer	Structure	Thickness cm	P_a %	ρ_f g/cm^3	VV %	VFA %	VMA %	MS kN	FL mm
Upper-layer	SMA-13 (SBS with Rubber Crumb Modifier)	4	6.3	2.412	3.7	78.7	17.4	8.9	8.0
Mid-layer	AC-20C (Rock Asphalt Modifier, with Internal content 20%)	8	4.2	2.418	4.3	69.3	13.6	9.9	3.2
Lower-layer	AC-25C (Rock Asphalt Modifier, with internal content 25%)	8	4.1	2.429	4.1	71.0	13.1	10.3	3.8

Table 3. Test results of core sample.

Asphalt mixture	Specimen thickness mm	Design thickness mm	Difference mm	Specimen density g/cm^3	Standard density g/cm^3	Degree of compaction %
SMA	50	40	10	2.393	2.42	98.9
AC-20C	75	80	−5	2.448	2.434	100
AC-25C	88	80	8	2.433	2.448	99.4

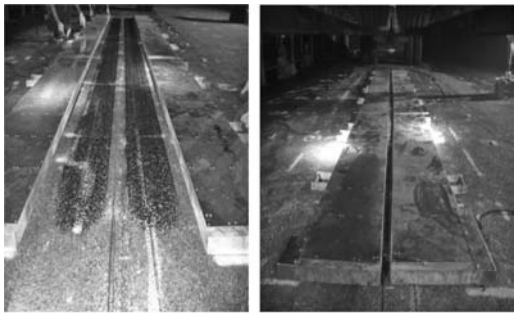

Figure 5. Heating process (a) Loading process during daytime; (b) Non-loading process at night.

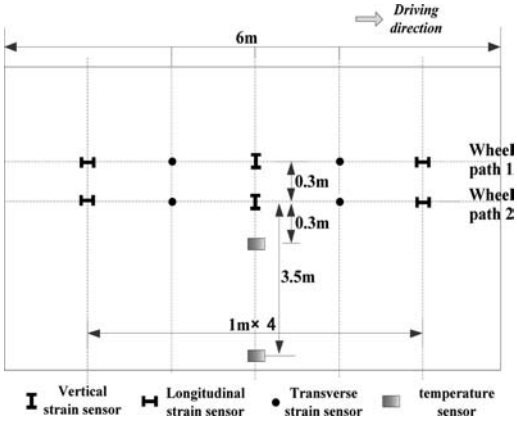

Figure 6. Schematic diagram of sensors layout.

The contact pressure was 0.801 MPa, equivalent circle diameter was 0.224 m, and the contact track footprint was 0.0467 m^2. Loading frequency was set to 6,000 load applications per hour. Hence the same point would be subjected to one load application every 0.6 second. Lateral wander was not considered.

Every night after trafficking was stopped, the surface profiles of the test tracks were measured with an MLS Profilometer Driver-P2003 and compared against the original profiles taken at the beginning of the APT testing. The loading area was divided into seven sections marked as 1#–7# from north to south with an interval of one meter (Figure 7). Each profile section was 1,500 mm in length which referred to

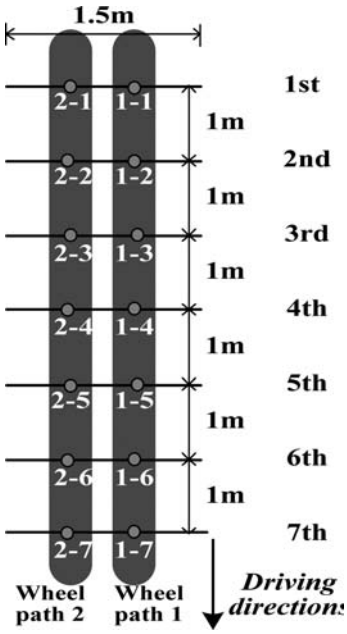

Figure 7. Rutting determination section.

the overall pattern of rutting along a transverse slice at each of the seven designated longitudinal sections shown in Figure 7. Data points were collected at 10 mm interval.

3 ANALYSES OF EXPERIMENTAL RESULTS

3.1 *Rutting curve*

Rutting depth is defined as the height from the highest profile point to the lowest profile point of the section curves, namely the sum of the upheaval and depression values. The seven profiles in each track had similar shapes, but the profiles near the equipment ends (Sections 6 and 7) had larger rutting depths, while the front sections (Sections 1 and 2) had smaller rutting depths. The reason for this was not specifically ascertained during testing. It could be related to unevenness of the original pavement surface since the trafficking profile of the MLS is linear and parallel to the levels of the machine footings at both ends. However the influence of this has been determined by the manufacturer and found to be less than five percent with a variation of

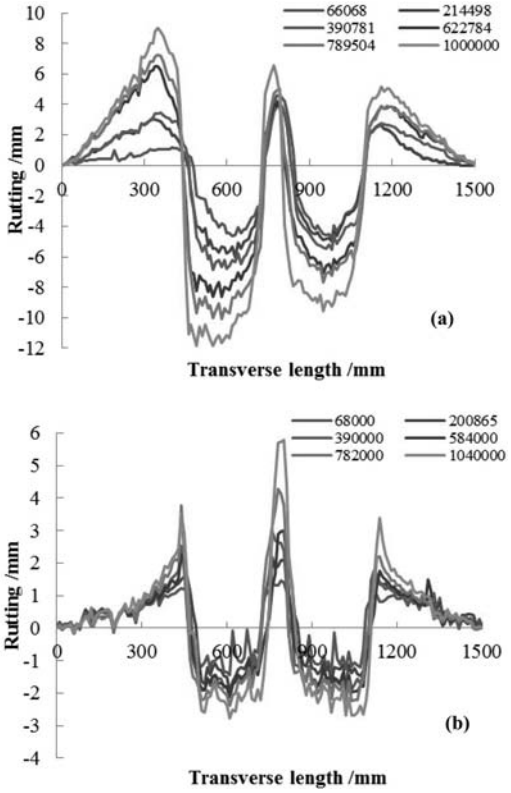

Figure 8. Relationship between rutting and number of load repetitions (a) 4th section of Track I; (b) 4th section of Track II.

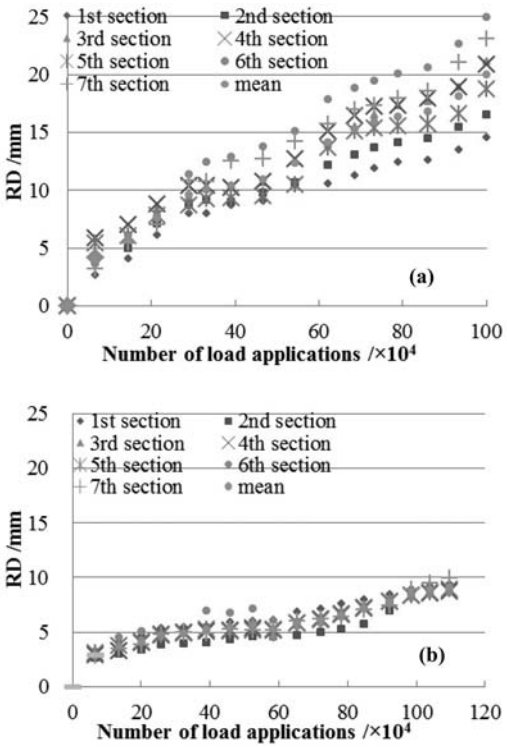

Figure 9. Relationship between maximum rutting depth and number of load repetitions (a) Track I; (b) Track II.

15 mm. A more likely cause could be temperature variation along the length of the pavement due to airflow during trafficking. This was not specifically monitored in this first trial. Figure 8 shows Section 4 as a typical example of the transverse profiles collected every 200,000 load applications.

Surface deformation was visually assessed and the rutting depth was one third to half of the total overall deformation after the first day's loading. The highest deformation recorded on nay one day was recorded on the first day, which was attributed to secondary compaction of the pavement material.

The final rutting depth of Track I and Track II was 25 mm and 11 mm, respectively. The rutting depth of Track II was much less than that of Track I, hence the importance of monitoring temperature during trafficking. The rutting result of Track II with ambient air temperature could meet the requirement of JTJ 073.2-2001 (2001), that the rutting depth should not be more than 15 mm. It is noteworthy that the rutting under heated trafficking with lateral wander would probably fall within the specified limit (Hugo et al, 2004). Therefore it was apparent that the fine-sand subgrade was acceptable despite the presence of the subsurface water. It was therefore concluded that it was feasible to use fine sand as subgrade fill material.

3.2 *Maximum rutting depth*

The rutting depth at different load applications obeyed the student t-distribution; accordingly the maximum (mean) rutting depth could be calculated by deleting significantly deviated points from the confidence interval of $(\overline{RD} - t/\sqrt{n}\ S,\ \overline{RD} + t/\sqrt{n}\ S)$ and averaging the remaining data based on Equation 2. The change of rutting depth with load applications for 14 sections of the two tracks is shown in Figure 9.

$$RD = \overline{RD} - \frac{t}{\sqrt{n}} S \tag{2}$$

where, RD = the rutting depth in mm; $\overline{RD}$ = the mean value of rutting depth in mm; t = the coefficient changed with guarantee rate (guarantee rate 95% was adopted); n = the number of effective data points in one type of load application (n = 7).

According to Figure 9, after one million load applications, the maximum rutting depth and mean maximum rutting depth of Track I were 25 mm and 20 mm, respectively and 11 mm and 8.5 mm, respectively for Track II. There was a statistically significant linear relationship between maximum deformation and number of load applications at each section, as shown in Equation 3.

The change of rutting can be divided into two periods on the basis of rutting development rate:

$$\begin{aligned}&\text{Track I:}\quad RD = 0.6\text{N}\ (R^2 = 1)\ (0 \le \text{N} \le 6.6)\\ &RD = 0.2\text{N} + 3.08\ (R^2 = 0.82)\ (6.6 \le \text{N} \le 100)\\ &\text{Track II:}\quad RD = 0.4\text{N}\ (R^2 = 1)\ (0 \le \text{N} \le 6.8)\\ &RD = 0.05\text{N} + 2.95\ (R^2 = 0.95)\ (6.8 \le \text{N} \le 110)\end{aligned} \tag{3}$$

where, RD = the maximum rutting depth /mm; N = the number of load applications /$\times 10^4$.

In Track I, the mean temperature at 2 mm distance below the surface in the trafficked area was approximately 60°C, while that of Track II was about 35°C. During the initial 60,000 load applications, the rate of rutting growth (defined as the rutting depth produced in 10,000 load applications, i.e. the slope in Figure 9) in Track I was 1.5 times of that in Track II. Thereafter, the difference increased to three times according to Equation 3. This was attributed to the difference in temperature.

Based on the assumption that the length of each subsection was 1.0 m (unit length), the relationship between rutting volume, including depression volume and upheaval volume and load applications was established as Equation 3. For a transverse profile curve of rutting, the depression volume was obtained from the graphic area below the original line multiplied by 1.0 m (Figure 8), and similarly the upheaval volume was obtained from the graphic area above the original line multiplied by 1.0 m.

The growth rate of displaced material (defined as the displacement after 10,000 load applications, i.e. the slope in Equation 4) in Track I was approximately twice that of Track II during initial trafficking and thereafter the difference increased to 4 times that of Track II.

$$\begin{aligned}&\text{Track I:}\quad RV = 262.5\text{N}\ (R^2 = 1)\ (0 \le \text{N} \le 6.6)\\ &RV = 60.69\text{N} + 1659.2 (R^2 = 0.99)\ (6.6 \le \text{N} \le 100)\\ &\text{Track II:}\quad RV = 137.59\text{N}\ (R^2 = 1)\ (0 \le \text{N} \le 6.8)\\ &RV = -0.44\text{N}^2 + 36.96\text{N} + 701.33\\ &(R^2 = 0.98)\ (6.8 \le \text{N} \le 110)\\ &RV = -0.44\text{N}^2 + 36.96N + 701.33\\ &\qquad (R^2 = 0.98)\quad (6.8 \le \text{N} \le 110)\end{aligned} \tag{4}$$

where, RV = the maximum rutting volume/mm^3; N = the number of load applications /$\times 10^4$.

According to the relative coefficients in Equation 3 and Equation 4, RV is a better index to reflect the rutting change compared to RD.

3.3 *Phase rate of rut development*

The phase rate of RD and RV is defined in Equation 5.

$$\begin{aligned}&\text{Phase rate of}\ \ RD = \frac{RD_2 - RD_1}{N_2 - N_1}\\ &\text{Phase rate of}\ \ RV = \frac{RV_2 - RV_1}{N_2 - N_1}\end{aligned} \tag{5}$$

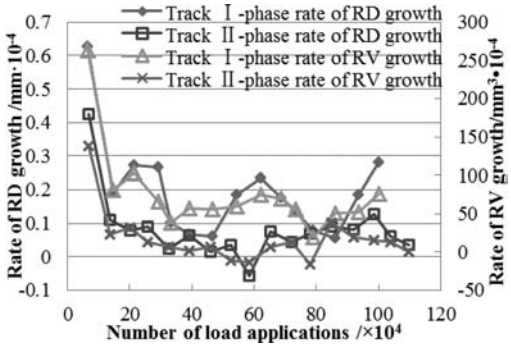

Figure 10. Relationship between the rate of deformation and number of wheel load applications.

where, N_1, N_2 = the number of load applications in the 1st phase or 2nd phase /$\times 10^4$; RD_1, RD_2 = rutting depth with number of load applications N_1 or N_2/mm·10^{-4}; RV_1, RV_2 = rutting volume with the number of load applications N_1 or N_2/mm^3·10^{-4}.

In Figure 10, the mean phase rate of RD and RV from the same test area showed a consistent trend during trafficking. During preliminary loading, the phase rate of RD of Track I was 1.5 times that of Track II, and the phase rate of RV of Track I was twice that of Track II. When the pavement material became more stable, the phase rate of RD of Track I was about twice that of Track II and the phase rate of RV of Track I was between 3 and 4 times that of Track II.

3.4 *Rutting upheaval analysis*

3.4.1 *Coefficient of lateral upheaval height*

In order to understand the law of rutting growth in the accelerated loading state, the coefficient of lateral upheaval height (UH_L) is defined as the proportion of the largest lateral upheaval height to the maximum rutting depth of each section curve. The results are plotted in Figure 11.

3.4.2 *Coefficient of upheaval volume*

In order to assess the movements of the asphalt surfacing in the accelerated loading state, the coefficient of upheaval volume (UV) defined as the ratio of upheaval volume to total rutting volume was calculated. The results are shown in Figure 12.

The coefficients of upheaval volume of seven sections in Track I had approximately similar changes in trend with increasing load applications, with no statistically significant relevance. In the first phase (0–66,000 repetitions), when the asphalt was compacted by trafficking, Track I had a large depression but relatively small upheaval. In the second phase (66,000–200,000 repetitions) the coefficients of upheaval volume reached maximum values, as the consolidation effect of trafficking was less obvious, and the asphalt heaved next to the wheel paths. In the third

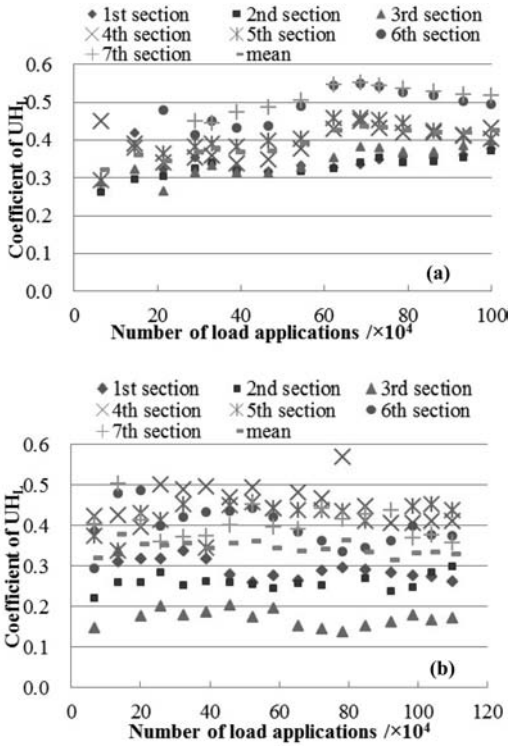

Figure 11. Relationship between lateral upheaval height coefficient and number of load applications (a) Track I; (b) Track II.

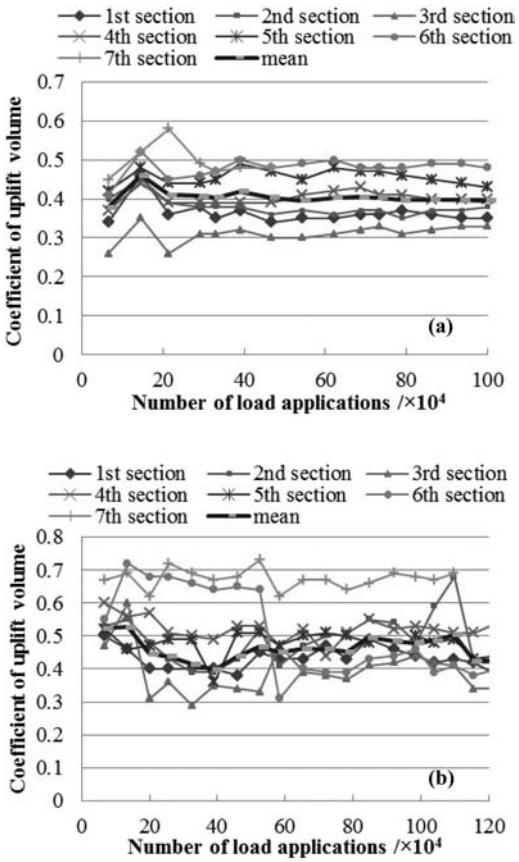

Figure 12. Relationship between upheaval volume coefficient and number of load applications (a) Track I; (b) Track II.

phase of trafficking (200,000–1,000,000 repetitions), down rut and upheaval values showed a steady growth, with a variation coefficient of between 2% and 4%. The coefficient of upheaval volume in Track I was concentrated between 0.3 and 0.5, with a mean of 0.41.

The coefficients of upheaval volume of seven sections in Track II had a similar trend and large variability. The coefficients of upheaval volume of all sections except Sections 6 and 7 were concentrated between 0.4 and 0.5, with a mean of 0.46. The data from Sections 6 and 7 deviated from the mean values significantly. This was attributed to the effects of tires lifting from the pavement surface.

An analysis of the results discussed in Sections 3.4.1 and 3.4.2, indicated that the upheaval height was two fifths of the rutting depth in Track I, and one third of the rutting depth in Track II. The upheaval volume was two fifths of the rutting volume in Track I, and close to half the rutting volume in Track II.

Table 4 compares the coefficient of variation of UH_L and UV. The coefficient of variation of UV was smaller than UH_L for the same section, indicating that the UV was less dependent on the number of load applications.

The coefficient's mean values of lateral upheaval height and upheaval volume coefficients are shown in Figure 13.

Table 4. Coefficient of variation of UH_L and UV.

	UH_L		UV	
Section	Track I	Track II	Track I	Track II
1st	7.4	10.8	7.9	7.8
2nd	8.3	7.3	6.1	15.8
3rd	11.5	11.7	7.8	18.5
4th	10.3	10.3	4.4	7.1
5th	10.7	9.0	4.4	7.7
6th	9.3	12.9	5.3	7.5
7th	7.3	9.6	8.6	4.3

The following conclusions are drawn with regard to the upheaval comparison analysis between the two tracks:

1. The coefficients of lateral upheaval height and upheaval volume were both insensitive to the number of load applications.
2. The coefficients of lateral upheaval height of the rutting sections were smaller than the upheaval volume but the variation coefficient was larger. The former discrete interval of 0.1 was much

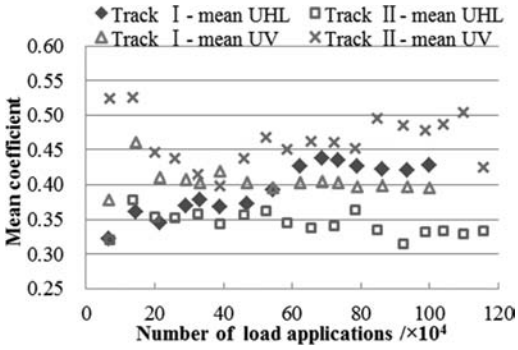

Figure 13. Relationship between upheaval coefficient and number of load applications in two tracks.

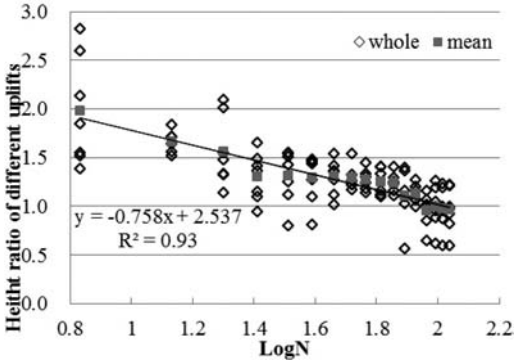

Figure 14. Relationship between upheaval height ratio and number of load applications in Track II.

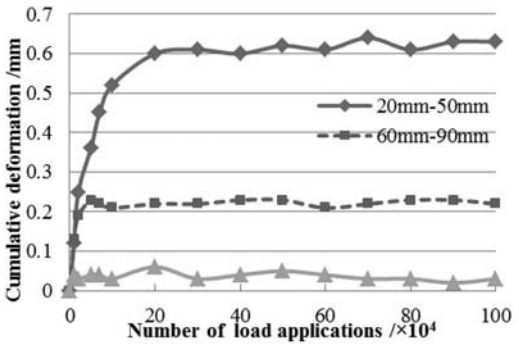

Figure 15. Permanent deformation of subgrade at different depths.

smaller than the latter 0.36. Consequently, use of the upheaval volume coefficient will be a more precise measure for analyzing and evaluating pavement structure rutting resistance.

3. The coefficient of upheaval volume in Track I was smaller than that in Track II. The latter was close to 0.5 which meant volume of upheaval and compaction of the asphalt layers were approximately equal under ambient air temperature conditions. In Track I, tested under high-temperature conditions, the coefficient of upheaval volume was 0.4, or two-thirds of the depression.

3.4.3 *Height ratio of different upheavals*

The ratio of the sum of two sides' upheaval height and that of dual-wheel clearance (i.e., the middle upheaval) in Track II, without artificial heating were calculated. The results are shown in Figure 14. A total of 119 data points (7×17, where 7 is the section number and 17 is the number of trafficking days) were collected.

An inverse correlation between the ratio and logarithm of loading times was observed and is stated by the following relation (Equation 6):

$$\frac{\text{Sum of lateral upheaval}}{\text{clearance upheaval}} = -0.76LogN - 0.00021T + 2.54 \quad \left(R^2 = 0.93\right) \tag{6}$$

where, N = the number of load applications /$\times 10^4$; T = mean temperature at 2 mm distance below the surface course /°C.

When testing under ambient air temperature, the ratio between upheaval height on both sides of wheel path and dual-wheel clearance changed very little with temperature. However, this may change with increasing load applications.

In early testing (0 to 200,000 load applications), the ratio rapidly changed from 2 to 1.6. Between 200,000 and 1,000,000 load applications, it changed from 1.3 to 1 at a slower rate, that is, upheaval height of the dual-wheel clearance was between 1 and 1.25 times that of the lateral upheaval height during initial trafficking (secondary compaction) compared to an upheaval height of between 1.54 and 2.0 times that of the lateral upheaval after initial trafficking. The mean ratio for the full duration of the test was 1.7.

3.5 *Influencing factors analysis*

3.5.1 *Subgrade height*

Dynamic deformation at different depths in the subgrade was consistent with the number of load applications. Data from Track I are shown in Figure 15 as an example.

From Figure 15 it follows that:

1. Dynamic deformation increased rapidly during the initial loading phase, then fluctuated within a certain range instead of increasing.
2. Permanent deformation at between 20 cm and 50 cm below the subgrade surface was approximately 0.6 mm (on Track II it was 0.67 mm); at between 60 cm and 90 cm it was approximately 0.2 mm (on Track II it was 0.23 mm); at between 100 cm and 130 cm it was approximately 0.05 mm (on Track II it was 0.03 mm).
3. Overall, the total permanent deformation of the fine sand subgrade with its top seal layer on both tracks was between 1 mm and 1.5 mm after completion of trafficking. However, total rutting depth reached 20 mm on Track I and 10 mm on Track II.

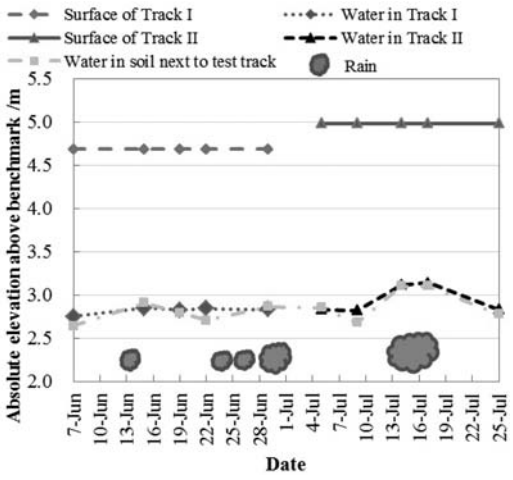

Figure 16. Variation in underground water table during testing of two tracks.

3.5.2 *Effect of underground water table*

The underground water table on the island where the tests were conducted was lowered during construction to construct the sand subgrade. Thereafter it stabilized at the levels indicated in Figure 16. During the trials the underground water level was not controlled but it was monitored. The respective levels during the trafficking are as indicated in Figure 16.

From Figure 16 it is apparent that the variation in the water table levels during trafficking did not appear to affect the deformation of the sand during trafficking to the extent that it was measureable and needed to be taken into account during analysis. This is confirmed by the very small deformations measured in the lower levels of the subgrade, discussed in Section 3.5.1 above.

There was no significant correlation between deformation and thickness of the subgrade or variation in underground water level. It was therefore concluded that the fine sand subgrade was unlikely to cause dynamic failure under vehicle wheel load at 50% overload.

The influence of cumulative deformation of subgrade on pavement structure was therefore ignored in further analysis.

The vertical instantaneous strain of the subbase was measured with the FBG sensors for 2 seconds with a collection frequency of 100 Hz. The results are shown in Figure 17.

The instantaneous response of vertical strain was about 16 με. Based on the Shell pavement design method, the allowable strain of vertical compression at the top of the subgrade can be calculated using Equation 7 with a confidence level of 95%.

$$\varepsilon_R = 0.018N^{-0.25} \quad (7)$$

where, ε = the allowable strain of vertical compression of subgrade top /με; N = the standard axle load

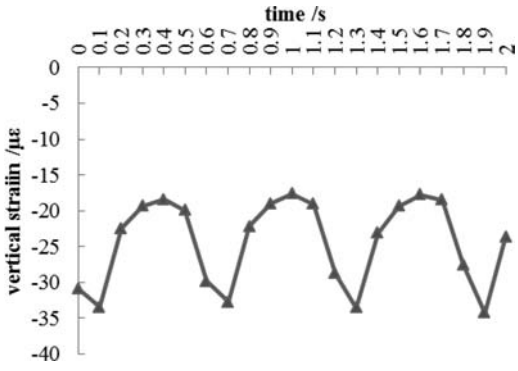

Figure 17. Vertical instantaneous strain of subbase in 2 s.

applications of each lane, and N = 100 × 10^4 × 12.18 (12.18 is the conversion coefficient).

Therefore,

$$\varepsilon_R = 0.018 \times \left(100 \times 10^4 \times 12.18\right)^{-0.25} = 305\mu\varepsilon$$

The vertical compressive strain at the top of the subgrade after testing was only 5% of the calculated allowable value. Consequently, it can be concluded that in this test, the influence of subgrade thickness had little effect on pavement rutting and was not considered in further analysis.

3.5.3 *Rutting depth and temperature*

Based on the findings of the rutting depth analysis discussed above, a strong linear relationship between rutting depth and load applications was found, as expected, with temperature a statistically significant factor influencing rutting resistance. The models described above were therefore refined to include temperature and are presented in Equation 8:

$$\text{Track I:} \quad RD = 0.16N + 0.003T + 3.84 \ (R^2 = 0.98)$$
$$\text{Track II:} \quad RD = 0.05N - 0.001T + 3.21 \ (R^2 = 0.95) \quad (8)$$

where, RD = the rutting depth /mm; N = the number of load applications /× 10^4; T = mean temperature at 2 mm below the surface course /°C.

3.5.4 *Permanent deformation and PSPA modulus*

With increasing temperature, the rheological property of asphalt changes, and the modulus of the asphalt surface layer significantly reduces. The pavement will undergo distress after the surface layer, absorbing most of the traffic load (Ou et al., 2008). Resilient modulus attenuation of the surface layer reflects the weakening process of the material's mechanical properties, and is an important parameter for assessing permanent deformation.

The Portable Seismic Property Analyzer (PSPA) is a field-deployable device for measuring sonic, ultrasonic, and resonant vibrations. This enables nondestructive evaluation of asphalt concrete and portland

cement concrete pavements and structures, including the base and subgrade materials (Nazarian et al., 1993; Gucunski, 2002). The PSPA hardware consists of a 'source', two 'receivers' and an electronics box packaged as a hand portable unit. The hardware is controlled by software running on a computer.

Guo (2010) proposed a prediction model for asphalt pavement rutting based on effective temperature, seismic modulus and traffic loading.

The seismic-wave modulus within the range of 4 cm to 18 cm from the top of the pavement was measured using the PSPA after taking rutting measurements on each section. The intersections of the two wheel tracks and seven rutting sections were taken as the measuring points as shown in Figure 7. The lateral and longitudinal PSPA modulus at each point was averaged as the true value.

Results from the two test tracks are summarized in Figure 18. Prior to trafficking a modulus of 8.3 GPa was recorded. After the first day of trafficking, this value dropped to 6.0 GPa, or about 70% of the original stiffness. These changes were mostly attributed to initial compaction by trafficking. Thereafter the rate of modulus reduction slowed and stabilized at about 5 GPa. Differences between Track I and Track II were attributed to temperature.

Because of the limited available data caused by equipment failure in Track II, Track I was used as an example to analyze the relationship between rut depth, temperature, and PSPA modulus. The curves are shown in Figure 19 based on the mean value of 16 groups from a total of 224 data groups (14 points per day × 16 days).

The equation for the above three parameters was developed as follows using *Matlab* software (Equation 9).

$$\text{Linear,}\quad R_P = 29.841 - 2.722M_P - 0.20T \quad (R^2 = 0.89)$$

$$\text{Nonlinear,}\quad R_P = 10.437 - 5.039M_P + 0.181M_P^2 + 1.131T - 0.017T^2 \quad (R^2 = 0.90) \qquad (9)$$

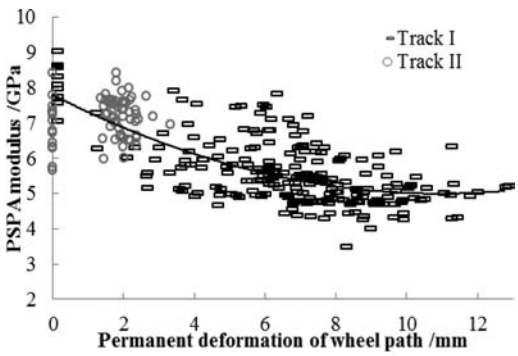

Figure 18. Relationship between rutting permanent deformation and PSPA modulus.

where, R_P = the permanent deformation /mm; M_P = the PSPA modulus /GPa; T = the mean temperature of surface /°C.

3.6 *Core samples and test pit analysis*

The test road was studied in a full-depth trench, schematically shown in Figure 20. It was found that rutting was the only form of distress in the upper and middle asphalt layer. No fatigue cracking was observed. The base and subgrade had no visible deformation. This further illustrated that plastic deformation of the asphalt mixture was the main cause of the rutting.

Cores were taken from the wheelpaths, from the deformed areas adjacent to the wheel paths, and from unaffected areas beyond any deformation. Actual positions are shown in Figure 21. Layer thicknesses were measured on all cores. Each specimen was then cut at the layer joins (SMA-13, AC-20C and AC-25C) and the volumetrics determined using the

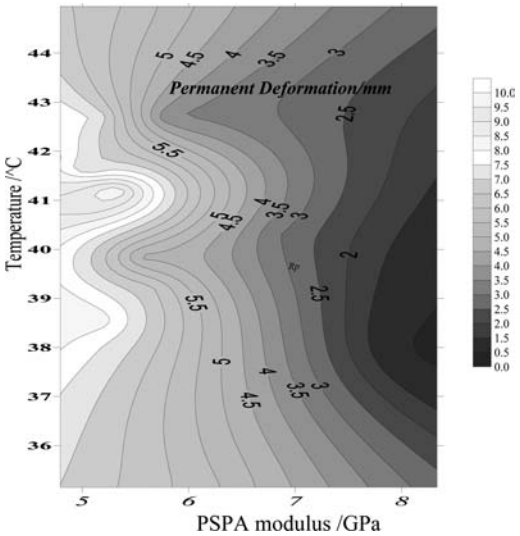

Figure 19. Relationship between permanent deformation (down rut only), PSPA modulus and temperature.

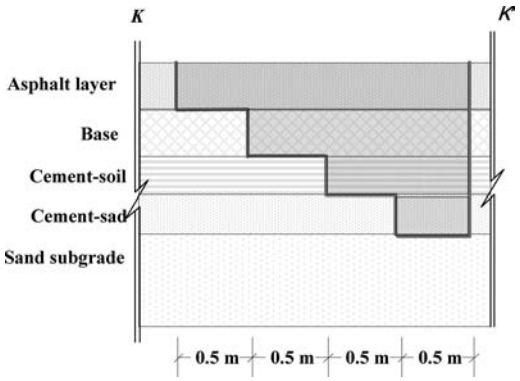

Figure 20. Test pit schematic.

Marshall Method. Table 5 lists the results. Unfortunately the cores from the deformed areas adjacent to the wheel tracks were discarded before measurements were taken.

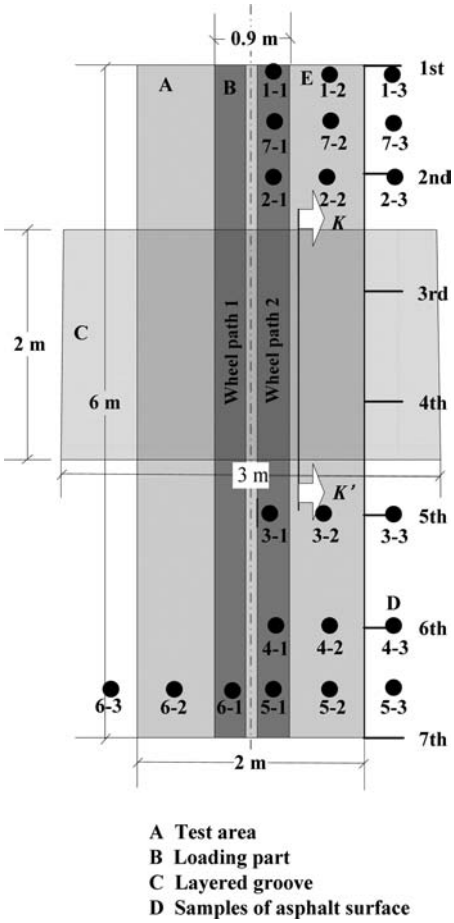

Figure 21. Core and test pit locations.

Variables such as specimen handling and accuracy of layer measurement, made it difficult to determine which specific layers were most affected by wheel trafficking. Consequently, void ratio was considered to be a more appropriate means of determining the degree of compaction of each layer. Accordingly, this was used for the analysis, rather than specimen height.

Reduction in void ratio in each asphalt layer in the cores removed from the wheelpaths was about 22% for both test tracks. Differences between layers could not be distinguished. In the cores taken from adjacent to the wheelpaths, the void ratio was different in the different layers, ranging between 27% in the top layer and 16% in the middle layer on Track 1, compared to 5.5% in the top layer and 15% in the middle layer on Track II.

The differences in results of reduction in void ratio between the two test tracks were again attributed to temperature.

4 CONCLUSIONS

The APT study to evaluate the performance of asphalt pavement structures with cement stabilized base and subbase layers on fine sand subgrades influenced by changing water table depth, proved to be successful. The conclusions are as follows:

- The influence of the depth of the fine sand subgrade on pavement rutting was negligible in terms of permanent deformation and vertical compression strain.
- Rutting occurred mostly in the top and middle layers of the asphalt. The middle layer was apparently more susceptible to rutting.
- As expected, the rate of rut depth accumulation increased with increasing temperature and increasing number of load repetitions.
- The coefficient of upheaval volume can be used for analysis and evaluation of rutting resistance more precisely with smaller discretion interval than that of upheaval depth.

Table 5. Test results of core samples from different positions.

	Position	Mean height cm	Relative ratio of height	Mean VV %	Relative ratio of VV
Track I	Upper layer-depression part	4.83	−0.04	4.08	−0.24
	Upper layer-upheaval part	4.36	−0.13	5.65	0.05
	Upper layer-untrafficked part	5.03	0	5.39	0
	Middle layer-depression part	7.14	0.01	1.95	−0.19
	Middle layer-upheaval part	7.63	0.08	2.77	0.15
	Middle layer-untrafficked part	7.1	0	2.41	0
	Lower layer-depression part	7.5	−0.07	4.08	−0.23
	Lower layer-upheaval part	8.64	0.08	5.65	0.06
	Lower layer-untrafficked part	8.03	0	5.32	0
Track II	Upper layer-depression part	3.96	0	4.09	−0.27
	Upper layer-untrafficked part	3.95	0	5.63	0
	Middle layer-depression part	6.42	−0.01	1.35	−0.15
	Middle layer-untrafficked part	6.49	0	1.59	0
	Lower layer-depression part	7.34	0.05	2.34	−0.16
	Lower layer-untrafficked part	7.02	0	2.8	0

– The phase rate discrepancy of rutting rate between high and ambient air temperature increased with number of load applications.
– High temperature caused continued lateral flow of asphalt mixture.
– The height of the upheaval adjacent to the wheelpaths was less than the depression in the wheelpaths, especially under high temperatures.
– Reduction in void ratio was higher in cores removed from the track tested at high temperature compared to those removed from the track tested at ambient temperature.
– At high temperature, permanent deformation grew linearly with the attenuation of PSPA modulus and the increase of temperature.

There are several issues that remain to be studied, such as the effect of different loading rate on rutting, the conversion relationship between conventional resilient modulus of asphalt and PSPA modulus, and the influence of lateral wander.

ACKNOWLEDGMENTS

The research was supported by the National Natural Science Foundation of China (No.50968016) and Shanghai Science and Technology Commission (No.2009DFA81630). The authors wish to acknowledge the support and contributions of the project sponsors, other participating institutions and their personnel.

REFERENCES

Epps-Martin, A, Walubita, L, Hugo, F. and Bangera, N. 2003. Pavement Response and Rutting for Full-Scale and Scaled APT. *Journal of Transportation Engineering, Vol. 129 No. 4: pp* 451–461.

Gucunski, N. and Maher, A. 2002. *Evaluation of Seismic Pavement Analyzer for Pavement Condition Monitoring*. Department of Civil and Environmental Engineering at Rutgers University.

Guo, Y. 2010. *Permanent Deformation Prediction Research of Asphalt Pavement in High Temperature Field*. Shanghai: Tongji University.

Heukelom, W. and Klomp, A.J. 1964. Road Design and Dynamic Loading. *Proceedings of the Association of Asphalt Paving Technologists, Vol. 33,* pp. 92–123.

Hua, B., She, Z. and Zhou, J. 2006. Experiment Study on the Pavement Structure Rutting Resistance of Huning Expressway with Circular Track Test. *Modern Transportation Technology*.

Huang, X., Zhang, X. and Deng, X. 2000. Asphalt Pavement Rutting Prediction of High-Grade Highway. *Journal of Southeast University (Natural Science Edition), Vol. 30, No. 5*, pp. 96–101.

Hugo, F. and Epps-Martin, A. 2004. *Significant Findings from Full-Scale Accelerated Pavement Testing.* Transportation Research Board, pp. 12–15.

Khaled, A.G. and White, T.D. 1999. INDOT-APT Test Facility Experience Paper #: CS8-4. Submitted for publication in *1st International Conference on Accelerated Pavement Testing*. Reno, Nevada.

Leif, G.W. 2001. *Accelerated Load Testing of Pavements.* VTI rapport 477A. Swedish National Road and Transport Research Institute.

Lu, Z. 2006. *Research on Prediction Method of Asphalt Pavement Rut.* Shanghai: Tongji University.

Lu, M. 2008. *High-temperature asphalt mixture rutting of the pilot study*. Lanzhou University of Technology.

Meng, Q., Cheng, J. and Li, L. 2008. Research on Hump of Asphalt Mixture Pavement by Accelerating Loading Facility. *Highway Engineering, Vol. 33, No. 4.* pp. 15–19.

MLS66 operation manual .2010. MLS Test System (Pty) Ltd, RSA.

Nazarian, S., Baker, M.R. and Crain, K. 1993. *Development and Testing of a Seismic Pavement Analyzer*. Report SHRP-H-375, Strategic Highway Research Program. National Research Council, Washington, D.C.

Ou, Y.W., Liu,Y. and Wang, L. 2008. *Experiment and Study on High Modulus Asphalt Mixture. Highway, No. 1.*

JTG E40-2007. 2007. Research Institute of Highway Ministry of Transport. *Test Methods of Soils for Highway Engineering.* People's Education Press.

JTJ 052-2000. 2000. Research Institute of Highway Ministry of Transport. *Standard Test Methods of Bitumen and Bituminous Mixtures for Highway Engineering*. People's Education Press.

JTJ 073.2-2001. 2001. Shanghai Highway Administration. *Technical Specifications for Maintenance of Highway Asphalt Pavement.* People's Education Press.

Su, K., Wang, C. and Zhou, G. 2008. Rutting Prediction Model for Asphalt Concrete Pavements Based on Accelerated Pavement Test. *Journal of Tongji University (Natural Science), Vol. 36, No. 4*. pp. 493–497.

Xu, Q. and Meng, S. 2004. Research on the Flexible Base of Asphalt Concrete Pavements Based on Accelerated Pavement Test. *Symposium on road projects in 2004*, pp. 205–210.

Yang, J., Cui, J. and Shi, X. 2006. Rutting Resistance Performance of Asphalt Pavement by Circle Tracking Test. *Journal of Southeast University (Natural Science), Vol. 36, No. 4*: pp. 576–579.

Zhang, H., Ling, J. and Jiang, X. 2008. Experimental Investigations of Highway Performance of Fine Sand of the Long River Estuary. *Highway Engineering Vol. 33, No. 3*: pp. 142–146.

Zhou, J. 1997. A Study of Domestic Asphalts High Temperature Performance on the Circular Testing Track. *Petroleum Asphalt, Vol. 11, No. 1*: pp. 13–18.

Zhou, F. and Scullion, T. 2002. *Vesys5 Rutting Model Calibrations with Local Accelerated Pavement Test Data and Associated Implementation*. Report No. FHWA/TX-03/9-1502-01-2. Texas Transportation Institute. Texas A&M University System.

Zhou, G., Zhou, J. and Hua, B. 2008. Study on Perpetual Deformation of Asphalt Pavement Structures by Circular Track Testing. *Journal of Tongji University (Natural Science), Vol. 36, No. 2*: pp. 187–192.

Advances in Pavement Design through Full-scale Accelerated Pavement Testing – Jones, Harvey, Mateos & Al-Qadi (Eds.)
© 2012 Taylor & Francis Group, London, ISBN 978-0-415-62138-0

Initial tests results from the MLS10 Mobile Load Simulator in Switzerland

M. Arraigada & M.N. Partl
Empa, Swiss Federal Laboratories for Materials Science and Technology, Duebendorf, Switzerland

A. Pugliessi
ITYAC S.A., Rosario, Argentina

ABSTRACT: The Mobile Load Simulator (MLS10) is a new type of Accelerated Pavement Testing (APT) equipment recently purchased by Empa, Swiss Federal Laboratories for Materials Science and Technology. This paper summarizes the results of the first calibration tests of the MLS10 in Switzerland. The objective was to evaluate the performance of the machine for testing pavements constructed with local materials under local guidelines. The focus of the study was the structure of the A4 motorway near Zürich. Three pavements were constructed and trafficked with a total of 1.6 million 65 kN load passes over a period of approximately seven months. To access the structural response throughout the loading history, the pavements were instrumented with different sensors. Transverse profiles of the surface were periodically taken. Falling Weight Deflectometer (FWD) and static deflection bowl measurements were taken before, during, and after trafficking to evaluate the structural condition. Finally, pavement samples were obtained from the section and tested in the laboratory. The pavement response was analyzed and validated with a model using the Finite Element Method (FEM). At the end of the tests almost no sign of distress was observed, showing the durability of the pavement.

1 INTRODUCTION

1.1 *Background and motivation*

In 2006, the University of Stellenbosch in South Africa developed a prototype APT device. In 2008 the Swiss Federal Laboratories of Material Science and Technology (Empa) purchased the prototype device, known as the MLS10 Mobile Load Simulator, a new APT technology that can apply 6,000 unidirectional load applications in one hour. This device is composed of four loading bogies running in a closed loop and powered by contactless linear induction motors (LIM) (Partl and Arraigada, 2011). Further, the machine is mobile and can be transported on standard low bed trucks. It also has the ability to move autonomously at walking speed to change position within the testing site. With the MLS10 it is possible to consider real climatic and construction conditions.

Since no previous experience with a mobile load simulator of this type was available in Switzerland, an experimental project to evaluate the performance of the machine with pavements constructed following local guidelines, with local materials and construction was planned. The primary objective was to test a typical Swiss pavement in order to know how many MLS10 loading cycles were necessary to produce distress in the structure. In addition, it was expected that these tests would provide some basic information about the design norms used in the country.

A second but equally important objective was to learn the operation of the MLS10 itself, detect possible operational shortcomings and technical defects, and to improve the performance of the machine, which is a prototype and the first of its class in the world.

Finally, the project was used to propose and evaluate pavement testing procedures as well as instrumentation and software to collect research data. Establishment and formalization of the data handling, formatting, processing, storage and backup protocols and software was also a goal.

A new motorway was chosen for the experiment. A dedicated testing site was constructed using the same materials and design used in the Zürich A4 motorway, considering four variations, as explained in the next section. The site was located just beside the motorway area to keep subgrade materials and climate as close as possible to real conditions.

Due to the restricted time window, problems with the prototype machine, and the lack of experience of the personnel in charge of the tests, the number of load repetitions applied to the test sections was limited to 1.6 million over a period of approximately seven months. Testing was carried out on three of the four test sections.

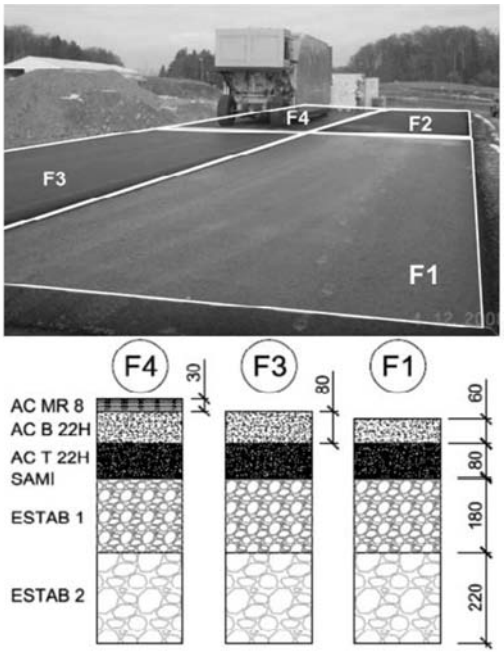

Figure 1. Layout of the sections and layers of the three pavements trafficked with the MLS10.

In situ tests were carried out to establish the subgrade properties before starting with trafficking. In order to evaluate the pavement deterioration, pavement response to MLS10 loading was monitored using strain gauges and accelerometers, as described later. Since temperature cannot be controlled while loading, several temperature sensors were installed in the structure. Other non-destructive pavement testing procedures were carried out on a regular basis, as described later.

After completion of trafficking of the sections, the pavement was cored and samples were tested in the laboratory. Parameters including temperature dependent elastic modulus and interlayer bonding between the asphalt layers of the trafficked and non-trafficked areas were assessed.

The analysis of all of these combined data was used to establish the degree of deterioration of the structure after APT with the MLS10. A finite element model was prepared to evaluate the stress conditions under load and compared with measured values.

2 EXPERIMENTAL SETUP

2.1 *Test section layout and construction*

The test site was constructed in September 2008 and comprised four different test sections. Each section consisted of a rectangular area 20 m × 5 m, totaling a paved surface of 10 m × 40 m, as shown in Figure 1a. The materials used in each section (Figure 1b) correspond to a heavy duty full-depth asphalt pavement described in the Swiss Norms (VSS, 1997; VSS, 2008). This pavement is the thickest structure in the design catalogue, prepared for the highest traffic loading calculated in Switzerland. The difference between each of the four sections was the number of layers. Section F4 was constructed following the exact design of the motorway pavement. Section F3 was built in the same way as Section F4, but without the top layer (AC MR 8). Finally, Section F1 was constructed with no top and second layers (AC B 22H). The base layer of all sections (AC T 22H) was placed on top of a stress absorbing membrane interlayer (SAMI) separating the asphalt layers from the two cement stabilized layers of 18 cm and 22 cm thickness, respectively. The concept behind test plan was to compare the response of each of the structures to evaluate the validity of the design norms. Each of the pavements in Section F1, Section F3 and Section F4 corresponds to a Structural Number (SN) of 128, 160 and 172, respectively.

For the tests, the MLS10 was regularly moved through the testing site to have, on average, the same temperature profile in each section. Due to time restrictions, Section F2 was not trafficked and therefore, is not discussed in this paper.

2.2 *Subgrade and base layer material properties*

During pavement construction, standard tests were carried out to evaluate the subgrade and base course performance. Load bearing capacity tests on the subgrade and compressive strength of the cement stabilization were performed prior to construction of the pavement.

2.3 *Test section instrumentation*

The response and deterioration of the pavement was evaluated using different methods. Sensors were installed in the structure to monitor the temperature of the materials and measure the deformation and deflection under the MLS10 loading. A schematic of the location of the sensors with their names is depicted in Figure 2 (only for Section F4). The name and the installation depth in all sections are shown in Table 1. Deflection was measured indirectly using capacitive accelerometers (A41 to A43 in the figure). Strain gauges were installed during construction to monitor deformation between the asphalt layers (BQ4, TQ4, BL4 and TL4). No strain gauges were installed in Section F1.

Kyowa (120 mm long) strain gauges were used. These are covered with acrylic and use three conductors for compensating resistance change due to temperature. The cables of the original sensor were changed for stranded silver-plated copper wires with Teflon insulation, capable of withstanding the high temperatures of the hot asphalt concrete during construction. Data acquisition was done with a *Spider 8* system. *Catman* software was used to control the system. Data was collected continuously and recorded every five minutes.

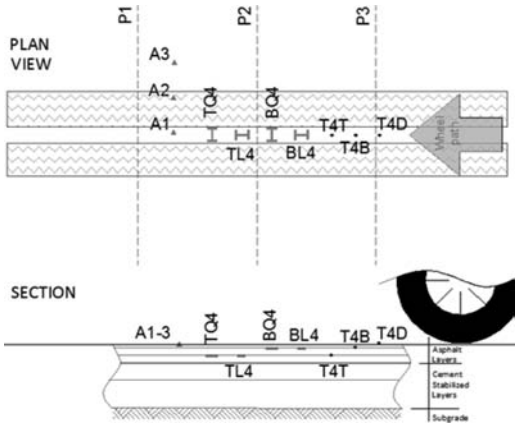

Figure 2. Schematic of the position of the sensors in Section F4.

Table 1. Location and naming of the sensors.

Section	Temp.	Depth (cm)	Strain gauge	Depth (cm)	Direction
F1	T1T	0	-	-	-
	T1S	-8	-	-	-
F3	T3B	0	TQ3	-8	
	T3T	-8	TL3	-8	
F4	T4D	0	BQ4	-3	
	T4B	-3	BL4	-3	
	T4T	-11	TQ4	-11	
	-	-	TL4	-11	

2.4 *Periodic measurements*

Permanent deformation of the structure was evaluated during periodic measurements with a profilometer in three transverse locations along the wheel path (P41 to P43 in Figure 2). Rutting profiles for each pavement were then calculated. Visual inspections of the pavement surface were carried out simultaneously with the profile measurements.

2.5 *Non-destructive tests*

Two types of non-destructive tests were carried out, before, during and after trafficking (Table 2). A Falling weight deflectometer (FWD) was used to measure pavement deflection using a grid of 45 points distributed in an area of 12 m × 2.5 m. Deflection bowl measurements were also taken with an ETH Delta device, which determines the deflection bowl produced by a static axle load. It has 12 high precision lasers that measure the rebound of the road surface when the loading axle moves away from the device (Rabaiotti, 2008). Measurements were taken in both the trafficked area and outside the trafficked area. Results are in the form of three dimensional deflection bowls that can be compared or can be used for backcalculation purposes.

Table 2. Date and number of MLS10 load repetitions for each non-destructive test.

	FWD tests			ETH delta tests		
	Section					
Date (2009)	1	3	4	1	3	4
29/06	0	0	353,000	–	–	–
15/09	188,000	427,000	396,000	–	–	–
16/09	–	–	–	188,000	427,000	396,000
22/10	439,000	427,000	550,000	–	–	–
10/11	–	–	–	439,000	–	740,000

3 TEST PROGRAM

The MLS10 is able to apply a maximum load of 65 kN, corresponding to a full-scale axle load of 130 kN. It can be converted to an equivalent single axle load with a destructive amplification factor of 8.46. In theory, to simulate 20 years of traffic it would be necessary to load the pavement with 8,630,000 MLS10 load repetitions. The goal of the first phase of the test program was to apply 3 million MLS10 65 kN load repetitions and after this, decide if an extension of the test period was required to fulfill the main objective of the project. Unfortunately, due to reasons already explained, a total of only 1,606,000 load applications were reached before the end of the project time period. Of that total, the load applications were distributed in each of the sections as summarized below:

- Section F1: 439,000 load repetitions
- Section F3: 427,000 load repetitions
- Section F4: 740,000 load repetitions

For these tests, the MLS10 was equipped with Goodyear 455/50 R22.5 dual tires. The speed of the moving tires was 22 km/h. In order to test under similar temperature profiles and have the results comparable, the machine was moved regularly from one section to the other.

4 DATA ANALYSIS AND INTERPRETATION

4.1 *Temperature*

Table 3 summarizes the average temperatures measured for the duration of the tests. The first column presents the total average temperature in the entire testing period whereas the second column considers only the temperature measured when the MLS10 was in

Table 3. Temperature in each section.

Sensor	Average temperature (°C)	Average temperature while trafficking (°C)
T4D	22.6	23.4
T4B	22.8	20.3
T4T	22.5	18.7
T3B	23.2	28.5
T3T	23.8	29.6
T1T	19.7	27.5
T1S	20.0	23.8

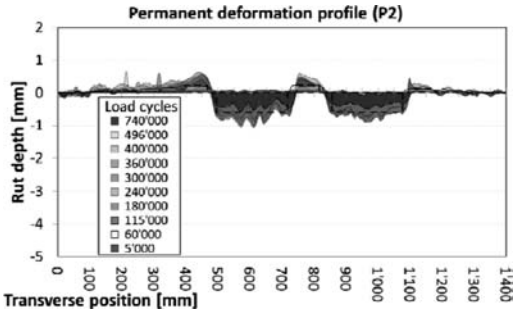

Figure 3. Example of one transverse pavement profile for different trafficking intervals.

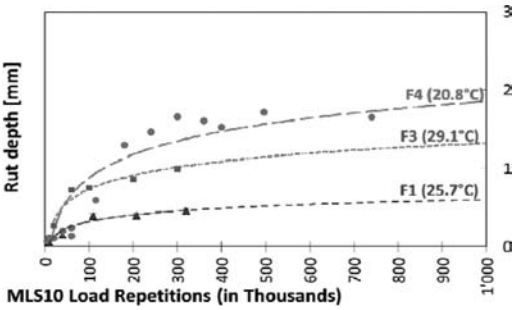

Figure 4. Progressive comparative rutting of all the sections.

service. Average surface temperatures in Section F3 were the highest of all sections, whereas Section F4 recorded the lowest temperature with 23.4°C.

4.2 *Transverse pavement profile*

Pavement permanent deformation for each section was calculated by analyzing the three profiles taken with the MLS profilometer. Figure 3 presents the accumulated deformation of the pavement surface of profile P42, corresponding to the second profile of Section F4. Figure 4 shows the progressive rutting in terms of load applications for all the test sections. The curves extrapolated to one million loading cycles show very small rutting depths of less than 2 mm for all sections trafficked. Section F4 had the highest rutting,

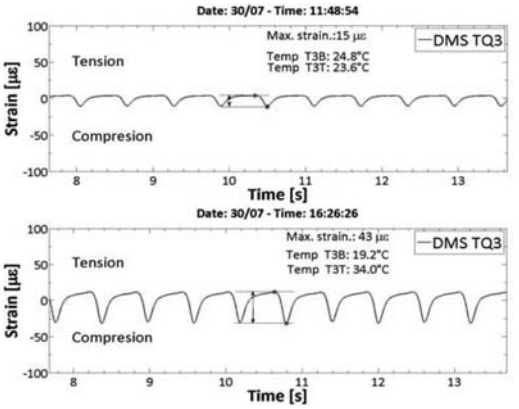

Figure 5. Deformation measured with the TQ3 strain gauge showing the deformation with increase in pavement temperature.

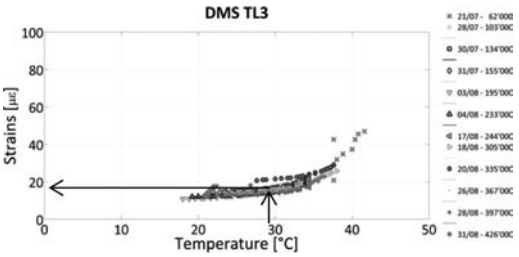

Figure 6a. Temperature dependent absolute deformation obtained with sensor TL3. Every marker type represents a day and a certain number of MLS10 loads.

despite the pavement having the most layers and lowest temperature during the tests.

4.3 *Strain gauges*

In order to analyze the deformation obtained with the strain gauges it was necessary to take into account the influence of speed of the MLS10 loads and the pavement temperature. Measurements were filtered and only those records taken at a trafficking speed of 22 km/h were considered. Temperature change during the day and the influence of tire friction on temperature were both taken into consideration as they both had an effect on strain under the same load, as shown in the example in Figure 5.

The average difference between tension and compression peaks was calculated for every valid file recorded and stored in a table together with the measured temperature, the timestamp and the number of accumulated loads. Then, for every day with records, curves of temperature dependent deformation were drawn and fitted with sigmoidal functions (Figure 6a). By repeating this procedure for everyday of the test, it was possible to build deformation curves dependent of the number of trafficking loads. An average temperature for all measurements was determined and the

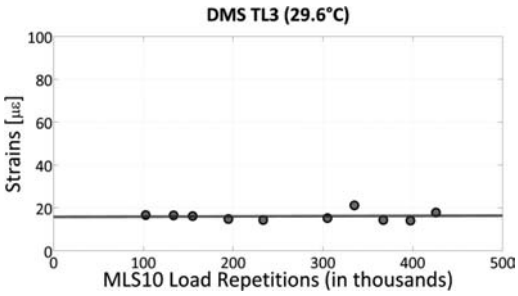

Figure 6b. Deformation vs. number of MLS10 load repetitions for average temperature.

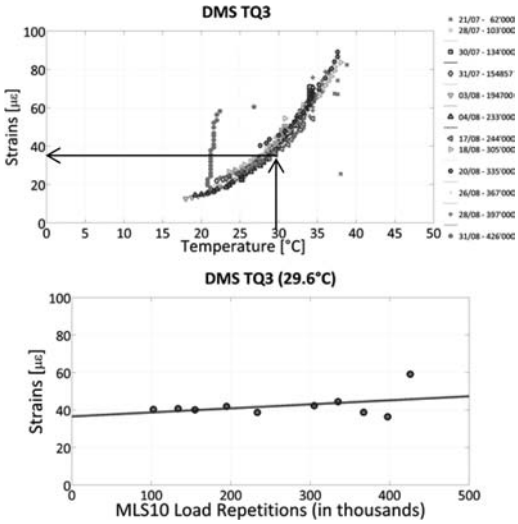

Figure 7. Strain gauge analysis for TQ3.

deformation was again calculated. This deformation was then plotted against the accumulated number of loads (Figure 6b). By evaluating the data in this way, it was possible to reduce the influence of temperature in the results.

Other calculations for Section F3 and Section F4 are presented in Figure 7 and Figure 8, respectively.

None of the strain gauge measurements showed a significant change in the deformation values. This can be interpreted as evidence that the structures tested with the MLS10 did not show any kind of distress after trafficking.

4.4 *Falling weight deflectometer*

Data obtained with the FWD was used to prepare deflection maps of the areas were the tests were carried out. This area, about 12 m long and 2.5 m wide had the MLS10 loading sector in its center (wheelpath). By taking the maximum deflection of each point of the measurement grid, the authors expected to identify relatively weak zones in the scoped area. Deflection maps for Section F1 and Section F4 are shown in Figure 9.

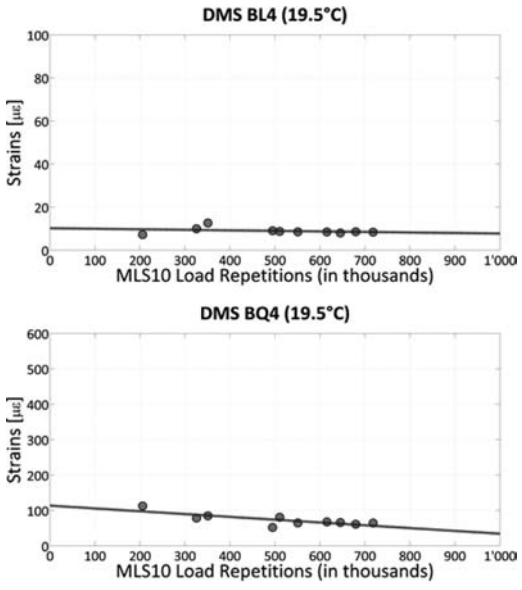

Figure 8. Strain gauge results for BL4 and BQ4.

The investigation revealed that no clear change could be detected in Section F1. On Section F4, however, relative deflection increased on the trafficked sector. Unfortunately, no further data could be collected in order to confirm this tendency.

4.5 *ETH Delta*

The data obtained with the ETH Delta device was used to prepare three-dimensional (3-D) deflection maps. Deflection maps for Section F1 and Section F4 are provided Figure 10 and Figure 11, respectively.

The shape and order of magnitude of the deflection bowls do not show clear signs of change after being trafficked. It can be seen that the amount of load repetitions were insufficient to induce a change in the structural response.

4.6 *Laboratory tests*

Bituminous layers on all sections were cored. No evaluation of the cement stabilized layers or subgrade was done after trafficking.

Laboratory testing on the three top layers included indirect tensile tests and evaluation of interlayer bonding.

4.6.1 *Indirect tensile test*

Temperature dependent elastic moduli of the bituminous layers were calculated for six cores taken from the wheel path and outside the trafficked area. An average elastic modulus for each condition was calculated and compared. Results are presented in Table 4 and Figure 12, and show that the difference between both loading conditions was negligible.

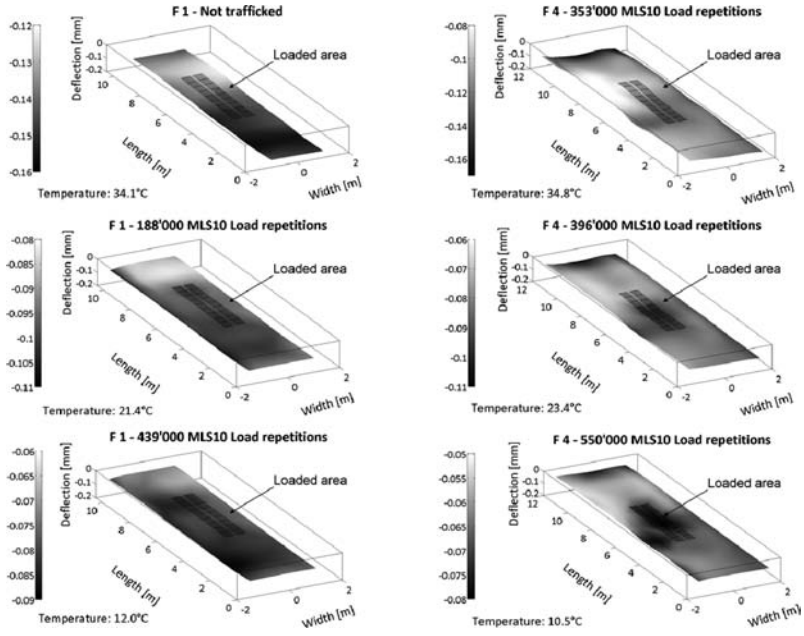

Figure 9. 3-D deflection maps for FWD tests on Section F1 and Section F4. The footprint of the dual tires is marked in the centre of the area.

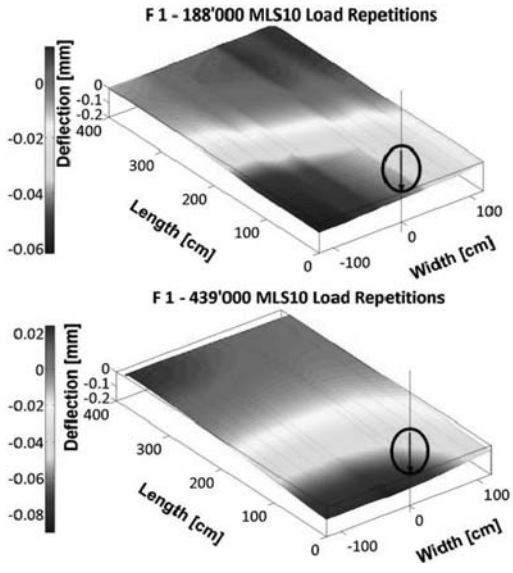

Figure 10. 3D deflection measured with ETH Delta for two trafficking conditions on Section F1.

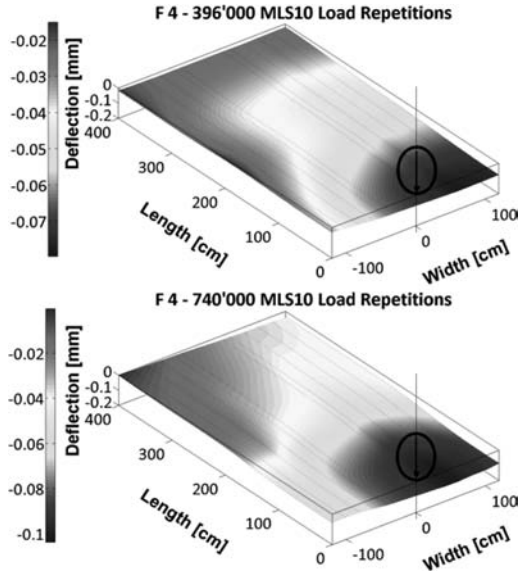

Figure 11. 3-D deflection measured with ETH Delta for two trafficking conditions on Section F4.

4.7 *Interlayer bonding*

Four cores taken from the loaded area were tested with the layer parallel shear test (LPDS) according to Leutner (VSS, 2000), and then compared with results obtained from untrafficked cores. Two interlayers were analyzed: between MR8 and AC B 22 H (top and second course) and between AC B 22 H and AC T 22 H. The results, summarized in Table 5, and plotted in Figure 13, show that the MR8 and AC B 22 H interlayer properties improved after trafficking. This confirms earlier research findings on this topic (Raab and Partl, 2007).

Table 4. Elastic moduli of the top layers.

Layer	Temp. (°C)	Non-trafficked (MPa)	Trafficked (MPa)	Difference %
AC MR8	5	9,543	9,395	1.6
	10	6,900	6,622	4.0
	15	4,442	4,594	−3.4
	20	3,435	3,481	−1.3
	25	2,367	2,449	−3.5
	30	1,128	1,187	−5.2
	35	859	871	−1.4
AC B22 H	5	18,948	19,490	−2.9
	10	14,668	13,561	7.5
	15	9,925	10,700	−7.8
	20	7,348	7,647	−4.1
	25	4,856	5,019	−3.4
	30	3,268	3,247	0.6
	35	2,231	2,175	2.5
AC T22 H	5	20,248	19,865	1.9
	10	15,985	14,279	10.7
	15	11,295	11,109	1.7
	20	8,060	7,927	1.7
	25	5,170	5,058	2.2
	30	3,522	3,332	5.4
	35	2,315	2,235	3.5

5 FINITE ELEMENT MODEL

In this section, a finite element (FE) model of the experimental phase is briefly discussed. The goal was to establish a relationship between the measured deformation on the test sections and the stress-strain field of the structure. The simulation attempts to represent as closely as possible the conditions of load dimension (footprint), speed, temperature of the structure, materials, etc. To that end, the commercial finite element software *ABAQUS* was used.

To take field conditions into consideration, a plug-in of *ABAQUS 6.8* was developed. A GUI (Graphical User Interface) coded in *Python* was used to generate and simulate the experiments automatically, as detailed below.

The GUI form was created in a way that the parameters were incorporated in each field through the different tabs. Data entry was arranged by completing five different forms, related to different stages of the organization of the model. The names of the forms, which are activated by selecting the appropriate tab are: Geometry and Materials, Loads, Interactions, Element Types + Mesh and Job + Visualization. This plug-in has the ability to create a structure of four layers with different thicknesses.

The material properties of each layer are stored in a file establishing a library of materials. A drop down menu in the materials form allows access to the list of materials available in the library. The form also allows incorporation of the influence of temperature in each layer separately.

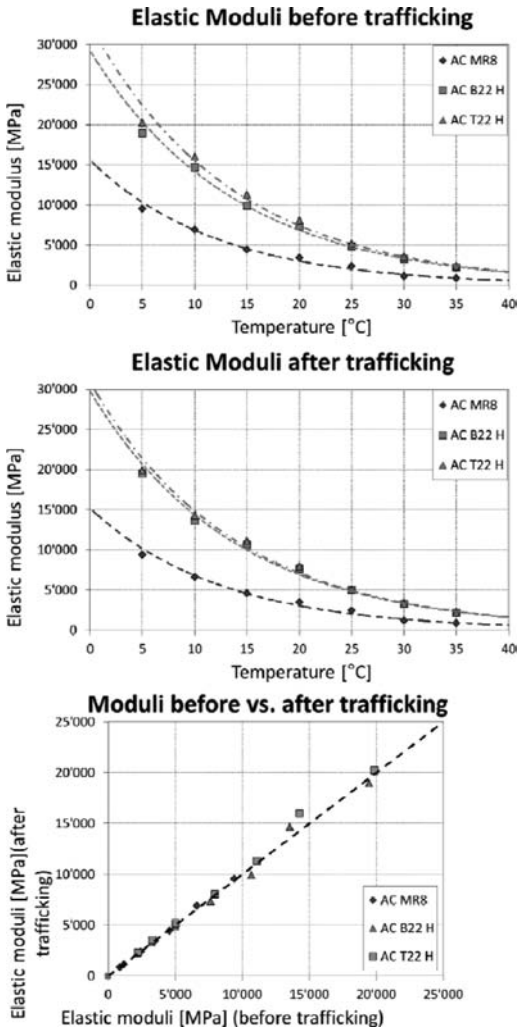

Figure 12. Top two diagrams show the moduli of trafficked and non-trafficked cores. Bottom diagram shows a comparison of both modules, with good correlation.

Table 5. Average results of the LPDS.

	MR8-AC B 22H		AC B 22H-AC T 22H	
Parameter	Trafficked	Un trafficked	Trafficked	Un trafficked
Load (kN)	41.9	32.9	37.1	39.5
Tension (kN/m^2)	2,373.0	1,864.3	2,099.5	2,235.3
Deform. (mm)	2.7	2.2	1.5	1.3

Loads were also stored in a load library. The GUI user chooses from a menu of loads of different type, shape, amplitude and speed. In the Interactions menu, different types of contact models are chosen. It is

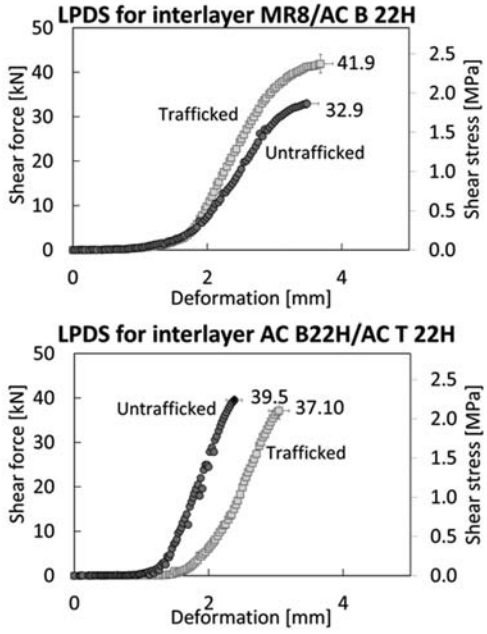

Figure 13. Comparison of the LPDS for both interlayers and loading condition.

possible to specify a coefficient of friction and tangential contact stiffness normal to the surfaces involved. It is also possible to select whether the simulated layers are bonded, creating a situation where no relative motion between them is possible.

An eight-node cubic element linear C3D8R was used to define the mesh. This form allows defining a refined element mesh directly under the load footprint and setting the number of elements in each direction of the model. In the last form Job + Visualization, the user can name the simulation and select the type of solver to use for resolution.

Figure 14 presents the FE model geometry for the Section F4 test. The four layers of the structure are displayed in different colors. By having similar characteristics, stabilized granular layer bonding (HGT) is considered as a single 400 mm (180 mm + 220 mm). The overall dimensions of the model are 2,250 mm long and 2,000 mm wide. These dimensions were defined during different runs to achieve an appropriate balance between accuracy and computation. The computing time for these models was on the order of four hours.

The mesh was designed to provide greater definition in areas where a reasonable accuracy is required. In total, 13,662 items were used to define the geometry of the pavement.

Figures 15 and 16 present two examples of calculated and measured strains. Figure 15 shows longitudinal strains at −30 mm depth with a pavement temperature of approximately 20° C. The curve calculated with the FE model is on the left. The window on

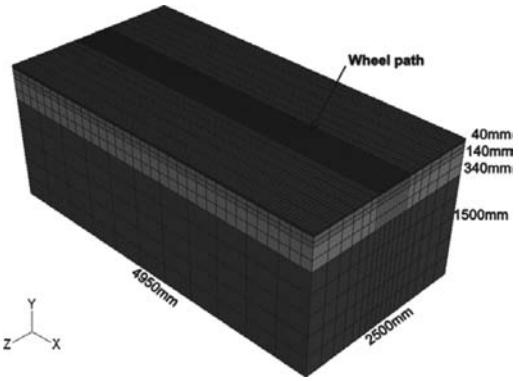

Figure 14. Geometry of the FE model.

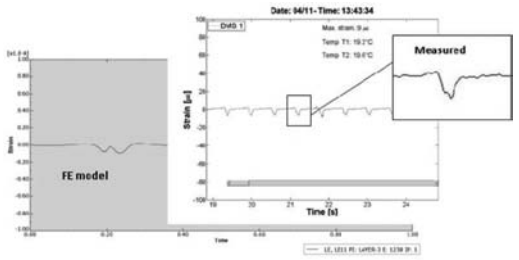

Figure 15. On left, the FE calculated strains. In the window, the measured strain. (Strain gauge BL4).

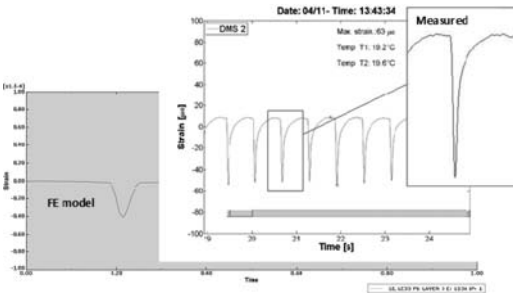

Figure 16. On left, the FE calculated strains. In the window, the measured strain. (Strain gauge BQ4).

the right shows one measured loading cycle. In Figure 16 the curve shows transverse strains for the same temperature and position.

Table 6 summarizes the results of the strain (absolute values) for each case: the real, as an average of several measurements, and the simulated for the same mentioned conditions of load speed and pavement temperature. The results show that, although there are still differences between the measured and calculated values, they are small and the model developed here can be used to estimate the pavement response. Further research on this topic will be presented elsewhere (Pugliessi, in prep.).

Table 6. Summary of measured and simulated strains.

Modeled strains ($\mu\varepsilon$)		Simulated strains ($\mu\varepsilon$)	
Longitudinal	Transverse	Longitudinal	Transverse
10	60	11	42

6 SUMMARY AND CONCLUSIONS

The main goal of the activities summarized in this paper was to calibrate the MLS10 which is a prototype for which there was no previous experience in Switzerland. To that end, the objective was to use MLS10 to traffic a typical Swiss pavement structure until signs of distress were observed. However, due to limited testing time, this objective could only be partially fulfilled, as there was no conclusive sign of distress shown in the data presented. An exception was the interlayer bonding between the top and second layers, where results show that bonding increased after MLS10 trafficking. FWD measurements on Section F4 also showed that relative deflection increased in the trafficked zone, which can be understood as the initiation of a distress mechanism in the structure. Almost no rutting was recorded on any of the sections, with measured deformation never exceeding 2 mm. It is interesting to note that rutting was worst on the pavement with multiple bituminous layers (Section F4). This shows that the permanent deformation resulted mostly from compaction of the asphalt layers and did not occur in the stabilized and subgrade layers.

Experience gained over the seven-month test period was, however, the most valuable offering of the project. During this time many shortcomings of the MLS10 were identified and improved. Instrumentation, data acquisition and analysis were all accomplished successfully, given that all sensors worked as required.

Finally, the development of a FE model capable of simulating the MLS10 loading with increasing accuracy was another asset of this project.

ACKNOWLEDGMENTS

The authors would like to thank the Swiss Federal Road Office (FEDRO) for financing the project. We would also like to express special thanks to Dipl. Ing. Martin Umminger, Dr.-Ing. Carsten Karcher and Dipl.-Ing. Plamena Plachkova from Karlsruher Institut für Technologie, who carried out the FWD measurements. Many thanks to Dr. Carlo Rabaiotti and ETH staff for the ETH Delta measurements. And also our gratitude to the operating staff of the MLS10 for their hard work.

REFERENCES

Partl, M.N. and Arraigada, M. 2011. Der neue Mobile Load Simulator (MLS10), *Strasse und Autobahn* 62(4):252–257 April 2011.

Pugliessi, A. in prep. *Relationship between Mobile Load Simulators MMLS3 and MLS10*, M Eng thesis, National University of Rosario (UNR), Argentina.

Raab, C. and Partl, M.N. 2008. Investigation on Long-Term Interlayer Bonding of Asphalt Pavements. *Baltic Journal of Road and Bridge Engineering*. 3(2):65–70.

Rabaiotti, C., Partl, M.N., Caprez, M. and Puzrin, A.M. 2008. APT device evaluation for road research in Switzerland: test campaign on a Swiss Highway with the MLS10, *3rd International Conference on Accelerated Pavement Testing*, Madrid October 2008.

VSS, 1997. *Schweizer Norm (SN) 640324a: Dimensionierung Strassenaufbaus, Unterbau und Oberbau.* Schweizerischer Verband der Strassen- und Verkehrsfachleute (VSS) VSS-Expertenkommission 5.03.

VSS, 2000. *Schweizer Norm (SN) 670461: Bituminöses Mischgut – Bestimmung des Schichtenverbunds (nach Leutner).* Schweizerischer Verband der Strassen- und Verkehrsfachleute (VSS) VSS-Expertenkommission 5.09.

VSS, 2008. Schweizer Norm (SN) 640430b: Walzasphalt – Konzeption, Ausführung und Anforderungen an die eingebauten Schichten. Schweizerischer Verband der Strassen- und Verkehrsfachleute (VSS). VSS-Expertenkommission 5.01.

This page intentionally left blank

Part 6: Accelerated pavement testing on portland cement concrete pavements

This page intentionally left blank

Advances in Pavement Design through Full-scale Accelerated Pavement Testing – Jones, Harvey, Mateos & Al-Qadi (Eds.)
© 2012 Taylor & Francis Group, London, ISBN 978-0-415-62138-0

Performance of thin jointed concrete pavements subjected to accelerated traffic loading at the MnROAD facility

T.R. Burnham & B.I. Izevbekhai
Minnesota Department of Transportation, Maplewood, Minnesota, US

ABSTRACT: With the growing trend in shrinking budgets, as well as increased concern for sustainable engineering, there is strong interest in determining how thin jointed concrete pavements can be constructed and still provide predictable long term performance. In 2008, five thin concrete test sections were constructed at the MnROAD pavement test facility toward addressing that question. Design slab thicknesses ranged from 130 to 165 mm (5 to 6.5 in.). The sections were constructed on the MnROAD mainline roadway, thus exposing them to accelerated loading in the form of live, high volume interstate traffic. Other than some variations in panel length and dowel type for the thinnest sections, all other design variables were kept constant. This paper summarizes the performance of the test sections after more than two years of traffic and environmental exposure. Several pavement performance parameters were analyzed, including visual distress, joint faulting and load transfer efficiency, panel deflections, and ride quality. Observed performance was also compared to performance predicted by the current Minnesota Department of Transportation pavement design procedure. Transverse and longitudinal cracking occurred on the thinner sections. Causes for each type of cracking are discussed. While the sections with slabs less than 150 mm (6 in.) thick in this study withstood over 1.5 million CESALS before cracking, it is clear the thicker sections have much greater capacity. The data and observations gathered from these cells will benefit the continuing development of mechanistic–empirical design procedures for thin concrete pavements.

1 INTRODUCTION

1.1 *Background*

Pavement engineers have always strived to balance structural capacity and economics to meet the needs of road agencies. With the growing trend in shrinking budgets, as well as increased concern for sustainable engineering, there is strong interest in determining how thin jointed concrete pavements can be constructed and still provide predictable long-term performance.

Recent studies (Steyn et al., 2005; Snyder, 2008) have demonstrated that thin concrete pavements can be successfully designed to serve specific applications. Most current concrete pavement design procedures however were not developed or calibrated to design sections with thicknesses less than 150 mm (6 in.). To address this shortfall, several thin concrete test sections were constructed at the MnROAD facility in 2008. The objective of this project was to gather performance data that can be used to expand the lower range of slab thickness in modern mechanistic-empirical design procedures.

The scope of this paper is to describe the observed performance of the MnROAD thin concrete test sections for the time period 2009 to 2011. The performance parameters examined include panel cracking, joint load transfer behavior, and ride quality. A comparison to predicted performance was also carried out.

1.2 *MnROAD facility*

Since the early 1990's, the Minnesota Road Research facility, commonly known as MnROAD, has continued to serve the purpose of validating pavement designs and methods of current interest, particularly those used in cold regions. With its unique layout, MnROAD can accommodate a variety of research projects, including short, long, and accelerated studies.

The MnROAD test facility is a full-scale test track, subject to real-time environment and traffic. Divided into two main segments, the MnROAD facility has one set of test sections or "cells" placed end-to-end that receive live traffic loading diverted from a parallel section of Interstate 94 near Albertville, Minnesota. Another portion of the facility contains a set of test sections arranged in a closed loop.

As MnROAD began Phase 2 operations in 2007, there was strong interest in understanding the capacity of thin concrete pavement sections. Utilizing the unique capability of shifting live traffic back to a parallel road in the case of early failures, several thin concrete pavement test sections or "cells" were constructed in 2008 on the "mainline" or interstate portion of MnROAD. Placement here allowed the opportunity to accelerate the evaluation of their performance.

Table 1. Test section design details.

Cell	Layer thickness (mm)			Panel size (m)		Dowel type
	Slab	Base	Subbase	Long	Wide	
113a	130	130	130	3.6	3.6	Round
113b	130	130	130	4.6	3.6	Round
213	140	130	115	4.6	3.6	Round
313	150	130	100	4.6	3.6	Round
413	165	130	90	4.6	3.6	Round
513a	130	130	130	4.6	3.6	Plate
513b	130	130	130	3.6	3.6	Plate

Unit conversion: 25 mm = 1 in.; 1 m = 3.28 ft.

2 TEST SECTION DESIGN

The concrete pavement test sections in this study are designated Cells 113–513. Design slab thicknesses range from 130 mm (5 in.) to 165 mm (6.5 in.). Standard panel dimensions are 4.6 m (15 ft.) long by 3.6 m (12 ft.) wide, except for two areas (Cells 113a and 513b) which each have three panels (in each lane) with a length of 3.6 m (12 ft.). It should be noted that in using 4.6 m (15 ft.) panels, the design length to slab thickness ratio for certain cells exceeds the recommended limits as suggested in ACI 302.1R-04 (ACI, 2004).

The base and subbase layers consist of a dense-graded granular material. The subgrade is a silty-clay material. Table 1 shows the design dimensions and dowel bar type in each cell.

The transverse joints in Cells 113–513 contain round or plate dowels. Table 3.1 of ACI 302.1R-04 (ACI, 2004) recommends against using 25 mm (1 in.) diameter bars in pavements less than 180 mm (7 in.) in thickness. The reason for this is to prevent excessive stresses in the concrete caused by the relatively stiff round dowel bars. To test whether those guidelines remain valid for current thin concrete pavement practices, the transverse joints in Cells 113–413 were constructed with 25 mm (1 in.) diameter by 380 mm (15 in.) long round dowel bars, spaced 305 mm (12 in.) on center. Recognizing the suitability of using plate dowels, which have demonstrated good long term performance in thin floor slabs, Cell 513 transverse joints were constructed with 9.5 mm (3/8 in.) thick by 305 mm (12 in.) long, tapered width (40–60 mm) steel plate dowels spaced 305 mm (12 in.) on center. Three #13 (12.7mm) tie bars were installed per panel along the longitudinal joint.

Due to the short duration of the experiment, joints and slab edges were not sealed. Both shoulders were constructed with asphalt.

As designed, the test cells were to be constructed with a difference in thickness of 12.5 mm (0.5 in.) between them. Given the inherent variation in the grade (base layer), and the practical tolerance achievable with a large slip-form paver, the as-built thickness of the cells varied from design values. Table 2 lists a summary of the results of thickness determination using core samples and magnetic tomography (Johnson et al., 2008). Except for Cell 413, each cell was built to an average thickness greater than the design value.

Table 2. As-built concrete slab thickness.

Cell	Outer wheelpath		Center-line (mm)	Average (mm)	Difference from design (mm)
	Drive (mm)	Pass (mm)			
113	145	151	132	143	+16
213	156	158	143	151	+11
313	158	159	157	158	+6
413	164	165	159	163	−2
513	156	150	144	149	+22

Unit conversion: 25 mm = 1 in.

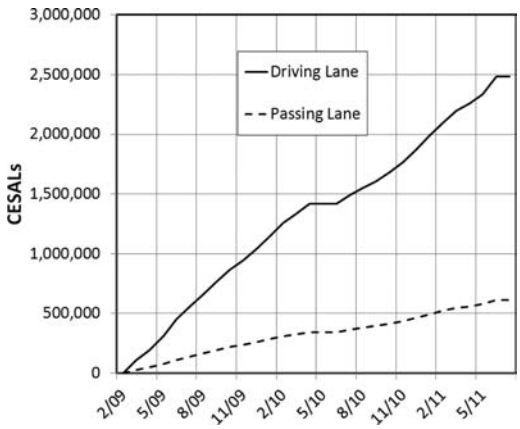

Figure 1. History of traffic loads, in CESALs, applied to Cells 113–513.

3 TRAFFIC

Traffic on the "mainline" or interstate portion of MnROAD consists of 24-hour live interstate traffic, diverted off of an adjacent interstate highway. Periodically, traffic is diverted off the test sections to conduct specific vehicle load tests, perform routine pavement performance measurements, or carry out maintenance or reconstruction activities.

Although the construction of Cells 113–513 was completed on October 10, 2008, they were not opened to live traffic until February 3, 2009. Traffic at MnROAD is characterized through the use of equivalent single axle loads (ESALs). Traffic loads applied to concrete test cells are further transformed into CESALs (Concrete Equivalent Single Axle Loads) using load equivalency factors to account for concrete pavement's unique response to applied loads. Figure 1 shows a plot of the cumulative CESALs applied to Cells 113–513 during the study period. As of June

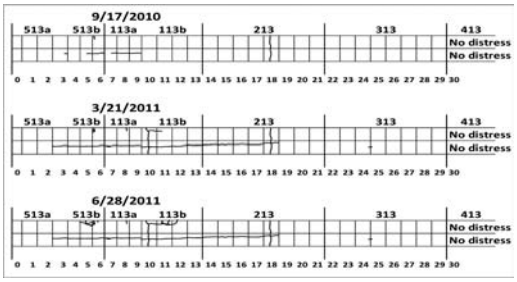

Figure 2. Cracking maps (plan view) from surveys conducted since September 2010.

Figure 3. Cracking in area of embedded sensors in Cell 513. Note condition of adjacent shoulder.

2011, the driving lane of each cell had received approximately 2.4 million CESALs, and the passing lane, approximately 614,000 CESALs (Mn/DOT, 2012).

4 TEST SECTION PERFORMANCE

4.1 *Panel cracking*

Traffic was first applied to Cells 113–513 on February 3, 2009. Visual distress surveys were conducted in the spring and fall of 2009 and 2010, and three times during the spring of 2011. The survey conducted on September 17, 2010 documented that the first slab cracking occurred in Cells 113, 213 and 513. Cracking maps from subsequent surveys are shown in Figure 2.

The amount of cracking in Cells 113, 213, and 513 rapidly accelerated during the spring of 2011. Two midpanel transverse cracks crossed both lanes in Cells 113 and 213. In the driving lane, short transverse cracks began to emerge, emanating from the edge of the panel near the shoulder. This typically indicates the onset of fatigue cracking. By June 2011, two areas in the driving lane of Cells 513 and 113 developed interconnected cracking which resembled punch-out type failures (Figure 3). Figure 4 shows that a crack in the sensor area of Cell 113 was detected in November 2010 near an embedded vibrating wire strain sensor.

To keep the sections in service, the panels in the sensor areas of Cells 513 and 113 were replaced with

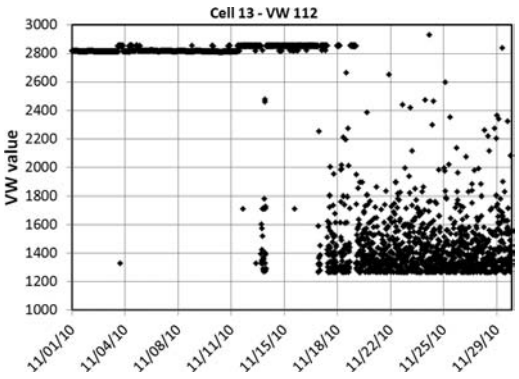

Figure 4. Crack formation indicated by disruption in smooth continuous trend of vibrating wire data.

Figure 5. Embedded sensor wires and supports along crack in Cell 513.

full depth repairs in August 2011. During the removal of the failed areas, it was noted that the cracks followed the sensor leads and supports that were routed within the pavement. It became evident that the concentration of sensor wires and supports likely formed a weak plane within the thin concrete slabs, which reduced their capacity to carry interstate type traffic. Figure 5 shows one such example.

In addition to the problems caused by embedded sensor wires, Cells 113, 213, and 513 show evidence of pumping of the underlying base materials. Figure 6 shows standing water in the deteriorated driving lane shoulder of Cell 513. Visual observations during the frequent rain events of spring and summer 2011 noted that water in these areas would squirt upward from the panel edges and unsealed transverse joints with each passing truck. The driving lane shoulder was often "stained" with mud pumped from the lane/shoulder joint.

Cracking in the passing lane of Cells 113, 213, and 513 differed from the driving lane. Longitudinal cracking progressed rapidly and in contiguous panels within these cells. This type of cracking is often associated with loss of panel support, either through settlement or pumping of base materials. Another possibility is damage from heavy trucks traveling over temperature curled thin slabs.

Figure 6. Standing water in deteriorated shoulder of Cell 513.

4.2 *Joint faulting*

Examination of the transverse joint faulting data for each cell in this study revealed that virtually no faulting had occurred through spring 2011. The average value of joint faulting had not yet exceeded 1.0 mm (0.04 in.), which indicates measurements are still within the range of surface texture depth.

4.3 *Joint load transfer efficiency and deflections*

The load transfer efficiency (LTE) history of transverse joints is an important indicator of their remaining service life. LTE values in this study were calculated using Equation 1 from the method outlined in Section 3.5.4 of the *AASHTO Guide for Design of Pavement Structures (1993)* (AASHTO, 1993).

$$\text{LTE}\ (\%) = d_{je} = d_u/d_l \times 100 \qquad (1)$$

where d_{je} is the load transfer efficiency in percent, d_u is the deflection at the joint of the unloaded slab, and d_l is the deflection of the loaded slab.

In addition to LTE, it is important to examine the total deflection at the joint. High values of LTE will not always indicate joints with excessive deflection, which can mask the potential for pumping of subsurface material.

Deflection measurements at MnROAD are accomplished using a falling weight deflectometer (FWD). FWD testing is done on a seasonal basis for all cells at MnROAD. To avoid artificially high LTE values (joints closed due to temperature expansion), transverse joints are only tested when pavement temperatures are below 25°C (77°F). For concrete test sections, the load levels applied are 26.7, 40, and 53.4 kN (6,000, 9,000, and 12,000 lbs.). For brevity, only the results from the 40 kN (9,000 lbs.) load level are reported in this paper.

Figure 7 shows the history of average LTE of all measured joints in the driving lane for each cell. Due to

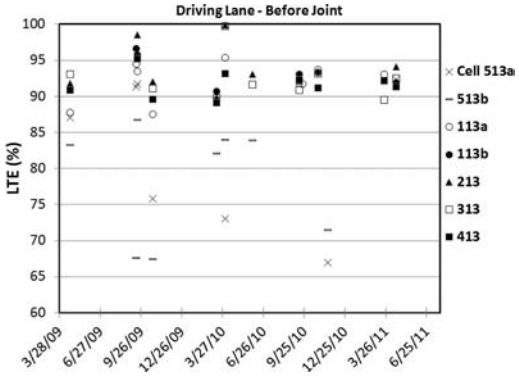

Figure 7. Average Load Transfer Efficiency (LTE) of transverse joints in Cells 113–513. FWD load level = 40 kN (9,000 lbs.).

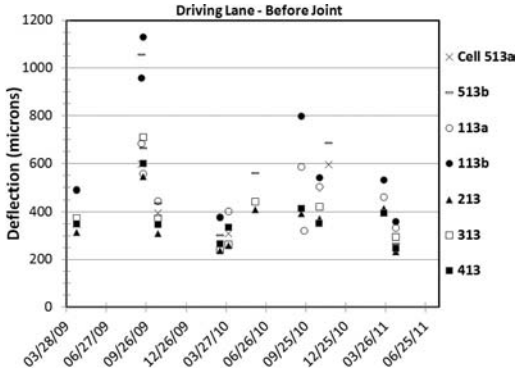

Figure 8. Average deflection of transverse joints in Cells 113–513. FWD load level = 40 kN (9,000 lbs.).

the wide variability in the measurements, caused either by seasonal effects on the panels and base layers, or the effect of cracks located near FWD test points, trend lines were not applied to the plots. In both lanes, the joints containing plate dowels (Cells 513a and 513b) exhibit lower LTE than joints containing round dowels, due to the lower inherent stiffness of plate dowels. No discernible difference in LTE was noticed between joints in the 4.6 m (12 ft.) or 3.6 m (15 ft.) long panels in Cells 113 or 513. The LTE trend does not yet appear to be declining for joints with round dowels.

Figure 8 shows the history of average deflection of the joints in the outer wheelpath of the driving lane (where LTE is measured). Similar to LTE, the deflections exhibit a wide range in magnitude, depending on the season. In the driving lane, joint deflections from thinner design Cells 113 and 513 were approximately one-third higher than Cells 213–413. The high measurement values in September 2009 appear to be related to measurement errors, rather than a trend in increasing joint deflections. Joint deflections in the passing lane were lower than those in the driving lane, and exhibit less variation. This is likely related to the passing lane receiving one-fourth the

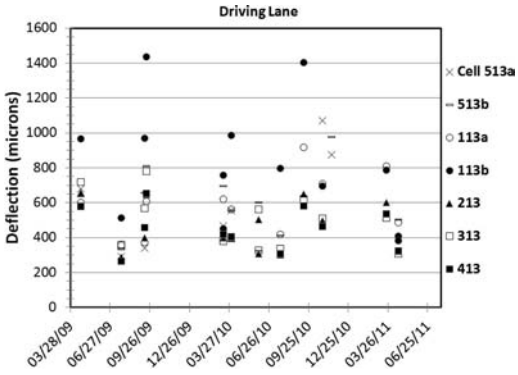

Figure 9. Average deflection of panel corners in Cells 113–513. FWD load level = 40 kN (9,000 lbs.).

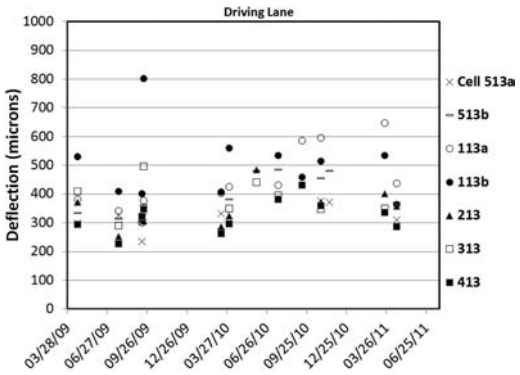

Figure 10. Average deflection of mid-panel edge in Cells 113–513. FWD load level = 40 kN (9,000 lbs.).

amount of traffic as the driving lane, and therefore material transport (pumping) occurs less frequently. The presence of longitudinal cracks is also likely having an effect on measured joint deflections.

4.4 *Other slab deflections*

Fatigue cracking in thin slabs usually begins with excessive deflections. It is important therefore to periodically measure deflections in critical panel locations throughout the life of a test cell. In addition to joint load transfer testing in the outer wheel paths, FWD tests at MnROAD are also conducted at concrete panel corners, center of panel, and mid-panel edge locations.

Figure 9 shows the history of average corner deflections of all measured panel corners in the driving lane of each cell. The corner deflections in this lane show large variation, particularly for the thinner cells 113 and 513. In fact, corner deflections in Cell 113b are consistently twice those of Cells 213–413. Corner deflections in the passing lane exhibit less variation, but are increasing with time, perhaps due to the effect the longitudinal cracks have on these measurements in Cells 113, 213, and 513.

Figure 10 shows the history of mid-panel edge deflections for measured locations in the driving lane of each cell. In this lane, the mid-edge panel deflections for Cell 113 are the highest. Those for Cell 513a exhibit lower deflections, most likely due to the higher as-built slab thickness. Mid-edge panel deflections in the passing lane also demonstrate an increasing trend for Cells 113, 213, and 513, likely due to the effect longitudinal cracks have on measurements in these locations.

4.5 *Ride quality*

The ride quality of a pavement is the predominant measure of its serviceability. It is also well understood that pavements built smooth remain smoother throughout their life (Smith et al., 1997). It is of great importance therefore to monitor and understand the ride quality behavior of Cells 113–513.

Figure 11. Lightweight profiler for measuring IRI and RN.

Ride quality measurements at MnROAD are accomplished using two methods. One set of measurements, conducted two times yearly, are taken by a network level type pavement management van. More detailed measurements, conducted on a more frequent and seasonal basis, are taken by a lightweight profiler device equipped with two laser types and two different accelerometers. Figure 11 shows the lightweight profiler device used at MnROAD. This device, in combination with Federal Highway (FHWA) "*PROval*" software, is used to determine both International Roughness Index (IRI) with units in in./mile (1 m/km = 63.36 in./mi.) and Ride Number (RN) data, whose different algorithms are shown in Figure 12 (Sayers and Karamihas, 1998). Unlike IRI, RN is dimensionless and increases with better ride quality. Measurements from this device were used to determine ride quality of the cells in this paper.

The objective of examining the ride quality trends in this paper was to ascertain whether the pavement thickness is in any way correlated to the measured pavement roughness. Moreover, it is of interest to determine the effect cumulative traffic had on the ride quality in each of the lanes, and how it differed between driving and passing lanes.

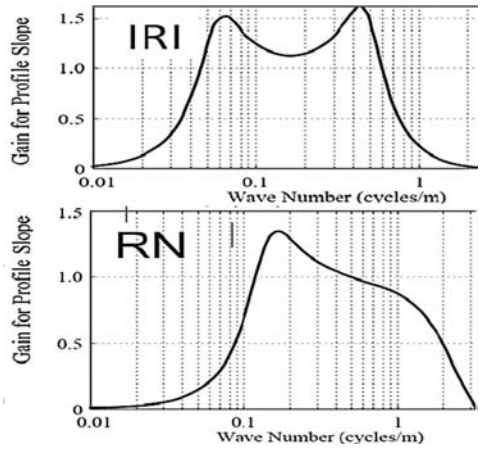

Figure 12. Different gain algorithms for IRI (Top) and RN (Bottom).

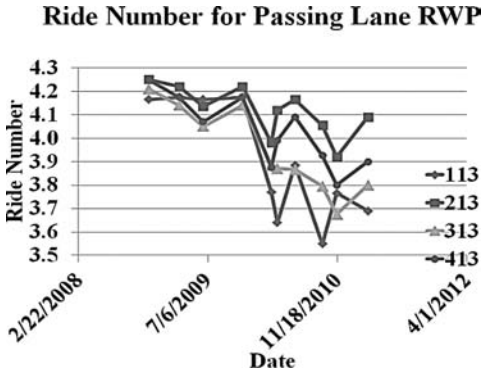

Figure 13. RN plot for passing lane, right wheelpath.

In Figure 13 the RN data for the passing lane, right wheel path, shows an overall decrease in RN in all the cells between 2008 and 2011. Note that for clarity, data from Cells 113 and 513 were combined, due to their equivalent design thickness. A drastic drop in RN was noticed with the measurements in June 2009, after which Cell 113 was consistently lower than the other cells. Cell 313 appeared to be similar to 113, likely due to the influence of one transverse joint, which had begun to exhibit a small crack and faulting. The other transverse joints in Cell 313 are performing much better. Cell 213 appeared to outperform Cell 413, but it is noteworthy that the entire RN ranged from 4.2 to 3.65, which is indicative of good performing pavements (Khazanovich et al., 2005).

In Figure 14 the IRI data for the passing lane, right wheel path, shows an overall increase in IRI in all the cells between 2008 and 2011. Cell 313 appeared to be the worst performing overall, again due to the one distressed transverse joint. Cell 213 appeared to outperform Cell 413. Note the IRI ranged from 40 to 90 in./mi. for all the cells, indicating good to fair performing pavements. Mn/DOT's terminal serviceability threshold in terms of IRI is 2.16 m/km (137 in./mi.).

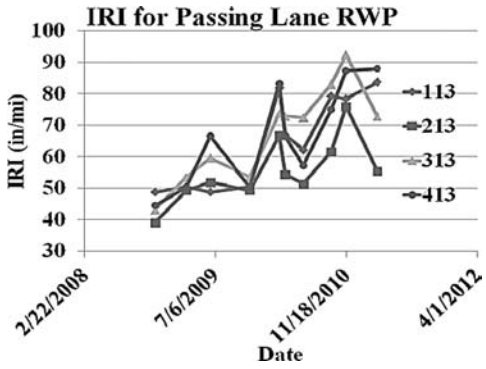

Figure 14. IRI plot for passing lane, right wheelpath.

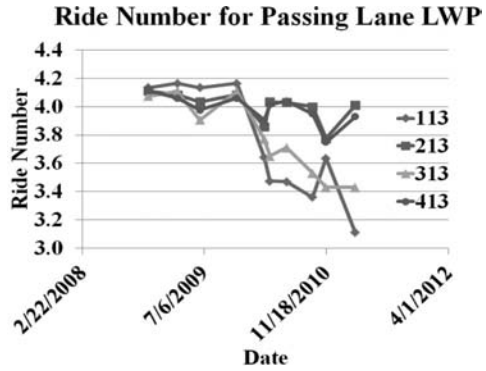

Figure 15. RN plot for passing lane, left wheelpath.

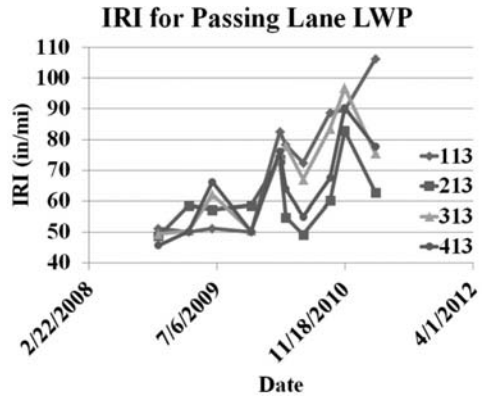

Figure 16. IRI plot for passing lane, left wheelpath.

In Figure 15 the RN data for the passing lane, left wheel path, shows a similar trend to Figure 13, but there is a slightly lower corresponding RN. Cell 313 also shows an unusually lower smoothness value considering its relative thickness, performing worse than Cells 113 and 213 until winter 2010. In Figure 16, the passing lane left wheel path IRI data was generally similar to Figure 14. Evidently the RN clearly shows Cell 113 as the worst performing section, but IRI shows Cell 313 to be performing in a similar way.

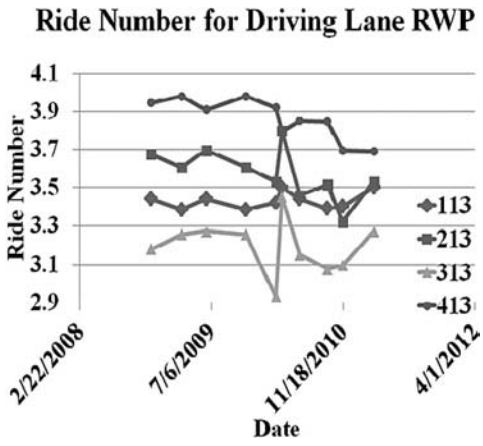

Figure 17. RN plot for driving lane, right wheelpath.

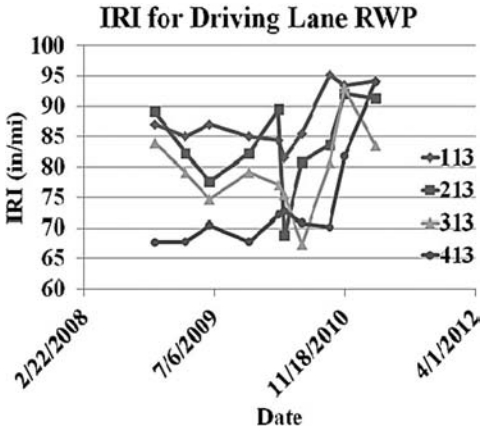

Figure 18. IRI plot for driving lane, right wheelpath.

In Figure 17 the RN data for driving lane, right wheel path, shows a slight overall decrease in RN in all the cells between 2008 and 2011. Unlike the passing lanes, a drastic drop in RN was not noticed following the June 2009 measurement. Cell 313 appears to be the worst performing section, likely due to subsequent pumping that was first observed in 2009. It is noteworthy that apart from Cell 313, where the RN fell to 2.9, the entire RN ranged from 3.9 to 3.1, indicative of good to fair performing pavements.

In Figure 18 the IRI data for driving lane right wheel path shows an overall increase between 2008 and 2011. Except in March 2010, cell 113 IRI was generally higher than the other sub cells. Cell 213 exhibited the next highest IRI. Cell 413 appeared to outperform cell 313 in most of the analysis period. The entire IRI ranged from 68 to 95, which is indicative of the limits of good to fair performing pavements.

In Figure 19 the driving lane, left wheel path, shows a general trend similar to Figure 17, but there is a slightly higher corresponding RN. Performance on Cell 113 dropped unexpectedly in 2010, perhaps due to the influence of some of the increasing distresses

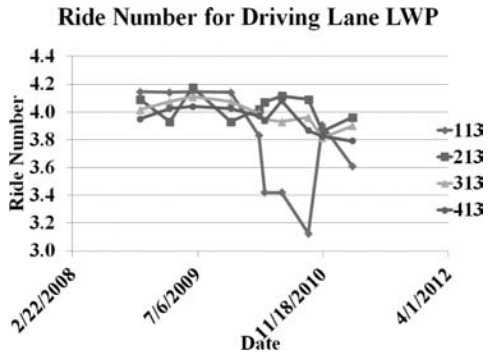

Figure 19. RN plot for driving lane, left wheelpath.

Table 3. Results of ANOVA and regression analysis of traffic ESALs, pavement thickness with IRI and RN.

	P-Values for dependent variables	
Independent variables	Ride number	IRI
Thickness (T)	0.0253	0.2606
ESAL	0.0010	0.0032
Log Thickness	0.0239	0.2293
LOG ESAL	0.0009	0.0031

in the driving lane. Cell 313 also shows an unusually lower smoothness value considering its relative thickness, performing worse than Cell 113 and occasionally worse than Cell 213.

Overall, it cannot be deduced that IRI and pavement thickness are correlated simply by observing the plots. It is also not easily detectable by observing the RN trends. Consequently a statistical method was utilized to better ascertain the extent to which the IRI and RN may be correlated to pavement thickness. This method identified the dependent variable as IRI in one case and RN in the next case. The independent variables were identified as pavement thickness *T* and ESALS. The AASHTO thickness design algorithm (AASHTO, 1993) being a function of LOG T and Log ESAL, suggested an investigation of LOG T and log ESAL as dependent variables, while maintaining IRI and RN as independent variables separately. Four separate multiple regressions were carried out based on an implicit confidence level of 95%, where it is hypothesized that the variables have no effect on IRI and on RN. Based on an α value of 0.05, the p-value of each independent variable was examined. A p-value less than 0.05 was thus considered sufficient evidence against the null hypothesis (Izevbekhai, 2012). Therefore, by having α less than 0.05, it can be concluded to a 95% confidence level that the independent variable is significant.

The result of the analysis of variance and regression analysis conducted is summarized in Table 3. It is evident that based on the traffic ESALs, pavement thicknesses examined, and their corresponding observed RN and IRI, Ride Number appears to be

Table 4. Predicted CESALs to terminal serviceability $P_t = 2.5$ using Mn/DOT design procedure.

Cell	As-built thickness (mm)	CESALs
113	143	560,000
213	151	720,000
313	158	905,000
413	163	1,050,000
513	149	685,000

Unit conversion: 25 mm = 1 in.

significantly correlated to the thickness and traffic ESALs in the cells examined. However, with IRI, pavement thickness was not significantly correlated, whereas ESAL was a significant variable. It may therefore be surmised that the distress features were in the wavelength regimes that are amplified more by the RN gain algorithm than by IRI. This is expected based on the characteristics of the RN algorithm that facilitates better detection of early distress features than IRI. Moreover, as both RN and IRI indicate significance of ESALs, the damage effects may be environmental. It may be extraneous to or independent of pavement thickness. A bias in the statistics may have been introduced by Cell 313 as a sub-cell with intermediate thickness exhibiting early distress before the thinner cells. It is probable that all the cells may have followed the form of Figure 18, in which the IRI appears to be negatively correlated to pavement thickness if Sub-cell 313 did not experience the unexplained early distress features. However, it is noteworthy that based on RN and IRI, the pavements are performing well, but their rate of roughness increase appears significant. Overall there is a lack of significant correlation between IRI and thickness.

While ride quality has not yet deteriorated to unacceptable service levels, the cracking in the thinnest sections is beginning to require frequent and costly repairs. An unacceptable service level at MnROAD is one in which there is a danger to the traveling public due to debris on the roadway from deteriorating cracks, or bumps or dips large enough to cause axles to lose traction from the pavement surface.

5 DESIGN PREDICTIONS

The premise for the design of test Cells 113–513 was to determine the performance levels provided by a range of slab thicknesses for a common panel dimension. It is certainly of interest to examine what a current pavement design procedure might predict for a design life for each of the sections.

For this study, the Minnesota Department of Transportation (Mn/DOT) concrete pavement design procedure (Minnesota Department of Transportation, 2010) was used to predict the performance of the test cells. This is a modified version of the AASHTO 1981 Interim Design procedure. Table 4 lists the predicted CESALs to an AASHTO terminal serviceability level of 2.5 for each test cell. Given that even the thinnest sections have provided satisfactory service levels beyond two million CESALs before major repairs were required, demonstrates the inherent conservatism in the Mn/DOT design procedure. A large part of the successful performance of the test cells is likely tied to the use of doweled transverse joints, something that is not always considered for thin concrete sections subject to much lower traffic levels.

6 SUMMARY AND CONCLUSIONS

In 2008, several thin concrete pavement test sections were constructed on the interstate portion of the MnROAD facility. The objective of these test cells was to determine the difference in performance of thin concrete pavement sections utilizing accelerated traffic loading. This paper examined several pavement performance parameters that characterize the performance of the sections for the time period of fall 2008 to spring 2011. Traffic was first applied to the sections in February 2009.

Visual distress surveys have documented several distinct types of cracking distress forming in the sections. Cells 113 and 213 have developed transverse cracks crossing both the driving and passing lanes. Cause for these cracks may be attributed to slab fatigue caused by continued pumping of base material toward the deteriorating driving lane shoulder. Areas in Cells 113 and 513 containing embedded sensors experienced punch-out type failures, likely caused by the concentrations of embedded wire leads and supports. The passing lanes of Cells 113, 213, and 513 have developed longitudinal cracks in contiguous panels, caused by loss of support or traffic damage to curled slabs. No distresses have formed in the thickest Cell 413.

An analysis of deflection measurements taken at several locations of the test slabs showed a clear distinction between the thinnest cells (113 and 513, 130 mm [5 in.] design) and the increasingly thicker cells (213–413, 140–165 mm [5.5–6.5 in.] design). Joint deflections in the thinnest cells are typically one-third higher than those in Cells 213–413. Confounding the joint deflection results however, is the fact that Cell 513 has plate dowels, which are more flexible than the round dowels used in the other test sections. This results in joint load transfer efficiency results that are markedly higher for Cells 113–413.

An analysis of the ride quality histories of the cells was carried out using both graphical and statistical methods. The graphical analysis proved to be inconclusive, due mainly to data influenced by an isolated distress in Cell 313. The statistical analysis concluded that Ride Number appears to be significantly correlated to the thickness and traffic ESALs in the cells examined. Also, based on RN and IRI, the pavements are performing well, but their rate of roughness

increase is increasing significantly. This seems reasonable, given the accelerated amount of traffic applied to the sections.

Whether due to their susceptibility to damage from overloaded axles, or their tendency toward higher amounts of panel warp and curl, thin concrete pavements must be carefully designed and located. Certainly a 130 mm (5 in.) thick concrete pavement would never be placed on an interstate route. An earlier report (Snyder, 2008) on another 130 mm (5 in.) thick concrete pavement test section, located on the MnROAD Low Volume Road, showed it could perform well under much lower volumes of traffic. The physical dimensions of that test section were different than those in this experiment, and the joints did not contain dowels. Therefore, a direct comparison of performance would not be appropriate here.

The original premise for this experiment was to rapidly determine "How Thin Can You Go?" in concrete pavement design and still achieve reliable and predictable performance. While the sections with slabs less than 150 mm (6 in.) thick in this study survived over 1.5 million CESALS before cracking, it is clear the sections 150 mm (6 in.) and thicker have much greater capacity. And while the ride quality has not yet deteriorated to unacceptable service levels, the cracking in the thinnest sections is beginning to require frequent and costly repairs. The data and observations gathered from these cells will certainly benefit the continuing development of mechanistic–empirical design procedures for thin concrete pavements.

REFERENCES

American Association of State Highway and Transportation Officials. 1993. *AASHTO Guide for Design of Pavement Structures (1993)*. Item Code: GDPS-4-M. ISBN Number: 1-56051-055-2.

American Concrete Institute. 2004. *ACI 302.1R-04.* http://www.concrete.org/General/f302.1(04)Chap3.pdf.

Izevbekhai, B.I. 2012. *Tire Pavement Interaction Noise of Concrete Pavements.* Dissertation of Doctor of Philosophy in Civil Engineering. Department of Civil Engineering, University of Minnesota.

Johnson, A., Clyne, T.R. and Worel, B.J. 2008. *2008 MnROADPhase II Construction Report. Report 2009–22.* Minnesota Department of Transportation, St. Paul, MN.

Khazanovich, L., Darter, M., Bartlett, R. and McPeak. 2005. *Common Characteristics of Good and Poorly Performing PCC Pavements.* Federal Highway Administration 1998 http://ntl.bts.gov/lib/6000/6300/6348/131.pdf. Database: TRIS Online AN: 00760483. ERES Consultants, Incorporated.

Minnesota Department of Transportation. 2010. *Section 5-3.0. Pavement Manual.* Maplewood, Minnesota.

Minnesota Department of Transportation. 2012. *Traffic and ESAL Summary for the MnROAD Mainline (July 1994 – June 2011).* MnROAD Data Release 1.0. Maplewood, Minnesota.

Sayers, M.W. and Karamihas S. M. 1998. *The little Book of Profiling.* URL: http://umtri.umich.edu/content/littlebook98R.pdf. Accessed 1/12/2011. University of Michigan.

Smith, K.L., Smith, K.D., Evans, L.D., Hoerner, T.E. and Darter, M.I. 1997. *Smoothness Specification for Pavements. (Final Report)* National Cooperative Highway Research Program (NCHRP 1-31). Transportation Research Board. Washington, D.C.

Snyder, M. 2008. Lessons Learned from Mn/ROAD (1992–1997): Five-Inch Concrete Pavement Study. *Proceedings from 9th International Conference on Concrete Pavements, Aug. 17–21, 2008.* International Society of Concrete Pavements.

Steyn, W.J., Strauss, P.J., Perrie, B.D. and du Plessis, L. 2005. The Roodekrans Trial Sections: The Role of Structural Support under Very Thin Jointed and CRC Pavements Subjected to Heavy Traffic. *Proceedings from 8th International Conference on Concrete Pavements, Aug 14–18, 2005.* International Society of Concrete Pavements.

This page intentionally left blank

Advances in Pavement Design through Full-scale Accelerated Pavement Testing – Jones, Harvey, Mateos & Al-Qadi (Eds.)
© 2012 Taylor & Francis Group, London, ISBN 978-0-415-62138-0

Accelerated pavement testing experiment of a pavement made of fiber-reinforced roller-compacted concrete

M.L. Nguyen & J.M. Balay
LUNAM University, IFSTTAR, Bouguenais, France

C. Sauzéat, H. Di Benedetto & K. Bilodeau
University of Lyon/ENTPE, Vaulx-en-Velin Cedex, France

F. Olard
EIFFAGE Travaux Publics, Research and Development Department, Corbas, France

B. Ficheroulle
Chaussées Technique et Innovation, Paris, France

ABSTRACT: Within the framework of the French National Research Agency (ANR), the project "Recyroute" aims to investigate the use of Fiber-reinforced Roller-Compacted Concrete (*FRCC*®) mixed with Reclaimed Asphalt Pavement (RAP) for heavy traffic road pavements. It comprises an accelerated pavement test conducted by means of the Accelerated Pavement Testing (APT) facility at IFSTTAR. Eight different structures were tested, including a reference section constructed with bituminous material, one structure constructed with *ERTALH*® gravel (RAP aggregate treated with hydraulic binder), and six other structures constructed with *FRCC*® materials. An associated laboratory test program was carried out to determine the mechanical properties of *ERTALH*® and *FRCC*® materials with respect to pavement design applications. This paper presents the main features and results of this APT experiment and the associated laboratory tests, leading to propose practical parameters for the thickness design of these innovative pavement structures, according to the French rational pavement design method.

1 INTRODUCTION

The experiment discussed in this paper is a part of the French National Research Agency (ANR) project named "Recyroute". This study aims to evaluate, from performance, environmental and economic points of view, "Fiber-reinforced Roller-compacted Concrete" (*FRCC*®) (Ficheroulle and Henin, 2004) mixed or not with reclaimed asphalt pavement (RAP) as a long lasting composite material for heavy traffic roads below a surface layer of thin asphalt concrete. This new and innovative material allows firstly to delay and control tensile cracking by inclusion of steel fibers and, secondly to preserve raw materials by using RAP, which respects sustainable development. One particular property of pavements made with *FRCC* in the base layer is the fact that the pavement structure is constructed continuously without any joints, which allows considerable reductions in construction time.

Laboratory material property characterization, production and placement of materials, realization and interpretation of the APT experiment, and its application to pavement design were conducted by seven teams involved in the Recyroute project: three private companies (EIFFAGE Travaux Public, Autoroutes Paris Rhin Rhône – APRR, Chaussée Technique et Innovation – CTI) and four public organisms (Institut Français des Sciences et Technologies des Transports, de l'Aménagement et des Réseaux – IFSTTAR – previously the LCPC -, University of Lyon/École Nationale des Travaux Publics de l'État – ENTPE, Laboratoire Régional de l'Ouest Parisien - LROP, and Paris City).

The accelerated pavement testing (APT) experiment was conducted at the accelerated load testing (ALT) facility of the IFSTTAR. More than two million of the French standard twin-wheel loads (65 kN) were applied on the eight structures over a period of nine months from January to September 2010. These accelerated loads are equivalent to about 20 years of service life of mean heavy traffic roads in France (210 heavy trucks per day). The evolution of structural behavior and damage of these pavement structures was surveyed by means of periodic measurements of different parameters such as deflection, deformation, and visual surface observation. Temperatures at different levels in the structures were also recorded every ten minutes. Periodic Falling Weight Deflectometer (FWD) measurements were also performed in order to evaluate changes in bearing capacity of the different structures.

This APT experiment had two main objectives:

– Acquire data for calibration of the French rational design method of new pavements for the design of this new innovative pavement structure;
– Study the influence of different design parameters (mainly the type of aggregate, and variation of base thickness) on the behavior and damage of tested pavement structures.

An associated extensive laboratory test program, divided into two parts, was carried out in order to determine the mechanical properties of tested materials with respect to pavement design application. The first part aimed to determine the classical mechanical properties obtained from standard tests. The second part consisted of a more comprehensive thermo-mechanical test program (complex modulus and fatigue tests) carried out to determine the viscous properties (by complex modulus tests) and fatigue resistance (by fatigue tests) of tested mixes as well as the effect of the RAP content in mixes.

This paper presents the main features and results of this APT experiment and summarizes the results of the associated laboratory study completed to date.

2 THE IFSTTAR ACCELERATED PAVEMENT TESTING FACILITY

The IFSTTAR's ALT facility, in Nantes, is an outdoor circular carousel dedicated to full-scale pavement experiments, carried out with public and/or private partners. The carousel consists of a central tower and four arms (each 20 m long) equipped with wheels, running on a circular test track (Figure 1). The experimental circular pavement has a mean radius of 17.5 m and a width of 6 m, and thus a total length of approximately 110 m. The position of the loading module can be adjusted for different radii on each arm, for instance to test simultaneously the effect of different load configurations. During loading, a lateral wandering of the loads can be applied to simulate the lateral distribution of loads of real traffic (Autret et al., 1988; IFSTTAR'ALT facility).

The arms can be equipped with various load configurations: single or dual wheels on single, tandem or triple axles. A large range of loads can be applied: from 45 kN to 80 kN on a single half axle, and up to 135 kN with multiple axles. The maximum speed in classical load configuration (65 kN twin-wheels) is 100 km/h. A low-stiffness suspension system enables control of the loads applied to the experimental pavements during the entire experiment, regardless of the state of distress of the pavement. The test facility comprises three circuits. The third one used for the Recyroute tests is equipped with a 3 m deep, 10.4 m wide concrete circular waterproof pit, ensuring the hydraulic insulation of the pavement subgrade from the external water table. The tested pavements were built by private pavement construction firms, using standard road building equipment.

3 DESCRIPTION OF THE EXPERIMENT

3.1 *Concept of experimental pavement structures*

Eight different structures were tested simultaneously, on two different radiuses of 16 m and 19 m (four structures each), and 3 m wide (Figure 2). Research in this experiment focused mainly on the evaluation of new pavement structures made of new base layer materials. The tested structures include one reference structure constructed with the French standard High Modulus Asphalt Concrete (EME2) with well-known behavior, one structure constructed with RAP aggregate treated with 5% hydraulic binders (*ERTALH*®), and six other structures constructed with *FRCC*® materials treated with 12% hydraulic binder and with and without RAP (three structures each). The three structures without RAP used two types of new aggregates, namely "Crain" (soft limestone) and the "Haut-Lieu" (hard limestone).

These structures were preliminarily designed using the French official pavement design method (LCPC-SETRA 1994), taking into account some additional design parameters for the innovative structures not considered by the official method. Nominal thicknesses of the base layer and the surface layer of each

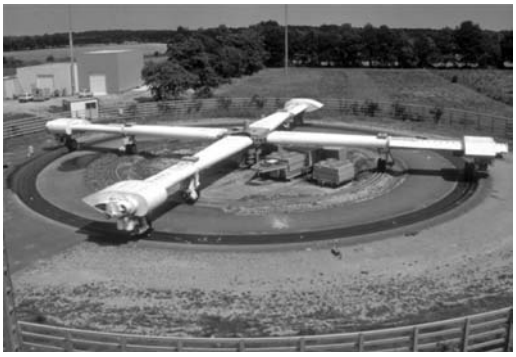

Figure 1. View of the IFSTTAR pavement testing facility.

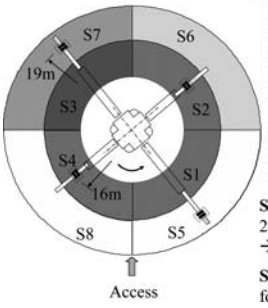

Structure	Base layer	Thickness
S1	FRCC with RAP	13 cm
S2	FRCC with RAP	12 cm
S3	EME2 (**reference**)	12 cm
S4	FRCC with RAP	15 cm
S5	FRCC Crain on cracked pavement	13 cm
S6	FRCC Haut-Lieu	12 cm
S7	ERTALH	20 cm
S8	FRCC CRAIN	15 cm

Subgrade:
2.7 m silty sand + 10 cm UGM
→bearing capacity of 95 to 110 MPa

Surface layer: 3.5 cm of thin HMA for all structures

Figure 2. Schematic of eight tested structures at the IFSTTAR's ALT facility.

structure are given in Figure 2. Actual thicknesses were measured at each phase of the pavement construction by means of topographical survey as well as from measurements on core specimens at the end of the experiment. These measurements allowed the identification of homogenous sections in each structure, which are helpful for the analysis and interpretation of results.

3.2 *Pavement materials*

The subgrade consists of a silty sand 2.7 m thick above the concrete raft of the APT facility. The bearing capacity of the subgrade was measured at different positions on each structure by means of a dynamic plate test, which gave values between 95 and 110 MPa. The materials used for base layer and surface layer are described below.

3.2.1 *Base layer materials*

Five different materials were used for the base layer of the eight experimental structures. The high modulus asphalt material EME2 was produced and transported from a nearby bituminous production plant. The four other materials were produced in an on-site production plant. The main characteristics of these four materials are given in Table 1. Mechanical performance laboratory tests on these materials are discussed below.

The fibers used were *Dramix*® RC-80/60-BN from Bekaert, consisting of curved filaments with hooked ends of high resistant steel (tensile strength 1,050 N/mm^2), 60 mm in length and 0.75 mm in diameter.

3.2.2 *Surface layer materials*

Two different bituminous materials were used for the surface layer of the eight experimental pavement structures:

- On structures S1 to S4 on the inner radius and structure S7 on the outer radius, the surface layer was hot mix asphalt (HMA) 0/10 with 35/50 ordinary bituminous binder.
- On structures S5, S6 and S8 on the outer radius, the surface layer consisted of HMA 0/10 with an SBS modified binder, called Orthoprene, developed by EIFFAGE Group, and used for the wearing course of the Millau viaduct (Héritier et al., 2005).

Table 1. Main characteristics of *FRCC* and *ERTALH* used for the base layers.

Material	*FRCC* Ht-Lieu	*FRCC* Crain	*FRCC* RAP	*ERTALH*
Sand 0/4	23%	23%	18%	–
Sand 0/6.3	35%	35%	–	25%
Gravel 6.3/14	30%	30%	–	–
RAP 0/14	–	–	70%	70%
Hyd. binder	12%	12%	12%	5%
Additive	0.50%	0.50%	0.50%	–
Steel fiber	30 kg/m^3	30 kg/m^3	20 kg/m^3	–

3.3 *Loading characteristics*

Total traffic of more than 2.15 million heavy loads was applied over nine months. It should be noted that loading started three months after construction of the pavements, to allow the cementitious materials used in the seven innovative structures to reach full strength. In addition, the first 100,000 loads were carried out with dual wheel loading of 45 kN (50,000 loads) and then 55 kN (50,000 loads). Thereafter, the reference French standard dual wheel configuration with 65 kN load was used for two millions passes. At the end of the experiment, an additional 21,000 dual wheel loads at 70 kN and 150,000 dual wheel loads at 75 kN were applied to study the overload effect on the experimental pavement structures (Figure 3).

According to the French rational design method, the aggressiveness of the loads on each structure depends on the slope of the fatigue law of the material used in the base layer, as follows:

$$NE = NP\left(\frac{P}{P_{ref}}\right)^{-1/b} \quad \text{with } P_{ref} = 65 \text{ kN} \tag{1}$$

where NP = number of passes of the load P; NE = number of reference loads (65 kN) equivalent to the NP passes of the load P; and b = slope of the fatigue law of the considered material.

Table 2 shows the cumulated equivalent traffic (standard loads of 65 kN) for each tested structure corresponding to a given base layer material, according to Equation 1.

For most applied loads, the speed was set at 10 rotations/min, which corresponds to a linear speed of 71.6 km/h on the 19 m radius, and 60.3 km/h on the 16 m radius. During measurements (deformation and dynamic deflection), the rotation speed of the carousel can be set at different speeds, from 0.6 to 10 rotations/min.

Lateral wandering of the loads was also applied during the experiment. The wheel path with lateral wander is 1.6 m wide, distributed according to an approximate normal law. The load modules were fixed at a 19 m radius on arms 1 and 3 of the carousel, for circulation

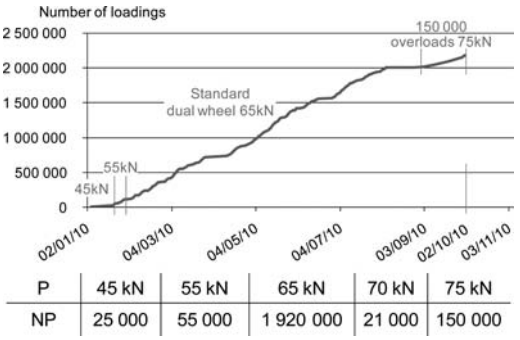

P	45 kN	55 kN	65 kN	70 kN	75 kN
NP	25 000	55 000	1 920 000	21 000	150 000

Figure 3. Evolution with time of the cumulative traffic during the Recyroute experiment.

Table 2. Cumulated equivalent traffic for each tested structure.

Structure	S1-S2-S4	S3	S5-S8	S6	S7
Material	*FRCC* RAP	EME2	*FRCC* Crain	*FRCC* Ht-Lieu	*ERTALH*
−1/b	9.9*	6.6**	16*	16*	10.7*
NE (65 kN)	2.6×10^6	2.4×10^6	3.5×10^6	3.5×10^6	2.7×10^6

*slope of the fatigue law for preliminary design of pavements
**slope of the fatigue law according to fatigue tests on EME2

on the structures S1 to S4, and a radius of 16 m on arms 2 and 4, for circulation on structures S5 to S8 (Figure 2).

3.4 *Instrumentation and pavement monitoring*

In each structure, at least ten horizontal strain gauges were placed at the bottom of the base layer for measuring longitudinal (5 sensors) and transverse (5 sensors) reversible strains. These ten sensors were positioned in both radii in the middle of the outer and the inner wheel-paths.

Thermocouple sensors were placed at different levels inside the three pavement structures constructed with bituminous material (S3 – EME2) and RAP (S4 – *FRCC* with RAP, S7 – *ERTALH*) in order to monitor the temperature in each layer. Two other thermocouples were used to measure air temperature in sunlight and in the shade.

In the middle of each structure, an anchored deflectometer was placed inside the structure for dynamic deflection measurement under load. Periodic deflection measurements were also performed after different levels of traffic by means of an FWD and Benkelman beam.

Visual surveys of the surface of the pavement were completed each day.

4 ASSOCIATED LABORATORY TESTS

The French pavement design method was used to design the reference structure EME2. No procedure is currently available in this guide for designing the *FRCC* and *ERTALH* structures. Therefore, these structures designed as cement treated materials. Preliminary design parameters of these composite materials were given by the patent holders (CTI for *FRCC*® and EIFFAGE Travaux Publics for *ERTALH*®) (Table 3), based on their past experience with the use of these techniques. In order to more accurately determine the mechanical properties of *FRCC* and *ERTALH* materials, an extensive laboratory test program, was carried out.

The mechanical behavior of the new composites was obtained from three different laboratory tests: tensile splitting tests, complex modulus tests and fatigue

Table 3. Preliminary design parameters and complex modulus test results for *FRCC* and *ERTALH* materials.

	Preliminary design parameters			
Material	−1/b	$\sigma 6$ (MPa)	Stiffness modulus E (MPa)	Complex modulus E* (15°C–10 Hz) (MPa)
FRCC Crain	16	2.47	39,000	30,340
FRCC Haut-Lieu	16	2.47	35,000	44,100
FRCC with RAP	9.9	1.26	12,000	23,360
ERTALH	10.7	0.68	10,260	14,110

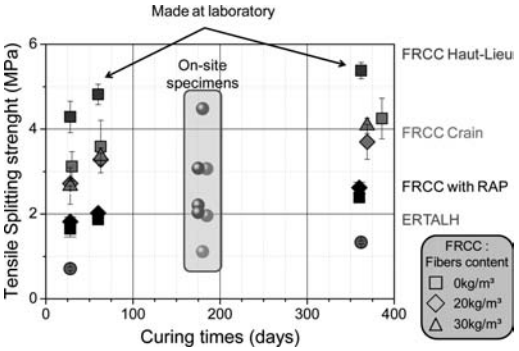

Figure 4. Tensile splitting strength.

tests performed on cylindrical samples. Only results from the tensile splitting and complex modulus tests are presented below.

4.1 *Tensile splitting test results*

Laboratory made samples using mixing similar to the APT Recyroute experiment materials were tested after three curing times (28, 60 and 360 days at constant relative humidity of 90% and temperature at 20°C). An extended laboratory test program was also performed to evaluate the effects of the fiber content on the *FRCC* made in the laboratory. A total of seven *FRCC* and *ERTALH* mixes were tested with the tensile splitting test on laboratory produced specimens:

- *ERTALH* (no fiber)
- *FRCC* with RAP and 0 kg/m^3 and 20 kg/m^3 of fibers
- *FRCC* Crain with 0 kg/m^3, 20 kg/m^3 and 30 kg/m^3 of fibers
- *FRCC* Haut-Lieu with 0 kg/m^3 of fibers

On-site specimens, extracted from the seven *FRCC* and *ERTALH* APT sections, were also tested after about 180 days.

Figure 4 shows the tensile splitting strengths for all tested specimens. As expected for materials treated with hydraulic binders, the strength increased with time. Laboratory prepared specimens showed about

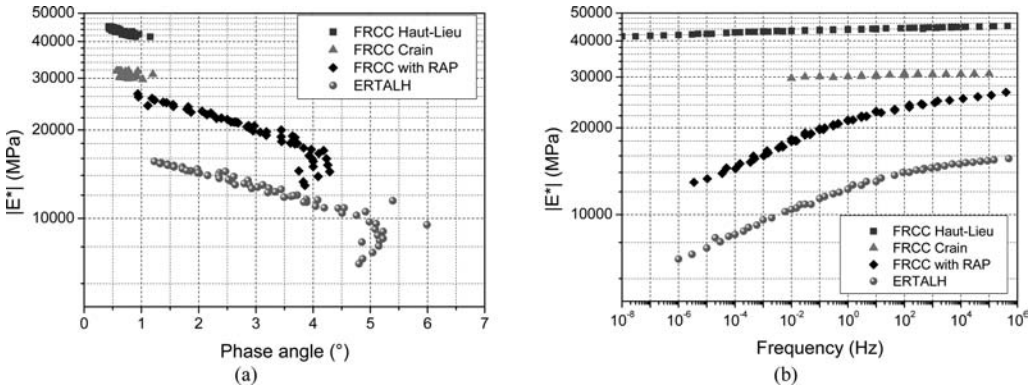

Figure 5. Complex modulus results: (a) Black diagrams; (b) Master curves at 15°C.

90% of final strength at 28 days, then about 94% at 60 days and finally 100% at 360 days. For the two *FRCC* materials with new aggregates (Haut-Lieu and Crain), strengths of the on-site specimens were about 8% lower than the laboratory prepared specimens. That can probably be explained by the difference in the curing process (on-site vs. humidity-temperature control room), fiber content, compaction, and specimen dimensions. Materials containing RAP did not seem to be affected by this change. Adding RAP materials into *FRCC* decreased strengths by about 35% in the *FRCC* Crain and by about 45% in the *FRCC* Haut-Lieu).

4.2 *Complex modulus results of extracted on-site specimens*

Complex modulus tests were performed on cylindrical core specimens (75 mm in diameter and 120 mm in length) extracted 200 days after construction from outside of the wheel path on the APT sections.

Black's curves of all tested materials are presented in Figure 5a. A unique curve was observed in the Black's diagram for *FRCC* with RAP, with behavior similar to that of thermo-rheological simple bituminous materials. The *FRCC* with RAP and *ERTALH* also satisfied the Time Temperature Superposition Principle (TTSP). A unique master curve at 15°C could be plotted for each material (Figure 5b).

According to the French pavement design method, the Young's modulus for the thickness computation is the modulus value at 15°C and frequency of 10 Hz, obtained from two points on the complex modulus curve. Table 3 presents the complex moduli (from tension-compression tests on cylindrical specimens) at 15°C and 10 Hz for the *FRCC* and *ERTALH* materials as well as the preliminary values used for the initial thickness design of the APT structures. The *FRCC* Crain, *FRCC* Haut-Lieu and *ERTALH*, preliminary stiffness values derived from past experience correlated well with the new values. However, this was not the case for the *FRCC* with RAP, where the modulus results appeared to be considerably higher than expected and have yet to be confirmed.

5 EVALUATION OF THE TESTED STRUCTURES

5.1 *Deflection measurements*

During the experiment, deflections on each structure were measured with three different methods: falling weight deflectometer (FWD), Benkelman beam, and anchored deflectometer.

5.1.1 *FWD Measurements*

FWD measurements were carried out five times at different load repetition counts at seven equidistant positions, on each structure. At each position, four levels of FWD force were applied, namely 25, 40, 50 and 65 kN.

Deflection bowl parameters were calculated with the following expressions (according to Horak and Emery, 2009):

- D_0: Deflection at the center of test load
- $RoC = L^2/[2(D_0 - D_{200})]$: Radius of Curvature, with $L = 200$ mm
- $BLI = D_0 - D_{300}$: Base Layer (performance) Index
- $MLI = D_{600} - D_{300}$: Middle Layer (performance) Index
- $LLI = D_{900} - D_{600}$: Lower Layer (performance) Index

where D_{200}, D_{300}, D_{600}, D_{900} are deflections at 200 mm, 300 mm, 600 mm, and 900 mm from the center of the test load, respectively.

Figure 6 shows results of mean values of these bowl parameters determined at the 40 kN FWD loading level (i.e., corresponding to an 80 kN single axle) at the beginning of the APT experiment before any loading has been applied. The values given in this figure are representative of a sound structural condition rating according to Horak and Emery for both cementitious base as well as bituminous base pavements (at the same 80 kN single axle loading level), which confirmed the very good performance of the tested structures at that time.

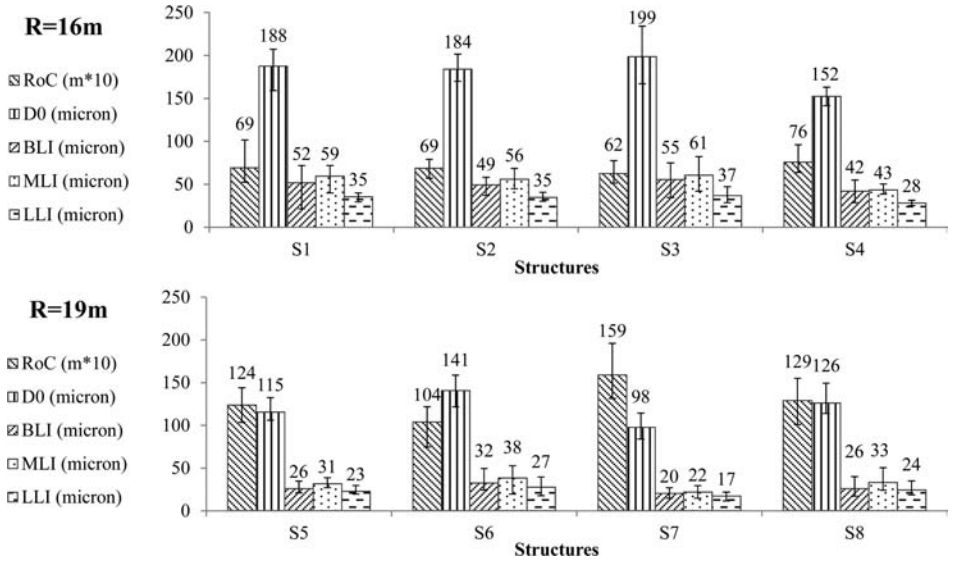

Figure 6. Deflection shape parameters from FWD measurement at a 40 kN load level (corresponding to an 80 kN single axle loading level) at the before the start of the APT, at a pavement temperature of 13°C.

The four sections on the inner ring (S1 to S4) had higher deflections (D_0) and lower RoC than the four sections on the outer ring (S5 to S8). This clearly shows the lower rigidity of the sections constructed with new bituminous materials (S3) or RAP materials (S1, S2, S4) compared with the sections constructed with thicker base course (S7) or more rigid new aggregates (S5, S6, S8). The bituminous structure (S3) was the most flexible pavement (highest D_0), and S7 (the thickest one) was the most rigid (lowest D_0). For the three structures made of RAP materials (S1, S2, S4), S1 and S2 had similar performance, but higher deflections compared to S4 (the thicker one). In the outer ring, performance on the two structures constructed with new aggregates (S5 and S8) was different to expectation, with the thicker structure (S8) having a higher deflection and RoC compared to the thinner structure (S5), as expected. S5 was also constructed on a platform of existing cracked pavement, which would typically also have higher deflections. At the end of APT testing, the S8 structure showed higher levels of distress compared to the S5 structure.

The FWD deflection measurements were used to backcalculate stiffness moduli of the individual layers in each structure. FWD data can also be used to calculate the degree of load transfer efficiency (LTE) (Al Qadi and Elseifi, 2006) near the joint between two pavement structures, or close to a crack. Interesting results from the modulus backcalculation as well as a dynamical analysis procedure for the FWD test were presented in Balay et al. 2010. Additional analyses on the FWD data, including deflection bowl shape parameters, backcalculation modulus, and change in these parameters during the APT will be presented in another paper.

5.1.2 *Benkelman beam measurements*

In parallel with the FWD measurements, deflections of experimental pavements under the 65 kN dual-wheel load of the carousel were measured with a Benkelman beam at very low speed. This method allows the rapid determination of pavement deflection response in a simple and inexpensive way.

Pavement deflections measured with the Benkelman beam were performed at the same seven positions used for FWD testing. Benkelman deflections compared well with the maximum deflections measured under the centre of the load plate (D_0) of the FWD at the same 65 kN loading level. This comparison is not detailed in this paper.

5.1.3 *Anchored deflectometer measurements*

The dynamic deflection of each structure was measured with an anchored deflectometer. The effects of the following parameters on dynamical deflection were studied:

- Speed of the load from 0.6 to 10 rotations/min (i.e., from 3.6 to 60 km/h at R = 16m and from 4.3 to 71.6 km/h at R = 19m)
- Distance between the load trajectory and the point of deflection measurement, from zero to 0.5 m, depending on the lateral wandering of the load modules.
- Weight of the load from 45 to 75 kN.

Deflections measured with the three different deflection measurement methods presented above were correlated with the temperatures measured continuously during the experiment. A synthesis of results of these three methods will be presented in another paper.

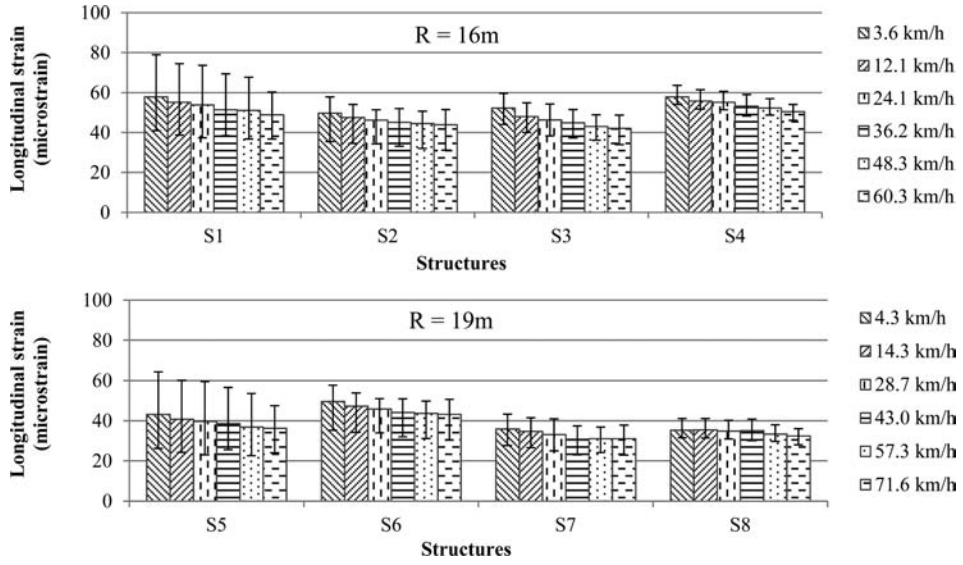

Figure 7. Effect of speed on strain measurement (45 kN wheel load, mean pavement temperature of 6.5°C).

Deflections determined by the three different methods did not show any increase in the mean values with the cumulated traffic in the bituminous pavement, or in the pavements constructed with and without RAP.

5.2 *Strain measurements*

Longitudinal and transverse strains at the bottom of the base layer were measured with strain gauges. The effects of the same parameters considered in the anchored deflectometer measurements (i.e., speed, lateral wandering position, and load) were also studied.

An example of the measurements collected showing effect of variation of the speed under the 45 kN wheel load at a temperature of 6.5°C is provided in Figure 7. This figure shows that the strains measured under different speeds on the sections in the inner ring vary more than those in the sections on the outer ring. In the structures made of *FRCC* RAP (S1, S2, and S4), strain measurements on the nominally thicker structures (S1, 13 cm and S4, 15cm) were similar, while the nominally thinner structure (S2, 12 cm) had lower mean values. This result is probably due to a difference in actual thickness of the pavement layers compared to the nominal thicknesses at the actual locations where strain gages were installed. Differences in the bearing capacity of the subgrade layer of these structures could also be a factor.

Like deflections, strain measurements are used to assess the validity of numerical modeling used for the application of the APT results to the design of *FRCC* structures. More analysis of these measurements needs to be undertaken and is not discussed further in this paper.

5.3 *Behavior and principal damage of tested pavement structures*

5.3.1 *Structural damage*

In terms of the structural functioning of the tested structures, the first general observation was the very encouraging performance, despite the generally low thicknesses of material used and the severity of the loading applied. The observed structural damage (Figure 8) was as follows:

Structure S2 (*FRCC* with RAP)
A transverse crack appeared at the surface of the pavement at the end of the experiment under the overload of 75 kN, after 2.3 million of the 65 kN standard dual-wheel load. The shrinkage, measured between both sides of the crack using a double sensor beam (Figure 8a), showed a value of 31 mm/100 revealing a rather low value of LTE. It has to be emphasized that *FRCC* with RAP was used in three other structures (S1, S2, and S4) over three-quarters of the inner ring. There was no joint between these structures (i.e., one 75 m long continuous pavement made of *FRCC* with RAP). Section S4 had the thickest *FRCC* layer. The other two structures (S1 and S2) were thinner and comparable to each other. However the load-bearing capacity of the subgrade under Section S2 was less than that under Section S1, which may explain the appearance of the crack through the surface layer on Section S2.

Structure S6 (*FRCC* with Haut-Lieu)
An open transverse crack appeared in the top 9 cm of actual thickness, 3 cm less than the nominal design of 12 cm. The mode of this degradation was initially attributed to shrinkage, which then developed into a fatigue crack (Figure 8b). Dust from abrasion of the aggregate on either side of the crack first appeared

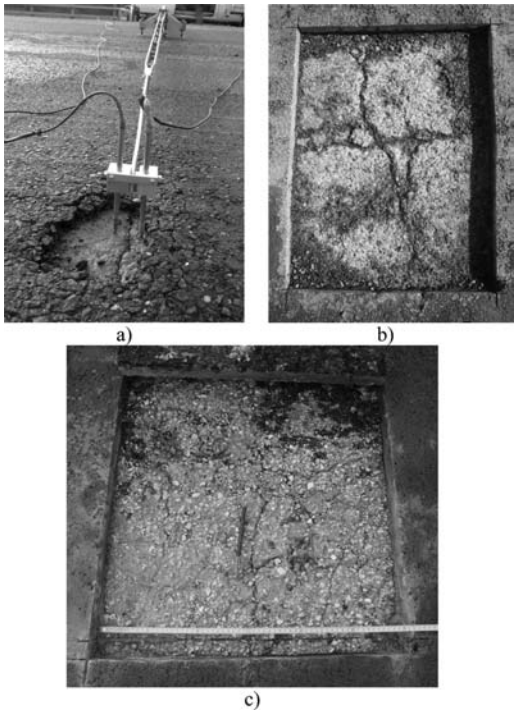

Figure 8. Structural damage of the structures: (a) S2 – *FRCC* with RAP; (b) S6 – *FRCC* Haut-Lieu; (c) S8 – *FRCC* Crain.

after 350,000 load cycles. Total loss of LTE between crack edges was recorded after 750,000 load cycles.

Structure S8 (*FRCC* with Crain)
A similar pattern of degradation to that recorded on Section S6 was recorded on Section S8. An 11 cm transverse crack (4 cm less than the nominal design thickness of 15 cm) appeared on the surface. LTE reduced with increasing load cycles and eventually formed a network of cracks (Figure 8c).

No structural damage was observed in the other five structures (S1, S3, S4, S5, and S7) at the end of the experiment.

5.3.2 *Non-structural damage*

Some non-structural damage was observed during the experiment, which affected thin HMA surface layer. This included potholes and the pumping of fines onto the road surface. Potholes were caused by:

- Poor homogeneity of the fiber mixing due to incorrect positioning of the fiber feeder plant (which generated balls of fiber) on Section S4. Four potholes resulted. This dosing defect was then corrected.
- Excess gravel on the curing layer of *FRCC*. One pothole on Section S1 and two on Section S2 were attributed to this.

The origin of fines on the surface came from two sources: abrasion of aggregates on either side of cracks in the *FRCC* base layer, or crushing of aggregates during high energy compaction, leading to a weak interface between the base and the surface layers. The presence of water and hydrostatic pressure caused by the passing wheel load pumps these fines to the surface. Crushing during compaction caused fines to be absorbed into the tack coat, explaining in part the low bonding quality of the surface layer in some of the sections. As a result of this, vacuum sweepers are now required on all *FRCC* construction sites to clean the surface prior to tack coat application.

6 PROPOSAL OF DESIGN PARAMETERS FOR FRCC PAVEMENTS

6.1 *Adjustment principle of pavement design model based on the Recyroute APT results*

According to the French pavement design method, the thickness design criterion for pavements treated with hydraulic binders only considers fatigue failure of the treated base layer, since plastic deformation (rutting) of the subgrade is not a determining factor due to the rigidity of the base layer. This fatigue criterion amounts to checking that the maximum calculated tensile stress $\sigma_{t,max}$ at the base layer is less than or equal to the admissible stress value $\sigma_{t,adm}$ given by the following equation (2):

$$\sigma_{t,\max} \leq \sigma_{t,adm} = \sigma_6 \left(\frac{NE}{10^6} \right)^b k_c k_d k_r k_s \qquad (2)$$

where:

- $\sigma_{t,max}$ = maximum calculated tensile stress at the base layer, using Burmister's multi-layer elastic model.
- σ_6 = mean value of the stress at which failure occurs in bending tensile conditions at 360 days for 10^6 loadings, determined from two point laboratory fatigue tests or correlated to indirect tensile strength.
- NE = number of equivalent standard loadings (130 kN axle load) calculated from the cumulated traffic (*NPL*) and the coefficient of mean aggressiveness (*CAM*) by the relationship: NE = NPL × CAM.
- b = slope of the fatigue law of the considered material (Wöhler bi-logarithmic law).
- k_c is a coefficient of adjustment intended to adjust the results of the calculation model to the observed behavior of pavements of the same type (feedback from real networks).
- k_d is a coefficient introduced to account for the effect of discontinuities in the base layer, which cannot be reproduced by Burmister's model.
- k_r, dependent on the "level of service" expected for the pavement, reflecting the capability of the road to meet the needs of both the users and the owners. k_r takes into account the allowable risk of pavement degradation at the end of the service life, and

the dispersion of both the base layer thickness and the fatigue behavior determined from laboratory testing.
- k_s is a coefficient of reduction to account for the low bearing capacity of the subgrade.

In the framework of the Recyroute experiment, the "known" data are as follows:

- $\sigma_{t,max}$ = determined using the *Alizé-LCPC* software, taking into account the actual thicknesses of the different layers and the modulus values determined by means of preliminary laboratory testing.
- NE = equivalent traffic at a considered time "t" (different stages from the beginning to the end of the tests).
- b is chosen as $-1/9.9$ for *FRCC* with RAP; $-1/16$ for *FRCC* Haut-Lieu and Crain; and $-1/10.7$ for *ERTALH* (preliminary design values).
- k_c is maintained at the value of 1.5 adopted for rigid and semi-rigid structures in the French pavement design manual, which means that final adjustment will be based on the value of the discontinuity coefficient k_d.
- k_r is based on risk calculation, representing the level of structural degradation of the pavement at a considered time "t".
- $k_s = 1$ because of the good homogeneity and well controlled bearing capacity level of the subgrade on the circular carousel.

The two remaining parameters are σ_6 and k_d which were determined by backcalculation based on the Recyroute APT results. The backcalculation of the product of $\sigma_6 \times k_d$ is discussed in Section 6.4.

6.2 *Need for APT vs. real pavement calibration*

In the reference structure EME2, the risk of degradation at the end of the Recyroute experiment was 27%. This value, backcalculated using the French design method, takes into account the thicknesses and mechanical performance of the materials used for the experiment. This theoretical value disagrees with the very good structural performance observed during the entire APT experiment (no damage observed) corresponding to a risk of damage below or equal to 5%.

As the design parameters of this reference structure cannot be questioned, the very good performance of the EME2 structure on the APT facility was attributed to the favorable test conditions, including:

- Good construction of the base layers, due to the high level of quality control and short construction length,
- Good homogeneity of the platform,
- Minimal aging effect of the materials,
- Favorable dynamic mode of loadings (no overload effect, no dynamic effect due to significant roughness of pavement surface, etc).

Therefore, an additional coefficient (k_h), which harmonizes the APT results with the behavior of actual pavements on in-service networks, was introduced into Equation 2. This coefficient, determined as a ratio of $k_{r27\%}$ (for risk of damage = 27%) and $k_{r5\%}$ (for risk of damage = 5%), is 1.10. This value will also be applied to the other structures tested in the Recyroute experiment.

6.3 *Effects of hypothetic wide shrinkage cracking on design parameters of FRCC*

The basic principle of *FRCC* is that the pavement works as a continuous structure, because the fibers should contribute to uniformly distribute the shrinkage cracking into a transversal micro-cracking network.

The openings of this micro-cracking remains so tight that load transfer at each micro-crack is considered as complete. This leads the promoters of the *FRCC* technique to consider, in the design of *FRCC* structures, the same value of coefficient k_d (= 1/1.07) as the value taken into account by the French *Catalogue of New Structures* (SETRA – LCPC 1998) for *FRCC* composite pavement placed on an asphalt concrete foundation. Despite the very encouraging behavior of *FRCC* observed all in this study, this mode of functioning has not yet been fully demonstrated by the APT experiment.

On the one hand, no microcracks were identified at the end of the test in a 20 m long trench excavated on Section S6, or in the many block specimens taken from the other sections for the final laboratory characterization of the materials. This, however, does not eliminate the possible existence of such micro-cracking, which is not easily detected. On the other hand, it should be noted that the short sections tested on the IFSTTAR APT facility – 27 m maximal length – are not necessarily representative of actual structures on in-service networks, which are significantly longer, and consequently the development mechanisms and distribution of cracks may be different.

Furthermore, international experience with roller-compacted concrete without fibers (RCC), particularly the ACI Committee 325 Report (ACI 2001) mentions that crack opening of RCC is at least 3 mm for cement contents of 280 kg/m^3 and crack spacing is about 20 to 25 m. For the same cement content and crack spacing, crack opening was less than 0.5 mm in *FRCC*, when observed on other *FRCC* site projects under heavy traffic. This comparison between RCC and *FRCC* crack opening provides significant indications in favor of microcrack and shrinkage crack control due to the high performance steel fibers in the *FRCC* material.

The remaining doubts concerning the validity of microcrack development are also due to the single transverse wide crack that appeared at the surface on the longer 75 m section (continuous pavement of the S1, S2, and S4 sections) at the end of the test, without being able to determine the precise origin or cause of this crack (i.e., shrinkage or fatigue crack, or combination of the two).

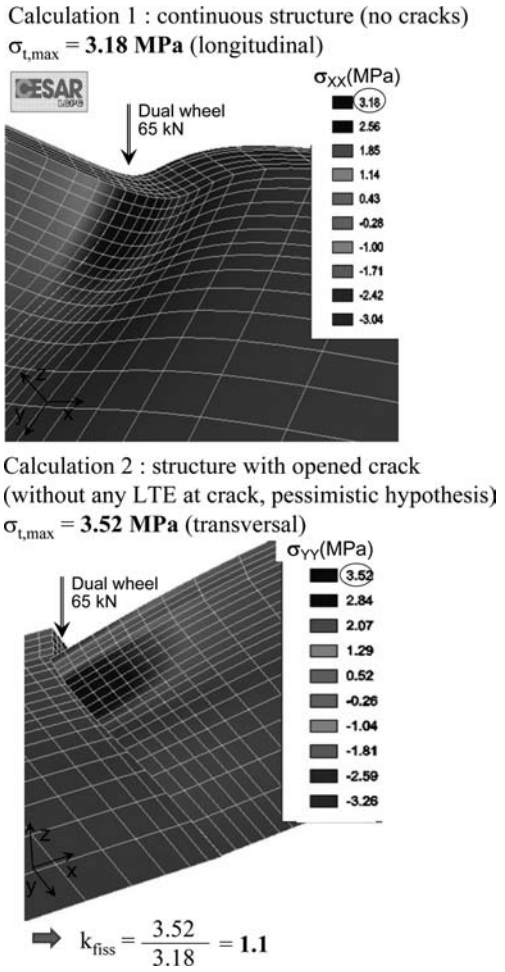

Figure 9. Transverse crack effect calculations: 3D-FEM modeling of the structure S6 – *FRCC* Haut-Lieu 12 cm with tensile stresses at the bottom of the base layer.

As a result of this uncertainly about the micro-cracking mechanism, which is not shared by the promoters of the *FRCC* technique, the IFSTTAR has undertaken numerical 3D-FEM modeling using the César-LCPC program, to evaluate the effect of a hypothetic, wide and transversal crack on the design parameters of *FRCC* pavements (Figure 9).

The results of the 3D FE calculations (Figure 10) taking into account a wide transverse cracking without any load transfer efficiency (pessimistic hypothesis) gives the following values of the coefficient k_{fiss}:

- 1.19 for the *FRCC* Haut-Lieu material (E = 35 GPa) at 15 cm thickness
- 1.07 for the *FRCC* with RAP material (E = 12 GPa) at 15 cm thickness

6.4 *Backcalculation of the product* $\sigma_6 \times k_d$

To backcalculate the product $\sigma_6 \times k_d$ for each structure represented for one base layer material used in this experiment, data needed to be collected based on the APT results (Table 4). On each structure, the risk of degradation was evaluated for a representative section. A number of core specimens were also extracted from each structure to determine actual thickness of pavement layers for this representative section.

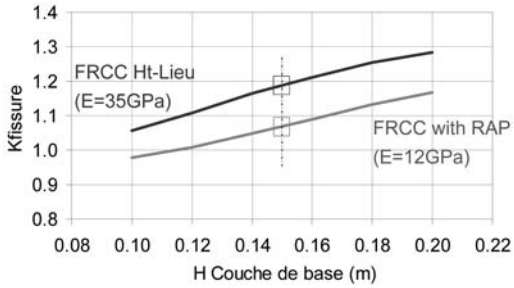

Figure 10. Transverse crack effect: Synthesis of FE calculations for *FRCC* Ht-Lieu and *FRCC* with RAP.

Backcalculation of the product $\sigma_6 \times k_d$ was determined using the pavement design program Alizé-LCPC. An example of the backcalculation for damaged and undamaged sections on the *FRCC* Haut-Lieu structure is presented in Figure 11. This figure shows that the value of $\sigma_6 \times k_d = 2.7$ MPa leads to a coherent simulation of the observed behavior on these sections:

- Risk of degradation equal to 50% with transverse crack at 350,000 cycles for the 9-cm thick damaged section.
- Risk of degradation close to 10% at the end of the experiment (e.g. 3.5 million equivalent loads for the 12 cm undamaged section).

The same procedure of backcalculation was followed for the other pavement structures. Table 5 summarizes results for each material.

Observations from these results include:

- These findings apply to *FRCC* structures on untreated platforms, such as those tested in this experiment.
- Two hypothesis concerning the mode of shrinkage cracking are considered:
  - Hypothesis *h*1 (continuous pavement): shrinkage develops within a closed micro-cracking transverse network without any open cracks. As full load transfer at the cracks remains unchanged over the pavement life, this hypothesis, advocated by the *FRCC* promoters, has to be considered as optimal; and still needs to be validated by further study before application to heavily trafficked or high service level pavements.
  - Hypothesis *h*2 (discontinuous pavement): shrinkage develops through opened cracks without load transfer, with a large distance of between 25 m and 40 m between cracks. This hypothesis has to be considered as pessimistic, leading to a probable increase in *FRCC* thicknesses in comparison

Table 4. Data needed for the backcalculation of $\sigma_6 \times k_d$.

		FRCC with RAP		*FRCC* Haut-Lieu		*ERTALH*	*FRCC* Crain	
		S1		S2		S6	S7	
Layer	Parameter	Undamaged	Transverse Crack	Damaged	Undamaged	Undamaged	Damaged	Undamaged
Surface	h (cm)	3.3	2.9	3	3	4.3	2.8	3.4
	E (MPa)	5,400	5,400	5,400	5,400	5,400	5,400	5,400
Base	h (cm)	3.3	2.9	3	3	4.3	2.8	3.4
	E (MPa)	12,000	12,000	35,000	35,000	10,000	39,000	39,000
	$-1/b$	9.9	9.9	16	16	10.7	16	16
	SN	0.5	0.5	0.5	0.5	0.5	0.5	0.5
	Sh (mm)	11	4	6	10	15	8	12
Platform	h (m)	2.9	2.9	2.9	2.9	2.9	2.9	2.9
	E (MPa)	141	118	95	95	121	105	133
	(MPa)	1.9	2.05	4.29	3.46	1.04	3.07	2.42
Other data	NE (loads)	2.6×10^6	2.6×10^6	0.35×10^6	3.5×10^6	2.7×10^6	0.45×10^6	3.5×10^6
	Risk (%)	<10	≈ 50	≈ 50	<10	<10	≈ 50	<10

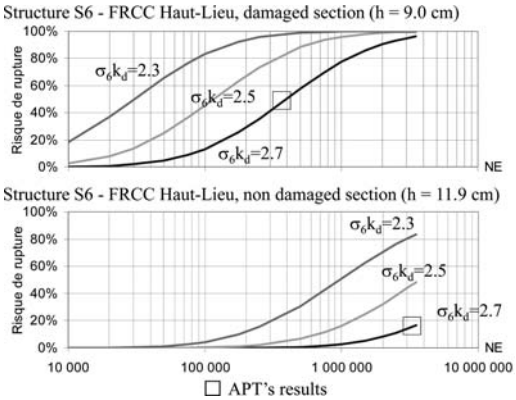

Figure 11. Backcalculation of the product $\sigma_6 \times k_d$ for the S6 Section (*FRCC* Ht-Lieu) for damaged section and undamaged sections, respectively.

with an optimized design taking into account the real performance of this innovative technique. However, as actual performance and mode of functioning of *FRCC* are not yet fully understood, IFSTTAR recommends that this second hypothesis should be taken into account for the thickness design of high service level pavements, in accordance with the precautionary principle, until the long-term performance of *FRCC* is fully understood.

– Difficulties in identifying the cracking process in *FRCC* pavements suggests the need for further research to understand microcracking behavior and evolution means to identify when it has occurred.
– Modulus of *FRCC* and slope of fatigue have a strong influence on the back-calculated values of $\sigma_6 \times k_d$.

Table 5. Synthesis of backcalculation of $\sigma_6 \times k_d$ and other adjustments.

Materials	$\sigma_6 \times k_d$ from APT	k_h	k_{fiss}	$\sigma_6 \times k_d$ for pavement design (h1)	$\sigma_6 \times k_d$ for pavement design (h2)
FRCC Haut-Lieu	2.7	1.1	1.19	2.45	2.06
FRCC Crain	2.0	1.1	1.19	1.82	1.53
FRCC with RAP	1.6	1.1	1.07	1.45	1.36
ERTALH	0.9	1.1	1	0.82	0.82

– A minimum value of $\sigma_6 \times k_d$ by default was proposed for the *ERTALH* material in the absence of any structural damage at the end of this experiment ($k_{fiss} = 1$).
– These proposed observations are provisional, until full results of the laboratory test program, including fatigue tests results, are available. In particular, the hypothesis about shrinkage cracking patterns may be reviewed based on the monitoring of experimental sites.

6.5 *Examples of thickness design of FRCC pavements in comparison with traditional solutions*

Based on the data in Table 4 and Table 5, four examples of *FRCC* pavement structures were evaluated for *FRCC* Haut-Lieu and *FRCC* with RAP respectively (Table 6). The two hypotheses concerning the shrinkage cracking distribution were considered. These *FRCC* pavement structures are compared to four French reference structures (SETRA – LCPC, 1998).

Table 6. Comparison on the total thickness of *FRCC* pavements with traditional structures.

For traffic of class TC5 (9.2 million in 30 years), on platform of class PF3 ($E \geq 120$ MPa)

	French pavement catalogue				*FRCC* structures			
			Sheet 20					
Layer	Sheet 2 GB3	Sheet 3 EME2	BC5g/BC2	BAC/GB3	*FRCC* Haut-Lieu	*FRCC* Haut-Lieu	*FRCC* with RAP	*FRCC* with RAP
Surface (cm)	8	2.5	19	2.5	4	4	4	4
	BB	BBTM	BC5g	BBTM	BB	BB	BB	BB
Base (cm)	21	19	15	15	15	17	16	17
	GB3	EME2	BC2	BAC	*FRCC*	*FRCC*	*FRCC*	*FRCC*
Subbase (cm)	–	–	–	9	–	–	–	–
	–	–	–	GB3	–	–	–	–
Htotal (cm)	29	21.5	34	26.5	19	21	20	21

GB: base asphalt concrete;
EME: high modulus asphalt concrete;
BC5g: dowelled concrete slabs;
BC2: foundation lean concrete;
BAC: CRCP – continuously reinforced concrete pavement

The pavement design examples presented in Table 6 identify several comparative points between *FRCC*, bituminous structures techniques, and reference rigid pavements:

- The *FRCC* with RAP had a lower modulus than the *FRCC* Haut-Lieu, and thus requires an increase in thickness of about 1 to 2 cm;
- The thickness of FRRC and high modulus asphalt concrete EME2 are similar. The competitive advantage varies in favor of one technique to another, depending on the traffic and directly related to the slope of fatigue that is flatter, particularly for the *FRCC* Haut-Lieu. This confirms the potential applicability of this technique for heavy traffic;
- Compared to the BAC (continuously reinforced concrete pavement) structure, the *FRCC* structures should allow significant reductions in thickness.
- The *FRCC* structures presented in Table 6 are still considered to be experimental. Production and construction will also need to be strictly controlled, and potential risks will need to be fully quantified.

7 CONCLUSIONS

The APT Recyroute experiment was carried out at the IFSTTAR's ALT facility. It investigated the use of an innovative material, *FRCC* with and without RAP, in pavement structures. More than 2 million 65 kN French standard dual-wheel loads were applied on the eight tested structures over a period of nine months.

The experiment showed encouraging behavior in the tested structures, despite the thin thicknesses of materials used in the base and surface layers and the severe loading conditions. Structural damage was limited to sections with very thin layers (less than 3 or 4 cm). However, it is well known that layers constructed with hydraulic binder-treated materials, must be optimally placed and compacted, and tack coat must be correctly applied, in order for the pavement to perform well. This is especially important if thin asphalt concrete surfaces, which are susceptible to different types of risk (potholes, stripping, etc), are used. These critical issues have been clearly highlighted by the Recyroute experiment.

Results from this APT experiment were used to backcalculate the product of $\sigma_6 \times k_d$ for each pavement material tested, in the absence of fatigue test results, which are not yet available. This parameter directly impacts the level of allowable flexural tensile stress according to the French rational design method. These values were largely influenced by the *FRCC* modulus and the slope of the fatigue curve. They still need to being confirmed with the results of dynamic fatigue tests presently being carried out in the ENTPE and IFSTTAR laboratories.

Based the on these APT results, two adjustments for the pavement design model of the tested pavements were proposed:

- Inclusion of a dynamic coefficient which takes into account the favorable dynamic mode of loading on the IFSTTAR's circular carousel;
- An adjustment coefficient taking into account that no "open" transverse cracks formed on the APT track, due to the limited length of the experimental sections. However, in comparison with roller-compacted concrete without fibers, international experience indicates that *FRCC* has significant benefits in terms of cracking control and limited presence of micro-cracks. Nevertheless a precautionary principle is recommended, especially for the design of new pavements with heavy traffic at high service levels, by using an additional coefficient (k_{fiss}), which reduces the allowable flexural tensile stress of *FRCC* materials. This security hypothesis proposed by IFSTTAR is considered to

be conservative and will be reviewed in the future, on the basis of the monitoring of further *FRCC* experiments on in-service pavements.

Pavement design examples show that the *FRCC* structures have thicknesses similar to those of high modulus asphalt structures (EME2) used in France, but exhibit significant reductions in thickness when compared to CRCP structures. The construction of these *FRCC* structures will have to be strictly controlled, with a proper assessment of the risks taken and efficient monitoring under heavy traffic. Results of laboratory tests currently being undertaken will help to confirm the above provisional proposals.

ACKNOWLEDGMENTS

The authors would like to acknowledge the French National Research Agency (ANR) for financing this project, as well as the other partners of the Recyroute project not directly involved in the IFSTTAR APT experiment, namely APRR, LROP and the Paris city. FWD testing performed by Regional Laboratory of Saint Brieuc is also appreciated.

REFERENCES

ACI. 2001. *State-of-the-art Report on Roller-Compacted Pavements*. Report of the Committee 325, reapproved.

Al-Qadi, I.L. and Elseifi, M.A. 2006. Mechanism and modeling of transverse cracking development in continuously reinforced concrete pavement. *International Journal of Pavement Engineering, Vol.7, N° 4*: 341–349.

Autret, P., Baucheron de Boissoudy, A. and Gramsammer, J.C. 1988. *Le manège de fatigue du Laboratoire Central des Ponts et Chaussées: Premiers résultats.* Bulletin de liaison des Laboratoires des Ponts et Chaussées, N° 155: 33–45.

Balay, J.M., Nguyen, M.L. and Gritti, R. 2010. *Dynamical analysis of FWD test on LCPC's accelerated load testing facility.* The 6th European FWD User Group Meeting – Structural Condition Assessment, BRRC, Brussels.

Ficheroulle, B. and Henin, M. 2004. *Compacted rolled fibre-reinforced concrete composition and method for producing a pavement based on same composition.* Patent EP1278925B1.

Héritier, B., Olard, F., Loup, F. and Krafft, S. 2005. Design of a specific bituminous surfacing for the World's highest orthotropic steel deck bridge: France's Millau viaduct. *Transportation Research Record, Journal of the Transportation Research Board, Vol. 1929*. Washington, DC. T141–148.

Horak, E. and Emery, S. 2009. Evaluation of airport pavements with FWD deflection bowl parameter benchmarking methodology. *2nd European Airport Pavement Workshop*, Amsterdam.

SETRA – LCPC. 1994. *French design manual for pavement structures – Technical guide*.

SETRA – LCPC. 1998. *Catalogue des structures de chaussées. The Dramix fibres*: http://pdf.directindustry.com/pdf/bekaert/dramix-rc-80-60-bn/5919-56674.html

The IFSTTAR's Alizé-LCPC software for the thickness design of pavement according to the French rational method: http://www.lcpc.fr/english/products/lcpc-products-alize-lcpc-routes/

The IFSTTAR's ALT. facility: http://www.lcpc.fr/english/presentation-209/human-and-financial-resources/lcpc-exceptional-testing-220/

The IFSTTAR's César-LCPC FEM software for the resolution of civil engineering and environmental problems: http://www.lcpc.fr/english/products/lcpc-products-cesar/

This page intentionally left blank

Advances in Pavement Design through Full-scale Accelerated Pavement Testing – Jones, Harvey, Mateos & Al-Qadi (Eds.)
© 2012 Taylor & Francis Group, London, ISBN 978-0-415-62138-0

Provisional results from accelerated pavement testing of roller-compacted concrete in South Africa

L. du Plessis & S.J.H. Louw
CSIR BE, Pretoria, South Africa

G. Rugodho
Gauteng Department of Roads and Transport, Pretoria, South Africa

S. Musundi
Cosal Consultants, Meyerton, South Africa

ABSTRACT: In conjunction with the Gauteng Department of Roads and Transport and Cosal Consultants CC in South Africa, the CSIR Built-Environment is evaluating the applicability of Roller Compacted Concrete (RCC) as an option for the upgrading and rehabilitation of low-volume residential and provincial roads. The ultimate aim of the study is to build confidence in the use of RCC, with cognizance being taken of the pavement structure, support conditions, construction, climate, and traffic. Whereas RCC is normally constructed with a relatively low labor component and with heavy mechanical equipment, the goal of this investigation was to evaluate the structural performance of RCC constructed with a relatively high labor component using hand-operated equipment. This is in line with the South African Government's drive towards sustainable job creation, together with the pressing need for the upgrading and maintenance of the low-volume road infrastructure. Full-scale Heavy Vehicle Simulator (HVS) tests were conducted to determine the structural capacity of the RCC. This paper summarizes the provisional results from the first Accelerated Pavement Test (APT) on the control section, constructed using conventional methods and equipment. Through APT testing it was shown that this type of pavement performed exceptionally well in the dry state, even though it was constructed on a substandard support system. Initial indications are that actual performance exceeded predicted performance. Sensitivity to water is an important factor that will be investigated in subsequent testing. Testing of the labor-intensive constructed sections will be documented in a separate paper.

1 INTRODUCTION

The upgrading of unsurfaced residential roads has become a priority for many metropolitan areas in South Africa. Coupled with this is the need to construct roads using labor-intensive construction techniques. In 2007 the South African Gauteng Department of Roads initiated its Expanded Public Works Program (EPWP). The goals and objectives of the EPWP are to alleviate unemployment, targeting especially women, youth, and the disabled (Gautrans, 2007; and Gautrans, 2010). This goal will be achieved by creating work opportunities in the following four constructive ways:

- Increasing the labor component of government-funded infrastructure projects;
- Creating work opportunities in public environmental programs;
- Creating work opportunities in public social programs, and
- Utilizing general government expenditure on goods and services to provide the work experience component of small enterprise learner ship/incubation programs.

In line with these objectives the EPWP embarked on a research program to evaluate Roller Compacted Concrete (RCC). Whereas RCC is normally constructed with a relatively low labor component and with heavy mechanical equipment, the main goal of this project was to evaluate the structural performance of RCC using a relatively high labor component and hand-operated equipment.

A short full-scale test section was constructed at the accelerated pavement testing (APT) facility of the Council of Scientific and Industrial Research (CSIR) in Pretoria, South Africa. The experiment was conducted in two phases. During Phase 1 a portion of the test section was constructed as a control section with normal heavy mechanical equipment and relatively low labor component. Phase 2 entailed the

construction and testing of a section using a high labor component and hand tools.

The primary objective of this project is to assess the performance of RCC under real field conditions using APT coupled with a laboratory-testing program. Comparative testing of the sections constructed by the two techniques will assist in the evaluation of labor-based RCC construction practices.

This study is aimed at building confidence in the use of RCC as a structural layer, with due cognizance being given to pavement structure, construction, climate, and traffic, by providing practitioners with reliable design information to enable them to make informed decisions.

Full-scale Heavy Vehicle Simulator (HVS) tests were conducted to determine the structural capacity of the RCC. This paper summarizes the provisional results from the first HVS test conducted during Phase 1 (conventional RCC construction) in the dry state. Subsequent testing will include the evaluation of the labor-intensive constructed sections (Phase 2).

2 ROLLER COMPACTED CONCRETE

RCC gets its name from the heavy vibratory steel drum and rubber-tired rollers used to compact it into its final form. RCC has similar strength properties and consists of the same basic ingredients as conventional concrete, including graded aggregates, portland cement, and water but has different mixture proportions (Harrington et al., 2010).

The largest difference between RCC mixtures and conventional portland cement concrete mixtures is that RCC has a higher percentage of fine aggregates, which allows for tight packing, low void content, and consolidation. Fresh RCC is stiffer than typical zero-slump conventional concrete. Its consistency is sufficiently stiff to remain stable under vibratory rollers, yet wet enough to permit adequate mixing and distribution of paste without segregation. The use of RCC on roads can potentially offer multiple benefits by comparison with more conventional approaches.

RCC is typically placed with and asphalt-type paver equipped with a standard or high-density screed, followed by a combination of passes with rollers for compaction. Final compaction is generally achieved within one hour of mixing. Unlike conventional concrete pavements RCC pavements are constructed without forms, dowels, or reinforcing steel. Joint sawing is not required, but when sawing is specified, transverse joints are spaced farther apart than in conventional concrete pavements.

Compaction is the process by which the aggregate particles in the RCC mixture are forced closer together, reducing the amount of air voids in the mixture and increasing the density of the layer. RCC mixtures should be dry enough to support the weight of a vibratory roller after placement, yet wet enough to ensure adequate hydration and even distribution of paste. Proper proportioning is essential for ensuring that the mix has sufficient paste to coat the aggregate particles and fill the voids of the compacted mix. Coating of the aggregate particles must be achieved in order to obtain a strong and durable pavement and to ensure load transfer through aggregate interlock at joints (Water resources, 2004).

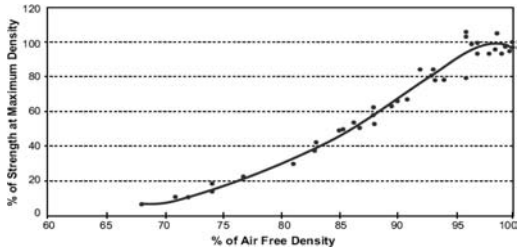

Figure 1. Strength versus density for various RCC mixes (after Schrader, 1992).

The increased density makes the pavement suitable for load bearing applications. Rolling must occur before cement hydration begins to harden the paste between the aggregate particles. Achieving proper density during the rolling process helps prevent non-uniform consolidation and isolated weak areas. Depending on the specific mixture and construction equipment used, external mechanical compaction by rollers may result in a 5 to 20 percent reduction in volume. Minimizing the air void content in the RCC mixture is crucial to the durability of RCC. Excess air voids allow the penetration of air and water. Non-entrained air weakens the mixture, while excessive water can cause material-related distresses in the aggregates, low field densities, and insufficient early strength gain. The strength of RCC decreases with reduced density as shown in Figure 1 (Schrader, 1992).

3 POSSIBLE BENEFITS

The use of RCC on roads can potentially offer multiple benefits by comparison with more conventional approaches. The primary benefit of RCC is that it can be constructed quicker and less costly than conventional concrete. Other beneficial characteristics of RCC include the following (Harrington et al., 2010):

- The lower paste content in RCC results in less concrete shrinkage and reduced cracking from shrinkage-related stresses.
- RCC can be designed to have high flexural, compressive, and shear strengths, which allow it to support heavy, repetitive loads without failure such as in heavy industrial, mining, and military applications, and to withstand highly concentrated loads and impacts.
- With its low permeability, RCC provides excellent durability and resistance to chemical attack, even under freeze-thaw conditions.
- RCC provides chemical and rut resistance in industrial areas where point loading from trailer dollies is a concern.

– Occasional light vehicles, such as cars and light trucks, can travel at low speeds on RCC pavements soon after completion without causing damage.
– Construction of RCC at ambient temperatures is suitable for labor-based construction and hence is ideally suited for Gauteng's EPWP.
– Apart from the basic road building equipment (grader, roller compactor, water cart), only simple, inexpensive construction equipment is required.
– The existing subgrade and alignment can be used.
– RCC can be used as an overlay on existing roads where there is no limitation on vertical alignment.
– A significant percentage of the cement in the mix can be replaced by fly-ash, a waste product from coal-fired power stations.
– RCC pavements require less lighting energy at night than bituminous surfaces because of the high surface reflectivity.
– Repairs of potholes and utility cuts are simple using the same material.
– Water demand is lower than that of conventional concrete, which is a benefit in water-scarce areas.

If the technology is proven to be appropriate, RCC can have:

– Lower life-cycle cost for comparable performance;
– Lower maintenance costs, and
– Better performance in difficult areas where heavy loads and stop-start traffic are common, such as container terminals and parking areas.

4 METHODOLOGY

– The general methodology followed for the laboratory and field evaluations of the RCC mixes was as follows:
– Two full-scale test sections with a total length of approximately 65 m and a width of 3.6 m were constructed. Structural design input parameters from laboratory testing such as flexural strength, fatigue life, and durability were determined.
– Accelerated pavement testing during which the RCC was subjected to a range of loading conditions and moisture regimes under the HVS (Figure 2) in channelized, bi-direction trafficking mode to assess the influence of the input parameters on the bearing capacity of the material.
– Analysis of laboratory and field data.

Although RCC is continuously cast and compacted, it is important to realize that, at the end of each working day, a construction joint will have to be made to finish the day's work. Formwork used to ensure correct compaction will be removed on the next day for the continuation of slab casting. The structural integrity of this construction joint will also be evaluated through HVS testing.

5 PAVEMENT CONSTRUCTION

The RCC test section was designed for local and provincial low-volume roads with design traffic of one to three million standard 80 kN axle loads (ESALs). The South African Mechanistic Pavement Design Method was used for the structural design of the pavement. Data from falling weight deflectometer (FWD), dynamic cone penetrometer (DCP), test pits, soil sampling, and laboratory material test results were all used to characterize the behavior of the pavement structure. The design specifications for the RCC test section were:

– Subgrade: Min. CBR of 25 at 95% modified AASHTO, PI < 12, Maximum swell 1%;
– Subbase: 150 mm thick in situ material compacted to 93% modified AASHTO;
– Base: 150 mm thick in situ material stabilized with 3% cement (of which 20% was replaced with fly-ash), compacted to 95% modified AASHTO, and
– RCC: 150 mm thick layer. Mix design according to consultant's specification.

In the Phase 1 construction process the subgrade was ripped and re-compacted. After compaction, the in situ material had an average CBR of 58 and a field density of 1,788 kg/m^3 (at 94% modified AASHTO), which was above the specified limit (minimum CBR of 25 at 95% modified AASHTO) (Figure 3).

The density of the subbase was measured with a nuclear density gauge after compaction and was

Figure 2. The Heavy Vehicle Simulator.

Figure 3. Subgrade preparation and compaction.

Figure 4. Subbase construction.

Figure 5. Mixing cement and fly ash with in situ material.

Figure 6. Compacting base with roller compactor.

determined to be 90.7% of the laboratory determined density, 2.3% short of the target density of 93% (see Figure 4)

The construction of the base material is shown in Figures 5 and 6. The in-situ material was stabilized with the addition of 2.4% cement and 0.6% fly-ash. Laboratory results indicated that after stabilization, the base material had an unconfined compressive strength (UCS) of 244 kPa. This is lower than the acceptable standard for a South African C4 type stabilized base, which requires a specified minimum UCS of 750 kPa. The field compaction was 92.3%, which was also lower than the specified minimum limit of 95%.

A tractor-loader-backactor (TLB) and 10 ton vibrating roller compactor were used to mix the stabilizer into the excavated in situ material for the base and imported materials for the RCC layer (Figures 7). Due to the short test section the contractor chose to use

Figure 7. Mixing RCC materials.

Figure 8. Spreading RCC materials.

Figure 9. RCC layer after Phase 1 construction (mechanical equipment).

the TLB for the placement of the RCC layer as well (Figure 8), instead of using an asphalt paver normally used in larger projects. Uniformity and possible segregation as a result of this equipment choice will be investigated after the completion of HVS testing.

The RCC layer was constructed with river sand and 9.5 mm crushed quartzite stone. The mix design consisted of a cement-to-sand-to-stone ratio of 1:2:3. As in the case of the stabilized base, 20% of the cement content was replaced with fly ash. CEM III A 32,5N cement was specified.

The sand, stone, cement, and fly ash were mixed according to the mix design and distributed over the base (Figure 8). The material was compacted with a 10

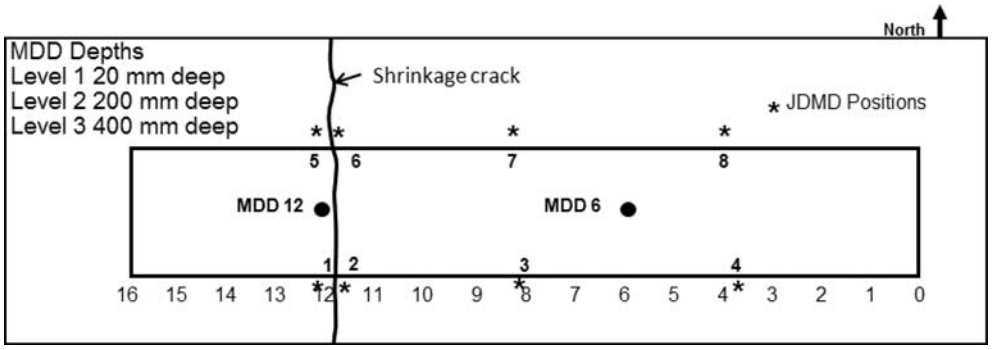

Figure 10. Test section layout.

ton steel roller while water was being added. The water: cement ratio was 0.36. The section was cured under plastic sheeting for 10 days. The final RCC surface is shown in Figure 9.

Laboratory tests were conducted on the RCC to determine the 7-day and 28-day cube strengths, which averaged 6.45 MPa and 9.74 MPa, respectively. This slow rate strength gain was attributed to the type of cement (CEM III) and the fly ash.

6 INSTRUMENTATION

Various instruments were used to record the performance of the RCC and the underlying layers during the test, including thermocouples (which measure air, surface, and layer temperatures), joint deflection measuring devices (JDMD), and multi-depth deflectometers (MDD).

6.1 *Joint Deflection Measuring Devices (JDMDs)*

JDMDs are linear variable displacement transducers (LVDTs) mounted vertically on the concrete slab (Figures 10 and 11). They record surface movements under the influence of traffic (deflections) and the environment (temperature-related curling effects). Several JDMDs were used to record deflections immediately adjacent to the trafficking wheel, as well as movements at longitudinal edges, transverse joints, and cracks.

JDMDs can also be used to measure the deterioration of load transfer across the construction joints and cracks under accelerated trafficking, by recording the relative movement of two JDMDs placed directly across a joint or crack as shown in Figure 11.

6.2 *Multi Depth Deflectometer (MDD)*

MDDs also use LVDTs and record surface as well as in-depth deflections. These LVDT modules are placed inside the pavement at various depths. In this experiment, the MDDs were placed at the surface, in the base layer 200 mm deep (MDD200) and in the subbase layer 400 mm deep (MDD400). MDDs were installed just before HVS testing started, after the

Figure 11. Shrinkage crack at Station 12 prior to trafficking.

formation of shrinkage cracks. Since the MDDs were only installed after the formation of shrinkage cracks it is believed that they did not have a significant influence in the deterioration of the shrinkage crack during HVS trafficking.

7 HVS TEST LAYOUT

The HVS test section covered the area on which a shrinkage crack had appeared. Instrumentation was concentrated around the shrinkage crack to enable the determination of cumulative damage in terms of deflections, load transfer efficiency (LTE), joint faulting, crack growth, and deformations. Although the entire test pad was instrumented, the results presented in this paper are focused on the damage which accumulated around the original shrinkage crack. The instruments described above, together with a laser profilometer were used to measure the response of the RCC under HVS loading. All loading was done in the dry state and no water was added. All trafficking was in a bi-directional, channelized mode.

8 HVS RESULTS

Only one test (Phase 1) was partially completed at the time this paper was submitted, and consequently only provisional results are presented. The section was tested in a dry state under a standard half axle load of 40 kN for one million repetitions. Because of time and

budgetary restraints and the slow rate of deterioration, the load was increased to 60 kN after the one million load repetitions had been applied. Using a damage factor of 4.2, the number of standard 80 kN axle load (ESALs) repetitions was equivalent to 5.5 for each 60 kN load repetition. The result of this increase in load level is clearly visible in the elastic response and permanent deformation of the pavement (Figures 12 and 13, respectively). To date, a total of 1.76 million repetitions had been applied, which equates to 5.18 million ESALs. This surpasses the design life of the pavement which was between one and three million ESALs.

8.1 *Elastic deflection response*

The variation in the elastic deflection (Figure 12) was mainly due to daily temperature variations and the increase in load to 60 kN after one million repetitions. The sudden drop in deflection at approximately

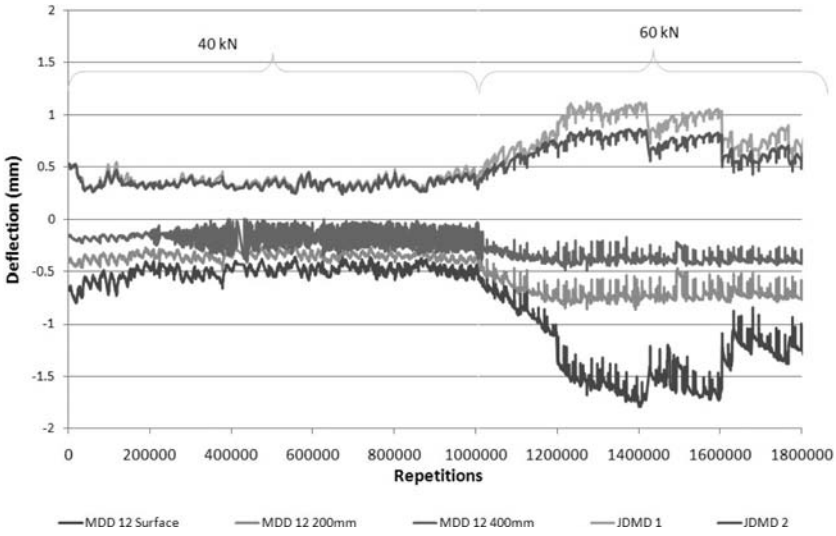

Figure 12. Elastic deflection data.

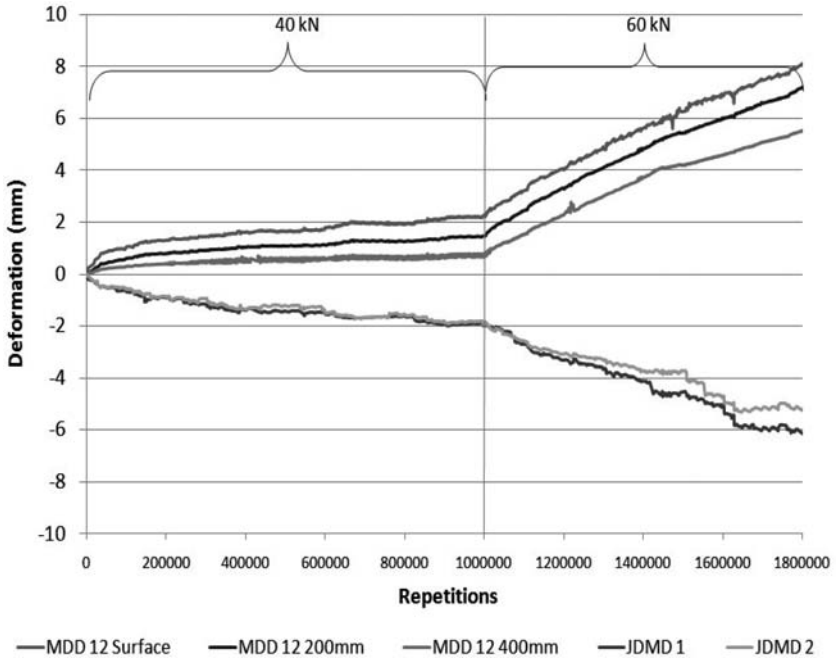

Figure 13. Permanent deformation data.

1.6 million repetitions was the result of an additional crack that formed around the instrumented shrinkage crack at Station 12 (Figure 12). The figure shows the data from JDMD 1 and JDMD 2 (placed across the shrinkage crack) and MDD 12 at three levels The MDD data is presented on a negative scale in the figure to differentiate between the JDMD data although both instruments recorded deflections positively downwards.

The measured deflections were high and are mainly due to the increase in the load level as well as the characteristics of the material, including concrete strength and the underlying base and subbase being weaker than designed. After the load was increased to 60 kN, the peak surface deflections increased to over 1.0 mm. MDD surface deflections were higher than JDMD data mainly because the instrument records data close to the load (between the HVS wheels) whereas JDMD deflections are recorded further from the loaded wheel. From the MDD data it can be seen that most of the early deflections originated from the base and deeper layers (surface deflections similar to deflections at 200 mm), but during the 60 kN phase most deflections originated between the top and the base at 200 mm inside the pavement.

Table 1. Average rate of deformation per 100,000 repetitions.

Phase	JDMD 1	JDMD 2
Embedment phase (mm/100,000 reps)	0.838	0.953
40 kN phase (mm/100,000 reps)	0.198	0.193
60 kN phase (mm/100,000 reps)	0.657	0.519

8.2 *Permanent deformation*

Permanent deformation in the pavement is illustrated in Figure 13 and shows a significant increase after the load was increased from 40 kN to 60 kN in line with the elastic deflections discussed above. The average rates of deformation per 100,000 load repetitions are shown in Table 1. The initial high rate of 0.84 mm/100,000 repetitions is termed the "embedment phase". This embedment phase is indicative of most APT tests, after which the pavement enters a stable phase of linear increase in deformation, as shown in Figure 13. The total average deformation of the slab was 6 mm after 1.76 million load applications, which is exceptionally high for a concrete pavement structure. This was attributed to the substandard base course which did not provide the required support.

Figure 13 also shows the permanent deformation recorded by the MDDs. Although all movements recorded were downwards, the MDD measurements are plotted positively upwards for clarity and to distinguish between JDMD and MDD plotted results.

The MDD recorded higher deformations mainly due to its location. It is interesting to note that even at a depth of 400 mm the granular layers had a significant amount of deformation. The total deformation recorded at this depth was 5.8 mm in relation to the total surface deformation of 8 mm after 1.8 million repetitions.

8.3 *Load transfer efficiency and relative movement*

Relative movements (RM) and LTE across the shrinkage crack at Station 12 are shown in Figure 14. LTE is a measure of the efficiency with which the load is

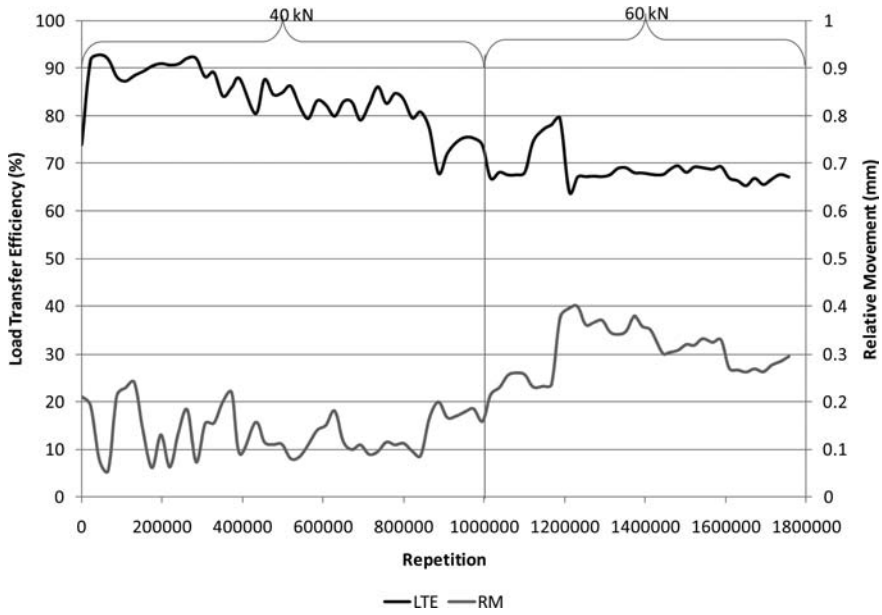

Figure 14. Load transfer efficiency and relative movement.

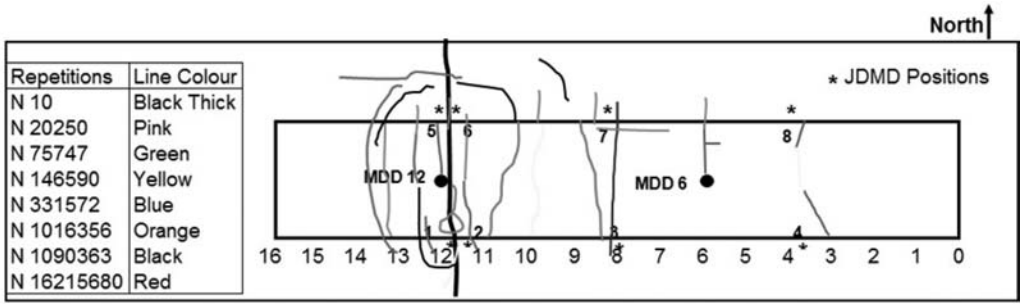

Figure 15. Crack formation.

transferred across a crack. It is defined as the relationship between deflection of the unloaded slab (Δ_U) and the deflection of the loaded slab (Δ_L) or:

$$LTE\ (\%) = \Delta_U/\Delta_L x100 \quad (1)$$

An LTE of 100 percent is consistent with full load transfer, and an LTE of zero percent indicates zero load transfer.

Relative movement is the movement of the loaded slab (Δ_L) relative to the movement of the unloaded slab (Δ_U), or:

$$RM\ (mm) = \Delta_L - \Delta_U \quad (2)$$

An RM of 0 mm indicates that both the loaded and unloaded slab had the same reaction to the applied load and corresponds to an LTE of 100 percent.

By considering the above two parameters, it is possible to quantify the effectiveness of the load transferred through pavement deflection across a crack or a joint. RM will measure a greater movement with high deflection at a certain LTE, but will measure smaller movement with a lower deflection given the same LTE. LTE will be higher with lower deflections at a certain RM, but lower with higher deflections at the same RM. These two factors underline the importance of considering both LTE and RM together with the elastic deflection behavior for crack movements.

The LTE was relatively high (above 80%) during the first 800,000 repetitions, with a maximum RM of approximately 0.2 mm. The LTE dropped to just below 70% after the load was increased to 60 kN, after which it remained fairly constant. The RM ranged between 0.25 mm and 0.4 mm.

The drop in LTE signifies a significant loss in aggregate interlock across the shrinkage crack after the application of approximately 1.2 million load applications.

8.4 *Crack formation*

Cracking caused by the repetitive HVS loading is shown in Figure 15. Cracks formed in quick succession during the embedment phase (0–100,000 load repetitions). Although clearly visible, crack widths were small (less than 0.2 mm) and were not considered to be structural cracks. Some additional cracks developed during the stable 40 kN trafficking phase.

Figure 16. Circular crack formation toward the end of the test.

Structural cracks wider than 0.3 mm appeared after the 60 kN loading phase (from one million repetitions onwards). They are shown in Figure 14 (orange, black and red cracks). These cracks encircled the original shrinkage crack at Station 12 (Figure 16).

9 CONCLUSIONS

This paper summarizes the initial findings of the first as-yet uncompleted HVS test conducted on a full-scale roller compacted concrete test section which was constructed using conventional methods. It reports on typical pavement performance measures, including deflections, crack growth, load transfer efficiency, permanent deformation, and crack faulting.

The initial results are promising. Although the RCC layer was constructed on a substandard base and subbase and the RCC strengths were below expectation for a CEM III cement mix, it has performed well in the dry state. The pavement has significant cracking, high surface elastic deflections and low LTE, but is still considered not to have failed even after the application of over 5 million equivalent 80 kN axle load applications.

Permanent deformation (rutting) is not a typical failure mechanism in concrete pavements, but was observed in this study due to the substandard granular layer works under the concrete, with base and subbase layers both not meeting their respective design specifications. More than 8 mm of surface deformation was recorded between the HVS wheels, all of which originated in the granular layers (per MDD measurements). Test pit analysis investigations will be carried out after the completion of the HVS testing to verify the extent and degree of layer deformation below the RCC.

An important factor not evaluated in this part of the study is the effect of water. The test discussed in this paper was conducted during the dry months when no rainfall was recorded. It is anticipated that the rate of deterioration will increase under the influence of water, especially with the presence of structural cracks, which will allow the ingress of water into the base.

Follow-up testing will include the evaluation of a labor-intensive constructed section, as well as the determination of the water sensitivity of this type of pavement construction.

ACKNOWLEDGEMENTS

This HVS research project was supported by the Gauteng Department Roads and Transport and their financial and technical contribution towards this study is greatly appreciated. The authors thank Mr. Steve Musundi, the managing director of Cosal Consultants CC, who did the foundational work and was responsible for the design and construction of the test pavement. He also provided crucial input during the execution of this research program.

REFERENCES

Gauteng Province Department of Infrastructure Development. 2007. www.did.gpg.gov.za/Pages/GEPWPBackground.aspx.2007

Gauteng Provincial Government. 2007. *Framework for Monitoring and Evaluation of the Expanded Public Works Program*

Harrington, D. Abdo, F., Adaska, W. and Hazaree, C. 2010. *Guide for roller-compacted concrete pavements*. National Concrete Pavement Technology Center, Iowa State University.

Portland Cement Association Water Resources. 2004, *Roller-Compacted Concrete Density: Principles and Practices*. Skokie, Illinois.

Schrader, E.K. 1992. Roller-compacted concrete for dams—State of the art. *Proceedings of the International Conference on Advances in Concrete Technology*. Athens, Greece.

This page intentionally left blank

Advances in Pavement Design through Full-scale Accelerated Pavement Testing – Jones, Harvey, Mateos & Al-Qadi (Eds.)
© 2012 Taylor & Francis Group, London, ISBN 978-0-415-62138-0

Accelerated pavement testing on slab and block pavements using the MLS10 Mobile Load Simulator

R. Blab, W. Kluger-Eigl & J. Füssl
Faculty of Civil Engineering, Vienna University of Technology, Vienna, Austria

M. Arraigada
EMPA Duebendorf, Duebendorf, Switzerland

ABSTRACT: To optimize the thickness of slab and block pavements and also to test new large-format slabs an Accelerated Pavement Test (APT) using the Mobile Load Simulator (MLS10) was carried out in Austria from September to October 2010. The APT was an international cooperation with the Swiss Federal Laboratories of Material Science and Technology, Semmelrock Ebenseer and the Vienna University of Technology. The experiment consisted of seven different slab and block pavements. Selected pavements were instrumented with soil pressure cells and horizontal strain gauges to assess primary responses under the wheel load. For the APT the MLS10 used Goodyear super single tires with a wheel load of 65 kN. The test speed was 22 km/h and no lateral wandering and no application of water was used during the tests. Falling Weight Deflectometer (FWD) measurements were taken after construction of the test sections and after completion of loading. Deformation of the surface (rut depth) was determined periodically. The results of the APT are intended to evaluate the parameters for a developed Finite-Element Model (FEM) for slab and block pavements, which enables simulation of the whole superstructure, traffic loads and thermal stresses. The FEM is the final tool to optimize the thickness of slabs and blocks for new designs and heavy traffic areas.

1 INTRODUCTION

Block pavements or slab pavements made of concrete or natural stones are mainly used for communal areas, where aesthetic variety (shape, color, texture) is welcomed. The economic efficiency and lifespan of the pavement are also very important.

At bus stops or pedestrian precincts for example, which are also trafficked by delivery trucks, high vertical and horizontal loads (braking and accelerating) often occur. If the layers of the pavement superstructure are not properly designed, the pavement often suffers damage and as a result of this expensive reconstruction is necessary. To avoid this in Austria, pavements with blocks or slabs for areas with light or medium traffic loads are designed according to the Austrian regulation RVS 03.08.63 (FSV 2008a). In this regulation the thickness of the layers for the superstructure can be determined depending on a given design traffic load and a chosen pavement type. The maximum sizes and the aspect ratio for blocks and slabs are also defined in this regulation. For heavy-duty trafficked areas, high traffic-loads and other formats, project specific structural designs are necessary.

To optimize the thickness of slab and block pavements for special areas of applications and also to design new large-format slabs, a research project was started in December 2009. A new finite element model (FEM) was created and evaluated with the data from an accelerated pavement test (APT). The APT was carried out in Austria from September to October 2010 using the Mobile Load Simulator (MLS10) from Switzerland.

This research project represented a challenge with no precedents for the partners involved and it was the first time an APT was undertaken in Austria on block pavements. The international cooperation involved two research institutes, the Technical University Vienna (TU) and the Swiss Federal Laboratories of Material Science and Technology (EMPA), and two industry partners, Semmelrock Ebenseer Baustoffindustrie GmbH & CoKG (SEB). The industry partners' main activity is the development and production of concrete block pavers.

2 CONCEPT FOR ACCELERATED PAVEMENT TEST

2.1 *Layout, construction and instrumentation of the test sections*

Seven different test sections were built for the APT in the summer of 2010 on privately owned land. TU and SEB designed and constructed the test sections,

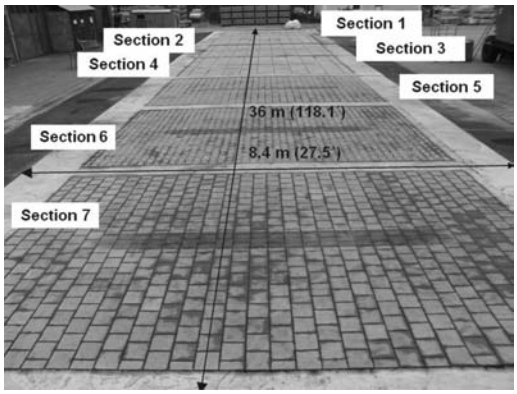

Figure 1. Layout of the seven test sections.

which included design and installation of the measuring devices. EMPA provided and operated the MLS10 with the support of SEB.

Slab pavement test sections were 6.4 m (21 ft.) long and 5.0 m (16.4 ft.) wide, and block pavement test sections were 6.4 m long and 4.0 m (13.1 ft.) wide (Figure 1). The length of each test section was adjusted to the length between the corner jacks of the MLS10, because the machine should not stand on the pavement itself during the traffic simulation. All sections were surrounded with a concrete foundation to support the MLS10 and to confine the pavement. Because of the design of the MLS10 (corner jacks) the maximum difference in height between the surface of the pavement and the foundation was limited to ±20 mm (0.79 in.). The test sections were built flat with no slope in longitudinal or cross direction.

The structural design of each test section was chosen according to the requirements in RVS 03.08.63 (FSV 2008a), depending on the calculated loading class (Table 1). For laying pattern a stretcher bond was selected for each test section. Bedding sand (2/4 mm), jointing sand (0/2 mm and 0/4 mm), base materials (0/63 mm and 0/32 mm), and porous concrete (C16/20) were chosen according to the requirements in regulations RVS 08.18.01 (FSV 2009) and RVS 08.15.01 (FSV 2008b).

Test sections 2, 4, 5 and 7 were instrumented in the main wheelpath of the MLS10 with the following devices to determine the response under loading conditions (Figure 2 and Figure 3):

- Strain gauges (type DMS LY 41-50/120) installed on the bottom of the slabs in the center and at the edge of the slab to monitor expansion.
- Soil pressure cells (type EBKE 20/30 K10 A) installed on the surface of the subgrade and the unbound base course to measure vertical pressure.
- Special strain gauges (type EKD 1002) installed on the bottom edge of the porous concrete to measure expansion.
- Thermocouples to measure air, surface and bedding sand temperatures.

Table 1. Test section design.

Section	Layer	Thickness (cm)	Instrument
1	Slab 100/50 cm	18	
	Bedding	3	
	Unbound base	20	
	Frost protection	30	
	Subgrade	–	
2	Interlocking slab 125/62.5	18	6 strain
	Bedding	3	
	Unbound base	20	2 pressure
	Frost protection	30	
	Subgrade	–	2 pressure
3	Interlocking slab 125/62.5	14	
	Bedding	3	
	Unbound base	20	
	Frost protection	30	
	Subgrade	–	
4	Interlocking slab 125/62.5	12	6 strain
	Bedding	3	
	Unbound base	20	2 pressure
	Frost protection	30	
	Subgrade	–	2 pressure
5	Interlocking block 20/20	10	
	Bedding	3	
	Unbound base	20	2 pressure
	Frost protection	30	
	Subgrade	–	2 pressure
6	Interlocking block DoubleT	10	
	Bedding	3	
	Unbound base	20	
	Frost protection	30	
	Subgrade	–	
7	Interlocking block 20/20	10	
	Bedding	3	
	Porous concrete	20	4 strain
	Frost protection	15	
	Subgrade	–	2 pressure

The exact position and designation of the instrumentation is show in Figure 2 with the following abbreviations:

- U Soil pressure cell on subgrade
- O Soil pressure cell on base course
- DMS Strain gauge on bottom edge of slab
- BD Special strain gauge on bottom edge of porous concrete

2.2 *Test program*

2.2.1 *Visual inspection*

Visual inspection was done before and after the APT and included the following checks on each test section:

- Laying pattern and width of joints
- Filling of joints
- Damage of blocks or slabs
- Surface evenness and rut depth (also done during maintenance stops of the MLS10)

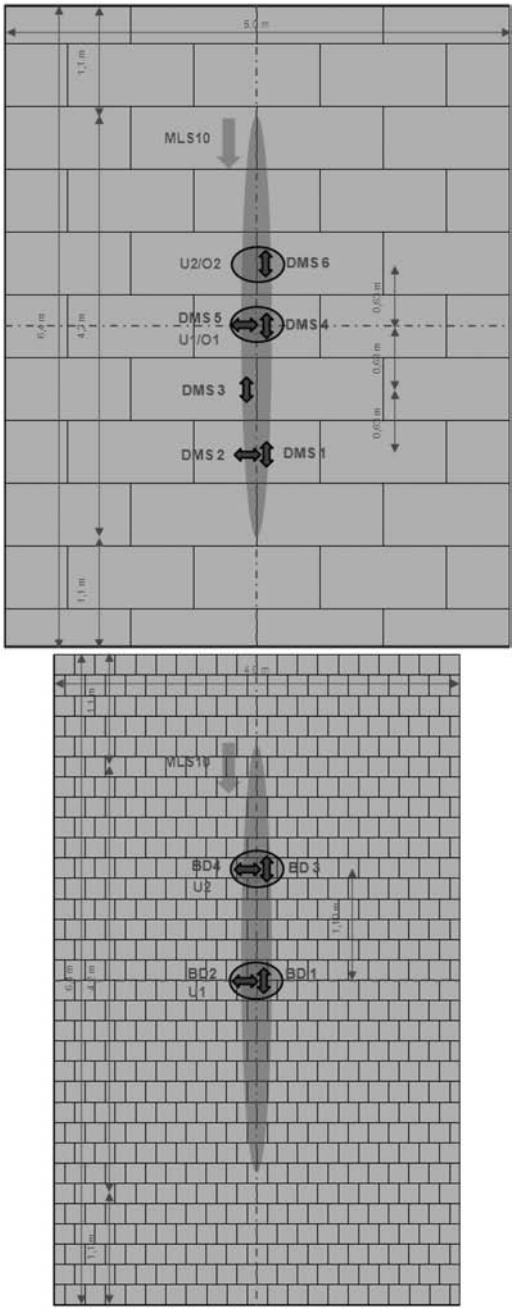

Figure 2. Layout of instrumentation on slab and block pavements.

2.2.2 *Falling weight deflectometer measurements*

Falling weight deflection (FWD) measurements were conducted on the surface of each pavement before and after the accelerated loading to assess the development of the bearing capacity of the test pavements. The measurements followed a fixed scheme as given in Figure 4 with an applied load of 50 kN. The following distances

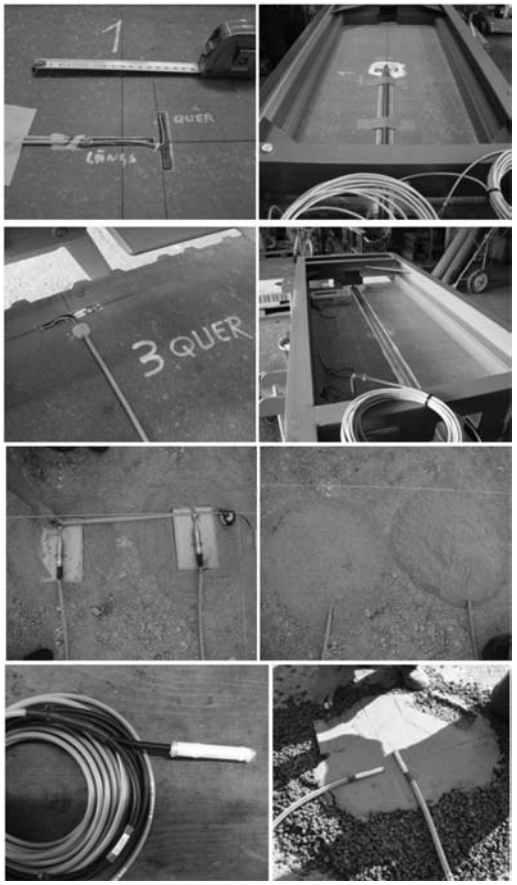

Figure 3. Strain and stress instrumentation.

between the geophones were chosen: 0–200–300–450–600–900–1,200–1,500–1,800 mm. Geophones were never positioned over a joint.

2.2.3 *Response measurements*

Four test sections were instrumented with different strain and stress measurement devices to determine the primary response under wheel load to verify the results of the developed FEM. A scan rate frequency of 100 Hz was used for all sensors. The maximum, minimum, average and standard deviation per minute were calculated for each sensor for later analysis.

2.3 *Traffic simulation with mobile load simulator*

The Mobile Load Simulator MLS10 from Switzerland (Partl, 2008) was used for the APT (Figure 5). Due to the given time and budget restrictions of two months for the tests it was necessary to increase the wheel load in order to reach the same amount of deterioration as for a standard axle load in Austria. Total testing was limited to a maximum of about 1.2 million load applications for all test sections.

The MLS10 was equipped with Goodyear 455/40 R22.5 super single tires with a tire pressure of

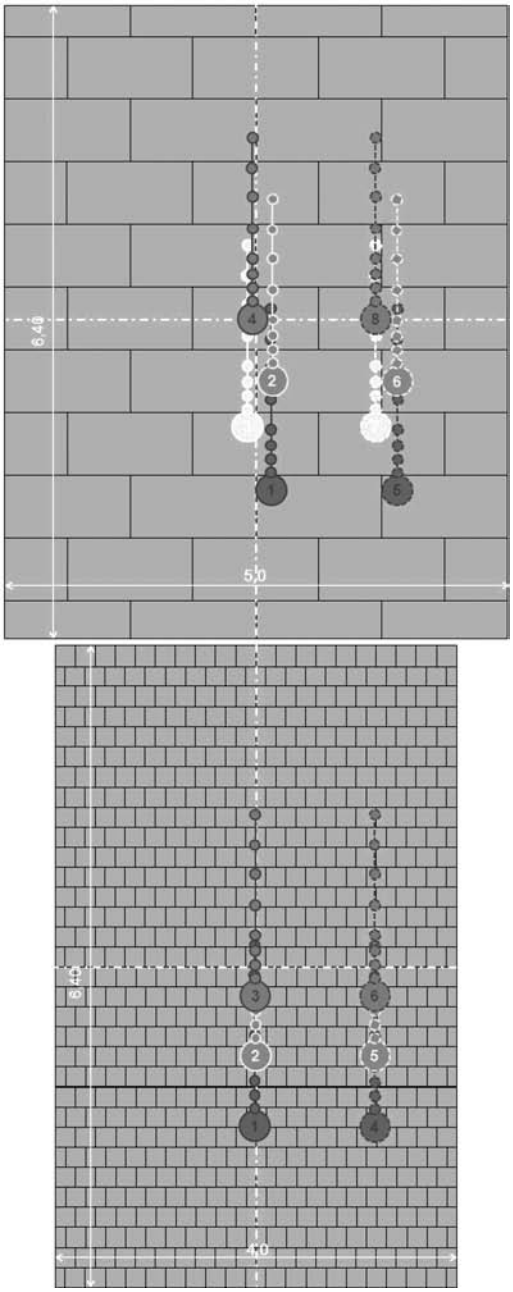

Figure 4. Scheme of FWD measurement points.

1.06 N/mm^2 (10.6 bar) and a wheel load of 65 kN. Changes in the geometry of the machine to accommodate these wheels were done prior to transporting the machine from Switzerland to Austria.

2.3.1 *Calibration of the MLS10*

At the start of the APT the wheel load was adjusted with a calibrated static scale and controlled with a mobile weigh-in-motion device (WIM) to achieve a wheel load of exactly 65 kN (Figure 6). Adjustment time for the first wheel was about three hours, and the same settings were used for the other three wheels. Although load checks were planned for after the test, scale availability and time restrictions prevented this being carried out. Operating staff adjusted the MLS10 manually during maintenance stops when required.

Figure 5. Mobile Load Simulator MLS10 with super single tires.

Figure 6. Static scale and weigh-in-motion.

2.3.2 *Preloading and continuous operation*

At the start of the traffic simulation a pre-loading phase with reduced wheel load and a speed of 7.2 km/h (4.5 mph) was completed on each test section for about 15 minutes (1,000 passes). During this time the MLS10 was not fully lowered to the pavement. After this initial phase, the MLS10 was lowered to the pavement and the speed was increased to 22 km/h (13.7 mph). During the tests no lateral wandering or application of water was performed.

The MLS10 was in Austria for 55 days and operated on 31 days with a total of 1,189,353 load applications distributed over the seven different pavements. This averaged 38,400 load cycles per day (Table 2).

Table 2. APT schedule.

Day	Test Section	Load Passes	Notes
01-Feb	01-Jul	0	First visual inspection and FWD
3	2	14,146	Sect. aborted due loss of jointing sand and swinging of slabs
4	6	20,052	Sect. aborted due strong rutting
5	5	5,042	Rut depth at 1,000 and 5,000
6	5	49,018	Rut depth at 35,000
7	5	44,280	Rut depth at 80,000
8	5	47,919	
9	5	50,241	Rut depth at 150,000
10	5	19,452	Rut depth at 200,000
11	5,7	51,641	Sect. 5 aborted due strong rutting at 250,000, Sect. 7 rut depth at 17,000
12	7	47,914	Rut depth at 43,000
13	7	49,430	Rut depth at 115,000
14	7	27,490	
15	7	56,680	Rut depth at 165,000
16	7	50,000	Rut depth at 200,000
17–18	1–6	0	2nd visual inspection and FWD
19	7	36,000	Finish at 285,000
20	6	50,026	Rut depth at 33,000
21	6	20,158	Rut depth at 70,000
22	6	48,376	
23	6	54,598	Rut depth at 130,000
24	6	50,015	Rut depth at 175,000
25	6	42,560	
26	6	19,422	Finish at 285,000
27	2	48,011	Rut depth at 5,000
28	2	49,121	Rut depth at 65,000
29	2,4	37,891	Sect. 2 finished at 100,000, Sect. 4 finished at 35,000
30	3	40,094	Rut depth at 26,000
31	3	46,694	Rut depth at 75,000
32	3	13,242	Finish at 100,000
33	1	42,271	Rut depth at 35,000
34	1	37,921	
35	1	19,830	Sect. 1 finished at 100,000
36–37	1–4,6,7	0	3rd visual inspection and FWD
Total	7 sections, 1,189,535 load applications, 31 operating days, average 38,400 load applications per day		

The authors had little experience with the use of APT on block and slab pavements and there is limited published information on the topic. This study was also the first use of the MLS10 for testing block and slab pavements; in the past it has only been used for asphalt or concrete pavements. The main concern was the possibility of exposing the machine, especially the loading system, to damage. If no lateral wandering is used, rutting on block pavements will depend on how the wheelpath of the APT device is located in relation to the laying pattern of the blocks. Some blocks will get the full load of the tires whereas others next to them have partial or no loading. This can result in uneven settlement/compaction of the bedding under the blocks resulting in an uneven surface with sharp borders that could be detrimental to the machine

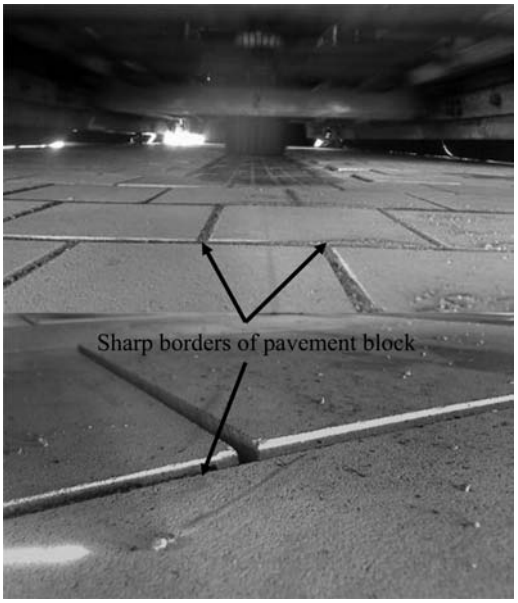

Figure 7. Uneven settlement of pavement.

(Figure 7). The most critical scenario would occur if a slab or block broke and was dislodged from the pavement and interfered with the loading action. To avoid this problem and to have a more representative situation of how loading distributes in real block pavements, the MLS10 was carefully positioned in order to set the wheelpath so that it covered as many blocks as possible. Regular visual inspections of the surface were also carried out to check that the surface did not have unevenness of more than 20 mm. This is also the threshold value for rut depth in Austria.

3 FINITE ELEMENT MODEL

3.1 *Description of the FEM*

In this section, a brief overview of the developed finite element model is provided to illustrate the use of the MLS10 test data for the validation of numerical simulation tools of the whole pavement structure.

The geometry and the boundary conditions of the FEM are illustrated in Figure 8. The thicknesses of the pavement layers are given in Table 1. The concrete slabs as well as the concrete blocks were modeled as linear elastic material. An anisotropic friction criterion in tangential direction and a nonlinear elastic material behavior in the normal direction were assigned to the vertical joints. A Drucker-Prager type yield function with a cap-hardening rule was assigned to all unbounded layers (2)–(4). All layers have continuous lateral elastic support.

The material parameters for the unbound layers were backcalculated from the FWD-measurements on the pavement surface and static plate load tests during

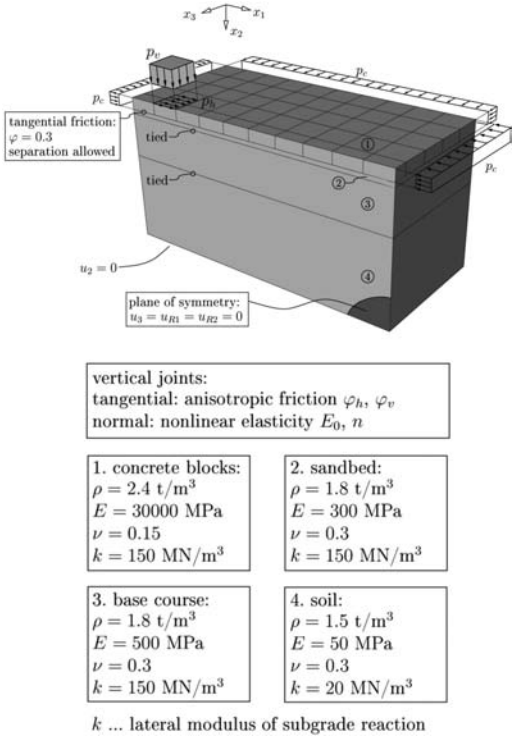

Figure 8. FEM for block pavement structures.

the construction of the layers. The linear elastic parameters of the concrete were determined from ultrasonic measurements. Different joint-tests were developed and conducted for the determination of the anisotropic friction behavior of the joints between the concrete slabs/blocks.

The full model is discretized with about 30,000 three-dimensional (3-D) finite elements and 50,000 contact elements, both having quadratic interpolation functions.

3.2 *Validation of FEM with sensor data*

Static calculations for different positions of the super single tire (65 kN wheel load) were conducted to validate the FEM. In Figure 9 the vertical deformation fields of a concrete slab pavement structure, for two different loading positions, obtained from FE-calculations are shown as an example.

The results were compared to the sensor data gained from the MLS10 tests. Both the strains measured with the strain gauges applied at the concrete slabs and the pressure measured in the unbound layers agreed well with the results obtained from the FE simulations (Table 3). A comprehensive comparison of the FE results with the experimental test data will be presented in a follow-up paper.

Mechanically-sound designs and optimization of the full pavement structure is now considered possible comes possible with this simulation tool, which has been validated using pavement tests with the Mobile Load Simulator MLS10, Realistic pressure and deformation states within all layers are also now available.

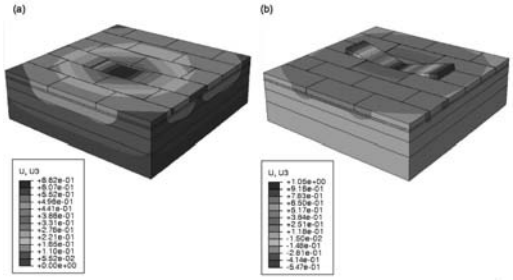

Figure 9. Vertical deformation of a concrete slab pavement structure loaded with a wheel load of 65 kN (a) in the middle of the slab and (b) at the edge of the slab.

Table 3. Sensor data and FEM results for slabs.

		Section 2		Section 4	
Sensor	Unit	Sensor	FEM	Sensor	FEM
DMS 1, 4	µm/m	20	21	40	50
DMS 2, 5	µm/m	65	52	80	95
DMS 3, 6	µm/m	35	30	55	66
O1	bar	0.80	0.43	0.60	0.64
O2	bar	1.70	2.00	0.40	2.40
U1	bar	0.40	0.35	0.40	0.39
U2	bar	0.55	0.54	0.50	0.57

4 EXPERIENCES AND CONCLUSIONS

4.1 *Execution of APT*

The main problem of the APT was the rapid loss of jointing sand, since the joints of the new surfaces had no time to consolidate. Therefore it was necessary to add jointing sand during the maintenance stops of the MLS10. However, inspection and refilling of joints are normal maintenance actions for block and slab pavements during their life time. For further tests on these types of pavements, it is recommended that new test sections are exposed to environmental conditions (rain, dust) for a few weeks before the start of the APT and until the jointing material consolidates.

Although a few slabs and blocks were damaged, and some surfaces were deformed during the APT, this had no influences on the operation of the MLS10. To minimize damage to moving parts of the MLS10 from jointing sand and water, the APT was undertaken without application of water to the pavement surface. The authors are aware of the unrealistic conditions for the test pavements, but the risk of damaging the MLS10 during the APT needed to be minimized.

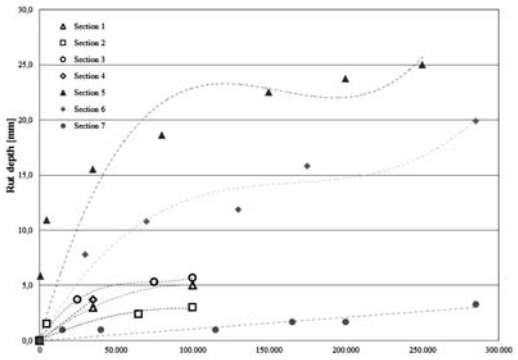

Figure 10. Rut depth of slab and block pavements.

In summary it can be said that the execution of the APT and the planned load applications were completed successfully and considerable time was saved compared to test sections on public roads with high traffic volumes.

4.2 *Performance of test sections*

The performance of Test Section 1 was as expected as it was a standard structure used in Austria. No slabs were damaged and vertical deformation was within the allowed tolerances. After the application of additional load passes deformation increased slightly and some slabs started to tip. The lager slabs used in Test Section 2 performed well, no slabs were damaged and vertical deformation was less than on Section 1 (Figure 10), although this design format is not standard in Austria.

The thinner slabs on Test Sections 3 and 4 broke in the center along the loading line of the MLS10. This was expected as these design formats are outside the regulations of the Austrian standards. However, the number of load passes could be determined up to the break. Vertical deformation was higher than on Sections 1 and 2, because of the loss of joint material and tipping of the slabs, which were loaded at the edge.

On Test Section 5, the APT was stopped before reaching the planned load passes because of a rut depth of more than 20 mm, which is the threshold value in Austria and also the maximum tolerance for the MLS10. The largest deformation was situated directly above the soil pressure cells in the unbound base course and it was concluded that the compaction of the base course around the instrumentation was unsatisfactory. Although considerable deformation was measured, no blocks were broken and only minimal spalling on two stones occurred. The width of joints in the middle of the load line was less than the allowable tolerances.

On Test Section 6 the rut depth was 20 mm at the planned end of the APT, but no damage was visible on the blocks. Some horizontal deformation and a little tipping of two pavers were observed in the touchdown area of the super single tires. The width of joints in the middle of the load line was mostly below 1 mm.

The structure with porous concrete on Test Section 7 is a new construction method in Austria for which there is only limited knowledge and experience. The performance of this pavement was excellent, with no measurable deformation and no visible damage.

In summary, it can be assumed that the performance of the test sections showed realistic behavior during the APT compared to real traffic loads. The only disadvantage of the MLS10 is that no horizontal forces can be applied on the pavement surface. For further tests an additional braking system for the MLS10 is recommended to evaluate the behavior of different block/slab pavements under brake load.

ACKNOWLEDGMENTS

The authors wish to express their thanks to Semmelrock Ebenseer Baustoffindustrie GmbH & CoKG and the Österreichische Forschungsförderungsgesellschaft (FFG) for financing the project. Special thanks also go to the operating staff of the MLS10 for their support and hard work.

REFERENCES

FSV. 2008a. *RVS 03.08.63: Straßenplanung – Bautechnische Details – Oberbaubemessung*, Vienna: Österreichische Forschungsgesellschaft Straße-Schiene-Verkehr.

FSV. 2008b. *RVS 08.15.01: Technische Vertragsbedingungen – Unterbauplanum und ungebundene Tragschichten – Ungebundene Tragschichten*, Vienna: Österreichische Forschungsgesellschaft Straße-Schiene-Verkehr.

FSV. 2009. *RVS 08.18.01: Technische Vertragsbedingungen – Pflasterarbeiten, Randbegrenzungen – Pflastersteinund Pflasterplattendecken, Randeinfassungen*, Vienna: Österreichische Forschungsgesellschaft Straße-Schiene-Verkehr.

Partl, M.N. 2008. *Full-Scale Accelerated Pavement Testing APT at EMPA – the New Mobile Load Simulator*, Dübendorf: EMPA Dübendorf.

This page intentionally left blank

Advances in Pavement Design through Full-scale Accelerated Pavement Testing – Jones, Harvey, Mateos & Al-Qadi (Eds.)
© 2012 Taylor & Francis Group, London, ISBN 978-0-415-62138-0

Environmental and load effect on dowelled and undowelled portland cement concrete slabs

S.M. Sargand & I. Khoury
Ohio Research Institute for Transportation and the Environment, Ohio University, Athens, Ohio, US

ABSTRACT: Two Portland Cement Concrete (PCC) slabs, one dowelled and one undowelled, were placed and instrumented in the Accelerated Pavement Load Test Facility in Lancaster, Ohio. The objectives of the study were to determine the forces generated in steel dowel bars and in the surrounding concrete resulting from PCC slab deformations during curing, thermal cycling, and moving wheel loads; monitor PCC slab shape during curing and thermal cycling with LVDTs and a *Dipstick*®; measure strain generated in the PCC slabs from moving wheel loads traversing the slab; and determine the magnitude of residual stress remaining in the slabs by taking cores at the rosette locations at the conclusion of testing. The slabs were cured at a constant temperature, and then subjected to temperature variations and wheel loads. Data were collected from the sensors and a *Dipstick*® was used to measure the shape of the slabs as they cured and when subjected to temperature gradients. It was found that slab temperature gradients were moderate during the curing period because of constant room temperature. LVDT data indicated that the amount of warping on undowelled slabs was much greater than on the dowelled slabs. As slab temperature gradients changed, the undowelled section had greater deflection than the dowelled section. Corner deflection increased with time during the period of constant temperature. Dowels restrained joint movement, thus reducing the amount of curling. Therefore, dowel bars not only transferred load but also reduced loss of support.

1 INTRODUCTION

1.1 *Overview*

During the curing of portland cement concrete (PCC) slabs, and as they are exposed to subsequent daily and seasonal temperature and moisture cycling, differential expansion and contraction change slab shape, and the magnitude and distribution of support under the slabs. Higher temperature and/or moisture in the upper portion of PCC slabs cause that stratum to expand relative to the lower portion of the slab, thereby forcing the slab edges down. Conversely, higher temperature and/or moisture in the lower portion of the slab results in the slab edges being raised. Slab distortion caused by differential temperatures is referred to as curling and slab distortion caused by differential moisture is referred to as warping.

Any differential vertical displacement of a PCC slab from its original as-placed elevation results in non-uniform support under the slab and bending stress induced in the slab. This distortion has a major impact on the long-term performance of rigid pavements. In locations where the slab surface is higher than its initial elevation, contact with the underlying support layer is significantly reduced, and dead load bending stresses will develop where the slab bridges these areas. Higher than normal live load bending stresses will then be superimposed on the dead load bending stresses in these areas when traffic passes over the unsupported slab. The extent of slab displacement and the magnitude of dead load bending stresses depend upon several factors, including: temperature and moisture gradients in the slab; concrete material properties; slab dimensions; and boundary conditions along the slab edges. Live load bending stresses will be dictated by these same parameters plus the weight and distribution of wheel loads on and around the slab.

One mechanism commonly used to stiffen PCC slab ends is the addition of dowel bars to distribute or transfer vertical shear and horizontal bending moments longitudinally across joints to adjacent slabs. These round, smooth bars are typically epoxy-coated steel, 32 mm (1.25 in.) to 38 mm (1.5 in.) in diameter, 460 mm (18 in.) long and spaced 300 mm (12 in.) on centers across the pavement width. They are installed as prefabricated baskets at the time of concrete placement, and one end of each bar is lubricated before coverage to prevent bonding with the concrete and to facilitate horizontal slab movement. While these bars provide additional stiffness to the slab ends, the forces they transfer are resisted by stresses generated in the bars and in the concrete surrounding the bars.

Mathematical models, including finite element methods, have been used to simulate the response of rigid pavements to dynamic loading. These models assume that PCC slabs are flat and in uniform contact with the underlying base material. Any loss of support from initial curing and from subsequent environmental

curling and warping has traditionally been ignored. However, research indicates that PCC slab edges begin to deform upward within a few hours after concrete placement and continue to deform throughout the traditional 28-day cure period and beyond, even when ambient conditions remain relatively constant. This displacement is caused primarily by a loss of moisture in the upper portion of the slab during the hydration process. As ambient temperature or moisture conditions change, further positive and negative displacements are superimposed on the slabs. Since the dynamic response of rigid pavements is affected by slab support, accurate response calculations require that the models properly account for non-uniform slab support.

When heavy traffic loads pass over deformed pavement slabs, significant live load stresses are added to environmental and dead load stresses already existing in the slabs. Various mathematical models have been developed to describe the combined response of rigid pavement slabs to environmental cycling and dynamic loading but, additional data is required to adequately verify and calibrate them.

1.2 *Objectives*

To verify results from previous studies and to quantitatively measure dowel bar and slab response under controlled conditions, dowelled and undowelled instrumented pavements were constructed in the Accelerated Pavement Loading Facility (APLF) in Lancaster, Ohio. Specific objectives for this study included the following:

1. Determining forces generated in steel dowel bars and in the surrounding concrete resulting from PC concrete slab deformations during curing, thermal cycling and moving wheel loads.
2. Monitoring PCC slab shape during curing and thermal cycling with LVDTs and a *Dipstick*®.
3. Measuring strain generated in the PCC slabs from moving wheel loads traversing the slab
4. Determining the magnitude of residual stress remaining in the slabs by taking cores at the rosette locations at the conclusion of testing.

1.3 *Facility*

The Accelerated Pavement Load Facility (APLF) located on the Lancaster Campus of Ohio University is a state-of-the-art research facility initially funded by the Ohio Board of Regents and designed for the testing of full-scale asphalt and concrete highway pavement sections under carefully controlled environmental and loading conditions. The initial investment in the facility by the Ohio Board of Regents was $1.1 million and since its construction in 1997 an additional $500,000 has been added in improvements and updates.

The pit where experimental sections of pavement are tested is 13.7 m (45 ft.) long by 11.6 m (38 ft.) wide by 2.5 m (8 ft.) deep. Large (4.3 m (14 ft.) high $\times$ 7.3 m (24 ft.) wide) doors are available on both ends of the building for easy access by standard construction equipment in order to construct pavements. Air temperature in the test chamber can be maintained between $-12°C$ ($+10°F$) and $+54°C$ ($+130°F$), and wheel loads of up to 13,000 kg (30,000 lbs.) can be applied at up to 8 km/h (5 mph) with either dual or super single tires.

Projects in the facility ranged from an Ultra White topping study to most recently studying various types of warm asphalt mixes and perpetual pavement designs.

In addition to the ability to control the environmental conditions, this unique facility includes the ability to change the underlying subgrade soil to depths up to 1.8 m (6 ft.), to vary the water table depth, and to add water from the top to simulate rain. The APLF is also equipped with monitoring cameras that allow users outside the facility to monitor all aspects of the experiment and give instant feedback to the technicians and engineers on location.

2 CONSTRUCTION, INSTRUMENTATION, AND LAYOUT

2.1 *Construction*

To define the impact of curing, environmental cycling, and wheel loading on the performance of PCC pavement, two separate 13.7 m (45 ft.) long by 3.7 m (12 ft.) wide by 250 mm (10 in.) thick jointed concrete pavements were constructed in the APLF. Each pavement was sawed into three slabs with joints spaced at 4.8 m (15 ft.) intervals. The pavements were separated with no constraints (e.g., tie bars) placed along the sides. One pavement contained dowel bars to transfer load across the joints between slabs and the other pavement was undowelled. The pavements were otherwise constructed in accordance with Ohio Department of Transportation (ODOT) specifications, with the 150 mm (6 in.) dense-graded aggregate base and the A-6 subgrade under the pavements being typical in Ohio. The pavement surfaces were finished smooth to facilitate the periodic measurement of surface elevations with a *Dipstick*®. Vertical plywood boards were placed at the bottom of the slab at all four joints to facilitate cracking of the pavements after joints were sawed to a depth of 75 mm (3 in.) at the same locations on the pavement surfaces. This joint treatment minimized aggregate interlock between adjacent slabs during curling and warping, which permitted a clearer definition of the effectiveness of dowel bars in resisting slab curvature. Table 1 summarizes the physical properties of concrete used in the two pavements.

2.2 *Instrumentation and layout*

Strain gauges and thermocouples were installed in both test pavements during concrete placement to measure strain in selected dowel bars, and strain and temperature in the concrete slabs. Precautions

were taken during construction to carefully place and vibrate concrete around these sensors without disturbing their alignment or damaging them. Linear variable differential transformers (LVDTs) referenced to a depth of 2.1 m (7 ft.) were installed along the pavement edges soon after placement to monitor vertical deflection at these locations.

2.2.1 *Concrete sensors*

Arrays of four equally spaced copper-constantan thermocouples were installed vertically at five locations in each pavement to measure temperature at depths of 25 mm (1.0 in.), 95 mm (3.7 in.), 160 mm (6.3 in.) and 230 mm (9.0 in.) below the PCC slab surface.

Two types of strain gauges were installed in the slabs to measure concrete strain. *Geokon VCE 4200* vibrating wire strain gauges were mounted 25 mm (1 in.) from the top and bottom of the end slabs along the centerline to monitor environmental strain caused by changing temperature and moisture in the slabs. *TML PMR-60* three-axis rosettes were mounted 25 mm (1 in.) from the top and bottom of the middle slabs to measure dynamic strain generated by a falling weight deflectometer (FWD) and the rolling test wheel. Eight *Schaevitz 121–500 DC* LVDTs were placed along each pavement edge to measure vertical deflection from environmental and dynamic effects. Instrumentation installed in the two slabs is shown in Figures 1 and 2.

Table 1. Physical properties of PCC.

Parameter	Result
Unit weight (kg/m^3 [pcf])	2,300 (143.6)
Poisson's ratio	0.22
Compressive strength (MPa [ksi])	
2-day	13.6 (1.97)
7-day	30.5 (4.43)
14-day	32.9 (4.77)
28-day	37.3 (5.41)
391-day	49.9 (7.24)
Modulus of rupture (MPa [ksi])	
28-day	3.6 (0.52)
Young's modulus (MPa [ksi])	
2-day	16,000 (2,320)
7-day	21,300 (3,085)
28-day	23,500 (3,415)

2.2.2 *Data acquisition*

Air temperature, relative humidity, and VCE 4200 vibrating wire strain gauges in the end slabs were monitored at 30-minute intervals throughout all phases of testing with *Campbell-Scientific CR10* data-loggers. The uniaxial dowel bar strain gauges LVDTs and thermocouples were monitored every 30 minutes during curing and temperature cycling with a *Campbell-Scientific CR7* data-logger. During dynamic load tests with the rolling wheel and the FWD, an *Optim Electronics Megadac 5108AC* data acquisition system was used to record responses of the uniaxial strain gauges and rosettes on the dowel bars, LVDTs along the slab edges, and PMR-60 rosettes in the concrete slabs at a rate of 1,200 samples per second per sensor.

2.2.3 *Dipstick®*

A *Dipstick®* 2000 was used to obtain slab profiles by measuring vertical elevations to a thousandth of an inch at 300 mm (12 in.) intervals. Slab profiles were monitored periodically along a fixed traverse to determine the environmental response of the pavement during curing and temperature changes. The traverse, consisting of a rectangle 3.4 m (11 ft.) by 4.3 m (14 ft.) and one diagonal across the rectangle, was drawn on the middle slab of both pavements (Figure 3).

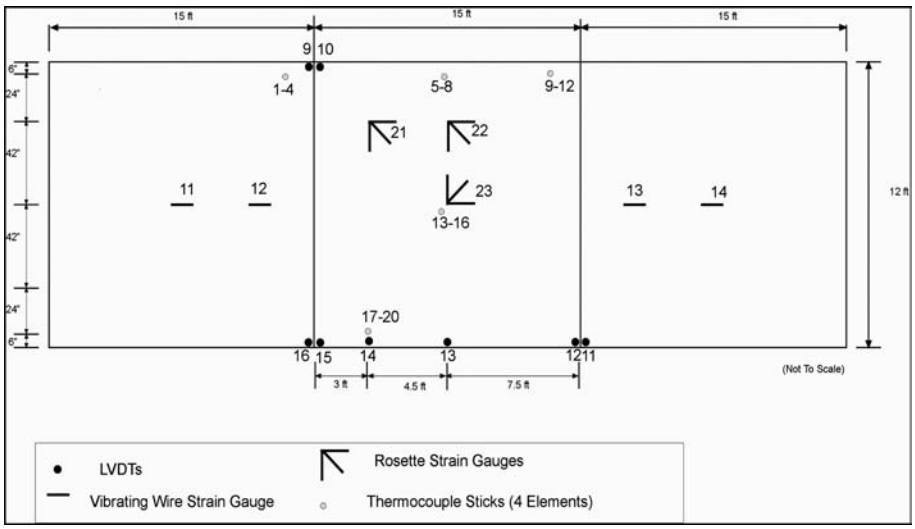

Figure 1. Undowelled slab instrumentation.

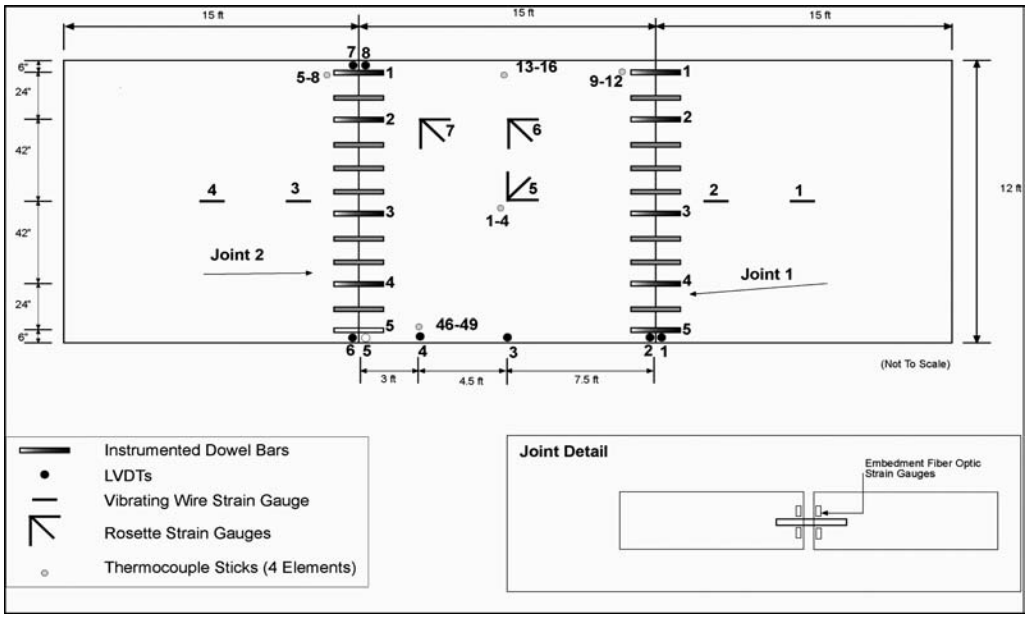

Figure 2. Dowelled slab instrumentation.

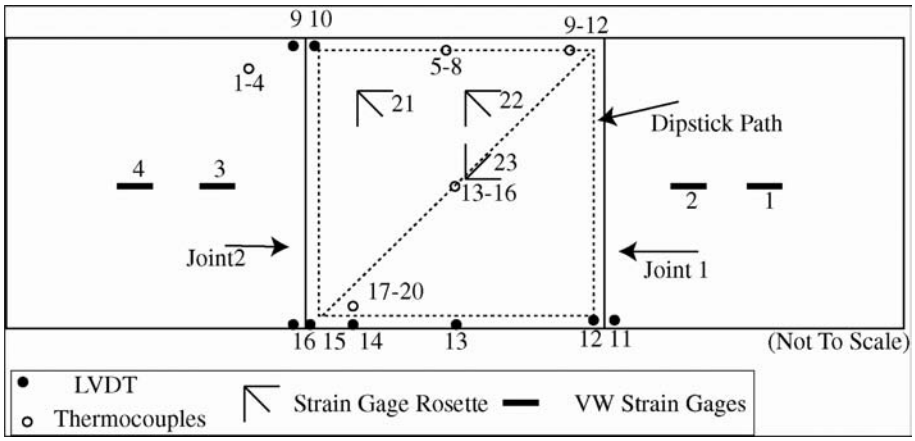

Figure 3. *Dipstick*® path on pavement.

3 ENVIRONMENTAL RESPONSE

Data analysis of the environmental response of the test pavements was measured during curing at constant air temperature and as air temperature changed after curing. Thermocouples were used to measure concrete temperature at different depths and locations in the slabs. LVDTs and the *Dipstick*® profiler were used to measure slab elevations, and strain gauges were used to measure strain in the concrete slabs and on the dowel bars during various induced environmental conditions.

3.1 *Curing under constant temperature*

3.1.1 *Slab temperature*

Slab heating during hydration

Temperatures at the center of the middle dowelled slab during the first five days after concrete placement are shown in Figure 4. The highest slab temperatures occurred approximately 15 hours after placement of the concrete and the maximum temperature difference measured between two thermocouples in the slab was approximately 4°C (7.2°F), which is moderate compared to gradients often observed in the field. During

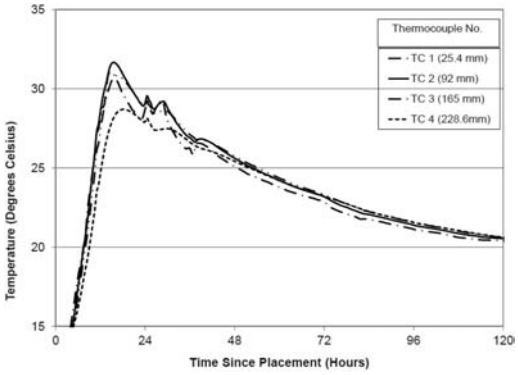

Figure 4. Initial temperature at center of the doweled slab at various depths as a function of time.

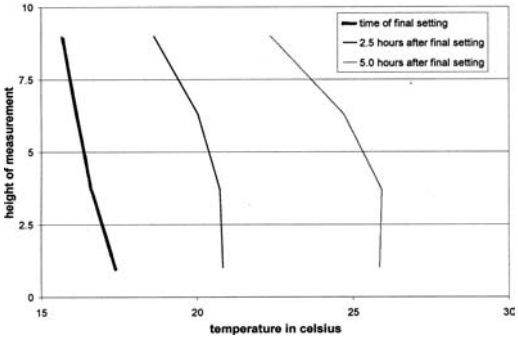

Figure 5. Temperature distributions in center of slab after final set.

hydration, the temperature gradients were nonlinear and fluctuations observed 24 hours after concrete placement were caused by changes in room temperature as the doors were opened for placement of the undowelled pavement section. After five days, the concrete and air temperatures were about the same and the temperature gradients in the slabs were essentially zero.

Temperature increases caused by concrete hydration varied between the corner and middle of the dowelled slabs. Differences in slab temperature at the two locations were approximately 2C° (3.6°F), which again is small compared to observations in the field. The temperature of newly placed slabs is affected by mix temperature, base temperature, and air temperature, hydration properties of the concrete, wind and solar radiation.

Determination of final set time

Generally, initial concrete set occurs when the heat of hydration causes concrete temperature to begin to rise, and final set occurs when concrete changes from a fluid to a rigid state. In accordance with Comité Euro (1993), initial and final concrete set times in minutes are related as follows:

$$\text{Final set time} = 90 + 1.2 \times \text{initial set time} \qquad (1)$$

On this project, final set time was used for monitoring the vibrating wire strain gauges.

Concrete was placed in the dowelled pavement at approximately 8:00 AM. The heat of hydration caused the temperature to begin rising at about noon, making the initial set time four hours; the final set time was determined to be 6.3 hours after placement, using Equation 1.

Temperature gradients

Slab temperatures measured in the dowelled and undowelled slabs were relatively similar, therefore conditions in the dowelled slab are considered to be representative of both sections in this study. Slab temperatures were higher on the bottom than on the surface during curing, thereby indicating a negative built-in gradient. Figure 5 shows temperature distributions in the slab center at the final set time, and at 2.5 and 5.0 hours afterwards.

3.1.2 *Slab shape*

Temperature and moisture gradients and concrete shrinkage are the main causes of slab deformation. Immediately after placement, fluidity of the green concrete allows it to flow as it expands with increasing temperature during early hydration. As the concrete changes from a fluid to a rigid state at the time of final set, it assumes a zero-stress state (Neville, 1997; Shah, 1998) dictated largely by internal environmental gradients generated within the concrete mix to that point in time. These gradients are, of course, affected by external environmental conditions imposed on the concrete during the cure period. All subsequent temperature associated stresses must be related to the zero-stress temperature gradient. Strength then increases rapidly in the concrete, and internal stresses develop as further temperature and moisture changes, and shrinkage of the concrete mix cause the concrete slab to alter its shape. When tensile stresses in the concrete exceed the tensile strength of the concrete, transverse cracks will appear and stresses elsewhere in the slab will be reduced. Transverse joints are sawed in the concrete before these cracks appear to control transverse cracking.

Joints were cut in the test pavements at approximately 10 hours test time, or four hours after final set. The temperature gradient at that time was assumed to be the zero-stress temperature gradient. Since the temperature gradient in the slab approaches zero as the heat of hydration dissipates, deformation from final set is downward curling. The magnitude of this temperature related deformation cannot be measured directly since shrinkage is occurring simultaneously.

Dipstick® data

Shrinkage causes upward warping as moisture is lost primarily from the top of the slab (Khan, 1997). In this test, slabs were cured under a constant temperature of 21°C (70°F). Thus, all changes in slab curvature after the slab temperature became uniform were caused by warping. The zero-stress gradient only defined the initial conditions for the warping process. Figure 6

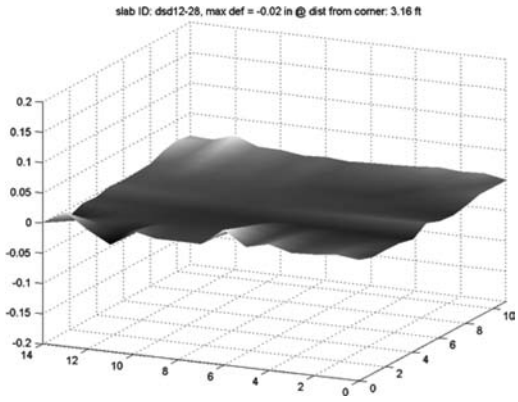

Figure 6. Dowelled slab shape after 1 week (x and y axis [ft.], z-axis [in.]; 1 in. = 25 mm, 1 ft. = 300 mm).

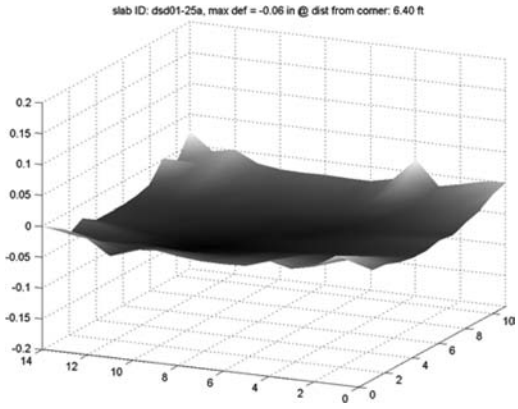

Figure 7. Dowelled slab shape after 5 weeks (x and y axis [ft.], z-axis [in.]).

through Figure 9 show typical slab deformation measured with the *Dipstick*® after one and five weeks for the dowelled and undowelled sections, respectively. The undowelled slab appeared to have a smoother shape than the dowelled slab. After five weeks, differences in elevation between the deepest point in the center and the highest corner were approximately 1.5 mm (59 mil) for both sections.

LVDT data

LVDT data presents a somewhat clearer description of the warping process. In general, the magnitudes of the *Dipstick*® and LVDT deflections were in agreement. The LVDT data, however, showed more corner deflection in the undowelled section than in the dowelled section. LVDTs were set in six corners of the undowelled and dowelled slabs as shown in Figures 1 and 2, respectively.

Figure 10 shows the rise of the corners in the dowelled section with data points for all six sensors and an average reading, while Figure 11 shows the same data for the undowelled section. These data indicate greater warping in the undowelled section where the corners

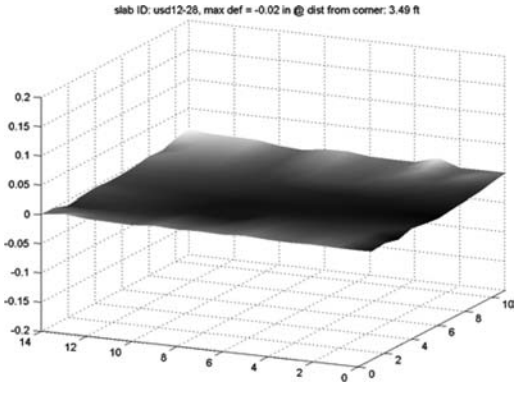

Figure 8. Undowelled slab shape after 1 week (x and y axis [ft.], z-axis [in.]).

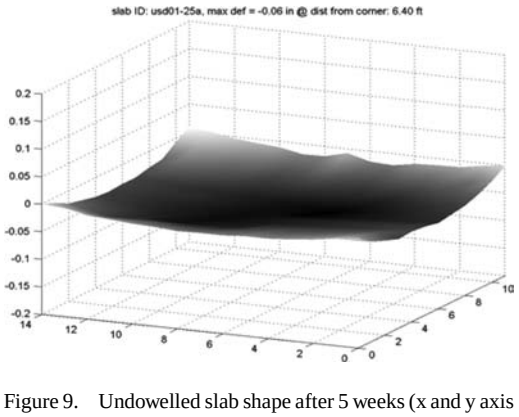

Figure 9. Undowelled slab shape after 5 weeks (x and y axis [ft.], z-axis [in.]).

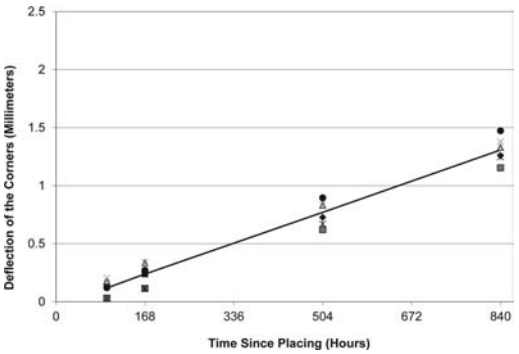

Figure 10. Deflection of the dowelled slab during the first five weeks (1 mm = 39 mil).

rose about 0.4 mm (16 mil) more than the dowelled section to an average of 1.7 mm (67 mil) after five weeks. The dowel bars appeared to reduce the amount of warping and improve the uniformity of corner deflections. It is interesting to note that in both sections deflection continued to increase steadily and showed no sign of slowing after five weeks.

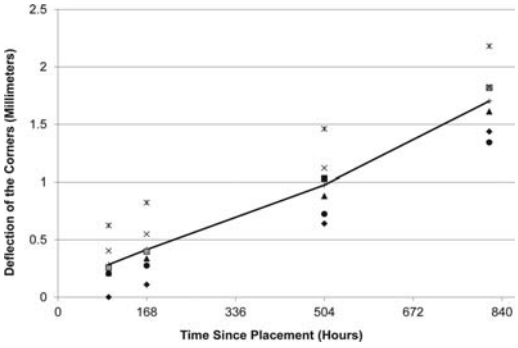

Figure 11. Deflection of the undowelled slab during the first five weeks (1 mm = 39 mil).

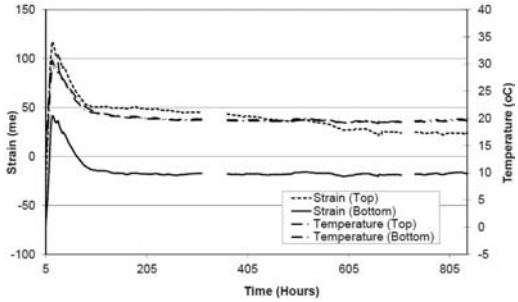

Figure 12. Strain development at center of the dowelled slab.

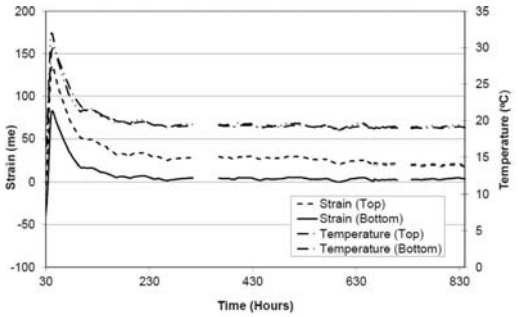

Figure 13. Strain development at center of the undowelled slab.

3.1.3 *Strain data*

Geokon Vibrating Wire Model 4200 strain gauges were installed during concrete placement at the center and third points of the outside slabs on both sections to measure longitudinal strain approximately 25 mm (1 in.) from the top and bottom of the slabs. Figure 12 and Figure 13 show strain in the slab center of the dowelled and undowelled sections respectively with the temperature gradient. The readings for comparable gauges in each section were very similar; discontinuities in the lines reflect missing data.

The gauges were zeroed about the time of final set (t = 6.3 hrs. and t = 30 hrs), thereby making the measured strains shown in Figures 12 and 13 relative to that point in time. In the first hours after final set, the gauges measured increasing positive strain (i.e., continued slab expansion due to heat of hydration). As the heat of hydration dissipated, reduced tensile strain indicated slab contraction, but friction at the pavement/base interface resisted the contraction and generated tensile forces in the slab. Joints were sawed in the slabs approximately 10 hours after placement to control transverse cracks that would develop when these internal tensile forces exceeded the tensile strength of the curing concrete mix. The presence of these external constraints affected slab movement and strain being monitored by gauge response.

Strain gauges near the top and bottom of the slabs behaved differently due to temperature and moisture gradients in the slabs, and bottom friction. Hydration temperatures were routinely higher on the slab bottom because of insulation from the lower air temperatures. Similarly, moisture was higher in the slab bottom because of surface evaporation into the air. Friction at the pavement/base interface retarded horizontal slab movement from environmental effects. After the heat of hydration dissipated in a few days, the bottom strain stabilized, but the top strain continued to drop as moisture continued to evaporate, causing an upward warping of the slab edges. Figures 10 and 11 show this warping to continue for at least five weeks. Because the dead weight of the slabs opposed this upward warping, slab deformation was less than expected for free shrinkage (Nagy, 1997). The differences between top and bottom strain suggest that slabs had greater curvature at the one-third point than at the center.

3.2 *Environmental response to temperature changes*

The eight-week long environmental response testing included a period of curing under constant temperature, which lasted approximately five weeks, and a period of controlled temperature changes, which lasted approximately three weeks. Temperature was first increased after 840 hours test time on the dowelled section. Since the undowelled section was placed one day later than the dowelled section, the time of the temperature increase began at 816 hours test time on the undowelled pavement.

3.2.1 *Temperature data*

After five weeks of curing under constant temperature, temperature changes were applied to both concrete sections, as follows: air temperature was increased from 20°C (68°F) to 35°C (95°F) for one week, decreased to 22°C (72°F) for three days, decreased further to 5°C (41°F) for three days and, finally, returned to 21°C (70°F).

The negative gradient of −6°C (−11°F) observed during this test was similar to maximum slab gradients measured in the field. In an annual distribution of hourly temperature gradients, this maximum negative gradient occurs less than 10 percent of the time.

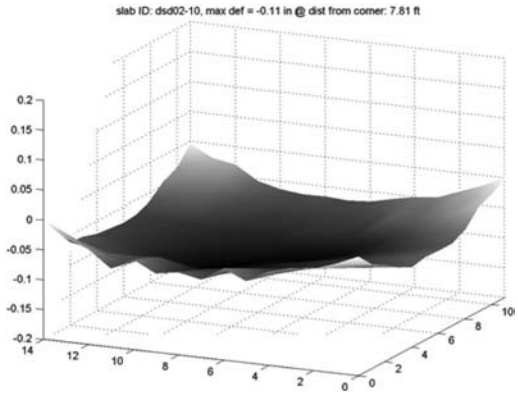

Figure 14. Slab profile at greatest negative gradient; dowelled section (x and y axis [ft.], z-axis [in.]).

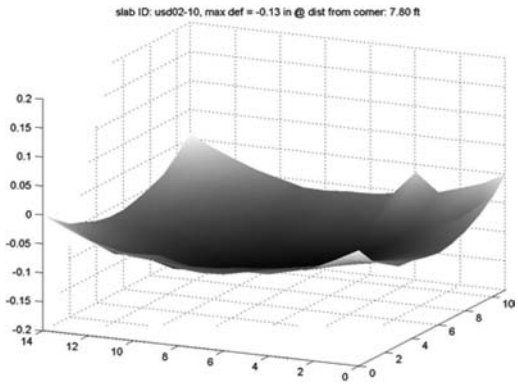

Figure 15. Slab profile at greatest negative gradient; undowelled section ((x and y axis [ft.], z-axis [in.]).

The positive gradient of $+6°C$ ($+11°F$) is a moderate value, in that gradients of $+6°C$ ($+11°F$) to $+12°C$ ($+22°F$) occur approximately 15 percent of the time in an annual distribution (Comité Euro, 1990; Khan et al., 1995).

3.2.2 *Slab shape*

Dipstick® data

The *Dipstick*®2000 was used to obtain slab profiles during the various temperature conditions. As stated earlier, however, LVDTs provide more precise measurements of slab deformation. The greatest slab deflection was observed at the $-6°C$ ($-11°F$) gradient. The slab profiles of the dowelled and undowelled sections, as measured with the *Dipstick*, are shown in Figures 14 and 15, respectively. The undowelled profile shows a slightly greater deflection than the dowelled section.

LVDT data

LVDTs mounted along the slab edges measured pavement curling resulting from positive and negative temperature gradients. Corner readings of LVDTs 9, 10, 11, 12, 15 and 16 on the dowelled and undowelled sections are shown in Figures 16 and 17, respectively.

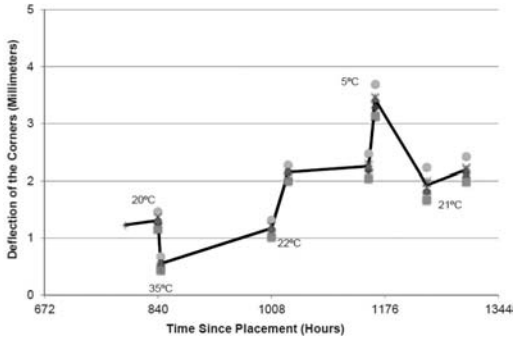

Figure 16. LVDT measurements of corner deflections during temperature cycling; dowelled section (1 mm = 39 mil).

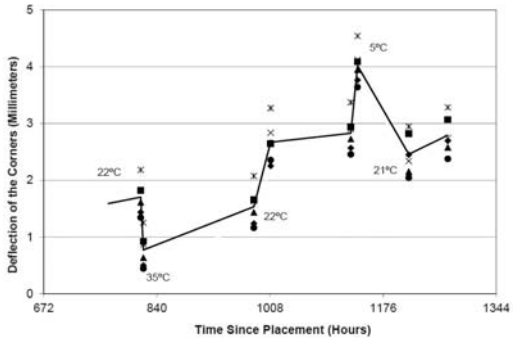

Figure 17. LVDT measurement of corner deflections during temperature cycling; undowelled section (1 mm = 39 mil).

The presence of dowel bars reduced slab edge deflection during changes in temperature, with the amount of curling being smaller in the dowelled section. The greatest deflection in the undowelled section occurred at 1,162 hours test time and was almost 4 mm. This was approximately 0.5 mm more than in the dowelled section.

The slab edges on both pavements continued to rise during periods of constant temperature. This suggests that upward warping continued as moisture was lost from the pavement surface. The variation in corner deflections was higher in the undowelled section than in the dowelled section and, the corners did not move simultaneously. Corners neither stayed in the same order nor did the difference in elevation between the points remain constant.

Furthermore, due to the aggregate interlock, the deflections in the undowelled slabs were more prominent during periods of cooler temperature gradients compared to the warmer temperatures. The effect of temperature gradient on pavement deflection during temperature cycling is illustrated best by plotting the average corner deflection versus temperature gradient. This relation for the undowelled section is shown in Figure 18.

Figure 18 shows the average corner LVDTs (9, 10, 11, 12, 15, and 16) versus the temperature gradient for the period between 800 hours and 1,300

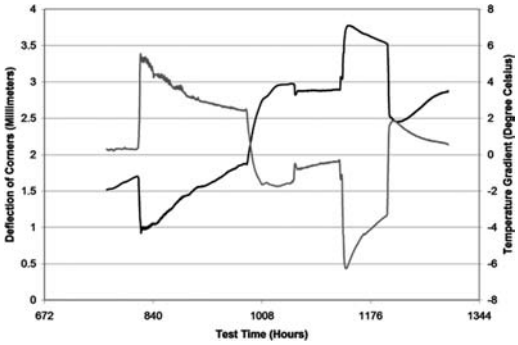

Figure 18. Average LVDT deflection reading (lower curve at left) vs. temperature gradient (upper curve at left); undowelled section (1 mm = 39 mil, 1°C = 1.8F°).

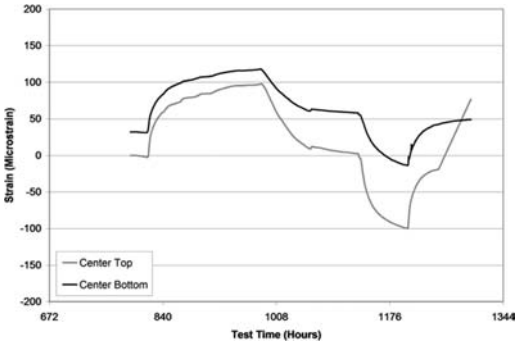

Figure 19. Strain readings during temperature change at center of undowelled slab.

hours, and demonstrates the gradient based curling of the pavement. However, it is also apparent that the corner deflections measured during the periods of temperature change were not solely driven by gradient. Although the gradient after approximately 1,300 hours was similar to the gradient after approximately 800 hours, the corner deflections differed significantly. In addition to the temperature gradient, two other influences affected slab curvature. The first influence is continuous warping caused by ongoing moisture loss in the upper portion of the pavement during temperature changes. The second is aggregate interlock at the slab joints, which tends to restrain slab warping, especially at higher temperatures.

3.2.3 *Strain data*

Vibrating wire strain gauge readings in the undowelled section during the temperature changes are shown in Figure 19. In general, strain in the slab is indicative of slab curling.

3.2.4 *Forensic studies*

At the conclusion of testing, two forensic experiments were performed on the dowelled section to evaluate slab condition. First, rosette gauges in the center slab were monitored as one joint was sawed to the top of the dowel bars to remove aggregate interlock above the

Figure 20. Cutting of doweled slab at contractor's yard.

bars. Plywood was installed vertically during placement of the concrete to eliminate aggregate interlock below the bars and the joints were sawed to a depth of 75 mm (3 in.) to facilitate cracking through the remaining slab thickness. The new saw cut was made to remove all interlock above the dowel bars. Any change in strain during the sawing would be indicative of how interlock above the bars affected internal slab stresses. The longitudinal legs of rosettes at the center of the slab recorded a reduction of about 200 $\mu\varepsilon$ as the joint was sawed. Strain in the transverse direction remained essentially unchanged as the joint was cut.

In the second experiment, a piece of intact concrete at a dowelled joint containing concrete from both sides of the joint and two dowel bars was removed and taken to the ORITE laboratory for examination. Figure 20 shows the cutting process and Figure 21 shows the pulled dowel bar. After removing the dowel bars from the concrete, the holes were measured with a micrometer and determined to be approximately 0.25 mm (10 mil) larger in diameter than the dowel bars. This difference in hole and bar diameters likely occurred soon after concrete placement as stresses generated in the bars during early slab warping caused the green concrete surrounding the bars to deform. As a result of this looseness, load transfer was lost across the joints and stresses were reduced in the slabs.

4 LOAD RESPONSE

4.1 *Slab response to falling weight deflectometer loads*

ODOT performed nondestructive testing on the test slabs with an FWD at three times when the pavement temperature was relatively uniform at 11°C (52°F), 22°C (71°F) and 30°C (86°F). Figure 22 shows the average effects of temperature on deflection under the load plate (Df1) and load transfer on the two joints of the dowelled pavement, while Figure 23 shows similar data on one undowelled joint. Theoretically, there should not have been any temperature effects on the undowelled sawed joint, since the width of

Figure 21. Dowel bar removed from the joint socket.

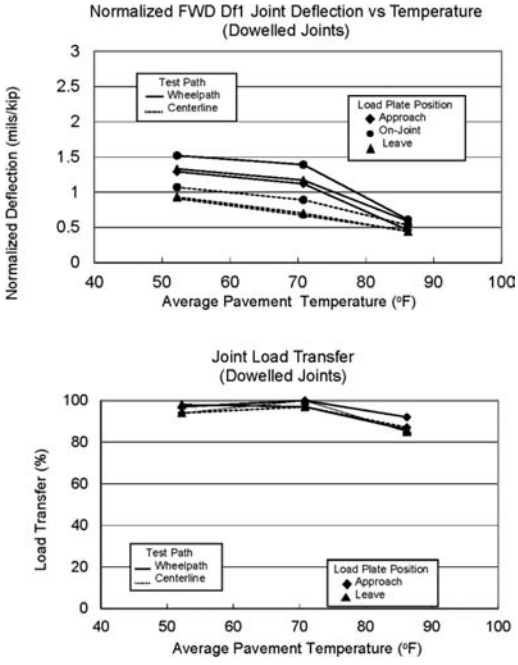

Figure 22. Normalized load plate deflection (top) and load transfer (bottom) vs. temperature at dowelled joints (1 mil/kip = 5.7 mm/MN; 52°F = 11°C, 71°F = 22°C, 86°F = 30°C).

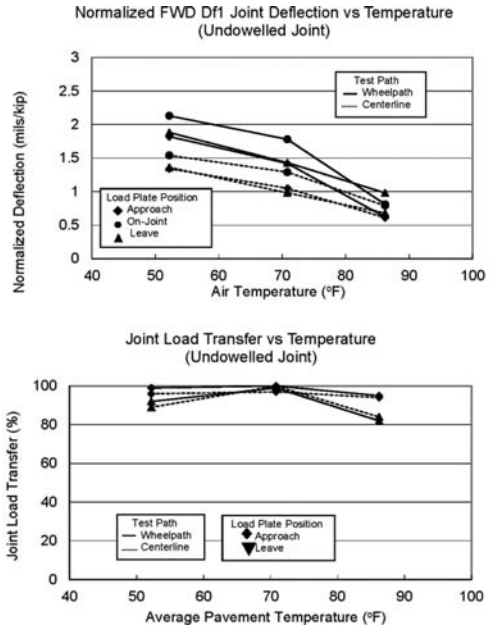

Figure 23. Normalized load plate deflection (top) and load transfer (bottom) vs. temperature at undowelled joints.

the saw cut was sufficient to prevent contact between adjacent slabs at the three test temperatures. An examination of the joint, however, revealed that much of the slurry created during the full-depth sawing of the joint remained in the joint and, upon hardening as it dried out, provided a mechanism for transferring vertical shear forces across the joint.

4.1.1 *Falling weight deflectometer analysis*

The following observations were made from the FWD analysis:

1. FWD deflection at slab ends decreased with increasing air temperature. This was likely due to temperature gradients existing in the pavements at the time of the measurements, and increased aggregate interlock at the joints. When the surface of the slab was cooler than the bottom, the slab edges tended to curl up away from the base, thereby reducing support and increasing deflections. Conversely, when the surface was warmer than the bottom, the slab edges curled downward against the base and negated some of the warping from reduced surface moisture.
2. Deflection in the wheel paths was higher than deflection along the slab centerline at the 11°C (52°F) and 22°C (71°F) temperatures, and about the same as the centerline at the 30°C (86°F) temperature. This trend also can be explained by slab curling resulting from temperature gradients in the slab.
3. Deflections were lower at the dowelled joints than the undowelled joint. This is consistent with the

mechanisms in place to transfer shear to adjacent slabs (e.g., dowel bars, aggregate particles and hardened slurry).

4. Load transfer in the dowelled and undowelled joints was high at all temperatures, again indicating good mechanisms were in place to transfer shear. Load transfer in the sawed undowelled joints increased significantly with temperature, indicating a compression of the hardened slurry as the slabs expanded.

5 CONCLUSIONS

From data collected on this project, it was found that slab temperature gradients were moderate during the curing period because of constant room temperature. After the heat of hydration had dissipated, slab temperature gradients approached zero. LVDT data indicated that the amount of warping on undowelled slabs was much greater and more erratic than on the dowelled slabs. Curvature was greatest at the one-third point of the slab, rather than at the center of the slab. As slab temperature gradients changed, the undowelled section had greater deflection than the dowelled section. Corner deflection increased with time during the period of constant temperature. Because built-in curling can be reduced but not overcome or eliminated by positive temperature gradients, permanent loss of support occurred. Dowels restrained joint movement, thus reducing the amount of curling. Therefore, dowel bars not only transferred load but also reduced loss of support. The forces in the dowel bars were not as large as expected from reports of previous investigations, particularly during the curing process. The reason is that during the curing process, the stiffness of the dowel bar forced an increase in the diameter of the hole.

REFERENCES

Bissonnette, B. and Pigeon, M. 1995. Tensile creep at early ages of ordinary, silica fume and fiber reinforced concretes. *Cement and Concrete Research, Vol. 25 (5).*

Comité Euro-International du Béton 1993. *CEB-FIB Model Code 1990. Design Code.*

Eisenmann, J. and Leykauf G. 1990. Simplified Calculation Method of Slab Curling Caused by Surface Shrinkage. *6th International Symposium on Concrete Roads*, Madrid.

Khan, A.A., Cook, W.D. and Mitchell, D. 1995. Early Age Compressive Stress-Strain Properties of Low-, Medium, and High-Strength Concretes. *ACI Mater. J. 92 (6).*

Khan, A.A., Cook, W.D. and Mitchell, D. 1997. Creep, Shrinkage, and Thermal Strains in Normal, Medium, and High-Strength Concretes during Hydration. *ACI Mater. J. 94 (2).*

Nagy, A. 1997. Determination of E-Modulus of Young Concrete with Nondestructive Method. *Journal of Materials in Civil Engineering, Vol. 9, No.1.*

Neville, A.M. 1997. Properties of Concrete. John Wiley & Sons, NY.

Sargand, S., Edwards, W. and Khoury, I. 2003. *Evaluation of Forces in Dowel Bars under Controlled Conditions.* Final report for U.S. Department of Transportation and Federal Highway Administration. Athens, OH: Ohio Research Institute for Transportation and the Environment.

Shah, S. 1998. Shrinkage Cracking of Restrained Concrete Slabs. *Journal of Engineering Mechanics, Vol. 124, No. 7.*

Springenschmid, R. and Fleischer, W. 1990. Effects of Temperature and Moisture on Concrete Pavements. *6th International Symposium on Concrete Roads, Madrid.*

Zachlehner, A. 1990. Restraint Stresses in Young Concrete Pavements. *6th International Symposium on Concrete Roads*, Madrid.

This page intentionally left blank

Advances in Pavement Design through Full-scale Accelerated Pavement Testing – Jones, Harvey, Mateos & Al-Qadi (Eds.)
© 2012 Taylor & Francis Group, London, ISBN 978-0-415-62138-0

Study of failure mechanisms in rubblized concrete pavements with hot mix asphalt overlays

N. Garg & G.F. Hayhoe
FAA Airport Technology Research and Development Branch, Atlantic City, New Jersey, US

L. Ricalde
Especialista Regional de Aeródromos y Ayudas Terrestres, OACI/ICAO South American Office, Lima, Peru

ABSTRACT: Full-scale traffic tests were completed on three rubblized rigid airport pavements overlaid with 5 in. (130 mm) of hot-mix asphalt at the FAA's National Airport Pavement Test Facility. Initially, the overlaid pavements were trafficked with a four-wheel landing gear (with wander) and 55,000-lbs (25-tonne) wheel load. No significant distresses were observed during the 5,000 passes, after which the wheel load was increased to 65,000 lbs (29.5 tonnes) and a six-wheel landing gear was used for testing. The rubblized concrete pavement on conventional base section (MRC) exhibited complete structural failure. The rubblized concrete on subgrade (MRG) section exhibited severe structural deterioration at the end of trafficking, but retained sufficient structural capacity to support the applied load. The rubblized concrete over econocrete base section (MRS) did not exhibit severe structural deterioration at the end of trafficking. Four trenches were opened perpendicular to the centerline of the test sections to conduct post-traffic investigation into the failure mechanism of the pavement structure. The trenching included testing for layer characterization (plate load tests, California Bearing Ratio tests, in situ densities, moisture contents, layer profile measurements, and visual evaluations) and removal of each pavement layer to reveal the subgrade interface and subsequent subgrade layers below. This paper summarizes the results from the post-traffic tests. The performance of the MRS test section suggests that rubblized concrete pavements with HMA overlay are a viable option on commercial airports. The results from post-traffic tests were useful in providing insight into the failure mechanism of rubblized concrete pavements.

1 INTRODUCTION

Rubblization of deteriorated concrete pavements is becoming a popular method of pavement rehabilitation because of its ability to prevent reflective cracking, and it being a cost-effective means of converting an existing failed or failing pavement into a superior base, thereby eliminating the expense of removal and replacement. The rubblized concrete layer behaves as a tightly keyed, interlocked, high-density unbound base. A number of airfield projects have used rubblization as a pavement rehabilitation technique (Buncher and Jones, 2006). The projects range from heavy-load military airfields to local general aviation (GA) airfields. Engineering Brief (EB) 66 (Airport Engineering Division, 2004) summarizes the guidelines for rubblized portland cement concrete (PCC) base courses. These guidelines are based on industry experience and although they provide interim guidance, full-scale testing is still needed to develop design standards. To study the performance of rubblized concrete pavements with hot-mix asphalt (HMA) overlays under heavy aircraft loading, three rigid airport pavement test sections (MRC, MRG, and MRS) at the FAAs National Airport Pavement Test Facility (NAPTF) with 12-in. (305-mm) thick concrete slabs on different support systems (slab on crushed stone base, slab on grade, and slab on stabilized base) were rubblized with a resonant pavement breaker and overlaid with 5 in. (127 mm) of P-401 HMA. The rigid pavements had been trafficked to complete failure, prior to rubblization, using dual-tandem and triple dual-tandem landing gear configurations at wheel loads of 55,000 lbs (25 tonnes). All three test sections were constructed on medium strength (California Bearing Ratio [CBR] $\approx$ 7–8) clay subgrades. The overlaid pavements were subjected to full-scale accelerated traffic loading until complete structural failure was attained. This was the first full-scale, accelerated pavement testing study conducted on rubblized concrete pavements with HMA overlays under heavy aircraft loading.

Four trenches were opened perpendicular to the centerline of the test sections to conduct post-traffic investigation into the failure mechanism of the pavement structure. The trenching included testing for layer characterization (plate load tests, CBR tests, in situ densities, moisture contents, layer profile measurements, and visual evaluations) and removal of each pavement layer to reveal the subgrade interface and subsequent subgrade layers below.

2 OBJECTIVES

The objectives of this research were to:

- Study the performance of rubblized concrete pavements with HMA overlays under heavy aircraft loading.
- Study the post-traffic trench results and failure mechanism of rubblized concrete airport pavements.
- Provide guidance for the characterization of rubblized concrete layers in the pavement thickness design procedure.

This paper summarizes the results from the post-traffic tests and provides some insight into the failure mechanism of rubblized concrete airport pavements.

3 NATIONAL AIRPORT PAVEMENT TEST FACILITY

The NAPTF is an indoor test facility located at the Federal Aviation Administration's (FAA) William J. Hughes Technical Center, Atlantic City International Airport, New Jersey. It is used to generate full-scale pavement response and performance data for development and verification of airport pavement design criteria. It is a joint venture between the FAA and the Boeing Company and became operational on April 12, 1999. The test facility consists of a 900-ft. (274.3-m) long by 60-ft. (18.3-m) wide test pavement area, embedded pavement instrumentation and a dynamic data acquisition system, environmental instrumentation and a static data acquisition system, and a test vehicle for loading test pavements with up to 12 aircraft tires at wheel loads of up to 75,000 lbs (34 tonnes). Additional information about the test facility is available elsewhere (*www.airport-tech.tc.faa.gov*). A construction cycle (CC) at the NAPTF involves test pavement construction, including instrumentation, traffic tests to failure, post-traffic testing (includes trenching activities and other tests), and pavement removal.

4 PAVEMENT STRUCTURES

Three rigid pavement test sections were constructed and tested during CC2 at the NAPTF. Each test section was 75 ft. long by 60 ft. wide (22.9 m by 18.3 m) with twenty 15- by 15-ft. by 12-in.-thick concrete slabs (4.6 m by 4.6 m by 30 cm). The slabs were doweled in both the transverse and longitudinal directions. The MRG test section was built directly on the subgrade, MRC was built on a crushed aggregate base on top of the subgrade, and MRS was built on an econocrete base over a crushed aggregate subbase. Each test section was separated into two 30-ft. wide traffic lanes, north and south. Construction was completed in April 2004. Detailed information on the design and construction characteristics of the pavement structures can be found in (Ricalde and Daiutolo, 2005). Traffic testing was completed in December 2004. More details about traffic tests and post-traffic tests on CC-2 test sections can be found elsewhere (Hayhoe and Garg, 2006). The structural condition index (SCI) of all the rigid pavement test sections, in both traffic lanes, was less than 20 (shattered slab condition) at the end of trafficking. However, most of the cracks were tight, with none rated worse than low severity. A detailed explanation on SCI computation and slab condition is given in (Brill, et al., 2005).

In January 2005, all the concrete slabs in the north traffic lane were rubblized with an RMI RB-500 resonant breaker operating at 44 Hz. In June 2005, the rubblized pavement was lightly wetted, rolled with a vibratory steel drum roller, and overlaid with 5 in. (127 mm) of P-401 HMA. Figures 1a and 1b show the vibrating foot of the resonant breaker and the test pavement surface after rubblization.

The pre-traffic test pits showed that the rubblization process induced cracks/fractures over the entire depth of the slabs and that the cracks were tightly held (Hayhoe and Garg, 2006). Figure 2 shows the pavement cross sections after the placement of the HMA overlay.

P-401, P-306, and P-154 are FAA standard specifications (Airport Engineering Division, 2005) for HMA surface, econocrete base, and uncrushed aggregate subbase (crushed aggregate screenings were used at NAPTF), respectively.

a. Rubblizing north traffic lane with resonant breaker.

b. Rubblized on left (north), as-trafficked on right (south).

Figure 1. Rubblized concrete pavement test sections at NAPTF.

5 TRAFFIC TESTS AND PAVEMENT PERFORMANCE

The traffic tests were started with a four-wheel, dual-tandem configuration (dual spacing of 54 in. [137 cm] and tandem spacing of 57 in. [145 cm]) on both traffic lanes. Wheel load was set at 55,000 lbs (25 tonnes) because this was the load applied to the original CC2 test sections, and although badly cracked at the end of trafficking, all the test sections were capable of structurally supporting the loads applied. Heavyweight deflectometer (HWD) tests were performed using the FAAs HWD equipment on a 10-ft. grid to study the uniformity of the pavement structures. The results showed that the pavement structure within each test section was fairly uniform (coefficient of variation less than 25 percent). MRC showed the highest deflections, followed by MRG, and then MRS. This order was counter to expectations because MRC had a crushed aggregate subbase and would normally be expected to have a higher stiffness than the MRG pavement built directly on the subgrade. Pretraffic measurements of subgrade strength in test pits excavated for material characterization showed that water had migrated from the crushed aggregate subbase into the subgrade of the MRC section and softened the top three or so inches. The CBR at the surface of the subgrade in the MRC test pits was four, whereas at 12 in. below the surface it was approximately eight. The subgrade CBR in the MRG and MRS test pits ranged from seven to eight, as constructed. The order of failure of the rubblized test sections also followed the order of the HWD deflection magnitudes. A detailed discussion on the HWD test results is presented elsewhere (Garg and Hayhoe, 2007).

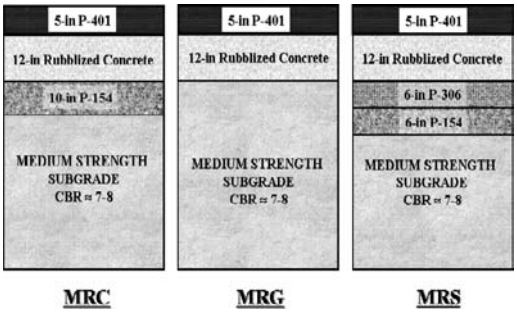

Figure 2. CC2 overlay pavement test sections (1 in. = 25 mm).

Trafficking started on July 7, 2005, and continued until October 6, 2005, following the schedule in Table 1. A fixed wander pattern was applied to the traffic during the tests. The wander pattern consisted of 66 repetitions, 33 traveling east and 33 traveling west. The transverse position of the gears was changed only at the start of the eastward repetitions. The wander pattern was designed to simulate a normal distribution with standard deviation of 30.5 in. (775 mm) (equivalent to a taxiway distribution for design). The distribution of the transverse wheel positions is not random, but consists of nine equally spaced wheel paths at intervals of 10.25 in (260 mm). Additional details about the wander pattern can be found elsewhere (Hayhoe et al., 2003). The temperature of the asphalt varied between 66°F and 85°F (19°C and 29°C) during the test period. The average temperature of the asphalt was about 78°F (26°C).

Traffic testing was continued until either structural failure occurred, or it was estimated that failure was unlikely to occur within a reasonable number of passes at the applied load. The failure criterion was the presence of at least 1.0 in. (25 mm) of surface upheaval adjacent to the traffic lane. This is the same as the criterion used by the U.S. Army Corps of Engineers in previous full-scale tests of flexible airport pavements and is indicative of shear failure in the subgrade. During the traffic tests, the test sections were monitored through a combination of visual surveys and nondestructive testing, including periodic straightedge rut depth measurements, surface profile measurements,

Table 1. Trafficking Schedule for CC2 Overlay Test Sections.

Dates (from-to)	Repetitions (from-to)	Test Sections Trafficked	Load on North Lane*	Load on South Lane*
07-07-2005 07/25/05	1 5,082	MRG-N, MRC-N, MRS-N MRG-S, MRC-S, MRS-S	4-wheel, 55,000lbs (25tonnes)	4-wheel, 55,000lbs (25tonnes)
07/26/05 08-12-2005	5,083 11,814	MRG-N, MRC-N, MRS-N MRG-S, MRC-S, MRS-S	6-wheel, 65,000lbs (29.5tonnes)	4-wheel, 65,000lbs (29.5tonnes)
08/15/05 08/18/05	11,814 14,256	MRG-N, MRC-NW**, MRS-N MRG-S, MRC-S, MRS-S	6-wheel, 65,000lbs (29.5tonnes)	4-wheel, 65,000lbs (29.5tonnes)
08/19/05 08/24/05	14,257 16,302	MRG-N, MRS-N MRG-S, MRC-S, MRS-S	6-wheel, 65,000lbs (29.5tonnes)	4-wheel, 65,000lbs (29.5tonnes)
09/13/05 10/06/2005	16,303 25,608	MRG-N, MRS-N MRG-S, MRS-S	6-wheel, 65,000lbs (29.5tonnes)	4-wheel, 65,000lbs (29.5tonnes)

*Cold, unloaded tire pressures: 220 psi (1.52 MPa) at 55,000 lbs (25 tonnes) and 260 psi (1.79 MPa) at 65,000 lbs (29.5 tonnes).
**After the localized failure in MRC-NE (northeast portion of the test section), only northwest portion (MRC-NW) of the test section was trafficked.

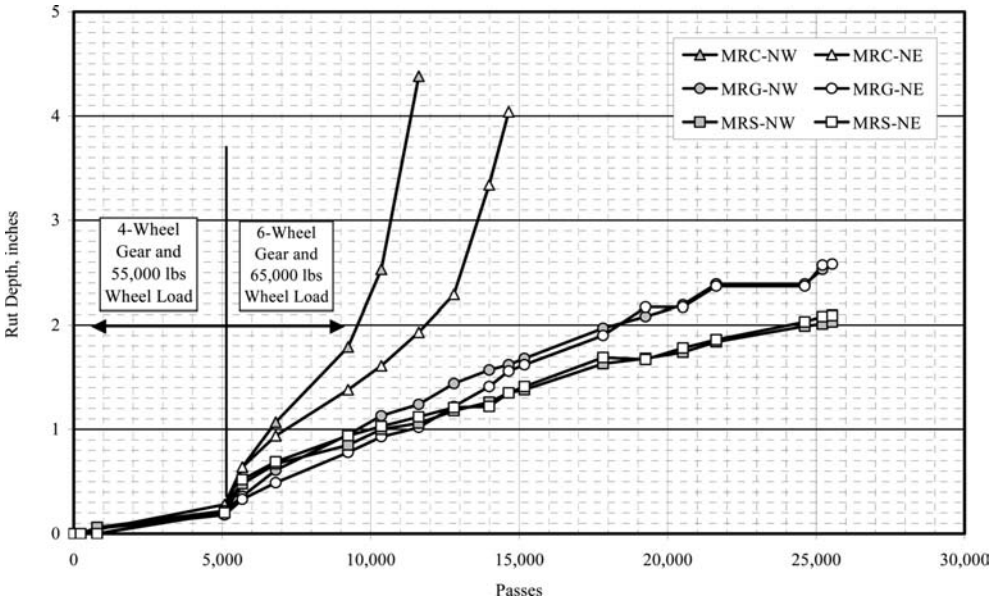

Figure 3. Rut depth measurements in rubblized concrete test sections (1 in. = 25 mm).

and HWD deflection measurements. A 16-ft. (4.8-m) long straightedge and laser profiler were used for rut depth measurements. In each test section, the rut depth and profile measurements were made at two different longitudinal positions located at one-third and two-thirds the distance into the test section. These locations were designated as NW and NE for the rubblized test sections (N stands for north side of the longitudinal centerline). Figure 3 shows the rut depth measurements during traffic tests (as computed from transverse surface profile measurements). All the test sections showed similar rut depths during the first 5,082 passes (55,000-lb wheel load, 4-wheel landing gear). Due to a minimal amount of distress (as shown in Figure 3), applied wheel loads were increased from 55,000 lbs (4-wheel dual-tandem landing gear) to 65,000 lbs (6-wheel triple-tandem landing gear). The 6- and 4-wheel configurations at increased loading both had the same dual and tandem spacings of 54 and 57 in. (137 and 145 cm), respectively.

After approximately 10,000 passes on the MRC section, 13,000 passes on MRG, and 15,000 passes on MRS, significant upheaval in the HMA layer at the longitudinal joints just outside the wheelpath was observed in the rubblized test sections. After these passes, the rut depth measurements (from straightedge) were exaggerated because the straightedge was resting on top of the upheaval outside the wheelpath. More accurate rut-depth measurements were computed from the surface profile measurements and are shown in Figure 3. Significant structural upheaval was also observed outside the wheel track in MRC-N, but neither the straightedge measurements nor the transverse profile measurements could separate the contributions of the underlying structural layers and the asphalt upheaval movement. Transverse trenches,

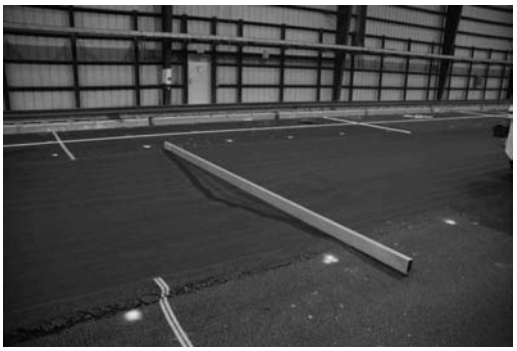

Figure 4. Pavement failure in the east end of the MRC rubblized test section.

were, therefore opened in the test sections so that transverse profiles of the structural layer interfaces could be measured. The NE end of MRC was the first area of the rubblized pavements to show signs of failure (Figure 4).

MRC-NW did not exhibit complete structural collapse as had MRC-NE. Trafficking on MRG and MRS was terminated after 25,608 passes. From a visual inspection at the end of trafficking, MRG-N appeared to have structural upheaval outside the wheel tracks, while MRS-N did not.

6 POST-TRAFFIC TESTS

Four trenches were dug in the rubblized test sections perpendicular to the centerline of test sections MRC (two trenches), MRG (one trench), and MRS (one trench) at the locations of the rut depth measurements

Table 2. Location of test trenches.

Section	Trench	Start Station (ft.)	End Station (ft.)
MRC	–	325	400
MRC	MRC-W	354	364
MRC	MRC-E	374	380
MRG	–	425	500
MRG	MRG	452	458
MRS	–	525	600
MRS	MRS	552	558

on the test pavements. The locations of the test sections and the trenches are summarized in Table 2.

The purpose of the trenches was to conduct post-traffic investigation into the failure mechanism of the pavement structure. The trenching involved removal of the P-401 HMA layer, the rubblized concrete layer, the P-209 crushed stone base and P-306 econocrete layer (in MRS), and the P-154 subbase layer (in MRC) to expose the subgrade interface and subsequent subgrade layers below. After removing the P-401 HMA surface, the rubblized concrete layer was exposed in all four trenches. Plate load tests (AASHTO Designation: T 222-81, 2000) were performed inside and outside the wheelpath on the surface of the rubblized concrete layer, and visual observations were made. Removal of the rubblized concrete layer exposed the P-154 surface in the MRC trenches, the subgrade surface in the MRG trench, and the P-306 econocrete base surface in the MRS trench. In the MRC trenches, plate load tests, CBR, and sand cone density measurements were taken on the surface of the P-154 layer. In the MRG trench (on the subgrade surface) the tests included CBRs, in situ density measurements (drive cylinder), and plate load tests. Only the plate load tests were performed on top of the P-306 econocrete layer in the MRS trench. After removing MRC P-154 subbase, CBRs and plate load tests were performed, and density measurements were taken on the subgrade surface. On the MRS section, the P-306 was removed to expose the P-154 subbase surface on which sand cone, plate load, and CBR tests were performed. Density, CBR and plate load tests were also performed on the subgrade surface after removal of the P-154 subbase. In all the trenches, CBRs and density measurements were also taken at a depth of 12 in. (300 mm) below the subgrade surface. After completing the test, the trench walls were cleaned to clearly expose the layer interfaces. Measurements of the pavement layer interface profiles were taken relative to a horizontal string line to quantify the contribution of each component layer to the total pavement rutting and upheaval. CBR tests on P-154 and subgrade were in situ CBR tests (ASTM D4429).

7 TEST RESULTS

The test results from different pavement layers in the four trenches are summarized in Table 3. One of the more significant observations relative to Table 3 was made from the subgrade CBRs in the four trenches. Pre-traffic/pre-overlay measurements of subgrade strength in the test pits showed that water had migrated from the crushed aggregate subbase into the subgrade of the MRC section and softened the top ± 3.0 in. of the subgrade. The CBR at the subgrade surface in the MRC test pits was approximately four, whereas the CBR at 12 in. (300 mm) below the subgrade surface was between six and eight. The MRG subgrade surface CBR was higher (about 11). It was assumed that this was due to water being drawn from the subgrade (since the slabs were directly cast over the subgrade) by hydration of the concrete during curing. This phenomenon was not observed in the MRC section (slab over crushed stone base) or the MRS section (slab over econocrete base). The results from trenches confirmed the observations/measurements from the pre-traffic test pits.

Performing any type of strength tests on the rubblized material only is very difficult (if not impossible) because of the nature of the material. In this project, plate load tests were performed on the top of the rubblized layer. Due to severe rutting in the MRC section, plate load tests could not be performed inside the wheelpath.

On the MRG test section, the 'k' value from the plate load test inside the wheelpath was lower ($k = 322$ pci [87.3 kPa/mm]) than the k value outside the wheelpath test ($k = 457$ pci [123.9 kPa/mm]). The lower k value inside the wheelpath could be the result of incipient failure in the MRG.

On the MRS test section, the k value from the plate load test inside the wheelpath was higher ($k = 780$ pci [211.4 kPa/mm]) than the k value outside the wheelpath ($k = 579$ pci [156.9 kPa/mm]).

8 LAYER PROFILES

After completing the tests, the trench walls were cleaned to clearly expose the layer interfaces. The pavement layer profile measurements were used to quantify the contribution of each component layer to the total pavement rutting and upheaval. Measurements of the pavement layer interface profiles were made relative to a horizontal string line. Figure 5 shows the layer profiles in the MRC test section.

The figure shows that the subgrade and the top of the rubblized layer (top 3 in. [75 mm] of finely rubblized material) contributed to rutting. Shear failure in the subgrade resulted in significant upheaval outside the wheelpath. Subgrade penetration into the subbase was observed. Significant shoving in the HMA layer was also observed.

Figures 6 and 7 show the pavement layer profiles for test sections MRG and MRS respectively. It is observed that most of the rutting was contributed by the top 3 in. of the thin rubblized layer and the HMA overlay. The top 3 in. (76 mm) of the rubblized layer was mainly composed of loose dust and stones with a

Table 3. Summary of test results from trenching study.

Section	Trench ID	Layer Type	Test Type	Test Results	
				Inside Wheelpath	Outside Wheelpath
MRC	MRC-W	Rubblized concrete	Plate load test (pci)	–	–
		P-154 subbase	Plate load test (pci)	144	92
			CBR	35.9	33.7
			In situ dry density (pcf)	122.4	122.1
		Subgrade surface	Plate load test	–	70
			CBR at (moisture content [%])[1]	5 (33.5)	4 (34.5)
			In situ dry density (pcf)	89.4	88.2
		1-ft. Below subgrade surface	CBR at (moisture content [%])[1]	7 (31.3)	6 (31.6)
			In situ dry density	93.1	93.2
	MRC-E	Rubblized concrete	Plate load test (pci)	–	270
		P-154 subbase	Plate load test (pci)	–	87
			CBR	–	–
			In situ dry density (pcf)	–	–
		Subgrade surface	Plate load test (pci)	–	60
			CBR at (moisture content [%])[1]	4 (36.1)	3 (38.5)
			In situ dry density (pcf)	89.4	86.8
		1-ft. Below subgrade surface	CBR at (moisture content [%])[1]	9 (30)	8 (30.7)
			In situ dry density (pcf)	91.8	93.5
MRG	MRG	Rubblized concrete	Plate load test (pci)	322	457
		Subgrade surface	Plate load test (pci)	106	149
			CBR at (moisture content [%])[1]	11 (30.6)	11 (30.5)
			In situ dry density (pcf)	91.7	92.9
		1-ft. Below subgrade surface	CBR at (moisture content [%])[1]	8 (31.5)	8 (31.5)
			In situ dry density (pcf)	92	91.5
MRS	MRS	Rubblized concrete	Plate load test (pci)	780	579
		P-306 econocrete base	Plate load test (pci)	409	504
		P-154 subbase	Plate load test (pci)	270	202
			CBR	–	–
			In situ dry density (pcf)	–	–
		Subgrade surface	Plate load test (pci)	171	101
			CBR at (moisture content [%])[1]	7 (32)	6 (33.4)
			In situ dry density (pcf)	91.3	90.7
		1-ft. Below subgrade surface	CBR at (moisture content [%])[1]	10 (30.4)	9 (30.2)
			In situ dry density (pcf)	90	89.7

[1]As constructed moisture content for subgrade was 30.7%
1 pcf $\sim$ 16 kg/m^3; 1 pci = 0.27 kPa/mm

top size of 1 in. (25 mm). The bottom 9 in. (230 mm) of the rubblized layer were composed of between 4 and 15 in (100 and 375 mm) tightly locked concrete pieces.

A considerable amount of shoving in the HMA layer was observed that resulted in significant upheaval just outside the wheelpath. The subgrade in test section MRG (Figure 6) showed indications of shear failure as evidenced by the subgrade upheaval outside the wheelpath.

9 FAILURE MECHANISM IN RUBBLIZED CONCRETE PAVEMENTS

The NE end of the MRC section was the first area of the rubblized pavements to show signs of failure (Figures 3 and 4). This failure was not representative of the structural performance of the test section as a whole because one of the pre-overlay test pits (for subgrade evaluation) was located where the pavement failed. A weakened support system resulted because the replaced subbase aggregate material could not be compacted to the same density as in the original construction. A depression in the pavement surface was observed at this location after about 400 load repetitions. The depression migrated longitudinally towards the east until it was about 15 ft. (4.6 m) long, but the structure continued to support the full traffic load until it appeared to be close to complete structural collapse at 11,814 passes. The weakened area did not migrate back into the west half of the test section and the declared structural life of 14,256 passes for the MRC-NW section is believed to be a true representation of the structural performance of the test section. The MRC-NW section also did not appear to be in danger of complete structural collapse as had MRC-NE. Trafficking on the MRG and MRS sections was terminated after 25,608 passes. A visual inspection at

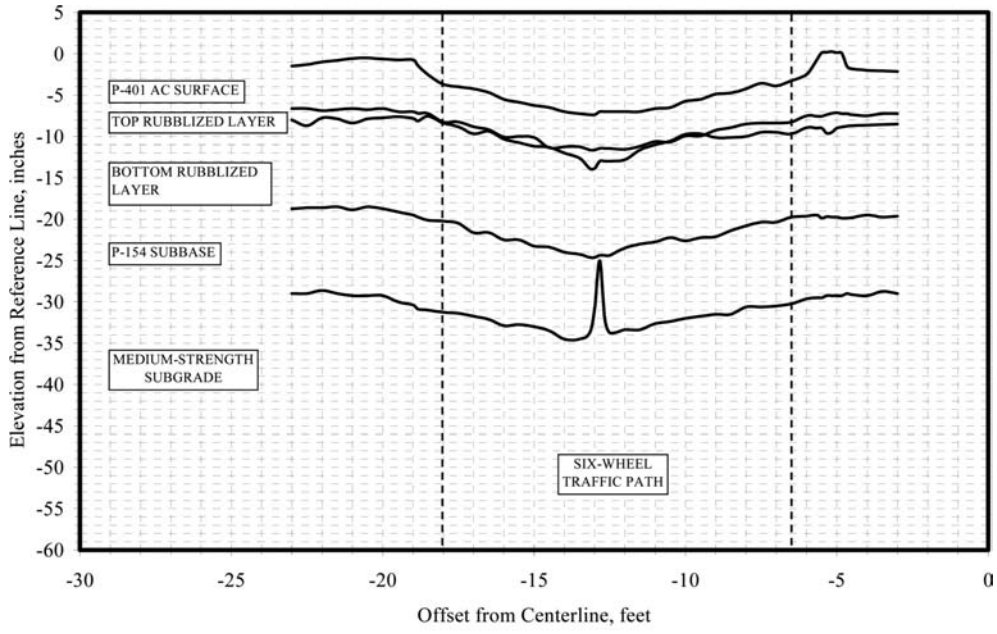

a. MRC-W trench

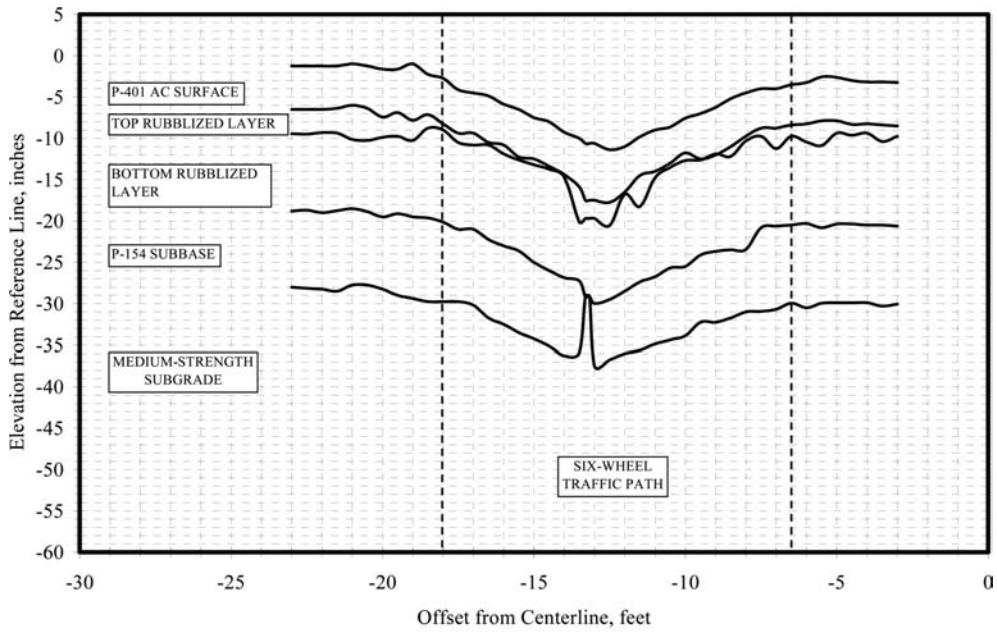

b. MRC-E trench

Figure 5. Pavement layer profiles from trenches in the MRC test section (1 in. = 25 mm).

the end of trafficking indicated that the MRG-N had structural upheaval outside the wheelpath, but the MRS-N section did not. Figures 8 through 11 are photographs of the trench faces in the MRC test section and close-ups of the failure zones. Figures 12 and 13 are photographs of the MRG and MRS section trenches, respectively.

Excluding the top 3 in. (75 mm) of finely rubblized material, the rubblized concrete layer behaved as a tightly interlocked, high-density unbound base. The strength of the rubblized concrete layer is derived from the tight interlock between the rubblized concrete pieces, the confinement provided by the HMA overlay, and the support system underneath (subbase and

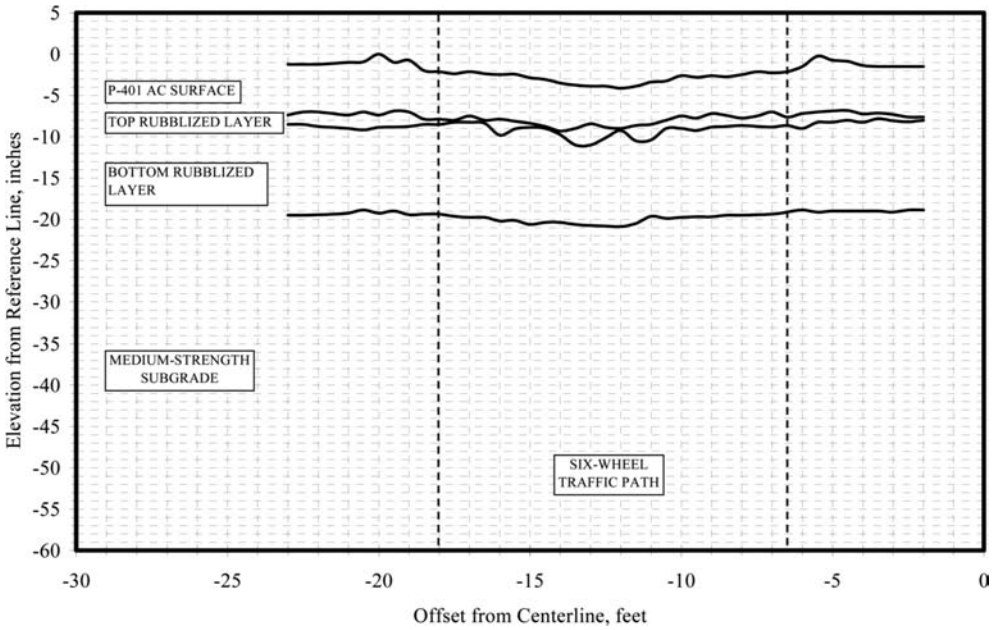

Figure 6. Pavement layer profiles from trenches in the MRG test section (1 in. = 25 mm).

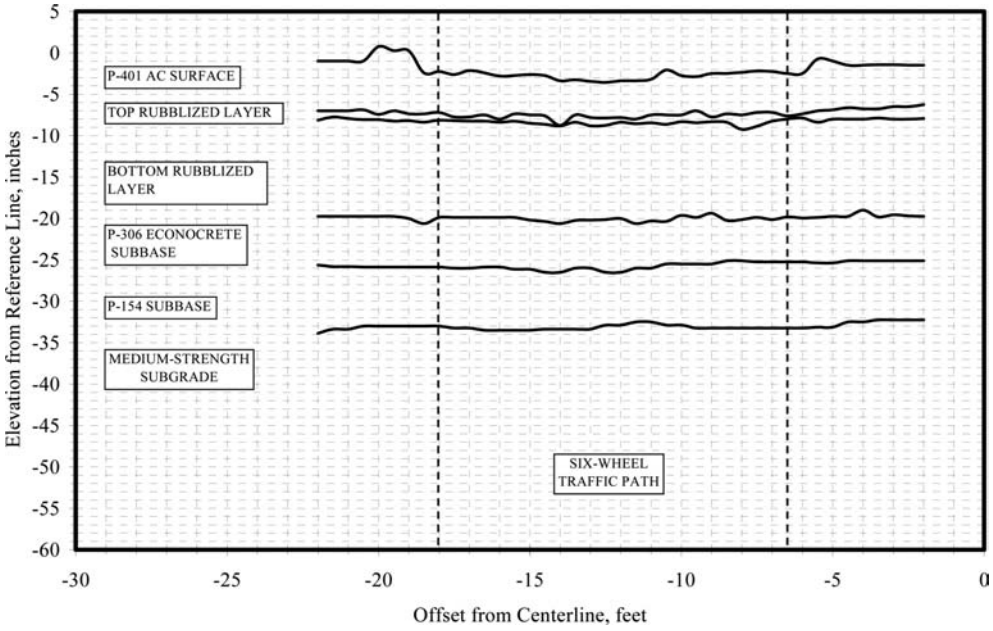

Figure 7. Pavement layer profiles from trenches in the MRS test section (1 in. = 25 mm).

subgrade). This interlock deteriorates under repeated wheel loads. The rate of deterioration is controlled by various factors, including:

- Magnitude and wander of the wheel loads;
- Loss of confinement due to fatigue cracks in the HMA overlay;
- Loss of confinement due to weak support system (underneath the rubblized concrete layer) allowing high vertical deflections in the pavement structure.
- Any moisture/water migration from base/subbase into the subgrade.

In the MRC test section, the top 3 to 4 in. (75 to 100 mm) of subgrade had reduced strength

Figure 8. MRC-W test trench.

Figure 9. MRC-E test trench.

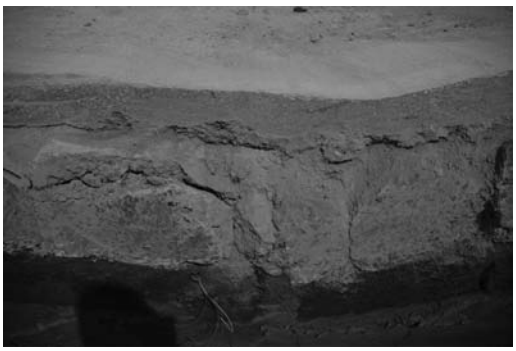

Figure 10. Close-up of failure zone in MRC-W trench.

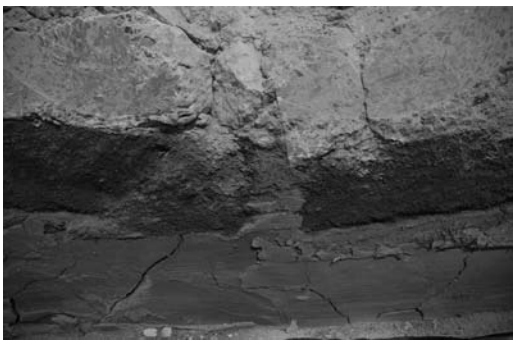

Figure 11. Subgrade intrusion into subbase on MRC-E trench.

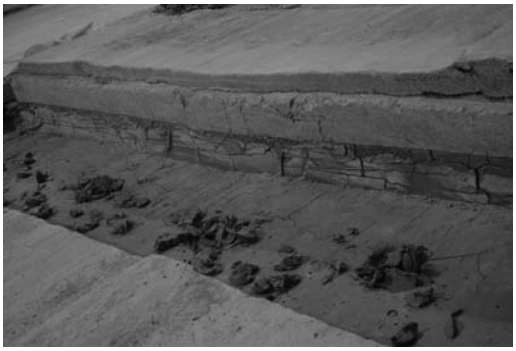

Figure 12. MRG test trench.

Figure 13. MRS test trench.

(CBR 3 to 4) because of moisture migration from the P-154 subbase into the subgrade. This weak area of subgrade allowed higher vertical deflection in the pavement structure, which resulted in a faster rate of deterioration of interlock between the rubblized concrete pieces and ultimate failure of the pavement structure. Figures 6 and 12 (for the MRG section) and Figures 7 and 13 (for the MRS section) show that the rubblized layer did not experience severe deterioration since the support system and the HMA overlay provided sufficient confinement and allowed limited vertical movement. This resulted in longer pavement structural life. The rubblization process also did not induce cracking in the underlying econocrete layer (as observed during the trenching study).

HWD tests were performed to study the variation in the backcalculated modulus of the rubblized concrete layer, impulse stiffness modulus, and the deflection basin shape factor AREA as the traffic tests progressed. The results indicate that the backcalculated modulus of rubblized concrete may not be a good predictor of pavement performance (see Garg and Hayhoe, 2007, for a detailed discussion on this topic).

10 SUMMARY AND CONCLUSIONS

Full-scale traffic tests were completed on three rubblized rigid airport pavements that were overlaid with

5 in. (130 mm) of HMA. This paper presents the performance of the three sections under full-scale traffic using heavy aircraft gear loads. All the rubblized pavements performed in a similar way to the original concrete sections under the same wheel load. Thereafter, the load was increased significantly to artificially induce failure by overloading. Of the three rubblized test sections, the MRC test section (original slab cast on crushed stone base) had the most severe structural distress. The MRG test section (original slab cast on the subgrade) was probably close to severe structural deterioration at the end of trafficking but retained sufficient structural capacity to support the applied load. The MRS test section (original slab cast on econocrete base) did not suffer severe structural deterioration at the end of trafficking despite having accumulated significant levels of rutting and shear flow in the asphalt layer. Poor drainage led to moist conditions and poor performance on the MRC section. The results from post-traffic tests were useful in providing some insight into the failure mechanisms of rubblized concrete pavements. The results also indicate that, for the conditions existing in the test pavements, the assumptions for design in EB66 are overly conservative ("When strength parameters are unknown, it is a fair assumption that most rubblized material will perform equal to or better than FAA standard Item P-209. Unless additional project specific information is available, a one-to-one substitution should be used in the design procedures provided that sufficient subgrade conditions exist to allow proper rubblization.").

For commercial airports serving wide-body aircraft (gross weights >100,000 lb), as per AC 150/5320-6E, rigid pavements are required to have a stabilized base. MRS is the most representative of the pavement structures that are encountered on a commercial airport in the U.S. The performance of MRS under a 65,000-lb wheel load suggests that rubblized concrete pavements with an HMA overlay are a viable rehabilitation option at commercial airports. The presence of a stabilized base underneath the rubblized concrete layer limits the vertical deflection in the layer below the rubblized concrete layer and helps in keeping the rubblized pieces tightly interlocked.

A thickness design procedure for HMA overlays over rubblized concrete pavement is now incorporated in FAARFIELD (FAA airport pavement thickness design procedure, AC 150/5320-6E). The recommended modulus values for the rubblized concrete layer range from 100 ksi (690 MPa) to 400 ksi (2,760 MPa). Some engineering judgment is required for the selection of an appropriate modulus value. Suggested ranges for selecting a design modulus value of rubblized PCC on airfields are provided in Table 4. The selected value is influenced by considerations such as level of conservatism in the design, exact slab thickness within the above ranges, pre-rubblized PCC modulus, anticipated particle size, steel debonding conditions, and relevant historical data. Further insights into selecting a design modulus of rubblized PCC are provided in Buncher (2008).

Table 4. Suggested design modulus ranges for rubblized PCC.

Slab Thickness		Design Modulus	
(in.)	(mm)	(ksi)	(MPa)
6 to 8	150 to 200	100 to 135	690 to 930
8 to 14	200 to 350	135 to 235	930 to 1,620
>14	>350	235 to 400	1,620 to 2,760

ACKNOWLEDGEMENTS

The work described in this paper was supported by the FAA Airport Technology Research and Development Branch, Dr. Satish K. Agrawal, Manager. The contents of the paper reflect the views of the authors who are responsible for the facts and accuracy of the data presented within. The contents do not necessarily reflect the official views and policies of the FAA or ICAO. The paper does not constitute a standard, specification, or regulation.

REFERENCES

Airport Engineering Division. 2004. *Rubblized Portland Cement Concrete Base Course.* Engineering Brief No. 66. Federal Aviation Administration, Washington, D.C., 2004.

Airport Engineering Division. 2005. *Standards for Specifying Construction of Airports*. Advisory Circular AC 150/5370-10A. Federal Aviation Administration, Washington, D.C.

Brill, D.R., Hayhoe, G.H. and Ricalde, L. 2005. Analysis of CC2 Rigid Pavement Test Data from the FAA's National Airport Pavement Test Facility, *Proceedings of the Seventh International Conference on the Bearing Capacity of Roads, Railways, and Airfields*, Trondheim, Norway.

Buncher, M. and Jones, H.W., 2006. Rubblization of Airfield Pavements – State of the Practice, *Rubblization of Portland Cement Concrete Pavements, Transportation Research Circular E-C087*, Transportation Research Board.

Buncher, M., Fitts, G., Scullion, T. and McQueen, R.D. 2008. *Development of Guidelines for Rubblization*., Final Report, Airfield Asphalt Pavement Technology Program Project 04-01, Asphalt Institute, Lexington, KY.

Garg, N. and Hayhoe, G.F. 2007. Characterization of Rubblized Concrete Airport Pavements at the NAPTF Using Non-Destructive Testing Methods. *Proceedings, 2007 FAA Worldwide Airport Technology Transfer Conference*. Atlantic City, New Jersey.

Hayhoe, G.F., Garg, N. and Dong, M. 2003. Permanent Deformation During Traffic Tests on Flexible Pavements at the National Airport Pavement Test Facility, *Proceedings, 2003 Airfield Pavement Specialty Conference.* Las Vegas, Nevada.

Hayhoe, G.F. and Garg, N. 2006. Characterization of Rubblized Concrete Pavements with HMA Overlays at the National Airport Pavement Test Facility, *Proceedings of the 2006 TandDI Airfield and Highway Pavement Specialty Conference.* Atlanta, Georgia.

Ricalde, L. and Daiutolo, H. 2005. New Rigid Pavement Construction and Testing at the FAA National Airport Pavement Test Facility (NAPTF), *Proceedings of the Fifth International Conference on Road and Airfield Pavement Technology*, Seoul, Korea.

Part 7: Accelerated pavement testing to evaluate functional performance

This page intentionally left blank

Advances in Pavement Design through Full-scale Accelerated Pavement Testing – Jones, Harvey, Mateos & Al-Qadi (Eds.)
© 2012 Taylor & Francis Group, London, ISBN 978-0-415-62138-0

Accelerated traffic load testing of seismic expansion joints for the new San Francisco–Oakland Bay Bridge

D. Jones & R.Z. Wu
University of California Pavement Research Center, University of California, Davis

T.J. Holland
California Department of Transportation

ABSTRACT: A relatively unique opportunity was recently identified for accelerated traffic load testing of a bridge expansion joint designed to withstand severe seismic activity. This study was part of the construction of the new East Span of the San Francisco–Oakland Bay Bridge and assessed whether the expansion joints (which were designed to function in harmony with the bridge decks in the event of a high magnitude earthquake) linking the Self-anchored Span with the Transition and Skyway spans would withstand traffic loading. A test structure incorporating one of the joints was constructed close to the actual bridge and tested with the California Department of Transportation/University of California Pavement Research Center Heavy Vehicle Simulator in a series of phases. On completion of three months of testing, no structural damage was recorded by any of the LVDTs or strain gauges installed on the steel plates, steel frames, bolts, or washers. There was also no visible damage on any of these components. Excessive overloading caused some damage to the Trelleborg unit towards the end of the test. Based on the results of this limited testing, it was concluded that the expansion joint would perform adequately under typical Bay Bridge traffic. The distress observed to the Trelleborg unit under the high loads in the last phase of testing is unlikely to occur under normal traffic. The findings from this study indicate that the Caltrans seismic expansion joint tested will be appropriate for typical Bay Bridge traffic. These joints will be used in the new bridge, due to be opened in 2013. The study also concluded that APT can be effectively used for testing bridge deck components to provide rapid answers for design and construction teams.

1 INTRODUCTION

The 13.5 km (8.4 mile) San Francisco–Oakland Bay Bridge connects the city of San Francisco with the East Bay cities of Oakland, Emeryville and Berkeley and is the start point of the Interstate 80 (I-80) corridor. The bridge carries approximately 280,000 vehicles per day (compared to the 100,000 carried by the Golden Gate Bridge). It currently consists of two separate bridges linked by a short tunnel on Yerba Buena Island. The existing East Span, a steel box girder design constructed in 1936, was damaged by the 7.1 magnitude Loma Prieta earthquake in 1989, during which a section of the top span, carrying the five west bound lanes, collapsed onto the lower east bound lanes. Although repairs were made and the bridge reopened approximately one month after the earthquake, a complete seismic retrofit of the East Span to withstand future similar or more severe earthquakes was not considered viable and construction of a new bridge was approved. The West Span, which consists of two suspension bridge spans connected at a center anchorage, was easier to retrofit to accommodate higher magnitude earthquakes. Retrofit work on this part of the bridge was completed in 2004 and retrofit work on the West Approach was completed in 2009.

The new East Span consists of four separate parts (Figure 1):

- The Oakland Approach and Touchdown, linking the new bridge to the existing I-80 infrastructure.
- The Skyway, two side-by-side 1.9 km (1.2 mile) long concrete spans (completed in 2008).
- The Main Span, a self-anchored suspension structure with two side-by-side 470 m (1,540 ft) long spans supported by a single tower, which was still under construction at the time this study was undertaken. It will be the longest bridge of its kind in the world. The span's single 160 m (525 ft) tall tower will match the height of the West Span's towers. Its placement closer to the west end of the structure creates a distinctive asymmetrical design, with the single 1.6 km (1.0 mile) long main cable presenting a sharper angle on the west side and a more sloping appearance on the east.
- The Yerba Buena Island Transition Structure (YBITS), still under construction, will connect the Self-anchored Suspension Span to Yerba Buena Island (YBI), and will transition the new East Span's side-by-side road decks to the upper and lower decks of the YBI tunnel and West Span.

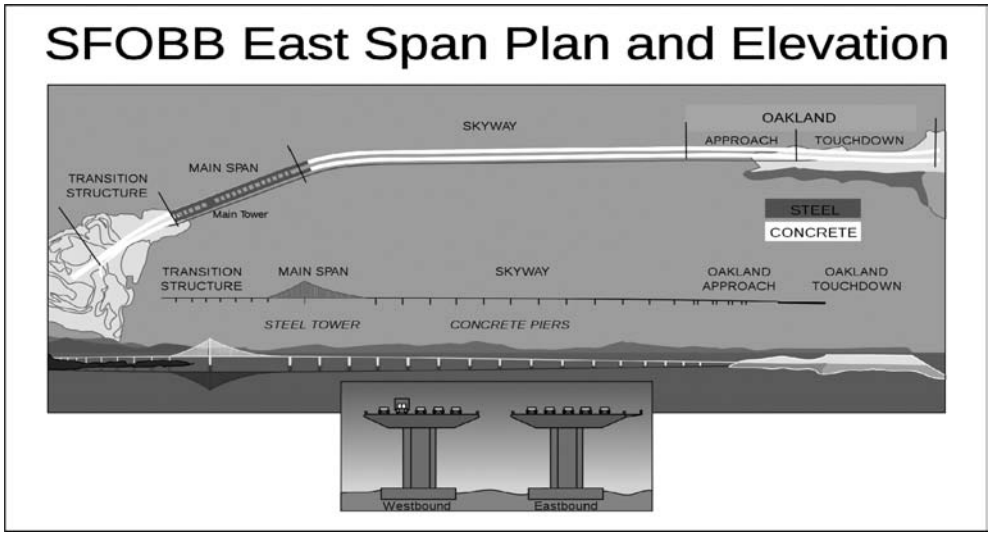

Figure 1. Schematic of the new East Span of the San Francisco Bay Bridge (http://en.wikipedia.org/wiki/File:SFOBBEast Span.svg).

The three radically different structures also require a new expansion joint design to link the three main parts (Skyway, SAS, and YBITS) while integrating with the seismic functioning of the entire bridge system. This expansion joint was subsequently designed and incorporates a *Trelleborg Transflex 2400* expansion joint, a steel connector plate, and fastening systems. The main focus of the design was to ensure that the joint acted in harmony with the three structures during seismic activity. A secondary focus was the requirement for separate joints for each lane, which would facilitate maintenance without major disruption to traffic. During review of the joint design, questions were raised with regard to how it would perform under traffic loading, given the focus on seismic and maintenance requirements. An accelerated loading test, using the California Department of Transportation/University of California Pavement Research Center Heavy Vehicle Simulator (HVS) was therefore undertaken to provide a quick indication of how the joint would perform under truck traffic.

This paper describes the accelerated traffic load study, summarizes the results, and relates performance in the accelerated test with expected performance on the actual bridge structure.

2 STUDY OBJECTIVE AND WORKPLAN

Two objectives were identified for this accelerated load study:

- Identify any fatal flaws in the design related to vehicle trafficking.
- Determine how the joint will fail under vehicle trafficking.

A project was consequently designed to meet these objectives (Jones and Wu, 2011). This included design and construction of a test structure, instrumentation of the test section, accelerated loading with a Heavy Vehicle Simulator (HVS), data analysis, and recommendations. The design of the test structure is provided in Figure 2. A prototype of the joint was manufactured and a replica of the joint support structures constructed to accommodate the testing.

A review of the literature found no published reference to any similar studies and given a testing period limitation of three months, best use of this time was taken into consideration in preparing a test plan to meet the study objectives. A phased approach was followed, starting with normal truck loads in the center of the joint to identify any fatal flaws, followed by incremental changes in loading and wheel position. A summary of the test plan is provided in Table 1.

In the first phase (Phase 1.1), testing at standard wheel loads for four weeks (i.e., equivalent to an 80 kN [18,000 lb] axle load), was included to identify any potential major flaws in the design. The following phases would then evaluate the joint response under wandering traffic, increasing wheel load, and different wheel path (specifically along the edge of the joint). Assuming that no damage was caused in the first two phases, the final phase would investigate impact loads and very high wheel loads and tire pressures with a view to identifying the weakest point of the design.

Load variations on a single day were included in the study to establish relationships between wheel load and structural response, and to identify any nonlinearity that might lead to structural damage.

Most trafficking was applied in a channelized, bidirectional mode using dual wheel truck tires (Goodyear G159 – 11R22.5 – steel belt radial inflated to 720 kPa [104 psi]) with these exceptions:

- Phase 1.3, which assessed the effects of bidirectional traffic wander using the dual tires.

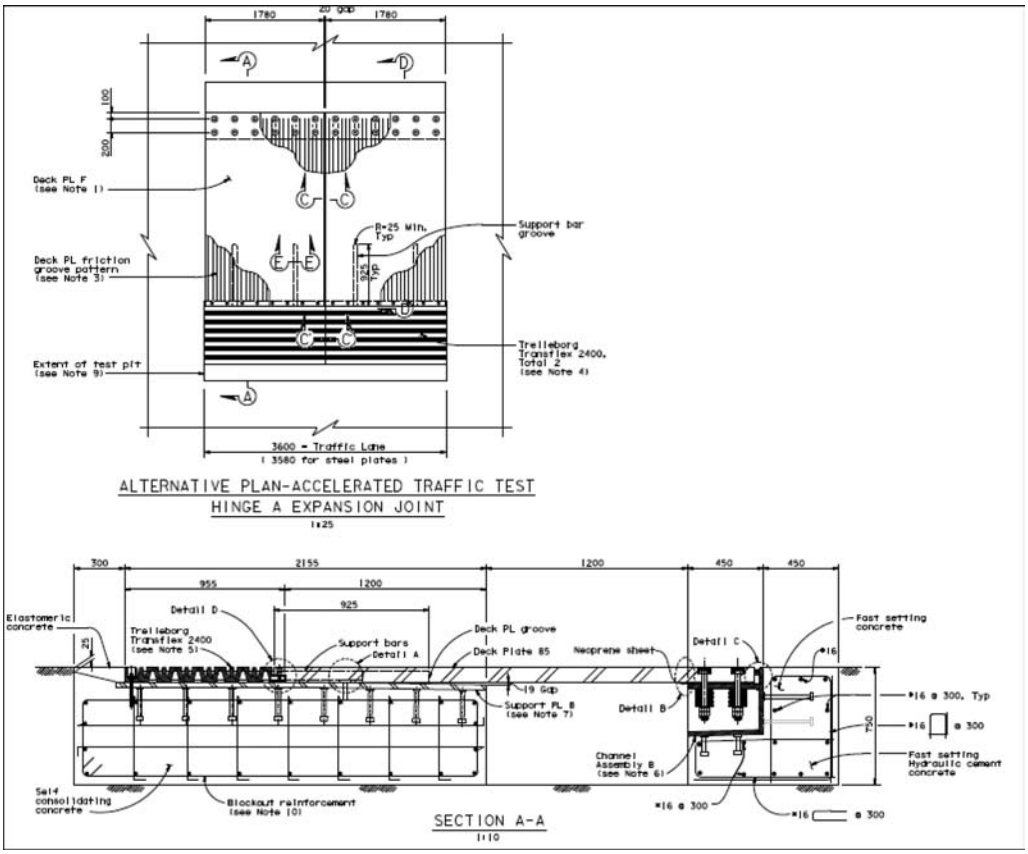

Figure 2. Test structure design.

Table 1. Loading Program for HVS Testing.

Phase No.	Test Section Location	Duration (days)	Half-Axle Wheel Loads (kN)	Repetitions Applied
1.1	Center	30	1day at 25, then 29 days at 40	5,18,000
1.2	Center	6	1 day each at 25, 40, 60, 80, and 100, then 1 day at 40	1,20,000
1.3	Center + Edge	7	1day each at 40, 80, 100, then 4 days at 60	1,20,000
2.1	Edge	11	2 days at 40, 1 day each at 60, 80 and 100, then 6 days at 80	1,89,000
3.1	Edge	3	60, impact load*	23,000
3.2	Edge	15	5 days at 60, 5 days at 80, and 5 days at 100, all with impact load	2,40,000
3.3	Edge	15	1 day at 100, then 14 days at 150	1,50,000
–	–	3	No test days	0
Total	–	90		13,60,000

*Impact load was applied by forcing the HVS wheel over a step in the wheelpath created by either a 13 mm (1/2 in.) neoprene pad or 19 mm (3/4 in.) hardwood board.

- Phase 3.1, which assessed the effects of an impact load in a unidirectional mode, and
- Phase 3.3, which assessed the effects of very high bidirectional loads using an aircraft tire (Boeing 737) inflated to 1,380 kPa (200 psi).

Load was checked with a portable weigh-in-motion pad at the beginning of each test and after each load change.

3 CONSTRUCTION

A suitable test site was identified on a temporarily vacant area close to the bridge construction offices at the Port of Oakland. Construction was started in March 2011 and completed in July 2011. Photographs of the construction are provided in Figure 3 and Figure 4 and completed project with the HVS in place in Figure 5 and Figure 6.

Figure 3. Formwork for test structure.

Figure 4. Deck joint installation.

Figure 5. Test structure prior to start of testing.

Figure 6. Test structure prior to start of testing.

4 INSTRUMENTATION

The expansion joint was comprehensively instrumented to monitor status and responses under HVS trafficking (Jones and Wu, 2011). Parameters monitored included: ambient and steel plate temperatures, vertical deflections at various locations, and longitudinal strain at the bottom of the steel plate. A layout of the instrumentation is shown in Figure 7. Instruments #1 through #9 are Linear Variable Differential Transducers (LVDTs), Instruments #11 to #13 are strain gauges, and Instruments #14 to #18 are thermocouples.

Figure 8 and Figure 9 show general views of the instruments on top and underneath the plate, respectively. Figure 10 and Figure 11 respectively show closer views of two LVDTs positioned on bolts on the surface of the steel plate, and how the movement of washers underneath the steel plate was monitored.

Permanent deformation of the Trelleborg unit was monitored daily using a laser profilometer that recorded surface profiles in a longitudinal direction (i.e., the trafficking direction) at 200 mm (8.0 in.) intervals in the transverse direction (Figure 12).

5 HVS TRAFFICKING

HVS trafficking commenced on August 08, 2011 and followed the test plan described earlier. The impact loads used in Phase 3.1 and Phase 3.2 were applied by creating a step in the wheel path using either a 12.5 mm (1/2 in.) neoprene pad or a 19 mm (3/4 in.) wood panel (Figure 13).

6 TEST RESULT SUMMARY

6.1 *Phase 1: Normal load and pavement response at center location*

This section covers the test results for Phases 1.1, 1.2 and 1.3 as listed in Table 1. The main objectives of these phases were identification of any major flaws in the joint design and evaluation of the strain and deflections caused by increasing wheel loads (Jones and Wu, 2011).

6.1.1 *Phase 1: Fatal flaw assessment*

No apparent damage was observed at the end of Phase 1.1. The permanent vertical settlement of the structure after testing was 0.2 mm, which was considered minimal and unlikely to influence joint performance. No permanent deformation in the steel plate occurred during this phase, based on the strain data recorded.

Example vertical deflection bowls and strain bowls measured at the mid-span of the steel plate are shown in Figure 14 and Figure 15, respectively. These figures show that the deflections and longitudinal strains induced by the 80 kN standard axle load (40 kN half-axle) at mid-span of the steel plate were approximately 0.9 mm and 60 microstrain, respectively, and

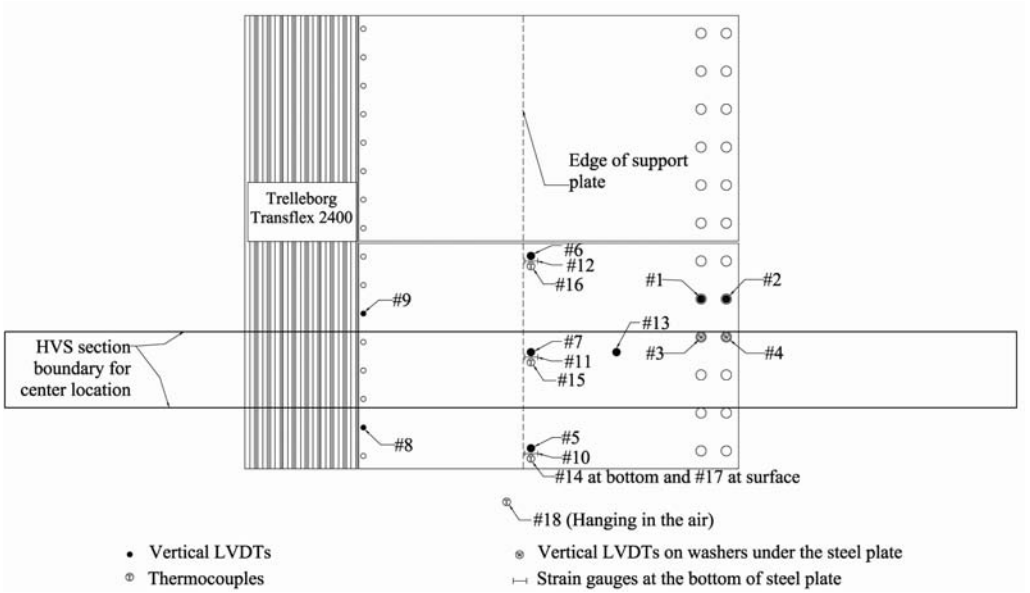

Figure 7. Layout of instrumentation during HVS testing on the center of the expansion joint.

Figure 8. General view of instruments on top of joint.

Figure 9. General view of instruments under the joint.

remained constant throughout the phase (i.e., deflections and strains did not increase with increasing load repetitions).

The vertical deflections at the bolts and washers were less than 0.1 mm, with washers deflecting a little more than the bolts. There was no distinct correlation between temperature and elastic response in the steel plate; however, very small changes in peak strain between the coldest and warmest periods each day were observed on the data plots on most days. Minor fluctuations in strain and deflection measurements were most likely caused by very small fluctuations in the actual load applied by the HVS. No fatal flaws in the deck joint design were identified.

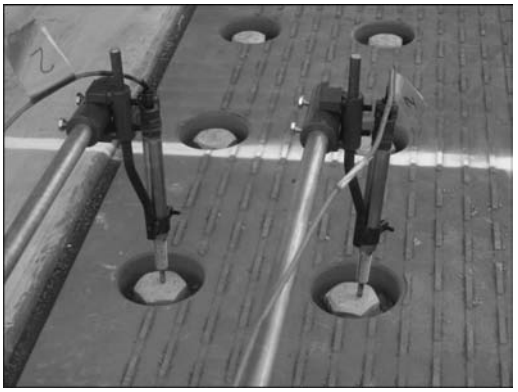

Figure 10. LVDTs for monitoring vertical movements of bolts on the steel plate.

6.1.2 *Phase 1.2: Load response on the center of the steel plate*

No damage was observed at the end of Phase 1.2. No permanent deformation in the steel plate occurred during this phase, based on the strain data recorded. Increases in peak deflection and peak strain showed a linear relationship with increasing load. The maximum

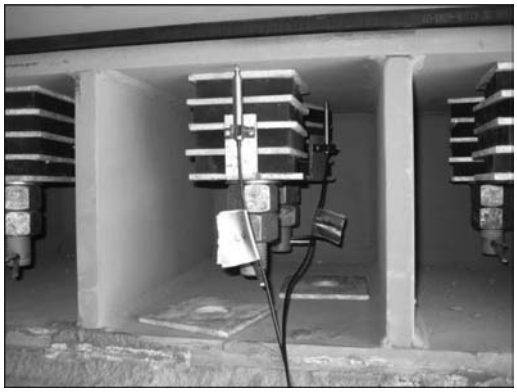

Figure 11. LVDTs for monitoring washer movements (Instrument #3 and #4 in Figure 7).

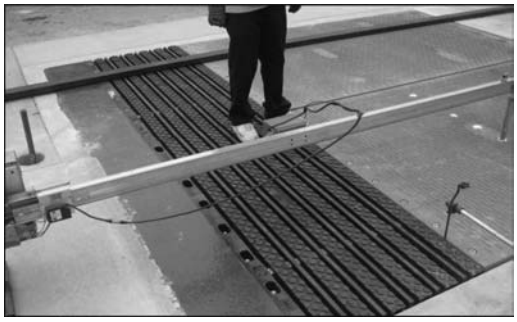

Figure 12. Laser profilometer recording surface profile of the Trelleborg unit.

Figure 13. Wooden step used for applying impact load.

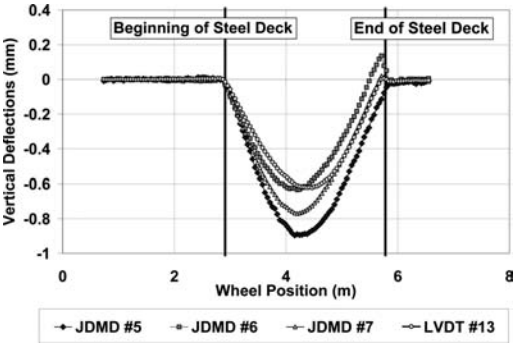

Figure 14. Deflection bowls (i.e., influence lines) measured during Phase 1.1. (Measurements for the three LVDTs [JDMD for DC LVDT and LVDT for AC LVDT] installed at mid-span of the steel plate. Legend indicates number corresponding to Figure 7).

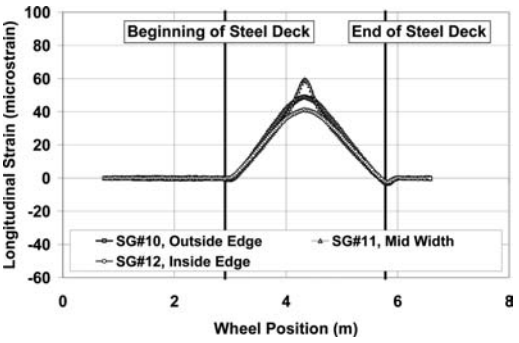

Figure 15. Strain bowls (i.e., influence lines) measured during Phase 1.1. (Measurements for the three strain gauges (SG) installed at mid-span of the steel plate. Legend indicates number corresponding to Figure 7).

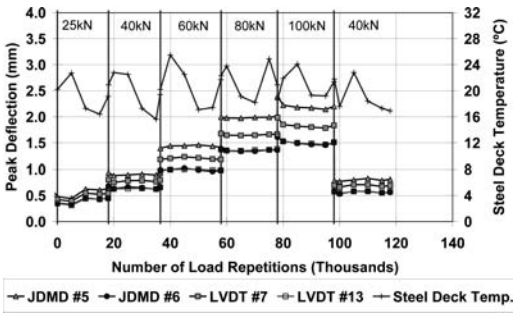

Figure 16. Vertical deflections measured by LVDT #5 during Phase 1.2.

deflection and maximum strain recorded was 2.3 mm and 135 microstrain respectively, both at the mid-point of the steel plate, under the 100 kN wheel load. Examples of the data recorded are shown in Figure 16 (peak vertical deflection against number of load repetitions) and Figure 17 (peak vertical deflection against load) for the LVDT corresponding to instrument #5 in Figure 7. Changes in deflection and strain with increasing wheel load showed similar trends. Very small daily variations in peak deflection and peak strain were consistent with daily temperature change on the data plots. Minor fluctuations in strain and deflection measurements were again likely caused by very small fluctuations in the actual load applied by the HVS.

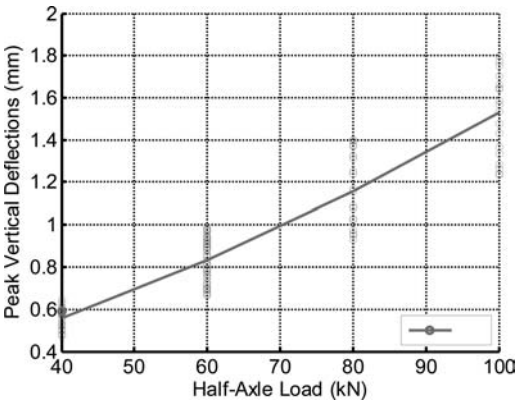

Figure 17. Vertical deflections measured by LVDT #5 during Phase 1.2.

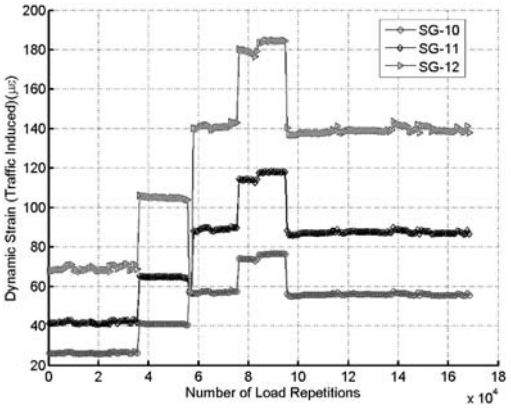

Figure 18. Histories of longitudinal strains at steel plate mid-span during Phase 2. (Legends indicate instrument type (SG for strain gauge) and instrument number shown in Figure 7.)

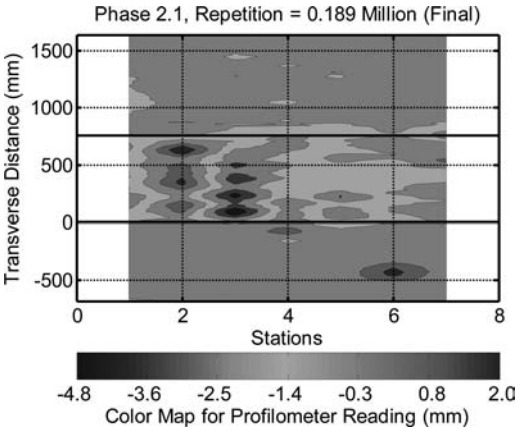

Figure 19. Permanent vertical deformation of the Trelleborg unit.

6.1.3 *Phase 1.3: Load response comparison at center and edge of the steel plate*

Phase 1.3 checked the joint response under wandering traffic. No damage was observed at the end of this phase and based on the deflection and strain data recorded, no permanent deformation in the steel plate occurred. Peak strain and deflection at any time was influenced by the position of the wheels in the wander pattern, as expected. Sensors furthest away from the wheels (i.e., on the edge of the steel plate) had larger differences between the lowest and highest deflection and strain (ratio of ∼2.5) compared to the sensors inside the wheelpath (i.e., at the mid-point of the steel plate), which had highest strain to lowest strain ratios of about 1.5. Increases in peak deflection and peak strain continued to show a linear relationship with increasing load. Very small daily variations in peak deflection and peak strain were consistent with daily temperature change on the data plots. Minor fluctuations in strain and deflection measurements were again likely caused by very small fluctuations in the actual load applied by the HVS. Based on the results and observations in this phase, it was concluded that there was no significant difference in the measurements recorded during traffic wander compared to those recorded during channelized traffic and that wander had very little effect on the behavior of the deck joint. Consequently all further testing was carried out in a channelized mode as this was considered more likely to induce damage given the concentrated nature of the loading.

6.2 *Phase 2: Higher loads at edge location*

During Phase 2, testing was carried out on the edge of one of the expansion joints as shown in Figure 7. The term "edge" was used because wheelpaths for this location were closer to the edge of one of the steel plates even though it was closer to the center of the entire lane width. Normal trafficking on the actual bridge would not occur in this way except when vehicles change lanes. The objective in this phase was to assess whether trafficking at higher loads on the edge of the plate would cause any damage to the expansion joint.

No damage was observed at the end of the phase and based on the deflection and strain data recorded, no permanent deformation in the steel plate occurred. Responses were similar to those recorded in earlier phases during loading on the center of the deck joint. Increases in peak deflection and peak strain continued to show a linear relationship with increasing load. Figure 18 shows the histories of longitudinal strains measured at the mid-span of the steel plate. The figure indicates some slight daily variation (attributed to temperature), but no significant increasing trend. Figure 19 shows the permanent vertical deformation of the Trelleborg unit, measured with the laser profilometer. Approximately 4.0 mm of downward deformation, caused by the HVS trafficking, was measured at the end of this phase of testing.

Based on the results and observations in this phase, it was concluded that there was no significant difference in the trends of measurements recorded during trafficking on the edge compared to those recorded during trafficking on the center. However, since higher deflections and strains were measured in this phase for the same loads, it was decided to undertake all further testing on the edge of the bridge deck joint as this was considered more likely to induce damage.

6.3 *Phase 3: Impact load and overloading*

After reviewing the Phase 2 results, it was concluded that continued trafficking at 80 kN and 100 kN was unlikely to cause any significant structural damage to the seismic joint in the time available. The study therefore proceeded to the third phase of the test plan, which required significantly heavier wheel loads (using an aircraft tire) and impact loading (caused by including a step in the wheel path).

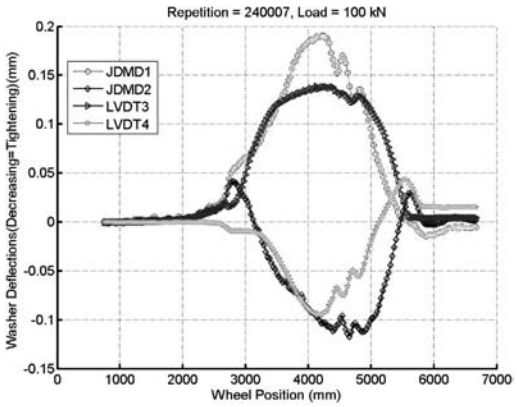

Figure 20. Example of vertical deflection bowls measured on the bolts and washers during impact loading.

6.3.1 *Phase 3.1: Edge test with impact load and unidirectional traffic*

A 60 kN impact load did not appear to influence response in the deck joint at the location of the sensors, and no damage was observed on completion of this short phase. Responses were similar to those recorded in earlier phases. There was also no difference observed between unidirectional and bidirectional trafficking and consequently all further testing was carried out in a bidirectional mode, which applies more wheel loads than unidirectional trafficking in a given period of time.

6.3.2 *Phase 3.2: Load response with impact load*

No damage was observed at the end of Phase 3.2 and based on the deflection and strain data recorded, no permanent deformation in the steel plate occurred. Responses continued to be the same as those recorded in earlier phases and increases in peak deflection and peak strain continued to show a linear relationship with increasing load.

Figure 20 shows an example of the deflections on the bolt washers (LVDT3 and LVDT4) and bolts (JDMD1 and JDMD2) caused by impact loading with a 100 kN half-axle wheel load. The impact load had some influence on the deflection bowls (influence lines) for each instrument, but did not result in an increase in the peak deflections. It was therefore concluded that this level of impact (the maximum possible without influencing the hydraulic load controls of the HVS) would not cause additional damage and consequently impact loads were not applied in Phase 3.3.

6.3.3 *Phase 3.3: Edge test with high load*

The objective of Phase 3.3 of the testing was to cause as much damage to the seismic joint as possible to identify the weakest part of the design. Loading was carried

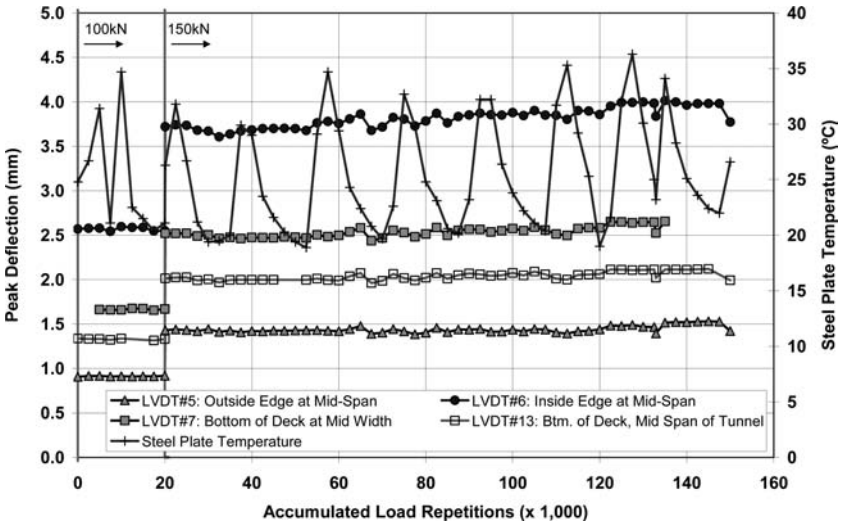

Figure 21. History of peak deflections at bottom of steel plate during Phase 3.3.

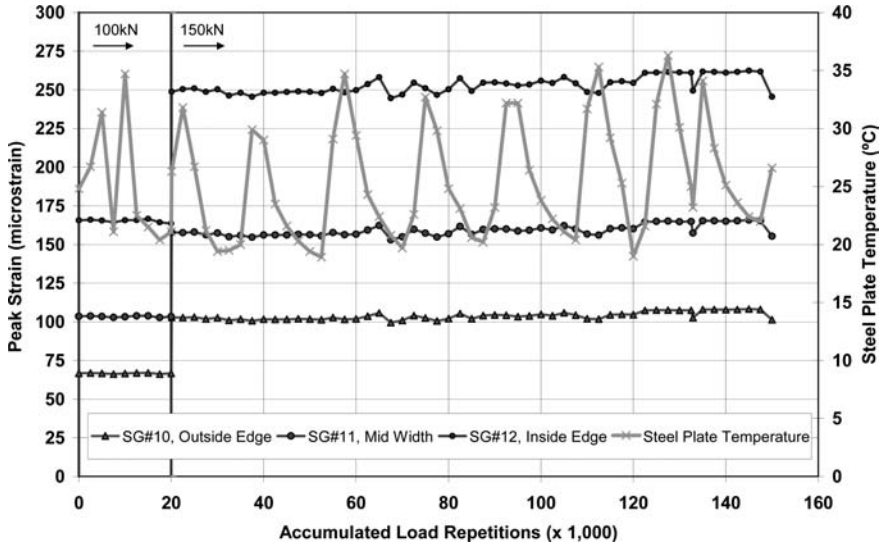

Figure 22. History of peak longitudinal strains at bottom of steel plate during Phase 3.3.

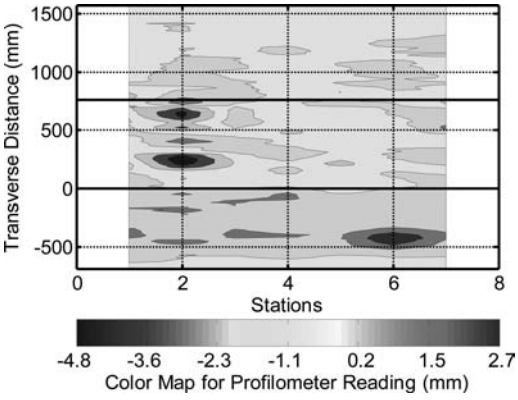

Figure 23. Contour plot of deformation at end of Phase 3.3

Figure 24. General view of structure after testing.

Figure 25a. Close-up view of damage to Trelleborg unit.

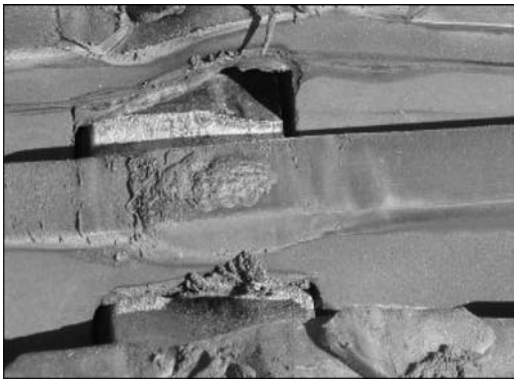

Figure 25b. Close-up view of damage to Trelleborg unit.

out with an aircraft tire with a half-axle load of 150 kN. On completion of this testing, the measured data from the LVDTs (Figure 21) and strain gauges (Figure 22) indicated that there was still no structural damage on any steel parts of the expansion joint. Observed damage was limited to the wheelpath over the Trelleborg unit only and consisted of significant wear and deformation on the rubber sections of the Trelleborg unit

and deformation and shearing in one of the steel ribs supporting these rubber sections. Some cracking was also observed in the concrete approach slab to the expansion joint, but this was not considered relevant to the study. Figure 23 shows the permanent vertical deformation of the Trelleborg unit, measured with the laser profilometer. Approximately 4.8 mm of downward deformation, caused by the HVS trafficking, was measured at the end of this phase of testing.

Photographs of the structure after completion of testing and a close up of damage to the Trelleborg unit are shown in Figure 24 and Figure 25, respectively.

The distress observed to the Trelleborg unit under the very high loads (almost four times the legal limit) applied in this last phase of testing is unlikely to occur under normal traffic on the Bay Bridge.

7 CONCLUSIONS AND IMPLEMENTATION

A relatively unique opportunity was recently identified for accelerated traffic load testing of a new bridge expansion joint designed to withstand severe seismic activity. This study was part of the construction of the new East Span of the San Francisco–Oakland Bay Bridge and assessed whether the expansion joints (which were designed to function in harmony with the bridge decks in the event of a high-magnitude earthquake) linking the Self-anchored Span with the Transition and Skyway spans would withstand traffic loading. A test structure incorporating one of the full-scale joints was constructed close to the actual bridge and tested with the California Department of Transportation/University of California Pavement Research Center Heavy Vehicle Simulator in a series of phases.

On completion of seven phases of testing over a three-month period, no structural damage was recorded by any of the LVDTs or strain gauges installed on the steel plates, steel frames, bolts, or washers. There was also no visible damage on any of these components. Excessive overloading with a 150 kN half-axle load (four times the standard axle load) on an aircraft tire in the last phase of the test caused some damage to the Trelleborg unit in the joint. The damage included abrasion, tearing, shoving and permanent deformation of the rubber inserts, and deformation and shearing of one of the steel supports directly under the wheel load.

Although no seismic or structural testing was undertaken and no recommendations towards its seismic or structural performance are made, and no vehicle suspension dynamics (i.e., vehicle bounce) or speed effects were considered, based on the results of this limited testing, it was concluded that the Caltrans seismic expansion joint would perform adequately under typical Bay Bridge traffic. The distresses observed on the Trelleborg unit under high loads in the last phase of testing are unlikely to occur under normal Bay Bridge traffic. However, the Trelleborg unit was found to be the weakest point of the expansion joint, as expected. On the actual bridge structure, these units will need to be checked periodically to confirm the findings of this study, and to assess any effects of higher speeds and vehicle dynamics that were not identified. The joints will require periodic maintenance and replacement in line with manufacturer's specifications.

This study also demonstrated and concluded that mobile accelerated pavement testing equipment can be effectively used for testing bridge deck components to provide rapid indications of how these will perform/behave under traffic loading. The results can be used by design, fabrication, manufacturing and construction teams to ensure safe and efficient performance of the bridge.

Based on the findings of this study and other studies carried out to assess seismic performance and skid resistance, the expansion joint design as tested in this study will be used in the new Bay Bridge, due to be opened to traffic in 2013.

ACKNOWLEDGEMENTS

This paper describes research activities that were requested and sponsored by the California Department of Transportation (Caltrans), Division of Research and Innovation. Caltrans sponsorship is gratefully acknowledged. The assistance and interest of Mike Whiteside, Jason Wilcox and Ric Maggenti of the Caltrans Toll Bridge Program, and the HVS test crew under the direction of Peter Miller is also gratefully acknowledged. The contents of this paper reflect the views of the authors and do not necessarily reflect the official views or policies of the State of California or the Federal Highway Administration.

REFERENCES

Jones, D. and Wu, R. 2011. *Accelerated Traffic Load Testing of Expansion Joints for the Self-anchored Suspension Section of the New San Francisco–Oakland Bay Bridge East Span*. Davis and Berkeley: University of California Pavement Research Center (Research Report RR-2011-06).

Advances in Pavement Design through Full-scale Accelerated Pavement Testing – Jones, Harvey, Mateos & Al-Qadi (Eds.)
© 2012 Taylor & Francis Group, London, ISBN 978-0-415-62138-0

Accelerated testing of noise performance of pavements

H. Bendtsen, J. Oddershede & G. Hildebrandt
Danish Road Directorate, Hedehusene, Denmark

R.Z. Wu & D. Jones
University of California Pavement Research Centre, University of California, Davis, California

ABSTRACT: Noise properties of road pavements change over time due to wear from traffic, impact of weather conditions, etc. With the introduction of noise reducing pavements in many countries, it has become increasingly important to understand how the noise properties of pavements change as they get older. The Danish Road Directorate and the University of California Pavement Research Centre have investigated the feasibility of using test results from Heavy Vehicle Simulator (HVS) test sections to predict the development of the noise properties of pavements. Pavement surface textures were measured at regular intervals with a three-dimensional scanner on a range of different HVS test sections on various projects. The Dutch Acoustical Optimization Tool (AOT), developed to predict the noise properties of road pavements based on texture data, and pavement type, was used for the analyses of the measured texture profiles.

1 INTRODUCTION

There are increasing demands for general improved environmental living conditions from modern society and communities living near roads are especially demanding reduced noise levels. Consequently there is increased pressure on road authorities to reduce noise levels. This has created a demand for durable and cost effective measures for noise abatement. The development of noise reducing road surfaces has in some countries proved to be an attractive solution that can be implemented by road authorities when constructing new roads or when maintaining, rehabilitating or widening existing pavements.

Noise emissions as well as noise reduction are often measured when a pavement is new. It is known from the literature (Lu, et al., 2009; Bendtsen, et al., 2009; Bendtsen, 2010) that noise emissions from pavements increase over time due to wear and environmental influence. However, reductions in noise levels have also been observed as pavements get older. When introducing quieter pavements, authorities need to know the expected average noise reduction over the lifetime of the new pavement type, which could be as long as ten to fifteen years. Long-term pavement performance studies measuring changes in noise levels over the life of the pavement, such as those being conducted by the Danish Road Directorate (DRD) in Denmark and University of California Pavement Research Center (UCPRC) in California, are important for research purposes, but of little immediate help to road authorities who need to make decisions on choice of pavement in a much shorter time frame.

In cooperation with the UCPRC, DRD recently performed a study of acoustical aging on asphalt pavements (Bendtsen, et al., 2009). This investigation concluded that there appears to be a linear relation between noise level and time/traffic. It also highlighted the need for measurements and analyses of the change in pavement texture over time to get a deeper insight and understanding of the ongoing noise level increases. In a follow-on study by the two institutions, a much faster method for predicting lifetime noise increases on pavements has been developed and tested. Some of the data used in the development of the prediction models was obtained from accelerated pavement tests (APT) at the UCPRC, where regular texture and other pavement surface property assessments could be taken on test pavements under controlled conditions.

2 EXPERIMENTAL LAYOUT

The UCPRC operates two Heavy Vehicle Simulators (HVS) to test the structural characteristics and durability of pavements. This equipment applies truck tire loads over a test pavement at a maximum speed of 8.5 km/h. An HVS Mk VI and close-up of the tires on the pavement are shown in Figures 1 and 2. Between 10,000 and 25,000 repetitions can be applied in a 24 hour period, depending on the trafficking configuration and time required to take measurements. Test duration depends on the purpose of the test, but are typically run until either an average maximum rut of 13 mm (high temperature rutting tests on asphalt) or a predetermined level of cracking is reached.

Figure 1. HVS at the UCPRC APT facility.

Figure 2. HVS dual tires in channelized mode on a test pavement.

The primary purpose of the HVS tests discussed in this paper was the comparison of rutting performance of seven different gap-graded rubberized warm-mix asphalt mixes against two hot-mix asphalt controls of the same mix design. In order to accelerate the rutting accumulation, pavement temperatures were maintained at 50°C at 50 mm depth. The pavement surfaces were kept dry during testing. Changes in rutting were measured on a daily basis with a laser profilometer at 500 mm intervals along the middle 6 m of the 8 m test section (the 1 m acceleration and deceleration zones at each end of the test section are excluded). The total rut, calculated as the difference in elevations between the top of the heaved material on the side of the section and bottom of the deformed area in the wheelpath, is derived from the profile measurements. The testing was stopped once the average total rut exceeded 13 mm.

The tests were carried out using a dual truck tire configuration, standard tire pressures, unidirectional trafficking, and half-axle loading starting at the legal load (40 kN) and increasing to 60 kN after completion of 160,000 load repetitions. An environment chamber around the HVS is used to maintain pavement temperature. Heaters are placed next to the test section radiating heat onto the pavement. Thermostats in conjunction with thermocouples in the pavement are used to control the heaters and maintain the pavement temperature at 50°C ± 2°C at 50 mm depth.

It was not possible to perform actual noise measurements during testing due to the noise generated by the HVS. The sections are also too short for testing with other noise measuring equipment at the required speeds (Close Proximity [CPX] noise trailer at 50 or 80 km/h [ISO/CD 11819-2:2000] or Onboard Sound Intensity [OBSI] equipment at 80 or 100 km/h [Standard Method, 2010]).

Figure 3. Ames Engineering Laser Texture Scanner used to measure pavement surface texture.

However, it is known from the literature (Sandberg and Ejsmont, 2002) that there is a close relationship between pavement texture and the tire rolling noise. Therefore, pavement texture was measured on each of the HVS test sections as an indicator for noise emission. These pavement textures were used as input to a model that predicts the noise emission from a pavement with a given surface texture (see description of the Acoustical Optimization Tool [AOT] below).

Pavement surface textures were measured with an *Ames Engineering Laser Texture Scanner* (Figure 3) for the duration of seven of the nine warm-mix asphalt tests in 2010 and 2011. The scanner is a stand-alone unit that is placed on the pavement surface. The device scans a surface directly under its base in multiple line scans with a scan line length of 100 mm and a maximum scan width of 75 mm. The number of lines scanned can be set by the user. Up to 1,200 lines with an average spacing between scan lines of as little as 0.064 mm can be scanned. It takes about nine seconds to complete one scan line. The greater the number of lines scanned, the longer it takes to complete one test. In this experiment a resolution of 100 scan lines was used.

Texture data were processed to create six 2,000 mm long strings of surface texture representing six lines of pavement texture in the direction of the wheelpath for input into the AOT model. This was achieved by randomly selecting 120 100 mm profile lines from a pool of scanned texture profiles and combining them into the six 2,000 mm long profile lines. Figure 4 shows a randomly selected example of 100 mm texture sections for one of the pavements after zero and 309,000 load repetitions.

3 WORKING HYPOTHESES AND NOISE GENERATING MECHANISMS

The working hypotheses for the experimental design of the project are:

– Pavement wear by the HVS creates pavement surface textures that are representative of pavements exposed to real traffic on roads.

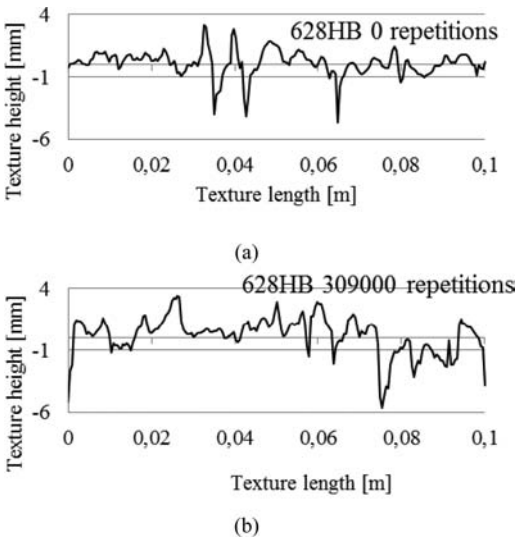

Figure 4. Example of 100 mm texture sections for one of the test pavements when new (top) and worn down after 309,000 repetitions (bottom) of the test tires passing over.

– AOT can be used to predict noise levels representative of the trafficked pavements based on the texture measured on these pavements.

The generation of noise when the tires are rolling on a road surface is mainly caused by the following mechanisms (Sandberg and Ejsmont, 2002). Other mechanisms may have a minor role:

– Vibrations in the tires: Vibrations are generated by the contact between the surface of the pavement and the rubber blocks of the tread pattern on the tire. Tire vibrations generate noise in the frequency range from 500 to 1,500 Hz. The noise increases with increasing roughness of the road surface. An increase in the maximum aggregate size generally leads to an increase in noise. The mean profile depth (MPD) can be regarded as a very general indicator for pavement roughness.
– Air pumping effect: When the rubber blocks on the tread pattern of the tire contact the road surface, air is pressed out of the cavities between the rubber blocks. When the rubber blocks leave the road surface, air is drawn back into the cavities. This air pumping generates noise at high frequencies above 1,000 Hz. If the road surface is open or porous the air will be pumped down into the pavement structure and the noise will be reduced.
– Horn effect: The curved tread pattern of the tires and the road surface act as an acoustical horn which amplifies the road noise generated around the contact point between the tire and the road surface. If the road surface is porous (and therefore sound absorbing) the amplification effect will be reduced.
– Absorption under propagation: The engine and road-tire noise propagate from the vehicles to the receivers. Under this propagation, the noise may be reflected from the road surface. If the road surface is porous, and therefore sound absorbing, the noise at some frequency bands will be reduced during propagation.
– Stiffness effect: The stiffness of the pavement is important for the determination of the noise generated by the contact between the surface of the pavement and the rubber blocks of the tread pattern on the tire. If the pavement has a low stiffness, the generated noise will be reduced.

Porous pavements have connected cavities and are open over the entire thickness of the layer, while open-textured pavements are open only in the upper part of the pavement with cavities having a depth less than the maximum size of the aggregate used. The basic concept of using open-textured pavements for noise reduction is to create a pavement structure, with as cavities as large as possible near the surface of the pavement to reduce to some extent the noise generated from the air pumping effect, and at the same time ensuring a smooth surface so the noise generated by the vibrations of the tires does not increase. These noise reducing open-textured pavements can be thin, since the mechanisms determining the noise generation only depend on the surface structure of the pavement.

4 ACOUSTICAL OPTIMIZATION TOOL

The texture profiles collected for the APT experiments were used to perform noise simulations/predictions using the Dutch Noise Optimization Tool (AOT, 2009) developed for the Dutch national road administration (DVS) between 2006 and 2008. AOT is an acoustical optimization tool for low-noise road surfaces (Kuijpers, 2008; AOT User's Manual, 2009). The AOT is based on models that describe the mechanisms generating tire road noise. Models included are a tire contact model, a tire interaction model, and a noise propagation model. The model framework was developed over a longer period and included theoretical development as well as empirical measurement results. A detailed presentation of the model framework is discussed in Kuijpers (2008).

AOT can simulate noise emissions caused by vehicles driving on a specific pavement surface at different speeds in the range from 50 to 120 km/h. There are four main input data describing the physical and acoustical properties of the pavement. These are presented below and related to the previously described noise generating mechanisms when a tire is rolling on a pavement (AOT User's Manual, 2009):

– Surface texture, which is a measure of the roughness of the road. The road surface texture is influenced by the size, shape, and arrangement of the road surface constituents (such as aggregates, binder, and additives). The surface texture influences the noise generated from vibrations in the tire.
– Acoustical impedance, which is a measure describing the influence of the road surface in terms of

reflection and absorption on the sound field that impinges on the surface. This term is related to the acoustic absorption of the road surface. Porous pavements have an absorbing effect on noise. The acoustical impedance of the road surface is used in the propagation part of the model. The acoustical impedance also influences the horn effect.

– Flow resistance, which is a measure of the resistance that the flow of air in the tire profile experiences in the rolling contact area. The flow resistance influences the noise generated from air pumping. The air flow resistance is the resistance that in the air that is expelled from the contact area between tire and road during the rolling process. If the airflow resistance is high, the air is effectively compressed in the contact area and might produce air pumping noise when the compressed air is released at the beginning or end of the contact patch. When the airflow resistance is low, for example on open-graded and porous pavements, then air is pressed down into the pavement structure with little resistance and the generation of air pumping noise is reduced.
– Mechanical impedance is a measure describing the influence of the road surface in terms of stiffness and damping on the vibrations of the tire. It has an influence on the noise generated from vibrations in the tire.

A series of measurement data from around forty Dutch test sections with many different kinds of noise reducing pavements are included in the AOT as default values, which can be selected by the user that has limited or no data. These test sections included amongst others single and double layer porous asphalt, thin overlays, poroelastic surfacings, dense-graded asphalt concrete, and standard stone-matrix asphalt (SMA) pavements. User can choose to use their own measured data for those parameters that they have available and then use AOT system data for the other parameters. In the study discussed in this paper, measured pavement texture data from the test sections were used in the analysis, together with AOT system data on acoustical impedance, flow resistance, and mechanical impedance. A standard SMA pavement with 11 mm maximum aggregate was selected as being closest to the tested asphalt pavements that had 12.5 mm aggregates.

Based on the selected input data, AOT predicts the noise for vehicles driving on the pavement described by the input data. The user can define the vehicle type used for the simulations (passenger cars or trucks) and can select results related to either the CPX measurement method (ISO/CD 11819-2:2000), or the SPB method (ISO 11819-1:1997), where the distance to the centerline of the road is 7.5 m and the receiver height is defined at 1.2 m, 3 m or 5 m.

The results are given as A-weighted noise levels (L_A) as well as the total noise in the third octave band spectra in the frequency range from 315 to 2,000 Hz. The spectral contributions from three individual noise generating mechanisms are also predicted. These are

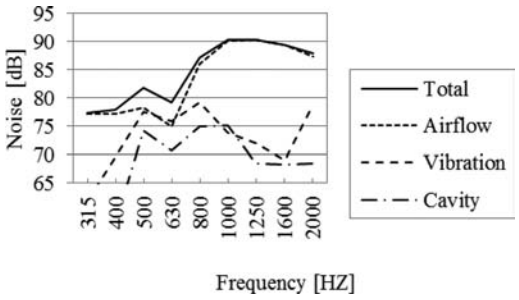

Figure 5. Example of the CPX spectra output from an AOT simulation of a dense-graded asphalt concrete (DGAC16). L_A is 96.6 dB at a speed of 100 km/h for passenger cars.

tire vibration generated noise (vibration), air pumping generated noise (airflow), and noise related to absorption (cavity).

Figure 5 is an example of the spectral output from an AOT simulation of a dense graded asphalt concrete (DGAC16) showing the total noise level as well as the contribution from the three noise generating mechanisms. The total noise level L_A is 96.6 dB (decibels) at a speed of 100 km/h for passenger cars. The frequency curve for the total noise level is shown with a black curve. In this example, the main contributor to the total noise level over 1,000 Hz is the airflow noise. At less than 1,000 Hz the noise from both vibrations and air flow have significance. The contribution from cavity or absorption is marginal as this pavement is dense with no high noise absorption.

Results related to the US OBSI method are not available as this is a European developed tool following ISO international standards. However, there is a close relation between the results measured by the CPX and the OBSI methods, depending on the reference tires used in the two methods. Consequently, the two methods will rank pavements in the same way in relation to noise. In principle, the noise levels and spectra that are predicted are the SPB and CPX levels for the tire group that was selected when the AOT was developed. They do not necessarily correspond to the standard indices for SPB and CPX (either survey or investigatory) methods. However, validation (Personal communication Kuijpers, 2009) has shown that, for example, the extended group of passenger car tires corresponds well with the "CPXcars" from the CPX standard. In this project CPX noise levels for passenger cars at a speed of 100 km/h was selected. The noise levels presented in this paper are A-weighted meaning that the noise at the different frequencies is weighted according to how the human ear perceives noise at these frequencies. The decibel unit "dB" is used and is the same as what is often denoted as "dB(A)" and "dBA".

To date, practical experience with the use of the AOT tool is relatively limited. Kuijpers (2008) evaluated the uncertainty of the AOT model, and based on a comparison of results of SPB and CPX measurements on five different pavements in the Netherlands and AOT noise predictions using measured pavement

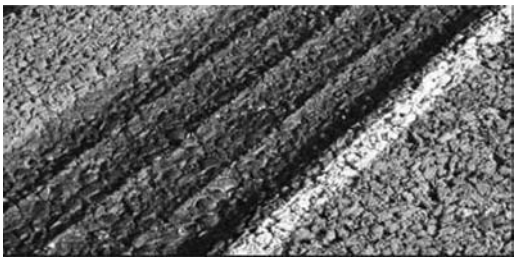

Figure 6. Close up of untested (beside the wheelpath) and tested pavement (in the wheelpath).

properties for these five pavements, it was concluded that in these cases the standard AOT modeling uncertainty was ±0.5 to 1.0 dB in the worst case. Noise emissions from road traffic are normally measured using the wayside SPB method or the Close-ProXimity (CPX) method. There is always uncertainty related to noise measurements. For measurements carried out according to the SPB standard, the uncertainty of the results for passenger cars is usually in the order of ±0.3 to 0.5 dB. For measurements carried out according to the CPX method the uncertainty is often stated to be in the order of ±0.5 to 0.7 dB. Based on this limited evaluation of AOT (Kuijpers, 2008) it would appear that the uncertainty of AOT predictions is higher than the uncertainty for actual SPB/CPX noise measurements.

5 TEST PAVEMENTS

The main objective of the HVS testing in this project was to compare the performance of different rubberized warm-mix asphalt technologies against a rubberized hot-mix asphalt control mix. The test pavements were all gap-graded aggregate with a maximum aggregate size of 12.5 mm and as-constructed air void contents ranging from 9 to 14% by volume. The five pavement sections discussed in this paper were 622HB, 623HA, 624HB, 625HA and 628HB.

Figure 4 shows a 100 mm section of the surface texture of an untested pavement and the same pavement after completion of HVS testing. Figure 6 shows the difference between the untrafficked and trafficked surface. From these two figures it can, as a first visual impression, be seen that the test pavement has a relatively rough surface texture before testing. After testing, the pavement surface appears to have a more convex surface structure where mortar and the smaller aggregates have been removed from the surface leaving the larger aggregates exposed. This can also be seen in Figure 7, which shows a horizontal view of the wheelpath after testing. In pavement acoustic analysis, the more convex a pavement surface is the more tire pavement noise is emitted.

6 RESULTS

As a very general indicator for the pavement surface structure, the mean profile depth (MPD) has been included in the data presented below. MPD generally does not correlate as well with noise as other pavement related factors like convex/concave texture, air void content, and aggregate size, etc., which also play an important role. Increasing MPD normally also leads to increases in tire/pavement noise. The measured MPD and the AOT predicted noise levels at different numbers of repetitions for the five sections tested are summarized in Table 1. Data from the SMA11 pavement used for the AOT predictions (SMA11-AOT) are also included. Between four and eight measurements were taken on each section depending on the number of repetitions to failure.

Bendtsen et al. (2009) concluded that a linear regression provides a good description of the relation

Figure 7. Horizontal view of the wheelpath after HVS testing.

Table 1. Measured MPD and the AOT predicted noise levels for the 5 pavements after different numbers of HVS repetitions. Data from SMA11 pavement used for the AOT predictions is included (SMA11-AOT).

Test section	Load Repetitions	MPD (mm)	Noise LA (dB)
622HA	15,000	0.91	97.5
	75,000	0.86	97.5
	1,29,000	–	98.1
	1,90,000	1.03	97.8
623HA	0	0.76	97.5
	10,000	0.87	98.0
	73,000	0.89	97.9
	1,71,020	0.94	97.8
	1,99,000	0.92	97.4
624HB	0	0.94	98.2
	10,000	0.83	97.6
	41,500	0.99	97.8
	73,000	0.78	98.5
	1,44,000	0.92	97.6
	1,60,000	0.88	97.7
	2,61,000	0.94	98.1
	3,20,000	1.03	98.1
625HA	0	0.92	97.8
	31,500	0.9	98.0
	43,000	0.93	98.6
	1,21,000	1.08	98.6
	2,60,000	0.86	96.8
	3,13,000	1.06	97.8
628HB	0	1.07	96.8
	20,000	1.01	98.4
	91,500	0.88	97.7
	2,70,000	1.07	97.8
	3,09,000		98.3
SMA11-AOT	0	1.01	97.3

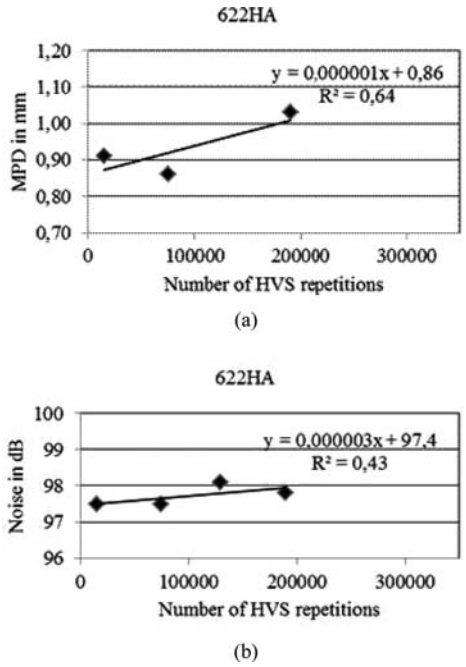

Figure 8. Development of MPD (measured) (a) and noise (predicted with AOT) (b) during the HVS testing on 622HA. Linear regression lines are included.

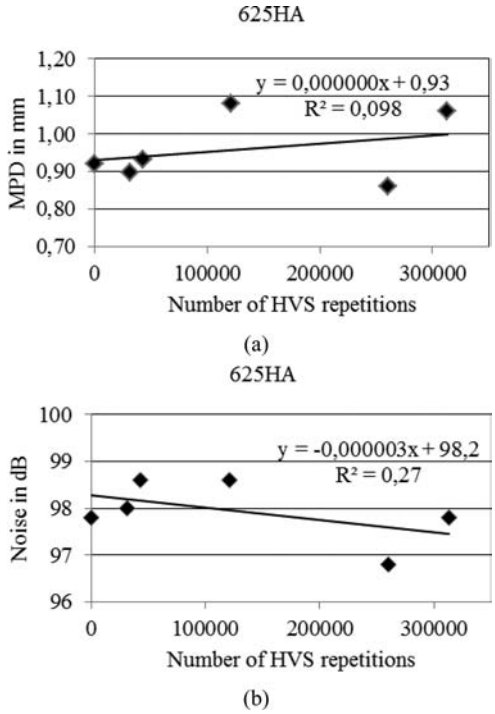

Figure 9. Development of MPD (measured) (a) and noise (predicted with AOT) (b) during the HVS testing on 625HA. Linear regression lines are included.

between noise level and the age of pavements, and that a logarithmic regression did not improve the result. Therefore linear regression has been used to analyze the relation between noise and the number of load repetitions with the HVS. Regression lines showing the results of the development of MPD and noise over the testing period are shown in Figures 8 and 9 for Sections 622HA and 625HA.

Figure 8 shows the development of the results for the 622HA pavement over a period of 190,000 repetitions. Increases in both MPD and noise are evident as the HVS testing continues. MPD increased around 0.1 mm and noise increased 0.5 dB during the testing.

Figure 9 shows similar results for the 625HA pavement over a range of 300,000 load repetitions. MPD increased around 0.07 mm, but for this pavement a decrease in noise of 0.8 dB was noted during HVS testing. The spread of the measured MPD levels on this section was high (R^2 is 0.10). This is reflected in the regression line for the AOT predicted noise, where R^2 is 0.27 and the standard deviation is 0.6 dB (Table 2).

In Figure 10, regression lines for the development of MPD (measured) during HVS testing on the five pavements are shown. The initial MPD of 1.01 mm for the SMA11 pavement, used as the standard pavement in the AOT predictions, is also shown. The SMA11 had a higher MPD than the five pavements (0.83 to 0.99 mm) before the start of HVS testing. MPD increased during testing on all pavements. This should be reflected by an increase in noise; however, as shown in Figure 11,

Table 2. Slopes for regression analyses of noise per 100,000 repetitions and per year (assuming 30,000 repetitions correspond to one year).

Test section	No. of measurements	Slope (dB/10^5 Reps)	Std. Dev. (dB)	Δ Noise/ year (dB/year)
622HA	4	0.3	0.3	0.1
623HA	5	−0.1	0.3	0
624HB	8	0.03	0.3	0
625HA	6	−0.3	0,6	−0.1
628HB	5	0.2	0.7	0.1

Std. Dev. = standard deviation

the noise increased on Sections 622HA, 624HB and 628HB, but decreased on the other two pavements (623HA and 625HA). All in all, the range of variation and development of noise for the five pavements during the testing was less than 1 dB. The initial noise levels for the five test pavements were 0.2 to 1.0 dB higher than the SMA11 pavement.

Table 2 shows an overview of the results of the regression analysis for the development of noise during the HVS testing. The standard deviations of the measured results in relation to the regression lines are included. For three of the pavements, the standard deviation was low at 0.3 dB (see also Figure 8 and 9),

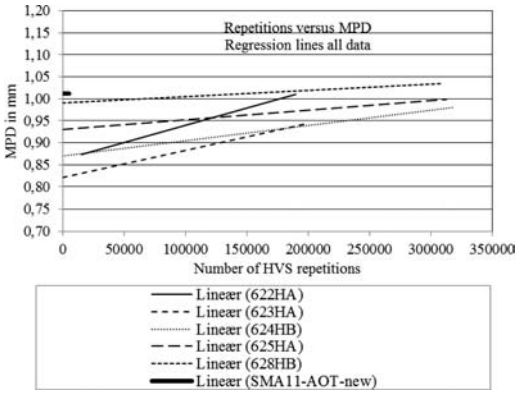

Figure 10. Regression lines for the development of MPD (measured) during the HVS testing on the five pavements.

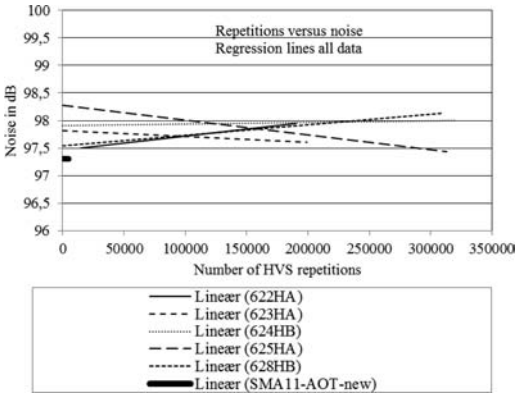

Figure 11. Regression lines for the development of noise predicted with AOT) during the HVS testing of the five pavements.

whereas for the 625HA and 628HA pavements, the standard deviation was 0.6 and 0.7 dB. The increase in noise per 100,000 load repetitions is also shown. In order to be able to express the development of noise as a change of decibels per year, it is necessary to define the lifetime of the tested pavements. For this study, it was generally assumed that the lifetime was ten years and equivalent to 300,000 HVS load repetitions. Using these parameters, the noise increase per year was calculated and is presented in Table 2. The results are presented with one decimal and vary from -0.1 dB/year to $+0.1$ dB/year with an average yearly increase on all five pavements of zero dB/year.

The spectral development of the noise can be seen in the figures below. Two examples are provided. Section 622HA had the highest increase of 0.30 dB/10^5 repetitions (Figure 12) and Section 625HA had the highest decrease of -0.30 dB/10^5 repetitions (Figure 13). The spectra are not broken down into the different components as in Figure 5; instead the total spectra are shown in the frequency range 315 to 2,000 Hz, as predicted by the AOT.

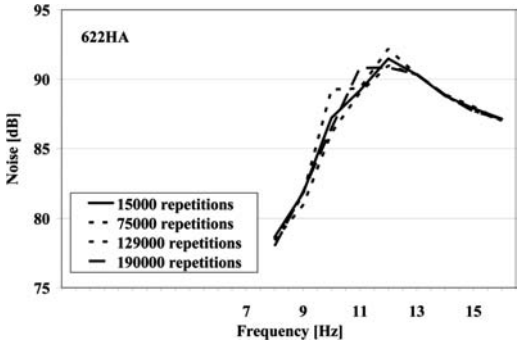

Figure 12. Spectral development (total noise) for 190,000 HVS repetitions on Section 622HA.

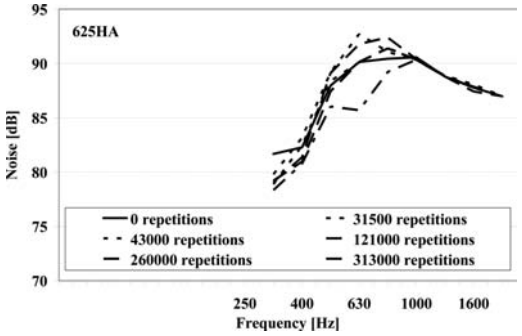

Figure 13. Spectral development (total noise) for 313,000 HVS repetitions on Section 625HA.

Figure 12 shows that the spectral change for the 622HA pavement occurs in the low frequency range below 1,000 Hz where a slight increase in noise can be seen with increasing load repetitions. This indicates that the pavement surface texture becomes rougher, which would increase the vibration generated noise. There was no change in noise levels over 1,000 Hz during the testing, indicating that the noise generated by air pumping did not change.

In Figure 13, the spectral change with a general noise decrease on the 625HA pavement can be seen. From zero to 121,000 repetitions, an increase of noise was predicted in the low frequency range below 1,000 Hz indicating that the pavement surface texture became rougher and increased the vibration generated noise, similar to the 622HA pavement. However, near the end of testing (i.e., after 260,000 repetitions) a remarkable decrease in the low frequencies of up to 4 dB can be seen. This indicates that the surface texture became smoother, which would decrease the generation of tire vibration noise. There was also no change in noise levels over 1,000 Hz indicating that the noise generated by air pumping did not change during the testing.

The AOT can separate the total noise spectra into the spectra related to vibration and air flow, respectively (see Figure 5). Examples of this for Section 622HA are provided in Figures 14 and 15. The main changes in

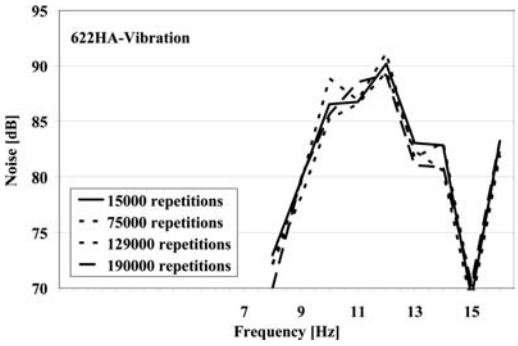

Figure 14. Spectral development (vibration component) for 190,000 HVS on Section 622HA.

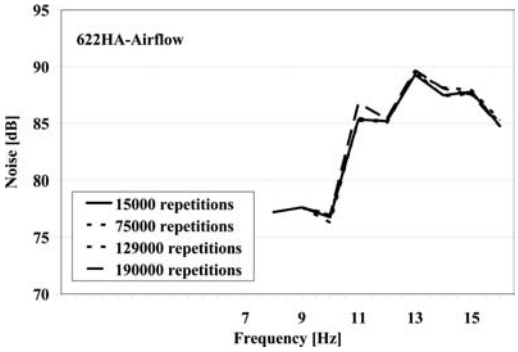

Figure 15. Spectral development (airflow component) for 190,000 HVS repetitions on Section 622HA.

Table 3. Prediction of the yearly increase of noise depending on different assumptions of the pavement lifetime.

	Pavement life		
Test section	5 years Δ noise/year (dB/year)	10 years Δ noise/year (dB/year)	15 years Δ noise/year (dB/year)
622HA	0.2	0.1	0.1
623HA	−0.1	0	0
624HB	0	0	0
625HA	−0.2	−0.1	−0.1
628HB	0.1	0.1	0

the spectra during the HVS testing were for the vibration noise (Figure 14), which increased slightly. There were no real changes in the spectra for air flow noise (Figure 15), which emphasizes the conclusions drawn above concerning the 622HA pavement.

The increase in noise during the HVS testing was converted to noise increase per year by assuming that 300,000 repetitions in the HVS testing corresponds to ten years of trafficking on a similar in-service pavement. Predictions for analysis periods of five and fifteen years were also considered. Results of this analysis are provided in Table 3.

7 DISCUSSION AND CONCLUSIONS

The visual impression looking at photographs of new pavements and the same pavements after HVS trafficking is that the pavement surface becomes rougher and acquires a more convex texture. This would be expected to result in a significant increase in the tire pavement noise generated. However, MPD measurements show only small increases in the pavements' general roughness, while noise predictions only show marginal increases for some of the pavement sections tested.

The predicted noise levels were 0.2 to 1.2 dB higher than the noise level predicted by AOT for the SMA11 pavement used as reference for the predictions. This was attributed in part to the tested pavements having a larger aggregate size (12.5 mm) than the SMA11 pavement (11 mm), and partly due to the channelized trafficking and relatively short nature of the test on pavements, which had not been exposed to extended environmental aging.

Assuming that 300,000 load repetitions is equivalent to ten years of in-service trafficking (very conservative), two of the pavements tested had a 0.1 dB/year increase in noise, two pavements had no increase, and one had a decrease of −0.1 dB/year. The average increase for all five pavements was 0.0 dB/year for passenger cars. These results are in the lower end of what has been observed in other investigations. In the European SILENCE project, DRD collected data from long-time noise measurements on pavements in Europe (Kragh, 2008). There was a large spread in the data, but the average results for passenger cars dense-graded asphalt concrete highways was an increase of 0.1 dB/year and 0.4 dB/year on porous pavements. The results of the study discussed in this paper are close to the results of this compilation of European results. In another project using Danish and Californian long-term noise measurement date (Bendtsen, 2009), the results for passenger cars on dense-graded asphalt concrete highways was an average increase of 0.4 dB/year. Research to obtain a better understanding of acoustic aging phenomena for asphalt pavements is still ongoing.

This study found a reasonable consistency in the development of the measured pavement textures expressed as MPD during the testing. The study also found a reasonable consistency in the noise levels predicted by the AOT using only texture measurements, in that the standard deviation of the results in relation to the regression line were generally low (0.3 to 0.7 dB). Based on these observations, it can be concluded that the selected method and the two hypotheses tested appear to produce reasonable results given the uncertainty related to the AOT and similar models.

There was, however, a spread in the individual results around the regression line, which is expected when using a limited number of data points (in this case, 3 to 8 texture measurements) to describe the full life cycle of a pavement. In these instances, the result

defined as the slope of the regression line can become very dependent on one "outlying" measurement point. The method could be improved by measuring texture at more frequent intervals (e.g., every 25,000 load repetitions), by testing on a wider range of pavements that are trafficked with wheel wander instead of channelized mode (as used in these tests), and testing on experiments of longer duration (e.g., fatigue cracking tests). This will result in the slope of the regression line being less dependent on individual measurement points. For practical reasons, it was not possible to obtain these types of measurements in the warm-mix asphalt rutting study.

ACKNOWLEDGMENTS

This project was performed as a part of a DRD project with entitled "Acoustical and structural durability of noise reducing pavements" with the objective of studying acoustical aging of asphalt pavements with a special focus on durability of noise reducing pavements. This project was partly financed by the Danish Ministry of Transport as a part of "A Green Transportation Policy" from January 2009. HVS testing was part of study into warm-mix asphalt, sponsored by the California Department of Transportation (Caltrans). The AOT model used in this project has been developed as a part of the Dutch Noise Innovation Program. The contents of this paper reflect the views of the authors and do not reflect the official views or policies of the Danish Ministry of Transport, the State of California, or the Federal Highway Administration.

REFERENCES

AASHTO, 2010. *Standard Method of Test for Measurement of Tire/Pavement Noise Using the On-Board Sound Intensity (OBSI) method.*

Acoustic Optimization Tool. 2009. Speron.net. CD ROM January 5th, 2009. M+P Consulting Engineers, the Netherlands.

AOT User's Manual. 2009. *Acoustic Optimization Tool.* Speron.net. CD ROM. M+P Consulting Engineers, The Netherlands.

Bendtsen, H; Kohler, E; and Lu, Q. 2009. *Acoustic aging of asphalt pavements. A Californian Danish comparison.* Report 171, 2009. Road Directorate/Danish Road Institute.

Bendtsen, H. 2010. *Noise reduction over time. Noise reducing thin layer pavements.* Status report 2010. Road Directorate/Danish Road Institute. See: www.roadinstitute.dk.

Dutch Noise Innovation Program, IPG: www.innovatieprogrammageluid.nl/gbdefault.asp.

ISO 11819-1: 1997. *Acoustics – Measurement of the influence of road surfaces on traffic noise – Part 1: Statistical Pass-by Method.*

ISO/CD 11819-2: 2000. *Acoustics – Measurement of the influence of road surfaces on traffic noise – Part 2: The close-proximity method.*

Kragh, J. 2008. Road Surfacings – Noise reduction time history. Report 161. Road Directorate/Danish Road Institute.

Kuijpers, A. et al. 2008. *Acoustic Optimization Tool. RE4 – modelling refinements in the SPERoN framework.* M+P Consulting Engineers, the Netherlands.

Kuijpers, A. 2009. Personal Communication. M+P Consulting Engineers, The Netherlands.

Lu, Q; Kohler, E and Harvey, J. 2009. *Investigation of Noise and Durability Performance Trends for Asphaltic Pavement Surface Types: Three-Year Results*. Davis and Berkeley: University of California Pavement Research Center.

Sandberg, U and Ejsmont, J.A. 2002. *Tyre/Road Noise Reference Book.* INFORMEX 2002. See: www.informex.info.

This page intentionally left blank

Advances in Pavement Design through Full-scale Accelerated Pavement Testing – Jones, Harvey, Mateos & Al-Qadi (Eds.)
© 2012 Taylor & Francis Group, London, ISBN 978-0-415-62138-0

Performance evaluation of unsurfaced pavements using the UIUC Accelerated Transportation Loading Assembly

D. Mishra & E. Tutumluer
University of Illinois at Urbana-Champaign, Illinois, US

ABSTRACT: Over 1.6 million miles of roads in the United States (US) are unpaved. In under-developed and developing countries, unpaved roads or unsurfaced pavements account for an even larger share in the total number of road miles. The absence of bound surface layers in these pavements results in direct application of traffic loads to the aggregate layer. Most methods used for thickness design of unsurfaced pavements are based on subgrade strength as the primary design consideration without giving much consideration to aggregate material quality. This paper presents findings from a recently completed research study at the University of Illinois aimed at investigating the effects of aggregate type and quality on unsurfaced pavement performance. Five full-scale unsurfaced pavement test sections were constructed at different combinations of aggregate quality and subgrade strength, and were tested to failure using the University of Illinois Accelerated Transportation Loading Assembly (ATLAS). Pavement performance was monitored through surface profile measurements as well as transverse scanning using Ground Penetrating Radar (GPR). The use of different field modulus measurement techniques was also pursued for identifying anomalies in construction conditions, and for justifying observed trends in test section performance. The performance of two different test "cells" constructed using uncrushed gravel with high fines and crushed limestone with low fines, respectively, were quite different.

1 INTRODUCTION

Unbound aggregate layers function as the primary load bearing component in unsurfaced pavements through distribution of traffic-imposed stresses. Design methods for unsurfaced pavements are commonly based on the principle of "subgrade protection" and recommend a minimum thickness of dense-graded aggregate layer based on the subgrade strength. Selection of aggregates for use in unsurfaced pavements is mostly based on economic considerations often resulting in the selection of aggregate sources associated with the lowest material hauling and transportation costs. In several parts of the United States, the only material processing requirement before use of aggregates in an unsurfaced pavement application involves the removal of large particles through screening (Skorseth et al., 2000). However, several researchers in the past have emphasized the significance of aggregate type and quality on the response and performance of unbound aggregate layers (Allen, 1973; Barksdale et al., 1989; Rowshanzamir, 1995; Lekarp et al., 2000; Mishra et al., 2010) in pavement systems.

In unsurfaced pavements characterized by direct application of heavy traffic loads on the unbound aggregate layer, the effect of aggregate quality on performance becomes even more pronounced (Garg and Thompson, 1998). For example, a recent Illinois Department of Transportation (IDOT) experimental study compared the performance of several unsurfaced pavement sections under truck loading, and observed that under similar loading conditions a 200-mm (8-in.) thick layer of crushed aggregate performed comparable to a 300-mm (12-in.) thick uncrushed gravel layer due to the better particle interlock and resulting higher shear strength in an aggregate matrix comprising crushed particles (Heckel, 2009).

This paper presents important findings from a recent study at the University of Illinois focused on accelerated testing of unsurfaced pavement test sections constructed using different aggregate types over weak subgrades of controlled strength. Five different test "cells" representing different combinations of aggregate quality and subgrade strength were constructed at the Advanced Transportation Research and Engineering Laboratory (ATREL), and were tested to failure using an Accelerated Transportation Loading Assembly (ATLAS). A summary of different aggregate material types used in construction of the full-scale test sections is presented first followed by the geometric layout and configuration details of individual test cells. Field trafficking performance of two of the test cells constructed over similar subgrade conditions are compared to identify different factors affecting unbound aggregate layer behavior.

2 OBJECTIVE AND SCOPE

The main objective of this paper is to evaluate the effects of aggregate type and quality on unsurfaced pavement performance through comparison of two

full-scale test cells constructed using different aggregate materials over similar subgrade conditions. The first cell was constructed using an uncrushed gravel with high amounts of nonplastic fines, whereas the second cell contained a crushed limestone with low amounts of plastic fines. Accelerated pavement testing was conducted through unidirectional application of a 44.5-kN (10-kip) wheel load using a super-single tire inflated to 758 kPa (110 psi) pressure. Test section performance was monitored through surface profile measurements and transverse scanning with ground penetrating radar (GPR). Visual analyses of pavement layer boundaries obtained from transverse trench excavations were conducted to distinguish between rut accumulation in aggregate and subgrade layers. Subgrade stress levels measured using earth pressure cells were used along with field-measured moduli of constructed subgrade and aggregate layers to justify observed trends in pavement performance.

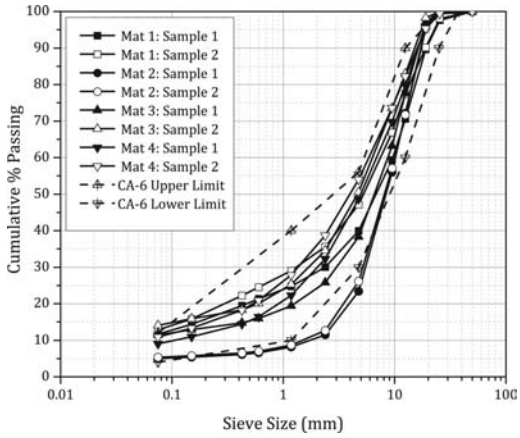

Figure 1. Particle size distributions of aggregate types used in full-scale test sections.

3 AGGREGATE MATERIALS TESTED

Four different aggregate materials commonly used in the state of Illinois for pavement applications were selected for construction of the full-scale unsurfaced pavement sections. The primary goal was to select aggregate types representing extreme combinations of aggregate physical properties as allowed by transportation agency specifications for pavement applications. Sources for the different aggregate materials were first identified through a preliminary survey of aggregate suppliers in the state of Illinois. Required quantities of the aggregates from individual sources were transported to the construction site and stockpiled with adequate precautions for minimizing moisture loss through evaporation and seepage. Each aggregate material was tested in the laboratory for grain-size distribution (ASTM C136), Atterberg limits (ASTM D4318), compaction characteristics (ASTM D698, D1557), unsoaked California Bearing Ratio (CBR) as a shear strength index (ASTM D1883), as well as permanent deformation and resilient modulus (AASHTO T307) characteristics.

Figure 1 presents the particle size distributions for the four aggregate types (two samples per material) along with the specification boundaries for a typical dense-graded coarse aggregate material (CA-6) used in Illinois for pavement applications. The percent fines content (fines defined as material passing the No. 200 sieve, or finer than 0.075 mm) and plasticity index (PI) of fines (measured on material passing sieve No. 40 or finer than 0.425 mm) for the four aggregate materials are listed in Table 1(a). Based on the particle shape and angularity (crushed or uncrushed), and type and amount of fines, the four aggregate materials were classified into the following four categories: (1) Uncrushed gravel with high amounts of nonplastic fines, (2) Crushed limestone with low amounts of plastic fines, (3) Crushed dolomite with high amounts of nonplastic fines, and (4) Crushed limestone with high amounts of nonplastic fines. Optimum moisture content (OMC) and maximum dry density (MDD) values for the four aggregate materials were determined using both the standard (ASTM D698) as well as modified (ASTM D1557) compactive efforts, and are summarized in Table 1b.

Table 1. (a) Aggregate materials selected for construction of full-scale test sections and (b) compaction characteristics.

(a)

Material	Average Fines Content (%)	Plasticity Index
1	12	0
2	5.2	5.7
3	13	0
4	10	0.2

(b)

	Optimum Moisture Content		Maximum Dry Density (kg/m^3/pcf)	
Material	ASTM D698	ASTM D1557	ASTM D698	ASTM D1557
1	8.6	8.2	2,140/136.2	2,200/140.0
2	6.5	7.3	1,810/115.2	2,150/136.9
3	7.7	5.5	2,220/141.3	2,250/143.2
4	8.1	5.7	2,210/140.7	2,260/143.9

Gradation curves for three of the four aggregate materials (except Mat 2) complied with the Illinois DOT dense aggregate CA-6 specification boundaries. The material used in Cell 2 (Mat 2) exhibited a coarser gradation compared to CA-6 specifications. Although the aggregate materials were obtained from sources commonly satisfying the CA-6 specification requirements, the particular “ledge” used as the source for

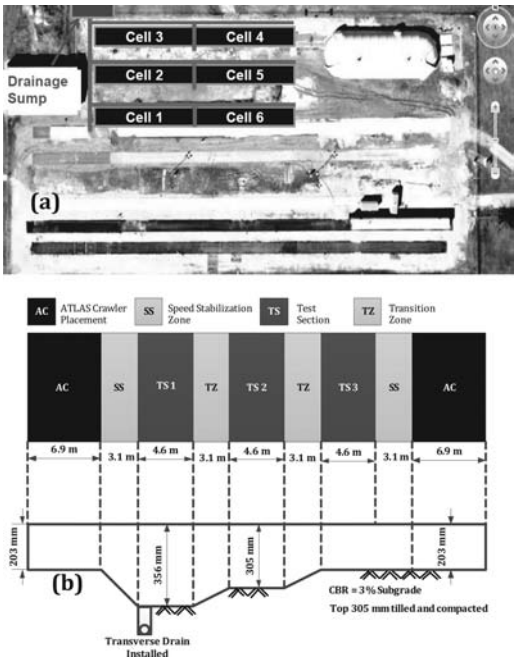

Figure 2. (a) Aerial map of test section layout, and (b) plan view (on top) and cross sectional details of the full-scale pavement test sections.

Mat 2 during this research project contained a significantly lower (5.2% compared to 12%) amount of fines than previously reported by the quarry. Note that verifying the particle size distributions in the laboratory was of particular importance as the aggregate gradations can change significantly with time depending on geological characteristics of the rock strata being quarried.

4 TEST SECTION LAYOUT AND CONFIGURATION

Six test "cells" (numbered 1 through 6) were constructed along three longitudinal strips (see Figure 2a) using the four aggregate materials listed in Table 1. However, Cell 6 was constructed using primary crusher type larger aggregate sizes, and its configuration will not be discussed in this paper. Cells 1, 2, 3 and 4 were constructed over engineered subgrades with a target CBR of 3% using aggregate materials 1 through 4, respectively. Identical subgrade conditions and aggregate layer thicknesses ensured that differences in pavement performance would be directly linked to aggregate quality. Cell 5 was constructed using the same aggregate material as Cell 2 (Mat 2) over a stronger subgrade of CBR 6%. The main objective behind this was to evaluate the effect of subgrade strength on unsurfaced pavement performance and mechanisms contributing to rut accumulation.

Figure 2a shows the layout of the test cells along three longitudinal strips 72.4 m (237.5 ft.) long and 5.5 m (18 ft.) wide separated by 3.7 m (12 ft.) wide access roads for construction equipment operation. Longitudinal edge drains were constructed along the north side of each cell and were connected to transverse drains near the west end of the cell. The edge drains sloped from east to west, and the discharge was carried by the long transverse drain along the west boundary to a sump pit. Water was continually pumped out from the sump pit to prevent accumulation of water in the drain pipes.

Figure 2b presents a schematic of the layout and cross-sectional details of individual test cells that were constructed 39.6 m (130 ft) long and comprised of three test "sections" with aggregate layers of thicknesses 355 mm (14 in.), 300 mm (12 in.), and 200 mm (8 in.), respectively. Each cell was separated from the adjacent cell (longitudinally) by a 6.9 m (22.5 ft.) long transition section for placement of the ATLAS tracks. From west to east, the 355mm (14-in.) thick aggregate section was named "Section 1" whereas the 200-mm (8-in.) thick aggregate section was named "Section 3". Each section was 4.6 m (15 ft.) long and was separated from adjacent sections by 3.1 m (10 ft.) long transition zones. At either end of the cell, 3.1-m (10-ft.) long speed stabilization zones were constructed to ensure uniform speed of loading on each section. As already mentioned, Cell 5 was constructed over a subgrade of CBR 6% and therefore the aggregate layer thicknesses for the three sections were 255 mm, 200 mm, and 150 mm, respectively.

5 SUBGRADE PREPARATION

The first step in construction of the full scale test sections involved laboratory characterization of the subgrade soil to quantify the change in CBR with moisture content, and ultimately determine the target moisture content in the field to achieve the target strength (CBR of 3% for Cells 1 through 4, and CBR of 6% for Cell 5). Samples were collected from twelve different locations at 150 mm (6 in.) intervals up to a depth of 1.2 m (48 in.). Visual classifications of the samples were first performed to divide them into four preliminary subgroups. Several laboratory tests were then conducted on the four sub-groups to characterize their physical and mechanical properties. All the four subgroups were characterized as low plasticity clayey silt (CL-ML). Since the four subgroups had similar properties, it was decided to use the average properties during the field construction. Important characteristics of the subgrade soil as determined from the laboratory tests are: Liquid Limit (LL) of 20, Plasticity Index (PI) of 5, Maximum Dry Density (MDD) from standard method (ASTM D698) test of 1,989 kg/m^3 (126.6 pcf) and Optimum Moisture Content (OMC) of 10.2%.

As the objective of the research study was to simulate unsurfaced pavement performance over weak subgrades, the top 300 mm (12 in.) of the subgrade layer was engineered through tilling and moisture addition to achieve a uniform strength (CBR of 3%

for Cells 1 through 4, and 6% for Cell 5). In-place CBR values were determined using the empirical relationship proposed by Kleyn et al. (1982) to correlate CBR with the penetration rate of a Dynamic Cone Penetrometer (DCP). The CBR-moisture characteristics as established in the laboratory served as the reference for determining moisture contents corresponding to the target CBR values. This procedure was repeated until the in-place CBR values (as determined from Equation 1) were obtained close to the target values. Note that the 'PR' term in Equation 1 denotes the DCP penetration rate (mm/blow). Details on the subgrade preparation procedure have been presented elsewhere (Mishra et al. 2012).

$$\text{Log (CBR)} = 2.61\text{-}1.26 \log (\text{PR}) \quad (1)$$

6 CONSTRUCTION QUALITY CONTROL AND IN SITU STIFFNESS MEASUREMENT

In situ constructed modulus values for the subgrade and aggregate layers were measured using *Dynatest® model 3031 Light Weight Deflectometer* (LWD), and *Humboldt® Soil Stiffness Gauge* (*GeoGauge*™). These devices have been identified by a recent NCHRP study (Von Quintus et al., 2009) as viable alternatives for non-nuclear quality assurance during flexible pavement construction and were used in the current study to investigate their adequacy in establishing links between as-constructed field moduli and pavement performance due to trafficking. In addition, in-place moisture-density values were also measured using a nuclear density gauge. Details of the in situ modulus measurement procedures and the mechanism of equipment operation have been reported elsewhere (Mishra, 2012).

7 EARTH PRESSURE CELL INSTALLATION AT AGGREGATE-SUBGRADE INTERFACE

To evaluate the effects of aggregate material type and quality on the dissipation of traffic-induced stresses with depth, earth pressure cells were installed on top of the subgrade at the aggregate-subgrade interface for monitoring the subgrade vertical compressive stresses. The earth pressure cells, manufactured by *Geokon*™ (model 3500), were circular in shape with a diameter of 230 mm (9 in.) and were rated for a maximum stress level of 400 kPa (58 psi). Two earth pressure cells (one each in Sections 2 and 3) were installed in each pavement test cell along the centerline of the wheel path. To install the pressure cells, a circular hole approximately 25 mm (1 in.) deep was first excavated in the compacted subgrade, and the cell was placed just below the finished subgrade surface. Trenches were excavated for connecting the pressure cell cables to the data acquisition system, and were filled with fine sand to ensure adequate protection against sharp aggregate particles. Pressure data during test section loading was acquired through a *LabView*™ virtual instrument at a frequency of 500 Hz. As the change in pavement layer temperature between installation of the pressure cells and the accelerated pavement testing was negligible, temperature corrections were not considered during analyses of the measured pressure levels. Figure 3 shows photos detailing the pressure cell installation procedure.

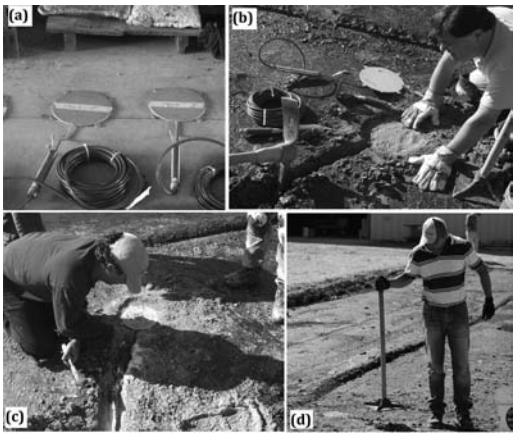

Figure 3. a) earth pressure cells, (b) excavation of circular hole in compacted subgrade, (c) embedding pressure cell cables in trenches using fine sand, and (d) tamping of soil on top of installed pressure cell to protect from sharp aggregate particles.

8 AGGREGATE PLACEMENT AND ACCELERATED PAVEMENT TESTING

After instrumentation of the test sections, aggregate layers were constructed by placing the material in two lifts and targeting a relative compaction of 95% with respect to the MDD values determined using the standard compaction (ASTM D698). Compaction of each lift was checked using a nuclear gauge, and moisture was added to the aggregate layer as necessary to aid the compaction process. Note that due to the weak subgrade conditions, it was not always possible to achieve the target value of 95% relative compaction. In such cases, the compaction process was continued until no significant increase in density was noticed from three consecutive passes of a vibratory compactor. The as-constructed moisture contents and dry densities of the compacted aggregate layers determined from nuclear gauge testing are summarized in Table 2.

The pavement test sections were constructed approximately 5.5 m (18 ft.) wide to accommodate loading along two different wheel paths. The sections were first tested under "as constructed" aggregate moisture conditions (north wheel path) before artificial flooding and testing along a wheel path (south wheel path) separated from the first one by a distance of 2.5 m (8 ft.). Note that the "as constructed" moisture contents of the aggregate layers were often

Table 2. In-place moisture-density and relative compaction (ASTM D698) values for the compacted aggregate layers.

	Moisture Content (%)			Dry Density (kg/m^3)/ Relative Compaction (%)		
Cell	S1	S2	S3	S1	S2	S3
1	7.6	7.3	6.9	2,040/95	2,030/95	2,060/96
2	3.6	3.5	3	1,880/104	1,930/107	1,970/109
3	6.1	6.1	5.8	2,040/92	1,980/89	2,040/92
4	3.6	4.2	4.1	2,000/90	2,040/92	2,080/94
5	3.6	4	3.6	1,960/108	2,030/112	1,950/108

S1, S2, and S3 denote test Sections 1, 2, and 3, respectively
1 kg/m^3 = 6.37 pcf.

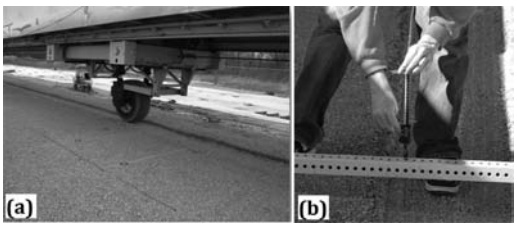

Figure 4. Photos showing unidirectional atlas loading and rut measurement.

similar to the optimum moisture contents (sometimes lower than the OMC by 1 or 2%) for the respective materials. Therefore, aggregate moisture conditions along the north wheel path have been referred to, as "near-optimum conditions" in this paper. Both the wheel paths were separated from the pavement edges by a distance of 1.5 m (5 ft.) to eliminate any possible edge effects induced by the unsupported aggregate boundaries. Performance of two test cells under near-optimum conditions only are presented in this paper. Effect of flooding on the test cell performance is presented elsewhere (Mishra, 2012).

9 ACCELERATED PAVEMENT TESTING AND PERFORMANCE MONITORING

After construction, the pavement sections were loaded to failure by a channelized, unidirectional application of a 44.5 kN (10 kip) wheel load through a super-single tire at a tire pressure of 758 kPa (110 psi). The development of rutting with load application for each test section was monitored through surface profile measurements using a digital caliper. Average surface profile for each test section was calculated using two measurements separated by a distance of 150 cm (5 ft.), located 150 cm (5 ft.) away from the section boundaries on either side. Figure 4 shows unidirectional loading of the test sections and the surface profile measurement using a digital caliper. Since the profile of an unsurfaced pavement is much more variable compared to that of a pavement with a bound surface layer, it

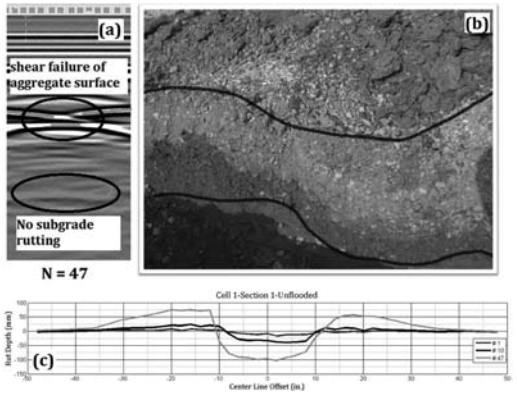

Figure 5. (a) GPR scan, (b) excavated trench, and (c) surface rut profile of the 355-mm thick uncrushed gravel aggregate section.

was important to take several adjacent measurements to develop the average surface profile around a particular point. The surface profile was measured for a distance of up to 1.22 m (4 ft.) on either side of the wheel path centerline.

Apart from surface profile measurements, performance under loading of the individual test sections was also monitored through transverse scanning using ground penetrating radar (GPR). Identification of the aggregate-subgrade layer interface from GPR scanning helped in distinguishing between aggregate and subgrade rutting. Strips of aluminum paint and thin aluminum strip foils were placed at the aggregate-subgrade interface to function as a pure reflector for electromagnetic (EM) GPR waves and clearly identify the layer boundaries. Detailed procedures for transverse GPR scanning of the test sections have been reported elsewhere (Mishra et al., 2012). After loading the test sections to failure, transverse trenches were excavated across the wheel paths for visual confirmation of different rut mechanisms contributing to failure. Important observations regarding the mechanisms contributing to the pavement failure of two different test cells are discussed in the following sections.

9.1 *Cell 1: Uncrushed gravel with high amounts of nonplastic fines*

Figure 5 shows the (a) GPR scan, (b) excavated trench section, and (c) surface rut profile for the 355-mm thick aggregate section (Section 1) in Cell 1 (uncrushed gravel with high amounts of nonplastic fines over a subgrade of target CBR of 3%). The first observation regarding the performance of this particular test section is that it failed (more than 100 mm rutting) after only 47 load applications (see Figure 5c) accompanied by significant surface heave adjacent to the wheel path. Note that heave development adjacent to the wheel path has been attributed by researchers to internal shear failure of aggregate layers (Dawson and Kolisoja, 2005). Close inspection of

the GPR scan (Figure 5a) and excavated trench section (Figure 5b) led to the following two important observations. Firstly, the amount of subgrade rutting (subgrade interface marked by the lower line in Figure 5a and lower trace in Figure 5b) is significantly lower compared to the surface rutting (aggregate surface shown by the upper line in Figure 5a and upper trace in Figure 5b). Moreover, the extent of heave development on the aggregate surface was more pronounced compared to the subgrade interface indicating internal shear movement of the aggregate layer. Secondly, as seen from the excavated trench section (see Figure 5b), rutting in the subgrade was laterally offset from the surface rut observed under the wheel path. The same was observed from the GPR scans (see Figure 5a), and indicated shear flow of material in the lateral direction.

Figures 6 and 7 show similar plots for Section 2 (300 mm gravel layer) and Section 3 (200 mm gravel layer), respectively. Similar to Section 1, the GPR scan of Section 2 (see Figure 6a) clearly showed higher rutting in the aggregate surface (upper line) compared to the subgrade (lower line). However, note that the subgrade rutting in Section 2 appeared to be more pronounced compared to Section 1 (confirmed by the cross-sectional profile obtained from the excavated trench). This phenomenon was attributed to the thinner aggregate layer in Section 2, and the lack of aggregate depth for the development of a complete shear surface within the layer. As a result, the depression in the subgrade for Section 2 was less offset from the wheel path compared to that in Section 1. Note that even for Section 2, the aggregate layer was the primary contributor to pavement failure.

The absence of significant heave development at the surface and the subgrade interface of Section 3 can be clearly seen in Figure 7. Lack of surface heaving indicated the absence of significant shear movement within the aggregate layer. Moreover, the subgrade deformation in Section 3 appeared to be less pronounced than in Sections 1 and 2. Lower accumulation of rutting in Section 3 was in contradiction with common intuition regarding thick aggregate layers ensuring better pavement performance, and could be justified through comparison of in-place subgrade modulus values measured using the LWD and GeoGauge^{TM}. As shown in Figure 8a, the subgrade

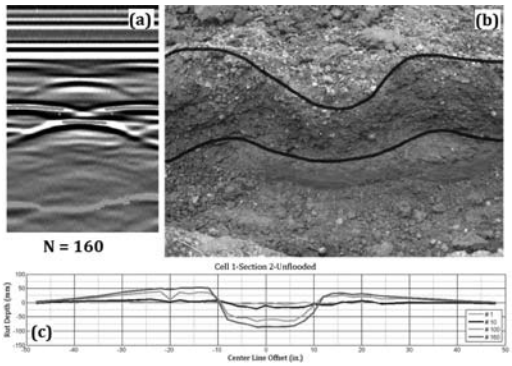

Figure 6. GPR scan, (b) excavated trench, and (c) surface rut profile of the 305-mm thick uncrushed gravel aggregate section.

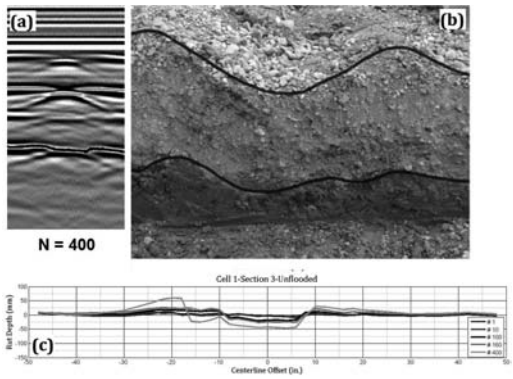

Figure 7. (a) GPR Scan, (b) Excavated Trench, and (c) Surface Rut Profile of the 200-mm thick Uncrushed Gravel Aggregate Section (1 in. = 25.4 mm).

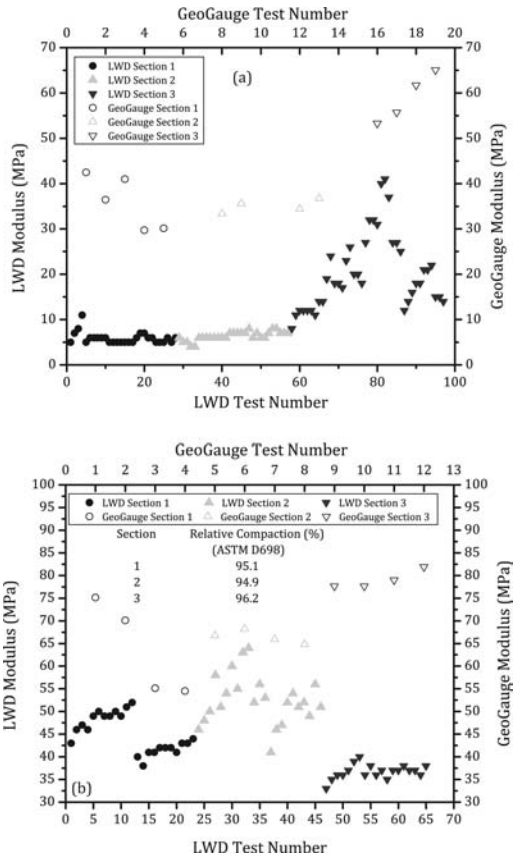

Figure 8. Field modulus values measured by LWD and GeoGauge^{TM} on (a) subgrade and (b) aggregate layers in Cell 1.

modulus values for Section 3 were consistently higher than those for Sections 1 and 2. This led to lower permanent deformation accumulation and hence resulted in the significantly better performance of Section 3 compared to Sections 1 and 2. Note that although the magnitudes of subgrade modulus values reported by the LWD and GeoGauge™ were different, both devices reported similar trends in the relative magnitudes of subgrade modulus in the three sections. This observation reinforced recent findings by Von Quintus et al. (2009) who presented the LWD and GeoGauge™ as viable non-nuclear alternatives for quality assurance during pavement construction.

Figure 8b shows modulus measurements on the compacted aggregate layer in Cell 1, constructed using the uncrushed "river-run" gravel with compaction targeting 95% of standard compaction (ASTM D698) maximum dry density. For Sections 1 and 2 (355-mm and 300-mm thick aggregate layers, respectively), the field moduli reported by the two devices were reasonably close to each other. However, for Section 3 (200-mm thick aggregate layer), the modulus values from LWD were significantly lower than those measured with the GeoGauge™. Note that the Section 3 subgrade for Cell 1 had significantly higher modulus/stiffness properties compared to Sections 1 and 2 (see Figure 8a). Moreover, from Figure 8b, the achieved degree of compaction for the aggregate layer in Section 3 was higher than those for the other two sections. As a higher degree of compaction usually corresponds to higher modulus values (Rowshanzamir, 1995; Tutumluer and Seyhan, 1998), the aggregate layer in Section 3 would then be expected to have higher moduli compared to Sections 1 and 2. Although the GeoGauge™ results followed this same trend, the LWD measured significantly lower modulus values for the aggregate layer in Section 3, which may be explained based on the depth of influence of the two devices. The depth of influence for LWD reported in the literature is between 270 and 280 mm (Nazzal, 2007; Nazzal et al., 2007), deeper than the 200-mm thick aggregate layer in Section 3. According to Von Quintus et al. (2009), LWD tests on thin pavement layers were significantly influenced by the underlying layer, and therefore, the results were consistently higher or lower than laboratory measured modulus values for those particular materials. Moreover, Mooney and Miller (2009) reported a depth of influence for LWD between 0.9 and 1.1 times the plate diameter. Therefore for the given study, the depth of influence for the LWD would be between 270 and 330 mm. Accordingly, the lower LWD-measured modulus values corresponding to the 200-mm thick aggregate layer in Section 3 were probably due to the influence of the weak underlying subgrade layer.

Significant material movement in the thick aggregate sections and the absence thereof in Section 3 was also established from the subgrade compressive stress data collected for Sections 2 and 3 at different numbers of load applications. Figure 9 shows subgrade vertical compressive stress values for Sections 2 and 3 plotted

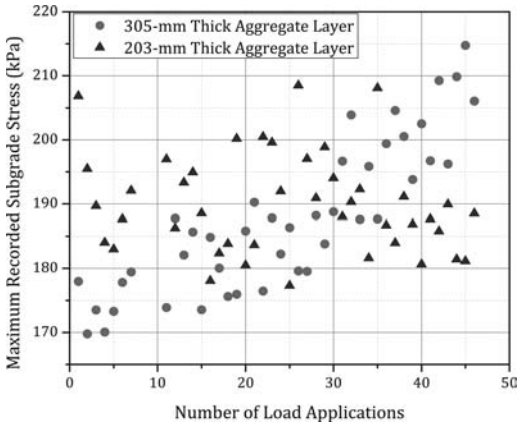

Figure 9. Change in subgrade stress levels with number of load applications for the uncrushed gravel test sections in Cell 1.

against different numbers of load applications (N). As shown in the figure, for low values of N, the subgrade stress levels under Section 2 (300 mm aggregate layer) were lower than those for Section 3 (200 mm aggregate layer) due to better lateral dissipation of stresses achieved in the thicker aggregate layer in Section 2. For example, for $N = 2$, the subgrade stress value in Section 2 was 169.8 kPa (24.6 psi), whereas the value for Section 3 was 195.5 kPa (28.4 psi). However as the number of load applications increased, the subgrade stress values for Section 2 gradually increased, and subsequently became greater than those for Section 3. Comparing the subgrade stress values at $N = 46$, it can be seen that the subgrade stress values for Sections 2 and 3 were 206 kPa (29.9 psi) and 188.5 kPa (27.4 psi), respectively. This was attributed to the significant shear movement within the aggregate layer in Section 2 which resulted in a reduction in the effective aggregate cover thickness subjecting the subgrade to higher stress levels. The 200-mm thick aggregate layer in Section 3 was constructed over a stiffer subgrade, and resisted internal shear movement supporting a significantly higher number of load applications without undergoing shear failure. Note that due to stiffer subgrade conditions, the aggregate layer in Section 3 could be compacted to higher densities than the other two sections (96% relative compaction for Section 3 compared to 95% relative compaction values for Sections 1 and 2, respectively).

9.2 *Cell 2: Crushed limestone with low amounts of plastic fines*

Cell 2 was constructed using a crushed limestone material with low amounts of plastic fines (Mat 2) over an engineered subgrade of target CBR of 3%. Performance of the test section under near-optimum aggregate moisture conditions was monitored through loading and surface profile measurements. Note that GPR scanning of this test cell could not be conducted

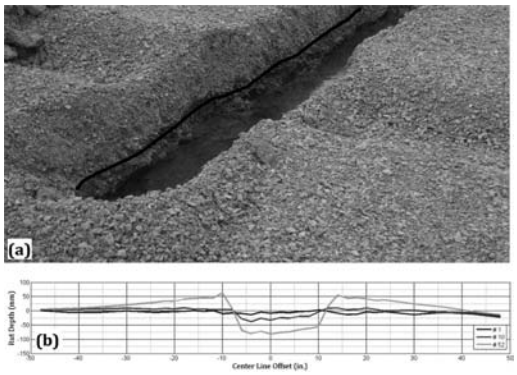

Figure 10. (a) Excavated trench and (b) surface rut profile of the 355-mm thick crushed limestone section in Cell 2.

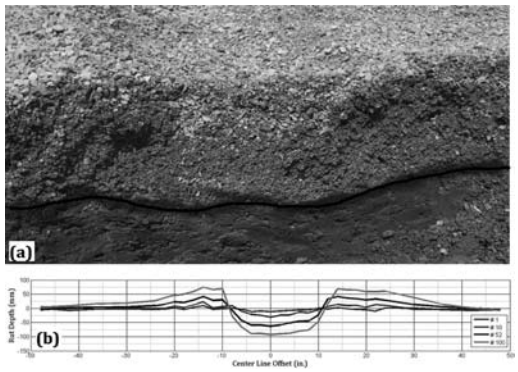

Figure 11. (a) Excavated trench and (b) surface rut profile of the 305-mm thick crushed limestone section in Cell 2.

due to unavailability of GPR equipment. Therefore, the mechanisms contributing to failure of this test cell were analyzed using surface profile measurements, and excavated trench sections only.

Figure 10 shows the (a) excavated trench section and (b) surface rut profile of Section 1 (355 mm aggregate layer) in Cell 2. As seen in Figure 10b, the test section failed after only 52 load applications by accumulating rut depths of 100 mm accompanied by significant heaving adjacent to the wheel path. As already mentioned, development of significant heave adjacent to the wheel path is often an indicator of shear movement within the aggregate layer, and presented the possibility of internal shear failure of the crushed limestone layer. Close inspection of the excavated transverse trench sections showed no significant deformation of the subgrade (see Figure 10a), with the aggregate-subgrade interface remaining essentially horizontal even after failure of the test section.

The deformation behavior was in contradiction with the commonly observed trends regarding crushed aggregate layers resisting permanent deformation due to better particle interlock. However, note that the crushed limestone material used in Cell 2 showed unstable matrix behavior under standard compactive efforts due to the significantly low fines contents, and could not be tested for permanent deformation characterization due to excessive bulging (Mishra, 2012). Moreover, the material showed very low CBR values (18 to 19%) under standard compaction conditions (ASTM D698). These laboratory test results supported the hypothesis of shear movement within the aggregate layer due to unstable matrix structure near standard compaction conditions. Figures 11 and 12 present the deformed profiles of Section 2 (305 mm aggregate layer) and Section 3 (200 mm aggregate layer), respectively.

As indicated in Figures 11 and 12, Sections 2, and 3 could sustain 100 and 350 load applications, respectively, before accumulating significant rutting. Moreover, close inspection of the surface profiles and the excavated trench sections clearly indicated

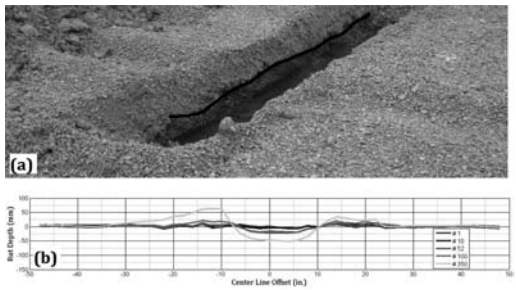

Figure 12. (a) Excavated trench and (b) surface rut profile of the 200-mm thick crushed limestone section in Cell 2.

increased subgrade heaving with decreasing aggregate layer thickness. The highest subgrade heaving was noted for the 200-mm (8-in.) thick aggregate layer in Section 3 (see Figure 12a).

Similar to the uncrushed gravel material in Cell 1, failure of the thickest aggregate section (Section 1) in Cell 2 was attributed to shear movement within the aggregate layer, which was also evident from the "wavy" nature of rut development along the wheel path. However, the crushed nature of the particles resulted in adequate stress reduction at the subgrade level, therefore, protecting the subgrade from excessive deformation before a significantly high number of load applications. Further investigation of the test cell performance was conducted through analysis of the field moduli measured using LWD and GeoGauge™ on the compacted subgrade and aggregate layers. Figure 13 shows the field moduli for the compacted (a) subgrade, and (b) aggregate layers for Cell 2.

The subgrade moduli for Sections 2 and 3 were similar in magnitude but were higher than those for Section 1 as highlighted from both the LWD and GeoGauge™ results. Although the lower subgrade moduli for Section 1 could possibly be a contributing factor resulting in rapid failure of the thickest aggregate section under loading, the difference between the performance of Sections 2 and 3 could not be

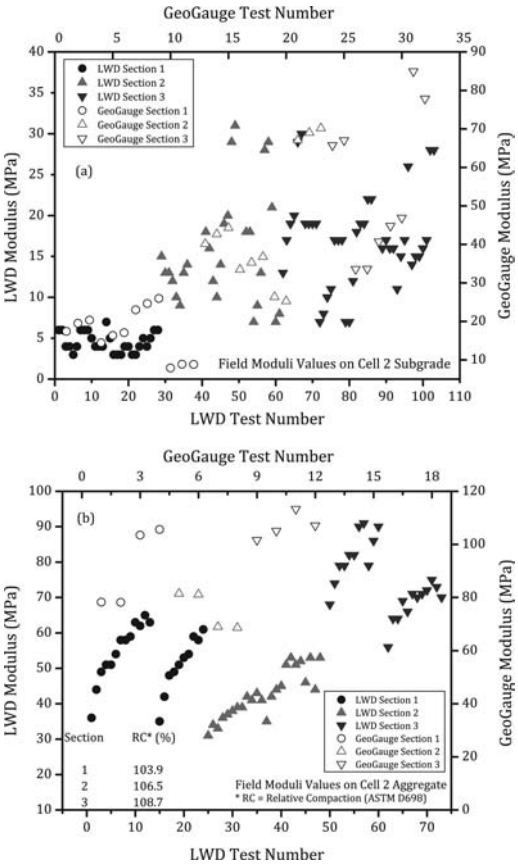

Figure 13. Field modulus values measured by LWD and GeoGauge^{TM} on (a) Subgrade and (b) aggregate layers in Cell 2.

explained on the basis of differences in subgrade moduli only. Close inspection of the aggregate field moduli (see Figure 13b) reflected significantly higher moduli for Section 3 compared to Sections 1 and 2. This was linked to the achieved relative compaction (ASTM D698) values for the three aggregate sections: 104%, 107%, and 109% for Sections 1, 2, and 3, respectively. Note that due to the free-draining nature of the crushed limestone aggregate used in Cell 2, the OMC and MDD values could not be easily established in the laboratory. Therefore, the laboratory-determined MDD value of 1,813 kg/m^3 was not indicative of the maximum achievable densities in the field. This explained the high relative compaction values (>100%) for all three test sections.

The 355-mm (14-in.) thick aggregate layer in Section 1 had the lowest relative compaction due to weaker subgrade conditions. Resulting inadequate particle interlock led to internal shear movement of the aggregate layer which ultimately failed after only 52 load applications. Sections 2 and 3 were both constructed over similar subgrade conditions, with the aggregate layer in Section 3 compacted to higher densities (109% MDD) compared to Section 2 (107%

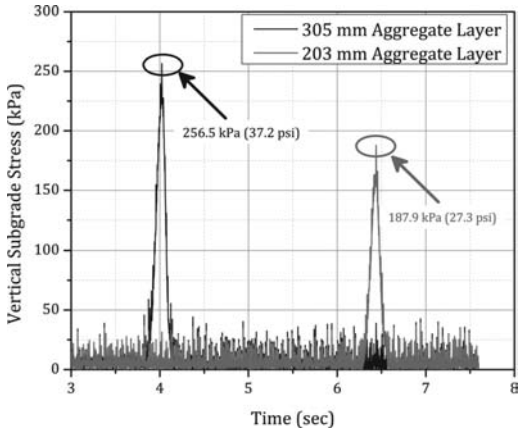

Figure 14. Subgrade stress levels below Section 2 (left) and Section 3 (right) of Cell 2 after N = 4 applications of unidirectional ATLAS loading.

MDD). Better compaction of the aggregate layer in Section 3 resulted in higher moduli values (adequately captured by the LWD and GeoGauge^{TM}), and better stress dissipation with depth. Reduced stress levels at the subgrade interface resulted in Section 3 sustaining a significantly higher number of load applications (350) compared to Section 2 (100) without accumulating excessive rutting. Higher compaction levels and in-place modulus values for Section 3 compared to Section 2 were also reflected in the subgrade stress levels as recorded by the earth pressure cells (see Figure 14). Figure 14 shows the subgrade vertical stress values for Sections 2 and 3 corresponding to N = 4 (relatively undeformed aggregate layer configuration) plotted against time. The first peak in Figure 14 (corresponding to time = 4 seconds) shows the subgrade stress level in Section 2, whereas the second peak (corresponding to time = 6.4 seconds) shows the stress on the Section 3 subgrade. As shown in the figure, higher subgrade stress values were recorded for Section 2 (305 mm aggregate layer) compared to Section 3 (200 mm aggregate layer). The same trend was observed at higher N values, and was attributed to the superior lateral dissipation of stresses within the stiffer aggregate layer in Section 3.

10 SUMMARY AND CONCLUSIONS

This paper has presented findings from a recently completed research project at the University of Illinois aimed at evaluating the effect of aggregate material type and quality on the performance of unsurfaced pavements. Full-scale test sections were constructed on a weak subgrade of controlled strength using different aggregate types and tested using the Accelerated Transportation Loading Assembly (ATLAS). The performance of two pavement test cells constructed using an uncrushed gravel with a relatively high percentage of nonplastic fines, and a crushed limestone with

a relatively low percentage of plastic fines, respectively, were compared to evaluate the effect of different factors affecting unsurfaced pavement performance.

For uncrushed gravel layers, internal shear movement of the aggregate layer was the primary mechanism contributing to pavement failure. Shear movement of the uncrushed gravel layer was more pronounced in the thick aggregate sections, and was not as significant in the thinner aggregate section constructed over a stronger subgrade. This was clearly confirmed by the increasing trend in subgrade stress levels with number of load applications for Section 2 (305 mm thick aggregate layer) and the absence of such a trend for Section 3 (200 mm thick aggregate layer).

The significantly better performance of the Section 3 (200 mm thick gravel layer) under near-optimum aggregate moisture conditions was questionable at first, but was later attributed to the significantly higher subgrade moduli for this section compared to the other two thicker aggregate sections. Higher subgrade moduli for Section 3 also enabled compaction of the corresponding aggregate layer to higher densities. Due to the combined effects of stiffer subgrade and denser aggregate layers, Section 3 of Cell 1 could withstand a significantly high number of load applications (400) without shear failure. This indicated that even an uncrushed gravel layer when constructed over stronger subgrades and compacted to high densities may result in adequate unsurfaced pavement performance.

Analysis of Cell 2 performance emphasized the importance of adequate compaction for crushed aggregates with low fines. Higher relative compaction percentages for the aggregate layers could be directly linked to better performance under loading. Laboratory testing of the aggregates showed similar trends, and have been reported elsewhere (Mishra, 2012). Although the crushed limestone matrix with low fines (used in Cell 2) was unstable under standard compaction conditions (ASTM D698), it performed comparably to other crushed aggregate materials with high fines, under modified compaction conditions (ASTM D1557).

For both the test cells, the Section 3 (200 mm thick aggregate layer) performed the best. In Cell 1, better performance of Section 3 was attributed to the higher subgrade modulus, whereas in Cell 2 the higher modulus of the aggregate layer was identified as the primary factor. In both cases, Section 3 achieved the highest relative compaction level (96% of MDD for Cell 1, and 109% of MDD for Cell 2) due to relatively low constructed lift thicknesses (approximately 100 mm). Research findings indicate that for relatively poor quality materials like uncrushed gravel with high fines, and crushed aggregates with very low fines adequate performance may be ensured through reduced lift thicknesses and increased compactive efforts.

Field modulus measurements using LWD and GeoGauge™ as well as substructure visualization using GPR were found to be effective in monitoring construction quality and identifying subsurface deformations respectively.

ACKNOWLEDGEMENTS

This paper is based on the partial results of ICT R27-81 "Field Performance Evaluations of Illinois Aggregates for Subgrade Replacement and Subbase" research study. ICT R27-81 project was conducted at the Illinois Center for Transportation (ICT) in cooperation with the Illinois Department of Transportation, Division of Highways, the U.S. Department of Transportation, and Federal Highway Administration. The authors would like to extend their acknowledgements to ICT research engineer James Meister and graduate students Hasan Kazmee, Huseyin Boler, Yu Qian, Marcus Dersch and Anthony Mareno for their help during the construction, testing, and performance monitoring of the full scale pavement sections. Special thanks are due to Maziar Moaveni and Yuanjie Xiao for their help with the in situ stiffness measurement during construction as well as the accelerated pavement testing. The authors are also thankful to Prof. Imad Al-Qadi, Dr. Zhen Leng, and Mr. Pengcheng Shangguan for their help in GPR scanning of the test sections. The contents of this paper reflect the views of the authors who are responsible for the facts and the accuracy of the data presented herein. The contents do not necessarily reflect the official views or policies of the Illinois Department of Transportation or the Federal Highway Administration. This paper does not constitute a standard, specification, or regulation.

REFERENCES

Allen, J. 1973. *The Effect of Non-Constant Lateral Pressures on the Resilient Response of Granular Materials*. Ph.D. Dissertation. University of Illinois at Urbana-Champaign.

Barksdale, R.D. and Itani, S.Y. 1989. Influence of Aggregate Shape on Base Behavior. In T*ransportation Research Record: Journal of the Transportation Research Board, No. 1227*, Transportation Research Board, Washington, D.C. pp. 173–182.

Dawson, A.R. and Kolisoja, P. 2005. Permanent Deformation. *ROADEX II Final Report*, Roadscanners, Rovaniemi, Finland.

Garg, N. and Thompson, M.R. 1998. *Mechanistic-Empirical Evaluation of the MnRoad Low Volume Road Test Sections*. Publication FHWA-IL-UI-262, University of Illinois at Urbana-Champaign, Urbana, Illinois.

Heckel, G. 2009. *Aggregate Subgrade Thickness Determination*. Final Report: Experimental Features Project IL 03-01, Physical Research Report # 154, Illinois Department of Transportation, Springfield, Illinois, 2009.

Kleyn, E.G., Maree, J.H. and Savage, P.F. 1982. The Application of a Portable Pavement Dynamic Cone Penetrometer to Determine in Situ Bearing Properties of Road Pavement Layers and Subgrades in South Africa. In *Proceedings of the 2nd European Symposium on Penetration Testing, Amsterdam, 1*, National Institute for Transport and Road Research, pp. 277–282.

Lekarp, F., Isacsson, U. and Dawson, A. 2000. State of the Art. I: Resilient Response of Unbound Aggregates. *Journal of Transportation Engineering*, ASCE, Vol. 126, No. 1, pp. 66–75.

Mishra, D., Tutumluer, E. and Butt, A.A. 2010. Quantifying Effects of Particle Shape and Type and Amount of Fines on Unbound Aggregate Performance through Controlled Gradation. In *Transportation Research Record: Journal of the Transportation Research Board, No. 2167*, Transportation Research Board, Washington, D.C. pp. 61–71.

Mishra, D., Tutumluer, E. and Heckel, G. 2012. Performance Evaluation of Uncrushed Aggregates in Unsurfaced Road Applications through Accelerated Pavement Testing. Accepted for Publication in *Transportation Research Record: Journal of the Transportation Research Board*.

Mishra, D. 2012. *Aggregate Characteristics Affecting Response and Performance of Unsurfaced Pavements on Weak Subgrades*. Ph.D. Dissertation. University of Illinois at Urbana-Champaign.

Mishra, D., Tutumluer, E., Leng, Z. and Al-Qadi, I.L. 2012. *Assessment of Subsurface Deformation in Unsurfaced Pavements using Ground-Penetrating Radar*. Paper No. 12-3439, Presented in Session No. 249, 91st Annual Meeting of the Transportation Research Board, Washington, D.C., January 22–26, 2012, Washington, D.C.

Mooney, M.A. and Miller, P.K. 2009. Analysis of Lightweight Deflectometer Test Based on In Situ Stress and Strain Response. *Journal of Geotechnical and Geoenvironmental Engineering, 135(2)*, pp. 199–208.

Nazzal, M.D. 2003. *Field Evaluation of In-Situ Test Technology for QC/QA During Construction of Pavement Layers and Embankments*. MS Thesis, Louisiana State University, Baton Rouge, Louisiana.

Nazzal, M.D., Abu-Farsakh, M.Y., Alshibli, K. and Mohammad, L. 2007. Evaluating the Light Falling Weight Deflectometer Device for In Situ Measurement of Elastic Modulus of Pavement Layers. *Transportation Research Record: Journal of the Transportation Research Board, No. 2016*, pp. 13–22.

Rowshanzamir, M.A. 1995. *Resilient Cross Anisotropic Behavior of Granular Base Materials under Repetitive Loading.* Ph.D. Dissertation. University of New south Wales, Australia.

Skorseth, K. and Selim, A.A. 2000. *Gravel Roads: Maintenance and Design Manual*. US Department of Transportation, Federal Highway Administration.

Tutumluer, E. and Seyhan, U. 1998. Neural Network Modeling of Anisotropic Aggregate Behavior from Repeated Load Triaxial Tests. In *Transportation Research Record: Journal of the Transportation Research Board, No. 1615*, Transportation Research Board, Washington, D.C., pp. 86–93.

Von Quintus, H.L., Rao, C., Minchin, R.E., Nazarian, S. Maser, K.R. and Prowell, B. 2009. *NDT Technology for Quality Assurance of HMA Pavement Construction*. NCHRP Report 626, Transportation Research Board.

This page intentionally left blank

Advances in Pavement Design through Full-scale Accelerated Pavement Testing – Jones, Harvey, Mateos & Al-Qadi (Eds.)
© 2012 Taylor & Francis Group, London, ISBN 978-0-415-62138-0

Use of accelerated pavement testing to validate Ride Quality Index data

T.R. Clyne
Minnesota Department of Transportation, Maplewood, Minnesota, US

ABSTRACT: Ride Quality Index (RQI) is the measure used by many state agencies to characterize pavement roughness for construction quality control or in their pavement management systems. The Minnesota Department of Transportation (MnDOT) uses RQI as a basis for determining what the driving public considers acceptable ride quality. To validate this concept, RQI measurements were analyzed for the 22 original asphalt test sections at MnROAD. These pavement test sections were built on the Mainline and Low Volume Road to study their performance under accelerated loading conditions. RQI data was collected twice per year on each section with a *Pathways* video inspection vehicle, similar to the data collected every year on 12,000 miles of the state highway network in Minnesota. Preventive maintenance treatments were applied at various times to various test sections to repair minor distresses and restore ride quality. This paper discusses the time required for each test section to reach a terminal serviceability level and compares it to the original three, five, or ten-year design life. The paper also considers the ride quality when microsurfacing was applied and the extension in life realized by the maintenance treatment. Finally, the paper examines the distress history within each cell to determine which surface distresses are most responsible for the deterioration in ride quality. The research shows how accelerated pavement testing can be used to validate ride quality concepts used in state pavement management programs. Although no statewide network data is presented in this paper, the MnDOT pavement management program does track the condition of highways over time and is able to quantify the benefits of extended life and reduced costs by applying preventive maintenance treatments.

1 INTRODUCTION

1.1 *MnDOT trunk highway network*

The Minnesota Department of Transportation (MnDOT), like many state highway agencies, surveys the condition of their pavement network on an annual basis. This survey evaluates statewide pavement performance trends and how they compare with established targets. In addition, the condition surveys aid in planning by identifying roadways that will need minor or major rehabilitation to maintain good ride quality. Pavement condition data is used to monitor the performance of the system as a whole, to help in selecting the best strategy to rehabilitate a particular pavement, and to identify pavements that need future maintenance and/or rehabilitation (MnDOT, 2011a).

MnDOT has performance targets in which a minimum percentage of roadway miles must be in the "good" category while limiting the percentage of miles in the "poor" category, based on functional classification of the roadway. MnDOT also identifies trigger values of ride quality for when a particular pavement is in need of rehabilitation. Finally, MnDOT uses pavement smoothness as a pay item in asphalt and concrete pavement construction (Wilde, 2007; MnDOT, 2011b).

1.2 *Ride Quality Index*

The index used to measure pavement smoothness by MnDOT is the Ride Quality Index (RQI). RQI is measured on a zero-to-five rating scale. The higher the RQI, the smoother the road. The RQI is intended to simulate the score that a typical driver would give to the pavement's smoothness as felt while driving in his or her vehicle. New construction projects generally have an initial RQI above 4.0, and pavements are normally designed for a terminal serviceability level of 2.5. This terminal RQI value does not mean that the road is impassable, but rather that it has deteriorated to the point where the ride has become uncomfortable and a major rehabilitation is necessary (Janisch, 2006).

The RQI is mathematically calculated according to Equation 1 below from a pavement's longitudinal profile, which is measured by a *Pathways* digital inspection vehicle. A parameter named the International Roughness Index (IRI) is then calculated to estimate the amount of vertical movement a standard vehicle would experience when driving down the road. IRI, as measured by the *Pathways* van, is directly correlated to the perceived roughness, RQI, as felt by a rating panel of the general public (Janisch, 2006). This is often referred to as the "seat-of-the-pants" ride

measurement. RQI values of 3.1 to 5.0 are considered "good" while RQI values of 0.0 to 2.0 are considered "poor." In between the ride quality is considered "fair."

$$RQI = 5.697 - (2.104) \times \sqrt{IRI} \quad (1)$$

1.3 *MnROAD Background*

The Minnesota Road Research Project (MnROAD) was constructed by the Minnesota Department of Transportation between 1990 and 1993 as a full-scale accelerated pavement testing facility, and opened to traffic in 1994. Located near Albertville, Minnesota (40 miles northwest of Minneapolis-St. Paul), MnROAD is one of the most sophisticated, independently operated pavement test facilities in the world. Its design incorporates thousands of electronic in-ground sensors and an extensive data collection system that provide opportunities to study how traffic loadings and environmental conditions affect pavement materials and performance over time. MnROAD consists of two unique road segments located parallel to Interstate 94:

- A 3.5-mile Mainline interstate roadway carrying "live" traffic averaging 28,500 vehicles per day with 12.7% trucks.
- A 2.5-mile closed-loop Low Volume Road carrying a MnROAD-operated 18-wheel, 5-axle, 80,000-lb tractor-semi-trailer to simulate the conditions of rural roads.

1.4 *MnROAD test sections*

MnROAD test sections are made up of various materials, designs, and drainage conditions and are constructed like any typical highway in MnDOT's network. This research only considers hot-mix asphalt (HMA) test sections built in the original MnROAD experiment in 1993. These sections, or cells, are on both the Mainline (Cells 1–4, 14–23) and Low Volume Road (Cells 24–31). Cells 24 and 25 were built on a sand subgrade with an R-value of 70; all other cells were constructed on a clay subgrade with an R-value of 12. Because MnROAD is an accelerated pavement testing facility, the design life of each test section is relatively short (three, five, or ten years). This allows researchers to observe pavement performance and realize the results of their studies in a reasonable time period, much shorter than a 20+ year design life on an in-service pavement. Figure 1 provides a schematic of each of the test sections investigated. Stroup-Gardiner and Newcomb (1997) describe detailed information about the test section construction and material properties.

Over the years MnROAD has applied a number of preventive maintenance treatments to various test sections including crack sealing, crack leveling with mastics, slurry seal, and microsurfacing. These maintenance treatments were applied primarily to address

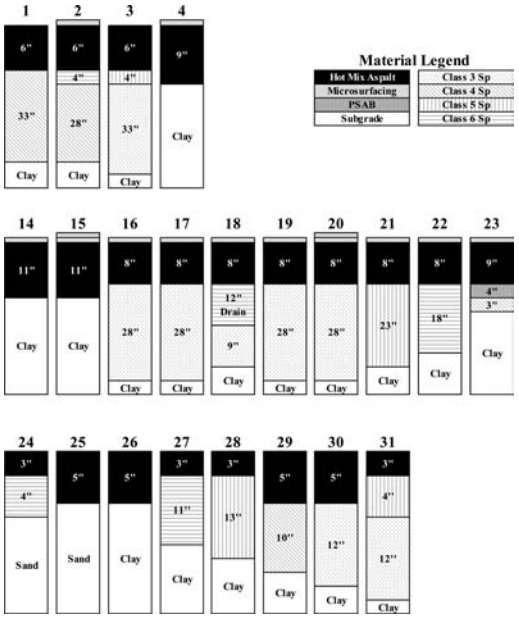

Figure 1. MnROAD HMA test cell schematics.

minor surface defects such as cracking and rutting, but also to evaluate different products side-by-side in a single location. Table 1 describes the maintenance activities performed at MnROAD (Palmquist et al., 2002; Zerfas et al., 2004; Johnson et al., 2007).

The traffic at MnROAD consists of equivalent single axle loads (ESALs) representative of both freeways and low volume roadways. Table 2 shows a summary of the traffic by year, roadway, and lane. For the Mainline test sections, the driving lane carries about four times the amount of ESALs as the passing lane. On the Low Volume Road, the ESAL counts between the inside and outside lanes are approximately equal. MnROAD lies within the wet-freeze climate zone in the north-central United States. Table 3 shows the typical temperature, humidity, and precipitation data from St. Cloud, MN, which is about 30 miles west of the MnROAD site (Minnesota Climatology Working Group, 2012).

1.5 *Objective*

The objective of this paper is to evaluate the ride quality of the original MnROAD asphalt test sections in the context of the overall MnDOT pavement network. MnROAD test sections were constructed with a three-, five-, or ten-year design life and will be considered against their actual lives when they reached a terminal serviceability level. Preventive maintenance (PM) treatments have been applied to many of the test sections, and the effect of these treatments on the extension of pavement service life will also be investigated. Finally, this paper will examine the distress history of each test section to determine which distress types most negatively affect pavement ride quality.

Table 1. MnROAD preventive maintenance activities.

Cell	Crack sealing (Both lanes)	Transverse crack repair (Both lanes)	MiniMac/Microsurfacing slurry seals	
			Passing lane (# Treatments)	Driving lane (# Treatments)
1	1998–2000–2003	–	–	–
2	2000–2003	–	2003 – MiniMac (1)	2003 – MiniMac (2)
3	Control Cell – No maintenance work performed			
4	2000–2003	2003 – Mastic	2003 – Micro (2)	2003 – Micro (2)
14	2000–2003	2003 – Mastic	2003 – MiniMac (2)	2003 – MiniMac (2)
15	2000–2003	2003 – MiniMac	2003 – Micro (1) over MiniMac (1) 2004 – Micro (1)	2003 – Micro (1) over MiniMac (1) 2004 – Micro (1)
16	1998–2000–2003	2003 – Mastic	2004 – Micro (1)	2004 – Micro (1)
17			2003 Control Cell 2004 – Micro (2)	No Maintenance Work 2004 – Micro (1)
18	2000–2003	2003 – Mastic	2003 – Micro (1)	2003 – Micro (2)
19	2000–2003	–	2003 – Micro (1)	2003 – Micro (1)
20	2000–2003	– –	1999 – Micro (2) 2003 – Micro (1)	1999 – Micro (2) 2003 – Micro (1)
21	2000–2003	–	2003 – Micro (1)	2003 – Micro (2)
22	2000–2003	–	2003 – Micro (1)	2003 – Micro (1)
23	2003	– –	1999 – Micro (2) 2003 – Crack Reseal Only	1999 – Micro (2) 2003 – Crack Reseal Only
24	2000–2003	–	2005 – Micro (1)	2005 – Micro (1)
25	2000–2003	–	2005 – Micro (1)	2005 – Micro (1)
29	2000–2003	–	2005 – Micro (2)	2005 – Micro (2)
30	2000–2003	–	2005 – Micro (2)	2005 – Micro (2)

Table 2. Annual MnROAD traffic data.

Year	Cumulative total ESALs			
	Mainline		Low volume road	
	Driving	Passing	Inside	Outside
1994	2,39,369	52,168	7,628	6,223
1995	7,55,498	1,77,231	25,813	26,810
1996	12,22,043	2,92,007	46,026	44,842
1997	15,24,322	3,66,640	62,187	60,046
1998	20,13,380	4,88,449	85,534	77,322
1999	25,37,115	6,31,668	96,549	90,027
2000	31,38,150	7,91,822	1,17,577	1,07,282
2001	37,49,492	9,61,563	1,36,448	1,24,579
2002	43,50,428	11,07,163	1,59,536	1,36,696
2003	49,61,403	12,53,129	1,72,542	1,49,905
2004	53,29,649	13,35,450	1,81,820	1,58,669
2005	60,51,316	15,27,434	1,95,536	1,73,243
2006	67,55,540	17,04,159	2,10,707	1,88,776
2007	75,16,069	18,92,828	2,22,210	1,95,601

2 RESEARCH METHODOLOGY

2.1 *Field data collection*

MnDOT staff typically collects pavement profile data on all of the MnROAD test sections with a *Pathways* digital inspection vehicle in the spring and fall of each year. Unfortunately for this project, MnDOT only obtained the *Pathways* equipment and began testing with it in 1997, three years after the test sections were opened to traffic in 1994. Nevertheless, there was a good body of data collected between 1997 and 2008, when the majority of the asphalt test sections at MnROAD were reconstructed (some Low Volume Road cells were reconstructed earlier – refer to Figure 1).

Table 3. Average MnROAD weather data.

Parameter	Jan	Feb	Mar	Apr	May	Jun	Jul	Aug	Sep	Oct	Nov	Dec
Air Temperature (°F)												
Normal Daily Maximum	18.7	25.7	37.7	54.9	69	77.3	81.7	78.9	69	56.3	37.2	23.2
Normal Daily Minimum	−1.2	6.4	19.1	32.2	44.1	52.9	57.9	55.5	45.7	34.3	20.4	5.5
Relative Humidity (%)												
Hour 6	79	81	82	81	82	86	90	92	91	86	84	82
Hour 12	70	68	63	50	50	55	57	59	59	58	68	72
Hour 18	74	70	64	50	48	53	57	60	62	61	74	77
Precipitation (inch)												
Normal	0.76	0.59	1.5	2.13	2.97	4.51	3.34	3.93	0.93	2.24	1.54	0.69
Maximum Monthly	2.52	2.76	3.43	8.42	8.01	10.52	8	7.55	9.48	6.16	3.83	2.04
Minimum Monthly	0.02	0.04	0.1	0.05	0.32	0.05	0.21	0.46	0.07	0.07	0.01	0.01
Maximum in 24 Hours	0.99	1.83	1.81	3.74	3.7	4.06	2.29	4.62	5.37	4.11	2.22	1.38
Normal # of Days With:												
Precipitation > 0.01″	8.8	6.9	8.3	9.4	11.1	11.4	10.6	10	9.3	8.5	8.3	7.9
Precipitation > 1.0″	0	0	0.1	0.2	0.4	1.2	0.8	1.1	0.6	0.6	0.2	0
Snowfall (inch)												
Normal	10.5	7.2	8.5	2.9	0.2	0	0	0	0	0.6	9.1	8.6
Maximum Monthly	29.9	21.6	51.7	11.1	3.2	0	0	0	1.8	6	26.9	25.4
Maximum in 24 Hours	9.4	12.2	14.5	7	3.2	0	0	0	1.8	4.9	11.4	10.2
Maximum Snow Depth	30	30	35	27	1	0	0	0	0	3	14	18
Normal # of Days With:												
Snowfall > 1.0″	3.4	2.6	2.8	1	0	0	0	0	0	0.1	2.5	3

The *Pathways* van collects pavement profile data, which is converted to an IRI and eventually an RQI value as discussed previously. Ride quality data is collected independently in each wheelpath, and for the purposes of this paper the two wheelpaths were combined to report an average RQI for each lane. This data is then plotted against time for each test cell in order to observe trends in the performance.

Distress surveys are also performed twice per year at MnROAD following a modified Long Term Pavement Performance (LTPP) protocol. These surveys quantify the extent and severity of various surface distress types. The primary distress modes that have been observed at MnROAD include cracking (transverse, longitudinal, edge or centerline joint, and fatigue) and patching. These distress types have also been summarized to observe how they change over time.

3 FIELD RQI MEASUREMENTS

3.1 *Description of raw data*

Table 4 summarizes information about the ride quality of the MnROAD test sections. The data shows which test cells correspond to a particular design life that was established during the early planning stages at MnROAD using the available design methods at that time. The design lives vary from three to ten years depending on the road section.

The initial RQI measurement taken with the *Pathways* van in June 1997 is presented for each cell. It should be noted that this value is not the true "initial" value of RQI, as the pavements were constructed in 1993 and opened to traffic in 1994. In almost every case, the ride quality early in the pavement life is categorized as good. Only two cases (the outside lanes of Cells 26 and 27) had slipped into the fair category. This is to be expected, as pavements should be smooth

Table 4. MnROAD RQI summary data.

	Driving or Inside			Passing or Outside		
Cell	June 1997 RQI	Years to 2.5	RQI at PM	June 1997 RQI	Years to 2.5	RQI at PM
1	3.59	9	NA	3.72	10	NA
2	3.4	8	2.39	3.63	12	2.63
3	3.08	8	NA	3.19	10	NA
4	3.03	7	1.64	3.13	7	2.21
14	3.76	7	NA	3.75	9	NA
15	3.65	7	1.66	3.73	9	2.56
16	3.59	7	1.24	3.81	8	2.44
17	3.49	7	1.36	3.81	8	2.06
18	3.41	6	1.82	3.56	7	2.24
19	3.56	7	2.09	3.64	8	2.45
20	3.96	12	3.6	3.99	14	3.75
21	3.94	15	3.32	3.99	15	3.6
22	3.43	9	2.66	3.76	15	3.14
23	3.38	9	2.91	3.56	12	3.13
24	3.96	15	3.35	3.44	15	3.35
25	4.05	15	2.97	3.75	15	3.09
26	3.16	7	NA	2.99	3	NA
27	3.12	5	NA	2.8	5	NA
28	3.5	5	NA	3.65	NA	NA
29	3.85	10	2.49	3.45	7	2.13
30	3.74	9	1.9	3.73	11	2.51
31	3.55	8	NA	3.63	NA	NA
Ave.	3.55	8.73	2.36	3.58	10	2.75

when they are built. The two cells in the fair category were already showing signs of pavement distress by the first ride measurements in 1997.

The next parameter noted in the table is the number of years that it took a particular test section to reach a terminal serviceability level of RQI = 2.5. Again it is noted that the initial data point was collected in 1997 (not 1994), but the number of years noted in the table is based on starting in 1994. The data becomes a lot more scattered when looking at this aspect of performance. Most cells fall within the five to ten year range, but there are many cases both above and below those values. The values listed as 15 years (or "NA") actually never reached a terminal serviceability level, yet were reconstructed in 2008 (or earlier) as new research opportunities presented themselves. Conversely, the outside lane of Cell 26 was already below 2.5 at its initial RQI measurement.

Maintenance treatments were performed at various times on various test cells to correct surface defects and restore ride quality. The ride quality of the pavements was generally near 2.5 at the time of treatment, but in many cases was much lower or higher than that. Again, many entries in the table are marked "NA" which indicates that no maintenance treatments (aside from occasional crack sealing) were applied to these cells.

In comparing between the two lanes of traffic in each test section, internal MnROAD data shows that on the Mainline the total traffic volumes are essentially equal between the two lanes, although the driving lane carries four times the amount of heavy truck traffic that the passing lane. For the Low Volume Road, this trend is essentially reversed: the inside lane sees four times the number of truck passes than the outside lane, yet because of the overloaded condition in the outside lane the Equivalent Single Axle Loads (ESALs) are roughly equivalent between the two lanes. In general the lane that sees the most heavy truck passes (driving or inside lane) also has a lower ride quality initially and over the life of each test section. On average the passing or outside lane shows a higher initial RQI value, and additional 1.25 years before reaching a terminal serviceability level, and a better ride quality at the time of the preventive maintenance treatment.

The comparison in ride quality between lanes is also shown in Figure 2. Of the 22 test sections evaluated, only five showed the driving or inside lane to have a higher ride quality than the corresponding passing or outside lane. Another four sections had essentially equal RQI values between the two lanes, while all of the remaining test sections had better ride quality in the passing or outside lane.

Another interesting performance trend to consider is shown in Figure 3, which shows that a pavement that has a high initial RQI value tends to remain smooth over a longer period of time. In short, "smooth pavements last longer." This finding is intuitively obvious and has been noted by other research in the past (Burnham, 2005). It is important to note that paying attention to detail during the construction process pays big dividends over the life of the pavement in terms of improved pavement performance.

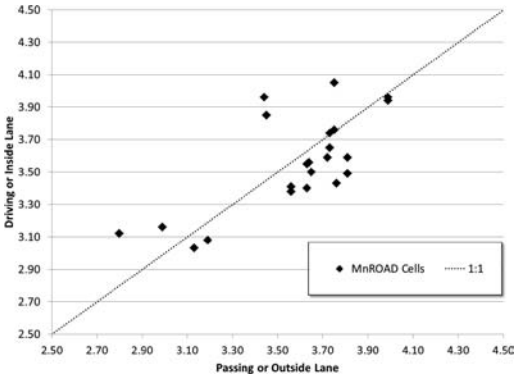

Figure 2. Ride quality index comparison between lanes.

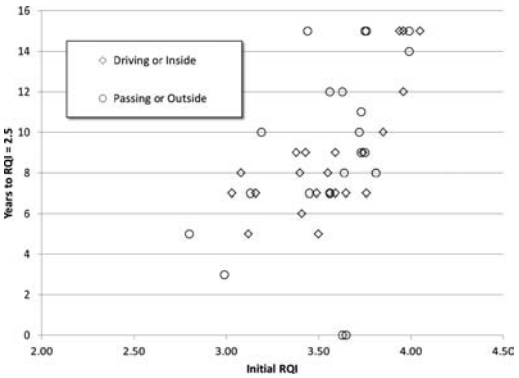

Figure 3. Pavement service life vs. initial ride quality index.

4 DATA ANALYSIS AND DISCUSSION

4.1 *Typical RQI curve*

Figure 4 shows a typical curve of RQI vs. time that was generated for this study. The plot was created for Cell 14, but it is indicative of plots for the other test sections. Both lanes are represented in the figure.

Early in the pavement life the slope of the curve is relatively flat, indicating that the ride quality is being maintained at a steady rate from the outset. Over time, the curve drops off more sharply, indicating that once the deterioration in ride quality begins, it accelerates rapidly. The preventive maintenance treatment is clearly identified by a large increase in the RQI, although not necessarily all the way back to the initial value. On average microsurfacing improved the RQI by about 1.0 for most of the MnROAD test sections. This is followed by a similar deterioration curve where it is relatively flat at the beginning and then accelerates in later years.

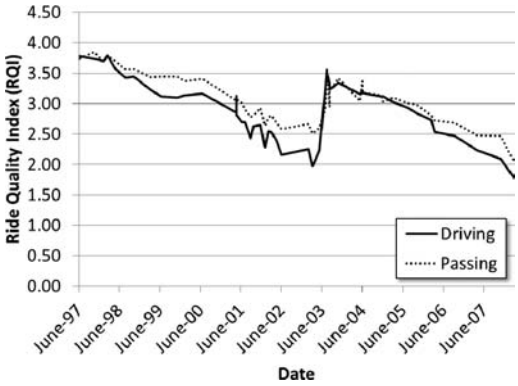

Figure 4. Typical RQI vs. Time Curve.

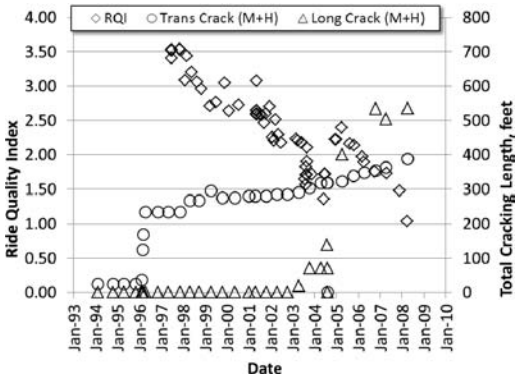

Figure 5. RQI and Distress vs. Time, ML Cell 17.

4.2 *Distress parameters that affect RQI*

It is apparent in reviewing the data for each test section that the ride quality deteriorates as the pavement condition deteriorates. Distress history data was gathered for each test section to determine which pavement distress types most affected the ride quality. These data were compared with ride history data against time. For each test section RQI values were plotted on the primary vertical axis, and multiple distress types were individually plotted on the secondary vertical axis.

For many of the distress types (e.g., total number and length of transverse cracks, number and total area of patches, and length of longitudinal joint cracking) no correlation was observed between the amount of distress and the decrease in ride quality. However, a few distress types stood out as being indicative of deteriorating ride quality. The total length of medium and high severity transverse cracks was clearly related to the deterioration in ride quality. This type of distress is common in cold regions like Minnesota and is caused by the inability of asphalt pavements to relax thermal stresses that build up with a decrease in temperature. Since the pavement sections developed initial thermal cracks early in their lives, the total amount of cracking has not changed significantly. However, the severity level of the cracks has increased under repeated traffic and environmental loads. This observation is in line with the work by Bae et al. (2007), which quantified the increase in IRI due to the prevalence and severity of transverse cracking. Another distress type that has a major effect on ride quality is the total amount of medium and high severity longitudinal cracking, which can eventually lead to fatigue cracking. This distress type shows a similar trend in that when the cracking rate accelerates, the rate of deterioration in RQI also accelerates. The amount of rutting was also directly related to the decrease in ride quality. As the rut depths increased at a linear rate, the ride quality started to decrease more rapidly. It is difficult to distinguish which of these distress types had the most effect on ride quality; however, the data shows that as each distress type increased the ride quality decreased accordingly.

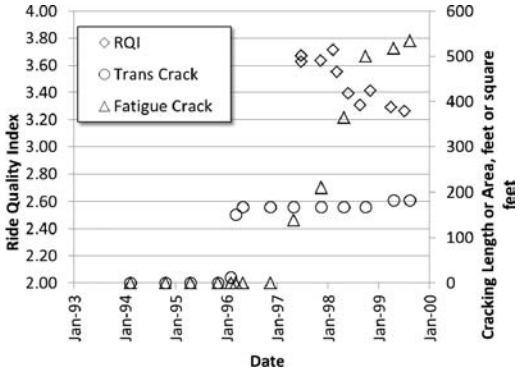

Figure 6. RQI and Distress vs. Time, LVR Cell 28.

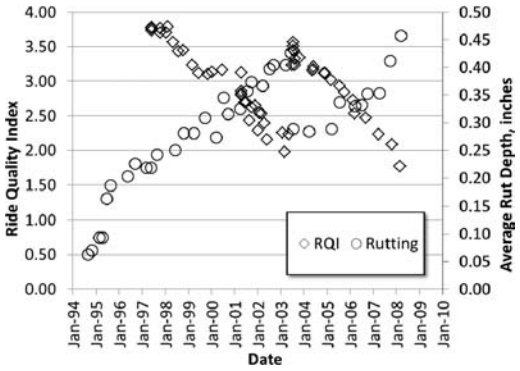

Figure 7. RQI and Rutting vs. Time, ML Cell 14.

Figures 5 through 7 display the trends that are discussed above for three different cells. Figure 5 shows the effects of preventive maintenance treatments on RQI. By examining the RQI values at the time of treatment and noting the time required to revert back to the same level, one can infer that a maintenance application extends the life of a pavement by three to four years in this particular case. This life extension is true even though both transverse and longitudinal cracks reappeared within six months of the treatment. This

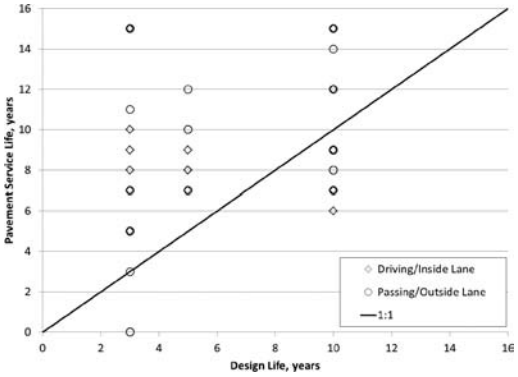

Figure 8. Pavement Service Life vs. Design Life.

implies that even though the maintenance treatment is unable to correct a cracking problem over the long term, it is able to restore ride quality for a certain period of time. The microsurfacing also noticeably reduced the surface rutting of the pavement, although within about four years the rutting returned to pre-treatment levels. The final note about the figures reiterates the fact that the roughness accelerates with the onset of medium and high severity transverse and longitudinal cracking.

4.3 *Performance vs. design life*

Figure 8 shows the service life of each test section in relation to its design life. It is rather concerning that the plot shows that there is virtually no correlation between the two values. However, it does show that the thinner pavements (three- and five-year design life) tend to have exceeded their design life while the thicker pavements (10-year design life) tend to have failed before the end of their design life. This data points to a need for revised pavement design procedures in Minnesota. Note that the MnROAD test sections were designed with empirical procedures developed in the 1960s, while the pavement design community is currently focused on the shift to mechanistic-empirical design methods.

5 CONCLUSIONS

Ride quality data was collected over the original 22 asphalt test sections at MnROAD twice per year from 1997 to 2008. The ride quality data was reported in terms of Ride Quality Index (RQI) to represent the way MnDOT evaluates their highway network on an annual basis. Surface distress data was also collected over time for each of the test sections, and the results considered in relation to ride quality. The data collected and analyzed in this study led to the following conclusions:

– MnROAD cells were generally smooth at the outset of their service lives, and those pavements with high initial RQI values remained smooth for a longer period of time.
– Increased traffic loadings tend to accelerate the distress and decrease in ride quality as evidenced by the comparison between driving/passing and inside/outside lanes.
– The application of preventive maintenance treatments extend the pavement life by at least three to four years based on the data in this study. While microsurfacing is only able to treat cracking and rutting over a short period of time, it does enhance pavement smoothness over a number of years.
– The deterioration of ride quality is most closely related to the increase in medium and high severity transverse, longitudinal, and fatigue cracks, as well as the increase in rut depths.
– The MnROAD test sections showed virtually no correlation between design life and actual pavement service life. New mechanistic-empirical design procedures that are calibrated to local conditions are more likely to accurately predict pavement performance.
– Although no statewide network data is presented in this paper, the MnDOT pavement management program does track the condition of highways over time and is able to quantify the benefits of extended life and reduced costs by applying preventive maintenance treatments. Accelerated pavement testing, whether at a pavement test track like MnROAD or by a linear or circular device, can be used to validate the ride quality concepts used in state pavement management programs.

ACKNOWLEDGEMENTS

The author gratefully acknowledges the data collection and processing work performed for this study by Dick Rude, Eric Peterson, and Keith Lindenfelser.

REFERENCES

Bae, A., Stoffels, S., Clyne, T., Worel, B. and Chehab, G. 2007. Direct Effects of Thermal Cracks on Pavement Roughness. *Journal of the Association of Asphalt Paving Technologists* 76: 59–83.

Burnham, T. 2005. Concrete Pavement Performance and Research at the Minnesota Road Research Project – The First Ten Years. *Eighth International Conference on Concrete Pavements: Innovations for Concrete Pavement: Technology Transfer for the Next Generation* 1, 2 & 3: 109–126.

Janisch, D. 2006. An Overview of Mn/DOT's Pavement Condition Rating Procedures and Indices. <www.dot.state.mn.us/materials/pvmtmgmtdocs/Rating_Overview_State.pdf> Accessed 10 March 2012.

Johnson, E.N., Wood, T.J. and Olson, R.C. 2007. Flexible Slurry–Microsurfacing System for Overlay Preparation: Construction and Seasonal Monitoring at Minnesota Road Research Project. *Transportation Research Record 1989: Journal of the Transportation Research Board*: 321–326.

Minnesota Climatology Working Group, <climate.umn.edu/pdf/normals_means_and_extremes/2005_Annual_LCD_STC_page_3.pdf> Accessed 13 March 2012.

Minnesota Department of Transportation. 2011. *2010 Pavement Condition Executive Summary.* Report #: MnDOT/OMRR-PM–2011-01. Office of Materials and Road Research, Pavement Management Unit.

Minnesota Department of Transportation. 2011. Specification 2399, Pavement Surface Smoothness. *Standard Specifications*.

Palmquist, D., Worel, B. and Zerfas, W. 2002. *2002 Mn/ROAD Hot-Mix Asphalt Mainline Test Cell Condition Report*. Minnesota Department of Transportation.

Stroup-Gardiner, M. and Newcomb, D.E. 1997. *Investigation of Hot Mix Asphalt Mixtures at Mn/ROAD*. Minnesota Department of Transportation. Final Report MN/RC – 97/06.

Wilde, W.J. 2007. *Implementation of an International Roughness Index for Mn/DOT Pavement Construction and Rehabilitation*. Minnesota Department of Transportation. Final Report MN/RC-2007-09.

Zerfas, W.J., Mulvaney, R. and Worel, B. 2004. MnROAD Mainline 2003 Maintenance Activities for Hot Mix Asphalt Test Cells. *2nd International Conference on Accelerated Pavement Testing*. Minneapolis, MN.

Part 8: Relating laboratory tests to performance using accelerated pavement testing

This page intentionally left blank

Advances in Pavement Design through Full-scale Accelerated Pavement Testing – Jones, Harvey, Mateos & Al-Qadi (Eds.)
© 2012 Taylor & Francis Group, London, ISBN 978-0-415-62138-0

Towards improved characterization of cemented pavement materials

R.E.Y. Yeo
ARRB Group, Melbourne, Victoria, Australia

W. Young
Monash University, Department of Civil Engineering, Clayton, Victoria, Australia

ABSTRACT: Increasing use of high productivity road freight vehicles combined with more sophisticated approaches to pavement analysis has led to the need for improved knowledge of the performance of pavement materials. This paper describes the development of laboratory tests intended for routine assessment of strength, modulus and fatigue properties of cemented pavement materials. The laboratory tests involved a four-point bending flexural beam test. Methods for preparation of beam specimens in the laboratory and from field-placed cemented material are described. In order to provide materials performance data needed to verify the improved laboratory tests, the Australian Accelerated Loading Facility (ALF) was used to assess the fatigue performance of two cemented materials. A comparison of laboratory characterization results and full-scale ALF trial results was favorable providing confidence in the use of the laboratory techniques. Two cases involving implementation of the laboratory strength and modulus tests with practical outcomes are presented.

1 INTRODUCTION

An essential element in understanding the performance of road pavements is understanding the performance of the constituent materials from which they are constructed. Cemented pavement materials, a sub-set of chemically stabilized materials, form a key component of a number of road pavement types. They are often used as a stiff subbase or as a semi-rigid base layer. Cemented materials are produced by the addition of a cementitious binder, such as general purpose (GP) cement, to a granular material to form a bound pavement material. A wide range of cemented materials are available for road construction comprising different host granular materials and different cementitious binders and binder addition rates. The absence of suitable laboratory tests for routine elastic characterization and fatigue assessment has led to a lack of knowledge on these properties for cemented materials in Australia.

Improved pavement design methods and materials characterization is essential given the growing demand for road freight. In Australia road freight is projected to nearly double between 2010 and 2030 (BITRE, 2011). A feasibility study is underway into the possibility of mass-distance-location charging as a means to enable high productivity freight vehicles to achieve optimal axle mass for any given freight task (NTC, 2010). These developments highlight the need for an improved understanding of materials properties and performance as the demands of road freight grow.

1.1 *Objective*

This paper presents improved approaches to the characterization of cemented materials in the laboratory. In the first section, the main knowledge gaps are identified and routine laboratory tests for strength, modulus and fatigue properties of cemented materials are proposed for use in Australia. In the second section, details of a full-scale accelerated pavement test used to provide verification of the laboratory characterization approach, is provided. In the third section, the paper discusses two case studies where early implementation of the laboratory processes for modulus characterization proved beneficial in addressing knowledge gaps for cemented materials.

2 BACKGROUND

2.1 *Mechanistic models*

Mechanistic models aim to incorporate a fundamental understanding of the effect, on each component material in a pavement structure, of any wheel loading applied to the material (Jameson and Sharp, 2004). Pure mechanistic models are preferred as they involve comprehensive constitutive equations with detailed requirements to fully characterize a situation. However, issues may arise in the application of pure mechanistic models for pavement design where material properties, traffic loading and operating environment are highly variable, and/or where the models are not fully developed. Although empirical design

approaches are less preferred, pragmatic pavement design methods often adopt a mechanistic-empirical approach allowing for substitution of empirical knowledge where the fundamental constitutive analysis is unavailable, too onerous and/or of limited additional benefit to an overall solution.

In a non-freeze thaw environment such as Australia, input requirements for mechanistic-empirical pavement design for cemented materials have for some time included elastic modulus and Poisson's ratio (Austroads, 2010). Other relevant parameters used may include modulus of rupture and minimum modulus of the cemented layer after fatigue cracking (NCHRP, 2011). However, as noted by Austroads (2010), there are no standard test procedures available in Australia for characterization of cemented materials in terms of modulus and fatigue. Further, the fatigue relationship for cemented materials proposed by AASHTO (NCHRP, 2011) (Equation 1) has not been field validated and AASHTO states that the required field calibration/validation data is non-existent. Scullion et al. (2008) aimed to address this knowledge gap but the key issue of the need for improved routine characterization of cemented materials remained.

$$\log N = \frac{\left(0.972\,\beta_{C1} - \left(\frac{\sigma_t}{\sigma_f}\right)\right)}{0.0825\,\beta_{C2}} \quad (1)$$

where N = fatigue life; σ_t = applied horizontal tensile stress; σ_f = modulus of rupture; and β_{C1} and β_{C1} are material constants which require field validation.

This paper reports progress towards improved characterization of cemented materials based on an ongoing research study in Australia.

2.2 *Theoretical approaches*

Zhong (1998) developed a constitutive fatigue model for cemented materials involving consideration of the cemented binder matrix and the bond between the cemented matrix and the coarse aggregate particles (Figure 1) rather than the bulk cemented material. A contact law approach using a statistical micromechanics process and the distinct element method for analysis of inter-particle behavior of the coarse aggregates connected by a cement binder matrix was developed. Zhong proposed that the overall damage behavior of cemented granular materials was a function of the stress-strain relationship, fracture strength, development of a damaged zone, and fatigue deformation. The primary parameters of interest identified were the microcrack length and density, binder toughness and the binder elastic constants. A limitation of the theoretical approach was that the constitutive model inputs required detailed knowledge of the initial crack length and a complex analytical process to enable crack growth prediction.

Theyse et al. (1996) identified three distinct phases for fatigue cracking of cemented materials being a pre-cracked phase, an effective fatigue life phase, and an equivalent granular phase. Thogersen et al. (2004) proposed the use of changes in cemented material modulus as an indicator of crack progression, rather than attempting a direct measure of cracking. This approach was applied to assess fatigue damage under accelerated pavement testing.

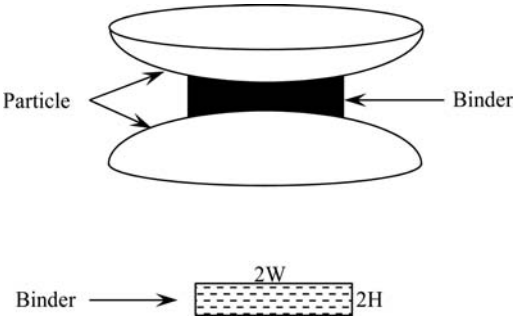

Figure 1. Configuration of a binder particle system (Zhong, 1998).

While theoretical approaches to characterization of cemented materials have been developed, there remains a significant gap in terms of application of these models. A particular issue is that cemented materials properties can be highly variable and this variability is dependent on the host material itself, the binder type and content, the construction process, the curing process, and the extent of cracking within the material. Methods for direct assessment of the extent and variability of initial cracking and crack progression, required for theoretical modeling, are not readily available for cemented materials. It was therefore proposed that laboratory assessment and accelerated pavement testing (APT) be used to provide an improved understanding of cemented materials properties to provide input to, and to facilitate, the further development and application of theoretical constitutive modeling for cemented materials.

3 LABORATORY CHARACTERIZATION

Austroads (2010) defined the design modulus for cemented materials as the flexural modulus at 28 days field curing and suggested use of the flexural beam test as it more closely simulated the stress/strain gradients generated in service. For highly bound cemented materials the preferred modulus test in the USA suggested by AASHTO (NCHRP, 2011) was the (compressive) modulus of elasticity at 28 days curing. However, the compressive test mode was not suited to fatigue assessment because the critical fatigue mode involves horizontal tensile stress at the bottom of the layer from repetitive heavy vehicle loading and the compressive strength of cemented materials is five to ten times higher than the modulus of rupture. For weaker cemented materials there was no AASHTO test method suggested for elastic modulus and correlations

with strength were proposed for use (NCHRP 2011, Scullion et al. 2008).

Several factors and constraints were identified and applied in the development of the laboratory protocols including:

- A focus on achieving a practical test that could be applied for a broad range of cemented materials.
- Use of test equipment that was generally available to pavement materials testing laboratories and fit for purpose.
- Ensuring a discerning test capable of providing an appropriate level of confidence on which decisions could be based.
- Drawing on the experience of others and existing methods and equipment where relevant.
- Verification through comparisons of the laboratory results with full-scale accelerated pavement testing performance data.

Two cemented materials were selected and tested to assist with the development of the laboratory protocols and specimen preparation techniques. Two sets of specimens for each cemented material were tested with one set manufactured in the laboratory and the second set sampled from plant-mixed, field-placed cemented material. The aim was to assess whether strength, modulus, and fatigue properties of field-placed materials could be simulated through manufacture of laboratory specimens as this would enhance the value of the laboratory testing. This approach had been used by Tayabji and Okamoto (1987) in their assessment of roller compacted concrete.

3.1 *Materials selected and compressive strength assessment*

The two cemented materials selected for this study were described as follows:

- Hornfels crushed rock (hornfels): 20 mm (0.8 in.) maximum sized crushed rock stabilized with 3% general purpose (GP) ordinary portland cement by dry mass. The source rock was a metamorphic hornfels from a quarry in Lysterfield, Victoria.
- Siltstone quartzite quarry rubble (siltstone): 20 mm (0.8 in.) maximum size quarry rubble stabilized with 4% GP ordinary portland cement by dry mass. The source rock was a siltstone quartzite sourced from the Para Hills quarry in South Australia.

Routine laboratory testing (maximum dry density, particle size distribution and Atterberg limits) was completed, followed by unconfined compressive strength (UCS) testing. The hornfels was found to have a UCS of 8.5 MPa (1.2 ksi) (field: five core specimens) and 7.1 MPa (1.0 ksi) (laboratory: three specimens) while the siltstone material UCS was 7.6 MPa (1.1 ksi) (field: six core specimens) and 6.5 MPa (0.9 ksi) (laboratory: three specimens) at 28 days cure. For both materials, the UCS increased with cure age as expected. Also, in both cases, the UCS for field specimens tended to be slightly higher than that for laboratory specimens.

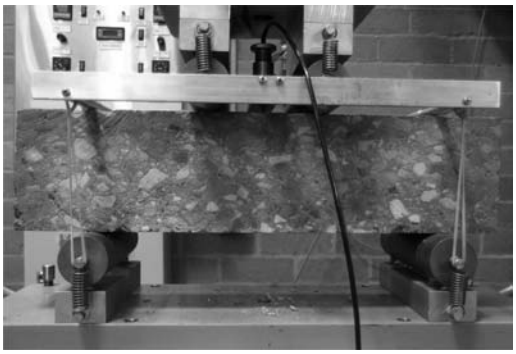

Figure 2. Four point bending flexural beam test arrangement.

The field UCS results were likely to be biased towards higher strength as weaker field material could not be retrieved because the cemented material disintegrated during core sampling.

Both the siltstone and hornfels were supplied and constructed in compliance with the relevant State Road Agency cemented materials specifications. The seven day UCS was 5.9 MPa (0.9 ksi) for the hornfels and 5.8 MPa (0.8 ksi) for the siltstone, which in both cases exceeded the minimum UCS requirement of 5 MPa (0.7 ksi) from the relevant specification based on triplicate laboratory test specimens. On this basis it would be expected that the hornfels and the siltstone would provide similar field performance.

3.2 *Development of improved laboratory tests for cemented materials*

A number of test modes were identified and considered for the assessment of strength, modulus, and fatigue properties of cemented materials. These included: direct tensile, indirect tensile, cantilevered bending, and four-point flexural bending. After consideration of the criteria listed above, a review of the literature and the conduct of initial experimentation using both indirect tensile and four-point bending (Yeo, 2008), the four-point bending flexural beam test was adopted (Figure 2). The test had been used in numerous earlier cemented materials studies (Mitchell et al., 1969; Otte, 1978; Litwinowicz, 1986; Raad, 1988; Litwinowicz and Brandon, 1994; Bhogal, 1995; Alderson, 1998; Sobhan and Das, 2007; Solanki, 2010). In addition, four-point bending was already in use for flexural strength (modulus of rupture) and it was the mode considered to simulate the actual loading most closely (Austroads, 2010).

Preparation and curing of uniform beam specimens in the laboratory or from field-placed cemented materials was an important aspect of the tests. This was resolved for laboratory specimens through use of a planetary concrete mixer and a segmental wheel slab compactor (slab size 400 mm [16 in.] long, 320 mm [13 in.] wide and 100 mm [4 in.] deep). It was considered that the equipment used was in

relatively widespread use in Australian pavement testing laboratories. After initial moist curing (about 7 days), the cemented slabs were demoulded and saw cut to size (100 mm [4 in.] square by 400 mm [16 in.] long) using a bench-mounted saw with a diamond tipped blade. Two beams were cut from the central portion of each slab then placed in a fog room for further moist curing. Field beams were prepared from constructed cemented material layers using a mobile pavement saw to cut slabs from the road bed. These slabs were trimmed to size in the laboratory and again cured in a fog room prior to testing. Beams used for modulus and fatigue testing were wrapped in thin plastic cling wrap to prevent moisture loss during testing. The four-point bending test involved use of stress control with a haversine pulse shape to simulate loading applied by heavy vehicle axles. For modulus and fatigue testing, the loading frequency was 2 Hz with a 250 ms haversine load pulse width and 250 ms rest period.

An initial set of beams was used to estimate breaking stress (modulus of rupture) and breaking strain. The failure load and breaking strain values were then used to guide the magnitude of the cyclic load applied for modulus and fatigue testing. As described by Sobhan and Das (2007) the approach of using paired specimens (one for strength and the pair for modulus/fatigue) can be problematic due to differences in properties between specimens. Such variations make it difficult to determine an accurate stress ratio or strain ratio for a given fatigue beam specimen. Modulus testing was conducted at a stress ratio of about 40% while a range of stress ratios of between 50% and 90% of the ultimate load were used to estimate fatigue life. This approach to specimen loading was used by Sobhan and Das (2007) and Gnanendran and Piratheepan (2010).

3.3 *Flexural strength*

In terms of flexural strength, the hornfels showed similar results for the field and laboratory specimens at 1 MPa (145 psi) at 28 days and between 0.7 MPa (102 psi) and 1.26 MPa (183 psi) at an extended cure age (greater than 70 days). For the siltstone, the field specimens showed higher strength at 1.3 MPa (189 psi) at about 30 days and 1.4 MPa (203 psi) at an extended cure age (greater than 70 days) compared to the laboratory specimens which showed about 1 MPa (145 psi) from about 30 days with no increase with cure age.

3.4 *Modulus and fatigue*

In the four-point bending test, the peak force applied and peak midspan deflection (measured with LVDTs) were used to estimate the extreme fiber stress and strain response. From these data the flexural modulus was estimated for each load pulse (Equation 2). This allowed modeling of the deterioration in modulus

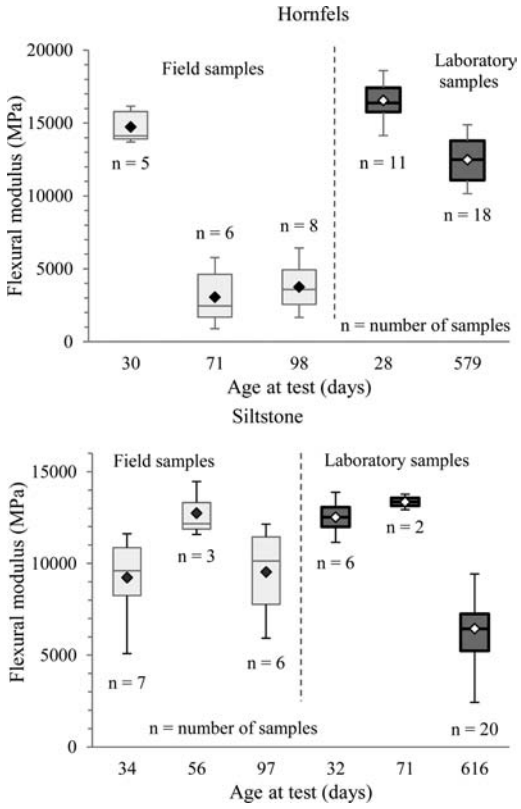

Figure 3. Summary of flexural modulus data.

in line with the incremental recursive approach (Thogersen et al., 2004).

$$E_{max} = \frac{\sigma_t}{\varepsilon_t} \times 10^3 = \frac{\frac{PL}{wh^2} \times 10^6}{\frac{108\delta h}{23L^2} \times 10^6} \times 10^3 \quad (2)$$

$$E_{max} = \frac{23PL^3}{108wh^2\delta h} \times 10^3$$

where E_{max} = flexural modulus (MPa); L = beam span (mm); σ_t = peak tensile stress (MPa); w = specimen width (mm); ε_t = peak tensile strain (microstrain); h = specimen height (mm); P = peak force, in kN; and δh = peak mid-span displacement (mm).

Both the cemented materials were plant mixed and constructed with the objective of achieving a uniform, well cured cemented base suitable for APT testing at different axle loads. The flexural modulus results are presented in Figure 3. For the hornfels, the limited number of field specimens were highly variable, some representing a weaker material with a low modulus at about 3,000 MPa (435 ksi) while others showed high quality with a modulus of about 15,000 MPa (2,175 ksi). This limited field data indicated a reduced modulus with cure age which is unexpected. However, the specimens representing each cure age were

sourced from a different location of the test pavement. While the cemented base was of uniform construction, the lower modulus beams were sampled from locations where shrinkage cracking was later identified, hence the lower modulus. In contrast, the siltstone modulus results were less variable falling in the range 9,000 MPa (1,305 ksi) to 13,000 MPa (1,885 ksi) for cure ages less than 100 days (Figure 3). This finding supports the need for an improved understanding and measurement of cemented materials properties as an input to theoretical constitutive modeling.

For the fatigue test, the aim was to develop a data set of applied stress or initial strain against fatigue life presented as cycles of load (N) to a defined fatigue state. The stress or strain parameter could also be a stress or strain ratio. Initial strain (S) was adopted for analysis of the fatigue test results as this was found to produce a higher correlation with fatigue life, compared to the use of stress and it aligned with the critical parameter identified in Australian pavement design (horizontal tensile strain [Austroads, 2010]). Fatigue performance was represented as an 'S–N' curve as used in classical materials fatigue assessment. The laboratory fatigue testing was expected to be useful in establishing the relative fatigue life of different cemented materials at a given initial strain under stress controlled loading.

The fatigue test duration was expected to be highly sensitive to the applied load as suggested by Molenaar and Pu (2008). At a low stress ratio, for example, less than 40%, fatigue life would be expected to be indefinite (Otte, 1978; Sobhan and Das, 2007; Scullion et al., 2008). While at high loading, fatigue could occur within a few cycles with the extreme case being the strength test which provided the failure load for a single application.

3.4.1 *Cure age for the fatigue test*

UCS testing often involves seven days curing to enable an early estimate of 28-day strength, a typical design parameter for concrete. Bhogal et al. (1995), Sobhan and Das (2007), Solanki (2010), and Gnanendran and Piratheepan (2010) used a 28-day cure period for investigation of the dynamic fatigue life of cemented materials. AASHTO (NCHRP 2011) suggested use of 28-day properties as a conservative estimate of longer-term properties of cemented materials. However, this study aimed to provide a comparison between field material and the laboratory specimens at the same cure age. Although the cementitious binder used in this study was general purpose (GP) ordinary portland cement, it was anticipated that changes to the cemented materials properties occurring well beyond the initial 28-day cure could significantly influence the fatigue performance of the materials. Testing of laboratory specimens was therefore conducted at an extended cure period representative of the cure age of the full-scale field experiments. It was noted that in France, cemented materials may be cured for up to 360 days prior to fatigue testing (LCPC, 1997). Testing at 28 days cure was also conducted to provide a comparison.

3.4.2 *Definition of fatigue life*

A suitable definition of the end of fatigue life was required for the laboratory test. Several options for this were considered including:

- Specimen rupture/fracture.
- Reduction in specimen modulus to a specified percentage of the initial modulus, for example 50%.
- Reduction in specimen modulus to a specified value, for example 500 MPa (70 ksi) which is considered representative of an unbound material.

In the absence of an established definition for the end of fatigue life, 'cycles to half initial modulus' was adopted as used by Jameson et al. (1992) and Gnanendran and Piratheepan (2010). The initial modulus and initial strain were defined as the mean value for the first 50 load cycles of the fatigue test. With the observed early rapid deterioration of modulus, this approach produced a lower and more consistent initial modulus, which allowed consideration of the majority of the second stage of crack progression under repeated loading prior to specimen fracture. A limitation of this definition was that fatigue tests were required to run in excess of 50 cycles.

The mean initial modulus for the hornfels laboratory specimens was 14,800 MPa (2,150 ksi) (28 days) and 10,300 MPa (1,490 ksi) (extended cure). The mean initial modulus for the siltstone laboratory specimens was 10,200 MPa (1,480 ksi) (28 days) and 5,700 MPa (830 ksi) (extended cure). It should be noted that there was a difference in the curing process for the 28-day specimens, which were cured in a fog room, compared to the extended cure specimens, which were subjected to a wet-dry-wet process. After an initial moist curing of about six months, the specimens were allowed to dry out over an extended period due to limitations with fog room capacity. Samples were subsequently wet-up again for a minimum of 48 hours in the fog room prior to testing. This process is likely to have introduced some micro-cracking in the specimens resulting in a lower modulus at the extended cure age compared with the 28-day modulus result.

The fatigue life for the laboratory specimens at the extended cure period is shown in Figure 4 together with the 28-day cure data. For both materials, the fatigue life at the extended cure age was found to be significantly greater than for the specimens cured for 28 days at a given initial strain.

3.4.3 *Initial approach to modeling fatigue*

The laboratory fatigue test data was analyzed and models based on Equation 3 were developed. The model was rearranged as shown in Equation 4 with fatigue life (N) as the dependent variable on the basis that, for the laboratory testing, the aim was to determine the fatigue life for a given initial strain.

$$N = \left[\frac{c}{S}\right]^{LDE} \tag{3}$$

$$\log(N) = -LDE \times \log(S) + d \tag{4}$$

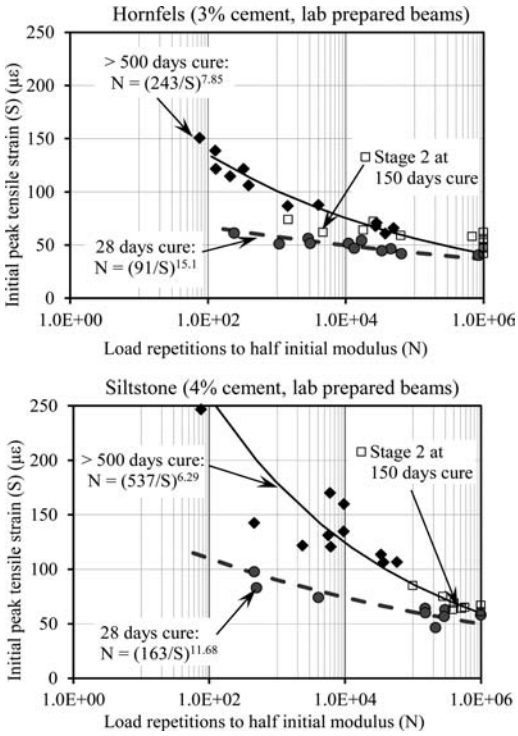

Figure 4. Beam fatigue results.

where N = fatigue life; S = the initial peak tensile strain (calculated as the mean of load cycles 1 to 50 of the four-point bending test); LDE = Load Damage Exponent and c and d are constants with d = LDE log(c).

For the extended cure fatigue data, the model fitted for the hornfels is shown in Equation 5 while Equation 6 shows the model for the siltstone. Equation 5 and Equation 6 indicated load damage exponents of 7.9 (hornfels) and 6.3 (siltstone). Looking at Figure 4 it is clear that the fatigue life of the hornfels is only one tenth or less of the fatigue life for the siltstone.

$$\log(N) = -7.85 \log(S) + 18.74 \quad (5)$$

(hornfels: n = 12, $R^2 = 0.96$)

$$\log(N) = -6.29 \log(S) + 17.18 \quad (6)$$

(siltstone: n = 11, $R^2 = 0.63$)

3.5 *Findings from the laboratory testing*

A four-point bending flexural beam test was proposed for assessment of the strength, modulus, and fatigue properties of cemented materials, and test results for two cemented materials were presented. The UCS was similar for both materials in the range of 6 MPa to 8 MPa (870 psi to 1,160 psi). For the laboratory prepared specimens the hornfels material showed a higher modulus (12,000 MPa to 16,000 MPa) (1,700 ksi to 2,300 ksi) compared to the siltstone (7,000 MPa to 13,000 MPa [1,000 ksi to 1,900 ksi]). A marked contrast was observed in the fatigue performance of the two materials with the hornfels showing only one tenth or less fatigue life compared to the siltstone material. Full-scale accelerated performance testing was used to provide verification of the laboratory tests. The observed contrast in fatigue performance predicted from the laboratory materials characterization was assessed as reported in the next section.

Figure 5. The Australian ALF operating indoors at Dandenong, Victoria.

4 ACCELERATED PAVEMENT TESTING

The full-scale load accelerated pavement testing experiment design involved use of the Australian Accelerated Loading Facility (ALF) (Sharp, 2004). The ALF (Figure 5) applies rolling half-axle wheel loads to pavement test strips 12 m (39 ft.) long at a constant speed of 20 km/h (12.4 mph) with one-way loading. Lateral wander based on a normal distribution with a standard deviation of 0.13 was introduced into the trafficking pattern such that the width of the trafficked area was about 1 m (3 ft.).

The experiment design involved (Table 1):

- Test sections with a 150 mm (6 in.) cemented base, a thin asphalt concrete surfacing and a uniform sand subgrade (Figure 6). The cemented base was moist cured for more than six months prior to trafficking.
- Up to six test sections, 12 m (39 ft.) in length, per material inside an enclosed shed.
- At least three half-axle load levels per material: 40 kN, 60 kN and 80 kN (9 kip, 13 kip and 18 kip).
- Performance measurement parameters included: visual inspection/surface cracking, deformation, falling weight deflectometer (FWD) deflection testing, and multi-depth deflectometer (MDD) deflection/deformation at depth.

Following construction of the test pavements, FWD deflection surveys were conducted to assess the cemented bases at various stages of curing. The FWD data indicated that the initial strengthening of the cemented material occurred rapidly within the first 100 days after placement followed by a slower, longer-term rate of strength gain. This observation supported

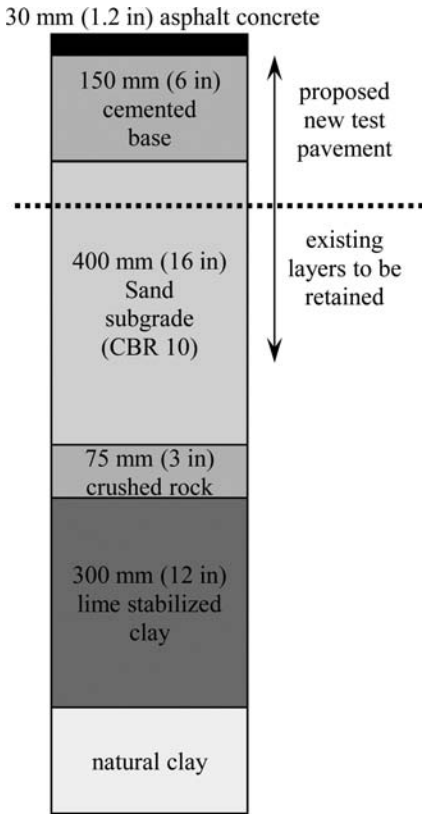

Figure 6. Nominal pavement structure.

Table 1. Test program and total ALF loading cycles.

Traffic Dates	Base Cure Age (months)	Expmt. No.	Half-axle Load (kN)	Load Reps (×1,000)
Siltstone				
01/12/05-23/01/06	12	3305	40	412.1
22/09/06-5/01/07	21	3302	50	645.6
15/09/05 7/11/05	9	3301	60	402.6
27/07/05 1/09/05	7	3304	80	209.2
Hornfels				
21/05/06-17/08/06	14	3307	40	641.2
17/08/06-23/09/06	17	3311	50	126.7
17/03/06-17/05/06	12	3308	60	476
31/01/06-14/03/06	11	3310	80	323
05/01/07-23/01/07	22	3309	80	114.6
			Total	3,351

Figure 7. Post mortem longitudinal trench face highlighting transverse fatigue cracking resulting from ALF trafficking.

the adoption of an extended cure age for the laboratory testing and for the accelerated pavement testing to ensure consistent and stable cemented materials properties. The FWD deflection data indicated a significant difference between the two cemented materials, with the hornfels found to have a more variable and higher mean deflection compared to the siltstone. The deflection results were compatible with the modulus data from field beam specimens tested.

There was minimal deterioration observed at the pavement surface during ALF trafficking. It was expected that fatigue cracking would reflect through the thin asphalt surfacing but this did not occur. As shown in Figure 7, the post mortem trenching of the test pavements highlighted that the fatigue cracks initiated at the bottom of the cemented base layer and progressed upwards but not through the asphalt.

While a range of performance measures were recorded for each ALF experiment, the most pertinent measure of the deterioration of the cemented base layers with loading was found to be the FWD deflection data. This was collected at the start and at regular stages during ALF trafficking without the need to move the mainframe off the test pavement (Figure 5). Backcalculation of the FWD deflection data was the main method used to assess changes in the cemented base layer modulus with trafficking. The ARRB backcalculation program *EfromD3* (an enhanced version of *EfromD2* [Vuong, 1991]) was used for the analysis. It was recognized that a key issue with backcalculation was that multiple possible solutions can result. To ensure the backcalculation provided consistent and useful outputs for the purposes of this study:

- Assigned modulus values were used for the thin asphalt surfacing. The modulus was based on laboratory testing of asphalt specimens at a range of temperatures (corrected for speed of loading) combined with a study of the back-calculated field asphalt modulus at one location of the test pavement on one day using FWD data taken at a range of asphalt concrete temperatures.
- An evaluation of the laboratory measured modulus of cemented field beams was completed to set bounds for the cemented base modulus (see Figure 8).
- Repeated-load triaxial testing was undertaken on the sand subgrade from which the modulus of the sand was found to vary between 150 MPa (22 ksi) and 200 MPa (29 ksi) for deviator stress

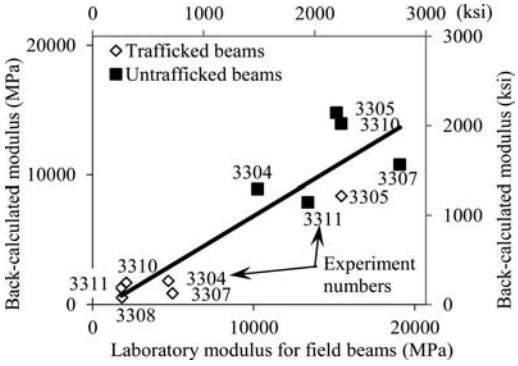

Figure 8. Comparison of laboratory measured and back-calculated cemented material moduli.

between 100 kPa (15 psi) to 200 kPa (30 psi) at 50 kPa (7 psi) confining stress. The underlying clay subgrade was evaluated in situ using a dynamic cone Penetrometer (DCP).

The backcalculation analysis assumed linear-elastic, homogeneous materials properties. This assumption was considered appropriate for the intact pavement prior to ALF trafficking. However, cracked and fragmented cemented materials are not generally considered linear-elastic or homogeneous. To address this limitation, an 'equivalent modulus' approach was adopted. In this approach, the cracked cemented material was modeled as a weakened equivalent linear-elastic layer. The backcalculated equivalent modulus was observed to drop rapidly with ALF load cycles. The analysis assumed that the equivalent modulus of the cemented layer was an indicator of fatigue crack progression with a reducing modulus indicating increased cracking.

The analysis of fatigue damage with ALF trafficking involved two main stages. In the first stage the mean modulus of the cemented material was back-calculated for each experiment and the reduction in modulus was determined as shown in Figure 9.

The second and main stage of the analysis involved a detailed assessment at each chainage location of each ALF experiment. This allowed multiple data-points from each ALF experiment because the test pavement length was 12 m (39 ft.). Locations of most interest in terms of fatigue were those where the cemented base was initially intact (i.e., not affected by non-load associated weakness) and where modulus reduced to about 50% or greater compared to the initial value. At these locations the observed reductions in modulus were again represented as a percentage of the initial modulus. This approach enabled an assessment of the relative rates of fatigue damage at different axle loads taking into account the unique properties at each test location (pavement layer thickness, applied stress, initial strain and materials properties). The definition of fatigue life adopted was load cycles to 50% of initial modulus.

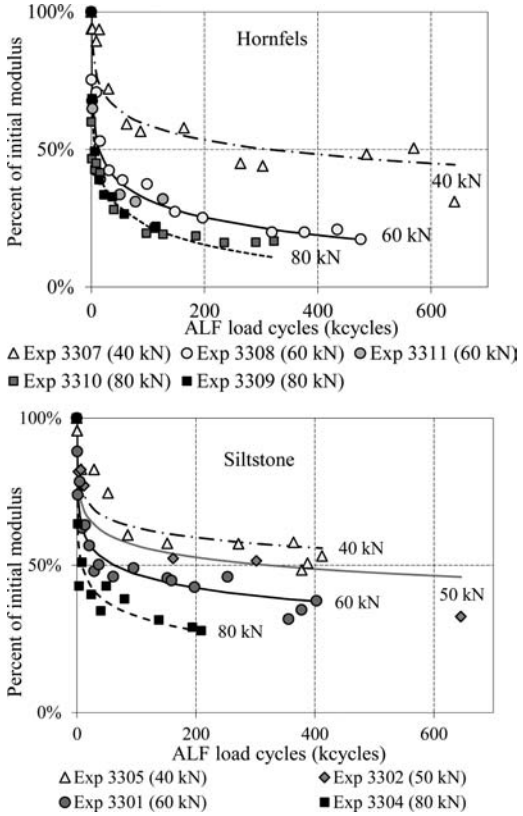

Figure 9. Cemented material change in modulus with loading.

The untrafficked backcalculated pavement layer moduli were used to estimate the initial horizontal tensile stress and strain at the base of the cemented layer in a forward calculation process using the *CIRCLY* program (MINCAD, 2004). The ALF dual tire loading was used rather than the FWD loading and the assigned asphalt modulus was adjusted down to account for the difference in load speed between ALF and the FWD. Figure 10 shows the data for initial strain (S) and ALF load cycles to fatigue failure (N) for the hornfels and the siltstone cemented materials. The multiple data-points for each ALF experiment shown in Figure 10 represent the results for individual chainage locations along each experiment.

Comparing the ALF results in Figure 10, the fatigue life of the hornfels was found to be up to one tenth that for the siltstone at the same initial strain. For the hornfels material the mean initial modulus was about 11,850 MPa (1,720 ksi) and the resultant fatigue model derived from the ALF performance data was:

$$\log(N) = -4.9 \times \log(S) + 14.0 \quad (7)$$

(hornfels: n = 27, $R^2 = 0.73$)

For the siltstone material, the mean initial modulus was about 11,000 MPa (1,600 ksi) and the resultant

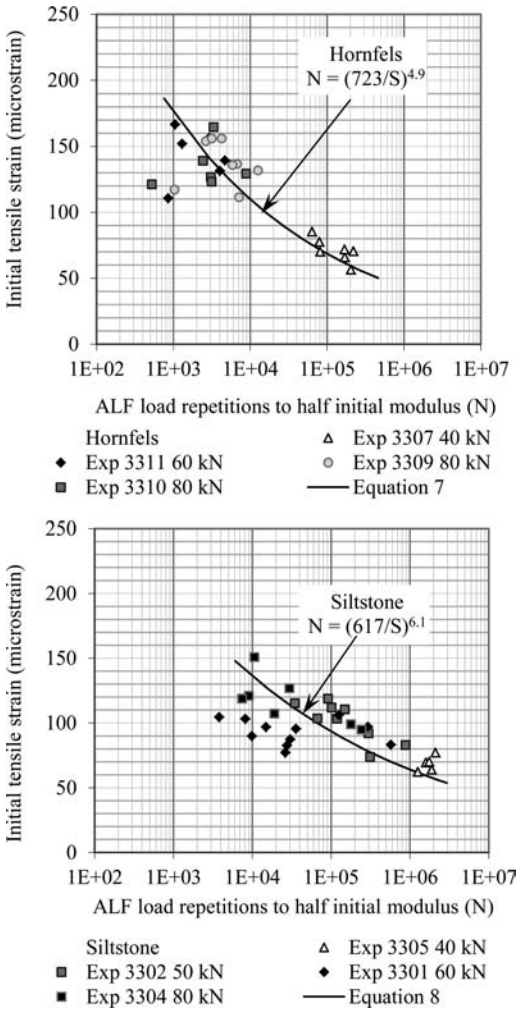

Figure 10. Initial peak tensile strain against ALF load cycles to 50% of the initial cemented layer modulus.

fatigue model derived from the ALF performance data was:

$$\log(N) = -6.1 \times \log(S) + 17.0 \quad (8)$$

(siltstone: n = 32, R^2 = 0.46)

The goodness-of-fit for Equation 8 may have been reduced as a result of the data from Experiment 3301 at the 60 kN loading although there was no clear explanation as to why this experiment differed from the other experiments on the siltstone.

4.1 *Summary of findings from the accelerated pavement testing*

The fatigue performance of two test pavements was assessed using accelerated pavement testing. The main performance measure was FWD deflection. The modulus of the cemented base layer was backcalculated from the FWD deflection bowl data and the results compared favorably with moduli determined in the laboratory for field beams. The reduction in the cemented base modulus was used as an indicator of crack progression and fatigue in the cemented base. Fatigue models were developed for the two cemented materials relating fatigue life (cycles to half initial modulus) to applied initial strain under the ALF loading. The fatigue models derived from the laboratory results and the accelerated pavement testing were almost identical for the siltstone. Also, the relative fatigue life of the two materials was found to be quite different with the hornfels showing only about one tenth the fatigue life compared to the siltstone material. The fatigue models for the hornfels material were similar but the laboratory model showed a much higher fatigue life compared to the ALF model. It was considered that the field hornfels material tested under ALF was of a weaker nature compared to the laboratory beam specimens and that this would explain the difference to a large extent. The hornfels field material was found to be affected by more variable and greater extents of initial cracking compared to the laboratory specimens. This was supported by the laboratory modulus results for the field-placed hornfels material which showed a greater range of moduli than for the laboratory prepared hornfels specimens (see Figure 3).

Overall, the laboratory test results were considered to compare very well with the ALF test results providing confidence in the proposed laboratory test protocols for characterization of cemented materials for strength, modulus, and fatigue.

In the third section of this paper, two examples of the early implementation of the laboratory test to improve knowledge of cemented materials modulus are provided. For these case studies, the specific details of the projects, the parties involved or the location are not relevant for this paper. Generic terminology is used such as ‘state road authority’ and ‘metropolitan area’ to avoid any sensitivity to release of the data.

5 IMPLEMENTATION: MATERIALS SPECIFICATION IMPROVEMENT

In the first case study, the test protocols for modulus described above were used to provide more in-depth information on cemented materials as a basis for revision of a state road authority specification requirement.

5.1 *Background*

In the early 1990s, following research into the UCS of a range of cemented materials, a new state road authority specification requirement was established. The specification covered cemented materials used as a bound subbase under asphalt concrete basecourses. The specification included three classes of cemented material with design moduli of 500 MPa

(70 ksi), 2,000 MPa (290 ksi) or 3,600 MPa (520 ksi). At that time, a range of cemented materials comprising different host crushed rocks (including recycled crushed concrete) and different binders (including GP cement and blended cements incorporating supplementary cementitious binders) had come into use. In order to ensure the integrity of the various blends of cemented materials, the new specification required a minimum UCS of 5.0 MPa (730 psi) at seven days moist curing and 100% modified compaction. Over time, it was found that, of eight commonly available cemented materials in use in a metropolitan area, a number were failing to meet the minimum UCS requirement. In particular, recycled crushed concrete and two granite materials produced a UCS of just below the minimum UCS with the commonly used GP cement binder at 3.0% addition by dry mass. This presented a dilemma for some sectors of the materials supply industry with an increased binder content required to meet the specification limit, potentially resulting in an uncompetitive product. As a result, a need for improved knowledge of the strength and modulus properties of a range of cemented materials was identified by the state road authority and the relevant industry association. This would enable a potential review of the specification requirement.

5.2 *Cemented materials properties*

With the development of the cemented materials test protocols described above, a laboratory test program was conducted to characterize eight different cemented materials. The aim of the study was to assess the cemented materials modulus and UCS, and any relationship between these properties and ultimately to assess the applicability of the minimum UCS specification requirement.

Bulk samples of the cemented materials components were obtained and beam specimens were prepared in the laboratory using 3.0% general purpose (GP) ordinary portland cement by dry mass. The UCS results are summarized in Figure 11, which shows that the recycled crushed concrete and both the granite materials had the lowest strength. For these materials, the minimum UCS requirement of 5 MPa (730 psi) at seven days was not satisfied.

A series of flexural beam specimens were manufactured and the flexural strength and modulus was determined with the results summarized in Figure 12. It was recognized that the laboratory modulus results represented ideal specimen preparation properties. A valid shift factor to allow for conversion of the laboratory moduli to field moduli was not available. Such a shift factor would be dependent on the construction quality, particularly compaction and curing and further research is required to better understand the relationships between field and laboratory properties of cemented materials. Litwinowicz and Brandon (1994) reported a field-to-laboratory modulus ratio of 50%. The field and laboratory results presented from the ALF test pavement (Figure 3) indicated that the shift

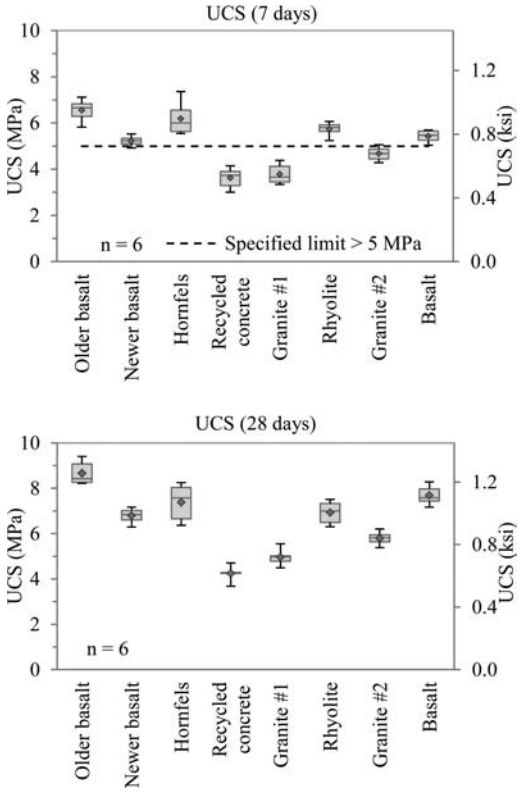

Figure 11. UCS results at 7 and 28 days curing.

factor could be 1.0, as for the siltstone or as low as one third to one quarter based on the results for the hornfels (Figure 3). As an interim approach, a conservative shift factor of one third was adopted for interpretation of the laboratory modulus data shown in Figure 12.

5.3 *Implementation summary – materials specification improvement*

The development of the four-point bending test protocols, supported by the accelerated pavement testing results enabled development of improved knowledge of the properties of a range of cemented materials. The existing state road authority materials specification required a minimum UCS of 5 MPa (730 psi) for cemented materials in three modulus classes (500 MPa (70 ksi), 2,000 MPa (290 ksi) and 3,600 MPa (530 ksi)). As a result of the laboratory test program, it was concluded that this requirement should remain for the two higher modulus classes of cemented materials. However, for the 500 MPa (70 ksi) modulus class, the evidence from the laboratory testing supported a reduction in the specified UCS requirement from 5 MPa (730 psi) to 4 MPa (580 psi). This was on the basis that the minimum modulus was estimated to be over 2,000 MPa (290 ksi) (based on one third of the modulus results in Figure 12) while the required modulus was 500 MPa (70 ksi) and, in addition, for

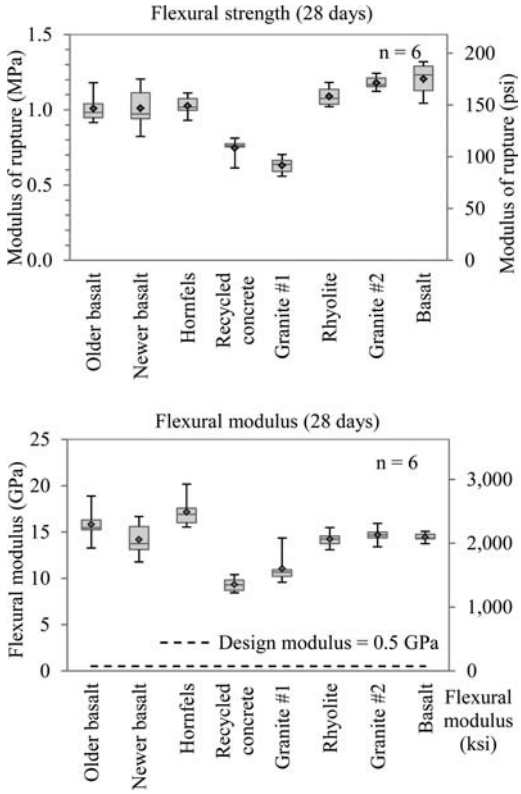

Figure 12. Flexural strength and modulus results at 28 days curing.

pavement design purposes this class of materials is modeled as having no fatigue life (similar to an unbound granular layer). The specification was amended in line with this finding and republished. It was noted that the 500 MPa (70 ksi) class of cemented material was most commonly used and that implementation of this research finding enabled full use of the range of cemented materials products available on the market.

6 IMPLEMENTATION: USE OF NON-STANDARD CEMENTED MATERIAL

The second example involved implementation of the flexural modulus test to support knowledge required for a major road construction project. The project involved four-lane dual-carriageway construction at a greenfields site. A typical composite pavement design comprising thick asphalt concrete supported by a 170 mm (7 in.) cemented subbase over the subgrade formation was proposed. The cemented subbase layer had been characterized with a 500 MPa (70 ksi) modulus based on conservative presumptive design inputs. Laboratory characterization of the cemented subbase modulus offered the possibility of consideration of alternative pavement materials through increased

Figure 13. Cemented material slabs extracted from the field trial.

knowledge of the materials properties. To this end, a field trial section was constructed and an assessment made of an alternative cemented subbase. The alternative material was a stabilized blend comprising recycled aggregate, a mix of high and low quality new aggregate with a slow setting cementitious binder. The blend of materials was mixed in situ with a pavement stabilizer to a depth of 300 mm (12 in.), compacted and left to cure for 28 days. A pavement saw was used to cut a series of cemented slabs from the field trial pavements for laboratory characterization (Figure 13). These were trimmed into beam specimens in the laboratory and the four-point bending test was used to determine the flexural strength and modulus. Samples of the constituent materials were also taken and a series of laboratory prepared beam specimens were tested.

6.1 *Implementation summary – use of non-standard cemented material*

The results of the testing of the field and laboratory beam specimens are shown in Figure 14. The data indicated that the material from the field trial had on average about 40% of the flexural strength of the laboratory prepared specimens and about 50% of the modulus. This information was useful in the development of a knowledge base comparing field-placed material properties with laboratory prepared material properties. Given the design modulus of 500 MPa (70 ksi) for the cemented subbase, the laboratory characterization results provided clear evidence that this could be achieved with the proposed alternative cemented material which showed a mean modulus of over 4,000 MPa (580 ksi). As the alternative cemented subbase incorporated components of recycled waste materials, both in the aggregates and the slow setting binder, apart from cost savings there were environmental benefits in terms of preserving scarce resources. In this case the laboratory protocols provided improved knowledge to support consideration of the use of alternative, lower cost cemented material with environmental benefits.

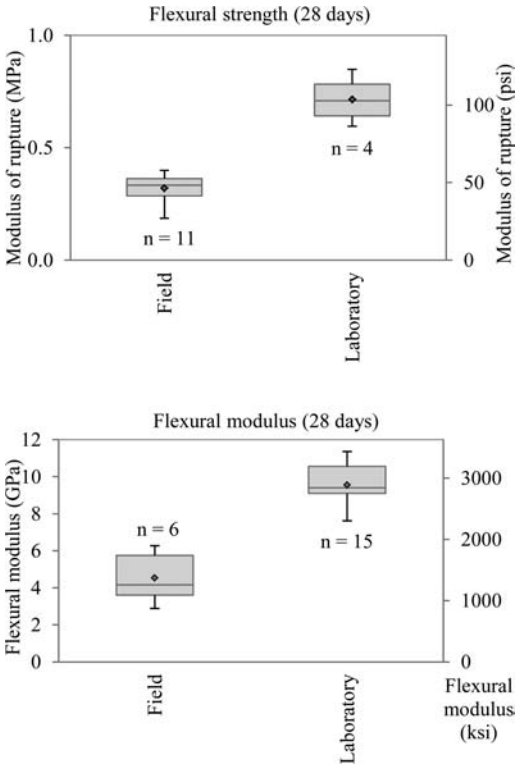

Figure 14. Summary of test results for strength and modulus.

7 CONCLUSIONS

This paper has presented improved approaches to cemented materials characterization involving development of standardized routine laboratory tests to characterize strength, modulus, and fatigue properties for use in Australia. Full-scale accelerated pavement testing was used to provide verification of the laboratory characterization approach. The properties and performance of two field trial test pavements were shown to compare favorably with laboratory characterization results. Two case studies, where implementation of the laboratory modulus characterization protocols proved beneficial in addressing knowledge gaps, were presented. In the first case study, an assessment of available cemented materials in a metropolitan area identified that some products may have been excluded from use due to a conservative specification requirement. On the basis of the laboratory characterization, the specification requirement was relaxed. In the second case study, implementation of the laboratory protocols enabled more informed consideration of an alternative cemented material for a major construction project.

Noting that specimens prepared under ideal laboratory compaction and curing conditions were likely to represent the highest achievable material quality, further research is required to establish links between the laboratory characterization results and the longer-term field properties of cemented materials. Routine implementation of the test protocols for major projects enabling comparisons of field and laboratory prepared specimens would be expected to assist. Further work should also focus on the means to pre-condition laboratory prepared specimens in a consistent manner such that they become representative of field properties for the strength, modulus, and fatigue characterization. The knowledge gained on cemented materials properties is considered important to facilitate the further development and application of mechanistic constitutive modeling for cemented materials.

ACKNOWLEDGMENT

The support from Austroads and my research colleagues at the Australian Road Research Board in Melbourne is gratefully acknowledged.

REFERENCES

Alderson, A. 1998. *Flexural modulus of selected cement treated crushed rocks*. ARRB Contract Report RC6015. ARRB Transport Research, Vermont South, VIC, Australia.

Austroads. 2010. *Guide to pavement technology: part 2 pavement structural design*. AGPT02/10 Austroads, Sydney, NSW, Australia.

Bhogal, B.S., Coupe, P.S., Davies, J. and Fendukly, L.M. 1995. Dynamic flexure tests of soil-cement beams. *Journal of Materials Science Letters*, Vol. 14, No. 4, p. 302–304.

Bureau of Infrastructure, Transport and Regional Economics (BITRE). 2011. *Truck productivity: sources, trends and future prospects*. Report 123. BITRE, Canberra, ACT, Australia.

Gnanendran, C.T. and Piratheepan, J. 2010. Determination of fatigue life of a granular base material lightly stabilized with slag lime from indirect diametral tensile testing. *Journal of Transportation Engineering*, Vol. 136, No. 8, p. 736–745.

Jameson, G. and Sharp, K. 2004. *Technical basis of Austroads pavement design guide*. AP-T33. Austroads, Sydney, NSW, Australia.

Jameson, G.W., Sharp, K.G. and Yeo, R. 1992. *Cement-treated crushed rock pavement fatigue under accelerated loading: the Mulgrave (Victoria) ALF trial, 1989/1991*. ARR 229. Australian Road Research Board (ARRB), Vermont South, VIC, Australia.

Laboratoire Central des Ponts et Chaussees (LCPC). 1997. *French design manual for pavement structures*. Laboratoire Central des Ponts et Chaussees, Paris, France.

Litwinowicz, A. and Brandon, A.N. 1994. Dynamic flexure testing for prediction of cement–treated pavement life. *Proceedings of the 17th Australian Road Research Board Ltd (ARRB) Conference, Gold Coast, Queensland*. ARRB, Vermont South, VIC, Australia, Vol. 17, No. 2, p. 229–247.

Litwinowicz, A. 1986. *Cement stabilised Pine Mountain crushed rock: assessment of properties and laboratory test procedures*. Materials Branch Research Project R533. Main Roads Department, Queensland, Australia.

MINCAD. 2004. *CIRCLY05 User manual*. MINCAD Systems, Richmond South, VIC, Australia.

Mitchell, J.K., Fossberg, P.E. and Monismith, C.L. 1969. *Behavior of stabilized soils under repeated loading: report 3: repeated compression and flexure tests on cement- and lime-treated buckshot clay, confining pressure effects in repeated compression for cement-treated silty clay*. Contract Report 3-145. Geotechnical Laboratory, U.S. Army Engineer Waterways Experiment Station, Vicksburg, Mississippi.

Molenaar, A.A.A. and Pu, B. 2008. *Prediction of fatigue cracking in cement treated base courses*. Delft University of Technology, Netherlands. http://citg.tudelft.nl/fileadmin/Faculteit/CiTG/Over_de_faculteit/Afdelingen/Afdeling_Bouw/-_Secties/Sectie_Weg_en_Railbouwkunde/-_Medewerkers/Profielen/doc/Prediction_molenaar.pdf. Accessed 9 September 2011.

National Cooperative Highway Research Program (NCHRP). 2011. *Mechanistic-empirical design of new and rehabilitated pavement structures*. NCHRP 1-37A. Transportation Research Board of the National Academies, Washington, D.C. http://www.trb.org/mepdg/guide.htm. Accessed 23 September 2011.

National Transport Commission (NTC). 2010. *Heavy vehicle pricing options: development and assessment framework*. NTC, Melbourne, VIC, Australia.

Otte, E. A. 1978. *Structural design procedure for cement-treated layers in pavements*. Thesis (D.Sc(Eng)). Faculty of Engineering, University of Pretoria, South Africa.

Raad, L. 1988. Behaviour of cement-treated soils in flexure. *In Transportation Research Record: Journal of the Transportation Research Board*, No. 1190, Transportation Research Board of the National Academies, Washington, D.C., p. 1–12.

Scullion, T., Uzan, J., Hilbrich, S. and Chen, P. 2008. *Thickness design systems for pavements containing soil-cement bases*. portland Cement Association, Skokie, Illinois.

Sharp, K.G. 2004. Full scale accelerated pavement testing: a southern hemisphere and Asian perspective. *Proceedings of the Second International Conference on Accelerated Pavement Testing, Minneapolis, Minnesota*. http://www.mrr.dot.state.mn.us/research/MnROAD_Project/index_files/pdfs/Sharp_K.pdf. Accessed 9 August 2011.

Sobhan, K. and Das, B.M. 2007. Durability of soil–cements against fatigue fracture. *Journal of Materials in Civil Engineering*. Vol. 19, No. 1, p. 26–32.

Solanki, P. 2010. *Characterization of cementitiously stabilized subgrades for mechanistic-empirical pavement design*. PhD Dissertation. School of Civil Engineering and Environmental Science, University of Oklahoma, Oklahoma.

Tayabji, S.D. and Okamoto, P.A. 1987. Engineering properties of roller compacted concrete. *In Transportation Research Record: Journal of the Transportation Research Board*, No. 1136, Transportation Research Board of the National Academies, Washington, D.C., p. 33–45.

Theyse, H.L., De Beer, M. and Rust, F.C. 1996. Overview of South African mechanistic pavement design method. *In Transportation Research Record: Journal of the Transportation Research Board*, No. 1539, Transportation Research Board of the National Academies, Washington, D.C., p. 6–17.

Thogersen, F., Busch, C. and Henrichsen, A. 2004. *Mechanistic design of semi-rigid pavements: an incremental approach*. Report No. 138. Danish Road Directorate, Hedehusene, Denmark. http://www.vejdirektoratet.dk/publikationer/VIrap138/index.htm. Accessed 23 August 2011.

Vuong, B. 1991. *EFROM2 user's manual. A computer based program for back-calculating elastic properties from pavement deflection bowls*. Version 1. ARRB Transport Research, Vermont South, VIC, Australia.

Yeo, R.E.Y. 2008. *The development and evaluation of protocols for the laboratory characterisation of cemented materials*, Technical Report AP-T101/08, Austroads, Sydney.

Zhong X. 1998. *Modeling for the mechanical behaviour of cementitious granular materials*. Doctor of Philosophy dissertation. University of Massachusetts, Amherst.

This page intentionally left blank

Advances in Pavement Design through Full-scale Accelerated Pavement Testing – Jones, Harvey, Mateos & Al-Qadi (Eds.)
© 2012 Taylor & Francis Group, London, ISBN 978-0-415-62138-0

Validating permanent deformation tests using accelerated pavement testing

M.A. Moffatt, G.W. Jameson & J.W.H. Oliver
ARRB Group, Vermont South, Victoria, Australia

ABSTRACT: Using two case studies, this paper demonstrates the role that controlled accelerated pavement tests can play in the development of performance based laboratory testing procedures. Firstly, the results of an evaluation of the rut-resistant properties of asphalt mixes under accelerated loading using the Accelerated Loading Facility (ALF) conducted between November 1993 and May 1995 are summarized. The performance ranking of the asphalt mixtures is compared to the ranking determined using a dynamic creep laboratory test. The relative rankings of the mixes were different. The laboratory creep test results suggested that the minimum creep slope could rank the relative performance under ALF loading of mixes having the same composition but different binder type but not the relative performance of mixes having different gradings and compositions. The results of the ALF testing correlated better with the results of laboratory wheel-tracking testing. Secondly, a similar deformation trial was conducted on four different spayed seal surfaced, unbound granular pavements between July 2007 and June 2008. The work was undertaken as a means of validating a Repeated Load Triaxial (RLT) test procedure. The RLT test results brought into question the usefulness of the axial permanent strains measured in the test method as these strains did not identify one of the four test materials as being unsuitable for base course due to its low resistance to lateral shoving. By contrast a wheel tracking test, similar to that adopted after the 1990s asphalt work, correlated reasonably well with the ALF results.

1 INTRODUCTION

Accelerated pavement testing (APT) facilities have been used for many different purposes. However, it is proposed that the uses can be classified into three distinct categories:

- Testing structures: where testing of an overall pavement system is undertaken, and an understanding of the pavement's performance is the primary goal.
- Testing materials: where testing of a specific material (or comparison between materials) is undertaken with the goal of determining the likely performance of the material in full pavement structures.
- Evaluating tests or theories: where the assessment of independent (usually laboratory) test processes or theories of pavement material/load interaction are examined by collecting performance data under controlled conditions.

The relevant international literature is dominated by descriptions of trials established primarily for the first two categories above, with very little for the last. In some cases APT data has been used subsequently to validate (or not) tests or theories, but there are very few documented APT experiments that were undertaken primarily for these purposes. This paper aims to highlight the role that APT can play in helping to develop laboratory-based tests. Two case studies are used to demonstrate the role that APT has played in assessing the ability of laboratory-based permanent deformation tests to predict field performance. There are strong similarities in both of the case studies.

2 TERMINOLOGY

2.1 *Accelerated Loading Facility*

The Australian Accelerated Loading Facility (ALF) is owned and operated by ARRB Group. ALF is a mobile, relocatable road testing machine which uses a directly driven load trolley to apply full-scale rolling wheel loads in a single direction to pavement test sections, at a constant speed, using a constant mass. The gravity load is applied to the test pavement through a load assembly trolley, consisting of a wheel assembly, chassis and weight bed. The load applied to the pavement can be varied from 40 kN to 90 kN in 10 kN increments, by adding ballast weights to the trolley above the axle assembly.

The cycle time for each load is about 10 seconds, which corresponds to approximately 350 load cycles per hour or, depending on the percentage of operating time, about 50,000 cycles per week (based on 22 hours operation per day). A normal distribution of transverse locations covering a 1.0 m wide trafficked area is commonly used to simulate typical traffic wander on a road.

2.2 *Asphalt*

This paper uses the term asphalt to denote the mixture of bituminous binder and aggregate with or without mineral filler. In Australia paving-grade bitumen binders are classified (Standards Australia, 1997) according to their viscosity at 60°C. The most common classes of bitumen used in asphalt mixes are:

- Class 320: viscosity in range 260–380 Pa.s
- Class 600: viscosity in range 500–700 Pa.s.

Class 320 and 600 binders would typically exhibit penetration (at 25°C) grades of 60/70 and 45/50 pen respectively.

2.3 *Austroads*

Austroads is an association of each of the state road authorities in Australia, and the national government transport agencies of both Australia and New Zealand. As a collective body it aims to maximize harmonization of practice amongst its members, to pool resources for research and other initiatives, and to provide a common voice in dialogues on issues such as road or vehicle reform. In the context of this paper, Austroads was the primary sponsor of both of the research trials discussed.

3 STUDY 1: DEFORMATION OF ASPHALT MIXES

3.1 *Research context*

Commencing in the late 1980s, a joint research program was developed by Austroads and the Australian Asphalt Pavement Association. The major aim of the program was the improvement of the quality and performance of asphalt mixes, obtained through developing a better understanding of their fundamental properties. This was to be achieved by developing new procedures and, where necessary, new equipment to better define asphalt properties.

By 1992 the first phase of the program was completed, having produced draft test methods, and appropriate laboratory equipment, for producing samples and determining the stiffness and creep properties of asphalt. At this stage, however, no information was available to link these new processes to observed field performance. Consequently, Austroads agreed to support an accelerated pavement testing field trial, using ALF. Associated with the ALF testing was an extensive laboratory evaluation program, the broad aim of which was to compare the anticipated performance of asphalt mixes as predicted by the new test processes with the actual performance obtained from ALF loading. In large part, the combined exercise was to be a validation, or not, of the dynamic creep assessment test method and equipment developed to date.

3.2 *Dynamic creep test*

The dynamic creep test used in Australia uses test equipment comprised of a load frame capable of applying up to a 4.5 kN loads for a set duration with a rest period. The short cylindrical samples used in the test are placed in a jig which measures the changing height of the sample as repeated cycles of loading/rest are applied during the test. The standard test result is the minimum slope of the loading cycles versus permanent deformation curve.

The test was based around an Australian variant of the Nottingham Asphalt Tester developed in the United Kingdom.

3.3 *Overview of ALF trial*

The ALF trial was conducted at a site near Beerburrum, approximately 70 km north of Brisbane, Queensland. As was common practice at this time, ALF trafficking was conducted in the open. Ultimately, the testing program consisted of three components:

- A Core trial during which the rut-resistant properties of seven asphalt mixes were evaluated under accelerated loading at summer/autumn ambient temperatures (November 1993 – May 1994)
- An Ancillary trial during which the rut-resistant properties of asphalt mixes nominated by asphalt/binder producers were evaluated, and compared to a control mix from the Core trial, under accelerated loading at controlled temperatures (January 1995 – April 1995)
- A Follow-up trial during which the rut-resistant properties of the original seven Core trial mixes were evaluated under accelerated loading at a controlled temperature of 50°C (November 1994 – May 1995).

Whilst the same asphalt mixes were used in the Follow-up trial as the Core trial, the physical pavements tested in the Follow-up trial had not previously been trafficked.

A pavement heating system for the ALF machine was installed and commissioned between the Core and Ancillary trials. The design of the heating system was primarily based on systems in use at the Federal Highway Administration's Turner-Fairbank Research Facility in McLean, Virginia. The system comprised 20 radiant heaters mounted to the ALF frame, with 10 each side of the test pavement area. The heaters were configured into four zones along the 12 m test length. Readings from infrared surface temperature sensors were used to selectively turn on or off the heaters in each zone. During the conduct of an experiment, separate data loggers were used to record the temperature of the asphalt at depths of 10, 40 and 80 mm. Measurements were recorded at five minute intervals. All pavement temperatures shown in this paper were recorded at 40 mm depth (i.e. mid-layer).

The asphalt mixes were all placed on a standard pavement structure:

- 75 mm of crushed rock subbase working platform placed over select subgrade.

– Two 150 mm layers of cement treated base (CTB) comprised of a 20 mm base quality crushed rock stabilized with a 3.5% (by mass) cement/flyash blend (a cement slurry was placed between the layers).
– Strain alleviating membrane interlayer (SAMI) placed on top of the CTB to inhibit reflection cracking through to the overlying asphalt.

All of the asphalt mixes tested were comprised of a nominal 10 mm asphalt compacted on the CTB in a 75 mm single layer, with the exception of a stone mastic asphalt (SMA) mix which was a 30 mm thick layer placed on top of a 45 mm thick ethylene vinyl acetate (EVA) modified mix. The test pavements were constructed 4 m wide in parallel with each other, and during testing the ALF was placed perpendicular to the direction of placement, allowing three mixes to be simultaneously trafficked with the 12 m test length of the machine. This arrangement allowed a higher productivity of trafficking, as well as a consistent environmental condition for the three mixes being tested (this was particularly important during the uncontrolled Core trial testing).

As the trial was examining the relative performance of asphalt mixes with the same predominant aggregate type, but different binders, the effect of trafficking pavements perpendicular to their direction of construction was considered to affect all sections equally.

3.4 *Asphalt mixes tested*

The different asphalt mixes tested are described in Table 1. The polymer modified binders (PMB) used in the C3 and C4 mixes were not the premium-grades commonly used in current asphalt mixes. The binders used were deliberately chosen with a view to obtaining high deformation rates for measurement purposes. The aggregate components and mix proportions used are shown in Table 2. Mixes C3, C4, C6 and C7 all contained the same aggregate components and grading as the C1 mix.

3.5 *Results of field testing*

The full details of the trafficking program and data collected are reported elsewhere (Sharp et al., 1996) and the full trial findings, including an extensive laboratory testing program were summarized in the international literature (Jameson et al., 1994; Oliver et al., 1997). Only a selected element of the trial works and findings are discussed in this paper.

In summary, almost all of the ALF trafficking was conducted using an 80 kN load on a half-single axle with dual tires placed at 330 mm centers. Loading was applied in one direction only and, as noted above, over three pavement structures with each cycle. A narrow distribution of transverse wander was used during trafficking, with the centre of the dual-wheels following a normal distribution spanning ± 150 mm, yielding a total loading width (i.e. to the outer extremities of the tires) of 900 mm.

The initial Core trial was conducted before asphalt temperatures could be controlled. To ensure, as far as possible, that all mixes were tested under comparable conditions, the following test sequence was adopted. A set of three mixes was first loaded for 100,000 cycles, the ALF was then moved and 100,000 cycles were applied to the other two groups of three mixes. ALF was then moved back to each of the three sites in turn to apply an additional 100,000 cycles of loading. A four to six week gap typically occurred between the two phases of loading for a given group of three mixes. Following implementation of the pavement heating system, trafficking during the Follow-up trial did not involve this two-stage loading regime.

A transverse profile measuring beam was used periodically during trafficking, recording the transverse profile of the 12 m long experiment strips at 0.5 m chainage. For each chainage the average deformation of the surface, resulting from the two loading tires, was calculated. For each asphalt mix section, the mean deformation was calculated as the mean of the averages determined at each chainage. Deformation was calculated based on the total downward movement of material, and did not include any upwards heave. Surface rutting measured using a straight-edge would have included the heave of the material. The exact relationship between deformation level and rutting level would depend on the material tested. For the asphalt mixes tested a rough rule-of-thumb was determined as surface rutting was approximately twice the deformation measurement. A typical failure criterion for flexible pavements in Australia is 25 mm of surface rutting. Typical relationships between mean surface deformation and cumulative ALF loading cycles are shown in Figure 1.

The data in Figure 1a typify that collected during the Core trial when asphalt temperature was not controlled. A general reduction in deformation between the end of the initial 100,000 cycles of loading and the start of the second 100,000 cycles is apparent. Evidently, relaxation of the pavement surface had occurred in the intervening four to six weeks.

Figure 1b shows typical data from the Follow-up trial, when control of the mid-depth asphalt temperature, at $50°C \pm 2°C$, was achieved using the heating system. The effect of maintaining this elevated temperature can be readily seen by comparison of the high deformations obtained with those observed during the earlier Core trial. As a result of these high deformation rates the trafficking durations for the Follow-up trial were much shorter.

As each group of three mixes tested included a mix that was subsequently tested as part of another group of three at a different temperature, sufficient data were available to allow the 'adjustment' of all deformation levels to a standard temperature condition for the Core trial (35°C).

Table 3 shows the average rate of deformation of the six mixes tested in the Follow-up trial at 50°C with

Table 1. Details of asphalt mixes tested.

Mix code	Description	Details
Core trial -– Phase 1		Temperature not controlled
C1	Control	Control mix – size 10 mm with Class 320 binder The mix was designed using the conventional 50 blow Marshall procedure, and was chosen to be representative of current (at the time) surfacing mixes. The nominal binder content was 5.5%.
C2	Austroads	Size 10 mm with Class 320 binder The mix was designed using the proposed Austroads mix design procedure, with the emphasis placed in the design process of improving rut resistance. The nominal binder content was 5.1%.
C3	SBS	Control mix grading with SBS binder The mix had the same aggregate grading as the control mix but used a styrene butadiene styrene (SBS) modified binder.
C4	EVA	Control mix grading with EVA binder The mix had the same aggregate grading as the control mix but used an ethylene vinyl acetate (EVA) modified binder.
C5	SMA	Stone mastic asphalt mix with Class 320 binder The mix was designed using the 50 blow Marshall procedure, and contained 0.3% (by mass) of cellulose fiber. The design binder content was 6.5%. The mix was placed in a 30 mm layer overlaying a 45 mm layer of the C4 mix, as it was thought that the C5 mix was insufficiently stable to be placed in a single 75 mm layer.
C6	Multi-grade	Control mix grading with multi-grade binder The mix had the same aggregate grading as the control mix but used a multi-grade (improved temperature susceptibility) binder.
C7	Class 600	Control mix grading with Class 600 binder The mix had the same aggregate grading as the control mix but used a Class 600 binder. This mix was included in an attempt to establish the extent to which the rut-resistant properties of a mix might be enhanced by the use of a stiffer conventional binder.
Core trial – Phase 2		Temperature controlled
C1a		C1 mix, but placed at higher air voids
C2a		C2 mix, but with 0.5% less binder (by mass)
C3a		C3 mix, but using a different SBS binder Some doubts had been raised as to whether the SBS binder used in C3 was representative of current practice, and as a result a different binder was used for the C3a mix.
Ancillary trial		Temperature controlled
A1	Control	Same control (C1) mixes used in Core trial Two strips of this mix were placed, designated A1-1 and A1-2.
Follow-up trial		Temperature controlled
C1, C2, C3, C4, C6, C7	as above	All of the Core trial mixes, with the exception of the C5 mix were retested in the Follow-up trial under controlled temperature conditions (50°C at mid-depth of asphalt).

those tested in the Core trial when temperatures were not controlled.

Laboratory creep testing had indicated that, based on the minimum creep slope, the C2 mix, designed using the Austroads mix design processes, should have been more rut-resistant than the control mix (C1), designed using the Marshall method. Additionally, experienced asphalt mix designers believed that the use of crusher fines in the C2 mix in place of the sand used in the C1 mix should also have ensured that the C2 mix was more rut-resistant than the C1 control mix. However, in all ALF tests the C2 mix demonstrated higher deformation rates than the C1 mix.

3.6 *Results of laboratory testing*

An extensive laboratory testing program (Oliver, 1994; Oliver et al., 1995) was conducted as part of the trial. A variety of asphalt specimen sets were tested including:

– Laboratory gyratory compacted specimens used during the mix design phase.

Table 2. Aggregate proportions and gradings of asphalt mixes C1, C2 and C3.

Percent of each fraction passing	10 mm rock	5 mm rock	Crusher fines	Coarse sand	Find sand	Filler pozzolanic
C1	24	22	7	25	18	4
C2	36	14	33	0	16	1
C5	52	19	15	0	5	9

Percent passing (combined gradings)

Sieve size (mm)	13.2	9.5	6.7	4.75	2.36	1.18	0.6	0.3	0.15	0.075
C1	100	96	79	64	47	36	25	15	8	5.4
C2	100	94	70	57	72	31	22	15	8	5.6
C5	100	92	57	39	26	20	18	15	12	9.6

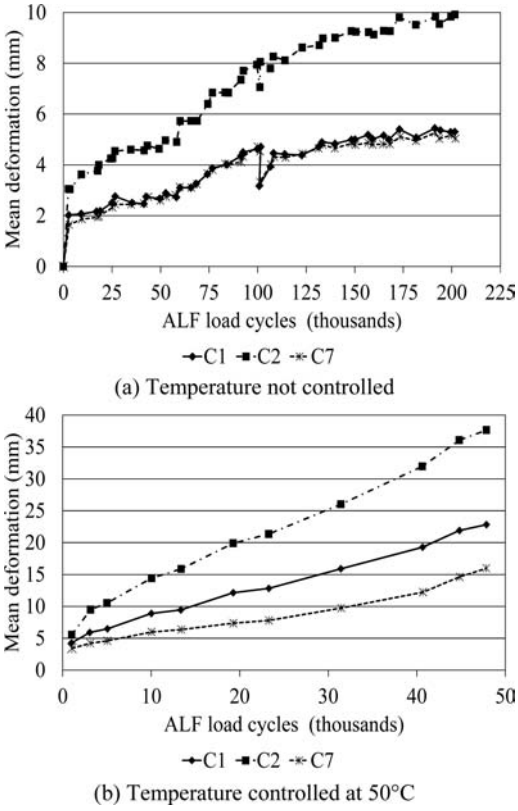

Figure 1. Typical relationship between surface deformation and ALF loading.

– Gyratory compacted samples of asphalt mixes sampled from trucks at the mixing plant.
– Cores extracted from untrafficked pavement sections.
– Cores extracted from the trafficked sections.

All samples were tested for density, and the majority for resilient modulus (indirect tensile) at 25°C and dynamic creep at 50°C using the then-draft procedures, which have subsequently been adopted as Australian standards. Some Marshall (50 blow) testing was conducted on selected specimens to provide comparative data, and a limited number of samples were also tested by the University of California using the Cox shear testing device. Additionally, slabs of the asphalt mixes were extracted from untrafficked areas of the test pavements and subjected to wheel-tracking using a device based on a UK Transport Research Laboratory design which was subsequently developed into an Austroads test method.

Table 3. Comparison of Core and Follow-up trial test results.

	Deformation rate (μm/kilocycle)	
Mix code	Core trial*	Follow-up trial
C1	12	373
C2	20	610
C3	18	197
C4	6	106
C5	15	
C6	9	99
C7	10	254

*Adjusted deformation rate.

This paper will focus largely on the findings related to the dynamic creep test.

As shown in Figure 2, dynamic creep tests conducted on gyratory compacted samples (of plant mixed materials) showed that the C2 mix had a lower creep slope, implying better rut-resistance, than the C1 mix over a range of air void contents. As noted above, this is contrary to the relative ranking of the deformation observed under ALF trafficking. Of additional interest is the large effect that air void content had on minimum creep slope; the creep slope for the C2 mix changed by a factor close to 800 between air void contents of 1% and 7.5% (Oliver et al., 1995).

Figure 2b shows that the creep slope continued to decrease with decreasing air void content below 3%, indicating increasing rut-resistance. However, general experience has shown that rapid shear failure occurs under field conditions for mixes with less than 3% voids. As a result of this testing, the creep test procedure was subsequently changed to specify that testing

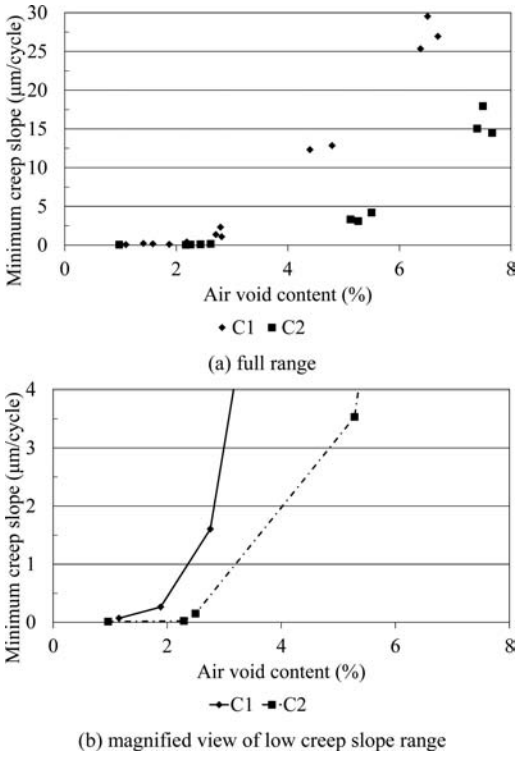

Figure 2. Comparison of air void content and creep slope for C1 and C2 mixes.

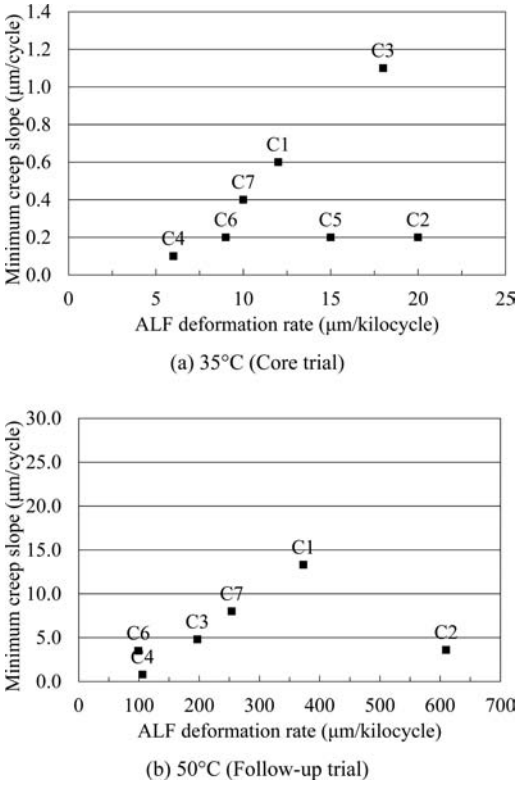

Figure 3. Comparison of minimum creep slope and ALF deformation rate.

be conducted at a void content of 5%. Nevertheless two issues remain:

- The possibility of misinterpretation of the dynamic creep test results from field extracted cores in which the control of air void content is more difficult.
- The inability of the dynamic creep test procedure to detect the propensity of low void mixes to rapid shear failure, thus casting some doubt on the utility of the test as a performance indicator of all of the mechanisms involved in asphalt mix deformation.

Table 4 summarizes the creep slopes and resilient modulus results for field cores and also the results of wheel-tracking conducted on field-extracted slabs. The dynamic creep slope is sensitive to air void content (Oliver, 1994). In order to compare dynamic creep data with both ALF deformation data and wheel tracking results on samples cut from the ALF pavement, the minimum creep slope for each mix was calculated at the air void content considered to be typical for that mix in the trial pavement. The procedure is described in more detail by Oliver (1994). The wheel-tracking results are discussed below.

Figure 3 compares the observed ALF deformation rates at 35°C (the typical value associated with the Core trial) and at 50°C (the controlled temperature used in the Follow-up trial) with the minimum creep slope of field cores (corrected to an air void content representative of ALF pavement conditions).

The results indicate that the dynamic creep test might be able to predict the relative ranking of mixes with the same grading and aggregate composition but different binders (i.e. mixes C1, C3, C4, C6, C7 and C1). However, the test does not appear to be able to correctly predict the performance of mixes having different aggregate gradings (i.e. C2, C5 and RS compared to C1).

The inability of the minimum creep slope to correctly rank the deformation resistance of mixes with different aggregate gradings was considered a major impediment to the widespread adoption of the test as the deformation performance indicator for use in mix design. Hoping that relatively minor adjustments to the test procedure would produce results more in line with the ALF field observations, some limited testing incorporating confining pressures was conducted. The results proved inconclusive.

As seen from Figure 4, a better match to the ALF deformation results was obtained from wheel-tracking tests (data listed in Table 4). A wheel-tracker, based on a Transport Research Laboratory design and similar to the small wheel-tracker used in current European standards was used.

As a result of this work, the use of wheel-tracking tests was included in the Austroads asphalt mix design process, with particular reference to their use in the design of heavy duty mixes.

Table 4. Summary of laboratory test results of field cores.

Mix code	Air voids (%)*	Resilient modulus at 25°C (MPa)	Dynamic creep testing at 50°C		Wheel-tracking at 60°C	
			Min. creep slope (μm/cycle)	Ranking of rut-resistance	Tracking rate (mm/kilocycle)	Ranking of rut-resistance
C1	3.7	3 950	13.3	7	2.04	6
C2	3.2	4 090	3.6	3	2.47	7
C3	3.1	1 320	(4.8)	4	0.75	2
C4	2.4	4 380	0.8	1	0.98	3
C5**	3.7	4 010	(6.1)	5	1.99	5
C6	5	3 750	3.5	2	0.57	1
C7	3.7	4 620	(8)	6	1.33	4

*Air voids determined on cores assumed to apply to ALF trafficked area.
**60/40 composite of SMA bonded to C4.
( )Estimate since regression line not significant or value outside range of data.

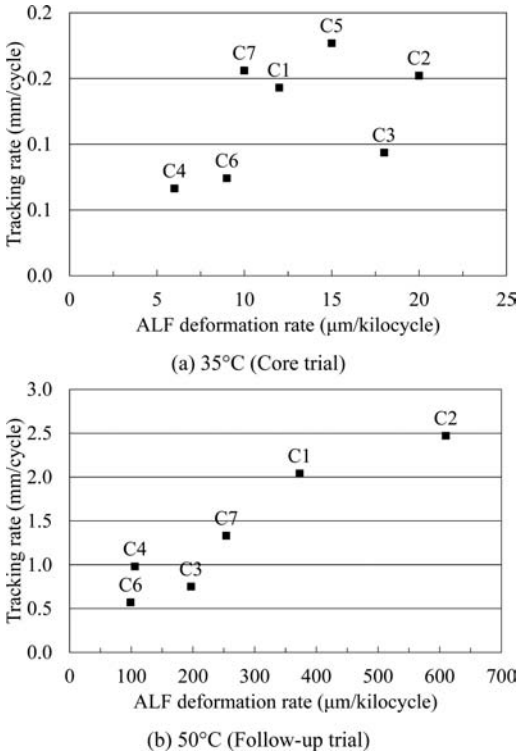

Figure 4. Comparison of wheel-tracking results and ALF deformation rate.

3.7 *Conclusions of deformation of asphalt mixes ALF trial*

The main findings of the trial were:

- Under controlled temperature ALF trafficking, clear differences in deformation were observed between different asphalt mixes.
- Multi-grade and PMBs demonstrated higher rut-resistance than conventional binders under ALF loading.
- Unexpectedly, the control mix (C1) designed using the established Marshall process outperformed the mix designed using the new performance-based mix design procedures (C2).
- Laboratory testing on gyratory prepared specimens showed that air void content highly affected both resilient moduli and minimum creep tests
- Significantly, the minimum creep slope continued to decrease with decreasing air void content below 3% voids, indicating that the test could not readily predict the rapid shear failures that commonly occur with extremely low void content mixes.
- The minimum creep slope of field extracted cores could rank the relative performance under ALF trafficking of mixes having the same composition but different binder types, but not the relative performance of mixes with different aggregate gradings and compositions.
- A reasonable correlation was found between the results of wheel-tracking at 60°C of slabs extracted from the field and the deformations obtained by ALF trafficking at a controlled temperature of 50°C
- The multi-grade and SBS mixes demonstrated a lower dependence of deformation rate under ALF loading on temperature than mixes with conventional binders.

In the context of this paper's underlying theme, the most significant outcomes were:

- The successful first use of ALF testing to validate (or not) laboratory test procedures for predicting the performance of pavement materials (all previous ALF trials had focused either on direct material behavior, construction techniques, or pavement design processes).
- A clear demonstration that, in isolation at least, the dynamic creep test was not as good a predictor of the deformation performance of asphalt mixes as had been expected – the test was poor at reflecting the (poor) performance of very low void mixes, and was unable to distinguish between different aggregate compositions between mixes.

– A rolling-wheel-based test, the wheel-tracking test, was able to provide a better prediction of the relative ranking of deformation under ALF loading than the pulsed dynamic creep test.

The use of accelerated pavement testing thus helped to ensure that an appropriate rutting test would be selected for use in asphalt mix design in Australia.

4 STUDY 2: DEFORMATION OF UNBOUND GRANULAR BASES

4.1 *Research context*

Road authorities in Australasia are coming under increasing pressure to deliver higher levels of serviceability to the road user, in a climate of continuing changes in traffic loadings (increasing volumes, high axle loads and new generation vehicles), scarcity of resources (reduction in high quality traditional materials and increased use of alternative materials such as recycled materials, and construction and industrial wastes), and moisture/thermal environments (increasing consumption of water for irrigation, changes in landscape, and climatic and thermal changes).

Currently most design, material specification, and construction technologies for sprayed sealed surfaced unbound granular pavements are still empirically based. Given the changes listed above, authorities are increasingly finding that they are pushing the boundaries of the empirical knowledge. One significant deficiency in the specification of granular materials is the lack of a reliable test to estimate the deformation of these materials in-service. This has led to a need to develop performance-based specification (PBS) approaches for unbound granular materials in Australia and New Zealand.

Austroads member authorities considered the repeated load triaxial (RLT) test to be the best candidate laboratory performance test to pursue new material measures (such as shear strength, resilient modulus, and pavement layer deformation) for use in PBS of granular material, and for predicting the performance of granular pavements with thin bituminous surfacing in a mechanistic pavement design procedure. In over a decade of development, a test procedure was written, relatively inexpensive testing equipment was developed, and the use of testing incorporated into some routine road authority practices. However, widespread use of the test has been hindered by the lack of data relating the laboratory RLT test results to observed field performance, and the lack of procedures for incorporating RLT results into the PBS and mechanistic design process.

In order to address this issue, Austroads funded a major research project centered upon the comparison of field results obtained by the use of ALF with an extensive laboratory testing program.

4.2 *Repeated load triaxial test*

The Austroads RLT test for granular materials characterizes the vertical permanent stress at three levels of dynamic deviator stress (σ_1–σ_2) conditions: 350, 450 and 550 kPa, and a static lateral stress of 50 kPa. Each stress condition is repeated for 10,000 repetitions (Austroads 2007). Based on the test results, stress-dependent characteristics of permanent strain for the material can be determined. Multiple tests at different density and moisture conditions may be required to assess the sensitivity to moisture and density of the material. The specimens are compacted in a split mould in five layers using a drop hammer to produce specimens 200 mm in height and 100 mm in diameter. Materials up to a maximum particle size of 19 mm may be tested.

4.3 *Overview of ALF trial*

Several test values (e.g. deformation rate per 1,000 cycles, and maximum deformation for each loading stage) can be extracted from the RLT test results for use in assessing the potential for permanent deformation of the material under field conditions. The main objective of the project was to determine which test values best correlated with performance under accelerated loading.

The ALF trial was conducted at the semi-permanent ALF site located at Dandenong South, an outer eastern suburb of Melbourne. As was common practice of the time, and remains current practice, the test pavements were constructed inside a large dedicated shed, and all trafficking took place within this enclosure. The shed, coupled with a drainage system, ensured that the moisture condition of the unbound bases was kept constant.

Four different bases were tested with the ALF between July 2007 and June 2008. After completion of ALF testing, laboratory tests were conducted at the same densities and moisture conditions present during the ALF trafficking. A simple comparison of laboratory test results with observed field performance under ALF could then be undertaken. Most trafficking was conducted with 60 kN dual wheel loading on a (half) single axle.

In order to ensure that the only mode of distress for the constructed pavement would be permanent deformation, and that this deformation would be restricted to the base material, and not occur in any subbase materials, a base course thickness of 350 mm was selected for all four materials. A cemented crushed rock subbase was placed under the granular bases for the following reasons (Moffatt and Eady, 2007):

– To ensure that the material underlying the granular base was deformation resistant, thus limiting the total pavement deformation to the overlying unbound granular base.
– To provide a stiff layer against which construction equipment could compact the granular material, thereby ensuring uniform densities were achieved both with pavement depth and also longitudinally along the test pavements.

A sprayed sealed surface was used instead of asphalt to further ensure that any surface deformation directly

reflected the deformation of the granular materials and that no contribution was made by the surfacing material. The sprayed double/double latex modified emulsion seal was designed using current Austroads seal design procedures (Moffatt and Eady, 2007; Holtrop and Moffatt, 2008).

4.4 *Unbound granular bases tested*

In order to ascertain which of the parameters from the RLT test best correlated with base performance under accelerated loading, it was important that the materials for testing be carefully selected to cover a wide range of material qualities. Twelve candidate materials were nominated by Austroads member authorities, and these materials were tested using both current empirical specification tests (e.g., Los Angeles abrasion [LAA], grading, plasticity index [PI], etc.) and advanced laboratory test methods for mechanical properties including permanent strain and resilient modulus using the RLT test (Vuong et al., 2007). Based on this testing, four base materials were selected as follows:

- Material A: Crushed rhyolite
- Material B: Crushed hornfels
- Material C: Crushed limestone
- Material D: Crushed tuff

The Victorian crushed rhyolite is a typical good quality 20 mm crushed rock produced commercially at a quarry in Melbourne. It is an angular, rough, hard, blue-grey crushed rock containing some dolomite and some blue-grey sand silt. This material is hard crushed rock with LAA of 12% but has added fines to improve its plasticity (PI of 4%). It meets VicRoads specification requirements for Class 1 crushed rock and has been widely used in Melbourne.

The Victorian crushed hornfels used in this study was obtained from a quarry in south-eastern Melbourne. It has a fines content of 18% (exceeding the limit of 13% passing the 0.075 mm sieve) and plasticity index of 9% and, therefore, is regarded as Class 3 material for subbase according to VicRoads specifications. Currently, this material is not used as crushed rock base material in Victoria.

The crushed limestone was obtained from a quarry near Port Wakefield in South Australia. The material has been used for granular overlays in several passing lanes on heavily trafficked roads (design life $>10^7$ ESA) during the last three years. This material is regarded as one of the better Class 1 materials available in South Australia.

The Victorian crushed tuff was obtained from a quarry in the south-western region of Victoria. Generally, tuff metamorphoses from volcanic ash. This ash was eventually buried to depths sufficient to produce temperatures and pressures necessary to petrify it into the tuff. Some tuff was later uplifted, and exposed to a secondary alteration with mordenite, which acted much like glue, changed the color, and gave it added strength. This material is soft (LAA of 45) and is high in fines. It is currently only used as base on lightly trafficked roads in south-western Victoria.

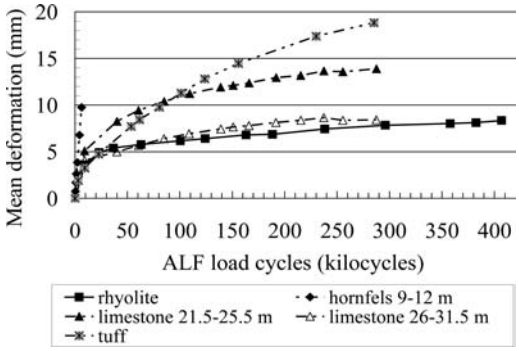

Figure 5. Summary of measured surface deformations under 60 kN ALF loading.

4.5 *Results of field testing*

The full details of the trafficking program and data collected are reported elsewhere (Jameson et al., 2010) and the full trial findings have been discussed at several international conferences (Jameson et al., 2010a, 2010b).

Figure 5 and Table 5 summarize the number of cycles of loading to 10 mm of surface mean deformation for each experiment (i.e. 12 m tested length). Some experiments were sub-divided into sub-sections if two distinct areas of performance were observed with the 12 m length (these are referenced using the site chainage in meters). For some experiments the deformation observed at the completion of trafficking was generally lower than the 10 mm terminal deformation criterion, and in these cases the cycles to reach 10 mm deformation have been extrapolated.

It is clear from this data that the crushed hornfels material failed rapidly under 60 kN loading (Experiments 3503 and 3504), and so repeat testing was conducted at 40 kN (Experiment 3405). Despite the lower loading level, the material again deformed rapidly. Post-trafficking forensic evidence indicated that the quick failure of the hornfels base was due to lateral shoving of the material rather than rapid densification.

4.6 *Results of laboratory testing*

4.6.1 *Austroads RLT method*

After the conclusion of ALF trafficking, RLT tests were conducted following the Austroads test method (Austroads, 2007) described above. For each of the materials, testing was conducted at densities and moisture contents that matched those that occurred in the field during the ALF trafficking. Table 6 summarizes the permanent axial strains recorded. It is apparent from this table that the strains in Stages 2 and 3 were poorly correlated with the deformation performance of the materials under ALF loading (Table 5). If the

Table 5. Estimated loading cycles to 10 mm mean surface deformation.

Material	Experiment	Mean density (t/m^3)[1]	Mean moisture content (%)[2]	ALF kilocycle to 10 mm deformation	
				60 kN	40 kN
Crushed rhyolite	3401	2.26	3.6	1,160*	–
Crushed hornfels	3403 Ch. 9 to 12 m	2.33	4.6	6.5	–
	3403 Ch. 12.5 to 19 m	2.33	4.7	3	–
	3404	2.33	4.7	3.6	–
	3405 Ch. 34 to 39 m	2.30	4.7	–	3.9
	3405 Ch. 39.5 to 44 m	2.28	4.7	–	8.7
Crushed limestone	3407 Ch. 21.5 to 25.5 m	2.27	4.9	74	–
	3407 Ch. 26 to 31.5 m	2.27	4.6	>1,000[3]	–
Crushed tuff	3409 Ch. 9 to 12 m	1.77	14.7	–	350
	3409 Ch. 12.5 to 19 m	1.76	15.3	–	135
	3410	1.76	15.3	83	–

[1]determined using nuclear density meter; [2]determined using oven dried samples; [3]extrapolated.

Table 6. Measured permanent axial strains at field densities and moistures (Austroads method).

Material	Permanent axial strain in stage 1[1] (microstrain)			Incremental permanent strain in Stage 2[2] (microstrain)	Incremental permanent strain in Stage 3[3] (microstrain)
	All cycles Stage1	Strain after first 50 cycles	Stage1 less strain after first 50 cycles		
Crushed rhyolite	5,540	3,050	2,490	1,060	2,720
Crushed hornfels	10,280	7,800	2,480	780	2,400
Crushed limestone	5,670	3,240	2,430	1,370	5,300
Crushed tuff	8,310	5,060	3,250	3,270	>7,000

[1]350 kPa deviator stress; [2]450 kPa deviator stress; [3]550 kPa deviator stress.

first 50 cycles of the test are ignored, then Stage 1 permanent strains were also poorly correlated to the ALF results. It was only the first 50 cycles of testing in Stage 1 that ranked the four materials in a manner consistent with their performance under ALF trafficking. Unfortunately, the deformation in the first 50 cycles is highly variable, being heavily influenced by the procedure used to finish the top of the test specimens, and as such it cannot be used as a reliable performance index.

4.6.2 *Alternative RLT methods*

Testing of samples was also conducted using two variations on the Austroads RLT method. Samples of the four materials were tested by the Department for Transport, Energy and Infrastructure (DTEI) in South Australia using their method which is a variation of the Austroads test method (DTEI, 2008). Pavespec Ltd tested the materials in accordance with the Transit New Zealand (now the NZ Transport Agency) method, which varies considerably from the Austroads method (Transit New Zealand, 2007). Both of these testing exercises yielded poor correlations of RLT deformation performance with the observed performance under ALF.

4.6.3 *Static shear tests*

The shear strength of the four bases was measured in accordance with the Standards Australia test (Standards Australia, 1998). Generally, shear failure tests should be conducted on three to four specimens for each material (compacted to a single density-moisture condition) at different constant confining pressures (e.g. 25, 50, 75 and 100 kPa) to enable derivation of general failure relationships, which are used to calculate shear strength (failure stress) at a given applied confining stress. However, the test method allows three levels of failure stress to be applied to a single test specimen (compacted to a specified combination of density and moisture content) to reduce the testing effort.

Table 7 summarizes Mohr-Coulomb criteria parameters and shear strength results for the four bases at their field densities and moisture contents. In principle, a material having a higher friction angle is more stable under a high confined stress condition, whereas a material having a higher cohesion value is more stable under a low confined stress condition. For the stress condition in the base layer, finite element method pavement analysis (Vuong, 1999) indicated that the highest shear stress would occur at a depth of between 75 and 100 mm, with typical mean stress of about 200 kPa

Table 7. Static shear strength results.

Material	Dry density (t/m^3)	Moisture content (%)	Frictional angle (°)	Cohesion (kPa)	Shear strength at mean stress of 200 kPa (kPa)	Shear strength at mean stress of 300 kPa (kPa)
Crushed rhyolite	2.28	3.0	60	70	590	820
Crushed hornfels	2.33	4.8	57	68	580	800
Crushed limestone	2.27	4.9	57	40	510	740
Crushed tuff	1.77	15.0	48	60	490	670

and a difference between principal stresses (or deviator stress, $q = \sigma 1 - \sigma 3$) of 450 kPa. Therefore, to characterize the four bases, the shear strengths were determined at the mean stress of 200 kPa (Table 7).

Table 7 shows that the measured static shear strengths of the rhyolite and hornfels were very similar at their field test densities and moistures. The laboratory test did not replicate the change in structure of the hornfels that occurred in the field under repeated ALF loading.

4.6.4 *Wheel-tracking tests*

A possible reason the permanent strains measured in the Austroads laboratory RLT test did not closely correlate with rutting under accelerated loading is that this laboratory test does not include rotating shear stresses. Given the findings of the asphalt deformation ALF trial a decade earlier, it was of interest to assess whether a laboratory wheel-tracker test would correlate more closely with the accelerated loading results. Initial tests conducted using the small-scale wheel-tracker did not prove helpful. The Roads and Traffic Authority, New South Wales uses a wheel-tracking device to test asphalt using a procedure similar to the European large wheel-tracking test (European Committee for Standardization, 2004). Table 8 shows the key characteristics of the small-scale wheel-tracker and the RTA large-scale machine.

Using the RTA machine, a single wheel-tracking test was conducted on each of the four base materials. The materials were compacted in a series of layers, at the field densities and moisture contents experienced during the ALF trafficking, in a mould 700 mm long, 500 mm wide and 300 mm deep. To prevent moisture evaporation during wheel-tracking, the top of the compacted specimens was sealed with polyurethane, which was cured overnight.

Wheel-tracking comprised 10,000 passes of a single, treadless, tire (125/75R) inflated to 700 kPa and loaded to 10 kN. The overall tire diameter was approximately 380 mm, and the resulting contact patch was 90 mm wide and 125 mm long, resulting in a contact stress of 1,060 kPa. Deformation of the surface of the specimen was measured regularly during the 10,000 cycles of applied load.

The results of this testing are presented in Table 9. It is apparent that the wheel-tracking test results are better correlated with the ALF trafficking results than the RLT test results.

Table 8. Characteristics of small-scale and large-scale wheel-trackers.

Characteristic	Small-scale	Large-scale
Wheel diameter	200 mm	380 mm
Wheel type	Steel with treadless rubber rim (80IRHD units)	Treadless pneumatic tire
Contact width	50 mm	90 mm
Contact length	–	125 mm
Load	0.7–1.5 kN	10 kN
Max. sample size	300 × 300 × 100 mm	700 × 500 × 300 mm

4.7 *Conclusions of deformation of unbound granular bases ALF trial*

The main findings of the trial were:

- There was a marked difference in the field performance of the materials, with the crushed rhyolite deforming an average 8 mm after 400,000 cycles of 60 kN loading, and the hornfels totaling less than 5,000 cycles to reach the same level.
- The bases were tested for rut resistance using variations of an RLT test by ARRB Group (Austroads method), DTEI (DTEI method), Pavespec Ltd (Transit NZ method), and none of these tests ranked the material performance in the same order as the observed behavior under ALF loading.
- There was no indication from any of the existing processes to interpret laboratory permanent axial strain data that the crushed hornfels would fail rapidly under accelerated loading.
- Both the DTEI and Transit NZ methods for assessing permanent deformation data would have allowed all four granular bases tested to be used for moderately trafficked roads ($>10^6$ ESA) even though the crushed tuff and particularly the crushed hornfels are not suitable for base on these roads at the test densities and moistures.
- After approximately 5,000 cycles of ALF loading, the hornfels material changed in structure and reduced to a low stiffness material – none of the permanent strain RLT tests was able to replicate this change in structure.
- The permanent axial strains measured in Stages 2 and 3 of the Austroads test suggested the hornfels

Table 9. Large-scale wheel-tracking test results.

Material	Deformation in first 50 cycles (mm)	Maximum deformation depth after 10,000 cycles (mm)	Deformation rate between 50 and 10,000 cycles (mm/log(kcycle))	Ranking from wheel-tracking test	Ranking from Austroads RLT test	Ranking under ALF
Crushed rhyolite	1.7	2.5	0.16	1	3	1
Crushed hornfels	3.4	11.8	2.8	4	1	4
Crushed limestone	1.9	4.8	0.52	2	2	2
Crushed tuff	4.8	10.9	1.23	3	3	3

would be the best performer, which was of concern given its inferior field performance.
- It was concluded that the Austroads RLT permanent strain test is not suitable for characterization of the deformation of unbound bases under thin bituminous surfacings (this is not to suggest that the RLT test is not suitable to assess the deformation of granular materials under thick asphalt layers where shear stresses are lower and densification rather than shear governs the rutting).
- The wheel-tracking results correlated reasonably well with the accelerated loading results, and it was concluded that a wheel-tracking test is the most suitable test for characterization of the deformation of unbound bases under thin bituminous surfacings.
- Further development of a wheel-tracking test is warranted.

The results of the trial support the contention that incorporating the aggregate interlock characteristics under the shear stress reversals that occur under rolling wheel loads is an integral part of a performance test for granular bases.

In the context of this paper's underlying theme, the most significant outcomes were:

- The successful further use of ALF testing to assess laboratory test procedures for predicting the performance of pavement materials.
- A clear demonstration that, in isolation at least, RLT permanent strain tests are not able to represent the susceptibility of an unbound granular material to fail when subject to high shear stresses, and are unable to replicate the relative ranking of material performance under accelerated loading.

5 SUMMARY

There are a series of common themes to the two case studies described, and some strong lessons to be learnt. In fact it could be argued that the lessons learnt from the asphalt deformation trial could have been better considered during the development of the RLT testing process for granular materials.

Both studies set out with the clear goal of verifying that the laboratory developed procedures represented good predictors of in-service performance. In both cases accelerated load testing was seen as the most time- and cost-efficient means of rapidly collecting performance data, and under controlled conditions. In both cases the laboratory tests were based around vertical axial loading, and in both cases the tests were found inadequate in predicting the relative performance of different aggregate structures under full-scale rolling wheel loads. Of note, wheel-tracking laboratory-based tests were found to be a better predictor of field performances.

Considerable effort was expended in developing the dynamic creep test, and the results of the ALF trial were a disappointment to many. Nevertheless at the end of the process, accelerated pavement testing had highlighted the shortcomings of the test, and had provided a data set against which other test processes could be assessed.

This paper suggests that when developing laboratory performance-based assessment tests, verification testing should be undertaken as early in the development process as possible, and that the role that accelerated pavement testing can play in that verification be strongly considered.

REFERENCES

Austroads. 2007. *Determination of Permanent Deformation and Resilient Modulus Characteristics of Unbound Granular Materials Under Drained Conditions*. Report AG-PT/T053. Austroads, Sydney, New South Wales, Australia.

Department of Transport, Energy and Infrastructure. 2008. *Determination of a Characteristic Value of Resilient Modulus and Rate of Deformation for Unbound Granular Pavement Materials*. Report MAT-TP 183. DTEI, Adelaide, South Australia, Australia.

European Committee for Standardization. 2004. *EN 12697-22: 2003: Bituminous Mixtures-Test Methods For Hot Mix Asphalt-Part 22: Wheel Tracking*. CEN, Brussels, Belgium.

Holtrop, W. and Moffatt, M.A. 2008. Design of Sprayed Seal Suitable for Accelerated Pavement Testing. *Proc. 1st International Sprayed Sealing Conference, Adelaide, South Australia*, 17 pp. ARRB Group, Vermont South, Victoria. Australia.

Jameson, GW., Oliver, J.W.H. and Sharp, K.G. 1994. Rut-Resistance of Asphalt Mixes Under Accelerated Loading. *Proc. 8th International Asphalt Conference. Sydney, Australia*. Australian Asphalt Pavement Association. Hawthorn, Victoria, Australia.

Jameson, G.W., Vuong, B.T., Moffatt, M.A., Martin, A. and Lourensz, S. 2010. *Assessment of Rut-Resistance of Granular Bases using the Repeated Load Triaxial*

Test. Report AP-R360/10. Austroads, Sydney, New South Wales, Australia.

Jameson, G.W., Vuong, B.T. and Moffatt, M.A. 2010a. Assessment of Rut-Resistance of Unbound Granular Bases. *Proc. 11th International Conference on Asphalt Pavements, Nagoya, Japan*. 10 pp. International Society for Asphalt Pavements, White Bear Lake, MN.

Jameson, G.W., Vuong, B.T. and Moffatt, M.A. 2010b. Assessment of Rut Resistance of Unbound Granular Bases, *Proc. 24th ARRB Conference, Melbourne, Victoria, Australia*. 14 pp. ARRB Group, Vermont South, Victoria, Australia.

Moffatt, M.A. and Eady, P. 2007. *Optimum Use of Granular Bases: Construction of Test Pavements*, Report AP-T93/08, Austroads, Sydney, New South Wales, Australia.

Oliver, J.W.H. 1994. *Laboratory Test Results on Asphalt Specimens from the Accelerated Loading Facility (ALF) Asphalt Deformation Trial*. APRG Report 10. ARRB Transport Research Ltd, Vermont South, Victoria, Australia.

Oliver, J.W.H., Alderson, A.J., Tredrea, P.F. and Karim, M.R. 1995. *Results of the Laboratory Program Associated with the ALF Asphalt Deformation Trial*. ARRB Transport Research report ARR 272 and APRG Report 12. ARRB Transport Research Ltd, Vermont South, Victoria, Australia.

Oliver, J.W.H, Jameson, G.W, Sharp, K.G. Vertessy, N.J., Johnson-Clarke, J.R. and Alderson, A.J. 1997. Evaluation of Rut-Resistant Properties of Asphalt Mixes Under Field And Laboratory Conditions. In*Transportation Research Record: Journal of the Transportation Research Board, No. 1590*, pp. 53–61, Transportation Research Board of the National Academies, Washington, D.C.

Sharp, K.G., Jameson, G.W., Oliver, J.W.H., Vertessy, N. J., Johnson-Clarke, J.R. and Alderson, A.J. 1996. *Rut-Resistant Properties of Asphalt Mixes Under Accelerated Loading: Final Summary Report*. ARRB Transport Research report ARR 287 and APRG report 17. ARRB Transport Research Ltd, Vermont South, Victoria, Australia.

Standards Australia. 1997. *AS 2008–1997: Residual Bitumen for Pavements*. Standards Australia. Sydney, New South Wales, Australia.

Standards Australia. 1998. *AS1289.6.4.1-1998, Methods of Testing Soil for Engineering Purposes- Soil Strength and Consolidation Tests-Determination of Compressive Strength of a Soil-Compressive Strength of a Specimen Tested in Undrained Triaxial Compression without Measure of Pore Water Pressure*. Standards Australia, Sydney, New South Wales, Australia.

Transit New Zealand. 2007. *Draft Specification for Repeated Load Triaxial (RLT) Testing of Unbound and Modified Road Base Aggregates*. Report TNZ T/15. Transit New Zealand, Wellington, New Zealand.

Vuong, B.T. 1999. *Technical Basis for Development of the Austroads Repeated Load Triaxial Test Method*. ARRB Transport Research Ltd, Vermont South, Victoria, Australia.

Vuong, B.T., Jameson, G.W. and Choummanivong, L. 2007. *Optimum Use of Granular Bases: Material Selection for Detailed Performance Evaluation*. Report AP-PT/T053. Austroads, Sydney, New South Wales, Australia

This page intentionally left blank

Advances in Pavement Design through Full-scale Accelerated Pavement Testing – Jones, Harvey, Mateos & Al-Qadi (Eds.)
© 2012 Taylor & Francis Group, London, ISBN 978-0-415-62138-0

The implementation of findings from accelerated pavement testing in pavement design and construction practice

J. Kwon & M.H. Wayne
Tensar International Corporation, Alpharetta, Georgia, US

G.J. Norwood & J.S. Tingle
U.S. Army Engineer Research and Development Center, Vicksburg, Mississippi, US

ABSTRACT: A series of laboratory and full scale Accelerated Pavement Tests (APT) were performed to quantify the effectiveness of geogrid stabilized flexible pavements. The measured responses at critical locations helped to improve understanding of the behavior and benefits associated with incorporation of a geosynthetic within unbound aggregate to form a Mechanically Stabilized Layer (MSL). The information obtained from APT combined with numerical modeling research helped to identify the key features that affect long-term performance of flexible pavements. Further, interpretation of the results generated from this combined approach was used to model the benefits of geogrids in pavement design. This paper presents a general approach to implement APT results in pavement design. This paper will also discuss other types of testing and research that can be used to reliably predict performance prior to establishing a full-scale APT program.

1 INTRODUCTION

Geosynthetics are commonly known to provide one or more of the following functions: (1) separation, (2) reinforcement, (3) filtration, (4) drainage, and (5) protection. Historically, laboratory and field pavement tests have been conducted to evaluate performance of geosynthetic stabilized flexible pavement systems. Improved traffic performance or reduced surface rutting performance reported from these tests are commonly used as the basis for development of empirical design methods. The logic employed for the empirical design method is related to geosynthetic products (or their index properties) and performance. A hypothesis employed in this empirical method is that the index properties such as aperture size, rib tensile strength, junction strength, and manufacturing process are reasonable metrics for determining which product to select for a given application. As the index properties increased there is an increase in predicted performance. However, there are experimental test and field study results which suggest that increased performance by geosynthetic index properties is not valid. The introduction of many different types of geogrid materials has made product selection difficult. The Federal Highway Administration (FHWA) offers a set of minimum properties required by geogrid reinforcement for stabilization and base reinforcement applications that are recommended. However, it is important to recognize that the geogrid index properties listed in the FHWA design manual (FHWA, 2008) are listed for survivability and are not provided as indicators of performance.

Another function that is critically important to punched and drawn geogrid, but less understood and less acknowledged as a key function, is stabilization. Lateral spreading of unbound aggregate is reduced by inclusion of a geogrid. A geogrid layer facilitates the optimal construction of a surrounding soil or aggregate by synergistically interacting with the soil or aggregate layer during construction in such a way that the soil or aggregate layer obtains its optimal engineering properties so that the performance of the aggregate layer is maximized. When the aggregate layer is in service the geogrid interacts with the aggregate particles and maintains optimal and/or enhanced performance during service. As a result, the composite consisting of aggregate and geogrid has enhanced properties over those of the original host material. The term mechanically stabilized layer (MSL) was introduced to define a composite structure (geogrid and aggregate) with enhanced stiffness in relation to a conventional, unbound aggregate layer.

A mechanistic based pavement design method better accommodates alternative materials to achieve a desired level of pavement performance. Implementation of the MSL in mechanistic designs requires a series of performance related data. Numerical studies using a discrete element method demonstrated that "enhanced" properties exist in the aggregate layer in a "zone of influence" that is generally in close proximity to the geogrid, and extends away from the geogrid for

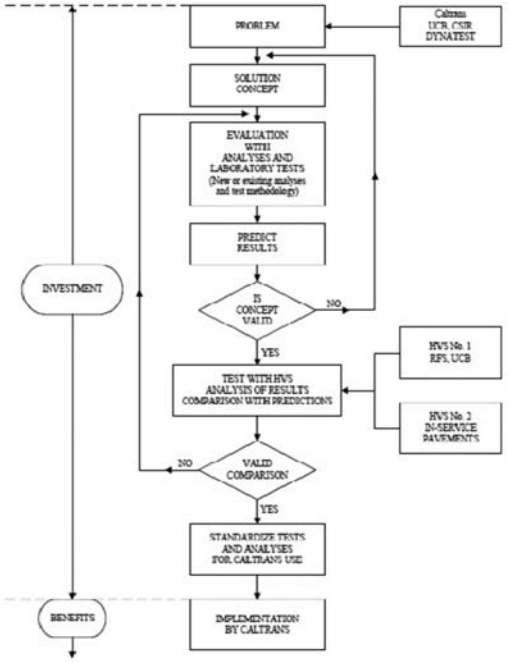

Figure 1. CAL/APT framework (Harvey, 2000).

a distance that will vary depending on aggregate type, geogrid type, and construction procedures (Konietzky et al., 2004; McDowell et al., 2006). It is believed that there is "an optimal" geogrid property that is dependent on the aggregate and conditions of use such as loading. This concept is very difficult to prove or measure due to the limitations of measuring aggregate properties in constructed structures.

Research activities for evaluation and validation of the mechanical stabilization concept and its influence on pavement performance are presented in this paper. This paper presents findings of both laboratory and APT test results. Laboratory tests were conducted to validate the MSL concept. Analyses of the laboratory and full scale APT could provide a guideline for MSL use in pavements. The impact of an MSL on pavement performance is investigated using the APT facility at the U.S. Army Corps of Engineers Engineer Research and Development Center (ERDC).

The research activity to quantify the effectiveness of geogrid stabilized flexible pavements follows the framework within which the Caltrans Accelerated Pavement Testing (CAL/APT) Program operates, which is summarized in Figure 1 (Harvey, 2000).

2 SOLUTION CONCEPT

When unbound granular materials are compacted in layers in pavements, the quality of the selected materials, (grading, angularity, durability, etc.) will normally improve. The various contributing material qualities can be agglomerated in a modulus value, (e.g. resilient

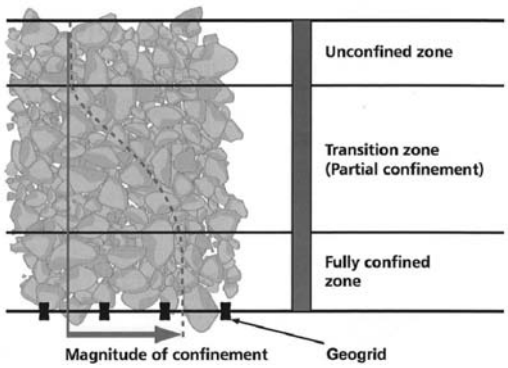

Figure 2. Graphic representation of the geogrid Mechanically Stabilized Layer (MSL).

modulus, surface modulus or elemental modulus). The modulus of overlaying layers is dependent upon quality of the underlying layer for a given quality and specification of a material and its thickness. This means that layers are interdependent and their combined effect is not the same as that employed in some empirical methods such as a structural layer coefficient as used in the AASHTO 1993 design method. This concept can be extended to Mechanistic – Empirical analysis by considering the influence of lateral confinement that develops through use of geogrids. In this regard, modulus enhancement is one of the more realistic options.

Based on the empirical and theoretical research conducted by Wayne et al. (2011a, 2011b, 2011c) and White et al. (2010a, 2010b) it is evident that lateral confinement of the aggregate promotes the ability for aggregate to carry more load that is distributed over a larger area. The lateral confinement mechanism is graphically depicted in Figure 2.

In mechanistic analysis, the road structure comprises a specific number of material layers which support the traffic load while, ultimately protecting the sub-grade. Each layer is defined by a thickness, a modulus and a Poisson's ratio. The analysis of the structure reveals a resulting critical stress and strain within each layer. The critical stress or strain values are then used within a transfer function equation to predict the traffic life of the individual layer. If the layer is an aggregate material, its serviceability is usually defined by rutting, and the critical parameter as vertical compressive strain at the top of the layer. There is one minor exception to this rule and that is the evaluation of the subgrade. The predicted life for the subgrade is based on the rutting, measured at the surface, and not within the subgrade alone, or the overlying layer.

Inclusion of a geogrid within the unbound aggregate will change the distribution of stresses and strains as a result of enhancing the modulus of the stabilized layer. The MSL provides long term performance benefits by delaying the onset of rutting and fatigue. Depending on the geogrid type, the performance benefit will vary for each geogrid based on behavior in full scale testing.

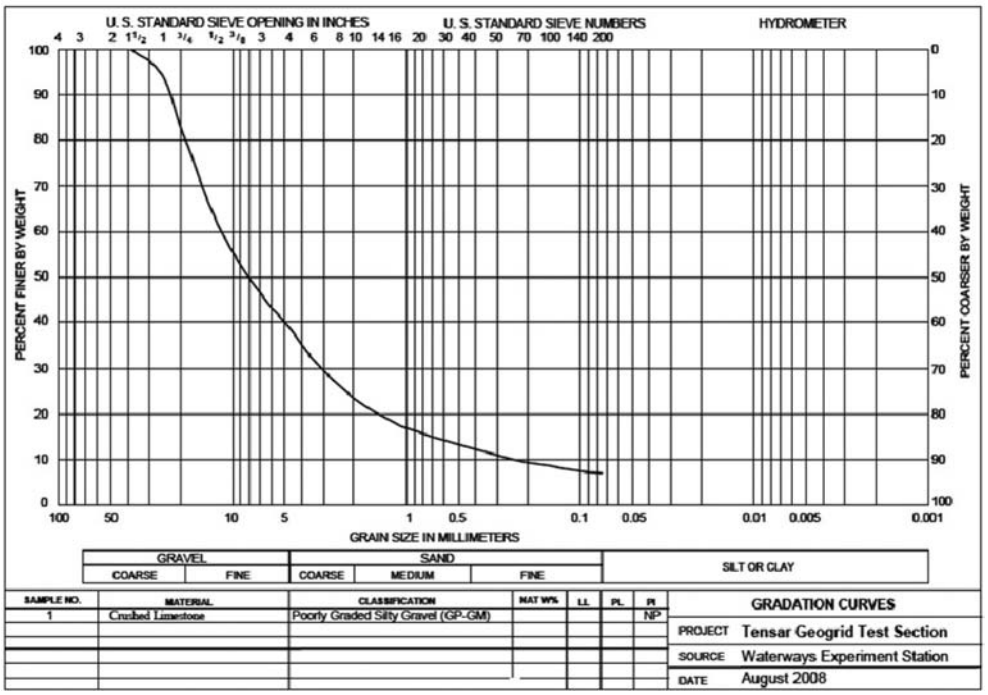

Figure 3. Gradation of aggregate base material.

Once the performance of a material subjected to full-scale repeated loading has been assessed to account for the presence and effect of a geogrid, then the MSL can be properly accounted for in the pavement design procedure to achieve an enhanced life, or its thickness can be altered to achieve equal performance to that of a thinner structural section.

3 PROOF OF CONCEPT – EVALUATION OF MSL WITH LABORATORY TESTS

The introduction of geogrid reinforcement and the complex phenomena of stabilization require mechanistic response validation. The interaction between the soil/aggregate and the geosynthetic during construction results in an increase in modulus of the base material soil/aggregate. Lateral confinement is the critical mechanism that determines the performance of a mechanically stabilized layer. A number of discrete element modeling (DEM) studies conducted to capture the true interactions between geogrids and aggregates, including load transfer mechanisms, deformation, damage, particle re-arrangements and more have been reported by Kwon et al. (2008). These studies reveal that the level of confinement achieved depends on a complex combination of geogrid properties including product geometry, rib and aperture shape, and stiffness. Results underscore that performance in base course reinforcement depends not only on a geogrid's actual properties, but also its ability to interact with, improve and ultimately create a stiffened aggregate layer above the geogrid capable of delivering enhanced overall pavement performance. The validity of the concept of mechanical stabilization is supported by triaxial test results.

In order to determine the effect of placing a geogrid within unbound aggregate, a test combination including AASHTO T307 (Determining the Resilient Modulus of Soils and Aggregates) and NCHRP 598 Repeated Load Permanent Deformation (Shear Strength of Aggregate by the Repeated Load Triaxial Test) was conducted on crushed limestone used in the APT research described later in this paper (Jersey et al. 2012). Both unstabilized and geogrid stabilized samples were tested. It is noted that both of these tests were conducted in series – first following AASHTO T307, then NCHRP 598 – for each test specimen fabricated (remolded to a specified dry density and moisture content).

Figure 3 shows the gradation of this aggregate. The crushed limestone was classified as poorly graded silty gravel (GP-GM) in the Unified Soil Classification System (USCS) and as A-1-a according to the AASHTO procedure (ASTM 2004).

The geogrid used in this study is a punched and drawn integrally formed polypropylene triaxial geogrid. Triaxial geogrids have triangular apertures and increased rib thickness when compared to geogrids with square apertures. Table 1 lists the index properties for the polypropylene triaxial geogrid used in laboratory test specimens.

Figure 4 shows the geogrid cut in a pattern to fit across the 6-inch diameter specimen cross section,

Table 1. Geogrid properties used in the tests.

Properties	Longitudinal mm	Diagonal mm	Transverse mm
Rib pitch	40	40	–
Mid-rib depth	–	1.4	1.2
Mid-rib width	–	1	1.1
Rib shape	Rectangular		
Aperture shape	Triangular		

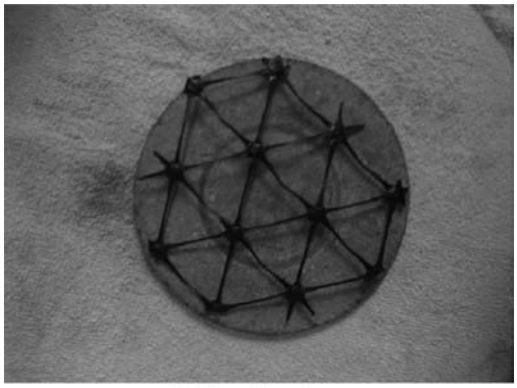

(a) Geogrid specimen

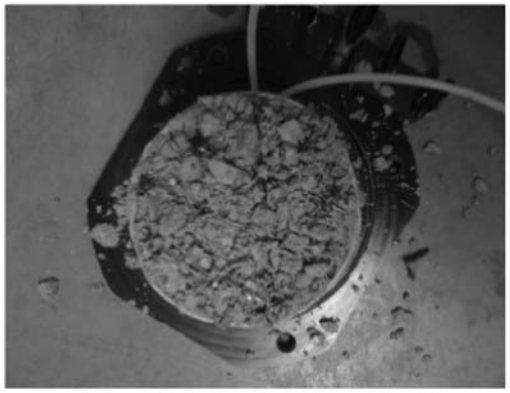

(b) Geogrid placed at the midpoint of the cell

Figure 4. Geogrid specimen preparation prior to placement in the triaxial cell.

which was placed at the interface between the top 6 in. specimen height and bottom 6 in. specimen height for the geogrid stabilized specimens. Figure 4 (b) demonstrates placement of the geogrid within the compacted specimen.

3.1 *Repeated load triaxial tests (AASHTO T307)*

The resilient modulus test was conducted in accordance with procedures contained within the referenced test standard. The specimen is subjected to a series of load pulses at a variety of axial stresses and confining pressures (15 specific combinations of stress levels),

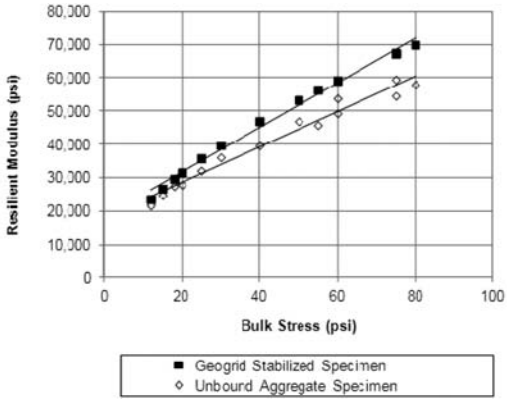

Figure 5. Resilient modulus predicted by the universal model.

and recoverable deformation resulting from these load pulses are measured. The data is used to fit a constitutive model, where resilient modulus can be predicted for any level of stress the pavement designer wishes to consider the design. Note that if density of the aggregate is not correctly achieved throughout the aggregate layer a noticeable reduction in resilient modulus can occur. Resulting resilient modulus equations can be easily established for any combination of aggregate and geogrid.

A comparison of the predictive modulus values between the unstabilized and stabilized materials shows that the stabilized specimen provides a stiffness benefit ranging from 5 to 20%, depending on the stress regime used for comparison (Figure 5).

While the differences in calculated modulus look to be small, these differences could in fact be significant when considering pavement performance. As an example, comparison is made between the stabilized and unstabilized materials at a bulk stress of 40 psi, which translates into a resilient modulus of 39,000 psi for the unbound aggregate material and 47,000 psi for the mechanically stabilized material.

3.2 *Repeated load permanent deformation (NCHRP 598)*

The permanent deformation test was conducted in accordance with procedures documented in NCHRP Report No. 598. Each of these specimens were tested immediately following the AASHTO T307 procedure, thus each specimen had been 'conditioned' with a specified number and amplitude of loadings, up to 40 psi axial stress.

The deformation response from the mechanically stabilized specimen and the unbound aggregate specimen are presented in Figure 6. This is an empirical representation of what would occur over time in a pavement system. As indicated by the shape of the curves versus load cycle (note that the test is commonly stopped at 10,000 load cycles for unbound aggregate specimens as shake down is readily achieved. If continued, plastic strain leads to failure of the specimen.

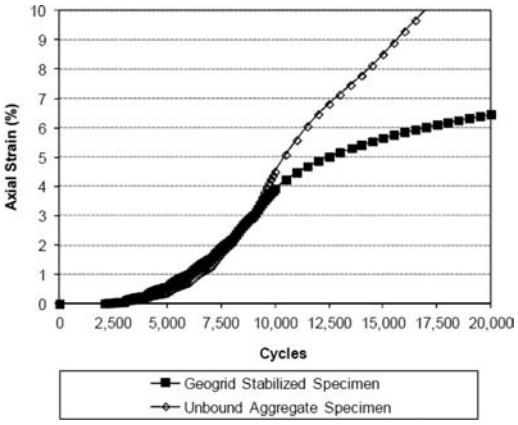

Figure 6. Repeated load permanent deformations (Based on NCHRP 598 results).

The mechanically stabilized specimen did not exceed the shake down limit even after an 8% axial strain deformation level.

3.3 *Discussion of laboratory test results*

These results highlight the fact that resilient modulus testing can be used to characterize MSL behavior. Although resilient modulus curves for the mechanically stabilized and unbound crushed limestone specimens were similar, repeated load permanent deformation curves were dramatically different.

The permanent deformation test shows that the unbound crushed limestone specimen was able to withstand the 10,000 cycles as prescribed by the NCHRP 598 test and showed a strain of only 4.5%. This same specimen was able to withstand an additional 6,690 cycles at 180 psi axial stress before reaching the 10% strain criteria. As a comparison, the mechanically stabilized specimen was able to withstand the 10,000 cycles as prescribed by NCHRP 598 and showed a strain of only 3.9%. This same specimen was able to withstand an additional 10,000 cycles at 180 psi axial stress and only reached 6.5% strain, indicating a greater resistance to permanent deformation compared to the same material without reinforcement.

4 FULL SCALE EVALUATION WITH ACCELERATED PAVEMENT TESTING

A full-scale test section was constructed and trafficked at the U.S. Army Engineer Research and Development Center to evaluate the performance of a geogrid used for base reinforcement in a thin, flexible pavement. Three test sections consisting of a geogrid-stabilized section and two unstabilized control test sections were constructed under controlled conditions. The reinforced section was paved with 2 in. of asphalt and the two control sections with 2 in. and 3 in. of asphalt, respectively. The asphalt was placed on a foundation which consisted of an 8 in. aggregate base layer and a design subgrade CBR of 3%. The strength profiles obtained after construction of the subgrade indicate a variation of 0.5% in the subgrade support values. The gradation of crushed limestone base course is shown in Figure 3. A punched and drawn integrally formed polypropylene triaxial geogrid was placed at the interface between the subgrade and the crushed limestone base. The test pavements were subjected to accelerated trafficking to evaluate the relative performance of the various pavement structures.

Table 2. Summary of ESALs at various levels of surface deformation.

	Number of ESALs to rut depth		
Rut Depth (in.)	Stabilized +2in. HMA	Control#1 +2in. HMA	Control#2 +3in. HMA
0.25	19,300	1,800	4,220
0.5	100,000+	8,100	16,300
0.75	100,000+	9,500	24,500
1	100,000+	13,000	27,870

Sensors were placed to measure pavement responses under traffic loading. Dynamic sensors included earth pressure cells at the top of the subgrade, single-depth deflectometers and geogrid strain gauges in the base, and asphalt strain gauges at the bottom of the asphalt layer. Environmental sensors were also placed in the subgrade to monitor changes in soil moisture (volumetric), temperature, and pore pressure.

5 ANALYSIS OF APT RESULTS

5.1 *Permanent surface deformation*

Permanent surface deformation was measured periodically throughout traffic testing. Rut depth is an indicator of a pavement's structural performance, particularly in thin pavements where subgrade failure is expected to govern rather than fatigue of the asphalt concrete surface layer. Rutting was measured at five locations along the length of each test section at selected traffic intervals throughout traffic testing. The average rutting measured at various traffic levels is shown in Table 2.

The results indicate that the onset of rutting occurred more rapidly in the unstabilized control sections than in the geogrid-reinforced pavement. Further, these data indicate that the pavement service life of the geogrid-stabilized test section exceeded that of the unstabilized test sections.

The unstabilized control with the 2 in. of asphalt concrete surface sustained the least traffic, followed by the section with 3 in. of asphalt concrete surface, and then the geogrid-stabilized section with 2 in of asphalt concrete. Following loading to failure of these sections, trenches were excavated through the pavement for further examination of the test section performance as shown in Figures 7a and 7b.

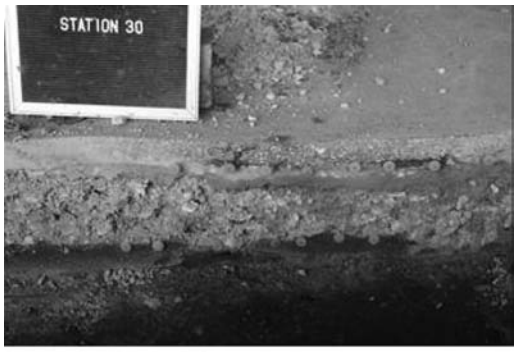

(a) Geogrid - stabilized section after 100,000 ESAL

(b) Control section with 2" AC after 24,000 ESAL

Figure 7. Pavement cross sections after testing.

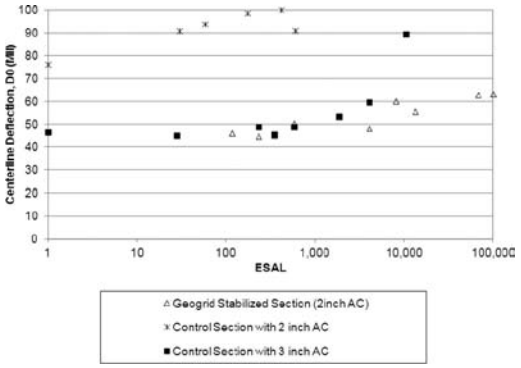

Figure 8. Comparison of centerline deflection (D0) versus applied traffic.

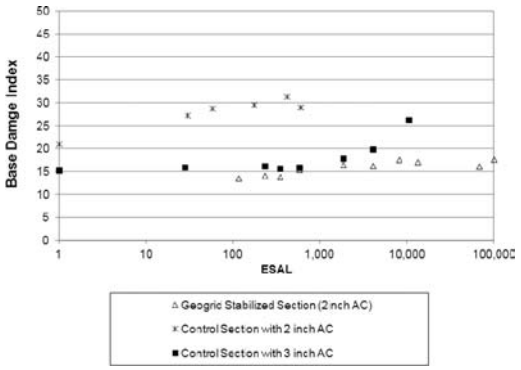

Figure 9. Comparison of Base Damage Index (BDI) versus applied traffic.

5.2 *Falling Weight Deflectometer (FWD)*

The use of FWD data to backcalculate pavement layer moduli is a cost-effective and widely used method. The deflection test data were analyzed by backcalculation to determine the resilient modulus of the subgrade and the effective pavement modulus (for the composite of the pavement components above the subgrade). The deflected shape of the channelized traffic basin is predominantly a function of the thickness of the pavement layers, the moduli of individual layers, and the magnitude of the load.

The FWD testing was performed periodically throughout traffic testing. The deflection basin parameters were used to investigate the enhanced rutting performance of geogrid stabilized pavements. Data were analyzed in terms of the centerline deflection and Base Damage Index (BDI). In general, higher centerline deflection values indicate weaker pavement layers.

The BDI was used to identify the strength and stiffness of the aggregate base.

Pavement stiffness increased due to inclusion of the geogrid mechanically stabilized layer as shown in Figure 8 and Figure 9.

In Figure 9, the base stiffness values for the reinforced test section appear to be higher than those computed for the control section. A significant drop in pavement stiffness or increase in base damage index occurred after 10,000 passes while the reinforced section retained its base stiffness. This information supports the fact that base stiffness was increased and maintained due to the presence of an MSL.

6 SUMMARY

Guidance on how to quantify the enhanced performance of an MSL layer was presented in this paper. The framework presented requires a series of laboratory and accelerated pavement tests. Laboratory tests can be used as an initial assessment of MSL performance and then used to predict how the MSL is expected to perform over time. The laboratory test results provide a fundamental understanding of the behavior of an MSL. Tests currently used for characterizing unbound aggregate materials can be used to characterize a particular combination of aggregate and geogrid.

APT provides a practical understanding of long-term performance of a pavement section stabilized with the geosynthetic. Observed performance, measured pavement responses, as well as monitored pavement stiffness should be used to quantify the effect of a particular geosynthetic on pavement performance.

The only limitation of the proposed method is that APT test results are required to calibrate design criteria to field performance condition. APT tests accelerate the cumulative effect of traffic loading, while the environmental effects on the pavement performance are not normally accelerated.

REFERENCES

American Society for Testing and Materials (ASTM). 2004. *Standard test methods for classification of soils for engineering purposes (Unified Soil Classification System).* Designation: D 2487-06. West Conshohocken, PA.

Harvey, J.T., Roesler, J., Coetzee, N.F. and Monismith, C.L. 2000. *Caltrans Accelerated Pavement Test (CAL/APT) Program Summary Report Six Year Period: 1994–2000.* Report No. FHWA/CA/RM-2000/15, Pavement Research Center, Institute of Transportation Studies, University of California, Berkeley.

Jersey, S.R., Tingle, J.S., Norwood, G.J., Kwon, J. and Wayne, M.H. 2012. *Full-Scale Evaluation of Geogrid Reinforced Thin Flexible Pavements.* Accepted for publication in the 2012 Transportation Research Record series (Journal of the Transportation Research Board).

Konietzky, H., te Kamp, L., Gröger, T. and Jenner, C. 2004. Use of DEM to Model the Interlocking Effect of Geogrids under Static and Cyclic Loading. *Numerical Modeling in Micromechanics via Particle Methods*. Shimizu, Y, Hart, R. and Cundall, P. (Eds.), A.A. Balkema, Rotterdam, pp. 3–12.

Kwon, J., Tutumluer, E. and Konietzky, H. 2008. Aggregate Base Residual Stresses Affecting Geogrid Reinforced Flexible Pavement Response. *International Journal of Pavement Engineering, Vol. 9, Issue 4*, pp. 275–285.

McDowell, G.R., Harireche, O., Konietzky, H., Brown, S.F. and Thom, N.H. 2006. Discrete Element Modelling of Geogrid-reinforced Aggregates. *In Proceedings of the Institution of Civil Engineers, Geotechnical Engineering 159*. pp. 35–48.

Wayne, M.H., Kwon, J. and Boudreau, R.L. 2011a. Resilient Modulus, Repeated Load Permanent Deformation and Plate Load Testing of a Mechanically Stabilized Crushed Miscellaneous Base Material. *CD-ROM Proceedings Transportation Research Board, 90th Annual Meeting,* Washington, D.C.

Wayne, M.H., Boudreau, R.L. and Kwon, J. 2011b. Characterization of a Mechanically Stabilized Layer Using Resilient Modulus and Permanent Deformation Testing. *In Transportation Research Record: Journal of the Transportation Research Board, No. 2011*. Transportation Research Board of the National Academies, Washington, DC. pp. 76–82.

Wayne, M.H., White, D.J. and Kwon, J. 2011c. *Field and Laboratory Evaluation of a Mechanically Stabilized Salvaged Base Course Used in the Construction of US 12 Marmarth, North Dakota.* Mid-Continent Transportation Research Symposium, Iowa State University, Ames, Iowa.

White, D.J., Vennapusa, P.K.R. Gieselman, H., Zhang, J. and Eidem, M. 2010a. *Accelerated Implementation of Intelligent Compaction Technology for Embankment Subgrade Soils, Aggregate Base, and Asphalt Pavement Materials: US 12 Marmarth, North Dakota*. Final Report ER10-08 US12, ND Field Project.

White, D.J., Gieselman, H., Zhang, C. and Vennapusa, P. 2010b. *In-Situ Compaction Measurements for Geosynthetic Stabilized Subbase: Weirton, West Virginia.* EERC Publication ER10-05, Iowa State University Institute for Transportation, Ames, IA.

This page intentionally left blank

Advances in Pavement Design through Full-scale Accelerated Pavement Testing – Jones, Harvey, Mateos & Al-Qadi (Eds.)
© 2012 Taylor & Francis Group, London, ISBN 978-0-415-62138-0

Recommended asphalt binder fatigue performance specification from full-scale accelerated pavement tests considering aging effects

N. Gibson
Federal Highway Administration, Turner-Fairbank Highway Research Center, McLean, Virginia, US

X. Qi & A. Andriescu
SES Group and Associates, Inc., Turner-Fairbank Highway Research Center, McLean, Virginia, US

A. Copeland
National Asphalt Pavement Association (contributions while at Federal Highway Administration), Lanham, Maryland, US

ABSTRACT: FHWA has completed a full-scale, accelerated loading experiment to identify an improved performance-based binder purchase specification for fatigue cracking in response to the shortcomings of $|G^*|\sin(\delta)$ in the current Superpave Performance Grading (PG) system. Nine candidate asphalt binder tests relating to fatigue cracking were evaluated and the statistical based selection procedure is described that identified the strongest candidate. A composite score calculated from multiple statistical parameters was utilized to select a test that provides a calculated critical Crack Tip Opening Displacement (CTOD) which evaluates a binder's strain tolerance in the presence of a crack. This paper summarizes the experimental results and recommendations from the original, principal experiment plus newer data collected from the test sections using full scale accelerated pavement aging. The test sections received an in-situ accelerated aging process, after being in place for more than five years of natural exposure, which heated the test sections to 74 C for eight weeks. The fatigue cracking performance of the aged test sections was measurably decreased when compared to the younger, less aged test sections with little effect on the ranking between material types. The accelerated-aged sections exhibited more top-down cracking than the younger, less aged sections at the same amount of passes. Extracted binder was recovered from the asphalt layers to quantify the variation of aging with depth for modified and unmodified asphalts from both natural aging conditions and the addition of accelerated aging. The relationships between in-situ CTOD in the younger, less aged sections and accelerated aged sections was much stronger than $|G^*|\sin(\delta)$ confirming the original recommendation from the principal experiment.

1 INTRODUCTION

Research has shown that the current Superpave Performance Grading (PG) specification for fatigue cracking, $|G^*|\sin(\delta)$, has limited ability to discriminate the performance of modified and unmodified asphalt binders (Bahia, et al. 2001). In the absence of a binder purchase specification that is "blind" to the type of modification, state highway agencies have developed a variety of localized specifications (commonly referred to as plus specifications) added to the Superpave PG binder specifications that can limit innovation and impact performance. The Federal Highway Administration (FHWA) initiated transportation pooled fund study TPF-5(019) to validate and refine changes proposed in the Superpave binder specification to properly grade modified binders (Gibson, et al. 2011).

2 PRINCIPAL EXPERIMENT

Figure 1 illustrates twelve lanes of pavements constructed with both unmodified and modified binders at FHWA's pavement test facility. The total thickness of the hot mix asphalt (HMA) and crushed aggregate base layers was 660 mm (26 in.). The HMA mix design for the test lanes was an identical, dense, coarse graded 12.5 mm nominal maximum aggregate mix, but the binder type was varied. Fatigue loading utilized a 425 super single tire with a 71 kN (16,000 lb) wheel load inflated to 827 kPa (120 psi). The wheel speed was nominally 18 km/h (11 mi/hr). Lateral wheel wander was programmed to produce a 133 mm (5.25 in.) standard deviation of the ALF transverse position.

Radiant heaters maintained the temperature of the HMA at 19°C (66.2°F) at a depth of 20 mm (0.79 in.) deep during cooler fall, winter and spring months.

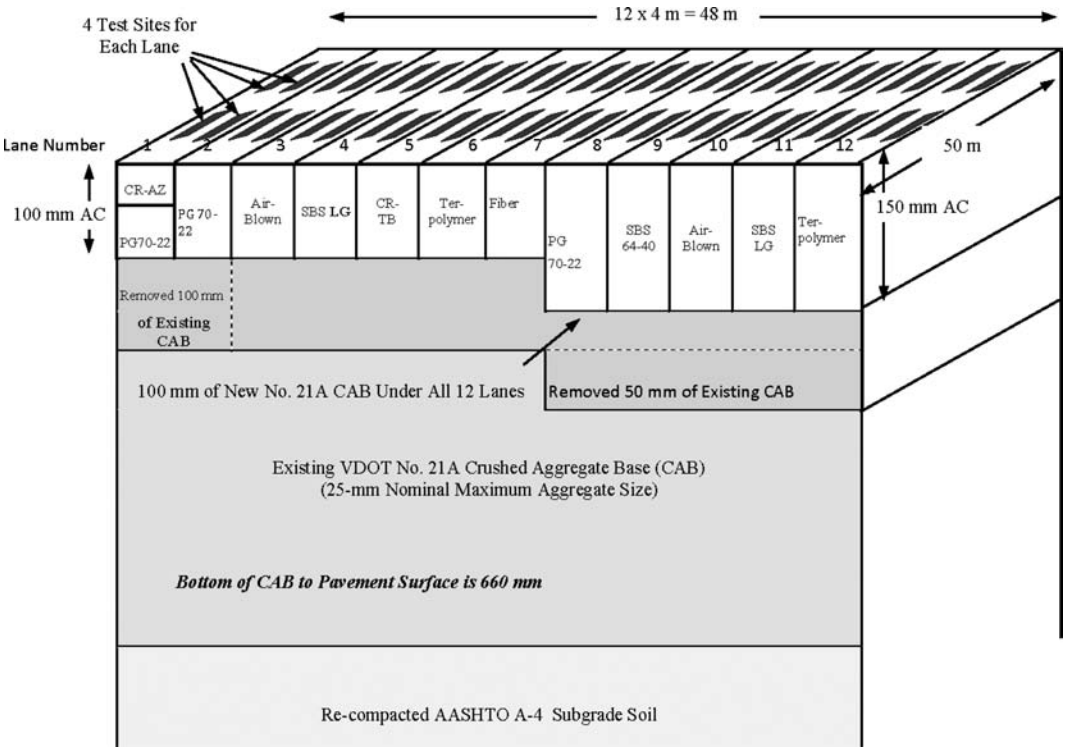

Figure 1. Materials and layout of APT experiment.

Table 1. Fatigue performance of modified and unmodified asphalts in principal experiment (without aging applied).

Binder type	Passes to surface crack	HMA thickness (mm)	Lane
Air Blown	6,648	100	Lane 3
Control PG70-22	22,728	100	Lane 2
CR-TB	40,178	100	Lane 5
Terpolymer	79,915	100	Lane 6
Air Blown	80,984	150	Lane 10
SBS-LG	1,40,857	100	Lane 4
Fiber	1,85,484	100	Lane 7
Control PG70-22	2,91,667	150	Lane 8
SBS 64-40	3,36,326	150	Lane 9
CR-AZ/Control	>375,000	100	Lane 1
Terpolymer	>400,000	150	Lane 12
SBS-LG	>673,000	150	Lane 11

Cracks were mapped manually so that cracked area and crack length could be quantified, but the ranking of those parameters has been found to be essentially identically and thus the passes to initial surface crack are summarized in Table 1.

3 CANDIDATE BINDER TESTS CONSIDERED FOR REPLACEMENT

Each of the binders was characterized with nine different tests. Comparisons were then made between the laboratory performance and full scale APT fatigue cracking to identify the relative strengths of each test. Brief descriptions of those tests are provided. Standard dynamic shear rheometer (DSR) tests were conducted to obtain the Superpave intermediate PG temperature and the $|G^*|\sin(\delta)$ loss modulus at a fixed temperature at 19°C by AASHTO T-315. Low temperature direct tension tests (DTT) were conducted to obtain the low temperature failure stress and strain by following AASHTO T-314 because low temperature fracture could provide some association with ductile intermediate temperature fatigue. Similarly, the low temperature creep stiffness and relaxation properties were included using bending beam rheometer tests following AASHTO T313. Martono and Bahia (2008) conducted stress sweep and time sweep fatigue testing on the ALF binders in the DSR. Time sweeps are cyclic tests where the imposed oscillatory strain amplitude is fixed throughout the test and fatigue damage is exhibited as the resultant peak-to-peak stresses decrease and thus the modulus decreases. As the name suggests, a stress sweep consists of multiple cycles of imposed stress magnitude causing the resultant cyclic strain to increase and the modulus to decrease. A special variation of stress sweep fatigue test was also developed by Martono and Bahia (2008) as a faster alternative to the time sweep. Instead of fixing the stress amplitude during the test, the stress was exponentially increased to reach failure sooner. Shenoy (2002) developed a technique to correlate and use

large-strain loss modulus as a surrogate for lengthy strain sweep tests.

Andriescu, et al. (2004) proposed evaluation of the energy needed for fracturing ductile materials to get a measure of the fatigue and crack resistance behavior of asphalt binders using double edged notched tension specimens. The essential work of fracture (EWF) approach has a history of application in the failure characterization of ductile materials such as plastics, certain metals, and composite materials (Broberg, 1995; Mai and Cotterell, 1980). The work necessary to fail a pre-notched elasto-plastic specimen is assumed to be divided into two parts; an essential portion of work performed in the local region of the advancing crack creating two surfaces and non-essential work away from the local region of cracking/tearing associated with ductility, plasticity and yielding. Johnson et al (2009) suggested the use of the yield energy measured in the DSR to identify the relative performance of asphalt binders. The method involves the evaluation of the amount of energy (stress-strain) to induce peak yielding in the asphalt binder. Data from Lane 1 composite crumb rubber and dense graded HMA and Lane 7 fiber are not considered any further in this paper because fibers do not lend themselves to the same evaluation using binder tests and tools. The composite, gap graded crumb rubber section does not allow a direct comparison of binder effects to the dense graded mixes and binders.

4 MAKING COMPARISONS TO JUDGE CANDIDATE TEST STRENGTHS

Ideally, a large number of data points are desired to make comparisons and judge the strength of various material properties against others; e.g., binder vs. mixture vs. full scale performance. This was not the case given only five data points were available for each HMA thickness under the ALF; 100 mm or 150 mm. Comparisons between the binder properties and laboratory axial fatigue performance measured on the mixtures (Kutay, et al. 2008) were incorporated in the comparative process. This was because there is much greater control over the density for laboratory fabricated specimens than full scale test pavements. However, the influence of HMA construction and unbound base and subgrade layer construction variability was analyzed and found not to be a significant factor in the ALF performance (Gibson, et al. 2011).

An assortment of comparative and statistical techniques and parameters were used. First, binder tests were screened by inspecting the direction of the paired data relationship in either the inverse direction or proportional direction and compared against the direction expected for a particular set of binder parameters. For example, an inverse relationship would be expected for two variables such as amount of cracking in the field versus number of cycles to reach failure in a laboratory test (binder or mixture). Any binder tests which did not have the correct direction compared to full-scale ALF cracking and laboratory mixture fatigue tests were not considered any further. The direction of the relationship was checked using the linear regression slope, correlation coefficient, and also the score calculated by the Kendall's Tau measure of association. The parameters listed below were calculated and transformed such that they ranged between 0 and 1 where 1 indicated the highest measure of association:

- Absolute value of Kendall's Tau measure of association score, $|-1 < \tau_K < +1|$
- ANOVA significance of the regression slope; (1-pvalue) from t-statistic
- SIGNIFICANCE of the Kendall's Tau association as a test for independence, like (1-pvalue)
- Absolute value of correlation coefficient, |R|

The Kendall's Tau measure of association is a distribution free or non-parametric, rank-correlation parameter (Washington et al. 2001). The Kendall's Tau parameter is better suited to small data sets than correlation coefficient, R, or coefficient of determination, R^2, which is more appropriate for larger data sets.

The four statistical parameters listed above were computed for binder vs. ALF cracking and again for binder vs. laboratory fatigue performance then summed and divided by eight to yield a single composite score. The individual and composite scores for the candidate binder tests for 100 mm thick ALF fatigue cracking are ranked from strongest to weakest in Table 2. The ranking reveals that there are more discriminating parameters than the Superpave $|G^*|\sin(\delta)$. Calculated CTOD has the strongest association with laboratory and full scale ALF fatigue cracking followed by the Binder Yield Energy. Both of these parameters mobilize the binder to very large strains and deformations, which research has identified as a needed mechanism to capture the beneficial effects from polymer modification rather than in the linear visco-elastic small strain region. Number of cycles to failure from the time sweep cyclic fatigue test is the third strongest parameter and takes place at a smaller strain but the approach illustrates that cyclic fatigue on binder and cyclic fatigue on mixture are equally valid. Brittle failure strain in direct tension test at temperatures much lower than the intermediate fatigue region discriminates fatigue cracking better than the standard Superpave fatigue parameter for these particular mixes, which could also support using deformations larger than linear visco-elasticity applied in Superpave $|G^*|\sin(\delta)$. The weaker parameters identified were the creep slope m-value from BBR and Essential Work of Fracture. BBR m-value was identified in the literature review as worthy of exploration but did not appear to provide any discrimination with these particular materials in this experiment, possibly due to the small deformations and low temperature region. The weaker Essential Work of Fracture is a necessary step in the calculation of CTOD by means of dividing EWF by the yield strength. This suggests the contributions of yield strength to Essential Work of Fracture to compute CTOD is important. The individual and ranked composite scores corresponding to the

Table 2. Ranked binder fatigue cracking parameters from 100-mm (4-in.) ALF lanes.

Binder test	Compare	1-p_{Reg} (%)	τ_K	1-$p_{\tau K}$ (%)	R	Score
CTOD	A.F.	99	1	99	0.95	0.99
	A.C	100	1	99	0.98	
Binder yield energy	A.F.	94	0.8	96	0.87	0.88
	A.C	90	0.8	99	0.8	
Time sweep	A.F.	89	0.8	96	0.79	0.88
	A.C	95	0.8	96	0.88	
DTT Failure Strain	A.F.	92	0.6	88	0.83	0.81
	A.C	93	0.6	88	0.85	
Superpave $\|G^*\|\sin\delta$	A.F.	84	−0.6	88	−0.73	0.75
	A.C	78	−0.6	88	−0.66	
Shenoy surrogate	A.F.	85	−0.4	76	−0.74	0.67
	A.C	78	−0.4	76	−0.67	
EWF	A.F.	53	0.4	76	0.43	0.55
	A.C	60	0.4	76	0.5	
Low Temp m-value BBR	A.F.	63	0.4	76	0.52	0.54
	A.C	47	0.4	76	0.38	
Stress sweep	A.F.	89	−0.4	76	−0.79	0.69
	A.C	83	−0.4	76	−0.73	

A.F. = Axial Fatigue (Laboratory), A.C. = ALF Cracking.

Table 3. Ranked binder fatigue cracking parameters from 150 mm (5.8-in.) ALF lanes with Lane 9 SBS 64-40.

Binder test	Compare	1-p_{Reg} (%)	τ_K	1-$p_{\tau K}$ (%)	R	Score
CTOD	A.F.	96	0.8	96	0.89	0.62
	A.C	12	0.4	76	0.1	
DTT Failure Strain	A.F.	94	0.6	88	0.86	0.55
	A.C	16	0.2	59	0.13	
Shenoy surrogate	A.F.	78	−0.8	96	−0.67	0.54
	A.C	38	0	41	−0.3	
Superpave $\|G^*\|\sin\delta$	A.F.	74	−0.8	96	−0.63	0.53
	A.C	38	0	41	−0.31	

A.F. = Axial Fatigue (Laboratory), A.C. = ALF Cracking.

150 mm thick ALF lanes are provided in Table 3 and Table 4 when data from Lane 9 SBS 64-40 is included and excluded respectively. More binder tests exhibited correct trends when the data from SBS 64-40, a very soft base asphalt with high polymer content that challenged the laboratory fatigue characterization ranking, was included or excluded. Consistent with the previous ranking, CTOD and Binder Yield Energy are present at the top of the ranking which further supports the discriminating ability of these tests.

Although the results are weaker than the ALF test results, the CTOD has the strongest association with the observed cracking while the Binder Yield Energy and Superpave $|G^*|\sin(\delta)$ are weaker and have incorrect trends altogether. These results combined with the ALF results help further identify and confirm that CTOD is a discriminating parameter for fatigue cracking.

Original binders and cracks maps from a test section built by the Ministry of Transportation of Ontario (2008) were able to provide another independent assessment of the ability of CTOD, binder yield energy and standard Superpave $|G^*|\sin(\delta)$ to discriminate fatigue cracking. Seven different asphalt binders were placed in the same pavement structure and mix design like the experimental design of the ALF experiment. Load associated cracking was approximated by subtracting detailed crack map data from the southbound lane from the northbound lane because heavy logging trucks are generally reported to travel loaded in one direction and unloaded in the other direction. Table 5 shows the same composite score and ranking analysis as followed by the ALF data.

5 CONSIDERATION OF AGING IN APT FATIGUE

A combination of natural and accelerated aging was utilized to gather additional performance data to verify the CTOD recommendation from the principal experiment and complement the younger, less aged fatigue performance. This aging program addressed how most APT loading takes place in the early stage

Table 4. Ranked binder fatigue cracking parameters from 150-mm (5.8-in.) ALF lanes without Lane 9 SBS 64-40.

Binder test	Compare	1-p_{Reg} (%)	τ_K	1-$p_{\tau K}$ (%)	R	Score
Binder yield energy	A.F.	79	1	96	0.79	0.83
	A.C	79	0.67	83	0.79	
CTOD	A.F.	29	0.67	83	0.29	0.75
	A.C	100	1	96	1	
Shenoy surrogate	A.F.	68	−0.67	83	−0.68	0.64
	A.C	65	−0.33	63	−0.65	
Superpave $\lvert G^*\rvert \sin\delta$	A.F.	67	−0.67	83	−0.67	0.63
	A.C	61	−0.33	63	−0.61	
DTT Failure Strain	A.F.	24	0.33	96	0.24	0.39
	A.C	21	0.33	63	0.21	

A.F. = Axial Fatigue (Laboratory), A.C. = ALF Cracking.

Table 5. Comparison between binder fatigue cracking test and Ontario total length of cracks.

Binder test	Compare	1-p_{Reg} (%)	τ_K	1-$p_{\tau K}$ (%)	R	Score
CTOD	Inv., Yes	79	−0.62	97	−0.54	0.73
Binder yield energy	Inv., No	18	0.05	50	−0.11	0.21
$\lvert G^*\rvert \sin(\delta)$ 25°C	Prop., No	63	0.24	72	−0.4	0.5
$\lvert G^*\rvert \sin(\delta)$ 16°C	Prop., No	80	−0.43	88	−0.55	0.66

Inv. = Inverse relationship expected, Prop. = Proportional relationship expected.

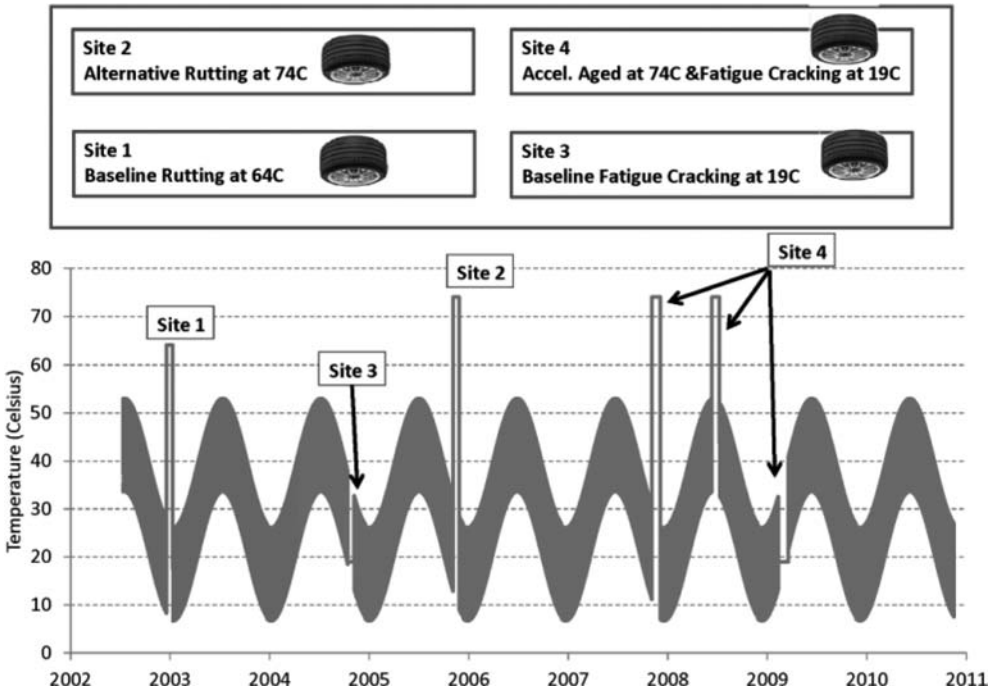

Figure 2. Representation of seasonal (and daily) pavement temperature change showing the imposed APT experiments temperature. Example for lane 2 PG70-22 Control.

of a pavement's life cycle rather than at a later time when the binder has become more brittle and less crack resistant. The pavement test sections received an in situ accelerated aging process, after more than five years of natural exposure, which used the radiant temperature control heaters to raise the temperature to 74°C for eight weeks; two separate sequences each at four weeks. Figure 2 puts into perspective the

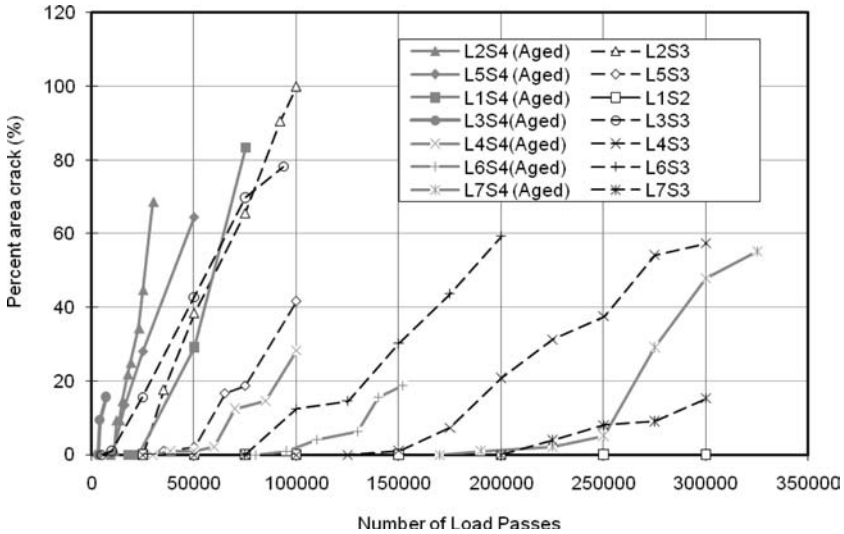

Figure 3. Full-scale fatigue cracking performance measured at two distinct aging levels.

time-temperature aspects of the imposed temperatures and natural temperatures at the ALF. Seasonal and hourly changes in pavement temperatures are represented using a daily sinusoid and annual sinusoid. These are summed together and fit to the quintiles of monthly climatic temperature changes, predicted by the enhanced integrated climatic model (EICM) from the mechanistic empirical pavement design guide methodology for the locality of the FHWA pavement test facility. The applied temperatures of 64°C and 74°C for rutting appear as spikes annotated for Site 1 and Site 2 while and 19°C fatigue for Site 3 and Site 4 appear as notches. Accelerated aging for Site 4 appears like the 74°C spikes from the rutting tests.

Table 6. Summary of asphalt binders' CTOD values (mm), extracted and laboratory PAV aged.

		Extracted top 25 mm		Extracted bottom 25 mm		
Lane	Binder	Acc. Aged	Nat. Aged	Acc. Aged	Nat. Aged	PAV
6	Terpolymer	9	12.8	20.3	20.1	15.7
4	SBS-LG	6.9	11.8	33.4	37.4	24
5	CR-TB	7.2	9.9	17.6	16.6	8.5
3	Air Blown	6.5	8.2	10	9.2	6.8
2	70-22 Control	6.6	7.7	11.8	14.4	7.5

6 IMPACT OF AGING ON FATIGUE CRACKING

Figure 3 graphically presents the early-aged and accelerated-aged fatigue results in terms of percent surface area cracked versus ALF loading passes. The legend indicates the designated lane/site and pavement aging condition. For example, L2S3 refers to Lane 2 Site 3 before accelerated aging and L2S4 (Aged) refers to Lane 2 Site 4 tested after accelerated aging. Asphalt aging and embrittlement significantly reduces fatigue life.

The in-situ binders' CTOD and $|G^*|\sin(\delta)$ properties for the 100 mm thick Lane 2 to Lane 6 were measured after solvent extraction and recovery following AASHTO T-319 using an 85 percent toluene/15 percent alcohol blend. Cores were taken from both Site 3 and Site 4 of each lane in 2009 after all accelerated aging and subsequent loading on Site 4 had been completed. Only the top and bottom 25 mm (1 in.) were cut from the cores for extraction and recovery. The results are summarized in Table 6 and plotted graphically in Figure 4. The CTOD properties after pressure aging vessel (PAV, AASHTO R-28) conditioning are shown in Figure 4 as the vertical line for comparison to the full scale aging responses. The natural aged and accelerated aged properties are plotted with square and triangle data points respectively.

The CTOD values on the x-axis are plotted in a reverse direction so as to be more consistent with stiffness or viscosity increasing to the right because a smaller CTOD corresponds to a less crack resistant, more brittle material. The particular binder type is included as a text inset to each sub-figure. The data illustrate how much less aging occurs at the bottom HMA layers relative to the surface where temperature swings are more extreme and more oxygen is available for oxidation. The data also illustrate that PAV aging exceeds the lower depths of HMA while PAV appears to underestimate surface aging responses near the surface.

Figure 5 and Figure 6 provide a graphical comparison between the principal experiment's fatigue cracking performance and accelerated aged fatigue cracking (cycles to 15% cracked area, see Figure 3) plotted against in-situ binder properties $|G^*|\sin(\delta)$ and

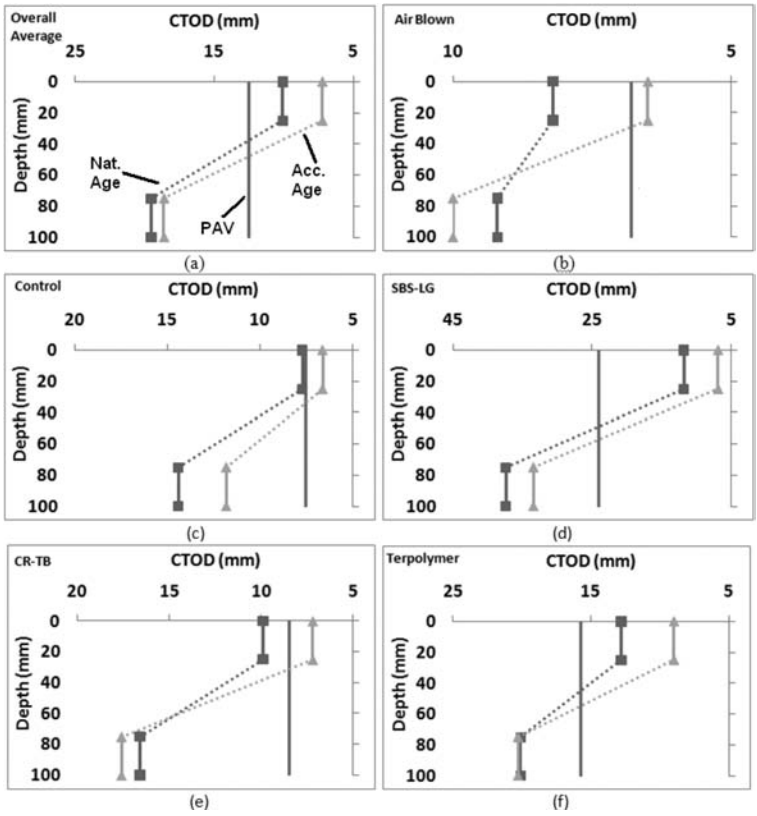

Figure 4. Change in binder CTOD due to age and depth.

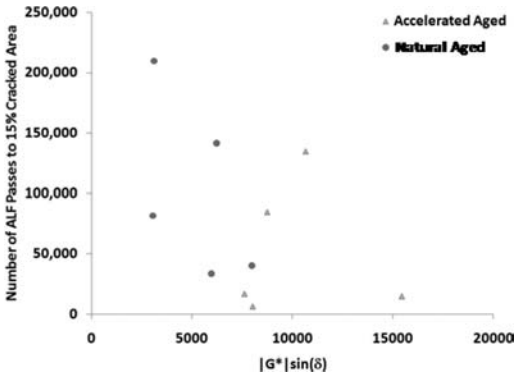

Figure 5. Comparison between $|G^*|\sin(\delta)$ and full-scale fatigue cracking for naturally aged and accelerated.

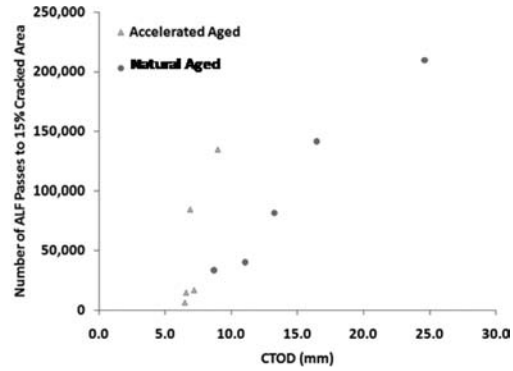

Figure 6. Comparison between CTOD and full-scale fatigue cracking for naturally aged and accelerated.

CTOD respectively. The accelerated aged data points represent the average for both Site 3 and Site 4 for the top 25 mm while the natural aged (principal experiment) data points represent the average of both Site 3 and Site 4 for the bottom 25 mm because coring of the test sections revealed that the cracking in the accelerated aged sections was top-down cracking as shown in Figure 7. It is clear the relationship between cracking and aging for CTOD is less scattered and has a greater level of association than the relationships observed for $|G^*|\sin(\delta)$ confirming CTOD is again a valid choice to replace $|G^*|\sin(\delta)$.

7 ESTIMATES ON EQUIVALENCY OF ACCELERATED AGING PROCESS

Estimates of the equivalent time that was simulated by the cumulative eight week, high temperature accelerated aging process have been calculated. The Western

Research Institute is developing improved aging models for asphalt binder based on individual binders' chemistry and the associated kinetics of oxidation (Western Research Institute, 2011).

An ongoing study is using high temperature, atmospheric pressure aging of thin 100 μm films and transmission infrared spectroscopy to track the carbonyl and sulfoxide products of oxidation. An FTIR cell with 1.0 mm path length characterizes binder dissolved in carbon tetrachloride at a rate of 50 mg/ml.

Original binders and cores from natural and accelerated ALF lanes have been included along with other national pavement test sections. Some preliminary estimates of the aging kinetics calculations using results from Lane 2 PG70-22 control are provided in Figure 8. The left axis provides the dimensionless absorbance of carbonyl and sulfoxide at wave numbers 1,693 cm^{-1} and 1,034 cm^{-1}, respectively, calculated based on the hourly pavement temperature profile with time and depth which is plotted and described by the right axis. The calculation of the aging products are compared for the temperature inputs with and without the accelerated aging period and suggest that eight weeks is equivalent to 12 to 18 months depending on the depth. Thus, it appears the difference in fatigue cracking performance between the accelerated aged and younger, less aged sections (Figure 3) is largely attributed to the natural aging process on the order of five years while the forced aging could account for a smaller portion of the change in fatigue cracking performance due to aging.

The thin film experiment more closely approximates surface aging while the conditions at the bottom of the asphalt layer are less comparable and reliable than the surface. As this research is completed, validated and the tools are implemented, full –scale accelerated aging to enhance accelerated pavement testing can become increasingly useful for durability and cracking studies.

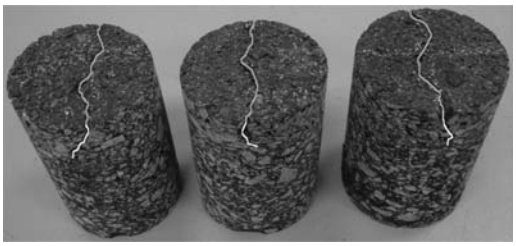

Figure 7. Photographs of cores showing top-down cracking in accelerated aged sections.

8 SUMMARY AND CONCLUSIONS

Using full-scale APT, FHWA has been able to recommend a replacement specification test for asphalt binders to control fatigue cracking performance. A series of test sections were constructed having the same mix design and thickness varying only the binder type/modification. Fatigue cracking performance under the ALF loading was measured and compared to the laboratory properties of the binder and mixtures. Given the number of data points available, a composite statistical score was used to screen nine candidate binder fatigue tests, which identified there were more discriminating parameters than $|G^*|\sin(\delta)$. The calculated CTOD was found to be the strongest parameter. Currently, a draft test method is available from the authors in AASHTO-style format for continued implementation of the research results.

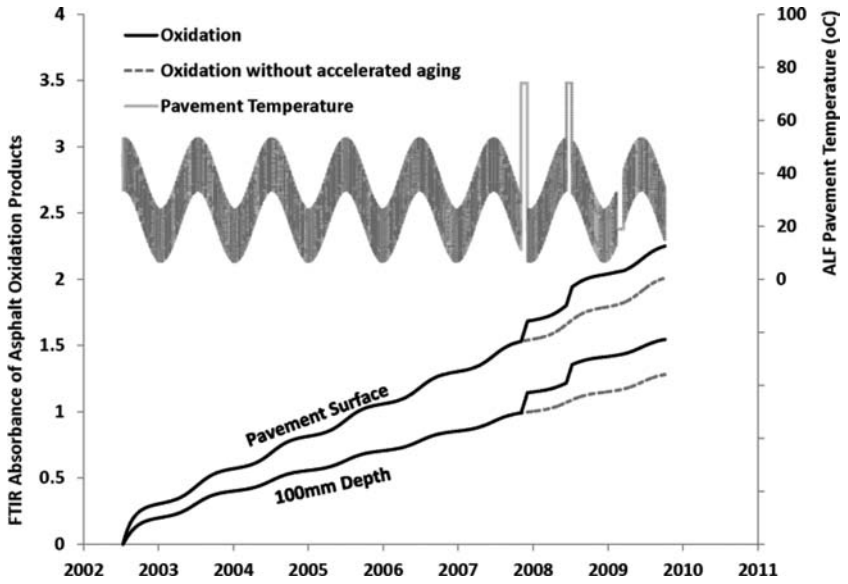

Figure 8. Illustration of the estimated equivalent increase in age simulated by two sessions of high temperature full scale accelerated aging calculated from chemistry and kinetics; Lane 2 PG70-22 Control binder.

To further validate and strengthen the recommendation, the same APT sections received full scale accelerated aging and then loading to assess the ability of the CTOD parameter to gauge performance of a more realistic scenario where older pavements are oxidized and more brittle and less crack resistant. The CTOD parameter was again shown to be the strongest discriminator. Accelerated aging produced more top down cracking and preliminary estimates on the equivalent aging time gained by accelerated aging followed a framework using chemistry and kinetics for the development of improved aging models.

ACKNOWLEDGEMENTS

The authors would like to acknowledge laboratory staff Scott Parobeck, Frank Davis, LaKesha Perry, Monte Simpson, Jason Metcalf, Dennis Lim, and Mario Tinio for specimen preparation and testing. National pooled fund study TPF-5(019) is funded by 16 State highway agencies (CT, FL, IL, IN, KS, MD, MI, MS, MT, NE, NV, NJ, NM, NY, PA and TX) with materials provided by the asphalt industry. The authors want to thank Western Research Institute's Ron Glaser and Mike Farrar for their expertise and collaboration on the aging kinetics as well as Shin-Che Huang, Will Grimes, Changping Sui, Ryan Boysen, Fran Miknis, Mark Pooler and Eric Kalberer.

REFERENCES

Andriescu, A., Hesp, S.A.M. and Youtcheff, J.S. 2004. Essential and Plastic Works of Ductile Fracture in Asphalt Binders, *Transportation Research Record, No. 1875*.

Broberg, K.B. 1975. On Stable Crack Growth, *Journal of the Mechanics and Physics of Solids, Volume 23, Issue 3*, Pages 215–237.

Bahia, H.U., Hanson, D.I., Zheng, M., Zhai, H., Khatri, M.A. and R.M. Anderson. 2001, Characterization of Modified Asphalt Binders in Superpave Mix Design, *NCHRP Report 459, Transportation Research Board – National Research Council*, National Academy Press, Washington, D.C.

Cotterell, B. and Reddel, J.K. 1977. The Essential Work of Plane Stress Ductile Fracture. *International Journal of Fracture, Vol. 13(3)*, pp. 267–277.

Gibson, N., Qi, X., Shenoy, A., Al-Khateeb, G., Kutay, M. E. and Andriescu, A. 2011. *Performance Testing for Superpave and Structural Validation.* Final Report FHWA-HRT-11-045, Federal Highway Administration, Washington, D.C. (Forthcoming).

Johnson, C., Wen, H. and Bahia, H. 2009. Practical Application of Viscoelastic Continuum Damage Theory to Asphalt Binder Fatigue Characterization, *Asphalt Paving Technology, Vol. 78*, pp. 597–638.

Kendall, M. and Gibbons, J. 1996. *Rank Correlation Methods.* Fifth edition, Oxford University Press.

Kutay, M.E. Gibson, N.H. and Youtcheff, J. 2008. Conventional and Viscoelastic Continuum Damage (VECD) Based Fatigue Analysis of Polymer Modified Asphalt Pavements, *Journal of the Association of the Asphalt Paving Technologists, vol. 77*, pp. 395–434.

Mai, Y.W. and Cotterell, B. 1980. Effects of pre-strain on plane stress ductile fracture in α-brass, *Journal of Materials Science, Vol. 15, No. 9, pp*. 2296–2306.

Martono, W. and Bahia, H. 2008. Developing a Surrogate Test for Fatigue of Asphalt Binders, *Transportation Research Board, 87th Annual Meeting Compendium of Papers DVD*.

Ministry of Transportation of Ontario. 2008. *Crack Mapping Survey for Highway 655 Phase 1 Trial.* Internal survey available upon request.

Shenoy, A. 2002. Fatigue testing and evaluation of asphalt binders using the dynamic shear rheometer, *ASTM – Journal of Testing and Evaluation, 30(4)*, 303–312.

Washington, S. Leonard, J., Manning, D.G., Roberts, C., Williams, B. and Bacchus, A.R. 2001.*NCHRP 20-45 – Statistics for Transportation Researchers, Scientific Approaches to Transportation Research*, November 7, http://onlinepubs.trb.org/onlinepubs/nchrp/cd-22/readme.html.

Western Research Institute. 2011. *Fundamental Properties of Asphalts and Modified Asphalts, III, Task 2-2.2 (R. Glaser and M. Farrar) Quarterly Technical Progress Reports*: April 1–June 30, 2011 and (forthcoming) July–September, 2011 http://www.westernresearch.org/transportation.aspx?id=2126

This page intentionally left blank

Part 9: Development and calibration of empirical and mechanistic-empirical pavement design procedures and models

This page intentionally left blank

Advances in Pavement Design through Full-scale Accelerated Pavement Testing – Jones, Harvey, Mateos & Al-Qadi (Eds.)
© 2012 Taylor & Francis Group, London, ISBN 978-0-415-62138-0

Calibrating full-scale accelerated pavement testing data using long-term pavement performance data

W.J.vdM. Steyn
University of Pretoria, Pretoria, South Africa

J.K. Anochie-Boateng & C. Fisher
CSIR, Pretoria, South Africa

D. Jones
University of California Pavement Research Center, University of California, Davis, US

L. Truter
Western Cape Provincial Administration, Cape Town, South Africa

ABSTRACT: Accelerated Pavement Testing (APT) has always been conducted with the objective of improving the understanding of real pavements under real traffic and environmental conditions. While APT provides an accelerated view of some of the major structural behavior to be expected from tested pavements, and while various environmental conditions can typically be simulated during APT, it is important to link the results obtained to real world pavement behavior to enable outputs from APT to be calibrated for use in general pavement design and analysis. One way of conducting this type of calibration is to conduct Long-Term Pavement Performance (LTPP) evaluations on similar pavements to those tested under accelerated conditions and to relate this information to the APT data to calibrate the them for general use (inclusive of normal traffic and environmental conditions). This paper evaluates six years of APT and LTPP data from two road sections in South Africa. The results of the APT tests are compared to the LTPP data and the pavement behavior models obtained from the APT calibrated to real-world outputs. Various concepts required to conduct these calibrations are discussed and the general procedure is reported. It is recommended that more LTPP sections be assessed in conjunction with APT, which should result in more realistic application of the APT data in that the effects of more real-time environmental and traffic applications will be incorporated into calibrated models.

1 INTRODUCTION

Accelerated Pavement Testing (APT) is the controlled application of a wheel loading, at or above the appropriate legal load limit, to a prototype or actual, layered, structural pavement system to determine pavement response and performance under a controlled, accelerated, accumulation of damage in a compressed time period (Metcalf, 1996). Long-term pavement performance (LTPP) focuses on evaluation of the in-service performance of pavements, incorporating normal traffic loads and typical environmental conditions affecting the pavement in a normal way. The calibration of APT data with LTPP data to allow for a realistic incorporation of normal traffic and environmental loading effects has been a topic of interest for APT practitioners for many years. It has been highlighted in two NCHRP synthesis documents (Metcalf, 1996; Hugo and Epps Martin, 2004) as one of the objectives of a comprehensive APT program, enabling the transposition of APT data to real-world applications. It should be appreciated that LTPP data resembles real life (real pavement, real traffic and real environment) while APT data are collected to understand behavior and to develop performance models in an accelerated period, and therefore the APT data should be adapted to the LTPP data.

Although the general aims and objectives of the combination of APT and LTPP data have been recognized for many years, the practical and economic aspects of such a combination of data have typically been the major hindrance in achieving this aim. From a practical viewpoint, it is important to ensure that the LTPP sections and the APT sections are located on the same pavement types and in the same environmental areas, and that the traffic on the LTPP section can be monitored in sufficient detail to use as input into the analysis process. This traffic should also resemble the traffic applied to the APT section within a reasonable period. From an economic viewpoint it should be appreciated that the operation of a quality LTPP program requires dedicated funding over a number of years, even though limited data are added to the database each year. The significance of the data

only materializes once sufficient data are available to compare realistically with the collected APT data.

This paper focuses on one application of a combination of the data from an APT and LTPP program in South Africa. There are currently two such programs running in South Africa, one for the Provincial Administration of the Western Cape (PAWC) on which this paper focuses, and one for the Gauteng Provincial Administration. The paper starts with background on the development of the LTPP guidelines used in the program, as well as some thoughts regarding the effective implementation of these guidelines into a provincial roads department environment. This is followed by a short methodology followed in developing this paper, and background information of the two pavements on which the APT and LTPP data were collected. The surface rut and elastic deflection data of the two pavements are compared and discussed, and conclusions and recommendations developed based on the data are provided.

2 PROJECT BACKGROUND

In 2003, when the South African initiative to relate APT to LTPP was started, very few formal comparative experiments had been undertaken anywhere in the world, although numerous ad hoc studies had been carried out in a number of countries. The primary reason given for this is usually the absence of sustained long-term funding.

Although committed funding had not been guaranteed for the South African Heavy Vehicle Simulator (HVS) APT/LTPP study program, the need for a protocol to standardize the methodology used for establishing and monitoring LTPP sections in conjunction with APT sections was identified, with a view to initiating such a study. The protocol, written in the form of a guideline was finalized in 2004 (Jones and Paige-Green, 2003) and a paper presented on it at the 2nd International Conference on Accelerated Pavement Testing (Jones et al., 2004). The protocol covers management responsibilities, section location and establishment, instrumentation, and data collection and reporting criteria. The protocol was developed for mobile facilities, but most aspects are also applicable to fixed facilities and test tracks.

In 2004, funding to conduct LTPP studies adjacent to two recently completed APT studies was provided by the Gauteng Department of Transport and Public Works to "test" the protocol. The first experiment included two sections where recycled materials (clinker ash) were used as base material with a thin chip seal surfacing. The second experiment was part of a full-depth reclamation with foamed bitumen study. Annual monitoring of these two sections continues today and interim reports have been published (Jones et al., 2007).

Additional funding was provided by the Department of Transport and Public Works (DTPW) of the Provincial Administration of the Western Cape (PAWC) in 2005 for an additional two studies to assess the performance of two pavements also rehabilitated using full-depth reclamation with foamed bitumen (Steyn et al. 2007, Anochie-Boateng and Fisher, 2010) after HVS tests were completed on a number of test sections on the two roads. The two sections, one on a National Highway (N7, equivalent to an Interstate highway in the United States) and one on a low-volume road (M538) were selected because of the differences in traffic loading, climate, and materials used. The studies on these two roads are the focus of the discussion in this paper.

Both long-term structural and functional performance of the two sections are being monitored, with the primary objective of providing appropriate, adequate data, information, and products (e.g., rutting and cracking performance models) to better understand pavement performance. The ultimate intention is to use LTPP data in the PAWC pavement design and pavement management systems. Based on the data collected to date, PAWC is currently extending the LTPP program by adding further pavement sections into the existing LTPP program.

3 PAPER METHODOLOGY

The methodology followed focused on a realistic calibration of the APT data using the available LTPP data. The overall objective is that the pavement performance models that were based on the original APT data be updated/calibrated through comparison with the data collected over a longer period using the LTPP process.

The two pavement sections used in the paper consist of a relatively high volume highway (N7) and a low-volume road (M538). The APT tests were conducted at load levels of both 40 kN and 80 kN, and allowance is firstly made for the calculation of equivalent traffic load repetitions for both the APT data and the LTPP data (based on traffic counts). No detailed environmental data were collected on the sections under investigation, although the seasonal changes are expected to be directly linked to the two main seasons (dry summer and wet winter) experienced in the Western Cape.

Once allowance was made for calculation of equivalent traffic loads, the actual data were compared graphically. At this stage of the process the calibration effort started, which essentially consisted of changes in the damage factor of the load equivalence equation, to allow the measured APT data to resemble the LTPP data as closely as possible. As pavement properties are variable, all data were shown as the average, as well as ± 1 standard deviation of the average data. The outcome of the calibration process was an improved load equivalence damage factor for application to all the data collected during APT tests on the specific pavement type and region (environmental effects). The rut and deflection data were treated separately in this calculation.

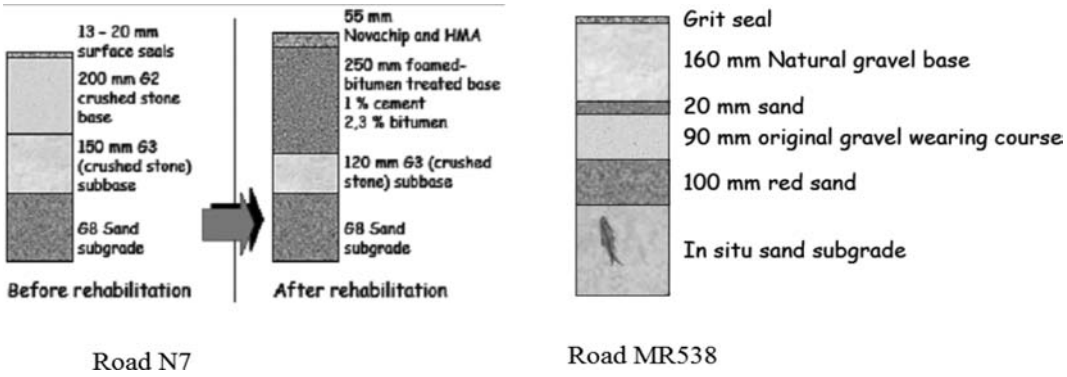

Figure 1. Nominal pavement structures of the two LTPP sections studied.

Table 1. Test conditions for HVS tests discussed in this paper.

Test conditions for Road N7 (HVS tests 415A5 and 416A5)					
		Wheel load (kN)/tire pressure (kPa)			
		Dry		Wet	
		40/620	80/800/850	100/880	80/800
Test section repetitions	415A5	0 to 48,628	48,628 to 423,374	423,374 to 498,863	–
	416A5	0 to 1,168,850	1,168,850 to 1,618,850	–	1,168,850 to 1,742,850
Test conditions for road M538 (HVS tests 419A5 and 420A5)					
		Wheel load (kN)/tire pressure (kPa)			
		Dry		Wet	
		40/620	80/820	40/620	80/820
Test section repetitions	419A5	0 to 15,268	15,268 to 310,000	–	–
	420A5	0 to 400,000	–	400,000 to 1,040,903	1,040,903 to 1,099,400

Apart from the rut and deflection data collected on the sites, in situ density and moisture content data were also collected during each monitoring visit. These visits are carried out approximately every six months to ensure that data are collected at the end of the dry and wet seasons. Logistics do not always allow for precise intervals in these data collection visits, and gaps may thus exist in the data.

The traffic levels on the two roads are approximately 17,000 (Average Annual Daily Traffic [AADT]) (23% heavy vehicles) for the N7 and approximately 200 AADT (15% heavy vehicles) for the low-volume road (M538) (2011 data).

4 TEST SECTION BACKGROUND

4.1 *Road N7*

The HVS study on Road N7 evaluated the performance of a rehabilitation strategy involving in-place full-depth reclamation of the existing pavement (thin surfacing over aggregate base (hornfels) using foamed bitumen and cement as a stabilizer and surfaced with hot-mix asphalt (HMA). Figure 1 shows the nominal pavement structures before and after construction, while the conditions under which HVS tests were conducted on the road section are shown in Table 1. The base was treated with 2.3% foamed bitumen and 1.0% cement by mass of dry aggregate. The subbase consisted of crushed stone and the subgrade of sand. Two HVS test sections (415A5 and 416A5) were investigated for Road N7 adjacent to the LTPP section (Theyse, 2004a). The site is located in a relatively flat sandy area with a moderate climate.

4.2 *Road M538*

The HVS study on Road M538 was initiated to assess the performance of a pavement structure with a very thin surface seal. Figure 1 shows the pavement structure, while Table 1 presents the conditions under which HVS tests were conducted on the road

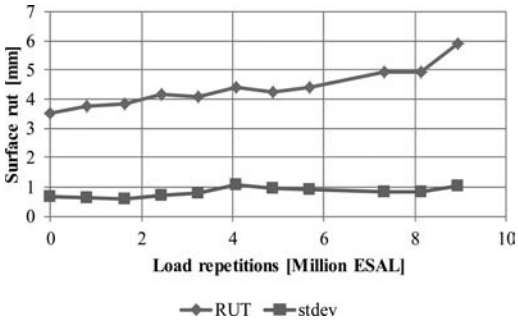

Figure 2. Rutting profile on N7.

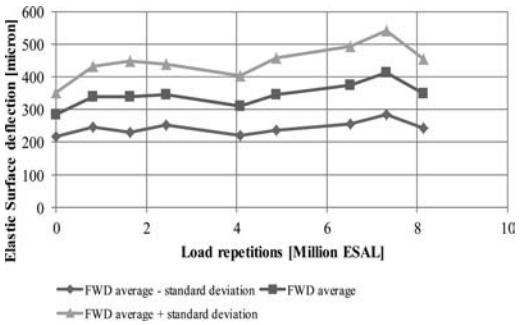

Figure 3. Average deflections on N7 LTPP section.

section. The base consisted of quartzitic sandstone while the subbase consisted of residual quartzitic sandstone fragments in a matrix of residual and windblown quartzitic sand. Two HVS tests were conducted on Road M538 (419A5 and 420A5) (Theyse 2004b). The site is located in a relatively flat sandy area with a moderate climate.

4.3 *General LTPP data*

An indication of the general form of both the rut and deflection data collected during the LTPP experiment are shown in Figure 2 (rut) and Figure 3 (deflection) for Road N7. Figure 4 shows typical trends of average elastic modulus at different depths in the Road N7 pavement. The stiffness values on the outer wheel path were consistently higher than the values for the inner wheel path. Figure 5 shows variations of density with pavement depth in the outer and inner wheel paths of the section. The figures indicate the general seasonal changes in the data. Similar trends were observed on the Road M538 pavement data.

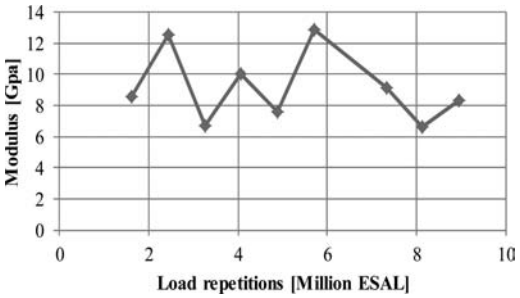

Figure 4. Stiffness trends on the N7 section at different depths.

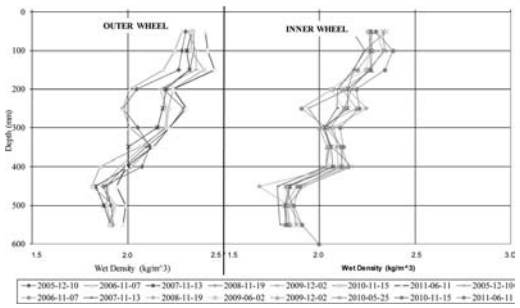

Figure 5. Variation of density with depth for LTPP section on N7 (refer to Figure 1 for layer thicknesses).

4.4 *Summary of findings from road N7*

The various analyses of the data collected from Road N7 (Figures 2 and 3) indicated that (Theyse, 2004a; Long and Brink, 2004):

- Backcalculated resilient moduli from both FWD and MDD deflection measurements indicated an increase in the resilient modulus of the base layer in the early stages of the investigation as a result of the stabilization process. However, under trafficking, the initial relatively high resilient modulus was reduced to values more representative of unbound crushed stone materials. As in the case of other stabilized materials, two modes of behavior were identified for the foamed-bitumen-treated base, the first mode consisting of a gradual reduction in the resilient modulus of the base layer, the second being the gradual permanent deformation of the layer;
- The structural bearing capacity of the pavement was ultimately determined by the permanent deformation and should be between 10 and 30 million standard axles (ES30 design traffic class) if the surfacing is well maintained. The permanent deformation increased and the structural bearing capacity decreased when water was allowed to penetrate the base layer during the wet test on Section 416A5;
- Water at the interface between the base layer and the HMA surfacing resulted in erosion of the base layer. This may lead to functional distress in the form of surface irregularity, and
- The dry density of the recycled base appeared to be less than that of the crushed stone base layer prior to recycling.

4.5 *Summary of findings from Road MR538*

The various analyses of the data collected from Road MR538 indicated that (Theyse, 2004a; Theyse, et al. 2006):

- The sandstone base layer material and light pavement structure performed well during the HVS tests, and laboratory results approaching those normally associated with crushed stone products were obtained for the sandstone gravel;
- The current CBR based material classification system correlated poorly to the performance of the sandstone gravel base layer in HVS tests. The shear strength and resilient modulus laboratory results were better indicators of performance and it is recommended that performance based specifications be developed for this class of pavement base layer;
- The light pavement structure of the HVS test sections was shown to be appropriate for application to low-volume roads and the structural bearing capacity of the pavement far exceeded the South African design traffic classes associated with low-volume roads (TRH4, 1996).
- The integrity and functional performance of the surfacing layer is a crucial aspect of pavement performance that will probably determine the service life of the road but could not be assessed with the HVS. LTPP projects are better suited to determining functional deterioration trends associated with the distress of the surfacing layer, especially on low-volume, light structures;
- The effect of density and degree of saturation was shown to be highly significant with regards to the mechanical properties of the sandstone gravel base layer material.

5 OUTCOME OF THE CASE STUDY

The analysis of the LTPP and APT data entailed a comparison of the surface rut and surface deflection measured for the respective sections. In the comparison, the average, as well as the average ± 1 standard deviation of the rut and deflection data, are shown for both the LTPP and APT data, to demonstrate the variability in pavement properties. The rut comparisons for the two roads (N7 and R538) are shown in Figures 6 and 7, while the deflection comparisons are shown in Figures 8 and 9.

Analysis of the data in Figures 6 to 9 indicates the following important points:

- Both the rut and the deflection data for the LTPP and APT sections on the higher trafficked section (N7) compare well;
- The damage exponent (used to calculate the equivalent traffic for the APT section on the N7 section) was 4.2 for both rut and deflection;
- The rut on the low-volume road (M538) showed significantly higher values for the LTPP (real traffic and environment) sections compared to the APT

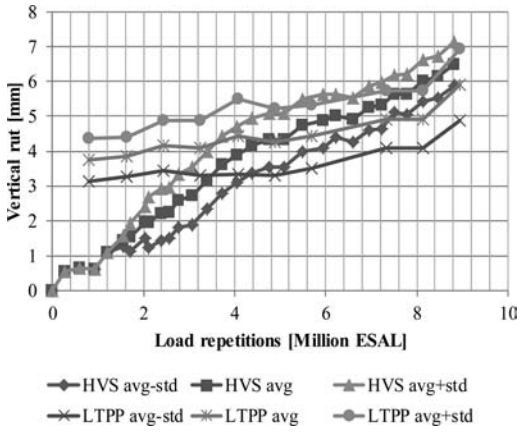

Figure 6. N7 rut correlation example.

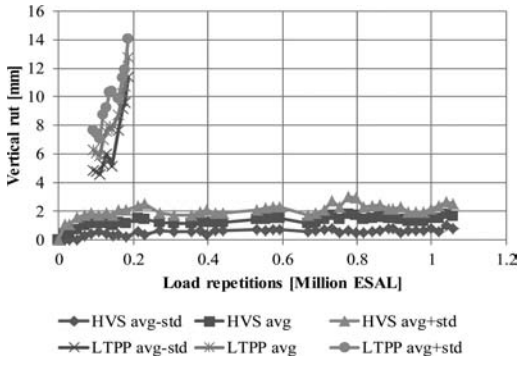

Figure 7. M538 rut correlation example.

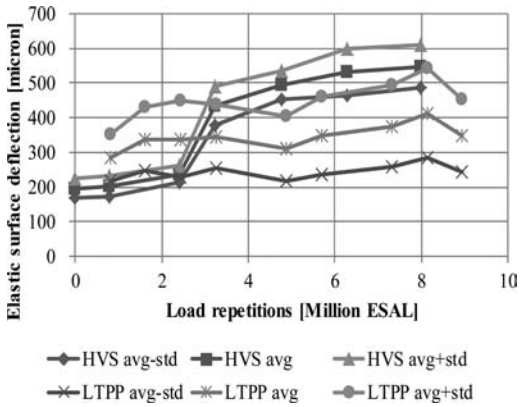

Figure 8. N7 deflection correlation example.

data. This may be linked to previous work in this regard where it was indicated that for low-volume roads, environmental factors may have a more significant role in the performance of the pavement than the actual applied loads (Steyn and Sadzik, 1998);

- The LTPP-measured deflections on the low-volume road (M538) were similar to the higher values

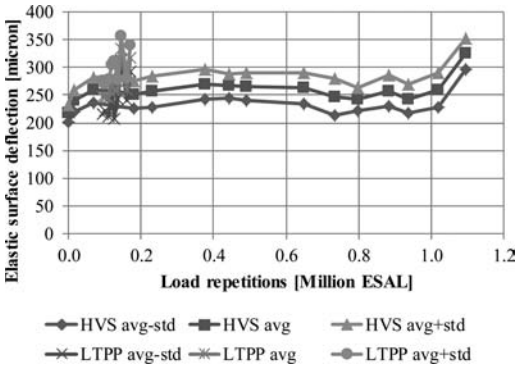

Figure 9. M538 deflection correlation example.

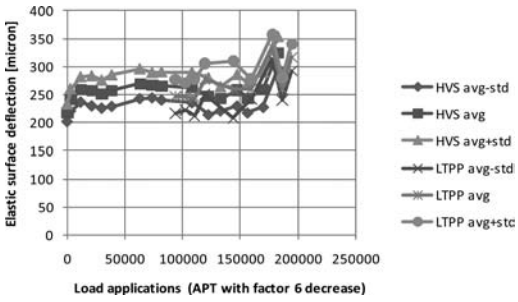

Figure 10. M538 deflection correlation example.

(average plus one standard deviation) recorded towards the end of the APT testing. This supports the theory that environmental factors often have a bigger influence on the performance of low-volume roads than traffic;

– For the low-volume road it appears that the APT rut needs to be adjusted by a factor of five to obtain similar data to the LTPP (real life) data, while the load applications should be adjusted (decreased) by a time factor of six for the APT elastic surface deflections to be equivalent to the LTPP data (M538 elastic deflection shown in Figure 10 with load application scale for APT decreased by a factor six);
– The time factor used for the M538 elastic deflection data is necessary to ensure that the effects of season and time on the low-volume pavement be attributed correctly to the APT data, as the APT data excludes the effect of these variables, which affect low-volume (light) pavements more significantly that higher volume (thicker) pavements.

6 CONCLUSIONS AND RECOMMENDATIONS

Based on the data analyzed for this paper the following conclusions are drawn:

– The effects of environmental changes are visible mostly on the low-volume road (M538) through seasonal changes in parameters such as deflection, moisture content, and density;
– Less environmental influences were identified on the more heavily trafficked, thicker Road N7 pavement;
– Comparison of the rut and elastic deflection data for the Road N7 pavement indicated that a standard damage factor of 4.2 was sufficient to convert the different traffic loads used in the APT test data to the LTPP data;
– The light pavement structure (M538) required a factor of five increase in rut data and a load time factor decrease of six for the elastic deflection for the APT data to resemble the LTPP data, and
– The major distresses on the two LTPP sections are believed to have been caused by seasonal variation in moisture identified during the evaluation periods.

Based on the analyses shown in this paper the following recommendations are made:

– The scope of LTPP programs needs to be expanded to obtain additional and essential data to help improve the applicability and accuracy of pavement performance models for diverse pavement conditions in southern Africa;
– There is a need to establish a database of mechanical properties of pavement materials on all LTPP sections. These data are typically collected as part of the laboratory testing phase in APT tests. Laboratory tests for stiffness (modulus), permanent deformation, and cracking as well as yield strength properties will be essential to develop calibrated Highway Development and Management (HDM-4) type models, and
– More LTPP sections are required close to APT sections covering a range of pavement types (light to heavy traffic design) to evaluate where the effect of environmental conditions start to become more important than that of traffic load equivalence.

ACKNOWLEDGEMENTS

The authors would like to acknowledge the financial support of the Western Cape Provincial Administration (PAWC) for conducting this research, as well as the permission of the PAWC and the executive director of CSIR BE to publish the paper.

REFERENCES

Anochie-Boateng, J. and Fisher, C. 2010. *Technical Memorandum: Monitoring of two LTPP experimental sections in the Western Cape.* Pretoria, South Africa: CSIR Built Environment. Contract Report CSIR/BE/IE/IR/2010/0021/B.

Hugo, F. and Epps Martin, A. 2004. *Significant findings from full-scale accelerated pavement testing.* Washington, DC: Transportation Research Board, National Research Council. Synthesis of Highway Practice 325.

Jones, D. and Paige-Green, P. 2003. *A protocol for the establishment and operation of LTPP sections.* Pretoria, South Africa: CSIR Built Environment. Contract Report CR-2003/11.

Jones, D., Paige-Green, P. and Sadzik, E. 2004. The development of a protocol for the establishment and operation of LTPP sections in conjunction with APT sections. In *Proc. 2nd International Conference on Accelerated Pavement Testing*, Minneapolis, MN, September 26–29, 2004.

Jones, D., Steyn, W.J.vdM. and Fisher, C. 2007. *Technical Memorandum: 2006/2007 monitoring of four LTPP experiments in association with HVS tests in Gauteng.* Pretoria, South Africa: CSIR Built Environment. CSIR/BE/IE/IR/2007/0108/B.

Long, F.M. and Brink, A.C. 2004. *2nd level analysis of the HVS data for the southbound carriageway of the N7 (TR11/1).* Pretoria, South Africa: CSIR Built Environment. Contract Report CR-2004/12.

Metcalf, J.B. 1996. *Application of full-scale accelerated pavement testing.* Washington, DC: Transportation Research Board, National Research Council. Synthesis of Highway Practice 235.

Steyn, W., Jones, D. and Fisher, C. 2007. *Technical Memorandum: Monitoring of two LTPP experimental sections in the Western Cape.* Pretoria, South Africa: CSIR Built Environment. Contract Report CSIR/BE/IE/IR/2007/0109/B.

Steyn, W.J.vdM. and Sadzik, E. 1998. Evaluation of superlight pavements under accelerated traffic. In *Journal of the Transportation Research Board. Transportation Research Record (TRR) 1639*. Washington, D.C. pp.130–139.

Theyse, H.L. 2004a. *First Level analysis report: HVS testing of the foamed-bitumen-treated crushed stone base on the slow lane of the southbound carriageway of the N7 near Cape Town.* Pretoria, South Africa: CSIR Built Environment. Contract Report CR-2003/23.

Theyse, H.L. 2004b. *HVS and laboratory testing of a light pavement structure on Main Road 538 between Leipoldtville and Lamberts Bay. Volume 1: Report.* Pretoria, South Africa: CSIR Built Environment. Contract Report CR-2004/36.

Theyse, H.L., Steyn, W.J.vdM, Sadzik, E. and Henderson, M. 2006. The use of the Heavy Vehicle Simulator and advanced laboratory testing to asses a light pavement structure for low-volume roads. *In Proc GeoShanghai International Conference 2006*, Geotechnical Special Publication 154, ASCE, Shanghai, China.

TRH4. 1996. *Structural design of interurban and rural road pavements.* Pretoria, South Africa: Committee for State Road Authorities, Department of Transport.

This page intentionally left blank

Advances in Pavement Design through Full-scale Accelerated Pavement Testing – Jones, Harvey, Mateos & Al-Qadi (Eds.)
© 2012 Taylor & Francis Group, London, ISBN 978-0-415-62138-0

Using point level accelerated pavement testing data for calibration of performance models

J.D. Lea
University of California Pavement Research Center, University of California, Davis, US

ABSTRACT: Accelerated Pavement Testing (APT) data is generally expensive to collect, and one section only yields one point or series of data for the calibration of performance models for mechanistic-empirical design methods. This data is typically the mean performance from a number of sets of measurements at various locations on the section. These raw data observations cannot be used directly for calibration because they are strongly correlated with one another. This paper details methods of using these points to calibrate performance models by controlling for this correlation. The paper uses examples from Heavy Vehicle Simulator (HVS) tests used to calibrate the *CalME* pavement design method for flexible pavements. Using all of the available data from a section can dramatically improve the quality of the calibration, and significantly enhance the value of APT testing.

1 INTRODUCTION

Accelerated pavement testing (APT) is generally used for two functions: proof testing of new materials or pavement design concepts, and for building a performance database to aid in the calibration of pavement design methods. However, the costs of testing are high and, even with the accelerated nature of the testing, it can still take time to perform the testing (although considerably less than long-term pavement performance [LTPP] monitoring). As a result, it is common to see comparisons of various materials made using a single test for each material and for performance models to be developed off extremely limited data sets. It must be assumed that the performance of a single small section is representative of the performance of a long section of pavement, which is not always the case.

On the other hand, the quality and quantity of data available is often very high, since the pavement is under continuous monitoring. While the latest mechanistic-empirical (ME) design methods, such as *CalME*, can take better advantage of this data, by using an incremental formulation that allows tracking the performance history and not just the 'failure' point, the assumption is still made that the section is representative.

This paper discusses strategies for using all of the available data to improve the calibration of models, so that the coefficients are more representative of the entire pavement, and so that better estimates of variability in performance can be made. In particular, it introduces the use of mixed effects models that have a spatial correlation structure. The application of these models to performance comparisons is also considered.

2 BACKGROUND

While some APT has been conducted on mainline pavements, most is on small, purpose built, test tracks. These tracks typically have a number of smaller cells of pavement (these are sometimes referred to as tracks or lanes), each with a slightly different pavement or mix design, and on each cell a number of sections might be tested, under different loading or environmental conditions. On each section, data is typically taken at a number of stations along the section, and at a number of fixed instrument locations. This is true for both machine-type APT devices and full-scale test tracks, although the details are slightly different. This paper will focus on the type of data collected in a Heavy Vehicle Simulator (HVS) test, simply to narrow the focus. The models described can be applied to any type of APT, and to LTPP or pavement management system (PMS) data.

At the section level, APT data often exhibits considerable within-section variability, due to differences in materials and structure, and minor differences in environment (such as variations in temperature). In the analysis of the results, the data from each section is typically averaged before between-section and between-cell results are compared. Because of the cost of testing, it is common for each section to have different testing conditions, and consequently differences in performance of a single section must be assumed to be caused by differences in loading, etc. rather than construction variation in the materials or structure.

However, when replicate tests are performed, large differences in performance are often noted. As part of the preparation for a sequence of HVS tests on reflective cracking performance, six test sections were

loaded with mostly identical loading, with the main goal of damaging the sections before an overlay was placed. In a sense, these sections were part of construction of the test track rather than tests themselves. The initial pavement design was 90 mm of dense-graded asphalt concrete (AC) on 410 mm of aggregate base (AB), on native subgrade (Bay Area mud). Details of the testing are available in Lea (2010) and Jones et al. (2007).

One of these sections (573RF) had an unexpected early failure and, as a result, the section was moved and the load lowered to prevent another failure. This section was thus discarded in this analysis. Another section (572RF) exhibits some behavior that is difficult to explain statistically (the rutting on this section occurred over a width greater than the measured profile width, resulting in the baseline moving), and consequently the data for this section was also discarded. On another section (567RF), the load was lowered at the end of the test since rutting was progressing too quickly without inducing cracking. The data after the load change was discarded.

Extensive data for this track was obtained, mostly after these sections were overlaid and tested further. This includes coring, test pits, dynamic cone penetrometer (DCP) and falling weight deflectometer (FWD) testing. For this paper, this data, the details of which can be found in Jones et al. (2007), was used to estimate the thickness of the AC, thickness of the AB and air-void ratio of the AC. A simple inverse distance weight interpolation scheme was used to predict the values at the center point of the section at each profilometer station. Profiles were taken transversely at 500 mm intervals along the section using a laser profilometer, at stations numbered zero through 16. Only stations 3 to 13 are used in this analysis, since the other profiles fall in the turn-around zone for the HVS wheel.

Figure 1 shows the rutting progression on the four remaining sections. The sections exhibit significantly different rutting performance. A simple equation of the form below is fitted to the rutting at each station, treating them as independent tests.

$$r = \alpha_0 R^{\alpha_1} \tag{1}$$

where r is the rut depth (in mm); R is the repetition count at the time of measurement; and α_0, α_1 are regression coefficients.

It is obvious that the results for each station are highly correlated, so using them to calibrate a design method would likely produce spurious results. It is typical to average the results for the section, resulting in four sets of data in this case, which are shown on Figure 2.

Three of the four sections have the same slope (since this is a log-log plot, this is the exponent above, so implies the shape of the rutting curve), while the fourth (569RF) has a higher slope. The intercepts of the lines are clearly different, implying different scales.

This much is clear from looking at the raw data. However, at this point, it is difficult to say why these results differ. Figure 3 shows a pair-wise plot of the slope and intercept with some possible explanatory variables (the average thickness of the AC and AB, the air-voids in the section, and the 'thickness' of voids in the AC: $V = h_{AC} \times AV/100$. The single result for 569RF dominates the correlation, so it is difficult to

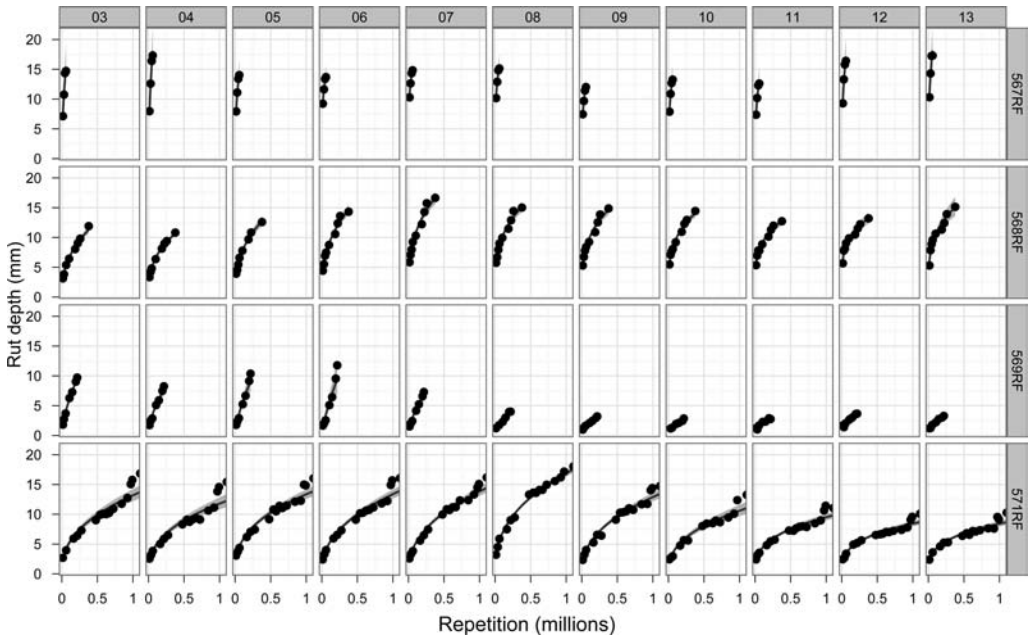

Figure 1. Rut depth progression on four identical sections at stations 3 through 13.

say if there is any effect from these variables. On the other hand, examination of the coefficients fitted to the individual data for each station (from Figure 1) in Figure 4, shows that there are significant correlations between the layer thicknesses and air-voids for some coefficients, and that these correlations are stable across the various sections.

However, examination of the two coefficients along each section, as shown on Figure 5, shows that they are not only correlated with one another (as one would expect from a regression model), but that they are also correlated spatially. In addition, because each station was fitted independently, the regression models are not particularly good (each of the 567RF models has only four data points).

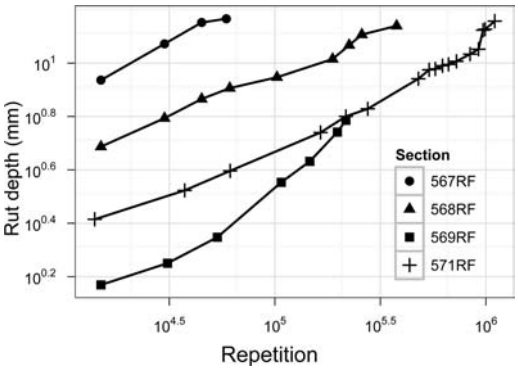

Figure 2. Average rut depth progression for four sections.

3 MIXED-EFFECTS MODELS

In the past many types of statistical model have been applied to pavement performance data. For the most part, these have been simple regression models. In statistical literature, there has been significant interest in a class of models known as mixed-effects models, which are ideal for handling the type of data generated by APT experiments (a multi-level panel data set). Unsurprisingly, these models have been applied to APT data several times, including Onar et al. (2006) and Hong and Prozzi (2010).

In a multi-level panel data set, the data are broken into a number of groups or panels (which in statistical literature are often referred to directly as individuals, although in APT these would be sections or stations). Below, a simple case of one level with groups $i = 1.N$ is used, although in some APT cases,

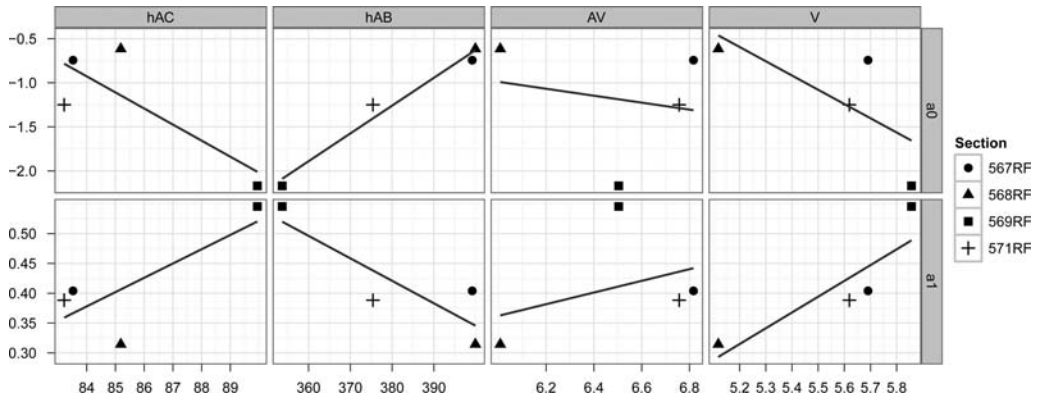

Figure 3. Correlation between regression coefficients for section models.

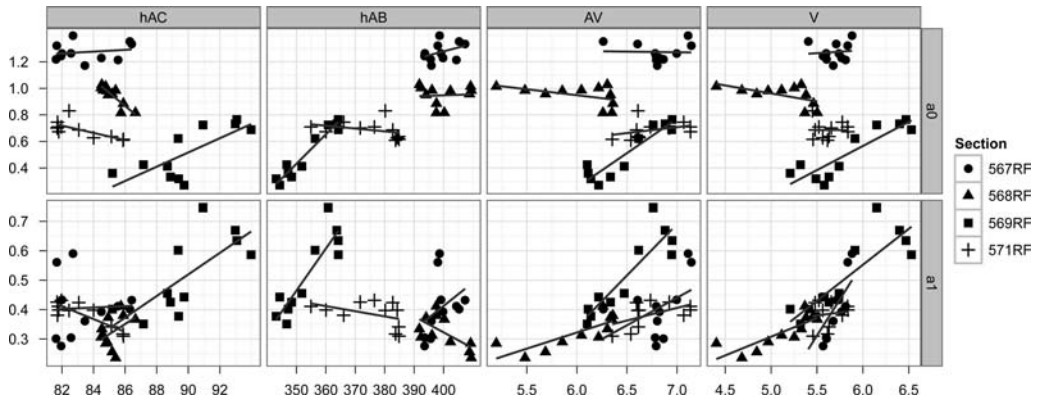

Figure 4. Correlation between regression coefficients for station level data.

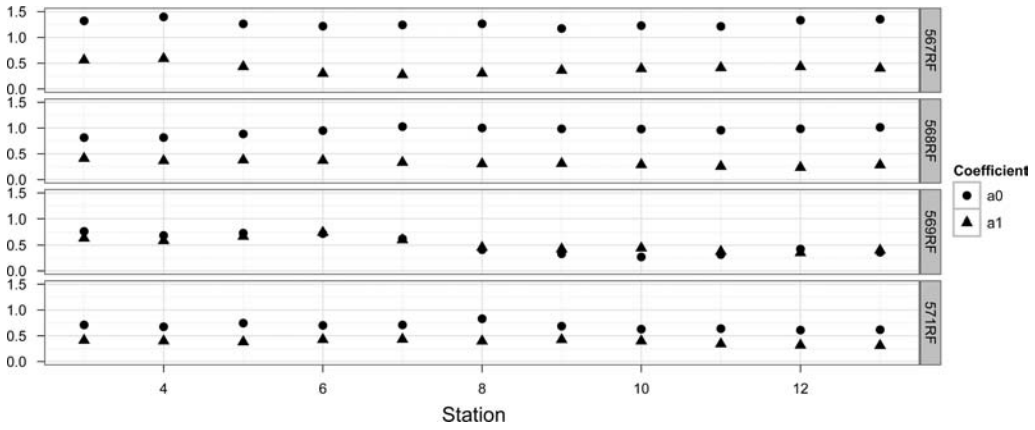

Figure 5. Spatial correlation between regression coefficients.

three or four levels may be used. The groups do not need to have the same number of members, although they should be similar. Each group has a set of data with time (or repetition in APT data) or space (on a continuous location scale). Each group i can have a different number of observations (n_i). The response variable of interest (the dependent variable) needs to vary within the panels (i.e. with time/repetition or position). In general, there should be some other explanatory (independent) variables observed, at least some of which are constant within the group. These are organized into two sets: fixed-effects and random-effects. In general, fixed-effects are those variables which are controlled between groups (e.g. different types of asphalt or different design thickness), while random-effects are uncontrolled differences between groups (e.g. the actual measured thickness on layers which should have all been the same). Since the model splits estimation into groups, the grouping variables must also be random-effects, which implies that grouping should not be by any experimental design parameters directly.

The classic form of a mixed effects model is:

$$\begin{aligned} &\boldsymbol{y}_i = \boldsymbol{X}_i\,\boldsymbol{\beta}_i + \boldsymbol{Z}_i\,\boldsymbol{b}_i + \boldsymbol{\varepsilon}_i \\ &\boldsymbol{b}_i \sim N\,(0,\,\boldsymbol{\psi}) \\ &\boldsymbol{\varepsilon}_i \sim N\,(0,\,\sigma^2\,\boldsymbol{\Lambda}_i) \end{aligned} \qquad (2)$$

where $\mathbf{y}_i$ = the $n_i \times 1$ vector of response variables in group i; $\mathbf{X}_i$ = a $n_i \times p$ matrix of explanatory variables in group i; $\boldsymbol{\beta}$ = the $p \times 1$ vector of fixed-effect coefficients; $\mathbf{Z}_i$ = a $n_i \times q$ matrix of explanatory variables in group i; $\mathbf{b}_i$ = the $q \times 1$ vector of random-effect coefficients for group i; $\boldsymbol{\varepsilon}_i$ = the $n_i \times 1$ vector of residual errors for observations in group i; $\boldsymbol{\Psi}$ = the $q \times q$ covariance matrix for the random effects; and $\sigma^2\boldsymbol{\Lambda}_i$ = the $n_i \times n_i$ covariance matrix for the errors in group i.

This form can be easily extended to more levels of groups if need. The independent variables are split into two groups ($\mathbf{X}$ and $\mathbf{Z}$), although the same variables can appear in both. Since the distribution of the random effects coefficients is defined to have zero mean, this implies that the mean of $\mathbf{Z}$ is effectively included as a fixed effect. The model is also split between a set of global coefficients that can be used for estimation, and a set of random effects that can only be used to fit the observed data. Since the groups must be random, this implies that one cannot assign any future observation of a new section to one of the groups.

The error structure of the mixed-effects model makes the model appealing. In the classic model there are two error distributions, both normally distributed with zero mean. The first is the within-group variance, which is governed by $\boldsymbol{\Lambda}_i$. This matrix is typically a structured matrix based on a combination of physical concerns or data observations. For example, if the within-group responses are over time, then it is common to use a time-series model, such as an autoregressive (AR) or moving average (MA) model. If the data are collected spatially, then a spatial autocorrelation model is used. This correlation model can also be augmented with a weighting model or a model that accounts for heteroskedastic variance. The role of this matrix is identical to the role of the covariance matrix in generalized least squares (GLS) models. If the matrix $\boldsymbol{\Lambda}_i$ is a function of some parameters $\boldsymbol{\gamma}_i$ then these can be included in the estimation process. σ^2 is retained outside of the matrix, since, after all of the model setup, it is still this parameter which is being minimised during the fitting process.

The random effects (or more strictly random coefficients) part of the model is determined by the vector $\mathbf{b}_i$. These allow each section or station to have a unique model. The matrix $\boldsymbol{\Psi}$ governs the correlation structure of the random effects, and is typically estimated along with the parameters. The random effects are typically correlated, since changing one effect requires changes to the others to maintain the fit of the model. The difference between a random effects model and fitting individual models to each group is in the structure of this matrix. Coefficients in individual models can often exhibit large variability, because of the effect of points with high errors. However, in a random effects model, these parameters are constrained by the

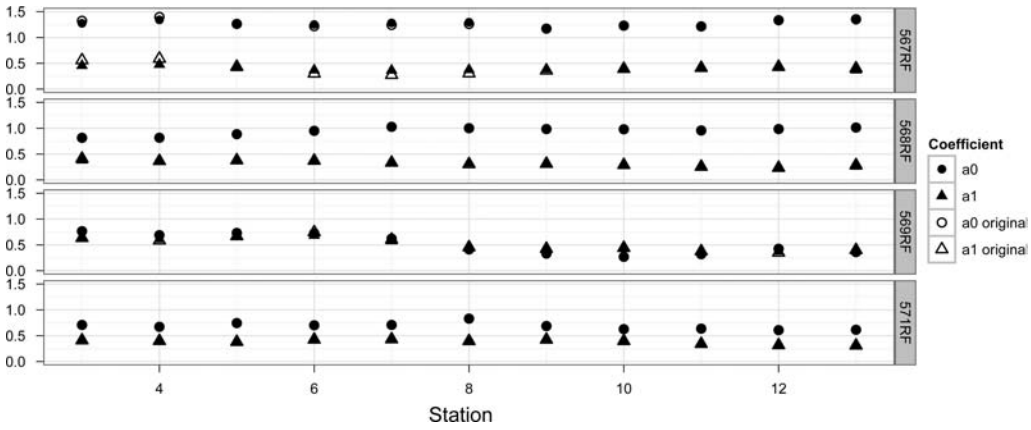

Figure 6. Spatial correlation of coefficients with random effects model.

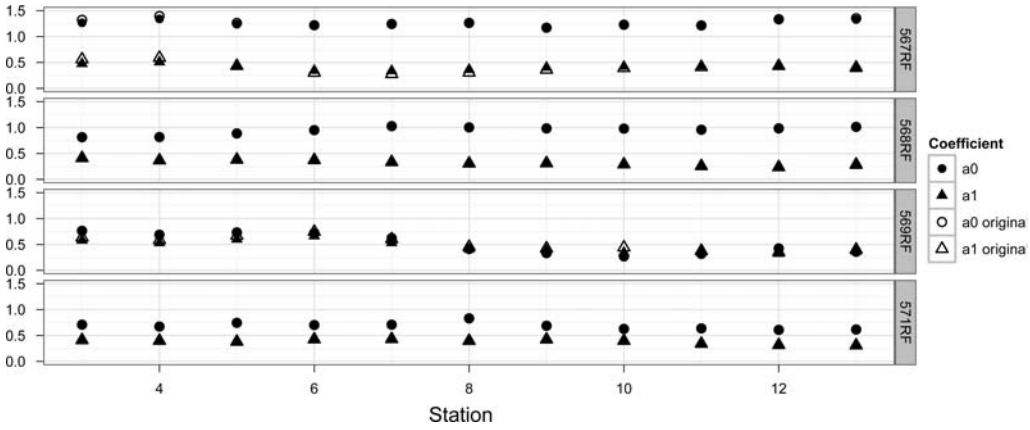

Figure 7. Spatial correlation of coefficients in random effects model with spatial correlation.

distribution, so there is a balance between the likelihood that a parameter is an outlier verses the individual data being an outlier.

What is missing from the classical model is the ability to specify a correlation structure between the random effects based on spatial distance. The assumption above is that the marginal distribution of each of the random effects in $\mathbf{b}_i$ is independent and identically distributed. The models fitted in the remainder of this paper follow the classic model, even though it is clear that the random effects are correlated spatially.

To begin, a two level mixed effects model, at both the section and station was fitted. The model in this case is:

$$\begin{aligned}\log_{10}(rut_{ijt}) = (&-1.634 + 0.155V_{ij} + 0.004hAB_{ij} \\ &+b0_i + c0_{ij}) + (-0.675 + 0.194V_{ij} \\ &+b1_i + c1_{ij})\log_{10}(\text{rep}_{ijt}) + \varepsilon_{ijt}\end{aligned} \quad (3)$$

where V_{ij} is the total voids in the AC at station j on section i; hAB_{ij} the thickness of the AB; rep_{ijt} the load repetition at time t; and the b and c coefficients are the per section and per station random coefficients.

Figure 6 shows the coefficients from this model with α_0 as the first bracket expression above and α_1 as the second, so that the total slope and intercept of the model can be compared to those on Figure 5. It is clear that coefficients are generally similar, although the model reduces the variability in the coefficient estimates for 567RF, since it is compensating for the lack of data on this section. It is still clear that there is spatial correlation in the model that is not being taken into account.

Although the software available cannot handle spatial correlation in the random-effects an attempt was made to "trick" the software by allowing a random effect for each observed repetition at each station, but forcing the data from the various stations to have a spatial correlation structure. Because this model has a large number of random coefficients, the structure of the correlation matrices had to be limited to enable the model to fit. In particular, this required not introducing correlation between the random intercept and random slope, which should be required. However, the model does show some interesting results. Figure 7 shows the coefficients for this model, which are similar to

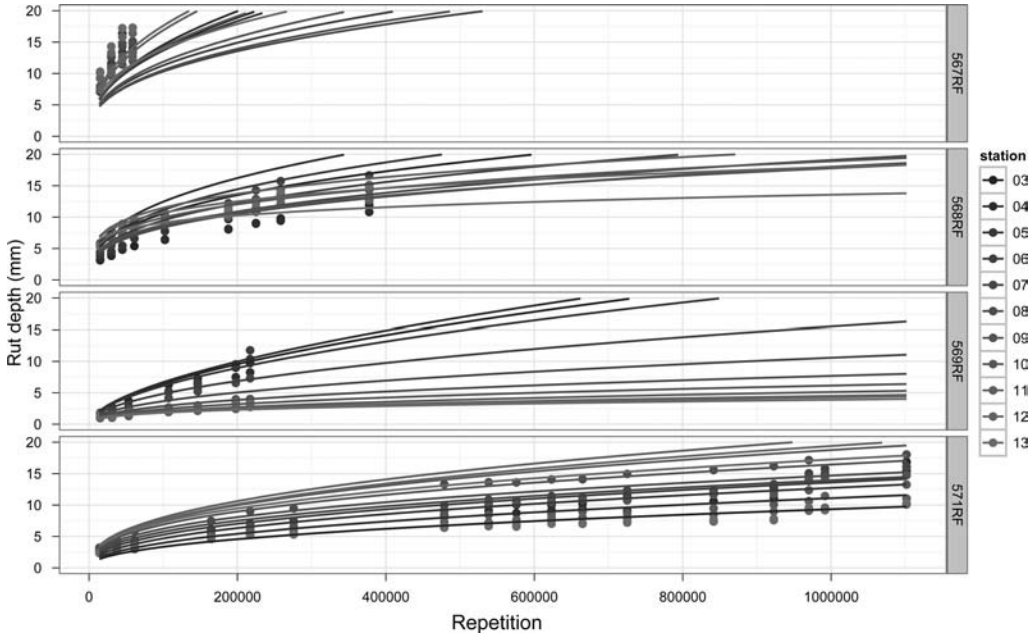

Figure 8. Random effects rutting model without random effects.

the previous model, except for what appears to be a slightly more logical slope at Station 10 on 569RF, and slightly more variance in the slopes at the earlier stations on this section. The change at Station 10 is a direct result of the model limiting the slope at this point because the rate of spatial change was higher than expected based on the estimates of the adjacent stations.

The model form in this case is similar; the only change is in the correlation structure of the random effects.

$$\log_{10}(rut_{ijt}) = (-5.953 + 0.239V_{ij} + 0.014hAB_{ij} + b0_{ijt}) + (-0.666 + 0.190V_{ij} + b1_{ijt})\log_{10}(\text{rep}_{ijt}) + \varepsilon_{ijt} \quad (4)$$

In this case the parameters for the voids in the AC and thickness of the AB have increased and the model now provides a good estimate of the range of performance of the sections. The estimates for this model are shown on Figure 8, without any random-effects.

Even with this 'tricked' model it can be seen that by controlling the correlation structure of the model, so that it accounts for both spatial and time based structure, can allow the development of models that extract additional information from the station level data which is not available at the section level. In this case there is a very clear indication that the total air voids in the AC is the main contributing factor for rutting.

This result is despite the estimates of thickness and air-voids at each station being made using a crude inverse distance weighted average from measurements around the section, rather than direct measurements at these points.

Figure 9 shows a comparison between a classic ordinary least squares model (what one would obtain fitting Equation 1 to all of the data with a spreadsheet or other simple program) and mixed effects model with the mean voids in the AC and thickness of the AB across the test track.

4 CONCLUSIONS

APT is an expensive process, which generates high quality performance data on small sections of pavement. In the past, the within-section variability of the data (as measured at points along the section) has largely been ignored and the section averages used for comparisons and calibration. Because there are typically a small number of sections, this results in a small number of data points for comparison or performance modeling, and it is difficult to attribute the differences in performance of the sections to the differences in the experimental design parameters alone. Best practice for APT already suggests that rather than comparing the raw data for the sections one should model the pavement using the best available mechanistic models to try to account for unintended differences between sections, to extract the true difference from changes in materials or structure.

However, fitting mixed-effects models to the station or point level data within each section, which can account for the correlation structure between observations in time and space, allows the differences in performance at each station to inform the analysis process. If there are significant differences between the station level data, and one can establish the reasons

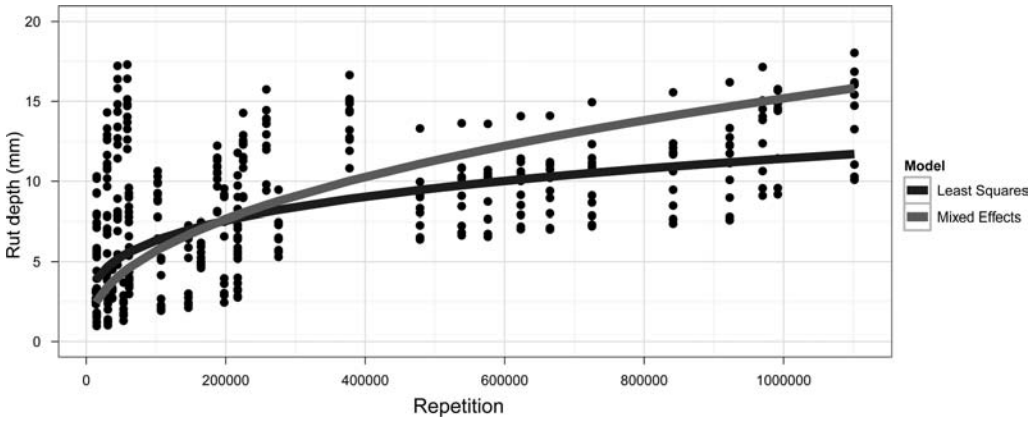

Figure 9. Comparison between ordinary least squares model and Equation 4 with mean AC voids and AB thickness.

for these differences (such as differences in layer thickness), then this can be used to correct and adjust the results from each section. This process extracts additional value from the APT data and can lead to better decision making, along with providing a method of correcting the section level data for minor differences in construction.

This process obviously relies on being able to extract some relationship between the station level performance and structural or material differences at each station, which can help to explain the changes in performance. In most tests, these will be differences in material thickness and density (and hence stiffness), although other factors such as differences in temperature, loading effects from the machine, binder contents, etc. might also play a role. On the one hand, the test track should be constructed to minimize these effects, to ensure the best possible comparison between sections, but, on the other hand, some variation is inevitable. Thus, even if the construction is closely controlled, as much data about each test track as possible should be gathered. This can be in the form of cores or other samples taken before, during or after the test, or non-destructive tests, such as ground penetrating radar. In all cases, the sampling should be spatial referenced, so that the exact location of each sample is known, and results can be extrapolated into the sections.

Further work needs to be performed on the available tools for mixed-effects modeling, since these tools do not allow spatial correlations in the random effects. This is not a major change to the methodology, since it merely adds another set of parameters to the covariance matrix. Of more importance, is that it is not currently possible to use this type of model in the calibration process for ME design methods, since the process typically does not involve statistical estimation of parameters.

ACKNOWLEDGEMENTS

This paper describes research activities that were requested and sponsored by the California Department of Transportation (Caltrans), Division of Research and Innovation. Caltrans sponsorship is gratefully acknowledged. The contents of this paper reflect the views of the author and do not necessarily reflect the official views or policies of the State of California or the Federal Highway Administration.

REFERENCES

Hong, F. and Prozzi, J.A. 2010. Roughness Model Accounting for Heterogeneity Based on In-Service Pavement Performance Data. *Journal of Transportation Engineering* 136: 205–213.

Jones, D.; Harvey, J.T. and Monismith, C.L. 2007. *Reflective Cracking Study: Summary Report.* Davis and Berkeley, CA: University of California Pavement Research Center. UCPRC-SR-2007-01.

Lea, J.D. 2010. *The Effect of Spatial Variability on the Reliability of Pavements.* PhD Dissertation, University of California, Davis.

Onar, A.; Thomas, F.; Choubane, B. and Byron, T. 2006. Statistical Mixed Effects Models for Evaluation and Prediction of Accelerated Pavement Testing Results. *Journal of Transportation Engineering* 132: 771–780.

This page intentionally left blank

Advances in Pavement Design through Full-scale Accelerated Pavement Testing – Jones, Harvey, Mateos & Al-Qadi (Eds.)
© 2012 Taylor & Francis Group, London, ISBN 978-0-415-62138-0

Use of mechanistic-empirical performance simulations to adjust and compare results from accelerated pavement testing

J.T. Harvey, D. Jones, J.D. Lea & R.Z. Wu
University of California Pavement Research Center, University of California, Davis

P. Ullidtz
Consultant, Copenhagen, Denmark

B. Tsai
University of California Pavement Research Center, University of California, Berkeley

ABSTRACT: This paper presents a discussion of the use of Mechanistic-Empirical (ME) analysis to simulate Accelerated Pavement Testing (APT) results in order to overcome problems with using APT data, such as differences in underlying conditions, construction quality, loading, and environmental control. This is particularly important when APT results are used for comparison studies between different pavement alternatives. In the process presented, APT results are first used to calibrate ME models so that the results from simulation of APT under actual conditions match the results predicted by the models. The APT results are then simulated with ME, this time assuming uniform conditions in the APT, to produce a ranking of the alternatives tested without the bias of differences between APT sections. Extrapolation of APT results to field conditions using ME analysis is also discussed. The paper presents a demonstration of this process from an experiment to compare different asphalt overlay treatments for reflective cracking and rutting performance.

1 INTRODUCTION

1.1 *Why are mechanistic-empirical simulations of APT results needed?*

Accelerated Pavement Testing (APT) is performed for a number of reasons. One of the most common is to quickly evaluate a new pavement technology that has shown promise in the laboratory and mechanistic analysis before going to more widespread implementation or pilot projects on the road network. The evaluation usually involves comparison with proven existing pavement technologies. Often there is some performance data from initial pilot projects in the field. However, the results from the field pilot projects are sometimes inconclusive for one or more of the following reasons:

- Differences in construction quality between the different sections, or problems with construction,
- Differences in the underlying pavement structure make direct comparison difficult,
- Insufficient time for the pavements to reach failure,
- Different traffic or climate from the control sections that new technologies are being compared to, because the pilot sections are in a different location,
- Pilot projects were placed in a location that is low risk in case of early failure (usually in a low traffic location), while the primary application will be in a different climate region or traffic level.

APT experiments intended to compare different types of pavement are often affected by the first and second problems listed above, which makes it difficult to provide a completely unbiased comparison. These problems occur because it is nearly impossible to construct exactly replicate subgrade and underlying pavement structures, achieve the same concrete curing conditions because of moisture and temperature differences at different times, or obtain the same compaction of asphalt, on different sections. These often occur because of factors such as the inevitable breakdowns at the materials plant, paver problems, clogged jets on the tack coat spray truck, and lost trucks full of hot asphalt or hydrating concrete.

In the process described in this paper, mechanistic-empirical (ME) models are used to help produce a ranking of the alternatives tested in an APT comparison study by accounting for the bias caused by differences in conditions that occurred between APT sections through ME simulation.

1.2 *Interaction between mechanistic-empirical analysis and APT*

The most common interaction of ME and APT has been the use of APT to calibrate ME models. Many mechanistic-empirical (ME) pavement design methods have been calibrated using at least some APT

data over the years. These include a number of the early methods that were calibrated in part using the AASHTO Road Test data, as well as more recent methods such as the AASHTO *Darwin*-ME models and software (*Mechanistic-Empirical Pavement Design Guide* [*MEPDG*], based on the NCHRP 1-37A [ARA, 2004]) and the *CalME* models and software (Ullidtz, 2008a, 2008b, 2010) that are the subject of this paper.

A less common interaction of ME and APT is to use ME to adjust APT results to help remove bias in APT comparison studies caused by the differences in construction, underlying structure, trafficking, and environmental control. The process for doing this was described in Harvey (2008) as follows:

"Once [ME] models are reasonably well validated and calibrated, they can be used to "re-run" the APT test sections through simulation with completely equal underlying conditions, temperature, water content, etc. Because there are inevitable differences in conditions that are supposed to be equal between APT sections, this simulation of the APT tests is extremely useful to confirm that the results of the initial empirical comparisons of performance do not change significantly under absolutely uniform conditions."

The synergetic interaction between APT and ME is greatly improved when the ME analysis method, such as the one used in this study, is capable of simulating the entire process of pavement damage and aging (or curing), and the changes in corresponding stress and strain responses throughout the entire pavement life for both the APT section and simulated field sections. This is very difficult to accomplish if the ME analysis method uses an approach, such as Miner's Law, that only considers the initial condition of the pavement and the final failure state. With the latter type of approach the ME method can only be calibrated based on the stress and strain responses at the initial state and the final failure distress level. The responses that occur in between these two points in time cannot be verified with data from APT instrumentation.

For example, the *MEPDG* (ARA, 2004) produces calculations of fatigue damage for the entire simulation starting from the first load. However, the asphalt master curve is not updated for damage (loss of stiffness for a given load, time of loading, and temperature) after each set of loads in each time increment (month) and responses of the pavement (stresses and strains) calculated for the undamaged state are therefore used for the simulation of the entire life of the pavement. (Note that although the master curve is not updated for damage, it is updated for aging so that the *MEPDG* predicts an increase in asphalt stiffness until the end of life, at which time the total damage calculated by Miner's Law is applied). Alternatively, a fully "incremental-recursive" analysis method (described in more detail in Ullidtz [2008a, 2008b]) is defined as one where the material properties are updated for damage, aging, and other processes (such as debonding) incrementally throughout the section life. With an incremental-recursive method, responses measured with APT instrumentation at intervals during the entire APT test can be used to calibrate and verify the damage processes simulated by the ME analysis method because they both reflect the incremental damage occurring during loading. The *CalME* analysis models used in the study described in this paper use an incremental-recursive method that updates the condition (fatigue and permanent deformation) of each layer of the pavement after each increment of loading for both aging and damage using the time hardening approach. Examples of the load increment can be each hour of a representative day of every month of the life for simulations of field loading, or each hour in an APT test. An additional advantage of incremental-recursive models is that data from APT and long-term pavement performance (LTPP) sections that never demonstrate distress on the surface can be used for calibration of the models because the damage (measured in terms of loss of stiffness such as in the asphalt master curve) can be measured by backcalculating the stiffness from measured deflections or strains and comparing it with the initial undamaged stiffness under the same load, time of loading, and temperature conditions. For example, some of the Heavy Vehicle Simulator (HVS) test sections in the study described in this paper never exhibited surface cracking, but had measurable damage to pavement layers backcalculated from deflections.

This paper presents an example of the three main steps in using an ME analysis method in conjunction with APT to greatly increase the benefit obtained from both of these research and development tools. These steps are:

1. Calibrate and verify the damage process models in the ME analysis method using instrumented APT data from the as-built comparison test sections and actual testing conditions (loading, temperature and moisture primarily). Once this is completed, the ME analysis should be capable of simulating the performance of the pavement test sections under a range of conditions.
2. Simulate the APT comparison test sections again, assuming exactly the same as-built structures, as-built construction quality, and as-tested loading, temperature, and moisture conditions. This will provide a "fair" comparison between alternatives tested under simulated equal conditions.
3. Simulate field sections for the same comparison of different pavements under different conditions of climate, traffic, materials, thicknesses, construction quality, and subgrade. This is essentially an extrapolation of the APT results, which must be treated with some caution and pavement engineering judgment. However, these simulations can be extremely useful because extreme temperature, loading, and moisture conditions are often used to accelerate pavement damage in APT and more realistic estimates are desired for the range of typical condition on the network.

2 OVERVIEW OF THE PROJECT AND APT RESULTS

The objective of the project used as an example in this paper was to develop improved rehabilitation treatments for reflective cracking for California, while also determining the risk of rutting for those treatments (Jones, et al., 2007a, 2008). Simulation of fatigue cracking of the original pavement prior to rehabilitation was also performed to help calibrate the ME models used for the evaluation of the rehabilitation treatments (Jones, et al., 2007b).

To provide a platform for evaluation of the rehabilitation treatments, a pavement was built to a single design on a compacted clay subgrade. The pavement was large enough (two lanes each 3.7 m wide by 80 m long) to provide adequate area for later placement of representative samples of six rehabilitation overlays with five different types of material produced at a commercial asphalt plant. All of the construction was performed using full-scale highway construction equipment, procedures and specifications using a qualified contractor selected based on low-bid.

The initial pavement was designed following standard Caltrans procedures and incorporated a 410 mm Class 2 aggregate base with a 90 mm dense-graded asphalt concrete (DGAC) surface. As was allowed by Caltrans District specifications, the Class 2 aggregate base included building waste, primarily crushed concrete, which was shown in the forensic trenching to still have reactive properties (Jones and Harvey, 2007c). The base was later found to have increased stiffness when left to cure with the light cementation coming from unhydrated cement in the crushed concrete that was activated by compaction water. The increased stiffness was substantially broken down when subjected to HVS loading, and showed renewed increases in stiffness whenever HVS loading was stopped, such as between completion of the initial cracking of the underlying pavement and the subsequent loading of the same locations after the overlay to test for reflective cracking. Six replicate sections of this structure were trafficked with the HVS between 2001 and 2003 to induce fatigue cracking in the DGAC. This trafficking of the initial pavement is summarized in Table 1, along with the overlay type later placed on the cracked DGAC pavement in each section.

Table 1. Summary of testing on the underlying DGAC layer and identification of overlay sections.

Under section	Load reps[1]	Final rut depth mm	Final crack density m/m^2	Overlay	overlay section
567RF	78,500	13.7	8.1	MB15-G	586RF
568RF	377,556	14.2	5.5	RAC-G	587RF
569RF	217,116	3.8	5.9	AR4000-D	588RF
571RF	1,101,553	14.1	6.2	MB4-G2	589RF
572RF	537,074	8.8	8.1	MB4-G3	590RF
573RF	983,982	15.3	4.1	MAC15-G	591RF

[1]at 20°C, 60 kN dual wheel load, 720 kPa tire pressure, bi-directional loading; [2]45 mm [3] 90 mm

The cracked DGAC sections were overlaid with six different treatments, with all but one placed with a thickness of half of the underlying DGAC (one type of asphalt overlay material was also constructed with full thickness) to assess their ability to limit reflective cracking. The treatments included:

- Half-thickness (45 mm) MB4-G gap-graded overlay, with a terminal blend rubberized binder containing both polymer and an unspecified amount of recycled tire rubber, and meeting Caltrans MB-4 binder specification;
- Full-thickness (90 mm) MB4-G gap-graded overlay;
- Half-thickness MB4-G gap-graded overlay with a terminal blend rubberized binder with minimum 15 percent recycled tire rubber (referred to as "MB15-G" in this paper);
- Half-thickness MAC15TR gap-graded overlay with a terminal blend rubberized binder with minimum 15 percent recycled tire rubber, similar to the MAC-10TR binder specified in the Southern California Greenbook section 600-5.2.1, except that it uses 15 percent tire rubber rather than 10 percent tire rubber. (referred to as "MAC15-G" in this paper);
- Half-thickness rubberized asphalt concrete gap-graded overlay (RAC-G) using a "wet" process binder containing at least 18 percent recycled tire rubber, included as a control for performance comparison purposes, and
- Full-thickness (90 mm) dense DGAC overlay with a conventional AR-4000 binder (now PG64-16), included as a control for performance comparison purposes.

Each of the overlay treatments was subjected to two APT tests. The first test was performed at high temperatures (asphalt heated to 50°C at 50 mm depth) to assess rutting performance. The second test was performed at moderate temperatures (asphalt temperature maintained at 20 C at 50 mm depth) on the overlay directly above the previously cracked underlying pavement section to assess reflective cracking. Table 2 shows the details of the APT tests on the overlays. A summary of the experiment and references to other project reports can be found in Jones et al. (2007a).

The results of the APT tests for rutting of the overlay are summarized in Table 3. It can be seen that the control overlays in the experiment typically used by Caltrans, conventional dense-graded overlay and RAC-G, were in the top three for best rutting performance, while the terminal blend mixes ranked second, fourth, fifth and sixth. These results suggested that caution should be used for placement of these mixes in locations with a higher risk of rutting based on the then current mix designs.

Table 2. Summary of HVS loading program on overlays.

Test Type	Section	Start Repetition	Total Repetitions	Wheel Load (kN)	ESALs	Temperature °C
Rutting	580RF	Full test	2,000	60	11,000	50°C ± 4°C
	581RF		7,600		42,000	
	582RF		18,564		102,000	
	583RF		15,000		83,000	
	584RF		34,800		191,000	
	585RF		3,000		17,000	
Reflective cracking	586RF (MB15-G)	0	2,492,387	60	88 million	20°C ± 4°C to one million repetitions;
		215,000		90		
		410,000		80		
		1,000,001		100		
	587RF (RAC-G)	0	2,024,793	60	66 million	
		215,000		90		
		410,000		80		
		1,000,001		100		
	588RF (AR4000-D)	0	1,410,000	60	37 million	
		215,000		90		
		410,000		80		
		1,000,001		100		
	589RF (45 mm MB4-G)	0	2,086,004	60	69 million	15°C ± 4°C the reafter
		215,000		90		
		407,197		80		
		1,002,000		100		
	590RF* (90 mm MB4-G)	0	1,981,365	60	37 million	
		1,071,004		90		
		1,439,898		80		
		1,629,058		100		
	591RF (MAC15-G)	0	2,554,335	40	91 million	
		215,000		60		
		410,000		80		
		1,000,001		100		

*590RF was the first HVS test on the overlays, and the 60 kN loading pattern was retained for an extended period to prevent excessive initial deformation (rutting) of the newly constructed overlay.

Table 3. Overlay rutting study results.

Overlay	rank	Reps to 12.5 mm avg max rut	Avg. max rut (mm)[1]	Avg. down rut (mm)
AR4000-D	1	8,266	15.6	8.1
MB4-G (45)	2	3,043	31.3	9.7
RAC-G	3	2,324	22.7	10.3
MB4-G (90)	4	1,522	23.3	11.9
MB15-G	5	914	18.8	7.1
MAC15-G	6	726	23.5	7.7

[1]Rut measured from highest point of upheaval to lowest point of deformation.

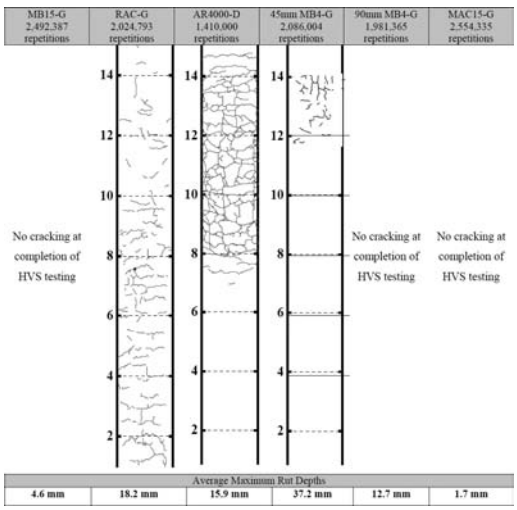

Figure 1. Cracking patterns and rut depths on the overlay sections.

With regard to reflective cracking, after millions of load repetitions, only three of the overlay sections showed surface cracking (DGAC, RAC-G and a small area of the MB15-G), as shown in Figure 1. The sub-sections with different levels of cracking seen in Figure 1 were modeled as separate sections. The other three sections had measureable damage, identified by increased deflections. The terminal blend overlay sections had the best reflective cracking performance with only one showing any surface cracking after more than two million load repetitions. Forensic trenches after HVS testing showed that all of the surface cracks were reflected from the cracked underlying DGAC, and that some of the DGAC cracks had begun to propagate

upward but had not reached the surface in the overlay sections that did not show surface cracking.

3 SIMULATIONS

Six sets of simulations were performed using the California mechanistic-empirical design and analysis software *CalME*, including five of the HVS tests and a sixth on a hypothetical set of typical Caltrans structures and traffic conditions in different climate regions in the state. The simulations are summarized as follows (Jones et al., 2007b):

1. Simulation of the tests on the original pavement structure using actual (in-situ) conditions;
2. Simulation of the moderate-temperature cracking tests on the overlaid pavement structure using actual conditions;
3. Simulation of the high-temperature rutting tests on the overlaid pavement structure using actual conditions;
4. Simulation of the high-temperature rutting tests on the overlaid pavement structure using design thicknesses for the overlays and identical conditions of underlying pavement structure and temperature across all of the tests;
5. Simulation of the moderate-temperature cracking tests on the overlaid pavement structure using design thicknesses for the overlays and identical conditions of underlying pavement structure and temperature across all of the tests; and
6. Simulation of rutting and cracking for a hypothetical set of typical Caltrans structures and traffic conditions in different climate regions in the state.

The first three sets of simulations served to validate the *CalME* models by comparing the calculated results from *CalME* models with the measured responses and performance. Simulations 4 and 5 provided objective ranking of the different asphalt overlays without the influence of underlying conditions, which varied in the actual HVS tests. The sixth set of simulations provided extrapolation of the HVS results to field conditions and an understanding of the sensitivity of the predicted performance of the different overlays.

3.1 *Input data and methodology*

To perform the simulations using actual conditions, data from each HVS test, reported in a series of first-level analysis reports (Jones, et al., 2007a), were imported into a *CalME* database. The data comprised information on loads (time of application and load level), temperatures at different levels, road surface deflectometer (RSD) results, multi-depth deflectometer (MDD) resilient and permanent deformations, and pavement profiles. Strain gauges were not used for the overlay testing because the cracking of the overlays was due to localized strains above cracks causing reflective cracking, not overall bending of the overlays. In fact, the bottoms of many of the thin overlays would have been above the neutral axis and in compression if analyzed using layer-elastic theory, but with high tensile and shear strains above the cracks.

The backcalculated layer moduli from the last falling weight deflectometer (FWD) tests undertaken before commencement of HVS loading on each section were used as the initial asphalt concrete layer moduli (reference temperature of 20°C). The master curve for the asphalt concrete layers was obtained from frequency sweep tests on beams in the laboratory, with the exception of the original DGAC layer where the master curve was based on FWD backcalculated moduli. The change in stiffness of the subgrade with changing stiffness of the pavement layers and with changing load level was obtained from FWD backcalculated values. These parameters were used with the layer-elastic response model to calculate stresses, strains, and deflections in the pavement structure. The tensile strain in an overlay over an existing cracked asphalt concrete layer was calculated using a regression equation based on finite element method modeling described in Ullidtz (2008a, 2010).

A number of models were used to predict the pavement performance, in terms of cracking and permanent deformation. Parameters for prediction of asphalt concrete damage for bottom up cracking (from the underlying DGAC sections) and reflective cracking (overlays) were obtained from controlled strain four-point fatigue tests on beams (AASHTO T 321). The model for the damaged asphalt master curve has the format:

$$\log(E)=\delta+\frac{\alpha\times(1-\omega)}{1+\exp(\beta+\gamma\log(tr))} \quad (1)$$

which is the *MEPDG* asphalt master curve equation for dynamic stiffness (E) where a, b, g and d are fitting parameters, tr is the reduced time of loading, and the damage (ω), is a function of the number of loads, the tensile strain, and current modulus.

Cracking at the pavement surface was calculated from the damage to the surface layer, using models shown below relating damage (ω) to crack initiation and crack propagation developed based on previous simulations of HVS tests and the FHWA WesTrack experiment in Nevada (Ullidtz, 2008b)) to initially simulate cracking from HVS testing on the underlying pavement and the later overlays. These parameters did not predict the relationship of damage to surface cracking for the overlays and were then re-calibrated to match the reflective cracking results on the overlays tested, resulting in the following:

$$\omega_{initiation}=\frac{0.42}{1+\left(\frac{h_{AC}}{250mm}\right)^{0}} \quad (2)$$

$$Crm/m^2=\frac{10}{1+\left(\frac{\omega}{\omega_o}\right)^{-3.8}} \quad (3)$$

Where $\omega_{initiation}$ is the damage at crack initiation, hAC is the thickness of the combined asphalt layers, Crm/m^2 is the crack density, and other values are calibrated constants.

Repeated simple shear tests at constant height (RSST-CH, AASHTO T 320) were used to determine the parameters for predicting permanent deformation in the asphalt concrete layers.

A crushing model was developed for the lightly cemented base layer, consisting of recycled material with a high content of old crushed concrete. The model was based on a model developed for cement-treated bases (CTB) at an HVS-Nordic experiment (Thoegersen et al., 2004). A model developed for subgrade materials in the Danish Road Testing Machine was used for permanent deformation of the unbound layers.

An incremental-recursive process in *CalME* was used to simulate the performance of the test sections. A one-hour time increment was used for the HVS test simulations. The modulus of the subgrade was adjusted to the stiffness of the pavement layers and to the load level. Wander was considered for the cracking sections, while the rutting sections had channelized traffic. For all load positions, the stresses and strains at the center line of the test section were calculated and used to determine the decrease in moduli and the increase in permanent deformation of each of the pavement layers. The output from these calculations were used, recursively, as input to the calculation for the next hour of loading, using a time hardening procedure, which takes changes in moduli, response, damage, and permanent deformation into consideration.

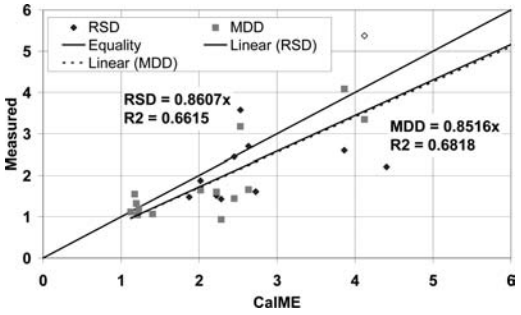

Figure 2. Increase in deflection (terminal deflection/initial deflection) during HVS experiments, as simulated and measured. (Note: some sections had both RSD and MDD measurements, others only one or the other, see Jones, et al., (2007b) for detailed results).

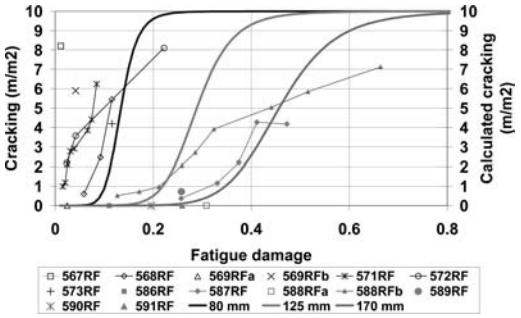

Figure 3. Observed surface cracking vs. damage for HVS tests on underlying DGAC and overlays with original parameters.

3.2 *Responses*

The first step in the simulation ensures that the calculated pavement response was reasonably close to the actual pavement response during the test. The calculated pavement response was used to predict the pavement performance (damage and permanent deformation) and if this response was not reasonably correct it would be futile to use it for calibration of the performance models. In this study, response measurements included resilient MDD deflections and/or RSD deflections.

Once the resilient deflections were predicted with reasonable accuracy during the simulations, the performance models were calibrated such that the permanent deformation of each layer, the decrease in layer moduli, and the observed surface cracking, were reasonably well predicted. The first important step in the simulations was to obtain good backcalculated stiffness values for all layers, and to compare those with measured values and laboratory test data. The best impression of the agreement (or lack of agreement) between the measured and calculated values is obtained from the deflection measurements from the entire duration of the HVS tests from start to finish, taken at various times during each test, which are shown in Jones et al., (2007b). A summary of the change in surface deflections between the initial and final deflections from HVS tests on both the underlying cracking tests and the cracking tests on the overlays from both MDD (one location) and RSD (average of 13 locations) measurements is provided in Figure 2. *CalME* tends to slightly overestimate the increase in deflection. The uncertainty on the measured values is illustrated by the difference between the deflections measured by the RSD and by the MDD, which in some cases is quite large.

3.3 *Simulations 1 and 2: Fatigue damage and cracking of asphalt concrete layers under actual conditions*

The damage calculated by *CalME* compared to the observed cracking on the test sections was reasonably accurate (see Figure 3), but the results were influenced by differences in the modulus of the underlying DGAC determined from FWD backcalculation and those determined from laboratory frequency sweep testing. This difference was attributed to early damage of the DGAC layer. Figure 4 shows that the surface cracking was fairly well predicted for the underlying sections (Sections 567 through 573) by cracking

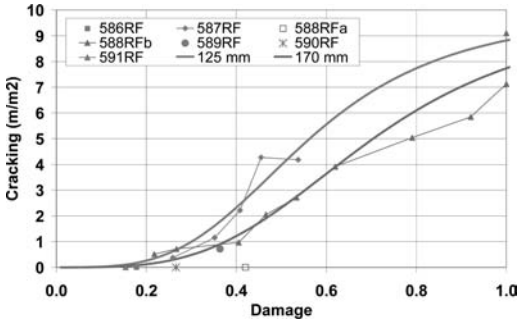

Figure 4. Observed surface cracking versus damage for overlays calculated using re-calibrated damage to cracking equation parameters to better fit overlay results.

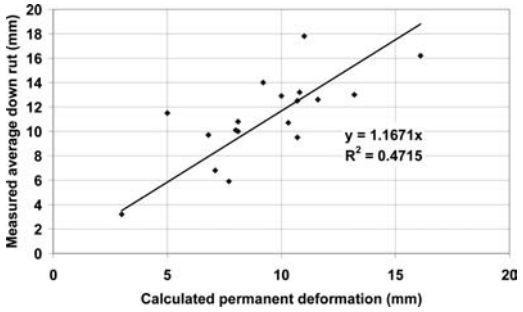

Figure 5. Calculated overall permanent deformation versus measured final down rut.

equation parameters that had been developed previously from other APT results, but not as well for the overlay reflective cracking sections that had surface cracking (Sections 587 through 589). In the figure the *CalME* calculation for a thickness of 80 mm should be compared with the HVS results for the underlying sections; the *CalME* calculation for a thickness of 125 mm should be compared to the 45 mm overlay results, and the *CalME* calculation for a thickness of 170 mm should be compared to the 90 mm overlay results, since those are the approximate thicknesses of the combined asphalt layers in each case.

In order to obtain a better fit to the measured reflective cracking in the overlay sections, the parameters in the equations developed for crack initiation and crack propagation that relate damage to surface cracking in *CalME* were re-calibrated in a series of iterations, using different constants. Cracking predicted using the re-calibrated equations is compared to the measured cracking for the overlays in Figure 4.

3.4 *Simulation 3: Permanent deformation under actual conditions*

The terminal overall permanent deformation calculated by *CalME* at the end of each HVS test and the average measured down rut (same as average deformation in Table 1) from profile measurements are shown in Figure 5. A similar plot for final down rut versus the permanent deformation of the top cap of the MDDs had a poorer correlation with *CalME* results because most of the permanent deformation was in the asphalt layer which was not captured because of positioning of the MDD sensors.

On average, *CalME* underestimated the overall permanent deformation by about seven percent, but the correlation coefficient was quite low. This should be seen in the light of the very large variation of down rut within some of the HVS sections. A difference of 5 mm to 10 mm between the minimum and the maximum down rut measured within the 6.0 m long test section was not unusual, and in one case (45 mm MB4-G) it reached 30 mm.

The permanent deformation of the top MDD includes the permanent compression of the aggregate base layers and the permanent deformation of the subgrade. The permanent deformation of the subgrade was usually very low, less than 1.0 mm, except for one section where one of the MDDs recorded final permanent deformations at the subgrade of 2.5 mm and another that recorded a value of 1.5 mm. In both cases, however, another MDD in the section recorded a permanent deformation close to zero.

3.5 *Simulation 4: Permanent deformation in overlaid sections with uniform conditions*

Experience has shown that the HVS testing conditions always have some influence on the performance of a particular section. This influence increases with increasing duration of the test. The rutting study was considered to consist of short duration tests since the test sections were on parts of the overlays that had not been trafficked previously with the HVS. As a consequence, the influence of the test conditions was less pronounced than it was in the fatigue experiment, which had a longer duration and took place on test sections located precisely above those trafficked with the HVS during Phase 1 of the experiment (HVS test on underlying DGAC). For completeness, the simulations were repeated for the rutting experiment using the same underlying structure used for the reflective cracking study discussed above, with the exception that the modulus of the underlying asphalt was assumed to be 3,200 MPa at 20°C, corresponding to the approximate layer moduli determined from FWD tests. The pavement structure and test conditions for HVS Test 584RF (90-mm MB4-G) were used for the simulation of uniform conditions. Almost 20,000 load repetitions (60 kN) were applied to this section. The ranking from best to worst was:

1. 90 mm MB4-G
2. AR4000-D (DGAC control)
3. RAC-G (control)
4. MAC15-G
5. 45 mm MB4-G
6. MB15-G

Table 4. Ranking of overlays for reflective cracking under uniform conditions.

Layer	Damage	Cracking (m/m^2)	Rank	
MAC15-G (591)	(45 mm)	0.48	3.1	1
MB4-G (589)	(45 mm)	0.56	5.0	2
MB4-G (590)	(90 mm)	0.75	5.5	3
MB15-G (586)	(45 mm)	0.69	6.7	4
RAC-G (587)	(45 mm)	0.76	7.4	5
AR4000 (588)	(90 mm)	1.00	7.7	6

This ranking differs from the actual results as can be seen by comparison with actual results in Table 3. Some mixes changed ranking by one place, and one mix changed ranking by two places.

3.6 *Simulation 5: Fatigue damage and cracking from reflection of overlays under uniform conditions*

Although the original pavement was built to provide uniform support for the reflective cracking study, the forensic investigation showed that there was some variation over the length of the structure, specifically with regard to layer thickness, composition of the recycled aggregate, and degree of re-cementation of the aggregate particles. The conditions of the underlying structure, wheel loads, and climate should be identical when ranking the different overlays. The simulations were therefore repeated using uniform conditions. The HVS loading and climate for Section 591RF (MAC15-G) were used, but the number of load applications was multiplied by 50. Thicknesses of 45 mm, 80 mm, and 400 mm were used for the overlay, underlying DGAC, and base respectively on all sections. Moduli of 3,580 MPa, 400 MPa, and 100 MPa were used for the underlying DGAC, base, and subgrade respectively. An intact modulus of 12,000 MPa with a damage of 0.253 was assumed for the underlying DGAC. The same factors for the effects of confining stiffness and nonlinearity of the aggregate base and the subgrade were assumed for all sections.

Damage and cracking were determined at the end of the (simulated) HVS loading, at 458 million ESALs. The values, ranked according to the amount of cracking from best to worst, are shown in Table 4. These rankings are the same for the AR4000 and RAC-G sections, which cracked, and places the third section, which showed some initial cracking (MB-4 45 mm overlay) in one place different from ranking from the HVS tests. These simulation results showed that the differing conditions under the overlays in the HVS sections did not substantially alter their ranking in performance. The simulations also provided an indication of the expected ranking of the sections that showed damage, but were not trafficked to a point where cracking reached the surface.

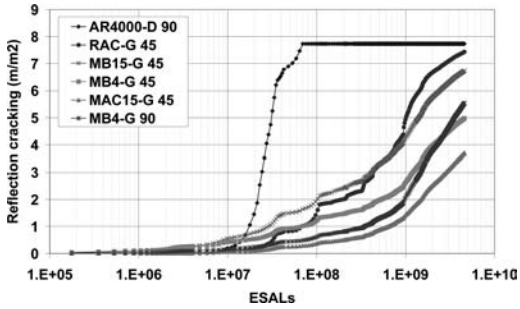

Figure 6. Simulated reflective cracking for identical testing conditions.

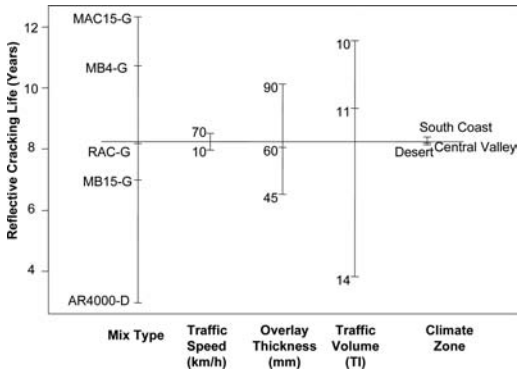

Figure 7. Design plot of reflective cracking life for asphalt overlays on cracked asphalt with using field mixed field compacted fatigue beam results. (Note: TI values are 2.4 million, 5.4 million and 41 million ESALs for TI = 10, 11 and 14, respectively).

The simulated reflective cracking is shown as a function of the number of loads (in ESALs) in Figure 6. The ranking depends to some extent on the number of load applications. The ranking would not change significantly if it was based on the reflective cracking predicted from fatigue damage of the overlay rather than surface cracking.

3.7 *Simulation 6: Extrapolation to field conditions and sensitivity studies*

Simulations were carried out to assess extrapolation of mix performance in the HVS tests to performance in the field. These results provided a preliminary assessment of expected field performance, considering the many limitations of the modeling and need to be checked with results from in-service pavements. An example of average values for reflective cracking life for each variable in the factorial of simulations for overlays on cracked asphalt pavement is shown in Figure 7. It shows that the effect of overlay mix type, climate region, and traffic level are more important than overlay thickness (for the ranges used).

Based on the simulation results, a number of observations were made based on simulations using the field

mixed field compacted materials placed on the HVS test sections:

- The relative ranking with respect to reflective cracking under field conditions was the same as the ranking under HVS test conditions, with the only exception being the RAC-G and MB15-G mixes. The RAC-G performed better than MB15-G in the field simulations but worse in the HVS tests.
- AR4000-D and MB15-G mixes had significantly shorter reflective cracking life under the Desert climate than under South Coast and Central Valley climates. The other mixes did not appear to be sensitive to climate conditions.
- Reflective cracking life was generally not sensitive to an increase in overlay thickness from 45 mm to 90 mm, and increasing the overlay thickness from 45 mm to 90 mm would not necessarily result in a longer reflective cracking life.
- Reflective cracking life decreased as traffic volume increased, but the life decreased at a rate much smaller than the increase in traffic volume.
- Increasing traffic speed from 10 km/h to 70 km/h approximately doubled the reflective cracking life for AR4000-D and MB15-G mixes. However, the reflective cracking life for the MB4-G, MAC15-G, and RAC-G mixes were less sensitive to traffic speed.

4 SUMMARY

This paper has presented a discussion of the synergistic interaction of mechanistic-empirical analysis and accelerated pavement testing. APT is used to calibrate ME analysis models, and calibrated ME analysis can then be used to solve problems with accelerated pavement testing results. These problems particularly occur when APT is used for comparison studies between different pavement alternatives, and include inevitable differences in underlying conditions, construction quality, loading, and environmental control. Calibrated ME analysis can then also be used to extrapolate APT results to a much wider range of conditions in the field than can practically and economically be considered by APT alone. This paper presented a demonstration of this process from an experiment to compare different asphalt overlay treatments for reflective cracking and rutting performance that included six different sets of simulations, from calibration through extrapolation.

ACKNOWLEDGEMENT

This paper describes research activities requested and sponsored by the California Department of Transportation (Caltrans), Division of Research and Innovation. Caltrans sponsorship is gratefully acknowledged. The contents of this paper reflect the views of the authors and do not reflect the official views or policies of the State of California or the Federal Highway Administration.

REFERENCES

ARA Inc., ERES Consultants Division. 2004. *Guide for Mechanistic-Empirical Design of New and Rehabilitated Pavement Structures.* Report to National Cooperative Highway Research Program, Project 1-37A. Washington, DC.

Harvey, J. 2008. Impacts and Benefits of APT: An APT Operator's Perspective. *Proceedings of the 3rd International Conference on Accelerated Pavement Testing*, Madrid, Spain, October.

Jones, D. Harvey, J. and Monismith, C.L. 2007a. *Reflective Cracking Study: Summary Report.* Davis and Berkeley, CA: University of California Pavement Research Center UCPRC-SR-2007-01.

Jones, D., Tsai, B. Ullidtz, P., Wu, R., Harvey, J. and Monismith, C.L. 2007b. *Reflective Cracking Study: Second-Level Analysis Report.* Davis and Berkeley, CA: University of California Pavement Research Center. UCPRC-RR-2007-09.

Jones, D. and Harvey, J. 2007c. *Reflective Cracking Study: HVS Test Section Forensic Report.* Davis and Berkeley, CA: University of California Pavement Research Center. (UCPRC-RR-2007-05).

Jones, D., Harvey, J. and Bressette, T. 2008. An Overview of an Accelerated Pavement Testing Experiment to Assess the Use of Modified binders to Limit Reflective Cracking in Thin Asphalt Concrete Overlays. *Proceedings, 6th RILEM International Conference on Cracking in Pavements*, Chicago, June. pp 45–54.

Thoegersen, F., Busch, C. and Henrichsen, A. 2004. *Mechanistic Design of Semi-Rigid Pavements—An Incremental Approach.* Report 138. Danish Road Institute, Fløng, Denmark.

Ullidtz, P., Harvey, J., Tsai, B. and Monismith, C.L. 2008a. Calibration of Mechanistic–Empirical Models for Flexible Pavements Using the California Heavy Vehicle Simulators. In *Transportation Research Record, 2087.* Washington, DC. Transportation Research Board. pp. 20–28.

Ullidtz, P., Harvey, J. Tsai, B. and Monismith, C.L. 2008b. Calibration of Mechanistic Empirical Models for Flexible Pavements Using the WesTrack Experiment. *Journal of the Association of Asphalt Paving Technologists. Vol. 77.* pp 591–630.

Ullidtz, P., Harvey, J., Basheer, I., Jones, D., Wu, R., Lea, J.D. and Lu, Q. 2010. *CalME*, a Mechanistic-Empirical Program to Analyze and Design Flexible Pavement Rehabilitation. In *Transportation Research Record, No 2153.* Washington, DC. Transportation Research Board. pp 143–152.

This page intentionally left blank

Advances in Pavement Design through Full-scale Accelerated Pavement Testing – Jones, Harvey, Mateos & Al-Qadi (Eds.)
© 2012 Taylor & Francis Group, London, ISBN 978-0-415-62138-0

Calibration of incremental-recursive rutting prediction models in *CalME* using Heavy Vehicle Simulator experiments

E. Coleri, R.Z. Wu & J.T. Harvey
University of California Pavement Research Center, University of California, Davis, US

J. Signore
University of California Pavement Research Center, University of California, Berkeley, US

ABSTRACT: The main objective of this study is to calibrate *CalME*, a Mechanistic Empirical (ME) analysis and design program for new flexible pavements and rehabilitation, rutting prediction models using the results of Heavy Vehicle Simulator (HVS) experiments. The methodology followed a shear-based Incremental-Recursive (IR) procedure using rutting model coefficients determined from laboratory shear testing. Calculated calibration coefficients for different HVS test sections were compared to evaluate the effects of asphalt mixture and structure type on predicted rutting performance. HVS rutting experiments were performed on four sections making up a full factorial of mix type (PG64-28PM [polymer modified dense-graded] and RHMA-G [rubberized gap graded]) and thickness (65 mm and 115 mm [2.5 and 4.5 in.]). HVS test results and early failure of RHMA-G mixes were also investigated to determine the changes in asphalt concrete microstructure with HVS trafficking using X-ray Computed Tomography (CT) images taken before and after HVS rutting tests. Three-dimensional images of deformed and un-deformed specimens were compared to determine the changes in air void content distributions for the PG64-28PM and RHMA-G mixes. Results of the analyses showed that shear related deformation controls the long term rutting performance of the test sections while densification was only an initial contributor at the very earlier stages of the trafficking. Laboratory shear testing was also determined to be an effective experiment for rutting performance evaluation. *CalME* was able to predict the early failure of the test sections constructed with the RHMA-G mix.

1 INTRODUCTION

Highways are an important component of civil infrastructure; they are essential to the economy and consume large amounts of natural and financial resources. Therefore, the most effective design and construction methods and the most efficient materials need to be used in order to minimize expenditures while maximizing the social benefits of mobility. Asphalt surfaced pavements make up the vast majority of pavements in California and the United States (US), and therefore have great importance in terms of roadway construction, rehabilitation and maintenance. Asphalt surfaced pavements include flexible pavements with granular bases, semi-rigid pavements with cement-treated soil bases, and composite pavements with underlying concrete. Asphalt surfaced pavements make up about 92 percent of roads in the US, and more than eight million km (5 million mi.) of highway across the United States. More than 500 million tons of hot-mix asphalt (HMA, another term for asphalt concrete [AC]) with the cost of nearly 18 billion dollars is used annually to improve and preserve the existing networks in the United States and to a lesser extent for the construction of new roadways (Epps et al. 2002). Even minor improvements in current design and construction methods can lead to large economic savings for the entire country, and decreases undesirable effects for the environment.

Rutting in the AC layers (White et al. 2002) appears to be a crucial part of the pavement failure problem. The risk of rutting of the AC is usually greater early in the life of the new asphalt surface layers before hardening occurs due to oxidation and trafficking, resulting in major increases in life cycle cost. Prediction of rutting performance is important to determine the most cost-effective design alternatives. Understanding of in situ deformation accumulation mechanisms is needed to develop effective performance prediction models and associated laboratory materials characterization tests in order to effectively design mixes to the appropriate level of risk for a given project. Appropriate tests and models are also needed to understand the reasons behind differences in the rutting performance of different asphalt mix types so that design methods can be improved.

Mechanistic-empirical (ME) design is a method of designing highway pavements by integrating the empirical relations relating distress to pavement response obtained from field data with the theoretical

predictions of pavement response from structural models (MEPDG, 2004). Structural models are developed based on generally accepted theories and methods (linear-elastic theory [LET], finite element [FE] method, etc.) to determine the response of pavements to environmental conditions, traffic levels, and material properties. Material characteristics, traffic, and climatic information are entered as inputs to predict pavement responses, such as strain, stress, and displacement at critical locations, by using theoretical structural models developed for predicting cracking or rutting distress potential. These responses are used as input to empirical transfer functions, which are generally developed from accelerated pavement testing and/or field test results (MEPDG, 2004; Ullidtz, 2006), to predict in situ distress distribution and pavement performance. Once it has been established that the pavement responses calculated by the theoretical models sufficiently match measured pavement response, the transfer function models are calibrated based on in situ performance measurements.

Accelerated pavement tests (APT) appear to be one of the most important initial sources of information for development and checking of ME models because the long-term performance of the pavement can be simulated in a short period of time (Brown, 2004). However, because APT is very expensive (although not as expensive as long-term field testing) and cannot be performed for all possible design alternatives, structural models and laboratory tests must be developed and/or improved to simulate actual pavement performance with a reasonable cost. Thus, results of APT should be used to improve these structural models and laboratory tests, rather than for development of empirical design criteria directly from the APT themselves.

The main objective of this paper is to summarize a study that calibrated *CalME* (an ME analysis and design program for new flexible pavements and rehabilitation), rutting prediction models using the results of Heavy Vehicle Simulator (HVS) experiments. The study followed a shear based incremental-recursive (IR) procedure using rutting model coefficients determined from laboratory shear testing. Calculated calibration coefficients for different HVS test sections were compared to evaluate the effects of asphalt mixture and structure type on predicted rutting performance. Rutting accumulation mechanisms for composite pavement sections were also investigated using X-ray Computed Tomography (CT) images taken before and after HVS rutting tests. Three-dimensional (3D) images of deformed and undeformed specimens were compared to determine the changes in air void content distributions, which were used to identify the contribution of densification to total accumulated downward rut. Changes in air void content distributions were also used to determine the significance of shear and densification related components of surface deformation in controlling rutting performance of AC layers. Results were further used to evaluate the effectiveness of repeated simple shear tests at constant height (RSST-CH) for rutting performance prediction of AC layers.

2 MECHANICS OF RUTTING ACCUMULATION

Pavement rutting can be divided into two categories: rutting of the asphalt surfacing, and rutting of the unbound layers. Rutting in the unbound layers usually results from subsidence caused by shearing and densification in unbound base, subbase and subgrade layers, and directly affects the total rutting accumulated at the surface. However, on existing pavements that are rehabilitated and where water has not been able to pass through to the unbound layers, most rutting (85 to 95 percent) is generally accumulated in the AC layers (Coleri et al., 2008). Rutting in the asphalt layers accumulates with increasing load applications and is highly sensitive to variations in temperature and traffic levels (Metcalf, 1996). Volume change (densification) and shape distortion (shear related deformation) are the two main deformation modes that control rutting accumulation. Volume change is the deformation of a material with equal principal strains in all dimensions. Bulk modulus (K) is the resistance of a material to volume change. Shear distortion can be defined as deformation without any change in volume. Resistance of a material to shear distortion is represented with the shear modulus (G^*) (Weisman et al., 2003). Typically, in situ rutting accumulation rates are higher under initial loading due to the combined effect of densification and shear distortion.

3 EXPERIMENT PROGRAM AND TEST RESULTS

3.1 *Heavy Vehicle Simulator testing*

The HVS is a mobile load frame that uses a full-scale wheel (dual or single) to traffic pavement test sections. The trafficked test section is 8 m (26 ft.) long, of which 1 m (3.3 ft.) on each end is used for turnaround of the wheel and is generally not included in analysis and reporting of results. This wheelpath length permits the testing of one slab of jointed portland cement concrete (PCC).

In this study, composite AC over PCC, full-scale pavement sections were constructed for HVS testing at the University of California Pavement Research Center facility at UC Davis (Coleri et al., 2012). Two asphalt mixture types were used in this study (Coleri et al., 2011), a dense-graded mixture with PG 64-28 polymer modified (PM) binder and a gap-graded mixture with asphalt rubber binder (PG 64-16 base binder modified with 18% crumb rubber [RHMA-G]). Both mixes were specified based on Caltrans specifications. Nominal maximum aggregate sizes (NMAS) for the

Table 1. Summary of HVS loading program.

Section	Mix Type	Design Thickness (mm)	As-built Thickness (mm)	Wheel Load (kN)	Temperature at 50 mm		Total Load Repetitions
					Average (°C)	Std Dev (°C)	
609HB	PG 64-28PM	115	116	40	49.5	1.1	63,750
				60			136,250
610HB	PG 64-28PM	65	72	40	49.8	1.0	64,000
				60			137.200
611HB	RHMA-G	115	118	40	48.7	1.1	18,503
612HB	RHMA-G	65	74	40	49.7	1.3	90,000

PG64-28PM and RHMA-G mixtures were 19 mm and 12.5 mm, respectively.

Two overlay thicknesses were tested for each of the two mix types placed on the HVS test sections: 65 mm (one lift) and 115 mm (two lifts) for thin and thick AC sections, respectively. All sections had 150 mm aggregate base layers and 180 mm thick PCC layers.

The HVS loading program for each section is summarized in Table 1. The failure criterion was defined as an average maximum rut of 12.5 mm over the full monitored section. Average maximum rut is defined as the summation of the downward deformation and upward deformation, or "humping", of material sheared to the sides of the wheelpath, averaged from 13 transverse profile measurements, at 0.5 m intervals along the 6 m wheelpath. The pavement temperature at 50 mm depth was maintained at 50°C ± 4°C to assess rutting potential under typical pavement conditions. All trafficking was carried out with a dual-wheel configuration with the centerlines of the two tires spaced 360 mm apart, using radial truck tires inflated to a pressure of 690 kPa. A channelized (no wander), unidirectional loading mode, in which the wheel travels one direction loaded and is lifted off the pavement for the return pass, was used. Channelized trafficking is used to simulate the tracking of radial tires in the wheelpath once a small rut forms, and is more aggressive than field conditions in the initial stages of rutting before tires begin to track in the ruts. Wheel speed for all tests was 8.7 km/h.

The rutting performance of the four sections is shown in Figure 1. Average maximum rut is given in Figure 1a and downward deformation only in (Figure 1b). Sections constructed with RHMA-G mix show earlier failure than the PG64-28PM mix, while the thick RHMA-G section (611HB) failed before reaching 20,000 load repetitions. Sections constructed with the PG64-28PM mix (609HB and 610HB) showed better rutting performance, with failure not observed after 200,000 load repetitions for both the thick and thin sections. The wheel load for the two sections with the PG 64-28PM mix (609HB and 610HB) was increased from 40 kN (9 kips) to 60 kN (13.5 kips) at around 64,000 repetitions. However, increasing the load did not have any significant effect on the rutting accumulation rate. The maximum rut depth, which considers both downward and upward deformation of material

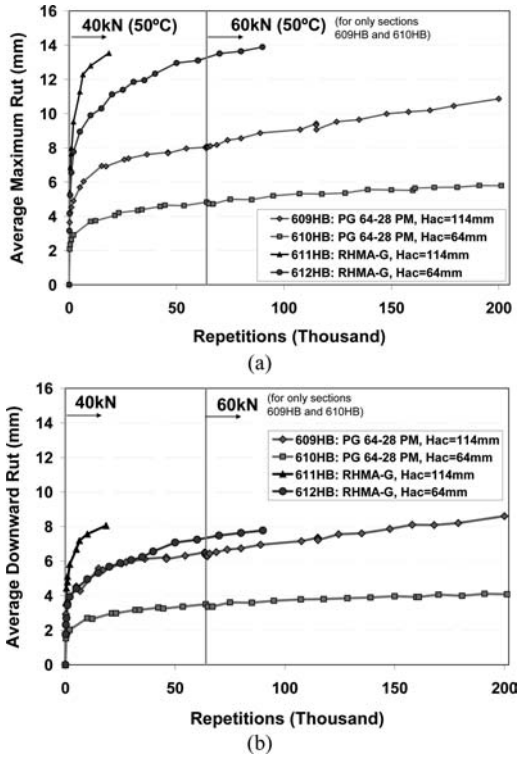

Figure 1. HVS test results (a) Average maximum rut (b) Average downward rut.

sheared to the sides of the wheelpath, is approximately 1.4 times greater than the average downward rut depth for both PG 64-28PM sections, and nearly 1.8 times greater for both RHMA-G sections, indicating that shearing of material to the side of the wheelpath is as important a contributor or more important than the downward rut.

In order to determine the contributions of shear and densification related deformations to total surface rutting, changes in air void distributions determined with X-ray CT imaging were analyzed for each section and is discussed later in this paper.

3.2 *Laboratory testing – Repeated Simple Shear Test at Constant Height (RSST-CH)*

The purpose of laboratory testing of the asphalt overlay mixes was to measure rutting performance and then use the results for the development of a laboratory performance model. RSST-CH tests were conducted on field-mixed, laboratory-compacted (FMLC) cores sawn from ingots compacted during the test section construction. Loose mix was sampled from the trucks with a skip loader immediately prior to it being tipped into the paver and then dumped next to the preparation area. The required volume of material, based on the theoretical maximum densities determined earlier in the contractor's laboratory, was weighed and then compacted, using a rolling wheel compactor, into moulds at the same temperatures as those recorded on the test track. Specimens were cored and then cut into 150 mm (6 in.) diameter and 50 mm (2 in.) thick cylindrical shear specimens.

Test specimens were subjected to repeated loading in shear using a 0.1-second haversine waveform followed by a 0.6-second rest period while the permanent (unrecoverable) and recoverable shear strains were measured. The permanent shear strain (PSS) versus applied repetitions is normally recorded until a five percent strain is reached, although AASHTO T-320 (AASHTO, 2003) calls for loading up to only 5,000 repetitions. A constant temperature is maintained during the tests.

Twelve shear tests were performed on the PG 64-28 PM mix and eighteen shear tests on the RHMA-G mix, the difference being the number of replicates, which differed based on the number of specimens available and the variability in test results for each mix. The full factorial experiment design was as follows:

- Two temperatures: 45°C and 55°C (113°F and 131°F)
- Three stresses: 70 kPa, 100 kPa, and 130 kPa (10.2, 14.5, and 18.9 psi)
- Three replicates for the RHMA-G mix and two replicates for the PG 64-28 PM mix.

Air void contents were measured using the *CoreLok* method (AASHTO, 2009). Table 2 summarizes the air void distribution categorized by mix type, test temperature, and test shear stress level. The differences in air void content distributions between the two mixes are clearly apparent. The mean differences for the mean air void content of the RHMA-G mix was 5.4 percent and 5.9 percent for the PG 64 28 PM mix. Laboratory compacted mixes had better compaction than the test track for both mixes. Significant differences between the field and laboratory compacted mix air voids was not expected to introduce bias into the test results because volume change (densification) is not permitted in RSST-CH tests.

Figure 2 shows the RSST-CH test results. Permanent deformation accumulation rate was extremely fast for the RHMA-G mix. This result indicated that early rutting failure was likely to be observed for that mix if exposed to pavement temperatures at 50 mm depth (2 in.) of 45°C to 55°C (113 to 131°F). The PG 64-28 PM mix showed better performance with a slower deformation accumulation rate.

Table 2. Summary of air void contents of FMLC shear test specimens.

		PG64-28PM		RHMA-G	
Temp (°C)	Stress (kPa)	Mean	SD	Mean	SD
45	70	4.1	0.4	8.5	0.6
	100	4.1	0.9	9.4	0.6
	130	3.9	1.2	8.5	0.4
55	70	4.9	0.3	7.8	1.2
	100	4.2	0.2	7.5	1.3
	130	2.9	0.4	7.5	0.3
Overall		4.0	0.8	8.2	1.0

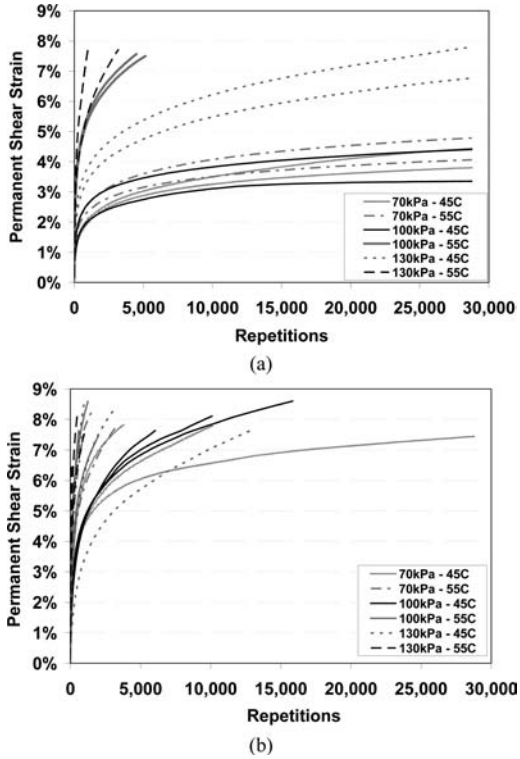

Figure 2. RSST-CH test results (a) PG64-28PM mix (b) RHMA-G mix.

4 RUTTING PERFORMANCE PREDICTION AND MODEL CALIBRATION

4.1 *Calibration of incremental-recursive rutting prediction models in CalME using HVS experiments*

4.1.1 *General procedure*

The mechanistic-empirical approach to pavement design makes use of fundamental physical properties

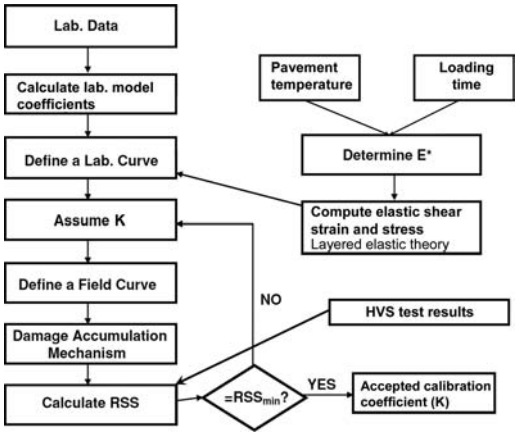

Figure 3. General framework for rutting model calibration. (Coleri, et al., 2008).

and a theoretical model to predict stresses, strains, and deflections, i.e., the pavement response, caused by a load on the pavement.

CalME uses a modified version of the shear based procedure developed by Deacon et al. (2002) to predict accumulated rut depth in HMA layers by considering the effects of temperature, material properties, load levels, and speed. *CalME* follows an increment-recursive (IR) procedure when simulating pavement performance where material properties are revised for each time increment by considering the changes in environmental conditions, traffic characteristics, and HMA stiffness. Calculated damage (permanent deformation for rutting, stiffness change otherwise) for each time increment is recursively accumulated to be able to predict the pavement condition at any point in time. The IR mechanism has been found to be an effective approach for considering damage accumulation, and has been implemented in *CalME* (Ullidtz et al., 2006), and to a partial extent in the MEPDG (MEPDG, 2004). The general framework followed for rutting performance model calibration is given in Figure 3.

The gamma function used to calculate permanent shear strain by using elastic shear strain, number of repetitions, and shear strain as the independent variables is given as follows (Ullidtz et al., 2008):

$$\gamma^i = \exp\left(A + \alpha \times \left[1 - \exp\left(-\ln(N)/\gamma\right) \times \left(1 + \ln(N)/\gamma\right)\right]\right) \times \exp\left(\beta \times \tau/\tau_{ref}\right) \times \left(\gamma^e\right)^{\delta} \quad (1)$$

where

γ^i = permanent shear strain

γ^e = elastic shear strain

τ = shear stress

N = number of load repetitions

τ_{ref} = reference shear stress (0.1 MPa = atmospheric pressure)

A, α, β, γ and δ are model coefficients determined from the RSST-CH results.

Table 3. Model Coefficients for *CalME* Rutting Model (Eq. 1) for Mixes, PG 64-28 PM and RHMA.

Mix	A	α	τ_{ref}	β	γ	δ
64-28PM	1.912	2.649	0.1	0	4.208	1
RHMA-G	0.359	3.943	0.1	0	1.719	1

Note: K = Calibration coefficient (Described in Equation 3); E* = Elastic modulus; RSS = Residual sum of squares (Described in Equation 4).

Model coefficients for Equation 1 for this study were calculated based on laboratory RSST-CH data for the HMA mixes of the HVS (PG 64-28 PM and RHMA-G) test sections by using nonlinear regression. Calculated model coefficients are given in Table 3.

Shear stresses at 50 mm (2 in.) depth at the edge of the tire were determined using the calculated stiffnesses, traffic-vehicle characteristics, and material properties as inputs to a layered-elastic program. Elastic shear strain values for each repetition interval were calculated by using the following equation (Ullidtz et al., 2008):

$$\gamma^e = \frac{\tau}{E_i/(1+\nu_i)} \quad (2)$$

where

τ = shear strain calculated from layer elastic theory

E_i = modulus of layer i

ν_i = Poisson's ratio for layer i (assumed to be 0.35 for all layers)

Calculated elastic strain values for the corresponding repetition interval are used in Equation 1 to calculate plastic shear strain. For the calibration of the model, the coefficient for the shear stress variable (β) is assumed to be equal to zero for all material types because the effect of shear stress on accumulated permanent shear strain is simulated using the elastic shear strain variable. *CalME* assumes that rutting is confined to the upper 100 mm of the asphalt layers (Ullidtz et al., 2008), therefore calculated plastic shear strains (from Equation 1) for each repetition interval are multiplied by 100 mm to calculate corresponding rutting deformation. Calculated rut depths for each repetition interval are accumulated based on the IR procedure to develop the final rutting curve.

The optimum calibration coefficient (K) is calculated by relating calculated permanent shear strain values to measured downward rut depths using the following equation and optimization:

$$dpi = K \times hi \times \gamma^i \quad (3)$$

where

K = calibration coefficient

h_i = thickness of layer i (up to 100 mm, assumed to be 100 mm for thicker asphalt layers)

dp_i = rut depth

The procedure given in Figure 3 can be repeated several times to develop rutting deformation curves for several calibration coefficients (K). The optimum calibration coefficient to calibrate between the laboratory regression equations and the measured rutting can be determined on the basis of a fitness function given as follows:

$$RSS = \sum_{i=1}^{n} (\text{Predicted Rut Depth} - \text{Measured Rut Depth})^2$$

where

n: number of rut depth measurements

RSS: residual sum of squares

The plot for calibration coefficient versus RSS can be fitted by a second order polynomial curve whose minimum RSS will correspond to an optimum calibration coefficient that can be used for design.

4.1.2 *Calibration results*

CalME rutting prediction models were calibrated using the results of HVS experiments by following the procedure described in the previous section and using the calculated rutting model coefficients that were determined from laboratory test results. Wheel speed (loading time) and collected asphalt temperature data were used for the prediction of stiffnesses. Shear stresses at 50 mm depth at the edge of the tire were calculated by using the calculated stiffnesses, traffic-vehicle characteristics, and material properties as inputs to a layered-elastic program. Calculated elastic strain values for the corresponding repetition interval were used to calculate plastic shear strain. Calculated rut depths for each repetition interval were accumulated based on the IR procedure to develop the final rutting curve. In this study, measured downward rut depths (layer compression compared to the original surface of the pavement) were used for model calibration.

HVS repetitions were converted to continuous time (year) for calibrations. Figure 4 shows the results of the calibrations.

The *Kcalib* rutting curve in each plot is the calibrated rutting prediction curve, while the *Kavg* curve is the predicted rutting curve using the calibration coefficient obtained by averaging the calibration coefficients of all four HVS test sections. *Kavg* was assumed to be the general calibration factor for composite pavements. It can be observed that *Kavg* gives reasonable predictions for all sections. Although the 115-mm thick RHMA-G section (611HB) showed early failure, it can be observed that measured performance can be effectively predicted with *CalME* models without having extreme differences in calibration coefficients. In other words, *CalME* was able to predict the early failure for that section with the same calibration coefficient used for the other sections.

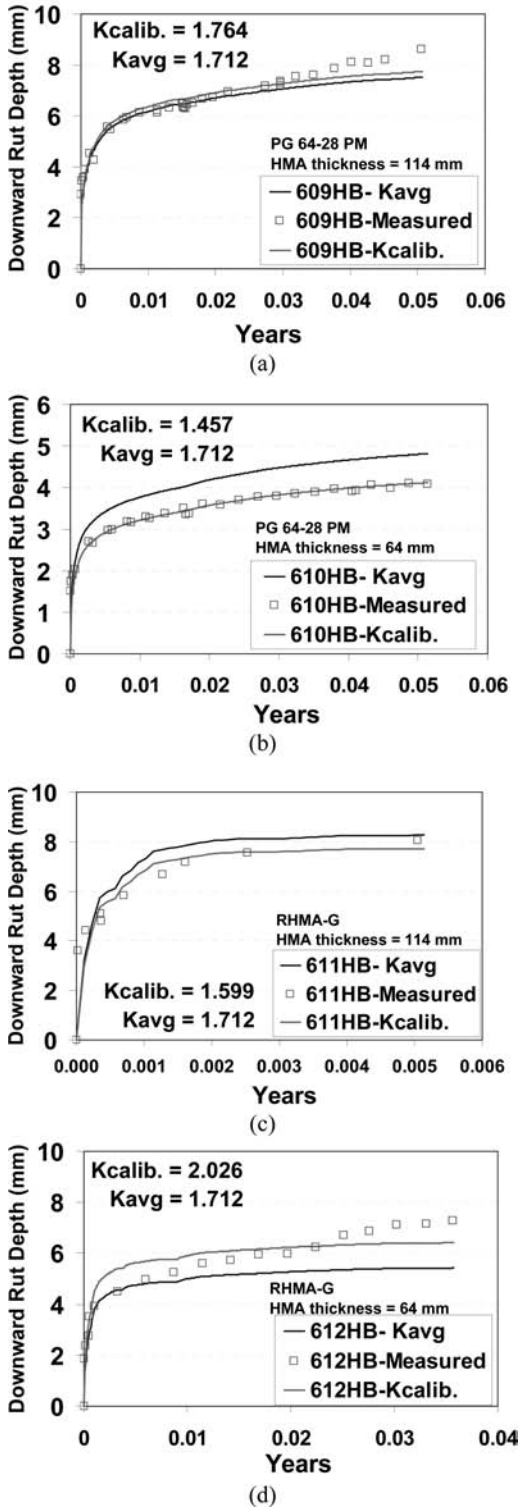

Figure 4. HVS test results compared with calibrated *CalME* rutting model predictions (a) 609HB – PG64-28PM – Thick (b) 610HB – PG64-28PM – Thin (c) 611HB – RHMA-G – Thick (d) 612HB – RHMA-G – Thin.

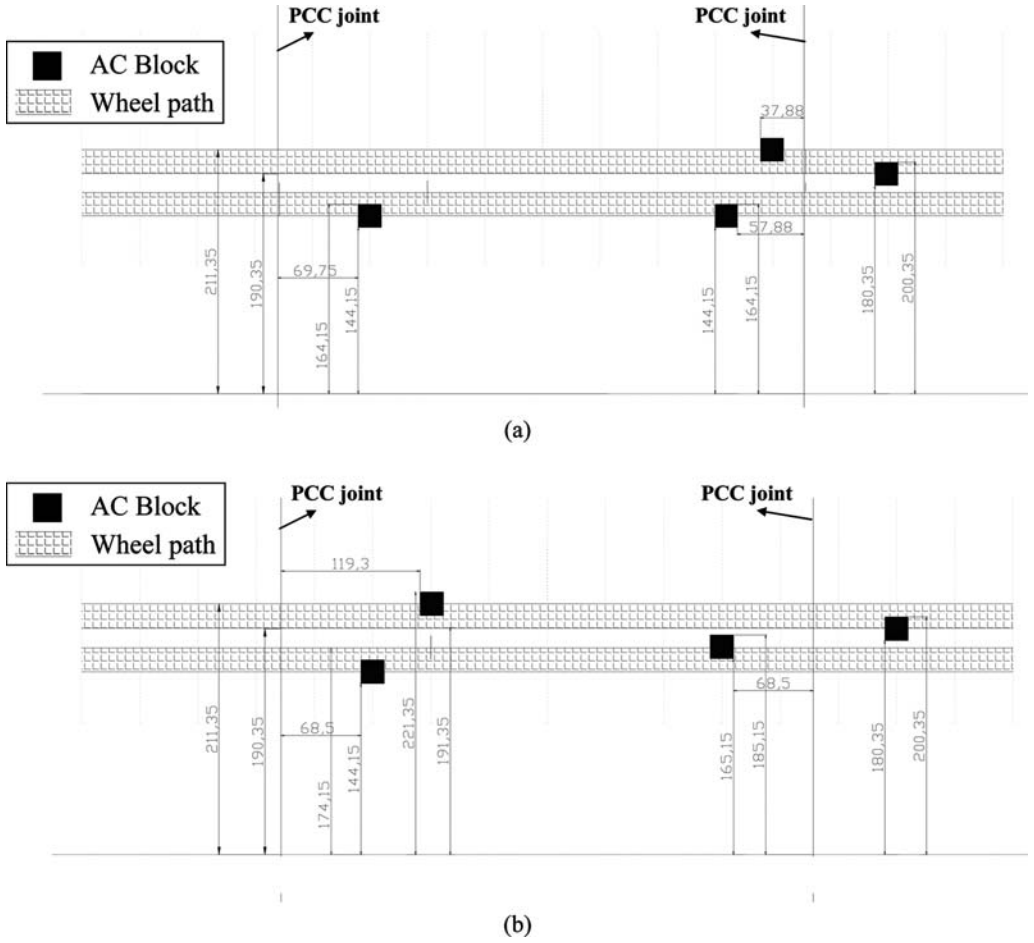

Figure 5. Locations for the AC blocks (scaled – Dimensions in cm) (a) Sections 609HB and 611HB with thick (115 mm) AC layer (b) Sections 610HB and 612HB with thin (65 mm) AC layer.

5 INVESTIGATION OF RUTTING MECHANISMS BY X-RAY COMPUTED TOMOGRAPHY IMAGING

5.1 *General procedure for X-ray CT image data collection*

The detailed procedure followed for X-ray CT image data collection for HVS samples (before and after HVS testing) is described by Coleri et al. (2011). Changes in AC microstructure with HVS loading were determined by comparing the X-ray CT images taken before and after HVS testing. Four blocks were sawn from each HVS test section (16 blocks from four HVS rutting sections) to obtain the complete deformation profile. AC blocks were distributed over the HVS test sections to avoid localized failure problems around the blocks. Figure 5 shows the locations for the AC blocks. Only one block was sawn from the upper wheel path of the thick-AC sections (609HB and 611HB) to prevent damage to the strain gauge cables (at 50 mm depth) in these sections. Therefore, only half of the inner wheelpath profiles were analyzed in this study for the thick-AC sections. The asphalt concrete blocks were scanned to determine the microstructure of the blocks before testing. Three dimensional (3-D) distributions of air voids were determined using these images.

Scanned AC blocks were replaced in their original locations using a fast-setting epoxy. HVS loading was applied until the surface rutting failure point was reached. Deformed AC blocks were re-sawn to perform after-testing X-ray CT scanning. Deformed and un-deformed 3-D air void distributions were compared to determine the changes in air void content distributions under HVS trafficking, which were used to identify the contribution of densification to total accumulated downward rut.

5.2 *X-ray CT Image Processing*

An X-ray CT image is simply the spatial distribution of the attenuation coefficients measured by the detectors.

A three dimensional image of a specimen can be generated by combining the image slices reconstructed by the X-ray CT imaging. The quality of the 3-D image will depend on the X-ray CT image resolution. In this study, horizontal sample images were taken at every 1 mm interval distance while the resolutions for the other two dimensions were 0.24 mm. At each sampling point within the sample volume the X-ray CT scanner measures a value that is related to the density and atomic number of the material at that particular point. These measured values are then converted to grayscale values (Simpleware, 2010). The gray scale intensities for the aggregates, air voids and mastic range from −1,000 to +3,095, but these values were rescaled to the range from 0 to 255. Because aggregates are denser than mastic and air voids, they will occupy the higher portion of the intensity scale, while air voids, with their low density, will be at the lowest intensity portion, and mastic intensity will be in between aggregate and air void intensities.

AC samples sawn from the HVS test sections were analyzed to evaluate the changes in microstructure with HVS trafficking. For that purpose, images taken before and after testing were processed to identify the distribution of air voids and aggregates within the sample block volume. Air void distributions were determined using the *Simpleware* software. Air void percentages for each asphalt mixture sample were determined using the standard *CoreLok* method. The total volume of the asphalt mixture sample was calculated for the complete zero to 255 intensity range. The upper limit for the air void intensity range was determined by trial and error to match the measured air void contents. The average range for the PG 64-28 PM mix AC blocks was determined to be zero to 119 with calculated average air void content of 9.9% while the average range for the RHMA-G mix AC blocks was zero to 102 with calculated average air void content of 13.6%. After the thresholds for the air void domain were determined, masks with specific colors were assigned to clearly visualize the distribution of air void domain in the total block volume. Figure 6 illustrates the air void distributions for Block 1 from HVS test section 609HB (PG64-28PM, 115-mm thick) before and after HVS trafficking.

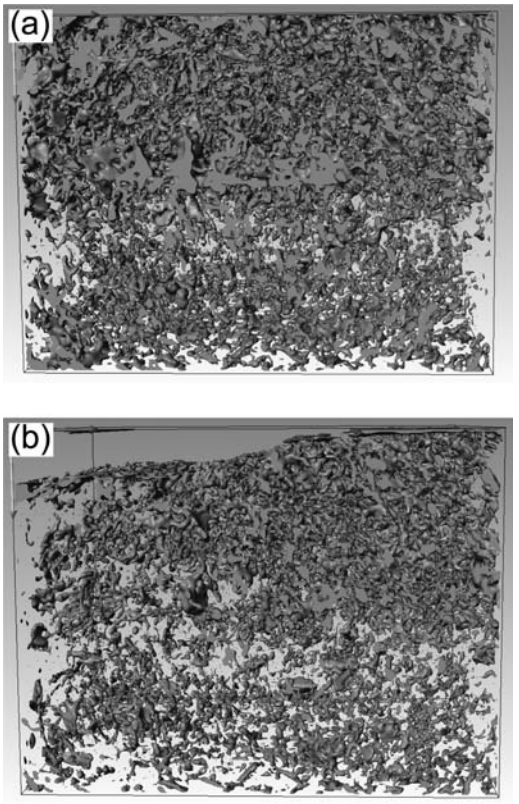

Figure 6. The changes in air void contents after HVS trafficking for the AC block from section 609HB – PG64-28PM – 115 mm (colored volumes are air voids) (a) Before trafficking (b) After trafficking. Note: HVS wheelpath is on the left half of the figures.

5.3 *Calculation of the contribution of air void reduction related deformation (densification) to the total accumulated surface deformation*

Changes in air void content profiles were determined by comparing the air void content distributions of the AC blocks before and after HVS testing. The three dimensional images were divided into 2.93 mm thick volumes along the horizontal direction. The calculated change in air void content percentages for each unit volume were multiplied by the height of the volume slice to calculate the air void content related surface deformation. Changes in block surface profile with HVS trafficking were also determined by taking surface profilometer measurements on the blocks before and after testing.

Laser profilometer-measured (total) and air void related surface deformation, calculated from X-ray CT images, profiles are given in Figure 7. Significant densification occurred under the wheelpaths, as expected. Air voids were also observed to be translated laterally by the shear stresses caused by HVS trafficking. On each block, the locations close to the humps (next to the wheelpath) were exposed to smaller densification related downward deformations, while even upward movements were observed for sections with thinner AC layers (Figure 7c and Figure 7d) as a result of the shear related air void movement.

The contribution of air void reduction related deformation (densification) to the total accumulated surface deformation was determined by comparing the profiles in Figure 7. The air void reduction related deformation in the wheelpath, was isolated from the complete block densification profile to calculate the average air void reduction related rutting under the HVS wheel. The ratio of densification related

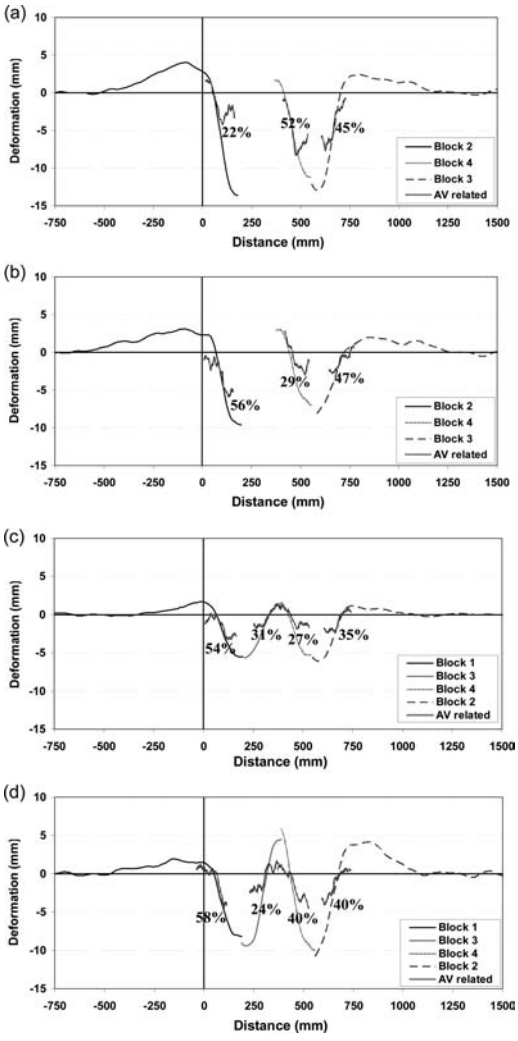

Figure 7. Comparison of profilometer-measured and air void related surface deformation profiles. (a) PG64-28PM, 155 mm; (b) RHMA-G, 115 mm; (c) PG64-28PM, 65 mm; (d) RHMA-G, 65 mm.

deformation to the total surface downward deformation was determined for each block and is shown as a percentage on the profile curves in Figure 7. The average contribution of densification related deformation to the total surface deformation was determined to be 40, 44, 37 and 41 percent for thick-PG 64-28PM, thick-RHMA-G, thin-PG 64-28PM and thin-RHMA-G sections, respectively. This result shows that a significant part of the measured downward rut was a result of densification. In addition, although the average air void content of the RHMA-G blocks was 37 percent higher than the PG 64-28PM blocks according to the *CoreLok* measurements, the contribution of air void reduction to total downward rutting was close for both mix types at both thicknesses. In other words, it is not possible to predict future rutting performance of the sections from the densification because it was approximately the same. Shear related deformation appeared to control the long-term rutting performance of the test sections while densification was an initial contributor at the very earlier stages of trafficking.

5.4 *Calibration of incremental-recursive rutting prediction models in CalME using the shear-related component of surface deformation*

RSST-CH simulates the shear performance of the AC mixes while densification is ignored. The general assumption is that shear related deformation controls the level of total surface deformation while densification is described as a minor contributor affecting the initial stages of the test. In this study, calibration coefficients were calculated to range from 1.46 to 2.03. A calibration coefficient that is equal to 1.0 suggests that in situ performance of the mix can be directly predicted based on the laboratory test results without using any HVS or field data (Equation 3). In this study, calculated calibration coefficients that are larger than 1.0 are attributed to the densification related component of the surface rutting, which cannot be simulated with RSST-CH.

In order to calculate the calibration coefficients for only the shear related component of surface rutting, the densification component of downward rut measurements were excluded from the surface downward rut using the contribution of densification percentages calculated in previous section. The assumption for this procedure is that contribution of densification to total surface rutting calculated by comparing X-ray CT images taken before and after HVS tests also holds for the intermediate repetitions. Although contribution of densification will be higher at the initial stages of the test, it is not possible to collect X-ray CT image data at intermediate repetitions to calculate the actual contribution. Thus, contribution of densification to total surface rutting calculated by comparing the before and after testing X-ray CT images is assumed to be an average contribution value for the overall HVS test and used for the calibration.

Calibration coefficients calculated for the shear related component of total surface rutting were 1.062, 0.897, 0.921 and 1.191 for thick-PG 64-28PM, thick-RHMA-G, thin-PG 64-28PM, and thin-RHMA-G sections, respectively. The calibration coefficients for all test sections were close to 1.0 after the exclusion of densification from total surface rutting. This result suggests that RSST-CH can effectively simulate the in situ shear performance of AC mixes. Figure 8 shows the predicted rutting curves for all test sections when calibration coefficients were assumed to be equal to 1.0 (in other words, not using the calibration coefficient in Equation 3 and directly predicting shear related surface rut from RSST-CH results). Results show that predicted rutting curves for a calibration coefficient of 1.0 are close to measured shear related rutting for all sections.

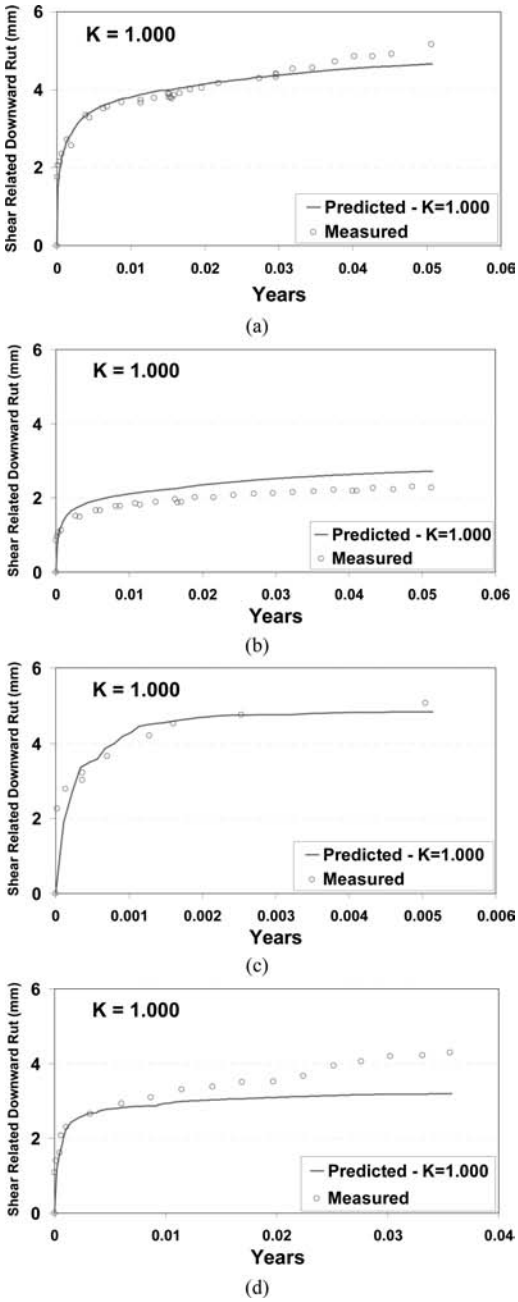

Figure 8. Predicted rutting curves for all test sections when calibration coefficients were assumed to be equal to 1.0. (a) 609HB, PG64-28PM, Thick; (b) 610HB, PG64-28PM, Thin; (c) 611HB, RHMA-G, Thick; (d) 612HB, RHMA-G, Thin.

6 CONCLUSIONS

In this study, *CalME* rutting prediction models were calibrated by using the results of HVS experiments and following a shear based IR procedure using rutting model coefficients determined from laboratory shear testing. Early failure of RHMA-G mixes were investigated by determining the changes in AC microstructure before and after HVS trafficking using X-ray CT images. Three-dimensional images of deformed and un-deformed specimens were compared to determine the changes in air void content distributions for PG64-28PM and RHMA-G mixes, and to quantify the contribution of air void reduction to total downward rutting. Measured contributions of air void reduction to total downward rutting for each HVS test section were used to calculate the shear related downward deformation, which was used to perform a shear based model calibration to determine the effectiveness of RSST-CH in predicting rutting performance of asphalt mixes.

Results of this study can be summarized as follows:

- Although the thick RHMA-G section (611HB) showed early failure, measured performance was effectively predicted with *CalME* models without having extreme differences in calibration coefficients.
- The average contribution of densification related deformation to the total surface deformation was determined to be 40, 44, 37 and 41 percent for thick-PG 64-28PM, thick-RHMA-G, thin-PG 64-28PM and thin-RHMA-G sections, respectively. This result shows that a significant part of the measured downward rut was a result of the densification.
- Although the average air void content of RHMA-G blocks was 37 percent higher than the PG 64-28PM blocks according to the *CoreLok* measurements, the contribution of air void reduction to total downward rutting was close for both mix types at both thicknesses.
- Shear related deformation appears to control the long-term rutting performance of the test sections, while densification was an initial contributor at the very earlier stages of the trafficking.
- Calibration coefficients for the *CalME* rutting model were calculated to range from 1.46 to 2.03. Calibration coefficients larger than 1.0 can be accepted to be a result of the densification related component of surface rutting, which cannot be simulated with RSST-CH.
- Calibration coefficients calculated for the shear related component of total surface rutting were 1.062, 0.897, 0.921 and 1.191 for thick-PG 64-28PM, thick-RHMA-G, thin-PG 64-28PM and thin-RHMA-G sections, respectively. Calibration coefficients for all test sections were close to 1.0 after the exclusion of densification from the total surface rutting. This result suggests that RSST-CH effectively simulates the in situ shear resistance of AC mixes.

Although the results obtained in this study provide considerable insight, further study is required to extend the analysis. Results should be validated by performing a field performance study. Falling weight deflectometer (FWD) tests should be conducted at

various locations on highway sections to determine the variability of stiffness for all pavement layers. In addition, pavement layer thicknesses should be measured by coring and/or ground penetrating radar. Rut depths should be measured at different time points by using profilometers. Rut depths, thicknesses and stiffnesses from these in situ measurements should be combined with data from weather and weigh-in-motion (WIM) stations to calibrate laboratory models. The effect of asphalt mix aging can also be incorporated into the calibration procedure by using the aging equations given in *CalME* and the results of the indirect tensile and FWD tests.

ACKNOWLEDGMENTS

This paper describes research activities that were requested and sponsored by the California Department of Transportation (Caltrans), Division of Research and Innovation. Test track construction and HVS testing were funded by SHRP II Project R21. Caltrans and SHRP II sponsorship is gratefully acknowledged. The contents of this paper reflect the views of the authors and do not reflect the official views or policies of the State of California, the Federal Highway Administration, or the SHRP II program.

REFERENCES

Brown, S.F. 2004. Accelerated Pavement Testing in Highway Engineering. *Proceedings of the Institution of Civil Engineers and Transportation*, 157(3), pp. 173–180.

Coleri, E., Tsai, B.W. and Monismith, C. L. 2008. Pavement Rutting Performance Prediction by Integrated Weibull Approach. In *Transportation Research Record: Journal of the Transportation Research Board*, No. 2087, Transportation Research Board, Washington, D.C., pp. 120–130.

Coleri, E., Wu, R. Signore, J.M. and Harvey, J.T. 2012. Rutting Performance Evaluation of Rubberized Gap-Graded and Polymer Modified Dense Graded Mixes under HVS Testing. *CD-ROM Proceedings 91st Transportation Research Board Annual Meeting*.

Coleri, E., Harvey, J.T. Yang, K. and Boone, J.M. 2011. A Micromechanical Approach to Investigate Asphalt Concrete Rutting Mechanisms. Submitted for Publication to *Construction and Building Materials*.

Deacon, J.A., Harvey, J.T., Guada, I., Popescu, L. and Monismith, C.L. 2002. Analytically Based Approach to Rutting Prediction. In *Transportation Research Record: Journal of the Transportation Research Board, No. 1806*. Transportation Research Board, Washington, DC.

Epps, J.A., Hand, A. Seeds, S., Schulz, T., Alavi, S., Ashmore, C., Monismith, C.L., Deacon, J.A., Harvey, J.T. and Leahy, R. 2002. *Recommended Performance-Related Specification for Hot Mix Asphalt Construction: Results of the WesTrack Project*. NCHRP Report 455, Transportation Research Board, Washington, DC.

MEPDG. 2004. *Guide for Mechanistic-Empirical Design of New and Rehabilitated Pavement Structures.* National Cooperative Highway Research Program, Report 1-37A.

Metcalf, J. 1996. *Application of Full-Scale Accelerated Pavement Testing*. National Cooperative Highway Program, Synthesis of Highway Practice Rep. No. 235.

Ullidtz, P., Harvey, J.T., Tsai, B.W. and Monismith, C.L. 2006. *Calibration of Incremental-Recursive Flexible Damage Models in CalME Using HVS Experiments.* Davis and Berkeley, CA: University of California Pavement Research Center. UCPRC-RR-2005-06.

Ullidtz, P., Harvey, J.T., Tsai, B.W. and Monismith, C.L. 2008. Calibration of Mechanistic-Empirical Models for Flexible Pavements Using the California Heavy Vehicle Simulators. In *Transportation Research Record: Journal of the Transportation Research Board, No. 2087*, Transportation Research Board, Washington, DC. pp. 20–28.

Weissman S.L., Harvey, J.T. and Monismith, C.L. 2003. *Rutting Characterization of Asphalt Concrete Using Simple Shear Tests*. Chapter Prepared for ASCE Publication, Modeling of Asphalt Concrete.

White, T., Haddock, J. Hand, A. and Fang, H. 2002. *Contributions of Pavement Structural Layers to Rutting of Hot Mix Asphalt Pavements.* NCHRP Report No. 468, Transportation Research Board Washington, DC.

Simpleware. *ScanIP and +ScanFE Software.* Simpleware Ltd, Innovation Centre, Rennes Drive. Exeter EX4 4RN, UK. http://www.simpleware.com; 2010.

This page intentionally left blank

Advances in Pavement Design through Full-scale Accelerated Pavement Testing – Jones, Harvey, Mateos & Al-Qadi (Eds.)
© 2012 Taylor & Francis Group, London, ISBN 978-0-415-62138-0

Lessons learned from the application of the *CalME* asphalt fatigue model to experimental data from the CEDEX test track

A. Mateos, J.P. Ayuso, B. Cadavid & J.O. Marrón
CEDEX Transport Research Center, Madrid, Spain

ABSTRACT: Predicting asphalt fatigue evolution in the field is difficult. Very few models are effective for this complex process, and even less where actual damage levels, determined from structural evaluations, can be efficiently incorporated to improve previous performance predictions. One model evaluated, *CalME* (California Mechanistic-Empirical Software for Structural Design of Flexible Pavements), incorporates an incremental-recursive procedure based on mechanistic-empirical principles and was used to study and reproduce the deterioration process at the CEDEX Test Track. Experimental data for this evaluation came from four full-depth pavements tested over 28 months at the track, during which bearing capacity and surface cracking data was collected. This provided detailed information regarding asphalt layer deterioration under changing environmental conditions. Special attention was paid to the accumulation of damage as a function of loads and temperature and how this damage, together with aging and post-compaction under traffic, determine the stiffness of the asphalt layer. This paper presents experimental evidence that supports the ability of the *CalME* model to reproduce the main aspects of asphalt performance in flexible pavements and to predict future asphalt mixture performance, after recalibration from field data. The model was initially calibrated from laboratory fatigue tests and later recalibrated based on FWD tests conducted at an early stage of the deterioration process. After this early recalibration, the model was able to predict future asphalt layer deterioration until an ultimate damage level was reached.

1 INTRODUCTION

Predicting asphalt fatigue evolution in the field is difficult. The large number of variables that contribute to the deterioration process, the complexity of the process itself, and the interaction with other distress mechanisms are some of the reasons for this. Preventing pavement failure has significant economic implications, not only at initial construction but also throughout the service life. Consequently, an accurate prediction of asphalt fatigue will allow optimization of design, maintenance, and rehabilitation actions to minimize the overall cost.

Figure 1 represents the typical evolution of asphalt layer modulus in a flexible pavement during its service life. Damage accumulation leads to this modulus reduction up to a point where cracking begins. This cracking process will continue until a "failure" condition is reached after N_f load applications. Prediction of N_f has been the goal of classical analytical design methods for at least two decades. However, the ultimate goal of an asphalt fatigue model should go further if it is deemed to be efficient in minimizing the significant costs of pavements construction and rehabilitation. These advanced goals can be stated as the ability to:

1. Predict asphalt modulus evolution.
2. Determine asphalt damage from actual modulus.
3. Determine asphalt cracking from damage.

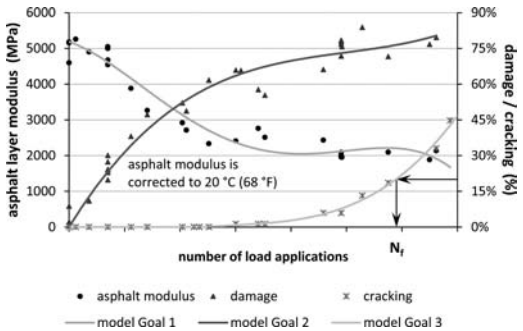

Figure 1. Evolution of asphalt fatigue during service life of a flexible pavement.

In theory, there are very few models that can achieve these goals. One of the few that can is the widely recognized *California Mechanistic-Empirical Software for Structural Design of Flexible Pavements* or *CalME* (Ullidtz et al. 2006). This program incorporates three design levels of increasing complexity; the most advanced being an incremental-recursive procedure based on mechanistic-empirical principles. *CalME* incorporates specific models for different distress mechanisms, including permanent deformation of asphalt, granular and soil layers, longitudinal unevenness, stabilized soils fatigue, and bottom-up asphalt fatigue.

A research effort has been conducted at CEDEX Transport Research Center, in cooperation with the University of California Pavement Research Center, to evaluate the potential of *CalME* asphalt fatigue model to predict actual performance observed from four flexible sections tested at the CEDEX Test Track. Important lessons have been learned from this research effort that help to understand the complex process of asphalt mixture deterioration in the field. The main lessons are described and analyzed in this paper, with special emphasis on the application of the *CalME* model to in-service pavements. The reason for this is the increasing importance of structural evaluation in Spain and other countries with a consolidated road network, where most investments are dedicated to maintenance and rehabilitation rather than new pavement construction. Under these circumstances, the assessment of actual pavement structural condition and the prediction of its future evolution become priorities, which are typically accomplished by conducting periodic structural evaluations. These evaluations provide large amounts of data that, if appropriately processed, can be incorporated into the fatigue model, thus improving previous performance predictions.

1.1 *Objective*

The objective of the research presented in this paper is the evaluation of the applicability of the *CalME* asphalt fatigue model as a tool for interpreting deflection testing data from in-service pavements and, based on this, for the prediction of future asphalt fatigue performance.

1.2 *Research approach*

The CEDEX Test Track is a linear-circular combined accelerated pavement testing (APT) facility located outdoors (Mateos, 2008). Traffic is simulated by two automatic vehicles that continuously move around a closed circuit, constructed in a test pit. Six asphalt surfaced sections (15–19 m long) were tested in a research project that focused on subgrade performance. The sections consisted of a 120 to 150 mm (4.5 to 6.0 in.) asphalt layer placed directly on top of medium to high quality subgrades, as shown in Figure 2. The two sections with cement-stabilized soils were not included in this particular research, since the critical distress mechanism was not conventional (bottom-up) fatigue cracking. Additional information about the test is as follows:

- Test period: 2007/08/29 through 2009/12/31
- Total number of passes: 1,323,600
- Vehicles loading: 65 kN (14.6 kip) dual wheel (corresponding to 130 kN axle)
- Transverse wander: ±195 mm (±7.7 in.)
- Vehicle speed: 30 to 40 km/h (19 to 25 mph)
- Environmental conditions: Open air; water table height changes with rainfall

Actual structural performance of the sections was periodically evaluated throughout the test. Bearing capacity was measured with a falling weight deflectometer (FWD) and surface cracking was measured by means of visual inspection. FWD testing was conducted at between 15 and 20 points along each section, and the average deflection bowl was used to backcalculate asphalt layer modulus using *Evercalc*. The temperature assigned to the asphalt modulus was the mean value from two thermocouples embedded in the asphalt layer (one at the top and one at the bottom).

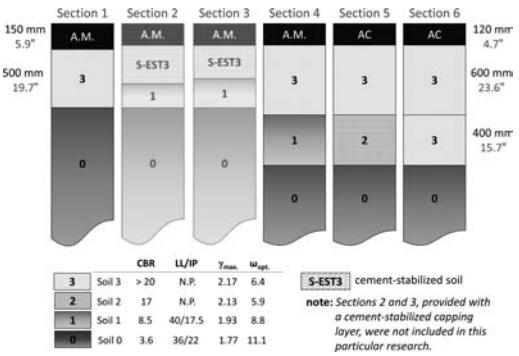

Figure 2. Flexible sections included in the test.

The pattern of the evolution of the stiffness of the asphalt layer, determined from FWD testing, was studied as a function of three main factors: damage, aging, and densification under traffic loads. The hypotheses of the *CalME* model concerning the effects of these three factors were evaluated by comparing the actual pattern with the pattern expected according to the model. The *CalME* asphalt fatigue model was initially calibrated in the laboratory, by conducting 4-point bending fatigue tests at 10°C, 20°C and 30°C. Fatigue tests were conducted in controlled-deflection mode following European Standard EN 12697-24 Annex D "*Four-point bending test on prismatic shaped specimens*". A shift factor was then introduced, according to the *CalME* approach, which takes into account the beneficial effects of rest periods between loads. The unknown part of the shift factor was determined on the basis of field data collected after 140,000 load repetitions on the track. The ability of the model to predict future performance was evaluated by comparing actual asphalt layer modulus evaluated from FWD testing to model predictions at this point.

The *CalME* transfer function for asphalt cracking was evaluated by comparing measured cracking to model predictions. Actual damage estimated from FWD testing was used as input to specifically evaluate this transfer function.

Finally, an application example is presented where the model is used to analyze the structural response of the sections in terms of deflection. Research is now under way to study other response variables that were measured by embedded sensors, in particular horizontal strain in the asphalt and vertical stress and strain in soils.

The actual *CalME* software was not used for this research, only the model for considering damage. This allowed some flexibility to work with available data, but required additional effort and missed some of the potential of *CalME*. The *CalBack* backcalculation program was also not used. This program incorporates specific unique features that optimize FWD testing data (Lu, et. al., 2009).

2 DETERMINATION OF ASPHALT DAMAGE FROM STRUCTURAL EVALUATIONS

The ratio of the actual modulus of the asphalt layer to the original value represents an indicator of the damage in the material. However, the quantification of damage from this ratio is not straightforward for two main reasons:

1. The evolution of asphalt modulus in the field is not only related to damage. It is widely accepted that aging and post-compaction under traffic are two main factors that must also be considered.
2. For a particular level of damage, the ratio $E_{actual}/E_{undamaged}$ is not independent of the temperature and frequency content of the FWD loading pulse.

CalME uses the *MEPDG* sigmoidal curve for the asphalt mixture dynamic modulus, according to Equation 1. Parameters for this equation are determined in the laboratory by conducting temperature and frequency sweep dynamic modulus tests.

$$\log(E) = \delta + \frac{\alpha}{1 + e^{\beta + \gamma \log(fr)}} \quad (1)$$

Original asphalt layer moduli can also be obtained by backcalculating FWD measurements taken immediately after construction, before trafficking. These values are representative of the undamaged asphalt mixture. A good correlation is typically found when these moduli are compared to master curve values, provided that a correct frequency is chosen that is representative of the FWD loading pulse. This frequency was 15 Hz for the particular load and buffer configuration of the Kuab device used for this particular study. Figure 3 shows the good agreement achieved for the four sections included in this study. It can be concluded that the original master curve constitutes a reliable reference to compare to FWD backcalculated moduli during the service life of the pavements.

Figure 4a shows the asphalt layer modulus values that were obtained by backcalculation from FWD testing throughout the study. Only results for Section 5 are presented in this paper, with results for the other sections in Mateos et al. (2012). Three issues in Figure 4a deserve special consideration:

1. When temperatures below 15°C (59°F) are considered, modulus reduction is clear during the test. In particular, modulus decreases consecutively throughout the following load application measurement intervals: 0, 140,000, 200,000, 275,000, 920,000, and 1,323,000.
2. When temperatures over 30°C (86°F) are considered, the modulus tends to converge to the original (undamaged) values.
3. No clear evolution can be observed for intermediate temperatures, except for the highly damaged material after one million cycles. The asphalt layer modulus actually tended to increase between 500,000 and 730,000 load repetitions. For this last cycle, the "apparent damage" appeared to be less than that recorded after 200,000 and 275,000 load repetitions.

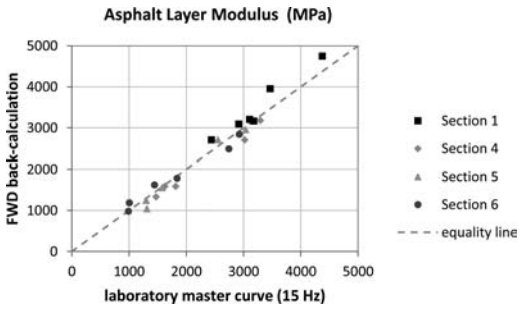

Figure 3. Comparison between laboratory and FWD backcalculated moduli

It is evident that this particular pattern is directly related to the specific sections that were tested and to the specific loading and environmental conditions under which the test was performed. However, the *CalME* approach actually shows that the pattern reflects different phenomena that take place to a greater or lesser extent in every flexible pavement during its service life. In particular, it reflects the combined effects of damage, aging and densification under traffic, as discussed below.

CalME introduces aging and densification under traffic by increasing the δ parameter in the master curve, as shown in Equation 2. This is equivalent to multiplying the modulus by the factor $10^{\Delta\delta}$ for any combination of temperature and frequency. Damage is introduced by multiplying the α parameter by $(1-\omega)$. As damage (ω) increases, the viscous part in Equation 2 decreases, and the modulus will be a constant value, $10^{\delta+\Delta\delta}$, for the maximum level of deterioration ($\omega = 1$).

$$\log(E) = \delta + \Delta\delta + \frac{\alpha \cdot (1-\omega)}{1 + e^{\beta + \gamma \cdot \log(fr)}} \quad (2)$$

According to Equation 2, the evolution of the asphalt mixture master curve follows the pattern reflected in Figure 5. Aging and densification shifts vertically on the master curve in the logarithmic scale, while damage effects are higher, in absolute and relative terms, for increasing reduced frequencies. As a result, structural evaluations conducted at high temperatures will mainly reflect aging and densification, thus hiding the real magnitude of the damage; the opposite

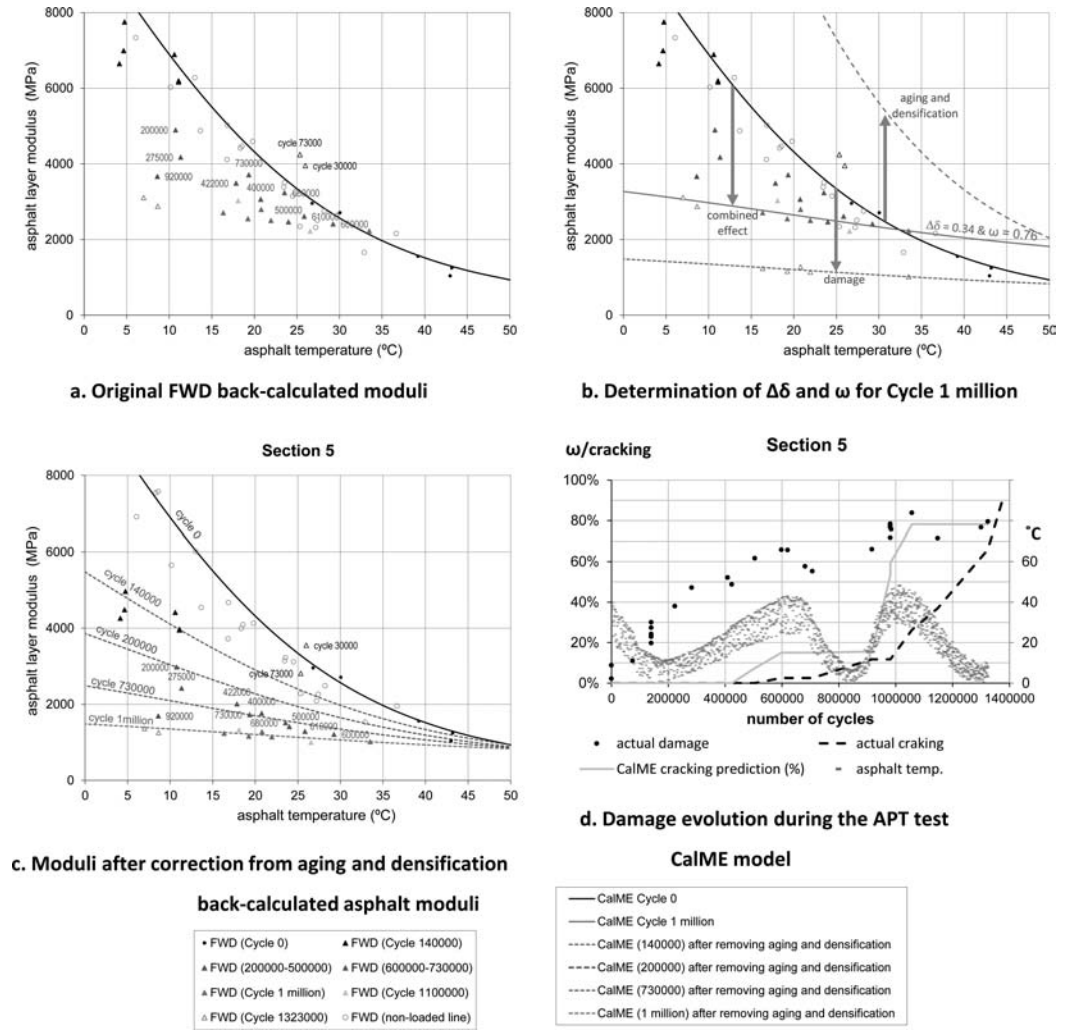

Figure 4. Asphalt layer modulus evolution throughout the test on Section 5.

will happen for low temperatures. This is the pattern that was observed in Figure 4a, supporting issues 1 and 2 listed above. It should be noted that each *CalME* model curve in Figure 4 is derived from a particular "actual master curve" as presented in Figure 5, by assuming the frequency corresponding to the FWD pulse (15 Hz for this particular study).

It should be noted that the prediction of $\Delta\delta$ during the service life of a flexible pavement constitutes a relatively complex problem. *CalME* software incorporates different aging and densification models, including sets of recommended parameters depending on the particular conditions of the pavement under consideration. These parameters can be readjusted later on the basis of actual performance evaluated from deflection testing.

In practice, $\Delta\delta$ can be estimated for an in-service pavement at a particular time, as soon as deflection testing is conducted over a wide temperature interval. These tests must be conducted over a relatively short period of time, where both $\Delta\delta$ and ω can be regarded as constant. For this particular research, the estimation was possible at the one million load repetition evaluation, when five FWD tests were carried out at different temperatures between 15°C and 35°C (59 to 95°F). An iterative process was followed by changing $\Delta\delta$ and ω in Equation 2 to fit actual backcalculated moduli. The *Excel Solver* tool was used, and results for Section 5 are presented in Figure 4.b. This process was also attempted after 140,000 load repetitions, but the resulting temperature range was too small and well below the highest temperatures that need to be used for the estimation of the increase in δ.

Once $\Delta\delta$ values were estimated for the four flexible sections, aging and densification model parameters were readjusted. This provided a reliable evolution of $\Delta\delta$ during the previous loading cycles as well as a reliable prediction of its future evolution. A detailed

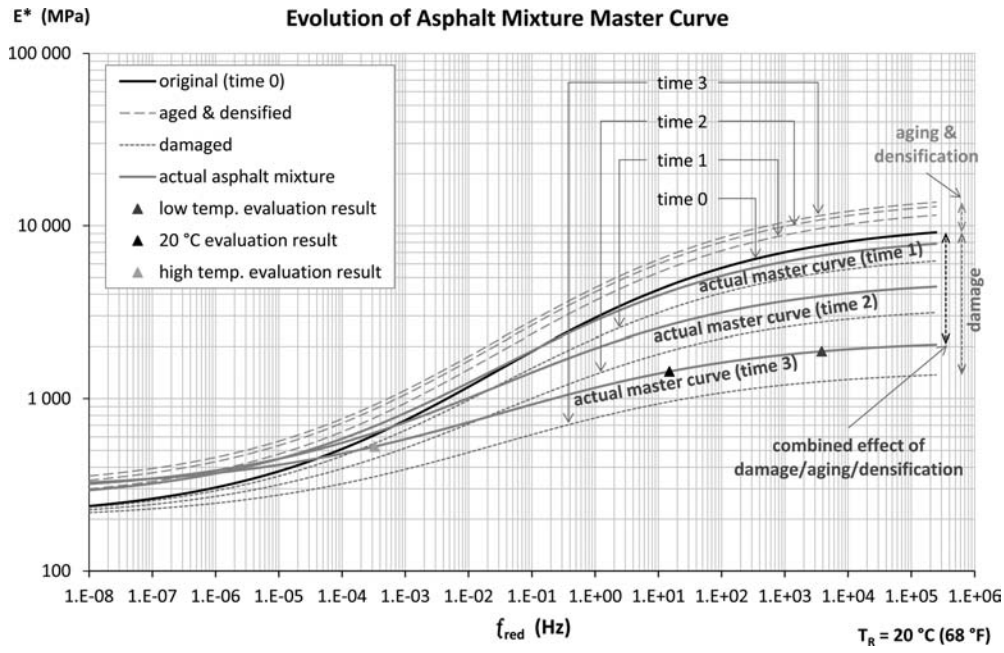

Figure 5. Asphalt master curve evolution according to *CalME*.

description of the approach can be found in Mateos et al. (2012). Results for Section 5, after removing both effects, are presented in Figure 4c, where damage evolution can be clearly seen for the full temperature range.

One of the main problems applying this approach to outdoor APT facilities is the difficulty in conducting FWD tests for a relatively wide temperature interval where both $\Delta\delta$ and ω remain relatively constant. For an in-service pavement, the slower rate of damage accumulation is a clear advantage, since it is possible to perform FWD tests over a longer time period to ensure that a wider temperature interval is obtained, as required for a reliable determination of $\Delta\delta$. Another problem when the approach is applied to APT is that the time required for stabilization of densification effects is of the same order of magnitude of the test duration. This means that the effects of this factor will coincide with asphalt fatigue, making it more difficult to discriminate between the two. For an in-service pavement, densification will mostly take place during the first years, while fatigue will continue until the end of the service life.

It is difficult to determine the actual period of time required for densification to stabilize in an in-service pavement, since it depends on numerous factors including traffic, environment and asphalt mixture properties. Several studies show that the mechanical properties of asphalt mixture remain fairly constant after the first two years (Seo et al., 2007, Hanson et al., 1994). The two-year period is also supported by observations from this research, where 87% of the permanent deformation of the surface layer at the end of the test had taken place during the first year, as

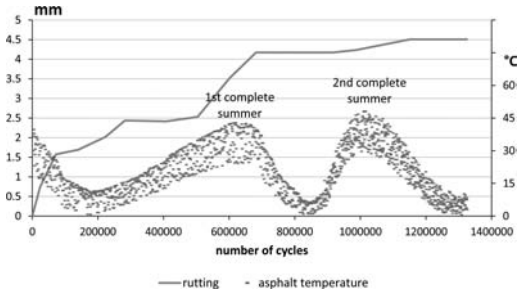

Figure 6. Evolution of permanent deformation of the surface layer during the test.

presented in Figure 6. Permanent deformation from the base course was negligible in this test.

It can be observed in Figure 6 that post-compaction effects concentrated at the beginning of the test and throughout the first summer, between about 500,000 and 700,000 load repetitions. This is believed to be the main reason behind the third issue that was previously observed in Figure 4a, i.e., the increase in backcalculated asphalt layer modulus during that interval.

Once FWD backcalculated moduli were corrected from aging and post-compaction effects, they could be compared to the original (undamaged) values in order to determine damage (ω), by applying Equation 3. Results obtained for Section 5 are included in Figure 4d.

$$\frac{E}{E_{original}} = \left(\frac{10^{\delta}}{E_{original}} \right)^{\omega} \quad (3)$$

Equation 3 can be deduced from Equation 2 and represents an assumption of the *CalME* asphalt fatigue model. This assumption, as well as those corresponding to aging and densification effects on asphalt mixture stiffness, have been validated for CEDEX sections within this research effort (Mateos et al. 2011, 2012).

It should be noted that aging, damage, and densification are considered as "overall" asphalt layer properties, but this is just a simplification, since they vary throughout the pavement thickness. This simplification is required when actual asphalt layer backcalculated moduli are used for the calibration, since current backcalculation techniques cannot distinguish between wearing and base asphalt courses.

3 FATIGUE OF THE ASPHALT MIXTURE: MOVING FROM LABORATORY TO FIELD

The *CalME* asphalt fatigue model presents an important advantage versus the classical fatigue laws employed in most mechanistic-empirical design procedures. This advantage is the ability to reproduce actual modulus reduction of the asphalt mixture due to damage. The model is calibrated in the laboratory by using the complete records of "modulus vs. cycles" obtained from fatigue tests, as shown in Figure 7. Once the model is calibrated in the laboratory, it can be used to predict asphalt modulus reduction throughout a fatigue test with changing load and temperature, as presented in the example in Figure 8. The model can also be used to predict asphalt layer modulus reduction in the field, under changing temperature and traffic loads, if horizontal strain at the bottom of the asphalt layer is known. *CalME* estimates this strain by taking into account pavement structure and axle configuration, temperature, actual damage, vehicle speed, and levels of aging and densification. Additional information on the *CalME* asphalt fatigue model can be found in the program help file (California DOT, 2010).

Laboratory calibration is best conducted for a wide temperature interval, as close as possible to the expected temperature range in the field. For this research, fatigue tests were conducted at 10, 20 and 30°C (50, 68 and 86°F), which still represents less than 50% of the actual temperature range on the sections during the test. A reasonably good agreement was found between the model and laboratory data for the three temperatures, with an overall error of 5.1% of the initial modulus. Details concerning this laboratory calibration can be found in Mateos et al. (2011).

The application of the model to in-service pavements is not straightforward, since numerous experimental studies show that asphalt fatigue life predicted from laboratory tests will systematically underestimate field performance (Bahia et al., 2010). It is widely accepted that a shift factor must be introduced that divides the actual number of load applications in the field, as presented in Figure 7. There are different reasons that explain the need for the shift factor, including

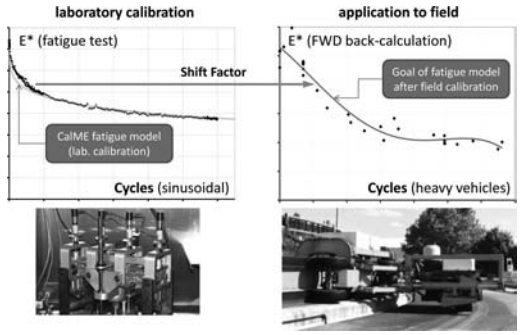

Figure 7. Application of laboratory data to field.

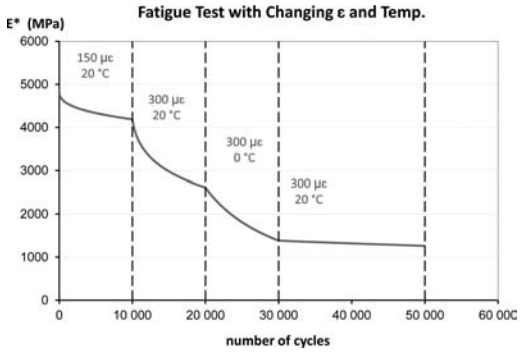

Figure 8. Example of application of *CalME* asphalt fatigue model to laboratory.

time required for cracks initiated at the bottom of the asphalt layer to reach the surface, traffic wandering across the wheelpaths, or rate of mixture densification. Probably the main reason is the existence of rest periods between traffic loads, during which asphalt healing takes place. This has been hypothesized by different authors (Bahia et al., 2010), and is fully supported by experimental evidence from this research, which shows that around 90% of the total shift factor was directly related to the beneficial effects of rest periods (Mateos et al. 2011). It should be indicated that this quantification was possible due to the approach used by *CalME*.

CalME incorporates the beneficial effects of rest periods into the shift factor, by using the concept of reduced rest period, as developed in the framework of the NCHRP 9-44 project (Advanced Asphalt Technologies, 2008). This reduced period results from the application of time-temperature correspondence principle to actual rest periods between traffic loads, as defined by Equation 4.

$$\log(RPr) = \log(RP) - \log(a_T) \quad (4)$$

where RP is the actual rest period between traffic loads; and a_T is the time-temperature shift factor for the temperature corresponding to the rest period.

According to this approach, the beneficial effect of a rest period will be larger for higher temperatures,

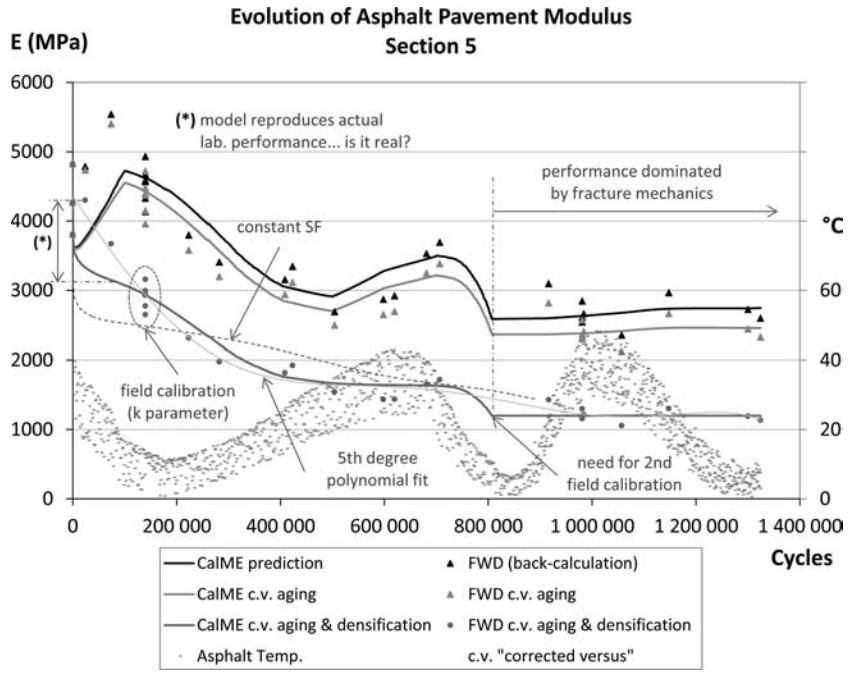

Figure 9. Application of *CalME* model to predict field performance.

which recognizes the well-known fact that healing potential increases with increasing temperature. This assumption entails important consequences concerning the rate of damage accumulation as a function of temperature. In particular, the critical periods with the highest rate of damage accumulation will no longer be the warmest periods, but the periods with the lowest temperatures. This pattern was observed for the flexible sections included in this research, as presented below.

Time-temperature relationship was determined for the asphalt mixture on the basis of dynamic modulus testing in the laboratory, and a shift factor was introduced according to Equation 5.

$$SF = k(1 + R\,\mathrm{Pr})^{\alpha} \quad (5)$$

where k is the unknown part of the shift factor (to be determined from field calibration); RPr is the reduced rest period; and α is a parameter that takes into account the nonlinear evolution of healing versus time.

Actual rest periods between loads of the two automatic vehicles were known. Asphalt temperature was measured from thermocouples embedded in the asphalt layer. Strain was estimated at the bottom of this layer by using *Bisar*, the well-known multilayer linear-elastic program developed by Shell. Damage was calculated in increments of 10 load repetitions, assuming constant temperature, speed and pavement conditions. Asphalt layer modulus was calculated for each 10-load repetition interval by applying Equation 2.

It should be noted that the unique unknown of the approach described above is the *k* parameter in Equation 5. This parameter was backcalculated, through a manual iterative process, in order to fit actual field performance. Values obtained for the four sections ranged from 0.5 to 1.7, when asphalt strain in fatigue tests was interpreted according to normative AASHTO T 321. Details of this approach can be found elsewhere (Mateos et al. 2011).

The ability of the *CalME* model to predict asphalt performance in the field is presented in the example in Figure 9. The *k* parameter was determined by fitting the actual modulus at 140,000 load repetitions with the model. The model reproduced almost exactly the reduction of asphalt layer modulus that took place during the following cycles. The figure also shows that the rate of damage accumulation was clearly higher at medium and low temperatures and not at high temperatures. FWD backcalculated modulus, after aging and densification correction, remained almost constant during the summer. The model was also applied by considering a constant shift factor ($\alpha = 0$ in Equation 5) but in this case an incorrect pattern of damage accumulation versus temperature was obtained, despite the fatigue model being calibrated in the laboratory for different temperatures. Some limitations of the model can be deduced from Figure 9, including the rapid decrease in modulus during the first cycles, which was not supported by experimental results. This was attributed to the model reproducing the pattern of the laboratory fatigue tests that were used for its initial calibration. It is widely known that

the initial reduction of the specimen modulus in these tests is mostly related to heating and thixotropy rather than actual damage (Di Benedetto et al., 2004), which explains the deviation observed. Problems were also experienced in predicting the asphalt performance during the second half of the test, probably due to the high level of damage and the presence of discrete cracking, which renders the hypothesis of continuity upon which *CalME* asphalt fatigue model is based unrealistic. As a consequence, a second calibration was required after 800,000 load repetitions.

It should be noted that in order to estimate asphalt strain under heavy vehicles, the moduli of the subgrade layers that were used in *Bisar* were the actual values obtained from FWD backcalculation and no prediction was carried out. The same can be stated for asphalt temperature, which were actual measurements from throughout the test. *CalME* incorporates models in order to predict these variables, but the use of them was not attempted in this research, since the objective was the specific evaluation of the asphalt fatigue model. It is obvious that achieving a satisfactory prediction in a real in-service pavement will be considerably more difficult, due to the uncertainties in the different variables that represent the inputs to the problem.

The third "model goal" included in Figure 1 is the ability to determine asphalt cracking from damage. *CalME* incorporates a transfer function that relates the ω parameter to cracking. A detailed description of this function is included in the program help file (California DOT 2010). Results for Section 5 are included in Figure 4.d, where a reasonably good agreement can be observed between measured and predicted cracking. Similar results were obtained for the other sections (Mateos et al., 2012). It should be noted that the damage values used for this calculation were the values determined from FWD testing, and consequently the transfer function was specifically evaluated. The good agreement observed for the different sections was, to some extent, unexpected, due to the inherent difficulty in predicting a variable such as cracking from a variable such as damage. Cracking is dominated by fracture mechanics while damage is based on continuum mechanics.

The *CalME* transfer function includes the variable h_{AC}, the combined thickness of the asphalt layers, in order to predict damage at crack initiation. The introduction of this variable recognizes that the time required for bottom-up cracks to reach the surface increases with layer thickness. As expected, the contribution of each layer to this combined thickness will depend on the characteristics of each asphalt mixture. For this particular test, the asphalt mixture used in the base course had an unmodified bitumen content of 4.0% by mass of aggregates, while the wearing course was a gap-graded mixture with 5.3% highly modified bitumen. This 30 mm-thick wearing course was expected to result in a significant delay in cracking, although it was a challenge to quantify how long this delay would be. Actual damage values were determined when cracking first appeared in the sections. Then, the equivalent thickness of the wearing course was obtained through an iterative analysis, where experimental values were fitted with the *CalME* transfer function. From this, it was determined that the modified binder wearing course mixture provided the equivalent crack propagation delay of a conventional mix six times thicker (i.e., 180 mm). This figure must be understood in comparison to the base course mixture.

4 APPLICATION EXAMPLE: STRUCTURAL RESPONSE IN TERMS OF DEFLECTION

Deflections measured under the FWD loading plate throughout the test are presented in Figure 10, together with predictions according to the *CalME* approach. Actual backcalculated moduli for the subgrade layers were used with *CalME* asphalt fatigue, aging, and densification models. As expected, a direct link exists between the pattern of deflections in this figure and the performance observed in Figure 4a in terms of the asphalt layer modulus. An additional factor, the moisture content of the subgrade soils, is introduced here. The test was conducted without cover and the water table fluctuated with the natural rainfall. The water table level was allowed to rise up to 1.0 m (3.3 ft.) below the top of the subgrade, which occurred after about 350,000 load repetitions. Thereafter the level was kept constant by either pumping or by adding water.

The effect of the water table can be assessed in Figure 10, by comparing experimental data for repetition-zero to data for the untrafficked zone, located 2.5 m (8.2 ft.) from the center of the wheelpath. FWD deflections in this zone correspond to the period after 350,000 load repetitions, when the water table level was constant. The introduction of the water table produced, as expected, a significant increase in deflection as well as an increase in temperature sensitivity. Additional aging took place from repetition-zero to about 350,000 repetitions, the effects of which are evident in this comparison. However, these effects are considerably reduced when compared to the water table effect, due to the relatively short period of time. It should be noted that the *CalME* model for the untrafficked zone was applied by considering two asphalt thicknesses: the mean asphalt layer thickness in this zone and the mean thickness along the center of the wheelpath (dashed line in Figure 10). This dashed line should be considered when comparing the *CalME* model predictions corresponding to the center of the wheelpath, especially for Section 6 where there was a significant difference in the two thicknesses.

Asphalt damage is clear for the low temperature range in Figure 10. This is the same issue that was previously observed in Figure 4a in terms of the asphalt layer modulus. Damage effects can be appreciated by comparing deflections for 920,000 and subsequent load repetitions to those corresponding to the

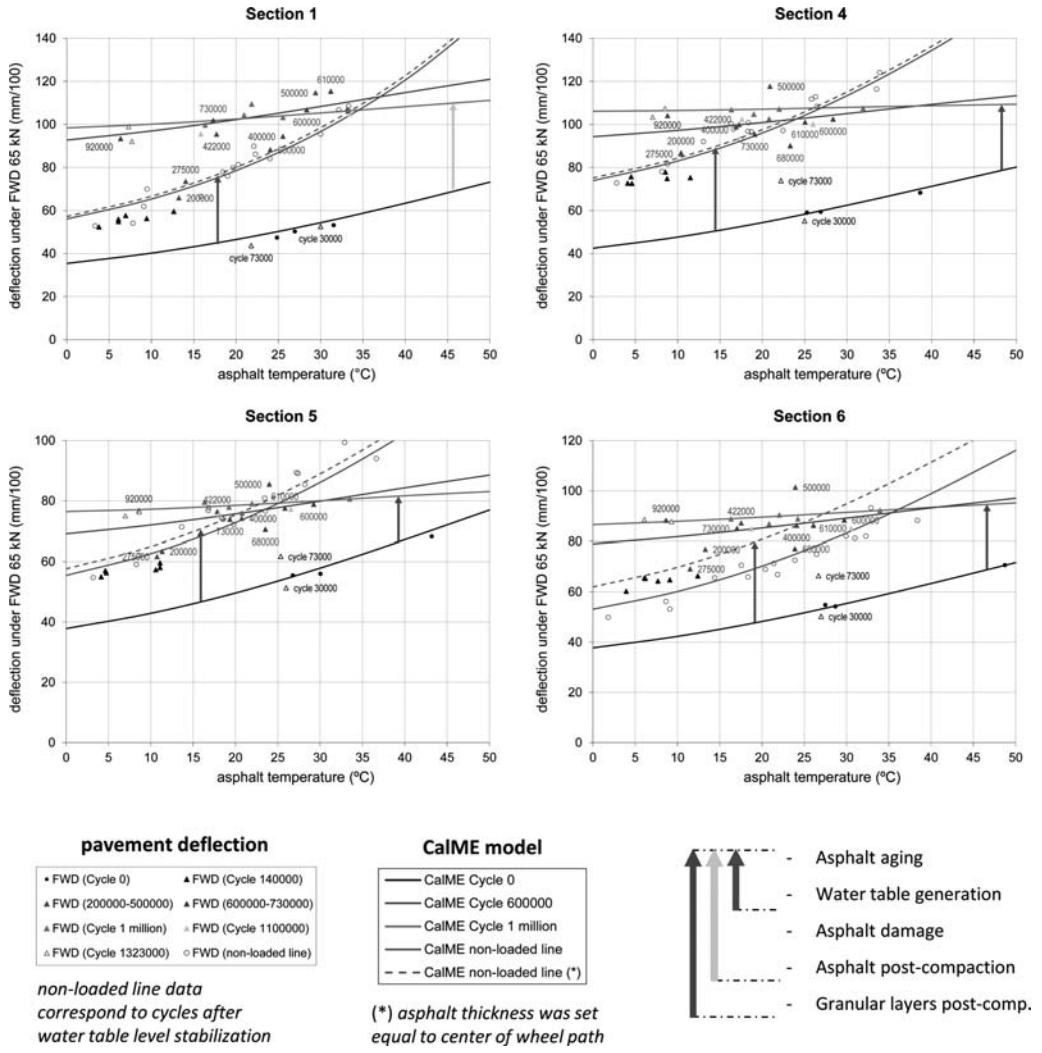

Figure 10. FWD deflection evolution throughout the test.

untrafficked zone. Data collected at 200,000 and 275,000 load repetitions, conducted at asphalt temperatures below 15°C (59°F), could not be included in this comparison since the water table had not reached its final level.

For the high temperature range (over 30°C [86°F]), damage evolution is not evident, as can be appreciated by comparing deflections along the wheelpath at one million load repetitions to values along the untrafficked zone (Figure 10). This is in part related to the asphalt layer modulus convergence to original values for high temperatures, as observed in Figure 4.a. This pattern was attributed to aging and densification of the asphalt mixture. An additional factor is present, namely the densification that took place in the capping layer under the pass of the vehicles. This densification was verified in terms of backcalculated modulus for Sections 4, 5 and 6, and also by means of penetrometer testing, which indicated that resistance to penetration was multiplied by a factor of about two. As a consequence, the deflections measured at high temperatures for these three sections were below those obtained along the untrafficked zone, where no damage had taken place.

The main conclusion that can be extracted from this application example is that the interpretation of FWD data, even if only in terms of the central deflection, represents a very complex process. This process will be more efficient and reliable if the different factors affecting asphalt mixture stiffness in the field are fully understood and accurately modeled.

5 CONCLUSIONS

The evaluation of four flexible sections at the CEDEX Test Track has provided detailed information concerning asphalt mixture deterioration in the field. The complexity of this process, together with its interaction

with aging, densification, and changing environmental conditions, have been the main obstacles, as well as challenges, of the research presented in this paper.

Experimental results from this test indicate that the rate of damage accumulation is strongly dependent on asphalt temperature. Most damage took place at medium to low temperatures, while very little damage took place during summer, even though strain at the bottom of the asphalt layer reached maximum values. This pattern was fully explained by the *CalME* models, as a consequence of the beneficial effects of rest periods, which are higher for increasing temperatures. This model incorporates a variable shift factor based on the concept of "reduced rest period". It should be noted that the pattern of damage accumulation that was observed in this test could not be explained by only the increase in asphalt fatigue life that results when temperature increases in laboratory fatigue tests conducted in controlled deformation. This implies that the introduction of a constant shift factor, used in most existing mechanistic-empirical procedures, will not be sufficient to bridge the gap between laboratory and field.

Important conclusions were also extracted from this test concerning how damage, in combination with asphalt aging and densification under traffic, affects the modulus of the asphalt layer. Damage caused a reduction in mixture modulus that was higher, in absolute and relative terms, at decreasing asphalt temperatures, while aging and densification effects appeared to multiply the asphalt layer modulus for any combination of temperature and frequency. This pattern was expected according to the *CalME* model, which employs a master curve format that incorporates the effects of the three factors: damage is introduced by decreasing the α parameter of the master curve (viscous term) and aging and densification by increasing δ (elastic term).

The *CalME* model was successfully used in this research as a tool for the interpretation of deflections from FWD testing. This was a complex process in that aging as well as densification effects had to be removed from the FWD backcalculated asphalt layer modulus. After removing the effects of both factors, modulus values could be compared to the original (undamaged) master curve to determine actual damage. These damage values were also used to predict asphalt cracking by using the corresponding *CalME* transfer function. The agreement between measured and predicted cracking was excellent.

The ability of the model to predict future performance, after recalibration from FWD testing results, has also been shown in this paper. The unknown part of the shift factor was determined on the basis of FWD results at 140,000 load repetitions. After this recalibration, the model was able to reproduce field performance up to 800,000 load repetitions, when an ultimate deterioration level was reached.

As a general conclusion, the *CalME* asphalt fatigue model was an indispensable tool in understanding the performance of the four flexible sections tested at the CEDEX Test Track. The validity of the assumptions of the model, together with the flexibility to incorporate results from FWD testing, make it a unique tool for obtaining the most out of structural evaluations.

ACKNOWLEDGEMENTS

Results presented in this paper come from a research effort conducted at CEDEX in cooperation with the University of California Pavement Research Center at the University of California, Davis. The authors of this paper would like to express their gratitude to this institution as well as to the California Department of Transportation. A special acknowledgment is given to Prof. Per Ullidtz for his advice and support, which was essential for conducting this study.

REFERENCES

Advanced Asphalt Technologies. 2008. An Experimental Plan for Validation of an Endurance Limit for HMA Pavements. *NCHRP Web-Only Document 134*, Transportation Research Board, Washington, DC.

Bahia, H., et al. 2010. Validating the Fatigue Endurance Limit for Hot Mix Asphalt. *NCHRP Report 646*, Transportation Research Board, Washington, DC.

California Department of Transportation. 2010. *CalME v.1.0 Help file.*

Di Benedetto, H., de La Roche, C., Baaj, H., Pronk, A. and Lundström, R. 2004. Fatigue of bituminous mixtures. *Materials and Structures*, p. 15, Vol. 37.

Hanson, D. I., Mallick, R.B. and Brown, E. R. 1994. Five-year evaluation of HMA properties at the AAMAS test projects. *Journal of the Transportation Research Board* No. 1454, National Research Council, Washington, DC.

Mateos, A. 2008. APT Update. *Proceedings of the Third International Conference on Accelerated Pavement Testing*, Centro de Estudios y Experimentación de Obras Públicas, Madrid, Spain. http://www.cedex.es/apt2008/html/english/apt_update.htm

Lu, Q., Ullidtz, P., Basheer, I., Chuzlan, K. and Signore, J. 2009. CalBack: Enhancing Caltrans Mechanistic-Empirical Pavement Design Process with New Back-Calculation Software. *Journal of Transportation Engineering*, Vol. 135, No. 7.

Mateos, A., Ayuso, J. and Cadavid, B. 2011. Shift Factors for Asphalt Fatigue from Full-Scale Testing. *Journal of the Transportation Research Board* No. 2225, National Research Council, Washington, DC.

Mateos, A., Ayuso, J., Cadavid, B. and Marrón, J. 2012. *Evolution of Asphalt Mixture Stiffness under the Combined Effects of Damage, Aging and Densification under Traffic.* 91st Annual Meeting of the Transportation Research Board, National Research Council, Washington, DC. *(pending publication in Journal of the Transportation Research Board)*

Seo, Y., El-Haggan, O., King, M., Lee, S. and Kim, Y.R. 2007. Air Void Models for the Dynamic Modulus, Fatigue Cracking, and Rutting of Asphalt Concrete. *Journal of Materials in Civil Engineering*, Vol. 19, No. 10.

Ullidtz, P., Harvey, J., Tsai, B.W. and Monismith, C. L. 2006. *Calibration of Incremental-Recursive Flexible Damage Models in CalME Using HVS Experiments.* UCPRC-RR-2005-06, California Department of Transportation. www.ucprc.ucdavis.edu

Advances in Pavement Design through Full-scale Accelerated Pavement Testing – Jones, Harvey, Mateos & Al-Qadi (Eds.)
© 2012 Taylor & Francis Group, London, ISBN 978-0-415-62138-0

Modeling of flexible pavement structure behavior – comparisons with Heavy Vehicle Simulator measurements

A.W. Ahmed
Pavement Technology, Swedish National Road and Transport Research Institute, VTI, Linköping, Sweden
Transport Infrastructure, Royal Institute of Technology, KTH, Stockholm, Sweden

S. Erlingsson
Pavement Technology, Swedish National Road and Transport Research Institute, VTI, Linköping, Sweden
Faculty of Civil and Environmental Engineering, University of Iceland, Reykjavik, Iceland

ABSTRACT: A response model to be employed in a mechanistic-empirical pavement performance prediction model based on multilayer elastic theory has been developed. An iterative approach using a method of successive over-relaxation of a stress dependency model is used to account for the nonlinear behavior of unbound materials. Asphalt and subgrade materials are assumed to be linear elastic. The response model was verified against two series of Heavy Vehicle Simulator (HVS) response measurements made under a variety of wheel load configurations and at different pavement temperatures. A comparison with Falling Weight Deflectometer (FWD) data was also carried out. The model was subsequently used to predict permanent deformation from the HVS testing using simple work hardening models. A time hardening approach has been adopted to combine permanent deformation contributions from stress levels of different magnitude. The response model outputs and the predicted permanent deformations were generally in good agreement with the measurements.

1 INTRODUCTION

A response model is one of the key components of all mechanistic-empirical (ME) performance prediction methods used to estimate the stresses, strains and displacements of a pavement structure subjected to traffic, and taking into account the material properties and prevailing environmental conditions. Several pavement response modeling approaches exist that might be utilized depending on the desired accuracy and computational speed.

The multilayer elastic theory (MLET) developed by Burmister has been employed in many engineering applications to calculate the responses of layered structures to external loading (Huang, 1968; Buffer, 1971; Maina and Matsui, 2005). As flexible pavements are layered structures composed of layers with different material properties, the Burmister theory can be utilized to simulate the response of pavement structures (Huang, 2004) and with the advent of high speed computers it is possible to use this method practically for multiple layers.

As a part of a new mechanistic-empirical performance prediction procedure for flexible pavement structures, a response model using MLET has been developed. The program outputs were compared with response measurements which were carried out in an accelerated pavement testing (APT) program using a Heavy Vehicle Simulator (HVS) under different pavement temperatures, different wheel configurations (single and dual wheels), and different tire pressures and wheel loads. The main objective of the research was to verify the results from the response and permanent deformation model with respect to the APT measurements.

2 MULTILAYER ELASTIC THEORY

Flexible pavements are layered structures with the stiffer layer conventionally placed at the top and weaker layers underneath. Their responses to external loading are well represented in analyses based on a multilayer elastic approach. The basics of the linear theory of elasticity for homogeneous half space have been well established by Boussinesq and their extension to a multilayer system has been presented by Burmister (Huang, 1968; Buffer, 1971).

An axisymmetric solution of a multilayer elastic system under a constant load q which is distributed over a circular area as shown in Figure 1 begins from the classical theory of elasticity where it is well known that axisymmetric problems can be solved by assuming a stress function that satisfies the governing differential equations together with the boundary

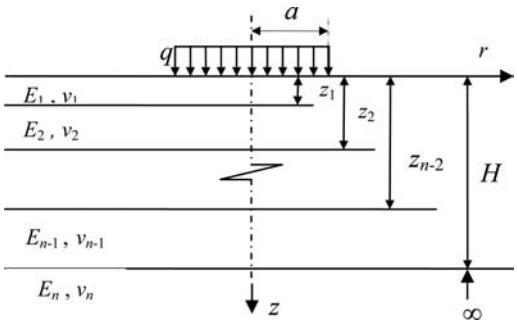

Figure 1. Layered system.

and continuity equations (Timoshenko and Goodier, 1951).

By introducing a stress function ϕ, the governing differential equation to be satisfied can be written as a fourth order differential equation:

$$\nabla^4 \phi = 0 \tag{1}$$

For a multilayer elastic structure, Equation 1 is assumed to be satisfied for each of the layers and for axially symmetrical stress distribution the Laplace operator ∇^4 can be written as:

$$\nabla^4 = \left(\frac{\partial^2}{\partial r^2} + \frac{1}{r}\frac{\partial}{\partial r} + \frac{\partial^2}{\partial z^2}\right)\left(\frac{\partial^2}{\partial r^2} + \frac{1}{r}\frac{\partial}{\partial r} + \frac{\partial}{\partial z^2}\right) \tag{2}$$

where r and z are radial and vertical cylindrical coordinates, respectively, as shown in Figure 1.

The axisymmetric responses, stresses and displacements, can be obtained from (Maina and Matsui, 2005; Timoshenko and Goodier, 1951)

$$\begin{bmatrix} \sigma_z \\ \sigma_r \\ \sigma_t \\ \tau_{rz} \\ w \\ u \end{bmatrix} = \begin{bmatrix} (2-\nu)\frac{\partial}{\partial z} & -\frac{\partial^3}{\partial z^3} \\ \nu\frac{\partial}{\partial z} & -\frac{\partial}{\partial z}\frac{\partial^2}{\partial r^2} \\ \nu\frac{\partial}{\partial z} & -\frac{\partial}{\partial z}\frac{1}{r}\frac{\partial}{\partial r} \\ (1-\nu)\frac{\partial}{\partial r} & -\frac{\partial}{\partial r}\frac{\partial^2}{\partial z^2} \\ \frac{1+\nu}{E}(1-2\nu) & \frac{1+\nu}{E}\left(\frac{\partial^2}{\partial r^2} + \frac{1}{r}\frac{\partial}{\partial r}\right) \\ 0 & -\frac{1+\nu}{E}\left(\frac{\partial^2}{\partial r \partial z}\right) \end{bmatrix} \begin{bmatrix} \nabla^2\phi \\ \phi \end{bmatrix} \tag{3}$$

in which ν and E are the Poisson's ratio and modulus of elasticity of the material, respectively; σ, τ, w, u, are normal stress, shear stress, vertical displacement and radial displacement, respectively.

The solution of the stress function ϕ for the ith layer which satisfies the governing differential equation is given as (Huang, 2004):

$$\phi_i = \frac{H^3 J_0(m\rho)}{m^2}\begin{bmatrix} A_i e^{-m(\lambda_i - \lambda)} - B_i e^{-m(\lambda - \lambda_{i-1})} + \\ C_i m\lambda e^{-m(\lambda_i - \lambda)} - D_i m\lambda e^{-m(\lambda - \lambda_{i-1})} \end{bmatrix} \tag{4}$$

where H denotes the distance from the pavement surface to the top of the lowest layer, $\rho = r/H$, $\lambda = z/H$, $\lambda_i = z_i/H$, z_i denotes the distance from the pavement surface to the bottom of the ith layer; A_i, B_i, C_i and D_i are the constants of integrations; J_0 is the Bessel function of first kind and order 0 and m is a parameter. The subscript (i) denotes the quantity corresponding to the ith layer and it varies from 1 to n. The coefficients A, B, C, and D in Equation 4 are obtained from a linear system of equations of the form as shown in Equation 5 which is formulated from the boundary and continuity conditions:

$$WX = Y \tag{5}$$

where W is a matrix of size ($4n$-2 x $4n$-2), X consists of the coefficients A, B, C and D of each layer arranged in columns, and Y includes known values from boundary and continuity conditions.

After solving for the coefficients in Equation 5, a numerical integration scheme is applied to determine the responses. The integration involves Bessel functions of the first kind which have an oscillatory nature. Several methods have been suggested for the integration, such as integrating between zeros of the Bessel function using the Gauss quadrature rule (Khazanovich, 2007; Huang, 2004) and double exponential integration (Maina and Matsui, 2005). In this paper Gauss-Kronrod rules, which are very effective and also provide error estimates (Lukas and Stone, 1994), have been implemented.

3 STRESS DEPENDENCY OF UNBOUND LAYERS

Unbound materials consist of granular aggregates. Their response behavior is affected by the applied stress level. Several studies have revealed that unbound granular materials (UGMs) show nonlinear elastic behavior and their stiffness increases with increasing confinement levels. This led researches to develop models that relate stiffness to the confining pressure (Lekarp et al., 2000; Gomes-Correia et al., 1999; Uzan, 1985; May and Witczak, 1981; Huang, 1968).

Unlike UGMs, subgrade materials are frequently composed of fine grained soils such as sandy, silty or clayey materials. Their response behavior is affected by the stress level as well as by the shear stress applied, frequently expressed as either the deviatoric stress or the octahedral stress (Thompson and Elliott, 1985).

The relationship used in this paper to take into account the nonlinear behavior of UGMs and subgrades is given as (ARA, 2004):

$$M_r = k_1 p_a \left(\frac{3p}{p_a}\right)^{k_2}\left(\frac{\tau_{oct}}{p_a} + 1\right)^{k_3} \tag{6}$$

where M_r denotes the resilient modulus, p denotes hydrostatic stress, which also includes the self weight

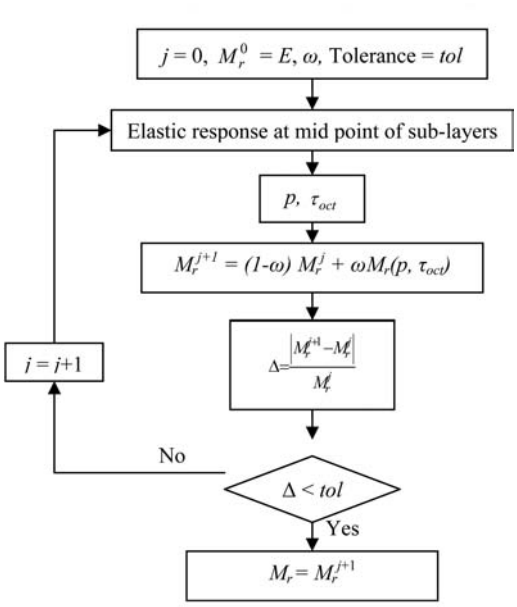

Figure 2. Flow chart for nonlinear iterations of unbound layers.

of the material and the lateral earth pressure denoted by $p = (\sigma_{kk} + (1 + 2k_o)\gamma z)/3$, using the summation convention, where σ_{kk} is the normal stress, k_o is the coefficient of lateral earth pressure, γ is the unit weight of the material and z is the depth, p_a is the atmospheric pressure (100 kPa); k_1, k_2 and k_3 are regression constants and τ_{oct} is the octahedral shear stress.

To take the stress dependency into account, the nonlinear layers are divided into a number of sub-layers and the stresses at the mid point of the sub-layers are used to compute the modulus. This procedure is repeated until the computed resilient modulus converges for successive iterations. For this particular task, only the points under one wheel are considered. This iterative procedure is depicted in Figure 2.

To speed up the convergence of the iteration, a method of successive over relaxation (Hadjidimos, 2000) of M_r is used; accordingly Equation 6 is written as:

$$M_r{}^{j+1} = (1-\omega)M_r{}^{j} + \omega\left(k_1 p_a\left(\frac{3p}{p_a}\right)^{k2}\left(\frac{\tau_{oct}}{p_a}+1\right)^{k3}\right)^{j} \qquad (7)$$

where $j = 0, 1, 2\ldots\omega$, $0 < \omega < 2$, is a relaxation factor and j is the iteration step. A value of $\omega = 0.5$ is used in this paper.

For the particular cases presented in this paper, the tolerance level is taken as $tol = 0.1\%$. Depending on the starting value of M_r used to compute the stiffness, the above method should converge within a maximum of 15 iterations with this tolerance level.

4 APT FACILITY

The Swedish National Road and Transport Research Institute (VTI) own an APT facility with an HVS. The HVS equipment is and can be used to study the behavior of pavement structures under controlled loading and environmental conditions which are similar to actual field conditions. The HVS can apply both single or dual wheel loading at wheel load magnitudes between 30 and 110 kN. The applied wheels travel in the longitudinal direction at a speed of up to 12 km/hr.

The wheels are also able to move in transverse directions (to simulate traffic wander). The HVS equipment has been used to perform a number of tests in both Sweden and Finland and occasionally in some other European countries. Environmental influences, such as pavement temperature and ground water table, are controlled through add-on facilities (Wiman and Erlingsson, 2008).

5 COMPARISON WITH APT RESULTS

The results of two series of APT structures (Figure 3), from the HVS – Nordic test program, were analyzed to verify the numerical approach against real response measurements.

The structures were named SE05-2 and SE06 and the tests were performed at VTI, Linköping, Sweden. SE05-2 was constructed from three layers including hot mix asphalt (HMA), a crushed aggregate base course and sand subgrade over a rigid bottom. SE06 was composed of an asphalt concrete surface, a bituminous base, granular base, granular subbase and sand subgrade over a stiff underlying structure. Figure 3 shows cross sections of the test structures. The structures were instrumented to measure the vertical stress and strain in the unbound layers and horizontal strain at the bottom of the asphalt layer. Both response and permanent deformation measurements were carried out in the test sections (Wiman, 2006). The response measurements were carried out at 0, 10 and 20°C while the permanent deformation measurements were made at 10°C. Falling weight deflectometer tests were also carried out during the different construction states of the structures.

The instruments (sensors) were located along the centre line of the loaded area. The following sensors were used in the tests (Wiman, 2006):

- H-shaped asphalt strain gauges.
- Soil pressure cells.
- Linear variable differential transducers (LVDTs) for vertical deflection and deformation.
- Inductive coils (εMU) for vertical deformation and strain (static and dynamic).
- Water content reflectometers.
- Temperature gauges.

Two or three sensors of each type were used at each measurement depth.

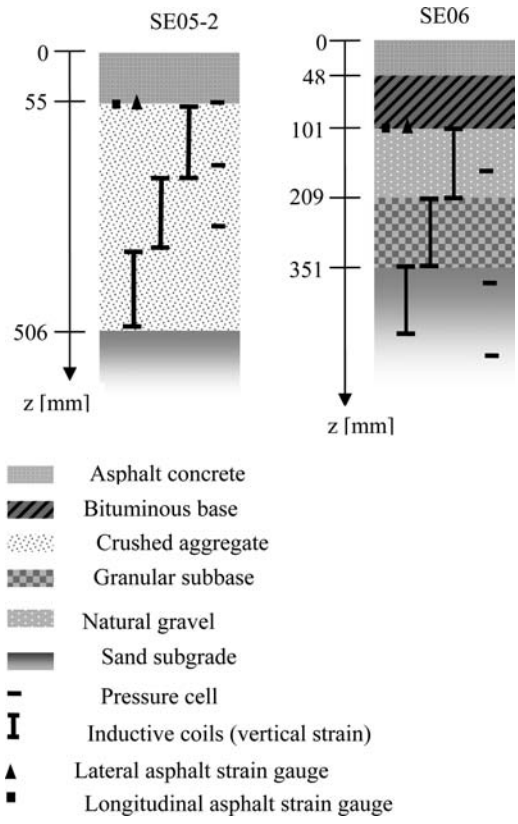

Figure 3. Cross sections of SE05-2 and SE06 HVS test structures.

5.1 *Material characterization*

This section discusses the material models and constitutive equations adopted for different layers which were used for modeling of the HVS sections. A detailed description of the selection of material properties is beyond the scope of this paper. Further information can be found in (Wiman, 2006; Erlingsson, 2010a).

5.1.1 *Asphalt concrete*

The surface layers of both structures were constructed with a dense graded HMA with a maximum aggregate size of 16 mm. The bound base layer of the SE06 consisted of bituminous road base with crushed rock aggregate of 22 mm maximum size (Wiman, 2006). The asphalt layers were considered as linear elastic materials and their stiffnesses were measured using an indirect tensile test (ITT). The stiffness was considered temperature dependent and it was adjusted to the desired temperature, T, according to the model given by (Erlingsson, 2010a):

$$E_T = E_{ref} e^{-b(T-T_{ref})} \tag{8}$$

where E_{ref} denotes the stiffness at reference temperature $T_{ref} = 10^{\circ}$C and the parameter $b = 0.065$ which has been obtained from the ITT.

Table 1. Material properties for the SE05-2 pavement structure.

Layer	Thickness h (cm)	Stiffness or Resilient modulus E (MPa)	k_1 (−)	k_2 (−)	k_3 (−)	Unit weight γ (kN/m^3)
AC	5.5	5,500	–	–	–	25.0
BC-1	10.0	–	700	0.3	0	22.0
BC-2	35.1	–	4,000	0.6	0	22.0
Sg	–	180	–	–	–	17.3

Table 2. Material properties for the SE06 pavement structure.

Layer	Thickness h (cm)	Stiffness/Resilient modulus E (MPa)	k_1 (−)	k_2 (−)	k_3 (−)	Unit weight γ (kN/m^3)
AC	4.8	5,500	–	–	–	25.0
BB	5.3	5,500	–	–	–	25.0
BC	10.8	–	284	0.4	0	23.0
Sb	14.2	180	–	–	–	22.5
Sg	–	140	–	–	–	17.3

5.1.2 *Unbound layers and subgrade*

The granular base course materials were considered as stress dependent elastic material for both structures (Erlingsson, 2007). The stress dependency model shown in Equation 7 was utilized for this purpose. A repeated load triaxial (RLT) test was used to estimate the nonlinear coefficients. However the granular subbase and subgrade materials used in this modeling were assumed to be linear elastic materials. Tables 1 and 2 present the geometry and material properties of the tested pavements (Erlingsson, 2010a).

In Tables 1 and 2, AC, BB, BC, Sb and Sg denote asphalt concrete, bituminous base, granular base course, subbase and subgrade, respectively, as shown in Figure 3. The coefficient of lateral earth pressure k_o was taken as a constant $k_o = 0.6$ for all layers in both structures. A poisons ratio of 0.35 was assumed for all layers.

Due to lack of compaction in the upper part of the base layer of SE05-2, the base layer was divided into two layers (BC-1 and BC-2) with different values of k_1 and k_2.

6 VERIFICATION OF RESPONSE MEASUREMENTS

The results of the response model for the HVS structures (SE05-2 and SE06), along with the corresponding measurements are discussed in this section. The responses considered include the vertical stress and

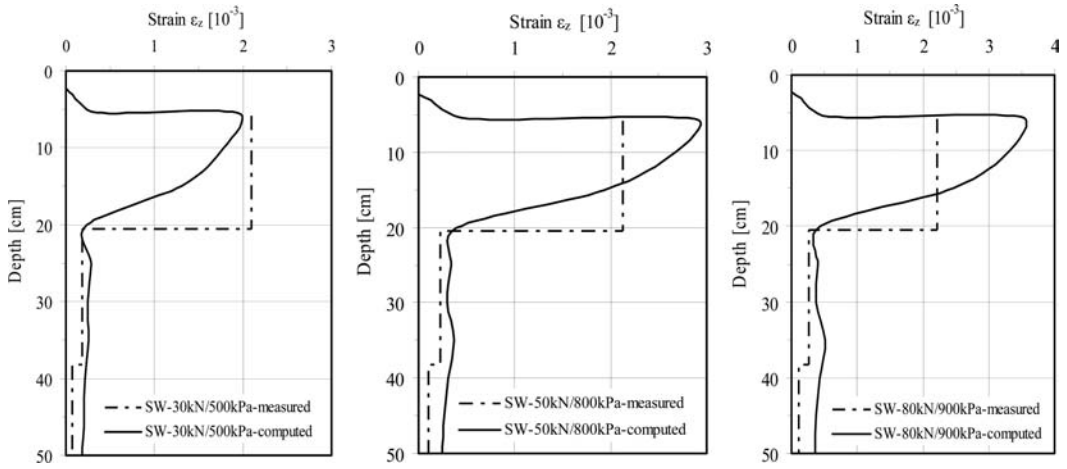

Figure 4. SE05-2 Vertical strain at 10°C for single wheel loading configurations.

strain, within the unbound layers, and the horizontal strain at the bottom of the asphalt layers. In order to study the response behavior of the test structures under various loading conditions, the measurements were performed for single and dual wheel loading configurations at different wheel loads and tire inflation pressures *p*. All the single wheel loading tests were performed at a pavement temperature *T* of 10°C, whereas 0, 10 and 20°C were used for dual wheel loadings. Unless otherwise specified, the responses shown were for the location under the centre of one of the wheels.

6.1 *Results from SE05-2*

Figure 4 presents a comparison between the measured and computed vertical strain for the SE05-2 test structure and Figure 5 compares the measured falling weight deflectometer (FWD) test results with backcalculated values.

6.1.1 *Vertical strain in the unbound layers*

The vertical strains under single wheel (SW) loads of 30, 50 and 60 kN and at tire pressures of 500, 800 and 900 kPa, respectively, are shown in Figure 4.

The results depicted in Figure 4 cover very light to heavy loading conditions. The measured strains represent the average strain for the portion of the pavement where the instruments were installed. At base course level, good agreement was obtained for medium to heavy loading conditions while at lower loading the model underestimated the strain. On the other hand, the strains at lower depths were slightly over-predicted.

6.1.2 *Falling weight deflectometer measurements*

FWD measurements were carried out after the HVS test. These measurements have been simulated and Figure 5 shows the comparison. The model underestimated the surface deflections in the vicinity of the centre of the plate and slightly over-predicted the deflections at farther distances from the centre. However, the overall agreement was acceptable.

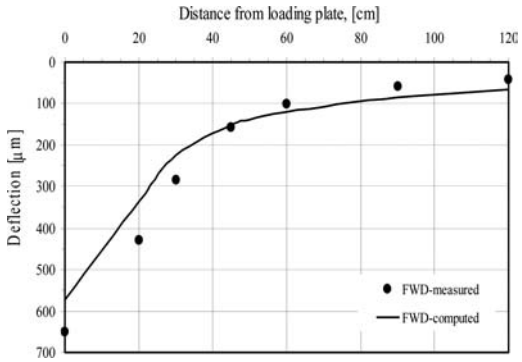

Figure 5. SE05-2 falling weight deflectometer measurement using a 50 kN load intensity on a 30 cm diameter steel plate.

6.2 *Results from SE06*

Figures 6 through 12 present the measured and computed responses for the SE06 test structure. The measurements shown were taken from two or more sensors installed at each measurement depth. For horizontal and vertical strain responses, the mean responses from sensors are presented.

6.2.1 *Vertical stress*

The measured and computed vertical stresses within the tested structure under single wheel (SW) loadings of 30, 50 and 80 kN and tire pressures of 500, 800 and 900 kPa, respectively, and at a pavement temperature of 10°C are presented in Figure 6.

The test results in Figure 6 cover light to heavy loading conditions and show a better agreement between the measured and computed responses for the lower part of the test structure.

The vertical stresses due to dual wheel loading of 60 kN at 800 kPa tire pressure for pavement temperatures of 0 and 20°C are presented in Figure 7.

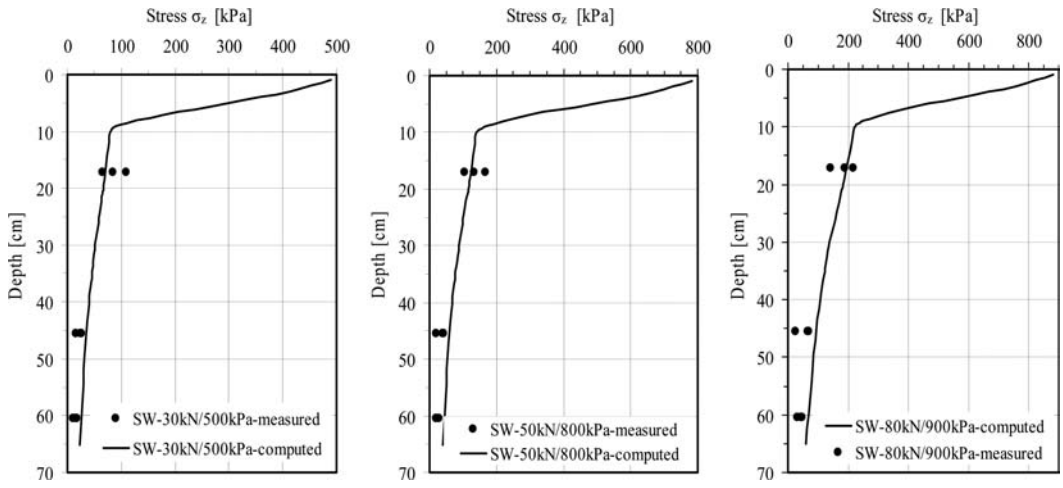

Figure 6. SE06 vertical stress under single wheel loading at T = 10°C for three loading cases ranging from low to high.

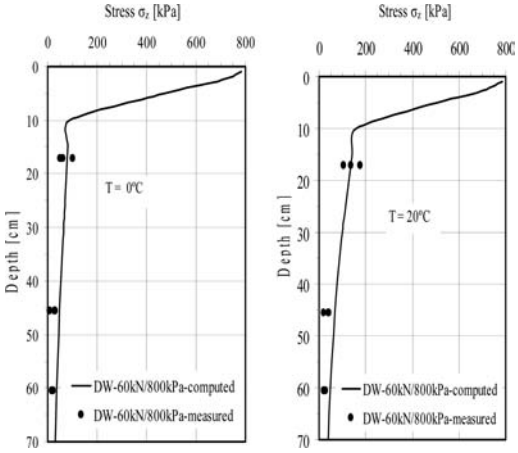

Figure 7. SE06 vertical stress under dual wheel loadings at T = 0 and 20°C.

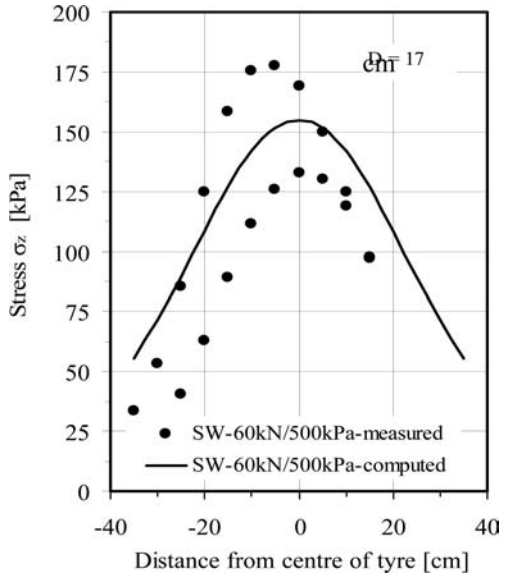

Figure 8. Vertical stress under single wheel loading at 500 kPa tire pressure and $T = 10°C$ for different radial locations.

The measured and computed vertical stresses at a number of radial locations at depth $D = 17$ cm under the surface are presented in Figures 8 and 9 for a single wheel loading of 60 kN at tire pressures of 500 and 900 kPa and at a temperature of $T = 10°C$.

The results in Figures 8 and 9 show the measurements from two pressure cells together with the computed values. The results from the two pressure cells were scattered; however the computed values appear to lie in between the measured values.

6.2.2 *Vertical strain*

The vertical strain within base, subbase and subgrade materials for dual wheel loadings of 50, 60 and 80 kN at tire pressures of 500, 800 and 900 kPa, respectively, are shown in Figure 10. The vertical strain measurements represent the average values from three sensors.

The results depicted in Figure 10 cover light to heavy loading conditions. As has been discussed for predicted strains for the SE05-2 structure, at lighter loading the response model somewhat under-predicts the strain. On the other hand there was good agreement for medium to heavy loading.

6.2.3 *Horizontal strain at the bottom of the bound layer*

Asphalt strain gauges were used to measure the horizontal strain at the bottom of the asphalt layer. Figure 11 shows selected measurements for single wheel loading at tire pressures of 500 and 800 kPa and varying wheel loads at temperature $T = 10°C$. As the transverse and longitudinal strains were equal on the

axis of symmetry of single wheel loading, only one curve is shown as a computed value in Figure 11.

Horizontal strains at the bottom of the asphalt layer under varying dual wheel loads at a tire pressure of 800 kPa and pavement temperatures of 0 and 20°C are shown in Figure 12.

From Figures 11 and 12, it can be observed that there was an acceptable agreement between the measurements and calculations. However the calculations somewhat over-predict the strains at high wheel loading. A better agreement was obtained at 0°C than at 20°C.

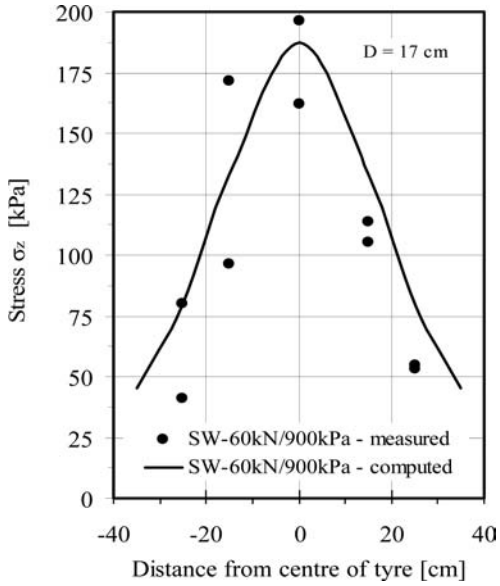

Figure 9. Vertical stress under single wheel loading at 900 kPa tire pressure and $T = 10°C$ for different radial locations.

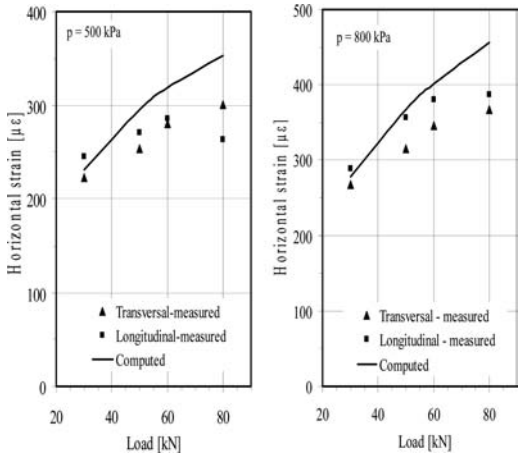

Figure 11. SE06 horizontal strains at the bottom of the asphalt layer due to single wheel loading at $T = 10°C$.

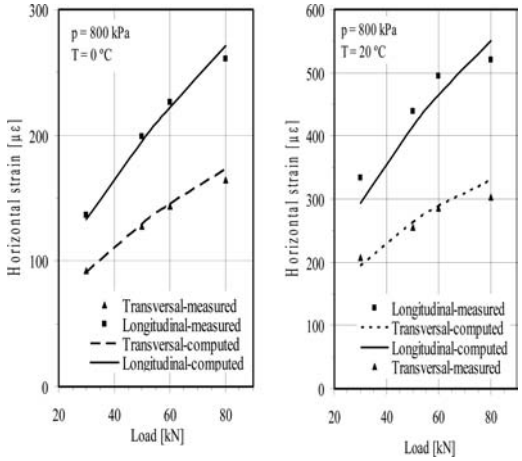

Figure 12. SE06 horizontal strains at the bottom of the asphalt layer for various dual wheel loads at two temperatures.

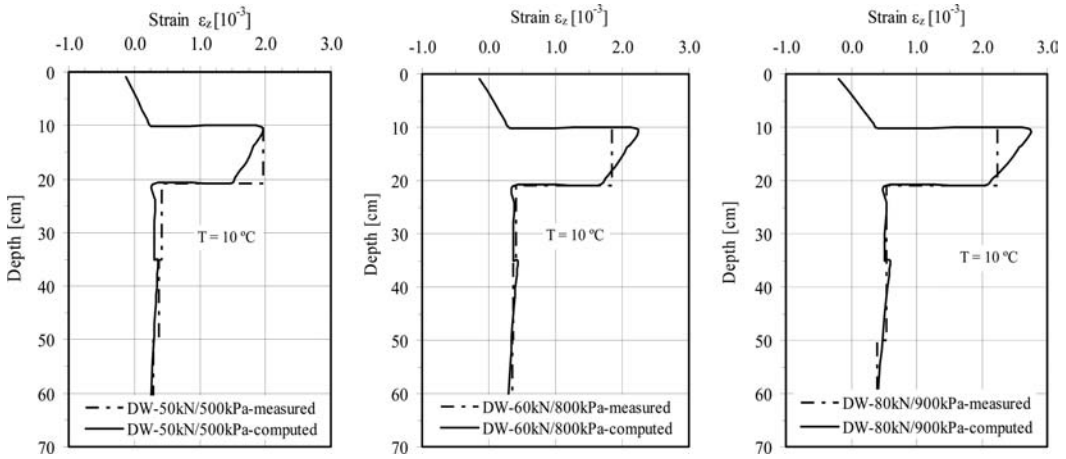

Figure 10. SE06 vertical strains in the unbound layers for three different load cases.

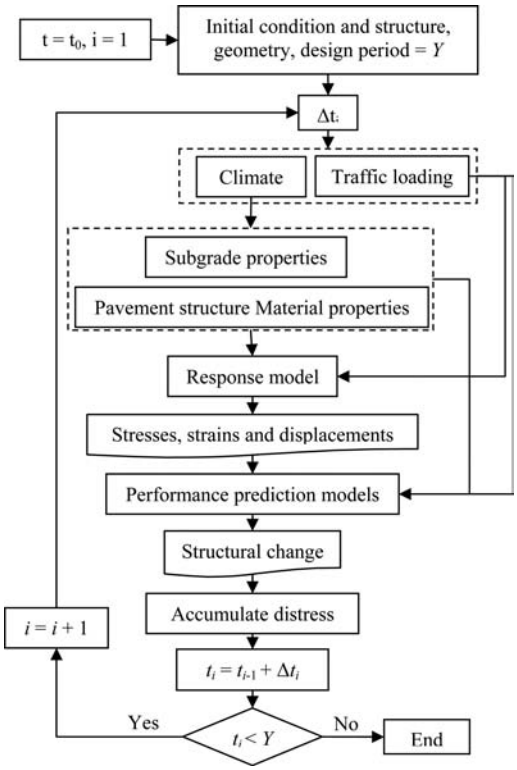

Figure 13. Mechanistic empirical performance prediction.

7 PREDICTION OF PERMANENT DEFORMATION FOR HVS TESTS

In this section, the HVS tested structures are studied for their permanent deformation behavior. The permanent deformation for these structures was measured under a dual wheel load of 60 kN and 800 kPa tire inflation pressure at a 10°C pavement temperature. To simulate traffic wandering, the applied load was normally distributed in the lateral direction through a width of 50 cm; −25 cm to +25 cm from the centre at intervals of 5 cm.

Figure 13 presents the flow chart for the mechanistic empirical performance prediction process where the design life of the pavement is divided into small time steps, Δt, that is characterized by specific material properties, climatic conditions, and traffic. These properties are introduced into the response model that performs the structural analysis and in return gives stresses, strains and deformations. These responses are thereafter used as an input to the performance prediction module which estimates the contribution of the distresses for the specified time step. These distresses are accumulated with time to obtain the performance history of the pavement. This procedure is repeated until the incremented time step reaches the design life. In this paper the response model developed has been used together with permanent deformation models, which are described below, to estimate the permanent deformation in HVS test structures.

Lateral wandering was considered in this study. Eleven locations were used at each depth level at 5 cm intervals to perform the calculations, distributed over a width of 0.5 m. To calculate the rutting at a given lateral wander location, x_i, for a given period, the responses at x_i due to the loads at each wander location were computed and their corresponding number of repetitions, from the distribution curve, were used to estimate their contribution to the permanent deformation at x_i. These contributions were summed to obtain the rutting at x_i. Similar procedures were followed for other wander locations.

In the above formulations, the nonlinear multilayer elastic responses were first modified according to the Mohr-Coulomb failure criterion, so that the stresses did not exceed the strength of the materials. The modified stresses were used for computing permanent deformation in the base, subbase and subgrade layers.

7.1 *Permanent deformation model for asphalt bound layers*

The permanent deformation model for asphalt concrete layers that has been developed for the *Mechanistic-Empirical Pavement Design Guide* (*MEPDG*) was used for this task, given as (NCHRP, 2004):

$$\varepsilon_p(N) = a_1 T^{a_2} N^b \Delta\varepsilon_r \tag{9}$$

where $\Delta\varepsilon_r$ is the induced resilient strain computed from the response model, ε_p is the accumulated permanent strain, T is the pavement temperature, N is the number of load repetitions and a_1, a_2 and b are regression constants.

7.2 *Permanent deformation model for unbound layers*

A model developed by Korkiala-Tanttu (2008) for predicting the permanent deformation in unbound layers was used. It is given by:

$$\varepsilon_p(N) = CN^b R/(A-R) \tag{10}$$

where C and b are material parameters, A is a parameter which is independent of the material ($A = 1.05$) and R is the deviatoric stress ratio given by

$$R = q_{\max}/q_f = q_{\max}/(s + mp_{\max})$$

where

$$m = 6\sin\varphi/(3-\sin\varphi)$$

and

$$s = 6c\cos\varphi/(3-\sin\varphi)$$

Table 3. Permanent deformation model constants for asphalt concrete.

Structure	a_1 (−)	a_2 (−)	b (−)
SE06	0.08	1.85	0.27
SE05-2	0.34	1.85	0.27

Table 4. Permanent deformation constants for base, subbase, and subgrade layers.

Structure	c (kPa)	ϕ (°)	C (−)	b (−)
Base layers				
SE06	15	40	4.0e-4	0.3
SE05-2	15	50	1.5e-4	0.3
Subbase layers				
SE06	20	50	2.0e-4	0.3
Subgrade				
SE05-2/SE06	20	36	2.0e-6	0.6

where ϕ is the angle of internal friction, c is the cohesion of the material and q_{max} and p_{max} are the maximum deviatoric and hydrostatic stresses of the load application respectively.

7.3 *Accumulation of permanent deformations*

To accumulate the permanent deformation at a given point due to different loading scenarios for a given cycle, a time hardening approach (Lytton et al., 1987) was applied, where for each season i the incremental permanent deformation $\Delta\varepsilon_p^i$ was computed from:

$$\Delta\varepsilon_p^i = \sum_{j=1}^{n} \varepsilon_{pj}^i (N=1)\left(\left(N_{eq,j}^i + \Delta N_j^i\right)^b - \left(N_{eq,j}^i\right)^b\right) \quad (11)$$

where $i, j = 1, 2, 3, \ldots$ and $N_{eq,j}$ is calculated from:

$$N_{eq,j}^i = \left[\frac{\varepsilon_p^{i-1}}{\varepsilon_{p,j}^i (N=1)}\right]^{1/b} \quad (12)$$

where $\varepsilon_{p,j}^i(N=1)$ is the permanent strain for the jth stress level (due to wander location or load level) for $N=1$, ΔN_j^i is the number of repetitions for the jth stress level in period i, ε_p^{i-1} is the accumulated permanent strain up to season $i-1$, and b is the material parameter corresponding to the permanent deformation model under consideration.

The accumulated permanent deformation at the end of period i is calculated from:

$$\varepsilon_p^i = \varepsilon_p^{i-1} + \Delta\varepsilon_p^i \quad (13)$$

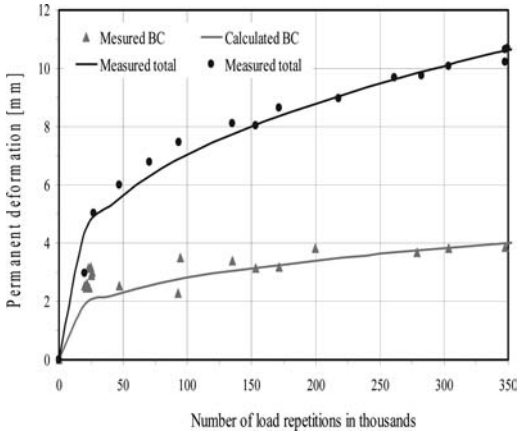

Figure 14. Measured and predicted permanent deformations for SE05-2.

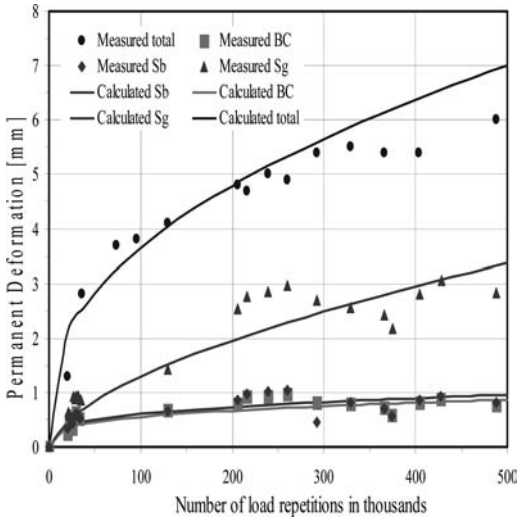

Figure 15. Measured and predicted permanent deformations for SE06.

7.3.1 *Material properties*

Tables 3 and 4 present the material properties used to calculate the permanent deformation of the HVS test structures (Erlingsson, 2010b).

7.4 *Results of permanent deformation modelling*

Figures 14 and 15 present the measured and predicted permanent deformation for both HVS test structures, shown in Figure 3. For SE05-2, only the permanent deformation of the base layer and the total surface rut are shown as the structure was instrumented that way. On the other hand the permanent deformation in the upper part of the subgrade, subbase, base course and total surface rut are depicted for the SE06 structure.

The figures show that the permanent deformation prediction models used in this study captured the development of the permanent deformation in the pavement layers.

8 DISCUSSION

The response behavior of two HVS test structures was studied under a broad range of axle loads and tire inflation pressures. The response measurements depicted in Figures 6 through 12 showed that there is fair agreement between the measured and the computed responses using the developed nonlinear multilayer elastic theory approach. In general the agreement was better for vertical strains than for stresses. This may be due to the fact that it is generally difficult to measure vertical stresses in granular materials due to the complex inherent inter-granular interactions between the aggregate particles. Furthermore the agreement in all responses increased with depth. This may be attributed to the influence of dynamic loading on the sensors, which diminished with depth due to the damping effect of the pavement materials.

The permanent deformation behavior of the HVS test structures was also studied. The two permanent deformation models considered in this study predicted the permanent deformation in the asphalt, base, subbase, and subgrade materials reasonably well.

9 CONCLUSIONS

In this research, a multilayer nonlinear elastic response model which takes the stress dependency of unbound granular materials into account was developed. The model was been verified using response measurements from two HVS tests, both of which included different load configurations and magnitudes at varying pavement temperatures. Furthermore, the response model was used in a performance prediction procedure. A three parameter work hardening model for all layers was employed. The following conclusions were drawn:

- Multilayer elastic theory in conjunction with the method employed to account for stress dependency in unbound layers captures the responses of real pavement structures with acceptable agreement under a broad range of axle loads and tire inflation pressures.
- Better agreement was observed between measured and calculated vertical strains compared to vertical stresses. This might be attributed to the fact that it is difficult to measure vertical stresses accurately in course grained materials at shallow depths.
- With regard to horizontal strains at the bottom of the asphalt layer, there was better agreement at a low temperature. This might be attributed to the fact that at low temperatures asphalt mixtures behave elastically, that is, their viscous nature becomes insignificant and is thus in better agreement with the assumptions made in this research.
- The results indirectly confirmed that the temperature correction model used in this work gives acceptable estimates of asphalt stiffness for a given temperature to estimate responses in the unbound layers.
- The permanent deformation that was predicted using the *MEPDG* model for asphalt layers and the model for unbound granular layers gave acceptable results with appropriate calibration.
- The permanent deformation contributions from stress levels of different magnitude can be combined using the time hardening approach.

REFERENCES

ARA 2004. *Guide for the mechanistic empirical design of new and rehabilitated pavement structures.* Report 1-37A, Washington, DC: Transportation Research Board of the National Academies.

Bufler, H. 1971. Theory of elasticity of a multilayered medium. *Journal of Elasticity* 1(2): 125–143.

Erlingsson, S. 2007a. Numerical modeling of thin pavements behavior in accelerated HVS tests. *Road Materials and Pavement Design 8(4)*:719–744.

Erlingsson, S. 2010a. Impact of water on the response and performance of pavement structure in an accelerated test. *Road Materials and Pavement Design 11(4)*:863–880.

Erlingsson, S. 2010b. *Pavement performance models. Part 2: Project level modeling of rutting performance – Comparison with LTPP road sections.* Nordic Cooperation Program.

Gomes-Correia, A., Hornych, P. and Akou, Y. 1999. Review of models and modeling of unbound granular materials, In: Gomes-Correia, ed.*Unbound granular material – Laboratory testing, in-situ testing and modeling*. Rotterdam: A.A. Balkema: 3–15.

Hadjidimos, A. 2000. Successive over relaxation (SOR) and related methods. *Journal of Computational and Applied Mathematics 123*:177–199.

Huang, Y.H. 1968. Stresses and displacements in nonlinear soil media. *The Journal of Soil Mechanics and Foundation Division 94(1)*. ASCE: 1–19.

Huang, Y.H. 2004. *Pavement analysis and design.* USA: Pearson Prentice Hall.

Khazanovich, L. and Wang, Q. 2007 High-Performance Layered Elastic Analysis Program. *Transportation Research Record: Journal of the Transportation Research Board, No. 2037*, Transportation Research Board of the National Academies, Washington, DC.

Korkiala-Tanttu L. 2008. *Calculation method for permanent deformation of unbound pavement materials.* PhD dissertation, Helsinki University of Technology, Finland.

Lekarp, F., Isacsson, U. and Dawson, A. 2000. State of the art I: Resilient response of unbound aggregates. *Journal of Transportation Engineering 126(1)*: 66–75.

Lukas, S.K. and Stone, H.A. 1994. *Evaluating infinite integrals involving Bessel functions of arbitrary order.* Division of Applied Sciences, Harvard University.

Lytton, R.L., Uzan, J., Fernando, E.G., Roque, R., Hiltumen, D. and Stoffels, S.M. 1993. *Development and validation of performance prediction model and specifications for asphalt binders and paving mixes*.

The Strategic Highway Research Program Project Rep. No. SHRP-A-357.

Maina, J. and Matsui, K. 2005. Elastic Multi-layered analysis using DE-Integration. *Publications of the Research Institute for Mathematical Sciences 41(5)*: 853–867.

May, R.W. and Witczak, M.W. 1981. Effective granular modulus to model pavement response. *Transportation Research Record 810*. Transportation Research Board, National Research Council Washington, DC. 1–9.

NCHRP, 2004. *Guide for the Mechanistic-Empirical Design of New and Rehabilitated Pavement Structures*, NCHRP Report 1-37A, Transport Research Board, Washington, DC. USA.

Thompson, M.R. and Elliott, R.P. 1985. *ILLI PAVE* based response algorithm for design of conventional flexible pavements. *Transport Research Record 1043*. Transportation Research Board, National Research Council. Washington, DC. 50–57.

Timoshenko, S. and Goodier, I.N. 1951. *Theory of Elasticity*. New York: McGraw-Hill.

Uzan, J. 1985. Characterization of Granular Materials. *Transportation Research Record 1022*. Transportation Research Board, National Research Council. Washington, DC. 52–59.

Wiman, L.G. 2006. *Accelerated load testing of pavements*: *HVS-NORDIC tests at VTI Sweden 2003–2004*. VTI Report 544A. Linköping: Swedish National Road and Transport Research Institute.

Wiman, L.G. and Erlingsson, S. 2008. *Accelerated pavement testing by HVS – a transnational testing equipment*, Transport Research Arena Europe, Ljubljana, 21–24 April, CD-ROM.

This page intentionally left blank

Advances in Pavement Design through Full-scale Accelerated Pavement Testing – Jones, Harvey, Mateos & Al-Qadi (Eds.)
© 2012 Taylor & Francis Group, London, ISBN 978-0-415-62138-0

Evaluation of the aggressiveness of different multi-axle loads using accelerated pavement tests

J.-P. Kerzrého, P. Hornych, A. Chabot, S. Trichet, T. Gouy & G. Coirier
UNAM Université, IFSTTAR, Bouguenais, France

L. Deloffre
Laboratoire Régional des Ponts et Chaussées de Strasbourg, Strasbourg, France

ABSTRACT: This paper presents results of a full scale accelerated test performed on the IFSTTAR pavement fatigue carrousel, to study the effect of various multiple axle combinations on bituminous pavements. The tested combinations correspond to the permissible maximum loads in France for the following axle systems: tridem axle (255 kN), tandem axle with dual wheels (210 kN), tandem axle with single wheels (170 kN) and single axle with dual wheels (130 kN). Recently, however, the French road carriers' federation was authorized to change the vehicle load from 400 kN to 440 kN. The consequences of this increase are also discussed. The test was performed on two thick bituminous pavement sections consisting of a 16-cm granular subbase and a 26-cm thick bituminous layer. Both pavements were instrumented with strain gages, vertical displacement and temperature sensors. The objective of this research is to compare the strain signals and the maximum strain levels obtained for different axle combinations and temperature conditions and then, to compare the results with classical pavement design calculations to assess the relative aggressiveness of the different axle systems. The fatigue life of the two pavements, however, was not studied because, owing to their thickness, too many load cycles would have been required to complete a full fatigue test.

1 INTRODUCTION

In France, transport of goods is currently divided up as 78% by road, 16% by waterway 5% by rail and 1% by pipeline or air. In order to absorb the expected traffic growth, the government is developing rail transport, which is considered safer and less polluting. To limit the number of heavy trucks, some Northern European countries have authorized alternatives including trains of loaded motor trucks, called ecocombis or EMS (European Modular Systems). They can haul up to 60 tons of goods, but can only be used for long distance transport and are considered more dangerous regarding traffic safety. In France, the search for a balanced transport policy was marked by the recent decision to increase vehicle maximum loads from 40 to 44 tons without modification regarding the number of axles of the vehicles. This concerns mostly five to six axle heavy goods vehicles carrying cereals, aggregates or liquids.

The impact of this gross weight legislation change on roads is not very well understood. Calculations were performed, using the French pavement design method (SETRA-LCPC, 1994; Corté and Goux, 1996) which is based on a simplifying hypotheses (linear elastic behavior, pavement design criteria based on maximum tensile strain values), but until now the problem has not been studied experimentally. This paper presents some first experimental studies, carried out on the circular test track at IFSTTAR Nantes, to compare the aggressiveness of the following different axle systems: tandem axle with single wheels, tandem axle with dual wheels, tridem axle with single wheels and single axle with dual wheels. The study was conducted to examine the performance of two thick bituminous pavements, for heavy traffic, under the above applied axle combinations adjusted to current permissible maximum loads. The pavements were instrumented with strain gages, vertical displacement sensors and temperature sensors, placed at different depths. The number of load cycles applied during this test was not sufficient to damage the thick structures. Pavement deformation and vertical displacement measurements, on the other hand, were used to assess the aggressiveness of the different axle systems.

2 PAVEMENT STRUCTURES AND LOAD COMBINATIONS

2.1 *The circular test track facility*

The IFSTTAR accelerated pavement testing facility, in Nantes (Autret et al., 1987; Gramsammer et al., 1999; IFSTTAR) is an outdoor circular carrousel dedicated to full-scale pavement experiments carried out

Figure 1. View of the IFSTTAR pavement testing facility.

with public and private partners (Figure 1). The carrousel is a one thousand horse-power electro-hydraulic facility, with a central tower and four 20-m long arms, which can run at a maximum speed of 100 km/hour. The experimental site includes three test rings, with the facility being moved from one ring to another in approximately one week.

Each arm can be equipped with different load combinations. The half-axle loads can vary from 40 kN on a single wheel to 135 kN on a triple axle system with single wheels, a tandem axle with dual wheels or a tandem axle with single wheels.

2.2 *Studied loads*

The different axle load combinations studied are presented in Figure 2. All combinations conform to the current permissible maximum loads per axle or group of axles in the French road regulations.

During the tests, a lateral wandering of the loads is applied, over a width of approximately 1.1 m (11 different lateral positions), with a Gaussian distribution over this width. The strain gages are always placed in the centre of the wheel path (Position 6).

2.3 *Pavement structures and instrumentation*

The tested pavements were thick bituminous structures commonly used for the construction of heavy traffic roads (Figure 3). Structure 1 is used for freeways with a traffic capacity of TC5-30 according to the French Catalogue of Pavement Structures (between 6 and 14 million heavy trucks over 30 years). Structure 2 is used for main or secondary roads with a traffic capacity of TC3-20 (between 0.5 and 1.5 million heavy trucks over 20 years). Both pavements were instrumented with strain gages, vertical displacement and temperature sensors during construction of the circular test track, to measure response under different load combinations. The location of the different instruments within each structure is presented in Figure 3.

The clay sand of the subbase contains approximately 10% water sensitive fines. The Unbound Granular Material (UGM) is a 0/31.5-mm crushed gneiss, classified as B according to French standards. The composition of the bituminous materials is presented in Table 1.

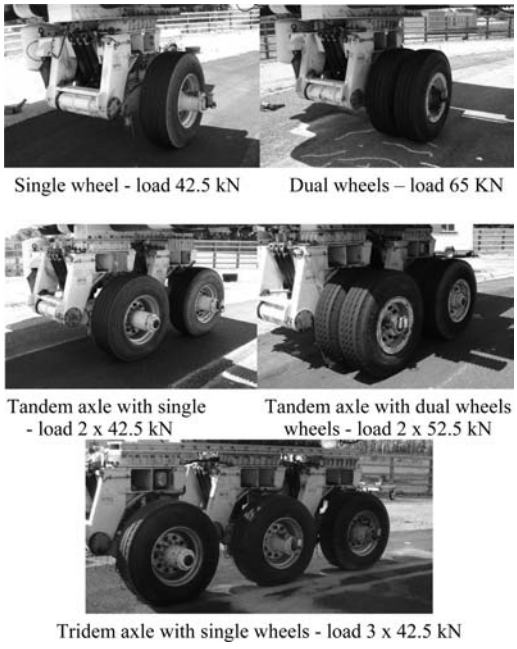

Figure 2. The circular test track facility equipped with the different axle systems studied.

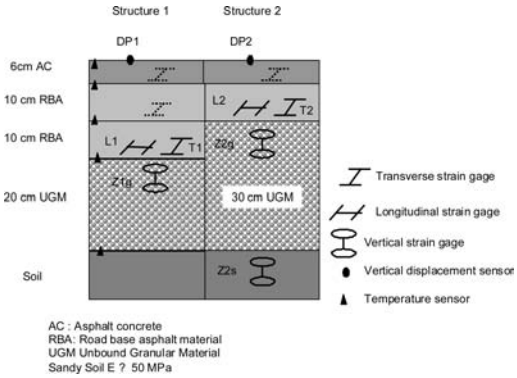

Figure 3. Instrumentation of the experimental pavements.

Table 1. Bituminous mix compositions.

Fractions	AC (Class 2) (%)	RBA (Class 3) (%)
0/2	34	35
2/6	16	20
6/10	49	10
10/14	–	35
Filler	1	–
Bitumen 35/50	5.7	4.6

Complex modulus tests on trapezoidal specimens (NF EN 12 697-31) were performed on the two bituminous mixes. The standard elastic moduli obtained for the two materials at 15°C and 10 Hz were respectively

Table 2. Huet Sayegh's model parameters obtained for the two bituminous mixes.

	E0 (MPa)	Einf (MPa)	δ	k	h
AC	20	29 843	2.194	0.217	0.658
RBA	20	22 980	1.985	0.174	0.578
	A0	A1	A2		
AC	20	29 843	2.194		
RBA	20	22 980	1.985		

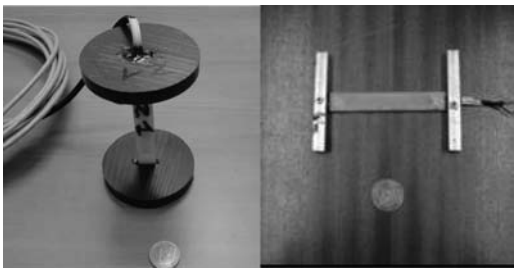

Figure 4. Strain gages used for vertical and horizontal strain measurements.

11,320 MPa and 10,700 MPa. The results of these tests were interpreted with the Huet-Sayegh visco-elastic model (Huet, 1963, 1999; Sayegh, 1965; Chailleux et al., 2006), and the model parameters obtained for the two mixes are summarized in Table 2.

The two pavement structures were instrumented with vertical strain gage sensors placed in the subgrade and the UGM, and horizontal strain gages placed at the bottom of the bituminous layers. Figure 4 shows the different gages used. An anchored vertical displacement sensor was also installed in each structure to record the vertical displacement of the pavement surface (vertical deflection). Finally, temperature sensors were placed at different depths in each structure to combine mechanical measurements with material temperature data (Figure 3).

2.4 *Axle load configurations*

The experiment was conducted in two successive phases, with different axle load combinations mounted on the four arms of the circular test track (Figure 5). The loads applied on the different groups of axles are summarized in Table 3 and correspond to the maximum permissible loads of the French road regulation.

These types of loads correspond to typical axle configurations of heavy trucks. Tridem axles with single wide wheels are those most commonly found on heavy trucks with a gross vehicle weight of 40 tons. The single wheel mounted on a single axle is never used at the rear of heavy vehicles, but only as the front axle, with a lower axle load around 70 kN. During the test, this axle was loaded at 42.5 kN and used as a reference load. The objective of the research was to

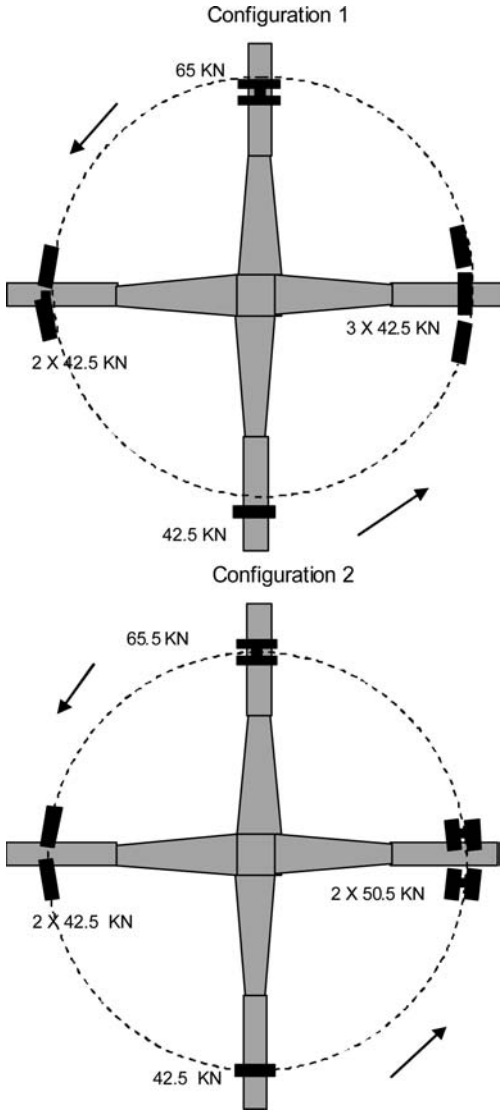

Figure 5. Two successive axle system configurations of the test.

Table 3. Current permissible maximum loads per axle or group of axles.

Axle type	Maximum load per axle (kN)
Dual wheels	130
Tandem axle with dual wheels	210
Single wide wheel	85
Tandem axle with single wide wheels	170
Tridem axle with single wide wheels	255

examine the effects, on the same sensors, of the four axle systems loaded at the maximum permissible load and to compare the results with those of the single reference wheel. Since the carrousel has only four arms,

two successive configurations were used to complete the test.

The tires chosen for the test were:

- Dunlop 385/65 R 22.5 tires for single wide wheels, inflated at 8.5 bars.
- Dunlop 12.00 R20 SP321 tires for dual wheels, inflated at 8.5 bars.

Tire imprints were determined under a load of 65 kN for the dual wheels and 42.5 kN for the single wheel (Figure 6). They can be approximated by rectangles, loaded with a mean vertical pressure of 0.62 MPa and 0.66 MPa respectively.

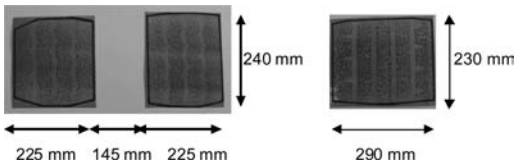

Figure 6. Dual and single wheel imprints at F = 65 kN and F = 42.5 kN, respectively.

Table 4. Maximum deflection and deformation values under a single wheel load of 42.5 KN. (speed v = 42 km /h, mean temperature T = 20°C).

	Structure 1	Structure 2
Vertical displacement at the surface of the pavement	0.32 mm	0.45 mm
Longitudinal strains at the bottom of the bituminous base layer	+90 μstrain	+150 μstrain
Transverse strains at the bottom of the bituminous base layer	+120 μstrain	+300 μstrain

3 EXAMPLES OF MEASUREMENT RESULTS

3.1 *Mechanical stiffness of the pavement structures*

The mechanical response of the tested pavements in terms of typical pavement surface deflection values and mean tensile strain values at the bottom of the bituminous materials obtained under the application of the reference load (single wheel loaded at 42.5 kN) are plotted in Table 4 (tensile strain values are positive).

Note that the transverse strains are higher than the longitudinal strains. The strain signals, presented below, also show that visco-elastic effects are more visible on the transverse strain gages.

3.2 *Examples of strain signals under the tridem axle load*

Figures 7 to 10 present examples of strain signals and displacement signals recorded as the tridem axle load (42.5 kN for each wheel) travels on both pavement structures. The distance between the wheels is 1.38 m for all the tandem and tridem combinations studied. The influence of the wheelbase on material deformations, though recognized, was not studied.

The signals were recorded under the centre of the wheels at a speed of 42 km/h and with a mean temperature within the bituminous materials of 18°C.

The signals from the longitudinal strain gages placed at the bottom of the bituminous layers always return to zero (Figure 8). The transverse strain gage signals distinctly reveal the visco-elastic behavior of the materials (Figure 9): the strains tend to cumulate under the passage of the three wheels, and the return to the zero state is slow. Some permanent deformation can sometimes be observed, in particular at high temperatures or low speeds. The transverse strains are in all cases greater than the longitudinal strains.

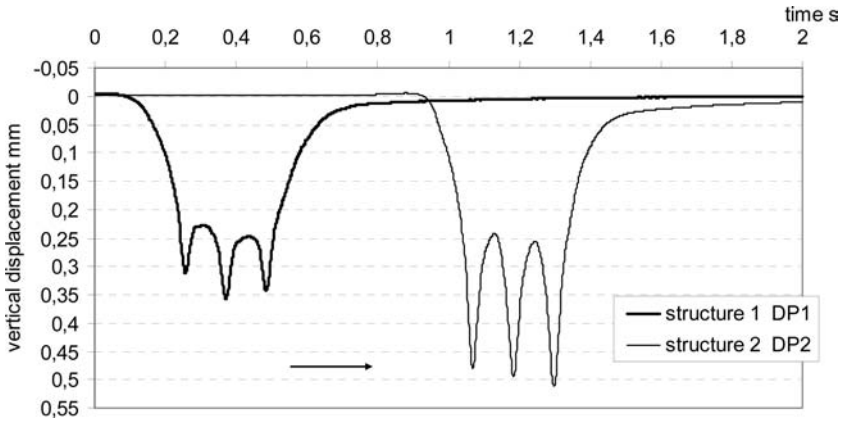

Figure 7. Vertical displacement signals at the pavement surface under tridem axle load.

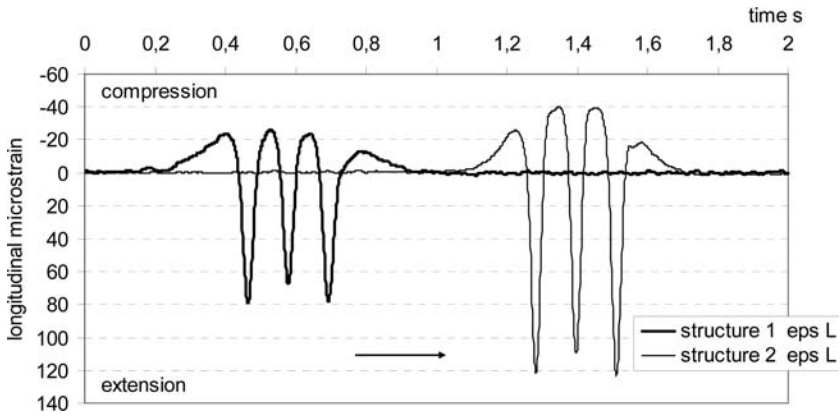

Figure 8. Longitudinal strain signals at the bottom of the bituminous materials under tridem axle load.

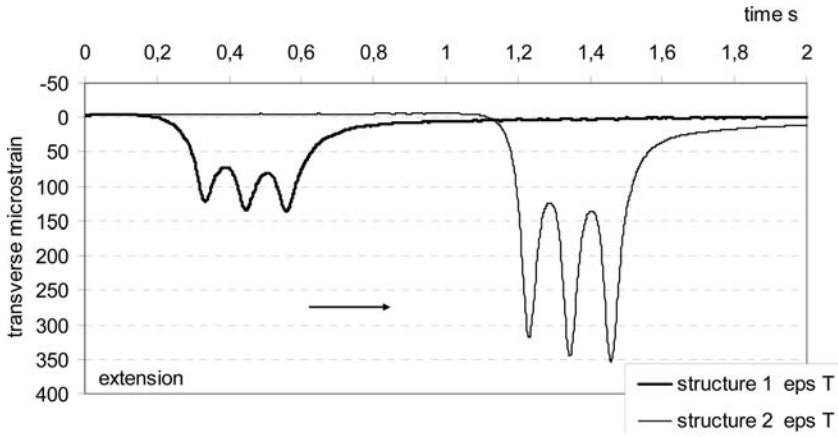

Figure 9. Transverse strain signals at the bottom of the bituminous materials under tridem axle load.

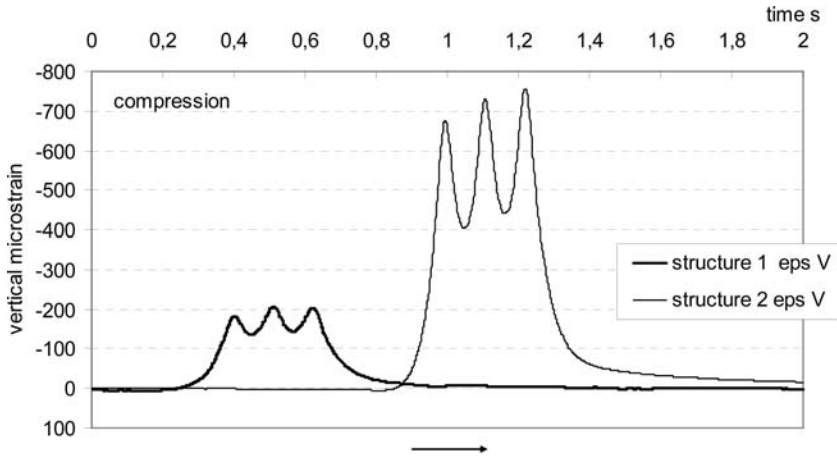

Figure 10. Vertical strain signals at top of the UGM, under tridem axle load.

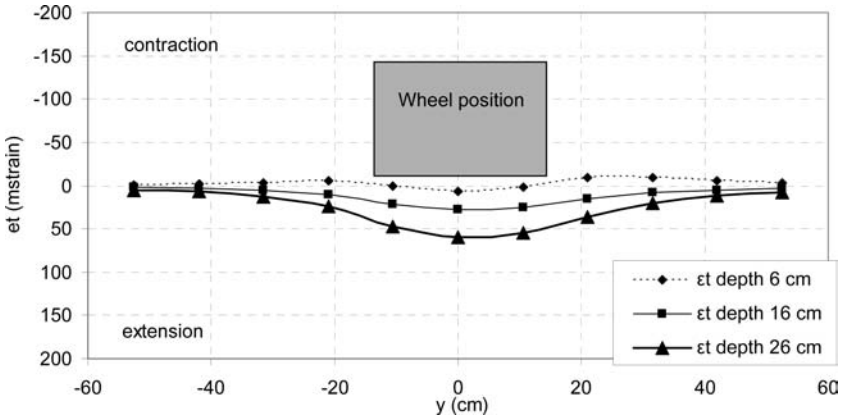

Figure 11. Maximum transverse strains under the reference single wheel load (42.5 kN) for different lateral positions (temp. 9°C).

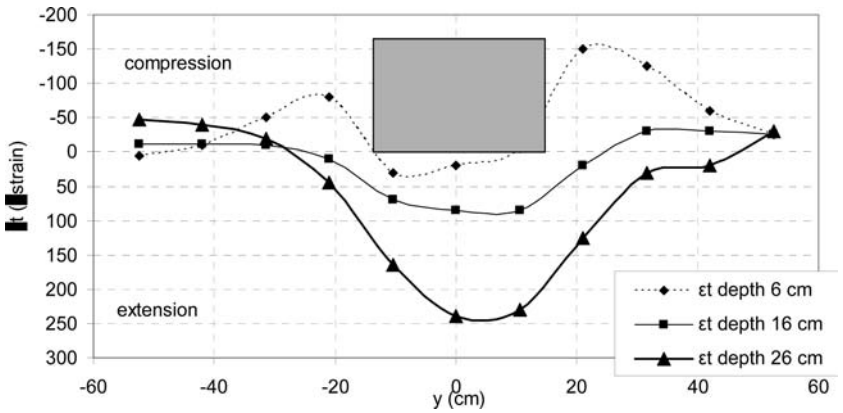

Figure 12. Maximum transverse strains under reference single wheel load (42.5 kN) for different lateral positions (temp 30°C).

4 COMPARISON OF PAVEMENT RESPONSE UNDER DIFFERENT AXLE COMBINATIONS

4.1 *Normalization of measurements recorded at different temperatures*

Figures 11 and 12 present, for Structure 1, the maximum transverse strain values measured at different depths in the bituminous layers, at two different temperatures (9°C and 30°C), under the single wheel load, for the eleven transverse positions of the wheel, due to the lateral wandering. The strain distributions change considerably with temperature. For instance, at the bottom of the bituminous base layer, under the centre of the wheel, the maximum transverse strains are about four times higher at 30°C than at 9°C. This demonstrates the high sensitivity to temperature of the response of bituminous pavements and underlines the difficulty of comparing strain measurements recorded under different axle load combinations at different temperatures.

Because of the visco-elastic, thermo susceptible behavior of bituminous materials, the recorded strain levels are highly dependent on temperature and loading speed. In this study, all the tests were performed at a constant speed of 42 km/h. (i.e., 7 revolutions/minute for loads running on the 19 m radius track). To eliminate the effect of temperature variations when comparing the effect of different axle systems, the maximum strain or displacement values obtained under different multiple axle loads were normalized by dividing them by the values obtained under the reference single wheel, at the same temperature (measurements carried out simultaneously).

4.2 *Comparison between the different axle load combinations and the single reference wheel*

As previously explained, two successive configurations were necessary to complete the test and compare the effects of the four multiple axle load combinations with those of the single 42.5 kN reference wheel. In both configurations, the reference wheel was mounted on one arm of the carrousel. The relative effect of the different axle combinations was assessed

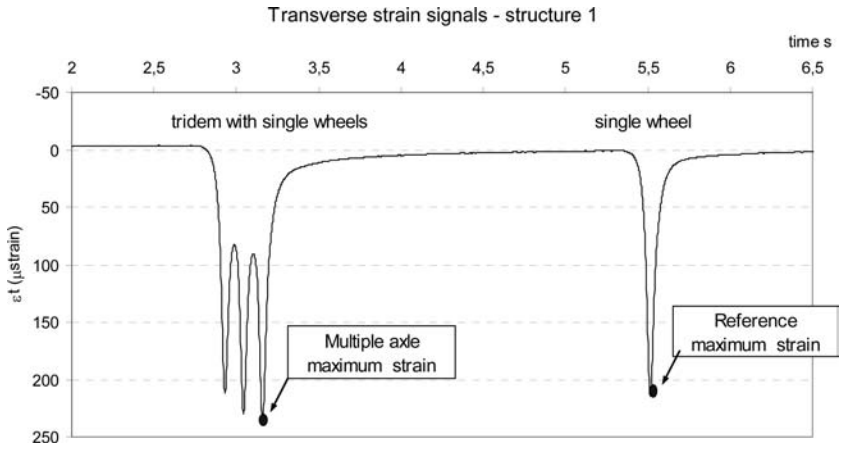

Figure 13. Example of determination of the maximum strain ratio R from measured strain signals (R = 1.14).

Table 5. Structure 1: Ratio R of the maximum strain recorded under multiple axle loads to that obtained under the reference single wheel load.

	Axle loads				
Measurement	42.5 kN single	65 kN dual	2 × 42.5 kN tandem single	3 × 42.5 kN tridem single	2 × 52.5 kN tandem dual
Vertical displacement DP1	1	1.25	1.16	1.26	1.19
Vertical strain Z1g	1	1.29	1.13	1.23	–
Longitudinal strain L1	1	1.25	0.91	0.97	0.90
Transverse strain T1	1	0.95	1.13	1.25	0.90

Table 6. Structure 2: Ratio R of the maximum strain recorded under multiple axle loads to that obtained under the reference single wheel load.

	Axle loads				
Measurement	42.5 kN single	65 kN dual	2 × 42.5 kN tandem single	3 × 42.5 kN tridem single	2 × 52.5 kN tandem dual
Vertical displacement DP2	1	1.25	1.08	1.13	1.2
Vertical strain Z2s	1	1.26	1.08	1.13	1.13
Vertical strain Z2g	1	1.12	1.06	1.14	1.18
Longitudinal strain L2	1	1.11	0.95	0.98	1.06
Transverse strain T2	1	0.93	1.08	1.1	0.98

by calculating the ratio of the maximum strain values recorded by the sensors under multiple axle loads to those obtained under the reference single wheel.

The strain or displacement ratios R are thus defined by:

R = maximum strain under multiple axle load/ maximum strain under single wheel load.

The approach for the calculation of the ratios R is illustrated in Figure 13. These ratios represent a simplification, because they only take into account the maximum strain level, and not the duration of the load signal, which is higher for a tridem axle than for a single axle.

The mean values of strain or displacement ratios R obtained for the different axle load combinations are summarized in Tables 5 and 6. These mean R values result from measurements made at different temperatures, varying between 10°C and 40°C. They were calculated for the two pavement structures, for the following sensors (Figure 3):

- Vertical displacement sensors (noted DP1 and DP2)
- Vertical strain gages placed at the top of the UGM layer (noted Z1g and Z2g)
- Vertical strain gages placed at the top of the subgrade Z2s (only for structure 2).
- Longitudinal strain gages placed at the bottom of the bituminous base layer (noted L1 and L2)
- Transverse strain gages placed at the bottom of the bituminous base layer (noted T1 and T2)

The results are similar for the two structures. In terms of the relative effect (strains) of the different axle combinations, compared with the reference single wheel, it can be concluded that:

- For the vertical deflection, and the vertical strains at the top of the subgrade, the tandem and tridem axles with 42.5 kN wheels are more aggressive than the single 42.5 kN wheel (the strains increase, due to interaction between the wheels). The most aggressive configuration is the single axle with dual wheels, with 65 kN load.
- For the transverse strains at the bottom of the bituminous layers, the tandem and tridem axles with single wheels are again, more aggressive than the single 42.5 kN wheel. The dual wheels, on the contrary, are less aggressive, in terms of transverse strains, than the single wheel.
- For the longitudinal strains at the bottom of the bituminous layers, the results are opposite to those obtained for the transverse strains: the strains are lower under tandem and tridem axles than under the single 42.5 kN wheel. The most aggressive configuration is the single axle with dual wheels, loaded at 65 kN

These results indicate that, depending on the strain criterion (or design criterion) considered, the same axle configuration is not always the most aggressive. In terms of vertical strain, and longitudinal tensile strain, the single axle with dual wheels was the most aggressive. However, the tridem axle was the most aggressive in terms of the transverse tensile strain (but the ratios R do not indicate whether longitudinal or transverse tensile strain was highest).

It should be added that these results were obtained for a given wheelbase (1.38 m) and given tire type. For tandem and tridem axles, a smaller wheelbase could lead to a higher aggressiveness (for tridem axles, the minimum wheelbase is about 1.12 m).

5 MODELLING OF MULTIPLE AXLE LOADS

The experimental results obtained on the test track were compared with pavement calculations, performed using two different models:

- A classical multi-layer linear elastic model, implemented in the software *ALIZE* (IFSTTAR).
- The software *VISCOROUTE© 2.0* (Chabot et al., 2010; Duhamel, 2005), based on a multi-layer visco-elastic model.

ALIZE is a pavement design software tool developed by IFSTTAR, based on the French pavement design method, and using a classical multi-layer linear elastic model developed by Burmister. *VISCOROUTE© 2.0* is a software tool developed for the modeling of pavements with visco-elastic layers, under moving wheel loads. It is based on the Huet-Sayegh visco-elastic model, which effectively describes the behavior of bituminous materials.

The two models were used for the two pavement structures, but due to space limitations, only the results obtained on Structure 1 are presented in this paper. Similar assumptions were used for both models:

- The thickness of the layers was equal to the real thickness measured on the pavement by leveling.
- The moduli of the unbound granular layer and subgrade were defined by back-calculation, from deflection tests, performed during and after construction.
- The comparisons were made for a series of measurements performed on the test track at an average temperature of 20°C, and a loading speed of 42 km/h.
- The properties of the bituminous layers were determined from laboratory complex modulus tests. With *VISCOROUTE©*2.0, the calculations were made with the Huet-Sayegh model parameters of the materials (Table 2), and a loading speed of 42 km/h.
- With *ALIZE*, the calculations were made with values of elastic modulus determined using the Huet Sayegh model, for the temperature and frequency of the tests (20°C, 6 Hz). This led to elastic moduli of 8,808 MPa for the wearing course bituminous concrete and 7,321 MPa for the road base asphalt.
- The loads were simulated by rectangular areas loaded by a uniform vertical pressure (Figure 6).

Figures 14 to 17 present comparisons between the longitudinal strains ε_l and transverse strains ε_t measured at the bottom of the asphalt layers, and the modeling results, for four different load combinations. The maximum strain values are presented in Table 7.

A difference can be observed between the dual wheel load at maximum measured longitudinal strains, and the loads with single wheels (1, 2 or 3 axles) at maximum transverse strains.

The following conclusions can be made concerning the prediction of the maximum tensile strains, for all the load types:

- The linear elastic model (*ALIZE*) predicts the longitudinal strains reasonably well (about 10% difference), but the transverse strains are strongly underestimated (about 50% difference).
- The visco-elastic calculations (*VISCOROUTE© 2.0*) predict much higher transverse strains than *ALIZE*, but better predict the experimental transverse strains (about 10 to 15% difference with the experimental values). The predictions are particularly accurate for the tandem and tridem axles (Figures 15 and 17).

It appears, therefore, that visco-elasticity affects transverse strains more than longitudinal strains, which has already been observed on the experimental measurements. Viscous effects tend to increase the transverse strains, compared with linear elastic behavior, and is confirmed both by the experimental measurements, and the *VISCOROUTE© 2.0* calculations. The increase of transverse strains is particularly

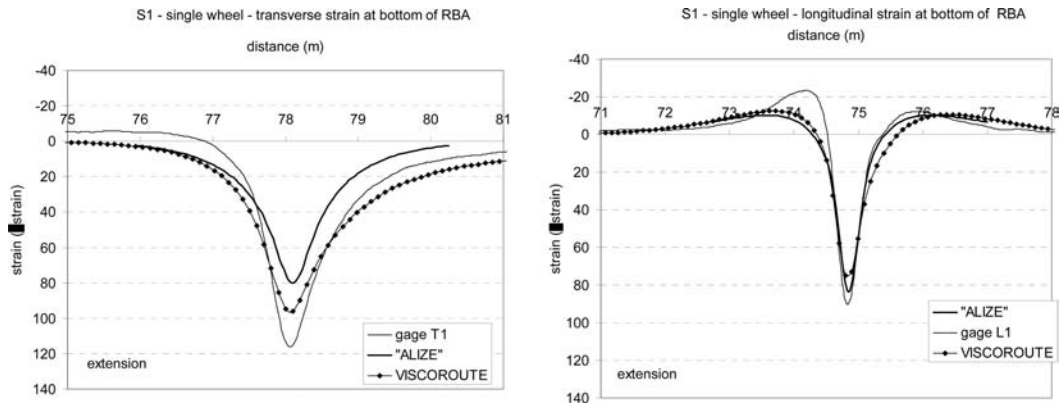

Figure 14. Structure 1 – comparison of measured and calculated strains under single wheel load.

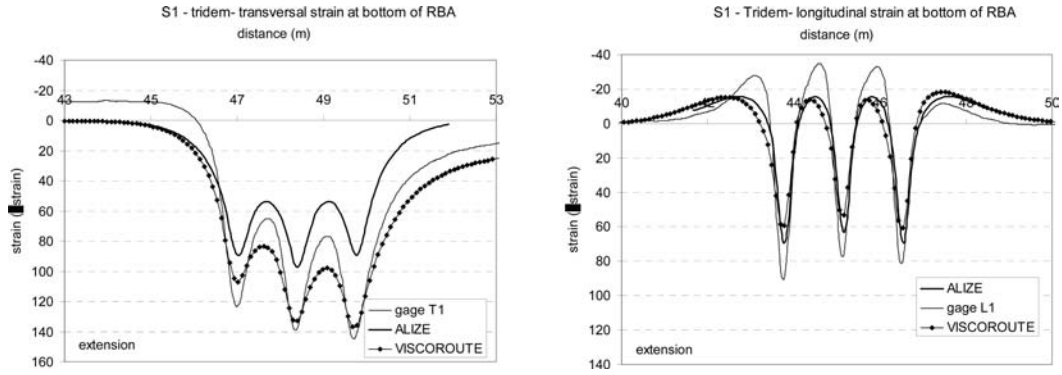

Figure 15. Structure 1 – comparison of measured and calculated strains under tridem axle.

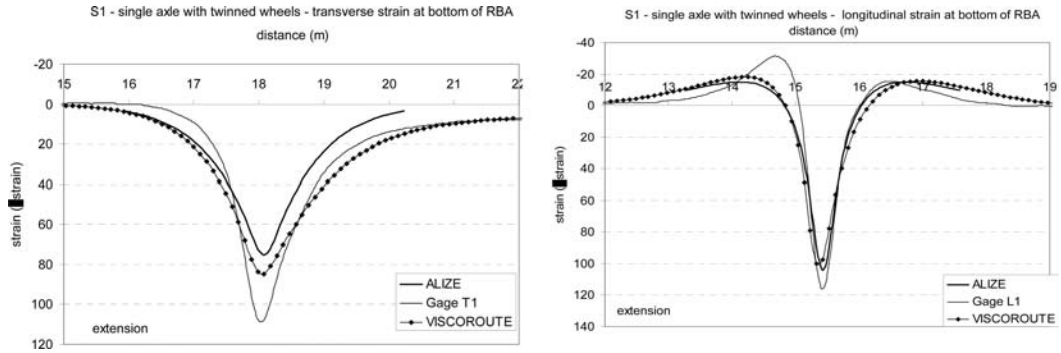

Figure 16. Structure 1 – comparison of measured and calculated strains under single axle with dual wheels.

important for the tandem and tridem axle loads. This result can have important implications on classical pavement design calculations, carried out with linear elastic models. It implies that these calculations can significantly underestimate the real maximum tensile strains (this is discussed in the next section).

The results show that the *VISCOROUTE© 2.0* software, based on the Huet-Sayegh model, simulates the response of the bituminous pavement reasonably well, for the conditions of the tests (temperature 20°C and speed 42 km/h), and the effects of different single or multiple axle loads. These satisfactory results were obtained with model parameters obtained from laboratory complex modulus tests. More detailed evaluations comparing *VISCOROUTE© 2.0* with results from this APT experiment are planned, specifically different

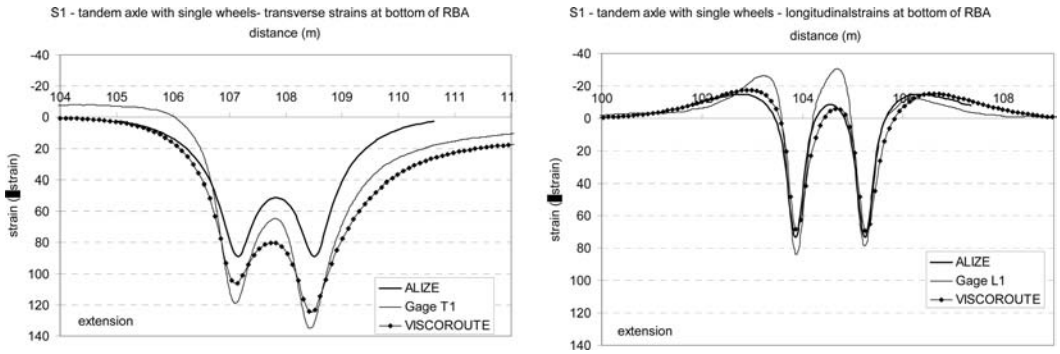

Figure 17. Structure 1 – comparison of measured and calculated strains under tandem axle with single wheels.

Table 7. Comparison of maximum measured and calculated tensile strains at bottom of bituminous layers under the different axle combinations.

Method	Strain	42.5 kN single	65 kN dual	42.5 kN tandem single	42.5 kN tridem single
Measured (μstrain)					
Gage L1	ε_l	89.7	116.2	83.8	91.0
Gage T1	ε_t	115.9	108.7	135.1	144.7
Predicted (μstrain)					
ALIZE	ε_l	83.6	104.2	73.3	69.4
	ε_t	80.3	75	88.6	97.3
	ε_l	75	100.2	69.1	60.5
VISCOROUTE	ε_t	96.1	84.7	124.3	136.6

speed and temperature conditions (measurements are available for temperatures between 10 and 40°C, and speeds from 3 to 70 km/h).

6 EVALUATION OF THE AGGRESSIVENESS OF THE DIFFERENT AXLE COMBINATIONS

The French pavement design method (SETRA-LCPC, 1994; Corté and Goux, 1996) is a mechanistic-empirical method, based on multi-layer linear elastic calculations. For bituminous pavements, such as those tested in this APT experiment, the main design criterion is based on the maximum tensile strain at the bottom of the bituminous layers. A second criterion, based on the maximum vertical strain at the top of the subgrade also exists. The tensile strain criterion is based on a fatigue law, for bituminous materials, determined experimentally from two point bending fatigue tests on trapezoidal specimens (Standard EN 12697-24). The expression of the fatigue law is:

$$\varepsilon = \varepsilon_6 \left(\frac{N}{10^6} \right)^b \quad (1)$$

where:

- ε_6 is the strain leading to fatigue failure for 10^6 load cycles;
- b is the exponent of the fatigue law; $b = -0.2$ for bituminous materials;
- N is the number of load cycles.

Inverting the fatigue law (Equation 1) leads to the following expression, for the number of load cycles $N_{failure}$ leading to failure:

$$N_{failure} = 10^6 \left(\frac{\varepsilon}{\varepsilon_6} \right)^{-5} \quad (2)$$

Using Equation 2, the relative aggressiveness A of two different loads, according to the French pavement design method, can be expressed, for bituminous pavements, by:

$$A = \frac{N_{failure}(load2)}{N_{failure}(load1)} = \left[\frac{\varepsilon(load1)}{\varepsilon(load2)} \right]^5 \quad (3)$$

A is defined as the ratio of the design lives (in terms of number of cycles leading to failure) for each load level, or as the ratio of the fatigue damage produced by one application of *Load-2*, in comparison with one application of *Load-1*. In the case of multiple axles groups, the coefficient *A* is calculated for each individual axle of the group.

Values of the relative aggressiveness *A* were determined for the different multiple axle loads, compared to the reference single wheel loaded at 42.5 kN. These values were calculated first using the maximum tensile strains ε_{tmax} obtained with the design software *ALIZE*, and also using maximum tensile strains measured experimentally on the test track. The results are presented in Table 8.

With the *ALIZE* calculations, the most aggressive load is the single axle with dual wheels ($A = 3.01$), followed by the tridem axle ($A = 2.14$). With the experimental measurements, the rating is quite different, with the most aggressive load being the tridem axle

Table 8. Relative aggressiveness coefficients obtained for the different multiple axle loads, in comparison with the single wheel loaded at 42.5 kN.

Parameter	42.5 kN single	42.5 kN tandem single	42.5 kN tridem single	65 kN dual
Measured				
ε_{tmax} (μ strain)	115.9	135.1	144.7	116.2
A value	–	2.15	3.03	1.01
ALIZE calculations (μ strain)				
ε_{tmax} (μ strain)	83.6	88.6	97.3	104.2
A value	–	1.34	2.14	3.01

Table 9. Typical wheelbases used on heavy truck rear axle systems.

	Tridem, single	Tandem, dual	Tandem, single	Tandem, single, very wide
Tires	385/65 R22.5	1200 R20	385/65 R22.5	445/65 R22.5
Wheel base (cm)	135	135	130	130
	130	130	–	–
	120	–	–	–
	116	–	–	–
	112	–	–	–

($A = 3.03$), and the least aggressive the single axle with dual wheels ($A = 1.01$). In conclusion, the standard linear elastic calculations again do not correctly predict the maximum tensile strains under multiple load configurations (due in particular to visco-elasticity), and can give misleading conclusions, concerning the aggressiveness of different axle configurations. In particular, it appears that the aggressiveness of tridem axles is underestimated by linear elastic calculations. The results obtained with *VISCOROUTE© 2.0* suggest that aggressiveness can be better evaluated using visco-elastic models.

For a given load type, there was also a large difference between the experimental and calculated maximum tensile strains (up to 50%). However, it appears quite difficult to compare directly, for one load type, the aggressiveness obtained with experimental and calculated strains, because in the French design method, calibration coefficients are introduced to correct the calculated fatigue life, in order to match the field behavior. Therefore, it is probable that these "calibration coefficients" already account for the difference between experimental and calculated strains. Consequently, only relative comparisons of damage caused by different axle configurations can be made, and not direct comparisons of damage due to the calculated and experimental strains.

7 DISCUSSION OF THE IMPACT OF AXLE WHEELBASE AND 10% INCREASE OF THE GROSS HEAVY VEHICLE WEIGHT

In France, measures have recently been taken to relax gross weight legislation for 210 kN tandem axles with dual wheels and 255 kN tridem axles with single wheels, and to authorize an increase of 10% of the gross weight. On the IFSTTAR test track, both axle systems were tested with a wheel base of 1.38 m. However, wheel base can vary depending on vehicle type. Table 9 presents the usual wheelbases used on heavy truck rear axle systems in France.

Table 9 shows that tridem rear axle systems in particular can have smaller wheelbases than 1.38 m, down to 1.12 m. These small wheelbases are often used on vehicles carrying heavy materials, like cereals or aggregates, which need to maneuver easily and discharge their load at the rear of the vehicle (Figure 18). Particular concerns are being raised about the possible increase of the gross weight on these vehicles, because they are usually loaded to the maximum authorized load. It is therefore interesting to evaluate the aggressiveness of these tridem axles with small wheelbase. For this purpose, calculations were performed using both standard linear elastic and visco-elastic models (to try to take into account the visco-elastic effects), for pavement Structure 1 from the APT experiment. Three cases were considered:

Figure 18. 44 ton heavy vehicle with tridem rear axle system, wheelbase = 112 cm.

1. The tridem axle with 1.38 m wheelbase with 3×42.5 kN load.
2. The tridem axle with 1.12 m wheelbase with 3×42.5 kN load.
3. The tridem axle with 1.12 m wheelbase with 3×46.75 kN load (10% overload)

The results are presented in Table 10. The first case was considered as the reference, and the relative aggressiveness of cases 2 and 3, compared with this reference was calculated. For the linear elastic calculations, the results indicate:

– Relative aggressiveness A of 1.56 for the tridem axle with 1.12 m wheelbase
– Relative aggressiveness A of 2.51 for the tridem with 1.12 m wheelbase and 10% overload.

Table 10. Prediction of aggressiveness with reduced wheelbase and 10% overload.

Parameter	42.5 kN tridem, 1.38 m wheelbase	42.5 kN tridem, 1.12 m wheelbase	46.75 kN tridem, 1.12 m wheelbase
ALIZE			
ε_{tmax} (μ strain)	97,3	106.4	117
A value	1	1.56	2.51
VISCOROUTE			
ε_{tmax} (μ strain)	132.5	146.4	161.3
A value	1	1.65	2.67

With the visco-elastic calculations, the values of A are slightly higher than for linear elasticity, but the difference is not significant ($A = 2.67$ for case 3 instead of 2.51). There is, again, a large difference between the maximum tensile strains given by the linear elastic and visco-elastic calculations. However, a direct comparison between aggressiveness obtained with linear elastic or visco-elastic behavior, for the same load, is not possible, because the design life calculations are calibrated only for the linear elastic model.

This last comparison is based only on model predictions, because these modified wheelbases and axle loads have not been tested on the accelerated test track. More APT tests clearly need to be carried out to improve understanding of the aggressiveness of different loads, including the effects of wheelbase, type of tires, loads and pavement structure, and to take into account the results in pavement design.

8 CONCLUSIONS

This paper presents the first pavement mechanics study carried out using the IFSTTAR's pavement circular test track with different axle system combinations mounted on each of its four arms.

The French road carriers' federation is currently exercising pressure on the government to increase the gross vehicle weight from 400 kN to 440 kN and more, without modifying the number of axles. Knowledge of the impact that such an increase may have on pavements is in great demand by society and the legislature.

The key finding from this study, as regards pavement mechanics, is that experimental strain measurements in pavement layers appear to provide the best information on the aggressiveness of an axle system. The results of the study concern mainly the tensile strains obtained at the bottom of bituminous layers, which are presently used as design criterion in the French and many other pavement design methods for bituminous pavements. The study has led to several interesting conclusions:

– Strain distributions under multiple axle loads are complex, and for the different axle combinations studied, the most critical tensile strains can be either longitudinal (for the dual wheels) or transverse (for the configurations with 1, 2 or 3 axles with single wheels).
– Visco-elastic behavior seems to have a particularly strong effect on the transverse strains, which tend to cumulate under the passage of several successive axles, and return more slowly to zero than the longitudinal strains.
– Due to this accumulation of transverse strains, tandem and tridem axles produce, experimentally, higher tensile strains than what would be expected from linear elastic response.
– Comparisons with linear elastic calculations indicate that linear elasticity predicts longitudinal strains reasonably well, but under-predicts the transverse strains, in particular under tandem or tridem axles with single wheels. If linear elasticity is used for pavement design calculations, the aggressiveness of certain axle combinations may be underestimated. In particular, linear elasticity indicates the highest aggressiveness for single axles with dual wheels loaded at 65 kN, whereas strain measurements indicate that the tridem with single wheels (42.5 kN per wheel) produces higher tensile strains, and is therefore more aggressive.
– Better predictions of the measured strains (essentially the transverse strains) were obtained with the software *VISCOROUTE© 2.0*, using the visco-elastic Huet Sayegh Model. Visco-elastic calculations appear particularly interesting for predicting the effects of multiple axle loads. They give the same ratios between longitudinal and transverse strains to those recorded in the experimental measurements, whereas linear elastic calculations can give the opposite.

Based on these results in this study, prediction of response of bituminous pavements using visco-elastic models clearly appears to be very promising, but further studies are still needed to confirm and validate these results for a larger range of experimental conditions, including for instance higher temperatures. Application of such calculations to design requires caution, because in the French design method, the failure criteria, material specifications, and the associated calibration coefficients are based on linear elastic modeling, and changing the pavement model is not possible without also adjusting the other elements.

The results obtained from this study are limited, because they were obtained for a given set of axle combinations, with identical tires. Other aspects such as load, tire type, tire pressure, and wheelbase were not studied. However, they show that APT tests have a great potential for studying the effects of aggressiveness of different axle systems, which represent a very important issue for the transportation sector, because they can influence the evolution of heavy vehicle configurations, and permitted vehicle weights.

It is also clear that experiments like the one presented here, centered on measurement of deformations under different loads are not sufficient, and that to

improve our understanding of axle system aggressiveness, it is necessary to undertake fatigue tests, until significant damage of the pavement structures is achieved. However, this implies some experimental constraints:

- Each load type must be tested on a separate pavement section (on the IFSTTAR facility, it is possible to carry simultaneous tests at two different radii, of 16 m and 19 m).
- Since the acceleration capacity of the circular test track is limited (about 1 million loads per month), such tests can be performed only on relatively thin pavements (15 cm of bituminous materials is approximately the maximum).

Another aspect which also needs to be investigated with accelerated testing is the effect of different axle configurations on the wear and deterioration of surface pavement layers.

ACKNOWLEDGMENTS

The authors would like to thank Jean-Maurice Balay and Didier Bodin from IFSTTAR for their active participation in this project.

REFERENCES

Autret, P., de Boissoudy, A.B. and Gramsammer, J.C. 1997. The circular test track of the Laboratoire Central des Ponts et Chaussées – First Results. *Proc. 6th Intern. Conf. on Structural Design of Asphalt Pavements,* Ann Arbor, June 13–17 1997. 1: 550–561.

Chabot, A., Chupin, O., Deloffre, L. and Duhamel, D. 2010. *Viscoroute 2.0*: a tool for the simulation of moving load effects on asphalt pavement. *IJRMPD Special Issue on Recent Advances in Numerical Simulation of Pavements 11(2)*: 227–250.

Chailleux, E., Ramond, G., Such, C. and de la Roche, C. 2006. A mathematical-based master-curve construction method applied to complex modulus of bituminous materials. *Roads Materials and Pavement Design 7* (EATA Special Issue): 75–92.

Corte, J.F. and Goux, M.T. 1996. Design of pavement structures: the French technical guide. *Transport Research Report*, 1539: 116–124.

Duhamel, D., Chabot, A., Tamagny, P. and Harfouche, L. 2005. *ViscoRoute*: visco-elastic modeling for asphalt pavements. *Bulletin des Laboratoires des Ponts et Chaussées* (http://www.lcpc.fr/en/sources/blpc/index.php), 258–259: 89–103.

Gramsammer, J.C., Kerzreho, J.P. and Odeon, H. 1999. The LCPC's A.P.T. Facility: Evaluation of Fifteen Years of Experimentations. *Proceedings of 1st International Conference on Accelerated Pavement Testing, October 18–20, 1999 Reno, NV.*

Huet, C. 1963. *Etude par une méthode d'impédance du comportement viscoélastique des matériaux hydrocarbonés.* PhD. Thesis. Université de Paris, France.

Huet, C. 1999. Coupled size and boundary-condition effects in viscoelastic heterogeneous and composite bodies. *Mechanics of Materials 31*: 787–829.

IFSTTAR. *The Accelerated Load Testing Facility*: http://www.lcpc.fr/en/presentation/moyens/manege/index.dml

IFSTTAR: *Alizé-Lcpc software for the design of pavements according to the French rational method*: www.lcpc.fr/en/produits/alize/index.dml

Sayegh, G. 1965. *Contribution à l'étude des propriétés viscoélastiques des bitumes purs et des bétons bitumineux.* PhD Thesis. Faculté des Sciences de Paris, France.

SETRA-LCPC 1994. *Conception et dimensionnement des structures de chaussée*. Guide Technique. Ministère de l'équipement des Transport et du Tourisme. Paris, France.

This page intentionally left blank

Advances in Pavement Design through Full-scale Accelerated Pavement Testing – Jones, Harvey, Mateos & Al-Qadi (Eds.)
© 2012 Taylor & Francis Group, London, ISBN 978-0-415-62138-0

Accelerated pavement testing-based pavement design catalogue

W.J.vdM. Steyn
University of Pretoria, Pretoria, South Africa

ABSTRACT: Full-scale Accelerated Pavement Testing (APT) is conducted by a number of international facilities with APT devices and who have funding to conduct this type of testing. There are a host of countries who cannot afford such programs and miss the opportunity of obtaining potential APT benefits. Although the objectives of each APT program differ, the results of different APT programs can often be complimentary when viewed holistically and not on a program by program or client by client basis. A compilation of the outputs from APT programs linked to the Heavy Vehicle Simulator International Alliance (HVSIA) has been used in this paper to generate an empirical pavement design catalogue for preliminary pavement thickness design. Surface rut was used as the failure condition for the catalogue. The paper focuses on the process followed and the outcomes of the study.

1 INTRODUCTION

Many Accelerated Pavement Testing (APT) experiments (using the Heavy Vehicle Simulator [HVS]) have been conducted by members of the Heavy Vehicle Simulator International Alliance (HVSIA) before and since its formation in 2003. These tests were conducted on a range of pavement structures considering a vast amount of material combinations. All of these studies contributed to reports written by the relevant testing agencies. Each report had a different focus, be it individual material or entire pavement structure performance, and relevant conclusions have been drawn on the different focus areas. Second-level analyses have been done with the objective of answering specific agency-based research questions.

The work described in this paper was conducted based on discussions in the HVSIA that focused on opportunities to compile the data from these tests into a more holistic research offering. The objective of the paper is to investigate the potential of using historic HVS data from a range of pavement structures to develop a new pavement design catalogue. The paper is based on analyses of available data from the HVSIA members regarding historic HVS test reports to develop a generic pavement design catalogue that can be used as a first-level indication of suitable pavement structures for various conditions (Jansen van Rensburg, 2009).

HVS test reports typically consist of relevant data on permanent deformation, fatigue cracking, environmental influences and construction details, all of which are relevant to the field of pavement engineering. Although all the above factors are important, only rut performance is considered in this paper, as this was the common parameter evaluated in all the studies. Expansion of the design catalogue will require incorporation of other failure conditions such as fatigue and thermal cracking. Evaluation included HVS test reports from the last 10 to 15 years with asphalt, granular, bitumen emulsion (or emulsified asphalt) stabilized granular, and asphalt treated base layers. The information obtained was combined into a three-dimensional matrix with traffic class, temperature, and base material being the respective axes of the matrix. The pavement material was evaluated and inferences drawn around the potential failure modes, and environmental influences that would accelerate or retard these modes. Where a particular test was stopped early or if water was added, conclusions had to be drawn on what the behavior of the base materials was before and after these influences to obtain the best possible behavioral indication.

The evaluation focused on rut performance of each test's base and surfacing combination as measured on the surface of the pavement. All the materials from the HVS test reports were evaluated according to their rut performance at 10 mm and 20 mm, defined as the warning and terminal levels of pavement performance, respectively. Where test data deviated from normal behavior, a statistical approach was taken to determine the final location of the base material in the three-dimensional matrix. The pavements were grouped according to their base course classification. Simulated environmental factors (i.e., changes in temperature and moisture content during the test) played a major role in the pavement material rut performance (as would be expected), and this was used as another parameter with traffic class to set up the three-dimensional matrix used as a pavement selection catalogue.

2 BACKGROUND

The HVSIA is a voluntary association of HVS users, established to promote interaction between users and to coordinate testing and the dissemination of test results. The HVSIA website (*www.hvsia.co.za*) captures pertinent information and displays meta-data with respect to the results of tests. The objectives of the HVSIA are to promote and share knowledge related to HVS technology; establish a structure for ongoing interactions focusing on HVS technology; establish mechanisms for funding, monitoring and completion of studies on common issues through participation of members; provide expertise to expeditiously define, manage and review studies of interest; and optimize resource use through coordination of HVS related research. All HVS owners continue with their own research programs while the HVSIA activities complement and support the efforts of individual members (Steyn, 2012). The current (October, 2011) members of the HVSIA are South Africa (Council for Scientific and Industrial Research [CSIR]/Gautrans), California (University of California Pavement Research Center [UCPRC]), Florida Department of Transportation (FDOT), US Army Engineer Research and Development Center – Cold Regions Research Engineering Laboratory (EDRC-CRREL), EDRC Geotechnical and Structures Laboratory (EDRC-GSL), Sweden VAG-OCH Transportforskningsinstitut (Swedish National Road and Transport Research Institute [VTI]), Costa Rica, China (Chang'an University), and India (Central Road Research Institute [CRRI]).

Collaboration between APT programs is often suggested as a method to encourage cost efficiencies, but is usually difficult to implement (Hugo and Epps Martin, 2004; Harvey, 2008). The HVSIA has, with no formal budget, been effective in encouraging interaction between users of HVS equipment. It has produced a number of useful products, including:

- The HVSIA activity matrix, which provides a quick reference to all research performed by HVSIA members by focus and competency area, with links to access reports that are available on this research. It also includes planned HVS research projects which are likely to lead to collaboration on actual research projects by HVSIA members, and, possibly, others (this matrix formed the data source for this paper),
- The HVSIA instrumentation matrix provides information on instrumentation used by HVSIA members, and
- Workshop and specialty sessions of interest to the HVSIA members including: HVS tests versus long-term field performance, analytical and performance issues, data collection issues, evaluation and quantification of HVS test benefits, stiffness related to structural design, linkages between APT and long-term monitoring (LTM) and mechanistic-empirical (ME) design and calibration.

The somewhat intangible benefit of ongoing interest and interaction between HVSIA members is viewed as the HVSIA's greatest success. This interaction is actively fostered within the HVSIA as members share a focused common interest.

APT is a process developed to bridge the gap between empirical design models and real life. This method evaluates a pavement structure under traffic conditions at an accelerated rate. APT provides a great deal of data ready for analysis that is very relevant to material performance (Du Plessis et al., 2008).

A pavement consists of a combination of layers that is placed on either a roadbed, or on the in situ subgrade material, to protect from the influences of traffic loading. It is important to evaluate the behavior of a pavement as a system, since the contribution of each of the layers in that system affects the ultimate reaction of the pavement structure to the applied loads and environmental conditions. The purpose of pavement design is to provide a pavement that is the most economical and still fulfills its requirements of providing a safe and desirable ride quality for at least its design life. A pavement structure is considered as unfit for use following one of two main failures, the first being functional failure and the other structural failure. It is considered a functional failure if it no longer fulfills its purpose of providing an acceptable riding experience to the road user with respect to riding quality, accident risk, and comfort. Structural failures are defined as a physical failure to one or more of the pavement layers contributing to the pavement structure. These failures include rutting, bleeding, cracking, etc.

A pavement catalogue design method is one that uses a catalogue instead of empirical or deterministic design procedures to give the final pavement structure. It typically consists of a selection of tables or graphs, from which a designer can use to select and appropriate road structure. The tables or graphs are grouped according to their base type, design traffic, and environmental conditions that can be expected (dry or wet regions). In these tables the material can be directly selected even if only the road category and the design traffic are known. In South Africa, the Technical Recommendations for Highways #4 (TRH4, 1996) document provides the basis for the structural design of pavements and contains a proposed catalogue design for typical South African traffic, environmental, and materials conditions. Typically, a catalogue design method will only define the applied loads in terms of the equivalent standard axle loads (ESALs) applicable for the specific pavement structure. An example of a catalogue design from TRH4 is shown in Figure 1. This catalogue design method option requires the user to determine the environmental conditions and traffic loading for the specific application, decide on the type of pavement structure (i.e., granular or stabilized base), and then select an appropriate design from the various applicable catalogues.

It should be noted that the South African National Roads Agency Limited (SANRAL) is in the process of substantially updating the existing SA pavement

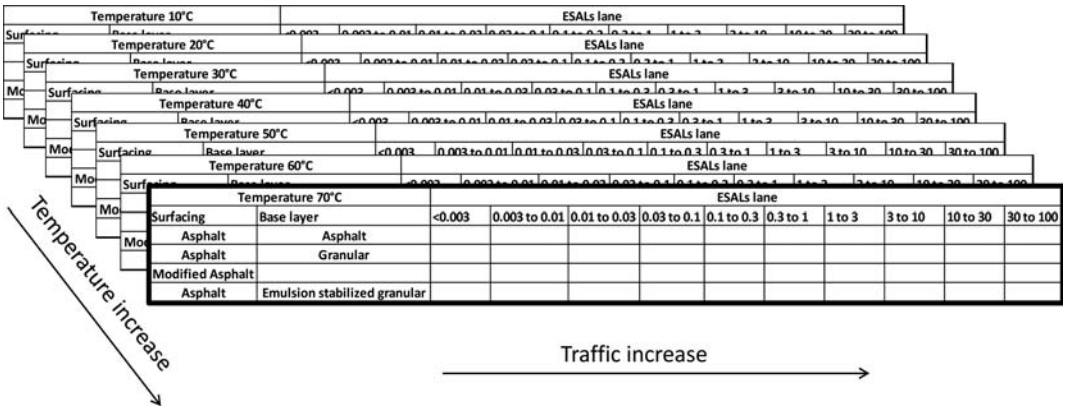

Figure 1. Three-dimensional structure with base layer, test temperature and traffic as respective axes.

design method, with a current expected implementation date around 2014 (Theyse et al., 2011), and the further use of the current TRH4 pavement catalogue design method will thus be affected by the outcome of this new design method.

The development of a pavement design catalogue is based on either an empirical selection process of pavement structures known to provide an acceptable level of performance, or an extensive mechanistic evaluation of potential pavement structures to develop potential structures to be used in the catalogue. The approach taken in the development of this APT-based catalogue design method is a hybrid method, where known pavement structures from APT experiments form the basis of the catalogue, while the various structures have been evaluated as part of the APT research to ensure that they provide mechanistically balanced structures.

3 METHODOLOGY

Permanent deformation data for the combined surfacing and base layers from selected HVS tests were collected from the HVSIA database to form the source material for the development of the catalogue. Data were grouped together according to the different base layer types (three options evaluated) and then evaluated to identify their appropriate locations in a three-dimensional catalogue.

3.1 *Three-dimensional matrix*

Available reports were studied to select categories that best described the fields relevant to pavement design. These categories included base layer type, cumulative traffic load, moisture conditions, and pavement test temperature. The types of base layers considered during the evaluation process included granular, bitumen emulsion stabilized granular, and bitumen-treated layers. The type of surfacing on the base layer was used as a secondary category under the type of base layer. The actual test temperature and moisture contents at which the specific HVS tests were conducted were used as input data. The temperature was mainly used to account for effects in the surfacings and bitumen emulsion stabilized and bitumen treated base layers, while the moisture conditions mainly affected the granular base layers' performance.

A method consisting of eight steps was developed to evaluate the data from the various HVS tests:

- Step 1: Data acquisition: Collect test data and evaluate HVS test reports to see if these tests have base layers consistent with that of the three-dimensional matrix.
- Step 2: Group all tests together that have base layers consistent with base layers in the matrix.
- Step 3: Identify tests that were not done at an applied load of 40 kN and use equivalency factors to transform the number of repetitions to compensate for the deviation in applied load, using the method developed by Kekwick (1985).
- Step 4: Identify in which manner each test's rut performance was reported. Inspect whether the test was stopped before a warning (10 mm) or terminal (20 mm) rut level was reached. If it was stopped prematurely, determine the rut rate for each test. Determine the number of repetitions each base layer could withstand before reaching 10 mm and 20 mm of rut.
- Step 5: Use the cumulative repetitions and testing temperature to place the test's base layer in the most appropriate cell in the three-dimensional matrix. Identify whether a test section was resistant to water that was added to the tests.
- Step 6: Evaluate the three-dimensional matrix and identify where more than one test's base layer occupies a single location in the matrix. Evaluate these data sets further to select the most appropriate base layer for a given cumulative traffic load and temperature.
- Step 7: Compare data in the three-dimensional pavement catalogue with pavement structures in the TRH4 catalogues.

Table 1. Summary of granular-based test sections used in developing pavement design catalogue.

Test data origin	Sections	Test temp. (°C)	Surfacing details	Base details	Test load (kN)	Tire pressure (kPa)
Florida	15	Ambient to 65	AC (PG67-22 & PG76-22)	Limerock; 225 mm	40	790
Gauteng	7	20 to 71	AC (PG64); single seal	Weathered granite; 150 mm (G4)	40; 70	520; 620
Finland/Sweden	2	10	AC (Pen 80)	Lusi/Teisko; 250 mm (Q1, Q2)	60; 80	800
Caltrans	1	20	AC (gap graded)	Granular; 350 mm (Class 2)	60 to 100	720

Table 2. Summary of bitumen emulsion stabilized base test sections used in developing pavement design catalogue.

Test data origin	Sections	Test temp. (°C)	Surfacing details	Base details	Test load (kN)	Tire pressure (kPa)
Gauteng HVS	7	Ambient	AC; single seal	Bitumen emulsion stabilized granular	40 to 100	520 to 850

– Step 8: Identify gaps in the three-dimensional catalogue and use a statistical approach together with the TRH4 catalogues to complete the gaps.

Steps 1 to 6 were completed for each of the three types of base layer. Where more than one data set occupied a single cell in the three-dimensional matrix, with temperature and ESAL being the respective axes, the data were evaluated after Step 6 had been completed for all tests, as the type of base layer was irrelevant in the two-dimensional matrix for ESAL against temperature. Step 7 and 8 were completed after completing Step 6 for all types of base layer.

3.2 *Determining rut rate*

When a particular test's rut performance was only available in a graphic form (as in the case of the 15 granular base layer tests from the Florida facility), a rut rate equation was determined by scaling the data from the graph, or through generating a creep curve based on the data. This process allowed for the calculation of expected ESALS to the 10 mm and 20 mm rut levels defined for the catalogue. The basic assumptions used were that the rut rates were constant when this process was followed, and that, without any extraneous effects (i.e., changes in traffic load or environmental condition) the rut rate would remain constant.

3.3 *Positioning data in the three-dimensional matrix*

The data were placed in the three-dimensional matrix by first considering only two axes at a time. The two two-dimensional structures were essentially base layer type versus traffic (ESALs) and temperature versus traffic (ESALs). In the first structure temperature, was not considered relevant and in the second structure base layer was not considered relevant in placing the data. The type of base layer was also categorized against the type of surfacing used as this can also influence the performance of the pavement structure. The two two-dimensional matrices are shown as one three-dimensional image in Figure 1.

To add a data point into the two-dimensional structure the temperature and ESAL would need to fall into the ranges described in the two-dimensional matrix. The temperature fields have a 10°C variance (based on inspection of all available tests). The ESAL categories are the same as the categories described in TRH 4 (based on a logarithmic increase in traffic).

3.4 *Details on specific layers*

As mentioned, the design method focused on pavement structures with granular, bitumen emulsion stabilized, and bitumen treated base layers. Granular materials include all natural and crushed aggregates used for normal base layer construction. The bitumen emulsion stabilized materials consist of granular materials stabilized with up to two percent residual bitumen to improve the material properties (Collings et al., 2009).

Tables 1 through 3 summarize the specific pavement structures used in the development of the pavement design catalogue. Details on each of the tests are available from the HVSIA activity matrix (www.hvsia.co.za).

The HVS facilities from which the data originated are as follows:

– Caltrans – California Department of Transportation HVS, located at the University of California, Berkeley at the time of testing;
– Gautrans – Gauteng Department of Public Transport, Roads, and Works, located in the Gauteng province of South Africa;
– Florida – Florida Department of Transportation HVS, located in Jacksonville, Florida, and

Table 3. Summary of bitumen treated base test sections used in developing pavement design catalogue.

Test data origin	Sections	Test temp. (°C)	Surfacing details	Base details	Test load (kN)	Tire pressure (kPa)
Gauteng HVS	13	20 to 40	AC	Bitumen treated granular	40 to 150	520

– Finland/Sweden – HVS initially jointly owned by Finland and Sweden Departments of Transport.

4 THREE-DIMENSIONAL MATRIX CATALOGUE

In general, pavements that are required to carry a high number of ESALs consist of thicker and or stronger layers of pavement materials. In the current TRH4 pavement design catalogue, the granular base layer type catalogue covers a full range of traffic spectra (low to high), while the bitumen stabilized and bitumen treated base layer type catalogues typically only cover higher traffic demands.

4.1 *Granular base layers*

Many of the HVS tests on granular base layers that were evaluated from Finland and Sweden, South Africa, and California were not conducted with an applied (half-axle) load of 40 kN. These tests' results had to be converted to equivalent 80 kN loads using a standard load equivalence factor. The load equivalence factors calculated and used for the 11 granular pavements ranged between 1 and 26 (average of 8.9), based on calculations using the respective rut rates obtained for the tests conducted at different load levels. The method developed by Kekwick (1985) was used to calculate these equivalence factors. Thirty-six of the granular base pavement tests had final rut values less than 10 mm and required extrapolation.

If more than one data set was available in some of the cells in the two-dimensional matrix, the best dataset needed to be chosen for each coordinate. Where more than one pavement structure was available for a specific location in the matrix, the pavement structure with the lowest final rut value, or with the highest number of repetitions before reaching a rut level of 10 mm or 20 mm (if these values were not reached in the test) was selected. This prevented using extrapolated data as far as possible.

4.2 *Bitumen emulsion stabilized base layers*

Most of the HVS tests conducted by Gautrans on bitumen emulsion stabilized base layer pavements used an applied (half-axle) load of 40 kN. For the remaining six tests the load equivalence factors calculated and used ranged between 1 and 39 (average of 11.9), based on calculation using the respective rut rates obtained for the tests conducted at different load levels.

Water was added to five test sections when the rut rate had reached a steady gradient. The values used to determine the rut rate for these tests were the values just before water was added, as this gave a constant creep rate in the secondary creep phase. The evaluated data were placed into the two-dimensional matrix with base layer type/ESAL axes. More than one data-set was available in some of the cells and the best was to be chosen for each coordinate in the matrix.

4.3 *Asphalt base layers*

Eight of the HVS tests conducted on asphalt base layers required conversion to standard 80 kN loads using an equivalency factor. The load equivalence factors calculated and used for these pavements ranged between 1 and 198 (average of 50, dual tire loads of 150 kN were used on selected sections), based on calculations using the respective rut rates obtained for the tests conducted at different load levels.

Twenty-five percent of the tests had final rut values less than 10 mm and required extrapolation. In tests where water was added, only those where the rut rate had reached a steady gradient before the water was added were used.

Based on the available information, the new catalogue was developed (Jansen van Rensburg, 2009). A section of the catalogue is shown in Figure 2 for the different base layer materials, showing the cells (traffic/base layer type) that were populated with pavement structures. Figure 3 shows the same information for the temperature axis of the three-dimensional catalogue (it should be noted that the details of the catalogues are not visible in these two figures due to size limitations). The typical format of the catalogue design guide is evident, with increasing pavement thicknesses corresponding to traffic volume increases. The ES designation denotes the traffic categories and is equivalent to the number of ESALs indicated for each of the categories (i.e., ES1 relates to a 0.3 to 1 million ESAL load category).

5 COMPARISON BETWEEN TRH4 CATALOGUE AND APT-BASED CATALOGUE

5.1 *Data acceptance evaluation*

In this part of the evaluation the data that were accepted for use in the three-dimensional matrix were evaluated against the existing TRH4 pavement design catalogue (developed based on the South African mechanistic design methods and the AASHTO design catalogue)

Base layer	Surfacing type	Category	ES0.003	ES0.01	ES0.03	ES0.1	ES0.3	ES1	ES3	
		ESAL	<0.003	0.003 to 0.01	0.01 to 0.03	0.03 to 0.1	0.01 to 0.3	0.3 to 1	1 to 3	etc.
Aphalt	Asphalt	No structure tested				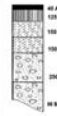			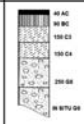	
Granular	Asphalt	No structure tested		Section 5A FDOT	Section 392A4 Gautrans	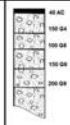	Section 4C FDOT	Section 387A4 Gautrans	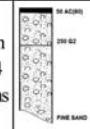	
	Modified asphalt				Section 1A FDOT	Section 3A FDOT	Section 2B FDOT	Section 1C FDOT		
Emulsion stabilized granular	Asphalt			No structure tested					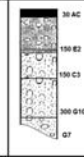	

Figure 2. Example of two-dimensional catalogue with base layer and traffic as respective axes.

Category	ESAL	Temperature					
		10	20	30	40	50	etc.
ES0.003	<0.003	No structure tested					
ES0.01	0.003 to 0.01						
ES0.03	0.01 to 0.03						
ES0.1	0.03 to 0.1	No structure tested			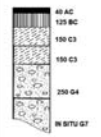	Section 3A FDOT	
ES0.3	0.01 to 0.3		392A4 Gautrans		Section 5C FDOT	Section 4C FDOT	
ES1	0.3 to 1	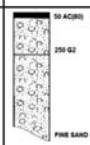	387A4 Gautrans	No structure tested			
ES3	1 to 3	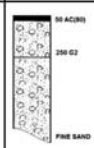	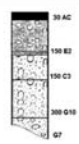	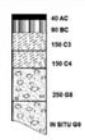	Section 3C FDOT	No structure tested	
	etc.						

Figure 3. Example of two-dimensional structure with test temperature and traffic as respective axes.

Table 4. Pavement structures for asphalt base layers – comparison between TRH4 and APT-based catalogues.

Design category	ES30		ES10		ES3	
Pavement structure origin	TRH4	3-D matrix	TRH4	3-D matrix	TRH4	3-D matrix
Surfacing description (Thickness mm)	AC (40)	AC (40)	AC (40)	AC (40)	AC (40)	AC (40)
Base description (Thickness mm)	BC (120)	BC (150)	BC (90)	BC (100)	BC (80)	BC (90)
Subbase description (Thickness mm)	C3 (400)	C3 (150)	C3 (300)	EG4 (150)	C3 (250)	C3 (150)
Upper selected description (Thickness mm)		C3 (150)		C3 (150)		C4 (150)

to determine whether they could be used in a generic pavement catalogue. This comparison would allow reasonable conclusions to be drawn about whether the data from these test reports were sufficiently adequate for preparing the design catalogue. Only the bitumen emulsion treated base layer example is considered in this paper as an example. Similar results were obtained in the comparison of the two remaining base layer types.

5.2 *Bitumen emulsion treated base layer*

Table 4 shows the pavement structures in the TRH4 pavement design catalogue and those in the three-dimensional matrix for asphalt base layer. The surfacing depths are the same and, as prescribed in the TRH4 pavement design catalogue, an asphalt concrete type surfacing can be used as a surfacing layer. The base thicknesses in the three-dimensional matrix are slightly higher than those in the TRH4 pavement design catalogue. This was attributed to the subbase and upper selected layers in the TRH4 pavement structure being of either better quality or slightly thicker than the sections tested in the HVS studies.

The pavement structures tested provided good results and are comparable to those in the TRH4 pavement design catalogue with asphalt base layers. The only outlier was in the ES0.1 category, where the pavement structure was the same as that of the pavement structure in the ES30 category; however, this was due to a higher test temperature. This shows that the pavement structure in the ES30 category can be used in regions with expected temperatures of 20°C to 30°C at design loads of ES30, or in regions with expected temperatures of between 20°C and 40°C at design loads of ES0.1. However, this is not recommended as the pavement structure would be very susceptible to high temperatures.

6 CONCLUSIONS AND RECOMMENDATIONS

Based on the information and discussion in this paper, the following conclusions are drawn:

- The basic concept of using APT data from a range of test programs to generate a rut-based preliminary thickness pavement design catalogue appears to be valid;
- Clear rules are required to ensure that the new catalogue is populated with data that are comparable in terms of the failure conditions of the different tests;
- Expansion of the catalogue to include other pavement failure conditions such as fatigue cracking is required, and
- The process of cooperation on further analyses, applications, and implementation of APT-based data can expand the benefit of limited APT test budgets and scope beyond the scope of the original APT test owner.

ACKNOWLEDGEMENTS

The assistance of Professor Joe Mahoney for initiating thoughts and discussions around the general concept of generating catalogue designs based on APT data from a range of HVS programs is acknowledged. The assistance of the various HVSIA members that contributed to this paper through access to their data on the HVSIA website is acknowledged. The assistance of Mr. Henning Jansen van Rensburg in developing the concept through an undergraduate project is gratefully acknowledged.

REFERENCES

Collings, D., Grobler, J., Hughes, M., Jenkins, K., Jooste, F., Long, F. and Thompson, H. 2009. A guideline for the design and construction of bitumen emulsion and foamed bitumen stabilised materials. *Technical Guideline 2: Bitumen Stabilised Materials.* Cape Town, South Africa: Asphalt Academy.

Du Plessis, L., Coetzee, N.F., Burmas, N. Harvey, J.T. and Monismith, C.L.. 2008. The Heavy Vehicle Simulator in accelerated pavement testing – A historical overview and new developments. In *Proc. 3rd International Conference on Accelerated Pavement Testing*, Madrid, Spain, October 1–3, 2008.

Harvey, J.T. 2008. Impacts and benefits of APT: An APT operator's perspective. *In Proc. 3rd International Conference on Accelerated Pavement Testing*, Madrid, Spain, October 1–3, 2008.

Hugo, F. and Epps Martin, A. 2004. *Significant findings from full-scale accelerated pavement testing*. Washington, DC: Transportation Research Board, National Research Council. Synthesis of Highway Practice 325.

Jansen van Rensburg, H.J. 2009. *Development of a generic pavement catalogue based on historic accelerated pavement test data.* Undergraduate research project report. Pretoria, South Africa: University of Pretoria.

Kekwick, S.V. 1985. *Derivation of pavement damage coefficients from Heavy Vehicle Simulator testing: methods and accuracy.* Pretoria, South Africa: National Institute for Roads and Transport Technology, CSIR. Technical Report RP/17.

Steyn, W.J.vdM. 2012. *Full-scale accelerated pavement testing, 2000 to 2011*. Washington, DC: Transportation Research Board, National Research Council. NCHRP Project 20-05. Synthesis Topic 42-08. (Final draft submitted at date of writing paper).

Theyse, H.L., De Beer, M., Maina, J.W. and Kannemeyer, L. 2011. Interim revision of the South African mechanistic-empirical pavement design method for flexible pavements, In Proc. *10th Conference on Asphalt Pavements for Southern Africa.* Champagne Sports Resort, KwaZulu-Natal, South Africa.

Technical Recommendations for Highways (TRH4). 1996. *Structural Design of Interurban and Rural Road Pavements.* Pretoria, South Africa: Committee for State Road Authorities, Department of Transport.

Part 10: Benefit-cost analysis of accelerated pavement testing

This page intentionally left blank

Advances in Pavement Design through Full-scale Accelerated Pavement Testing – Jones, Harvey, Mateos & Al-Qadi (Eds.)
© 2012 Taylor & Francis Group, London, ISBN 978-0-415-62138-0

Developments in evaluating the benefits of implemented accelerated pavement testing results in California

W.A. Nokes, M. Mahdavi, N.I. Burmas & T.J. Holland
California Department of Transportation, Sacramento, California, US

L. du Plessis
CSIR, Pretoria, South Africa

J.T. Harvey
University of California Pavement Research Center, University of California, Davis, US

ABSTRACT: This paper describes and discusses methods, measures, and indicators—drawn from within and outside transportation research and from international sources—that may be suitable for evaluating benefits from Accelerated Pavement Testing (APT). The authors' intent is to aid in translating technical pavement benefits well-known to APT experts into quantitative measures and qualitative indicators so the public, decision-makers, and others who lack pavement expertise (but who may have interests such as funding and staffing APT activities) can understand and appreciate the benefits from their investments in APT research. APT researchers and owners/operators both individually as well as the broader APT research community comprise the intended audience for this paper. The paper (1) reviews and compares qualitative and quantitative techniques including direct economic benefits assessments, (2) describes challenges to the evaluation process, (3) highlights trends that make evaluating benefits of APT an emerging priority, and (4) outlines new directions and potential actions for individual APT owners/operators and for the broader APT community. This paper aims to stimulate dialogue and investigations to advance the use and development of approaches that better identify, evaluate, and communicate the benefits of APT.

1 INTRODUCTION

Accelerated Pavement Testing (APT) programs continue to expand worldwide. APT has produced significant technical outputs of interest to pavement engineers including validating performance of advancements such as long-life pavements, mechanistic-empirical design methods, and modified asphalt mixes. Implementing APT results like these lead to positive technical outcomes such as longer pavement service life, more robust design methods, and lower environmental emissions. These technical outcomes are of interest to capital improvement and maintenance/preservation engineers and managers (usually the APT "customers") who often understand the APT results and their implications on design, construction, operations, and road users.

This level of technical understanding is unusual for non-technical decision-makers, administrators, and elected officials who control or influence APT funding, program planning, and project approvals. It is also rare for most of the public, who fund most APT programs. How the technical improvements from implemented APT results translate into non-technical benefits that can be characterized and communicated to (and ultimately understood by) non-technical audiences is problematic and is an emerging priority for the APT community.

Evaluating non-technical (mainly economic) benefits has been a topic of discussion at two previous APT international conferences. At the Second International Conference in 2004, results were presented from a cost-benefit analysis of Accelerated Load Facility (ALF) testing by the Louisiana Department of Transportation and Development (King and Rasoulian, 2004). From a three-year analysis period, life cycle cost savings were calculated at approximately US$8.17M and costs for construction, operations, and of research were about US$1.55M, resulting in a benefit-cost ratio (BCR) of 5.3.

The Third International Conference in 2008 focused on the impacts and benefits of APT. The funding challenges and continuing need for high benefit-to-cost ratios of pavement research in Europe were emphasized in a keynote paper (Hildebrand and Dawson, 2008). To better inform participants and encourage dialogue, one workshop was dedicated solely to cost-benefit analysis basics and case studies (Du Plessis and Prozzi, 2008). An introductory workshop on APT described the value of pavement testing and analysis

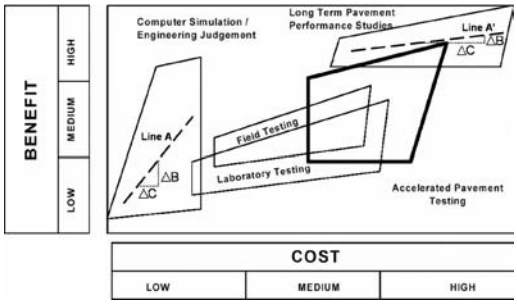

Figure 1. Benefits vs. costs of pavement test and research tools. (Based on Coetzee and Mateos [2008]; Horak et al., [1992]).

methods in terms of benefits vs. costs as shown in Figure 1, with a range of benefits shown on the vertical axis and costs on the horizontal axis (Coetzee and Mateos, 2008). Figure 1 provides an insightful representation of the relationship of benefits vs. costs, in contrast to the traditional portrayal of data/quantity of results vs. time/effort expended as presented originally in (Horak et al., 1992). Two dashed lines (shown as Lines A at left and A' at right) in Figure 1 have been added to illustrate the conceptual potential for quantification and comparison of benefits vs. costs of various research methods—which could be compared if sufficient benefits and cost data actually were available.

In this illustrative example, the steeper positive slope of Line A indicates a higher benefit vs. cost relationship than for Line A'. However, the magnitude of benefits and costs of Line A are lower than for Line A'. Review of Figure 1 clarifies the need for discerning the economic efficiency (e.g., benefit-cost ratio [BCR]) as well as effectiveness (e.g., magnitude of cost savings) when evaluating economic benefits of research. It also conveys a sense of the potential difficulties in evaluating benefits of research.

Technical papers at the 2008 conference were presented for case studies in a technical session devoted to "Benefits and Economic Evaluation of APT Programs". Minnesota's MnROAD program reported total economic benefits estimated at US$396M and a BCR of 8.9 (Worel et al., 2008). Case studies of HVS testing in South Africa reported BCR values ranging from approximately 2.0 to 10 (Samson et al., 2008). Project reports for the South African case studies on which the technical papers are based give details and "best practices" for assessing research benefits (Jooste and Samson, 2004; Jooste and Samson, 2005; Jooste et al., 2004). Preliminary draft findings were presented from California's APT program reporting BCR values ranging from approximately 3.0 to 10 (Du Plessis et al., 2008).

This paper presents findings since 2008 of a pilot study by the California Department of Transportation (Caltrans) and its research partners, the University of California Pavement Research Center (UCPRC), Dynatest Consulting, Inc., and the CSIR (Council for Scientific and Industrial Research) in South Africa. The approaches described here were identified in the study, which focuses on direct economic benefits in a retrospective evaluation of California's APT program (Du Plessis et al., 2011; Nokes et al., 2011). The paper focuses on practical applications instead of discussions from the academic literature and is indicative rather than exhaustive. Indicators of qualitative benefits are described but quantitative methods and measures are emphasized. The paper does not discuss macroeconomic impacts.

The purpose of this paper is to give APT researchers and owners/operators expanded and updated information on evaluating the benefits of APT research made available since the Third International conference in 2008.

This paper has three objectives. First, it aims to stimulate dialogue within the APT "community" to advance understanding and improvements in evaluating and describing the benefits of APT. This is aided by presenting (1) a brief overview and discussion of evaluation techniques and (2) challenges to assessing benefits of research. Second, the paper examines APT benefits evaluation as an emerging priority. The expanded discussions of this topic at the previous two APT international conferences and the ongoing impacts from the global recession suggest the evolution of a "new normal" context, to which APT research programs must adapt. Third, the paper outlines new directions and potential actions for individual APT owners/operators as well as the broader APT community to move forward.

2 PAST AND CURRENT DEVELOPMENTS

Technical APT research outputs culminate in technical and non-technical benefits to transportation agencies and road users as well as industry and other stakeholders. The term "benefits" as used in this paper are the positive and/or negative impacts or outcomes from implemented APT research results, i.e., outputs.

Methods for evaluating benefits are generally categorized as quantitative and qualitative. Quantitative measures have a numerical value, e.g., savings in dollars and lives, which can be viewed as objective. Qualitative indicators are descriptive and typically lack implicit numerical value and hierarchy (though numbers are sometimes assigned for analytical purposes) but reflect more subjective assessment such as satisfaction and quality.

Evaluation techniques have advantages and disadvantages that present trade-offs depending on project-specific circumstances. For example, research outputs are clearly linked to benefits in a case study but difficult to determine using econometrics, which applies mathematics and statistics to determine economic relationships and is better suited to larger scale economic studies (RAND, 2006). Choosing a method is context-sensitive, reflecting specific needs such as determining whether a line of research should be terminated, if

results are within accepted quality standards, or if there are direct economic benefits. Techniques to evaluate indirect benefits and larger-scale economic impacts of a project on the economy such as jobs and construction are described in the literature but are not in this paper, which focuses on direct benefits of APT.

2.1 *Qualitative and quantitative techniques*

Evaluation of research outcomes and their effects has a long history in the past half century (Roessner, 2002). Steadily increasing scrutiny and demands for justification of public expenditures have caused continuing efforts at evaluating research benefits. Highlights of previous studies are presented here.

2.1.1 *Office of Technology Assessment (1986)*

Findings from the US Congress Office of Technology Assessment (OTA) study identified various approaches for evaluating research outputs used in government and industry (OTA, 1986). The study, which remains a landmark of the past quarter century, found qualitative assessment was dominated by peer review. The study examined non-economic measures including bibliometrics (which quantitatively analyze publications in terms such as citation and content analysis) and "indicators" (such as educational degrees, personnel, and awards). Quantitative evaluation consisted of a wider set of methods including economic evaluation (in terms of macroeconomic and investment analysis) and output measurement (in terms of published information). The study examined retrospective as well as prospective evaluations and found economic analysis in both.

The study found one of the basic challenges to evaluating research benefits in terms of return on investment (ROI) is that the reason for most government research is not economic benefits but, instead, non-economic aspects of public interests such as safety, security, and health. The study found that most (two-thirds) of federal expenditures on applied research were related to production of public goods "whose primary value is not measured in economic terms".

Especially relevant to APT research, OTA concluded that quantitative economic assessment was potentially useful for evaluating applied research and development and research facilities within a single, focused discipline (OTA, 1986).

2.1.2 *Federal Highway Administration (1996)*

A review of benefits of research and technology applications by the Federal Highway Administration (FHWA) Office of Technology Applications described many of the challenges and obstacles reported generally in the literature in and outside of the transportation field (Harder, 1995). The FHWA study focused on research results in 12 technology areas from 1984 to 1993. A major objective of the review was to identify techniques to document the payoffs of research and technology transfer, with an emphasis on quantifying benefits in terms of dollars. The study elicited information including cost data, savings, and other benefits from a survey of state Departments of Transportation (DOTs). Survey responses "expressed repeatedly that the tools simply did not exist to quantify cost and savings data" (Harder, 1995). Respondents found quantitative benefits for high visibility concerns such as improving air quality and avoiding catastrophic events (e.g., a bridge collapse) extremely difficult to quantity. Respondents' reluctance to assign values to benefits was attributed to lack of detailed cost analyses.

2.1.3 *National academies (1999)*

Several of the same approaches identified in (OTA, 1986) are prominent in a 1999 report by the National Academy of Sciences Committee on Science, Engineering, and Public Policy (COSEPUP) (National Academies, 1999). COSEPUP conducted studies and workshops with Federal agencies, the research community, industry, states, and agencies in other nations. The goal was to identify and analyze the most effective ways to assess research results. The study identified advantages and disadvantages for each method. Like more recent studies, the COSEPUP findings suggest that a multi-faceted approach, which combines measures and indicators in a complementary manner, should enable analysis of outcomes and impacts from many types of research.

2.1.4 *Transportation Research Board (2001)*

Soon after the COSEPUP report, the Transportation Research Board (TRB) National Cooperative Highway Research Program (NCHRP) Synthesis 300 reported on a review of approaches to measure the performance and effectiveness of transportation research and development (Sabol, 2001). Results from a survey of US state DOTs found 25 percent used performance measures for projects after implementation. All measures relied on qualitative information, though respondents described them as quantitative.

The report describes survey responses from state DOTs, private sector research programs, and academia. The study found peer review to be the standard for qualitative assessment. Results showed substantial differences in the approaches to and concerns about assessing benefits of research in public, private, and academic sectors. Most state DOTs were not satisfied with their cost-benefit techniques and said many issues would need to be resolved to provide useful and reliable benefits information over a long-term assessment period. Quantifying benefits by cost-benefit analysis in the private sector also was problematic but aided by higher quality and more extensive cost data as well as a more customer-driven business environment. Less quantification of benefits of research in the academic sector was attributed to greater concern about productivity and quality. The study reported that neither college faculty nor administrators frequently discuss cost-benefits of academic research activities. High priorities for development included measuring

payoffs from implemented research results and providing guidance on the use of cost-benefit analysis (Sabol, 2001). Most if not all of the gaps that were reported in 2001 still exist.

2.1.5 *Review of non-transportation (2002)*

A review of the state-of-the-art in measuring outcomes of non-transportation research in the US describes peer review as the standard against which other methods are judged for both retrospective and prospective evaluation (Roessner, 2002). The review recommends developing methods that better capture non-economic benefits of research. In discussing the usefulness of conducting surveys it cautions against potential bias from surveying individuals who benefit from research. The review recommends more emphasis on long-term qualitative benefits and suggests evaluating research "nuggets" (referred to as "big winners" in Lay [2006]), which are high payback projects that produce direct economic benefits that may far exceed the cost of an entire research program.

2.1.6 *Comparisons from reviews (2003–2008)*

Several reviews of evaluation approaches have been published in the past decade. A sampling of reviews from two European reports (RAND, 2006; Marjanovic et al., 2009) and two US reports (Krugler et al., 2006; FHWA, 2003) shows a wide variety of methods used within and outside of transportation research. The US reports focus on transportation research whereas the European publications reflect health and medical research assessment methods, which have been described as more advanced than in other fields (including transportation research). These reviews indicate the following.

- Use of qualitative and quantitative measures is widespread.
- Cost-benefit/savings analysis, peer review, and surveys are the most common methods.
- These common methods are used in transportation as well as non-transportation research.

The choice of approach is driven by the purpose and conditions of the study as well as time, resources, and other constraints. Each technique offers advantages and disadvantages. Analysts face challenging trade-offs in choosing an approach best suited for a specific study. Findings suggest that evaluations of research may be more representative if they combine qualitative and quantitative information. Some analysts suggest that relying on one indicator can mislead analysts and decision-makers (Georghiou and Roessner, 2000).

2.1.7 *"Toolkit" methods*

Approaches that enable characterization of benefits using more than one measure have been evolving in recent years with the development of "toolbox" or "toolkit" frameworks, which consist of many quantitative measures and qualitative indicators. Toolkits have been developed in the US and are in different stages of implementation for transportation research (Krugler et al., 2006) and non-transportation areas, such as federal energy research at the Department of Energy (Ruegg and Jordan, 2007) and technology development at the National Institute of Standards and Technology (NIST) (Powell, 2006; Ruegg and Feller, 2006). A European review highlights the NIST toolkit and refers to it as "one of the most influential reference works, practical aids and planning guides for practitioners of research evaluation" (Marjanovic et al., 2009). The NIST toolkit was developed from extensive evaluations of 45 NIST research projects between 1990 and 2000.

2.1.8 *Non-APT transportation research*

Federal research case study

In assessing the federal investment in infrastructure research and development from 2006 through 2009, TRB Special Report 295 observed that evaluations of past FHWA research in materials and structures found substantial savings and extension of service life far in excess of the cost of the research (TRB 2008). The observation is based largely on a US report of retrospective evaluations of benefits from FHWA-sponsored research in three separate research areas (FHWA, 2003).

- Highway Safety Information System (information system/database) – evaluated by bibliometrics, survey, and expert peer review.
- *Quickzone* (software) – evaluated by survey.
- Infrastructure research and development – evaluated by quantitative and qualitative methods.

The FHWA's report observed that estimating cost savings was "…the most demanding part of the assessment…". However, those projects with cost data available had very high agency, road user, and safety cost savings. The report estimated costs savings at a national level that was more than 10 times the total annual research funding (FHWA, 2003). This is an example of research "nuggets" and "big winners" mentioned above (Roessner, 2002; Lay, 2006).

NCHRP project 20-63 toolbox

A relatively recent addition to the toolkit approach is the NCHRP Project 20–63 toolbox (Krugler et al., 2006). The main objectives of the initial project were to define performance measures for transportation research projects and to assemble a useful and practical toolbox of performance measures (with examples) for use by state DOTs.

Analysts conducted a survey of state DOTs as well as federal and private sector research managers. The survey showed return on investment or benefit-cost ratio tied for third rank (tied with agency cost savings), just following behind lives saved and reduction in crashes. The study identified 30 performance measures to include in the toolbox. The report does not analyze or provide guidance on cost-benefit analysis.

Performance measures were programmed in software made available for state DOTs. It allows users to import other performance measures and to customize

the toolbox for specific needs. The performance measures (mostly quantitative) are categorized under five major headings as follows:

- Outputs – products, reports, graduate students.
- Outcomes – cost savings, lives saved.
- Stakeholders – customer satisfaction and input.
- Efficiency – BCR, projects on time and in budget.
- Resources – funding and contractor issues.

Several state DOTs are interested in the NCHRP Project 20-63 toolbox, which has attracted international interest as well (Elston et al., 2009). NCHRP 20-63 was completed in 2010 and followed by Phase II (designated NCHRP 20-63B), which began in July 2010. Phase II focuses on enhancements and refinements in functionality. The ultimate goal is to expand access for routine use. Phase II is scheduled to be completed in 2014 (NCHRP, 2011a).

2.2 *Evaluating direct economic benefits*

There are many publications on quantifying the benefits of transportation *improvement* projects (capital as well as maintenance/rehabilitation). In contrast, information on quantifying benefits of transportation *research* projects (especially economic benefits) remains much rarer. Approaches proposed for measuring economic returns on research investments have been categorized into three groups: macroeconomic, microeconomic, and direct outputs (Georghiou and Roessner, 2000). Direct economic benefits (on which this paper focuses) are immediate, first order impacts often expressed in terms of savings in agency costs (e.g., lower capital and maintenance costs) and users costs (e.g., less travel delay and lower vehicle operating costs).

2.2.1 *Transportation research*

SHRP case study evaluations

Direct economic benefits (in terms of agency and user cost savings) were calculated for various products developed in the Strategic Highway Research Program, SHRP (Little et al., 1997; Epps and Ardila-Coulson, 1997). The evaluation was a prospective assessment focused on specific research products in case studies. Expected future benefits were calculated as an assumed percentage of future expected costs.

The SHRP research assessment was conducted and completed by 1997, just as SHRP results were being communicated and product implementation was getting underway. Because of the timing of the assessment, the evaluation relied on the best available information plus assumptions for projecting expected benefits. The SHRP evaluations applied a deterministic approach for benefits projected to occur over a time horizon of up to 20 years.

TRB Special Report 260 (TRB, 2001) reviewed the results of the SHRP evaluation case studies, which it identified as providing estimates of potential benefits from SHRP based on various implementation scenarios as detailed in (Little et al., 1997). When compared to the costs of SHRP research, development, and implementation, projected BCRs of SHRP research products ranged from 1.0 to 43 for transportation agencies and from 6.0 to 173 for users.

Florida DOT synthesis

A 2002 study sponsored by the Florida DOT (FDOT) investigated techniques to assess direct economic benefits of transportation research (Concas et al., 2002). The overall goal was to recommend a method for *retrospective* assessment of benefits and *prospective* valuation of research for project selection. Investigators reviewed past FDOT-sponsored projects, searched the literature (including non-transportation sources), and evaluated which techniques appeared well suited to transportation research. The literature review identified techniques within transportation (DOTs and private sector) and outside transportation including medical, chemical, agricultural, and telecommunications. University transportation research did not rely on quantitative economic assessments, but instead preferred qualitative measures or bibliometrics.

For transportation research, the study found cost-benefit analysis, net present value (NPV), and ROI dominated. Techniques and measures outside of transportation varied widely and included utility analysis and financial indicators such as ROI, internal rate of return, and payback period. The FDOT study also described a financial approach, called *Real Option*, used mainly to evaluate non-transportation research in highly competitive fields (e.g., telecommunications and pharmaceuticals) that views research investment opportunities as financial options and applies investment theory to evaluate potential returns. None of the approaches were suitable for all categories of research. To address diverse needs and conditions, the study developed and recommended a matrix of techniques including economic analysis using benefit-cost ratio, NPV, and ROI for most categories (Concas et al., 2002).

2.2.2 *APT research*

In addition to technical assessments presented at previous APT International Conferences, other evaluations of implemented APT results have been reported.

CAL/APT program evaluation

Research outputs from the Caltrans Accelerated Pavement Testing Program (CAL/APT) were evaluated in an economic assessment of three pavement recommendations for hot-mix asphalt (HMA) (Gillen et al., 2001). Recommendations based on HVS testing were to increase compaction, require tack coats between all HMA lifts, and use a rich asphalt bottom layer if multiple lifts of HMA were to be placed. Based on HVS-derived expected increases in pavement service life of 10 to 50 percent, a full-cost model (direct agency costs plus user and safety costs) was applied to typical Caltrans construction and rehabilitation projects.

Extrapolation showed total cost savings on the order of several hundred millions of dollars for a sample

of projects, with even higher cost savings if improvements were adopted statewide. The study highlighted the need to go beyond characterizing benefits of APT research only in technical terms such as "increased axle repetitions" or "years between required rehabilitation" and concluded the following:

"These pavement measures must be rationally converted to monetary measures so that the public and managers without pavement training can evaluate the return on their investment in pavement research" (Gillen et al., 2001).

APT-focused NCHRP projects

APT activities and outputs are the focus of several NCHRP projects. In 2004 NCHRP Synthesis 325 reported results from a review of APT programs around the world. The report included direct economic benefits in terms of benefit-cost ratio and net savings (Hugo and Epps-Martin, 2004). Survey responses from APT owners/operators to a questionnaire showed monetary benefits (cost savings) exceeded US$2M for six of the seven agencies that responded. BCRs reported by respondents varied from 1.0 to higher than 20 (no upper limit was set in the questionnaire). Savings and BCRs were presented in the report as respondents provided them with no additional analysis and few details about procedures and assumptions.

The Synthesis 325 report gives anecdotal highlights of economic assessments prepared for various APT programs. The anecdotal highlights were meant to supplement findings presented in the 1996 NCHRP Synthesis 235 report, which described the diverse APT technologies in use and reviewed the state-of-the-practice (Metcalf, 1996). The study found "few formal evaluations" of cost-benefit had been published and that "evaluation of APT…cost-benefit is historically limited and only rarely been rigorously quantified". However, it concluded that "shrinking budgets and privatization of facilities may result in more frequent, formal, and quantitative assessments in the future". Assessments of benefits from APT actually did not become more frequent since 1996, but studies described in this paper show some efforts at formal and quantitative evaluation.

Syntheses 235 and 325 are foundational for the more recent NCHRP Synthesis 20-05/Topic 42-08 project, which focuses on providing an update on APT activities, outputs, and impacts (NCHRP, 2011b). This latest project builds on the framework established in Synthesis 325, updates APT developments since 2000, and examines new/expanded categories of work including cost-benefit analysis of APT outputs. The project report is expected to be published in 2012.

3 CHALLENGES TO EVALUATING BENEFITS

3.1 *Widespread and recurring challenges*

Reviews of methods from a wide variety of fields are reported in the literature. Challenges begin with three

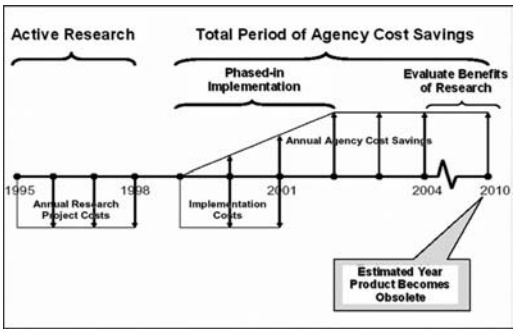

Figure 2. Example of publicly-funded research project timeline and cash-flow. (Adapted from [Krugler et al., 2006]).

wide-spread expectations by those unfamiliar with the benefits of the evaluation process.

1. The process will lead to a "right" answer.
2. The process will produce an "objective" analysis.
3. The process will remove discomfort in determining benefits.

The literature suggests current and future techniques will not meet these expectations. However, information is presented in this paper to help APT owners/operators move forward in evaluating benefits from their research outputs.

Those who attempt to evaluate benefits of implemented APT results face several potential challenges including:

– Lack of familiarity with this topic.
– Long time domain for benefits to accrue.
– Scale of evaluation.
– Complexity and context-sensitivity.
– Recurring procedural challenges.

Lack of familiarity with this subject is not surprising due to widespread lack of knowledge about evaluation methods and lack of opportunity or motivation to use them. Evaluation efforts have less influence in the literature than they deserve and reports on the best work are not easy to obtain (Georghiou and Roessner, 2000).

The long timeline for performing research and implementing results is a significant barrier to evaluating benefits. Examining a typical research project's life cycle helps illustrate this barrier. Figure 2 outlines the typical activities and cash-flow (both costs and benefits) for a research project. Not shown are the time, costs, and processes in identifying and scoping a project, incorporating it into the research program, and obtaining funding and other resources (all occurring before "Active Research"). Pre-research activities typically are led by staff who do not perform research or implement the results. This research management staff usually is tasked to process the research program and projects, not to evaluate benefits from research outputs.

In the "Active Research" phase the researchers naturally take lead responsibility. In the "Implementation" phase the researchers and research management

staff may participate, but often the implementers take lead responsibility, typically working in operational functions such as design, maintenance, and construction. Implementing research results produces benefits (shown in Figure 2 as "Annual Agency Cost Savings") that accrue many years after completing the research. This example shows (1) the research project life cycle is long, (2) monetary benefits accumulate long after research is completed, and (3) lead responsibilities change, but no one is assigned to evaluate benefits.

The scale of evaluation (i.e., test-specific, project-specific, or program-level) must be decided at the outset. The purpose of the evaluation determines its scale. Program-level assessments are reported in the literature in terms of determining whether a research program has achieved some pre-set targets or goals. APT research evaluations have been reported for all three levels. Challenges are inherent for each level of evaluation.

Complexity is another challenge. Like the research process itself, evaluating benefits is a complex and difficult effort with uncertain outputs. Benefits may be very difficult to characterize. Evaluators of research benefits must decide what is significant that should be measured, how and when to measure, and how to interpret results. The evaluation process can be costly because it is time- and labor-intensive. Deciding whether to evaluate benefits and how to proceed is also context-sensitive, reflecting the attributes and constraints of the research outputs as well as those of the evaluators, the organization, and users. This partly explains why no universal technique has been recommended.

Regardless of the approaches used, several recurring procedural challenges to evaluation have been observed including (Marjanovic et al., 2009):

- Attributing impacts, which requires linking outcomes to a specific research project and discerning previous research that influenced it as well as other projects that were influenced by it.
- Setting boundaries, which requires identifying the starting point of all contributing research (in retrospective studies) and identifying the timeframe for analysis (in prospective studies).
- Bias in selecting projects for case studies.
- Unclear descriptions of techniques in data collection and analysis.
- Non-uniform definition of terms and concepts.

Attributing impacts and benefits to a specific research project is one of the biggest procedural challenges. A clear cause-and-effect linkage between research outputs from one specific project (versus other projects or non-research sources) and subsequent benefits is exceptional. One review of international practice in assessing research impacts characterized the attribution of impacts as a main reason why such assessments usually are considered "too hard" to perform (Grant et al., 2009). Case studies that focus on evaluating a few benefits where the path from research outputs to benefits is distinct have been successful in mitigating this challenge (Marjanovic et al., 2009; Grant et al., 2009). Case studies such as described in (Du Plessis et al., 2011) also might provide a way to meet a challenge that several APT owners/operators may be familiar with: determining the value of learning "what not to do" in technical or operational terms as well as the economic value of cost-avoidance. Evaluation methods that overcome this challenge warrant further investigation and development.

3.2 *An emerging priority*

If there is substantial literature presenting methods for benefits assessment and this topic has been a focus of previous APT papers and conferences, then why are such evaluations of APT research results not done more routinely? One explanation is the cost, time, and labor commitments required to evaluate benefits. Another possibility is that opportunities for evaluation occur infrequently if at all. This may be related to assignments and changes in lead roles—which do not include benefits evaluation—described above in regard to Figure 2. A related explanation is lack of motivation; there may be no need (real or perceived) to evaluate benefits of APT research. APT owners/operators naturally focus on performing research and may dissociate themselves from assessing the value of that research. In regard to such dissociation in road research, Lay (2006) observed that "part of the valuation problem lies with researchers who do not pay sufficient attention to the end value of their research". However, the opportunities as well as motivation for evaluating benefits may grow in the rapidly changing conditions affecting most publicly-funded expenditures, including funding of APT research.

Evaluating benefits of research is an emerging priority due to the worldwide recession, mandates for measuring effectiveness and performance, and increasing global competition and collaboration.

The recession has affected all areas of publicly-funded activities and budgets. Accountability for public expenditures has steadily grown, leading to demands for greater transparency, more scrutiny of public agency processes, and greater need for use of state-of-the-practice methods. Clear (non-technical) justifications that emphasize costs and benefits such as a cost-benefit analysis may even increase public confidence in decision-makers (Baron and Gurmankin, 2009). European road researchers in the COST-347 study suggested that applying methods to evaluate costs and benefits of accelerated load testing may increase funding because of better marketing of transportation research activities and results (COST-347, 2005).

Mandates to measure effectiveness of governments' expenditures of public funds are on the rise. At the US federal level, passage of the Government Performance and Results Act (GPRA) of 1993 required federal agencies to develop performance plans and report performance periodically (Roessner, 2002). Federal transportation funds that contribute to federal

and state DOT APT programs are subject to GPRA requirements. After more than 15 years of experience the GPRA Modernization Act (GPRAMA) of 2010 improved on the GPRA requirements (GAO, 2011a) and may again affect many US APT programs. The trend for performance evaluation of state government expenditures is expanding as well.

The "changing dynamics of global interdependence" (including competition and collaboration) is one of eight major trends described recently by the Comptroller General of the US General Accountability Office (GAO, 2011b). One anticipated impact is greater emphasis on performance evaluation. Similarly, a 2009 TRB report focusing on efforts at coordination between transportation research agencies in Europe and the US observed that the lack of credible evaluation methods could have adverse impacts on international collaboration (TRB-ECTRI, 2009).

Responsive to the trends highlighted above, the US Department of Transportation (USDOT) Research and Innovative Technology Administration (RITA) provides a potentially helpful example for benefits evaluation of APT. RITA hosts a knowledge resource "portal" to help measure and document benefits in specific goal areas, e.g., safety, energy, and environmental impacts (RITA, 2011). Their activities are linked to the International Benefits, Evaluation and Costs (IBEC) Working Group, which coordinates and expands evaluation of benefits and costs, international evaluation efforts, and information exchange (IBEC, 2011).

The context for APT research will continue to evolve in a rapidly changing environment. Requirements to evaluate benefits of publicly-funded programs such as APT research are likely to grow as part of that evolution. Efforts such as those by RITA and IBEC provide the APT community with potential models to help APT programs adapt, survive, and possibly grow.

4 POTENTIAL ACTIONS GOING FORWARD

This paper has described previous use of existing benefits evaluation techniques by individual APT owners/operators. This section looks to the future, outlining new directions and next steps building on past efforts. Potential actions are presented for individual APT owners/operators and for the broader APT community. These actions are intended to help provide a structured approach for applying and improving on existing techniques in showing the benefits of APT research.

4.1 *Potential actions for APT owners/operators*

APT researchers and owners/operators may want to consider the following in conducting an evaluation of benefits from their tests, projects, or overall program.

- Consult the literature to understand approaches suitable for the specific evaluation.
- Consider starting small through a pilot study focused on an APT project that has well-defined and narrow benefits that are clearly linked to specific APT project outputs (an example of this is presented in Du Plessis et al., [2011]). This may help in attributing benefits to specific APT outputs, which is a key challenge.
- Document and acknowledge other sources that contributed to outputs and benefits.
- Identify benefits in detail, e.g., specific improvements and innovations in practices, technology, specifications, and/or policies. Researchers responsible for performing the work as well as their technical collaborators and research project contacts may be good sources of this information.
- While researchers can help identify best performing projects and their outcomes and benefits, practitioners who use the APT research results are well suited to provide estimates of actual benefits. Surveys or interviews with knowledgeable practitioners in the subject area can help elicit their assessment of benefits.
- Document the reasons for choosing projects evaluated in case studies.
- Consider selecting the best performing projects to quantify benefits. Benefits from a few projects (i.e., "nuggets" or "big winners") may exceed the cost of the entire APT program.
- Determine what techniques are best for your organizational context and for specific outputs and subsequent benefits. Evaluation may require the use of different methods if there are changes in context, outputs, or benefits.
- Consider more than one measure or indicator of benefits such as presented in the NCHRP 20-63 toolbox (Krugler et al., 2006) or the FDOT matrix (Concas et al., 2002).
- Identify and document assumptions and subjective aspects in the evaluation process.
- Document the process in determining inputs and assumptions such as setting useful life of research products, the analysis period (for economic and qualitative evaluation), and selection of base year (for costs).
- Document techniques used in data collection and analysis.
- Clearly define terms and concepts used in the evaluation.
- For process improvement, during evaluations note deficiencies, unnecessary steps, and problems that need resolution. Also note what worked well. Compile these records to provide feedback and "lessons learned" for future reference and sharing.
- When evaluating economic benefits of APT, use standard economic principles including discounting of costs and benefits. Present the magnitude of benefits in terms of NPV and economic efficiency in terms such as BCR.
- Apply sensitivity analysis, e.g., a range of discount rates, to examine impacts on results from variations of inputs and assumptions.

– In economic assessments consider reporting ranges of results instead of a single value of economic benefits.

4.2 *Future steps for the APT community*

In the larger context of APT organizations at various levels (e.g., state, regional, national, and international), research organizations (e.g., TRB) or consortia, and professional societies, the following may help guide future use and advancements in benefits assessment for the APT field as a whole. Noteworthy efforts that provide potential models for future APT evaluation developments include the RITA knowledge resource portal and international activities by the IBEC Working Group.

– Recognize potential gains from benefits assessment and advocate for coordinated evaluation of quantitative and qualitative assessments of APT research. Consider efforts to promote wider recognition in the APT field such as a working group similar to the IBEC Working Group (IBEC, 2011). A similar "working group" for APT could coordinate efforts to identify methods, measures, and indicators best suited for various types of APT research contexts, results, and benefits.
– Evaluate previous and existing efforts at establishing frameworks to assess research benefits.
– Scan fields of study outside of APT, pavement, and transportation research for advances in evaluation techniques.
– Organize and perform coordinated studies of specific evaluation methods (perhaps beginning with cost-benefit analysis) for APT research.
– Investigate methods suitable for retrospective as well as prospective assessments.
– Identify or pursue development of approaches that help determine the value of learning what *not* to do and the associated economic cost-avoidance value.
– Compile information about the state-of-the-practice in evaluating benefits of APT including techniques for various outputs and benefits. Identify the following: (1) Tools and evaluations by APT programs that have performed benefits evaluations who can share tools, information, and lessons learned; (2) Evaluation approaches that represent agreement or consensus between APT owners/operators and their sponsors, decision-makers, and clients; (3) Tools for accurate and consistent data collection that are suitable for various types of APT research products; and (4) Ways to bundle tools for benefits assessment along with APT research products during implementation.
– Investigate ways to balance the advantages and disadvantages of quantitative and qualitative evaluation. For example, focusing only on ROI might lead to emphasis on projects with high payback when low (or even zero) payback innovations may be better for environmental, safety, or other reasons.
– Identify conditions and criteria for assessing APT at various levels of evaluation (test, project, and program).
– Develop a website (similar to the RITA portal (RITA, 2011)) focused on APT benefits assessments that coordinates and aids in compiling and sharing information as well as hosting a database of costs, benefits, and "lessons learned".
– Identify required data to collect on costs and benefits. Investigate the availability of data as well as procedures for identifying or calculating necessary data.
– Pursue and promote systematic and consistent practices for evaluating APT research results, which could start with developing guidance on the use of cost-benefit analysis of APT.
– Develop standardized and commonly accepted approaches (between APT programs) for evaluating costs and benefits of APT research.
– Evaluate new approaches such as the NCHRP Project 20-63 toolbox to determine suitability for assessing benefits of APT. Investigate potential development of a multi-faceted, complementary approach that uses quantitative measures and qualitative indicators. Evaluation of alternate approaches such as *Real Option* analysis could be included in these investigations.
– Consider development of guidance in a resource document including concepts, terms, and techniques for APT owners/operators to consult in performing benefits evaluations.
– Plan for ultimate development of guidelines of practice for evaluating benefits of research that APT owners/operators may consult. Techniques developed and applied outside (as well as inside) the transportation field that may be suitable for APT benefits evaluation should be identified and considered for including in the guidelines.
– Identify the need and potential for training APT specialists on benefits, e.g., through webinars and documents at web portal/websites.
– Identify and promote use of evaluation techniques that are acceptable as "best practice" across state and national boundaries and suitable for collaboration in international evaluations of APT research.

5 CONCLUSIONS

This paper shows the substantial variability in approaches used worldwide to evaluate benefits of research in and outside of transportation research. No universal approach is recommended because there is no "one size fits all" technique, but developments during the past decade appear promising.

The most prominent qualitative indicators continue to be peer review and surveys. For quantitative assessment, cost-benefit analysis and bibliometrics continue to dominate. Evaluations of benefits from APT results have focused on direct economic

assessments, although qualitative indicators have been reported.

Efforts to evaluate benefits of research face many challenges. However, dynamic conditions and trends highlighted in this paper suggest evaluation of benefits from implementing APT results is an emerging priority. The future appears likely to bring increased focus on evaluating benefits of implemented APT research results. This paper provides information that should help APT owners/operators interested in evaluating benefits of their research.

The authors' overall intent in this paper is to raise awareness and increase familiarity with evaluating benefits of APT research results. The authors hope this paper will encourage dialogue on how to use and enhance existing evaluation approaches, stimulate further efforts on developing new ones, and adapt suitable methods to assessing benefits of implemented APT results. The ultimate goal is to help better evaluate, understand, and communicate the benefits of APT.

ACKNOWLEDGEMENTS

Foundational work and efforts by various APT owners/operators in evaluating benefits is acknowledged and much appreciated including publications by investigators in Australia, Europe, South Africa, and the US. Studies initiated, led, and completed under the leadership of Dr. Fritz Jooste are especially recognized for their catalytic effects in expanding awareness, knowledge, and sparking far-reaching actions. HVS testing and associated research in California described in this paper was funded by the FHWA and Caltrans, which sponsor work performed by Caltrans' research partners at the UCPRC, Dynatest Consulting, Inc., and the CSIR. The authors thank the Caltrans Library staff for their assistance.

DISCLAIMER

The contents of this paper reflect the views of the authors who are responsible for the facts and accuracy of the data presented herein. The contents do not necessarily reflect the official views or policies of the State of California or other agencies. This paper does not constitute a standard, specification, or regulation.

REFERENCES

Baron, J. and Gurmankin, A. 2009. *Cost-benefit analysis can increase trust in decision makers*. University of Pennsylvania. www.sas.upenn.edu/∼baron/papers.htm/cba.html. Accessed March 18, 2010.

Coetzee, N.F. and Mateos, A. 2008. Introduction to Accelerated Pavement Testing. *3rd International Conference on Accelerated Pavement Testing, Madrid, 1–3 October 2008*. www.cedex.es/apt2008/html/docs/workshops/workshop2.pdf. Accessed April 5, 2009.

Concas, S. Reich, S. and Yelds, A. 2002. *Valuing the Benefits of Transportation Research: A Matrix Approach*. Final Report on Contract #BC-353-24 to Florida DOT. Center for Urban Transportation Research at the University of South Florida.

COST347. 2005. *Work Package 5: Future use of ALT*. Working Group 5: Report on Improvements in Pavement Research with Accelerated Load Testing. European Co-operation in the Field of Scientific and Technical Research (COST action 347). www20.vv.se/fudresultat/Publikationer_000001_000100/Publikation_000039/W P%205%20Final%20report.pdf. Accessed March 18, 2010.

Du Plessis, L. and Prozzi, J. 2008. A Logical Framework Approach to the Evaluation of Benefits Derived from Accelerated Pavement Testing (APT) Studies. *3rd International Conference on Accelerated Pavement Testing, Madrid, 1–3 October 2008*. ww.cedex.es/apt2008/html/docs/workshops/workshop3.pdf. Accessed April 5, 2009.

Du Plessis, L. Nokes, W. Mahdavi, M. Burmas, N. Holland, J. and Lee, E. 2011. A Case Study of Economic Benefits Assessment of APT Research in California. *Transportation Research Record: Journal of the Transportation Research Record 2225* (1): 137–146.

Du Plessis, L. Rust, F.C. Horak, E. Nokes, W.A. and Holland, T.J. 2008. Cost Benefit Analysis of the California HVS Program. *3rd International Conference on Accelerated Pavement Testing, Madrid, 1–3 October 2008*. www.cedex. es/apt2008/html/docs/TS07/Cost_benefit_analysis_of_the_Ca lifornia_HVS.pdf. Accessed April 5, 2009.

Elston, D., Huft, D. Harder, B. Curtis, J. Evans, M. Jenks, C. McGinnis, L. Paul, H. Roberts, G. Wingfield, E. and Wlaschin, J. 2009. *Transportation Research Program Administration in Europe and Asia, Final Report*. FHWA-PL-09-015. FHWA, US Department of Transportation. www.international.fhwa.dot.gov/pubs/pl09015/pl09015.pdf Accessed November 12, 2009.

Epps, J., and Ardila-Coulson, M. 1997. *Summary of SHRP Research and Economic Benefits of Asphalt*. FHWA-SA-98-012. Prepared by Nevada Transportation Technology Transfer Center at the University of Nevada, Reno for FHWA, US Department of Transportation.

FHWA. 2003. *Synthesis of RandD Benefits Case Studies*. Non-numbered (unpublished) report. Office of Research, Development, and Technology, FHWA, US Department of Transportation.

GAO. 2011a. *GOVERNMENT PERFORMANCE – GPRA Modernization Act provides Opportunities to Help Address Fiscal, Performance, and Management Challenges*. Testimony Before the Committee on the Budget, US Senate. US Government Accountability Office, GAO-11-466T, Washington, DC., March 2011. www.gao.gov/products/GAO-11-466T. Accessed September 15, 2011.

GAO, 2011b. *Meeting Accountability Challenges in a Dynamic Environment*. US Government Accountability Office, GAO-12-167CG, Washington, DC., October 2011.

Georghiou, L., and Roessner, D. 2000 Evaluating Technology Programs: Tools and Methods. *Research Policy* 29: 657–678.

Gillen, D. Harvey, J. Cooper, D. and Hung, D. 2001. Assessing Economic Benefits from Implementation of New Pavement Construction Methods. *Transportation Research Record: Journal of the Transportation Research Record 1747* (1): 71–78.

Grant, J. Brutscher, P. Kirk, S. Butler, L. and Wooding, S. 2009. *Capturing Research Impacts – A Review of International Practice*.: Documented Briefing DB-578-HEFCE. Prepared for the Higher Education Funding Council for England. RAND Europe. Cambridge, United Kingdom. www.rand.org/pubs/documented_briefings/DB578. Accessed April 7, 2011.

Harder, B.T. 1995. *Stewardship Report Documenting Benefits of Research and Technology Efforts.* FHWA-SA-96-044. FHWA, U.S. Department of Transportation.

Hildebrand, G. and Dawson, A. 2008. ALT in Europe Following COST 347. *3rd International Conference on Accelerated Pavement Testing, Madrid, 1–3 October 2008*. www.cedex.es/apt2008/html/docs/keynote%20and%20plenary/ALT_in_Europe_following_COST_347.pdf. Accessed April 5, 2009.

Horak, E. Kleyn, E. du Plessis, J. de Villiers, E. and Thomson, A. 1992. The Impact and Management of the Heavy Vehicle Simulator (HVS) Fleet in South Africa. *Proceedings of the 7th International Conference on Asphalt Pavements, Nottingham, England, 16–20 August 1992.*

Hugo, F., and Epps-Martin, A. 2004. *NCHRP Synthesis 325 Report: Significant Findings from Full-Scale Accelerated Pavement Testing*. Transportation Research Board of the National Academies, Washington, DC.

IBEC. 2011. International Benefits, Evaluation and Costs (IBEC) Working Group. www.ibec-its.co.uk. Accessed March 15, 2011.

Jooste, F. J. and Sampson, L. 2004. *Assessment of Gautrans HVS Programme Benefits – Pilot Study Report (Draft)*. Report prepared by Modelling and Analysis Systems for Gauteng Provincial Government, Department of Public Transport, Roads and Works, Gauteng, South Africa.

Jooste, F.J. and Sampson, L. 2005.*The Economic Benefits of HVS Development Work on G1 Base Pavements*. Report prepared by Modelling and Analysis Systems for Gauteng Provincial Government, Department of Public Transport, Roads and Works, Gauteng, South Africa.

Jooste, F. Sampson, L. and Shaw, A. 2004. *Assessment of Gautrans HVS Programme Benefits – Inception Report*. Report to Gauteng Provincial Government, Department of Public Transport, Roads and Works, Gauteng, South Africa.

King, W. and Rasoulian, M. 2004. Experimental and Operational Progress with a Benefit/Cost Analysis for Louisiana's Pavement Research Facility. *2nd International Conference on Accelerate Pavement Testing, Minneapolis, 26–29 September 2004*. www.mrr.dot.state.mn.us/research/mnroad_project/index_files/pdfs/king.pdf. Accessed June 27, 2010.

Krugler, P., Walden, M. Hoover, B. Lin, Y. and Tucker, S. (Texas Transportation Institute). 2006. *NCHRP Project 20-63 Report: Performance Measurement Tool Box and Reporting System for Research Programs and Projects*. NCRHP Web-Only Document 127. Contractor's Final Report. Transportation Research Board of the National Academies, Washington, DC. onlinepubs.trb.org/onlinepubs/nchrp/nchrp_w127.pdf. Accessed June 22, 2009.

Lay, M.G. 2006. Why invest in road research? – A review of past outcomes. *Road and Transport Research* 15(4) 79-96.

Little, D., Memmott, J. McFarland, F. Goff, Z. Smith, R. Wootan, C. Zollinger, D. Tan, T. and Epps, J. 1997. *Economic Benefits of SHRP Research*. Research Report 596-1F. Texas Transportation Institute, College Station, Texas.

Marjanovic, S., Hanney, S. and Wooding, S. 2009. *A Historical Reflection on Research Evaluation Studies-Their Recurrent Themes and Challenges*. Technical Report 789 Prepared for Project Retrosight. RAND Europe. Cambridge, United Kingdom. www.rand.org/pubs/technical_reports/TR789/ Accessed March 17, 2010.

Metcalf, J. 1996. *NCHRP Synthesis 235 Report: Application of Full-Scale Accelerated Pavement Testing*. Transportation Research Board of the National Academies, Washington, DC.

National Academies. 1999. *Evaluating Federal Research Programs: Research and the Government Performance and Results Act*. Committee on Science, Engineering, and Public Policy. National Academy of Sciences, National Academy of Engineering, Institute of Medicine, Washington.

NCHRP. 2011a. *NCHRP 20-63B (Phase II) – Performance Measurement Tool Box and Reporting System for Research Programs and Projects*. Transportation Research Board of the National Academies, Washington, DC., (Active). http://rip.trb.org/browse/dproject.asp?n=24519. Access July 27, 2011.

NCHRP. 2011b. *NCHRP Synthesis 20-05/Topic 42-08 – Full-Scale Accelerated Pavement Testing, 2000-2011*. Transportation Research Board of the National Academies, Washington, DC., (Active). rip.trb.org/browse/dproject.asp?n=26246. Accessed June 25, 2011.

Nokes, W.A. du Plessis, L. Mahdavi, M. and Burmas, N. 2011. Techniques and Case Studies for Evaluating Benefits of Accelerated Pavement Testing. *Transportation Research Record: Journal of the Transportation Research Record 2225* (1) 147–154. Transportation Research Board of the National Academies, Washington, DC.

OTA. 1986. *Research Funding as an Investment: Can We Measure the Returns? – A Technical Memorandum*. OTA-TM-SET-36 (NTIS #PB86-218278). US Congress, Office of Technology Assessment, Washington, DC. www.fas.org/ota/reports/8622.pdf. Accessed May 26, 2009.

Powell, J. 2006. *Toward a Standard Benefit-Cost Methodology for Publicly Funded Science and Technology Programs*. Report NIST IR-7319. National Institute of Science and Technology, Gaithersburg, Maryland. www.atp.nist.gov/eao/ir-7319/contents.htm. Accessed February 12, 2009.

RAND 2006. *Measuring the Benefits from Research*. Research Bulletin 9202. RAND Europe. Cambridge, United Kingdom. www.rand.org/pubs/research_briefs/2007/RAND_RB9202.pdf. Accessed March 17, 2010.

RITA. 2011. Research and Innovative Technology Administration. US Department of Transportation. www.benefitcost.its.dot.gov/its/itsbcllwebpage.nsf/krhomepage. Accessed March 15, 2011.

Roessner, D. 2002. Outcome Measurement in the United States: State of the Art. *American Association for the Advancement of Science, Annual Meeting, Boston, Massachusetts, 17 February 2002*. www.prism.gatech.edu/~sc149/reseval/html/boston.pdf. Accessed January 5, 2009.

Ruegg, R. and Feller, J. 2006. *A Toolkit for Evaluating Public RandD Investment*. Report NIST GCR 03-857. National Institute of Science and Technology, Gaithersburg, Maryland. www.atp.nist.gov/eao/gcr03-857/contents.htm. Accessed February 12, 2009.

Ruegg, R., and Jordan, G. 2007. *Overview of Evaluation Methods for RandD Programs*. Report prepared by TIA Consulting, Inc. for Office of Energy Efficiency and Renewable Energy, US Department of Energy, Washington, DC. www1.eere.energy.gov/ba/pba/pdfs/evaluation_methods_r_and_d. pdf. Accessed June 10, 2009.

Sabol, S.A. 2001. *NCHRP Synthesis 300 Report: Performance Measures for Research, Development and Technology Programs*. Transportation Research Board of the National Academies, Washington, DC.

Samson, L. Sadzik, E. and Jooste, F. 2008. A Cost-Benefit Analysis of Heavy Vehicle Simulator Testing and Related Technology Development. *3rd International Conference on Accelerated Pavement Testing, Madrid, 1–3 October 2008*. www.cedex.es/apt2008/html/docs/TS07/A_cost_benefit_analysis_of_Heav y_Vehicle. Accessed April 5, 2009.

TRB. 2001. Committee on a Study for a Future Strategic Highway Research Program. *Strategic Highway Research: Savings Lives, Reducing Congestion, Improving Quality of Life.* Special Report 260. Transportation Research Board of the National Academies, Washington, DC.

TRB. 2008. *The Federal Investment in Highway Research 2006-2009: Strengths and Weaknesses*. Special Report 295. Research and Technology Coordinating Committee. Transportation Research Board of the National Academies, Washington, DC.

TRB-ECTRI. 2009. *Working Group 10 Report on European-United States Transportation Research Collaboration – Challenges and Opportunities*. Report of the TRB-ECTRI Working Group on EU-U.S. Transportation Research Collaboration. TRB (Washington, DC) and European Conference of Transport Research Institutes (Lyon, France and Brussels, Belgium). www.ectri.org/Documents/Publications/Strategic-documents/WG10report_EU-UScooperation_pub_EN.pdf. Accessed March 3, 2010.

Worel, B. Jensen, M. and Clyne, T. 2008. Economic Benefits Resulting from Road Research Performed at MnROAD. *3rd International Conference on Accelerated Pavement Testing, Madrid, 1–3 October 2008*. www.cedex.es.ex/apt2008/html/docs/TS07/Economic_Benefits_Resulting_from_Road.pdf. Accessed April 5, 2009.

Advances in Pavement Design through Full-scale Accelerated Pavement Testing – Jones, Harvey, Mateos & Al-Qadi (Eds.)
© 2012 Taylor & Francis Group, London, ISBN 978-0-415-62138-0

Results of a case study determining economic benefits of accelerated pavement testing research in California

L. du Plessis
CSIR BE, Pretoria, South Africa

W.A. Nokes, M. Mahdavi, N.I. Burmas & T.J. Holland
California Department of Transportation, Sacramento, California, US

J.T. Harvey
University of California Pavement Research Center, University of California, Davis, US

ABSTRACT: This paper highlights findings of a case study using cost-benefit analysis to determine economic benefits resulting from Accelerated Pavement Testing (APT) with a Heavy Vehicle Simulator (HVS) in California. The University of California Pavement Research Center (at UC Davis and UC Berkeley) and its research partners started APT in 1994 on behalf of the California Department of Transportation and is now in its 17th year of existence. The results presented in this paper follow a pilot study intended to define a method suitable for measuring the direct economic benefits from APT. The method used was initially developed and applied in Australia and later enhanced in South Africa for the respective APT programs. Enhancements to the Australian/South African methods and application to California APT program are discussed. The case study evaluated benefits (in terms of agency and road user cost savings) from HVS tests performed to validate innovative pavement mixes and designs. The method was successfully applied and showed benefit-cost ratios ranging from about 2:1 to 17:1 (depending on discount rate), which is in the range of previous studies in Australia and South Africa. Due to the uncertainties and subjective nature of this technique, sensitivity analysis is recommended to determine a range of savings instead of a single benefit-cost ratio.

1 INTRODUCTION

The California Department of Transportation (Caltrans) established an accelerated pavement testing (APT) program and in 1994 with the purchase of two Heavy Vehicle Simulators (HVS). The original program, abbreviated as CAL/APT, evolved into the University of California Pavement Research Center (UCPRC), a partnership between Caltrans, UC Davis, UC Berkeley, South Africa's CSIR, and, Dynatest Consulting. The APT program has been very productive for the past 17 years and has significantly helped with the advancement of pavement technologies in California.

The need for assessing benefits from APT in California comes from many sources including Caltrans' commitment to its strategic goal of effective stewardship of California's resources and assets. In managing HVS tests and pavement research overall, the Caltrans Division of Research and Innovation, supports the Department's vision, mission, and strategic goals through processes that include:

- Feedback – to ensure that sound investments are made in the pavement research program.
- Continuous improvement – to identify and overcome barriers in the research process.
- Accountability and performance measurement – to identify and communicate benefits of research.

The first step in assessing benefits from APT in California was to conduct a pilot project that included a case study, which is described in this paper. The primary goal of this case study was to assess a cost-benefit analysis (CBA) method, developed in Australia to assess their APT program and later enhanced in South Africa for evaluating the economic benefits from their HVS testing. The ultimate purpose of the pilot project was to determine the potential for adapting the method to California conditions.

The work described in this paper accompanies research efforts on methods and measures for the evaluating benefits of transportation research (Nokes et al., 2011). The objectives of this paper are to:

- Briefly outline the cost-benefit methodology used in this study;
- Detail the project which was selected to test the method;
- Describe all the analysis actions and methods to calculate the direct quantifiable economic benefits stemming from the successful implementation of APT research; and

– Present the results together with suggestions on possible improvements and enhancements.

The project is continuing and the results are being updated as more reliable data becomes available. The results presented in this publication stem from the latest analysis completed in early 2011.

2 BACKGROUND

Use of economic analysis such as CBA provides many benefits. In addition to showing research managers and decision-makers the return on investment and cost-effectiveness, CBA can help inform stake-holders and the public. The process of quantifying and assigning value to benefits and costs also provides documentation about the decision-making process. When applied retrospectively, CBA can clarify the forces and barriers that led to a project decision reveal opportunities and lessons learned, and possibly lead to process improvements for future projects.

Horak et al. (1992) presented an investigation of the benefits from HVS testing in South Africa. Horak details a comprehensive list of specific technical impacts from the HVS program at the time. These included the improved use of new and innovative construction materials and methods, improved design and analysis procedures, and specific rehabilitation investigations. The analysis found an overall benefit-cost ratio (BCR) of 12.8 and reported that "It should be appreciated that such economic quantification, in this instance attempting to realistically compare the "with HVS" and "without HVS" scenarios, is invariably both imprecise and conservative (the latter to minimize potential contention)."

The subjectivity in determining benefits (though conservative) and the lack of benchmarking with other expert opinions make the 1992 study difficult to update. Building on the work of Horak, Jooste and Sampson (2004, 2005) presented a methodology in 2004 where the direct economic benefits of HVS work done in South Africa to develop a high-quality crushed aggregate base pavement design (termed G1 base) were evaluated. Their methodology was largely based on initial development work done by Rose and Bennett (1994) and BTA Consulting (1992) who calculated BCR values for the evaluation of the Australian APT program. Enhancements to the methodology are described in Jooste and Sampson (2004, 2005).

This pilot project investigates BCR as one of the many ways to evaluate the economic efficiency of a project. The Federal Highway Administration (FHWA) also recommends BCR (or net present value) for most economic evaluations of projects (California Department of Transportation, 2007). The method used in this pilot project is consistent with Caltrans practices in evaluating economic benefits and life-cycle analysis of transportation projects and procedures presented in the FHWA Economic Analysis Primer (FHWA, 1998).

2.1 *Terms in economic assessment*

BCR is the quotient of total discounted benefits divided by total discounted costs. Projects with a BCR higher than one have greater benefits than costs, i.e. positive net benefits. The higher the ratio, the greater the benefits relative to the costs. BCR is insensitive to the magnitude of net benefits and therefore may favor projects with small costs and benefits over those with higher net benefits. This can be overcome by also presenting the net present value (NPV), which results when the total discounted costs are subtracted from the total discounted benefits. Both measures are used in this case study.

Because of time-related separation between a project's development, completion, and its ultimate impacts and benefits realization, it is important to account for the time value of money and to compare discounted costs and benefits. Agencies across the world rely on a basic set of key cost–benefit indicators, including:

– NPV (net present value);
– PVB (present value of benefits);
– PVC (present value of costs);
– BCR (benefit-cost ratio) = PVB/PVC), and
– Discount rate.

The discount rate is the interest rate used in discounted cash flow analysis to determine the present value of future cash flows. The discount rate takes into account the time value of money (the idea that money available now is worth more than the same amount of money available in the future because it could be earning interest). In this study the NPV of the benefits is presented in relation to the costs as the BCR, using a discount rate of four percent (as prescribed by Caltrans for all their transportation life-cycle cost analyses).

3 APPROACH FOR BENEFIT ASSESSMENT OF UCPRC PROJECT

Evaluation of the economic returns of research and development is difficult. An economic benefit can only be calculated if the outcome of a technology development effort can be compared with a scenario that would have existed had the development not been undertaken. Such an assessment includes a significant amount of uncertainty and subjective judgment. The methodology adopted for this study takes this uncertainty into account as suggested by the framework in the Australian and South African studies, with some modifications.

3.1 *Approach background*

The approach applied in this case study was developed by the Australian Road Research Board (ARRB) and applied to retrospective evaluation of research results from APT in their Accelerated Load Facility (ALF) program (Rose and Bennett, 1994, BTA Consulting,

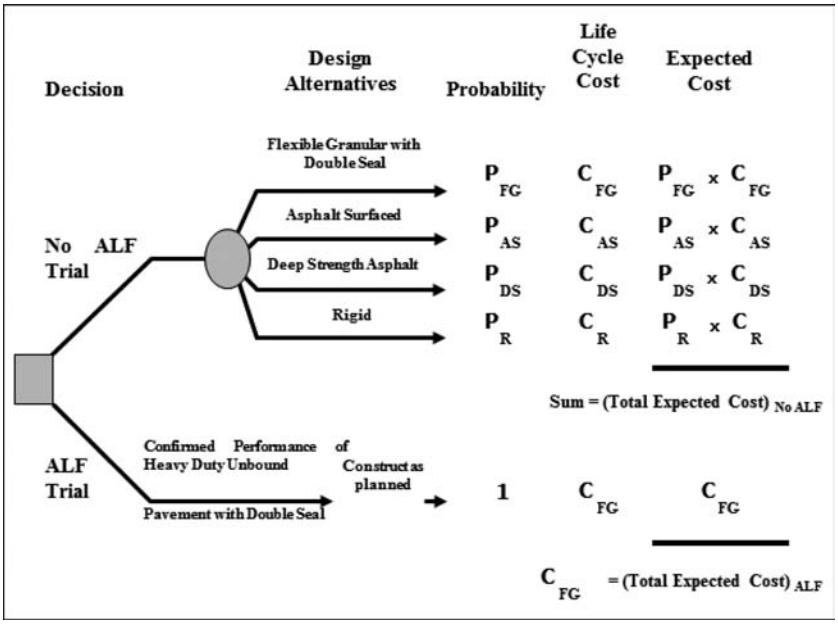

Figure 1. Decision tree for Benalla ALF trial benefits assessment. (Rose and Bennett, 1994).

1992). The goal of ARRB's original study was to provide an evaluation of dollar value benefits and costs of the first seven ALF trials. The ARRB approach calculated road agency costs under two scenarios: (1) costs resulting from outputs of the ALF trials and (2) costs expected in the absence of ALF trials. Comparison of the two costs would be straightforward except for the uncertainty about the likelihood of events (such as selecting alternative materials and/or designs) in the "ALF trial" vs. "no ALF trial" scenarios. The ARRB approach takes uncertainty into consideration by using the concept of expected value, which is a tool for decision-making under uncertainty. The uncertainties were represented by using probabilities for all alternatives. These subjective probabilities (based on input from pavement experts) were then multiplied by the cost of each alternative to yield an expected cost. The ARRB analyses focused on specific outcomes of each ALF trial that were linked directly to agency costs.

Decision tree diagrams were used to represent the decision-making process including alternatives, probabilities, and costs. The diagram for the Benalla ALF trials of heavy duty unbound pavement with a double seal (shown in Figure 1) illustrates the method (Rose and Bennett, 1994). The bottom branch in the diagram indicates positive results from the ALF trial, which led to construction of the heavy duty unbound pavement. Figure 1 also shows (on the top branch) four design alternatives that would likely be used in the absence of the ALF trial. Probability values were derived from interviews with individuals who were working in the pavements area of the Victoria state road agency at the time. For each alternative, the interviewees gave their estimate of the probability that the agency would have chosen that alternative. The probabilities sum to 1.00 for each of the two separate branches. ARRB reported that interviewees assigned probabilities that were collectively consistent for each alternative and presented results from sensitivity analyses that helped evaluate the effects from using various probabilities and discount rates. The expected cost of each alternative was calculated as the product shown at far right in Figure 1.

The total expected cost of the "no ALF trial" scenario is calculated as the sum of the expected costs of the four alternatives on the upper branch. The total expected cost of the "ALF trial" scenario equals the cost of the design shown (CFG) on the lower branch. Benefits (in terms of savings of agency costs) are calculated by subtracting these two total expected costs. In the ARRB case studies these savings represent the direct economic benefits attributed to the ALF trial. The quotient of benefits divided by costs of testing produced a range of BCR values depending on inputs and assumptions. Results were reported as showing a "healthy return" on research investments in the ALF programs (BTA Consulting, 1992)

3.2 *Enhancement and use in South Africa*

The ARRB methodology was used in South Africa to assess direct economic benefits from HVS APT (Jooste and Sampson, 2004, Jooste and Sampson 2005). In 2003, road budget constraints at the Gauteng Provincial Government's Department of Public Transport, Roads and Works (Gautrans), in the South African province of Gauteng, led to an evaluation of benefits from HVS tests. In searching for approaches to evaluate the program, the ARRB's ALF program evaluation was identified and determined to be an approach that provided "a well-documented record"

and used "many of the best practice aspects" for assessing research benefits. It also was conceivable that the approach could help establish a framework for evaluating future tests (Jooste and Sampson, 2004).

Just as in the ARRB's retrospective analysis, case studies were performed to assess benefits in terms of Gautrans' agency costs. One study evaluated benefits from the use of a high quality crushed stone base (called "G1"), which had been implemented and in use for many years after extensive research including HVS testing (Jooste and Sampson, 2005). Like the ARRB's case studies, the G1 study relied on input from pavement experts to set probabilities. The probabilities for each alternative were collectively consistent. Benefits (agency cost savings) were calculated by subtracting total expected costs of the "HVS test" from the "no HVS test" total expected costs. Sensitivity analyses were performed to determine the effects of discount rate on benefits.

The Gautrans studies introduced an enhancement to the ARRB approach that resulted from questions in South Africa about how much of the benefits were attributable to the HVS tests. The Gautrans study acknowledged that most pavement advancements have more than one contributing source, and consequently benefits from advancement should be attributed proportionally to the sources. To enable attribution, they augmented the ARRB approach by introducing the use of a "contribution ratio", which ranges from 0 to 100 percent and is derived from input from interviews with pavement experts. A 100 percent contribution ratio would mean that the HVS research was solely responsible for the technology development and all the credit for this development belongs to the HVS research program. In the Gautrans study the contribution ratio values were collectively consistent. The total expected cost savings were multiplied by the contribution ratio to calculate total savings attributed to the HVS tests. These adjusted benefits were divided by the cost of HVS testing to calculate the benefit-cost ratio for the HVS tests. The Gautrans study report recommended sensitivity analysis to evaluate the effects of contribution ratio on the calculated benefits.

3.3 *Further enhancement and use in California*

Caltrans learned of the Gautrans study through the UCPRC – CSIR, South Africa research partnership. Having conducted HVS testing in California since 1994, there was interest in determining the direct economic benefits from the HVS program. The successful use of the evaluation method in South Africa, plus its subsequent enhancement suggested potential suitability for use in California. A previous study in California (Du Plessis, 2008) had estimated projected, larger-scale benefits from early HVS tests in California, but subsequent interest changed to a more narrowly focused assessment that examined impacts long after APT results were implemented such as was done in the Gautrans study.

Caltrans initiated a pilot effort that, like the previous work by the ARRB and Gautrans, included a case study. This paper presents further enhancement of the method and results from its use to evaluate benefits from a specific HVS project.

3.4 *Best practices and key steps in the methodology*

Like the pilot project in California, the South African HVS evaluation needed a suitable method for determining benefits from HVS testing. In an initial effort to meet Gautrans' needs, South African investigators developed a "best practice approach". Elements of best practice include the following (Jooste and Sampson, 2004, 2005):

- Select the best performing project to quantify benefits.
- Collect information and validate estimates of benefits from road authorities and practitioners who will implement the research results (not from the researchers).
- Explicitly address uncertainty through methods such as calculating a range of values and using probability measures, and
- Acknowledge other sources that contribute to technology advances and ask practitioners how much they believe the research results (i.e., from HVS tests) contributed to the advances.

The adopted method is based on decision analysis, value of information concepts, and the use of expected values, which are the product of probabilities of outcomes multiplied by the cost of each outcome (De Neufville, 1990; Samson, 1988). The method is based on "Bayesian" statistics. This approach consists of procedures and measures for events in non-repeatable random experiments or when the process of sampling is mooted by circumstances (oil-well drilling is a typical example in the literature). Unlike the frequentist approach, which emphasizes underlying population and sample distributions and confidence intervals for hypothesis testing, the Bayesian approach relies on states of knowledge and beliefs (including probabilities) given by knowledgeable individuals. In this case study, pavement experts who had first-hand knowledge and experience of the rehabilitation project and associated HVS testing provided input. The use of sensitivity analysis is strongly recommended to examine and understand the range of potential impacts from reliance on subjectivity. This paper follows the method for Bayesian analysis as described in the literature and as applied in Australian and South African studies.

A payoff table or decision tree is a framework for calculating expected costs for a decision. Each decision, such as conducting a test, or not conducting a test, results in its associated expected cost. Conducting a test may provide more information which might produce a lower expected cost than not testing. Depending on the cost of testing, the difference in expected costs may show a cost savings (i.e., benefit). If savings exceed the cost of testing then the benefits

are worth the cost of the test. The BCR of conducting a test can then be calculated (Jooste and Sampson, 2004). Details of the method and its application in the case study are given below.

The steps in applying the adapted methodology are summarized below:

1. Situations with and without the benefit of HVS testing are identified. This includes clearly describing the benefit(s) attributable to specific research output(s).
2. Uncertainty in assumptions and outcomes is accommodated by assigning a probability (based on input from interviews) to each alternative outcome.
3. Cost (life-cycle) of each alternative outcome is calculated.
4. Expected value (cost) of each alternative outcome is calculated by multiplying its probability by its cost.
5. Total expected value for each decision (with HVS test and without HVS test) is calculated as the sum of expected costs of alternatives.
6. Benefit (expressed as NPV of cost savings) of the information from the HVS test is determined by subtracting the total expected cost without the HVS test from the total expected cost with the HVS test.
7. BCR is derived by dividing the benefit by the total cost of the HVS test.

A key part of the assessment and validation effort is estimating the likelihood of technical advances that would have occurred if HVS testing had not been performed. To explicitly address alternative scenarios of technology development, Jooste and Sampson adopted decision tree analysis, which takes uncertainty into account and has been successfully used in previous analyses (Rose and Bennett, 1994, BTA Consulting, 1992). The decision tree format for HVS tests in South Africa is shown in Figure 2.

The expected cost of each design alternative is determined by multiplying the life-cycle cost for each alternative by its assigned probability. Note that the sum of all probabilities must equal one in each decision branch.

The total expected cost for each decision (with and without HVS testing) is calculated as the sum of the expected cost of the alternatives. The difference of these two total expected costs represents the benefit (cost savings) due to the HVS investigation. The calculated benefit along with the cost of HVS testing can then be used to determine an economic indicator such as the benefit-cost ratio.

For benchmark objectivity and credibility, each of the impacts identified were validated through formal interviews with pavement engineers within and outside of Caltrans. These engineers had firsthand knowledge of the HVS test and rehabilitation project that are the subject of this case study. During these interviews the various rehabilitation alternatives, probabilities for implementation, costs, and perceived impacts and benefits were discussed (Jooste and Sampson, 2005). Interviews provided a wide range of opinions as well

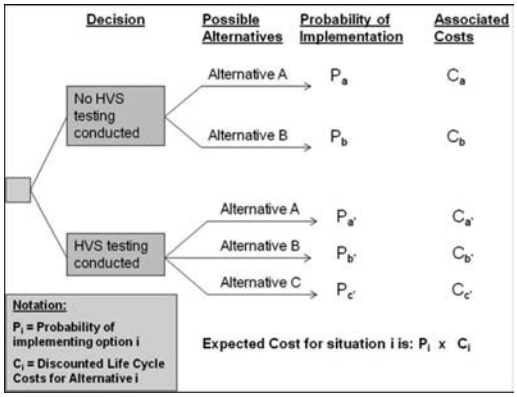

Figure 2. Approach for assessing HVS testing benefits assessment in South Africa.

as the inputs needed for analysis such as the probability for each alternative and the extent to which the HVS test contributed to benefits. To accommodate the variability in the perceptions of the interviewees, sensitivity analysis was conducted to examine how the range of their inputs affects the CBA results.

It is also important to take consideration of the fact that benefits (e.g., from a less expensive design) cannot be realized over the whole road network where an innovation is applicable and certainly not immediately after validation. The potential benefit would be phased in based on needs of the road network, budgets, and other priorities.

Savings in road user cost and other user benefits can make a significant contribution to total economic benefits. This paper reports on both the direct agency and user benefits (reduced road user delay), determined using the methodology described above.

4 CASE STUDY

To evaluate the cost-benefit analysis methodology, a case study was conducted on an HVS test on hot-mix asphalt concrete (AC) pavement associated with the Long-Life Pavement Rehabilitation Strategy (LLPRS) program started by Caltrans in 1998. Criteria for the LLPRS program were fast construction (within a limited number of 55-hour weekend closures), at least a 30-year service life, and minimal maintenance. The project selected was a rehabilitated section of heavily-trafficked Interstate 710 (I-710) in Long Beach, California (Monismith and Long, 1999a; Monismith and Long, 1999b).

HVS testing was conducted to validate the innovative mix designs for rutting and fatigue cracking (Wu et al., 2006). This pilot study focuses only on evaluating the economic benefits of that series of HVS testing to validate the mix designs used during the reconstruction of the first phase of the I-710 project.

The HVS tests are highlighted here as needed for this pilot study. Further details are provided in project reports (Wu et al., 2006; Monismith et al., 2009). After extensive and ongoing discussions, by June 2000 the UCPRC had prepared an HVS test plan for the validation of the I-710 long life innovative mixes, HVS test sections were built, and the first HVS test started. The HVS would test these experimental sections to provide data for validation of the AC mix overlay design and comparison of rutting performance of the AC mixes. Of longer term interest was pavement performance data for development and validation of refinements in mechanistic-empirical procedures for predicting rutting of AC mixes.

HVS tests were performed by the UCPRC at UC Berkeley's Richmond Field Station. Results provided validation performance data that Caltrans used in deciding to move forward with implementing the innovative mixes and pavement designs for the I-710 rehabilitation project.

4.1 *I-710 Long Beach rehabilitation project*

The I-710 LLPRS rehabilitation project was completed in 2003. The 30-year design loading of the rehabilitated pavement is 200 million equivalent 80 kN standard axle loads (ESALs). At that time, with approximate average daily traffic of 155,000 during weekdays with 13 percent trucks, asphalt concrete pavements based on the (then) standard Caltrans design method could not meet the LLPRS criteria. This provided an opportunity to develop and implement innovations validated through HVS testing. Details about the development and specifications for the innovative mixes and designs were reported by Monismith and Long (2009).

The project consisted of three full-depth asphalt concrete (FDAC) replacement sections (approximately 8.7 lane-miles total) under freeway overpasses with minimum lower vertical clearances required by federal standards. Two sections (approximately 15.8 lane-miles) between overpasses were rehabilitated with crack, seat, and asphalt concrete overlay (CSOL) of existing 50-year old portland cement concrete (PCC) slabs. The three overcrossings are shown in Figure 3 at the southern, northern, and intermediate locations on the project. The FDAC under the overcrossings and the CSOL between them produced distinct benefits that are described and evaluated in this paper.

4.1.1 *Rehabilitation alternatives*

Through various interviews a list of possible rehabilitation strategies for LLPRS projects with similar climatic and traffic demands as the I-710 were identified. These alternative strategies were:

1. Standard Caltrans CSOL;
2. Innovative CSOL;
3. Standard Caltrans FDAC replacement;
4. Innovative FDAC replacement; and
5. Long-life PCC lane and slab replacement.

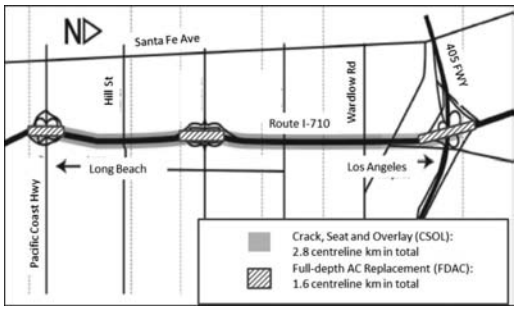

Figure 3. Plan view of I-710 Phase 1 rehabilitation project.

Innovative mixes and designs for CSOL and FDAC (shown as alternatives 2 and 4 in the list above) were developed based on mechanistic-empirical design (Monismith and Long, 1999a; Monismith and Long, 1999b), laboratory testing, and professional engineering judgment. HVS testing was performed subsequently to validate the performance of the mixes and designs (Wu et al., 2006).

Two different designs were required. Substandard vertical clearances under the overcrossings required lowering the existing grade. The innovative mixes placed in the FDAC designs were expected to meet this need. Between the overcrossings, where there were no clearance concerns, a different design could be used. The innovative mixes placed in the CSOL designs were planned for this purpose. Though two different pavements structures were developed, both designs used innovative mixes and both had to meet the LLPRS criteria mentioned above. The two benefits identified for this case study reflect the two different design approaches:

- Benefit #1: Innovative mixes enabled the improvement of vertical clearance under overcrossings while meeting LLPRS criteria.
- Benefit #2: Innovative mixes enabled meeting the LLPRS criteria where no vertical clearance constraints existed.

4.2 *Benefit-cost analysis*

The steps detailed below were followed to determine the savings and BCR. The base year for all cost comparisons was 2000 and the Caltrans' standard four percent discount rate was used. The decision tree diagram for the I-710 case study is shown in Figure 4 (Du Plessis, 2011).

1. Validation interviews were conducted with pavement engineers within and outside of Caltrans who had first-hand knowledge of the HVS test and I-710 rehabilitation project. They identified likely alternative designs (with and without HVS tests), probabilities of construction of each alternative, maintenance and rehabilitation schedules for the design life, and the percentage contribution of HVS tests to innovative designs.

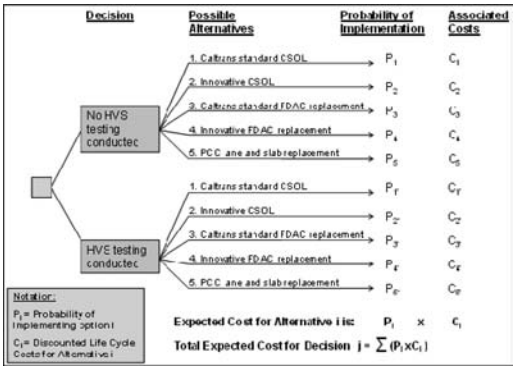

Figure 4. Decision tree used in the I-710 case study.

2. The costs (NPV) for each alternative were calculated using the Caltrans *Life-cycle Cost Analysis (LCCA) Procedures Manual* (2007) and *RealCost 2.2* software (California Department of Transportation, 2007; FHWA, 1998). The *CA4PRS* software developed at UCPRC was used to calculate construction schedules, work zone user costs, and agency costs for initial and future maintenance and rehabilitation (Harvey et al., 2005; Lee, 2011). Costs were discounted to determine the present value of agency and road user costs for each alternative.
3. Applying the costs and probabilities from above, the total expected cost (discounted NPV) was determined for the two decisions, with and without HVS testing. Sensitivity analyses were conducted to assess the range of probabilities from the interviewees' perceptions. (Note that $\sum(p1.p5) = 1.0$ and similarly for $p1'$ to $p5'$).
4. The maximum expected payoff (i.e., cost savings in this case) is the greater total expected cost of the two decisions.
5. The benefit (cost saving) is the difference in the total expected cost of the two decisions and is determined by subtracting the total expected costs of the "with HVS" decision from the "without HVS" decision. A positive value indicates a positive net benefit.
6. Scaling-up the benefit is based on the projected number of lane-miles where the innovation may be implemented. Projecting the likely number of lane-miles requires input from interviews, programmed roadway improvements, and judgment. The total benefit is then calculated by scaling-up the benefit to the correct expected lane-miles suitable for these rehabilitation strategies.
7. Determining the development costs requires identifying historical records along with judgment about the costs of operations, testing, and analysis in developing the I-710 innovative mixes and designs.
8. The BCR is determined by dividing the total scaled-up benefits by total development costs.

4.2.1 *Assumptions*

Life-cycle cost analysis using *RealCost* software requires several inputs (California Department of Transportation, 2007; FHWA, 1998). Values for several input parameters are listed below. Because the I-710 rehabilitation is a LLPRS option an analysis period of 60 years was selected in accordance with the guidelines in the Caltrans LCCA Procedures Manual. Zero salvage value is assumed at year 60 and the cost of any maintenance treatments at year 60 is excluded from the LCCA. The assumptions and inputs including all costs (agency and road user) are detailed in Lee (2011).

Traffic data

Caltrans annual average daily traffic (AADT) data for the period from September 2001 to March 2002 was used for the analysis:

- AADT: 137,500 weekday and 97,300 weekend.
- Trucks: 15%/5% weekday/weekend of AADT.
- Annual growth rate of traffic: 0.5%.
- Capacity of free flow: 2,000 vehicles per hour per lane (vphpl).
- Capacity of queue dissipation: 1,800 vphpl.

Road User Cost calculations

The values of time for user costs were $11.51/hour for passenger cars and $27.83/hour for trucks.

Maintenance/preservation and rehabilitation costs

Apart from the initial construction required for the rehabilitation of the I-710, various capital maintenance and rehabilitation strategies are planned to keep the facility in a serviceable condition for the duration of the 60-year design life-span. These maintenance interventions are shown in Table 1 for all five rehabilitation options including the standard and innovative designs between and under the over-crossings. Timelines of the various alternative maintenance and rehabilitation strategies are also shown in Table 1. These were derived from the suggested Maintenance and Rehabilitation Strategies in the LCCA Procedures Manual, input from interviewees, and judgment. Due to space limitations abbreviated actions are listed in Table 1. More complete descriptions can be found in the Manual.

Table 1 shows milling and replacing the open-graded friction course (OGFC) as well as the dense-graded asphalt concrete (DGAC) for the standard and innovative asphalt concrete alternatives. These are part of the various capital maintenance (CAPM), routine maintenance, and preservation activities. Also shown are the levels of concrete pavement rehabilitation (CPR), which includes surface grinding, spall and joint seal repair, and slab replacement, and which range from minor (indicated as "a"), and moderate ("b"), to significant ("c") depending on the extent of slab cracking.

The costs for the various designs were based on the project scope of the I-710 (24.5 lane-miles) using 2000 as the base year. The initial construction costs and the recurring maintenance costs per annum are shown in

Table 1. Maintenance and rehabilitation strategies for standard and innovative alternatives.

Year	Standard ACP Alternative[1]		Innovative ACP Alternative		Standard PCC
	Alt 1: CSOL	Alt 3: FDAC	Alt 2: CSOL	Alt 4: FDAC	Alt 5: Long-life PCC
10	1st CAPM (a) 30 Mill&rep OGFC 60 Mill DGAC 90 rep DGAC	1st CAPM 30 Mill&rep OGFC 60 Mill&fill DGAC	1st CAPM 30 Mill&rep OGFC	1st CAPM 30 Mill&rep OGFC	N/A
15	2nd CAPM (b) 30 Mill OGFC 30 Mill&rep DGAC 30 rep OGFC	N/A	N/A	N/A	N/A
20	1st Rehab 30 Mill&rep OGFC 90 Mill DGAC 120 rep DGAC	2nd CAPM 30 Mill&rep OGFC 60 Mill&fill DGAC	2nd CAPM 30 Mill&rep OGFC	2nd CAPM 30 Mill&rep OGFC	N/A
30	3rd CAPM 30 Mill&rep OGFC 60 Mill DGAC 90 rep DGAC	3rd CAPM 30 Mill&rep OGFC 60 Mill&fill DGAC	1st Rehab 30 Mill&rep OGFC 75 Mill&fill PBA-6a	1st Rehab 30 Mill&rep OGFC 75 Mill&fill PBA-6a	1st CAPM CPR (C) Random slab (2%) Diamond grinding Joint sealing
35	4th CAPM 30 Mill OGFC 30 Mill&rep DGAC 30 rep OGFC	N/A	N/A	N/A	2nd CAPM (CPR B) CPR (B) Random slab (5%)
40	2nd Rehab 30 Mill&rep OGFC 90 Mill DGAC 120 rep DGAC	4th CAPM 30 Mill&rep OGFC 60 Mill&fill DGAC	3rd CAPM 30 Mill&rep OGFC	3rd CAPM 30 Mill&rep OGFC	N/A
45	N/A	N/A	N/A	N/A	3rd CAPM (CPR A) CPR (A) Random slab (7%) Diamond grinding Joint sealing
50	5th CAPM (a) 30 Mill&rep OGFC 60 Mill DGAC 90 rep DGAC	5th CAPM 30 Mill&rep OGFC 60 Mill&fill DGAC	4th CAPM 30 Mill&rep OGFC	4th CAPM 30 Mill&rep OGFC	1st PCC Rehab 300 PCC
55	6th CAPM (b) 30 Mill&rep OGFC 30 Mill DGAC 30 rep DGAC	N/A	N/A	N/A	N/A

[1] All thicknesses in millimeters

Table 2. Agency and road user costs (RUC) for maintenance and rehabilitation strategies are both shown in the table (Lee, 2011) for the five rehabilitation alternatives.

The LCCA results specific to the initial phase of the I-710 project are based on costs for various pavement rehabilitation types as of 1999 to 2003 and a discount rate of four percent as used by Caltrans for LCCA cost-benefit analysis.

The results would be expected to change depending on factors including different materials cost changes (such as differences in inflation rate between asphalt and portland cement concrete costs), changes in project configuration (such as the ratio of truck lanes needing replacement relative to passenger car lanes not needing rehabilitation), different discount rates, and other project-specific factors.

The total life-cycle costs represent the NPV of each of these alternatives and is shown for agency, road user, and total costs in Table 3. The table shows the NPV in terms of $/lane-mile or $/lane–km of all alternatives including the total of all rehabilitation interventions, annual maintenance costs, and user costs.

Ranking the NPV of the five alternatives reveals the most cost-effective rehabilitation option at the time was alternative 4 (Innovative FDAC) with a total life-cycle cost of $17.27M followed by alternative 2 (innovative CSOL) with a total life-cycle cost of $21.75M.

The most expensive rehabilitation option at the time was the PCC alternative with a total life-cycle cost of $59.81M. It should, however, be noted that alternatives 4 and 2 are not directly comparable with one another as these alternatives are for different designs for between and under the overcrossings. A more logical comparison would be to compare alternative 1 (standard CSOL) with alternative 2, and alternative 3 (standard FDAC) with alternative 4. In terms of both benefits #1 and #2, the NPV of the innovative I-710 rehabilitation strategies were lower than the (then) standard Caltrans rehabilitation alternatives for LLPRS.

4.3 *Analysis of benefits*

The net benefit of implementing the HVS-validated innovative mixes and designs for both benefits are

Table 2. Maintenance and rehabilitation costs (in millions) for standard and innovative alternatives (agency and road user cost).

	Alt 1: Standard ACP Alternative				Innovative ACP Alternative				Alt 5: Long-Life PCC Alternative	
	Alt 1: CSOL		Alt 3: FDAC		Alt 2: CSOL		Alt 4: FDAC			
Year	Agency Cost	RUC	Agency Cost	RUC	Agency Cost	RUC	Agency Cost	RUC	Agency Cost	RUC
0	$5.35	$0.55	$13.94	$1.67	$11.92	$0.56	$10.72	$1.30	$43.67	$5.22
	1st CAPM		1st CAPM		1st CAPM					
10	$3.95	$1.57	$1.86	$0.80	$1.20	$0.58	$0.69	$0.33		
	2nd CAPM									
15	$1.83	$0.83								
	1st Rehab		2nd CAPM		2nd CAPM					
20	$3.52	$1.60	$1.26	$0.63	$0.81	$0.46	$0.46	$0.26		
	3rd CAPM		3rd CAPM		1st Rehab				1st CAPM (CPR C)	
30	$1.80	$0.96	$0.85	$0.49	$2.15	$0.99	$1.20	$0.56	$1.14	$0.33
	4th CAPM								2nd CAPM (CPR B)	
35	$0.84	$0.50							$0.64	$0.65
	2nd Rehab		4th CAPM		3rd CAPM					
40	$1.61	$0.96	$0.57	$0.38	$0.37	$0.28	$0.21	$0.16		
									3rd CAPM (CPR A)	
45									$1.06	$0.67
	5th CAPM		5th CAPM		4th CAPM				1st PCC Rehab	
50	$0.82	$0.57	$0.39	$0.29	$0.25	$0.21	$0.14	$0.12	$2.36	$2.77
	6th CAPM									
55	$0.38	$0.30								
Sub-Total	$20.09	$7.84	$18.87	$4.26	$16.70	$3.08	$13.42	$2.73	$48.87	$9.64
Annual Cost	$0.98		$1.12		$1.97		$1.12		$1.29	
Total Life-cycle Cost	$21.07M (Agency) + $7.84M (RUC) = $28.91M		$19.99M (Agency) + $4.26M (RUC) = $24.25M		$18.67M (Agency) + $3.08M (RUC) = $21.75M		$14.54M (Agency) + $2.73M (RUC) = $17.27M		$50.16M (Agency) +$9.64M (RUC) = $59.81M	
Note:	4% discount rate, 2000 base year				Costs at year 0 represent the initial rehabilitation costs					

Table 3. Final cost comparison: NPV (per lane-mile, 4% discount rate, 2000 base year).

Item cost	Standard AC Alternative 1 CSOL	Alternative 3 FDAC	Innovative AC Alternative 2 CSOL	Alternative 4 FDAC	Long-life PCC Alternative 5 PCC (Overlay)
Agency Cost	$20,094,652	$18,870,000	$16,700,000	$13,420,000	$48,873,142
Annual Cost	$980,000	$1,120,000	$1,970,000	$1,120,000	$1,290,000
User Cost	$7,840,000	$4,260,000	$3,080,000	$2,730,000	$9,644,522
Total Cost	$28,914,652	$24,250,000	$21,750,000	$17,270,000	$59,807,664
Lane-km	25.90	14.80	25.90	14.80	40.70
Total Unit-cost ($/lane-km)	$1,116,396	$1,638,514	$839,768	$1,166,892	$1,469,476
Total Unit-cost ($/lane-mile)	$1,786,233	$2,621,622	$1,343,629	$1,867,027	$2,351,161

shown in Table 4. Values in the table include agency and road user costs as well as the range and mean values of probabilities.

As expected, the probabilities of implementing an untested pavement design are low, as reflected by the low probabilities assigned to the innovative CSOL and FDAC designs without HVS testing. For example, for Benefit #1, without HVS testing PCC lane replacement was assigned a high probability (70%) of implementation and the innovative FDAC was given only a 5% probability. These mean values contrast with those associated with validation through HVS testing in that the innovative FDAC was assigned a 70% probability of implementation and PCC lane replacement only 25%. This reversal pattern is consistent for both benefits.

Given the various probabilities of implementation, the value of benefits from HVS testing can be calculated by subtracting the total expected cost of the "with HVS" situation from the "without HVS situation". The following cost savings for both benefits (agency and road user costs) were realized:

Table 4. Expected costs (based on probabilities and life-cycle costs) for benefits 1 and 2.

Benefit 1: Innovative mixes enabled the improvement of vertical clearance under overcrossings while meeting LLPRS-AC criteria Discount Rate of 4%								
		Probability of implementation				Expected cost ($)		
Decision	Rehabilitation alternatives	Mean	Low	High	Total LCC ($)	Mean	Low	High
Without HVS test	Alt 1: CA std CSOL	0	0	0	1,116,396	1,496,606	1,479,702	1,513,510
	Alt 2: Innovative CSOL	0	0	0	839,768			
	Alt 3: CA std Full Depth AC	0.25	0.15	0.35	1,638,514			
	Alt 4: Innovative Full Depth AC	0.05	0.05	0.05	1,166,892			
	Alt 5: PCC Lane replacement	0.7	0.8	0.6	1,469,476			
With HVS test	Alt 1: CA std CSOL	0	0	0	1,116,396	1,266,119	1,296,377	1,235,861
	Alt 2: Innovative CSOL	0	0	0	839,768			
	Alt 3: CA std Full Depth AC	0.05	0.05	0.05	1,638,514			
	Alt 4: Innovative Full Depth AC	0.7	0.6	0.8	1,166,892			
	Alt 5: PCC Lane replacement	0.25	0.35	0.15	1,469,476			
Unit costs Savings (Saving per lane-km)						230,487	183,325	277,649
Unit costs Savings (Saving per lane-mile)						368,779	293,320	444,239
Benefit 2: Innovative mixes enabled meeting the LLPRS-AC criteria where no vertical limits existed								
Without HVS test	Alt 1: CA std CSOL	0.45	0.35	0.55	1,116,396	1,272,427	1,307,735	1,237,119
	Alt 2: Innovative CSOL	0.05	0.05	0.05	839,768			
	Alt 3: CA std Full Depth AC	0.05	0.05	0.05	1,638,514			
	Alt 4: Innovative Full Depth AC	0.05	0.05	0.05	1,166,892			
	Alt 5: PCC Lane replacement	0.4	0.5	0.3	1,469,476			
With HVS test	Alt 1: CA std CSOL	0.05	0.05	0.05	1,116,396	1,098,805	1,161,776	1,035,835
	Alt 2: Innovative CSOL	0.55	0.45	0.65	839,768			
	Alt 3: CA std Full Depth AC	0.05	0.05	0.05	1,638,514			
	Alt 4: Innovative Full Depth AC	0.05	0.05	0.05	1,166,892			
	Alt 5: PCC Lane replacement	0.3	0.4	0.2	1,469,476			
Unit costs Savings (Saving per lane-km)						173,622	145,959	201,284
Unit costs Savings (Saving per lane-mile)						277,795	233,534	322,055

– Benefit 1: a cost saving of $368,779 (range $293,320–$444,239) per lane-mile.
– Benefit 2: a cost saving of $277,795 (range $233,534–$322,055) per lane-mile.

Although not shown here, the above calculations were repeated isolating the agency costs from the road user costs. The agency cost savings alone were:

– Benefit 1: agency cost saving of $297,893 (range $238,975–$356,812) per lane-mile.
– Benefit 2: agency cost saving of $141,286 (range $126,431–$156,141) per lane-mile.

In the context of the various pavement rehabilitation alternatives available for LLPRS strategies, the HVS tests resulted in more cost-effective pavement designs with substantial savings depending on the degree of implementation.

4.3.1 *Scaling-up*

The determination of the total potential benefit depends on the degree of market penetration. Information available as of early 2011 suggests a minimum of 115 lane-miles will be rehabilitated using the innovative mixes and designs. This includes subsequent rehabilitation phases on the I-710 corridor rehabilitation. Assuming future projects have a proportion of lane-miles that require a similar distribution of dig-out sections (36.4% in the I-710 project) with remaining sections (63.6%) not requiring dig-out, then the total mean cost savings above can be scaled-up as follows:

$$\text{Total cost savings (mean)} = 115 \text{ lane-miles} \times [(36.4\% \times \$368{,}779) + (63.6\% \times \$277{,}795)]$$

This results in total cost savings (sum for Benefits 1 and 2) of $35,755,012 (mean) with extremes of $29,359,074 and $42,150,951 depending on the range of probabilities as shown in Table 4.

Table 5. Net present values and benefit-cost ratios.

Summary of benefits for Caltrans Investment in HVS technology development & implementation (at 4% discount rate)								
Benefit	Contribution Ratio	Range of Probabilities			Contribution Ratio	Range of Probabilities		
		Mean	Low	High		Mean	Low	High
Benefit 1: Innovative mixes enabled the improvement of vertical clearance under overcrossings while meeting the LLPRS-AC criteria	20%	3,087,420	2,455,674	3,719,167	85%	13,121,537	10,436,614	15,806,460
Benefit 2: Innovative mixes enabled meeting the LLPRS-AC criteria where no vertical constraints existed	20%	4,063,582	3,416,141	4,711,023	85%	17,270,224	14,518,599	20,021,848
Total Benefit (2000 base year):		7,151,002	5,871,815	8,430,190		30,391,760	24,955,213	35,828,308
Total HVS Testing Cost (2000 base year)		2,113,200	2,113,200	2,113,200		2,113,200	2,113,200	2,113,200
Benefit Cost Ratio		3.4	2.8	4.0		14.4	11.8	17.0
Summary of benefits excluding RUC for Caltrans Investment in HVS technology development & implementation (at 4% discount rate)								
Benefit 1: Innovative mixes enabled the improvement of vertical clearance under overcrossings while meeting the LLPRS-AC criteria	20%	2,493,964	2,000,695	2,987,233	85%	10,599,346	8,502,952	12,695,740
Benefit 2: Innovative mixes enabled meeting the LLPRS-AC criteria where no vertical constraints existed	20%	2,066,726	1,849,427	2,284,025	85%	8,783,585	7,860,065	9,707,105
Total Benefit (2000 base year):		4,560,690	3,850,122	5,271,258		19,382,931	16,363,017	22,402,845
Total HVS Testing Cost (2000 base year)		2,113,200	2,113,200	2,113,200		2,113,200	2,113,200	2,113,200
Benefit Cost Ratio		2.2	1.8	2.5		9.2	7.7	10.6

4.4 *Analysis of HVS test costs*

In order to calculate the BCR, the total costs of HVS testing and related activities must be calculated and compared with the benefits. Separating the innovations developed for the I-710 rehabilitation from the UCPRC's other research is complex. Reasonable assumptions are, therefore, required before an estimate can be made of the total development cost.

The bulk of the implementable research used for the I-710 rehabilitation project took place during the four years from 1997 to 2000. The total costs of the HVS tests, associated laboratory tests, and analysis for the I-710 project are estimated at $2,113,200, which consists of:

- $1,011 million for the HVS testing to validate the innovative mixes and designs (this includes operational costs, instrumentation, data collection, analysis and reporting);
- $250,000 for the mechanistic-empirical design of the two pavement rehabilitation designs;
- $300,000 for development of CA4PRS and subsequent modeling of the I-710 project;
- $250,000 for the laboratory studies which went towards the characterization of the materials used in the I-710; and
- 20% of all the above added for managerial, analysis, reporting, and administrative costs.

4.5 *Calculation of benefit-cost ratio*

The final step in the determination of the quantifiable benefits from HVS testing is comparison of the total costs of the research to benefits derived after implementation. Table 5 shows results of the final calculations for both benefits.

It should also be borne in mind that the HVS was not solely responsible for the development of the cost-saving innovative mixes and designs in the I-710 project. However, the interviews revealed that full-scale validation provided by HVS tests was a key contributor to the decision to use the innovative mixes

and designs in the I-710 rehabilitation. The extent of cost savings that may be attributed to the HVS tests is accounted for by assigning a contribution ratio, which is multiplied by total cost savings presented above. The contribution ratio is an indicator of how much of the savings from implementing the innovative mixes and designs are due to the HVS tests. The contribution is estimated to be between 20% and 85%, as determined in accordance with inputs from the interviews. Interviewees who assigned low contribution ratios acknowledged that the innovative mixes and designs would not have been implemented without HVS tests.

Table 5 shows that the NPV of the final potential cost saving realized is between $5,872 and $35,828 million depending on the range of probabilities and the contribution ratios. The BCR calculation varied between 2.8 and 17.0 depending on the same probability ranges and contribution ratios.

If road user costs are excluded then BCR values are still positive and varied between 1.8 and 10.6 depending on the probability ranges and contribution ratios.

4.6 *Discussion of results*

Results from the case study are examined from several perspectives including comparisons with economic benefits of APT reported in the National Cooperative Highway Research Program (NCHRP) Synthesis 325 report (NCHRP, 2004). The report is a summary of significant findings from full-scale accelerated pavement testing of APT programs worldwide. Included in the report are direct economic benefits in terms of net savings and BCR benefit-cost ratio and net savings.

In comparing this case study results with that published in NCHRP 325 it should be noted that the NCHRP investigated APT program-wide benefits whereas this case study investigated the quantifiable benefits stemming from project specific HVS testing. It is realized that the results from program-wide investigations will be different from project specific investigations but it is nevertheless important to gauge the results of this study with what has been reported on a world wide scale.

A questionnaire survey of the programs indicated cost saving benefits higher than US$2M for eight of the nine agencies that responded (Figures 5 and 6). BCRs reported by respondents varied from one to higher than 20. Savings and BCRs were reported as provided by respondents and compared in the report without additional analysis. Few details of methods and assumptions for these values are available.

NCHRP Synthesis 325 reported "overall estimated savings/benefits in monetary terms" from survey respondents at two levels. No maximum value for savings/benefits was set. Information about discounting of costs and savings/benefits is not available.

– Savings/benefits ranging from $500k to $1M for one APT program (ISETH, in Switzerland).

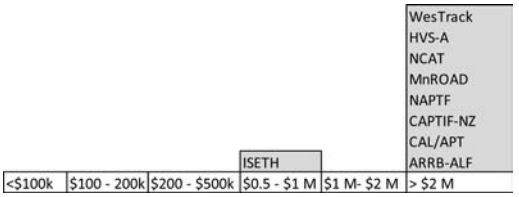

Figure 5. Overall estimated savings/benefits in monetary terms.

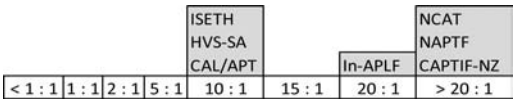

Figure 6. BCR of APT programs (NCHRP, 2004).

– Savings/benefits higher than $2M for eight programs including WesTrack, HVS-Corps of Engineers (Vicksburg, MS), NCAT, MnROAD, FAA, CAPTIF, CAL/APT, and ARRB.

BCR values were reported at three different levels by seven APT programs. No maximum BCR value was defined in the questionnaire.

– BCR of 10 for three APT programs including ISETH, HVS-South Africa, and CAL/APT.
– BCR of 20 for one program (Indiana APT).
– BCR higher than 20 for three programs including NCAT, FAA, and CAPTIF.

Cost savings from this case study are consistent with the highest level of savings (higher than $2M) reported from the NCHRP 325 survey. BCR values from the case study span the range of values reported in NCHRP 325. BCRs for an assumed low contribution ratio from the case study are in the lower end of values (approximately from 2:1 to 5:1) reported in the Synthesis. For assumed high contribution ratios, BCRs from this case study are in the upper range (from 15:1 to 20:1) of values reported in the Synthesis.

5 COMPARISONS WITH PREVIOUS STUDIES AT 4% DISCOUNT RATE

Comparing BCR values for a discount rate of 4% that was used in the I-710 case study and also reported in the Australian and South African cost-benefit analysis studies reveals the following:

– The Australian ALF program reported a BCR of 4.9 for the overall APT program and BCRs of between 1.4 and 11.6 for individual ALF tests (Rose and Bennett, 1994; BTA Consulting, 1992).
– The South African HVS study involved BCR calculations on provincial and national levels (managed by the South African National Roads agency). On the provincial level the use of the G1 base course technology was measured by Gautrans. BCR values of between 2.2 to 5.6 (low contribution ratio) and

Table 6. NPV and BCR from the South African study (Jooste and Sampson, 2005).

Benefit	Lower Contribution Ratio: Contribution Ratio	Discount Rate of 4%	Discount Rate of 8%	Discount Rate of 12%	Higher Contribution Ratio: Contribution Ratio	Discount Rate of 4%	Discount Rate of 8%	Discount Rate of 12%
Benefit Summary for Gautrans Investment in HVS Investigations on G1 Base Pavements								
Increased use of G1 base pavements	50%	535,117	410,881	318,534	80%	856,187	657,409	509,654
Increased use of 150 mm thick G1 Layers	20%	55,267	42,436	32,898	30%	82,900	63,653	49,347
Improved Maintenance and construction practices	30%	183,504	140,900	109,233	60%	367,007	281,801	218,465
Total Benefit (in 1978 SA Rand)		773,887	594,217	460,665		1,306,094	1,002,863	777,467
Total Costs (in 1978 SA Rand)		358,261	340,669	324,813		358,261	340,669	324,813
Benefit Cost Ratio		2.2	1.7	1.4		3.6	2.9	2.4
Total Benefit (in 2004 SA Rand)		2,145,579	4,395,036	8,771,091	N/A	3,621,107	7,417,530	14,803,024
Benefit Summary for SANRAL Investment in HVS Investigations on G1 Base Pavements								
Increased use of G1 Base Pavements	50%	488,451	375,049	290,756	80%	781,522	600,079	465,209
Increased use of 150 mm thick G1 Layers	20%	85,307	65,501	50,780	30%	127,960	98,252	76,169
Improved Maintenance and Construction Practices	30%	656,590	504,152	390,842	60%	1,313,179	1,008,303	781,684
Total Benefit (in 1978 SA Rand)		1,230,347	944,702	732,378		2,222,661	1,706,634	1,323,063
Total Costs (in 1978 SA Rand)		218,277	194,911	174,765		218,277	194,911	174,765
Benefit Cost Ratio		5.6	4.8	4.2		10.2	8.8	7.6
Total Benefit (in 2004 SA Rand)		3,411,101	6,987,351	13,944,522		6,162,261	12,622,867	25,191,213
Benefit Summary for Combined Gautrans and SANRAL Investment in HVS Investigations on G1 Base Pavements								
Increased use of G1 Base Pavements	50%	1,023,568	785,930	609,290	80%	1,637,709	1,257,488	974,864
Increased use of 150 mm thick G1 Layers	20%	140,573	107,937	83,678	30%	210,860	161,905	125,517
Improved Maintenance and Construction Practices	30%	840,093	645,052	500,075	60%	1,680,187	1,290,104	1,000,149
Total Benefit (in 1978 SA Rand)		2,004,235	1,538,919	1,193,042		3,528,755	2,709,497	2,100,530
Total Costs (in 1978 SA Rand)		576,538	535,580	499,578		576,538	535,580	499,578
Benefit Cost Ratio		3.5	2.9	2.4		6.1	5.1	4.2
Total Benefit (in 2004 SA Rand)		5,556,680	11,382,386	22,715,611		9,783,368	20,040,396	39,994,235

3.6 to 10.2 (high contribution ratio) were reported (Jooste and Sampson, 2005).

– The California I-710 HVS tests calculated BCR values from 2.8 to 4.0 (low contribution ratio) and 11.8 to 17.0 (high contribution ratio) which include RUC benefits.

Although the California study has a higher variability of BCR values, these results are similar to the other two APT programs. As mentioned the benchmark credibility of this type of analysis lies in the acceptance of the results by road authorities and practitioners. Their input and the variability of their responses are the main reasons behind the range of BCR values calculated. One of the criticisms of BCR (and CBA itself) is the effect of inputs, assumptions, and subjectivity (e.g., probabilities) on results as shown in the sensitivity analysis. However, sensitivity analysis is recommended because it enables examination of these effects for interpretation and use of CBA results.

Another possible reason for differences in the BCR values in the California study is the inclusion of road

Table 7. NPV and BCR from ARRB trails and program (BTA Consulting, 1992).

	Banalla	Beerburrum	Prospect	Callington	Mulgrave	Brewarrina	Total
Cost ($M, $1992)	0.9	2.2	1.8	2.4	1.8	0.7	9.8
Benefits ($M, $1992) at discount rate of							
4%	5.4	13.9	2.5	8.3	10.1	8.1	48.3
6%	4.8	11.4	2.3	6.9	9.3	7.7	42.4
8%	4.6	9	2.1	5.8	8.7	7.3	37.5
Benefit-Cost Ratio at discount rate of							
4%	6	6.2	1.4	3.5	5.7	11.6	4.9
6%	5.4	5.1	1.3	2.9	5.2	11	4.3
8%	5.1	4	1.2	2.5	4.9	10.4	3.8

user costs. Neither the Australian nor South African study evaluated user costs and instead included only agency costs in their investigations. Excluding the road user costs from the case study, the California I-710 HVS tests calculated BCR values from 1.8 to 2.5 (low contribution ratio) and 7.7 to 10.6 (high contribution ratio) which are more in line with both the Australian and South African studies (see bottom of Table 5).

5.1 *South Africa – variability of BCR based on contribution ratio and discount rate*

Results from the South African study are shown in Table 6 for low and high contribution ratios as well as various discount rates. Costs and benefits were adjusted in that study using discount rates of 4, 8, and 12 percent. The BCR data for the Gautrans investment in G1 base technology differs from the results of the SANRAL BCR data due to the differences in the degree of implementation and other differences such as construction costs, etc. For low contribution ratios, BCR values varied from 1.4 (at 12 percent) to 5.6 (at 4 percent). For high contribution ratios, BCRs ranged from 2.4 (at 12 percent) to 10.2 (at 4 percent).

5.2 *Australia – economic benefits of ALF trials and ALF program*

Results from the ARRB evaluation are shown in Table 7 for the overall ALF program and for individual trials. Costs and benefits (reported in Australian dollars) were adjusted using discount rates of 4, 6, and 8 percent. Benefits for the overall ALF program ranged from $48.3M (at 4 percent) to $37.5M (at 8 percent). Benefits for individual trials ranged from $2.1M to $13.9M. BCR values for the overall ALF program were 3.8 to 4.9 and for individual trials ranged from 1.2 to 11.6. ARRB concluded that these results provided evidence of a "healthy return" on investments in the ALF program (Rose and Bennett, 1994; BTA Consulting, 1992).

The results illustrate the variability of benefits produced from different APT projects as well as the contrast with benefits when calculated for an entire APT program. BCR values for individual ALF trials vary from 1.2 to 11.6 depending on discount rate. In contrast, the BCR for the ALF program ranged from 3.8 to 4.9.

5.3 *UCPRC – comparing project benefits to program costs*

Published studies have suggested evaluating research benefits by comparing the costs of an entire research program with the economic benefits of a few outstanding projects referred to as "big winners" or "nuggets" (Nokes et al., 2011). Such projects are evident when economic benefits from research outputs far exceed not only the cost of the project but total costs of the research program as well.

The HVS tests were pivotal to validation and use of the innovative mixes on the I-710 rehabilitation project, which was expected to produce substantial technical benefits—and has met or exceeded performance expectations in the years since opening to traffic. But economic benefits of HVS testing of those mixes have not been compared previously to the total cost of the CAL/APT program during the period (1997–2001) evaluated in this case study.

Positive results would suggest that the I-710 HVS testing project was a "nugget" as described in the literature. Total costs for the CAL/APT program from 1997 to 2000 were determined to be $9.836M. NPV of benefits from Table 5 were used to calculate BCRs. Assuming a low contribution and a low probability, the NPV of the benefits of the I-710 HVS test is between $5.87M and $8.43M, amounting to at least half of the costs for the entire APT program during this four-year period (1997–2000). Looking at higher contribution ratios and higher probabilities, the benefits stemming from the HVS project are over $35M (Table 5). The project's direct economic benefits are high (using any of these assumptions) in contrast to the cost of the whole program, suggesting that the HVS testing for the I-710 project mixes was indeed a "nugget" and "big winner" for the California APT program.

6 CONCLUSIONS

This paper summarizes a study to determine the direct economic benefits stemming from the validation tests of innovative materials and pavement designs using the

HVS in California. Developed and tested in Australia, applied and enhanced in South Africa, and subsequently adapted to California conditions for evaluating benefits from APT, the method shows promising results.

The net present value of cost savings is between $5,872 and $35,828 million with associated benefit-cost ratios of between 2.8 and 17.0 depending on the range of probabilities and contribution ratios as determined through an extensive interview process. The study highlights the importance of sensitivity analysis to determine ranges of savings instead of a single benefit-cost ratio value.

ACKNOWLEDGEMENTS

The authors thank the pavement practitioners who provided crucial input for this pilot study, the foundational work done by the ARRB, and subsequent work by South African engineers. Caltrans' research partners at the UCPRC, Dynatest Consulting Inc., and the CSIR performed HVS testing and research, which was funded by Caltrans and the FHWA. The authors thank the Caltrans Library for assistance in acquiring references. The contents of this paper reflect the views of the authors, who are responsible for the facts and the accuracy of the data. The contents do not necessarily reflect the official views or policies of the CSIR or the State of California. This paper does not constitute a standard, specification, or regulation.

REFERENCES

BTA Consulting. 1992. *Economic evaluation of the ALF program*. APRG Report 5, Austroads Pavement Research Group/ARRB, Victoria, Australia.

California Department of Transportation. 2007. *Interim Life-Cycle Cost Analysis Procedures Manual*. www.dot.ca.gov/hq/esc/Translab/OPD/DivisionofDesign-LCCA.htm. Accessed July 17, 2008.

De Neufville, R. 1990. *Applied Systems Analysis: Engineering Planning and Technology Management*. McGraw-Hill, New York, 1990.

Du Plessis, L., Rust, F.C. Horak, E. Nokes, W.A. and Holland, J.T. 2008. Cost Benefit Analysis of the California HVS Program, *3rd International Conference on Accelerated Pavement Testing*, Madrid, Spain.

Du Plessis, L., Nokes, W.A., Mahdavi, M., Burmas, N., Holland, J.T. and Lee, E.B. 2011. A Case Study of Economic Benefits Assessment of APT Research in California. *Transportation Research Record: Journal of the Transportation Research Board, 2225*. The Transportation Research Board of the National Academies. Washington, DC. pp. 137–146.

FHWA, U.S. Department of Transportation Office of Asset Management. 1998. *Life-Cycle Cost Analysis in Pavement Design*. Publication FHWA-SA-98-079, Interim Technical Bulletin, Washington, DC. www.fhwa.dot.gov/infrastructure/asstmgmt/lcca.htm. Accessed April 28, 2008.

Harvey, J.T., Santero, N., Lee, H., Du Toit, W. and Fermo, G. 2005. *Evaluation of I-710 Long Beach (07-1384U4) Long-Life Pavement Rehabilitation Costs*. Davis and Berkeley, CA: University of California Pavement Research Center. UCPRC-TM-2005-06.

Horak, E., Kleyn, E.G., Du Plessis, J.A., De Villiers, E.M. and Thompson, A.L. 1992. The Impact and Management of the Heavy Vehicle Simulator (HVS) Fleet in South Africa. In Proceedings of the *7th International Conference on Asphalt Pavements, Nottingham, Vol. 2*, UK.

Jooste, F. and Sampson, L. 2004. *Assessment of Gautrans HVS Programme Benefits – Pilot Study Report*. Modeling and Analysis Systems for Gauteng Provincial Government, Department of Public Transport, Roads and Works, Gauteng, South Africa.

Jooste, F. and Sampson, L. 2005. *The Economic Benefits of the HVS Development Work on G1 Base Pavements*. Modeling and Analysis Systems for Gauteng Provincial Government, Department of Public Transport, Roads and Works, Gauteng, South Africa.

Lee, E.B. Kim, C. and Harvey. J.T. 2011. Implementation of Construction Analysis Tools on Life-Cycle Cost Analysis of Highway Rehabilitation: A Case Study of California Interstate 710 Long Beach Project. Paper 11-1127. In *CD-ROM Proceedings of the 90th Annual Meeting of the Transportation Research Board*. Washington, DC.

Monismith, C.L. and Long, F. 1999. *Mix Design and Analysis and Structural Section Design for Full Depth Pavement for Interstate Route 710*. Davis and Berkeley, CA: University of California Pavement Research Center. TM-UCB-PRC-99-2.

Monismith, C.L. and Long. F. 1999. *Overlay Design for Cracked and Seated Portland Cement Concrete (PCC) Pavement – Interstate Route 710*. Davis and Berkeley, CA: University of California Pavement Research Center. TM-UCB-PRC-99-3.

Monismith, C.L., Harvey, J.T., Tsai, B.W., Long, F. and Signore, J. 2009. *Summary Report: The Phase I I-710 Freeway Rehabilitation Project: Initial Design (1999) to Performance after Five-plus Years of Traffic*. Davis and Berkeley, CA: University of California Pavement Research Center. UCPRC-SR-2008-04.

Nokes, W., Du Plessis, L., Mahdavi, M. and Burmas, N. 2011. Techniques and Case Studies for Evaluating Benefits of Accelerated Pavement Testing. *Transportation Research Record: Journal of the Transportation Research Board, 2225*, The Transportation Research Board of the National Academies. Washington, D.C., pp. 147–154.

Rose, G. and Bennett, D. 1994. Benefits from Research Investment: Case Study of Australian Accelerated Loading Facility Pavement Research Programme. *Transportation Research Record: Journal of the Transportation Research Board, 1445*, The Transportation Research Board of the National Academies. Washington, D.C., pp. 82–90.

Samson, D. 1988. *Managerial Decision Analysis*. Irwin, Homewood, IL.

Wu, R. Harvey, J.T. and Bejarano, M. 2006. *Performance of Asphalt Concrete Overlay of PCC Pavement under Accelerated Loading-Summary Report*. Davis and Berkeley, CA: University of California Pavement Research Center. UCPRC-RR-2005-07.

This page intentionally left blank

Internationally, full-scale accelerated pavement testing, either on test roads or linear/circular test tracks, has proven to be a valuable tool that fills the gap between models and laboratory tests and long-term experiments on in-service pavements. Accelerated pavement testing is used to improve understanding of pavement behavior, and evaluation of innovative materials and additives, alternative materials processing, new construction techniques, and new types of structures. It provides quick comparisons between current and new practice and the ability to rapidly validate and calibrate models with quality data, with minimal risk at relatively low cost.

Advances in Pavement Design through Full-scale Accelerated Pavement Testing is a collection of papers from the 4th International Conference on Accelerated Pavement Testing (Davis, CA, USA, 19-21 September 2012), and includes contributions on a variety of topics including:

- Overview of accelerated pavement testing
- Establishment of new accelerated pavement testing facilities
- Review of the impact of accelerated pavement testing programs on practice
- Instrumentation for accelerated pavement testing
- Accelerated pavement testing on asphalt concrete pavements
- Accelerated pavement testing on portland cement concrete pavements
- Accelerated pavement testing to evaluate functional performance
- Relating laboratory tests to performance using accelerated pavement testing
- Development and calibration of empirical and mechanistic-empirical pavement Design procedures and models
- Benefit-cost analysis of accelerated pavement testing

Advances in Pavement Design through Full-scale Accelerated Pavement Testing will be useful to academics and professionals involved in pavement engineering.

CRC Press
Taylor & Francis Group
an **informa** business
www.crcpress.com

6000 Broken Sound Parkway, NW
Suite 300, Boca Raton, FL 33487
Schipholweg 107C
2316 XC Leiden, NL
2 Park Square, Milton Park
Abingdon, Oxon OX14 4RN, UK

ISBN 978-0-415-62138-0

an **informa** business